V. 19

NUCLEAR PHYSICS

JOURNAL DEVOTED TO THE EXPERIMENTAL AND THEORETICAL STUDY OF THE FUNDAMENTAL CONSTITUENTS OF MATTER AND THEIR INTERACTIONS

EDITOR: L. ROSENFELD - COPENHAGEN
ASSOCIATE EDITOR: O. NATHAN - COPENHAGEN

VOLUME XIX

NORTH-HOLLAND PUBLISHING COMPANY - AMSTERDAM

NUCLEAR PHYSICS

EDITORIAL BOARD

AUSTRALIA & NEW ZEALAND:	H. Messel (Sydney), M. L. Oliphant (Canberra)
AUSTRIA:	B. Karlik (Vienna), H. Thirring (Vienna)
BELGIUM:	M. de Hemptinne (Louvain), J. Verhaeghe (Ghent)
CANADA:	G. Volkoff (Vancouver)
DENMARK:	C. Møller (Copenhagen), S. Rozental (Copenhagen), G. E. Brown (Copenhagen)
FINLAND:	L. Simons (Helsinki)
FRANCE:	A. Berthelot (Saclay), S. Gorodetzky (Strasbourg)
GERMANY (DEM. REP.):	G. Hertz (Leipzig)
GERMANY (FED. REP.):	W. Gentner (Freiburg i. B.), J. H. D. Jensen (Heidelberg)
GREAT BRITAIN:	S. Devons (Manchester), T. H. R. Skyrme (Harwell)
HUNGARY:	L. Janossy (Budapest)
INDIA:	H. Bhabha (Bombay), R. Ramanna (Trombay)
IRISH REPUBLIC:	J. McConnell (Maynooth)
ISRAEL:	G. Racah (Jerusalem)
ITALY:	E. Amaldi (Rome)
JAPAN:	S. Kikuchi (Tokyo), S. Tomonaga (Tokyo)
MEXICO:	M. Moshinsky (Mexico)
NETHERLANDS:	H. Brinkman (Groningen), S. R. de Groot (Leiden)
NORWAY:	E. Hylleraas (Oslo), A. Lundby (Oslo), H. Wergeland (Trondheim)
POLAND:	L. Infeld (Warsaw)
PORTUGAL:	J. M. Araújo (Porto), J. R. de Almeida Santos (Coimbra)
SOUTH AMERICA:	G. Beck (Saõ Paulo), J. Leite Lopes (Rio de Janeiro)
SPAIN:	J. M. Otero (Madrid), C. Sanchez del Rio (Madrid)
SWEDEN:	O. Klein (Stockholm), K. Siegbahn (Uppsala), I. Waller (Uppsala)
SWITZERLAND:	P. Huber (Basel), P. Scherrer (Zürich)
U.A.R. & ARAB COUNTRIES:	F. El Bedewi (Alexandria), M. G. Nooh (Cairo)
U.S.A.:	H. H. Barschall (Madison, Wisconsin), V. Weisskopf (Cambridge, Mass.)
U.S.S.R.:	M. A. Markov (Moscow), I. S. Shapiro (Moscow), D. V. Skobeltzyn (Moscow)
YUGOSLAVIA:	I. Supek (Zagreb)

NUCLEAR PHYSICS

JOURNAL DEVOTED TO THE EXPERIMENTAL AND THEORETICAL STUDY OF THE FUNDAMENTAL CONSTITUENTS OF MATTER AND THEIR INTERACTIONS

EDITOR: L. ROSENFELD - COPENHAGEN

VOLUME XIX

SEPTEMBER 1960 — DECEMBER 1960

NORTH-HOLLAND PUBLISHING COMPANY-AMSTERDAM

PRINTED IN THE NETHERLANDS

1.D.2:
1.E.1

Nuclear Physics **19** (1960) 1—17; © *North-Holland Publishing Co., Amsterdam*
Not to be reproduced by photoprint or microfilm without written permission from the publisher

LOW LEVELS OF Al^{27}

E. ALMQVIST, D. A. BROMLEY, H. E. GOVE and A. E. LITHERLAND

Chalk River Laboratory, Atomic Energy of Canada Limited, Chalk River, Ontario, Canada

Received 8 March 1960

Abstract: The de-excitation radiation from the 0.84 and 1.013 MeV levels in Al^{27} has been studied at a number of resonances in the reaction Al^{27} (p,p'γ) with proton energies between 1.7 MeV and 2.8 MeV. The data support assignments $\frac{1}{2}^+$ and $\frac{3}{2}^+$ to the 0.84 and 1.013 MeV states. The 1.013 MeV state is observed to be de-excited, 2.4 ($\pm$ 0.3)% via a 0.170 MeV transition to the 0.84 MeV level and the remainder to the ground state. It is shown that either one or both of these radiations have an E2/M1 amplitude ratio $\gtrsim$ 0.2. These results and other properties of the low levels of Al^{27} are discussed in terms of the rotational collective model which is found to give a good qualitative description of most of the known data.

1. Introduction

The results of previous investigations[1, 2]) of the low energy levels of Al^{27} are summarised in fig. 1. The excitation energies have been computed from the precise measurements[2]) of the energies of protons scattered inelastically by aluminium. The level assignments are based on the results of a number of researches reviewed by Endt and Braams[1]). They include the measurements described in this paper of which only a preliminary report has been made earlier[3]). These studies were undertaken to determine the properties of the first

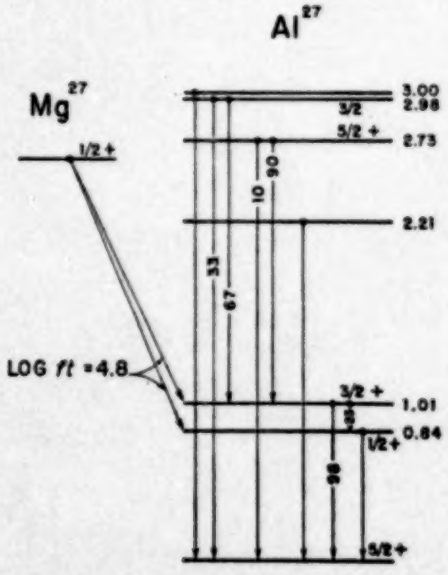

Fig. 1. Low energy levels of Al^{27}. The present data establish $J = \frac{3}{2}$ for the 1.013 MeV state and show that either one or both transitions from the 1.013 MeV state has a ratio E2/M1 width $\gtrsim$ 0.03

and second excited states of Al^{27} and to gain information about the applicability of the rotational collective model to mass 27 nuclei. This model was applied with considerable success to Al^{25} by Litherland *et al.*[4]) and has been found to give a good qualitative description of many other d-shell nuclei[5]).

The ground state properties of Al^{27} are known to be $\frac{5}{2}^+$ from the spectrographic measurements of Brown and Williams[6]). The absence of a beta transition to this state in the decay of Mg^{27} supports the shell model assignment of $\frac{1}{2}^+$ to the latter nuclide. This assignment together with the allowed nature of the beta transitions to the 0.84 MeV and 1.013 MeV states strongly suggests that they have spin either $\frac{1}{2}$ or $\frac{3}{2}$ and even parity. These assignments are supported by the measurements of internal conversion coefficients by Rankin *et al.*[1]).

In order to obtain information about the multipole mixing in the radiations use is made of a relation among the angular distribution coefficients of two competing radiations arising from the de-excitation of a single state. The relation follows from angular correlation theory[7,8]) provided that the nature of the gamma-ray de-excitation of the state is assumed to be independent of its mode of formation in which case the ratio of the coefficients a_k/a_0 in the Legendre polynomial expansion of the angular distribution of the gamma radiation may be factored into two main terms. If the state is formed by the inelastic scattering of protons and the scattered particles are unobserved the ratio may be expressed by[8])

$$\frac{a_k}{a_0} = \alpha_k = \left\{\frac{\sum (-1)^\lambda Z(l_1 j_1 l_1' j_1', s_1 k)\, W(j_1 j_2 j_1' j_2, L_1 k)}{\sum (-1)^\lambda Z(l_1 j_1 l_1' j_1', s0)\;\; W(j_1 j_2 j_1' j_2, L_1 0)}\right\} \left\{\frac{\sum Z_1(L_2 j_2 L_2' j_2, I_2 k)}{\sum Z_1(L_2 j_2 L_2' j_2, I_2 0)}\right\}, \quad (1)$$

provided that the gamma-ray de-excitation is independent of the method of forming the state. The Z and W coefficients[7,8]) are functions of the orbital angular momenta l, channel spins s, and nuclear spins j involved in the inelastic scattering process. These parameters, collected in the first bracket which concerns the process leading to the formation of the gamma emitting state, in general are not known but are independent of the multipolarities L_2 and spins I_2 involved in the gamma ray de-excitation. When the quotient α_k^1/α_k^2 is taken for a pair of competing transitions from a given state the identical terms in Z and W cancel and the result is a function of Z_1 coefficients only:

$$\frac{\alpha_k^1}{\alpha_k^2} = \frac{\sum Z_1(\xi^1 k)}{\sum Z_1(\xi^1 0)} \Big/ \frac{\sum Z_1(\xi^2 k)}{\sum Z_1(\xi^2 0)}, \quad (2)$$

where ξ^1 has been written for all the quantum numbers describing one transition and ξ^2 for those describing the other. The sums are taken over all values of ξ compatible with the conservation laws. If the spins are known the quotient defined by eq. (2) can be computed as a function of the multipole mixing in the

radiation to yield a contour plot such as shown in fig. 2 for the radiations from the 1.013 MeV state in Al^{27}.

In fig. 2 the contour lines represent the loci of points with a constant value of the quotient defined by eq. (2). The corresponding E2/M1 amplitude ratios for the two competing de-excitation radiations may be obtained from the

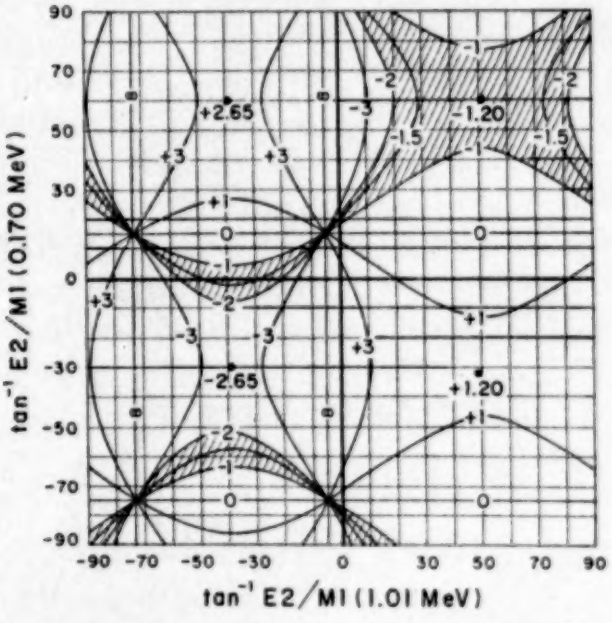

Fig. 2. Plot of the E2/M1 amplitude ratio of the 0.170 MeV transition against that of the 1.013 MeV ground state transition as a function of the ratio $\alpha_2(0.170)/\alpha_2(1.013)$ discussed in the introduction. The contour lines represent loci of points with constant value of the ratio of α_2 coefficients. For convenience in plotting, the ordinate and abscissa are $\tan^{-1}$E2/M1 (amplitude ratio). The measured ratio of α coefficients allows points in the cross-hatched area lying between $\alpha_2(0.170)/\alpha_2(1.013)$ equal -1 and -2. This area does not contain the origin which represents pure M1 radiation for both transitions and lies on $\alpha_2(0.170)/\alpha_2(1.013)$ equal $+5$.

abscissa and ordinates; the numerical scales give the values of the angle defined by $\tan^{-1}$ E2/M1 (amplitude ratio) which forms a convenient representation of the multipole mixing ratio over the entire range from zero to infinity. The 1.013 MeV state of Al^{27} de-excites[3,9]) both by a ground state transition and by a weak branch to the 0.84 MeV state; the measured angular distributions together with the contour plot of fig. 2 are used to obtain information about the multipole mixing in these transitions.

2. Apparatus

2.1. TARGET ARRANGEMENT

The Chalk River 3 MeV Van de Graaff generator was used with an experimental arrangement similar to that reported in previous communications[10]) except for modifications made to facilitate the study of the 0.17 MeV cascade radiation from the state at 1.013 MeV to that at 0.842 MeV. Since this soft

radiation is highly absorbed in materials of high atomic number, the target chamber walls were made of 0.32 cm lucite and the targets were evaporated on to backings of 0.16 cm pure graphite. The graphite backing had the additional advantage of avoiding the prolific yield of low energy radiations which result from Coulomb excitation of many elements of higher atomic number commonly used as target supports.

2.2. GAMMA-RAY DETECTORS

The gamma ray detectors were two NaI scintillator assemblies (12.7 cm diameter, 10.2 cm deep), mounted on arms that allowed them to be moved in a horizontal plane to any angle with respect to the beam. For direct measurements the front face of the detectors were at 26 cm from the target while for coincidence correlations they were moved in to 12 cm. The outputs of the detectors were amplified using conventional electronics and the pulse-height distributions displayed on a 30-channel pulse-height analyser. Energy calibrations were obtained using the following radioactive sources:

$$\text{RdTh} - 2.62 \text{ MeV}; \text{Na}^{22} - 1.275 \text{ MeV and } 0.511 \text{ MeV}; \text{Zn}^{65} - 1.112 \text{ MeV};$$

$$\text{Cs}^{137} - 0.661 \text{ MeV}; \text{Pr}^{144} - 0.134 \text{ MeV}.$$

2.3. COINCIDENCE ARRANGEMENT

Coincidence measurements were made using a "slow-fast" coincidence arrangement which allowed any portion of the pulse height spectrum of one detector to be selected by a single-channel analyser. The pulses from the second detector which were in time coincidence with the selected pulses from the first could be recorded on the 30-channel analyser. Measurements of this type will be referred to later as "gated" coincidence studies. A coincidence resolving time $2\tau = 40 \times 10^{-9}$ s was used.

When making coincidence measurements it is important to eliminate coincidences caused by radiation from the target which is Compton scattered from one detector into the second. In the present measurements the scattering of low energy radiation from either crystal into the other was prevented by a sheet of lead 2 mm thick placed in front of one crystal. The detector with the lead in front of it could not detect low energy radiation but retained adequate sensitivity for the 0.84 MeV gamma rays; at this energy the lead is computed to reduce the efficiency to 82% of its normal value.

The fact that without the lead shield coincidences could be observed between Compton recoils in one crystal and back scattered radiation reaching the second crystal was employed to test the circuitry and to obtain an additional calibration point. The detector arrangement shown in the inset in fig. 3 was used with a Cs^{137} source in the target position. The lead sheet in front of crystal A was removed and the "gated" coincidence circuitry arranged so that only pulses

from crystal B were recorded that were coincident with the most energetic Compton recoils from 0.661 MeV radiation in crystal A. The backscattered radiation which is computed to have an energy of 0.184 MeV results in the pulse height distribution shown in the upper part of fig. 3 together with the 0.134 MeV peak from a Pr^{144} source. When the lead sheet was re-installed in front of

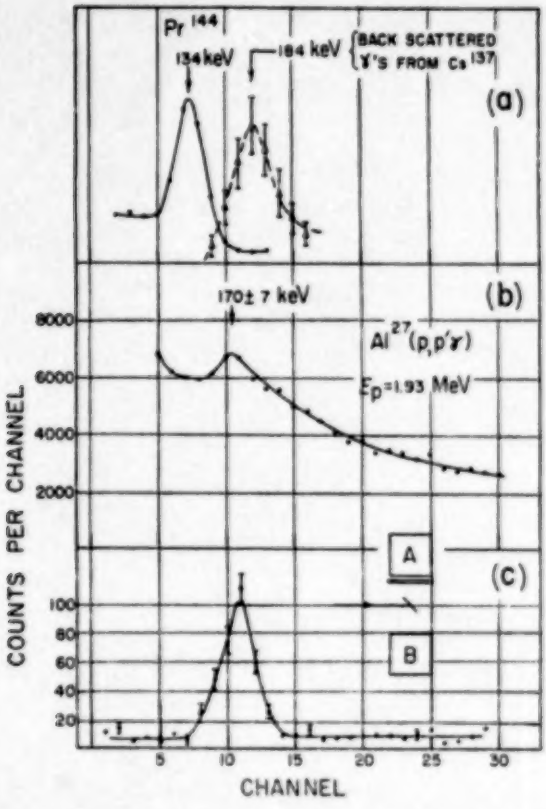

Fig. 3. Part (a) shows the low energy calibration data discussed in the text. Part (b) shows evidence for a 0.170 MeV transition in direct radiation from $Al^{27}(p,p'\gamma)$ and part (c) shows 0.170 MeV radiation detected in coincidence with 0.84 MeV radiation using two 12.7 × 10.2 cm crystals arranged as indicated.

crystal A there were no coincidences observed in the same time interval although the counting rate in the Compton peak was 82% of its original value thus demonstrating the efficiency of the lead shield in stopping backscattered radiation.

3. Results

3.1. GENERAL

Fig. 4 shows typical spectra obtained at three different resonances in the Al^{27} $(p,p'\gamma)$ reaction. Because this work is concerned only with radiations from states in Al^{27} at 1.013 and 0.84 MeV the pulse-height scale shown does not extend above 1.4 MeV energy. The peak which appears near the upper end of the pulse spectrum in each curve is the 1.368 MeV gamma ray from the reaction Al^{27} $(p,\alpha\gamma)$ Mg^{24}. In addition there are radiations of still higher energy which

fall above the top end of the analyzer from the relatively low yield capture reaction Al^{27} (p,γ)Si^{28}. Pair production by this high energy radiation results in annihilation radiation which causes the peak in channel five. The remaining peaks are from the Al^{27}(p,p'γ) reactions; in the upper curve only the 1.013 MeV radiation is clearly visible while at the other resonances that are illustrated both

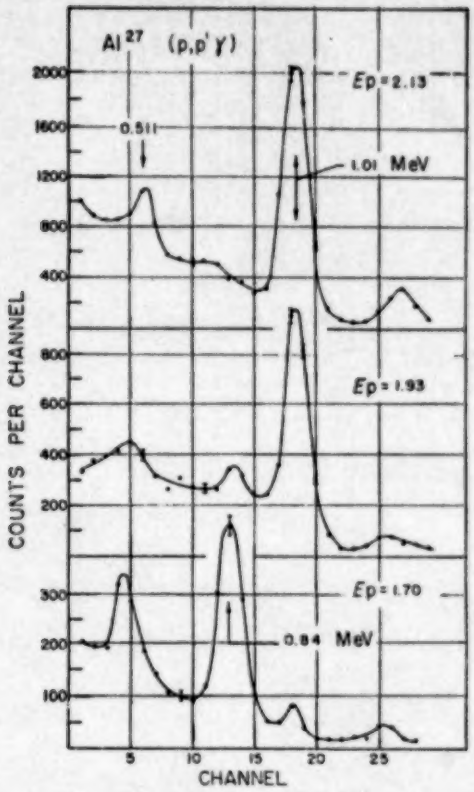

Fig. 4. Typical gamma-ray pulse spectra at three resonances. Peaks corresponding to gamma rays of 0.84 and 1.01 MeV from Al^{27}(p,p'γ) together with 1.37 MeV radiation from Al^{27}(p,$\alpha\gamma$)Mg^{24} and 0.51 annihilation radiation are seen.

the 1.013 and the 0.84 MeV gamma ray peaks appear.

As already discussed in the introduction, the Mg^{27} beta decay is consistent only with spins $\frac{1}{2}$ or $\frac{3}{2}$ for both the 0.84 and 1.013 MeV states; the observation of an anisotropy of the angular distribution in this case is sufficient to rule out the $J = \frac{1}{2}$ possibility and consequently determine the spin of the corresponding state. To search for an anisotropy two gamma-ray detectors were arranged to measure the yield simultaneously at 0° and 90° to the beam. In table 1 are given the results of these measurements made at several resonances. For 9 of the 15 cases studied significant deviations from isotropy are observed for the 1.013 MeV radiation leaving spin $\frac{3}{2}$ as the only possibility for this state. For all 8 cases where the 0.84 MeV radiation had sufficient intensity for significant comparisons to be made isotropy is observed which strongly favours spin $\frac{1}{2}$ for this state. These assignments are assumed in the discussion that follows.

TABLE 1

The ratio of the intensity at 90° to that at 0° of the 1.013 and 0.84 MeV radiations excited in the reaction Al^{27} (p,p'γ)

Proton Energy MeV	Ratio 90°/0° Yields	
	1.013 MeV	0.84 MeV
1.74†	1.20††	0.98††
1.77	1.26	0.98
1.82	1.10	
1.94†	1.00	
1.99	1.03	
2.13†	0.85	0.99
2.34	0.99	
2.39	0.89	1.00
2.43	1.01	
2.47	1.03	1.00
2.51	1.08	0.97
2.56	0.88	1.00
2.60	1.01	1.00
2.70	1.15	
2.78	1.25	

† Detailed studies made at these resonances.

†† The limits of error in the second and the third column are everywhere ± 0.04.

3.2. COINCIDENCE STUDIES

In order to confirm the existence of a cascade transition from the 1.013 MeV level through that at 0.84 MeV the measurements shown in fig. 5 were made using the two detectors arranged as in fig. 3. The gain of detector A was adjusted to display the region near 1 MeV on the analyzer while detector B was adjusted to display the region near 0.170 MeV; the direct spectra from the detectors are shown in figures 5(a) and (b) respectively. In addition to a strong 1.013 MeV ground state transition there is evidence for a weak transition measured to be 0.170 ± 0.007 MeV energy; the corresponding 0.84 MeV cascade transition is obscured by the Compton edge of the intense 1.013 MeV gamma ray in the direct spectra. However the coincidence spectra of figs. 5(c) and (d) discussed below verify that a 0.84 MeV transition is in cascade with that of 0.170 MeV.

Figures 5(c) and (d) show the distribution of pulses which are in time coincidence with pulses in the gates indicated by the cross hatched areas in figs. 5(b) and (a) respectively. The curve of fig. 5(d) clearly shows the 0.170 MeV radiation coincident with the gate (fig. 5(a)) set on the 0.84 MeV region in the other detector. When the gate is set on the 0.170 MeV region indicated in fig. 5(b) the 0.84 MeV radiation clearly appears in the coincident distribution of fig. 5(c) together with annihilation radiation from higher energy radiations whose pulse distribution tails fall in the gate. As an additional check a coinci-

dence measurement was made with the gate set on the 1.013 MeV peak; for the same irradiation as above only 4 coincidence counts attributed to chance were obtained. These measurements show that within the experimental resolving time 2τ equal 40×10^{-9} s the 0.84 and 0.170 MeV radiations are coincident and consequently must be in cascade.

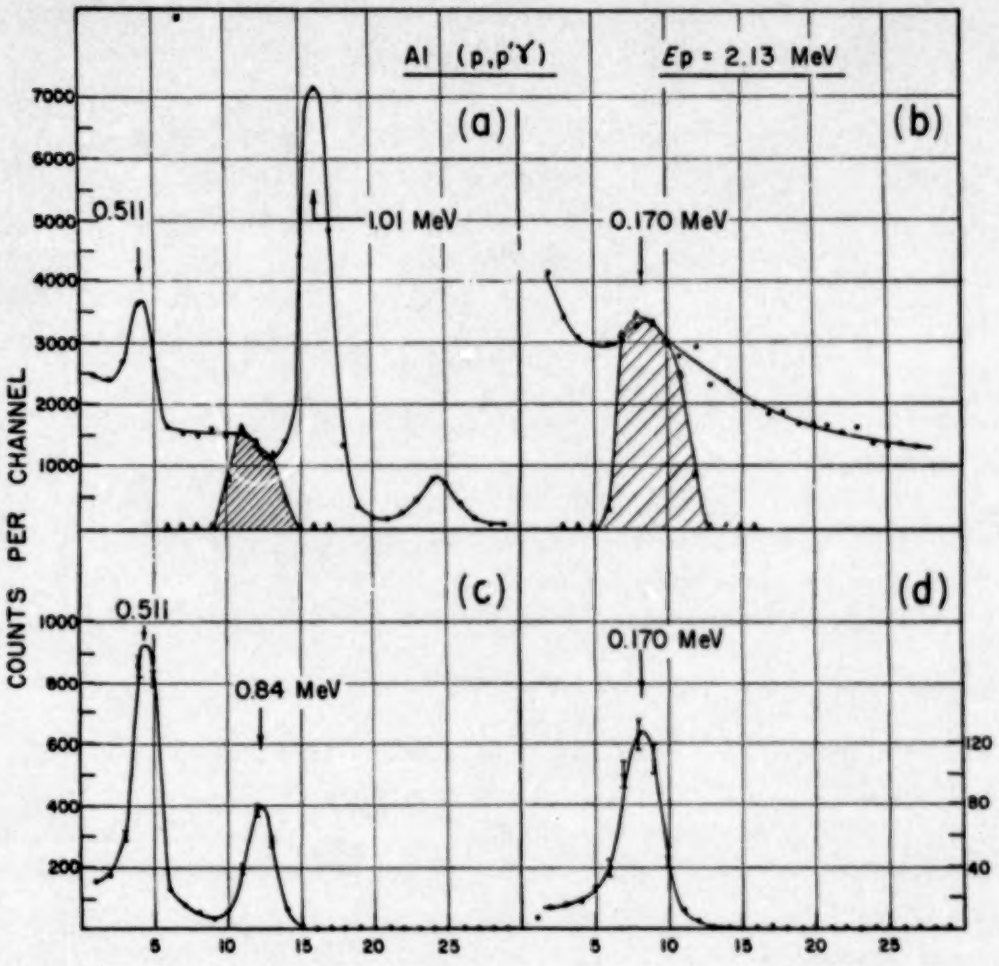

Fig. 5. Parts (a) and (b) show direct pulse-height distributions in crystals A and B arranged as shown in inset of fig. 3. The cross-hatched areas represent the portion of the pulse distributions that fall within the windows of single channel analysers set to select primarily the 0.84 MeV and 0.170 MeV radiations. The pulse distributions (c) and (d) were observed in time coincidence with pulses in the windows indicated by parts (b) and (a) respectively.

3.3 ANGULAR DISTRIBUTIONS

The detailed angular distribution measurements on the de-excitation radiations from the 1.013 MeV state are summarised in fig. 6 and table 2. The measurements were carried out at the three resonances indicated by the asterisks in table 1 which strongly favour formation of the 1.013 MeV state. The distribution of the 1.013 MeV radiation was measured directly and in this case the statistical errors are less than the size of the triangles used to indicate the points. The 0.170 MeV radiation however, was not sufficiently well resolved in the direct

spectrum to permit a direct measurement. Instead the coincident arrangement was used and the coincidence counting rate of the 0.170 MeV radiation in detector B measured as a function of the angle between detector B and the beam while detector A was kept at 90°. This coincidence angular distribution is equivalent to the direct distribution provided that the spin of the 0.84 MeV

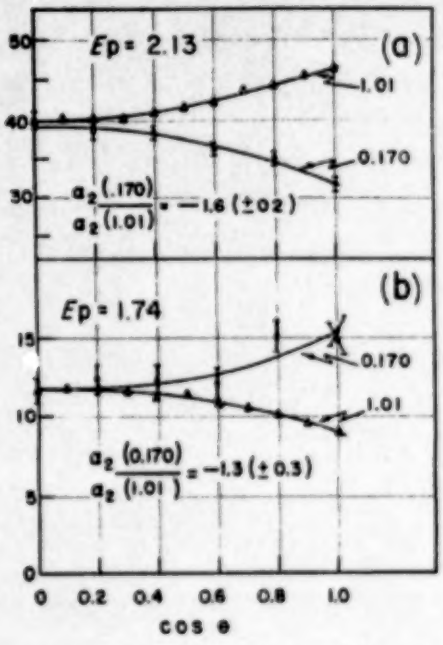

Fig. 6. Angular distributions of the 1.013 MeV and 0.170 MeV radiations. The solid curves are least squares fits obtained by fitting a Legendre polynomial of the form $a_0P_0 + a_2P_2$ to the data.

state is $\frac{1}{2}$ as suggested by all the available data. The necessity for the coincidence arrangement of course reduces the counting efficiency which is the reason for the relatively large statistical errors shown on the 0.170 MeV points. The solid curves in fig. 6 represent the least squares fit to the experimental points of a Legendre polynomial expansion of the form $a_0P_0 + a_2P_2$. The spin $\frac{3}{2}$ assignment to the 1.01 MeV state precludes the possibility of terms of higher order than P_2 (cos θ) occurring in the angular distribution of the de-excitation

TABLE 2

Angular distribution coefficients for the 0.170 MeV and 1.013 MeV radiations. See text for definitions

Proton Energy (MeV)	$a_2/a_0 = \alpha_2$		$\frac{\alpha_2(1)}{\alpha_2(2)}$
	(1) 0.170	(2) 1.013	
1.74	$+0.21 \pm 0.04$	-0.159 ± 0.01	-1.32 ± 0.3
1.94	$+0.04 \pm 0.06$	$+0.01 \pm 0.01$	
2.13	-0.20 ± 0.02	$+0.124 \pm 0.003$	-1.60 ± 0.2

radiation. Experimentally there is no significant improvement of the fit obtained by including a P_4 term. The results of the data analyses are summarised in table 2 where the last column is the ratio defined in the introduction. A correction for the attenuation of the a_2 coefficients owing to the finite size of the detectors has been applied; the factors are 1.041 for the 1.01 MeV radiation and 1.9 for the 0.170 MeV case. The larger value of the latter results from the smaller target to detector distance used in the coincidence measurements.

3.4. BRANCHING RATIO

The ratio of intensity of the cascade (0.170 MeV) to that of the ground state (1.013 MeV) transitions from the 1.013 MeV level can be obtained from the values of the a_0 coefficients of the Legendre polynomial fit to the angular distributions. The ratio is

$$\frac{I^{0.170}}{I^{1.01}} = \frac{a_{0(0.170)}}{\varepsilon_{0.84}\,\varepsilon_{0.171}}\,\frac{\varepsilon_{1.01}}{a_{0(1.01)}}\,, \tag{3}$$

where I is the intensity of the indicated transition and the ε's are detector efficiencies for the indicated gamma ray energies. The ratio $\varepsilon_{1.01}/\varepsilon_{0.84}$ was taken from the measured efficiency curve of the gamma ray detectors corrected for the effect of the lead absorber. The value of $\varepsilon_{0.17}$ was obtained from the computations of Wolicki, Jastrow and Brooks assuming that 0.9 of the total number of pulses are in the unresolved total absorption and iodine X-ray escape peaks. The result is that 2.4 $\pm$ 0.3 % of the de-excitations are via the cascade branch in good agreement with the value 2.2 % obtained by Lyons and Lazar[9]) in studies of Mg^{27} beta decay to Al^{27}.

4. Discussion of Results

4.1. GENERAL

The assignments of spin and parity to the lowest levels in Al^{27} shown in fig. 1 and discussed in the introduction are almost certain. The measured isotropy of the 0.84 MeV radiation in every case and the anisotropy of the angular distribution of the 1.01 MeV radiation support spin assignments $\frac{1}{2}$ and $\frac{3}{2}$ to the respective states. The measured de-excitation branching of the 1.01 MeV level of 2.4 ($\pm$ 0.03) % via a 0.170 MeV transition to the 0.84 MeV state is in good agreement with the result 2.2 % reported by Lyons and Lazar[9]). This branching value is in fair agreement though somewhat larger than the estimate of 0.5 % based on most probably single particle widths[11]). However, it should be noted that if the shell model assignments of $d_{\frac{5}{2}}$, $s_{\frac{1}{2}}$ and $d_{\frac{3}{2}}$ are made to the three lowest levels in Al^{27} respectively, an M1 transition between the $d_{\frac{3}{2}}$ and $s_{\frac{1}{2}}$ states is l-forbidden. Such forbiddeness if effective in inhibiting the 0.170 MeV transition would result in a branching value expected to be lower than the above estimate in contradiction to the measured result. Similarly, on the basis

of these assignments the β-decay of Mg^{27} ($s_{\frac{1}{2}}$) would favour transitions to the $s_{\frac{1}{2}}$ (0.84 MeV) state over l-forbidden transitions to the $d_{\frac{3}{2}}$ (1.01 MeV) state whereas experimentally[1]) the log ft values are equal. The qualitative expectations based on the above simple shell model assignments therefore are not in good accord with the experimental data. This is not surprising since considerable mixing of single particle states is expected to occur particularly in view of the large nuclear deformations that are known to exist in this mass region.

The single particle estimates[11]) suggest essentially pure M1 radiations from the 1.013 MeV state; the estimated E2 widths are 2×10^{-9} and 7×10^{-8} of the M1 widths of the 0.170 MeV and 1.01 MeV transitions respectively. These estimates can be compared with the information regarding the E2/M1 multipole mixing which is deduced from the observed value of the ratio of the angular distribution coefficients $\alpha_{2(0.170)}/\alpha_{2(1.01)}$. The measured mean value of this ratio from table 2 is $-1.46(\pm 0.3)$ which rules out the result $+5$ obtained by assuming pure M1 radiations. Inspection of fig. 2 shows that either one or both of the 0.170 and 1.01 MeV radiations must have a multipole amplitude ratio E2/M1 $\gtrsim$ 0.2 in strong contradiction to the single particle estimates given above.

In the discussion that follows, it will be shown that the β-decay results and at least the qualitative feature of the branching ratios measured for electromagnetic de-excitation of certain of the states in Al^{27} follows naturally from an application of the rotational collective model[12]), which has been successfully used in the mass 25 region. The large enhancement of E2 widths, or alternatively, diminution of M1 widths indicated by the measurements reported herein is characteristic of the predictions of this model. On the basis of this model, the ground state of Al^{27} is assigned the quantum numbers $(J,\pi,K) = (\frac{5}{2}, +, \frac{5}{2})$ (orbit 5) and is derived from the $d_{\frac{5}{2}}$ shell model state. Similarly the 0.842, 1.013 and 2.730 MeV states are assigned the quantum numbers $(J,\pi,K) = (\frac{1}{2}, +, \frac{1}{2})$, $(\frac{3}{2}, +, \frac{1}{2})$ and $(\frac{5}{2}, +, \frac{1}{2})$ respectively, and comprise the lowest three members of the $K = \frac{1}{2}$ (orbit 9) rotational band derived from the $s_{\frac{1}{2}}$ shell model state. The orbit numbers noted are those tabulated by Nilsson[13]). An examination of the level energy diagram given by Nilsson shows that the thirteenth proton will fall into orbit 5 to give a $J = \frac{5}{2}$ ground state for values of the distortion parameter η between 0 and $+3$ suggesting a prolate shape of Al^{27}.

4.2. QUADRUPOLE MOMENT

The measured quadrupole moment for Al^{27} is positive and has the value $Q_s = 0.16$ b. As given by Bohr and Mottleson[12]),

$$Q_s = \frac{3K^2 - J(J+1)}{(J+1)(2J+3)} 1.15\, ZA^{\frac{2}{3}} \varkappa\eta (1 + \tfrac{2}{7}\varkappa\eta) \times 10^{-26} \text{ cm}^2 , \qquad (4)$$

where $\varkappa$ is the Nilsson parameter[13]) proportional to the strength of the spin orbit term in the nuclear potential and η is the usual distortion parameter. Substituting in eq. (4) results in $\varkappa\eta \approx 0.275$. In the original papers on this model, $\varkappa$ was chosen to be 0.05 in order to achieve the best overall fit to the shell model level ordering at zero distortion. It was recognized however that, particularly in the light nuclei, a larger value of $\varkappa$ might be appropriate[4, 5]); in O^{17} for example $\varkappa = 0.13$ is required to fit the $d_{\frac{5}{2}}$–$d_{\frac{3}{2}}$ splitting of 5.08 MeV. A value of $\varkappa = 0.08$ was selected by Litherland *et al.*[4]) in their study of the mass 25 system. Depending upon the value of $\varkappa$ selected, a range $2.1 \leqq \eta \leqq 5.5$ is indicated for the equilibrium distortion of Al^{27}, corresponding to a relatively large prolate deformation. This result is similar to the value $2.5 \leqq \eta \leqq 6.6$ derived from the shape factor for Al^{27} given by Osborn and Klema[14]) who made a detailed analysis of quadrupole moments using a kinematic model.

4.3. LEVEL SEQUENCE

From the measured excitations of the members of the $K = \frac{1}{2}$ rotational band it is possible to deduce values for the nuclear moment of inertia I appropriate to the band and the decoupling parameter a characteristic of the $K = \frac{1}{2}$ band. The appropriate relation given by Bohr and Mottelson[12]) is

$$E_J = \frac{\hbar^2}{2I}\{J(J+1) + a(-1)^{J+\frac{1}{2}}(J+\tfrac{1}{2}) - B\}. \qquad (5)$$

The correction term B for vibration rotation interaction to leading order is given by[12])

$$B = 4\left\{\frac{3}{(\hbar\omega_\beta)^2} + \frac{1}{(\hbar\omega_\gamma)^2}\right\}\left[\frac{\hbar^2}{2I}\{J(J+1) + a(-1)^{J+\frac{1}{2}}(J+\tfrac{1}{2})\}\right]^2.$$

In this compution a value of $\hbar\omega_\beta = \hbar\omega_\gamma = 12$ MeV has been assumed; this value for the vibrational quanta has been found appropriate to nuclei in this region of the d shell[4, 5]). The values thus found from a numerical solution of equation 5 are $a = -0.7$ and $A = 210$ keV. Comparing this value of the decoupling parameter with the model predictions (see fig. 12 of ref. [4])) a very large prolate distortion $\eta \approx 10$ beyond the range of the Nilsson tabulated wave functions is found. This value which is in quantitative disagreement with the preceding data results from the observed close spacing of the two lowest levels assigned to the $K = \frac{1}{2}$ band followed by a large gap to the third level. The reason for the depression of the $\frac{3}{2}$ level is not known; in the absence of a nearby level of the same spin and parity it seems unlikely that rotational particle coupling effects[15]) can account for the observations but sufficient data are not available to permit detailed analysis of this possibility.

The value of $A = 210$ keV is in good agreement with results[4, 16]) obtained in

Mg^{24}, Al^{25}, Si^{28} and Si^{29} and corresponds to a nuclear moment of inertia equal to 50% of the corresponding rigid rotator value. Ratios ranging from 25% to 89% have been reported in the d shell[4, 16]).

The second member of the rotational band based on the $\frac{5}{2}^+$ ground state has not been identified as yet. It is interesting to note that if the same moment of inertia is assumed for this $K = \frac{5}{2}$ band as for the $K = \frac{1}{2}$ band, the $\frac{7}{2}^+$ member is predicted at an excitation of 1.85 MeV. The state at 2.205 MeV has suggested assignment of $\frac{3}{2}^-$ based on measurements by Van der Leun *et al*[1]) on the Mg^{26} (p,γ)Al^{27} reaction, however, a $\frac{7}{2}^+$ assignment would accord with much of the available experimental data. Measurements on the angular distributions of inelastically scattered deuterons, at $E_d = 9$ MeV[17]) do in fact indicate positive parity for the 2.205 MeV level in contradiction to the (p,γ) measurements. A determination of the assignment to this state would be of considerable interest. If, in fact, the $\frac{3}{2}^-$ assignment is shown to be correct, one of the states at $\approx$ 3.0 MeV excitation is the only remaining candidate for the $\frac{7}{2}^+$ assignment corresponding to $A = 430$ keV and $I/I_{\text{rigid}} = 0.27$.

4.4. DE-EXCITATION OF THE 1.013 MeV STATE

As noted previously, the 0.170 MeV transition via the 0.842 state occurs in only 2.4 ± 0.3% of the de-excitations of the 1.01 MeV state. From the angular distributions of the gamma radiations, one or both of the transitions has a significant E2 admixture although in single particle estimates this admixture is completely negligible.

Additional information on the amount of multipole mixing in the 1.013 MeV radiation has recently been obtained by McCallum[18]) from the measurements of the linear polarization of the radiation at the 1.74 and 2.13 MeV resonances. These data set limits on the E2/M1 amplitude ratio of —0.3 to —1.0 which on the inverse tangent scale of fig. 2 corresponds to —17° to —45°. Since the internal conversion coefficients measured by Rankin *et al.*[1]) suggest nearly pure M1 radiation it appears likely that the real value is nearer —17° than —45°. The corresponding ranges of the E2/M1 amplitude ratio of the 0.170 MeV radiation obtained from fig. 2 are either from +0.16 to 0 or —2.3 to —1.2.

Using the Nilsson eigenfunctions and the expressions quoted previously for the de-excitation widths[4, 5]) to include both collective and single particle components for the E2 transition, a branching ratio ranging from 0 at $\eta = 0$ to 26 at $\eta = 6$ is predicted for the 1.013 MeV state. This ratio is expressed as the total width for the cascade de-excitation divided by that for the direct transition to the ground state. The experimental value of 0.024 ($\pm$ 0.003) would thus correspond to a very small deformation.

It should be noted, however, that in this model transitions which correspond to $\Delta K = 2$, such as those from the 1.013 and 2.730 MeV levels to the ground

state of Al^{27} are predicted to have zero M1 width Empirically, it has been found that this K selection rule is not a strong one in the d shell, corresponding to an inhibition factor in the range of 10 to 20. The fact that this selection rule is not an absolute one is reflected in the discrepancy between the predictions just quoted for the 1.013 MeV state branching ratio and the experimental value. To obtain a perhaps more realistic prediction for the branching for the 1.013 MeV state ratio, it is possible to use the collective model predictions for the interband transition between the 1.013 and 0.842 MeV states and to reduce the most probable[11]) single particle width for the M1 ground state transition by the empirical K inhibition factor ≈ 20. This results in a predicted branching ratio $\approx 0.5\%$ for $\eta \approx \pm 3$. The fact that this is equal to the direct single particle estimate is due to the collective model inhibition of the 0.170 MeV M1 width as compared to the single particle estimate. Since a factor of ≈ 7 uncertainty exists in the "most probable" widths, this agreement is quite satisfactory.

In the case of the 0.170 MeV transition between two $K = \frac{1}{2}$ levels both the M1 and E2 amplitudes can be computed using the Nilsson eigenfunctions to yield an E2/M1 amplitude ratio in the range 0.11 to 0.14 for η in the range $+2$ to $+4$. These values lie within the limits 0 to 0.16 obtained from experimental data.

4.5. DE-EXCITATION OF THE 2.730 MeV STATE

Measurements on the $Mg^{26}(p,\gamma)Al^{27}$ reactions[1, 19]) and studies of the gamma radiation from $Al^{27}(p,p'\gamma)$ by Rankin *et al.*[1]) have shown that the 2.73 MeV state de-excites 90% via the 1.013 MeV state and fewer than 2% via the state at 0.84 MeV while the remainder is to the ground state. Fig. 7 presents the widths for these three transitions as functions of the nuclear deformation computed using Nilsson eigenfunctions. A value of $\eta \lesssim 2.3$ results in transition B (fig. 7) having a width less than 2% of that of transition A in accord with measurements. Also for the assignments indicated in fig. 7, the ground state

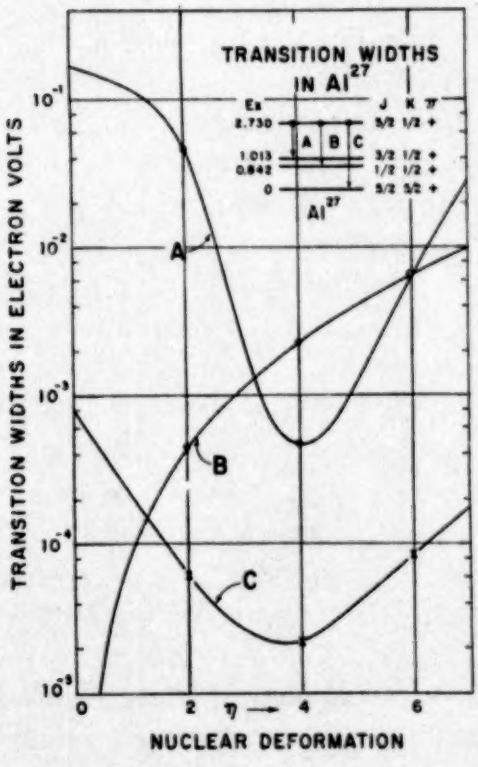

Fig. 7. The transition widths for de-excitation of the 2.73 MeV state in Al^{27} computed as functions of the nuclear deformation using Nilsson's eigenfunctions[13]). These functions yield only the E2 width for transition C for which $\Delta K = 2$. Both M1 and E2 components are included in curve A.

transition C corresponds to $\Delta K = 2$ which as discussed above leads to zero M1 width on the rotational model and to an underestimate of the total width of this transition. The weakening of the K selection rule which occurs in the d shell is reflected in the discrepancy between the measured ratio of widths of transitions C to A of 0.09 as compared with the computed ratio of 0.002 for $\eta = 2.3$. Values of $\eta \lesssim 2.3$ are therefore in qualitative accord with the known properties of the 2.73 MeV state.

The computed E2/M1 amplitude ratio for transition A lies in the range 0.04 to 2.7 for η between 2 and 4 but there is no experimental measure with which to compare this result.

4.6 Mg^{27} β DECAY BRANCHING

As shown in fig. 1, the Mg^{27} β-decay branches almost equally to the 1.013

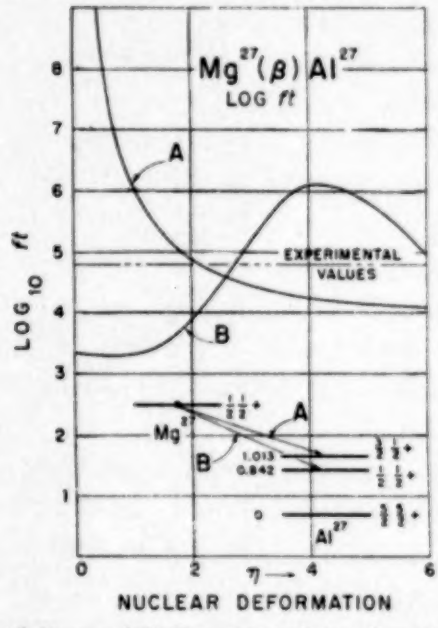

Fig. 8. The log ft values for the β-decay of Mg^{27} computed as a function of the nuclear deformation using the formalism of Nilsson[13]). The experimental values for both the indicated transitions are each 4.8.

and 0.842 MeV levels in Al^{27}. Using the Nilsson formulae and the values of the beta decay coupling constants obtained by Gerhart[20]), the predicted log ft values for these transitions have been calculated as functions of the nuclear deformation. The results are shown in fig. 8 together with the experimental value, equal to 4.8 for both branches. Here again a value of $\eta \approx 2.5$ results in agreement between prediction and experiment.

4.7. Si^{27} β^+ DECAY

From the experimentally determined[1]) half life of 4.14 sec and the positon end point of 3.786 MeV deduced from the 5.800 ± 0.008 MeV threshold for

the $Al^{27}(p,n)Si^{27}$ reaction, a log ft value of 3.69 is obtained for the Si^{27} ground state positon decay, characteristic of a super-allowed mirror transition. The Nilsson model prediction is log $ft = 3.63$ and is independent of the nuclear distortion, thus precluding the extraction of any information on the equilibrium deformation.

4.8. Al^{27} GROUND STATE MAGNETIC MOMENT

Similarly in this case the predicted magnetic moment is independent of nuclear deformation, equal to 3.75 nuclear magnetons, in good accord with the experimentally determined value of 3.64 nuclear magnetons.

5. Conclusions

The rotational collective model[12, 13]) gives a good qualitative description of many of the properties of the low lying levels of Al^{27} with the exception of the level energies. The ground state spin, the quadrupole moment, the de-excitation branching of the 1.013 MeV and 2.73 MeV states as well as the available data on E2/M1 mixing are in good qualitative accord with the model predictions. Quantitative agreement is obtained for the Al^{27} magnetic moment and for the log ft values of the Si^{27} β decay and of the Mg^{27} β decay to the 0.84 and 1.013 MeV states. The analysis suggests a prolate distortion for Al^{27} corresponding to $\eta = 2.5$ or $\Delta R/R = 0.275$ if R and ΔR are defined as the mean value of the semi-axes of the Al^{27} spheroid and the difference between the axes respectively. It is interesting to note that for Al^{25} a larger prolate distortion corresponding to $\eta = 4.5$ is found[4]) whereas for Si^{29}, on the other hand, an oblate distortion of $\eta = -3$ is obtained[5]). These results are in qualitative agreement with the expectation that the deformation should reach a maximum value near the middle of a nuclear shell or sub-shell and should decrease and change sign in passing through the closed shell nuclei.

References

1) P. M. Endt and C. M. Braams, Rev. Mod. Phys. **29** (1957) 700;
W. A. Rankin, T. W. Bonner, R. Castillo-Behena, M. V. Harlow and T. A. Robson, Phys. Rev. **112** (1958) 239;
C. Van der Leun, P. M. Endt, J. C. Kluyver and L. E. Vrenken, Physica **22** (1956) 1223

2) C. P. Browne, S. F. Zimmerman, and W. W. Buechner, Phys. Rev. **96** (1954) 725;
D. J. Donahue, K. W. Jones, M. T. McEllistrem and H. J. Richards, Phys. Rev **89** (1953) 824;
W. C. Porter, M. A. Rothman and O. M. Van Patter, Bull. Am. Phys. Soc. **2** (1957) 143

3) E. Almqvist, D. A. Bromley, H. E. Gove and A. E. Litherland, Bull. Am. Phys. Soc. **2** (1957) 178

4) A. E. Litherland, E. B. Paul, G. A. Bartholomew and H. E. Gove, Phys. Rev. **102** (1956) 208;
A. E. Litherland, H. McManus, E. B. Paul, D. A. Bromley and H. E. Gove, Can. J. Phys. **36** (1958) 378

5) D. A. Bromley, H E. Gove and A. E. Litherland, Can. J. Phys. **35** (1957) 1057;
E. B Paul, Phil. Mag. **15** (1957) 311;
L. K. Peker, L. V. Gustova and O. V. Chubinskii, Isvestii a Akademic Nauk USSR **21** (1957) 1013;

R. K. Sheline, Nuclear Physics **2** (1957) 382;
C. Broude, L. L. Green and J. C. Willmott, Proc. Phys. Soc. **72** (1958) 1122;
E. B. Paul and J. H. Montague, Nuclear Physics **8** (1958) 61;
H. E. Gove and A. E. Litherland, Phys. Rev. **113** (1959) 1078;
R. Batchelor, A. J. Ferguson, H. E. Gove and A. E. Litherland, Nuclear Physics **16** (1960) 38
6) L. C Brown and D. Williams, J. Chem. Phys. **24** (1956) 751
7) L. C. Biedenharn and M. E. Rose, Rev. Mod. Phys. **25** (1953) 729
8) W. T. Sharp, J. M. Kennedy, B. J. Sears and M. G. Hoyle, Chalk River Report CRT-556 (unpublished) 1954
9) W. S. Lyons and N. H. Lazar, Phys. Rev. **101** (1956) 1524
10) H. E. Gove, G. A. Bartholomew, E. B. Paul and A. E. Litherland, Nuclear Physics **2** (1956) 132; A. E. Litherland, E. Paul, G. A. Bartholomew and H. E. Gove, Phys. Rev. **102** (1956) 208
11) D. H. Wilkinson, Phil. Mag. **1** (1956) 127
12) A. Bohr and B. Mottelson, Mat. Fys. Medd. Dan. Vid. Selsk. **27**, No. 16 (1953); **30** No. 1 (1955); Beta and Gamma-Ray Spectroscopy, Ed. Kai Siegbahn (North-Holland Publishing Company, Amsterdam, 1955) Ch. 17
13) S. G. Nilsson, Mat. Fys. Medd. Dan. Vid. Selsk. **29**, No. 16 (1955)
14) R. K. Osborn and E. D. Klema, Nuclear Physics **2** (1956) 454
15) A. K. Kerman, Mat. Fys. Medd. Dan. Vid. Selsk. **30**, No. 15 (1956)
16) G. Rakavy, Nuclear Physics **4** (1957) 375;
D. A. Bromley, Proc. Rehovoth Conf. on Nuclear Structure (1957), ed. H. J. Lipkin, (North-Holland Publishing Company, Amsterdam, 1958)
17) S. Hinds and R. Middleton, Proc. Phys. Soc. A **69** (1956) 347L
18) G. J. McCallum, to be published
19) A. J. Ferguson, H. E. Gove, A. E. Litherland and D. A. Bromley, private communication
20) J. B. Gerhart, Phys. Rev. **95** (1954) 288

1.D.2:
1.E.1

Nuclear Physics **19** (1960) 18—39; © *North-Holland Publishing Co., Amsterdam*
Not to be reproduced by photoprint or microfilm without written permission from the publisher

THE W^{187} DECAY SCHEME AND POSSIBLE VIBRATIONAL LEVELS IN AN ODD-MASS NUCLEUS

C. J. GALLAGHER, Jr.†, W. F. EDWARDS†† and G. MANNING*

Norman Bridge Laboratory of Physics, California Institute of Technology, Pasadena, California **

Received 20 February 1960

Abstract: The transitions and levels of Re^{187} populated by W^{187} β^- decay have been investigated with a bent crystal spectrometer, an iron-free homogeneous-field spectrometer, an iron-free 180°-focusing spectrometer and a fast-slow coincidence angular-correlation unit. There have been observed 17 transitions, which are interpreted to establish 8 excited levels in Re^{187}. An analysis of the levels in terms of the Nilsson description shows that certain definite discrepancies exist between the theoretically expected level order and that observed. It is therefore suggested that 2 of the levels observed may correspond to the coupling of single particle states to gamma vibrations.

1. Introduction

The low-lying levels of strongly-deformed odd-mass nuclei in the region $150 \lesssim A \lesssim 190$ have been described very successfully as single particle states in a deformed potential well with rotational states based upon them[1,2]). For nuclei with smaller deformations, where the division between intrinsic and rotational states is not so clear-cut, the applicability of the model is not as yet so well established, and further experimental information is required.

Mottelson and Nilsson[2]) have recently classified the single particle levels of nuclei in the $150 \leqq A \leqq 190$ region. According to their classification Re^{185} and Re^{187} have the smallest deformations in this region. Such small deformations imply that strong coupling may no longer be a good approximation. Additional support for such a supposition is provided by the energies of the first rotational states in Re^{183}, Re^{185} and Re^{187}, which increase from 114 to 134.25 keV, although the assigned ground state configuration for all three isotopes is the same[2,3]). It thus seemed that a knowledge of the levels of Re^{187} would be useful for testing the predictions of the Nilsson wave functions near the limits of the region where the strong coupling model is known to be applicable.

A review of the previously reported data on the levels of Re^{187} from W^{187} β-decay showed considerable agreement in the energies of the transitions, but disagreement as to the level scheme based on these transitions[3-6]). Under such

† Present address: Institute for Theoretical Physics, Copenhagen, Denmark.
†† Present address: Dept. of Physics, Utah University, Logan, Utah.
* Present address: Dept. of Physics, AERE, Harwell, Berkshire, England.
** Work supported by the United States Atomic Energy Commission.

circumstances we decided that a study of W^{187} decay utilizing the high accuracy and resolution provided by the DuMond bent-crystal spectrometer would be useful for eliminating some of the reported permutations.

W^{187} has been studied by many workers, the most recent and most comprehensive studies being those of Cork, Brice, Nester, LeBlanc and Martin[4]), Dubey, Mandeville, Mukerji and Potnis[5]), and Vergnes[6]). A review of the work on this isotope until 1953 has been given by Cork *et al.* and will not be reported here. The transitions reported by Cork *et al.*, Dubey *et al.* and Vergnes, are summarized in table 1. As can be seen from the table there is agreement in all

TABLE 1

Transitions in Re^{187} following W^{187} beta decay, as reported in recent investigations of this isotope

Cork *et al.*		Dubey *et al.*			Vergnes			
Energy of gamma (keV)	K/L ratio	Energy of gamma (keV)	Photon intensity	K/L ratio	Energy of gamma (keV)	Photon intensity	Conversion coefficients	
							Sub-shell	Value
72.1		72			72 [a]	≈ 175 [b]	α_K [c]	≦1.6
106.2		136	2	5.0 ± 0.5				
113.8		206	4	4.5 ± 0.5	107			
134.3	5.5 ± 0.5	224			114			
206.3	4.0 ± 0.5	241			134	35	α_K [d]	1.5 ± 0.4
239.2		249	2					
246.4		482	100	4.0 ± 0.5	206	— [e]	— [f]	
480.0	4.2 ± 0.5	510	12		480	100	α_K	1.95×10^{-2}
513.5		552	40		550	20 to 35	α_K	$\leqq 2.9 \times 10^{-2}$
619.2	4.0 ± 1.0	621	30	3.8 ± 1	630	20 to 35	α_K	$< 6 \times 10^{-2}$
625.8		627	15		686	100	α_K	$\leqq 6.9 \times 10^{-3}$
686	5.0 1.0	686	185		775	≈ 10	α_K	4.7×10^{-2}
774		775	20		870	0.75 to 1		
866		866	12					

[a] E1 ≧98.5%, M2 ≦1.5%
[b] Includes K X-ray intensity
[c] $\alpha_{L_I} + \alpha_{L_{II}} = 0.23 \pm 0.13$
[d] $\alpha_L = 0.3 \pm 0.1$
[e] $I_{\gamma 206}/I_{\gamma 134} \leqq 0.1$
[f] $I_{e_{K206}}/I_{e_{K134}} \leqq 0.01$

TABLE 2

Coincidence results reported for transitions in Re^{187} following W^{187} beta decay

Worker / Gating transition (keV)	Sunyar	Dubey *et al.*	Vergnes
	Coincident transitions (keV)	Coincident transitions (keV)	Coincident transitions (keV)
K X-rays and 72.00			no 620 (≦90% I_γ 620), no 690, no 770
134.25	552, ≈ 780, 480		K X-rays and 72, 480, 550
479.5	206	K X-rays, 72, 136, 210	K X-rays and 72, 205
> 750		72, 136	
867		K X-rays, 136, no 72	

strong transitions, but several differences exist over weaker lines. The decay schemes proposed by Cork *et al.*, Dubey *et al.* and Vergnes are shown in fig. 1 (a, b and c). The coincidence results reported by Sunyar[7]), Dubey *et al.* and Vergnes are shown in table 2. As can be seen from the table, the question whether the 773, 625 and 618.2 keV gamma-rays feed to the 206.25 or 134.25 keV levels is not settled, Sunyar and Dubey *et al.* having reported that they are

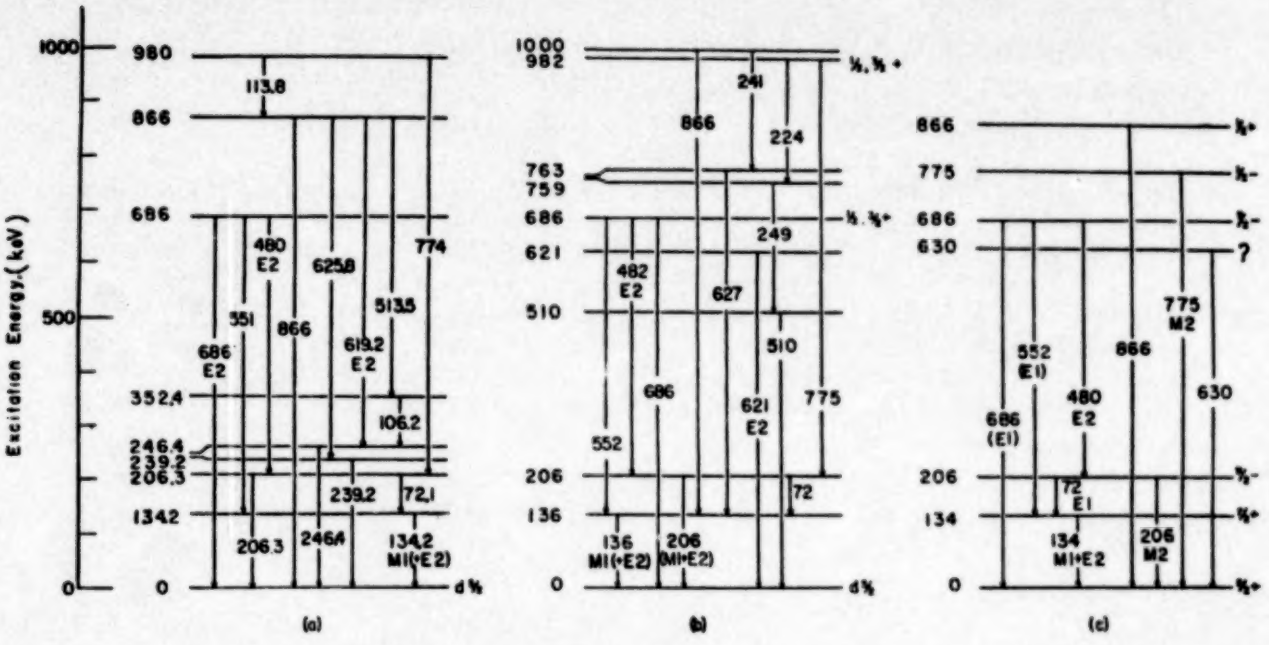

Fig. 1. Level schemes of Re^{187} proposed by previous workers. (a) Cork *et al.* (b) Dubey *et al.* (c) Vergnes.

in coincidence, and Vergnes that they are not. In addition to these studies, Coulomb-excitation experiments have excited the 134.25 keV level and a $\frac{9}{2}^+$ rotational level based on the ground state at $\approx$ 300 keV.†

2. Apparatus and Techniques

In the present experiment we used the DuMond iron-free homogeneous-field spectrometer[9]) and a 180°-focusing iron-free spectrometer[10]) to study the electron spectrum. The detectors in both spectrometers were G-M tubes; the end-window counter in the homogeneous-field spectrometer had a 0.9 mg/cm² mica window, and in the present experiment the side window counter in the 180° spectrometer was used with an approximately 30 μgram/cm² Formvar window.

Thin sources of high specific activity were prepared for the electron spectrometers by vacuum evaporation of W^{187} onto $\approx$ 2 mg/cm² aluminized mica.

† See the references quoted in ref.[3]) for the data on Coulomb-excitation of Re^{187}; see also refs.[28,29]).

The W^{187} activity was prepared by high flux irradiation of WO_3 (Oak Ridge sample, W^{186} enrichment = 97.4%) in the MTR at Arco, Idaho.

The gamma-ray spectrum was studied at high resolution with the DuMond bent-crystal spectrometer. The WO_3 sources (same enrichment as above) were also irradiated at Arco. Both "line" ($\approx$ 4 mg of WO_3) and "extended" sources (100 mg of WO_3) were used. Line sources are made by packing the material to be irradiated into quartz capillaries of 0.023 cm internal diameter; the extended source holder was milled from very pure aluminium and has inner dimensions 0.025 cm wide by 0.64 cm deep by 2.5 cm high.

Gamma-gamma coincidence measurements and an angular correlation study of the 551.7–134.25 keV gamma-ray cascade were made using a conventional fast-slow coincidence circuit of $\approx 2 \times 10^{-8}$ sec resolving time. The sources for the angular-correlation experiment were prepared by suspending WO_3 in dilute nitric acid.

3. Experimental Results

3.1. GAMMA-RAY MEASUREMENTS

The gamma-ray intensities were measured with the bent-crystal spectrometer, using a 12.7 cm diameter by 7.6 cm NaI(Tl) crystal detector and a 100-channel pulse-height analyzer. The statistical accuracy is 2% on most of the lines and less than 15% in all cases. The gamma-ray intensities were corrected for absorption in the source, quartz-capillary source holder, air path, bent crystal and aluminium window of the NaI detector. The absorption coefficients calculated by Grodstein[11] were used for all computations. The photopeak efficiency for a parallel beam of photons impinging on the NaI crystal was calculated from the formulae of Berger and Doggett[12]). A correction for the iodine escape peak was made where necessary. The reflectivity of the bent quartz crystal has a $1/E^2$ dependence. The energy dependence of the reflectivity has been the subject of considerable study in this laboratory and will be discussed in more detail elsewhere[13]).

3.2. ELECTRON MEASUREMENTS

The electron spectrum from 60 to 1400 keV was studied at 0.7% momentum resolution with the homogeneous-field spectrometer. A Fermi-Kurie analysis of the high-energy beta spectrum is shown in fig. 2. This plot is linear between $\approx$ 700 and 1250 keV. Such a conclusion disagrees with the $\Delta I = 2$, yes, shape reported by Dubey *et al.*, although both sets of results are consistent with the calculated value for this transition log $ft = 7.9$. The spectrum also provides evidence for the absence, or at least weakness, of a β^- group or groups directly populating the 134.25 and 206.25 keV levels. This is consistent with previous measurements of the beta spectrum and with our measured gamma-ray

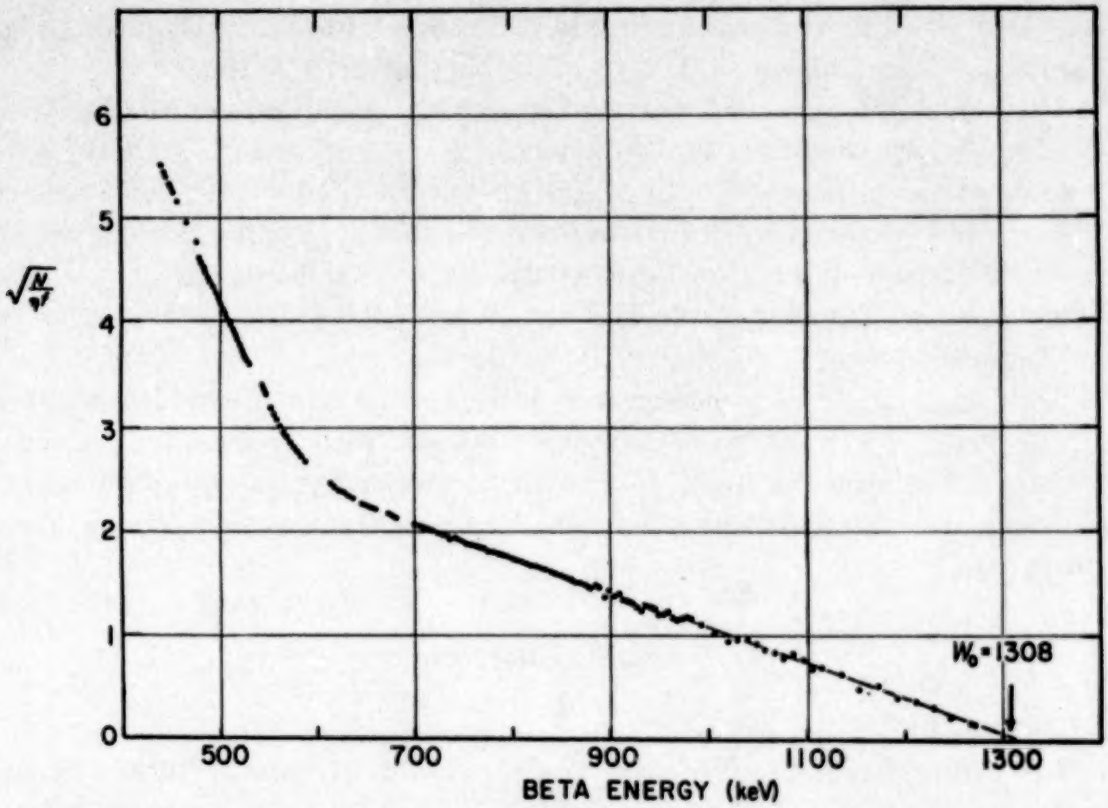

Fig. 2. Fermi-Kurie analysis of the high-energy beta spectrum of W^{187}. The spectrum shown above is linear between 690 and 1308 keV. The endpoint energy, $W_0 = 1308 \pm 10$ keV, was determined by a least squares analysis of the data between 700 and 1250 keV.

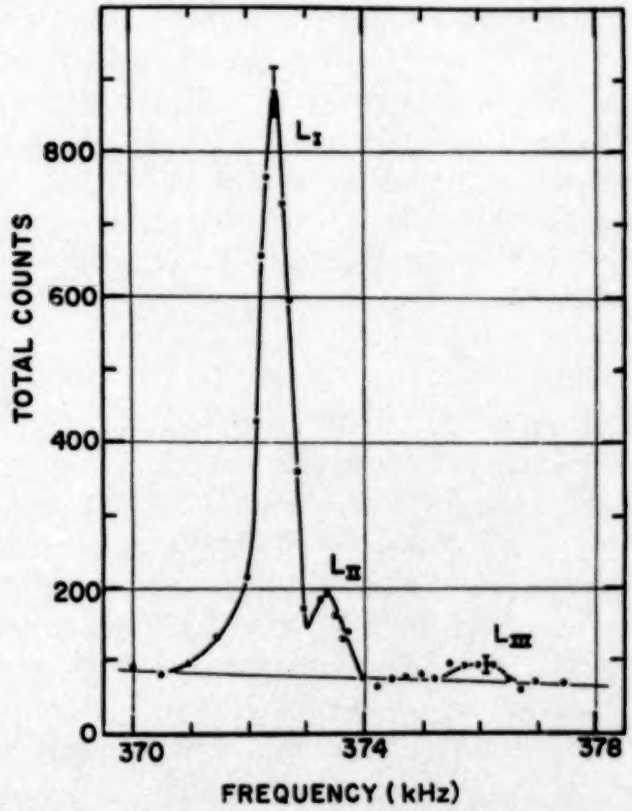

Fig. 3. The L-subshell conversion lines of the 134.25 keV transition at 0.15 % momentum resolution.

branching to and from these levels. The energy of the highest-energy beta group was calculated by a least-squares fit to the data between ≈ 700 and 1250 keV. The value of 1308 ± 10 keV that we obtained is within experimental error of the energies previously reported for this group, although some 15 keV lower.

The conversion electrons were studied for the most part at 0.7% resolution. In several cases, where higher resolution was required to determine intensities of close-lying lines, 0.3% and 0.15% resolution was employed. Figure 3 shows the L_I, L_{II} and L_{III} lines of the 134.25-keV transition at 0.15% resolution. The M1 to E2 admixture we report for this transition was determined from this run.

The intensities of the electron lines from 60 to 1400 keV were determined by integrating areas of peaks on an $N/H\rho$ versus $H\rho$ plot. They have statistical errors of ≦ 5% for the intense lines and ≦ 20% for the weaker lines. Intensities of only 3 of these lines (the L_I, L_{II} 72.00 keV, and the K 134.25 keV) had to be corrected further, for window absorption. A 12% correction was applied, using the correction curve for an effective mica window of 1.1 mg/cm² determined by Murray[14]). Because the effective window thickness was 1.3 mg/cm² for our 0.9 mg/cm² window (the electrons enter the counter at 45°), we determined the correction to the correction curve. This was estimated from the absorption curves for mica quoted by Saxon[15]) to be roughly ≦ 3% additional correction to the total intensity, and was therefore neglected. Because these three electron lines are at essentially the same energy the same correction was applied to all three.

3.3. CONVERSION COEFFICIENTS

The electron and gamma-ray data discussed above were used to obtain a set of relative conversion coefficients. These were normalized so that the measured K-conversion coefficient of the 686 keV transition equals Sliv and Band's[16] K-conversion coefficient for a pure E1 of this energy ($\alpha_K = 0.00323$). This normalization was checked by several absolute methods which will be discussed below. The results are presented in table 3.

The intensities of the K-conversion lines of the 96.0, 106.61 and 113.74 keV transitions, and the KL_IL_{II} KL_IL_{III}–$KL_{II}L_{III}$ and $KL_{III}L_{III}$ Auger-electron peaks were measured at 1% resolution in the 180° spectrometer. The relative line intensities, which were weak compared to the beta background, are only peak-height measurements and are less accurate than the results in table 3. They are shown in table 4. The normalization used in obtaining the conversion coefficients listed in table 4 is discussed below.

3.4. PRIMARY BETA BRANCHING

The relative beta branchings to the levels that we propose in Re^{187} have been deduced from differences between the intensities of the transitions populating and depopulating the levels. The relative populations thus deduced, normalized

TABLE 3. Transition energies and photon and electron int

Energy of gamma (keV)	Photon intensity	Relative conversion			co
		α_K	α_{L_I}	$\alpha_{L_{II}}$	
72.00 ± 0.01	48.5 ± 1.9	1.01 ± 0.14	0.063 ± 0.007	0.021 ± 0.003 [e]	
96.0 ± 0.5 [f,g]	≦0.12				
106.61 ± 0.06	0.17 ± 0.02				
113.74 ± 0.05	0.35 ± 0.03				
134.25 ± 0.02	39.3 ± 1.2	1.7 ± 0.2	0.33 ± 0.04	0.045 ± 0.005	
206.2 ± 0.2	0.48 ± 0.05	2.3 ± 0.3	0.7 ± 0.2		
239.3 ± 0.3	0.34 ± 0.05	0.7 ± 0.3			
246.3 ± 0.3	0.52 ± 0.05	0.3 ± 0.1			
479.4 ± 0.4	100	0.016 ± 0.002		$\alpha_L = 0.0043$	±
511.3 ± 0.7	2.6 ± 0.2	0.013 ± 0.003			
529 ± 3 [f]	≦0.4	≥0.048 ± 0.010			
551.7 ± 0.7	21.2 ± 0.7	0.0056 ± 0.0006			
618.2 ± 0.6	26 ± 1	0.030 ± 0.003			
625 ± 1.6	4.3 ± 0.2	0.010 ± 0.004			
686.1 ± 0.4	116 ± 5	(0.00323)			
773 ± 1	16.2 ± 0.8	0.018 ± 0.003			
867 ± 3	1.54 ± 0.25	0.014 ± 0.006			
Re $K\alpha_1$ X-ray	50.5 ± 2.0				

The conversion coefficients are normalized to the theoretical (Sliv and Band) K-conversion coefficient for a pure E1 transition of this energy ($\alpha_K = 0.00323$). The normalization has been checked by several absolute methods. The percentage of the total decay intensity carried by each transition is calculated assuming the total beta and gamma decay into the ground state is 100, using the reported 20% primary beta branching to the ground state.

[a] The normalization of these conversion coefficients has been checked by two absolute methods.

[b] This is the sum of the measured conversion coefficient, and does not include corrections for higher-shell conversion coefficients which were not measured.

[c] The decay fraction is proportional to $(1 + \alpha_{tot.})I_\gamma$, and is normalized so that 100% of all decays feed the ground state. $\alpha_{tot.}$ is as in (b). We have assumed 20% of the primary beta decay feeds the ground state.

TABLE 4. Conversion coefficients of the low-energy transitions whose conversion electron lines were measured in the 180° spectrometer

Energy photon (keV)	Intensity photon	Electron assignment	Electron intensity	Conversion coefficient α	Multipolarity
Re K X-rays	100 ± 5.0 [a]	$KL_I\,L_I$	0.81 ± 0.12	0.053 ± 0.006 [b]	
		$KL_I\,L_{III}$ — $KL_{II}\,L_{III}$	1.10 ± 0.16		
		$KL_{III}\,L_{III}$	0.41 ± 0.06		
96.0	≦0.12 ± 0.02	K	0.39 ± 0.06	≥3.8 ± 0.9	Not E1, E2
106.61	0.17 ± 0.02	K	0.48 ± 0.07	3.3 ± 0.6	M1 (+ E2)
113.74	0.35 ± 0.3	K	1.0 ± 0.15	3.3 ± 0.7	M1 (+ E2)

The conversion coefficients have been normalized absolutely to the measured K-Auger coefficient for $Z = 75$ (0.053).

[a] Assuming the $K\alpha_1$ intensity shown in table 3 and that $K\alpha_2/K\alpha_1 = 0.56$, $(K\beta_1 + K\beta_3)/K\alpha_1 = 0.34$ and $K\beta_2/K\alpha_1 = 0.08$ (from the tables of Wapstra *et al.*[18]).

[b] K Auger coefficient for $Z = 75$. The total K-Auger electron intensity $I_T = I_{KLL} + I_{KLX} + I_{KXY}$, where I_{KLL} = 1.2 times the sum of the Auger electron intensities indicated (correction for $KL_I\,L_{II}$ intensity) and KLX/KLL = 0.59, KXY/KLL = 0.065 (from the tables of Wapstra *et al.*[18]). We assumed these ratios have a 20% error.

intensities measured in this investigation

coefficients [a]		Decay fraction [c]	Multi-polarity	Mixing ratio [d]
$\alpha_{L_{III}}$	α_{total} [b]			
	1.11	27	E1	>99% E1, <1% M2
			— [h]	
		0.13 [i]	M1 + E2	
		0.26 [i]	— [j]	
0.011 ± 0.002 [k]	2.2	33	M1 + E2	2.6 ± 1.4% E2
	3.0	0.50	M2	>80% M2, <20% E1
	0.7	0.16	M1 (+ E2)	
	0.3	0.20	M1 + E2	
± 0.0005	0.021	28.5	E2	100% E2
	0.013	0.73	E2	>99% E2, <1% M1
	≥ 0.048		— [h]	
	0.0056	5.9	E1	$\leq$ 1% M2
	0.030	7.5	M1	>85% M1, <15% E2
	0.010	1.2	E2	
	0.00323	32.4	E1	
	0.018	4.6	M1	>85% M1, <15% E2
	0.014	0.43	M1	

[d] Mixing ratios, or limits on mixing ratios, are given for transitions where the error on the experimental conversion coefficient warrants such calculations.

[e] $\alpha_{L_I}/\alpha_M/\alpha_{N+O} = 1/0.3/0.1$.

[f] Energy deduced from electron line only.

[g] K line of 96.0 keV transition can possibly be assigned as L line of 36.2 keV transition.

[h] The limit on the conversion coefficient from table 4 rules out E1 or E2.

[i] Electron intensities measured only with 180° spectrometer. See table 4.

[j] In our analysis of the decay scheme we have assigned this transition as pure M1.

[k] $I_{L_I}/I_M/I_N/I_O(\text{estimated})/I_{K\ 206\cdot2} = 1/0.24/0.07/0.02/0.048$.

[l] $I_L/I_M/I_{N+O}(\text{estimated})/I_{K\ 551\cdot7} = 67/28/11/15$, where $I_{K\ 551\cdot7} = 26 - I_{N+O}(\text{estimated})$.

TABLE 5. Classification of the beta groups populating levels in Re^{187}

Initial state [a]	Final state [a]	Energy of state (keV)	Primary beta branching (percent)	Log *ft*	Asymptotic quantum no. classification
512 ↓	402 ↑	0	(20) [b]	7.9	1u
		511.6	$\leq$0.38	$\geq$9.0	
	411 ↓	625.3	4.0	7.7	1h
		618.2	6.7	7.4	1h
		686.1	64.0	6.3	
	402 ↓	773	4.1	7.3	1u
		864.5	$\approx$0.80	$\approx$7.8	

The relative beta group intensities are calculated from the difference in intensity of the populating and depopulating transitions, assuming 20% of the primary beta decay is to the ground state. The classification is based on the asymptotic selection rules for beta decay.

[a] Asymptotic-quantum number limit.

[b] Branching reported by Cork *et al.*[4]) and Dubey *et al.*[5]). In calculating primary branching to the upper states, the sum of the intensities of the electromagnetic transitions feeding the ground state was set equal to 80% of the total primary beta branching.

so that 100% of all beta- and electromagnetic transitions populate the ground state, are shown in table 5. We have assumed that the 20% beta-branching to the ground state reported by Cork *et al.*[4]) and Dubey *et al.*[5]) is correct. The log *ft* values reported in this table are calculated assuming the relative populations we report, a total decay energy of 1308 keV, and the reported half-life[3]) of 24.0 h.

3.5. COINCIDENCE MEASUREMENTS

Gamma-gamma coincidence measurements were made to determine whether the 773, 625 or 618.2 keV gamma-rays feed the 206.25 or 134.25 keV levels. As stated previously, the experimental evidence on this point conflicts. Our measurements were made by observing those high energy gamma-rays in coincidence with the 134.25 keV gamma-rays. Resolving times of 2×10^{-8} and $\approx 10^{-7}$ seconds were used to distinguish between those transitions which feed the 134.25 keV level directly and those which feed it via the long-lived ($t_{\frac{1}{2}} = 5.3 \times 10^{-7}$ sec) 206.25 keV level[7]). For both resolving times random coincidences were measured, delays of 10^{-7} and 1.6×10^{-6} sec being added to the signals from the high energy detector for resolving times of 2×10^{-8} and $\approx 10^{-7}$ seconds respectively.

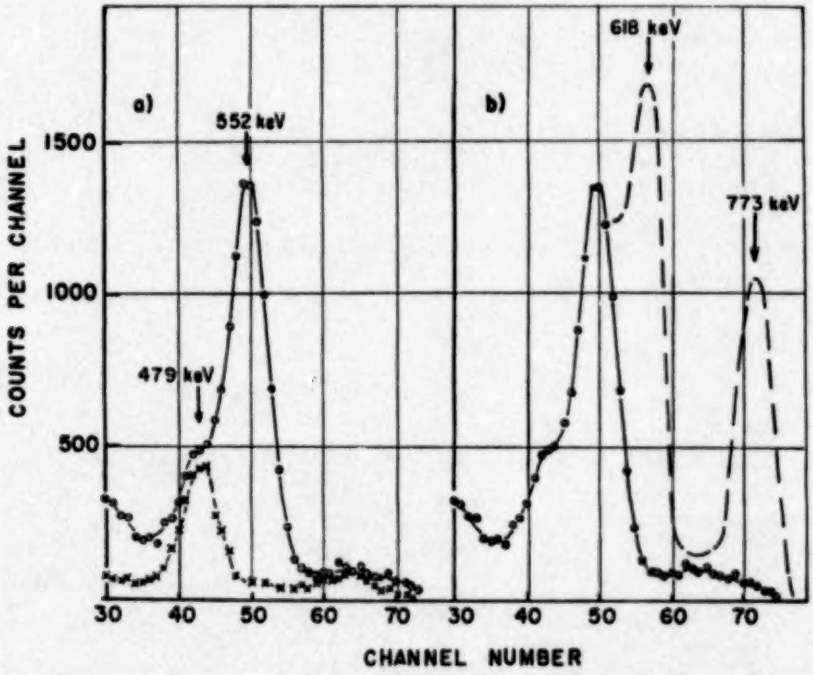

Fig. 4. (a) Spectrum in coincidence with the 134.25 keV gamma ray using a resolving time of $\approx 2 \times 10^{-8}$ sec. (b) The dotted line indicates the spectrum expected in coincidence with the 134.25 keV gamma-ray if the 618.2, 625 and 773 keV gammas fed the 134.25 keV level directly.

Figures 4a and 5a show the spectra in coincidence with the 134.25 keV gamma-rays for resolving times 2×10^{-8} and $\approx 10^{-7}$ seconds respectively. The

delayed coincidence spectra for each resolving time is also shown. The results with $\tau = 2 \times 10^{-8}$ sec (fig. 4a) show prompt coincidence for the 551.7–134.25 cascade, and delayed coincidences for the 479.4–134.25 cascade. The small peak observed at $\approx$ 686 keV is due to random coincidence and is in agreement with the computed random rate. Figure 4b shows the observed spectrum and the approximate spectrum that would be expected if the 773, 625 and 618.2 keV gamma-rays fed the 134.25 keV level directly. The results clearly disprove this. Figure 5b, the analogue of fig. 4b for a resolving time of 10^{-7} seconds, shows the

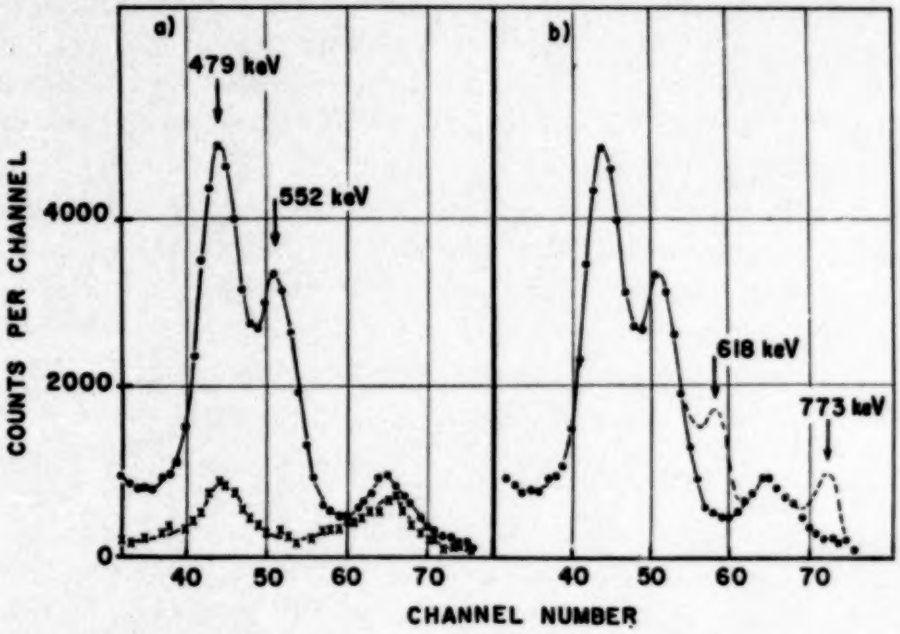

Fig. 5. (a) Spectrum in coincidence with the 134.25 keV gamma-ray using an resolving time of $\approx 10^{-7}$ sec. (b) The dotted line indicates the spectrum expected in coincidence with the 134.25 keV gamma-ray if the 618.2, 625 and 773 keV gamma rays fed the 206.25 keV level.

observed spectrum and the approximate spectrum that would be expected if the 3 gamma-rays fed the 206.25 keV level. The results prove that this assumption is also incorrect. We therefore agree with Vergnes[6]) that the 773, 625 and 618.2 keV gamma-rays do not feed the 206.25 and 134.25 keV levels, in contradiction to the results of Sunyar[7]), and Dubey *et al.*[5]).

The angular correlation measurement of the 551.7–134.25 cascade was observed to be isotropic to within 1%.

4. Absolute Normalization of Conversion Coefficients

We have checked the normalization of our conversion coefficients by two independent methods. The first was to measure the intensity of K X-rays and 134.25 keV gamma-rays in coincidence with the 551.7 keV gamma-ray. After correcting the K X-ray intensity for the fluorescence yield, the value $\alpha_{K\ 134.25} = 1.6 \pm 0.3$ was obtained. The ratio x of this value to the normalized value in

table 3, is $x = 0.94 \pm 0.21$. The second method is to equate the intensities of the populating and depopulating transitions for each level. Because the 206.25 and 134.25 keV levels are populated only by transitions from other levels, we have an overdetermined system which can be used to determine both the normalization constant and the value $\alpha_{K\ 72.00}$. (We have not been able to determine $\alpha_{K\ 72.00}$ directly because the K-conversion electrons only have ≈ 300 eV energy). The values obtained are $x = 0.96 \pm 0.11$ and $\alpha_{K\ 72.00} = 1.01 \pm 0.14$. (This is the value of $\alpha_{K\ 72.00}$ listed in table 3). These values depend on the assumption that the mica absorption of the K line at the 134.25 keV transition and the L lines of the 72.00 keV transition is as quoted, and that there is no β^--branching to the 134.25 and 206.25 keV levels. The average value $x = 0.95 \pm 0.12$ obtained from these two methods, is in excellent agreement with the normalization chosen.

A third check is to determine the number of K-holes from the number of K X-rays and (because we are dealing with a β^- decay) this must equal the K-holes created by K-shell conversion (except for β^--fluorescence excitation, which we discuss below). However, this would not be as reliable as the two above methods in our case because it depends on the value of $\alpha_{K\ 72.00}$ determined above and a second, more subtle, correction. As a consequence of these uncertainties we have only determined the value of x as a consistency check on the K X-ray intensities.

It is necessary to mention here that beta particles passing through a thick source such as ours can cause fluorescence excitation of K X-rays in the source. We have determined that the number of K-holes in Re created by this method is negligible compared to that created by the internal conversion process. We can do this because we know the ratio of W to Re atoms in the sample ($\approx 10^4$) and because we resolve the W K X-rays and the Re K X-rays. With the additional assumption that the cross sections for fluorescence excitation of W and Re are equal, we obtain the result above.

The second correction mentioned above is fundamental to high resolution instruments and is a consequence of the fact that the natural line width of the K X-rays is larger than that of most gamma-rays. In most instruments used in gamma-ray spectroscopy this is of no importance, as the window width of the measuring instruments is large compared to the natural line width. This is not true for the DuMond bent-crystal spectrometer, however, for while the window is large compared to the natural line width of the gamma-ray it is comparable to that of the K X-ray. As a consequence the method we have used to measure photon intensities does not yield directly the ratio of gamma-rays to K X-rays but involves a correction factor to account for the folding of the crystal window and the X-ray line. The folding procedure used and checks on it will be discussed elsewhere[13]).

The intensity of the $K\alpha_1$ X-ray obtained, on the same scale as the gamma-ray

intensities, is shown in table 3. The $K\alpha_2$ and $K\beta$ X-rays were measured, but not as accurately. Their contribution to the total intensity was estimated by determining the ratio of their intensities to that of the $K\alpha_1$, and was based upon a mean of our values, those of Beckman[17]) and those reported in Wapstra, Nijgh and Van Lieshout[18]). The ratios were taken to be $K\alpha_2/K\alpha_1 = 0.56$, $(K\beta_1 + K\beta_3)/K\alpha_1 = 0.34$ and $K\beta_2/K\alpha_1 = 0.08$. Using the fluorescence yield of 0.95 as interpolated from the computed values of Wapstra *et al.*, the value of x obtained is $x \approx 0.85$. The $K\alpha_1$ X-ray intensity reported in table 3 is therefore in reasonable absolute agreement with the gamma-ray intensities.

The conversion coefficients of the low energy transitions were normalized by what could be considered a fourth method, which has the property of separating nuclear and atomic internal conversion. The method consists of comparing the K X-ray and gamma-ray intensities measured on one scale with the K-Auger and K-shell internal-conversion electrons measured on another. When the (K-Auger electron)/(K X-ray) ratio is normalized to the fluorescence yield, the absolute normalization of the nuclear internal conversion coefficients is established directly. We have determined the absolute normalization factor for the low-energy electrons in table 4 by this method. The total K-Auger electron intensity has been calculated from the measured KLL intensities using the KLX/KLL and KXY/KLL ratios reported by Wapstra *et al.* The relative KLL Auger intensities have been compared to those reported by Gallagher, Strominger and Unik[19]) in W^{184} as a consistency check, and are in reasonable agreement with them.

5. Interpretation of Results

5.1. DECAY SCHEME

The decay scheme deduced from the data is shown in fig. 6. Level spin and parity assignments are based on the measured $\frac{5}{2}$ spin and positive parity assignment of the Re^{187} ground state, and the transition multipolarities obtained in the present study. In cases where the limits of error on the sum or difference of two gamma-ray energies is less than that of the crossover transition, the energy indicated in the figure is that with the smaller error. We have attempted to illustrate the transition intensities by the width of the transition in fig. 6.

In the following discussion we assume that W^{187} has spin $\frac{3}{2}$, negative parity. Such an assignment is the only assignment consistent with the observed branching, the neutron levels observed in W^{183} and those predicted by the Nilsson diagram[2, 20]).

The spins of the 134.25, 206,25 and 686.1 keV levels are unambiguous. The 106.61, 113.74, 239.3, 246.3, 511.3, 618.2, 625 and 867 keV transitions form an interrelated group of levels which are placed as indicated because the coincidence results show that the high energy transitions are not in coincidence with

the 134.25 and 72.00 keV transitions, and intensity arguments and energy considerations preclude their decay to any but the ground state (or a state of $\lesssim 20$ keV). The spins and parities of the group are related by the crossover transitions. Assuming the 511.3 and 625 keV transitions are pure E2 and the spin change of the 625 keV transition is $\Delta I = 2 = L$, two mutually exclusive sets of spins are possible for this group. The set of lower spins has been assigned because no branching from these levels to the 134.25 keV level is observed. If we do not assume that the E2 transition changes ΔI by 2 units, then the alternative spins shown in parentheses in fig. 6 are possible for these levels. On the basis of pure E2 between the 511.6 keV level and the ground state, the spin of the 511.6 keV level is probably $\frac{1}{2}$.

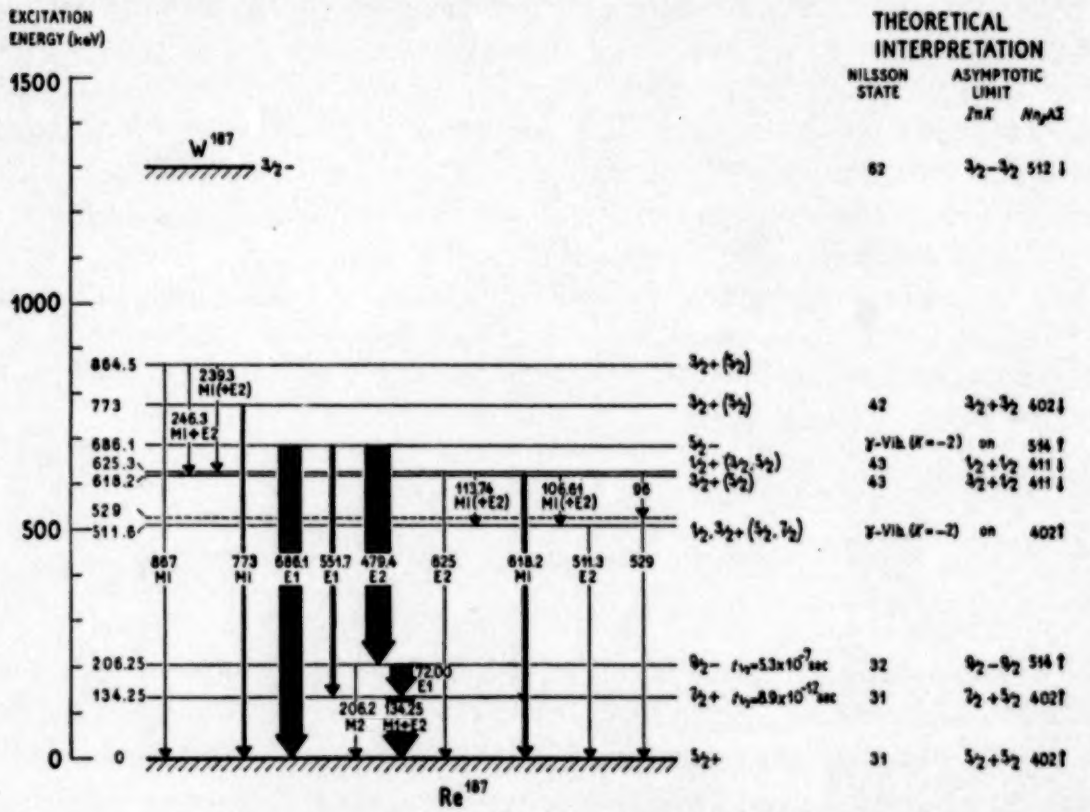

Fig. 6. Levels of Re^{187} based on the results of the present investigation. On the right of the figure is given our analysis of the levels of Re^{187} in terms of the asymptotic-quantum-number description of the Nilsson states assigned to them.

The level at 773 keV is established by only a single M1 (E2 admixture < 15%) transition, which, on the basis of energy and intensity considerations and our failure to detect it in coincidence with the 134.25 keV transition, we assign to populate the ground state. The $\frac{3}{2}^+$ assignment is made because the level is fed directly by beta decay from a $\frac{3}{2}^-$ state, decays directly to a $\frac{5}{2}^+$ state by an M1 transition, and is not observed to decay to the 134.25 keV $\frac{7}{2}^+$ state.

The level at 529 keV is postulated only tentatively as it is based on only two weak transitions.

5.2. INTERNAL CONVERSION COEFFICIENTS

The conversion coefficients measured in the present study which have the smallest limits of error are shown in table 3. A comparison of the theoretical K-conversion coefficients of Sliv and Band[16]) with our values shows that within experimental error no significant deviations exist between the theory and the K-conversion coefficients of the 551.7 and 686.1 keV transitions (pure E1), the 479.4, 511.3, and 625 keV transitions (pure E2), the 618.2 and 773 keV transitions (pure M1) and the 206.2 keV transition (pure M2). The experimental K-conversion coefficient of the 134.25 keV transition is within the experimental error of the theoretical K-conversion coefficient calculated for a $2.6 \pm 1.4\%$ E2 admixture (where we have used the $L_I/L_{II}/L_{III}$ subshell ratio shown in fig. 3 to determine the admixture). The K-conversion coefficient of the 72.00 keV transition is somewhat larger than a linear extrapolation of the K-conversion coefficients would indicate, but this probably indicates that such an extrapolation is not valid so near the binding energy.

As has been pointed out previously[6]), the 72.00 keV transition is delayed 3.5×10^{-6} times single particle rates, a factor somewhat larger than is ordinarily observed for a $\nu = 1$ K-forbiddeness ($\Delta K - L = \nu$). In this respect the agreement between the theoretical and experimental L_I and L_{II} subshell conversion coefficients is of interest, as Nilsson and Rasmussen[21]), and Asaro, Stephens, Hollander and Perlman[22] have shown that strongly delayed E1 transition may have anomalous conversion, although such anomalous conversion is not predicted for K-forbidden transitions[21]). In this respect it is unfortunate that we did not measure the L_{III} intensity in a high resolution run (it almost coincides in energy with the K 134.25), as Asaro *et al.*[22]) have recently shown that the L_{III} conversion coefficient is generally unchanged in such transitions and the $L_I/L_{II}/L_{III}$ subshell ratio would thus serve as a further check on our conclusions. The absolute value of the L_I conversion coefficient also indicates that if there is any M2 component in the 72.00 keV transition the M2/E1 admixture is $\leq 1\%$. As a further check on our M2/E1 branching ratio we estimated the intensity of the M2 component of the 72.00 keV transition theoretically, which is possible because the ratio of reduced transition probabilities for decay of a state to two states of the same rotational band is just the ratio of squares of Clebsch-Gordan coefficients (*if* K is a good quantum number)[23]). Basing our calculation on the intensity of the pure M2 206.2 keV photon intensity, we find that the intensity of the M2 component of 72.00 keV photon should be 2.6×10^{-3} times the intensity of the 206.2 keV photon, or the M2 admixture of the 72.00 keV transition should be $5.2 \times 10^{-3}\%$.

5.3. ANGULAR CORRELATION DATA

It is a consequence of the Bohr-Mottelson theory that if it is possible to measure the sign of the relative phases of the M1/E2 matrix element ratio of a

rotational transition, it will be possible to determine information about the magnetic moment of the rotational state. As Alder *et al.*[24]) have shown,

$$\text{sign } \delta = \text{sign } (g_\Omega - g_R)/Q_0$$

Thus, if we can determine the sign of δ_{134} we will be able to learn something about the gyromagnetic ratio of the first rotational state in Re^{187}, because the quadrupole moment is known to be positive.

The sign of δ can sometimes be determined from an angular correlation experiment if information as to the multipole mixtures of the transition is available from independent measurements. In our case we have been able to set limits on the multipole mixtures of both the 551.7 and 134.25 keV transitions from conversion-coefficient measurements. It therefore seemed worthwhile to calculate whether the sign of δ_{134} (the δ of the 134.25 keV transition) could be determined unambiguously from our data.

Before trying to interpret angular-correlation results it is necessary to estimate what the attenuation of the true correlation by electric and magnetic fields in the source will be. From elementary considerations it is clear that the amount of attenuation will be related to the mean life of the intermediate level. We therefore estimated the partial E2 radiation width of the 134.25 keV level from the Coulomb-excitation cross-section[8]). Using the M1 to E2 admixture we have observed to determine $|\delta_{134}|^2$, we were able to estimate that the total mean life of the state is 1.3×10^{-11} sec. With a lifetime this short and any reasonable estimate of the expected fields in the source the attenuation coefficients (see Abragam and Pound[25]) should be of the order of unity, i.e. no attenuation of the angular correlation.

Figure 7 is a contour plot of the coefficient $P_2(\cos\theta)$ expected for a $\frac{5}{2}$-$\frac{7}{2}$-$\frac{5}{2}$ cascade, the first transition an E1/M2 admixture (δ_{552}) and the second an

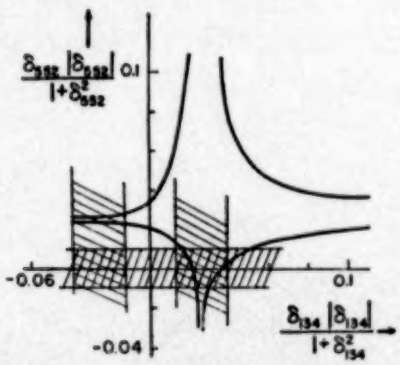

Fig. 7. Comparison of the absolute value of the electric quadrupole content in the 134.25 keV transition (abscissa) and the magnetic quadrupole content in the 551.7 keV transition (ordinate) determined from conversion coefficient data with the limits on these quantities deduced from angular correlation data. The crossing of the three experimental points in the first quadrant indicates that the ratio of the M1 and E2 matrix elements is positive. The positive value of this quantity indicates that $(g_\Omega - g_R)$ is positive, in agreement with the theoretical predictions for the 134.25 keV state.

M1/E2 admixture (δ_{134}). Contours for the coefficient of $P_2(\cos\theta) = \pm 0.015$ are shown. Limits set on $|\delta_{134}|$ and $|\delta_{552}|$ from the conversion-coefficient measurements are also shown. The areas common to the cross-hatched regions indicate the possible values of δ_{134} and δ_{552}. These values are $\delta_{552} = \pm 0.1$ and $\delta_{134} = 0.17 \pm 0.05$. The positive sign of δ_{134} can now be compared with the predictions of the Bohr-Mottelson model through the relationship given above. Computing the value of g_Ω for the ground state from Nilsson's wave functions, we obtain $g_\Omega = 1.6$, which indicates that $(g_\Omega - g_R)/Q_0$ is positive, if $g_R \approx Z/A$. Thus the positive sign of δ_{134} is in agreement with the theoretical predictions.

It has been noted by Huby[26]) that some ambiguity exists about the sign convention for the matrix element ratio δ. We have been careful in our analysis to use the same sign convention as Alder *et al.* in order to compare the sign we have determined with their theoretical results.

6. Comparison with Previous Results

A comparison of fig. 1 with fig. 6 shows the similarities and differences between the previously reported level schemes of Re^{187} and that which we propose. Our decay scheme is similar to that proposed by Cork *et al.*[4]) but we have inverted the level order of the group of levels based on the transitions which sum to the 864.5 keV level because of the relative transition intensities. We place their 774 keV transition to populate the ground state, and their 513.5 and 113.8 keV transitions fit into the group of levels beginning with the 864.5 keV level. The parity they assign to the 686.1 keV level does not agree with our results. The similarity between our results and those of Dubey *et al.*[5] is limited to the energies of the first five of their 9 excited levels. For the most part the difference in interpretation seems to arise from the question as to the correct place of the 773 keV transition in the decay scheme. Our results do not agree with their assignment of mixed M1 and E2 multipolarities to the 206.2 keV transition. Although the shape of the beta spectrum we have observed shows no indication of the $\Delta I = 2$, yes, shape reported by these authors, we do not believe this question has been answered finally yet, because we have not checked our measurement by measuring a spectrum with a well-established $\Delta I = 2$, yes, shape, nor completely evaluated the sources of scattering in our spectrometer, which must be done accurately before definite conclusions on spectral shapes can be made.

The energy levels proposed by Vergnes[6]) are in agreement with our proposals, although he has assigned a multipolarity to the 775 keV transition, and hence a spin and parity to his 775 keV level, and a spin to his 866 keV level with which we disagree.

In addition to these determinations of the decay scheme, Behrend and

Neuert[27]) have measured the angular correlation for the 72–134 cascade and obtained $W(\theta) = 1 \pm 0.008 - (0.229 \pm 0.033)P_2(\cos\theta) + (0.091 \pm 0.045)P_4(\cos\theta)$. It must be noted here that the 1.5 % M1 and E2 admixture reported by these authors for the 134.25 keV transition is based upon assignments by Dubey *et al.* of pure E2 multipolarity to the 72.00 keV transition and a spin and parity of $\frac{3}{2}^+$ to the 206.25 keV level, which have now been shown to be incorrect. Thus in order to compare the results of Behrend and Neuert with the present results, we recalculated the mixing ratios using the now established $\frac{9}{2}$-$\frac{7}{2}$-$\frac{5}{2}$ sequence for this cascade. Using our $\delta_{134} = 0.17 \pm 0.05$ and the above spin sequence we find that these results agree with our results only if the ratio of $\delta_{72.00}$ of the M2/E1 matrix elements for the 72.00 keV transition is $\delta_{72.00} \geqq 0.5$.

As stated previously, our experimental results indicate that the 72.00 keV transition has $\leqq 1\,\%$ admixture ($\delta_{72.00} \leqq 0.1$), which result is in agreement with that calculated from reduced transition probability arguments. Predictions based on our results therefore clearly differ from the value measured by Behrend and Neuert.

A check on our results, in this case δ_{134}, is provided by the Bohr-Mottelson theory. A consequence of this theory is that the ratio of the M1/E2 matrix elements of the transitions within a rotational band should be equal. We have been able to check our results (or the theory, if our results are taken as correct), because the δ_{167} of the 167 keV $\frac{9}{2}^+$ to $\frac{7}{2}^+$ rotational transition in this band has been measured by McGowan and Stelson[28]) and de Boer, Martin and Marmier[29]) by means of Coulomb-excitation experiments. The ratio of the square of our value ($|\delta_{134}|^2 = 0.027 \pm 0.014$) to the square of the values reported for the 167 keV transition (McGowan and Stelson: $|\delta_{167}|^2 = 0.0256 \pm 0.015$; de Boer *et al.*: $|\delta_{167}|^2 = 0.030 \pm 0.002$) yields values of 1.1 ± 0.8 and 0.9 ± 0.4 respectively, in agreement with the theoretical ratio, $|\delta_{134}|^2 / |\delta_{167}|^2 = 1.035$. McGowan and Stelson, and de Boer *et al.* have also measured the sign of δ_{167} and found that it is positive. This indicates that the sign of g_Ω for the first two rotational states is in agreement with theory.

7. Analysis of the Decay Scheme

In order to determine whether any differences exist between the observed levels in Re^{187} and those predicted by Nilsson[1]) we have calculated, using the Nilsson wave functions, all those properties that we have been able to measure or which have been measured elsewhere and reported. In doing so we have noted that certain states exist which cannot be explained as intrinsic states predicted by Nilsson or rotational states based upon such states. In the first section of the analysis we compare the experimental results with Nilsson's predictions. In the second part we point out those states of the level scheme

which appear to us to be unexplained as intrinsic states or rotational states, and a possible interpretation of them.

7.1. NILSSON STATES

The ground state, which has a measured spin $\frac{1}{2}$, is assigned as Nilsson state 31 (see fig. 6 for the asymptotic-quantum number assignments for these states), as this is the only $\frac{1}{2}$ state expected in this region. The parity is then positive. The calculated values for the magnetic moment for state 31, and the quadrupole moment for a spin $\frac{1}{2}$ state are shown as a function of deformation in figs. 8a and 8b. The experimental values (references [30]) and [31]), respectively) are as reported in Strominger *et al.*[3]. A comparison between experimental and theoretical values has been made previously by Mottelson and Nilsson[2]), who assigned the ground state a deformation $\delta \approx 0.19$ ($\eta \approx 3$).

The state at 134.25 keV is assigned as the $\frac{7}{2}^+$ rotational state based on state 31. The dependence of the M1/E2 admixture of the 134.25 keV transition as a function of deformation is shown in fig. 8c. The observed ratio has limits of error which preclude an exact assignment of the deformation, but the deformation predicted is similar to that of the ground state.

The $\frac{9}{2}^-$ state at 206.2 keV is assigned as Nilsson state 32. The calculated transition probability for the 206.2 keV M2 transition from the $\frac{9}{2}^-$ level to the ground state is equal to the experimental value deduced from the reported 5.3×10^{-7} sec half-life[7]) and the relative 72.00/206.2 photon intensities (fig. 8d) for $\eta \approx 5$. For a smaller deformation ($\eta = 2$) it is delayed by only a factor of 10. Because th[e] ingle particle estimates[32]) of this half-life indicate it is ≈ 500 times delayed, the correct prediction of the order of magnitude of the transition probability by the Nilsson description seems to be a reasonable check on the theory.

The probable assignments of $\frac{3}{2}^+$ and $\frac{1}{2}^+$ to the 618.2 and 625.3 keV levels suggest that these levels may be the base state and first rotational state of a $K = \frac{1}{2}$ level with a large negative decoupling factor. We have calculated the decoupling factors for the $K = \frac{1}{2}$ states expected in this region (fig. 8e). The results allow us to select state 43 as the probable assignment. We assumed that the $K = \frac{1}{2}$ band has the same moment of inertia as the ground state band in calculating the decoupling factor.

The 773 keV level has been assigned as state 42. The E2 and M1 admixture in the decay of this state 31 is expected to be small if this state is state 42. This is observed (fig. 8h). The failure to observe E2 branching from this level to the 134.25 keV rotational state to state is in agreement with this small ratio and the theoretical reduced transition probabilities shown in table 6.

A possible assignment for the 864.5 keV level is state 33, because of its decay to the 618.2 and 625.3 keV levels. The strong M1 to ground would then be also in agreement with the theoretical prediction (fig. 8h). However, we have not definitely assigned this state a configuration in fig. 6.

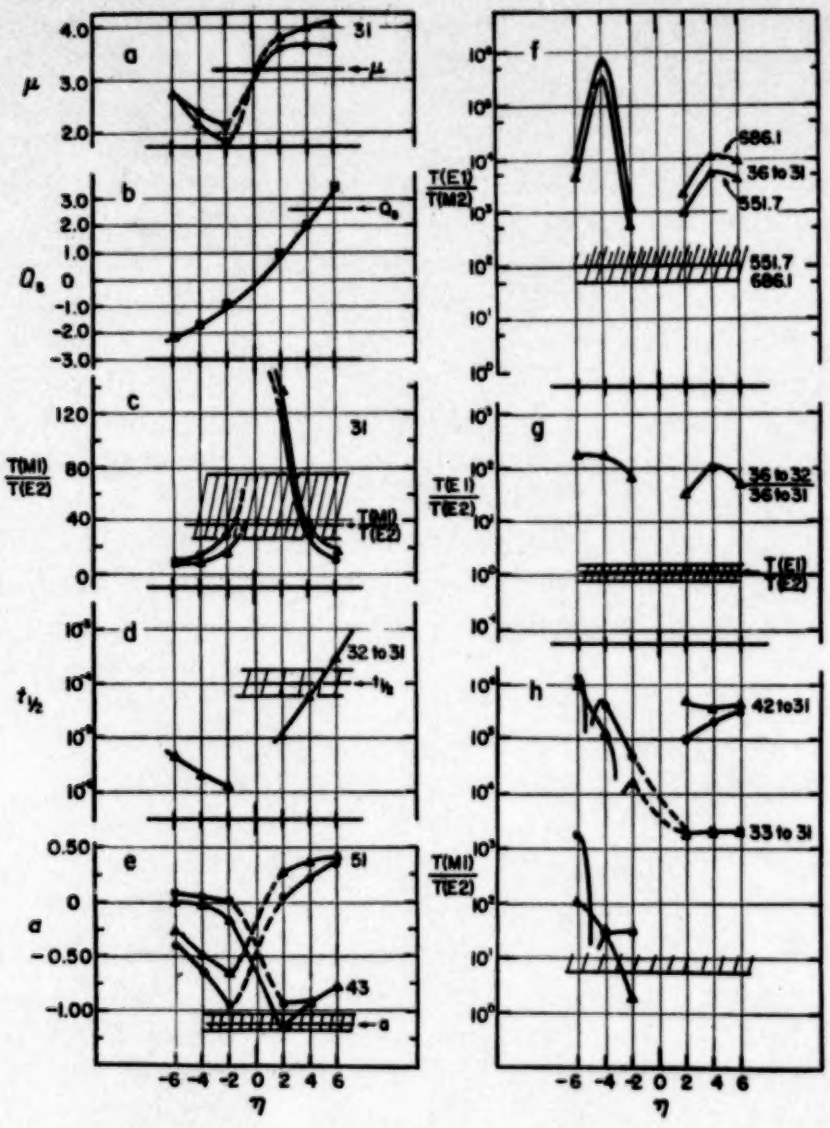

Fig. 8. Comparison of experimental results with theoretical predictions for several of the levels in Re^{187} as a function of deformation. The theoretical values are calculated using the expression and wave functions reported by Nilsson. Two values of Nilsson's quantity μ, 0.45 and 0.55, are used in cases where both were available (triangles: $\mu = 0.45$; circles: $\mu = 0.55$). (a) The ground state magnetic moment of Re^{187}, assuming state 31. The experimental value is that quoted in ref. [3]). (b) The quadrupole moment of the Re^{187} ground state calculated with $I = \frac{5}{2}$. The experimental value is that quoted in ref. [3]). (c) The ratio of M1 to E2 transition probabilities for the decay of the 134.25 keV state, assuming it is the first rotational state based on state 31. Only the collective E2 transition probability was calculated. (d) The radiative M2 transition probability for the decay of the 206.25 keV state to ground (states 32 to 31). The half-life of the 206.25 keV state is that quoted in ref. [3]). (e) Decoupling factors for states 51 and 43. The experimental value was calculated assuming the $K = \frac{1}{2}$ state has the same moment of inertia as the ground state. (f) The ratio of E1 to M2 transition probabilities for the 686.1 keV and 551.7 keV transitions, assuming the initial state is number 36 and the final states are respectively state 31 and the rotational state based on 31. (g) The ratio of the electric dipole transition probability between states 36 and 31 (686.1 keV transition) to the E2 transition probability between states 36 and 32 (479.4 keV transition). (h) The ratio of the M1 and E2 transition probabilities between the $\frac{3}{2}^+$ intrinsic states 42 and 33, and state 31 for $E_\gamma = 773$.

TABLE 6

Comparison of experimental and theoretical reduced transition probabilities for transitions from some of the levels in Re^{187}.

Energy of initial state (keV)	Reduced transition probability	Theoretical value	Experimental value
206.25	$\frac{B(M2; \frac{9}{2}^- \rightarrow \frac{7}{2}^+)}{B(M2; \frac{9}{2}^- \rightarrow \frac{5}{2}^+)}$	0.485	≤ 190 [a]
686.1	$\frac{B(E1; \frac{5}{2}^- \rightarrow \frac{7}{2}^+)}{B(E1; \frac{5}{2}^- \rightarrow \frac{5}{2}^+)}$	0.40	0.33
773	$\frac{B(E2; \frac{5}{2}^- \rightarrow \frac{7}{2}^+)}{B(E2; \frac{5}{2}^- \rightarrow \frac{5}{2}^+)}$	1.33	— [b]

[a] Upper limit based on upper limit of 1 % M2 admixture in the 72.00 keV transition. Theoretically we can thus expect a $\approx 5.2 \times 10^{-3}$ % M2 admixture in the 72.00 keV gamma.

[b] The upper limit of 15 % E2 admixture in the 773 keV transition establishes an upper limit on the intensity of the 639 keV $\frac{3}{2}^+ \rightarrow \frac{7}{2}^+$ transition of 7.5 % of the intensity of the 733 keV gamma. We can, in addition, set an experimental limit of 6.8 % of the intensity of the 773 keV gamma on the intensity of the 639 keV gamma. The data are thus consistent.

7.2. DEVIATIONS FROM THE PREDICTED NILSSON STATES

The levels discussed above seem well described as intrinsic states with rotational states based upon them. The 686.1 keV level, on the other hand, while manifesting some of the expected properties of the Nilsson hole state 36 (fig. 8f), has these pecularities: (1) it occurs at a much lower energy than is expected; (2) although it is very strongly populated, it does not populate the $\frac{7}{2}^-$ hole state which theoretically must occur between it and the $\frac{9}{2}^-$ hole state if it is an intrinsic state. Unless the energies of the $\frac{5}{2}^-$ and $\frac{7}{2}^-$ states are nearly degenerate, the lack of transitions between them is most unusual, because the M1 matrix element between such like states should be large. The transition is not observed, even in competition with the strong E2 to the $\frac{9}{2}^-$ level (fig. 8g), and we can exclude any transition of the expected intensity that would have an electron line between 8 and 480 keV. We are therefore forced to conclude that either the $\frac{5}{2}^-$ and $\frac{7}{2}^-$ states are nearly degenerate, or the $\frac{5}{2}^-$-state cannot be described as an intrinsic state in the Nilsson description. We believe the latter possibility is more likely.

Similarly, the velel at 511.6 keV is most difficult to fit into the Nilsson scheme. If it has a spin and parity $\frac{3}{2}^+$, it could possibly be the particle-excitation state 42 or the hole-excitation state 33. However, if it is either of these states, it is not easy to explain its almost pure E2 decay to ground. In addition, because the E2 branching to ground is so strong, it is difficult to explain why the E2 branch to the $\frac{7}{2}^+$ level at 134.25 keV is not observed. (Such E2 transitions to various members of a rotational band are related only by geometrical factors[28]). Furthermore, if it is hole-excitation state 33 it should occur at a higher excita-

tion energy than hole-excitation state 43, which we assign as the 773 keV level. If, however, it is $\frac{1}{2}^+$, as we believe likely, the latter query would be answered, but then, assuming we continue to insist that the 625.3 keV level is the hole-excitation state 43, it is not possible to explain the level on the basis of the Nilsson model. This is because the only other intrinsic state of spin $\frac{1}{2}^+$ (state 51) is a particle-excitation and must occur at a higher excitation energy than the $\frac{3}{2}^+$ particle-excitation state 42. Because no level below 511.6 keV can be assigned as $\frac{3}{2}^+$ (and such a level should definitely be observed) we are forced to conclude that this level is also not an excited intrinsic level.

At the present time we can only speculate on this deviation from the expected intrinsic-rotational state spectrum. However, because Re^{187} is in the region where rotational-vibrational spectra occur, it seems logical to look for an explanation within the framework of the collective model. A well-known prediction of the model is that collective core excitations of a vibrational nature can occur in odd-mass nuclei, although to date none have been reported. If these states are not intrinsic or rotational states it therefore seems probable that they are single particle states coupled to a $K = 2$ vibrational state (the $K = 0$ vibrational states being expected from the systematics of energy levels in nearby even-even nuclei to be somewhat higher in energy). The possible spins of particle-gamma-vibrational excitations are $I - 2$ and $I + 2$. We believe that the anomolous states observed in Re^{187} might well belong to this category, the $\frac{1}{2}^+$ state at 511.6 keV being associated with the ground state ($\frac{5}{2}^+ - 2^+ = \frac{1}{2}^+$) and the level at 686.1 keV with the $\frac{9}{2}^-$ state at 206.2 keV ($\frac{9}{2}^- - 2^+ = \frac{5}{2}^-$). The strong E2 transitions between these pairs seem to support such a speculation. It should also be noted that, if these levels are postulated to be the $I - 2$ excitations of the levels quoted, the excitation energies, 511.6 and 479.4 keV, are sufficiently close to the energies of the gamma-vibrational states in Os^{186} (768 keV) and Os^{188} (633 keV) to make such assignments seem reasonable.

8. Conclusion

From the data we present it seems that although Re^{187} lies on the edge of the region where the strong coupling model is expected to be valid, the Re^{187} levels that are populated by W^{187} beta decay can be interpreted within the framework of the model if we postulate that, in addition to the well-established intrinsic state-rotational state pattern, two vibrational states based on intrinsic states also occur.

We thank Mr. R. L. Cohen and Mr. J. Rogers for help in making some of the measurements, and Professor J. W. M. DuMond for the excellent working conditions in his laboratory. One of us (CJG) acknowledges an interesting discussion with Dr. B. R. Mottelson and Dr. S. G. Nilsson.

Note added in proof: Klimentovskaya and Shavrin[33]) have reported the results of γ–γ angular correlation measurements on the 522–134, 480–72–134 and 72–134 gamma-ray cascades in Re^{187}. The spins of the 686, 206 and 134 keV levels reported by these authors agree with those reported here. The only apparent discrepancy between their work and ours is that they report that $\delta_{134} < 0$. However, because the experimental results reported in their paper are otherwise in agreement with our results, we believe that the discrepancy may be the result of the use of different phase conventions in the two cases.

References

1) S. G. Nilsson, Mat. Fys. Medd. Dan. Vid. Selsk. **29**, No. 16 (1955)
2) B. R. Mottelson and S. G. Nilsson, Mat. Fys. Skr. Dan. Vid. Selsk. **1**, No. 8 (1959)
3) See, for example, the references listed in Strominger, Hollander and Seaborg, Revs. Mod. Phys. **30** (1958) 585
4) Cork, Brice, Nester, LeBlanc and Martin, Phys. Rev. **89** (1953) 1291
5) Dubey, Mandeville, Mukerji and Potnis, Phys. Rev. **106** (1957) 785
6) M. Vergnes, J. Phys. Rad. **19** (1958) 947
7) A. W. Sunyar, Phys. Rev. **90** (1953) 387A
9)† J. W. M. DuMond, Annals of Physics **2** (1957) 283
10) Special Report No. 24, United States Atomic Energy Commission Contract AT(04-3)-63, J. W. M. DuMond contract supervisor (California Institute of Technology, Pasadena, California)
11) G. W. Grodstein, National Bureau of Standards Circular, NBS-583 (1957)
12) M. J. Berger and J. Doggett, J. Research Natl. Bureau Standards **56** (1956) 355
13) W. F. Edwards, Thesis, California Institute of Technology, 1959 (unpublished)
14) J. J. Murray, Thesis, California Institute of Technology, 1954 (unpublished)
15) D. Saxon, Phys. Rev. **81** (1951) 639
16) L. A. Sliv and I. M. Band, Leningrad Physico-Technical Institute Reports (1956 and 1958); reproduction: Reports 57 ICC K1 and 58 ICC L1, issued by Physics Department, University of Illinois, Urbana, Illinois (unpublished)
17) O. Beckman, Arkiv för Phys. **9** (1955) 495
18) Wapstra, Nijgh and Van Lieshout, Nuclear Spectroscopy Tables, (North-Holland Publishing Company, Amsterdam, 1959)
19) Gallagher, Strominger and Unik, Phys. Rev. **110** (1958) 725
20) Murray, Boehm, Marmier and DuMond, Phys. Rev. **97** (1955) 1007
21) S. G. Nilsson and J. O. Rasmussen, Nuclear Physics **5** (1958) 617
22) Asaro, Stephens, Hollander and Perlman, Phys. Rev. **117** (1960) 492
23) Alaga, Alder, Bohr and Mottelson, Mat. Fys. Medd. Dan. Vid. Selsk. **29**, No. 9 (1955)
24) Alder, Bohr, Huus, Mottelson and Winther, Revs. Mod. Phys. **28** (1956) 432
25) A. Abragam and R. V. Pound, Phys. Rev. **92** (1953) 943
26) R. Huby, Proc. Phys. Soc. A **67** (1959) 1103
27) H. J. Behrend and H. Neuert, Z. für Naturforschung **13A** (1958) 208
28) F. K. McGowan and P. H. Stelson, Phys. Rev. **109** (1958) 901
29) de Boer, Martin and Marmier, Helv. Phys. Acta **32** (1959) 377
30) H. E. Walchi, Oak Ridge National Laboratory Report ORNL-1469 (April, 1953) and Supplement II Feb. 1955 (unpublished);
H. Kopferman, Kernmomente (Akademische Verlagsgesellschaft, Frankfurt am Main, 1956)
31) J. E. Mack, Revs. Modern Phys. **22** (1950) 64
S. L. Segel and R. S. Barnes, Phys. Rev. **107** (1957) 638; and others
32) S. A. Moszkowski, in Beta- and Gamma-Ray Spectroscopy, edited by K. Siegbahn (North-Holland Publishing Company, Amsterdam, 1955) Chap. XIII, p. 391
33) M. V. Klimentovskaya and P. I. Shavrin, JETP **36** (1959) 1360

† There is no ref. 8).

2.D:2.F

Nuclear Physics **19** (1960) 40—51; © *North-Holland Publishing Co., Amsterdam*
Not to be reproduced by photoprint or microfilm without written permission from the publisher

MECHANISM OF THE $Zn^{64}(n, p)Cu^{64}$ REACTION AT INCIDENT NEUTRON ENERGIES OF 8 AND 14 MeV†

ALICE H. ARMSTRONG and LOUIS ROSEN††

Los Alamos Scientific Laboratory, University of California, Los Alamos, New Mexico

Received 29 February 1960

Abstract: The $Zn^{64}(n,p)Cu^{64}$ reaction was studied at incident neutron energies of 8 and 14 MeV. These experiments were part of an investigation of the adequacy of the statistical model concept of the compound nucleus to describe interactions when complex nuclei are bombarded by neutrons of energies in the region of nuclear binding energies. The spectral and spatial distributions of most of the protons indicate that the compound-nucleus hypothesis may be satisfied. The high-energy proton distributions are in sharp contrast with the predictions of the statistical model and contradict the compound-nucleus hypothesis.

For 8-MeV neutron bombarding energy, there is an inordinately large probability for the emission or protons with energies considerably lower than that of the Coulomb barrier.

1. Introduction

The present experiments were undertaken as part of an attempt to delineate the extent to which the statistical model of the compound nucleus[1]) provides a valid description of the interaction of neutrons with complex nuclei in the energy region of nuclear binding energies

The striking success of Bohr's compound nucleus concept, at energies where the levels in the compound nucleus are well separated, is in itself sufficient to establish the validity of this concept. At higher energies the situation is however far less clear. There has, in fact, been accumulating in recent years a large body of information which not only casts doubt on the general validity of the statistical theory but also on the compound nucleus hypothesis which serves as the foundation for this theory.

The compound nucleus assumption which is brought into question is the very fundamental one of the uncorrelated formation and decay of a compound system, which implies a very short mean free path for nucleons in nuclear matter so that a statistical distribution of energy among all the nucleons is achieved during the lifetime of the compound system. The point here, which is subject to some kind of experimental verification, is that the incident nucleon is so thoroughly amalgamated within the compound system that it loses its identity as the incident particle. The additional assumptions of the statistical model which are at least as suspect as the compound nucleus hypothesis are:

† Research performed under the auspices of the U. S. Atomic Energy Commission.

†† Now a Guggenheim Fellow at le Centre d'Études Nucléaires de Saclay, France.

(a) the phase relationships between the levels in the intermediate nucleus are random so that interference effects cancel (statistical assumption); (b) the probabilities for the various modes of disintegration of the compound nucleus are determined only by the total energy and angular momentum of the compound system; (c) transitions to all levels of a given residual nucleus are equally probable.

On the basis of the above assumptions it is possible to predict the main features of the energy and angular dependence of the differential non-elastic cross sections for a great variety of nuclear reactions and, in particular, for nucleon-induced reactions. For example, when the incident nucleon energy spread encompasses many levels of the compound nucleus, as is the case in the present experiments, the emitted nucleons are predicted to have a Maxwellian-like energy distribution and an angular distribution which is symmetrical about 90° in the centre-of-mass coordinate system. Also, the charged particle yield from medium and heavy nuclei should be small compared to the neutron yield, and should fall off rapidly with increasing atomic number. Furthermore, the total and differential cross sections for a given mode of decay of the compound nucleus should be independent of how the compound nucleus is formed.

A large number of experiments have yielded results which are indeed characterized by one or more of the above features. In this category would be the energy distributions of neutrons from proton[2]) and neutron induced[3]) reactions, the energy dependence of level densities from (p,p′) reactions[4]) at 11 to 23 MeV, and, perhaps most spectacular of all, the excitation functions for neutron emission from proton and alpha induced reactions which proceed through the same compound nucleus[5]). But some of the very same experiments which seemed to confirm the predictions of the statistical model also foreshadowed serious difficulties with this theory. Both (p,n)[2] and (n,n′)[3]) experiments yielded more high energy neutrons than predicted and large anisotropies were observed for the high energy neutrons produced in 14-MeV (n,n′) reactions[6]). In this case there was no question of confusion due to the Coulomb barrier; so here was very strong evidence that the high energy neutrons, which are unaccounted for by the statistical model, do, in fact, "remember" something about the energy and direction of the incident neutrons. In fact, all of these experiments indicate a correlation between the mode of formation of the compound nucleus and its subsequent decay. Similar difficulties for the statistical model were found in the energy and angular distributions of the protons from (p,p′)[4]) reactions. These experiments also indicated both an excess of high energy protons and a strong forward asymmetry. If any doubt remained about the inadequacy of the statistical model, it was completely removed by the demonstration of an angular correlation between the recoil direction of the residual nucleus and the gamma rays emitted in (p,p′) processes[7]). It still remains, however, to delineate which nuclear processes are adequately described

by the statistical model and which are not, and why the division occurs in the way that it does.

Perhaps no reaction is more difficult to describe within the framework of the statistical model than the (n,p) reaction for intermediate and heavy nuclei. It has been shown by Paul and Clarke[8]) and, subsequently, Coleman and co-workers[9]) that (n,p) cross sections are much larger than can be deduced from the statistical theory. Since (n,p) cross sections are large, it appeared that this reaction might be amenable to the kind of detailed study which could give considerable insight into that part of the reaction mechanism which is at variance with the statistical model.

By now a substantial number of (n,p) experiments have been performed in which were measured the energy and angular distributions of the emitted protons[10]), most of them at 14-MeV neutron energy and a few at somewhat higher energies. In the present experiments we have concentrated on a detailed analysis of the energy and angular distributions of the protons from the Zn^{64}(n,p) reaction for incident neutron energies of 8 and 14 MeV. The choice of 8 MeV was based on the fact that it represents the highest energy at which one can avoid confusion arising from the emission of two nucleons as well as from (n,d) processes.

2. Experimental Arrangement

The experimental arrangement appropriate to the 14-MeV experiment is shown in fig. 1. The neutrons were generated by means of the d–T reaction using 200 keV deuterons. The large iron collimator permits the Zn^{64} target to

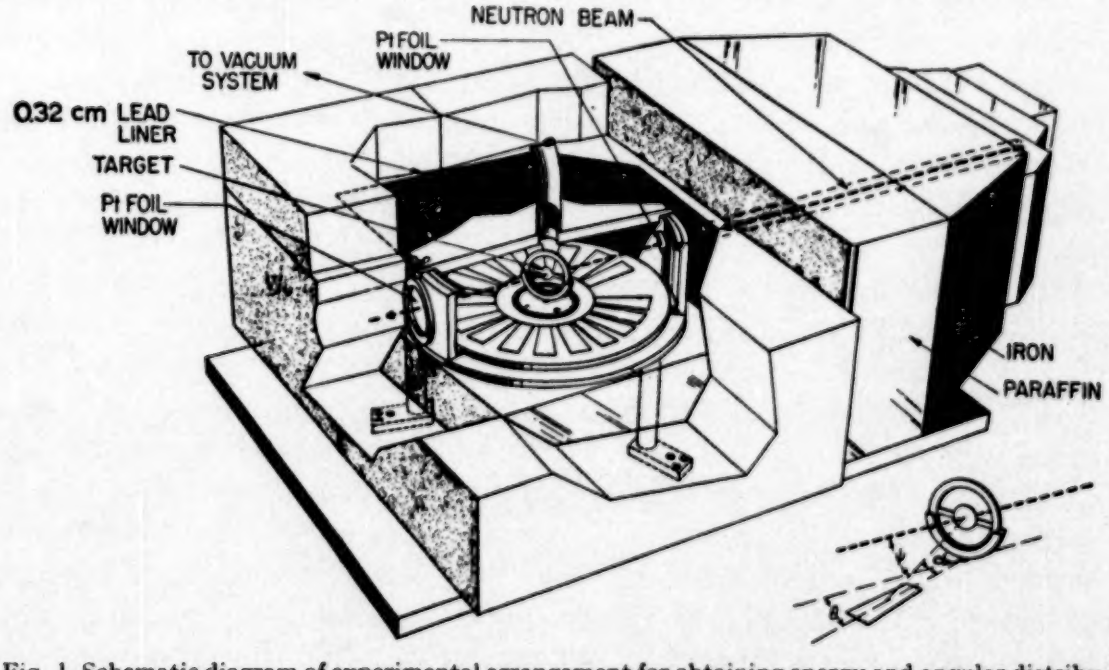

Fig. 1. Schematic diagram of experimental arrangement for obtaining energy and angular distributions of protons from interaction of 14-MeV neutrons with Zn^{64}.

be irradiated by a narrow beam of monoenergetic neutrons while simultaneously shielding the detectors from direct and room-scattered neutrons. The detectors were 400 μ C–2 emulsions arranged along the periphery of a circle centered about the target. The Zn^{64} was electrodeposited on a gold backing. Background runs were made with a blank gold target. Two runs were required for the complete angular distribution, with the target rotated through 180° around a vertical axis through the centre of the target for the second run. The selection criteria discarded tracks whose line of direction did not intersect the target.

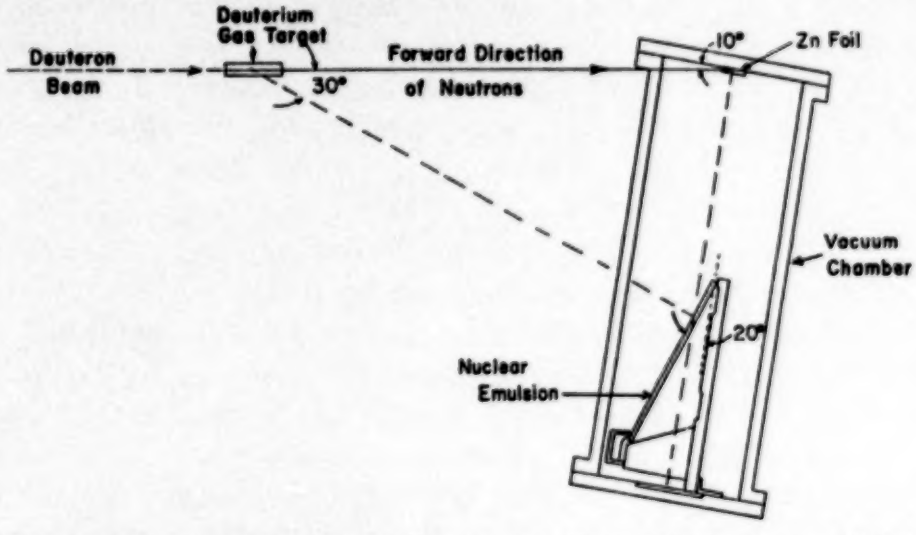

Fig. 2. Schematic diagram of experimental arrangement for obtaining energy distribution of protons emitted at 90° to the incident neutron beam, for interaction of 8-MeV neutrons with Zn^{64}.

At 8 MeV two experiments were performed. In one of them we measured only the energy distribution of the protons emitted at 90° to the incident neutron beam. Fig. 2 shows this geometry. In the second experiment the Zn^{64} was placed in contact with a nuclear emulsion. The geometry of the exposure was such that the plane of the emulsion was orthogonal to the neutron beam direction. This permitted angular and energy distributions over the angular region 0° to 70°. The 8-MeV neutrons were generated by the d–D reaction, the deuterons being accelerated to the appropriate energy by an electrostatic accelerator. The same Zn^{64} target was used in both experiments and all data were corrected for the target thickness which was 0.4 MeV for 10-MeV protons.

3. Results and Discussion

Since it is convenient to present our results within the framework of the statistical model, we shall briefly review the formalism[1]). The conventional equations which describe the energy distributions of emitted particles are based on a thermodynamic analogy whereby the excited residual nucleus is treated as a degenerate Fermi gas of independent particles, confined to the nuclear

volume, whose level density is given by $\omega(E') = \text{const. exp } [2(aE')^{\frac{1}{2}}]$, where a is a constant and E' is the excitation energy of the residual nucleus. Considering now an (n,p) process, the number of protons emitted with energy between E and $E + \mathrm{d}E$ is given by

$$N(E)\,\mathrm{d}E = \text{const. } \sigma_p\, E\omega(E')\,\mathrm{d}E\,, \tag{1}$$

where σ_p is the cross section for the formation of a compound nucleus by protons of energy E incident on the residual nucleus at excitation $E' = E_{max} - E$. In this latter relation E_{max} is the maximum energy available for proton emission and is equal to $E_0 + Q$ for incident neutrons of energy E_0. By use of the entropy relation $S = \int \mathrm{d}E/T = \ln \omega$ one obtains a relation between E' and T, namely $E' = aT^2$, where T now represents the temperature of the residual nucleus prior to de-excitation. For values of $E_{max} \gg E$, $\omega(E')$ may be approximated by $\mathrm{e}^{-E/T}$

It is apparent from eq. (1) that a plot of $\ln(N(E)/\sigma_p E)$ versus E' is equivalent to the variation of level density with excitation energy.

The 14-MeV data are presented in figs. 3–5 and the 8-MeV data in figs. 6 and 7. We first consider the 14-MeV data. Spectra were measured at 10 angles between 17.5° and 160° in the c.m. system. Figure 3 represents the space-integrated energy spectrum while fig. 4 shows the angular dependence of three energy-groups of protons: 2–7 MeV, 7–10.5 MeV and 10.5–14.5 MeV. It is apparent that whereas the low energy group, and perhaps also the intermediate group, is symmetrical about 90° (a minimum requirement for processes which proceed through a compound nucleus), the high energy protons are unmistakably peaked in the forward direction. Figure 5 displays the data in such a way as to yield a straight line according to eq. 1. However, the data are seen to resolve themselves into three straight lines. The reason for this becomes at least partially clear when we consider the energy diagram for Zn^{64} plus a 14-MeV neutron. This is illustrated in fig. 8. The curve labelled "first neutrons" is calculated on the basis of the statistical model using $T = 0.8$ MeV, which is consistent with the previous results[3]) on Cu, after correction is made for (n,2n) processes. It is seen from fig. 8 that all neutrons of energy between 2.4 and 6.4 MeV must lead to proton or gamma-ray emission from the residual Zn^{64*} nucleus. We assume that it is these protons that are represented by curve A (fig. 5), contaminated, to be sure, by a small number of "evaporation" protons from the (n,p) reaction. However, we think it a reasonable assumption, on the basis of the qualitative appearance of the data, that most of the evaporation protons are encompassed by curve B, again contaminated with "direct process" interactions as indicated by the forward peaking of the high energy protons. Curve C is attributed to a superposition of "evaporation" protons on "direct interaction" protons. The apparent temperatures for the various energy regions are indicated in fig. 5. The fact that the energy dependence of the level

density, if indeed the data can be so interpreted, for the regions A, B and C in fig. 5 appears to increase exponentially with E' rather than with $(E')^{\frac{1}{2}}$, is not significant since almost as good straight lines are obtained by plotting $\ln[N(E)/\sigma_p E]$ against $(E')^{\frac{1}{2}}$. In order to test the hypothesis, first put forward

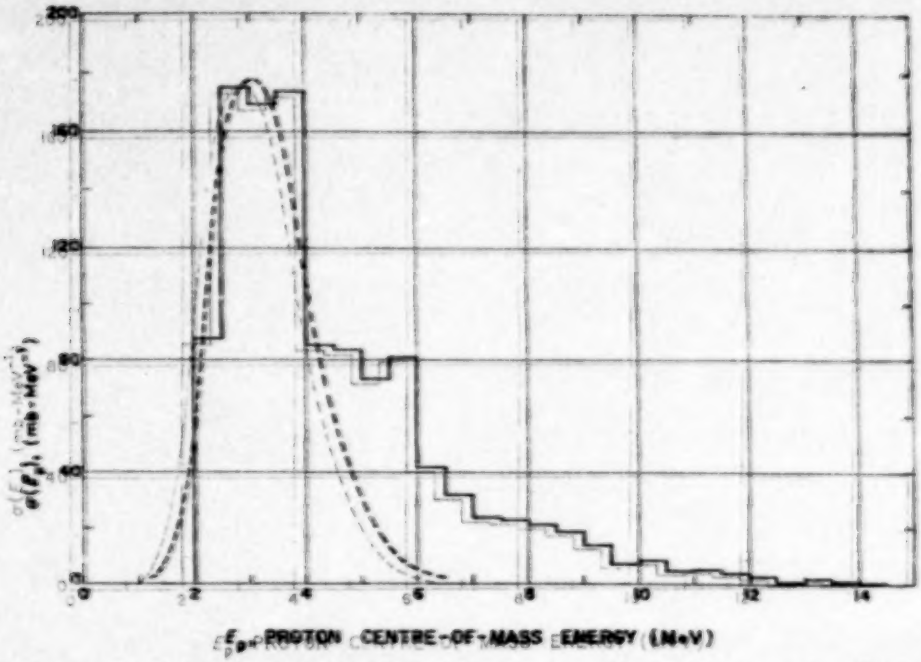

Fig. 3. Solid curve: proton emission (integrated over 4π solid angle), as a function of proton energy, from the interaction of 14-MeV neutrons with Zn^{64}, (lower limit of 2 MeV imposed by absorption in target). Dashed curve: protons from the (n,n'p) reaction calculated from the computed "first neutrons" distribution.

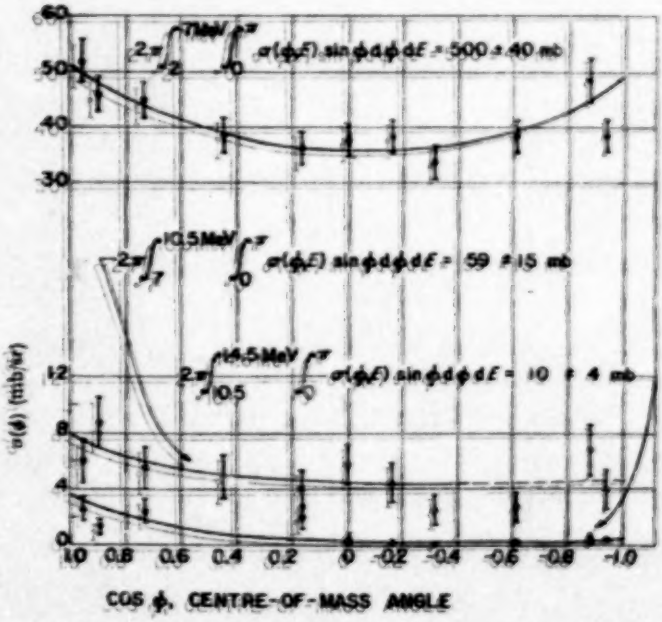

Fig. 4. Angular distributions of three energy groups of protons from the interaction of 14-MeV neutrons with Zn^{64}: 2–7 MeV, 7–10.5 MeV and 10.5–14.5 MeV.

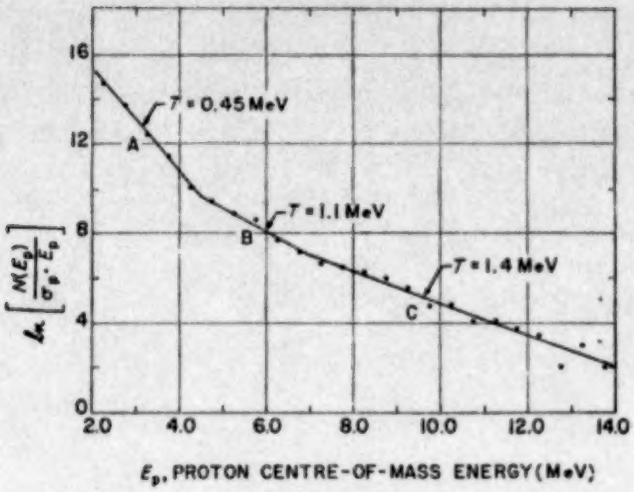

Fig. 5. Proton spectrum from the interaction of 14-MeV neutrons with Zn^{64}, corrected for barrier penetration.

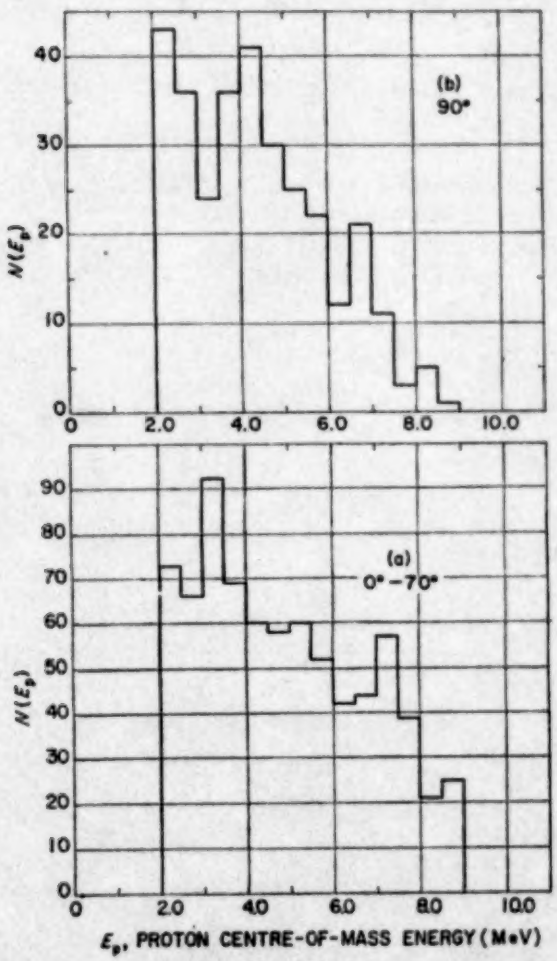

Fig. 6. Proton emission as a function of proton energy from the interaction of 8-MeV neutrons with Zn^{64}: (a) from 0°–70°; (b) at 90°, using apparatus illustrated in fig. 2.

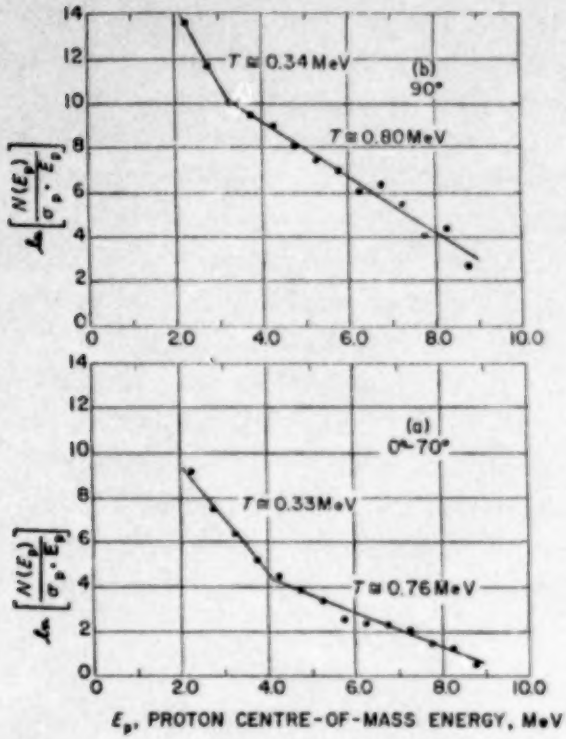

Fig. 7. Proton spectrum from the interaction of 8-MeV neutrons with Zn^{64}, corrected for barrier penetration: (a) from 0°–70°; (b) at 90°.

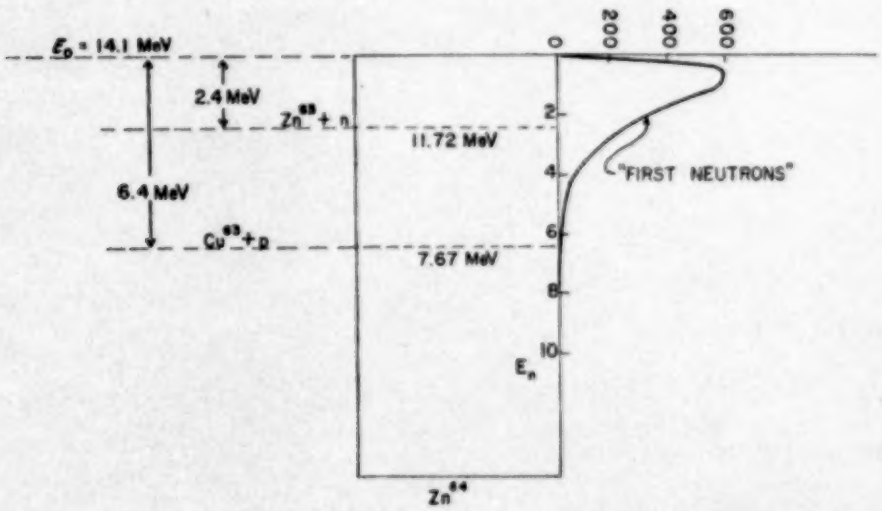

Fig. 8. Energy level diagram for Zn^{64} plus a 14-MeV neutron; with energy spectrum of "first neutrons" calculated on basis of statistical model with $T = 0.8$ MeV.

by Allan[10]), that region A comprises protons from the (n,n'p) reaction, we have calculated the expected energy spectrum of such protons. The results of our calculations are shown as the dashed curve in fig. 3. The assumptions made were the following: (a) the "first neutron" spectrum is represented by $N(E_n)dE_n = \text{const.}\ E_n\, e^{-E_n/T}\, dE_n$ with $T = 0.8$ MeV; (b) the proton spectrum is given by eq. (1) in which the maximum energy available to the proton is E_0 —

$E_n - Q$, where Q represents the binding energy of the last proton in Zn^{64}. σ_p values were taken from the tables of Shapiro[11]) assuming $R = 1.5 \times 10^{-13} A^{\frac{1}{3}}$ cm; (c) $T = \text{const.}\,(E_0 - E_0 - Q)^{\frac{1}{2}}$. The agreement between the shapes of the observed and calculated spectra in fig. 3 is seen to be excellent giving credence to the hypothesis that the low energy protons arise from evaporation of protons from Zn^{64} when its excitation, as a result of inelastic neutron scattering, is below the energy at which a second neutron can be emitted. The fact that the angular distribution of the low energy protons is symmetric about 90° (fig. 4) lends added weight to this interpretation. On the other hand, the large value of T associated with the high energy protons, together with their strong forward peaking, might logically be ascribed to the consequence of "direct interaction". From fig. 3 it may be deduced that the cross section for the Zn^{64}(n,n'p) process at 14 MeV is ≈ 370 mb, leaving a cross section of roughly 200 mb for the (n,p) reaction. If we make the logical assumption that the cross section for (n,n'x) processes is equal to the total non-elastic cross section for Zn^{65} less 200 mb, we arrive at an observed ratio

$$\frac{\sigma_{n,p}}{\sigma_{n,n'x}} = \frac{200\ \text{mb}}{1260\ \text{mb}} = 0.16 \qquad (2)$$

We now compute this ratio on the basis of the statistical model. We then have

$$\sigma_{n,p} = \sigma_n(14\ \text{MeV}) \frac{F_p}{F_p + F_n + F_\alpha + \ldots} \qquad (3)$$

and

$$\sigma_{n,n'x} = \sigma_n(14\ \text{MeV}) \frac{F_n}{F_p + F_n + F_\alpha + \ldots}, \qquad (4)$$

where $F_p, F_n, \ldots$, are proportional to the respective probabilities for emission of "first" particles indicated by the subscript. Since the Q for the Zn^{64}(n,p) reaction differs from zero by only 0.2 MeV,

$$\frac{F_p}{F_n} = \frac{\int_0^{14\ \text{MeV}} E_p \sigma_p(E_p)\, \omega_{Cu}(E_0 - E_p)\, dE_p}{\int_0^{14\ \text{MeV}} E_n \sigma_n(E_n)\, \omega_{Zn}(E_0 - E_n)\, dE_n}, \qquad (5)$$

in which ω_{Cu} and ω_{Zn} are the level densities of the residual nuclei Cu^{64} and Zn^{64}, as a function of excitation energy. If we now assume, still following the statistical model, that the energy dependence of ω_{Cu} is the same as ω_{Zn}, but that an odd-odd nucleus has 8 times the density of levels at any given excitation energy as an even-even nucleus, we compute a value for F_p/F_n which is consonant with the observed value. There exists, of course, the possibility that some of the observed particles are deuterons. It is argued, however, that they would not significantly affect our results, since the (n,d) reaction would be

characterized by strong forward peaking and since the region of small angles does not contribute much to the energy distribution as obtained in this experiment.

Our results at 14 MeV are characterized by the same features that have been observed by investigations[10]) of other elements in the same region of the periodic table and also agree with our preliminary results[12]).

We conclude that the greater part of the cross section for the non-elastic interaction of 14-MeV neutrons with Zn^{64} probably goes through a compound nucleus and is well described by the statistical model. This conclusion even applies to most of the reactions in which protons are emitted, especially when they are emitted following neutron emission. On the other hand, the anisotropies observed for the high energy protons not only violate the statistical assumption of random phases but are extremely difficult to reconcile with the compound nucleus hypothesis as well. It is, of course, possible to obtain asymmetries, within the framework of the compound nucleus assumption, if one postulates that relatively few levels are excited in the compound nucleus and that there is interference between various modes of decay from levels of different parity. However, we believe the above eventuality unlikely and, in harmony with other investigators[10, 13]), ascribe the high energy protons to direct interaction. The significant contribution from such reactions may be interpreted as implying that interactions between the nucleons in a compound system are not as strong as was originally thought to be the case. This would be in accord with the success of the "optical" representation of the nucleon-nucleus interaction in which the nucleus is pictured as a "cloudy crystal ball"[14]) which acts like a complex potential. This representation has been extremely successful in describing neutron cross sections at 1 to 3 MeV and both charged particle and neutron cross sections at higher energies. Also, the success of the shell model[15]) is explaining regularities in nuclear ground states might lead one to suspect that nuclear transparency is important in the energy region under consideration and that "direct" reactions involving only a small number of nucleons will be superimposed on the "evaporation" spectrum predicted by the statistical theory.

Austern, Butler and McManus[16]) have made extensive calculations on the assumption that the direct-interaction processes have their origin in surface interactions in which a particle is ejected directly from the surface of the target nucleus. However, if mean free paths for nucleons in nuclear matter are not much smaller than nuclear sizes, it may not be sufficient to confine the direct process to the nuclear surface. A number of theoretical investigations have been carried out on the degree to which the nuclear interior might be involved in such direct interactions[17]) but the conclusions drawn from the various calculations differ rather widely.

We turn now to a consideration of our 8-MeV results. The energy spectrum

of protons emitted between 0° and 70° is shown in fig. 6a, while fig. 6b displays the 90° spectrum. These data were treated in the same way as the corresponding data at 14 MeV, with the results shown in fig. 7a and 7b, respectively.

The 8-MeV data are difficult to explain for two reasons: the abundance of quite low-energy protons and the apparent group structures of the energy distributions. Nor is it possible, at this energy, to invoke the (n,np) process, as we did at 14 MeV. The only reasonable explanations that we can advance are based on: (a) the work of Kikuchi[18]) who calculated the effect of a diffuse nuclear boundary on the evaporation of protons and found it to be considerable; and (b) the demonstration by Németh[19]) that surface oscillations, in the compound nucleus, could account for the energy distribution of the protons emitted when Rhodium is irradiated by 13.2-MeV neutrons. Either or both of the above mechanisms would have the effect of reducing the Coulomb barrier, thus permitting evaporation of lower energy protons than would otherwise be possible. The phenomenon of surface oscillations, as proposed by Németh, has the additional features that it can give rise to anisotropic angular distributions and to multiple peaks in the energy distributions. Both of these features are quite in accord with the results of the present experiments.

The authors thank Dr. J. H. Coon and R. W. Davis for making available the 14-MeV neutron source, Dr. J. L. McKibben, R. A. Nobles and R. K. Smith for providing and operating the 8-MeV neutron source. They acknowledge also the plate analyses performed by the staff of the nuclear plate laboratory. They are indebted further to Mrs. Virginia Stovall and Mrs. Majorie Work, who carried out the earlier stages of the calculations, and especially to Mrs. Ferne Agee who took responsibility for completing the data analysis.

References

1) V. F. Weisskopf, Phys. Rev. **52** (1957) 295;
V. F. Weisskopf and D. H. Ewing, Phys. Rev. **57** (1940) 472;
J. M. Blatt and V. F. Weisskopf, Theoretical Nuclear Physics (John Wiley, New York, 1952) pp. 365–374;
J. M. B. Lang and K. J. LeCouteur, Proc. Phys. Soc. A **67** (1954) 586;
K. J. Le Couteur and D. W. Lang, Nuclear Physics **13** (1959) 32
2) P. C. Gugelot, Phys. Rev. **81** (1951) 51
3) E. R. Graves and L. Rosen, Phys. Rev. **89** (1953) 343
4) P. C. Gugelot, Phys. Rev. **93** (1954) 425;
B. L. Cohen and A. G. Rubin, Phys. Rev. **113** (1959) 579
5) S. N. Ghoshal, Phys. Rev. **80** (1950) 939;
W. John, Jr., Phys. Rev. **103** (1956) 704
6) L. Rosen and L. Stewart, Phys. Rev. **107** (1957) 824
7) H. A. Lackner, G. F. Dell and H. J. Hausman, Phys. Rev. **114** (1959) 560
8) E. B. Paul and R. L. Clarke, Canadian J. Phys. **31** (1953) 267
9) R. F. Coleman, B. E. Hawker, L. P. O'Connor and J. L. Perkin, AWRE-NR/P-10/58
10) D. L. Allan, Proc. Phys. Soc. A **68** (1955) 925;
L. Colli and U. Facchini, Nuovo Cimento **4** (1956) 671;

C. Badoni, L. Colli and U. Facchini, Nuovo Cimento **4** (1956) 1618;
L. Colli, U. Facchini and S. Micheletti, Nuovo Cimento **5** (1957) 502;
L. Colli, U. Facchini, I. Iori, G. Marcazzan and A. Sona, Proceedings of the Seond International Conference on Peaceful Uses of Atomic Energy (United Nations, New York, 1958) **14**, p. 147;
P. V. March and W. J. Morton, Phil. Mag. **3** (1958) 143;
P. L. Allan, Nuclear Physics **6** (1958) 464, **10** (1959) 348;
H. P. Eubank, R. A. Peck, Jr. and M. R. Zatzick, Nuclear Physics **10** (1959) 418

11) M. M. Shapiro, Phys. Rev. **90** (1953) 171
12) L. Rosen and A. H. Armstrong, Bull. Am. Phys. Soc. **1** (1956) 224
13) J. Terrell and D. Holm, Phys. Rev. **109** (1958) 2031
14) H. Feshbach, C. E. Porter and V. F. Weisskopf, Phys. Rev. **96** (1954) 448
15) M. G. Mayer and J. H. D. Jensen, Elementary Theory of Nuclear Shell Structure (John Wiley, New York, 1955)
16) N. Austern, S. T. Butler and H. McManus, Phys. Rev. **92** (1953) 350;
G. R. Satchler, Proc. Phys. Soc. A **68** (1955) 1037;
S. T. Butler, Phys. Rev. **106** (1957) 272;
G. Brown, G. C. Morrison, H. Muirhead and W. T. Morton, Phil. Mag. **2** (1957) 785
17) S. Hayakawa, M. Kawai and K. Kikuchi, Prog. Theoret. Phys. (Japan) **13** (1955) 415;
J. R. Lamarsh and H. Feshbach, Phys. Rev. **104** (1956) 1633;
G. Brown and H. Muirhead, Phil. Mag. **2** (1957) 473;
L. R. B. Elton and L. C. Gomes, Phys. Rev. **105** (1957) 1027
18) K. Kikuchi, Prog. Theoret. Phys. (Japan) **17** (1957) 643
19) J. Németh, Nuclear Physics **6** (1958) 686

2.A.1:
3.A

Nuclear Physics **19** (1960) 52—61; © *North-Holland Publishing Co., Amsterdam*
Not to be reproduced by photoprint or microfilm without written permission from the publisher

GAMMA RAYS FROM THE INTERACTION OF 14-MeV NEUTRONS WITH BERYLLIUM

J. BENVENISTE, A. C. MITCHELL, C. D. SCHRADER and J. H. ZENGER

Lawrence Radiation Laboratory, University of California, Livermore, California

Received 3 March 1960

Abstract: The cross section for the $Be^9(n,t')Li^{7*} \rightarrow Li^7 + \gamma$ (0.477 MeV) reaction has been measured in the vicinity of 14 MeV by detecting the gamma-rays at scattering angles from 30° to 150°. A time-of-flight technique was used to distinguish the gamma-rays from the high neutron background. The cross section drops from 20 mb at 13.6 MeV to 10 mb at 14.1 MeV and then rises to 30 mb at 14.7 MeV.

1. Introduction

A time-of flight technique has been employed for the study of gamma rays originating in the interaction of 14 MeV neutrons with various nuclei. We have previously used this technique to measure the spectral lines and angular distributions from several elements. (Some of this work was mentioned in a preliminary paper[1])). The present full report will be confined to our observations on Be for two reasons: (1) the simplicity of the gamma-ray spectrum, and (2) the relative ease of making calculations necessary to correct for contributions due to secondary processes. Previous efforts by others to detect gamma rays in the presence of high, continuous neutron fluxes have been hampered due to the discouragingly low signal-to-noise ratio. Through the use of short neutron bursts and a suitable flight path between the scatterer and the detector however, the difference in time of arrival between the gamma rays and any other reaction products can be easily distinguished. The system described below exploits this fact to reduce the background substantially. In brief, the spectrometer is gated on only during those intervals in which gamma rays are being received at the detector.

2. Description of Experiment

The accelerator used was a 500-keV Cockcroft-Walton machine. The deuteron beam emanating from the rf ion source was accelerated, then swept and bunched into pulses of 3 ns duration at a repetition rate of 5 MHz, which finally impinged on a titanium-tritium target producing 14-MeV neutrons through the reaction

$$D + T \rightarrow n + He^4 .$$

The reaction was monitored by counting the alpha particles in a gas pro-

portional counter mounted on the beam pipe. It detected alphas which were emitted at an angle of 174° with respect to the deuteron beam.

The gamma rays resulting from the interaction of the neutrons in the scattering ring placed near the tritium target were detected by a scintillation counter which was shielded on the sides by a 10 cm thick cylinder of lead. The scattering geometry is shown in fig. 1. In order to eliminate changes in pulse-height output due to temperature changes in the scintillator and photo-multiplier, the entire detector and lead shield were maintained at a temperature of 15° C, by cooling water from a portable refrigeration unit. A 28 cm long copper slug, suspended between the target and the detector, attenuated the direct flux of neutrons reaching the detector by a factor of 30.

The Be ring had an outside diameter of 33 cm, an inside diameter of 23 cm and a thickness of 5 cm. It was suspended from a cart on a track that was elevated enough above the target so that no unshielded path existed between the track and the detector. By remote control the ring could be moved so that the angle θ, between the incident neutron and the detected gamma ray, could be varied continuously between 30° and 150°. As a consequence of moving the ring with repect to the source, the energy of the incident neutrons also changed with angle over a range of about 1 MeV.

A block diagram of the detector-analyzer system is shown in fig. 2. The

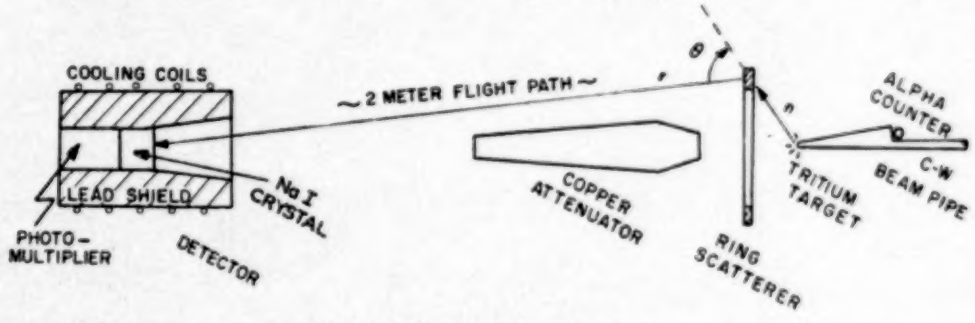

Fig. 1. Scattering geometry.

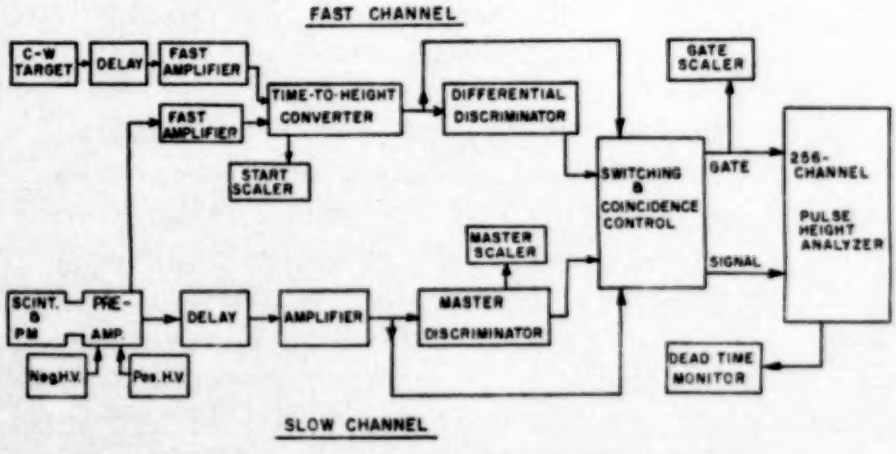

Fig. 2. Block diagram of detector electronics.

detector proper consisted of a 5.23-cm-long by 4.52-cm-diam. NaI(Tl) cylinder mounted on a 6810A RCA photomultiplier tube. Each signal from the photomultiplier was split into a fast signal (taken from the anode and clipped to a width of 50 ns) used in the gating system, and a slow signal (taken from the 9th dynode) which was analyzed. In order to isolate the fast signal from the slow, two high-voltage supplies were used. Negative voltage was applied across the first ten dynodes and positive voltage across the last four with the ground point at the tenth dynode.

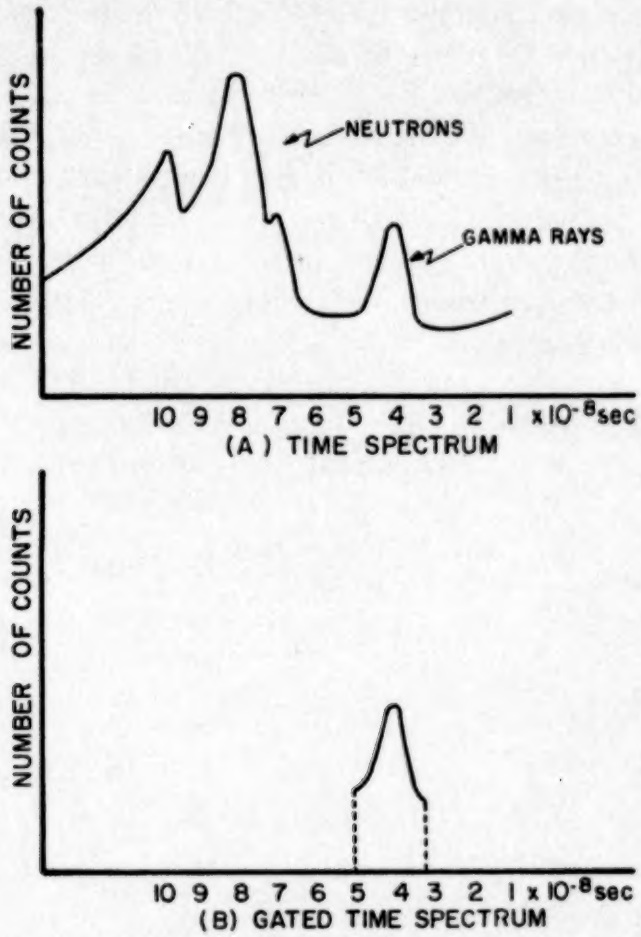
NUMBER OF COUNTS
NEUTRONS
GAMMA RAYS
10 9 8 7 6 5 4 3 2 1 x10⁻⁸sec
(A) TIME SPECTRUM
NUMBER OF COUNTS
10 9 8 7 6 5 4 3 2 1 x 10⁻⁸sec
(B) GATED TIME SPECTRUM

Fig. 3. Time and gated time spectra.

The fast signal, after amplification by Hewlett-Packard wide-band amplifiers, entered a modified Los Alamos type[2]) time-to-height converter as the "start" signal and triggered the discharge of a condenser. The zero-time Cockcroft-Walton target pulse was amplified and delayed and, upon entering the converter, served to stop the condenser discharge. This produced output pulses from the converter whose heights were proportional to the times of arrival of start pulses at the detector. By suitable use of the switching and coincidence control these output pulses could be analyzed and displayed on a 256-channel pulse-height analyzer. Such a "time spectrum" is shown in fig. 3(A). As seen in the figure

the difference between times of traversal of the approximately 2-meter flight path for the gamma rays and the elastically scattered 14-MeV neutrons was about 3.5×10^{-8} s. The converter output pulses could also be sent through a differential discriminator. When the output from the differential discriminator was used as a gate for the analyzer, the discriminator window could be visually set to bracket the gamma peak as shown in fig. 3(B). This was the procedure used to select the gate pulses which allowed the analyzer to accept the slow signal just during that interval of time when gammas were being detected. To insure good time resolution the high voltages were adjusted so that the fast pulses produced by the 60-keV gammas from an Am^{241} source were saturated. Thus all pulses originating from gammas which deposited more than this energy in the scintillator should certainly be saturated. The leading edges of such signals which trigger the condenser discharge in the time-to-height converter, would have nearly identical rise times. A start signal discriminator at the input to the converter was set just below the Am^{241} peak to eliminate lower energy pulses with consequently longer rise times. During the selection of the timing gate the output of the differential discriminator was required to be in coincidence with the output of a master discriminator in the slow channel in order to reduce contributions from electronic noise. The master discriminator was set at the same level as the input discriminator of the multichannel analyzer.

In order to insure time coincidence between the differential discriminator gate pulses and the slow-channel signal pulse arriving at the analyzer, delay was introduced in the slow channel until the 1-μs signal pulse was well centered within the 2-μs gate pulse. This provided enough overlap so that no signals were lost due to the small amount of jitter present.

Scalers at various points in the circuit enabled the counting of start, master and gate pulses. The analyzer also had a scaler output indicating the dead time within the analyzer. This, plus the information from the other scalers, was used to determine the total dead time of the detector-analyzer system.

3. Preliminary and Auxiliary Experiments

A number of preliminary and auxiliary experiments were performed which included the following:

1. *Photopeak Efficiency.* Measurements of the photopeak efficiency and the peak-to-total ratio as a function of energy for gamma-ray interactions in the shielded scintillator were made. The precision of these measurements at the energy of the Be gamma ray was $\pm$ 4%.

2. *Counting Rate.* A thorough test of all electronic components to determine any possible change in gain of the system with varying counting rate was performed. No noticeable change in gain occurred for counting rates below 17 kHz. The counting rates actually used, however, were kept below this maximum by

at least a factor of 4 so that the dead times in the time-to-height converter and the analyzer would be kept to reasonably low values.

3. *Alpha Counter Calibration.* If the D–T reaction is monitored by an alpha counter located at 90° with respect to the deuteron beam, the total neutron yield can be calculated from the number of observed alphas. It is very difficult, however, to calculate the neutron yield per 174°-alpha, since any errors in the input information to the calculations tend to become magnified at angles far from 90°. Therefore using a neutron detector as monitor, the number of alpha counts per neutron was measured for 90° and 174° assemblies separately. The ratio of these two numbers yields the 174° calibration constant in terms of the calculable 90° constant. Background in each counter (about 2% of the total counts), due mainly to the interaction of neutrons in the counter walls, was determined by introducing a shutter in front of the entrance window. The ratio of the counts in the two counters was determined to within 1%. A complete description of this calibration procedure has appeared before[3]).

4. *Angular Distribution of Neutrons from the Target.* An experimental measurement of the relative angular distribution of the neutrons from the target yielded the experimental points shown in fig. 4. The theoretical curve

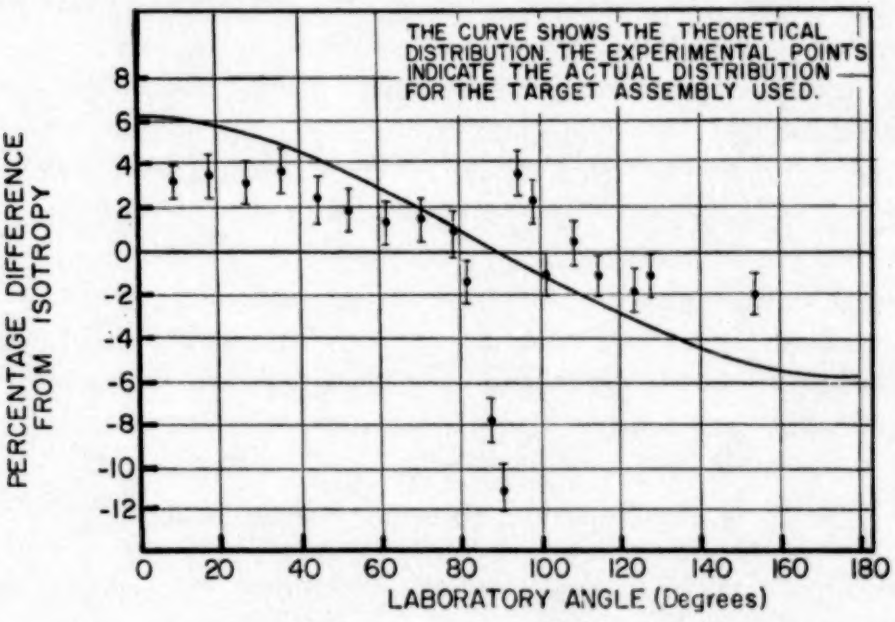

Fig. 4. Angular distribution of target neutrons.

is shown for comparison. Some of the features of the angular distribution may be understood as follows: (a) The observation that the anisotropy is less pronounced than that of the theoretical curve is due partly to the fact that in the forward direction neutrons must penetrate the target backing (0.51 mm of tungsten). (b) The large dip near 90° is due to absorption of neutrons going edgewise through the target backing. (c) The rise observed at about 90° is

due to the extra contribution of small-angle elastic scattering from the target disc.

5. *Geometrical Effects.* The possibility of target neutrons scattering from the Cu slug, and thus forming a secondary source of neutrons, was investigated. Although a difference of ½% between the number of neutrons received at a plastic scintillator located at various ring positions with the slug in and the number received with the slug out could have been detected, no effect was observed. Also, since it was inconvenient to remove the ring completely from its suspension in order to make background runs, it was moved to a position where it was essentially "out" both in time (signals would not arrive at the proper time to make a gate) and in space. In any event, the experimentally measured backgrounds with the ring in the out position and with the ring completely removed did not differ by more than ½%.

6. *Crystal Activity.* It was found that, if the neutron-induced activity in the NaI crystal (mainly from the 25-min I^{128}) were allowed to build up for at least 25 minutes before taking data, the small number of counts which by chance occurred at the proper time to produce a gate was constant and could easily be subtracted with the rest of the background.

7. *Energy Calibration.* An energy calibration of the entire system was made using various radioactive sources with gamma rays of known energy. After such calibration the energies of unknown gamma rays could be determined with a precision of 1%.

4. Procedure

Before every individual run all of the following routine checks were made: (a) The alpha spectrum was displayed on the multichannel analyzer, the gain was adjusted so that the alpha peak was located in a certain channel, and an integral discriminator was set on a "plateau" position. Observation of a similar spectrum after each run immediately showed any change in gain or discriminator setting. Any appreciable observed drift was cause for rejection of the run. (b) The gain of the entire detector-analyzer system was adjusted so that the photopeak of a Cs^{137} source occurred in a chosen channel of the analyzer. A check of the photopeak position immediately after a run showed whether any shift in gain had taken place. (The Cs^{137} source could be positioned in front of the counter, or removed, by remote control.) (c) The time spectrum was analyzed and the differential discriminator setting was examined for proper bracketing of the gamma peak.

The angular order of the runs was randomly staggered in order to expose any other possible change of conditions with time, since a monotonic change in angle coupled with a progressive change in some other parameter might result in a false asymmetry. Background runs were made every second angle run. Con-

sistency of the background data gave an additional check on the stability of the entire system since the background was expected to remain constant with time.

After a run was completed the information in the analyzer was printed out on paper tape, and the readings on the clock and the various scalers were recorded. A picture of the spectrum displayed on the analyzer was taken with a Polaroid Land camera for quick reference before the final data were plotted.

5. Treatment of the Data

Dead-time corrections were computed and applied to all raw data. The backgrounds were then subtracted and the corrected spectra were plotted. Base lines were then drawn under the peaks to separate each peak from the remainder of its spectrum. From drawing various reasonable base lines under the same peak it is estimated that a possible error of 7% could be introduced in the number of peak counts.

Monte Carlo calculations on an IBM 704 gave corrections for both multiple scattering of neutrons and self-absorption of gammas in the ring scatterer. The correction factors ranged from 1.25 at 30° to 1.15 at 150°. This variation with angle occurred because the energy of the incident neutrons was different at different angles and because the geometrical aspect which the ring presented to the neutron source changed with angle.

6. Results

An example of the gamma-ray spectra produced by 14-MeV neutrons on beryllium is shown in fig. 5. The simplicity of the spectrum may be understood from the following considerations: Of the energetically possible non-elastic neutron interactions, by far the major one is the (n,2n) process. (Ordinary inelastic scattering would leave Be^9 in a state unstable to neutron decay so that these events are just the prelude to (n,2n) processes.) Since the residual Be^8 is unstable to breakup into two alpha particles, for which no excited states have been observed, it is clear that this process yields no mechanism for the emission of gamma rays. The Be^9 (n,α) reaction could conceivably leave He^6 in one of the excited states at 1.71 and 3.35 MeV but these too are unstable to particle decay. And finally, the Be(n,t) reaction could leave Li^7 in the well-known 0.477-MeV level which would subsequently emit a gamma ray of this energy. In fact, the gamma ray from this reaction is the only one observed. The part of the spectrum above, and a portion of the spectrum below, the 0.477-MeV line are due to gammas from the C–W target which were Compton-scattered in the Be ring. This background has no bearing on the cross sections reported in this paper because only the peak counts were used.

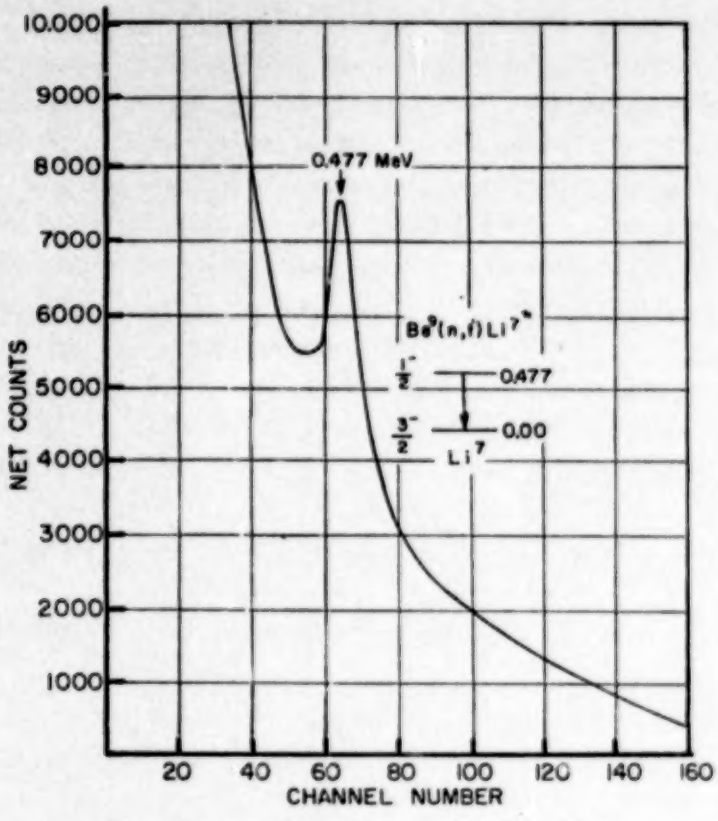

Fig. 5. Gamma-ray spectrum from beryllium.

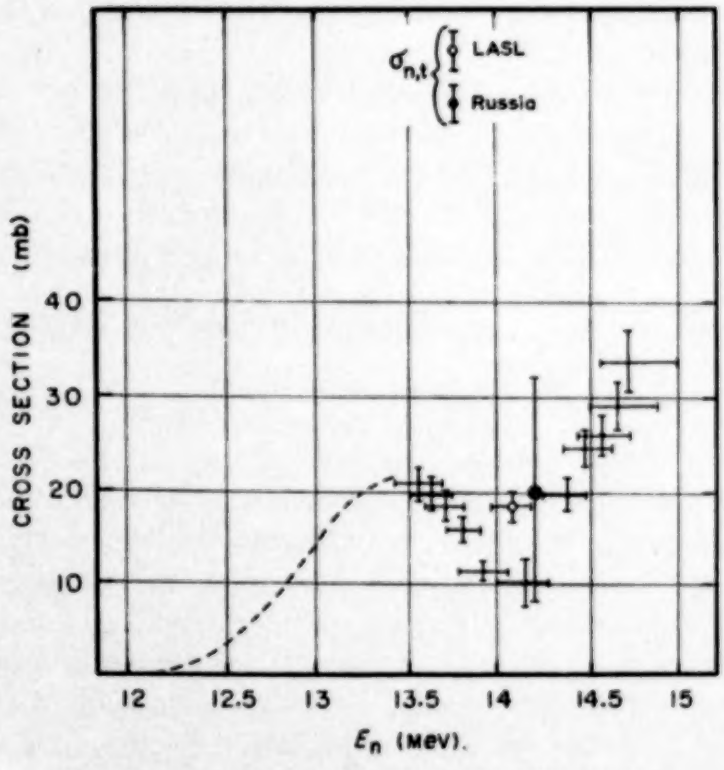

Fig. 6. Cross section for the $Be^9(n,t',\gamma)Li^{7*}$ reaction.

Since the spin of the 0.477-MeV state in Li^7 is $J=\frac{1}{2}$, the γ rays from this state must be isotropic[4]), and the apparent angular dependence observed in this case actually shows the energy dependence. Fig. 6 is obtained by multiplying each observed differential cross section by 4π and plotting the result versus incident neutron energy. The horizontal bars indicate the spread in incident neutron energy due to both the finite angle subtended by the scatterer at the source and the inherent energy spread[5]) of neutrons emitted at any particular angle. The vertical lines represent the uncertainty introduced into each measurement as determined by the root-mean-square of the following individual sources of error:

1. Statistics contributed between 6 and 25% to the probable error.
2. The calibration of the neutron source and its angular dependence introduced about 2%.
3. The penetrability calculations used in the Monte Carlo determination of the contribution of secondary events introduced 3–5% error.
4. The determination of our detector efficiency for 0.477-MeV gamma rays introduced another 4%.

The marked structure observed in this excitation curve is suggestive of resonances in the Be^{10} compound nucleus. The dotted portion of the curve has been drawn to indicate how one might expect the cross section to approach threshold, taking into account the barrier penetration. It is not clear whether the peak at 13.5 MeV represents a level in Be^{10} at about 10 MeV or whether it is a result of the barrier penetration factor acting on the tail of the known peak at the 18.43-MeV level.

Other results pertinent to this investigation have recently been reported from LASL[6]) and from Russia[7]). Although these two studies measured the total amount of tritium produced in the reaction (including transitions to the ground state as well as to the first excited state of Li^7), the data have been included in fig. 6 for ease of comparison. The data indicates that the branching ratio

$$n + Be^9 \rightarrow \frac{t' + Li^{7*}\,(0.477)}{t + Li^7\,(\text{gnd.})} \approx 1 .$$

It is a pleasure to acknowledge the invaluable contributions of Dr. Donald H. Davis to the analysis of the multiple scattering phenomenon. We would also like to express our gratitude to A. B. Williams who helped with much of the data analysis, to Vernon Ehlers who helped in the early phases of the work, and to the operating crew of the Cockcroft-Walton Accelerator under the capable guidance of Roy V. Cedarlund. Finally, we express our appreciation for mechanical engineering support from H. E. Brooks and his group, and for electronic support from L. E. Gibson of R. C. Kaifer's counting group, and from H. R. Buddingh and his maintenance group.

References

1) C. D. Schrader, J. Benveniste and J. H. Zenger, Bull. Am. Phys. Soc. **2** (1957) 309
2) W. Weber, C. W. Johnstone and L. Cranberg, Rev. Sci. Instr. **27** (1956) 165
3) J. Benveniste, A. C. Mitchell, C. D. Schrader and J. H. Zenger, UCRL-5619 (June 23, 1959)
4) F. Ajzenberg-Selove and T. Lauritsen, Nuclear Physics **11** (1959) 28
5) Jack Benveniste and Jerry Zenger, UCRL-4266 (Jan. 1954)
6) M. E. Wyman, E. M. Fryer and M. M. Thorpe, Phys. Rev. **112** (1958) 1264
7) S. S. Vasil' ev. V. V. Komarov, and A. M. Popova, JETP **33** (1957) 527 (English translation JETP **6** (1958) 411

4.C

Nuclear Physics **19** (1960) 62—67; © *North-Holland Publishing Co., Amsterdam*
Not to be reproduced by photoprint or microfilm without written permission from the publisher

β-γ CORRELATION OF THE 3^--2^+-0^+ CASCADE IN THE DECAY OF Eu^{152}

J. W. SUNIER, P. DEBRUNNER and P. SCHERRER

Department of Physics, Federal Institute of Technology, Zurich

Received 1 March 1960

Abstract: The $\beta - \gamma$ directional correlation of the $3^- - 2^+ - 0^+$ cascade in the decay of Eu^{152} has been measured as a function of beta particle energy. The anisotropy factor $\varepsilon(W)$ in the $\beta - \gamma$ directional correlation $N(W,\theta) = 1 + \varepsilon(W)\, P_2(\cos\theta)$ was fouhd to be $\varepsilon(3.5\ m_0c^2) = -0.46 \pm 0.02$ near maximum beta energy. The nuclear matrix elements involved in the observed beta transition have been computed from the measured values of $\varepsilon(W)$ and from the shape correction factor. The data imply that the relative contribution of the $\int B_{ij}$ matrix element is unusually large, as was expected on the basis of the large deviation from the allowed shape of the beta spectrum. The reduction of the matrix elements other than $\int B_{ij}$ can be caused by a selection rule effect.

1. Introduction

The theory of beta interaction has been greatly simplified by the experimental evidence that only V and A coupling exist[1]), with $C_A = C_A'$ and $C_V = C_V'$[2]).

A first forbidden non unique beta transition is characterized by the six nuclear matrix elements:

$$\int \sigma\cdot r\,,\ \int i\gamma_5\ (\lambda = 0);\ \int i\sigma \times r\,,\ \int i\alpha\,,\ \int r\ (\lambda = 1)\ ;\ \int B_{ij}\ (\lambda = 2)\,.$$

Experimental determination of these nuclear matrix elements is required for comparison with the predictions of nuclear models. Such a determination is somewhat facilitated in the case of a $\Delta I = 1$ beta transition, where only 4 matrix elements contribute. A measurement of the energy dependence of both the shape correction factor and the $\beta - \gamma$ directional correlation yields in general sufficient information for that purpose.

According to Kotani[3]) the $\beta - \gamma$ correlation is given by

$$N(W, \theta) = 1 + \varepsilon(W)\, P_2\,(\cos\theta)\,,$$

where

$$\varepsilon(W) = \frac{p^2}{W}\,(R_3 + eW)\,[C'(W)]^{-1}$$

and the shape correction factor can be expressed by

$$C(W) = kC'(W) = k\left(1 + aW + \frac{b}{W} + cW^2\right).$$

The coefficients R_3, e, a, b and c have been defined by Kotani[3]). For a $\Delta I = 1$ transition they depend on the parameters ηu, ηx, $\eta \xi' y$, ηz given by

$$\eta u = C_A \int i\sigma \times r \,,$$

$$\eta x = -C_V \int r \qquad (\lambda = 1) \,,$$

$$\eta \xi' y = -C_V \int i\alpha \,,$$

$$\eta z = C_A \int B_{ij} \qquad (\lambda = 2) \,,$$

where we assume the V, A interaction as the dominating one. For the computation we shall rather use, instead of $\xi' y$, the parameter $Y = \xi' y - \xi(u + x)$, where $\xi = \alpha Z/2\rho$.

From the experimental determination of the $\beta - \gamma$ directional correlation and the shape correction factor the coefficients R_3, e, a, b, c can be extracted, and the ratios of the nuclear matrix elements involved in the beta transition can be calculated.

2. Experimental Arrangement and Procedure

The present investigation is concerned with the β_1 transition ($3^- - 2^+$, $W_0 = 3.9\, m_0c^2$) in the decay of Eu^{152}, where a large log ft value and a deviation from the allowed shape had been observed. The directional correlation of the beta particle emitted in this transition with the succeeding γ-ray (344 keV) was measured as a function of the beta energy. Fig. 1 shows the decay scheme which has been proposed by Nathan and Hultberg[4]).

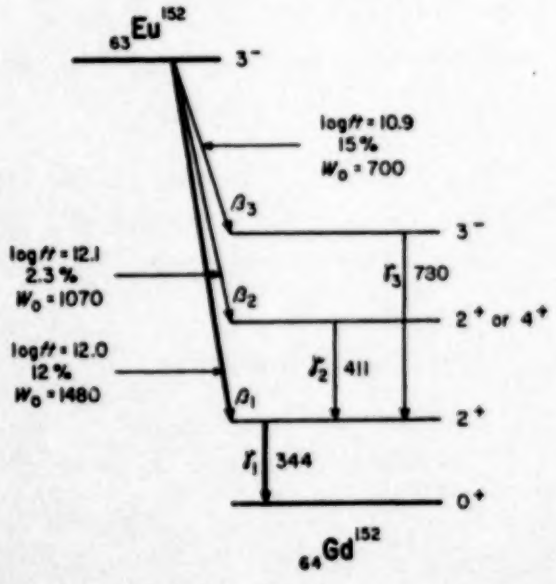

Fig. 1. Decay scheme of Eu^{152}.

The Eu^{152} source of high specific activity (90 c/g) was prepared by drying a drop of aqueous $EuCl_3$ solution on an aluminium foil of 0.8 mg/cm². The source was of rectangular shape (1 mm × 6 mm) and had a surface density of 8 μg/cm². It was mounted in the center of an aluminium vacuum chamber (wall thickness 0.5 mm) which is shown in fig. 2.

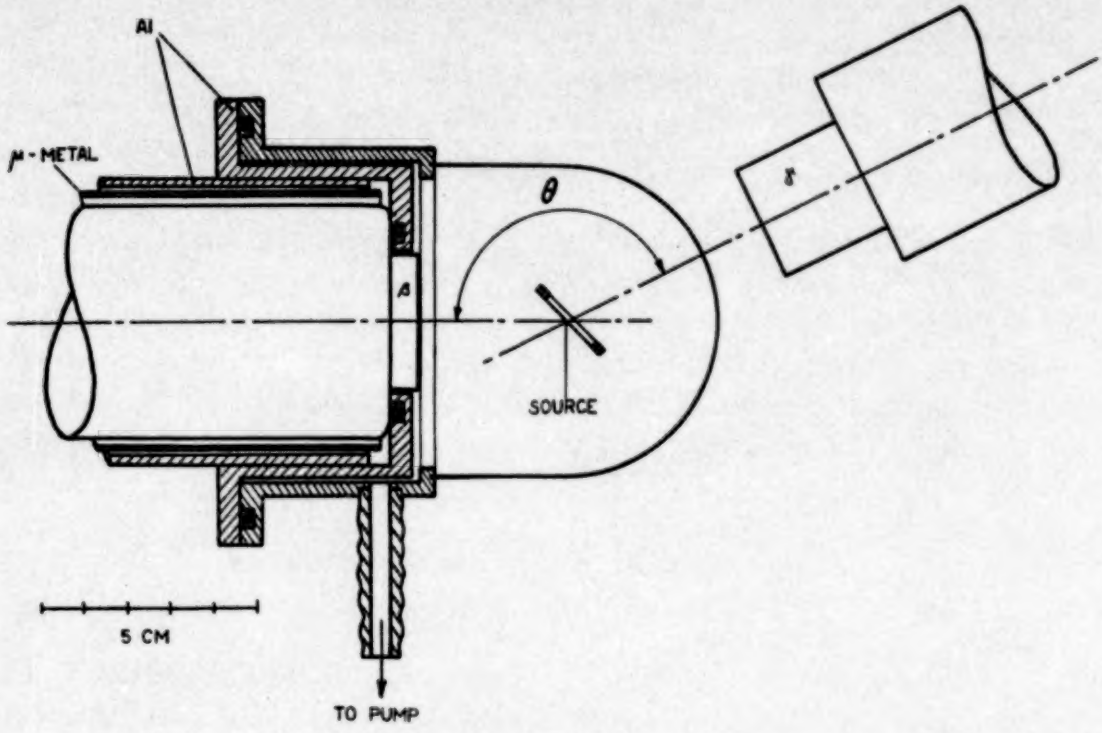

Fig. 2. Vacuum chamber and detectors.

The beta particles were detected by a plastic scintillator (Nuclear Enterprises NE 102) of 6.5 mm thickness covered by an evaporated aluminium film. Four single-channel analysers were used in parallel. The resolution of the 624 keV conversion line of Cs^{137} was 20%. The γ detector was a NaI(Tl) crystal of 2.5 cm × 2.5 cm.

The source was centered such that the counting rate deviation between the different positions of the movable detector (γ) was less than 1%.

The overall resolving time of the coincidence analyser was $2\tau_R = 4 \times 10^{-7}$ sec.

3. Results

The anisotropy

$$A(W) = \frac{CR(\pi) - CR(\frac{1}{2}\pi)}{CR(\frac{1}{2}\pi)},$$

where $CR(\theta)$ is the coincidence counting rate corrected for chance coincidences, was measured in steps of 100 keV from $E_\beta = 500$ keV to $E_\beta = 1400$ keV. For

each energy setting the weighted average $\bar{A}$ was computed. The consistency of the measurements was checked by the χ^2-test.

From $\bar{A}$ the values of $\varepsilon = 2\bar{A}/(3 + \bar{A})$ were computed taking into account the corrections for finite solid angles and for the finite size of the source.

For beta energies $E_\beta \leqq 1070$ keV an additional correction must be applied since the measured correlation contains admixtures of the cascades $\beta_2 - \gamma_2$ and $\beta_2 - (\gamma_2) - \gamma_1$. (Refer to fig. 1). It was assumed that the 756 keV level of Gd^{152} has spin $I = 2$ and that the ratios of the matrix elements of both beta transitions have the same order of magnitude. The errors have been increased correspondingly (fig. 3). No correction for the $\gamma_3 - \gamma_1$ and $\gamma_2 - \gamma_1$ directional

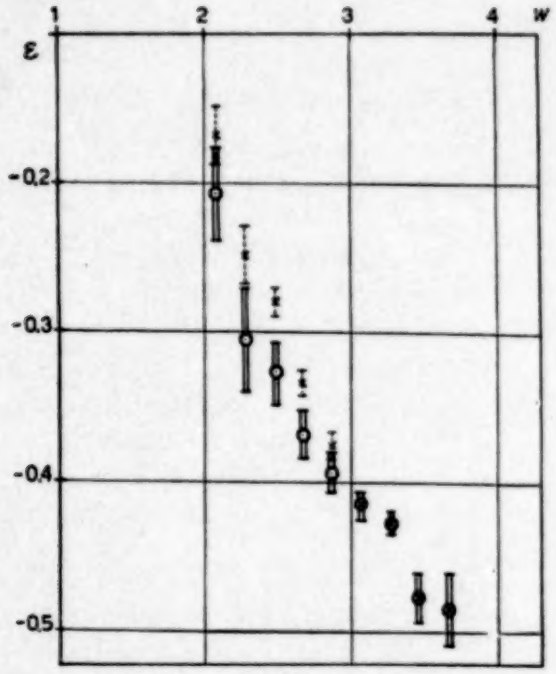

Fig. 3. The $\beta - \gamma$ directional correlation coefficient ε as a function of W (W in units of m_0c^2)
× Measured values without corrections for other cascades.
⊙ Measured values with corrections for other cascades.

correlations have been considered since the γ-efficiency of the β-crystal is negligibly small.

In order to test our experimental arrangement we have measured the $\beta_3 - \gamma_3$ correlation which should be isotropic. The measured value of the anisotropy $\bar{A} = -0.006 \pm 0.009$ confirmed that electron scattering in the vacuum chamber does not result in counting rate asymmetries.

4. Interpretation

Langer, Smith and Klein[5]) have measured the shape correction factor of the β_1 transition in the energy region $3.2\ m_0c^2 < W < 3.9\ m_0c^2$. The result is

$$C(W) = (W_0 - W)^2 + 0.791\,(W^2 - 1) + 5 \pm 2\,,$$

or

$$C(W) = \text{const.}\; C'(W) = (W_0^2 + 4.21 \pm 2)\left[1 - \frac{2W_0}{W_0^2 + 4.21 \pm 2}\,W + \frac{1.791}{W_0^2 + 4.21 \pm 2}\,W^2\right].$$

With their value of $C'(W)$ and our measurement of $\varepsilon(W)$, we have been able to compute the values of the parameters Y, x, u, z which are consistent with both measurements, using the theoretical expressions of Kotani[3]).

Taking $\eta = C_A \int B_{ij}$ as normalisation factor ($z = 1$) we find

$$Y = 0.68 \pm 0.12\,,$$

$$x = \frac{-\,C_V \int r}{C_A \int B_{ij}} = 0.14 \pm 0.06\,,$$

$$u = \frac{C_A \int i\sigma \times r}{C_A \int B_{ij}} = -\,0.015 \pm 0.015\,,$$

$$\xi' y = Y + (u + x)\xi = \frac{-\,C_V \int i\alpha}{C_A \int B_{ij}} = 2.18 \pm 1.02\,.$$

In fig. 4 the experimental values of $\varepsilon(W)$ and $C'(W)$ are compared with the calculated theoretical functions for the following values of z, Y, x, u:

$z = 1,\ Y = 0.68,\ x = 0.14,\ u = -\,0.015$ (curve a of fig. 4),

$z = 1,\ Y = 0.80,\ x = 0{,}20,\ u = \quad 0$ (curve b of fig. 4),

$z = 1,\ Y = 0.56,\ x = 0.08,\ u = -\,0.030$ (curve c of fig. 4).

The curves d' and d'' of fig. 4 represent the extreme values of $C'(W)$ consistent with the measurements of Langer *et al.*

According to Nathan and Hultberg[4]) the log *ft* value for the β_1 transition is 12.0. Taking into account the correction for the non-allowed shape of the β_1 spectrum, we can compute the absolute value of the normalisation matrix element $\eta = C_A \int B_{ij}$,

$$|\,\eta\,|^2 = \frac{\pi^3 \ln 2}{f_c t}\,.$$

Using the system of natural units $\hbar = m = c = 1$ (unit of time: $\hbar/m\,c^2 = 1.29 \times 10^{-21}$ sec and unit of length: $\lambda\!\!\!^{-}_c = \hbar/m\,c = 3.87 \times 10^{-11}$ cm), with the values of the coupling constants $C_V = 1.43 \times 10^{-49}$ erg cm^3 $= 3.0 \times 10^{-12}$ $\hbar^3/mc^2$ and $C_A = -\,1.2\,C_V$, we find

$$\left|\frac{\int B_{ij}}{R}\right| = (3.0 \pm 0.3) \times 10^{-3}\,,\quad \left|\frac{\int r}{R}\right| = (5.1 \pm 2.0) \times 10^{-4}\,,$$

$$\left|\frac{\int i\sigma \times r}{R}\right| = (0.45 \pm 0.45) \times 10^{-4}\,,\quad \left|\int i\alpha\right| = (1.3 \pm 0.6) \times 10^{-4}\,.$$

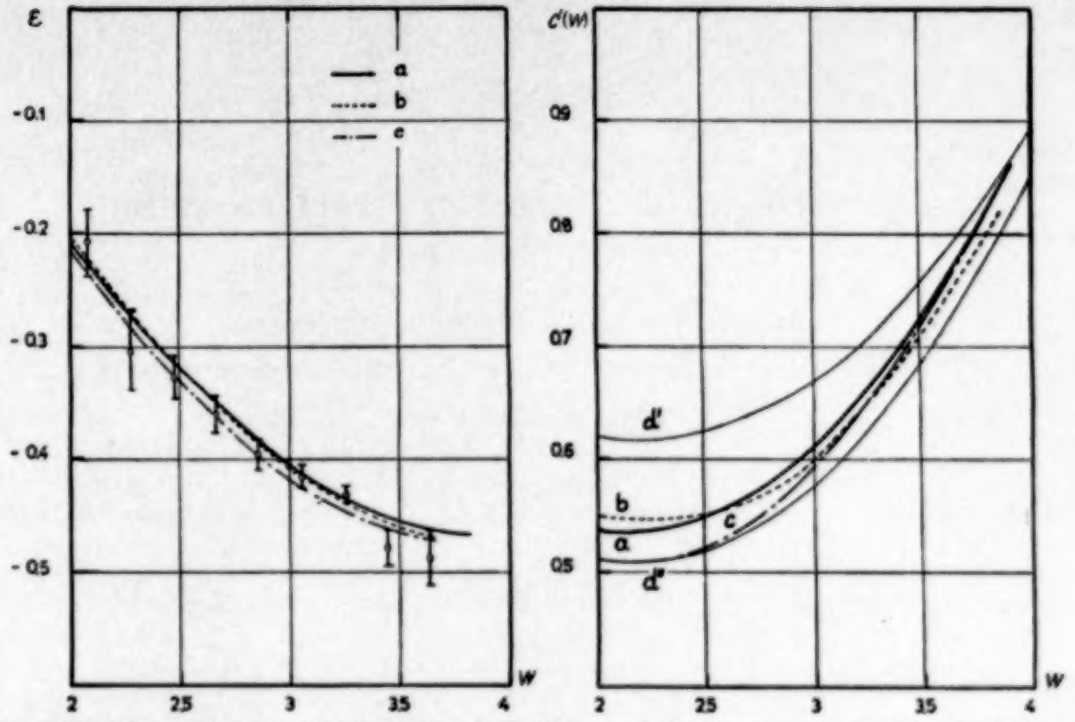

Fig. 4. The $\beta - \gamma$ directional correlation coefficient ε and the shape correction factor $C'(W)$ as a function of W (W in units of m_0c^2) for the three different sets of the nuclear parameters z, Y, x, u. The circles represent the experimental values of $\varepsilon(W)$. The curves d' and d'' represent the extreme values of $C'(W)$.

The $\int r$, $\int \sigma \times r$, $\int B_{ij}$ matrix elements have been normalised in terms of the nuclear radius $R = r_0 A^{\frac{1}{3}} = 3.1 \times 10^{-3} A^{\frac{1}{3}} \lambda_c$.

All the matrix elements are much smaller than those for a general first forbidden transition with $\log ft = 6$ to 7. The relative reduction is much less for the $\int B_{ij}$ matrix element than for the others. The data suggest that the dominance of the $\int B_{ij}$ matrix element is caused by a selection rule effect. This behaviour, however, cannot be assigned to K-forbiddenness, since the final nucleus Gd^{152} has a spherical shape so that the quantum number K cannot be defined.

Measurements of the circular polarisation of the $\beta_1 - \gamma_1$ cascade are in progress[6]).

We would like to express our sincere thanks to Professor R. M. Steffen and to Professor T. Kotani for stimulating discussions and for their interest in our measurements.

References

1) Herrmannsfeldt, Maxson, Stähelin and Allen, Phys. Rev. **107** (1957) 641;
Goldhaber, Grodzins and Sunyar, Phys. Rev. **109** (1958) 1015;
Burgy, Krohn, Novey, Ringo and Telegdi, Phys. Rev. **110** (1958) 1214
2) Wu, Ambler, Hayward, Hoppes and Hudson, Phys. Rev. **105** (1957) 1413
3) T. Kotani, Phys. Rev. **114** (1959) 795
4) O. Nathan and S. Hultberg, Nuclear Physics **10** (1959) 118
5) L. M. Langer, D. R. Smith and M. P. Klein, Bull. Am. Phys. Soc. **7** (1959) 426
6) J. Berthier and M. Lambert (to be published)

1.E.5:
7.B

Nuclear Physics 19 (1960) 68—78; © *North-Holland Publishing Co., Amsterdam*
Not to be reproduced by photoprint or microfilm without written permission from the publisher

AN EXPERIMENTAL SEARCH FOR DIPOLE STRUCTURE OF THE ELECTRON

GEORGE R. BURLESON and H. W. KENDALL

High-Energy Physics Laboratory, Stanford University, Stanford, California†

Received 16 March 1960

Abstract: By measuring absolute cross sections for the elastic scattering of electrons from the α particle, a determination of the quantity $\alpha(q) = [\lambda^2(q) + \mu^2(q)]^{\frac{1}{2}}$ has been found, where $\lambda(q)$ and $\mu(q)$ are structure form factors of an electric dipole moment and an anomalous magnetic dipole moment of the electron. They are functions of the four-momentum transfer q. The result is $\alpha(Q) = (9.3 \pm 6) \times 10^{-5}\ e\hbar/m_0c$, with an additional uncertainty of $\pm 7 \times 10^{-5}$ $(e\hbar/m_0c)$, for $Q \leqq 2.25 \times 10^{13}$ cm.

The experiment also determines the charge form factor of the α particle. The data correspond to the scattering from a Gaussian charge distribution having an rms radius of $(1.68 \pm 0.04) \times 10^{-13}$ cm.

1. Introduction

It has been shown[1-3]) that the existence of an electric dipole moment in any elementary particle would constitute a violation of space-reflection and time-reversal invariance in electrodynamics. Recent experiments[4]) on the formation and decay of positonium renewed interest in the possible existence of intrinsic electric dipole moments in the elementary particles. Experimental upper limits on the size of an electric dipole moment for the negaton[5-8]), the positon[6]), the proton[9]), the neutron[10]) and the muon[11]) have been found. A summary of these limits is given in ref. [8]), and a theoretical study of the implication of non-zero values of these moments has been published by Sachs[12]) and Sachs and Schwebel[13]).

The atomic effects that would result from the existence of an electronic electric dipole moment aligned parallel to the electron spin have been considered by Feinberg[5]) and Salpeter[6]). Measurements on the g-factor of the free electron by Pidd, Louisell and Crane[14]), and Schupp, Pidd and Crane[15]) have set an upper limit on the magnitude of an electronic electric dipole moment. These experiments were analyzed by Garwin and Lederman[7]) and by Nelson, Schupp, Pidd and Crane[8]). This limit is $\lambda \lessapprox 8 \times 10^{-5}$, where the dipole moment λ is expressed in units of $e\hbar/m_0c$. This limit is lower than those placed by the Lamb-shift experiments[5,6] and the absence of non-parity-conserving atomic transitions[6]).

† Supported by the Office of Naval Research, the U.S. Atomic Energy Commission and the Air Force Office of Scientific Research.

The elastic scattering of high-energy electrons from the α particle is sensitive to an electric dipole moment and to the charge and magnetic moment structure of the electron. As in the case of electron scattering from the proton[16-18]), the charge form factor of the electron cannot be separated from that of the α particle[19]).

The scattering of electrons having (a) an electric dipole moment or (b) an anomalous magnetic dipole moment can be distinguished by a characteristic alteration of the angular distribution of the scattered electrons from that predicted by the Mott scattering cross section. First Born approximation calculations have been completed by Margolis, Rosendorff and Sirlin[20]), who considered (a) and (b), and by Avakov and Ter-Martirosyan[19]), who considered (b).

The differential cross section for the elastic scattering of high-energy electrons having both an electric and an anomalous magnetic dipole moment from the α particle is given by

$$\sigma(\theta) = \sigma_{\mathrm{M}}(\theta) \mid F(q) \mid^2 \left[1 + \alpha^2(q) \left(\frac{\hbar q}{m_0 c}\right)^2 \frac{1}{\cos^2 \frac{1}{2}\theta}\right], \tag{1}$$

where q is the four-momentum transfer, $\sigma_{\mathrm{M}}(\theta)$ the Mott scattering cross section (including recoil), $F(q)$ the nuclear structure form factor, θ the angle of scattering in the laboratory and $\alpha^2(q) = \lambda^2(q) + \mu^2(q)$, where $\lambda(q)$ and $\mu(q)$ are the structure form factors of the electric and anomalous magnetic dipole moments measured in units $e\hbar/m_0 c$. It can be shown[21]) that no term linear in $\lambda(q)$ and $\mu(q)$ appears in eq. (1). The quantities $\lambda(q)$ and $\mu(q)$ are the strengths of the moments; they reduce to the static values as $q \to 0$.

The electron anomalous magnetic moment as observed in experiments with $q \approx 0$ arises from radiative corrections and has a spatial structure of characteristic length $\approx \hbar/m_0 c$ and a form factor which varies as[22]) $(m_0 c/\hbar q)^2 \ln(\hbar q/2m_0 c)^2$ for $\hbar q \gg m_0 c$; its effect is negligible for the momentum transfers involved in this experiment. The present experiment is sensitive to moment structure of much smaller size.

The explicit θ dependence of the term containing α may be used to determine limits on $\alpha(q)$ in the presence of the form factor $F(q)$. Define

$$R(q, \theta_1, \theta_2) \equiv \frac{\sigma(\theta_2)\,\sigma_{\mathrm{M}}(\theta_1)}{\sigma(\theta_1)\,\sigma_{\mathrm{M}}(\theta_2)} = \frac{1 + \alpha^2(q)\,(\hbar q/m_0 c)^2 \cos^{-2} \frac{1}{2}\theta_2}{1 + \alpha^2(q)\,(\hbar q/m_0 c)^2 \cos^{-2} \frac{1}{2}\theta_1}, \tag{2}$$

where the cross sections $\sigma(\theta_1)$ and $\sigma(\theta_2)$ are taken at a constant four-momentum transfer q. Let $R(q) = R(q, \theta_1, \theta_2)$, where $\theta_1 = 60°$ and $\theta_2 = 135°$. The quantity measured in this experiment is $R(q)$. The values of q involved range from 1.25 to 2.25 f^{-1}, where $f = 10^{-13}$ cm.

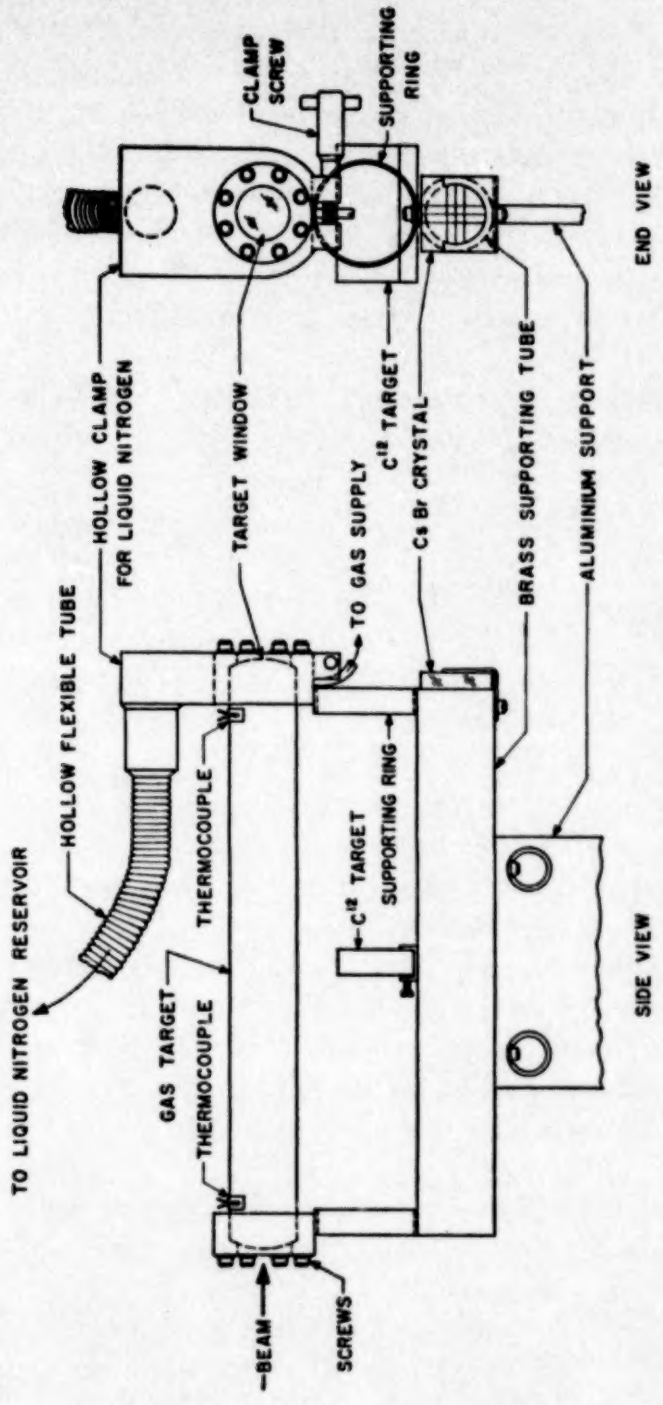

Fig. 1. Diagram of the target assembly. The pressure vessel, labeled "gas target", is 2.5 cm in diameter and 23 cm long. The figure is drawn to scale.

2. Experimental Procedure

Cooled, compressed helium gas was used as the target material. The pressure vessel was similar to one described before[16]). The walls of the vessel were of 0.051 cm thick stainless steel and the windows of 0.025 cm thick stainless steel. It was cooled by a hollow metal muffle fitted over one end which was supplied with liquid nitrogen from a reservoir. The vessel and the reservoir were thermally insulated by vacuum. The target temperature was monitored during data-taking by means of thermocouples placed at the ends of the vessel. A temperature differential of about 2–8° K was caused by the cooling method. The temperature of the gas was taken to be the average of the two temperatures. The variation in this average temperature was fairly large, from 102° K to 145° K, but the variation of temperature during a single run was usually only a few degrees. The gas pressure was monitored continuously during data taking and was maintained at 136 ($\pm$ 1 %) atm.

The target assembly consisted of the high-pressure gas target and two other targets mounted below the gas target on the same holder. Remote controls allowed any of the three targets to be moved to the electron beam line. The other targets were a C^{12} target 0.996 cm thick and a CsBr(Tl) scintillator which was used to observe the incident electron beam. A diagram of the target assembly is shown in fig. 1.

The target was placed in the momentum-analyzed beam of the Stanford Mark III linear accelerator, and the scattered electrons were analyzed by the 91 cm double-focusing magnetic spectrometer[16, 23]). The detector was a 10-channel array of counter telescopes[24]).

Absolute elastic cross sections[18]) were determined for each point by direct comparison with elastic scattering from hydrogen gas used in the same target assembly. In order to minimize errors caused by energy-dependent geometrical effects at the target and energy-dependent spectrometer transmission or detector efficiency, the primary electron energy was altered so as to keep the recoil electron energy the same as in the helium runs.

The uniform operation of the electronics was checked by taking data at the flattest part of the inelastic spectra of electrons scattered from the C^{12} target. Correction factors were computed from these data to correct for variations in the dectection efficiencies of the various channels.

Data from the helium and hydrogen runs were corrected, channel by channel, using these factors. Elastic peak measurements were interrupted at intervals of from 2 to 3 hours to allow a C^{12}-target calibration run.

By a comparison of the number of counts per channel per unit of integrated electron beam for the calibration runs, which spanned an absolute cross-section measurement, fluctuations in the detection efficiencies could be determined. Approximately 1000 events per channel per calibration run were ac-

cumulated, and the variation of the channel efficiencies was not outside what would be expected from statistical fluctuations in the number of detected events.

The elastic peaks were about 3 or 4 channels wide ($\Delta p/p$ was 0.003 for each channel), and consequently a run taken at a single setting of the spectrometer current gave a profile of the major part of a peak. In order to measure the low-energy tail of a peak, a second profile was always taken with the spectrometer current reduced. Occasionally more than two profiles of a curve were taken. A typical peak, corrected for channel efficiencies, is shown in fig. 2.

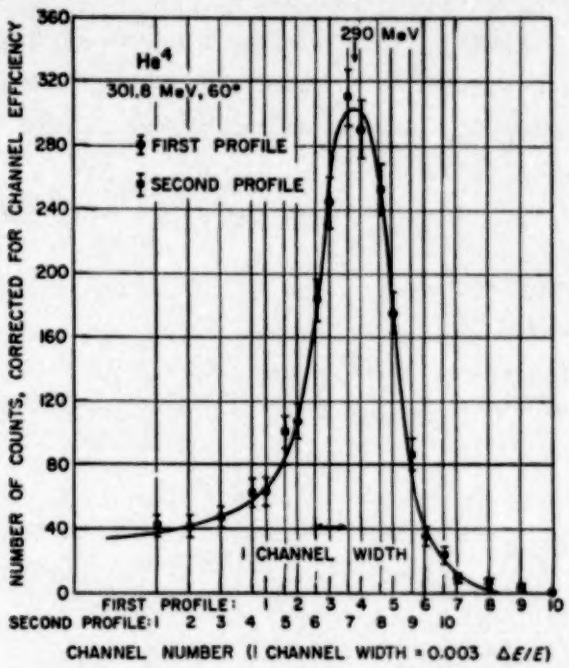

Fig. 2. The He^4 elastic peak found at 301.8 MeV, 60°. The number of counts detected in each channel, corrected for channel efficiency, is plotted as a function of channel number on the detector. The errors shown are standard deviations arising from counting statistics. Two partly overlapping profiles of the peak are shown.

Whenever possible, the He^4 peak and its normalizing proton peak were taken during the same machine run. If this was not possible, each peak was normalized to some hydrogen or helium elastic peak taken once during each of the two runs involved in the comparison.

3. Treatment of the Data

The total number of counts found in each elastic peak was determined by the following procedure: The number of counts recorded in each channel was corrected by dividing by the measured relative efficiency of the channel. A plot of the points was then made, and a curve profile was drawn. The curve was cut off seven channel widths below the point of maximum counting rate, which corresponds to a $\Delta p/p$ of 0.021. The peaks were integrated by summing the

counts for scattered electron energy greater than the cutoff. The curve was occasionally used to interpolate between measured values when two 10-channel profiles failed to be staggered properly.

Data from the elastic peak integrations were corrected for loss of events from electron bremsstrahlung in the target material and radiative effects during the scattering process. These corrections have been discussed previously[16]). In traversing the gas target assembly, an electron passed through approximately 0.06 radiation length of material. A typical correction factor for bremsstrahlung was about 1.40 and for radiation during the scattering process about 1.17. The corrections applied to a helium elastic peak and its associated proton peak differed in all cases by only a few percent.

The density of the gas enters directly into the calculation of the cross sections and also into the calculation of the radiation length the electrons traversed. The densities of helium and hydrogen gas at 136 atm as a function of temperature were calculated from virial coefficients taken from ref. [25]). As a check, the density of hydrogen gas at 100 atm as a function of temperature was calculated and compared with accurate density measurements made by the U.S. National Bureau of Standards[26]); the agreement was better than 1%.

A correction amounting to $\approx$ 1–2% for the energy variation of the efficiency of secondary-emission monitors[27]) was also applied to the data.

4. Results and Conclusions

The experimental values found for $R(q)$ at five values of q are shown in fig. 3 with their standard deviations. Table 1 presents the experimental cross sections found for He^4 at 135°, together with the incident beam energies used for the He^4

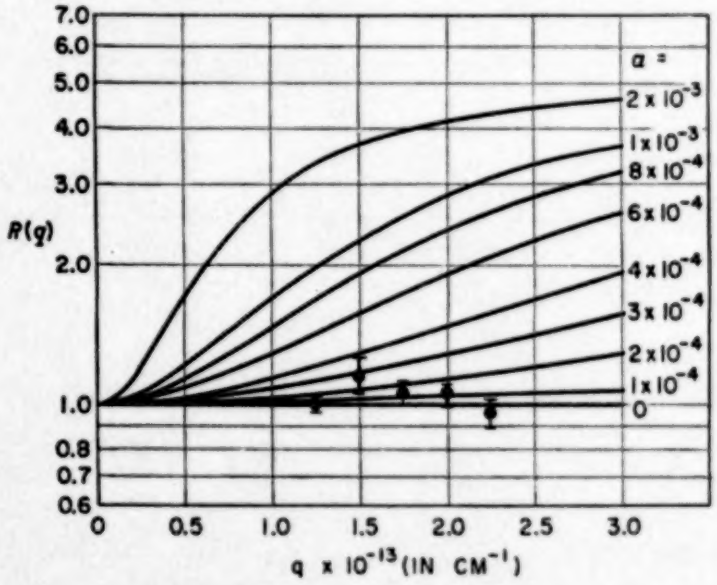

Fig. 3. The experimental values of $R(q)$. The errors shown are standard deviations. Theoretical curves of $R(q)$ for various constant values of $\alpha(q)$ are also shown.

and the normalizing hydrogen curves. Table 2 presents the same information for the 60° points, and table 3 presents the values of $\sigma(\theta)/\sigma_M(\theta)$ found at both angles and the resulting values of $R(q)$.

TABLE 1

The experimental He^4 cross sections found at 135°. The errors shown are standard deviations arising from counting statistics

q ($\times 10^{13}$cm^{-1})	Energy of He^4 peak (MeV)	Energy of proton peak (MeV)	$\sigma(135°)$ (cm^2/sr)
1.25	137.6	169	$(4.60 \pm 0.13) \times 10^{-32}$
1.50	166.1	215	$(2.05 \pm 0.06) \times 10^{-32}$
1.75	195.0	267	$(5.99 \pm 0.20) \times 10^{-33}$
2.00	224.2	325	$(1.88 \pm 0.03) \times 10^{-33}$
2.25	253.6	387	$(4.37 \pm 0.26) \times 10^{-34}$

TABLE 2

The experimental He^4 cross sections found at 60°. The errors shown are standard deviations arising from counting statistics

q ($\times 10^{13}$cm^{-1})	Energy of He^4 peak (MeV)	Energy of proton peak (MeV)	$\sigma(60°)$ (cm^2/sr)
1.25	250.6	281	$(8.55 \pm 0.24) \times 10^{-30}$
1.50	301.8	343	$(3.32 \pm 0.26) \times 10^{-30}$
1.75	353.2	410	$(1.05 \pm 0.03) \times 10^{-30}$
2.00	405.0	483	$(3.42 \pm 0.09) \times 10^{-31}$
2.25	457.1	559	$(8.95 \pm 0.32) \times 10^{-32}$

TABLE 3

The experimental values of $R(q)$. The errors shown are standard deviations arising from counting statistics

q ($\times 10^{13}$cm^{-1})	$\sigma(135°)/\sigma_M(135°)$	$\sigma(60°)/\sigma_M(60°)$	$R(q)$
1.25	$(2.22 \pm 0.07) \times 10^{-1}$	$(2.23 \pm 0.06) \times 10^{-1}$	0.995 ± 0.050
1.50	$(1.46 \pm 0.05) \times 10^{-1}$	$(1.08 \pm 0.09) \times 10^{-1}$	1.160 ± 0.104
1.75	$(5.83 \pm 0.19) \times 10^{-2}$	$(5.50 \pm 0.15) \times 10^{-2}$	1.060 ± 0.053
2.00	$(2.51 \pm 0.11) \times 10^{-2}$	$(2.38 \pm 0.06) \times 10^{-2}$	1.062 ± 0.063
2.25	$(7.52 \pm 0.45) \times 10^{-3}$	$(7.86 \pm 0.28) \times 10^{-3}$	0.956 ± 0.076

The standard deviations of the cross sections were computed from the total number of events in the elastic peaks. For the hydrogen curves these errors amounted to $\approx$ 2–3% and for the He^4 curves to $\approx$ 2–4%.

The error in setting the primary beam energy was about $\frac{1}{2}\%$, which corresponds to an error of about 1% in $\sigma(\theta)/\sigma_M(\theta)$ at the largest q values. Errors in densities of the gases and in the radiative corrections are difficult to estimate accurately, but the former is believed to be of the order of a few percent and the latter 1–2%. A sample of the helium gas used was mass-spectrometer analyzed and found to contain the following impurities, measured in percent by volume: H_2, 0.1%; H_2O, 0.1%; O_2, 0.04%; N_2, 0.25%; CO_2, $< 0.01\%$. An estimate of the scattering caused by the impurities indicated that the error introduced was less than 2%. The uncertainty in the absolute value of the proton cross sections, $\approx 8\%$ at the largest q value[18]), introduced additional error in the absolute cross-section measurements.

The data were analyzed by a series of χ^2 tests to determine the value of α corresponding to the minimum value of χ^2. This minimum value occurs for $\alpha = 9.3 \times 10^{-5}$, for which the Pearson probability P is 0.5. The value of α for which $P = 0.10$ is 18×10^{-5}, using the errors derived from statistical fluctuations only. The value of α determined in this experiment is

$$\alpha = (9.3 \pm 6) \times 10^{-5}\, e\hbar/m_0c,$$

where the error is estimated from the series of χ^2 tests, using the errors found from statistical fluctuations only. Additional uncertainties in α were estimated to be about 7×10^{-5} from other effects described above. In developing these results it was assumed that $\alpha(q)$ is independent of q for $q \leq 2.25\, f^{-1}$. This result is clearly consistent with $\alpha = 0$, and the following limit may be set:

$$\alpha(q) \leq 2 \times 10^{-4} \frac{e\hbar}{m_0c} \quad \text{for } q \leq 2.25\, f^{-1}.$$

The limits set on $\lambda(q)$ and $\mu(q)$ are separately the same as set on $\alpha(q)$. A non-zero value of α would not necessarily imply the existence of a non-parity-conserving interaction, for the experiment does not distinguish between the electric dipole scattering and the anomalous magnetic dipole scattering.

A failure of the first Born approximation would introduce corrections to the static nuclear scattering cross section which would, for virtual magnetic transitions, have an explicit angular dependence. Corrections to the charge scattering from virtual electric multipole transitions have been evaluated by Krall and Salpeter[28]). The maximum value of the corrections pertinent to the present experiment is $\approx 6\%$. The contributions from virtual magnetic transitions, including both spin and orbital currents, are being investigated by Goldberg[29]); he finds that corrections to the present experiment arising from spin currents are less than 1%.

We wish to point out that the experiment is sensitive to dipole moment distributions of approximate dimensions 0.5×10^{-13} cm or less. Thus the limit on α should not be compared directly with the limit found in the $q = 0$ experi-

ments, for, in analogy to the determination of the charge structure of the neutron by electron scattering[30]), dipole moment distributions can be constructed[31]) which are observable in the present experiment but unobservable in a low q measurement. We interpret the limitations on the size of the electron as determined here more conservatively than Avakov and Ter-Martirosyan[19]). Although the electron may well have[32]) structure extending to $0.5\,f$, the present experiment is sensitive only to that structure associated with an electric dipole moment or an anomalous magnetic moment not arising from the usual radiative corrections.

If it is assumed that there is no scattering due to either type of moment in the electron ($\alpha = 0$), the absolute values found for $\sigma(\theta)/\sigma_M(\theta)$ then define the

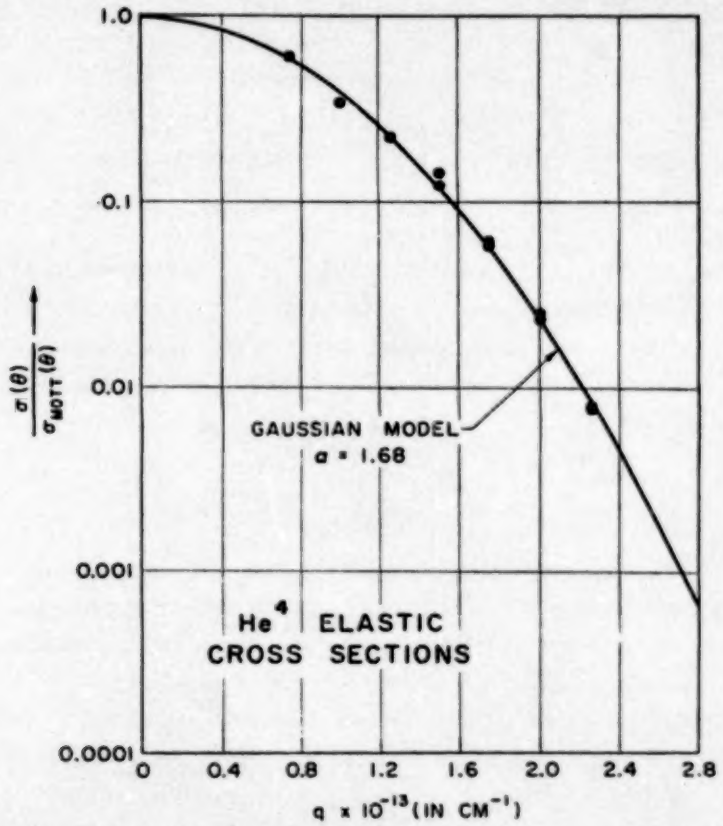

Fig. 4. The experimental values of $\sigma(\theta)/\sigma_M(\theta)$. The curve shown is the form factor for a Gaussian charge distribution with an rms radius of 1.68 f. The statistical errors are about as large as the points as they are shown.

function $F(q)$, the nuclear charge form factor for the α particle. A plot of these points as a function of q is given in fig. 4. Also shown are points taken at q values of 1.00 and $0.75\,f^{-1}$ at 45°, using the techniques described above. Table 4 presents the incident energies used and the experimental cross sections and values of $\sigma(\theta)/\sigma_M(\theta)$ found for these. The points can be fitted satisfactorily by

form factor curves corresponding to a Gaussian charge distribution having rms radii of $(1.68 \pm 0.04)\,f$; the curve drawn in fig. 4 is the form factor for a radius of $1.68\,f$. The analytical form of this charge distribution is

$$\rho(r) = \frac{3\sqrt{6}}{4\,\pi^{\frac{1}{2}}\,a^3} \exp\left(-\frac{3r^2}{2a^2}\right), \tag{3}$$

which corresponds to the form factor

$$F(q) = \exp\left(-\tfrac{1}{6}q^2a^2\right), \tag{4}$$

where a is the rms radius. This is the charge distribution predicted for the α particle by an independent particle model of the nucleus assuming an harmonic oscillator potential[17]). A previous measurement of elastic scattering from the α particle by Blankenbecler and Hofstadter[16]) gave the same analytic form for the charge distribution, but a different value for the rms radius ($a = 1.61\,f$) was reported. In view of the errors involved in these determinations, the agreement between the results can be considered satisfactory.

TABLE 4

The experimental He^4 cross sections found at 45°. The errors shown are standard deviations arising from counting statistics

q ($\times 10^{13}$cm^{-1})	Energy of He^4 peak (MeV)	Energy of proton peak (MeV)	$\sigma(45°)$ (cm^2/sr)	$\sigma(45°)/\sigma_M(45°)$
0.75	194.7	204	$(1.28 \pm 0.03) \times 10^{-28}$	0.627 ± 0.016
1.00	260.3	277	$(4.06 \pm 0.11) \times 10^{-29}$	0.341 ± 0.009

We wish to thank Dr. B. Margolis and Dr. K. A. Ter-Martirosyan for providing us with preprints of their articles. Discussions with Dr. S. D. Drell, Dr. J. D. Bjorken, Mr. C. N. Lindner, and Mr. A. Goldberg on the theoretical aspects of the experiment were very helpful. We also wish to thank Dr. J. I. Friedman for some calculations and several discussions. Finally, we acknowledge the help of Mr. C. N. Davey, Mr. W. C. Ewings, and the Hansen Laboratories Machine Shop under Mr. E. A. Wright in the design and construction of the target assembly, of Mr. M. Ryneveld in setting up the experimental apparatus, and of the accelerator crew under Dr. R. F. Mozley for the operation of the accelerator.

References

1) T. D. Lee and C. N. Yang, Brookhaven National Laboratory Report BNL-443 (1957) (unpublished)
2) Lee, Oehme and Yang, Phys. Rev. **106** (1957) 340
3) L. Landau, Nuclear Physics **3** (1957) 127

4) F. E. Obenshain and L. A. Page, Phys. Rev. **112** (1958) 179
5) G. Feinberg, Phys. Rev. **112** (1958) 1637)
6) E. E. Salpeter, Phys. Rev. **112** (1958) 1642
7) R. L. Garwin and L. M. Lederman, Nuovo Cimento **11** (1959) 776
8) Nelson, Schupp, Pidd and Crane, Phys. Rev. Letters **2** (1959) 492
9) R. M. Sternheimer, Phys. Rev. **113** (1959) 828
10) Smith, Purcell and Ramsey, Phys. Rev. **108** (1957) 120
11) Berley, Garwin, Gidal and Lederman, Phys. Rev. Letters **1** (1958) 144; D. Berley and G. Gidal, Phys. Rev. **118** (1960) 1086
12) M. Sachs, Annals Phys. **6** (1959) 244
13) M. Sachs and S. L. Schwebel, Annals Phys. **8** (1958) 475
14) R. W. Pidd, Bull. Am. Phys. Soc. **7** (1958) 364
15) Schupp, Pidd and Crane, Bull. Am. phys. Soc. **4** (1959) 250
16) R. Hofstadter, Revs. Modern Phys. **28** (1956) 214
17) R. Hofstadter, Ann. Rev. Nuc. Sci **7** (1957) 231
18) Hofstadter, Bumiller and Yearian, Revs. Modern Phys. **30** (1958) 482
19) G. V. Avakov and K. A. Ter-Martirosyan, Nuclear Physics **13** (1959) 685
20) Margolis, Rosendorff and Sirlin, Phys. Rev. **114** (1959) 1530
21) J. D. Bjorken, A. Goldberg and C. N. Lindner (private communication)
22) S. D. Drell and F. Zachariasen, Phys. Rev. **111** (1958) 1727
23) E. E. Chambers and R. Hofstadter, Phys. Rev. **105** (1956) 1454
24) H. W. Kendall, Trans. I.R.E. **5** (1958) 190
25) W. Wien, ed., Handbuch der Experimentalphysik (Akademische Verlagsgesellschaft, Leipzig 1929), vol. 7, part 2
26) J. Hilsenrath, Tables of thermal properties of gases, NBS Circular no. 564 (U.S. Government Printing Office, Washington, 1955)
27) F. Bumiller (private communication)
28) N. A. Krall and E. E. Salpeter, Phys. Rev. **115** (1959) 457
29) A. Goldberg (private communication)
30) L. I. Schiff, Revs. Modern Phys. **30** (1958) 462
31) S. D. Drell (private communication)
32) Katayama, Taketani and Leal Ferreira, Prog. Theoret. Phys. **21** (1959) 818

4.E *Nuclear Physics* **19** (1960) 79—84; © *North-Holland Publishing Co., Amsterdam*
Not to be reproduced by photoprint or microfilm without written permission from the publisher

THE 85 MINUTE ACTIVITY OF Ba^{139}

W. H. KELLY, G. B. BEARD, W. B. CHAFFEE†* and J. M. GONSER
Michigan State University, East Lansing, Michigan††

Received 20 February 1960

Abstract: The decay scheme of Ba^{139} has been studied using scintillation detectors. The half-life is found to be 85 ± 3 min. Beta-gamma and gamma-gamma coincidence measurements show this decay to consist of three beta groups of 2.38, 2.23 and 0.95 MeV, leading to the ground state and two excited states of La^{139}, the energies of the excited states being 0.167 ± 0.003 and 1.43 ± 0.05 MeV. Transitions from these two states are to the ground state. Branching ratios of 0.72, 0.26 and 0.02 were found for the 2.38, 2.23 and 0.95 MeV beta groups, respectively. Beta-gamma delayed coincidence measurements made on the 0.167 MeV state show the half-life of this state to be 1.7 ± 0.2 ns.

1. Introduction

The 85 minute activity of Ba^{139} has been studied by a number of investigators[1–4]) and a decay scheme proposed. According to this scheme there are three levels in La^{139} at energies 0, 0.163 and 1.43 MeV, populated by negaton groups of 2.38, 2.23 and 0.820 MeV with branching ratios of 15%, 66% and 19%, respectively. Both gamma transitions are to the ground state. Considering these energies, one would expect the 1.43 and 0.163 MeV gammas to be in coincidence. However, no gamma-gamma coincidences have been reported. The large branching to the 1.43 MeV state implies the 0.820 MeV beta is an allowed transition so that the 1.43 MeV state has a negative parity. Such a state is not expected in this mass region. The 66% branching of the 2.23 MeV beta is in disagreement with the value of 23% determined by Macklin *et al.*[5]) from neutron activation experiments. The experiments reported here were undertaken in an attempt to resolve these discrepancies. They included beta-gamma and gamma-gamma coincidence measurements using scintillation techniques.

2. Source Production

Several samples of "specpure" $BaCO_3$ and a sample of $BaCO_3$ isotopically enriched to 98.04% Ba^{138} were irradiated for periods of 2–3 hours in the

† Part of the work reported here will be used in a thesis for the M.S. degree by W.B.C.
* Permanent address: Bismark Junior College, Bismark, N.D.
†† Supported in part by the United States Air Force under contract AF49(638)-10 monitored by the Air Force Office of Scientific Research of the Air Research and Development Command.

University of Michigan Ford Nuclear Reactor. These sources were dissolved in dilute HCl to facilitate handling. Approximately 3 hours elapsed after each irradiation before the sources could be examined.

3. Measurements and Results

3.1. GAMMA RAY SPECTRUM

The gamma spectra of the sources made from "specpure" $BaCO_3$ were examined periodically with a 4.45 cm diameter × 5.1 cm NaI(Tl) crystal mounted on a DuMont 6292 photomultiplier. A 0.64 cm thick aluminium absorber was used to prevent the betas from entering the detector. These spectra were recorded with an RIDL 256-channel pulse-height analyzer. From the energies and half-lives, gammas due to the 11.6 day Ba^{131}, 39 h Ba^{133} and 29 h Ba^{135} activities were identified besides those of the desired Ba^{139}. In addition, three peaks of energies 0.850, 1.78 and 2.10 MeV were present and could not be attributed to any of the barium isotopes. These peaks were relatively weak and had the same half-lives (2½–3 h) within experimental error. Their energies, relative intensities and half-life are suggestive of a Mn^{56} contamination. The activity noted for this would correspond to 10^{-2}% manganese impurity which is below the limits of analysis of the sources†.

In addition to the above mentioned gamma rays there was a strong one at 167 ± 3 keV and a weak one at 1.43 ± 0.05 MeV. These were observed over a period of several hours to have half-lives of 85 ± 3 min and 90 ± 10 min, respectively. The measurement of the 1.43 MeV gamma has a large error associated with it because of its weak intensity and because of the presence of the higher energy gammas of comparable intensity. These two gammas are tentatively assigned to the Ba^{139} activity.

Gamma ray spectra obtained with the isotopically enriched source are shown in figs. 1 and 2. The peaks due to the Ba^{131}, Ba^{133} and Ba^{135} activities are greatly reduced from those seen with non-enriched sources. The sizes of the 0.850, 1.78 and 2.10 MeV peaks relative to those of the 0.167 and 1.43 MeV gammas are reduced by almost a factor of 2 for the enriched source, indicating these three peaks are due to an impurity. The ratios of the area of the 0.167 MeV peak to that of the 1.43 MeV peak are the same for the two sources to within experimental error. After correction for relative efficiencies[6,7]) the 0.167 MeV gamma is found to be 12 times more intense than the 1.43 MeV transition.

3.2. GAMMA-GAMMA COINCIDENCES

The first gamma-gamma coincidence measurement was carried out using two 3.8 cm diam. × 2.5 cm NaI(Tl) crystals mounted on DuMont 6292 photomultipliers and a conventional fast-slow coincidence circuit with a resolving

† The spectrographic analysis of the enriched Ba^{138} sample obtained from Oak Ridge National Laboratories gives a limit of detection of Mn as 0.04 %.

time of 0.05 μsec. The second experiment made use of a 12.7 cm diam. $\times$ 10.2 cm NaI(Tl) summing crystal with the source placed in a copper tube of 0.08 cm wall-thickness to help stop the betas. The summing crystal was used with the enriched source and the other arrangement with the unenriched sources. No coincidences between the 0.167 and 1.43 MeV gammas were observed.

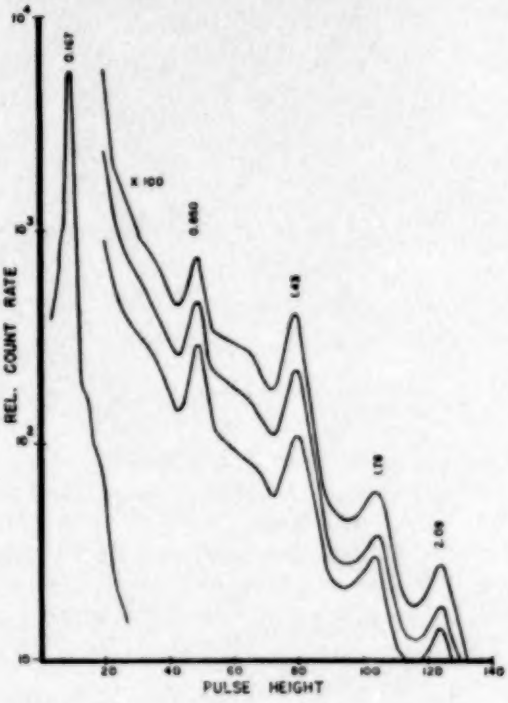

Fig. 1. High energy region of the Ba^{139} spectrum. These were taken for 5 minutes each at 202, 284 and 400 minutes after the source was removed from the reactor. The 0.167 MeV peak is shown only for the run at 202 minutes. These spectra have not been corrected for background.

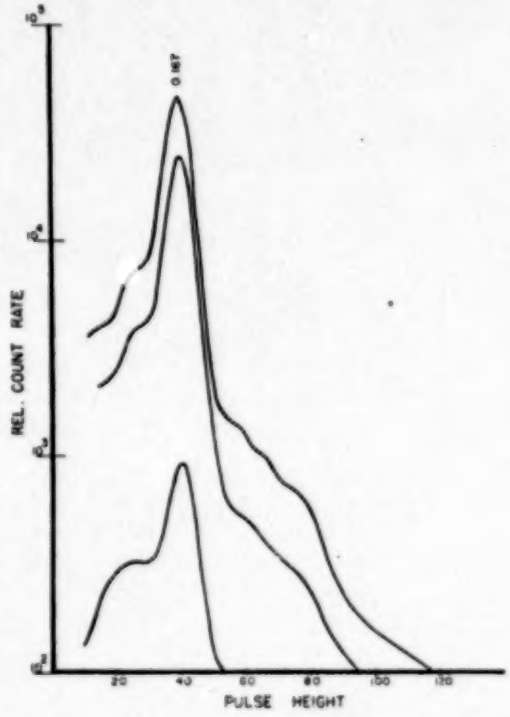

Fig. 2. Low energy region of the Ba^{139} spectrum. These spectra were taken for 1 minute each at 211, 303, and 720 min after source was removed from the reactor. These spectra have not been corrected for background.

3.3. BETA-GAMMA COINCIDENCE MEASUREMENTS

Beta-gamma coincidence experiments were performed to check on the above gamma ray assignments and to determine the branching ratios. Of the barium isotopes, only Ba^{139} decays by negaton emission. The suspected impurity Mn^{56} also decays by negaton emission. In the first beta-gamma experiment, performed with a non-enriched source, the beta detector was a 3.8 cm diam. $\times$ 0.2 cm NaI(Tl) crystal with a 0.013 cm thick beryllium window. The fast-slow coincidence circuit used for the gamma-gamma measurements was also used here. The beta detector was biased to accept betas above 175 keV. Coincidences were obtained between these betas and the 0.167, 0.850, 1.43, 1.78 and 2.10 MeV gammas.

Branching ratios to the excited states of La^{139} were determined by another

beta-gamma coincidence experiment. Here the source was sandwiched between two Pilot B plastic scintillators 4.45 cm diam. × 1.27 cm and the scintillations observed by two 6292 photomultipliers. The outputs of these were summed and

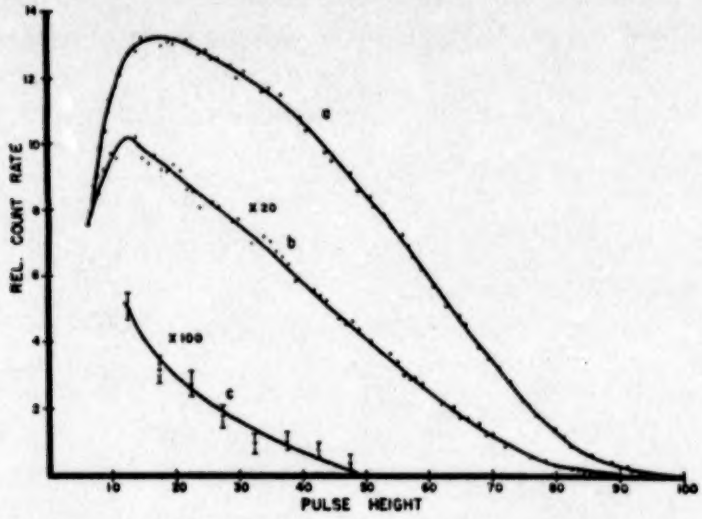

Fig. 3. Beta spectra of Ba^{139} taken with the source sandwiched between two 4.45 cm diam. × 1.27 cm Pilot B plastic scintillators. Curve a shows the singles spectrum obtained in a 1 min run. Curve b shows the betas in coincidence with the 0.167 MeV gamma obtained in a 30 min run. Curve c shows the betas in coincidence (corrected for accidental coincidences) with the 1.43 MeV gamma obtained in a 30 min run. Statistical counting errors are indicated on curve C. The data for curves a, b and c were taken 447, 452 and 514 min after the source was removed from the reactor.

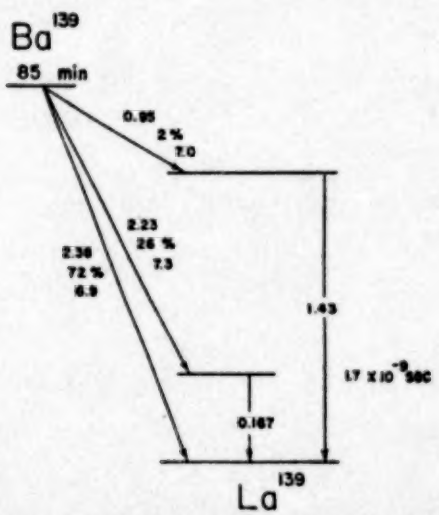

Fig. 4. Decay scheme of Ba^{139}. Energies are given in MeV. Log *ft* values are indicated.

displayed on the 256-channel analyzer. The 12.7 cm × 10.2 cm NaI(Tl) crystal used in the summing experiments was located about 15 cm from the centre of the above arrangement and was used as the gamma detector. Fig. 3 shows the spectra obtained for beta singles and the betas in coincidence with the 0.167 and 1.43 MeV gammas. The singles run was for 1 minute and the coincidence runs were for 30 minutes each. The coincidence spectra were corrected

for accidental coincidences. The counting rates obtained, adjusted for solid angles, efficiencies and an internal conversion coefficient[1,4,8,9]) of 0.21 for the 0.167 MeV gamma, give branching ratios of 72 ± 6%, 26 ± 6% and 2 ± ½% to the ground state, 0.167 and 1.43 MeV states, respectively. This experiment was performed with both enriched and non-enriched sources. The values obtained for the two sources agreed to within experimental error and the ratios listed are an average of the two. The branching to the 1.43 MeV state obtained here agrees with that obtained from the relative intensities of the gammas quoted in section 3.1. The response of the summing beta detector was not such as to permit accurate end point energies or spectral shape determinations. Therefore, no Kurie plots of the spectra were made.

Separate beta-gamma delayed coincidence measurements using Pilot B plastic scintillators and the above fast-slow coincidence circuit with 3 ns resolving time and also using a time-to-pulse-height converter[10]) gave an average half-life of 1.7 ± 0.2 ns for the 0.167 keV state. This is in agreement with the result reported by Gerholm and de Waard[11]).

4. Discussion of Results

The above results indicate that the decay scheme proposed by Mitchell and Hebb[1]) is essentially correct. Fig. 4 gives this decay scheme with the gamma energies and branching ratios found here. Since accurate beta energy determinations were not possible here, the values obtained by Mitchell and Hebb are given for the two high energy groups. The end point energy of 0.95 MeV for the weak, low energy group is the difference between the ground state beta transition and the high energy gamma transition. Log *ft* values for the 2.38, 2.23 and 0.95 MeV beta groups are 6.9, 7.3 and 7.0, respectively, indicating that all three are probably first forbidden and hence the three states in La^{139} excited by the beta decay of Ba^{139} have positive parity.

The internal conversion coefficient[1,4,8,9]) of the 0.167 MeV gamma and the fact this state is not Coulomb excited would seem to indicate this is predominantly an M1 transition. Since the lifetime obtained is approximately 400 times the Weisskopf single particle value, the transition is probably *l*-forbidden[13]) in agreement with the conclusion reached by the Nuclear Data Group[14]).

The authors wish to express their appreciation to Dr. C. W. Ricker and the staff of the University of Michigan Ford Nuclear Reactor for providing the irradiations. The loan of the 12.7 cm diam. × 10.2 cm NaI(Tl) summing crystal by Prof. M. L. Wiedenbeck of the University of Michigan is gratefully acknowledged. One of the authors (WBC) is grateful to the NSF for summer support in its Summer Institute for College Teachers of Science.

References

1) A. C. G. Mitchell and E. Hebb, Phys. Rev. **95** (1954) 727
2) H. J. Born and W. Seelman Eggebert, Naturwiss. **31** (1948) 201
3) L. R. Shepherd and J M. Hill, Nature **162** (1948) 566
4) R. H. Nussbaum and R. Van Lieshout, Physica **20** (1954) 440
5) R. L. Macklin, N. H. Lazar and W. S. Lyon, Phys. Rev. **107** (1957) 504
6) E. A. Wolicki, R. Jastrow and F. Brooks, U. S. Naval Research Laboratory Report 4833 (October 5, 1956)
7) M. J. Berger and J. Doggett, Rev. Sci. Instr. **27** (1956) 269
8) C. H. Pruett and R. G. Wilkinson, Phys. Rev. **96** (1954) 1340
9) B. H. Ketelle, H. Thomas and A. R. Brosi, Phys. Rev. **103** (1956) 190
10) W. Weber, C. W. Johnstone and L. Cranberg, Rev. Sci. Instr. **27** (1956) 166
11) T. R. Gerholm and H. de Waard, Physica **21** (1955) 601
12) N. P. Heydenburg, G. M. Temmer, Phys. Rev. **100** (1955) 150
13) H. de Waard and T. R. Gerholm, Nuclear Physics **1** (1956) 281
14) Nuclear Level Schemes, National Research Council, NRC-58-10-72 La^{139}-1

1.D.2 *Nuclear Physics* 19 (1960) 85—93; © *North-Holland Publishing Co., Amsterdam*
Not to be reproduced by photoprint or microfilm without written permission from the publisher

THEORY OF E0 TRANSITIONS OF SPHEROIDAL NUCLEI

JOHN O. RASMUSSEN

Lawrence Radiation Laboratory and Department of Chemistry, University of California, Berkeley, California†

Received 7 March 1960

Abstract: The nuclear matrix elements for E0 transition probabilities associated with beta-vibrational transitions of spheroidal nuclei are derived by two different models. The first model, previously studied by Peaslee and by Reiner, involves the volume-conserving quadrupole surface oscillations of a uniformly-charged spheroid about an equilibrium deformation of β. The second model sums over the coherent contributions of all the proton orbitals involved in an individual particle representation of the collective motion. The second model when corrected for volume-conservation gives about twice the ratio of E0 to E2 for Sm^{152} and Pu^{238} given by the first model. A brief comparison with experiment is made, showing satisfactory agreement for Pu^{238} and serious disagreement for Sm^{152}.

1. Introduction

In recent years Church and Weneser have given attention to the theory of internal conversion of orbital electrons by nuclear electric monopole transitions[1]). Reiner[2]) has also considered the theory in detail and has surveyed the experimental data. Striking cases of such transitions were found by Asaro and Perlman[3]) to be associated with the decay of excited 0+ states in deformed even nuclei, and Albridge and Hollander[4]) have assigned conversion electron lines in the decay of Np^{238} as 2 + to 2 + and 4 + to 4 + transitions. Reiner cites work on Sm^{152}, Gd^{154} and Th^{232} as also indicating E0 transitions. All the abovementioned experimental cases are classified as proceeding from the first excited beta-vibrational band to the ground band.

It is of interest first to consider the model of a uniformly charged spheroid undergoing quadrupole oscillations without change of volume. From the form of the E0 matrix element $\langle r^2 \rangle$ it can readily be appreciated that quadrupole surface oscillations about a spherical equilibrium shape have a vanishing E0 matrix element, since the excursion outward of some charge elements is always counterbalanced by inward motion of other charge. When the oscillation occurs about a deformed equilibrium shape, the cancellation is not complete and there is a certain collective contribution to the E0 matrix element. Peaslee carried out a calculation[5]) of the ratio of E0 to E2 transitions depopulating a 0+ beta vibrational state. Reiner has made the same calculation but in greater detail.

It is the purpose of this paper to repeat the vibrating spheroid derivation

† This work was done under the auspices of the U.S. Atomic Energy Commission.

with attention to some higher order terms of significance (sect. 2) and carry out a derivation in terms of single proton contributions in the asymptotic (anisotropic harmonic oscillator) representation (sect. 3). A serious failure of these models might give proof of and fundamental information on the involvement of compressional modes of oscillation.

2. Vibrating Spheroid Model

Church and Weneser give E0 transition rates in terms of a reduced transition probability ρ^2 defined as

$$\rho^2 = |\sum_p \varphi_f^* \left(\frac{r_p^2}{R^2} - \sigma\frac{r_p^4}{R^4} + \dots\right)\varphi_i \, d\tau|^2 , \tag{1}$$

where R is the nuclear radius, taken as $1.20 \times 10^{-13} A^{\frac{1}{3}}$ cm, and the summation is taken over all protons.

Let us consider a uniformly charged spheroidal nucleus of charge Z and surface defined by the equation

$$R(\theta) = R_0\left(1 + \alpha Y_{20}(\theta) - \frac{\alpha^2}{4\pi}\right). \tag{2}$$

The third term is included to make the nuclear volume independent of α to second order.

A nucleus in the spheroidally deformed region will have an energy minimum at some finite value of α, designated β. Let γ measure the excursion of the shape from its equilibrium value, i.e., $\beta + \gamma = \alpha$.

We take the usual convention for the Hamiltonian for vibrational motion as a harmonic oscillator

$$H_{coll} = \tfrac{1}{2}B|\dot{\gamma}|^2 + \tfrac{1}{2}C|\gamma|^2 .$$

With this definition the oscillator energy quantum is $\hbar\omega = \hbar(C/B)^{\frac{1}{2}}$. With this definition the matrix element of γ connecting the ground and first excited oscillator state is

$$\langle \gamma_{01} \rangle = (\tfrac{1}{2}\hbar)^{\frac{1}{2}} (BC)^{-\frac{1}{4}} . \tag{3}$$

To evaluate ρ^2 we note that the charge density is the atomic number Z divided by the volume and carry out the integration below:

$$\begin{aligned}\langle \sum_p r_p^2 \rangle &= \int_0^{\pi}\int_0^{2\pi} \sin\theta d\theta d\varphi \int_0^{R(\theta)} r^2 \left(\frac{Z}{\frac{4}{3}\pi R_0^3}\right) r^2 \, dr \\ &= \left(\frac{3ZR_0^2}{20\pi}\right)\int_0^{\pi}\int_0^{2\pi}\left(1 + \alpha Y_{20}(\theta) - \frac{\alpha^2}{4\pi}\right)^5 \sin\theta d\theta d\varphi \qquad (4) \\ &= \tfrac{3}{5}ZR_0^2\left(1 + \frac{5\alpha^2}{4\pi} + \dots\right),\end{aligned}$$

neglecting terms of higher power in α. Our result is $\frac{5}{7}$ that of Peaslee's[4]) and Reiner's[2]), since we included the second order volume-conserving term in the surface expansion in the numerator. Reiner discusses the question of the inclusion of this term and decides against it; we feel a true test of the volume-conserving oscillation model requires its inclusion as we have done. Substituting $\beta + \gamma$ for α we obtain for the linear term in γ, which is the only one connecting the nuclear states in question,

$$\langle \sum_p r_p^2 \rangle = \frac{3}{2\pi} Z R_0^2 \beta\gamma + \dots \tag{5}$$

From eqs. (3), (5) and (1) we have the result

$$\rho^2 = \frac{9}{8\pi^2} Z^2 \beta^2 \hbar (BC)^{-\frac{1}{2}} \left(\frac{R_0}{R}\right)^4. \tag{6}$$

We may well choose our R_0 the same as Church and Weneser's R, and the last factor will be unity. The contribution of the higher order term in eq. (1) can be similarly evaluated, and its effect can be expressed by an additional factor of $[1 - 2\sigma(R_0^2/R^2)]^2$ multiplying the right hand side of eq. (6).

The reduced E2 transition probability from the 0+ first beta-vibrational state to the 2+ state in the ground band is, according to eqs. (V.33) and (V.34) of Alder *et al.*[6]),

$$B(\mathrm{E2}; 0 \to 2) = \frac{9}{32\pi^2} Z^2 e^2 R_0^4 \hbar (BC)^{-\frac{1}{2}}. \tag{7}$$

We see from eqs. (6) and (7) that the dimensionless ratio

$$X = \frac{\rho^2 e^2 R_0^4}{B(\mathrm{E2}; 0 \to 2)}$$

is independent of B, C, R_0 and Z. Thus, the ratio of E0 to E2 depopulation may be compared with theory, even in the absence of knowledge of B and C. We have

$$X = 4\beta^2. \tag{8}$$

The quantity $(BC)^{-\frac{1}{2}}$ is essentially the zero-point amplitude of vibration. That the ratio in eq. (8) is independent of it simply means that the dependence of E0 and E2 transition probabilities on the vibration amplitude is the same.

3. Individual Particle Description

The model of the nucleus as a uniformly charged body undergoing quadrupole oscillations neglects many significant details in describing the motion of the nuclear charge. It would be preferable to describe the motion as a coherent superposition of individual excitations of the more easily polarizable protons

near the Fermi surface. For calculations of only the E2 to E0 ratios and not the absolute transition probabilities it is sufficient to evaluate only the relative weight of the various proton excitations making up the "vibrational" motion. We shall evaluate these weights by separating off one at a time each single proton in the quadrupole vibrational field provided by the other $A - 1$ nucleons. This approach bears a close analogy to formulation of rotational properties of nuclei in terms of single nucleon excitations[7]). The calculation of absolute transition probabilities by this model would raise many fundamental questions (regarding self-consistency, etc.) not easily answered, but we believe the calculation of the relative probabilities as outlined here is valid.

Bohr and Mottelson in their comprehensive paper[8]) in 1953 outlined a perturbation approximation as well as the widely-used strong coupling approximation for the coupling of individual particle and collective surface motions. The latter approximation has proved applicable in greater detail to a larger group of nuclei and in that sense has been more fruitful. We should like to apply here a hybrid of these approximations for treatment of the "vibrational excitations" of strongly deformed nuclei about their spheroidal equilibrium shape. The basis functions of the individual nucleons are to be chosen appropriate to the spheroidal well, and for simplicity we shall use harmonic oscillator functions separated in cylindrical coordinates z, ρ, φ. (The "asymptotic representation" of eqs. (4) and (6) of Alaga[9])). The wave functions are labelled by the familiar asymptotic quantum numbers N, n_z, Λ and Σ.

For description of the beta vibration the contribution of the $A - 1$ nucleons will be considered collectively via creation and destruction of phonons. The amplitude of each individual proton excitation in the wave function of the first excited vibrational state will be proportional, by perturbation theory, to a matrix element divided by an energy denominator $(\varepsilon'_p - \varepsilon_p - \hbar\omega + \Delta)$, where ε'_p and ε_p are upper and lower orbital energies for the excited proton in question, $\hbar\omega$ is the phonon quantum energy which is approximately the energy of the vibrational state, and Δ is a term to represent the energy loss in breaking a proton pair. The matrix element of interest is of the form of Bohr and Mottelson's[8]) eq. (II.12), but we consider for the interaction Hamiltonian H_{int} not a surface interaction as in their eq. (II.9) but a volume interaction appropriate to quadrupole motion of the harmonic oscillator potential well, i.e.

$$H_{\text{int}} = -M\omega_0^2 \gamma r^2 Y_{20}(\theta) , \tag{9}$$

where γ is as defined in section 2, M is the nucleon mass, ω_0 is related to the energy separation of major shells and may be taken, after Nilsson, as $\hbar\omega_0 \approx 41\, A^{-\frac{1}{3}}$ MeV[10]); r and θ are position coordinates of the proton in the well. In cylindrical coordinates we have

$$H_{\text{int}} = -M\omega_0^2 \gamma \sqrt{\frac{5}{4\pi}} (z^2 - \tfrac{1}{2}\rho^2) . \tag{9a}$$

The distance coordinates r, z, ρ are to be understood as having the dimensions of distance and are not the dimensionless parameters often introduced in harmonic oscillator calculations. It could be argued that H_{int} might better use a higher power of r than the square, if the interaction is predominantly on the surface.

The interaction (9a) involves a single particle operator which cannot change the projections Σ and Λ of the angular momenta. It does have off-diagonal elements in n_z and n_ρ, where n_ρ will be defined as twice the number of cylindrical nodes in the nucleon wave function and is identically equal to $N - n_z - \Lambda$ and can have only even integral values. The selection rules of H_{int} are $\Delta n_z = 0, \pm 2$ with $\Delta n_\rho = 0$; also $\Delta n_\rho = 0, \pm 2$ with $\Delta n_z = 0$. The matrix elements of z^2 for the one-dimensional harmonic oscillator and of ρ^2 for the two-dimensional case have been taken from a paper of W. H. Shaffer[11]) and are as follows:

$$\langle n_z \mid z^2 \mid n_z - 2 \rangle = \tfrac{1}{2}\hbar\,(M\omega_z)^{-1}\,[n_z(n_z-1)]^{\frac{1}{2}}, \tag{10a}$$

$$\langle n_\rho, \Lambda \mid \rho^2 \mid n_\rho - 2, \Lambda \rangle = -\tfrac{1}{2}\hbar\,(M\omega_\rho)^{-1}\,[n_\rho(n_\rho + 2\Lambda)]^{\frac{1}{2}}. \tag{10b}$$

Thus, the relative amplitude in the first beta-vibrational state of the proton excitation leaving two odd protons in orbitals of $\mid N, n_z, n_\rho\ \Lambda\rangle$ and $\mid N-2, n_z-2, n_\rho, \Lambda\rangle$ is as follows:

$$a_{\tau\tau'}(\Delta n_z = 2) \approx \frac{\langle H_{\text{int}}\rangle}{\Delta E} \approx -\frac{\omega_0^2}{8\omega_z^2}\left[\frac{5\hbar\, n_z(n_z-1)}{2\pi\,(BC)^{\frac{1}{2}}}\right]^{\frac{1}{2}}, \tag{11a}$$

where we have simplified the energy denominator by considering $\Delta \approx \hbar\omega$, a reasonable assumption, and that $\varepsilon'_p - \varepsilon_p \approx 2\hbar\omega_z$. Similarly, the amplitude in the excited vibrational state of the configuration with two odd protons in orbitals $\mid N, n_z, n_\rho, \Lambda\rangle$ and $\mid N, n_z, n_\rho - 2, \Lambda\rangle$ is

$$a_{\tau\tau'}(\Delta n_\rho = 2) \approx \frac{\omega_0^2}{16\omega_\rho^2}\left[\frac{5\hbar\, n_\rho\,(n_\rho + 2\Lambda)}{2\pi\,(BC)^{\frac{1}{2}}}\right]^{\frac{1}{2}}. \tag{11b}$$

We wish to calculate the ratio of E0 to E2 transition probability for this model, hence the ratio X of Church and Weneser's ρ^2 to the dimensionless quantity $B(\text{E2})/e^2R^4$, where R is the nuclear radius. The contribution to E0 of a particular proton excitation with orbitals specified by $\tau\tau'$ will be

$$a_{\tau\tau'}\left\langle \frac{r^2}{R^2}\right\rangle_{\tau\tau'} = \frac{a_{\tau\tau'}}{R^2}\langle z^2 + \rho^2\rangle_{\tau\tau'},$$

and its contribution to the corresponding E2 transition probability will be

$$\frac{a_{\tau\tau'}}{R^2}\langle r^2\, Y_{20}\rangle_{\tau\tau'} = \frac{a_{\tau\tau'}}{R^2}\sqrt{\frac{5}{4\pi}}\langle z^2 - \tfrac{1}{2}\rho^2\rangle_{\tau\tau'}.$$

The contributions of these components of the total wave function will add coherently, since they are coupled in phase to the collective shape oscillation

of the well. Contributions arise only from pairs of orbitals one of which is occupied and one unoccupied in the ground configuration. We have

$$X = \frac{4\pi}{5} \frac{\left| \sum_{\tau\tau'} \frac{n_z(n_z-1)}{\omega_z^3} \delta_{n_z,\, n_z'+2}\, \delta_{n_\rho,\, n_\rho'} - \frac{n_\rho(n_\rho+2\Lambda)}{2\omega_\rho^3} \delta_{n_z,\, n_z'}\, \delta_{n_\rho,\, n_\rho'+2} \right|^2}{\left| \sum_{\tau\tau'} \frac{n_z(n_z-1)}{\omega_z^3} \delta_{n_z,\, n_z'+2}\, \delta_{n_\rho,\, n_\rho'} + \frac{n_\rho(n_\rho+2\Lambda)}{4\omega_\rho^3} \delta_{n_z,\, n_z'}\, \delta_{n_\rho,\, n_\rho'+2} \right|^2}. \tag{12}$$

It can be verified that the numerator vanishes for summation over all transitions from a closed oscillator shell where $\omega_z = \omega_\rho$, the spherical limit. As one goes beyond the closed shell, filling successive levels in a spheroidal well, the numerator will increase in value but will again decrease as the next closed shell is approached.

In any practical example there will be a great number of terms in the summations in eq. (12). We have evaluated the expression numerically for Pu^{238} and Sm^{152}. In Pu^{238} we have taken the deformation parameter δ as 0.24, and have used the following equation from Nilsson[10]):

$$\frac{\omega_z}{\omega_\rho} = \sqrt{\frac{1-\frac{4}{3}\delta}{1+\frac{2}{3}\delta}}\,. \tag{13}$$

Taking the level schemes from Nilsson and Mottelson's figs. 3 and 5[7]), there are 3 occupied proton levels with $N = 6$ and 9 with $N = 5$. Lower shells are completely occupied. There are thus 6 terms between $N = 6$ and $N = 8$, and 18 terms between $N = 5$ and $N = 7$. There are 12 terms between the completely filled $N = 3$ and the partially unoccupied $N = 5$. There are 27 terms between $N = 4$ and $N = 6$. Using eq. (12) we calculate for Pu^{238} the ratio $X = 0.86$. Similarly we calculate for Sm^{152} at the same deformation the value $X = 0.98$.

These values are to be compared with a value of 0.23 from eq. (8) for the vibrating spheroid model. How is this considerable difference in predictions to be understood? It seems most likely that the protons in only slightly filled shells are contributing especially heavily to the E0 transition probability, because they lie predominantly in the tips of the nuclear well.

Some additional insight into this individual particle model is afforded by examining the contributions from a completely filled oscillator shell N to a completely empty shell $N + 2$. It can be shown in such a case that the numerator of eq. (12) vanishes when $\omega_z = \omega_\rho$, the case of no deformation. Thus, in terms of ω_z and ω_ρ,

$$X_{\text{closed shell}} = \frac{4\pi}{5} \frac{\left(\frac{1}{\omega_z^3} - \frac{1}{\omega_\rho^3}\right)^2}{\left(\frac{1}{\omega_z^3} + \frac{1}{2\omega_\rho^3}\right)^2}.$$

Substituting from eq. (13) and expanding for small δ in powers of δ we have to lowest order

$$X = \frac{16\pi}{5}\delta^2 + \ldots$$

Using from Nilsson[10]) the relation

$$\delta = \tfrac{3}{2}\sqrt{\frac{5}{4\pi}}\beta$$

we have

$$X = 9\beta^2 + \ldots \tag{14}$$

That this result is over twice that for the vibrating spheroid model in eq. (8) probably reflects the fact that the volume-conserving second order term was specifically included there and was not taken into account in the individual particle model here. It is possible to include the volume-conserving term in the derivation of eq. (12) by reducing the matrix elements of $\langle z^2 \rangle$ by the factor $[1 - (\beta/\sqrt{5\pi})]$ and increasing the matrix elements of $\langle \rho^2 \rangle$ by the factor $[1 + (2\beta/\sqrt{5\pi})]$. This alteration reduces the Pu^{238} calculation of X to 0.50 and the Sm^{152} value of X to 0.61. Thus, the individual particle model here predicts X values about twice that of eq. (8).

From a theoretical standpoint it certainly seems proper to introduce the higher order volume-conserving factors discussed above; at least the formulation is appropriate for testing what we set out to test, whether volume-conserving collective motion can explain the observed E0 to E2 ratios without explicitly involving compressional modes of vibration.

To the extent that the surface interaction has anharmonic terms such as $r^4 Y_{20}$ there will be an involvement of proton excitations within the same oscillator shell (i.e. via $\langle z^2\rho^2 \rangle$). These excitations will contribute to the second term of eq. (1) and further decrease the individual particle estimate of X. The matrix elements will be much smaller than the harmonic terms previously considered, but the energy denominators will be an order of magnitude smaller, being about equal to 2 $(\hbar\omega_\rho - \hbar\omega_z)$. The model also suffers from the use of pure cylindrical wave functions and the neglect of the pairing interaction, which blurs the Fermi surface. Corrections for the effects mentioned in this paragraph would probably not be very large but would be in the direction of further reducing the relative strength of the monopole transitions.

4. Comparison with Experiment

Only a preliminary comparison with experiment is appropriate here, since the experimental work is still largely unpublished and results are not in final form.

Asaro and Perlman[12]) have worked out the ratio of E0 to E2 deexcitation

of the 941 keV 0+ state in Pu^{238} and find the ratio 0.5 between K electrons (E0) to ground and E2 photons to the 44 keV 2+ state. Choosing $R_0 = 1.20\ A^{\frac{1}{3}} \times 10^{-13}$ cm the dimensionless ratio $X = \rho^2 e^2 R_0^4 / B(E2) = 0.14$.

Nathan[13]) has measured the similar ratio in Sm^{152} following electron capture of Eu^{152m} and finds the K/photon ratio from the 687 keV 0+ state to be 0.013. Recently Graham, Ewan and Geiger[14]) have beta spectrometrically resolved the E0 K line from a very near-lying line, finding the two lines to be of about equal intensity. Thus, the K/photon ratio of Nathan's report should be reduced a factor 2, to 0.0065, yielding the ratio $X = 0.016$.

Table 1 summarizes the results of this paper.

TABLE 1

Summary of theoretical and experimental reduced E0: E2 ratios X

Nucleus	Assumed deformation δ	Uniform spheroid model		Individual proton model		Experiment
		Without vol. conserv.	With vol. conserv.	Without vol. conserv.	With vol. conserv.	
Pu^{238}	0.24	0.32	0.23	0.86	0.50	0.14
Sm^{152}	0.24	0.32	0.23	0.98	0.61	0.016

The agreement of theory with experiment is satisfactory in the Pu^{238} case, and we may conclude that volume-conserving quadrupole surface oscillations are of predominant importance in the E0 transition here and that monopole compressional modes certainly must make a considerably lesser contribution.

The bad disagreement in the Sm^{152} case is not easy to explain. We note that Sm^{152} is on the very borderline of the region of strongly deformed nuclei, and the model may be breaking down in ways which would either depress the E0 transition or enhance the competing E2 transition. One such effect, capable of treatment, would enhance the E2 transition in the following way: The nuclear spheroid for the first excited state (2+) will be somewhat more distended than in the ground state by virtue of centrifugal effects (vibration-rotation interaction). In other words the vibration-rotation interaction causes configuration mixing between the 2+ state in the ground rotational band and the 2+ state in the beta-vibrational band. This mixing causes an enhancement of the E2 matrix element between the excited 0+ and the 2+ state of the ground band. Our preliminary estimates[15]) set this enhancement of the order of a factor of 5, not sufficient to explain the observed E0 to E2 ratio. This effect is quite small in Pu^{238} with its considerably larger moment of inertia. It will be of interest to Coulomb excitation considerations from ground to the β-vibrational band that this configuration-mixing effect depresses the E2 transition probability here below expectation from the simple vibrating spheroid formulas.

I am grateful to Drs. Perlman, Asaro, Nathan and Graham for communication of their unpublished results and to Dr Gaja Alaga for helpful discussions.

References

1) E. L. Church and J. Weneser, Phys. Rev. **103** (1956) 1035
2) A. S. Reiner, Structure Effects in the Interaction between Nuclei and Atomic Electrons (Thesis, University of Amsterdam, 1958), unpublished
3) F. Asaro, unpublished results given by Reiner in ref. [2])
4) R. G. Albridge and J. M. Hollander, The Decay of Neptunium-238, UCRL-8034 (1958), unpublished; also R. G. Albridge, Ph. D. Thesis (Univ. Calif., 1960)
5) D. C. Peaslee, Nuclear Monopole Matrix Elements, UCRL-3523 (1957) unpublished
6) Alder, Bohr, Huus, Mottelson and Winther, Revs. Mod. Phys. **28** (1956) 432
7) B. R. Mottelson and S. G. Nilsson, Mat. Fys. Skr. Dan. Vid. Selsk. **1**, No. 8 (1958); S. T. Belyaev, Mat. Fys. Medd. Dan. Vid. Selsk. **31**, No. 11 (1959)
8) A. Bohr and B. R. Mottelson, Mat. Fys. Medd. Dan. Vid. Selsk. **27**, No. 16 (1953)
9) G. Alaga, Nuclear Physics **4** (1957) 625
10) S. G. Nilsson, Mat. Fys. Medd. Dan. Vid. Selsk. **29**, No. 16 (1955)
11) W. H. Shaffer, Revs. Mod. Phys. **16** (1944) 245
12) F. Asaro and I. Perlman, to be published
13) O. Nathan, private communication (1959)
14) R. L. Graham, G. T. Ewan and J. S. Geiger, private communication (1959)
15) L. Person and J. O. Rasmussen, unpublished results

1.D.2:
2.I

Nuclear Physics **19** (1960) 94—100; © *North-Holland Publishing Co., Amsterdam*
Not to be reproduced by photoprint or microfilm without written permission from the publisher

THE $Mg^{24}(\gamma, n)Mg^{23}$ REACTION

J. D. KING† and W. J. McDONALD

Department of Physics, University of Saskatchewan, Saskatoon, Saskatchewan

Received 15 February 1960

Abstract: The $Mg^{24}(\gamma, n)Mg^{23}$ reaction has been studied by irradiating a magnesium sample in the X-ray beam of a 25 MeV betatron and measuring the Mg^{23} positon decay by coincidence detection of the annihilation radiation. The cross section has a small peak at 17.2 MeV with the giant resonance appearing at 19.2 MeV; there is a pronounced high energy tail. These results are compared with recent investigations of the $Na^{23}(p,\gamma)Mg^{24}$ inverse photonuclear reaction. Both cross sections show a small peak below the giant resonance region. An attempt is made to interpret the cross section shapes in terms of the deformation of the Mg^{24} nucleus, but the results are inconclusive.

1. Introduction

Spicer[1]) has pointed out that the splitting of the photonuclear giant resonance predicted by Danos[2]) and Okamoto[3]) should be readily observable in the region of mass 25. The collective model of the nucleus has been applied successfully to many nuclei in this mass region[4-7]). Recent data indicate a rotational character for the excited states of Mg^{24} [4,7,8]). Thus, the Danos-Okamoto theory, which is based on a strong interaction model of the nucleus, should be applicable to Mg^{24}.

The intrinsic quadrupole moment Q_0 of Mg^{24} has been reported by Rakavy[4]) to be 0.66×10^{-24} cm², by Deliagin and Shpinel[9]) to be 0.7×10^{-24} cm², and by Gugelot and Rickey[10]) to be 0.45×10^{-24} cm². These results lead to a value of approximately 1.6 for the ratio a/b of the half-axes of the spheroidal nucleus. If the Mg^{24} nucleus is actually so deformed, the low energy component of the giant resonance, on the Danos model, would be below the (γ,n) threshold which is at 16.6 MeV, assuming the high energy component to be at 19.5 MeV[11,12]). In this case, only the higher energy resonance would be observed, although the behaviour of the (γ,n) cross section near threshold might provide some information as to the characteristics of the photon absorption cross section at energies below the (γ,n) threshold.

The $Mg^{24}(\gamma,n)Mg^{23}$ reaction has been studied by Katz and Cameron[11]) who detected the 12 second Mg^{23} activity, and by Nathans and Yergin[12]) who detected the neutrons emitted from a sample of MgO enriched to 99.59% Mg^{24}. The presence of oxygen in the sample prevented an accurate measurement of

† Present address: Physics Department, McMaster University, Hamilton, Ontario, Canada.

the (γ,n) cross section shape for Mg^{24} in the latter experiment. The residual activity experiment[11]) was complicated by the presence of 60 second Na^{25} originating from a (γ,p) reaction in Mg^{26} and by the high betatron room background. In the present work the Mg^{23} positon activity is measured by coincidence detection of the 0.511 MeV radiation emitted by positons annihilating in the sample.

2. Experimental Procedure

The annihilation radiation was detected by two 5.1 cm × 5.1 cm NaI crystals integrally mounted on RCA 5819 photomultiplier tubes. Pulses from the phototubes were amplified by non-overloading amplifiers. The output from one amplifier was applied to a transistorized 100-channel pulse-height analyser and counted in coincidence with the output from the second amplifier.

Because of the high neutron flux during irradiation, the NaI crystals had to be shielded from neutrons as well as from X-rays. The experimental arrangement is shown in fig. 1. The crystals were contained inside a 56 cm long lead cylinder. The walls of the cylinder were 2.5 cm thick with an inside diameter of

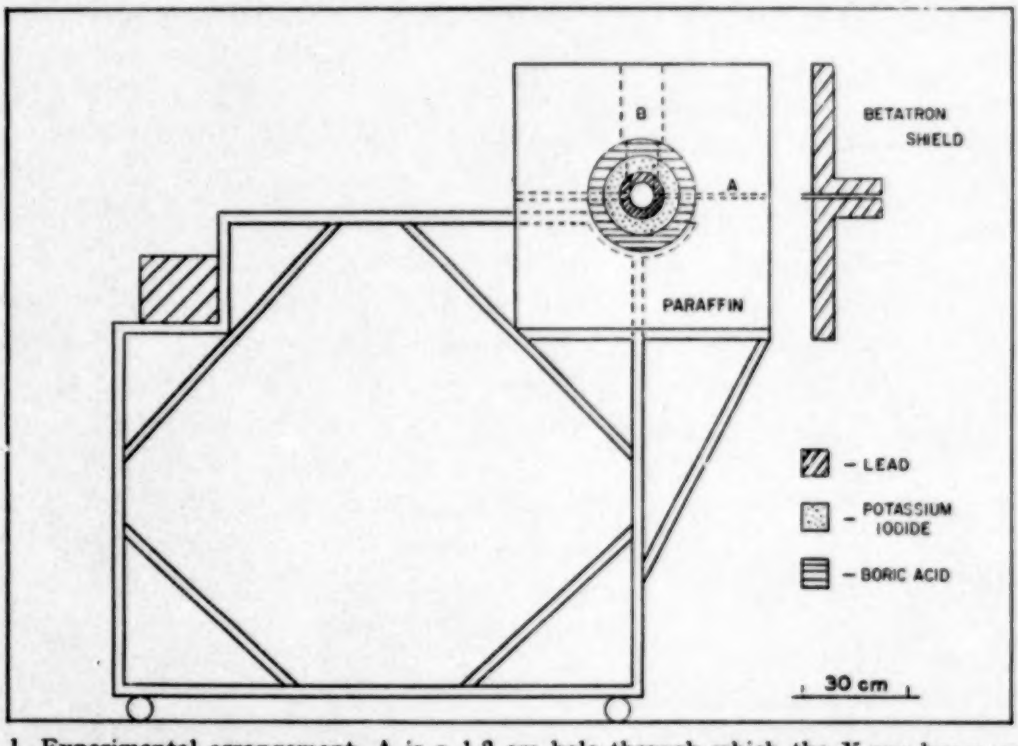

Fig. 1. Experimental arrangement. A is a 1.3 cm hole through which the X-ray beam passes before striking the sample. B is a removable plug which allows the sample to be changed easily.

7 cm. The cylinder was covered on the outside by a thin sheet of cadmium metal plus 5 cm of potassium iodide and 5 cm of boric acid. The cylinder so formed was enclosed in boron-loaded paraffin in a plywood box of dimensions 100 cm × 74 cm × 74 cm. A 1.3 cm hole (A in fig. 1) was provided for the X-ray beam. Removable pieces were provided at each end and above the centre (B in fig. 1)

of the central lead cylinder to allow for removal of the crystals and for sample changing. The box was mounted on one end of a movable cart 150 cm long, 90 cm wide, and 145 cm high. Collimation of the X-ray beam was provided by a thick lead shield which covered the front of the betatron. The lead shield contained a 0.64 cm central collimator which provided 23 cm of lead shielding in the region of the X-ray beam.

It was hoped that the presence of a large amount of iodine immediately outside the central lead cylinder would remove most of the neutrons leaving the moderator with energies corresponding to the energies of several large resonances observed in the (n,γ) cross section for I^{127} between 40 and 200 eV[13]).

A cylindrical magnesium sample (99.9% pure) of mass 47.04 g, diameter 2.2 cm, and length 6.9 cm was placed between the two NaI crystals as shown in fig. 2. Irradiations were performed at energy intervals of 0.2 MeV from 16.6 MeV to 25.0 MeV. The dose was measured in terms of the charge passed to a condenser by an aluminium-walled ionization chamber mounted in the X-ray beam. The condenser was shunted by a resistance whose value was chosen to compensate for the decay of the sample activity during irradiation. The dosemeter had previously been calibrated against a Victoreen thimble in an 8 cm lucite block. Periodic irradiations were made at a setting of the energy control circuit corresponding to 22.0 MeV according to the calibration equation, and the variation in counts per unit dose at this setting was noted; small corrections to the activation points were made when necessary. Corrections for background due to random coincidences were made for all points; counting loss corrections were applied when necessary.

In order to determine the scale of the yield curve, thin discs of copper and magnesium 0.5 cm thick and 2.2 cm in diameter were irradiated and counted with the coincidence system. The discs were positioned between the NaI crystals as shown in fig. 2. Corrections for attenuation of the X-ray beam in the samples, for loss of counts due to finite irradiation time, for loss of positons from the samples (Roalsvig and Haslam[14])), and for attenuation of 0.511 MeV γ-rays in the samples were made. The yield of Cu^{62} at 22 MeV was assumed to be 2.25×10^8 disintegrations per g-atom and per 100 roentgens[15]).

3. Results

The yield of Mg^{23} per unit monitor response as a function of the maximum energy in the X-ray spectrum is shown in fig. 3. The cross section was obtained from the unsmoothed yield curve by the inverted matrix method of Penfold and Leiss[16]) using a bin width of 0.2 MeV. The resulting cross section curve was smoothed by drawing a smooth curve through the running integral of the cross section[16]). The running integral of the cross section and the smoothed cross section curve are shown in fig. 4 and 5, respectively.

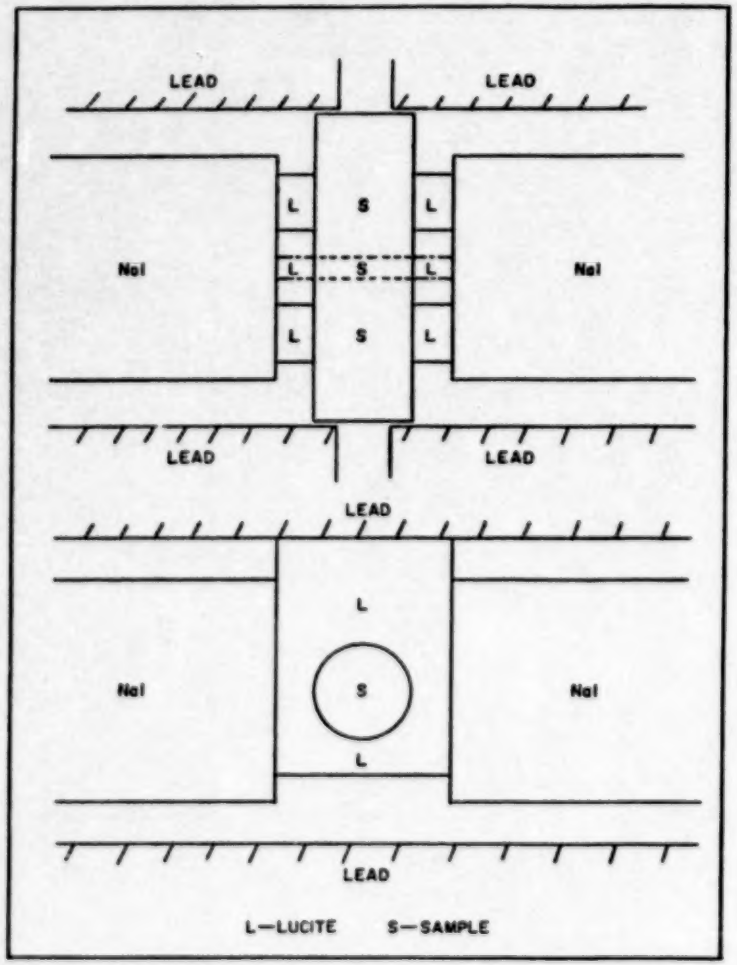

Fig. 2. Sample position. The X-ray beam passes along the central axis of the cylinder. The dotted lines indicate the position of the magnesium or copper disc and its lucite holder during the normalization irradiations.

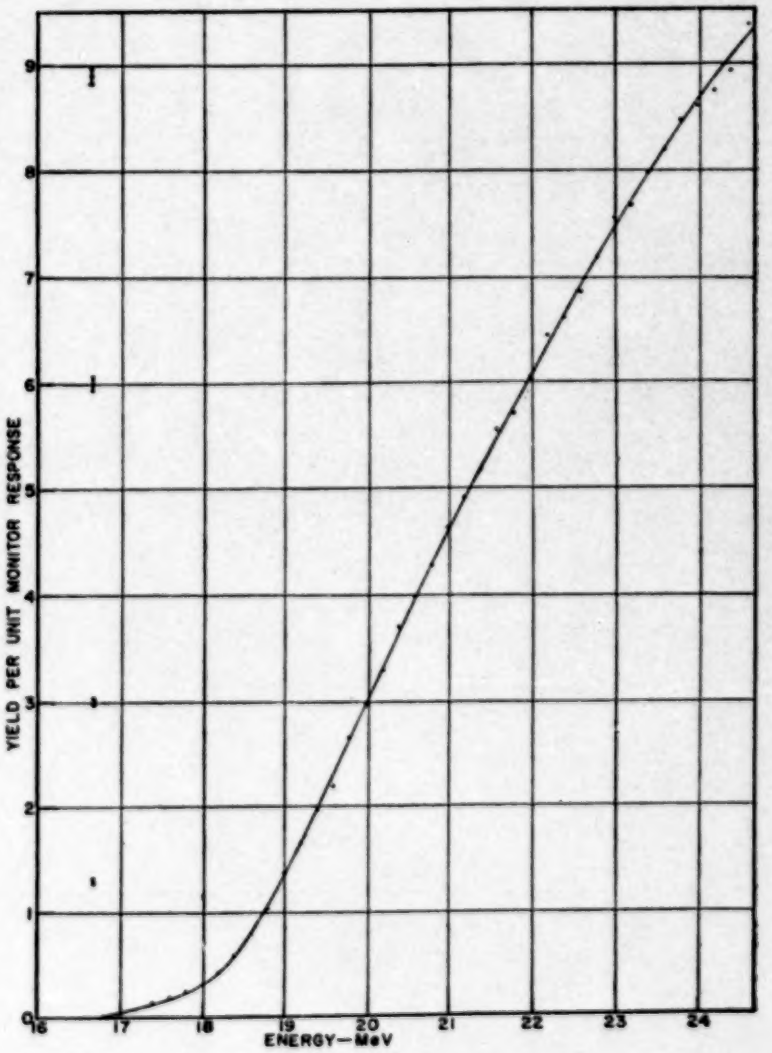

Fig. 3. Yield of Mg^{23} per unit monitor response as a function of the maximum energy in the X-ray spectrum.

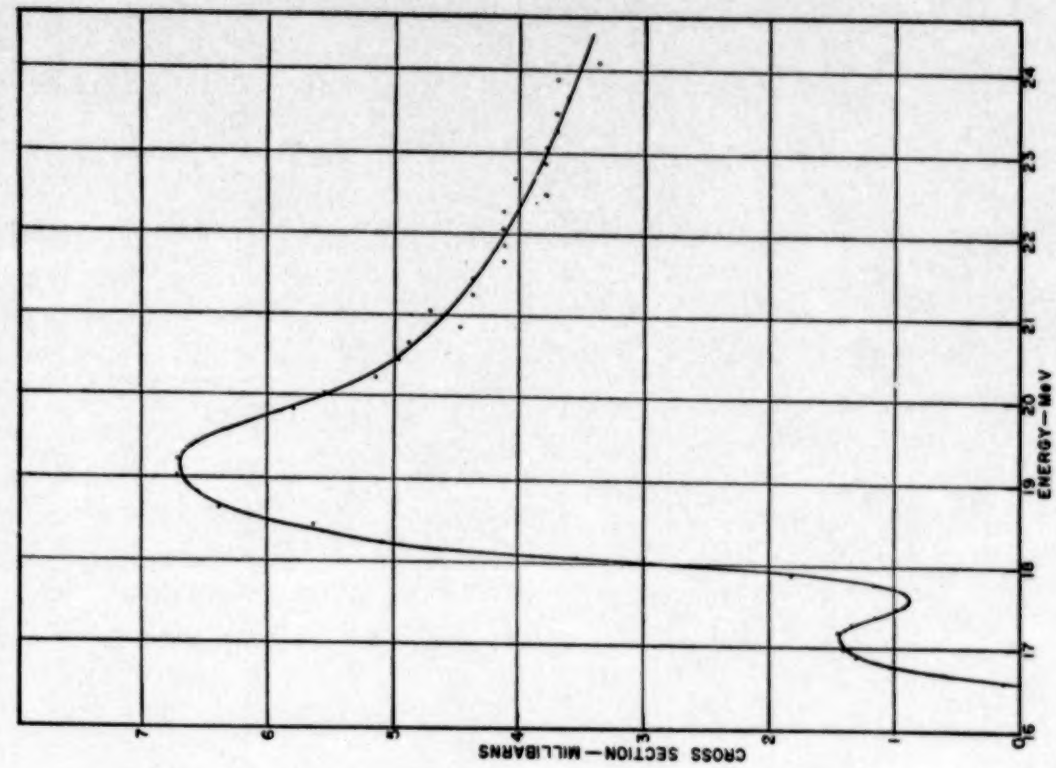

Fig. 5. Cross section for $Mg^{24}(\gamma,n)Mg^{23}$.

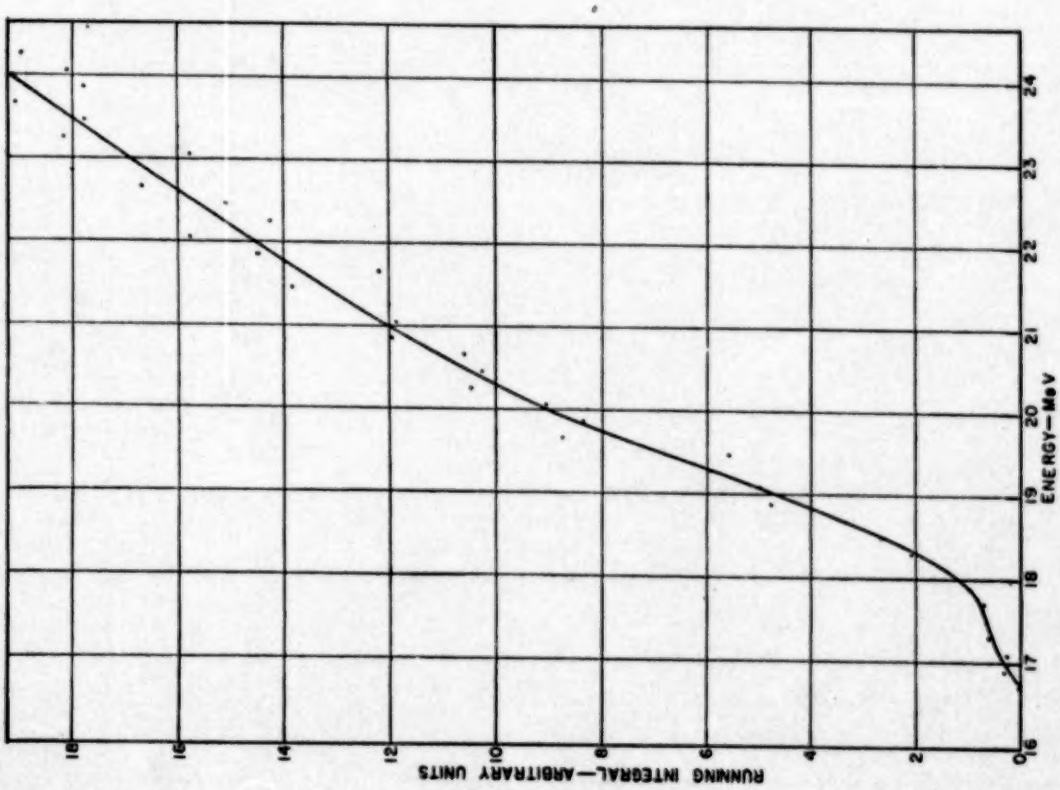

Fig. 4. Running integral of the unsmoothed cross section points as a function of the maximum energy in the X-ray spectrum. The full line is a smooth curve drawn through the points by inspection.

The cross section curve has peaks at 17.2 ± 0.2 MeV and at 19.2 ± 0.2 MeV. The position and height of the low energy peak are not well known because of poor statistics near threshold. However, there is no doubt as to the existence of a peak in this energy region, as it was found in two different determinations of the yield curve. The cross section does not fall to zero above the peak at 19.2 MeV as there is a pronounced high energy tail.

The yield of Mg^{23} at 22 MeV was found to be 1.62×10^7 disintegrations per g-atom and per 100 roentgens.

4. Discussion

The peak at 17.2 MeV has not been observed previously. A peak in the yield curve for $Na^{23}(p,\gamma)Mg^{24}$ at 5.95 MeV proton energy has been observed by Gemmel *et al.*[17]) and was confirmed recently by the Chalk River Tandem Accelerator Group[18]). This proton energy corresponds to an excitation energy of 17.4 MeV for the Mg^{24} nucleus. The agreement between this peak and the $Mg^{24}(\gamma,n)Mg^{23}$ peak at 17.2 MeV is quite good, considering the uncertainty involved in the determination of the position of the (γ,n) peak. An examination of the (γ,n) calculations shows that the peak position could be as high as 17.4 MeV.

Calculations of E1 transition widths for Mg^{24} using the Nilsson model[19]) of the nucleus have recently been carried out. The calculations show that the E1 transitions cluster into two well-separated groups. The agreement between the calculations and the observed shapes for the $Na^{23}(p,\gamma)Mg^{24}$ and $Mg^{24}(\gamma,n)Mg^{23}$ cross sections is good. The lifetime of the first excited state of Mg^{24} has been obtained recently by heavy-ion Coulomb excitation[21]) and by nuclear resonance fluorescence methods[9, 22]). These experiments indicate the mean life of the excited state to be of the order of 10 to 15 $\times 10^{-13}$ sec, yielding a value of Q_0 of approximately 0.6×10^{-24} cm² for Mg^{24}. This value of Q_0 is 2 to 3 times larger than the value of Q_0 obtained from the $Mg^{24}(\gamma,n)Mg^{23}$ and $Na^{23}(p,\gamma)Mg^{24}$ cross sections assuming splitting of the giant resonance according to the Danos-Okamoto theory. This theory, however, applies only to the total photon absorption cross section. A detailed study of the $Mg^{24}(\gamma,p)Na^{23}$ reaction would be of considerable interest as the (γ,p) threshold is at 11.7 MeV.

The peak value of the (γ,n) cross section obtained from this work is 6.7 mb, somewhat lower than the values of 9.8 and 8.4 mb reported previously[11, 12]). This is due to the fact that the Leiss-Penfold method of cross-section analysis yields lower values for the cross section than the photon difference method used previously. The yield at 22 MeV is 1.62×10^7 disintegrations per g-atom and per 100 roentgens, in good agreement with the average value of 1.70×10^7 for the yield of neutrons from the natural element[20]).

The apparatus described in section 2, is presently being modified to permit

the sample activity to be counted between X-ray bursts from the betatron. The increased statistical accuracy of this method will allow a more precise measurement of the $Mg^{24}(\gamma,n)Mg^{23}$ cross section near threshold.

The authors would like to thank Dr. R. N. H. Haslam whose constant interest and guidance have made this work possible, and Dr. H. E. Gove for communication of the Chalk River results before publication.

References

1) B. M. Spicer, Australian J. Phys. **11** (1958) 490
2) M. Danos, Nuclear Physics **5** (1958) 23
3) K. Okamoto, Phys. Rev. **110** (1958) 143
4) G. Rakavy, Nuclear Physics **4** (1957) 375
5) A. E. Litherland, E. B. Paul, G. A. Bartholomew and H. E. Gove, Phys. Rev. **102** (1956) 208
6) D. A. Bromley, H. E. Gove and A. E. Litherland, Canadian J. Phys. **35** (1957) 1057
7) A. E. Litherland, H. McManus, E. B. Paul, D. A. Bromley and H. E. Gove, Canadian J. Phys. **36** (1958) 378
8) B. L. Birbrair, Soviet Physics (JETP) **6** (1958) 951
9) N. N. Deliagin and V. S. Shpinel, Soviet Physics (Doklady) **3** (1958) 789
10 P. C. Gugelot and M. Rickey, Phys. Rev. **101** (1956) 1613
11) L. Katz and A. G. W. Cameron, Phys. Rev. **84** (1951) 1115
12) R. Nathans and P. F. Yergin, Phys. Rev. **98** (1955) 1296
13) D. J. Hughes and J. A. Harvey, Neutron Cross Sections (BNL 325, 1955)
14) J. P. Roalsvig and R. N. H. Haslam, Canadian J. Phys. **37** (1959) 499
15) J. P. Roalsvig, R. N. H. Haslam and D. J. McKenzie, Canadian J. Phys. **37** (1959) 607
16) A. S. Penfold and J. E. Leiss, Analysis of Photo Cross Sections (Physics Research Laboratory Report, University of Illinois, Chicago, 1958)
17) D. S. Gemmel, A. H. Morton and W. I. B. Smith, Nuclear Physics **10** (1959) 45
18) H. E. Gove, private communication (December 1959)
19) S. G. Nilsson, Mat. Fys. Medd. Dan. Vid. Selsk. **29** (1955) no. 16
20) L. Katz, R. N. H. Haslam, J. Goldemberg and J. G. V. Taylor, Canadian J. Phys. **32** (1954) 580
21) D. G. Alkhazov, A. P. Grinberg, G. M. Gusinskii, K. I. Erokhina and I. Kh. Lemberg, Soviet Physics (JETP) **8** (1959) 737
22) S. Ofer and A. Schwarzschild, Phys. Rev. Letters **3** (1959) 384

1.E.1 *Nuclear Physics* 19 (1960) 101—109; © *North-Holland Publishing Co., Amsterdam*
Not to be reproduced by photoprint or microfilm without written permission from the publisher

THE 9.63 MeV STATE OF C^{12}

F. C. BARKER, E. BRADFORD and L. J. TASSIE†

Research School of Physical Sciences, The Australian National University, Canberra, Australia

Received 2 March 1960

Abstract: An analysis of the data from experiments involving the 9.63 MeV state of C^{12} suggests that this state may be 3^-, and not 1^- as previously supposed. An experiment to distinguish between these possibilities is suggested.

1. Introduction

From an analysis of the results of several experiments, the 9.63 MeV state of C^{12} has been tentatively assigned[1]) the spin, parity and isobaric spin values $J^{\pi} = 1^-$, $T = 0$. Since this is probably the lowest state of negative parity in C^{12}, it is of interest to fix its spin definitely. In this paper we give a brief summary of the relevant experimental data (sect. 2), an analysis of part of this data (sect. 3) and a simple shell-model calculation for the low-lying negative parity states (sect. 4), and suggest an experiment which may lead to a definite spin assignment (sect. 5).

2. Experimental Data and Previous Spin and Parity Assignments

Most of the experimental data are given in ref. [1]). It is fairly definite that the 9.63 MeV state is predominately $T = 0$, as the lowest $T = 1$ state is expected at about 15 MeV. Also[2]) it decays, at least in part, by emission of an α-particle to the Be^8 ground state, giving $J^{\pi} = 0^+, 1^-, 2^+, 3^-, 4^+, \ldots$; from the width of the state, it is unlikely that $J > 4$.

We summarize below the results of certain other experiments which have been used to assign spin and parity values to the 9.63 MeV state.

B^{11} (d,n) C^{12}

At $E_d = 9$ MeV, Maslin *et al.*[3]) have fitted the angular distribution of the neutrons to the 9.63 MeV state with an $l_p = 2$ stripping pattern, giving $J^{\pi} = 0^-, 1^-, 2^-, 3^-$ or 4^-; there is little evidence for any $l_p = 0$ contribution. Also at $E_d = 0.85$ MeV, Graue[4]) has obtained an $l_p = 2$ pattern††.

† On leave at The Weizmann Institute of Science, Rehovoth, Israel.

†† From the arguments of Wilkinson[5]) on stripping at low energies, a better stripping pattern might be expected for the 9.63 MeV state than for the ground state, in agreement with Graue's results.

C^{12} (e,e′) C^{12}

Excitation of the 9.63 MeV state by inelastic scattering of 187 MeV electrons has been observed[6,7]). The shape of the form factor for small momentum transfer was taken[7]) to indicate an E0 or E2 transition, $J^{\pi} = 0^+$ or 2^+. Ferrell and Visscher[8]) found that the shape could also be fitted by assuming an E1 or E3 transition, $J^{\pi} = 1^-$ or 3^-, with the magnitude of the form factor favouring 1^-.

C^{12} (p,p′) C^{12}

Peelle[9]) has observed the angular distribution of protons of initial energy 18 MeV scattered inelastically from C^{12}. By comparing with the direct surface interaction theory which predicts a $j_l^2(KR)$ angular distribution, where j_l is the l^{th} order spherical Bessel function, l is the magnitude of the orbital angular momentum change of the incident particle, $\hbar K$ is the magnitude of the momentum transfer and R is the interaction radius, Peelle concluded that his results for the 9.63 MeV state were best fitted with $l = 1$, giving $J^{\pi} = 0^-, 1^-$ or 2^-.

C^{12} (α,α′) C^{12}

The angular distributions for inelastic scattering of 40 MeV α-particles from C^{12} were obtained by Yavin and Farwell[10]). They compared their results with the direct surface interaction theory, with $l = J =$ spin of final state of C^{12}, and found agreement for the 9.63 MeV state with $J^{\pi} = 0^+$ or 2^+, but not with 1^- or 4^+, while 3^- was not considered.

Thus there has been most support for the 1^- assignment, with 3^- as the only alternative if the interpretation of the B^{11}(d,n) C^{12} results is correct. In the next section, we consider in more detail the data for the last three experiments mentioned above, to compare the fit possible in each case for 1^- and 3^- assignments.

3. Analysis of Inelastic Scattering Experiments

C^{12} (e,e′) C^{12}

In his analysis of the inelastic scattering of high energy electrons on nuclei, Schiff[11]) has three types of contributions (i) EL transitions with $\Delta M = 0$, (ii) EL transitions with $\Delta M = \pm 1$, (iii) ML Transitions with $\Delta M = \pm 1$. Here ΔM is the change in component of the spin of the nucleus along the direction of momentum transfer. ML transitions do not concern us here as the 9.63 MeV state of C^{12} is α-unstable. In EL transitions the $\Delta M = \pm 1$ contributions are usually neglected. By an order of magnitude calculation Schiff justified this for collective excitations, but for single particle excitations found $\Delta M = \pm 1$ and $\Delta M = 0$ contributions of the same order. In his estimate, however, Schiff took $r \times \nabla$ operating on $j_l(qr)\, Y^*_{l\pm 1}\ (\theta\phi)$ as of order qR,

whereas it should be of order 1, leading to ratios of $\Delta M = \pm 1$ contributions relative to $\Delta M = 0$ contributions $\frac{1}{2}(q\hbar/Mc)\,(Q'/Q)$ and $\frac{1}{2}(1/qR)\,(v/c)\,(Q''/Q)$ for the magnetization and current terms respectively. With Schiff's estimates $q\hbar/Mc \approx \frac{1}{3}$, $Q'/Q \approx 1$, $qR \approx 3$, $v/c \approx \frac{1}{3}$, $Q''/Q \approx 1$, these ratios become $\frac{1}{6}$ and $\frac{1}{30}$ respectively. Thus neglect of the $\Delta M = \pm 1$ contributions in EL transitions is probably justified.

Then, as pointed out by Fregeau[7]), for small momentum transfer $\hbar q$, the form factor is proportional to q^2 for E0 and E2 transitions, to q^3 for E1, $\Delta T = 0$ transitions in selfconjugate nuclei and E3 transitions, and to q^L for other EL transitions. The experimental form factor for excitation of the 9.63 MeV state[6, 7]) is plotted in fig. 1, and is consistent with q^2 or q^3 dependence[7, 8]). This implies $J^\pi = 0^+, 1^-, 2^+$ or 3^-.

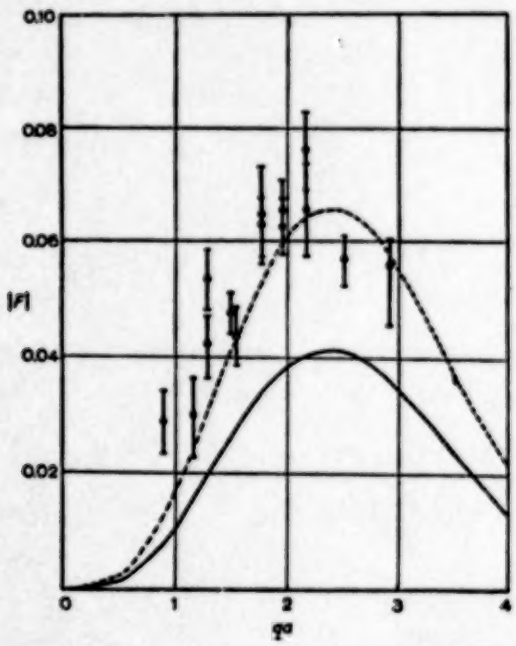

Fig. 1. Magnitude of form factor F for electron excitation of 9.63 MeV state of C^{12} as a function of qa. Experimental points are from refs. [6, 7]). Continuous and dashed curves are respectively $|F'_{1,\max}|$ and $|F'_3|$, which are given in eq. (6). $a = 1.63 \times 10^{-13}$ cm, $a_p = 0.72 \times 10^{-13}$ cm.

The data on the elastic scattering of electrons from C^{12} have been closely fitted using an harmonic oscillator well in a shell model treatment[12]). The length parameter of the well is $a = 1.63 \times 10^{-13}$ cm. We use the same model for the 1^- or 3^- excited state of C^{12}.

Initially we work in the $L - S$ coupling limit. Then the C^{12} ground state is

$$\Psi_0 = \Psi(1s^4 1p^8[44]000,0)\,, \tag{1}$$

where the numbers following the configuration are values of $[\lambda]\,TSL,J$. The only 3^-, $T = 0$ state with one unit of excitation which is coupled to Ψ_0 by the E3 operator is

$$\Psi_3 = \Psi((1s^4 1p^7[43]\tfrac{1}{2}\tfrac{1}{2}1,1d)003,3)\,, \tag{2}$$

while there are three 1^- states coupled by the E1 operator,

$$\begin{aligned}\Psi_{1a} &= \Psi((1s^3[3]\tfrac{1}{2}\tfrac{1}{2}0, 1p^9[441]\tfrac{1}{2}\tfrac{1}{2}1)001,1)\,,\\ \Psi_{1b} &= \Psi((1s^4 1p^7[43]\tfrac{1}{2}\tfrac{1}{2}1, 2s)001,1)\,,\\ \Psi_{1c} &= \Psi((1s^4 1p^7[43]\tfrac{1}{2}\tfrac{1}{2}1, 1d)001,1)\,.\end{aligned} \tag{3}$$

The form factors, taken as the matrix elements of $Z^{-1}\sum_{i=1}^{A} e_i \exp(i\mathbf{q}\cdot\mathbf{r}_i)$ between Ψ_0 and these states, with r_i measured from the well centre, are then

$$F_3 = \frac{\sqrt{15}}{180} i^3 q^3 a^3 \, e^{-\frac{1}{4}q^2a^2},$$

$$F_{1a} = -\frac{\sqrt{6}}{36} iqa \, e^{-\frac{1}{4}q^2a^2},$$

$$F_{1b} = -\frac{\sqrt{2}}{18} iqa \, (1 - \tfrac{1}{4} q^2a^2) \, e^{-\frac{1}{4}q^2a^2},$$

$$F_{1c} = -\frac{\sqrt{10}}{18} iqa \, (1 - \tfrac{1}{10} q^2a^2) \, e^{-\frac{1}{4}q^2a^2}.$$

Now Ψ_3 is a non-spurious state, in the sense of Elliott and Skyrme[13]), but we have to take a combination

$$\Psi_1 = \alpha\Psi_{1a} + \beta\Psi_{1b} + \gamma\Psi_{1c}\,, \tag{4}$$

which also contains no spurious states, and this corresponds to choosing α, β, γ so that, in $F_1 = \alpha F_{1a} + \beta F_{1b} + \gamma F_{1c}$, the coefficient of $\exp(-\frac{1}{4}q^2a^2)$ proportional to qa vanishes. This gives $F_1 \propto q^3$ for small q, as stated by Fregeau[7]). Then

$$F_1 = Ciq^3a^3 \, e^{-\frac{1}{4}q^2a^2}, \tag{5}$$

where C attains a maximum value of $\sqrt{210}/1080$ for $(\alpha, \beta, \gamma) = (-2\sqrt{35}/21,\ 5\sqrt{105}/63,\ -2\sqrt{21}/63) = (-0.563,\ 0.813,\ -0.145)$. The effects of the motion of the centre of mass of the nucleus relative to the well centre and of the finite proton size are simply to multiply the form factors F_1 and F_3 by $\exp(q^2a^2/48 - q^2a_p^2/6)$, where a_p is the root-mean-square radius of the proton[14]). We then obtain for the form factors

$$\begin{aligned}|F'_{1,\max}| &= \frac{\sqrt{210}}{1080} q^3a^3 \, e^{-11q^2a^2/48 - q^2a_p^2/6},\\ |F'_3| &= \frac{\sqrt{15}}{180} q^3a^3 \, e^{-11q^2a^2/48 - q^2a_p^2/6},\end{aligned} \tag{6}$$

which are plotted in fig. 1. It is seen that $|F_3'|$ roughly fits the experimental points, while $|F_{1,\max}'|$ is about 40% too low.

Ferrell and Visscher[8]) calculated similar form factors in the $j-j$ coupling limit and favoured a 1^- assignment, but their expression for $|F_{1^-}'|$ contained an error and also they did not eliminate the spurious 1^- state. After correction, the maximum ratio of $|F_1|$ to $|F_3|$ is again $\sqrt{14}/6$, as in the $L-S$ coupling limit, although the F_3 value in $j-j$ coupling is only $\sqrt{\frac{2}{3}}$ times that in $L-S$ coupling. In fact it can be shown that, even in intermediate coupling, as long as one assumes the ground state of C^{12} belongs only to the configuration $1s^4 1p^8$, no values of $|F_1|$ or $|F_3|$ greater than those obtained in the $L-S$ coupling limit can be obtained. Thus this experimental evidence favours the 3^- assignment rather than the 1^-.

$C^{12}(p,p')C^{12}$

Peelle's[9]) analysis of his data on the inelastic scattering of protons on C^{12} was based on the direct surface interaction theory with an interaction radius $R = 3.3 \times 10^{-13}$ cm. This gave a very poor fit for the excitation of the 4.43 MeV state, known to be 2^+. Levinson and Banerjee[15]) used a direct (volume) interaction theory with distorted waves and obtained good agreement with experiment for the excitation of the 4.43 MeV state of C^{12} for proton energies from 14 to 185 MeV. Their calculations show that the direct surface interaction theory is probably inadequate for a nucleus as light as C. Thus it is doubtful if much weight can be attached to Peelle's spin assignment for the 9.63 MeV state. In any case for a larger value of R, say $R = 4.8 \times 10^{-13}$ cm which fits the observed position of the minimum in the angular distribution for the 4.43 MeV state, the 9.63 MeV state angular distribution is fitted somewhat better for spin 3^- than for 1^-, though the fit is still not satisfactory.

$C^{12}(\alpha,\alpha')C^{12}$

Although there are objections to the direct surface interaction theory for α-particle scattering similar to those for proton scattering, the theory is probably more reliable in the α-particle case, as is shown by the better agreement with experimental results. Thus in the scattering of 40 MeV α-particles on C^{12}, the positions of the first few maxima of the diffraction type angular distribution can be fitted fairly closely, for the elastic scattering and for excitation of the 2^+, 4.43 MeV and 0^+, 7.66 MeV states[10, 16]). These give R values of $(5.52 \pm 0.10) \times 10^{-13}$ cm for the elastic scattering[16]), $(5.45 \pm 0.15) \times 10^{-13}$ cm for excitation of the 4.43 MeV state[10]) and $(5.9 \pm 0.2) \times 10^{-13}$ cm for the 7.66 MeV state[16]). For the 9.63 MeV state, fits similar to those obtained by Yavin and Farwell[10]) for spins 0^+ and 2^+ are obtained for spins 1^- and 3^- with R values 6.5×10^{-13} cm and 6.0×10^{-13} cm respectively. The value of R for the 3^- case is closer to those required for the lower states.

Thus the evidence of this section is slightly in favour of the 3⁻ assignment, without being conclusive.

4. Shell Model Calculation for Negative Parity States

We calculate the excitation energies of the lowest 1⁻ and 3⁻ states of C^{12}, using a simplified shell model treatment. The Hamiltonian is taken as

$$H = K + V^c + V^{so} + V_{conf} ,$$

where

$$K = -\frac{\hbar^2}{2M} \sum_{i=1}^{A} \nabla_i^2 ,$$

$$V^c = \sum_{i<j=1}^{A} [W + MP_{ij}^x - AP_{ij}^r + BP_{ij}^\sigma] \frac{V_0 e^{-\kappa r_{ij}}}{\kappa r_{ij}} ,$$

$$V^{so} = \sum_{i=1}^{A} \xi_{n_i l_i} (l_i . s_i) ,$$

and V_{conf} is a diagonal operator depending only on the configuration of the state involved, which is introduced to correct for deficiencies in the oscillator potential wave functions which are used[17]). The matrix elements of V_{conf} are determined by fitting the lowest positive parity states of C^{13}.

The ground state of C^{12} is expected to consist mainly of the wave function (1), as a large spin-orbit coupling is necessary to cause appreciable departure from the $L - S$ coupling limit[18]). By analogy with the calculations of Elliott and Flowers[19]) on the negative parity states of O^{16}, it is expected that the lowest 1⁻ and 3⁻ states of C^{12} will consist mainly of the basic wave functions (3) and (2) respectively. Similarly the ground state of C^{13} is taken as

$$\Psi_{\frac{1}{2}^-} = \Psi(1s^4 1p^9 [441] \tfrac{1}{2}\tfrac{1}{2}1, \tfrac{1}{2}) .$$

Lane[20]) has shown that the $\frac{1}{2}^+$, 3.09 MeV and $\frac{5}{2}^+$, 3.85 MeV states of C^{13} can be well represented as the C^{12} ground state plus a 2s or 1d neutron respectively, giving the wave functions

$$\Psi_{\frac{1}{2}^+} = \Psi((1s^4 1p^8 [44]000, 2s) \tfrac{1}{2}\tfrac{1}{2}0, \tfrac{1}{2}) ,$$

$$\Psi_{\frac{5}{2}^+} = \Psi((1s^4 1p^8 [44]000, 1d) \tfrac{1}{2}\tfrac{1}{2}2, \tfrac{5}{2}) .$$

Only the basic states given above have been included in the calculation of the energy differences of the various states. Inclusion of other basic states as in a full intermediate coupling calculation would probably not seriously change our estimates of excitation energies in C^{12}, because of the way in which

the matrix elements of V_{conf} are calculated. From the observed excitation energies of the $\frac{1}{2}^+$ and $\frac{5}{2}^+$ states of C^{13}, values are obtained for $V_{conf}(1s^4 1p^8 2s) - V_{conf}(1s^4 1p^9)$ and $V_{conf}(1s^4 1p^8 1d) - V_{conf}(1s^4 1p^9)$ in terms of the parameters occurring in V^c and V^{so}. The same values are assumed for $V_{conf}(1s^4 1p^7 2s) - V_{conf}(1s^4 1p^8)$ and $V_{conf}(1s^4 1p^7 1d) - V_{conf}(1s^4 1p^8)$ which are required in the C^{12} calculations. Also $V_{conf}(1s^3 1p^9) - V_{conf}(1s^4 1p^8)$ is required; this is arbitrarily taken as zero but the results are not sensitive to this choice.

Then the excitation energies of the 3^- and the lowest non-spurious 1^- states of C^{12} can be calculated in terms of the parameters of V^c and V^{so}. We take $\kappa a = 1.2$, $V_0 = 50$ MeV, $\xi_{1p} = -4.4$ MeV, $\xi_{1d} = -2$ MeV and two sets of exchange parameters: (i) $W = 0.1\dot{3}$, $M = -0.9\dot{3}$, $H = 0.2\dot{6}$, $B = -0.4\dot{6}$, the Rosenfeld interaction, (ii) $W = -0.485$, $M = -0.365$, $H = -0.265$, $B = 0.115$, suggested by Elliott and Flowers[19]) from their analysis of the negative parity states of O^{16} and N^{16}. These give for the excitation energies in MeV

(Rosenfeld)	$E_1 - E_0 = 9.78$,	$E_3 - E_0 = 9.26$,
(Elliott and Flowers)	$E_1 - E_0 = 10.08$,	$E_3 - E_0 = 9.20$.

Thus a 1^- and a 3^- state might be expected in the neighbourhood of 10 MeV.

It is of interest to consider the composition of these states. The 3^- wave function is given by eq. (2), while the 1^- wave function is given by eq. (4) with $(\alpha, \beta, \gamma) = (-0.028, 0.916, -0.399)$ for the Elliott and Flowers interaction. This is close to the wave function giving a maximum value of C in the form factor (5); actually it gives a C which is 0.819 times the maximum value, and therefore a form factor $|F_1| = 0.511\,|F_3|$. If the 9.63 MeV state is taken as 3^-, then it might be possible to identify one of the states at 10.84, 11.1 and 11.81 MeV with the 1^- state, as this would be consistent with the observed excitation of these states by electron scattering[6]).

If the ground state of B^{11} is taken as $\Psi(1s^4 1p^7\,[43]\,\frac{1}{2}\frac{1}{2}1, \frac{3}{2})$, we see that mainly $l_p = 0$ stripping is expected in $B^{11}(d,n)\,C^{12}$ to the 1^- state, and $l_p = 2$ to the 3^- state. The observed $l_p = 2$ pattern for the 9.63 MeV state[3, 4]) favours it being 3^-. Maslin *et al.*[3]) suggest that there are $l_p = 0$ components in transitions to higher states, consistent with taking the 1^- state as one of the states near 11 MeV. The intensity of the transition to the 9.63 MeV state[3]) gives $(2J+1)\,\gamma^2 = 1.9 \times 10^{-13}$ MeV cm. For $J = 3$, this leads to a single particle reduced width for d-wave emission $\theta_d = 0.05$. This is somewhat smaller than the d-wave single particle reduced widths obtained in other stripping reactions, but the difference is probably due to the ground state of B^{11} being not entirely $\Psi(1s^4 1p^7[43]\,\frac{1}{2}\frac{1}{2}1, \frac{3}{2})$.

5. $B^{11}(p,\gamma)\,C^{12}(\alpha)\,Be^8$

In proton bombardment of B^{11}, there is a resonance at $E_p = 0.163$ MeV from which γ-rays are observed to the ground and 4.43 MeV states of C^{12}.

This state[1]) of C^{12} at 16.11 MeV is fairly definitely 2^+ and probably the $T = 1$ analogue of the first excited state of B^{12}. One therefore expects E1 γ-radiation from this state to the 9.63 MeV state, assumed to be 1^- or 3^- with $T = 0$, which then decays by α-emission to the ground state of Be^8. Then it may be possible to observe the $\gamma - \alpha$ angular correlation, which should depend on the spin of the 9.63 MeV state. Because of the low energy of the proton and the small momentum of the γ-ray, there is a clear distinction between the energy of the first emitted α-particle ($\approx$ 1.5 MeV) and the maximum energy of the α-particles coming from the Be^8 breakup ($\approx$ 0.7 MeV).

The experimental upper limit[21]) to the radiation width for the transition to the 9.63 MeV state is of order 5 eV. We can estimate the radiation width on the basis of the shell model, using simple wave functions for the states involved. The 16.11 MeV state, being the second lowest $T = 1$ state, presumably belongs mainly to the configuration $1s^4 1p^8$, and in the $L - S$ coupling limit would be $\Psi(1s^4 1p^8[431]111,2)$. There is no E1 radiation from this state to the 9.63 MeV state, given by eq. (2) or eq. (4), nor any E2 radiation to the ground state, given by eq. (1). The largest E2 radiation width is obtained by taking the 16.11 MeV state as $\Psi(1s^4 1p^8[431]102,2)$, but it is only 0.54 eV compared with the observed value[21, 22]) of about 2 eV. Then the E1 radiation widths to the 1^-, 3^- states are 2.3 eV, 13.2 eV respectively. It is not unreasonable therefore to hope that there is an appreciable intensity of γ-radiation to the 9.63 MeV state, which will show up clearly in coincidence with α-particles of 1.5 MeV.

The $\gamma - \alpha$ angular correlation can be calculated uniquely for each spin assignment of the 9.63 MeV state, since[1]) the resonance is due to p-wave protons with known channel spin ratio ($\chi = 0.42$). For α-particles observed at 90° to the proton direction, and γ-rays observed in the plane formed by protons and alphas, and at an angle θ to the proton direction, the angular correlations are

$$W(\theta) \propto 1 - 0.08 \cos^2\theta \quad \text{for } J^\pi = 1^- ,$$

$$W(\theta) \propto 1 + 0.66 \cos^2\theta \quad \text{for } J^\pi = 3^- .$$

Thus a definite spin assignment may be possible from this experiment.

References

1) F. Ajzenberg-Selove and T. Lauritsen, Nuclear Physics **11** (1959) 1
2) R. A. Douglas, J. W. Broer, R. Chiba, D. F. Herring and E. A. Silverstein, Phys. Rev. **104** (1956) 1059
3) E. E. Maslin, J. M. Calvert and A. A. Jaffe, Proc. Phys. Soc. A **69** (1956) 754
4) A. Graue, Phil. Mag. **45** (1954) 1205
5) D. H. Wilkinson, Phil. Mag. **3** (1958) 1185
6) J. H. Fregeau and R. Hofstadter, Phys. Rev. **99** (1955) 1503
7) J. H. Fregeau, Phys. Rev. **104** (1956) 225
8) R. A. Ferrell and W. M. Visscher, Phys. Rev. **104** (1956) 475

9) R. W. Peelle, Phys. Rev. **105** (1957) 1311
10) A. I. Yavin and G. W. Farwell, Nuclear Physics **12** (1959) 1
11) L. I. Schiff, Phys. Rev. **96** (1954) 765
12) R. Hofstadter, Annual Review of Nuclear Science (Annual Reviews, Inc., Stanford, 1957) Vol. 7, p. 231
13) J. P. Elliott and T. H. R. Skyrme, Proc. Roy. Soc. A **232** (1955) 561
14) L. J. Tassie and F. C. Barker, Phys. Rev. **111** (1958) 940
15) C. A. Levinson and M. K. Banerjee, Annals of Physics **2** (1957) 471;
M. K. Banerjee and C. A. Levinson, Annals of Physics **2** (1957) 499;
C. A. Levinson and M. K. Banerjee, Annals of Physics **3** (1958) 67
16) S. F. Eccles and D. Bodansky, Phys. Rev. **113** (1959) 608
17) J. P. Elliott and B. H. Flowers, Proc. Roy. Soc. A **229** (1955) 536;
E. C. Halbert and J. B. French, Phys. Rev. **105** (1957) 1563
18) A. M. Lane, Proc. Phys. Soc. A **68** (1955) 197
19) J. P. Elliott and B. H. Flowers, Proc. Roy. Soc. A **242** (1957) 57
20) A. M. Lane, Phys. Rev. **92** (1953) 839
21) T. Huus and R. B. Day, Phys. Rev. **91** (1953) 599
22) D. S. Craig, W. G. Cross and R. G. Jarvis, Phys. Rev. **103** (1956) 1414

1.D.2:
1.E.1

Nuclear Physics **19** (1960) 110—112; © *North-Holland Publishing Co., Amsterdam*
Not to be reproduced by photoprint or microfilm without written permission from the publisher

CALCULATION OF SPLITTING OF $3s_{\frac{1}{2}}$ NEUTRON LEVELS

F. C. BARKER

Research School of Physical Sciences, The Australian National University, Canberra, Australia

Received 29 February 1960

Abstract: A simple calculation of the separation of the levels produced by addition of a $3s_{\frac{1}{2}}$ neutron to an odd proton nucleus gives satisfactory agreement with the observed separation.

There is evidence[1]) that the addition of a $3s_{\frac{1}{2}}$ neutron to a nucleus containing an odd proton of low j produces two levels of spin $j + \frac{1}{2}$ and $j - \frac{1}{2}$ which are separated by about 60 keV. Thus this is true for the 0^- and 1^- states formed in Rh and Y, which have an odd $2p_{\frac{1}{2}}$ proton, and is probably true of the 4^+ and 5^+ states formed in Nb and In, with proton configurations $1g_{\frac{9}{2}}$ and $(1g_{\frac{9}{2}})^{-1}$ respectively[1]). This separation can be calculated on the basis of a simple shell model description of the nuclear states and a central interaction between the odd proton and the added neutron.

The target nucleus of spin j is described by

$$\Psi\left((\text{core}\{TM_T0\}, nl\{\tfrac{1}{2} - \tfrac{1}{2}j\})j\right),$$

where triads of numbers represent values of $\{TM_TJ\}$. The nl_j nucleon is assumed to be always a proton. No change in the results is caused by introducing a mixture of T values for the core. The state of spin J formed by adding a neutron in the state $3s_{\frac{1}{2}}$ is then

$$\Psi_J = \Psi\left(\left((\text{core}\{TM_T0\}, nl\{\tfrac{1}{2} - \tfrac{1}{2}j\}), , 3s_{\frac{1}{2}\frac{1}{2}\frac{1}{2}}\right)J\right).$$

By the use of Wigner coefficients and Racah functions, this can be rewritten as a linear combination of states in which the proton and neutron are coupled together to form states of definite isobaric spin, spin and orbital angular momentum

$$\Psi_J = \sum_{T_2} \Psi\left((\text{core}\{TM_T0\}, (nl_j\, 3s_{\frac{1}{2}})\{T_20J\})J\right)(\tfrac{1}{2}\tfrac{1}{2} - \tfrac{1}{2}\tfrac{1}{2} \mid T_20)$$

$$= \sum_{T_2S_2} \Psi\left((\text{core}\{TM_T0\}, (nl\,3s)[\lambda_2]\,T_2S_2l, J)J\right)(\tfrac{1}{2}\tfrac{1}{2} - \tfrac{1}{2}\tfrac{1}{2} \mid T_20)$$
$$(-)^{S_2+J-J-\frac{1}{2}}\, U(l\tfrac{1}{2}J\tfrac{1}{2}, jS_2);$$

$[\lambda_2]$ is [2] or [11] for the proton-neutron system in the symmetric or antisymmetric orbital state respectively. The central interaction between proton and neutron is taken as

$$V^c_{pn} = [W + MP^x_{pn} - HP^r_{pn} + BP^\sigma_{pn}]\, V(r_{pn}),$$

so that

$$V^c_J \equiv (\Psi_J \mid V^c_{pn} \mid \Psi_J)$$
$$= \sum_{T_2 S_2} (\tfrac{1}{2}\tfrac{1}{2} - \tfrac{1}{2}\tfrac{1}{2} \mid T_2 0)^2\, U^2\, (l\tfrac{1}{2} J \tfrac{1}{2}, jS_2)\, A_{T_2 S_2}$$
$$\langle (nl\,3s)\,[\lambda_2]\, l \parallel V \parallel (nl\,3s)\,[\lambda_2]\, l \rangle,$$

where

$$A_{01} = W + M + H + B, \quad A_{10} = W + M - H - B,$$
$$A_{00} = W - M + H - B, \quad A_{11} = W - M - H + B.$$

Then

$$V^c_J = \tfrac{1}{2}\left[A_{01}H_+ + A_{11}H_- - \{(A_{01} - A_{10})H_+ - (A_{00} - A_{11})H_-\}\delta_{Jl}\frac{2j+1}{2(2l+1)}\right],$$

where

$$H_+ = \langle (nl\,3s)\,[2]\, l \parallel V \parallel (nl\,3s)\,[2]\, l \rangle, \quad H_- = \langle (nl\,3s)\,[11]\, l \parallel V \parallel (nl\,3s)\,[11]\, l \rangle.$$

Thus for

$$j = l - \tfrac{1}{2}: \quad V^c_{l-1} - V^c_l = \tfrac{1}{2}\frac{l}{2l+1}\{(A_{01} - A_{10})H_+ - (A_{00} - A_{11})H_-\},$$

$$j = l + \tfrac{1}{2}: \quad V^c_{l+1} - V^c_l = \tfrac{1}{2}\frac{l+1}{2l+1}\{(A_{01} - A_{10})H_+ - (A_{00} - A_{11})H_-\}.$$

The orders of magnitude of these separations are calculated for the cases $nl_j = 2p_{\frac{1}{2}}$, $1g_{\frac{9}{2}}$. The values of $A_{T_2 S_2}$ obtained by Elliott and Flowers[2]) from a study of the nuclei with $A = 16$ to 19 have been used; those values are

$$A_{01} = -1, \quad A_{10} = -0.7, \quad A_{00} = -0.5, \quad A_{11} = 0.26.$$

For calculating $H_\pm$, single particle wave functions for an harmonic oscillator potential have been used, the length parameter a being adjusted to fit the nuclear mean square radius $\overline{r^2} = \frac{3}{5}(1.2\, A^{\frac{1}{3}})^2 \times 10^{-26}$ cm^2; with A taken as 100, this gives $a = 2.13 \times 10^{-13}$ cm. The interaction energy $V(r)$ is taken as a Yukawa potential $V_0 \exp(-\kappa r)/\kappa r$, with $\kappa^{-1} = 1.33 \times 10^{-13}$ cm, so that $\kappa a = 1.6$ and $V_0 = 41$ MeV[2]). Then for

$$nl_j = 2p_{\frac{1}{2}}: \quad H_+ = 1.41 \text{ MeV}, \quad H_- = 0.85 \text{ MeV}, \quad V^c_0 - V^c_1 = 37 \text{ keV};$$

$$nl_j = 1g_{\frac{9}{2}}: \quad H_+ = 0.75 \text{ MeV}, \quad H_- = 0.49 \text{ MeV}, \quad V^c_5 - V^c_4 = 41 \text{ keV}.$$

Thus the separations calculated in this way are of the same order of magnitude as the observed separations of about 60 keV.

A similar calculation gives a much larger splitting ($\approx$ 400 keV) of the levels

produced by addition of a $3s_{\frac{1}{2}}$ neutron to an odd neutron nucleus. For the same nl_j values, however, the $3s_{\frac{1}{2}}$ levels occur at higher excitation energies for the odd neutron nuclei than for the odd proton nuclei, and so would be more difficult to observe.

It is to be noted that definite isobaric spin values are not assigned to these heavy nuclei; in particular states of the proton-neutron system with $T_z = 0$ and 1 are taken as equally likely.

Thanks are due to Dr. D. C. Peaslee for suggesting this calculation and for discussions on the treatment of isobaric spin.

Note added in proof: The wave functions assumed above are not antisymmetrized between the core particles and the odd proton and neutron. I am indebted to Professor J. B. French for pointing out that if complete antisymmetry is assumed and provided the nl_j neutron shell is completely filled, the isobaric spins of the target and final nuclei are determined uniquely by their neutron excesses. The formula for the splitting is unchanged, however, as the filled nl_j neutron shell does not give any contribution to the relative energies of the levels[3]).

References

1) B. L. Cohen and R. E. Price, Nuclear Physics **17** (1960) 129
2) J. P. Elliott and B. H. Flowers, Proc. Roy. Soc. A **242** (1957) 57
3) O. M. Bilanink and J. B. French, Nuclear Physics **17** (1960) 435

1.E.1:
3.A

Nuclear Physics **19** (1960) 113—139; © *North-Holland Publishing Co., Amsterdam*
Not to be reproduced by photoprint or microfilm without written permission from the publisher

THE DECAY MODES OF THE 9.17-MeV EXCITED STATE IN N^{14}

H. J. ROSE

Physikalisches Institut der Universität Freiburg, Freiburg, Germany†

Received 31 March 1960

Abstract: A search has been made for the gamma rays and gamma-cascade transitions resulting from the decay of the 9.17-MeV excited state in N^{14} using the reaction $C^{13}(p,\gamma)N^{14}$ at the 1.75-MeV resonance. The main purpose of the investigation was to gain information about the "missing" (2,0) and (2,1) levels arising from the p^{-2} configuration in mass 14 by obtaining a detailed decay scheme for the 9.17-MeV state. For that purpose, three-crystal pair spectrometer techniques have been applied in order to search for gamma rays too weak to be detected by singles spectra measurements in the presence of the strong 9.17 MeV → ground-state transition. In addition to the previously reported transitions from the 9.17-MeV state to the ground state and the 6.44-MeV excited state, a transition was observed to the 7.03-MeV excited state. Furthermore, three-crystal pair spectra measurements and coincidence measurements indicate a transition from the 9.17-MeV excited state to the (presumably) odd-parity $T = 0$ state at 5.83 MeV and possibly to the 5.69- and 5.10-MeV states. Upper limits on the transitions to the 5.69- and 5.10-MeV states have been placed. Observation of gamma rays with energies of 1.64 MeV and 2.49 MeV in three-crystal pair spectra measurements and in several coincidence measurements give evidence that the 6.44-MeV excited state branches to the 3.95-MeV (1,0) state. To obtain anisotropies and intensities relative to the 9.17 MeV → ground-state transition for the gamma rays observed, three-crystal pair spectra have been taken at 0° and 90° relative to the proton beam. The results of these measurements (combined with results about the 9.17 → 6.44 MeV → ground-state transition published recently) lead to spin assignments of $J = 2$ to the 9.17-MeV level and of $J = 3$ to the 6.44-MeV level. Furthermore, they lead to a spin assignment of $J = 2$ to the 7.03-MeV excited state in N^{14}. The latter assignment and comparison of the strength of the 9.17 → 7.03 MeV transition with results of calculations obtained by Warburton and Pinkston suggest that the 7.03-MeV excited state arises from the p^{-2} configuration as (2,0) level and that the 9.17-MeV level at least in part arises from p^{-2} as (2,1) level. Comparison of the dipole-quadrupole mixture ($0.13 < |\delta| < 3.5$) in the 7.03 MeV → ground-state transition, which was determined from the measured anisotropy of this transition, with theoretical results of Warburton and Pinkston agrees with this conclusion.

1. Introduction

In order to explain the anomalously long lifetime of the C^{14} beta decay extensive intermediate coupling shell model calculations of the levels arising from the p^{-2} (i.e. s^4p^{10}) configuration in mass 14 have been made[1,2]). As a consequence of these calculations and comparison with available experimental data, for instance, the doublet splitting of the N^{15} nucleus and the three lowest states of the p^{-2} configuration—which have been identified as the N^{14} ground

† Work supported in part by the German Ministerium für Atomkernenergie. A summary of the results of this paper has been presented at the Munich meeting of the "Fachausschuss Kernphysik der Deutschen Physikalischen Gesellschaft" in April 1959.

state $(J, T) = (1, 0)$, the 2.31-MeV (0,1) and the 3.95-MeV (1,0) excited states—it appears that a (2,0) level should be expected around 6 MeV excitation energy in N^{14} and a (2,1) level around 10 MeV. In fact, Elliott's results[1]) show that the strength of the tensor force in the interaction of the two p holes very sensitively depends on the position of the (2,0) level.

For the identification of the (2,1) and the (2,0) levels theoretical and experimental information has been obtained recently: Elliott[3]) has calculated that the gamma width $\Gamma_\gamma^{\dagger}$ for the decay of the (2,1) state to the ground state should be 25 eV and a branch is predicted to the (2,0) level with an intensity between 2 and 12 % of the intensity of the (2,1) → ground-state transition, if the (2,1) and (2,0) states are assumed in the energy regions between 9 and 10 MeV and between 6 and 7 MeV, respectively. A branch to the 3.95-MeV (1,0) state should be smaller than 1 %. Thus it appears that the gamma transition connecting the (2,1) with the (2,0) p^{-2} level should be extremely helpful for the identification of both these states.

During the course of the experimental investigations described in the present paper Warburton and Pinkston (referred to in the remainder of this paper as WP) have made extensive calculations† concerning the radiative transitions in mass 14. Some of the experimental results presented in the following sections of this paper have already been considered by them in a comparison of present available experimental knowledge with the results of calculations they have made in order to give shell model assignments to the levels in C^{14} and N^{14}. In view of the comprehensive discussion WP give not only for the identification of the even parity p^{-2} and s^4p^8(s, d) states but also for the $T = 0$ and $T = 1$ lowest odd-parity states arising from s^4p^9s and s^4p^9d, it hardly seems necessary to repeat all the arguments which have lead to the conclusion that—if there is a (2,1) state arising from p^{-2} in the group of levels known between 8 and 10.5 MeV—it seems that it must be the 9.17-MeV or 10.43-MeV state (or both).

The 9.17-MeV level has recently been found to have even parity[5]). Also it has been assigned (2,1)[6]). Thus, from these assignments, it seems that the 9.17-MeV state could quite well be the (2,1) p^{-2} state in question. However, the radiative width of the 9.17-MeV → ground-state transition is reported[7]) to be $\Gamma_\gamma^{\dagger} = (8.7 \pm 1.5)$ eV† which corresponds to a matrix element for M1 radiation of $|M(\mathrm{M1})|^2 = 0.53$ Weisskopf units, corresponding to a transition strength[4]) $A(\mathrm{M1}) = 4.1$. This value is to be compared to the theoretical results of Elliott (or of WP) which predict $A(\mathrm{M1}) = 12$. Furthermore, the proton reduced width θ_p^2—assuming p-wave formation of the 9.17-MeV state and using the total width $\Gamma = (77 \pm 12)$ eV obtained by Hanna and Schützmeister[7])—is about

† See ref. [4]). The author is greatly indebted to E. K. Warburton for communicating results to him before publication.

† The value referred to in ref. [6]) was taken from another paper by S. S. Hanna and L. Meyer-Schützmeister[7a]).

10^{-4}, which is more than two orders of magnitude smaller than the value Elliott (or WP) estimated. Elliott (or WP) obtained $\Theta_p^2 \approx 0.03$ from a choice of eigenfunctions which yield the right matrix element for the C^{14} beta-decay and the right spacing of the three lowest levels in N^{14}.

Thus it seems necessary to obtain further information from a study of the decay scheme of the 9.17-MeV state, especially since the $T = 0$, 6.44-MeV state has been found to have $J = 3$[6]), which excludes this state from being (2,0) p^{-2}. The reported[8]) 10 % branch from the 9.17-MeV to the 6.44-MeV level would have been in satisfactory agreement with the predicted branch from the (2,1) p^{-2} state to the (2,0) p^{-2} state if the 9.17-MeV level were this (2,1) p^{-2} state. Therefore, if the 9.17-MeV state shall still be considered as a possible candidate for the (2,1) p^{-2} state, one might expect a branch to some other state around 6 MeV excitation energy in N^{14}. It is not surprising that such a branch might have escaped previous detection, for its intensity could easily be less than half the itensity of the branch from the 9.17-MeV level to the 6.44-MeV excited state, and less than 5 % of the intensity of the 9.17 MeV → ground-state transition. In fact, establishing the existence of such a low intensity gamma ray by singles spectra measurements in the presence of a high intensity ground-state transition and the ever present fluorine contamination would be extremely difficult.

2. Gamma Ray Spectrum from the Decay of the 9.17-MeV State

In order to accomplish a detection of gamma rays between 1.5 and 10 MeV relatively unaffected by the strong 9.17 MeV → ground-state transition, three-crystal pair spectrometer techniques have been applied. The design of the spectrometer was essentially the same as in previous investigations[9, 10]) except that the centre crystal in the present investigations is a 3.2 cm diameter and 6.4 cm long NaI(Tl) crystal. A lead collimator of 10 cm length has been used with an entrance hole of 0.5 cm and an exit hole of 2 cm diameter. The distance from the beam spot on the target has been chosen as approximately 1 cm to accomplish optimum collimating effects. The target consisted of 70 % C^{13} enriched elemental carbon deposited on a 0.013 cm platinum foil. The profile and thickness of the target have been determined using the fact that the 1.75-MeV resonance of the reaction $C^{13}(p, \gamma)N^{14}$ has a total width of only 77 eV[7]) (Doppler broadened approximately 500 eV) and, therefore, can be assumed to be small compared to the target thickness. Varying the proton bombarding energy in steps of 2 keV and going over the 1.75-MeV resonance the target profile was found to consist of a well defined rise to peak yield in 5 keV on the low energy side with a "long tail" on the high energy side which resulted in a target half-width of 20 keV. Unless stated differently in a figure caption this target also has been used for most of the coincidence measurements. The protons were accelerated in the Freiburg University research van de Graaff

accelerator. By means of crossed counter techniques using the $Li^7(p, n)$ threshold the energy spread of the beam was determined to be less than 0.5 keV.

Figs. 1 and 2 show three-crystal pair spectra taken at 0° to the proton beam with an integrated charge of 0.36 C and 0.20 C, respectively. The average beam intensity was 10 μA. The spectrum shown in fig. 1 was taken at a proton energy E_p corresponding to maximum yield from the 1.75-MeV resonance while the spectrum shown in fig. 2 was taken at a proton energy 12 keV below this energy. Considering the target profile and the extremely small proton width of the 1.75-MeV resonance, this choice of proton energy guarantees that the spectrum of fig. 2 will show no contributions from the 1.75-MeV resonance. From a comparison of figs. 1 and 2 it is seen that all the gamma rays shown in fig. 1 except those at 3.5, 4.4 and possibly 5.1 MeV are due to the decay of the 9.17-MeV state in N^{14}. The gamma rays at 3.5 MeV which show up on- and off-resonance are almost entirely due to the 1.70-MeV resonance in the reaction $C^{12}(p, \gamma)N^{13}$. However, for reasons which will be described later, a small fraction of the 3.5-MeV gamma rays shown in fig. 1 are believed due to transitions from the 9.17-MeV level to the 5.83- and 5.69-MeV levels. The gamma rays at 4.4 MeV are—within the experimental errors—just as strong in the off-resonance spectra as in the on-resonance spectra. Therefore it is believed that they are not due to the decay of the 9.17-MeV state in N^{14} but due to some contaminant. The gamma rays at 5.1 MeV may contain small contributions from off-resonance.

Figs. 3 and 4 show three-crystal pair spectra taken at 90° with respect to the proton beam with an integrated charge of 0.33 C and 0.44 C, respectively. These spectra were taken under the same conditions as that for the corresponding spectra at 0°. It was checked that the target shape did not change appreciably during these runs except for a build up of C^{12}. The spectra displayed in figs. 1 to 4 were taken in the sequence 1, 3, 4, 2. Before taking the last one (i.e. the spectrum of fig. 2) the spectrum of fig. 1 was repeated with an integrated charge of 0.055 C to check reproducibility. The yield of 9.17-MeV gamma rays was found to be the same while the yield of 3.5-MeV gamma rays increased by approximately 30 %.

The gamma rays observed in the three-crystal pair spectra shown in figs. 1 and 3 and the transitions believed responsible for these gamma rays are listed in table 1. Also listed in table 1 are the anisotropies and relative intensities obtained from analysis of the three-crystal pair spectra measurements. The assignments for the 9.17-MeV and 6.44-MeV gamma rays follow previous work[8]). The value of the anisotropy given in table 1 for the 9.17 MeV → ground-state transition was taken from measurements investigating the 9.17 MeV → ground-state and the 10.43 MeV → ground-state transition distributions in N^{14} by singles spectra measurements[11]). The 9.17 MeV → ground-state transition anisotropy obtained from singles spectra measurements (ref. [11])) was used for normalization of the pair spectra shown in figs. 1 and 3.

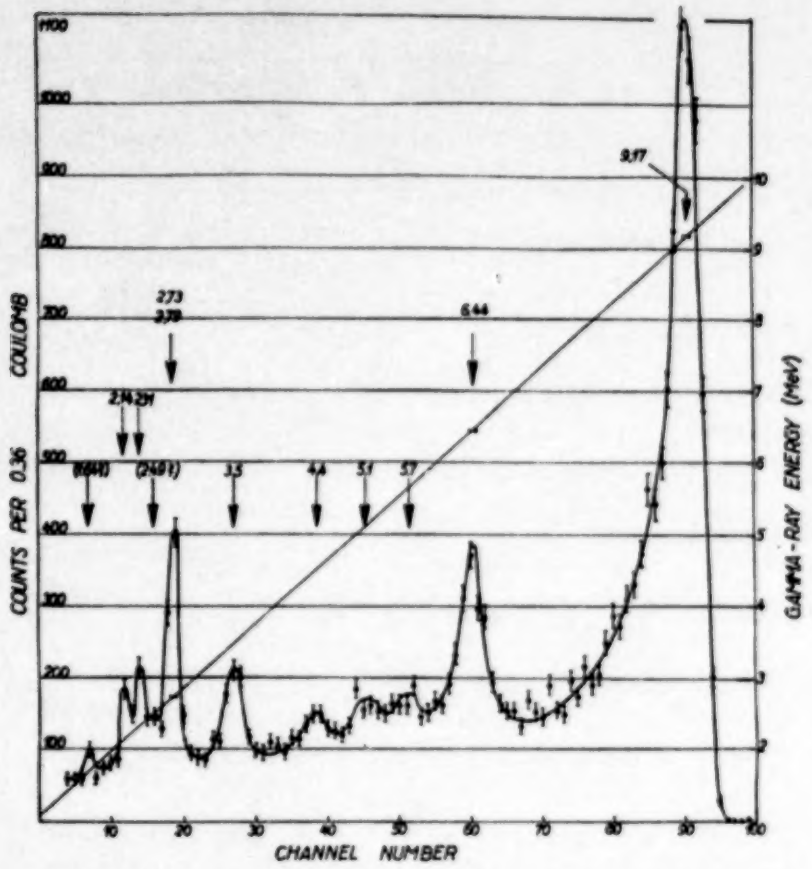

Fig. 1. Three-crystal pair spectrum of the gamma rays from a 20-keV thick C^{13} target bombarded by 1.75-MeV protons. The centre crystal of the spectrometer was placed at 0° to the beam and 11 cm from the target. The spectrum corresponds to an integrated charge of 0.36 C and was taken with a 10 μA proton beam. Side crystal shielding was accomplished using a lead collimator.

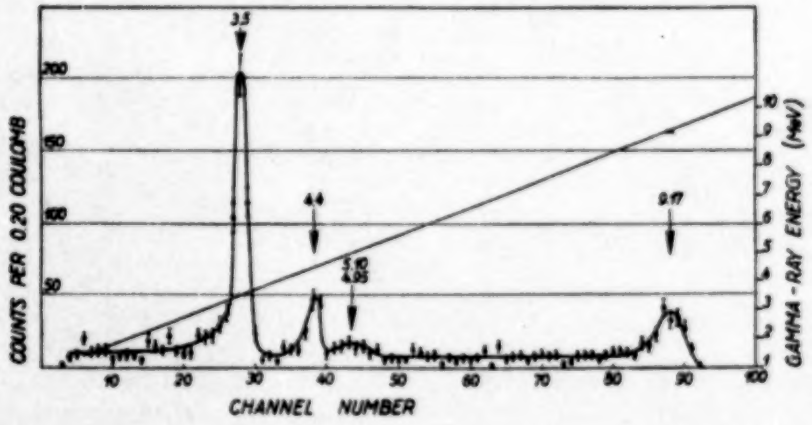

Fig. 2. Three-crystal pair spectrum of the gamma rays from a 20-keV thick C^{13} target bombarded by 1.738-MeV protons (i.e. 12 keV below the 1.75-MeV $C^{13}(p,\gamma)N^{14}$ resonance). The centre crystal of the spectrometer was placed at 0° to the beam and 11 cm from the target. The spectrum corresponds to an integrated charge of 0.20 C and was taken with a 10 μA proton beam. Side crystal shielding was accomplished using a lead collimator.

The errors listed for the intensities in table 1 are due to counting statistics and uncertainties in the background substraction. Corrections have been made for anisotropies as well as for pair spectrometer efficiency and off-resonance contributions. The corrections for anisotropy were performed assuming all

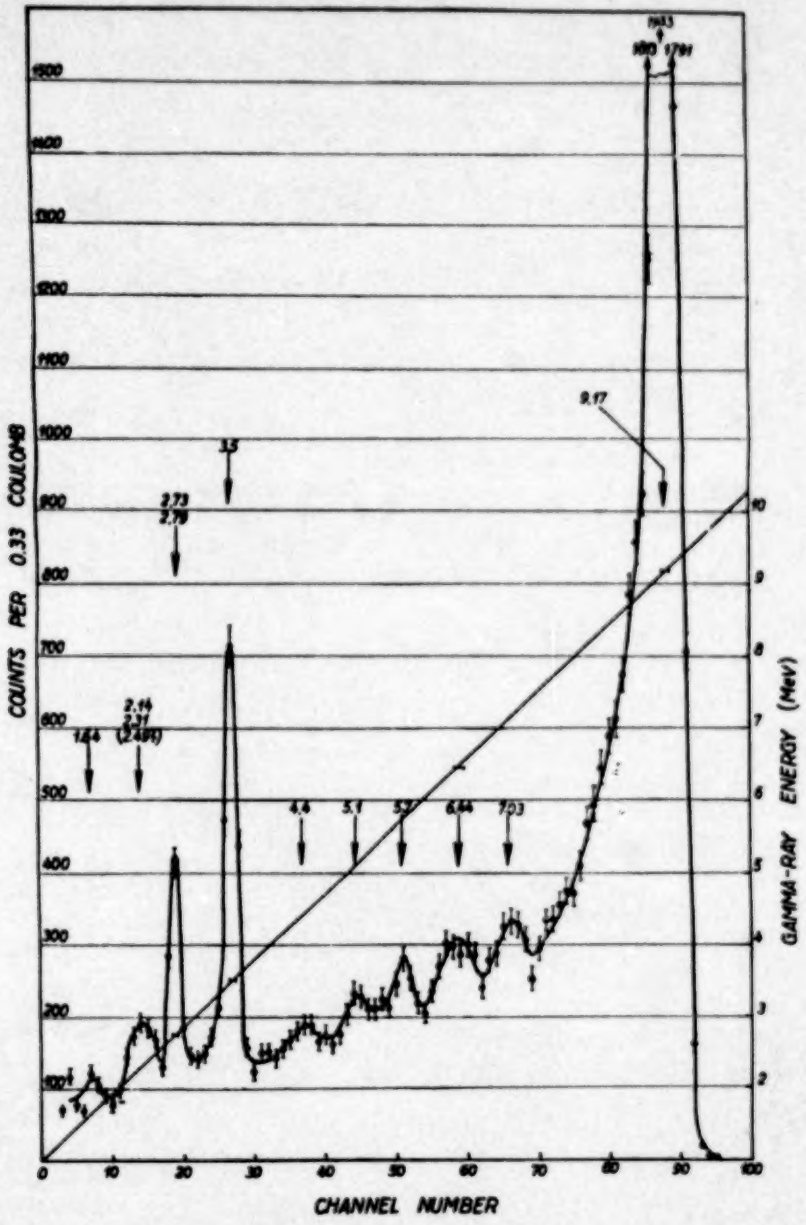

Fig. 3. Three-crystal pair spectrum of the gamma rays from a 20-keV thick C^{13} target bombarded by 1.75-MeV protons. The centre crystal of the spectrometer was placed at 90° to the beam and 11 cm from the target. The spectrum corresponds to an integrated charge of 0.33 C and was taken with a 10 μA proton beam. Side crystal shielding was accomplished using a lead collimator.

angular distributions were of the form $W(\Theta) = 1 + A\cos^2\Theta$, where A is the anisotropy. In performing the corrections for pair spectrometer efficiency, estimates were obtained for deviations from the pair peak efficiency curve.

This was found necessary in view of the high energy gamma rays from the 9.17 MeV → ground-state transition which predominate the spectra of figs. 1 and 3. The escape of bremsstrahlung and—to a smaller extent—electrons from the centre crystal will cause "long tails" on the two-quantum escape peaks

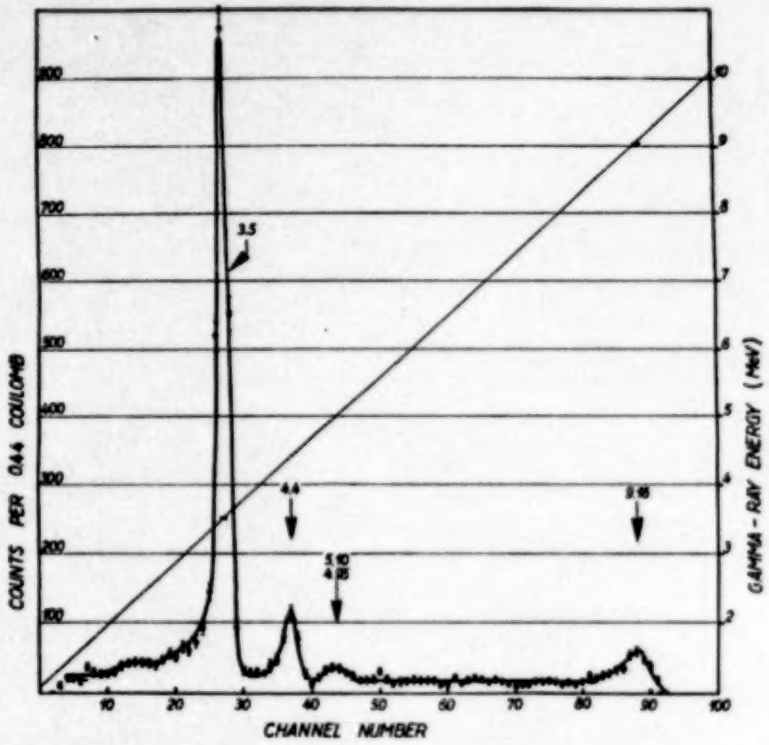

Fig. 4. Three-crystal pair spectrum of the gamma rays from a 20-keV thick C^{13} target bombarded by 1.738-MeV protons (i.e. 12 keV below the 1.75-MeV $C^{13}(p,\gamma)N^{14}$ resonance). The centre crystal of the spectrometer was placed at 90° to the beam and 11 cm from the target. The spectrum corresponds to an integrated charge of 0.44 C and was taken with a 10 μA proton beam. Side crystal shielding was accomplished using a lead collimator.

detected in three-crystal pair spectra measurements. Gamma rays which should contribute to the two-quantum escape peaks will appear at lower energies because of such escapes. To obtain estimates for the deviations from the "true" (relative) efficiency curve of the pair spectrometer (as given by the pair cross section) measurements† were carried out on the dominating gamma rays at 4.4 MeV and 11.7 MeV produced at the 160 keV resonance of the reaction $B^{11}(p,\gamma)C^{12}$. These measurements were made to obtain the energy dependence of the ratio of peak intensity of "tail" intensity. In addition the peak to tail ratio of the N^{14} 9.17 MeV → ground-state transition was used.

The ratios of peak intensity to total intensity for the three-crystal pair

† These measurements have been carried out by U. Stierlin, P. Paul and W. Scholz at the Freiburg University Cockcroft-Walton accelerator. The author is grateful for the permission to use their data.

spectrometer used in the present investigations are given in fig. 5. It is seen from this figure that linear interpolation seems to be justified in order to obtain values for total intensities from peak intensities (which are more easily distinguished in a complex spectrum) for photon energies different from the ones for which measurements could be made. It also appears from this figure that corrections on the relative efficiency of a spectrometer may become quite appreciable at higher photon energies. No attempt has been made to include corrections for positon escape from the centre crystal.

TABLE 1

Decay scheme assignments, relative intensities and anisotropies of gamma rays following proton bombardment of an approximately 20 keV thick, 70% enriched C^{13} target with 1.75 MeV protons

Gamma ray energy[a] (MeV)	Assignment[b]	Relative intensity	Anisotropy $\left(\frac{I(0°)}{I(90°)} - 1\right)$
9.17	N^{14}(9.17 — 0)	100 ± 5[c]	—0.55 ± 0.02[d]
7.03	N^{14}(7.03 — 0)	3 ± 1	$A < -0.35$
6.44	N^{14}(6.44 — 0)	7 ± 2	+0.61 ± 0.32
5.7	N^{14}(5.69 — 0)	3 ± 2	—0.55 ± 0.30
5.1	N^{14}(5.10 — 0)	3 ± 2	—0.32 ± 0.20
4.4	contaminant	3 ± 2	—0.44 ± 0.20
3.5	N^{14}(9.17 — 5.69)[e]	17 ± 2	—0.72 ± 0.10
	N^{14}(9.17 — 5.83)		
	N^{14}(5.69 — 2.31)		
	N^{13}(3.51 — 0)		
2.73 + 2.79	N^{14}(9.17 — 6.44)	12 ± 2	—0.02 ± 0.15
	N^{14}(5.10 — 2.31)		
2.49[e]	N^{14}(6.44 — 3.95)	2 ± 1	
2.31	N^{14}(2.31 — 0)	6 ± 2	—0.04 ± 0.16
2.14	N^{14}(9.17 — 7.03)	4 ± 2	$A > 0$
1.64[e]	N^{14}(3.95 — 2.31)		

[a] The energies listed were computed from the known positions of the energy levels of N^{14} (see ref. [13])). The value of 9.17-MeV has been adapted instead of 9.16 MeV according to the new report of Ajzenberg and Lauritsen[13]).

[b] The assignments were made on the basis of energy measurements and coincidence measurements.

[c] Normalization standard for intensities.

[d] Normalization standard for anisotropies. The value was obtained from singles spectra measurements of the angular distribution of the 9.17-MeV gamma rays[11]).

[e] Doubtful.

Assignments and relative intensities of the gamma rays obtained from the off-resonance spectra displayed in figs. 2 and 4 are listed in table 2. For convenience of comparison with the results listed in table 1 the intensities given in table 2 have been normalized relative to the value of 100 given for the intensity of the 9.17 MeV gamma rays in table 1.

It is seen from table 2 that of all the gamma rays which have been assigned in table 1 as due to the decay of the 9.17-MeV excited state, only the 5.10-MeV

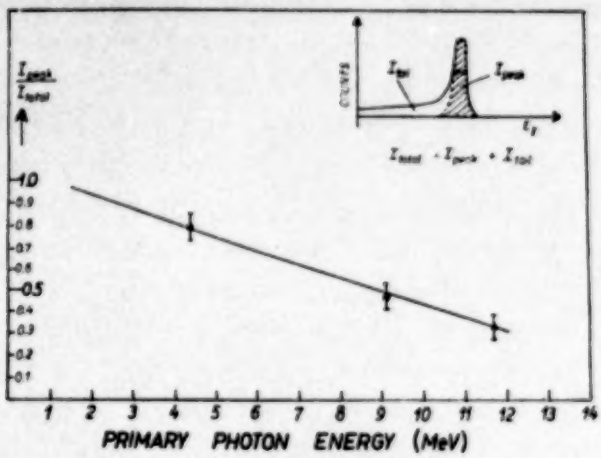

Fig. 5. The ratio of peak intensity to total intensity I_{peak}/I_{total} for a three-crystal pair spectrometer using a 3.2 cm diameter by 6.4 cm long NaI(Tl) crystal as centre crystal. The values at 4.4 MeV and 11.7 MeV have been obtained by the Freiburg Cockcroft-Walton accelerator group from measurements using the reaction $B^{11}(p,\gamma)C^{12}$ at the 160-keV resonance. The value at 9.2 MeV has been obtained from measurements using the reaction $C^{13}(p,\gamma)N^{14}$ at the 1.75-Me resonance. In all experiments the centre crystal has been placed 11 cm from the target and the side crystals have been 7.6 by 7.6 cm NaI(Tl) crystals which were shielded against direct irradiation from the target. For each measurement I_{peak} has been obtained summing up all counts which contribute to the two quantum escape peak itself. This was accomplished using the width of the peak at half maximum and drawing the peak as a curve symmetrical with respect to the maximum as indicated on the insert of the figure. I_{total} has been obtained summing up all counts in peak and tail together.

TABLE 2

Assignments and relative intensities of gamma rays following proton bombardment of an approximately 20 keV thick, 70% enriched C^{13} target below [a] the 1.75-MeV $C^{13}(p,\gamma)N^{14}$ resonance

Gamma ray energy (MeV)	Assignment[b]	Relative intensity[c]
9.17	$N^{14}(8.70 - 0)$	1.5 ± 0.2
	$N^{14}(8.06 - 0)$	
5.7	$N^{14}(5.69 - 0)$	< 0.2
5.1	$N^{14}(5.10 - 0)$	0.5 ± 0.2
	$N^{14}(4.91 - 0)$	
4.4	contaminant	2 ± 1
3.5	$N^{13}(3.51 - 0)$	20 ± 3

[a] Bombarding energy 12 keV below maximum yield from the 1.75-MeV resonance, i.e. (taking into account the profile of the target) protons more than 7 keV below the 1.75-MeV resonance.

[b] Assignments have been made on the basis of energy measurements only.

[c] Normalization standard as in table 1.

gamma rays contain appreciable contributions (approx. 10 %) from off-resonance. A possible contribution to 5.69-MeV gamma rays from off-resonance

is smaller than 5% of the intensity these gamma rays show on-resonance. Considering the extremely small proton width of the 1.75-MeV resonance and the target profile it has been pointed out that the gamma transition from the decay of the 9.17-MeV state cannot contribute to gamma rays observed in the off-resonance spectra. Therefore, the intensity of the 9.17-MeV gamma rays given in table 2 will be mostly due to the ground-state transitions of the broad 8.06-MeV and 8.70-MeV levels. Using the $C^{13}(p, \gamma)N^{14}$ cross section obtained by Seagrave[12]) in the proton energy region between 0.4 and 2.8 MeV, and considering that both the 8.06-MeV and the 8.70-MeV states decay about 80 % to the ground-state, a cross section of 28 μb is estimated for the production of 9.17-MeV gamma rays at $E_p = 1.74$ MeV. For reasons which are not related to the present paper the cross sections for production of 5.10 (+ 4.91)-MeV and 5.69-MeV gamma rays shall be given from a comparison of the relative intensities of the 9.17-, 5.10(+ 4.91)- and 5.69-MeV gamma rays given in table 2. A value of (9 $\pm$ 3) μb for the production of 5.10 (+ 4.91)-MeV gamma rays is obtained at 1.738-MeV bombarding energy and an upper limit of 4 μb can be placed on the production of 5.69-MeV gamma rays at this bombarding energy. These values do not take into account the branching ratios of the 5.10- and 5.69-MeV levels and, therefore, will have to be corrected if cross sections for the gamma rays populating the 5.10- and 5.69-MeV levels are desired. Direct observation of these gamma rays is prevented by the presence of 3.5-MeV and 4.4-MeV radiation (table 2).

Gamma rays observed at 3.5 MeV have been assigned in tables 1 and 2 as due to the 3.51-MeV transition from the reaction $C^{12}(p, \gamma)N^{13}$ at the 1.70-MeV resonance. These 3.5-MeV gamma rays show up somewhat stronger off the 1.75-MeV resonance as is expected since the off-resonance spectra of figs. 2 and 4 were taken at a proton energy closer to the maximum yield of the $C^{12}(p, \gamma)N^{13}$ 1.70-MeV resonance than the spectra of figs. 1 and 3. It was estimated from the profile of the target used and the energy dependence of the $C^{12}(p, \gamma)N^{13}$ cross section[12]) that the yield of 3.5-MeV gamma rays due to the reaction $C^{12}(p, \gamma)N^{13}$ should increase by approximately 30 % when changing the bombarding energy from 1.75 MeV to 1.738 MeV. Considering the sequence in which the spectra were taken together with the build up of C^{12} on the target, one should expect (in the on-resonance spectra) approximately 12 of the intensity units used in table 1 to be contributions from off-resonance. Thus it appears that a small fraction of the 3.5-MeV gamma rays listed in table 1 could be due to other transitions than to the N^{13} 3.51-MeV $\rightarrow$ ground-state transition.

The gamma rays at 5.10 MeV have been assigned in table 1 as due to the decay of the 5.10-MeV state to the ground state. As a consequence of the known branching ratio[13]) of the 5.10-MeV state to the 2.31-MeV level it then appears that gamma rays of 2.79 MeV and 2.31 MeV should also be expected. Gamma rays of 2.31 MeV are clearly observed while the corresponding 2.79-MeV

radiation would be covered by the comparatively strong 2.73-MeV radiation from the decay of the 9.17-MeV state to the 6.44-MeV level. From the spectra of figs. 1 and 3 it appears that the 5.10-MeV state is not populated directly from the 9.17-MeV level via a 4.07-MeV gamma transition. The upper limit on the intensity of a gamma ray of 4.07 MeV obtained from the spectra shown in figs. 1 and 3 is half the intensity of the 5.10-MeV gamma rays which, in turn, means that the 5.10-MeV state (taking into account the branch to the 2.31-MeV level) must be populated to at least two thirds via an intermediate state. It is suggested that this intermediate state is the 5.83-MeV state since this state decays almost completely (85 %) to the 5.10-MeV state[13, 10]) via a 0.73-MeV gamma transition. The 3.34-MeV gamma rays populating the 5.83-MeV level would then have an intensity of 4 ± 2 units of table 1 and, therefore, would be hidden by the strong 3.5-MeV gamma radiation due to the reaction $C^{12}(p, \gamma)N^{13}$. In section 3 coincidence measurements on the 0.73-MeV and 3.34-MeV gamma rays which support this suggeststion will be described.

The 5.7-MeV gamma rays observed in the spectra of figs. 1 and 3 have been assigned in table 1 as most likely arising from the decay of the 5.69-MeV level. This assignment is suggested by coincidence measurements which will be described in sect. 3. The gamma rays labelled as 7.03-MeV in fig. 3 have been assigned in table 1 as due to the decay of the 7.03-MeV excited state to the ground state. The gamma rays of the transition populating the 7.03-MeV level are also clearly observed in the spectra of figs. 1 and 3 and have been labelled there as 2.14-MeV gamma rays. The intensities of the 2.14-MeV and 7.03-MeV radiation given in table 1 agree within the experimental errors. The gamma rays labelled as 2.49-MeV and 1.64-MeV radiation in figs. 1 and 3 are — for intensity reasons — not well defined. Coincidence measurements described in sect. 3 indicate that they could be due to a branch in the decay of the 6.44-MeV state.

3. Coincidence Measurements

In order to confirm the assignments given in table 1 to the gamma rays observed in three-crystal pair spectra measurements and to search for low energy gamma rays to weak to appear in singles spectra measurements various coincidence measurements have been carried out. In these measurements combinations of two 7.6 by 7.6 cm NaI(Tl) crystals or one 7.6 by 7.6 cm and one 10.2 by 10.2 cm have been used to obtain display and gate spectra. In searching for the population mode of the 5.10-MeV state via a 0.73-MeV transition from the 5.83-MeV excited state some of the measurements were carried out using a 5.1 by 5.1 cm NaI(Tl) crystal for display and a 7.6 by 7.6 cm for gating. Conventional fast-slow coincidence techniques were applied in the associated circuitry. The fast coincidence circuit had a time resolution of 1×10^{-7} sec. A single-channel pulse-height analyser could be adjusted to count

any portion of the total gate spectrum. This analyser window which determines the energy dependence of the gate signals was adjusted by "self-gating" as described in a previous paper[9]). The spectra were displayed on a RIDL 100-channel pulse height analyser. The average beam intensity during the coincidence runs was 5 μA; some of the spectra were repeated with a beam of 1 μA to check on random coincidence effects. The gate crystal used in a measurement was placed at a distance as close to the target as permitted by the maximum

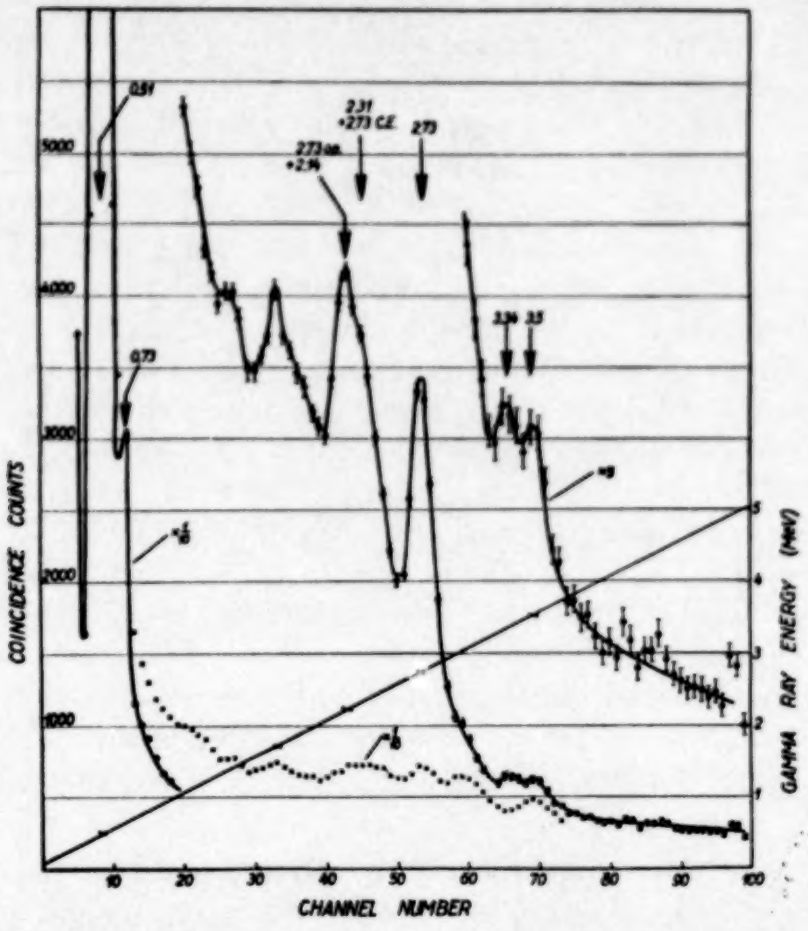

Fig. 6. Spectrum of the gamma rays from the $C^{13}(p,\gamma)N^{14}$ reaction at the 1.75-MeV resonance in coincidence with 4.7- to 7.5-MeV radiation. The crystal used to obtain the display spectrum was a 7.6 by 7.6 cm NaI(Tl) crystal and was placed at 90° to the proton beam and 3 cm from the target. The crystal used to obtain gate signals was a 10.2 by 10.2 cm NaI(Tl) crystal and was placed at 90° to the beam and 3 cm from the target. The spectrum corresponds to an integrated charge of 40 mC and was taken with a 6 μA beam. Peaks not especially labelled are one or two quantum escape peaks. C.E. = Compton edge, o.e. = one-quantum escape peak. The dotted line (crosses) shows a singles spectrum obtained with the display crystal without coincidence condition.

counting load the associated circuitry could take and was, in most of the measurements, approximately 3 cm. As a further check on random coincidences and back-scattering effects several of the measurements were repeated under varying conditions as—for instance—change of the distance of the crystals

from the target or collimation and shielding of one or both the crystals. Only those coincidence spectra will be shown in this section which seem necessary for the conclusions which are to be drawn. For these spectra the experimental conditions are specified in the figure captions.

In figs. 6 and 7 singles spectra have been displayed in coincidence with gamma radiation from 4.7 to 7.5 MeV and from 1.0 to 4.7 MeV, respectively. A full energy loss peak at 2.73 MeV together with its one and two quantum escape peaks shows up as the most prominent radiation in coincidence with gamma rays between 4.7 and 7.5 MeV. The "reverse" experiment with the analyser window on the low energy portion of the gate spectrum (1.0 to 4.7 MeV) yields a full energy loss peak at 6.44 MeV with its one and two quantum

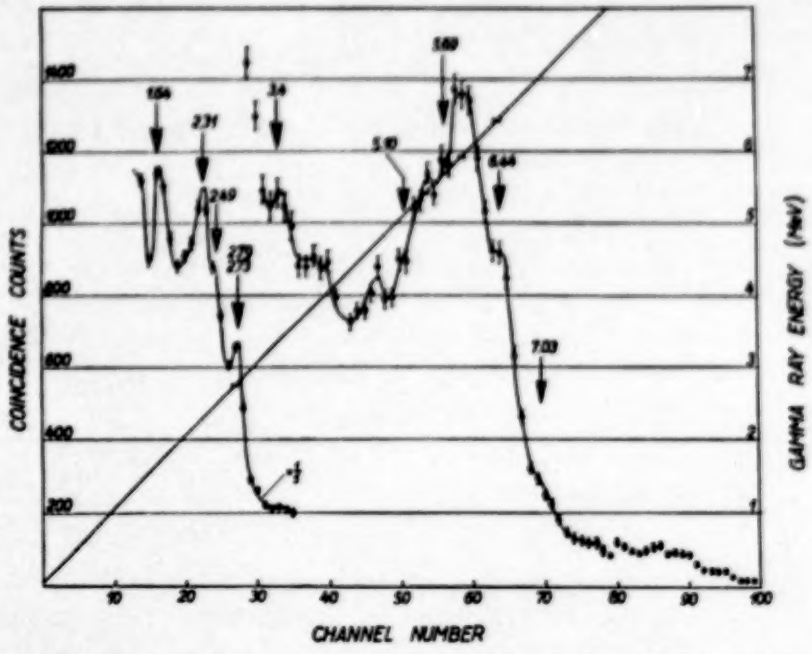

Fig. 7. Spectrum of the gamma rays from the $C^{13}(p, \gamma)N^{14}$ reaction at the 1.75-MeV resonance in coincidence with 1.0- to 4.7-MeV radiation. The crystal used to obtain the display spectrum was a 7.6 by 7.6 cm NaI(Tl) crystal and was placed at 0° to the proton beam and 5 cm from the target. The crystal used to obtain gate signals was a 7.6 by 7.6 cm NaI(Tl) crystal and was placed at 120° to the beam and approximately 5 cm from the target. The spectrum corresponds to an integrated charge of 36 mC and was taken with a 7 μA beam. Peaks not especially labelled are one or two quantum escape peaks. The spectrum shown in this figure was taken using a 1.3-keV thick target which had been prepared by cracking C^{13}-enriched methyl iodide onto a 0.2 mm platinum foil and which was found uniform. Unfortunately most of the experimental work described in the present paper had been finished before it was possible to prepare targets by cracking of methyl iodide.

escape peaks (fig. 7). These gamma rays correspond to the well known cascade 9.17 → 6.44 MeV → ground state.

Also apparent in fig. 6 are gamma rays of 3.34 and 3.5 MeV which are approximately one tenth of the intensity of the 2.73-MeV radiation. These values for the intensities of the 3.34-MeV and 3.5-MeV gamma rays relative to the

intensity of the 2.73-MeV radiation are smaller than expected from the intensities of the 5.10-MeV and 5.69-MeV gamma rays observed in three-crystal pair spectra measurements (table 1) if the 3.34-MeV and 3.5-MeV radiations corresponded to the transitions 9.17 → 5.83 MeV and 9.17 → 5.69 MeV. However, the analyser window contains full energy loss, one and two quantum escape peaks of the 6.44-MeV radiation and part of the Compton background of this radiation, while it contains only the full energy loss peak of the 5.10-MeV gamma radiation. Therefore, neglecting anisotropy effects which were shown to bring no appreciable change when using different geometrical arrangements of the detectors, a value for the intensity of the 3.34-MeV radiation should be expected in this measurement which may be less than one third of the intensity of the 5.10-MeV radiation given in table 1, or (compared to the intensity of the 2.73-MeV radiation) between, say, 10 and 20 % of the intensity this radiation shows in fig. 6. A similar argument may be given to explain the low intensity of the 3.5-MeV radiation in fig. 6 if this radiation were due to the transition 9.17 → 5.69 MeV. However, in this case the analyser window would contain full energy loss and one quantum escape peak of the 5.69-MeV radiation and, therefore, the 3.5-MeV peak should show up approximately twice as strong as the 3.34-MeV peak, because the intensities of the 5.10-MeV and 5.69-MeV gamma rays as obtained from three-crystal pair spectra measurements (table 1) are the same. Contributions of N^{13} 3.51-MeV gamma rays due to random coincidences in the spectrum of fig. 6 have been estimated from the counting rate in the analyser window and the known resolving time of the coincidence circuit and have been found to be small compared to the 3.5-MeV gamma ray intensity observed in the spectrum of fig. 6. Of course, all these arguments concerning the population modes of the 5.10-MeV and 5.69-MeV levels implicitly disregard the high errors which had to be quoted on the intensities of the 5.10-MeV and 5.69-MeV radiation in table 1.

So, as to obtain further information on the transitions feeding the 5.10-MeV and 5.69-MeV states, a coincidence experiment was made with an analyser window centered at 3.5 MeV and a width of only 0.7 MeV. This experiment may be understood as the "reverse" to the experiment which yielded the spectrum shown in fig. 6 as far as the corresponding transitions to the 5.1-MeV and 5.7-MeV gamma rays are concerned. The spectrum obtained in this manner is displayed in fig. 8. The 2.31-MeV peak is the most prominent radiation in this spectrum as would be expected since both the 5.10-MeV and the 5.69-MeV states are known to branch to the 2.31-MeV first excited state. Furthermore, a peak at 2.79 MeV shows up which hardly can be explained as due to the 2.73-MeV radiation from the transition 9.17 → 6.44 MeV (the analyser window, of course, also will contain some Compton background of the 6.44-MeV radiation) by reason of its higher energy and strong intensity. Therefore this peak is believed to correspond to the gamma transition from the 5.10-MeV to the

2.31-MeV level. Some 5.10-MeV radiation also shows up in the spectrum of fig. 8. The analyser window also would detect gamma rays resulting from the 63 % branch of the 5.69-MeV state to the 2.31-MeV level if the 3.5-MeV gamma rays observed in the spectrum of fig. 6 were due to the 3.48-MeV transition feeding the 5.69-MeV state. Therefore it should be expected that a relatively strong gamma ray should show up in the spectrum of fig. 8 at an average

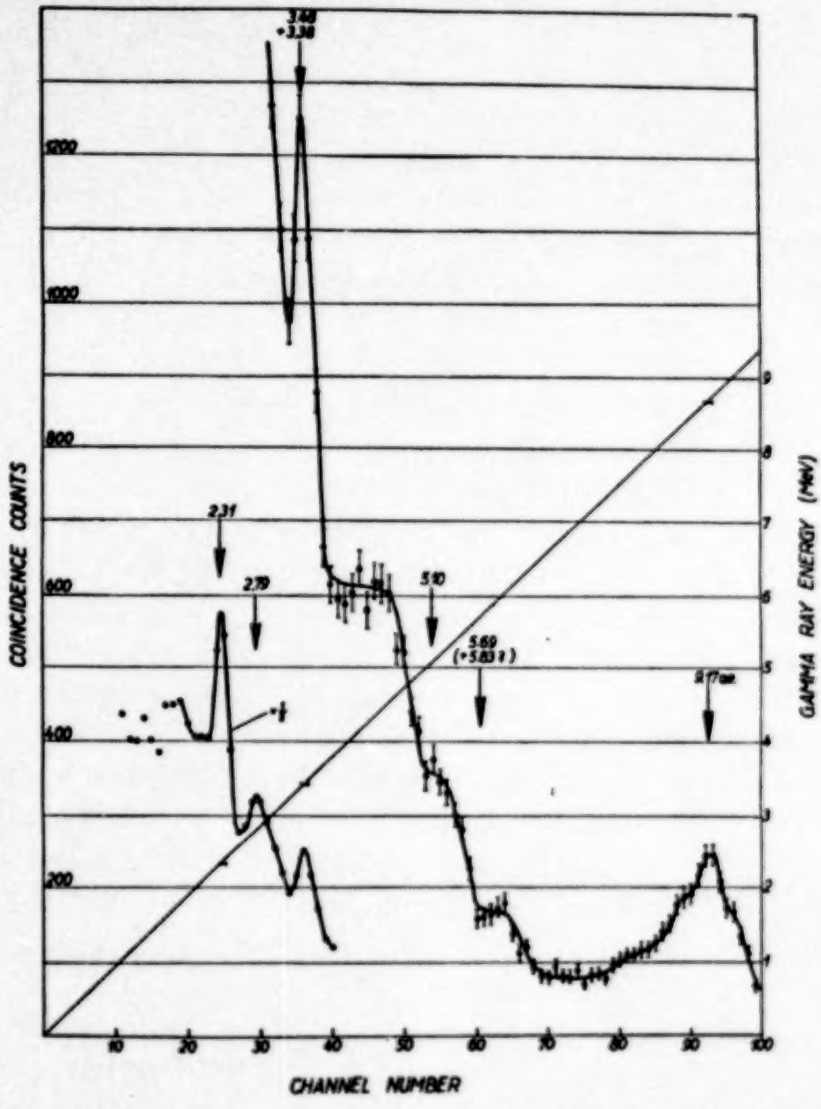

Fig. 8. Spectrum of the gamma rays from the $C^{13}(p,\gamma)N^{14}$ reaction at the 1.75-MeV resonance in coincidence with 3.0- to 3.7-MeV radiation. The crystal used to obtain the display spectrum was a 7.6 by 7.6 cm NaI(Tl) crystal and was placed at 90° to the proton beam and approximately 3 cm from the target. The crystal used to obtain gate signals was a 7.6 by 7.6 cm NaI(Tl) crystal and was placed at 90° to the beam and approximately 4 cm from the target. The spectrum corresponds to an integrated charge of 60 mC and was taken with a 2.5 μA beam. The spectrum shown in this figure was taken with a 90-keV thick target. An almost identical spectrum using a 10.2 by 10.2 cm NaI(Tl) crystal for gating had been obtained earlier from the 20-keV thick standard target described in sect. 2. When taking the spectrum shown it was observed that the gamma rays labelled as 3.48 + 3.38 showed up somewhat lower in energy than the 3.51-MeV radiation from N^{13} which shows up when the coincidence condition is taken out.

energy of 3.43 MeV which should contain approximately equal parts of 3.38-MeV and 3.48-MeV gamma rays. This peak clearly is observed in the spectrum of fig. 8. Furthermore, a peak between 5.7 and 5.9 MeV shows up which is believed to be due to the 5.69 MeV → ground-state transition with contributions from the 5.83 MeV → ground-state transition.

In summary, the coincidence measurements described so far have presented evidence that the gamma rays observed at 5.1 and 5.7 MeV in the three-crystal pair spectra measurements (figs. 1 and 3) are due to gamma transitions from the 5.10-MeV and 5.69-MeV levels to the ground state. Comparison of the intensities of the transitions populating these levels shows that it is possible—if not proved—that the 5.10-MeV level is populated via a 3.34-MeV transition to the 5.83-MeV state, while the question of wether or not the 5.69 MeV level is populated 100 % via a direct transition from the 9.17-MeV state is still open. It seems that either there is some other population mode of this state or else the intensity of the 5.69-MeV radiation is of the lowest limit permitted by the errors quoted in table 1.

From sect. 4 it will be seen that a transition to the 5.83-MeV state is of great importance for a confirmation of the spin assignment of the 9.17-MeV state. Therefore the population mode of the 5.10-MeV state has been investigated in a further experiment. The absence of gamma rays at 4.07 MeV in the coincidence spectra of figs. 6 and 8 supports the conclusion obtained from three-cystal pair spectra measurements that the 5.10-MeV level is populated via an intermediate state. Evidence has been presented which indicates that this state is the 5.83-MeV level. This is supported by the fact that the coincidence spectrum of fig. 6, which was obtained with the broad analyser window on the high energy gamma rays, shows a small peak on the side of the 0.51-MeV annihilation peak at 0.7 MeV. To prove that these 0.7-MeV gamma rays are due to the transition 5.83 → 5.10 MeV coincidence measurements were carried out on and off the 1.75-MeV resonance with different energy adjustments of a narrow analyser window between 3 and 9 MeV. The results of these measurements, which have been displayed in fig. 9, exclude the possibility that the 0.7-MeV peak is caused by random coincidences of 0.51-MeV annihilation quanta and low energy radiation from Coulomb excitation of the platinum of the target backing. Also they exclude the possibility that the 0.7-MeV peak could be due to "real" coincidences between gamma rays of cascade transitions of which one is registered by the analyser window and the other one is converted by pair production in the target material and surroundings. This latter one would cause annihilation quanta. If one of these annihilation quanta is back-scattered to the display-crystal and the other one is directly detected by this crystal it could yield a peak at 0.69 MeV.

Besides the 2.73, 3.34 and 3.5 MeV gamma rays, gamma rays at 2.14 MeV have been labelled in fig. 6. These gamma rays have been resolved more com-

pletely from the 2.73-MeV radiation one-quantum escape peak in spectra obtained with a higher gain. To confirm these 2.14-MeV gamma rays as due to the transition feeding the 7.03-MeV excited state from the 9.17-MeV level, a narrow analyser window has been placed counting gamma rays from 6.7 to

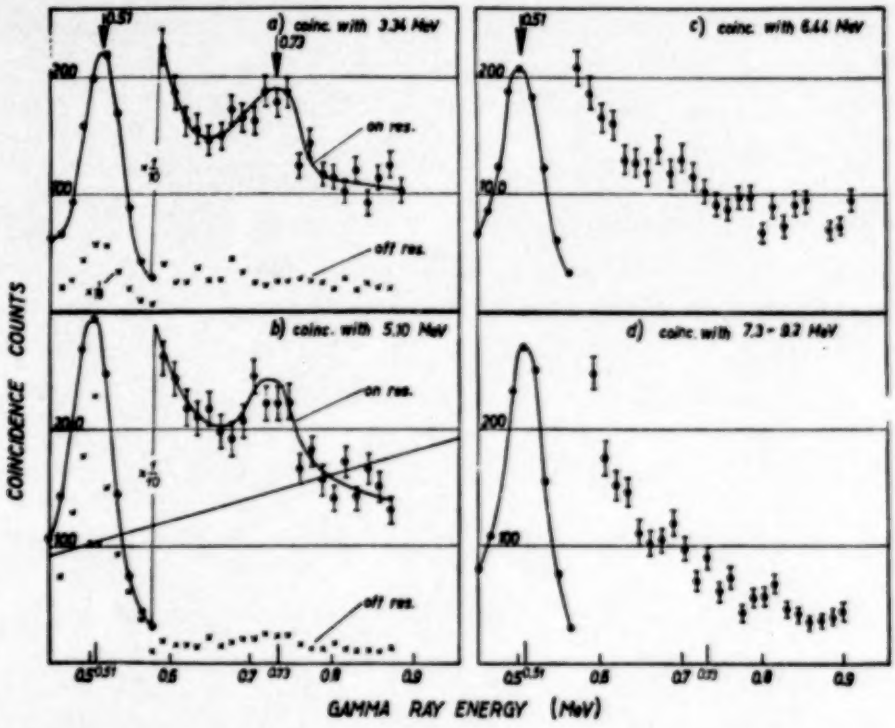
a) coinc. with 3.34 MeV
c) coinc. with 6.44 MeV
b) coinc. with 5.10 MeV
d) coinc. with 7.3 - 9.2 MeV
on res.
off res.
COINCIDENCE COUNTS
GAMMA RAY ENERGY (MeV)

Fig. 9. Coincidence spectra of the 0.73-MeV gamma rays on and off the 1.75-MeV resonance. All spectra were taken using a 5.1 by 5.1 cm NaI(Tl) crystal to obtain the display spectrum at 90° to the beam and 4 cm from the target and a 7.6 by 7.6 cm NaI(Tl) crystal to obtain the spectrum for gating at 90° to the beam and 4 cm from the target. All spectra correspond to an integrated charge of 36 mC and were taken with a 2.5 μA beam. The target used had a thickness of 10 keV and—although not prepared by a cracking process—was found close to uniformity. The spectra in figs. 9a and 9b labelled as off-resonance spectra were taken at a proton energy a few keV below the 1.75-MeV $C^{13}(p,\gamma)N^{14}$ resonance; all other spectra shown were taken on the 1.75-MeV resonance. Energy adjustments of the analyser window to obtain gate signals: a) 2.8 to 3.8 MeV; b) 4.0 to 5.35 MeV; c) 5.5 to 6.8 MeV; d) 7.3 to 9.2 MeV.

7.3 MeV. The result of this experiment is shown in fig. 10; it is seen from this figure that the peak due to 2.73-MeV gamma rays has disappeared while a peak at 2.14-MeV appears. This experiment confirms that the 2.14-MeV gamma rays are due to a transition from the 9.17-MeV level to the 7.03-MeV excited state. A peak at 7.03 MeV is also observed in the spectrum of fig. 7 (where the analyser window had been placed on the low energy gamma rays).

Gamma rays showing up on the side of the 2.73-MeV one-quantum escape peak in fig. 6 have been labelled as 2.31-MeV radiation and as the 2.73-MeV Compton edge. By replacing the target by a RaTh-source which emits gamma rays of 2.62 MeV, it was shown that the Compton edge yields an appreciable

contribution to the one-quantum escape peak at this energy and a spectrum is obtained which shows a broadened one-quantum escape peak similar to the one observed in fig. 6 for the 2.73-MeV radiation. However, it seems quite possible that some 2.31-MeV radiation also shows up in fig. 6 because this level is populated in so many different ways that gate signals might be expected due to coincident gamma rays belonging to a cascade transition leading to the 2.31-MeV state.

The coincidence spectrum taken with the analyser window counting the low energy portion of the spectrum which is shown in fig. 7 agrees with the conclusions drawn previously. All the gamma rays which have been labelled in this figure have been discussed above except the gamma rays labelled as 1.64-MeV and 2.49-MeV radiation. Possible gamma rays of this energy were also observed in the three-crystal pair spectra shown in figs. 1 and 3; however, the presence of these gamma rays could not be conclusively established. Comparison of the

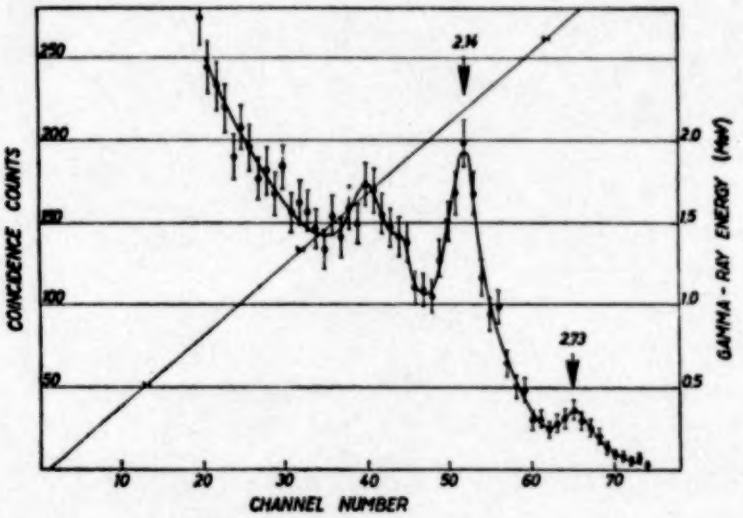

Fig. 10. Spectrum of the gamma rays from the $C^{13}(p,\gamma)N^{14}$ reaction at the 1.75-MeV resonance in coincidence with 6.7- to 7.3-MeV radiation. The crystal used to obtain the display spectrum was a 7.6 by 7.6 cm NaI(Tl) crystal and was placed at 90° to the proton beam and approximately 3 cm from the target. The crystal used to obtain gate signals was a 10.2 by 10.2 cm NaI(Tl) crystal and was placed at 90° to the beam and approximately 3 cm from the target. The spectrum corresponds to an integrated charge of 6.5 mC and was taken with a 1.2 μA beam.

intensities of 6.44-MeV and 2.73-MeV radiation given in table 1 yields some argument that these gamma rays could be due to a decay of the 6.44-MeV state to the 3.95-MeV second excited state. A possible contribution of 2.79-MeV gamma rays to the 2.73-MeV radiation is too small to bring the intensities of the 2.73-MeV and 6.44-MeV radiations into agreement, provided one does not overemphasize the errors. In order to obtain further information about the 1.64-MeV and 2.49-MeV gamma rays coincidence measurements were made with a narrow analyser window on the 2.73-MeV radiation full energy loss peak

counting gamma rays from 2.6 up to 2.9 MeV. A spectrum obtained in this manner has been displayed in fig. 11 and it is seen that the 1.64-MeV peak shows up strongly together with a peak at 2.31 MeV. The full energy loss peak caused by 2.49-MeV gamma rays is not resolved from the 2.31-MeV peak. The analyser window will also register 2.79-MeV gamma rays due to the 5.10 → 2.31 MeV

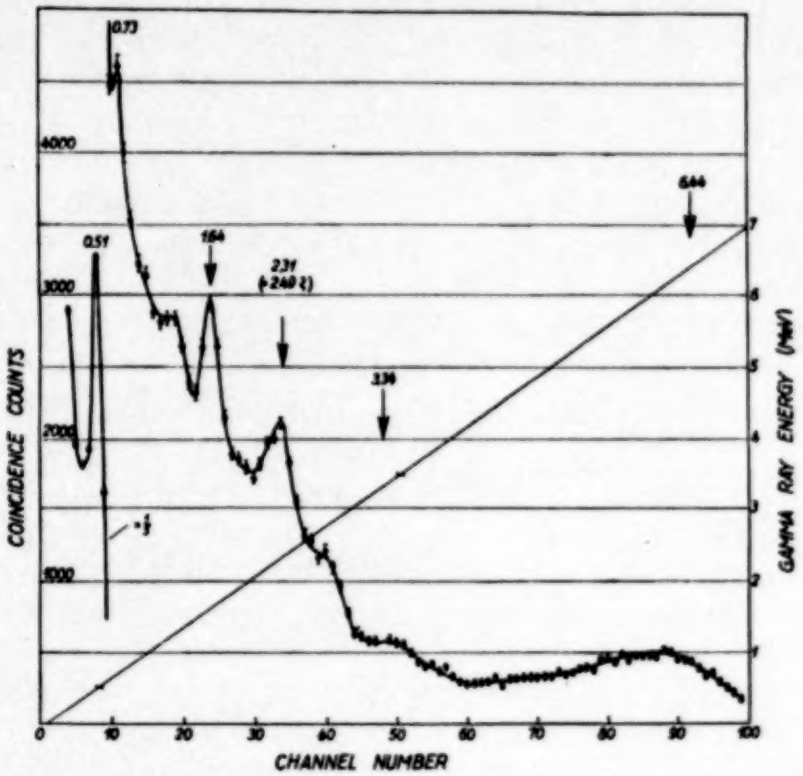

Fig. 11. Spectrum of the gamma rays from the $C^{13}(p,\gamma)N^{14}$ reaction at the 1.75-MeV resonance in coincidence with 2.6- to 2.9-MeV radiation. The crystal used to obtain the display spectrum was a 7.6 by 7.6 cm NaI(Tl) crystal and was placed at 90° to the proton beam and approximately 3 cm from the target. The crystal used to obtain gate signals was a 10.2 by 10.2 cm NaI(Tl) crystal and was placed at 90° to the beam and approximately 3 cm from the target. The spectrum corresponds to an integrated charge of 60 mC and was taken with a 6 μA beam.

transition and—in addition—part of the one-quantum escape peak due to the 3.34-MeV radiation populating the 5.83-MeV level. Therefore, the 2.31-MeV radiation observed in the spectrum of fig. 11 will be stronger than expected from the decay of the 3.95-MeV state to the 2.31-MeV level alone, and therefore stronger than the 2.49-MeV gamma radiation. Furthermore, one quantum escape peaks due to the 3.38- and 3.48-MeV gamma radiations will also cause coincidence signals and, therefore, some radiation at an average energy of 3.43 MeV will be detected (as has been described in the explanation of the spectrum shown in fig. 8). Finally the 6.44-MeV gamma rays—of course—will be gated too. The experiment has been repeated using a different gain and spreading the low energy portion of the spectrum such that the well-isolated 1.64-MeV

peak appeared at channel 80 of the 100-channel analyser. This spectrum also showed the 0.73-MeV gamma rays which have been discussed above. Now, the analyser window was adjusted to count gamma rays between 3.3 and 3.6 MeV. The 1.64-MeV peak disappeared while the 0.73-MeV peak stayed the same. Therefore it seems very likely that the 1.64-MeV radiation is due to a decay mode of the 6.44-MeV level. If this level branches to the 3.95-MeV second excited state via a 2.49-MeV gamma ray, both the 2.49-MeV and 1.64-MeV radiation can be explained, because the 3.95-MeV state is known to decay to 95 % to the 2.31-MeV first excited state[13]).

From fig. 6 (and possibly fig. 11) it also seems possible that some radiation of approximately 1.35 MeV is present in the spectra shown in these figures, although at approximately this energy the two-quantum escape peak of the 2.31-MeV radiation and the Compton edge of the 1.64-MeV gamma rays are expected. If the 1.35-MeV radiation really is present, the source of this radiation has not been determined. It would therefore be a rather speculative suggestion that this radiation could be related to a population mode of the 5.69-MeV state from the 7.03-MeV level (it has been pointed out above that the 5.69-MeV state might be populated in part via an intermediate state), especially since this radiation does not seem to be present in the spectrum of fig. 8. All further coincidence measurements using narrow analyser windows with a width of 0.5 MeV counting gamma rays lower in energy than the strongest low energy radiation of 2.73 MeV failed. The reason for this is that a window adjusted this way counts Compton background and escape peaks due to all gamma rays higher in energy. Thus the spectrum obtained in this manner is too complex to yield any reliable information.

4. Analysis of Results and Conclusions

In fig. 12 is shown the decay scheme of the 9.17-MeV level obtained from the investigations described in sects. 2 and 3. The branching ratios were calculated from the relative intensities given in table 1. The branch to the 6.44-MeV excited state was previously obtained by Woodbury *et al.*[8]), who reported the intensity of this branch to be 10 % of the intensity of the 9.17 MeV → ground-state transition. The result given in fig. 12 is in perfect agreement with the observations of Woodbury *et al.* The spin assignments of the 9.17- and 6.44-MeV levels have been taken from ref. [6]). The spin assignments given to the 5.83- and 5.10-MeV levels were obtained recently[10]). The parity assignments of the 9.17-MeV level and proposed parity assignments of the 5.83- and 5.69-MeV levels have been taken from refs. [5]) and [10]), respectively. The spin assignment of the 5.69-MeV level and the spin-parity assignments of the 2.31, 3.95 MeV levels and the ground state have been taken from ref. [13]).

The value for the branch to the 5.69-MeV excited state is given in fig. 12 as an

upper limit. It was pointed out in sect. 2 that the intensity of the 3.5-MeV gamma rays observed in three-crystal pair spectra measurements is due at least 75 % to the 3.51-MeV gamma radiation from N^{13}. If, therefore, the 5.69-MeV level were populated 100 % by a direct transition from the 9.17-MeV state via a 3.48-MeV gamma transition, 8 of the 17 intensity units of the 3.5-MeV gamma rays in table 1 would be needed to explain the intensity of 3 units of the 5.69-MeV gamma rays given in table 1 (taking into account that the

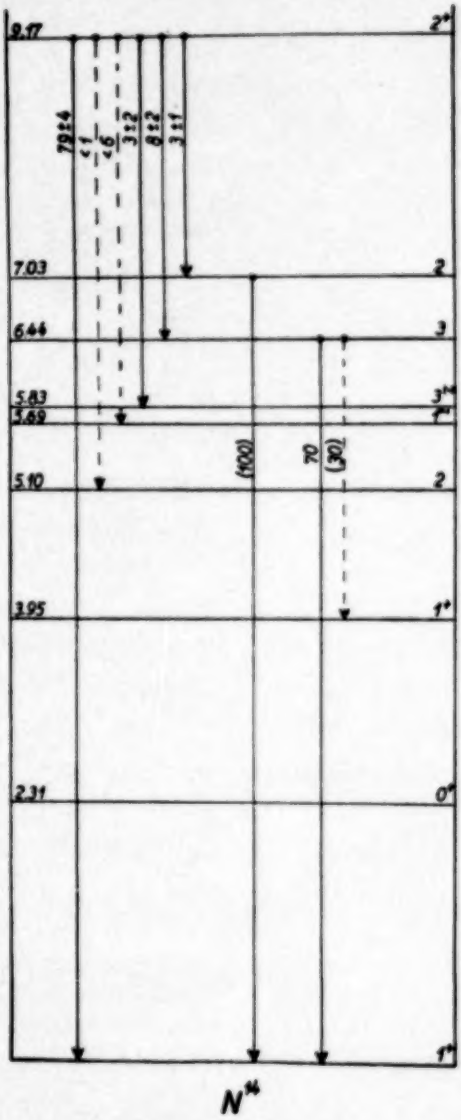

Fig. 12. The decay scheme of the N^{14} 9.17-MeV level as determined in the present work. Only the levels involved in the decay of the 9.17-MeV level are shown. The spin and parity assignments are discussed in the text. Broken arrows denote uncertain transitions.

branch 5.69 → 2.31 MeV, also yields gamma rays of 3.38 MeV which contribute to the 3.5-MeV peak). Also the coincidence measurements described in sect. 3 gave some reason to believe that it is quite well possible that the 5.69-MeV

state is populated indirectly via a level between 9.17 and 5.69 MeV. The transitions associated with this cascade could easily have escaped observation because of their weakness and because the various gamma rays observed in coincidence measurements could easily cover them. Although the coincidence measurements described in sect. 3 gave reason to believe that at least part of the population of the 5.69-MeV state is due to a direct transition from the 9.17-MeV state, the transition has been represented in fig. 12 by a dotted line.

The presence of transitions to the 5.83- and 7.03-MeV states was confirmed by the coincidence measurements described in sect. 3. It is not certain if an extremely weak direct transition exists to the 5.10-MeV state and an upper limit on such a transition has been placed in fig. 12 from three crystal pair spectra measurements described in sect. 2 and from the lack of observation of 4.07-MeV gamma rays in the coincidence measurements described in sect. 3.

A branch of the 6.44-MeV state to the 3.95-MeV level has not been assigned for certain in fig. 12. This is because 1.64-MeV and 2.49-MeV gamma rays were not established for certain. Coincidence measurements described in the last paragraphs of sect. 3 suggest this branch in the decay of the 6.44-MeV state.

Partial gamma widths Γ_γ^f and matrix elements $|M|^2$ in Weisskopf units for the primary transitions from the 9.17-MeV excited state calculated for the lowest two multipolarities possible in each case are given in table 3. The matrix element $|M|^2$ is defined as the ratio Γ_γ^f to the Weisskopf single particle estimate[14]) of the radiative width of the transition. The values have been calculated from the branching ratios given in fig. 12 and the known gamma width Γ_γ^f of the 9.17 MeV → ground-state transition[7]). By comparison with available experimental and theoretical information[15, 16, 17]) it appears from table 3 that all the transitions are—at least partially—dipole in character. An upper limit of 25 (i.e. collective enhancement by all the protons outside the 1s shell) can be assumed as a conservative limit for the matrix element $|M|^2$ for quadrupole radiation[10]). Since the 5.83-MeV level has an assignment of $J = 3$

TABLE 3

Partial gamma widths and Weisskopf matrix elements for the primary gamma rays observed at the 1.75-MeV resonance

Transition	Γ_γ^f (eV)	$\|M\|^2$			
		E1	M1	E2	M2
9.17 — 0	8.7[a]	0.018	0.53	33.2	1060
9.17 — 5.69	< 0.65	< 0.024	< 0.74	< 314	< 10000
9.17 — 5.83	0.33	0.014	0.42	196	6200
9.17 — 6.44	0.87	0.066	2.03	1700	54000
9.17 — 7.03	0.33	0.053	1.60	1820	57500

[a] See ref. 7).

and since the strength of the ground-state transition limits the spin of the 9.17-MeV excited state to $J \leq 2$ the transition 9.17 → 5.83 MeV supports the assignment $J = 2$ given recently to the 9.17-MeV state on the basis of angular correlation measurements[6]).

The 5.69-MeV level has a spin assignment[13]) of $J = 1$ and a favoured odd parity assignment[10, 4]). Only an upper limit on the strength of the transition 9.17 → 5.69 MeV could be placed in the present paper and consequently no confirmation of these assignments can be gained from this transition. The 5.83-MeV and 5.69-MeV states have been proposed[10, 4]) as members of the four $T = 0$ lowest odd parity states in N^{14} arising from $(p_{\frac{1}{2}}\, s_{\frac{1}{2}})$ and $(p_{\frac{1}{2}}\, d_{\frac{1}{2}})$. The transitions to these states from the 9.17-MeV $J^\pi = 2^+$ state may lead to further understanding of the eigenfunctions as well of the odd parity states as of the 9.17-MeV state.

The transition 9.17 → 6.44 MeV is proved by the results of table 3 to have negligible quadrupole admixture. This fact has been used in assigning the 9.17-MeV state $J = 2$ and the 6.44-MeV state $J = 3$[6]). Furthermore, it is seen from table 3 that the 9.17 → 7.03 MeV transition must be predominantly dipole. Any quadrupole admixture will be much too small to influence the conclusions which are to be drawn from the anisotropy of this transition.

TABLE 4

Comparison of the experimental and theoretical anisotropies corresponding to the decay scheme of fig. 12

Transition	A (experimental) [a])	A (theoretical)
9.17 — 0	-0.55 ± 0.02	−0.45
9.17 — 6.44	-0.12 ± 0.20 [b]	−0.14
9.17 — 7.03	$0 < A$	0.64
7.03 — 0	$A < -0.35$	−0.24
6.44 — 0	0.61 ± 0.32	0.62
5.69 — 0	-0.55 ± 0.30	0.28
5.10 — 0	-0.32 ± 0.20	−0.32 [c]
2.31 — 0	-0.04 ± 0.16	0

[a] See table 1.
[b] Corrected for contributions from 5.10 → 2.31.
[c] If populated via the 5.83-MeV state.

Using the spin-parity assignment $J^\pi = 2^+$ of the 9.17-MeV state and assuming p-wave formation of this state with negligible f-wave admixture, the angular distribution of the gamma rays about the beam have been calculated. The anisotropies of these distributions have been given in table 4 for pure transitions of lowest multipole order. For convenience of comparison the experimentally determined anisotropies from table 1 have been repeated in table 4. The known

spin assignments[6, 13]) of the levels involved as given in fig. 12 have been used for the calculations of the distributions. An assignment of $J = 2$ has been given to the 7.03-MeV level on the basis of the positive anisotropy of the 9.17 → 7.03 MeV transition determined in the present investigation. It can easily be shown that for pure dipole radiation following the capture of a p-wave proton by the C^{13} nucleus into a $J = 2$ state the anisotropy is positive only if the initial and final state of the (primary) transition have the same spin. The distribution of the 9.17 → 7.03 MeV transition shows positive anisotropy and, therefore, the spin of the 7.03-MeV state is $J = 2$. This conclusion agrees with the spin assignment proposed in a previous paper[10]) and remains valid even if f-wave admixture in the formation of the 9.17-MeV state is taken into account. In case the 7.03-MeV state were $J = 3$ the anisotropy stays between —0.19 and —0.12 for any mixture of p- and f-waves. If the 7.03-MeV state were $J = 1$ the anisotropy also stays negative with values between —0.57 and —0.37. These values are obtained for pure dipole character of the 9.17 → 7.03 MeV transition (compare table 3) and taking into account the phase shift between p- and f-waves when forming the 9.17-MeV state by proton capture. It is seen from table 4 that —with the exception of the 5.69 MeV → ground-state transition and the 7.03 MeV → ground-state transition†—the experimentally determined anisotropies agree with the theoretical ones for pure dipole radiation. The anisotropy of the 3.5-MeV gamma rays (table 1) has not been included in table 4 because of the many different contributions to this radiation.

The measured anisotropy of the 5.69 MeV → ground-state transition does not agree with the theoretical one. A high quadrupole admixture would be needed to give agreement. This is true if the 5.69-MeV level is directly populated from the 9.17-MeV state. Since the 5.69-MeV state has $J = 1$ and proposed odd-parity assignment[4, 10, 13]) this admixture would have to be M2. However, it has been pointed out that the 5.69-MeV state might be populated in part via an intermediate state.

As to the anisotropy of the 2.73-MeV radiation due to the 9.17 → 6.44 MeV transition, it should be mentioned that the experimentally determined anisotropy given in table 1 is caused not only by the angular distribution of the 9.17 → 6.44 MeV transition but also by the angular distribution of the 2.79-MeV gamma rays due to the 5.10 → 2.31 MeV transition. The influence of the 2.79-MeV radiation on the anisotropy given in table 1 can be calculated because all spins in the cascade transition 9.17 → 5.83 → 5.10 → 2.31 MeV are known and because the 5.10 → 2.31 MeV transition must be pure quadrupole. Admixtures of higher multipole orders in the preceeding transitions 9.17 → 5.83 → 5.10 MeV will enter only with δ^2, where δ is the ratio of the reduced matrix elements of quadrupole and dipole radiation in a preceding transition. From

† The 9.17-MeV → ground-state transition anisotropy has no concern with the present paper.

table 1 it appears that 2 ± 1 of the intensity units of the (2.73-MeV + 2.79-MeV) radiation are due to 2.79-MeV gamma rays from the transition 5.10 → 2.31 MeV. The anisotropy of the 2.79-MeV gamma ray distribution is calculated to be $A = 0.62$. Using these values and the value for A given in table 1 the anisotropy of the 2.73-MeV radiation alone is obtained to be $A_{2.73} = -(0.12 \pm 0.2)$. This value definitely excludes that the 9.17-MeV and the 6.44-MeV states both have $J = 2$, which fact has been used[6]) when assigning spins to the 9.17-MeV and the 6.44-MeV states. ét has been shown in ref. [6]) that this conclusion remains valic even if f-wave contributions in the formation of the 9.17-MeV state are taken into account.

The theoretical value for the anisotropy of the 5.10 MeV → ground-state transition given in table 4 has been calculated assuming that the 5.10-MeV level is populated via the 5.83-MeV excited state. Analysis of the angular distribution of the 5.10 MeV → ground-state transition following the capture of protons into the N^{14} 9.50- and 8.90-MeV levels[10]) yielded $0.1 < |\delta| < 0.2$ as the value for the quadrupole-dipole mixture in the 5.10 MeV → ground-state transition. This analysis did not take into account octupole admixtures. WP have pointed out that—in the case that the 5.10-MeV state arises from $(p_{\frac{1}{2}}\, d_{\frac{5}{2}})$ as $J^\pi = 2^-$, $T = 0$ state—a contribution of E3 radiation should be expected in the 5.10 MeV → ground-state transition. Therefore, the assumption made in general for the calculations of the theoretical anisotropies given in table 4, namely that admixtures of higher multipole orders can be neglected, could be violated in the case of the 5.10 MeV → ground-state transition. No further information about admixtures of higher multipole orders in this transition can be gained from the present investigation because of the large experimental uncertainties.

In view of the large experimental errors only in one case an attempt has been made to put limits on the higher multipole admixtures. From table 4 it is seen that the 7.03 MeV → ground-state transition shows an anisotropy which is stronger than expected if the transition were pure dipole in character. In fig. 13 the anisotropy A of the 7.03 MeV → ground-state transition following the formation of the 9.17-MeV level by p-wave protons and assuming a spin sequence 2 — 2 — 1 for the transition 9.17 → 7.03 MeV → ground state has been plotted. The figure shows the dependence of the anisotropy on the multipole mixture $|\delta|$. Furthermore, the limit on A imposed by the experimental result given in table 4 has been included in fig. 13. From this figure limits on the quadrupole-dipole mixture of $0.13 < \delta < 3.5$ in the 7.03 MeV → ground-state transition are obtained.

It has been pointed out in the introduction that—if the 9.17-MeV state is a possible candidate for the missing (2,1) state arising from p^{-2}—there should be expected a branch to a 2^+ state around 6 MeV. The intensity of this branch is expected between 2 and 12 % of the intensity of the 9.17 MeV → ground-state

transition (the specific value—of course—depending on the location of the levels). The only level with $J = 2$ for which a branch from the 9.17-MeV state is observed is the $J = 2$, 7.03-MeV state. Furthermore, this state almost certainly is $T = 0$ (compare for instance WP). Assuming the 9.17-MeV and the 7.03-MeV states as (2,1) and (2,0) states arising from p^{-2} and using the transi-

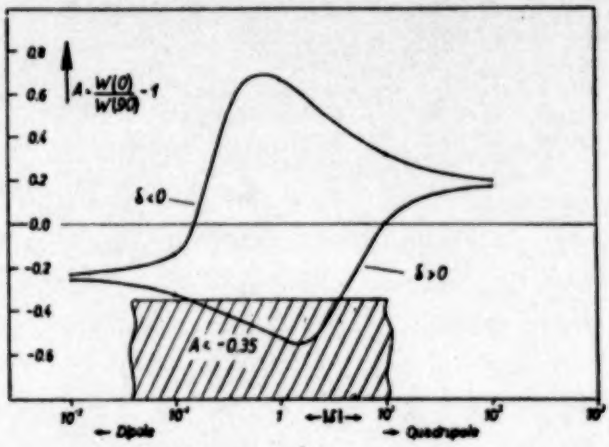

Fig. 13. The anisotropy of the 7.03 ($J = 2$) → ground-state ($J = 1$) gamma transition following the formation of the 2^+, N^{14} 9.17-MeV level by p-wave protons. The transition is assumed to be a mixture of dipole and quadrupole radiation with an intensity ratio $\delta^2 = \Gamma_\gamma^\gamma(2)/\Gamma_\gamma^\gamma(1)$. This figure shows a function of $|\delta|$ the anisotropy A of the angular distribution of the gamma transition relative to the proton beam. Each one of the two curves corresponds to a definite sign of δ. The two curves were calculated from the theoretical angular distribution function:

$$W(\Theta) = 1 - (0.175 + 0.784\delta - 0.125\delta^2)\,(1 + \delta^2)^{-1} P_2(\cos\Theta).$$

The measured anisotropy is also shown and limits the possible values of δ to $0.13 < \delta < 3.5$.

tion strengths A (which essentially are identical with reduced matrix elements) WP give for the (2,1) → (2,0) and (2,1) → (1,0)-ground-state transitions a branching ratio of 2 % is calculated. This is in good agreement with the experimental result of the present paper (table 1). It therefore seems very likely that the 7.03-MeV level is the (2,0) p^{-2} state in question and—vice versa—that the 9.17-MeV level arises at least partially from p^{-2}.

This conclusion does not preclude contributions from other configurations to the total eigenfunction of the 9.17-MeV level. In fact, the disagreement of the observed gamma width of the 9.17 MeV → ground-state transition with the value expected if the 9.17-MeV state were pure p^{-2} (cf. sect. 1) and the observed proton width indicate that the total eigenfunction of the 9.17-MeV state contains considerable contributions from other configurations (most likely from p^8sd). This point has been discussed extensively by WP.

A comparison of the experimentally determined value for the quadrupole-dipole mixture δ (fig. 13) with the theoretical results of WP should yield a check on the conclusion that the 7.03-MeV state (very likely) arises from p^{-2}. Unfortunately such a comparison can be made only in so far as $|\delta|$ is concerned. This is due to the fact that the phase conventions, which have been

used in the existing publications on triple angular correlation theory, have not been stated unambiguously to the extent that a comparison could easily be made amongst different authors. The value for $|\delta|$ obtained from fig. 13 is to be compared to the theoretical values for $|\delta|$ of 0.42, 0.30 and 0.25 which can be calculated from the relative strengths of quadrupole to dipole radiation in the transition $(2,0)p^{-2} \rightarrow (1,0)p^{-2}$ WP obtained from *jj*-coupling, Elliott or Visscher-Ferrell eigenfunctions, respectively.

In conclusion, the author wishes to express his sincere thanks to his friend E. K. Warburton at Princeton for many helpful comments and for invaluable discussions in a continual exchange of letters during the progress of this work. Furthermore, he should like to express his thanks to F. Riess and W. Trost for their active help in taking and evaluating the data and for many discussions about their interpretation.

References

1) J. P. Elliott, Phil. Mag. **1** (1956) 503
2) W. M. Visscher and R. A. Ferrell, Phys. Rev. **107** (1957) 781
3) J. P. Elliott, private communication
4) E. K. Warburton and W. T. Pinkston, Phys. Rev. **118** (1960) 733
5) A. A. Strassenburg, R. E. Hubert, R. W. Krone and F. W. Prosser, Bull. Am. Phys. Soc. **3** (1958) 372
6) H. J. Rose, W. Trost and F. Riess, Nuclear Physics **12** (1959) 510
7) S. S. Hanna and L. Meyer-Schützmeister, Phys. Rev. **115** (1959) 986
7a) S. S. Hanna and L. Meyer-Schützmeister, Phys. Rev. **108** (1957) 1644
8) H. H. Woodbury, R. B. Day and A. V. Rollestrup, Phys. Rev. **92** (1953) 1199
9) E. K. Warburton and H. J. Rose, Phys. Rev. **109** (1958) 1199
10) E. K. Warburton, H. J. Rose and E. N. Hatch, Phys. Rev. **114** (1959) 214
11) H. J. Rose, F. Riess and W. Trost, Nuclear Physics (in print)
12) N. Jarmie and J. D. Seagrave, Charged Particle Cross Sections, Los Alamos Report 2014
13) F. Ajzenberg-Selove and T. Lauritsen, Nuclear Physics **11** (1959) 1
14) V. F. Weisskopf, Phys. Rev. **83** (1951) 1073
15) D. H. Wilkinson, Phil. Mag. **1** (1956) 127 and Proceedings of the Rehovoth Conference on Nuclear Structure, edited by H. J. Lipkin (North-Holland Publishing Company, Amsterdam, 1958), Session 4, p. 175
16) G. Morpurgo, Phys. Rev. **110** (1958) 721
17) E. K. Warburton, Phys. Rev. **113** (1959) 595

I.D.1: E.1 *Nuclear Physics* **19** (1960) 140—147; © *North-Holland Publishing Co., Amsterdam*
Not to be reproduced by photoprint or microfilm without written permission from the publisher

THE NUCLEAR SPINS OF I^{126}, I^{132}, I^{133} AND I^{135}

HUGH L. GARVIN† and EDGAR LIPWORTH

Lawrence Radiation Laboratory and Department of Physics, University of California, Berkeley, California††

Received 8 April 1960

Abstract: This paper reports some recent results of a continuing program to determine the nuclear spins, magnetic moments and electric quadrupole moments of the radioactive halogen isotopes by the method of atomic beams. The determination of the ground-state spins of radioactive isotopes is particularly important for the interpretation of radioactive decay patterns, and the measurements of nuclear spins and moments provide experimental evidence for the formulation and evaluation of nuclear-structure theories. This work completes the measurement of the nuclear spins of the series of iodine isotopes I^{123} to I^{135} with the exception of the 52-min I^{134} isotope. The nuclear spins of I^{126}, I^{132}, I^{133} and I^{135} are 2, 4, $\frac{7}{2}$ and $\frac{7}{2}$, respectively. The nuclear spins of the iodine isotopes I^{123} to I^{135} are now know with the exception of the 52 min I^{134} isotope.

1. Method

The atomic-beam apparatus used for these measurements was especially designed for use with radioactive volatile materials. Although similar in principle to the standard Atomic-Beam "flop-in" apparatus[1]), it differs from it in many constructional details, which have been described in a previous report[2]). The method of determination of spin of radioactive isotopes in atomic-beam experiments has also been discussed in detail in several recent publications[2–4]) and only a brief summary is presented here.

The electronic ground state of all halogen atoms is $^2P_{\frac{3}{2}}$, and thus, with normal ordering of the hyperfine levels, there are in general two observable flop-in transitions for which the resonance frequencies are unique functions of the value of nuclear spin and magnetic field. For $I > 0$ these transitions, designated α and β, are

$$\alpha\colon\quad (F = I + \tfrac{3}{2}\,,\quad M_F = -I + \tfrac{1}{2}) \longleftrightarrow (F = I + \tfrac{3}{2}\,,\quad M_F = -I - \tfrac{1}{2})$$

and

$$\beta\colon\quad (F = I + \tfrac{1}{2}\,,\quad M_F = -I + \tfrac{3}{2}) \longleftrightarrow (F = I + \tfrac{1}{2}\,,\quad M_F = -I + \tfrac{1}{2})\,,$$

where F is the total angular-momentum quantum number of the atom, I the nuclear-spin quantum number, and M_F the projection of the total angular momentum along the direction of quantization. In order to determine the spin of an isotope unequivocally, these resonances are observed at several different

† Present address: John Jay Hopkins Laboratory for Pure and Applied Science, General Atomic Division of General Dynamics Corp., San Diego, California.

†† Work done under the auspices of the U.S. Atomic Energy Commission.

values of the magnetic field. The resonances are detected by allowing the beam to fall upon silver-coated collection buttons which are subsequently counted in continuous-flow proportional counters. The magnitude of the resonance signal is indicated by the counting rates of the buttons. The isotope contributing to the signal is identified by its radioactive decay properties.

The beam of iodine atoms is formed by attaching a vial containing a mixture of radioactive and natural iodine to a heated platinum dissociation tube heated by electron bombardment to about 700° C to dissociate the iodine molecules to atoms[5]). The vapour pressure of iodine at room temperature is adequate for the maintenance of the beam. On some occasions a radio-frequency discharge tube has been employed[2]).

2. Sample Preparation

Owing to the wide range of masses embraced by the isotopes studied here, several different methods are required for the production and separation of the radioactive samples.

IODINE-126

The bombardment of a foil of natural tellurium metal by 12-MeV protons produces 28-min I^{128}, 12.6-h I^{130}, 4-d I^{124} and 13-d I^{126} by the (p, n) reaction. Following a bombardment in the Berkeley 152 cm cyclotron, the tellurium target is dissolved in HNO_3 with some iodine carrier (NaI) and the solution made basic with NaOH. Formic acid is added to precipitate the tellurium as TeO_2, leaving the active iodine in solution. The solution is made slightly acidic with H_2SO_4 and $NaNO_2$ solution is added to oxidize the iodine to its elemental state so that it can be readily extracted into CS_2. Natural iodine carrier is dissolved in the CS_2. The solution is mixed thoroughly and the CS_2 is evaporated off, leaving the crystalline mixture of active and natural iodine in a glass vial which is attached directly to the atomic-beam apparatus.

IODINE-132

The 2.3-h I^{132} is conveniently obtained by a "milking process" from the 77-h Te^{132} parent in an iodine generator provided by the Brookhaven National Laboratory[6]). The tellurium is adsorbed in an alumina mesh within the generator, and the iodine is removed by flushing with 25 ml of 0.01 *M* NH_4OH solution. The active iodine is oxidized and extracted from the solution as described above. The generator regains its secular equilibrium in approximately 12 hours, and fresh samples of I^{132} may be removed at 12-hour intervals if desired. One iodine generator originally charged with 108 mc of I^{132} provided sufficient amounts of I^{132} to measure the nuclear spin and to obtain preliminary values of the nuclear moments.

IODINE-133

The 21-h I^{133} isotope is obtainable as a reactor fission product from the Brookhaven National Laboratory. It is received as NaI in aqueous solution from which the I^{133} is easily extracted. Some I^{131} (8-d activity), whose spin is also $\frac{7}{2}$, is present with the I^{133} in the sample, and decay analysis was necessary to ensure correct identification of the observed resonance signals.

IODINE-135

The iodine isotopes I^{131} to I^{135} are obtained as fission products after the deuteron bombardment of U^{238}. The uranium targets used were in the form of thin uranium foils. As I^{132} and I^{133} are more easily and economically obtained in the ways already described, the method of uranium bombardment was used only for the production of 6.7-h I^{135} and 52-min I^{134}. The target foils of uranium are bombarded with 24-MeV deuterons in the Berkeley 152 cm cyclotron and then dissolved in HCl. The solution (to which carrier has been added) is diluted and $NaNO_2$ added to oxidize the iodine to elemental form. The final extraction proceeds as described earlier. This method of separation, though simple, yielded sufficient activity for successful measurements on I^{135} but a more rapid method would be advantageous for measurements on the short-lived I^{134}.

3. Results

The results of spin measurements on I^{126}, I^{132}, I^{133} and I^{135} are summarized in table 1. The magnetic field values at which α and β resonance were observed

TABLE 1

Results of spin measurements

Isotope	Half life	Spin value	Magnetic field at which resonances (both α and β) were observed (gauss)				
I^{126}	13 d	2	0.71	1.42	6.92		
I^{132}	2.3 h	4	2.82	6.92	13.42	25.39	46.08
I^{133}	21 h	$\frac{7}{2}$	2.82	6.92	13.42		
I^{135}	6.7 h	$\frac{7}{2}$	2.82	6.92	10.87		

are indicated. Fig. 1 shows the results of a spin search on a radioactive iodine sample produced by the (p, n) reaction on tellurium. The high-counting resonance buttons at spins 5(α) and 5(β) were decayed and the signals found to be due[7]) to 12.6-h I^{130}. The signal at spin 2 is due to contributions from both a 2(α) and a 2(β) transition, and its decay was consistent with published half-life values for I^{126}. Complete radio-frequency resonances were traced at magnetic fields where the 2(α) and 2(β) resonances were resolved (see fig. 2).

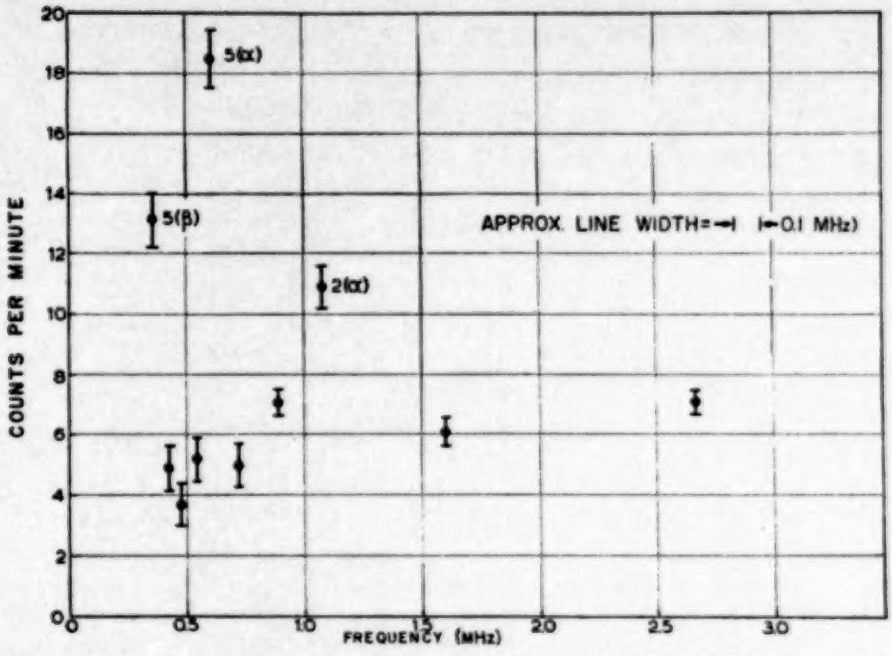

Fig. 1. Spin search on a radioactive iodine sample at a field of 1.43 G. The high counting buttons at 0.35, 0.62 and 1.14 MHz are due respectively to resonances 5(α), 5(β) in I^{130} and to a resonance 2(α) in I^{126}.

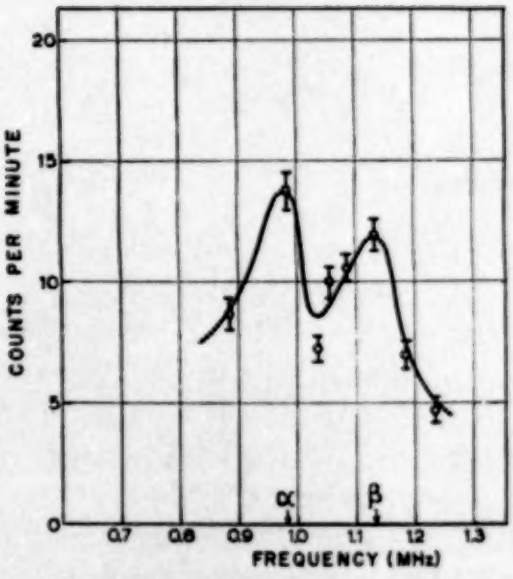

Fig. 2. Resolved 2(α) and 2(β) resonance observed in I^{126}.

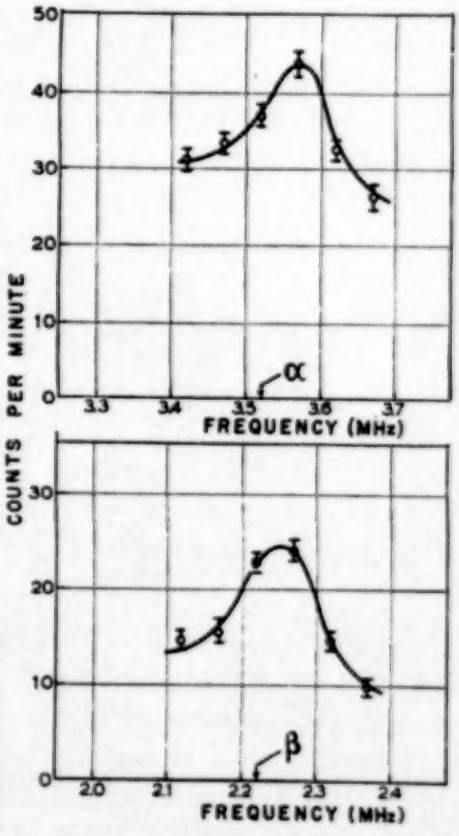

Fig. 3. Complete radio-frequency resonance for I^{132}.

Figures 3, 4 and 5 show radio-frequency resonances observed in I^{132}, I^{133} and I^{135}. The fission-produced samples contain some I^{131}, I^{133} and I^{135} and each has spin $\frac{7}{2}$ therefore, as mentioned earlier, the decays of the spin-$\frac{7}{2}$ resonance are complex because of the several components present.

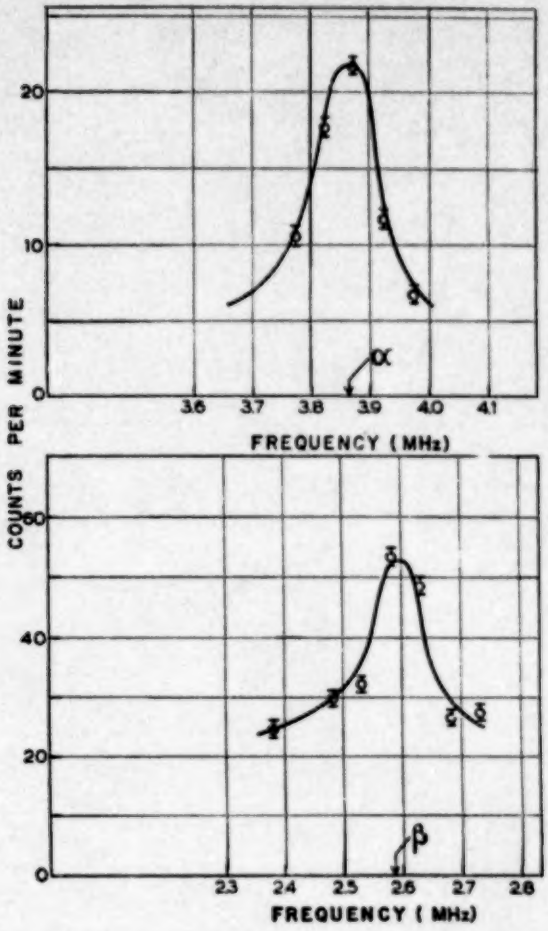

Fig. 4. Complete radio-frequency resonance for I^{133}.

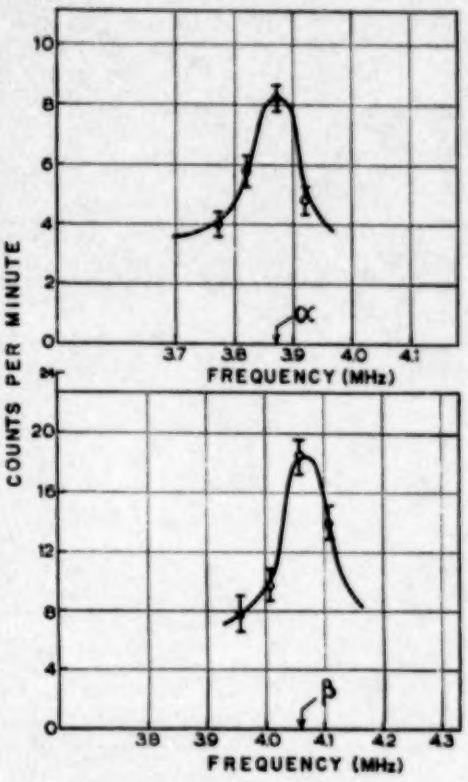

Fig. 5. Complete radio-frequency resonance for I^{135}.

4. Discussion

With the exception of I^{134}, the nuclear spins of the iodine isotopes I^{123} to I^{135} are now known. The results are summarized in table 2 together with odd-proton and odd-neutron level assignments that lead at least to the correct spin values of the ground states if not in all cases to the correct parity where it is known. In those instances in which the neutron number N is even the unpaired 53rd proton in iodine is reasonable assigned to the $4d_{\frac{3}{2}}$ level for $N < 76$, while for $N > 76$ the most reasonable assignments is to the level $5g_{\frac{7}{2}}$.

The nuclear spins of the odd-neutron nuclei are consistently $\frac{1}{2}$ for $N = 65$ to $N = 75$, but from $N > 76$ to $N < 82$ the observed spins are $\frac{3}{2}$. It is not unreasonable to suppose that these spin values arise from the $3s_{\frac{1}{2}}$ and $4d_{\frac{3}{2}}$ levels

TABLE 2

Known spins of iodine isotopes I^{123} to I^{135}

Proton assignment	Neutron assignment	Shell-model or Nordheim-rule spin prediction	Observed spins (and references)												
			I^{123} [a]	I^{124} [a]	I^{125} [b]	I^{126} [c]	I^{127} [d]	I^{128} [e]	I^{129} [f]	I^{130} [g]	I^{131} [h]	I^{132} [c]	I^{133} [c]	I^{134}	I^{135} [c]
$(5g_{\frac{7}{2}})^2\,(4d_{\frac{5}{2}})$	even	$I = \frac{1}{2}$	$\frac{1}{2}$		$\frac{1}{2}$		$\frac{1}{2}$								
$(5g_{\frac{7}{2}})^3$	even	$I = \frac{7}{2}$							$\frac{7}{2}$		$\frac{7}{2}$		$\frac{7}{2}$		$\frac{7}{2}$
$(5g_{\frac{7}{2}})^2\,(4d_{\frac{5}{2}})$	$(3s_{\frac{1}{2}})$	$2 < I \leqslant 3$ weak		2		2									
	$(4d_{\frac{3}{2}})$	$I = 1$ strong						1							
$(5g_{\frac{7}{2}})^3$	$(3s_{\frac{1}{2}})$	$I = 3$ strong													
	$(4d_{\frac{3}{2}})$	$2 < I \leqslant 3$ weak								5		4		?	

The single-particle shell-model configurations for I^{124} and I^{126} do not give rise to the ground-state parity believed correct (see text), but are included because of the simple spin classification that results.

[a] Garvin, Green and Lipworth, Phys. Rev. **111** (1958) 534
[b] P. C. Fletcher and E. Amble, Phys. Rev. **110** (1957) 536
[c] This paper
[d] K. Murakawa, Sci. Papers Inst. Phys. Chem. Research (Tokyo) **20** (1933) 285; Z. Physik **109** (1938) 162
[e] J. W. Sherwood and S. J. Ovenshine, Phys. Rev. **114** (1959) 858
[f] Livingston, Gilliam and Gordy, Phys. Rev. **76** (1949) 149
[g] Garvin, Green and Lipworth, Phys. Rev. Letters **1** (1958) 292; J. E. Sherwood and S. J. Ovenshine, Phys. Rev. **114** (1959) 858
[h] Livingston, Benjamin, Cox and Gordy, Phys. Rev. **92** (1953) 1271; Garvin, Green and Lipworth, Phys. Rev. **111** (1958) 534

respectively. The spin value 2 of I^{124} and I^{126} can be explained by assuming that the odd neutrons (71, 73) are in the $3s_{\frac{1}{2}}$ level and that they couple with the $d_{\frac{3}{2}}$ proton in accordance with Nordheim's "weak" rule. However, the parities of the ground states in these two cases are thought to be negative[9, 10]; the present assignment would class them as positive. At I^{128} ($N = 75$) the observed spin 1 can be explained only by assuming that the odd neutron lies in the $4d_{\frac{3}{2}}$ level, though this is not the case in Xe^{120}, which also has 75 neutrons and exhibits a spin $\frac{1}{2}$.

It is of interest to note that if this assumption is made, the resultant spin 1 is in agreement with the "strong" rule of Nordheim[8]). The spins of I^{130} and I^{132} are consistent with a weak rule coupling between an odd proton in the $5g_{\frac{7}{2}}$ level and an odd neutron in the $4d_{\frac{3}{2}}$ level. The spin of I^{126} has been the subject of some discussion. Stevenson and Deutsch, on the basis of a ($\beta\gamma$) angular correlation experiment, concluded that I = 2 (negative parity)[11]), but Marty *et al.*[12]), who studied the shape of the β spectrum made the assignment 1^+. Perlman and Welker[13]), after a more exact determination of the comparative half lives of the β transitions, concluded that 2^- was the more reasonable assignment, a result strongly supported by the later and more detailed work of Koerts *et al.*[10]). The work reported here definitely established the correctness of the spin value $I = 2$.

The decay scheme of I^{132} has been investigated by Funston and Bernstein[14]). Though Funston and Bernstein do not make a spin and parity assignment to the ground state of I^{132}, Cheever *et al.*[15]) in a study of the decay of Te^{132} suggest the assignment 4^+; this spin value is confirmed by the experiment reported here. The most recent work on I^{133} is that of Holm and Ryde[16]), but the decay scheme is not completely analyzed. The result presented here should aid in this analysis. There appears to be little or no published work on the spectrum of I^{135}.

The disagreement between the experimental parity assignments to I^{124} and I^{126} and those resulting from the classification scheme of table 2 is probably more apparent than real. It is certainly possible to pick single-particle model neutron and proton states which give rise in all cases to the correct spins and parities, as it is also possible to reconcile the discrepancy by a suitable choice of states resulting from a deformed-core nuclear model such as the Nilsson model. However, in the absence of a measurement of the nuclear magnetic moment and nuclear electric quadrupole moment of the isotopes involved it is hardly more than speculative to list the alternative orbitals.

The authors wish to acknowledge the assistance of Messrs. Larry M. Cohen and John R. Padilla, who helped operate the atomic-beam apparatus. Members of the Lawrence Radiation Laboratory Chemistry Division and Health Chemistry Group made substantial contributions to the success of this work.

References

1) Norman F. Ramsey, Molecular Beams (Oxford University Press, London, 1956) Chapters I, V, XIII and XIV
2) Garvin, Green and Lipworth, Phys. Rev. **111** (1958) 534
3) William A. Nierenberg, in Annual Review of Nuclear Science (Annual Reviews Inc., Stanford, 1957) Vol. **7**, p. 349
4) Kenneth F. Smith, Progr. Nucl. Phys. **6** (1957) 52
5) Garvin, Green, Lipworth and Nierenberg, Phys. Rev. Letters **1** (1958) 74
6) Stang, Tucker, Banks, Doering and Mills, Nucleonics **12**, No. 8 (1954) 22
7) Garvin, Green and Lipworth, Phys. Rev. Letters **1** (1958) 292
8) L. W. Nordheim, Phys. Rev. **78** (1950) 294;
Mitchell, Juliano, Creager and Kocher, Phys. Rev. **113** (1959) 628
9) R. K. Girgis and R. Van Lieshout, Physica **25** (1959) 133
10) Koerts, Macklin, Farrelly, Lieshout and Wu, Phys. Rev. **98** (1955) 1230
11) D. T. Stevenson and M. Deutsch, Phys. Rev. **84** (1951) 1071
12) Marty, Langevin and Hubert, J. Phys. Radium **14** (1953) 663
13) M. L. Perlman and J. P. Welker, Phys. Rev. **95** (1954) 133
14) H. L. Funston and W. Bernstein, Phys. Rev. **96** (1954) 71
15) Cheever, Koski, Tilley and Madansky, Phys. Rev. **110** (1958) 922
16) G. Holm and H. Ryde, Arkiv Fysik **15** (1959) 387

1.D.2:
1.E.4

Nuclear Physics **19** (1960) 148—153; © *North-Holland Publishing Co., Amsterdam*
Not to be reproduced by photoprint or microfilm without written permission from the publisher

MULTIPOLE ORDER OF THE 869 keV GAMMA RAY IN Sm^{152}

OVE NATHAN†

Physics Department, University of Pennsylvania, Philadelphia, Pennsylvania††

Received 15 February 1960

Abstract: The angular correlation of the 869–244 keV gamma-electron cascade in Sm^{152} has been measured and the multipole mixture of the 869 keV transition has been deduced to be 98.8 % E2, 1.2 % M1. The influence of the rotation-vibration coupling on the E2 and M1 transitions from the γ-vibrational states in Sm^{152} is discussed. The value of the coupling parameter z is found to be 0.08.

Only in comparatively few cases among the deformed even nuclei has it been possible to test accurately the prediction of the unified model that M1 radiation should be forbidden in the decay of vibrational states of such systems. This is in particular true for the often observed rotational 3^+ states associated with 2^+ γ-vibrational excitations, because the multipolarity of the transitions from such states usually must be estimated from measurements of the internal conversion coefficients, and such measurements are rarely precise enough to allow an accurate determination of the mixing. Sm^{152} is a case where somewhat more precise data are available (see fig. 1) and the decay of the 3^+ state has been studied both by high resolution γ- and β-ray spectroscopy[1,2]) and by γ–γ angular correlation techniques[3,4]). These measurements are in agreement as regards the multipolarity of the $3^+ \rightarrow 2^+$ transition to the 2^+ member of the ground state rotational band (predominantly E2, less than 1 % M1), but conflicting evidence is present on the multipole order of the 869 keV transition to the 4^+ rotational state. The internal conversion data indicate predominantly M1[2]) while the γ–γ angular correlation results give 97.9 % E2, 2.1 % M1[4]). In both sets of measurements, however, large corrections had to be applied to the measured data because of interference from other radiations in the very complex Eu^{152} decay.

In this experiment, the multipolarity of the 869 keV γ-ray was examined by means of an angular correlation experiment in which the 869 keV γ-ray was observed in coincidence with the K-conversion line of the 244 keV transition, selected in a magnetic lens spectrometer. This method offers certain advantages over the γ–γ method due to the higher resolution of the β-ray spectrometer and the reduction of the number of spurious coincidences from Compton scattering events.

† On leave from the Institute for Theoretical Physics, University of Copenhagen.

†† This work has been supported in part by the National Science Foundation.

The properties of the lens spectrometer and associated coincidence equipment have been described in detail elsewhere[5]). The source was produced by vacuum evaporation of Eu_2O_3 enriched to 98% in Eu^{151}† onto a 150 $\mu g/cm^2$ Al foil and subsequent irradiation for one week in the MTR reactor. The source strength was $\approx$ 100 μc and, with a diameter of 2 mm, this corresponds to a thickness of $\approx$ 25 $\mu g/cm^2$. At this thickness, scattering effects should be very small for

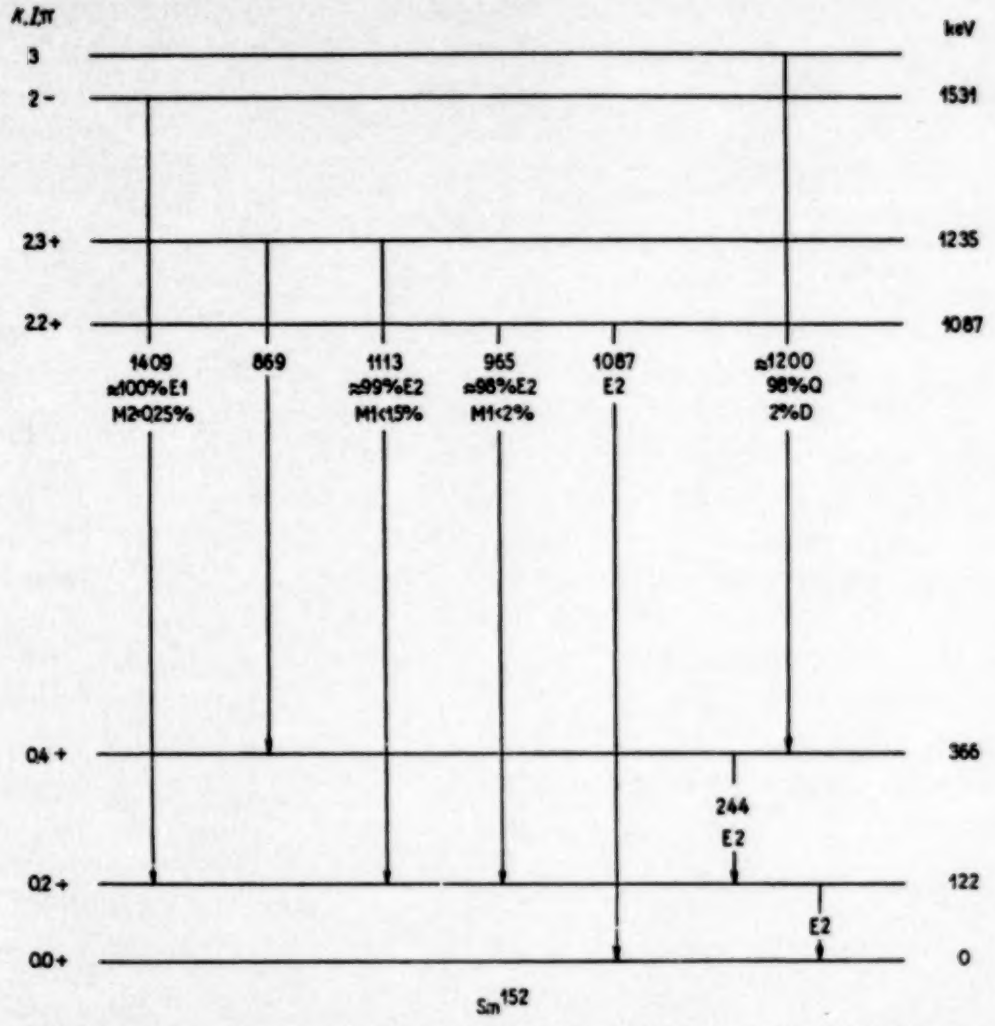

Fig. 1. Pertinent part of the level scheme of Sm^{152}. The indicated multipole mixtures are those which seem to be reasonably well established from the works of Ofer, and of Lide and Wiedenbeck.

200 keV electrons and this was verified experimentally by additional angular correlation measurements which will be discussed below. Because of the relatively large source strength which was necessary to obtain sufficient counting statistics, the coincidence resolving time was reduced to 5.5×10^{-9} sec, giving a true to chance ratio of 40:1.

Measurements were made at 0°, $\pm$ 45° and $\pm$ 90° with the γ-ray counter set to accept events between 810 and 930 keV. A total of about 5000 coincidences

† Supplied by Stable Isotope Division, Oak Ridge National Laboratory.

was recorded at each angle. The data were corrected for coincidences due to the β-continuum underneath the line, for random coincidences, and for the geometry of the detectors. No corrections were applied for counts due to the very weak 1200 keV γ-ray which is also coincident with the 244 keV transition. According to the spectrum given by Lide and Wiedenbeck[4]), about 10–15% of the coincidences in the selected channel should be due to this photon, but a γ–γ coincidence experiment which was performed to check this point resulted in a $\approx 50\%$ lower intensity of the 1200 keV γ-ray relative to the 869 keV γ-ray than indicated by these authors. Furthermore, the 1200–244 keV and the 869–244 keV correlation functions seem to be nearly identical[4]).

By using mean values of the data obtained at positive and negative angles, the correlation function was found to be

$$W(\theta) = 1 + (0.187 \pm 0.026)\, P_2(\cos\theta) + (0.167 \pm 0.064)\, P_4(\cos\theta)\,.$$

Due to a small instrumental asymmetry the errors quoted are somewhat larger than the counting errors. This effect is discussed in detail in ref. [5]) and there it is shown that the average of the correlations at positive and negative angles probably represent a good fit to the true correlation.

We have assumed the electric quadrupole attenuation effects on the measured correlation to be small in view of the short half-life of the 4^+ state ($T_{\frac{1}{2}}$ may be estimated from the collective description of the state and the measured half-life of the 122 keV state. One finds $T_{\frac{1}{2}} \approx 10^{-10}$ sec). No accurate additional correlation experiment involving the 4^+ state seemed feasible to prove this statement directly. Another source of attenuation of the correlation is electron scattering whose magnitude depends critically on the thickness of the radioactive source and on the electron energy[6]). To examine the scattering properties of the source two additional experiments were performed, involving the 1409–122 keV γ-e_K^- and γ-γ cascades. The γ-γ cascade has been investigated by several groups and is found to involve only P_2 terms[3,4]). The ratio of the correlation coefficients measured in the two different experiments can be written

$$\frac{A_2(\gamma\text{-}e_k^-)}{A_2(\gamma\text{-}\gamma)} = b_2 G_2\,,$$

where b_2 denotes the particle factor and G_2 the scattering factor, both occurring in the γ-e_K^- correlation. In this case $b_2 \approx 1.90$, a result which is found by extrapolation from Rose and Biedenharn's tables[7]). The measured correlation coefficients were $A_2(\gamma\text{-}e_K^-) = 0.260 \pm 0.025$ and $A_2(\gamma\text{-}\gamma) = 0.124 \pm 0.013$, from which we deduce $G_2 = 1.10 \pm 0.16$. Thus, the scattering factor in the 1409–122 γ-e_K^- correlation may at the highest be 0.96, which, according to the diagram presented in ref. [6]), corresponds to a source thickness of ≈ 20 μg/cm^2. From this estimate of the source thickness we calculate the scattering

corrections in the 869–244 keV correlation to be about 0.99 for the P_2 term and about 0.97 for the P_4 term. These numbers are, of course, not to be taken as more than rough estimations, but they clearly show that scattering does not affect the measured correlation in a significant way.

Since, previously, the spins and parities of the 1235, 367 and 122 keV states have been firmly established[3,4]) to be 3^+, 4^+ and 2^+, and since the 244 keV γ-ray is known to be[3]) pure E2, the measurement of the 869–244 keV angular correlation may be used to determine the M1–E2 mixture ratio in the 869 keV transition. The situation is illustrated by fig. 2 which shows the theoretically expected values of A_2 and A_4 in the γ-e_K^- correlation plotted with δ as parameter, where δ denotes the ratio of the E2 to the M1 matrix element in the mixed transition. The particle parameters b_2 and b_4 for the 244 keV transition, which are needed for the calculation of A_2 and A_4, were taken from the work of Biedenharn and Rose[7]). It appears from fig. 2 that only one value of δ can fit the measurements and we find $\delta = +9.1^{+1.8}_{-1.3}$, corresponding to $(98.8 \pm 0.3)\%$

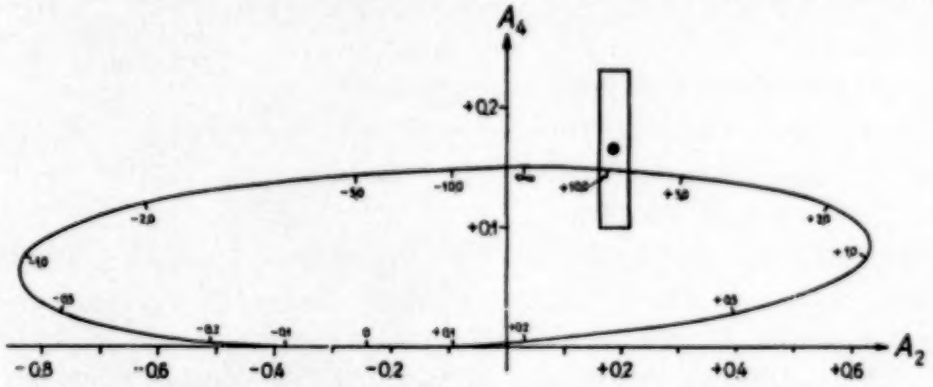

Fig. 2. Directional correlation of the 869–244 keV gamma-electron cascade. The ellipse represents calculated values of A_2 and A_4 with δ as parameter for a 3^+(M1,E2)4^+(E2)2^+ cascade. The particle parameters b_2 and b_4 in the second transition were found by interpolation from the tables of Biedenharn and Rose. We have used $b_2 = 1.73$ and $b_4 = -0.82$. The experimental correlation is indicated by the dot and the uncertainties are shown by the surrounding rectangel.

E2 radiation. This result is close to that of Lide and Wiedenbeck, but disagrees with the internal conversion data. However, as pointed out in ref. [2]), the internal conversion coefficient is poorly known in this case, the uncertainty apparently being associated mainly with the determination of the internal conversion intensity. The uncertainty in the evaluation of the γ-ray intensity is estimated in ref. [2]) to be about 30%.

Having established the multipolarity of the 869 keV transition, we can calculate the E2 γ-ray branching ratio in the decay of the 3^+ state. Using the γ-ray data of Nathan and Hultberg, we obtain for the ratio of the reduced transition probabilities

$$\frac{B(\mathrm{E2};3^+ \to 4^+)}{B(\mathrm{E2};3^+ \to 2^+)} = \frac{9 \pm 3}{49 \pm 7} \times \left(\frac{1113}{869}\right)^5 = 0.64 \pm 0.24\,.$$

For a pure $K = 2$ state the theoretical expectation value is 0.4. The branching from the 2^+ γ-vibrational state is known with greater accuracy, since here

$$\frac{B(\mathrm{E2};2^+ \to 2^+)}{B(\mathrm{E2};2^+ \to 0^+)} = 2.27 \pm 0.07 .$$

The theoretical value for a $2,2^+$ state is 1.43.

In an attempt to explain similar discrepancies associated with the decay of γ-vibrational states in Gd^{156}, Gregers Hansen *et al.*[8]) examined the effect of a coupling between the $K = 2$ vibrational band and the ground state $K = 0$ band. This effect is taken into account by multiplying the theoretical transition probabilities with a correction factor f, which depends upon the initial and final spins in the transition and upon the degree of admixture, characterized by a quantity z. If the interpretation is correct, the same mixing parameter z should apply for all transition rates between the two bands. In the case of Tb^{156} a common value of $z = 0.03$ was found to give a good fit to the observed branching ratios associated with the γ-band.

Using the table of correction factors f given in ref. [8]), we find that the data for the 1087 keV 2^+ state in Sm^{152} imply a value of $z = 0.08$. Using this to correct the theoretical branching from a pure $K = 2$, 3^+ state, we obtain the corrected prediction 0.88 which is compatible with the observations, although the agreement is marginal. Without overemphasizing the quantitative aspects of this procedure, we may conclude that the apparent discrepancies observed for the branchings of E2 transitions in the decay of the γ-band in Sm^{152} may be explained, at least qualitatively, in a similar way as for other deformed nuclei in the rare earth region.

The coupling of $K = 0$ and $K = 2$ bands may also be kept responsible for the weak M1 radiations observed in the transitions between the two bands. One can test the consistency of the description by comparing the observed M1/E2 branching ratio with a theoretical expectation based on the above choice of the coupling parameter z. An approximate theoretical prediction may be obtained by the following argument.

The M1 transition rate will, apart from spin factors of the order unity, be the single-particle rate times $A^2(g_R - g_K)^2$, where A is the amplitude of the $K = 2$ admixture to the $K = 0$ state in the ground state band, g_R is the g-factor which characterizes the rotational motion, and g_K is the g-factor of the vibrational motion. A is related to the coupling factor z by $z = A\,(Q_0/Q_2)$, where Q_0 is the mean quadrupole moment of the two rotational bands, and Q_2 denotes the quadrupole transition amplitude from the $K = 2$ band to the $K = 0$ band. The E2 transition rate will be the single-particle value times Q_2^2, where again we have neglected the spin factors. Thus, we arrive at the following approximate

expression for the M1/E2 branching ratio:

$$\frac{1}{\delta^2} \approx (g_R - g_K)^2 z^2 \left(\frac{Q_2}{Q_0}\right)^2 \frac{1}{Q_2^2} \left(\frac{M1}{E2}\right)_{s.p.} = (g_R - g_K)^2 \frac{z^2}{Q_0^2} \left(\frac{M1}{E2}\right)_{s.p.} .$$

In the case of the 869 keV transition in Sm^{152}, the single-particle prediction for the M1/E2 intensity ratio is ≈ 300, and Q_0^2 is known from experiments to be ≈ 150 times the single-particle value. Consequently,

$$\frac{1}{\delta^2} \approx 2\,(g_R - g_K)^2 z^2 = 0.013\,(g_R - g_K)^2 .$$

Assuming $(g_R - g_K)$ to be a quantity of the order unity, we conclude that this estimate is indeed consistent with the experimental value for $1/\delta^2$ which is 1.2×10^{-2}.

Finally, we compare the observed branching from the 3^+ state with the prediction of another "collective" model, namely the axially asymmetric model of Davydov and Filipov. Using the energies of the 122 and 1087 keV states, an axial asymmetry of $\gamma = 13°.5$ is deduced for the ground state of Sm^{152}, and from this γ-value Davydov and Rostovsky[9]) calculate the following E2 branching from the 3^+ state:

$$\frac{B(E2;3^+ \to 4^+)}{B(E2;3^+ \to 2^+)} = 1.37 .$$

Davydov and Rostovsky compared this number with the earlier, less precise data of Nathan and Waggoner[10]) and found tolerable agreement. Using the better γ-ray data of Nathan and Hultberg[2]), however, the prediction of Davydov and Rostovsky deviates by a factor 2 from the observed branching.

The author is much indebted to Dr. S. Frankel for advice concerning the experiment and to Dr. Ben Mottelson and Dr. Aage Bohr for helpful suggestions regarding the results. The hospitality of the Physics Department, University of Pennsylvania, is gratefully acknowledged.

References

1) B. V. Bobykin and K. M. Novik, Izv. Akad. Nauk SSSR, Ser. Fiz. **21** (1957) 1556
2) O. Nathan and S. Hultberg, Nuclear Physics **10** (1959) 118
3) S. Ofer, Nuclear Physics **4** (1957) 477
4) R. W. Lide and M. L. Wiedenbeck, Phys. Rev. **113** (1959) 840
5) B. I. Deutch, Thesis (1959), Physics Department, University of Pennsylvania (unpublished)
6) R. K. Golden and S. Frankel, Phys. Rev. **102** (1956) 1053
7) L. C. Biedenharn and N. E. Rose, Revs. Mod. Phys. **25** (1953) 729
8) P. Gregers Hansen, O. B. Nielsen and R. K. Sheline, Nuclear Physics **12** (1959) 389
9) A. S. Davydov and V. S. Rostovsky, Nuclear Physics **12** (1959) 58
10) O. Nathan and M. A. Waggoner, Nuclear Physics **2** (1956/57) 548

1.C *Nuclear Physics* **19** (1960) 154—163; © *North-Holland Publishing Co., Amsterdam*
Not to be reproduced by photoprint or microfilm without written permission from the publisher

REACTION MATRIX SINGULARITIES AND THE ENERGY GAP IN AN INFINITE SYSTEM OF FERMIONS

V. J. EMERY

Physics Department, University of California, Berkeley, California

Received 17 February 1960

Abstract: It is shown that the presence of a singularity in Brueckner's t-matrix for an infinite system of Fermions is a sufficient (but not necessary) condition for the existence of a gap in the energy spectrum of the system. On the other hand there are singularities in Galitskii's t-matrix if and only if the system has an energy gap.

Furthermore there are both singularities and an energy gap if the solution of a Schrödinger equation with modified kinetic energy has a positive phase shift δ at the Fermi momentum.

The results are illustrated by deriving approximate expressions for the energy gap and the distances of the singularities from the Fermi surface in terms of the phase shift δ.

1. Introduction

In a previous paper[1]) (hereafter called I), it was shown that, for a wide class of potentials, the Brueckner t-matrix for an infinite system of fermions possesses singularities. At that time, it had been speculated that these singularities were associated with the existence of a gap in the energy spectrum of the system and that the low-lying states had a highly collective character—although the relationship between the various phenomena had not been clarified.

Recently, however, Cooper, Mills and Sessler[2]) and Bogoliubov[3]), using a generalization of the superconductivity theory of Bardeen, Cooper and Schrieffer[4]), derived a criterion for the existence of an energy gap which appears to be quite different from the condition for the existence a singularity of the Brueckner t-matrix, discussed in I. It is therefore of great interest to compare the two criteria in order to see it they are indeed related and to determine the range of validity of the Brueckner method.

In this paper, it will be shown that, if the Brueckner t-matrix possesses singularities, then the Fermi system is in a highly correlated state, but that, in general, the converse is not true.

On the other hand, it will be seen that the t-matrix introduced by Galitskii[5]), is singular if and only if there is an energy gap. This result is physically reasonable since, in contrast to the convential Brueckner method, both Galitskii's theory and the Bardeen-Cooper-Schrieffer theory treat holes and particles symmetrically (see also Iwamoto[6]).

It is therefore to be expected that Galitskii's approach provides a more

accurate description of the normal state in that, in the absence of an energy gap, it may well be a good approximation to a more general theory which is applicable to both correlated and uncorrelated states. This conclusion is of interest since the collective effects are not expected to be of importance far away from the Fermi surface or when two particles have a total momentum very different from zero, so that calculations with the Galitskii t-matrix could give some useful results even when there is an energy gap.

In section 2, the criterion for the existence of a phase transition of a Fermi system to a highly correlated state is introduced and it is expressed in a form suitable for the comparison with the t-matrix equations which is effected in sections 3 and 4. In section 5 the magnitude of the energy gap and distances of the singularities from the Fermi surface are expressed in terms of the Schrödinger equation phase shift to illustrate the results of the previous sections. Section 6 contains a discussion of the results.

2. The Existence of an Energy Gap

In order to avoid the use of the non-linear equation whose solution determines the existence of an energy gap[2]), we use the criterion[7]) that an infinite Fermi system will undergo a phase transition to a highly correlated state at a temperature $T_c = 1/k\beta_c$. If this criterion is satisfied, the energy spectrum possesses a gap.

A Fermi system has a phase transition if the equation

$$| \chi_K \rangle = -\frac{\tanh(\frac{1}{4}\beta H_0)}{H_0} v | \chi_K \rangle \tag{1}$$

has a non-trivial solution for some value β_c of β.

Here, v is the two-particle potential and, in momentum representation,

$$\langle k | H_0 | k' \rangle = | \varepsilon_0(k) | \delta(k - k') , \tag{2}$$

with

$$\varepsilon_0(k) = e(k) - e(k_F) , \tag{3}$$

where

$$e(k) = k^2 + 2V(k) \tag{4}$$

is the "normal state" energy of a pair of particles with relative momentum k and total momentum zero; $V(k)$ is the single-particle potential, k_F the Fermi momentum, $\hbar = 1$ and the particle mass is unity.

In eq. (2), $| k \rangle$ is the radial part of the solution with angular momentum l and momentum k of the free-particle Schrödinger equation, i.e.

$$\langle r | k \rangle = krj_l(kr) \tag{5}$$

for some l. Here, r is the separation of the particles and $j_l(kr)$ is the spherical Bessel function of order l. (In the following, the angular momentum label l will be suppressed and it is to be understood that all states refer to a fixed but arbitrary angular momentum l.)

Eq. (1) may be rewritten as an eigenvalue equation

$$| \chi_{K_i} \rangle = - \mu_{K_i}(\beta) \frac{\tanh (\frac{1}{2}\beta H_0)}{H_0} v | \chi_{K_i} \rangle , \tag{6}$$

and the condition for a phase transition is that there be a value β_c of β for which

$$\mu_{K_i}(\beta_c) = 1 \tag{7}$$

for some value of i.

Throughout the discussion it will be assumed that the matrix elements $\langle k | v | k' \rangle$ of v are finite although they may be arbitrarily large so that there is no essential physical restriction on v.

Then, by using the methods of I, it may be shown that, for each value of l, there is a set of eigenvalues $\mu_{K_i}(\beta)$ having the following properties:

I. The eigenvalues are real and discrete and $\mu_{K_i}(\beta) \neq 0$ for finite β.

II. $\partial/\partial\beta \, | \mu_{K_i}(\beta) | < 0$ for all β and i.

III. (a) When $\langle k_F | v | k_F \rangle \neq 0$, $\mu_{K_i}(\beta) \to 0$ as $\beta \to \infty$ for one and only one value n of i. If $\langle k_F | v | k_F \rangle < 0$, $\mu_{K_n}(\beta) \to 0$ through positive values, otherwise through negative values.

(b) When $\langle k_F | v | k_F \rangle = 0$, $\mu_{Ki}(\beta) \to 0$ as $\beta \to \infty$ for at least two values of i. In general, there are exactly two such values and one tends to zero from above and the other from below.

IV. $| \mu_{K_i}(\beta) | \to \infty$ as $\beta \to 0$.

It follows at once that when $\langle k_F | v | k_F \rangle \leqq 0$, eq. (7) can be satisfied for at least one value n of i, so that there is a phase transition.

When $\langle k_F | v | k_F \rangle > 0$, every positive eigenvalue $\mu_{K_i}(\beta)$ remains non-zero as $\beta \to \infty$, so that it is necessary to show that, for some value of l, at least one eigenvalue is less than unity at $\beta = 0$. This possibility is most conveniently discussed eq. (6).

Define

$$\langle k | \Delta | k' \rangle = \sqrt{| \varepsilon_0(k) |} \, \delta(k - k') \tag{8}$$

and

$$\langle k | \bar{\chi}_{K_i} \rangle = \begin{cases} \operatorname{Lim}_{\beta \to \infty} \langle k | \dfrac{1}{\Delta} v | \chi_{K_i} \rangle & \text{for } k \neq k_F , \\ 0 & \text{for } k = k_F , \end{cases} \tag{9}$$

for all $i \neq n$ ($\mu_{K_n}(\beta) \to 0$ for $\beta \to \infty$). By using the methods of I, it can be shown that $\langle k_F | v | \chi_{K_i} \rangle \to 0$ as $\beta \to \infty$, for $i \neq n$ (so that $\langle k | \bar{\chi}_{K_i} \rangle$ is a continuous

function of k) and that in the limit as $\beta \to \infty$ all eigenfunctions and eigenvalues of eq. (6), except those with $i = n$, are given by solutions of

$$| \bar{\chi}_{K_i} \rangle = \mu_{K_i} G | \bar{\chi}_{K_i} \rangle , \tag{10}$$

where

$$G = -\frac{1}{\Delta}\left\{v - \frac{v | k_F \rangle \langle k_F | v}{\langle k_F | v | k_F \rangle}\right\}\frac{1}{\Delta} \tag{11}$$

and

$$\mu_{K_i} = \operatorname*{Lim}_{\beta \to \infty} \mu_{K_i}(\beta) .$$

We have now to determine the conditions under which the lowest positive eigenvalue μ_{Kp} is less than unity.

3. The t-Matrix and Free-Space Equations

In this section, we introduce the t-matrix and free-space equations which are to be compared with eqs. (10) and (11).

In I, it was shown that the criterion for the existence of a singularity in the Brueckner t-matrix for total momentum zero and relative momentum $m < k_F$ is that the equation

$$| \chi_{B_i} \rangle = -\mu_{B_i(m)} \frac{Q}{H_1(m)} v | \chi_{B_i} \rangle \tag{12}$$

has a non-trivial solution with

$$\mu_{B_i} = 1 \tag{13}$$

for some values of m and i.

Here

$$\langle k | H_1(m) | k' \rangle = \delta(k - k')\, \varepsilon_1(k, m) , \tag{14}$$

$$\varepsilon_1(k, m) = e(k) - e(m) \tag{15}$$

and

$$\langle k | Q | k' \rangle = \begin{cases} \delta(k - k') & \text{for } k > k_F , \\ 0 & \text{for } k, k' < k_F . \end{cases} \tag{16}$$

Eq. (12) refers to a state of any fixed angular momentum l (although it was derived for $l = 0$ in I).

Galitskii's t-matrix (which includes "hole-hole" scattering as well as "particle-particle" scattering (see also Iwamoto[6]) has a singularity for total momentum zero and relative momentum m, if the equation

$$| \bar{\chi}_{G_i} \rangle = -\mu_{G_i}(m) \frac{P}{H_1(m) - i\varepsilon} v | \chi_{G_i} \rangle \tag{17}$$

has a non-trivial solution with

$$\mu_{G_i}(m) = 1 \tag{18}$$

for some values of $m < k_F$ and i.

Here

$$\langle k \mid P \mid k \rangle = \begin{cases} \delta(k - k') & \text{for } k > k_F, \\ -\delta(k - k') & \text{for } k < k_F. \end{cases} \tag{19}$$

Using the methods of I, it may be shown that both eqs. (13) and (18) can be satisfied if $\langle k_F \mid v \mid k_F \rangle \leqq 0$ and that when $\langle k_F \mid v \mid k_F \rangle > 0$, it is necessary to show that $\mu_{B_i} = \mu_{B_i}(k_F)$ and $\mu_{G_i} = \mu_{G_i}(k_F)$ are less than unity† for some value p of i.

Now define

$$\langle k \mid \bar{\chi}_{B_i} \rangle = \begin{cases} \operatorname{Lim}_{m \to k_F} \langle k \mid \frac{Q}{\Delta} v \mid \chi_{K_i} \rangle & \text{for } k \neq k_F, \\ 0 & \text{for } k = k_F, \end{cases} \tag{20}$$

and

$$\langle k \mid \bar{\chi}_{G_i} \rangle = \begin{cases} \operatorname{Lim}_{m \to k_F} \langle k \mid \frac{1}{\Delta} v \mid \chi_{G_i} \rangle & \text{for } k \neq k_F, \\ 0 & \text{for } k = k_F, \end{cases} \tag{21}$$

for all $i \neq n$ ($\mu_{B_n} = 0 = \mu_{an}$). Then, as in section 2, $\langle k \mid \bar{\chi}_{B_i} \rangle$ and $\langle k \mid \bar{\chi}_{G_i} \rangle$ are continuous functions of k and in the limit as $m \to k_F$, all eigenfunctions and eigenvalues of eqs. (12) and (17) are given by

$$\mid \bar{\chi}_{B_i} \rangle = \mu_{B_i} QGQ \mid \bar{\chi}_{B_i} \rangle \tag{22}$$

and

$$\mid \bar{\chi}_{G_i} \rangle = \mu_{G_i} G \mid \bar{\chi}_{G_i} \rangle \tag{23}$$

respectively. Finally, for purposes of comparison with a Schrödinger equation phase shift, δ, we introduce the factor λ_0 by which v has to be multiplied in order that the Schrödinger equation

$$\mid \psi \rangle = \mid k_F \rangle - \frac{P}{H_0} \lambda_0 v \mid \psi \rangle \tag{24}$$

with kinetic energy $e(k)$ should have zero phase shift for momentum k_F, i.e. that

$$\langle k_F \mid v \mid \psi \rangle = 0. \tag{25}$$

† It is also necessary that both $\mu_{Bp}(0)$ and $\mu_{Gp}(0)$ be greater than unity. A sufficient condition for this would be that v have no bound state or at most a weakly bound state. This property is a feature of systems of physical interest, and it will be assumed here.

Using eqs. (8) and (25) and defining

$$|\bar{\psi}\rangle = \begin{cases} \langle k | \frac{1}{\Delta} v | \psi \rangle & \text{for } k \neq k_F, \\ 0 & \text{for } k = k_F, \end{cases} \tag{26}$$

eq. (24) may be rewritten as

$$|\bar{\psi}\rangle = \lambda_0 GP |\bar{\psi}\rangle . \tag{27}$$

It is not hard to see that if $\delta(k_F) > 0$ and $\langle k_F | v | k_F \rangle > 0$, then $\lambda_0 < 1$. Considering the arbitrary coupling constant λ, we find, for $\lambda \ll 1$,

$$\tan \delta(k_F) \approx -\lambda \langle k_F | v | k_F \rangle , \tag{28}$$

which is small and negative so that $\delta(k_F) < 0$. However, when $\lambda = 1$, $\delta(k_F) \geqq 0$ by assumption, so that there is a value of λ_0 of λ in $0 < \lambda_0 < 1$ for which $\delta(k_F)$ is zero for the potential $\lambda_0 v$.

Eqs. (22), (23) and (27) are to be used in the next section.

4. Conditions for an Energy Gap

In this section, it will be assumed that $\mu_{Gi}(0) \geqq 1$ and $\mu_{Bi}(0) \geqq 1$ for all i. This condition is satisfied very well for systems of physical interest and is sufficient to ensure that the t-matrices are singular when $\mu_{Gi} < 1$ and $\mu_{Bi} < 1$.

By using the results of section 3, the following theorems may be proved (for all relative angular momentum states):

A. The conditions for a singularity in the Galitskii t-matrix and for an energy gap are identical.

B. The presence of a singularity in Brueckner's t-matrix is a sufficient (but not necessary) condition for the existence of and energy gap.

C. A sufficient condition for the existence of a singularity in Brueckner's t-matrix and hence for an energy gap is that the phase shift at momentum k_F in the solution of Schrödinger equation with kinetic energy $e(k)$ be positive.

The remainder of this section is devoted to proving the theorems.

Eqs. (10) and (23) are identical, which is just the content of theorem A.

Let μ_{Bp} and μ_{Gp} be the smallest positive values of μ_{Bi} and μ_{Gi} respectively. It is not hard to show that

$$\frac{1}{\mu_{Kp}} \geqq \frac{\langle \chi | G | \chi \rangle}{\langle \chi | \chi \rangle} \tag{29}$$

and

$$\frac{1}{\mu_{Bp}} \geqq \frac{\langle \chi | QGQ | \chi \rangle}{\langle \chi | \chi \rangle} \tag{30}$$

for any trial function $|\chi\rangle$. Then, replacing $|\chi\rangle$ in the inequality (29) by $|\bar{\chi}_{Bp}\rangle$ from eq. (22), we find that

$$\frac{1}{\mu_{Kp}} \geqq \frac{1}{\mu_{Bp}} > 0\,, \tag{31}$$

so that

$$\mu_{Bp} \geqq \mu_{Kp} \tag{32}$$

and theorem B follows at once.

Finally, consider the eigenvalue equation

$$|\psi_1\rangle = \lambda_1 (GP + PG)\,|\psi_1\rangle\,. \tag{33}$$

Then, using the trial wave function $Q|\psi_1\rangle$ in the inequality (30), we find (since $2Q = 1 + P$)

$$\frac{1}{\mu_{Bp}} \geqq \frac{1}{2\lambda_1}\,. \tag{34}$$

Then, using $|\bar{\psi}\rangle$ of eq. (27) as trial wave function,

$$\frac{1}{\lambda_1} \geqq \frac{\langle\bar{\psi}|\,GP + PG\,|\bar{\psi}\rangle}{\langle\bar{\psi}|\bar{\psi}\rangle} = \frac{2}{\lambda_0} > 0\,, \tag{35}$$

so that $\lambda_0 \geqq \mu_{Bp}$, which is tantamount to theorem C, since $\lambda_0 < 1$.

5. Expression for the Energy Gap

The rather formal results of section 4 may be made plausible by deriving an expression for the magnitude of the energy gap and also for the distance of the singularities from the Fermi surface.

First an expression for the transition temperature is obtained. We introduce the function $|\phi\rangle$ as the solution of

$$|\phi\rangle = |k_F\rangle + Fv\,|\phi\rangle\,, \tag{36}$$

where

$$F = -\frac{\tanh\,(\frac{1}{4}\beta H_0)}{H_0} + L(\beta)\,|k_F\rangle\langle k_F| \tag{37}$$

and

$$L(\beta) = \int_0^\infty \mathrm{d}k\,\frac{\tanh\,(\frac{1}{4}\beta\varepsilon_0(k))}{\varepsilon_0(k)}\,. \tag{38}$$

Then, from eqs. (1) and (36),

$$\langle\phi|v|\chi_K\rangle = -\langle\phi|v\frac{\tanh\,(\frac{1}{4}\beta H_0)}{H_0}v|\chi_K\rangle = \langle k_F|v|\chi_K\rangle + \langle\phi|vFv|\chi_K\rangle.$$

Thus

$$\langle k_F | v | \chi_K \rangle = -L(\beta) \langle \phi | v | k_F \rangle \langle k_F | v | \chi_K \rangle \tag{39}$$

and either

$$\langle k_F | v | \chi_K \rangle = 0 \tag{40}$$

or

$$L(\beta) = \frac{-1}{\langle \phi | v | k_F \rangle}. \tag{41}$$

For finite β, eq. (40) is not satisfied in general unless $| \chi_K \rangle$ is identically zero, i.e. there is no phase transition. When there is a phase transition, the transition temperature is given by the value β_c of β for which eq. (41) is satisfied.

Since $L(\beta)$ is positive, $\langle \phi | v | k_F \rangle$ must be negative. This requirement could be satisfied by a repulsive potential, but then $| \chi_K \rangle$ would be zero and eq. (41) would not follow. For a very strongly attractive potential, $\langle \phi | v | k_F \rangle$ could be positive for large values of β but it would then be singular for some value β_0 of β and negative for some $\beta < \beta_0$.

The function $L(\beta)$ has been evaluated elsewhere[7]) and it is found to be sensitive to the form of $e(k)$ only through the effective mass M^* at the Fermi surface. It is found that

$$kT_c = 2.28 \frac{k_F^2}{M^*} \exp\left\{ \tfrac{1}{2}\pi \frac{k_F}{M^*} \frac{1}{\langle \phi | v | k_F \rangle} \right\}. \tag{42}$$

In situations of physical interest, v is weakly attractive in that $| \chi_K \rangle$ is not zero and $\langle \phi | v | k_F \rangle$ is negative and the calculated value of β_c is very large. For large β, F is only weakly dependent on β and, to a good approximation, we may let $\beta \to \infty$ in eq. (37). Let

$$F_0 = \lim_{\beta \to \infty} F = -\int_0^\infty dk \frac{| k \rangle \langle k | - | k_F \rangle \langle k_F |}{| \varepsilon_0(k) |} \tag{43}$$

and let $| \phi_0 \rangle$ be the solution of the equation obtained by replacing F by F_0 in eq. (36).

If

$$F_1 = -\int_0^\infty dk \frac{| k \rangle \langle k | - | k_F \rangle \langle k_F |}{\varepsilon_0(k)}, \tag{44}$$

the equation for the wave matrix Ω for the Schrödinger equation with kinetic energy $e(k)$ is

$$\Omega = 1 + F_1 v \Omega, \tag{45}$$

from which

$$v | \phi_0 \rangle = v\Omega | k_F \rangle + \Omega^\dagger v (F_1 - F_0) v | \phi_0 \rangle. \tag{46}$$

This integral equation may be expressed as a convergent interation series in $v\Omega$, of which the first term gives a good approximation, so that

$$\langle \phi | v | k_F \rangle \approx \langle \phi_0 | v | k_F \rangle \approx \langle k_F | v\Omega | k_F \rangle = -k_F \tan \delta(k_F). \tag{47}$$

Using the result of Bardeen, Cooper and Schrieffer[4]) for the relationship between the magnitude ΔE of the energy gap and the transition temperature (which is obtained by linearizing the equation[2]) for the energy gap) and combining eqs. (42) and (47), we find

$$\Delta E = 3.5\, kT_c \approx \frac{8k_F^2}{M^*} \exp\left\{ -\tfrac{1}{2}\pi \frac{\cot \delta(k_F)}{M^*} \right\}. \tag{48}$$

In a similar manner, it may be shown that if the singularities in Brueckner's t-matrix and the *real part* of Galitskii's t-matrix occur for momenta m_1 and m_2 respectively, then

$$| \varepsilon_0(m_1) | \approx \frac{k_F^2 - m_1^2}{M^*} \approx \frac{4k_F^2}{M^*} \exp\left\{ -\pi \frac{\cot \delta(k_F)}{M^*} \right\} \tag{49}$$

and

$$| \varepsilon_0(m_2) | \approx \frac{k_F^2 - m_2^2}{M^*} \approx \frac{4k_F^2}{M^*} \exp\left\{ -\tfrac{1}{2}\pi \frac{\cot \delta(k_F)}{M^*} \right\} \tag{50}$$

in the effective mass approximation and for m_1 and m_2 near to k_F.

Within the range of validity of the approximations (48), (49) and (50), it is clear that $\delta(k_F)$ has to be positive for there to be both an energy gap and t-matrix singularities. The quantity $| \varepsilon_0(m_2) |$ is equal to $\frac{1}{2}\Delta E$ but $| \varepsilon_0(m_1) |$ is smaller than $\frac{1}{2}\Delta E$ (as a result of the absence of the factor $\frac{1}{2}$ in the exponent of eq. (49) compared to eqs. (48) and (50). This fact suggests that, in a more correct expression, a weaker interaction would be required to give an energy gap than to give a singularity in Brueckner's t-matrix. These results are an approximate expression of the content of the theorems proved in section 4.

Eqs. (48), (49) and (50) cannot be used directly to obtain approximate expressions for ΔE, $| \varepsilon_0(m_1) |$, and $| \varepsilon_0(m_2) |$ from known phase shifts since $\delta(k_F)$ is to be calculated with kinetic energy $e(k)$. The further approximation of replacing $e(k)$ by k^2 is too drastic in general (since it introduces an error into the exponent) although it may be useful for discussing the qualitative features of actual physical systems. (For applications to liquid He^3 and to Nuclear Matter see Emery and Sessler[7,8]).

Finally it should be noted that, in the low-density limit, we can put M^* equal to unity and replace $\tan \delta(k_F)$ by $(-k_F a)$ (a being the scattering length) in eq. (49) to obtain the result of Van Hove[9]).

6. Discussion

The results of sections 3, 4 and 5 show that Brueckner's theory of an infinite Fermi system and Galitskii's extension of the theory meet with difficulties when the low-lying energy states of the system have a significantly collective character.

At the same time, if the energy gap is small, Brueckner's approach probably gives an adequate description of states far away from the Fermi surface or of pair states with total momentum appreciably different from zero, and it should therefore be able to reproduce many properties of the system.

For this purpose, it seems to be more accurate to use Galitskii's t-matrix instead of Brueckner's t-matrix and, indeed, the former has summed more terms of the complete perturbation series (although it is not clear without further discussion that this would result in an improved value of the energy). Consequently it is important to see if the two t-matrices predict significantly different properties of many-Fermion systems, since it may be necessary to amend the extensive calculations already carried out[10, 11]).

In this connection it should be noted that the exclusion principle in intermediate states is doubled in the Galitskii equation with the result that the total potential energy would be decreased in magnitude and the rearrangement energy[12]) increased. These two effects compensate to some extent and, without further calculation, it is not possible to give a quantitative estimate of the changes.

I wish to thank Dr. A. M. Sessler for many stimulating discussions and to acknowledge the hospitality of the Lawrence Radiation Laboratory of the University of California. This work was carried out during the tenure of a Harkness Fellowship from the Commenwealth Fund of New York.

References

1) V. J. Emery, Nuclear Physics **12** (1959) 69
2) L. N. Cooper, R. L. Mills and A. M. Sessler, Phys. Rev. **114** (1959) 1377
3) N. N. Bogoliubov, V. V. Tolmachev and D. V. Shirkov, A New Method in the Theory of Superconductivity (Consultants Bureau, New York, 1959)
4) J. Bardeen, L. N. Cooper and J. R. Schrieffer, Phys. Rev. **108** (1957) 1175
5) V. M. Galitskii, Soviet Physics JETP **34** (1958) 104
6) F. Iwamoto, Progr. Theoret. Phys. (Kyoto)
7) V. J. Emery and A. M. Sessler, Phys. Rev.
8) V. J. Emery and A. M. Sessler, Phys. Rev.
9) L. Van Hove, Physica **25** (1959) 849
10) K. A. Brueckner and J. L. Gammel, Phys. Rev. **109** (1958) 1040
11) R. J. Eden and V. J. Emery, Proc. Roy. Soc. A **248** (1958) 266;
R. J. Eden, V. J. Emery and S. Sampanthar, Proc. Roy. Soc. A **253** (1959) 177, 186
12) N. M. Hugenholtz and L. Van Hove, Physica **24** (1958) 363

1.E.1: 2.G

Nuclear Physics **19** (1960) 164—172; © *North-Holland Publishing Co., Amsterdam*
Not to be reproduced by photoprint or microfilm without written permission from the publisher

ENERGY LEVELS OF Si^{29}, Si^{30} AND Si^{31} FROM (d, p) REACTIONS

C. P. BROWNE and J. T. RADZYMINSKI†

University of Notre Dame, Notre Dame, Indiana††

Received 10 March 1960

Abstract: The Si^{28} (d,p)Si^{29} reaction was used to locate nuclear energy levels in Si^{29} in the range of excitation energy between 3.5 and 9.1 MeV. The bombarding energy was 7.03 MeV and the MIT broadrange spectrograph was used to resolve the particle groups. Identification was based on a change of observation angle and a change of isotopic abundance in the target. A total of 65 levels of Si^{29} was found in the range covered, 54 of which have not been reported before. In addition, 16 particle groups were assigned to the reaction Si^{29}(d,p)Si^{30} and 7 groups to the reaction Si^{30}(d,p)Si^{31}. The Si^{30} levels lie in the range of excitation of 6.4 to 10.8 MeV and have not been reported before, whereas the Si^{31} levels lie between 2.3 and 5.5 MeV and two of these are new. Q-values and excitation energies are listed for all these groups. The uncertainty in Q-value for most of the levels is ± 5 keV.

1. Introduction

In the course of experiments on the Si^{28}(d, α)Al^{26}, O^{16}(d, α)N^{14} and O^{16}(d, p)O^{17} reactions[1]), SiO_2 targets on Formvar backings were bombarded with 7.03 MeV deuterons and all reaction products analyzed with the MIT broad-range magnetic spectrograph and recorded on nuclear track plates. These plates have now been read for all proton groups, the reaction energies computed and the groups assigned to the proper reactions.

This paper reports on the energy levels of Si^{29} and a few levels found in Si^{30} and Si^{31}. Twelve levels in Si^{29} were previously known from the Si^{28}(d, p)Si^{29} reaction[2, 3]), run at bombarding energies of 1.8 to 2.1 MeV. Seven of these levels were seen with the P^{31}(d, α)Si^{29} reaction[4]) at a bombarding energy of 1.8 MeV. Gamma rays have been observed from the Si^{28}(n, γ)Si^{29} reaction and some of them have been assigned to transitions in Si^{29} on the basis of the level structure found from charged particle spectra. These data are summarized by Endt and Braams[5]). Two resonances in the silicon total neutron cross section are assigned to levels in Si^{29} in the region of excitation covered by the present work[6]). Earlier work with low resolution and experiments giving information about spin and parity of some of the levels are summarized elsewhere[5]).

The region of excitation in Si^{30} in which levels are found in this experiment has been surveyed previously only with the Al^{27}(α, p)Si^{30} reaction using low

† Now, Lieutenant, United States Marine Corps.

†† Supported in part by the joint program of the Office of Naval Research and the United States Atomic Energy Commission.

resolution. Seven levels were tentatively assigned to Si^{30} between 6.5 and 10.8 MeV[7]). Five levels were known in Si^{31} in the region of present interest, all through the Si^{30}(d, p)Si^{31} reaction[3]).

2. Procedure

Experimental details concerning the apparatus, target preparation, and data analysis procedure, have been given elsewhere[1, 8]). Seven of the runs used in this work were made on natural silicon targets at observation angles of 15°, 30°, 40°, 50°, 60°, 70° and 90°. One run at 30° was made on a target enriched in Si^{29}. For each run, the input energy was precisely determined by measuring the energy of protons from the O^{16}(d, p)O^{17} reaction and using the well known Q-value for this reaction. This method automatically corrects for the energy lost by the deuterons in passing through the target backing when the target is set in the transmission position as it must be for forward angles of observation. Energy loss of protons in the SiO_2 layer was shown to be negligible both by noting that the peak shapes are just those caused by instrumental effects and deuteron energy spread and by the fact that Q-values calculated for runs with the target in transmission position agree with Q-values from runs with the target in reflection position.

The assignment of proton groups to the appropriate reaction was based mainly on the shift of output energy with change of observation angle but was confirmed in many cases by comparing the intensity of groups from the enriched target with the intensity of groups from the natural target. This procedure could not be used for the groups from the higher excited states because of an intense deuteron background on the plate exposed with the enriched target. This background, which prevented counting the α-particle tracks, arose from elastic scattering, by the target and backing, of deuterons in the beam which had lost energy by slit edge scattering.

To be consistent with all earlier work on the MIT spectrographs, all energies given in this paper are based on a value of 5.298 MeV for the energy of Polonium alpha-particles. If the polonium alpha energy is actually higher, as it seems to be[9]) all the energies listed here should be raised by the appropriate percentage.

3. Results

Figure 1 shows the proton spectrum taken at 50°. On the scale used for this figure many of the data points in the background regions and on small peaks are excluded by space limitations. The figure is as accurate a representation of the spectrum as can be made on this scale but more detail of peak shapes is available in the original data. The numbered groups are those assigned to Si^{29} levels, the numbers increasing with excitation and beginning with one for the

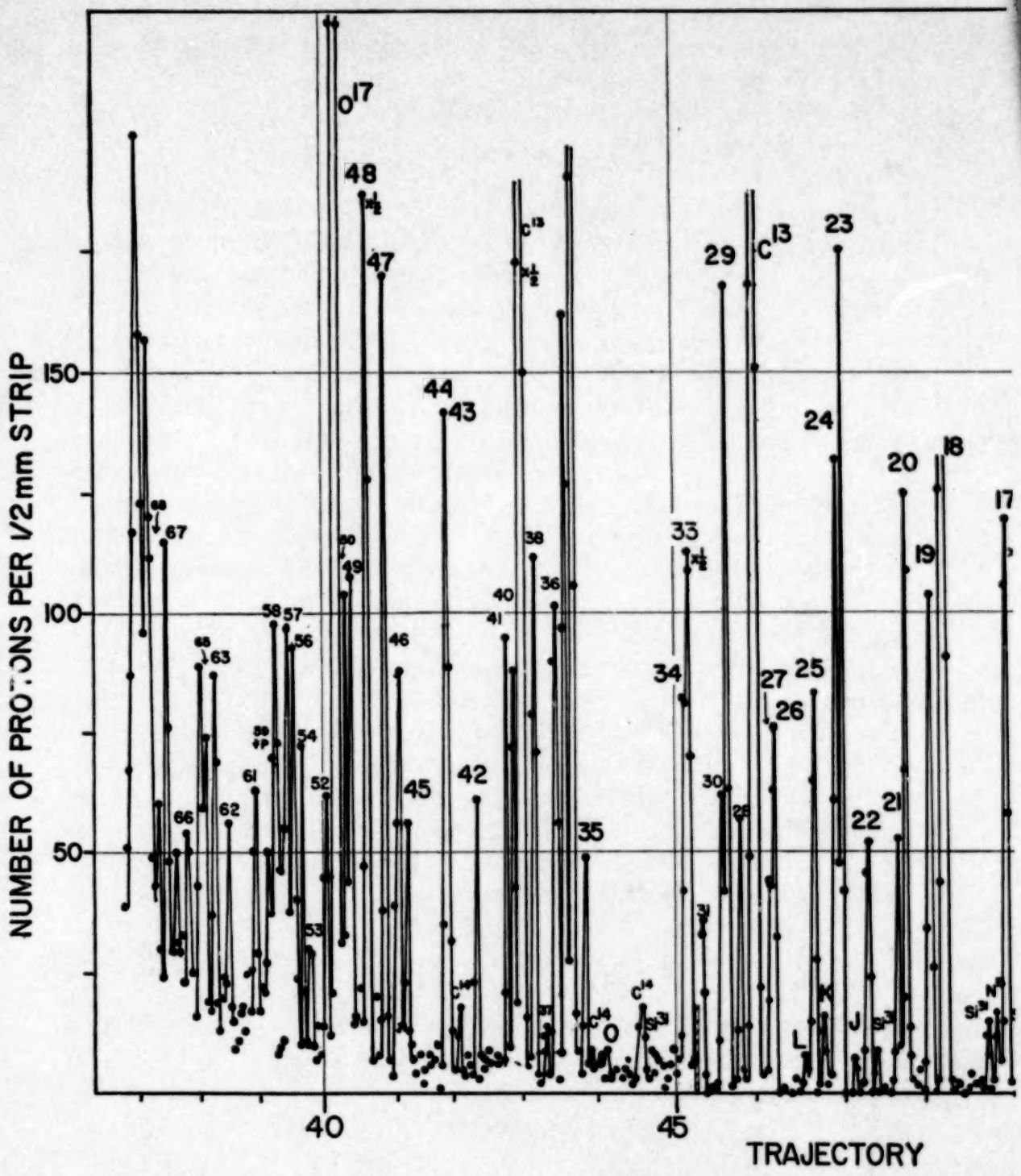

Fig. 1. Spectrum of protons observed at 50° from a SiO_2 on Formvar target bombarded with 7.034 MeV deuterons. In the regions between peaks, only representative points can be shown on this scale. Open topped peaks indicate groups of uncountable intensity. Numbered groups arise from levels in Si^{29}, lettered groups from levels in Si^{30}. Other groups are labelled with the symbol of the residual nucleus to which they lead.

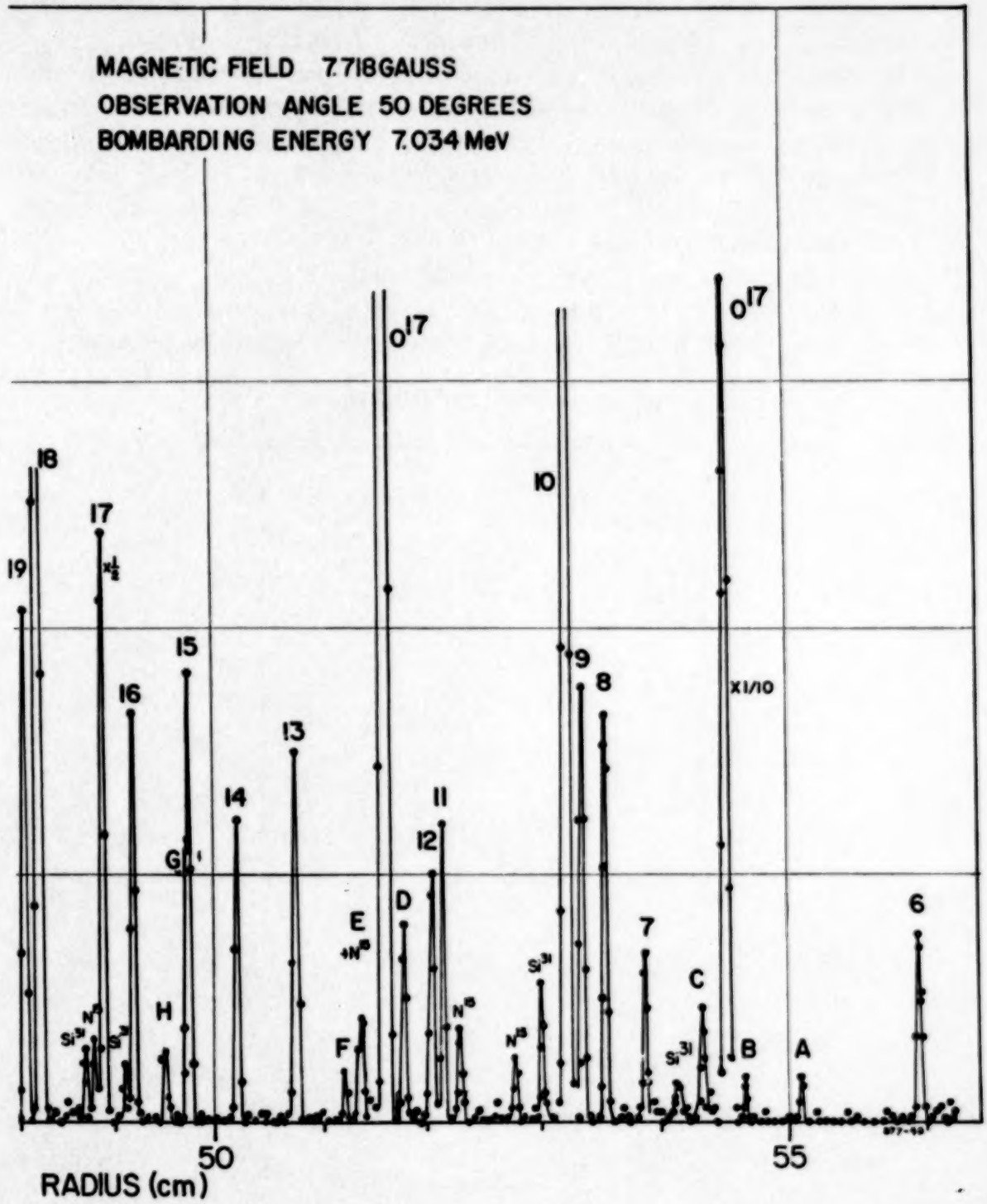

first excited state (not seen in fig. 1). The lowest energy level that could be seen at any of the field settings used in this experiment was the fifth excited state found by Endt *et al.*[2,3]). This numbering is continued here. Beyond level 6 the present numbers no longer correspond to those of Endt, because additional intermediate groups appear. It has been assumed, however, that there are no

unreported levels below the fifth. Groups assigned to the $Si^{29}(d, p)Si^{30}$ reaction are labelled alphabetically in fig. 1 in order of increasing excitation energy. Only those levels of Si^{30} having excitation energies between 6.0 and 12 0 MeV could give proton groups in the energy range covered by this experiment. Other groups in fig. 1 are labelled with the symbol for the residual nucleus to which they correspond. These include, in addition to the groups expected from the known target and backing materials, groups leading to N^{15} levels from a small nitrogen contamination in the target.

In several cases groups lie so close together that they are not resolved. An example of such a case and the procedure used to obtain the positions of the groups is illustrated in fig. 2. The peak shape caused by all instrumental and

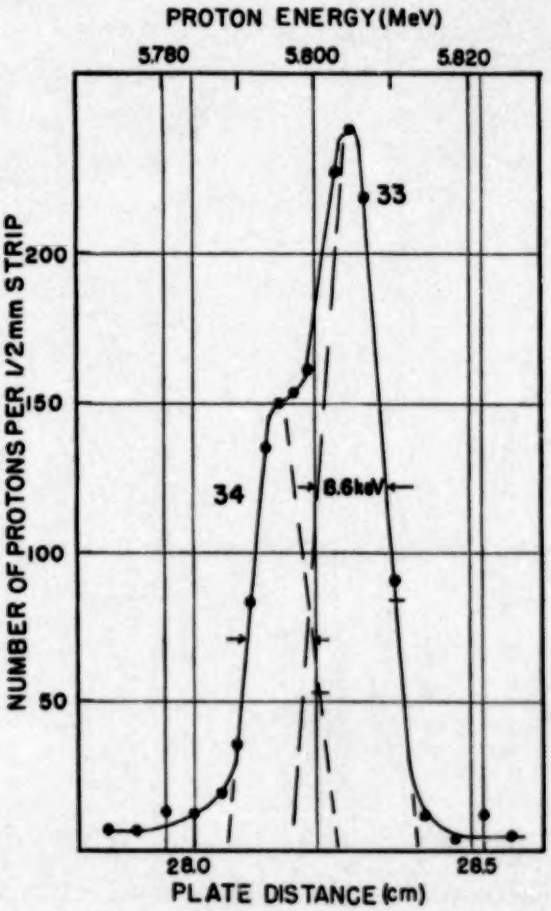

Fig. 2. Large scale plot of proton groups 33 and 34 illustrating resolution of combined groups into components.

target factors combined was well known from isolated groups near the unresolved groups. This peak shape is essentially a triangle with a width at half-maximum of 1.1 to 2.0 mm depending on the position along the plate. The corresponding spread in energy of the protons is about 8.6 keV. Practically all spread arises from the energy spread in the deuteron beam. Under the

conditions used here the effective resolution is about 700. The proper superposition of two or more such peaks, required to give the observed peak shape, was found and thus the correct group position was ascertained.

TABLE 1

Q-values and excitation of levels in Si^{29}

Group number	Number of runs	*Q*-value (MeV)[a]	Excitation energy (MeV)		Group number	Number of runs	*Q*-value (MeV)[a]	Excitation energy (MeV)
			Endt *et al.*[b]	Present work[c]				
1			1.278		36	6	−1.376	7.622
2			2.027		37	5	−1.402	7.648
3			2.426		38	6	−1.447	7.693
4			3.070		39	6	−1.489[d]	7.735[e]
5	3	2.625	3.623	3.621	40	6	−1.520	7.766
6	4	2.168	4.078	4.078	41	6	−1.541	7.787
7	5	1.509		4.737	42	7	−1.646	7.892
8	5	1.410	4.840	4.836	43	5	−1.740	7.986
9	5	1.353	4.897	4.893	44	5	−1.749	7.995
10	3	1.315	4.934	4.931	45	5	−1.889	8.135
11	5	0 994		5.252	46	4	−1.913	8.159
12	4	0.964		5.282	47	5	−1.962	8.208
13	6	0.596		5.650	48	4	−2.024	8.270
14	6	0.434		5.812	49	5	−2.085	8.331
15	6	0.299	5.946	5.947	50	5	−2.101	8.347
16	6	0.139	6.105	6.107	51	3	−2.122	8.368
17	6	0.054		6.198	52	4	−2.172	8.418
18	2	−0.132[d]	6.380	6.378	53	4	−2.233	8.479
19	6	−0.174		6.420	54	4	−2.259	8.504
20	6	−0.249		6.495	55	4	−2.280	8.526
21	6	−0.276		6.522	56	5	−2.293	8.539
22	6	−0.368		6.614	57	5	−2.310	8.556
23	5	−0.449		6.695	58	5	−2.355	8.601
24	5	−0.466		6.712	59	4	−2.363[d]	8.609
25	4	−0.535		6.781	60	2	−2.398[d]	8.644[e]
26	5	−0.660		6.906	61	4	−2.423	8.669
27	4	−0.673		6.919	62	4	−2.514	8.760
28	6	−0.771		7.017	63	4	−2.568	8.814
29	6	−0.812		7.058	64	5	−2.602	8.848
30	6	−0.828		7.074	65	4	−2.614[d]	8.860
31	7	−0.894		7.140	66	3	−2.662	8.908
32	5	−0.912		7.164[e]	67	5	−2.740	8.986
33	8	−0.937		7.183	68	3	−2.767	9.013[e]
34	4	−0.946[d]		7.192	69	2	−2.794[d]	9.040
35	5	−1.277		7.523	70	2	−2.807	9.053

[a] All *Q*-values have an uncertainty of ± 0.005 MeV except where noted specially.
[b] See ref. [2]) in text.
[c] Excitation energies based on a ground state *Q*-value of 6.246 MeV.
[d] These *Q*-values have an uncertainty of ± 0.008 MeV.
[e] Assignment to Si^{29} is doubtful.

3.1. Si^{29}

Q-values for the levels found in Si^{29} are listed in column 3 of table 1. The first column of this table shows the group number corresponding to the plot of fig. 1, and column 2 the number of independent measurements of the given Q-value. As the ground state group was not observed in this experiment, the ground state Q-value found in earlier work[3]) was used to calculate excitation energies. The value used is 6.246 MeV, and the resulting excitation energies appear in column 5 of table 1.

Errors in the present measurements are given for the Q-values. These do not include the uncertainty in the polonium α-energy used for calibration. In most cases the error listed is $\pm$ 5 keV but for some of the unresolved groups the uncertainty is estimated to be $\pm$ 8 keV as shown in the table. The assignment of four of the groups to the Si^{28}(d p)Si^{29} reaction is uncertain because of their low intensity and the presence of overlapping groups. Level 39 is particularly uncertain. From the run on the enriched target it seems that there are one or two groups leading to Si^{30} that overlap this group. The resulting mixture of peaks seen at the various observation angles does not yield a constant Q-value for either Si^{28}(d, p)Si^{29} or Si^{29}(d, p)Si^{30}. The fit is somewhat better for the former reaction so the group has been assigned to a Si^{29} level. Where assignments are uncertain the Q-values in table 1 have been so marked.

Column 4 in table 1 shows the excitation energies previously measured[2]) with the (d, p) reaction. It is seen that agreement in energy is excellent although some of the intermediate levels were missed at the lower bombarding energy. Of the levels measured in the present work, the ones numbered 5, 6 and 10 had been observed with the P^{31}(d, α)Si^{29} reaction[4]) with excitations of 3.619 $\pm$ 0.017, 4.078 $\pm$ 0.018 and 4.937 $\pm$ 0.020 MeV respectively. The agreement is again excellent. Levels above number 53 are unstable to neutron emission. Two resonances in the total neutron scattering cross section of Si^{28} correspond to levels 61 and 68. Taking 8.873 MeV for the neutron binding energy[5]) and adding the observed resonance energies[6]), one obtains 8.668 and 9.043 MeV respectively for the excitation energy; remarkably close to the present values. An energy level diagram for Si^{29} appears in fig. 3.

3.2. Si^{30}

Table 2 gives Q-values and excitation energies for sixteen levels found in Si^{30}. This is only a partial list of the levels in this nucleus, even in the range of excitation energies covered because only those groups with sufficient intensity to be seen with the natural silicon targets are recorded. Other groups appeared in the spectrum from the enriched target; but as only one exposure was made with this target, these groups could not be definitely assigned to the proper nucleus. None of the levels listed in table 2 correspond to levels suggested by earlier work[7]).

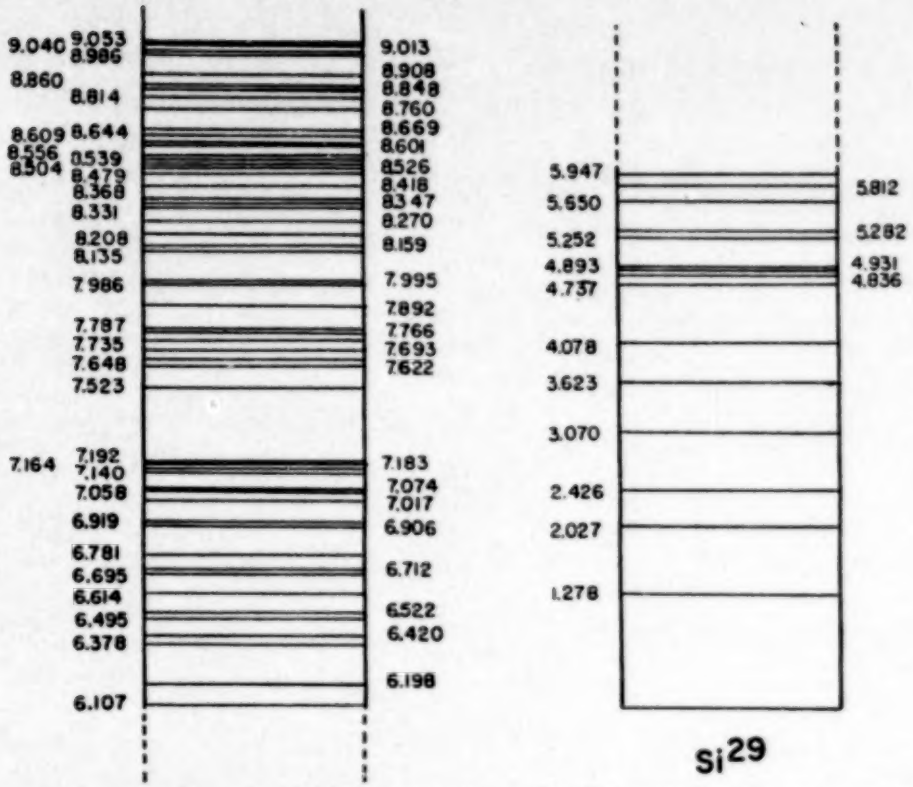

Fig. 3. Energy level diagram of Si^{29}. The levels from the fifth excited state up were observed in this experiment.

TABLE 2

Q-values and excitation energies of some levels in Si^{30}

Group letter	Number of runs	*Q*-value (±0.005) (MeV)	Excitation energy [a] (MeV)
A	3	1.891	6.494
B	3	1.755	6.630
C	4	1.651	6.734
D	6	0.888	7.497
E	3	(0.772)[b]	(7.613)[b]
F	5	0.727	7.658
G	2	0.292	8.093
H	4	0.236	8.149
I	2	−0.186	8.571
J	4	−0.405	8.790
K	4	−0.505	8.890
L	3	(−0.562)[b]	(8.947)[b]
M	4	−0.713	9.098
N	3	−0.861	9.246
O	4	−1.205	9.590
P	5	−2.375	10.760

[a] Excitation energy based on a ground state *Q*-value of 8.385 MeV.
[b] Assignment of this group is uncertain.

3.3. Si^{31}

Seven groups leading to levels in Si^{31} were seen and are listed in table 3. The group number in column 1 of this table corresponds to numbering of levels found in earlier work[3]) and the excitation energies from that work are given in column 4. A ground state Q-value of 4.364 MeV was used to calculate excitation

TABLE 3

Q-values and excitations of some levels in Si^{31}

Group	Number of runs	Q-value ($\pm$ 0.006) (MeV)	Excitation energy (MeV)	
			Van Patter[a]) ($\pm$ 0.008)	Present work[b])
3	1	2.042	2.319	2.322
4	3	1.576	2.791	2.788
5	3	1.227	3.140	3.137
6	4	0.829	3.539	3.535
7	4	—0.022	4.381	4.386
8	4	—0.361		4.725
9	3	—1.083		5.447

[a]) See ref. [3]) in text.

[b]) Excitation energy based on a ground state Q-value of 4.364 MeV.

energies from the presently measured Q-values and the results are listed in column 5. The agreement with the previous values is considerably better than the stated errors would indicate.

Angular distributions can be deduced from these data; but as a more ambitious program on angular distributions of several reactions involving the silicon isotopes is underway at MIT[10]), it was decided to give this separate report of the level positions.

The authors wish to thank Mr. George Pogue for doing much of the plate scanning.

References

1) C. P. Browne, Phys. Rev. **104** (1956) 1598; **108** (1957) 1007; **114** (1959) 807
2) Endt, Van Patter, Buechner and Sperduto, Phys. Rev. **83** (1951) 491
3) Van Patter and Buechner, Phys. Rev. **87** (1952) 51
4) Van Patter, Sperduto, Endt, Buechner and Enge, Phys. Rev. **85** (1952) 142(L)
5) P. M. Endt and C. M. Braams, Rev. Mod. Phys. **29** (1957) 683
6) Fields and Walt, Phys. Rev. **83** (1951) 479 (L);
Hughes and Harvey, BNL 325 (1955);
Day, Johnsrud and Lind, Bull. Am. Phys. Soc. **1** (1956) 56
7) Hassler, Steigert and Pieper, Bull. Am. Phys. Soc. **1** (1956) 280;
Brolley, Sampson and Mitchell, Phys. Rev. **76** (1949) 624
8) C. P. Browne and W. W. Buechner, Rev. Sci. Inst. **27** (1956) 899
9) Collins, McKenzie and Ramm, Proc. Roy. Soc. A **216** (1953) 219;
White, Rourke, Sheffield, Schuman and Huizenga, Phys. **109** (1958) 437;
Browne, Galey, Erskine and Warsh, Bull. Am. Phys. Soc. **5** (1960) 263
10) R. E. White, private communication

2.I *Nuclear Physics* **19** (1960) 173—183; © *North-Holland Publishing Co., Amsterdam*
Not to be reproduced by photoprint or microfilm without written permission from the publisher

RÉACTIONS SECONDAIRES DE SPALLATION

Marc LEFORT, Gabriel SIMONOFF et Xavier TARRAGO

Laboratoire de Physique Nucléaire de la Faculté des Sciences de Paris, ORSAY, B.P. n° 1 (S. et O.)

Reçu le 20 février 1960

Abstract: In the spallation nuclear reactions induced by 150 MeV protons on bismuth and thallium, light fragments are produced. Alpha particles induce secondary reactions. By radio-chemical study of astatine isotopes, cross sections for (α,2n) to (α,6n) reactions are measured. A cross section of 60 ± 10 mb is calculated for the production of helion fragments, and the energy distribution given. An upper limit is estimated for the production cross sections of lithium and beryllium fragments.

1. Introduction

Au cours du bombardement de noyaux lourds par des protons d'énergie élevée, plusieurs auteurs ont observé, outre l'émission de protons et de neutrons, celle de tritons, hélions, et même de fragments plus lourds comme des noyaux de lithium, beryllium, bore et carbone. Les sections efficaces des processus qui conduisent à ces fragments ne sont pas négligeables, du moins aux énergies supérieures à 300 MeV, et le problème s'est posé d'examiner l'origine de ces émissions. On a pu expliquer au moins une partie de la formation de tritium par évaporation des noyaux résiduels disposant d'une énergie d'excitation de plusieurs centaines de MeV. Aux énergies plus basses, un phénomène d'interaction directe décrit sous les termes de "pick up" et "double pick up" rend compte des sections efficaces relativement élevées et de la distribution anisotrope des tritons[1]). Par contre, la formation de fragments plus lourds pose le problème de la probabilité d'existence de ces fragments dans les noyaux et de leur expulsion à un instant donné, par un processus d'interaction directe.

La plupart des travaux relatifs[2,3]) à cette question ont été faits en examinant les traces des fragments projetés dans des émulsions nucléaires. Deutsch[4]) a étudié la distribution angulaire en énergie de He^3, He^4, $Li^{6\text{ à }9}$, $Be^{8\text{ à }12}$ et $C^{10\text{ à }14}$ produits par des protons de 332 MeV sur diverses cibles, dont l'or et l'uranium.

Nous nous sommes intéressés à un autre aspect: la plupart de ces fragments sont émis avec une énergie suffisante pour provoquer à leur tour sur les noyaux cibles des réactions nucléaires que l'on qualifiera de *secondaires*. Les noyaux excités ainsi formés évaporent un nombre de nucléons qui dépend de l'énergie d'excitation, donc de l'énergie du fragment au moment de la réaction. C'est ainsi que Marquez et Perlman[5]) ont observé la formation d'iode dans le bombardement d'étain par des protons de 335 MeV et l'ont expliquée par la réaction

secondaire de fragment Li sur l'etain. Batzel *et al.*[6]) puis Lavroukhina[6]) ont observé que du germanium et du gallium étaient formés lors du bombardement de cuivre par des protons de 130 à 480 MeV. Turkevich et Sugerman[7]) ont également observé le gallium, le germanium et aussi l'arsenic produits sur le cuivre par des protons de 2.2 GeV.

Metzger et Miller[8]) ont récemment fait une étude très complète sur les réactions secondaires des fragments hélions, lithium et beryllium produits sur l'or par des protons de 380 MeV. Par la mesure de plusieurs isotopes du thallium, du plomb et du bismuth, ils ont pu accéder à la section efficace de formation de ces fragments. Enfin Kurchatov *et al.*[9]) ont procédé au même genre d'étude pour les hélions produits à partir du bismuth par des protons de 480 MeV, en mesurant les sections efficaces apparentes des astates 211 et 210. Nous avons entrepris un travail sur les réactions secondaires induites sur le bismuth et le thallium par des protons d'énergie plus faible que celles utilisées par les auteurs précédents (150 MeV), et nous pouvons considérer comme très petite la probabilité d'émission d'hélions ou de fragments plus lourds par évaporation.

En mesurant les sections efficaces de plusieurs réactions secondaires correspondant à plusieurs nombres de neutrons émis, on peut calculer la section efficace de formation et la distribution en énergie des fragments F, moyennant la connaissance ou l'estimation des fonctions d'excitation des réactions (F,n) (F,2n) . . . (F,xn).

Si on appelle $\sigma_{(p,F)}$ la section efficace de formation du fragment F, sa variation en fonction de l'énergie est $\sigma_{(p,F)}\,\mathrm{d}E$. Ces fragments de diverses énergies initiales E sont ensuite ralentis dans la cible et leur probabilité de produire une réaction secondaire (F,xn) dépend de leur énergie au moment de la réaction. La section efficace de la réaction (F,xn) varie donc elle-même le long du parcours du fragment. Si l'on désigne par $\mathrm{d}l$ un élément de parcours au cours duquel l'énergie varie de $\mathrm{d}E$, la section efficace "apparente" de formation du produit d'une réaction secondaire (F,xn) sera donnée par

$$\sigma_s = \int_0^{E\,\max} \int_E^0 \sigma_{(p,F)}\,\sigma_{(F,xn)}\,\mathrm{d}l/\mathrm{d}E\,,$$

le ralentissement étant lui-même lié à l'énergie par les relations classiques parcours-énergie.

2. Irradiation, Séparations Chimiques et Conditions de Mesures

Les cibles de bismuth ont été préparées en fondant du bismuth sous atmosphère d'azote pour éviter l'oxydation et en le refroidissant brusquement dans l'air liquide. On obtient ainsi un lingot malléable que l'on peut laminer facilement en feuilles de 0.1 mm d'épaisseur. La pureté de ce bismuth fourni par Johnson-Matthey, est de 99.99%.

Les cibles de thallium étaient préparées en laminant de petits lingots de

thallium très pur (99.999%) (Johnson-Matthey). Elles étaient conservées en absence d'oxygène pour éviter l'oxydation.

Pour mesurer une section efficace de produits secondaires qui ait une signification, il faut que l'épaisseur des cibles soit grande devant le parcours des fragments les plus énergiques. Mais l'attaque chimique de feuilles très épaisses est longue et difficile, de sorte que nous avons irradié des empilements de plusieurs feuilles, dont chacune est relativement mince (0.1 mm), et nous avons traité celles pour lesquelles les fragments susceptibles de s'échapper sont remplacés par des fragments issus des feuilles précédentes. On a vérifié ainsi que la section efficace apparente augmentait depuis la première feuille jusqu'à la troisième, puis restait constante. Ceci montre par ailleurs que les fragments énergiques sont émis vers l'avant, au moins pour une grande partie.

Le bismuth et le thallium fondent à des températures assez basses et évacuent assez mal la chaleur. Par ailleurs, l'astate est très volatil. Pour éviter le risque de perte d'astate ou même de polonium dans la chambre à vide du synchrocyclotron, on a irradié en faisceau externe, à une intensité d'environ 0.1 μA. Le flux de protons était mesuré grâce à des moniteurs d'aluminium de 0.02 mm d'épaisseur, placés en avant et en arrière des feuilles de bismuth et de thallium. On avait placé entre le bismuth et le moniteur des feuilles de garde contre le recul des produits de fission. On a pris comme section efficace de la réaction Al (p, 3pn) la valeur de 9.0×10^{-3} barns, trouvée par Hicks *et al.*[10]). Cette valeur a d'ailleurs été vérifiée en utilisant comme moniteurs secondaires des lames de polystyrène et de plexiglass, grâce auxquelles on a trouvé une section efficace de 45 mb $\pm$ 2 pour la réaction ^{12}C (p, pn) ^{11}C, valeur superieure de 8 % à celle indiquée par Crandall *et al.*[11]). Après irradiation, on séparait l'astate du bismuth et de tous les produits susceptibles d'être formés (principalement polonium, plomb, thallium, mercure et or). Cette méthode doit être particulièrement poussée en ce qui concerne le polonium, puisque celui-ci posède des isotopes émetteurs alpha comme l'astate, qui sont produits par réactions primaires (p, xn) avec des sections efficaces plusieurs milliers de fois supérieures à celles des astates. Après attaque du bismuth par l'acide nitrique concentré, on ajoute de l'acide chlorhydrique diliué et de l'acide tellurique comme entraîneur. On précipite par le chlorure stanneux tellure, astate et polonium. Le précipité est redissous après lavages, dans une goutte d'HNO_3, puis HCl 3N. Une solution de chlorhydrate d'hydrazine saturée de SO_2 précipite alors tellure et astate, le polonium restant en solution. Ce précipité dissous par HNO_3 est mis en solution alcaline par addition de soude. Une nouvelle séparation par précipitation par le stannite de sodium en milieu alcalin élimine le tellure et éventuellement le polonium restant. Dans le filtrat l'étain est complexé par addition de fluorure et la solution est remise en milieu acide par addition d'HCl. Le fluorure empêche la précipitation de l'étain en milieu neutre, précipitation au cours de laquelle l'astate s'adsorberait. Enfin on fait tourner une lame d'argent dans la solution

environ 0.5 N HCl et l'astate se dépose à 75 % en moins d'une heure. On contrôle ce dépôt de façon à déterminer son rendement exact, en exécutant l'opération de dépôt plusieurs fois successives sur la même solution. On a pu vérifier ainsi que moins de 1/1000 du polonium initial est présent sur la lame d'argent.

Le rendement total de l'extraction est contrôlé par un dépôt sur argent sans séparation préalable, et mesure du polonium 211 issu de l'astate 211.

Le traitement des cibles de thallium pourrait être beaucoup simple. En effet aucun émetteur alpha ne peut être produit par réaction primaire et la séparation polonium-astate n'est pas indispensable car ils doivent être formés en quantités comparables. La spectrométrie alpha permet alors de les distinguer. Cependant il est nécessaire d'éliminer les isotopes de l'or, du mercure et du thallium, car les électrons de conversion sont émis en grand nombre au cours de leur désintégration γ, et empêchent le fonctionnement régulier de la chambre à impulsion détectrice des rayons α. Après l'attaque, on précipite donc le thallium avec de l'acide chlorhydrique. Le chlorure mercureux et le chlorure d'or sont entraînés alors que le polonium et l'astate restent en solution sans adsorption. On procède ensuite à leur dépôt spontané sur une lame d'argent. Comme nous nous sommes bornés à rechercher l'astate 211 et les polonium 210 et 206, la séparation chimique entre At et Po n'ést pas utile.

La détection et le comptage des désintégrations α des produits formés ont été faits avec une chambre à boule à collection électronique. La chambre à boule est remplie d'un mélange d'argon et de 3 % de gaz carbonique à une pression de 3.5 atm et la tension entre les électrodes est de 5000 V. Les impulsions sont analysées après amplification sur un sélecteur à 100 canaux. Le pouvoir de résolution correspond à une largeur à mi-hauteur de 90 keV pour les rayons α du polonium (5.3 MeV) et l'étalonnage en énergie a été fait avec le depôt actif du thoron.

L'astate 211 est identifié par son rayonnement α de 5.86 MeV (40.9 %) et par celui du polonium 211 de très courte période (7.44 MeV) issu de la desintégration par capture électronique de ^{211} At. L'astate 210 est mesuré grâce au polonium 210 accumulé après la séparation. De même l'isotope 208 de période 6.3 h conduit à ^{208}Po, émetteur α de 2.93 ans. On a obtenu quelques indications sur ^{209}At qui conduit à ^{209}Po par capture, ce dernier ayant une période de 103 ans et émettant des rayons alpha de 4.8 MeV. ^{207}At, de période 1.8 h, se désintègre par émission alpha pour 10 % et a pu être approximativement mesuré. Enfin, l'isotope 206 forme ^{206}Po par capture. Celui-ci se désintègre partiellement par émission alpha avec une période totale de 9 jours. La valeur la plus probable du rapport d'embranchement est de 5 % $\pm$ 1, selon Momyer et Hyde[12]).

3. Résultats

Pour la formation d'astate dans le bismuth, on a obtenu les valeurs indiquées dans le tableau 1. Ces valeurs sont comparées à celles de réactions équivalentes

mesurées sur l'or pour des protons de 380 MeV par Metzger et Miller[8]), et sur le bismuth pour 480 MeV par Kurchatov *et al.*[9])†.

TABLEAU 1

Sections efficaces pour la formation d'astate dans le bismuth.

Énergie des protons (MeV)	Référence	Produit	Sections efficaces en microbarns					
			$\sigma_{\alpha,2n}$	$\sigma_{\alpha,3n}$	$\sigma_{\alpha,4n}$	$\sigma_{\alpha,5n}$	$\sigma_{\alpha,6n}$	$\sigma_{\alpha,7n}$
150		^{206}At à ^{211}At	5 ± 0.5	5 ± 0.5	4 ± 1	1.1 ± 0.2	0.5 ± 0.2	0.5 ± 0.1
180	[9])	^{210}At, ^{211}At	21					
480	[9])		63	20				
380	[8])	^{195}At à ^{201}Tl	22.5 ± 4.7	42 ± 8	1.71 ± 0.27	17 ± 7	13.6 ± 0.9	

On remarquera que la formation d'astate 211 pourrait être interprétée aussi bien comme une réaction (α, 2n) sur le bismuth que comme une réaction (^{3}He, n). Cependant, on a négligé cette dernière contribution, car Deutsch[4]) a montré que la production de ^{3}He représente moins de 4% de celle de l'ensemble des fragments d'hélium émis.

Le thallium irradié n'étant pas monoisotopique (^{205}Tl 75% — ^{203}Tl 25%) on ne peut plus faire correspondre à un seul isotope de l'astate ou du polonium une seule réaction. On a trouvé que la section efficace apparente de ^{210}Po qui correspondrait aux réactions (^{8}Li, 3n) et (^{8}Li, n), (^{7}Li, 2n), (^{7}Li, γ) et (^{6}Li, n), était de 5×10^{-3} μb. Pour ^{206}Po, la limite de détection correspond à une section efficace maximum de 10^{-4} μb.

Nous n'avons pu détecter d'astate. D'après l'évaluation de la sensibilité de nos mesures faites pendant 24 heures, on a pu calculer que si une réaction secondaire avait lieu avec le beryllium, sa section efficace apparente ne pouvait dépasser 2×10^{-7} μb (2×10^{-13} b).

Si l'on compare aux valeurs trouvées par Metzger et Miller[8]) sur l'or, on constate que la diminution d'énergie de 380 à 150 MeV diminue d'un facteur 30 les sections efficaces de réactions attribuables au lithium et d'un facteur 10^4 celles dues au beryllium, si toutefois de telles réactions ont lieu. Ces auteurs trouvaient en effet 0.131 μb pour ^{199}Pb et 0.0026 μb pour ^{203}Bi et ^{204}Bi.

4. Discussion et Analyse Relative à la Formation de Fragments

4.1. FONCTIONS D'EXCITATION DES REACTIONS (α,xn) SUR LE BISMUTH

On peut en principe remonter à la section efficace de formation de fragments alpha ($\sigma_{(p,\alpha)}\,dE$), et à la variation de cette section efficace en fonction de l'énergie

† *Note ajoutée sur épreuve*: Tout récemment Kalkine et ses collaborateurs[23]) ont indiqué pour ^{211}At et ^{210}At à 130 MeV les valeurs de 5.2 et 3.3 μb en très bon accord avec les notres.

de ces fragments, à partir de la mesure des sections efficaces apparentes de plusieurs isotopes de l'astate. Il est nécessaire pour celà de connaître les fonctions d'excitation des réactions (α, xn) qui conduisent aux isotopes 206 à 211 de l'astate. Kelly et Segré[13]) ont établi expérimentalement ces fonctions pour (α, 2n) et (α, 3n). Sur la figure 1 nous avons porté ces deux courbes ainsi que celles calculées pour x allant de 4 à 6. La construction de ces courbes est faite selon la méthode de Jackson[14]) qui permet d'obtenir la probabilité d'évaporation de x neutrons d'un noyau disposant d'une énergie d'excitation donnée. Si E_0 est l'énergie de la particule incidente et $\sigma_c(E_0)$ la section efficace de capture de cette particule conduisant au noyau composé, on a la section efficace

$$\sigma_{(\alpha,xn)} = \sigma_c(E_0) \sum_{i=0}^{x} q\,(i, 0)\, P\,(E, x - i)\ ;$$

$q\,(i, 0)$ est la probabilité d'émission directe de i neutrons et 0 protons et $P\,(E, x - i)$ la probabilité moyenne d'évaporation de $(x - i)$ neutrons. Le calcul de Jackson est fait pour des protons incidents La même énergie d'excitation est produite dans le noyau composé par des protons et par des particules alpha, si l'énergie de ces dernières est plus élevée d'environ 11 MeV pour le bismuth, en raison de l'énergie de liaison des protons B_p que l'on admet d'environ 5 MeV, alors que pour les particules alpha $B_\alpha = -28 + 2B_p + 2B_n$ est d'environ −6 MeV.

Les valeurs de $\sigma_c(E_0)$ ont été prises d'après les tables de Blatt et Weisskopf[15]) en extrapolant lorsque $Y = E_0/V$ est supérieure à 1.8 (V étant la barrière de potentiel). Il faut remarquer que les calculs de Jackson ont été faits pour un

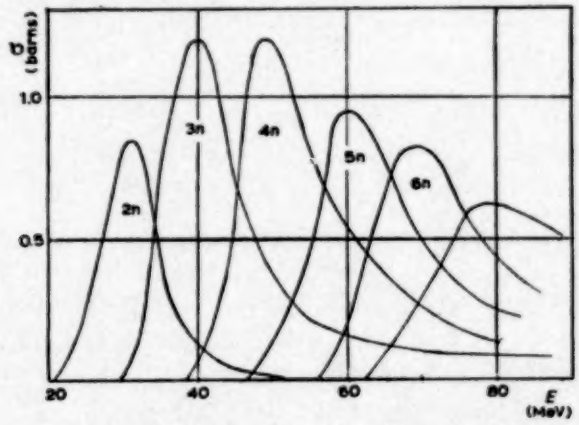

Fig. 1. Fonctions d'excitation (α, x n).

rayon $R = 1.35 \times 10^{-13}\, A^{\frac{1}{3}}$ cm. Shapiro[16]) a souligné un léger désaccord entre les résultats de Kelly et Segrè et les calculs de section géométrique σ_c, lorsqu'on prend $r_0 = 1.35 \times 10^{-13}$ cm. Il faut utiliser $r_0 = 1.5 \times 10^{-13}$ cm pour obtenir un accord avec les fonctions expérimentales d'excitation (α, 2n) et (α, 3n). Nous avons donc tracé les courbes pour (α, 4n), (α, 5n) et (α, 6n) avec $r_0 = 1.5 \times 10^{-13}$ cm (fig. 1).

Nous n'avons apporté aucune autre modification aux calculs de Jackson, conformément aux résultats obtenus par John[17]). Cet auteur a en effet montré que les fonctions d'excitations ^{206}Pb (α, xn) et ^{209}Bi (p, xn) étaient pratiquement confondues à condition de translater de 12 MeV l'échelle des abcisses pour les particules alpha.

Par ailleurs nous avons été guidés par les indications données par Igo[18]), selon lesquelles la section efficace de toutes les réactions (α, xn) est relativement constante en fonction de l'énergie à partir de 35 MeV et ne dépasse pas 2 b.

4.2. RALENTISSEMENT ET DISTRIBUTION DES FRAGMENTS ALPHA

Si l'on considère maintenant sur une de ces fonctions d'excitation un petit intervalle d'énergie ΔE, on voit que le nombre d'evenements correspondant à la formation d'un produit de réaction secondaire dans cet intervalle ΔE, est égal au produit de la section efficace différentielle de la réaction (α, xn) à l'énergie comprise entre E et $E + \Delta E$, par le nombre de particules α se trouvant à cette énergie et réagissant le long d'un parcours défini par le ralentissement de $E + \Delta E$ à E. Ce nombre dépend lui-même du nombre de fragments α ralentis à l'énergie $E + \Delta E$, du nombre de noyaux cibles par cm^3 et de l'épaisseur traversée, c'est à dire du parcours Δl nécessaire pour ralentir de $E + \Delta E$ à E. On peut l'écrire $\sigma_\alpha(E) n \Delta l$. $\sigma_\alpha(E)$ dépend elle-même de la section efficace de formation des fragments alpha par le bombardement des protons $\sigma(\mathrm{p},\alpha)$, de la distribution initiale en énergie de ces fragments et de la façon dont ils sont ralentis.

On pourrait en principe trouver cette distribution initiale à partir des sections efficaces apparentes de plusieurs isotopes issus des réactions secondaires. Nous avons procédé plus empiriquement en essayant diverses relations de distribution en énergie des fragments et en choisissant celle qui conduisait au meilleur accord avec les résultats.

C'est par une méthode analogue qu'ont procédé Kurchatov *et al.*[9]). Cependant ils ont choisi comme distribution initiale celle donnée par la théorie de l'évaporation et ils ont utilisé pour les hélions la relation de Le Couteur[19])

$$P(E) = \frac{E - V}{\tau^2} \, \mathrm{e}^{-\frac{E-V}{\tau}}$$

(V représenté la barrière de potentiel pour les α et τ la température nucléaire). Une telle distribution paraît discutable, même pour des protons incidents de 480 MeV, car elle implique le processus d'évaporation et une distribution isotrope des noyaux d'hélium. Cette répartition favorise les particules de faibles énergies et les auteurs soviétiques ont dû prendre une température nucléaire très élevée ($\tau = 5$ MeV) pour obtenir un accord avec leurs résultats. A 150 MeV, ce type de distribution n'est plus du tout utilisable, car il exclurait presque

complètement la production d'astate 208 à 206 qui nécessite des particules alpha de plus de 60 MeV. D'autre part nos expériences ont bien montré une distribution vers l'avant des fragments alpha, qui semble indiquer un processus d'interaction directe.

Nous avons essayé une relation empirique du type $P(E) = P(E_s)\, e^{-k(E-E_s)}$ entre $E_s = 20$ MeV et 100 MeV. (E_s correspond approximativement au seuil de la réaction $(\alpha,2n)$ et k est une constante.) $P(E_s)$ et k ont été déterminés en essayant diverses valeurs et en comparant le résultat du calcul avec les sections efficaces secondaires expérimentalement mesurées pour $(\alpha,2n)$ à $(\alpha,6n)$. La courbe de la figure 2 est celle qui coïncide le mieux avec ces résultats. On a

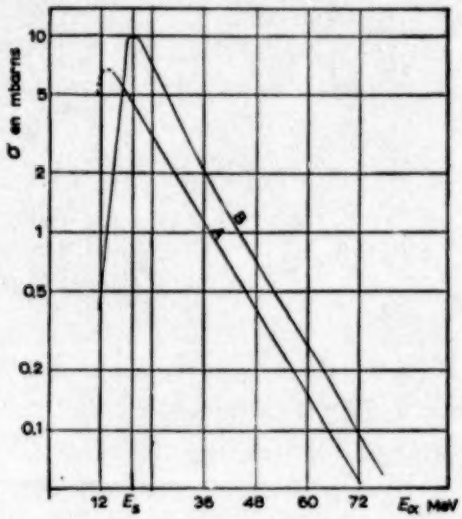

Fig. 2. Distribution en énergie des fragments α. A: Protons de 150 MeV. B: Protons de 190 MeV (Bailey[20]).

choise $\sigma_s = 5 \times 10^{-3}$ b et $k = 0.09$. La forme de cette distribution est d'ailleurs très voisine de celle observée par Bailey[20]) par mesure directe des hélions projetés par des protons de 190 MeV sur l'or, courbe reproduite aussi sur la figure 2. La distribution des particles α de moins de 20 MeV n'a pas d'influence puisque le seuil de la première réaction étudiée $(\alpha,2n)$ est déjà à 21 MeV.

Sur la courbe de la figure 2, on a pris des intervalles d'énergie de 6 MeV en 6 MeV entre 78 et 21 MeV et on a porté la section efficace partielle de production des fragments α. D'après les tables de pouvoir de ralentissement données par Aron *et al.*[21]) pour le plomb, on a calculé l'épaisseur nécessaire au ralentissement dans le bismuth pour chaque intervalle. Pour une bande d'énergie de 6 MeV comprise entre E_i et $E_i + 6$ MeV, on ajoute au nombre de particules α produites dans cette bande celles qui ont été ralenties jusqu'à cette valeur E_i. On obtient la probabilité de réaction des particles α d'énergie comprise entre E_i et $E_i + 6$ MeV en multipliant leur nombre par la portion de parcours Δl_i correspondant à ces 6 MeV et par le nombre de noyaux de bismuth par cm³. On multiplie enfin par la section efficace dans cette bande d'énergie de la réac-

tion (α, xn) considérée, section efficace déterminée d'après les courbes de fonctions d'excitations expérimentales pour $(\alpha, 2n)$ et $(\alpha, 3n)$ et calculées pour $x > 3$ (fig. 2). En faisant la somme des valeurs calculées pour chaque bande de 6 MeV comprise entre 78 et 21 MeV, on obtient la section efficace apparente de la réaction secondaire envisagée. On trouve dans le tableau 2 les valeurs ainsi

TABLEAU 2

Sections efficaces du réaction secondaire

Réaction secondaire	Produit	Section efficace (μb)	
		Expérience	Calcul
$\sigma_{\alpha,3}$	^{211}At	5 ± 0.5	5.2
$\sigma_{\alpha,3}$	^{210}At	5 ± 0.5	5.3
$\sigma_{\alpha,4}$	^{209}At	4 ± 1	3.2
$\sigma_{\alpha,5}$	^{208}At	1.1 ± 0.2	1.0
$\sigma_{\alpha,6}$	^{207}At	0.5 ± 0.2	0.35

calculées pour $x = 2, 3, 4, 5$ et 6 comparées aux valeurs expérimentales en prenant la distribution initiale des fragments α

$$\sigma(E)\,\mathrm{d}E = 6(\mathrm{mb/MeV})\,\mathrm{e}^{-0.090\,(E-E_0)} \quad (E, E_0 \text{ en MeV}) .$$

On obtient une section efficace totale de production de fragments alpha de 60 ± 10 mb, l'énergie de ces α étant comprise entre 20 et 78 MeV. D'après la distribution de Bailey on peut évaluer à 100 mb cette section efficace, l'énergie des protons étant de 190 MeV au lieu de 150.

Par ailleurs, Perfilov et Ostroumov[3]) ont trouvé 150 à 160 mb pour les α de plus de 20 MeV produits dans le bismuth par des protons de 480 MeV, par la mesure directe des traces des fragments α dans les émulsions nucléaires.

Il faut enfin remarquer qu'une traine de fragments alpha de grandes énergies semble exister puisque nous trouvons encore 0.5 μb pour ^{206}At, qui correspondrait à $(\alpha, 7n)$.

4.3. LITHIUM ET BERYLLIUM

La formation de lithium, beryllium et fragments plus lourds n'a été observée que pour des énergies de particules incidentes beaucoup plus élevées que 150 MeV. On l'a considérée initialement comme un phénomène de fission[6]), mais l'étude de la répartition angulaire a montré une forte distribution vers l'avant[4]). La production de beryllium par bombardement par des particules α accélérées entre 30 et 40 MeV a été expliquée par un processus de pick-up, les hélions captant dans le noyau cible un fragment ^{3}He pour donner ^{7}Be[22]). Mais ce phénomène a une importance très faible pour les noyaux lourds.

D'après l'évaluation de la sensibilité de nos mesures sur les réactions secondaires on peut essayer d'estimer l'ordre de grandeur de la section efficace maximum de ces fragments. On ne connaît pas les fonctions d'excitations des réactions (Li,xn) et (Be,xn), ni les proportions de chacun des isotopes formées pour chaque élément. On peut seulement calculer $\bar{\sigma}_c$, section géométrique moyenne globale de capture des fragments par les noyaux de thallium pour des énergies comprises entre 40 et 100 MeV. Le ralentissement dans le thallium des fragments de lithium varie de 3×10^{-4} à 5×10^{-4} cm par MeV, celui du beryllium de 2 à 3×10^{-4} cm par MeV. On peut calculer grossièrement la section efficace maximum de production de ces fragments

$$\sigma_F = \frac{\sigma_s}{\int_{40}^{100} n\sigma_c dl},$$

où n est le nombre de noyaux par cm^3. On obtient ainsi que la section efficace des beryllium est inférieure à 3×10^{-3} μb et celle des lithium est d'environ 30 μb. Ces valeurs sont très faibles et laissent peu d'espoir pour une mesure directe, même par la technique des émulsions nucléaires pour la détection de ^{7}Be radioactif. En comparant aux résultats obtenus par Metzger et Miller[8]) on s'aperçoit, que la baisse d'énergie des protons incidents de 380 à 150 MeV diminue dans des proportions considérables la production de fragments béryllium.

Nous remercions Madame Brun pour l'aide précieuse qu'elle nous a apportée au cours de ce travail, l'equipe de conduite du synchrocyclotron et le service d'électronique du laboratoire pour leur concours bienveillant.

Bibliographie

1) Voir par exemple Chew et Goldberger, Phys. Rev. **77** (1950) 470
2) S. Katcoff, Phys. Rev. **114** (1959) 903;
S. C. Wright, Phys. Rev. **79** (1950) 838;
S. O. C. Sorensen, Phil. Mag. **40** (1949) 947;
D. H. Perkins, Proc. Roy. Soc. **203** (1950) 399
3) N. A. Perfilov et V. A. Ostroumov, Dokl. Akad. Nauk **103** (1955) 227
4) R. W. Deutsch, Phys. Rev. **97** (1955) 1110
5 L. Marquez et I. Perlman, Phys. Rev. **81** (1951) 953
6) R. E. Batzel, D. R. Miller et G. T. Seaborg, Phys. Rev. **84** (1951) 671;
Lavroukhina, Thèse, Geochim. Acad. Sci. URSS (1955)
7) A. Turkevich et N. Sugerman, Phys. Rev. **94** (1954) 728
8) A. E. Metzger et J. M. Miller, Phys. Rev. **113** (1959) 1125
9) B. V. Kurchatov, V. N. Mekhedov, L. V. Chistiakov, M. Ia. Kuznetsova, N. I. Borisova et V. G. Soloviev, JETP **35** (1958) 56;
V. V. Kuznetsova, V. N. Mekhedov et V. A. Khalkin, Rapport du centre international de recherche nucléaire à Dubna, URSS (1957)
10) H. G. Hicks, P. C. Stevenson et W. E. Nervick, Phys. Rev. **102** (1956) 1390
11) W. E. Crandall, G. P. Millburn, R. V. Pyle et W. Birnbaum, Phys. Rev. **101** (1956) 329

12) F. F. Momyer et E. K. Hyde, J. Inorg. Nucl. Chem. **1** (1955) 274
13) E. L. Kelly et E. Segré, Phys. Rev. **75** (1949) 999
14) J. D. Jackson, Can. J. Phys. **34** (1956) 767
15) J. M. Blatt et V. F. Weisskopf, Theoretical Nuclear Physics (John Wiley, New York, 1952) pp. 352, 353
16) M. H. Shapiro, Phys. Rev. **90** (1953) 171
17) W. John, Phys. Rev. **103** (1956) 704
18) G. Igo, Phys. Rev. **115** (1959) 1665
19) K. J. Le Couteur, Proc. Phys. Soc. A **65** (1956) 718
20) L. E. Bailey, UCRL 3334 (1956), cité par réf. [8])
21) Aron, Hoffman et Williams, AECU 663 (1949)
22) G. H. Bouchard, Phys. Rev. Letters **3** (1959) 407
23) Van Youn Yu, V. V. Kuznetsov, M. Ia. Kuznetsova et V. A. Kalkine, Rapport de l'Institut unifié de Recherches Nucléaires, Dubna (1960), p. 471

2.D *Nuclear Physics* **19** (1960) 184—198; © *North-Holland Publishing Co., Amsterdam*
Not to be reproduced by photoprint or microfilm without written permission from the publisher

RADIATIVE PROTON CAPTURE IN Ni^{58}

J. H. CARVER

Australian National University, Canberra

and

G. A. JONES

A.E.R.E., Harwell

Received 31 March 1960

Abstract: The resonance structure of the reaction $Ni^{58}(p,\gamma)Cu^{59}$ has been studied by measuring the positon activity of 81 sec Cu^{59}. There have been observed 153 new resonances for proton energies between 1.8 and 4.3 MeV. The results can be fitted to a level spacing formula of the form $D(U) = 3.8 \times 10^4\, U^2 \exp\{-2\sqrt{5U}\}$ keV (U is in MeV). The nuclear temperature, and hence the slope of the $D(U)$ curve, is in agreement with Cameron's semi-empirical formula which, however, underestimates the absolute spacings by a factor ≈ 15. The data are interpreted as giving the spacings of levels of all spins. The spacings of the $\frac{1}{2}^+$ and $\frac{3}{2}^+$ states of Cu^{59} are known from previous proton inelastic scattering measurements and combining the two sets of data determines the moment of inertia for Cu^{59} as 0.35 ± 0.12 of the rigid body value. The total radiation widths $g\Gamma_\gamma$ have been determined for the levels with excitations $U = 5$ to 7.5 MeV and the average value $\overline{g\Gamma_\gamma}(U)$ is found to increase systematically with U. The photon strength function $\overline{g\Gamma_\gamma}(U)/\overline{D}(U)$ also increases with U. The shape, but not the absolute value, of the strength function is correctly given by a statistical calculation in which the radiative probability is determined from photodisintegration data. After removing the average energy dependence the frequency distribution of the total radiation widths $g\Gamma_\gamma/\overline{g\Gamma_\gamma}$ is found to be χ-squared with (2.9 ± 0.6) degrees of freedom. This is consistent with the Porter-Thomas theory since only a few partial radiation widths comprise the bulk of the total radiation width.

1. Introduction

Radiative proton capture has been widely used as a tool for studying the properties of the excited states of light nuclei. The extension of such studies to the middle-weight nuclei is limited by the rapid increase of level density with increasing atomic weight. While useful information can be obtained from radiative capture studies in the region of unresolved levels, the resolution of most electrostatic generators is such that a detailed study of the level structure is possible only if the spacing exceeds about 2 keV. Such situations are most likely to occur near the closed shells where the level spacings are unusually large.

In the present experiments, the reaction $Ni^{58}(p,\gamma)Cu^{59}$ has been studied for proton energies between 1.8 and 4.3 MeV and the resonances have been resolved throughout this energy range. Previous work[1]) at lower energies showed the

presence of 17 resonances below a proton energy of 1.84 MeV with an average spacing of $\approx$ 60 keV. This wide spacing arises partly from the low Q-value (3.42 MeV) and more importantly, from the near-magic properties of Cu^{59} with 2 neutrons and 1 proton outside the $N = Z = 28$ shells. An unusually wide spacing for the levels of Cu^{59} is also indicated by the results of inelastic proton scattering experiments[2]) which, however, select compound states of a very limited number of spins. Between proton energies of 3.3 and 4.5 MeV the average spacing of the inelastic scattering resonances is 18 keV[2]). A more complete spectrum of levels is observed in the present $Ni^{58}(p, \gamma)$ experiments and the level structure and radiation widths can be studied over an energy range of some 2.5 MeV.

This paper reports on the $Ni^{58}(p, \gamma)$ cross-section as obtained by measuring the radioactive yield of Cu^{59}, which has the conveniently short half-life of 81 sec[3]). This radioactive method leads to a determination of the total radiative capture cross-section which is a very convenient way of studying the energy levels of Cu^{59}. The results are therefore independent of variations in the quality of the capture gamma-rays and lead to a determination of the total radiation widths.

2. Experimental Method

The targets consisted of isotopically separated Ni^{58} enriched to 94 % and electroplated onto 0.25 mm gold backing. Measurements were made with targets of 1, 3, 10 and 500 keV thickness for 3 MeV protons. The most detailed observations were made with the 3 keV targets but, in preliminary measurements, complete excitation functions were obtained with the 10 and 500 keV targets. The 1 keV targets were used in some energy regions where the levels were difficult to resolve with the 3 keV targets. In order to limit the deposition of impurities onto the surface of the target, the last 90 cm of the beam tube were cooled to liquid nitrogen temperature. The targets were bombarded with proton beams of 3μA from the Harwell Van de Graaff and the induced Cu^{59} activity was measured with 3.8 cm diam. $\times$ 2.5 cm long NaI(Tl) crystal.

Cu^{59} decays by positon emission with a half-life of 81 sec[3]). At each proton energy the target was bombarded for 1 min and after an interval of $\frac{1}{2}$ min the annihilation radiation was counted for three successive 1 min periods. After another $\frac{1}{2}$ min interval the cycle was repeated at the next proton energy. The 81 sec Cu^{59} component was separated from the background positon count by comparing the activities in the three 1 min counting periods and small corrections were applied for the carry-over of 81 sec activity from one run to the next. The decay of the background activity was investigated in detail at a number of proton energies and the chief contribution was found to have a half-life of about 10 min. This probably corresponds to N^{13} produced in the $C^{12}(p, \gamma)$ reaction despite the precautions taken to keep the targets clean. Owing to its longer half-

life the background built up during the course of several 1 min bombardments. The background was more serious at the higher proton energies and is the chief source of uncertainty in the measured excitation function.

3. Results

The measured excitation function for the reaction $Ni^{58}(p, \gamma)Cu^{59}$ is shown in fig. 1. There have been observed 153 new resonances for proton energies between 1.8 and 4.3 MeV. In addition 17 resonances have previously been observed by Butler and Gossett[1]) at lower proton energies. Near 1.8 MeV the energy scale of fig. 1 is fixed accurately by the known[1]) energy of the 1843.7 ± 0.9 keV resonance. At 4.3 MeV the energy scale may be in error by ± 20 keV but the relative spacing of neighbouring resonances is probably accurate to ± 3 keV.

It is assumed that the natural width of the resonances is small compared with the target thickness and beam inhomogeneity. The yield Y per proton is therefore related to the radiative capture cross-section σ by the expression

$$Y = \frac{n}{k} \int_R \sigma(E) \mathrm{d}E ,$$

where n is the number of capturing nuclei per cm^3, $k = -\mathrm{d}E/\mathrm{d}x$ is the rate of energy loss of a proton in the target and the integration is continued over the resonance R. The Breit-Wigner one level formula leads to the result

$$Y = \frac{n}{2k} \frac{h^2}{2mE} \frac{g\Gamma_\gamma \Gamma_p}{\Gamma} ,$$

where for the present reaction the statistical factor $g = J + \frac{1}{2}$.

The quantity $g\Gamma_\gamma \Gamma_p/\Gamma$ can therefore be obtained from the measured reso-

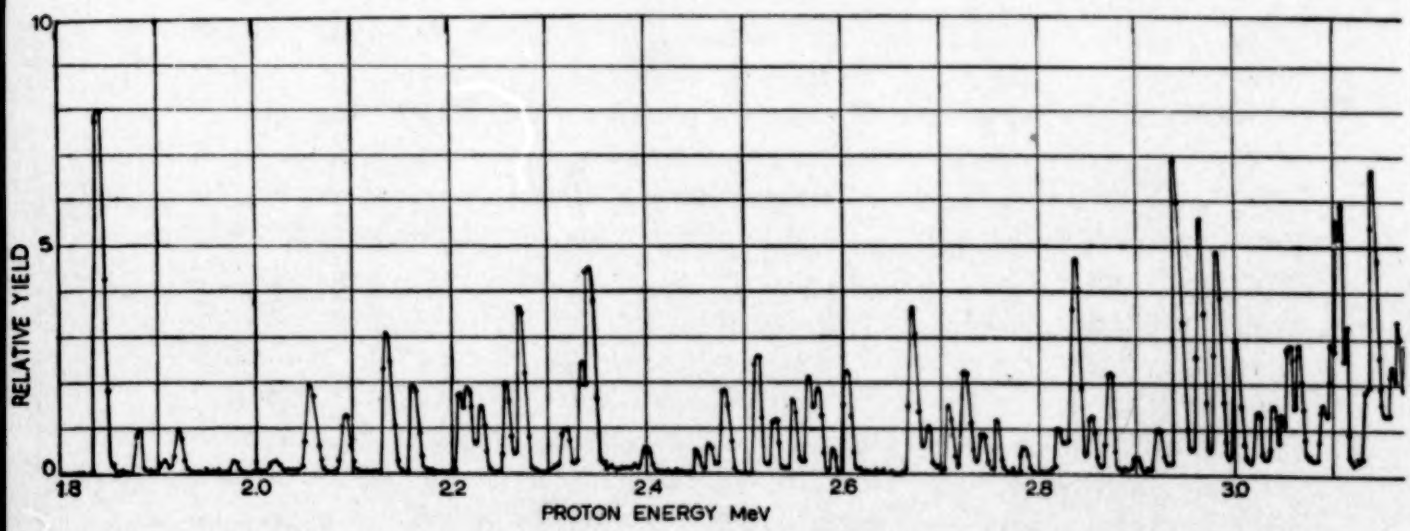

Fig. 1. Excitation function for the reaction $Ni^{58}(p, \gamma)Cu^{59}$ obtained

nance yields. At proton energies that are not too low ($E_p \gtrsim 1.6$ MeV) it is plausible to assume[1]) $\Gamma_p \gg \Gamma_\gamma$. In the range of excitation energies of these experiments the only other competing process is inelastic proton scattering. This process has been studied by Schiffer *et al.*[2]) for $3.0 < E_p < 4.5$ MeV and following their analysis we also assume $\Gamma_p \gg \Gamma_{p'}$. Thus $\Gamma_p \approx \Gamma$ and $g\Gamma_\gamma \Gamma_p/\Gamma \approx g\Gamma_\gamma$ for $E_p > 1.6$ MeV.

The resonance parameters are listed in table 1. The data for the first 17 resonances have been taken from the work of Butler and Gossett[1]) and the absolute values for the widths are based on their value for the 1.844 MeV resonance (assumed $J = \frac{1}{2}$)

4. Level Spacings

The total number N of resonances occurring below an excitation energy U is plotted as a function of U in fig. 2. A value of 3.42 MeV has been taken for the Q-value of the $Ni^{58}(p, \gamma)$ reaction[1]). The positive curvature of fig. 2 clearly shows the increase of the level density with increasing excitation energy. The (p, γ) resonance-energy data provide information about the level spacings for $U = 5$ to 7.5 MeV. The positions of 7 of the low-lying states of Cu^{59} are known[1]) from studies of the gamma-ray cascades in the (p, γ) reaction and this provides information about the spacing near $U = 1$ MeV.

According to the statistical theory[4]) D and U are expected to be related by an expression of the form

$$D(U) = CU^2 \exp\{-2\sqrt{aU}\}, \qquad (1)$$

where C and a are constants. This expression is fitted to the present experimental

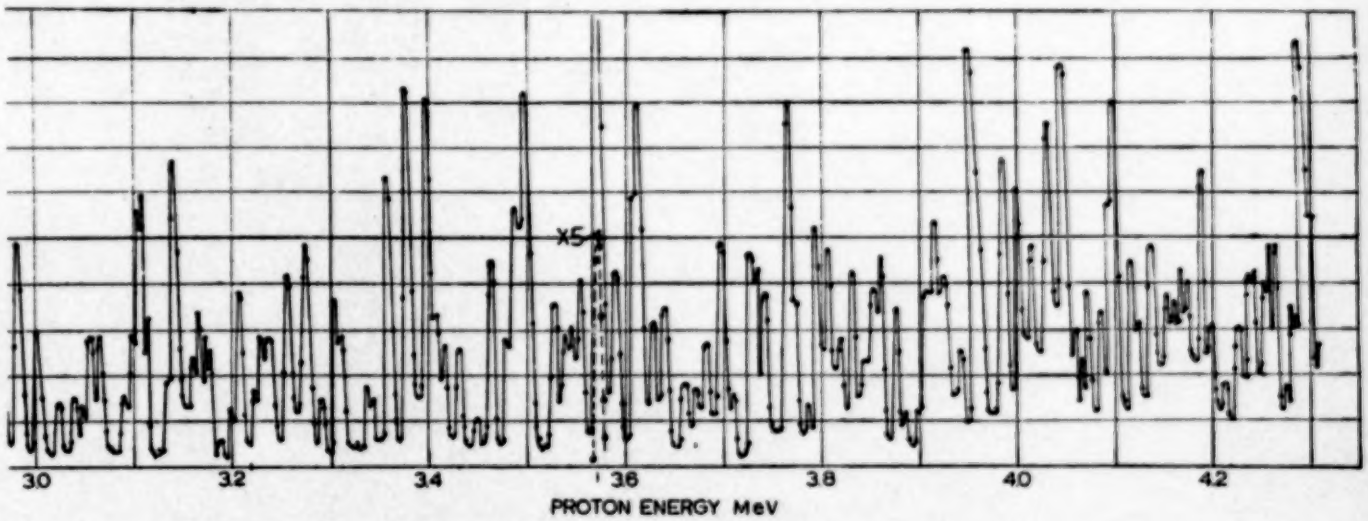

by measuring the yield of annihilation radiation of 81 sec Cu^{59}.

TABLE 1

Resonance parameters for the reaction $Ni^{58}(p,\gamma)Cu^{59}$

Resonance number N	Proton energy E_p (MeV)	$g\Gamma_\gamma \Gamma_p/\Gamma = g\Gamma_\gamma$ eV for $E_p > 1.6$ MeV	Resonance number N	Proton energy E_p (MeV)	$g\Gamma_\gamma \Gamma_p/\Gamma = g\Gamma_\gamma$ eV for $E_p > 1.6$ MeV
1	0.855	0.002	45	2.603	0.30
2	0.947	0.035	46	2.668	0.50
3	1.010	0.002	47	2.684	0.13
4	1.100	0.014	48	2.704	0.21
5	1.227	0.014	49	2.721	0.32
6	1.308	0.037	50	2.741	0.12
7	1.316	0.027	51	2.756	0.16
8	1.376	0.065	52	2.784	0.07
9	1.424	0.62	53	2.820	0.14
10	1.522	0.004	54	2.835	0.68
11	1.540	0.008	55	2.851	0.17
12	1.582	0.027	56	2.869	0.32
13	1.653	0.019	57	2.896	0.03
14	1.663	0.065	58	2.918	0.13
15	1.716	0.15	59	2.935	1.02
16	1.833	0.030	60	2.960	0.82
17	1.844	1.00	61	2.978	0.72
18	1.883	0.12	62	2.999	0.43
19	1.907	0.03	63	3.020	0.20
20	1.923	0.12	64	3.038	0.22
21	1.980	0.03	65	3.045	0.19
22	2.021	0.03	66	3.051	0.42
23	2.057	0.25	67	3.062	0.42
24	2.095	0.16	68	3.088	0.22
25	2.136	0.40	69	3.096	0.42
26	2.161	0.25	70	3.101	0.82
27	2.210	0.22	71	3.106	0.62
28	2.221	0.20	72	3.111	0.33
29	2.232	0.19	73	3.133	0.25
30	2.256	0.26	74	3.139	1.00
31	2.269	0.48	75	3.160	0.35
32	2.317	0.12	76	3.165	0.41
33	2.332	0.32	77	3.173	0.25
34	2.339	0.60	78	3.177	0.25
35	2.398	0.07	79	3.189	0.08
36	2.450	0.08	80	3.197	0.19
37	2.463	0.09	81	3.206	0.56
38	2.480	0.25	82	3.225	0.25
39	2.512	0.35	83	3.230	0.33
40	2.529	0.16	84	3.238	0.29
41	2.548	0.22	85	3.255	0.63
42	2.566	0.29	86	3.275	0.73
43	2.574	0.20	87	3.290	0.21
44	2.589	0.07	88	3.305	0.54

TABLE I *(continued)*

Resonance number N	Proton energy E_p (MeV)	$g\Gamma_\gamma\Gamma_p/\Gamma =$ for $E_p > 1.6$ $g\Gamma_\gamma$ eV MeV	Resonance number N	Proton energy E_p (MeV)	$g_\gamma\Gamma\Gamma_p/\Gamma =$ $g\Gamma_\gamma$ eV for $E_p > 1.6$ MeV
89	3.311	0.25	130	3.856	0.53
90	3.337	0.26	131	3.873	0.53
91	3.343	0.12	132	3.883	0.18
92	3.355	0.96	133	3.893	0.18
93	3.374	1.26	134	3.903	0.62
94	3.396	1.22	115	3.911	0.72
95	3.405	0.50	136	3.919	0.62
96	3.414	0.26	137	3.941	0.40
97	3.431	0.38	138	3.951	1.48
98	3.449	0.15	139	3.986	1.08
99	3.464	0.68	140	3.998	0.98
100	3.477	0.42	141	4.015	0.77
101	3.484	0.86	142	4.032	1.24
102	3.494	1.02	143	4.046	1.42
103	3.523	0.55	144	4.059	0.45
104	3.535	0.42	145	4.066	0.27
105	3.541	0.29	146	4.069	0.58
106	3.550	0.47	147	4.086	0.54
107	3.568	3.77	148	4.092	0.72
108	3.585	0.66	149	4.099	1.08
109	3.603	0.93	150	4.117	0.72
110	3.608	0.78	151	4.124	0.27
111	3.625	0.47	152	4.140	0.77
112	3.638	0.54	153	4.156	0.59
113	3.660	0.27	154	4.164	0.54
114	3.668	0.21	155	4.170	0.68
115	3.681	0.40	156	4.178	0.63
116	3.695	0.76	157	4.192	1.04
117	3.709	0.21	158	4.201	0.50
118	3.737	0.72	159	4.214	0.28
119	3.735	0.61	160	4.228	0.50
120	3.741	0.52	161	4.243	0.68
121	3.767	1.28	162	4.248	0.46
122	3.774	0.44	163	4.259	0.64
123	3.787	0.20	164	4.264	0.55
124	3.794	0.82	165	4.270	0.73
125	3.807	0.74	166	4.281	0.28
126	3.819	0.44	167	4.288	0.55
127	3.829	0.66	168	4.291	0.37
128	3.844	0.36	169	4.298	1.55
129	3.851	0.58	170	4.308	0.73

data† in fig. 3 in which $D(U)/U^2$ has been plotted as a function of $\sqrt{U}$. The lowest energy point in fig. 3 has been obtained from the average spacing of the low-lying states of Cu^{59}. The remaining points have been obtained from the averages of the local spacings of the observed resonances. From 10 to 30 resonances are included in each local average, the number being larger at the

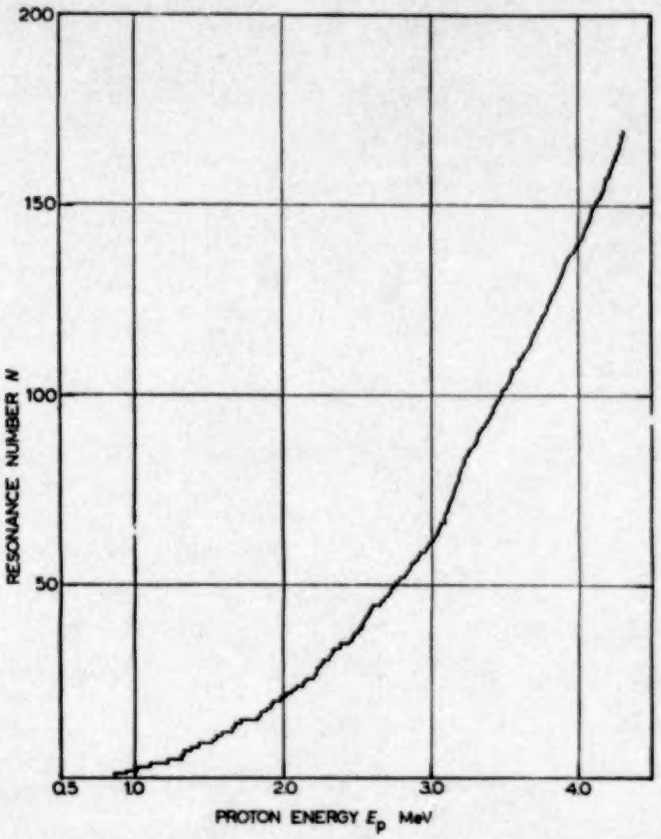

Fig. 2. The number N of $Ni^{58}(p, \gamma)$ resonances observed below an excitation energy U.

higher energies. The first of the points obtained from the resonance data is expected to be high since it corresponds to $E_p < 1.5$ MeV where the (p, γ) resonances may be small, and therefore missed, owing to a break-down of the assumption $\Gamma_p \gg \Gamma_\gamma$. Some levels will be missed because of the finite resolution of the experiment. The "dead space" can be estimated from the observed spacings and the target thickness which essentially determines the resolution. The loss depends on the proton energy and on the size of the resonances and is estimated to be 4 % at $E_p \approx 2$ MeV and 15 % at $E_p \approx 4.3$ MeV if we assume a χ-squared distribution with $\nu = 3$ as suggested by the analysis of section 7.

The straight line fit of fig. 3 indicates that equation (1) gives an adequate

† Figure 3 should not be taken as experimental confirmation of the theoretical expression for $D(U)$. The data can also be fitted to a simple exponential dependence of level spacing on energy of excitation.

account of the level spacing data which may be expressed as

$$D(U) = 3.8 \times 10^4 \, U^2 \exp\{-2\sqrt{5U}\} \text{ keV}, \tag{2}$$

where U is in MeV.

The nuclear temperature τ is defined by[4])

$$\tau^{-1} = \frac{\mathrm{d}}{\mathrm{d}U} \log D^{-1}, \tag{3}$$

and a plot of log D against U indicates an approximately constant temperature of 1.7 MeV for $5 < U < 7.5$ MeV. This is of course consistent with the values obtained by differentiating equation (2) which gives $\tau = 1.7$ MeV at $U = 6$ MeV and a change in τ of 0.15 MeV in going from $U = 5$ to $U = 7.5$ MeV.

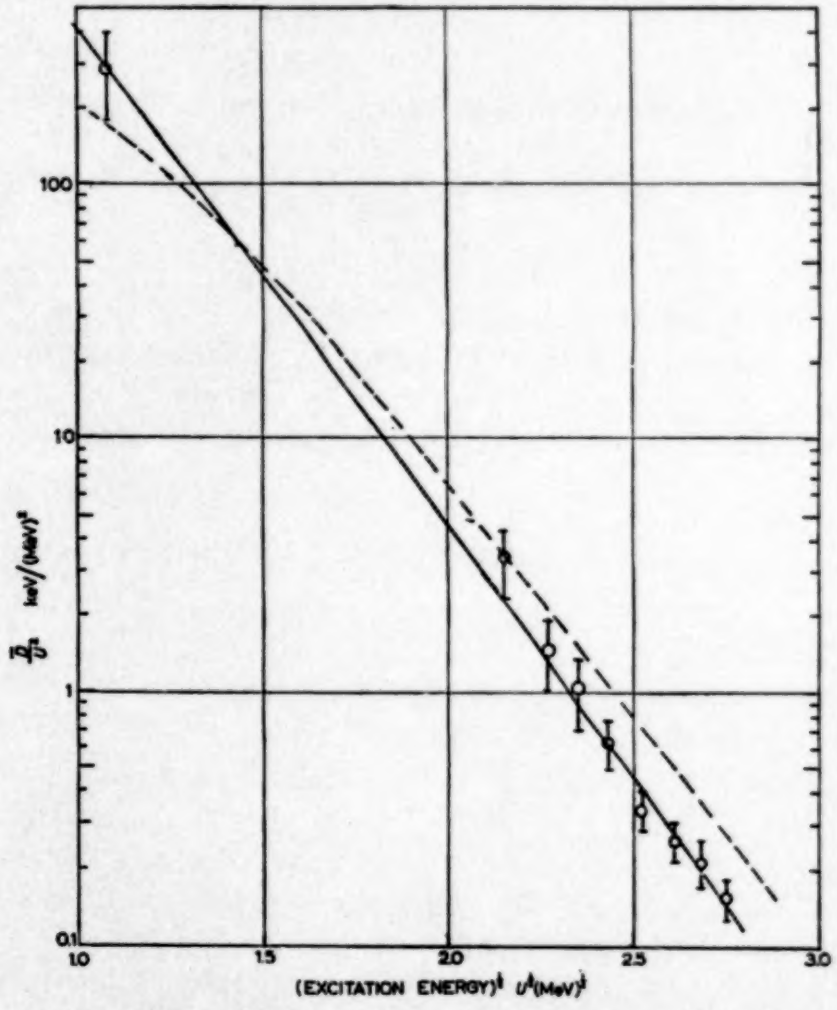

Fig. 3. Cu^{59} average level spacing $\overline{D}$. The lowest energy point is obtained from the average spacing of the low-lying states of Cu^{59}; the remaining points are obtained from the average spacing of the observed resonance. $\overline{D}/U^2$ is plotted as a function of $U^{\frac{1}{2}}$. The full line is the best fit to the data and is given by $D(U) = 3.8 \times 10^4 \, U^2 \exp\{-2\sqrt{5U}\}$. The dotted line is obtained from Cameron's[5]) semi-empirical formula with $J = 0$.

These temperatures may be compared with those given by Cameron's semi-empirical formula[5]) which indicates a "thermodynamic" temperature $t = 1.4$ MeV at $U = 6$ MeV. The distinction between τ and t has been pointed out by Lang and Le Couteur[4]) who show that

$$\tau^{-1} = t^{-1} - \frac{3}{4U} . \tag{4}$$

Thus, Cameron's formula gives $\tau = 1.7$ MeV at $U = 6$ MeV in agreement with the present results. Cameron's expression for the level density for $J = 0$ is also plotted in fig. 3 and is seen to have the same slope as the measured curve. However, according to the analysis of the next section, the measured values are expected to include nearly all spin states and, according to eq. (6) and (9), $D_{\text{total}} \approx \frac{1}{24} D_0$ so that the semi-empirical formula underestimates the spacings by a factor ≈ 15.

5. *J*-Dependence and Nuclear Moment of Inertia

Theoretically[4,6]) the J-depencence of the level density is expected to be given by

$$D_J^{-1} = D_0^{-1} (2J + 1) \exp \{ - J(J + 1)/2ct \} , \tag{5}$$

where D_J and D_0 are the spacings for levels of a given parity and spin J and spin 0. $c\hbar^2$ is the nuclear moment of inertia. The total level density can easily be obtained from equation (5) if we replace the sum over J by an integral and assume equal probability for states of either parity. The result is

$$D^{-1} = 4ct\, D_0^{-1} . \tag{6}$$

It is convenient to refer the moment of inertia to the rigid body value

$$c_0 h^2 = \tfrac{2}{5} MAR^2 , \tag{7}$$

and write[4])

$$c = B^2 c_0 = B^2 A^{\frac{5}{3}}/75 \text{ MeV}^{-1} \tag{8}$$

for $r_0 = 1.2 \times 10^{-13}$ cm.

We expect $B^2 < 1$, especially near closed shells in accordance with the trends found in nuclear moments of inertia from studies of the rotational bands[7]). Proton penetration factors should not unduly restrict the number of different spin states which are observed in the present experiments owing to the approximate constancy of the radiation widths. Thus, if $B^2 = 0.7$, 90 % of the levels can be excited by incoming waves having $l < 5$ and these waves should all be effective above proton energies of ≈ 2 MeV. The black nucleus approximation[8]) with $r_0 = 1.45 \times 10^{-13}$ cm was used to reach this conclusion†.

† The larger radius $r_0 = 1.45 \times 10^{-13}$ cm seems more appropriate for calculations of reaction cross-sections, but we have used the smaller value $r_0 = 1.2 \times 10^{-13}$ cm to evaluate the moment of inertia.

It was assumed that levels would be observed if the proton width Γ_p exceeded the average radiation width $\overline{\Gamma_\gamma}$ ($\overline{\Gamma_\gamma} \approx 0.2$ eV at $E_p = 2$ MeV). Size resonance effects may alter the calculated proton width but should have only a small effect on the energies at which the various partial widths become effective.

The radiation widths for states of high spin might be severely reduced if there were only a few low-lying states of suitable spin. Seven states of Cu^{59} are known below an excitation of 2.4 MeV and the ground state and first excited state are $\frac{3}{2}^-$ and $\frac{1}{2}$. As noted in section 7 transitions from the capturing state to these low-lying states are expected to play a major role in determining the total radiation widths. Since there are so few low-lying states their actual spin distribution may be very different from the average which obtains at higher energies. In the absence of direct measurements of the spins of the other low-lying states, such as it is hoped to obtain from a study of the capture gamma-rays, it is assumed provisionally that such effects do not appreciably limit the spin of the observed resonances.

With these reservations we shall assume that the measured (p, γ) resonances do indicate the total level density for states of all spins, at least at the higher proton energies. It is possible then to combine these results with those of Schiffer *et al.*[2]) on inelastic proton scattering to estimate the moment of inertia of Cu^{59}. Schiffer *et al.*[2]) determined the spins of 37 inelastic scattering resonances between proton energies of 3.0 and 4.5 MeV. This was about half the total number of such resonances observed in this range. They found 1 resonance with $J = \frac{1}{2}$, 17 with $J = \frac{3}{2}$ and 18 with $J = \frac{5}{2}^+$. The parity of the $\frac{3}{2}$ states could not be assigned definitely but was somewhat more likely to be positive, as will be assumed here. The level, spacing for all the observed inelastic scattering resonance is approximately constant for $E_p = 3.5 - 4.5$ MeV and is 18 keV. The spacing for levels of a given spin and parity is

$$D_{\frac{1}{2}}^+ = D_{\frac{3}{2}}^+ = 60 \pm 20 \text{ keV},$$

where the upper limit is obtained from the number of states identified with a given spin and the lower limit assumes that only two spin states are involved for all the observed resonances. The total level density as obtained from the (p, γ) resonances is for the same energy range

$$D_{\text{total}} = 10 \pm 3 \text{ keV}.$$

These data impose the following limits on the allowed values of ct, which determines the spin dispersion (eq. (5)):

(a) $D_{\frac{1}{2}}^+/D_{\frac{3}{2}}^+ = 1.0 \pm 0.2$ implying $4 < ct < 12$,
(b) $D_{\frac{1}{2}}^+/D_{\text{total}} = 6.0 \pm 2.7$ implying $0.6 < ct < 8$,
(c) $D_{\frac{3}{2}}^+/D_{\text{total}} = 6.0 \pm 2.7$ implying $2.5 < ct < 9$.

Combining these conditions gives

$$ct = 6 \pm 2. \tag{9}$$

The measured nuclear temperature $\tau = 1.7$ MeV (section 4) so that at a mean excitation of 7.5 MeV the thermodynamic temperature $t = 1.45$ MeV (equation (4)) and $c = 4.1 \pm 0.14$ (MeV)$^{-1}$. In terms of the rigid body value (equation (8))

$$c = (0.35 \pm 0.12)\, c_0 \,. \tag{10}$$

The reduction in the moment of inertia below the rigid body value is in agreement with what is known from studies of nuclear rotational bands[7]).

6. The Average Total Radiation Widths

The measured total radiation widths are listed in table 1. There is a systematic tendency for the widths to increase with increasing excitation energy U as shown in fig. 4 in which the local average of the widths $\overline{g\Gamma_\gamma}$ is plotted as a function of U. The local averages were obtained by grouping the data in the same way as for the determination of the average spacings (section 4) and 10 to 30 widths are included in each local average. For $U < 5$ MeV the result is uncertain since the assumption $\Gamma_p \gg \Gamma_\gamma$ may break down. The measurements of the widths and the spacings have been combined in fig. 5 to obtain the photon strength function $\overline{g\Gamma_\gamma}/\overline{D}$ which is also an increasing function of U.

It is of interest to compare the measured strength function with that calculated by means of the statistical theory. We consider only electric dipole radiation and assume that the cross-section for the inverse process of gamma-ray excitation can be taken from the data of nuclear photo-disintegration. Explicitly, we use Steinwedel and Jensen's expression[9]) to extrapolate the photonuclear cross-section below the well-known giant resonance region. The total width is obtained by integrating over all possible partial gamma-ray transitions from the capturing state. We note that the total width, as measured by induced radioactivity, excludes those transitions in which the primary emission of a (low) energy gamma-ray is followed by particle emission. Thus the integration is to be extended only to some energy T such that for residual energies $R > T$ competition from particle emission prevents the development of a gamma-ray cascade. In the present case this is determined by proton re-emission so that $T > 3.4$ MeV and we assume $T \approx 4$ MeV.

The details of the calculation have been given previously[10]) where the approximation $D_J^{-1} = (2J + 1)D_0^{-1}$ was made. It follows from this approximation that the widths are independent of the spin of the capturing state and the result for Cu^{59} is

$$\frac{\Gamma_\gamma^0(U)}{D(U)} = 1.12 \times 10^3 \int_0^T \frac{y^4\, dR}{D(R)\,\{y^2 - 1)^2 + 0.084\, y^2\}}, \tag{11}$$

where R is in MeV, Γ_γ^0 in eV and $y = (U - R)E_m$, introducing E_m = photonuclear peak energy = 19 MeV.

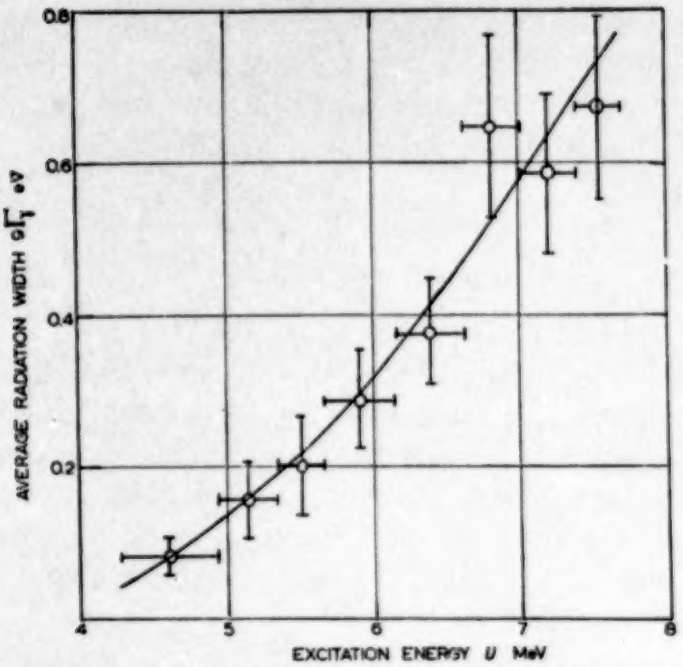

Fig. 4. The average radiation width $\overline{g\Gamma_\gamma}$ for Cu^{59} as a function of the excitation energy U.

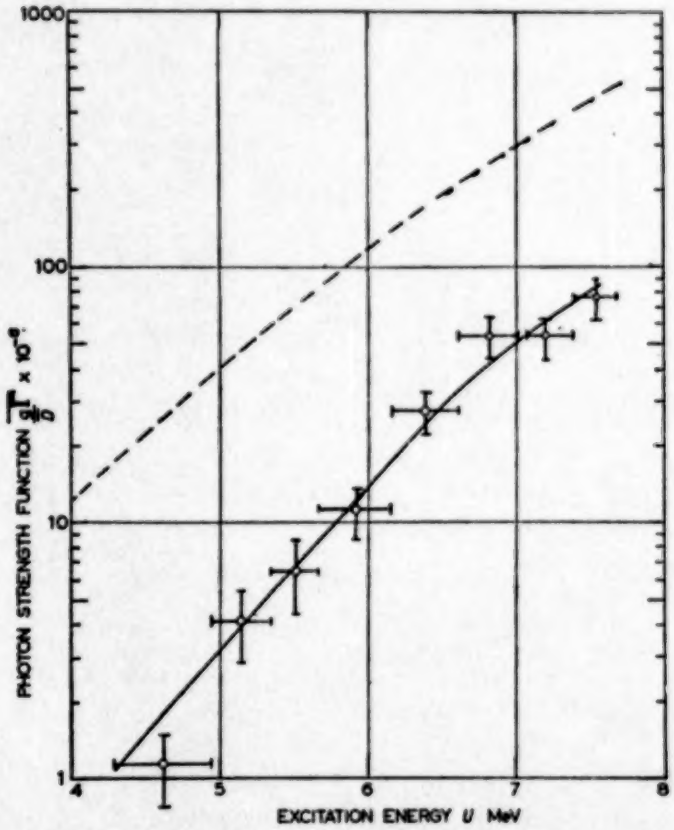

Fig. 5. Photon strength function $\overline{g\Gamma_\gamma}/\overline{D}$ for Cu^{59}. The dotted curve corresponds to the statistical calculation (see text).

For comparison with the present results, we need $g\Gamma_\gamma/D$ where $g = J + \frac{1}{2}$ is the statistical weight factor and the $(2J + 1)$ approximation is not sufficient. Instead, we average $g\Gamma_\gamma^J$ over the spins using the spin dependence given by eq. (5) with $ct = 6$ as found in section 5.

The result is

$$\frac{\overline{g\Gamma_\gamma(U)}}{D(U)} = 2.9\,\frac{\Gamma_\gamma^0(U)}{D(U)},$$

where the right hand term is given by eq. (11).

The measured level spacing is used to evaluate these expressions and the calculated photon strength function is compared with experiment in fig. 5. It is seen that the slopes of the two curves are similar but the calculated values are too large by a factor of ≈ 10. It should be noted that, as stated in section 7, most of the radiation takes place to the first 6 or 7 levels in Cu^{59}, and a statistical calculation can therefore be taken only as a very rough approximation.

7. Distribution of the Total Radiation Widths

The measured total radiation widths show considerable fluctuations from level to level. The nature of this variation is most clearly seen by removing the average energy dependence and plotting the frequency distribution $P(x)dx$ where $x = g\Gamma_\gamma/\overline{g\Gamma_\gamma}$. This is done in fig. 6 for the 157 resonances with $E_p > 1.6$

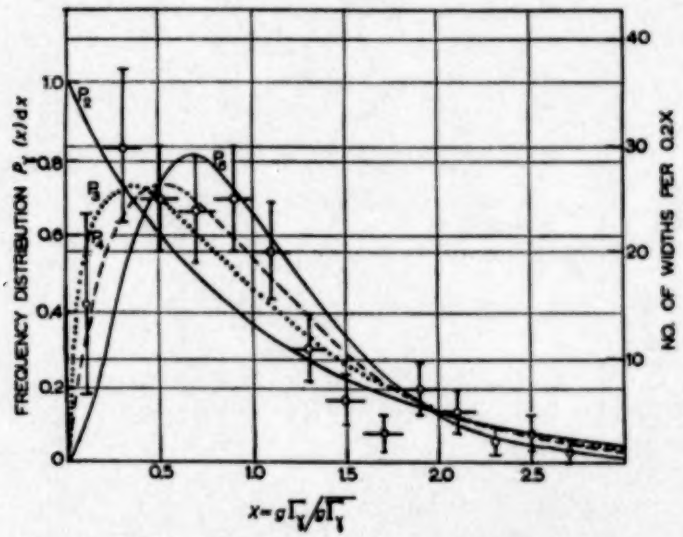

Fig. 6. Frequency distribution of 158 total radiation widths of Cu^{59} as a function of $x = g\Gamma_\gamma/\overline{g\Gamma_\gamma}$. Corrections have been made for the loss of small levels. The smooth curves are the chi-squared distributions $P_\gamma(x)dx$. Two observed widths with $6 < x < 7$ are not shown on the figure.

MeV for which the assumption $\Gamma_p \gg \Gamma_\gamma$ is excepted to hold. The distribution has been corrected for the loss of small levels by multiplying the observed numbers by the estimated probability of observing a level of a given size at a

given energy. This correction amounts to a factor of two for the first point in fig. 6, and is negligible for all but the first two points. The errors include the estimated uncertainties in the loss correction as well as statistical uncertainties.

Following the analysis of Porter and Thomas[11]) we compare the observed distribution with the χ-squared distributions of $\nu = 2\rho$ degrees of freedom

$$P_\gamma(x)\mathrm{d}x = \Gamma(\rho)^{-1}\,(\rho x)^{\rho-1}\,\mathrm{e}^{-\rho x}\,\rho\,\mathrm{d}x\,, \tag{12}$$

where $\Gamma(\rho)$ is the gamma function. The comparison is made in fig. 6. A maximum likelihood fit to the observed distribution gives $\gamma = 2{,}9 \pm 0.6$ with the uncertainty arising mainly from the loss correction.

The total radiation width is the sum of n partial widths such that

$$\Gamma_\gamma = \sum_{i=1} \Gamma_i\,.$$

Porter and Thomas[11]) assume that the distributions of the individual Γ_i are independent and χ-squared with one degree of freedom. If all the partial widths had the same average value $\overline{\Gamma}_i$ the distribution for the total widths would be χ-squared with $\gamma = n$ degrees of freedom. In the general case of unequal $\overline{\Gamma}_i$ the distributions are more complicated but the main conclusion remains unaltered namely, that the dispersion in the total widths becomes smaller as the number of partial widths increases.

The large dispersion of the present set of total radiation widths is in marked contrast with the almost constant values which have been found in neutron studies of the heavy nuclei[12]). The small dispersion for the heavy nuclei is a consequence of the large number ($\approx$ 100) of partial radiation widths. The present data can be fitted by a χ-squared distribution with $\nu = 2.9 \pm 0.6$ degrees of freedom. If the Porter-Thomas theory[11]) is correct, this result implies that, on the average, three partial widths make up the bulk of the total width. This is not unreasonable in view of the sparseness of the low-lying states of Cu^{59}. We recall that the total radiation width as measured in these radioactive experiments refers only to those gamma-ray transitions which are not followed by particle emission and exludes those low-lying primary gamma-ray transitions which leave the nucleus with more than $\approx$ 4 MeV residual excitation. Further, the more energetic gamma-ray transitions are favoured by the shape of the inverse cross-section for gamma-ray excitation. The qualitative conclusion is the same if we use an ε^3 dependence or the giant resonance shape used in deriving eq. (11). In the latter case, for excitations of 4.5 — 7.5 MeV, 80–65 % of the transitions are expected to populate the seven known[1]) levels of Cu^{59} lying below 2.4 MeV. This is qualitatively in agreement with the result $\nu \approx 3$ since spin factors will further reduce the effective number of partial widths. A direct confirmation can only be obtained by experimental investigation of the partial

widths and preliminary measurements indicate that on the average less than five partial widths comprise the bulk of the total radiation width. It is concluded that the present data are in agreement with the Porter-Thomas theory[11]).

One of us (J. H. C.) wishes to thank Dr. E. Bretscher and Dr. E. B. Paul for the facilities made available to him while visiting Harwell.

References

1) J. W. Butler and C. R. Gossett, Phys. Rev. **108** (1957) 1473
2) J. P. Schiffer, M. S. Moore and C. M. Class, Phys. Rev. **104** (1956) 1661
3) J. W. Butler and C. R. Gossett, Phys. Rev. **109** (1958) 863
4) J. M. B. Lang and K. J. Le Couteur, Proc. Phys. Soc. A**67** (1954) 586
5) A. G. W. Cameron, Can. J. Phys. **36** (1958) 1040
6) T. Ericson and V. Strutinski, Nuclear Physics **8** (1958) 284
7) A. K. Kerman, in Nuclear Reactions, ed. by P. M. Endt and M. Demeur (North-Holland Publishing Company, Amsterdam, 1959)
8) J. M. Blatt and V. Weiskoff, Theoretical Nuclear Physics (Wiley, 1952)
9) H. Steinwedel and J. H. D. Jensen, Z. Naturforsch. **5a** (1950) 413
10) J. H. Carver and G. A. Jones, Nuclear Physics **11** (1959) 400
11) C. E. Porter and R. G. Thomas, Phys. Rev. **104** (1956) 483
12) J. S. Levin and D. J. Hughes, Phys. Rev. **101** (1956) 1328

7.C *Nuclear Physics* **19** (1960) 199—220; © *North-Holland Publishing Co., Amsterdam*
Not to be reproduced by photoprint or microfilm without written permission from the publisher

ELASTIC SCATTERING OF NUCLEONS AND PIONS AT VERY HIGH ENERGY

Z. KOBA†, A. KRZYWICKI,

Institute for Nuclear Research, Warsaw, Poland

R. RĄCZKA

Warsaw University, Warsaw, Poland

and

Z. CHYLIŃSKI

Institute for Nuclear Research, Kraków, Poland

Received 25 February 1960

Abstract: Theoretical considerations concerning the elastic scattering of nucleons and pions in the GeV region are presented. Criteria for the validity of the simplest picture and a formula for constructing the optical potential from known phase shifts are given. The comparison with existing data reveals a sharp discrepancy in the case of p—p scattering at 8.5 GeV (this has been reported by Veksler in Kiev). Various possibilities to get rid of this disagreement are discussed: introduction of the real part of phase shifts (for which the dispersion relations would give a direct check), spin-dependence of nuclear interactions (which leads to predominance of the singlet state interaction), and quasi-resonance. Some remarks are added on relevant topics.

1. Introduction and Summary

The scattering of nucleons and pions in the energy region of several GeV has been studied by many authors††. Here we shall refrain from repeating the explanation on the importance of this investigation. The usual approach to this problem is either by the partial wave analysis or by the optical model, which are closely related to each other.

So far the experimental material in this domain is not very rich and only a small number of quantities have been measured. Owing to this situation there is still much freedom in constructing theoretical pictures. The analysis of the experimental data now available can be carried out in an exact and unambiguous way only when the scattering is assumed to be purely absorptive (i.e. the real parts of all the phase shifts are assumed to vanish) and, moreover,

† On leave of absence from the Research Institute for Fundamental Physics, Kyoto University, Japan.

†† A most comprehensive and systematic survey on this field has been given by Veksler[1]). An extensive list of existing literature can be found in this report. Here we are recapitulating some of his main arguments.

certain strongly simplifying assumptions concerning the spin-dependence of the nuclear interaction are introduced†. This is one of the main reasons why this simple approach has been the subject of many studies.

On the other hand, this simple picture was more or less supported by the increasing predominance of inelastic events over the elastic ones with increasing energy, and it appeared to be rather successful for the energy region above, say, 5 GeV for p-p collisions and 1.3 GeV for π-p collisions. The experiment of Markov and others[3]) at 8.5 GeV, however, has revealed a sharp contradiction with this simple theory††. Thus a systematic investigation of other theoretical possibilities has become necessary. In this work we should like to carry out a preliminary examination of such possibilities and their implications.

We begin with the simple theory and give in sect. 2 general criteria of this theory without making use of the optical approximation. Most of them are already known, but we formulate them here for the sake of completeness. Comparison with the existing experimental data leads to the same results as have been given in Veksler's report[1]): for proton-proton scattering the simple picture fails both in the lower energy region (< 5 GeV) and in the experiment of Markov *et al.*, while for pion-nucleon scattering no discrepancy is found above 1.3 GeV. Further, the problem of the determination of the optical potential from a given set of phase shifts is solved.

Then we go over to the study of various possibilities of overcoming the discrepancy with the simple theory revealed by the experiment of Markov and others. The first of them is to introduce real parts of phase shifts. Sect. 3 is devoted to the estimation of the real part of the scattering amplitude by means of dispersion relations. Such a calculation would be the most direct check of the existence of potential scattering (i.e. elastic scattering not due to the shadow effects accompanied by inelastic events). Before more detailed calculations are performed, we cannot make a definite statement on its consequences; it seems likely, however, that at present this approach will not be so sensitive as to give a clear-cut conclusion.

The second possibility is to admit spin-dependence of the nuclear interaction†††. If we are to attribute the disagreement of the experimental data with the simple theory to this effect alone, we are obliged to assume an overwhelming predominance of the singlet state interaction. Although recent work of Shahbazyan[3a]) has shown that such an assumption will lead to another discrepancy, its consequences may remain qualitatively valid, if we wish to

† For p—p scattering one introduces either the assumption of no spin-dependence, or that of a degeneracy of the scattering amplitude, which is otherwise to be regarded as a matrix in the spin-space. See e.g. ref. [2]).

†† This experimental result has been confirmed with better statistics by recent studies made in Dubna. We are indebted to Professor M. Danysz and Dr. P. Zieliński for information concerning experimental data.

††† According to Veksler's report, this possibility was first pointed out by D. I. Blokhintsev.

minimize the contribution from potential scattering. One of them might be observed in the scattering of protons by certain light nuclei. A third mechanism, which may account for the puzzling situation, is the presence of a quasi-resonant state with large angular momentum. This hypothesis implies a drastic energy-dependence and could be tested without difficulty. These two possibilities are investigated in sect. 4, as an application of the optical theorem to more general cases.

In the final section we present two relevant remarks, firstly concerning the connection of the nucleon structure to the optical potential, and secondly on the nature of the possible quasi-resonance.

2. Simple Theory

2.1. CRITERIA FOR THE VALIDITY OF THE SIMPLE THEORY

First of all we discuss the simplest case, in which the possibility of spin-dependence and "quasi-resonances" (see sect. 4.5) is neglected and, moreover, it is assumed that the real parts of all the phase shifts vanish. As is well known, we can then carry out the phase shift analysis by the following formula:

$$1 - \eta_l = k \int_{-1}^{1} \left(\frac{\mathrm{d}\sigma_{el}}{\mathrm{d}\Omega} \right)^{\frac{1}{2}} P_l (\cos\theta)\, \mathrm{d}(\cos\theta) . \tag{1}$$

Here we have assumed that the scattering amplitude does not change sign. This assumption fails when the differential cross section of elastic scattering (as a function of the angle) consists of more than two parts separated by vanishing values. In such a case we have to choose properly the sign of the square root $\pm (\mathrm{d}\sigma_{el}/\mathrm{d}\Omega)^{\frac{1}{2}}$ for these parts.

Sometimes it is more convenient to go over to the optical limit, $l \gg 1$, and work with the approximate expression

$$1 - \eta(\rho) = k \int_{-1}^{1} \left(\frac{\mathrm{d}\sigma_{el}}{\mathrm{d}\Omega} \right)^{\frac{1}{2}} J_0 (k\rho \sin\theta)\, \mathrm{d}(\cos\theta) ,$$

where we have put $l + \frac{1}{2} = k\rho$ and made use of the relations

$$\lim_{n\to\infty} P_n \left(\cos \frac{z}{n} \right) = J_0(z) ,$$

and

$$\lim_{k\rho, k\rho' \to \infty} \int_0^{\pi} J_0(k\rho \sin\theta)\, J_0(k\rho' \sin\theta)\, \mathrm{d}(\cos\theta) = \frac{1}{k\rho}\, \delta(k\rho - k\rho') = \frac{1}{k^2\rho}\, \delta(\rho - \rho') .$$

It should be noticed, however, that these are not correct for small $\rho \approx l/k$; in such a case we have to go back to eq. (1).

The necessary and sufficient conditions for the consistency of the method of analysis based on eq. (1), or the assumption of vanishing real parts of the phase

shifts, are as follows (these three conditions, if they are satisfied, show that the results obtained with eq. (1) are one possible set of phase shifts, but by no means exclude the possibility of other solutions):

A) From the definition of imaginary phase shifts

$$0 \leq \eta_l \leq 1 \qquad \text{for all values of } l\,. \tag{2}$$

Further, from physical considerations, it is natural to require

$$\eta_l = 1 \qquad \text{for all values of } l \geq l_0\,, \tag{3}$$

where $l_0 = kR$, and R a quantity comparable to $1/\mu$.

B) From the optical theorem it follows that

$$\sigma_{\text{tot}} = \frac{4\pi}{k}\left(\frac{\mathrm{d}\sigma_{\text{el}}}{\mathrm{d}\Omega}\right)^{\frac{1}{2}}_{\theta=0} \tag{4}$$

In the case of n-p scattering we have a second relation[5])

$$[\sigma_{\text{tot}}(\text{p}-\text{p}) - \sigma_{\text{tot}}(\text{n}-\text{p})\,] = \frac{4\pi}{k}\left(\frac{\mathrm{d}\sigma_{\text{el}}(\text{n}-\text{p})}{\mathrm{d}\Omega}\right)^{\frac{1}{2}}_{\theta=\pi} \tag{5}$$

The proof of this relation is given in sect. 4.4.

C) No polarization effects are to be observed (this is proved in sect. 4.3).

In practice it is often convenient to make use of the following necessary (but not sufficient) conditions as criteria of the assumption $\operatorname{Re}\delta_l = 0$ (conditions I), II) replace condition A), while III) replaces B)):

I). The condition[6])

$$\sigma_{\text{inel}} \geq \sigma_{\text{el}}\,, \tag{6}$$

which can be verified in the following way. Under the assumption $\operatorname{Re}\delta_l = 0$, we have

$$\begin{aligned}
\sigma_{\text{el}} &= \frac{\pi}{k^2}\sum_{l=0}^{\infty}(2l+1)\,(1-\eta_l)^2\,,\\
\sigma_{\text{inel}} &= \frac{\pi}{k^2}\sum_{l=0}^{\infty}(2l+1)\,(1-\eta_l^2)\,,\\
\sigma_{\text{tot}} &= \sigma_{\text{el}} + \sigma_{\text{inel}} = \frac{2\pi}{k^2}\sum_{l=0}^{\infty}(2l+1)\,(1-\eta_l)\,.
\end{aligned} \tag{7}$$

The relation (2) leads to

$$(1-\eta_l)^2 \leq (1-\eta_l) \qquad \text{for all values of } l\,,$$

which with eq. (7), gives

$$\tfrac{1}{2}\sigma_{\text{tot}} \geq \sigma_{\text{el}}\,,$$

whence we get the condition (6).

This relation can be also easily seen from fig. 1, which shows $\sigma_{el}^{(l)}/\sigma_{inel}^{(l)}$ for any l as a function of the phase shift: the various curves correspond to different values of Re δ_l; the lowest curve represents the case Re $\delta_l = 0$.

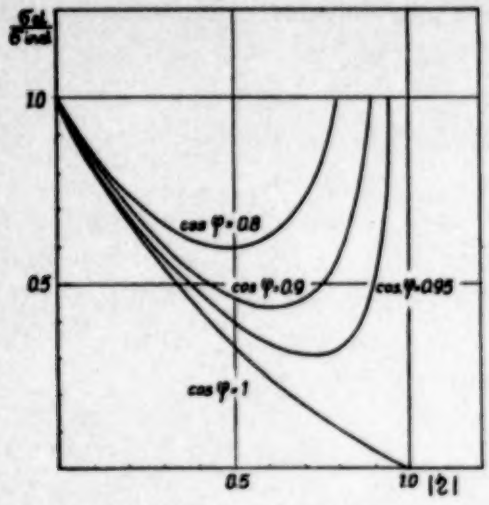

Fig. 1. The ratio of the elastic to the inelastic scattering cross section for a certain partial wave with arbitrary l) as function of the phase shift. The abscissa represents the absolute value $e^{2i\delta_l}$ and the various curves correspond to a different ratio of the real to the imaginary part. The lowest curve, which stands for the case of Re $\delta_l = 0$, never exceeds 1. $\varphi = 2$ Re δ.

The condition (6) is almost always satisfied at high energy and thus turns out to be a rather trivial restriction.

II) Further[4]),

$$\int_{-1}^{1} \left(\frac{d\sigma_{el}}{d\Omega}\right)^{\frac{1}{2}} d(\cos\theta) \leqq \frac{1}{k}. \tag{8}$$

We can obtain this condition from eq. (1), by requiring that $\eta_0 \geqq 0$. As will be shown later, the expression $(1 - \eta_l)$ usually takes its largest value when $l = 0$. If the above condition is satisfied, therefore, it is almost sure that $\eta_l \geqq 0$ is satisfied for all values of l.

Since the integrand of the left-hand side of the inequality (8) is the square-root of the differential cross section, the contributions from large angles, which are not essential for the total elastic cross section, are relatively important, and better statistics is required for small values of the differential cross section.

III) The requirement of the optical theorem can be more conveniently put into the following form:

$$\left(\frac{k}{4\pi}\sigma_{tot}\right)^2 \geqq \left(\frac{d\sigma_{el}}{d\Omega}\right)_{\theta}, \tag{9}$$

where θ can be *any* angle. This last condition can be derived from eq. (5) with the help of

$$\left(\frac{d\sigma_{el}}{d\Omega}\right)_{\theta=0} \geqq \left(\frac{d\sigma_{el}}{d\Omega}\right)_{\theta \text{ arbitrary}} \tag{10}$$

The latter inequality is obvious, since in the expression

$$\frac{d\sigma_{el}}{d\Omega} = \frac{1}{4k} \left| \sum (2l+1)(1-\eta_l) P_l(\cos\theta) \right|^2$$

the quantities $P_l(x)$ have their maximum values when $x = 1$. (Generalization of the inequality (9) to the case $\mathrm{Re}\,\delta_l \neq 0$ is discussed in sect. 3.1).

The criterion (9) means that even one experimental point (in any angle or in a region of angle) which surpasses the value specified by the total cross section is sufficient to disprove at least one of the assumptions made in the simple theory.

While II) is concerned practically with large angles, III) is related essentially to the smallest angles.

Generally speaking, the more spread the angular distribution, the more concentrated is the absorbing region. Concerning this point we can say that the imaginary phase shifts decrease, or, in other words, η_l increases with l at least up to

$$l \leqq \frac{\pi}{\theta_0}, \tag{11}$$

when the differential cross section vanishes outside a certain angle:

$$\frac{\mathrm{d}\sigma_{el}}{\mathrm{d}\Omega} = 0 \quad \text{for } \theta \geqq \theta_0 . \tag{12}$$

This statement can be proved in the following way. From eq. (1) we have

$$\eta_l - \eta_{l-1} = k \int_{-1}^{1} \left(\frac{\mathrm{d}\sigma_{el}}{\mathrm{d}\Omega}\right)^{\frac{1}{2}} [P_{l-1}(\cos\theta) - P_l(\cos\theta)]\, \mathrm{d}(\cos\theta) . \tag{13}$$

With the help of the formula[7])

$$P_n(\cos\theta) = \frac{2}{\pi} \int_0^{\theta} \frac{\cos(n + \frac{1}{2})\phi}{[2(\cos\phi - \cos\theta)]^{\frac{1}{2}}}\, \mathrm{d}\phi , \tag{14}$$

we get

$$P_{l-1}(\cos\theta) - P_l(\cos\theta) = \frac{4}{\pi} \int_0^{\theta} \frac{\sin l\phi \sin \frac{1}{2}\phi}{[2(\cos\phi - \cos\theta)]^{\frac{1}{2}}}\, \mathrm{d}\phi . \tag{15}$$

If we now restrict l by the inequality (11), we have

$$P_{l-1}(\cos\theta) - P_l(\cos\theta) > 0 \quad \text{for all } \theta \leqq \theta_0 . \tag{16}$$

Our result is obtained from eq. (13), if (12) and (16) are taken into account. (A similar argument can be applied to the second difference,

$$(\eta_l - \eta_{l-1}) - (\eta_{l-1} - \eta_{l-2}) = \eta_l - 2\eta_{l-1} + \eta_{l-2} ,$$

and we find that this remains positive at least up to $l \leqq \pi/2\theta_0 + \frac{1}{2}$).

As is seen from the above proof, the inequality (12) is a sufficient condition. The monotonic increase of η_l is usually true for much larger values of l than those permitted by (12). In most cases η_l never decreases for any l.

In connection with the spread in the angular distribution, we note further

that if all the phase shifts above a certain value of $l = l_0$ vanish, or, in other words, $\eta_l = 1$ for $l \geqq l_0$, the differential cross section cannot vanish for angles $\theta \leqq \theta_0$, where

$$\theta_0 = \frac{\pi}{2l_0 + 1} . \tag{17}$$

(Here of course it is assumed that at least one phase shift does not vanish, otherwise there would be no scattering at all.) The proof of this statement is based on the well-known expression

$$\left(\frac{\mathrm{d}\sigma_{\mathrm{el}}}{\mathrm{d}\Omega}\right)^{\frac{1}{2}} = \frac{1}{2k} \sum (2l + 1)\,(1 - \eta_l)\, P_l\,(\cos\theta)\ ; \tag{18}$$

we make use of eq. (14) and find that no negative terms can appear in the summation of the right-hand side of eq. (18), while there is at least one positive term.

The inequality $\theta \leqq \theta_0$ is again a sufficient condition, and usually the non-vanishing region spreads far outside of θ_0.

2.2. ANALYSIS OF EXPERIMENTAL DATA

We apply the criteria I), II) and III) to the experimental data now avaiable. The results are shown in table 1. As is seen, the p-p collision data at energies less than 5 GeV do not satisfy the criterion II), while that of 8.5 GeV contra-

TABLE 1

Comparison between the experimental data and the criteria of sect. 2.1

Author	Kinetic energy in GeV	$\lambda\!\!\!^{-} \times 10^{14}$ cm	$\int_{-1}^{1} \left(\frac{\mathrm{d}\sigma_{\mathrm{el}}}{\mathrm{d}\Omega}\right)^{\frac{1}{2}} \mathrm{d}(\cos\theta)$	σ_{tot} (mb)	$\left(\frac{\sigma_{\mathrm{tot}}}{4\pi\lambda\!\!\!^{-}}\right)^2$ (mb)	$\left(\frac{\mathrm{d}\sigma_{\mathrm{el}}}{\mathrm{d}\Omega}\right)_{\mathrm{max}}$ (mb)
p-p collision						
Cork *et al.*	2.24	1.94	3.06	$41.6^{+4}_{-1.6}$	28.9^{+6}_{-2}	20.8
Cork *et al.*	4.40	1.37	1.56			20.5
Cork *et al.*	6.15	1.16	0.836			27.7
Kalbach *et al.*	6.20	1.15	1.03	31.4 ± 7.3	$47.1^{+24.2}_{-19.9}$	40.4
Markov *et al.*	8.50	0.99	0.59 ± 0.07	29.6	57.1	123 ± 18
π-p collision						
Eisberg *et al.*	1.37	2.66	2.0 ± 0.7	34.6 ± 2.7	$10.7^{+1.8}_{-1.7}$	9 ± 2
Van Gan Chiang *et al.*	6.8 ± 0.6	1.14 ± 0.05	0.80 ± 0.16	30 ± 5	44^{+22}_{-16}	19 ± 5

dicts III). Thus, these discrepancies at lower and high energy are due to different causes. In the pion-proton collision we do not find disagreement above 1.3 GeV.

2.3. DETERMINATION OF THE OPTICAL POTENTIAL FROM EXPERIMENTAL DATA IN THE CASE Re $\delta_l = 0$

The quantity $\eta_l = \exp(2i\delta_l)$ can be obtained from the present experimental data when we put $\operatorname{Re}\delta_l = 0$. In the framework of the optical model, the limiting transition $l + \frac{1}{2} \to k\rho$ corresponds to the substitution of a function of the impact parameter $\delta(\rho)$ for δ_l. The coefficient of absorbtion[8]) of the optical model $K(\rho)$ is related to Im $\delta(\rho)$ by the well known equation

$$\operatorname{Im}\delta(\rho) = \tfrac{1}{4}\int_{-\sqrt{R^2-\rho^2}}^{+\sqrt{R^2-\rho^2}} K(\sqrt{\rho^2+\xi^2})\,\mathrm{d}\xi\,. \tag{19}$$

where R is the range of action of the potential. We assume, what is plausible from the physical standpoint, $K(\rho)$ and $\delta(\rho)$ to be functions defined in the whole space, sufficiently rapidly vanishing when $\rho \to \infty$. We shall now treat δ and K as functions of ρ^2. Then the equation (19) takes the following form:

$$\operatorname{Im}\delta(\rho^2) = \tfrac{1}{4}\int_{-\infty}^{+\infty} K(\rho^2+\xi^2)\,\mathrm{d}\xi\,. \tag{20}$$

We define the functions $\bar{\delta}$ and $\bar{K}$ by

$$\delta(x) = \begin{cases} \delta(x) & \text{for } x > 0 \\ \delta(|x|) & \text{for } x < 0 \end{cases}, \qquad \bar{K}(x) = \begin{cases} K(x) & \text{for } x > 0 \\ K(|x|) & \text{for } x < 0 \end{cases}, \tag{21}$$

and assume that $\bar{\delta}$ and $\bar{K}$ can be expanded into Fourier integrals. We look for the function $\bar{K}$ satisfying the equation

$$\operatorname{Im}\bar{\delta}(x) = \tfrac{1}{4}\int_{-\infty}^{+\infty} \bar{K}(x+\xi^2)\,\mathrm{d}\xi\,. \tag{22}$$

Inserting the Fourier expansions of $\bar{\delta}$ and $\bar{K}$ into (22) we obtain after simple calculations

$$\bar{K}(x) = -\frac{4}{\pi}\int_x^\infty \frac{\partial}{\partial y}[\operatorname{Im}\delta(y)]\frac{\mathrm{d}y}{\sqrt{y-x}}\,. \tag{23}$$

From the form of the original equation it is seen that if Im δ has a step-like behaviour, K must have a singularity. This is an important point since the experiment gives us Im δ in the form of a histogram, which must be replaced by a suitable smooth curve. The solution (23) can be formally applied also in the case when the real part of the potential is present. The function[8]) k_1 of the optical model theory is in this case expressed by Re δ in the following way

$$k_1(x) = -\frac{2}{\pi}\int_x^\infty \frac{\partial}{\partial y}[\operatorname{Re}\delta(y)]\frac{\mathrm{d}y}{\sqrt{y-x}}\,. \tag{24}$$

We have written "formally", since in this case the phase shift analysis cannot be carried out if we know the differential cross section only, which is the present situation. It must be noted that the relation (19) between phase shifts and potential is a consequence of the WKB approximation, which is not applicable for small l. Since the experimentally measured quantities are just the phase shifts, the part of the potential corresponding to small ρ cannot be taken literally. Inserting the solution (23) into the equation (20) we see that this solution is a very general one, since as far as the integral in (23) is meaningful this expression satisfies the original equation identically.

The applicability of the optical model requires $\lambda\!\!\!^{-} \ll d$ where $\lambda\!\!\!^{-}$ denotes the de Broglie wave length of the colliding particle in the c.m. system and d is a linear dimension characterising the "obstacle". Denoting by $\lambda\!\!\!^{-}_{\mathrm{N}}$, $\lambda\!\!\!^{-}_{\pi}$ the wave lengths in these collisions we get

$$\frac{\lambda\!\!\!^{-}_{\pi}}{\lambda\!\!\!^{-}_{\mathrm{N}}} = \left[\frac{\dfrac{E}{\mu} + 4.45}{\dfrac{E}{\mu} + 2}\right]^{\frac{1}{2}} \approx 1 \text{ for } E > 1 \text{ GeV},$$

μ being the rest mass of the pion. Thus we have practically the same energy threshold for application of the optical model in both collisions. That is true of course only if the characteristic dimensions of the "obstacle" are the same in n-n and in π-n collisions.

3. Estimation of the Real Part of the Proton-Proton Scattering Amplitude by means of the Dispersion Relations

3.1. CONSEQUENCES OF THE p—p SCATTERING EXPERIMENT

As was emphasized by Veksler[1]) the result of the experiment of Markov *et al.* with the Dubna accelerator on the proton-proton scattering at the energy 8.5 GeV is in contradiction to the assumption that the real part of the scattering amplitude vanishes if the scattering is spin-independent. This discrepancy cannot be removed even if we take into account the Coulomb correction to the scattering. Veksler describes one of the possible solutions, which consists in assuming the existence of a potential scattering even at such high energy. Calculations performed with a square-well complex potential, assuming spin-independence of the scattering, gives, for a definite value of the real part of the optical potential Re V, results in accordance with the experiment. Here Re V as a function of distance has a definite sign. It is understandable that the addition of some real part to the potential improves the situation, since it always raises the curve $\mathrm{d}\sigma_{\mathrm{el}}(\theta)/\mathrm{d}\Omega$. The question, however, arises whether the value of Re V, required in order to reproduce the experimental cross section, is not too large. It is thus of great interest to estimate the ratio

$|\operatorname{Re} f| / |\operatorname{Im} f|$. At present, this is in principle possible at one point only, namely at the point $\theta = 0$, by means of the dispersion relation.

Such an estimation, if possible, would permit us to decide whether the assumption of non-vanishing spin-independent Re V, constant in sign, is compatible with the present experimental knowledge. The constancy in sign of Re V is an important point, since it has an intimate connection with the shape of the curve $\mathrm{d}\sigma_{el}(\theta)/\mathrm{d}\Omega$, which we know, down to about $\theta = 2°$, to be a decreasing function of the angle. For small angle the optical model is applicable and we have

$$f(\theta) = \frac{i}{k} \int_0^R (1 - \mathrm{e}^{2i\delta})\, J_0(k\rho \sin\theta)\, \rho \mathrm{d}\rho\,. \tag{25}$$

Im f always takes its largest value at $\theta = 0$, but the shape of Re f depends on the behaviour of the sign of Re δ. If this sign is constant Re f is largest at $\theta = 0$, but if the sign of Re δ changes, Re f can have the largest value in a point different from $\theta = 0$. In the optical model

$$\operatorname{Re}\delta = \tfrac{1}{2} \int_{-\sqrt{R^2-\rho^2}}^{+\sqrt{R^2-\rho^2}} k_1 \left(\sqrt{\rho^2 + \xi^2}\right) \mathrm{d}\xi\,,$$

where

$$k_1(\rho) = k \left[\left(1 + \frac{\operatorname{Re} V(\rho)}{E} \right)^{\frac{1}{2}} - 1 \right].$$

We see that Re δ can change its sign only when Re V changes its sign, and if the maximum of Re f lies in the region of very small θ, Re V must change its sign in a region very far out. The experiment of Markov and others is in disagreement with the condition (9), but the latter is not valid when Re $V \neq 0$. When the sign of Re V is constant this condition is replaced by the following one:

$$\left(\frac{k}{4\pi}\sigma_{tot}\right)^2 \left(1 + \left|\frac{\operatorname{Re} f(0)}{\operatorname{Im} f(0)}\right|^2\right) \geqq \frac{\mathrm{d}\sigma_{el}(\theta)}{\mathrm{d}\Omega}\,. \tag{26}$$

3.2. ESTIMATION OF Re f

Now we should like to give a preliminary discussion of the possibility of estimation of Re f based on the dispersion relations. The numerical results of our calculation are of a rather rough character, because our calculational possibilities are limited.

Let us make some introductory remarks. A similar calculation in the case of π-p scattering was performed by Sternheimer[9]), up to a pion kinetic energy equal to 2.5 GeV. We shall not continue his calculation for higher energies, since the discrepancy between simple theory and experiment in the small angle region is apparent only in the case of p-p scattering. We just notice that, according to his results, the ratio $|\operatorname{Re} f(0)| / |\operatorname{Im} f(0)|$ at the energy 2.5 GeV

is approximately equal to $\approx \frac{1}{3}$; the contribution from Re f to $d\sigma/d\Omega$ for small θ is thus about 10 % of the contribution from Im f.

In the case of proton-proton scattering, the scattering amplitude is a matrix in spin space and from general invariance requirements we obtain it in the following form (we use the notation of Goldberger, Nambu and Oehme[10]):

$$f = \frac{m}{E}[\alpha + \beta(\sigma^1 \cdot n)(\sigma^2 \cdot n) + i\gamma(\sigma^1 + \sigma^2)\cdot n + \delta(\sigma^1 \cdot m)(\sigma^2 \cdot m) + \varepsilon(\sigma^1 \cdot l)(\sigma^2 \cdot l)], \tag{27}$$

where

$$l = \frac{k + k'}{|k + k'|}, \quad m = \frac{k - k'}{|k - k'|}, \quad n = \frac{k \times k'}{|k \times k'|}.$$

The quantities α, β, γ, δ and ε are scalar functions of invariants. It is possible to write down the dispersion relations for these functions. However, the experimentally measured quantity which is known in the GeV region and which appears simultaneously in the dispersion relations is only the total cross section σ_{tot} for the scattering of unpolarised particles. It is related by the optical theorem to Im α ($\theta = 0$):

$$\sigma_{tot} = \frac{4\pi}{k}\frac{m}{E}\,\mathrm{Im}\,\alpha(\theta = 0)\,. \tag{28}$$

The physical meaning of α is the following: if the scattering were spin-independent in some energy region, we should have there $f = (m/E)\alpha$; generally for unpolarized incident beam and unpolarized target, when the system is described by the density matrix ρ, we have

$$\alpha = \frac{E}{m}\,\mathrm{Tr}\,(\rho f)\,, \tag{29}$$

α being thus proportional to the average value of f. We make now two assumptions of a rather general character. Firstly we assume the dispersion relations for nucleon-nucleon scattering, which have not been proved rigorously, to be valid. Secondly we assume the validity of these relations in the GeV energy region. We take the dispersion relations from the work of Goldberger *et al.*[10]):

$$\begin{aligned}\mathrm{Re}\left[\alpha(\lambda_1) + \frac{\lambda_1 - \lambda_2}{\lambda_2 - m}\alpha(m) - \frac{\lambda_1 - m}{\lambda_2 - m}\alpha(\lambda_2)\right] &= (\lambda_1 - \lambda_2)(\lambda_1 - m)\left\{\frac{f^2}{16\pi}\frac{1}{(\lambda_\mu + \lambda_1)(\lambda_\mu + \lambda_2)(\lambda_\mu + m)}\right. \\ &+ \frac{1}{8\pi^2}\mathrm{P}\int_m^\infty d\lambda\sqrt{\lambda^2 - m^2}\left[\frac{\sigma_{tot\ pp}(\lambda)}{(\lambda - \lambda_1)(\lambda - \lambda_2)(\lambda - m)}\right. \\ &\left.\left. + \frac{\sigma_{tot\ p\bar{p}}(\lambda)}{(\lambda + \lambda_1)(\lambda + \lambda_2)(\lambda + m)}\right] + \frac{1}{\pi}\mathrm{P}\int_{\lambda(2\mu)}^\infty d\lambda\,\frac{\mathrm{Im}\,\alpha_{p\bar{p}}(\lambda)}{(\lambda + \lambda_1)(\lambda + \lambda_2)(\lambda + m)}\right\},\end{aligned} \tag{30}$$

where

$$\lambda = \frac{2E^2}{m} - m\,.$$

Two subtractions are necessary, to make the integrals converge, if we extrapolate σ_{tot} to the energy region which is beyond the present experimental possibilities. Of course the existence of the unphysical contribution in eq. (30) is a defect of our estimation. As λ_2 we choose the point corresponding to the laboratory kinetic energy 310 MeV, which is the proton energy in the experiment of Chamberlain *et al.*[11]). For this energy the phase analysis was done by Stapp *et al.*[12]) and several sets of phase shifts were obtained. As Smorodinski[13]) stated the present experimental data are in conformity with Stapp's solutions no. 1 and no. 2 only. Our calculations have been done for these two solutions, and correspondingly we have obtained two values for Re $\alpha(\theta = 0)$. The experimental points for p-p scattering are taken from the paper by Hess[14]) and Veksler's report at the Kiev conference. The very low ($E_{lab} < 6$ MeV) p-p cross section is taken from the text-book of Blatt and Weisskopf, where the singlet cross section is calculated with the use of the effective range approximation. Up to 450 MeV $\sigma_{tot\ pp}$ is approximated inside three energy intervals (0 — 9.7 MeV, 9.7 — 95 MeV, 95 — 450 MeV) by easily integrable functions of the type

$$\frac{a + bE_{lab}}{1 + c(E_{lab} - E_1)(E_{lab} - E_2)} \qquad (E_1 \leq E_{lab} \leq E_2)$$

with an accuracy of 5 — 10 %. For $E > 450$ MeV, $\sigma_{tot\ pp}$ is approximated by linear functions of energy inside three intervals (450 — 800 MeV, 0.8 — 9 GeV, 9 GeV — ∞). For $E > 9$ GeV we put $\sigma_{tot\ pp} = \text{const.} = 29.5$ mb. As to the p-$\bar{\text{p}}$ scattering the data are taken from Segrè's report at the Kiev conference and from papers cited in it. Inside the energy intervals 5 — 160 MeV, 160 — 2000 MeV, 2 GeV — ∞ we approximate $\sigma_{tot\ p\bar{p}}$ by linear functions, putting $\sigma_{tot\ p\bar{p}} = \text{const.} = 88.9$ mb for $E > 2$ GeV. There is some difficulty with the low energy interval. The lowest energy total cross section measurement known to us is that done by Horwitz *et al.*[16]). These authors obtained from 6 points lying inside the energy interval 5 — 80 MeV the mean total cross section $\sigma_{tot\ p\bar{p}} = 210 \pm 70$ mb and the mean elastic cross section $\sigma_{el\ p\bar{p}} = 96 \pm 43$ mb for the mean energy $E = 50$ MeV in accordance with the calculations of Ball and Fulco[17]) ($\sigma_{tot\ p\bar{p}} = 232$ mb, $\sigma_{el\ p\bar{p}} = 91$ mb). For very low energy, when only the S-wave scattering occurs, we expect the validity of the relation $\sigma_{ann} \approx 1/k$ (with a black hole of radius $r_0 = \frac{3}{2}\mu^{-1}$ the condition of applicability of this relation is $1/k \gg r_0$, that is, $E_{lab} \gg 84$ MeV). We assume $\sigma_{el\ p\bar{p}} = \text{const} = 91$ mb for $E_{lab} < 50$ MeV. Finally, for $E_{lab} \leq 5$ MeV we obtain $\sigma_{tot\ p\bar{p}} = 91 + \beta/\sqrt{E_{lab}}$. Down to 5 MeV we extrapolate linearly the energy dependence of the total cross section. The constant β is determined from the continuity of $\sigma_{tot\ p\bar{p}}$.

The final numerical results obtained by our calculation are not satisfactory, however. This is due to the cancellation of large numbers, which are not known exactly, so that we are left with a number which involves an error comparable to its own value. To speak more concretely let us discuss below the result of

the calculation of Re α at the energy corresponding to Markov's experiment ($\lambda_1 = m + 8.5$ GeV). The main contribution to the integral over the physical region in eq. (30) is due to the integration of

$$\frac{\sqrt{\lambda^2 - m^2}\, m\, \sigma_{\text{tot pp}}}{(\lambda - \lambda_1)(\lambda - \lambda_2)(\lambda - m)}$$

from $\lambda = m$ to $\lambda = m + 450$ MeV, which is equal to ≈ 301 mb. The integration of the same quantity from $\lambda = m + 450$ MeV to infinity gives ≈ -36 mb. The integration of

$$\frac{\sqrt{\lambda^2 - m^2}\, m\, \sigma_{\text{tot p}\bar{\text{p}}}}{(\lambda + \lambda_1)(\lambda + \lambda_2)(\lambda + m)}$$

from $\lambda = m$ to infinity gives ≈ 12 mb. The right-hand side of eq. (30) without the unphysical integral is equal to $\approx 133 \times 10^{-13}$ cm. The left-hand side of eq. (30) without Re α ($\lambda_1 = m + 8.5$ GeV) is equal to $\approx 147 \times 10^{-13}$ cm. To estimate the unphysical integral we make the additional, physically plausible assumption that

$$\lim_{\lambda_1 \to \infty} \frac{\text{Re}\, \alpha(\lambda_1)}{\lambda_1} = 0 .$$

Since λ_1 is large we write

$$\int_{\lambda(2\mu)}^{m} \frac{\text{Im}\, \alpha_{\text{p}\bar{\text{p}}}(\lambda)\, \text{d}\lambda}{(\lambda + \lambda_1)(\lambda + \lambda_2)(\lambda + m)} = h(\lambda_1) \int_{\lambda(2\mu)}^{m} \frac{\text{d}\lambda}{(\lambda + \lambda_1)(\lambda + \lambda_2)(\lambda + m)} \approx h_0 \int_{\lambda(2\mu)}^{m} \frac{\text{d}\lambda}{(\lambda + \lambda_1)(\lambda + \lambda_2)(\lambda + m)} , \tag{31}$$

where

$$h_0 = \lim_{\lambda_1 \to \infty} h(\lambda_1) .$$

We find h_0 from the condition mentioned above† and obtain the contribution from the unphysical part $\approx 22 \times 10^{-13}$ cm. Thus Re $\alpha \approx 7 \times 10^{-13}$ cm.

It may be interesting to note that one obtains nearly the same result for the two phase shift sets of Stapp. The obtained value for Re α is large (Im $\alpha = 5.62 \times 10^{-13}$ cm) but we must take into account the error due to the experimental uncertainty in our knowledge of the cross sections which is of the same order of magnitude. If the error were small this result would rather support the explanations given in Veksler's report; but the conclusion essentially depends on the estimation of the error so that it is impossible to say anything definite. We have to do with the cancellation of large numbers since we have

† In our calculations $\sigma_{\text{tot pp}}$ and $\sigma_{\text{tot p}\bar{\text{p}}}$ are not equal to each other at infinity, as they should be. In practical calculations it turns out more convenient to extrapolate cross sections in such a manner, since the contributions from very high energy regions are negligible and at present the difference between those two cross sections at the highest energies available experimentally is very large. However, in calculating lim $\alpha(\lambda)/\lambda$ we have to omit the logarithmically divergent terms. For the meaning of these terms see the paper by I. Pomeranchuk[18]).

chosen the point $\lambda = m$ as one of the subtraction points. However, in order to choose a definite point for subtraction, it is necessary that we are able to calculate Re α at this point, or in other words the phase analysis at this point must be done. The phase shift analysis has been done as yet in few suitable points (for very low energies we obtain too large a value of Re α). We calculated Re α at 95 MeV, which is the energy corresponding to the phase analysis of Phillips[19]). For Phillips' solutions 1b and 3c we obtained Re α equal to 0.1941×10^{-13} cm and 0.1267×10^{-13} cm respectively. We see that the result can depend strongly on our choice of the set of phase shifts. A calculation of the magnitude of Re α at large energies, starting with different subtraction points and phase shift sets would be of interest. Such a calculational program should be, however, the subject of a separate work.

4. Spin Dependence and Quasi-Resonance

4.1. APPLICATION OF THE OPTICAL THEOREM UNDER GENERAL CONDITIONS

In sect. 3 we have investigated the first possibility of getting rid of the discrepancy between the simple theory and the experiment of Markov *et al.* In this section we shall discuss the second and third possibilities.

As we have seen in the previous sections the optical theorem imposes a strict restriction on the magnitude of the elastic cross section at small angles. Now we shall examine its application under more general conditions.

We should like to emphasize that the relation between the elastic cross section and the total cross section derived by the optical theorem is a non-linear one. We must be careful, therefore, when we have not to do with a pure state and have to carry out an averaging procedure.

For a pure state we have

$$\left(\frac{\mathrm{d}\sigma_{\mathrm{el}}}{\mathrm{d}\Omega}\right)_{\theta=0} = \left(\frac{\sigma_{\mathrm{tot}}}{4\pi\lambda}\right)^2 \left[1 + \left(\frac{\mathrm{Re}\, f(0)}{\mathrm{Im}\, f(0)}\right)^2\right]; \tag{32}$$

if we are to average over a number of states, however, we get instead an inequality,

$$\left(\overline{\frac{\mathrm{d}\sigma_{\mathrm{el}}}{\mathrm{d}\Omega}}\right)_{\theta=0} \geqq \left(\frac{\bar{\sigma}_{\mathrm{tot}}}{4\pi\lambda}\right)^2 \left[1 + \left(\frac{\overline{\mathrm{Re}\, f(0)}}{\overline{\mathrm{Im}\, f(0)}}\right)^2\right], \tag{33}$$

because, in general,

$$\overline{[\mathrm{Im}\, f(0)]}^2 \leq \overline{[\mathrm{Im}\, f(0)]^2}. \tag{34}$$

A special case of the relation (33) was formulated by Rarita as "minimum theorem"[20]). As examples of such an averaging procedure we shall discuss two cases described in sects. 4.2 and 4.5, respectively.

4.2. SPIN DEPENDENCE OF THE NUCLEON-NUCLEON INTERACTION

When the incident beam is unpolarized, we have to do with a statistical mixture of singlet and triplet states. Consequently,

$$\sigma_{\mathrm{tot}}^{(\mathrm{exp})} = \tfrac{1}{4}\,\sigma_{\mathrm{tot}}^{(\mathrm{s})} + \tfrac{3}{4}\,\sigma_{\mathrm{tot}}^{(\mathrm{t})} \tag{35}$$

and

$$\left(\frac{\mathrm{d}\sigma_{\mathrm{el}}^{(\mathrm{exp})}}{\mathrm{d}\Omega}\right)_{\theta=0} = \tfrac{1}{4}\left(\frac{\mathrm{d}\sigma_{\mathrm{el}}^{(\mathrm{s})}}{\mathrm{d}\Omega}\right)_{\theta=0} + \tfrac{3}{4}\left(\frac{\mathrm{d}\sigma_{\mathrm{el}}^{(\mathrm{t})}}{\mathrm{d}\Omega}\right)_{\theta=0}, \tag{36}$$

where the superscripts (exp), (s) and (t) denote respectively the experimentally measured values for the unpolarized beam and those corresponding to the singlet and triplet states.

It is to be remarked that the scattering matrix is reduced to a diagonal form in the case of forward scattering, and $\mathrm{d}\sigma_{\mathrm{el}}^{(\mathrm{t})}/\mathrm{d}\Omega$ in (36) represents actually a mean value of contributions from the three triplet components (two of them being equal).

It may here be noticed, too, that the value of the total spin remains a good quantum number of a two-nucleon system even in a rigorously relativistic treatment. We can verify, for instance, that the operator $(\boldsymbol{\sigma}_1 \cdot \boldsymbol{\sigma}_2)$, whose eigenvalues characterize singlet and triplet states, commute with the general expression (27) for the scattering matrix†.

Assuming again that $\mathrm{Re}\, f_{ij} = 0$ for all i, j (the quantities f_{ij} are elements of the scattering matrix in the total spin representation of the two-nucleon system), we can apply the simple form of the optical theorem to the singlet and the triplet state separately:

$$\left(\frac{\mathrm{d}\sigma_{\mathrm{el}}^{(\mathrm{s})}}{\mathrm{d}\Omega}\right)_{\theta=0} = \left(\frac{\sigma_{\mathrm{tot}}^{(\mathrm{s})}}{4\pi\lambda\!\!\!^{-}}\right)^2, \qquad \left(\frac{\mathrm{d}\sigma_{\mathrm{el}}^{(\mathrm{t})}}{\mathrm{d}\Omega}\right)_{\theta=0} = \left(\frac{\sigma_{\mathrm{tot}}^{(\mathrm{t})}}{4\pi\lambda\!\!\!^{-}}\right)^2. \tag{37}$$

Let us introduce the ratio

$$\xi = \frac{\sigma_{\mathrm{tot}}^{(\mathrm{s})}}{\sigma_{\mathrm{tot}}^{(\mathrm{s})} + \sigma_{\mathrm{tot}}^{(\mathrm{t})}}, \qquad 0 \leq \xi \leq 1\,. \tag{38}$$

Then we can get from eqs. (35)–(38) a relation between experimental quantities:

$$\left(\frac{\mathrm{d}\sigma_{\mathrm{el}}^{(\mathrm{exp})}}{\mathrm{d}\Omega}\right)_{\theta=0} = Q(\xi)\left(\frac{\sigma_{\mathrm{tot}}^{(\mathrm{exp})}}{4\pi\lambda\!\!\!^{-}}\right)^2, \tag{39}$$

where

$$Q(\xi) = \frac{4(4\xi^2 - 6\xi + 3)}{(3 - 2\xi)^2}\,. \tag{40}$$

† This fact can be understood more physically by the help of the exclusion principle if we take into account the conservation of the isobaric spin in the strong interaction. We are grateful to Dr. A. Deloff for his remarks concerning this point.

The behaviour of this function is shown in fig. 2. It is easily seen that only in the case $\sigma_{tot}^{(s)} = \sigma_{tot}^{(t)}$ the relation (39) coincides with eq. (4).

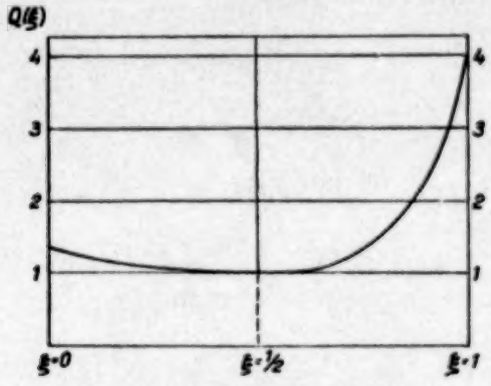

Fig. 2. The behaviour of the function $Q(\xi)$ defined by eq. (40). $\sigma_{tot}^{(t)} = 0$: $Q(1) = 4$; $\sigma_{tot}^{(t)} = \sigma_{tot}^{(s)}$: $Q(\frac{1}{2}) = 1$ (minimum); $\sigma_{tot}^{(s)} = 0$: $Q(0) = \frac{4}{3}$.

If we wish to ascribe the difference of the experimental value of Markov *et al.* from the prediction of the simplest theory (no-spin-dependence and $\mathrm{Re}\,\delta_l = 0$ being assumed) to the effect of spin-dependence alone, we are obliged to put

$$Q(\xi) \approx 2 \text{ to } 3\,, \tag{41}$$

whence

$$\xi \approx 0.8 \text{ to } 0.95\,. \tag{42}$$

This would mean, of course, an overwhelming predominance of the singlet interaction in the proton-proton collision at this energy. We can see, however, from a recent work of Shahbazyan[3a]), who has carried out a detailed phase-shift analysis taking account of the spin-dependence, that the extreme assumption of the absence of the triplet interaction is certainly in disagreement with experimental data. The reason is that if we assume the presence of singlet interaction alone, we must at the same time modify the criterion (8) into the following form:

$$\int_{-1}^{1} \left(\frac{\mathrm{d}\sigma_{el}^{(exp)}}{\mathrm{d}\Omega}\right)^{\frac{1}{2}} \mathrm{d}\,(\cos\theta) \leqq \frac{1}{2a}\frac{1}{k}\,, \tag{8'}$$

where the correction factor 2 comes from the fact that the "true" cross section is 4 times as large as the experimental unpolarized beam value, and $a \geqq \sqrt{2}$ is meant to take into account the absence of odd orbital angular momentum states. Then the numerical values given in table 1 show that (8') is not fulfilled.

In the following subsection we shall examine some consequences of the hypothesis that $\sigma_{tot}^{(t)} \approx 0$, because this feature will probably remain qualitatively valid if we wish to minimize the contribution from the potential scattering.

4.3. IMPLICATIONS OF THE HYPOTHESIS $\sigma_{tot}^{(1)} \approx 0$

Let us put, for orientation,

$$\sigma_{tot}^{(1)} \approx 0\,, \tag{43}$$

and see what conclusion we can derive in such an extreme case. From the requirement that the differential cross section for elastic scattering of the triplet state should vanish everywhere, we get the following conditions imposed on the coefficients of (27):

$$\gamma = 0\,, \quad \beta = \delta = \varepsilon = -\alpha\,. \tag{44}$$

Consequently (27) takes the form

$$f = \frac{\alpha m}{E}\{1 - (\sigma_1 \cdot \sigma_2)\}\,, \tag{45}$$

which includes, as it should, the projection operator on the singlet state.

The absence of the triplet state in the scattered wave requires, of course, non-existence of any polarization effects. But this does not mean much, because even if the triplet state existed, still the original assumption $\mathrm{Re}\, f_{ij} = 0$ should lead to the conclusion that all the polarization effects vanish. This can be seen, for instance, from the following expression for the polarization of the scattered wave, when the incident beam is unpolarized:

$$P = \frac{\mathrm{Tr}\,(f^{\dagger}\,\sigma f)}{\mathrm{Tr}\,(f^{\dagger} f)} = n\,\frac{2\,\mathrm{Im}\,(\alpha^{*}\gamma + \beta^{*}\gamma)}{|\alpha|^2 + |\beta|^2 + 2|\gamma|^2 + |\delta|^2 + |\varepsilon|^2}\,. \tag{46}$$

This expression is a non-relativistic one; it is known, however, that a rigorous relativistic treatment gives in this case the same result[21]). The right-hand side of eq. (46) vanishes by the assumption $\mathrm{Re}\, f_{ij} = 0$, which leads to purely imaginary values of α, β and γ, as well as by the absence of the triplet interaction, which requires, among others, that $\gamma = 0$.

The expression (45) for the scattering matrix shows that we have only one function of angle, α, at our disposal. The elastic scattering of the incident proton by a proton bound in a nucleus will give, therefore, the same angular distribution as in the free proton-proton scattering if we assume that the boundary condition imposed by the rest of the nucleus can be regarded to restrict the freedom of spin change.

On the other hand, the absolute magnitude of the elastic scattering cross section by a bound proton might depend on the details of the boundary condition. If we imagine that the target proton forms a spin singlet or triplet with a third nucleon in the nucleus and this state is not to be changed by the collision[22]), we have (it would be necessary to confirm that the nucleus is not left in an excited state):

$$\left(\frac{d\sigma_{el}}{d\Omega}\right)_{bound} = 4 \times \tfrac{1}{8}\,\mathrm{Tr}\left[\left(\frac{1-\sigma_2\cdot\sigma_3}{4}\right) f^{\dagger}\left(\frac{1-\sigma_2\cdot\sigma_3}{4}\right) f\right] = \left(\frac{\alpha m}{E}\right)^2 = \tfrac{1}{4}\left(\frac{d\sigma_{el}}{d\Omega}\right)_{free} \tag{47}$$

for the singlet binding and

$$\left(\frac{d\sigma_{el}}{d\Omega}\right)_{bound} = \tfrac{3}{4} \times \tfrac{1}{8}\,\mathrm{Tr}\left[\left(\frac{3+\sigma_2\cdot\sigma_3}{4}\right) f^{\dagger}\left(\frac{3+\sigma_2\cdot\sigma_3}{4}\right) f\right] = 3\left(\frac{\alpha m}{E}\right)^2 = \tfrac{3}{4}\left(\frac{d\sigma_{el}}{d\Omega}\right)_{free} \tag{48}$$

for the triplet binding.

It may be expected, therefore, that the elastic scattering cross section of a proton by such a nucleus as He^4 or C^{12} will be much reduced compared to the free proton-proton case, if the contribution to the proton-neutron scattering from the isobaric singlet part is not very large.

4.4. SECOND OPTICAL THEOREM FOR THE PROTON-NEUTRON SCATTERING, WHEN THE INTERACTION IS SPIN-DEPENDENT

The relations (37)–(40) can be applied to proton-neutron scattering as well as to proton-proton scattering. In the former case, however, there is an additional relation, which can be obtained by applying the above argument to the second optical theorem (5).

The theorem is valid for the spin singlet and triplet cases:

$$\left(\frac{d\sigma_{el}^{(s)}(n\text{–}p)}{d\Omega}\right)_{\theta=\pi} = \left[\frac{\sigma_{tot}^{(s)}(p\text{–}p) - \sigma_{tot}^{(s)}(n\text{–}p)}{4\pi\lambda}\right]^2, \tag{49}$$

$$\left(\frac{d\sigma_{el}^{(t)}(n\text{–}p)}{d\Omega}\right)_{\theta=\pi} = \left[\frac{\sigma_{tot}^{(t)}(p\text{–}p) - \sigma_{tot}^{(t)}(n\text{–}p)}{4\pi\lambda}\right]^2. \tag{50}$$

The remark made after (36) concerning the meaning of $\sigma^{(t)}$ remains valid for eq. (50).

In the same way as we derived (39) and (40), we have, for the unpolarized beam,

$$\left(\frac{d\sigma_{el}^{(exp)}(n\text{–}p)}{d\Omega}\right)_{\theta=\pi} = Q(\varepsilon)\left[\frac{\sigma_{tot}^{(exp)}(p\text{–}p) - \sigma_{tot}^{(exp)}(n\text{–}p)}{4\pi\lambda}\right]^2, \tag{51}$$

where the function Q is given by (40) and its argument by

$$\varepsilon = \frac{\xi\xi'(1-\zeta)}{\xi' - \xi\zeta}. \tag{52}$$

Here ξ and ξ' denote the ratio (38) for the proton-proton and proton-neutron interaction respectively, while ζ is given by

$$\zeta = \frac{\sigma_{tot}^{(s)}(p\text{–}p)}{\sigma_{tot}^{(s)}(n\text{–}p)}. \tag{53}$$

For $\xi = \xi'$, the parameter ε is independent of ζ and is equal to ξ. Consequently, $\xi = \xi' = \frac{1}{2}$ gives the minimum value of $Q = 1$. For $\xi \neq \xi'$, Q can have a minimum value if $(\xi - \frac{1}{2})(\xi' - \frac{1}{2}) > 0$, and it is reached when

$$\zeta = \frac{\xi'}{\xi} \frac{\xi - \frac{1}{2}}{\xi' - \frac{1}{2}} . \tag{54}$$

4.5. SHARP QUASI-RESONANCE AS A SECOND EXAMPLE OF THE AVERAGING PROCEDURE DESCRIBED IN SECT. 4.1

Suppose that the energy of the incident beam is determined up to a spread ΔE. We should like to examine the effects of a sharp resonance-like behaviour of certain partial waves with angular momenta $l'_1, l'_2, \ldots$, when the width of the resonance Γ is small compared to ΔE. The amplitudes $\eta_{l'}$ of the outgoing waves corresponding to these partial waves are represented by

$$\eta_{l'} = \eta^0_{l'} + \eta^1_{l'} e^{i\xi} \tag{55}$$

(the quantities ξ and η have different meanings from those in sect. 4.4), while those of other partial waves are given by

$$\eta_l = \eta^0_l . \tag{56}$$

Here η^0_l does not change appreciably within the energy range of ΔE, but $\eta^1_{l'}$ and ξ change very rapidly within this region. For instance, we can put

$$\xi = \operatorname{arc\,tg} \frac{\Gamma}{E_0 - E} , \qquad \frac{\Delta E}{\Gamma} \gg 1 . \tag{57}$$

For simplicity ξ is taken as a function common for all values of l'.

The scattering amplitude is then given by

$$f(\theta) = \frac{i}{2k} \sum_{\text{all } l} (2l + 1)(1 - \eta^0_l) P_l(\cos\theta) + \frac{i}{2k} \sum_{l'} (2l' + 1) \eta^1_{l'} e^{i\xi} P_{l'}(\cos\theta) \tag{58}$$

Now the averaging procedure yields†

$$|\overline{f(0)}|^2 = \frac{1}{4k^2} |\sum (2l + 1)(1 - \eta^0_l)|^2 , \tag{59}$$

$$|\overline{f(0)}|^2 = \frac{1}{4k^2} |\sum (2l + 1)(1 - \eta^0_l)|^2 + \frac{1}{4k^2} \sum_{l'} \sum_{l''} (2l' + 1)(2l'' + 1) \overline{\eta^1_{l'} \eta^1_{l''}} . \tag{60}$$

In this way we get a relation between cross sections which are measured by experiment:

$$\left(\overline{\frac{d\sigma_{el}}{d\Omega}}\right)_{\theta=0} = \left(\frac{\bar{\sigma}_{tot}}{4\pi\lambda}\right)^2 + \frac{1}{4k^2} \sum_{l'} \sum_{l''} (2l' + 1)(2l'' + 1) \overline{\eta^1_{l'} \eta^1_{l''}} . \tag{61}$$

† If we assume independent functions ξ for different values of l', the cross terms in the last sum of eq. (60) vanish.

If we want to ascribe the whole discrepancy between the experiment of Markov and others and the simple theory to this effect alone, it is necessary that the last term of eq. (60) should have a magnitude of 70 to 100 mb. We should be obliged, therefore, to assume a resonance-like behaviour involving at least 2 to 3 angular momentum states with relatively large l.

The above argument can also be expressed in the following way: after averaging over the energy region, a certain part of the elastic scattering behaves as if it were incoherent, and by including this part into the inelastic (reaction) cross section, we can apply the usual formalism.

5. Final Remarks

5.1. OPTICAL POTENTIAL AND NUCLEON STRUCTURE

The optical model investigations of the collision processes in the GeV energy region can give us information concerning the structure of colliding particles, especially of the nucleon. It would be necessary, however, to note that in the framework of the optical model we are treating the scattering of two particles as a one-body problem (scattering of a particle in an external potential, which we shall call a one-body potential). Actually the scattering problem is a two-body one. We shall not discuss here the concept of potential in the relativistic quantum field theory. We assume that the physical situation is such that the motion is described by a two-body equation involving a potential, which is obtained for instance[6]) by the elimination of all amplitudes of states except one, corresponding to the two particles in question, from the Schrödinger equation (such a potential we shall call a two-body potential). As is well known, in the non-relativistic case the two-body problem is reducible to the one-body problem, the one-body equation being written in terms of relative coordinates. The reducibility in the relativistic case is so far an open question. If we know the initial states of both particles and the final state of one of them, however, the conservation laws permit us to find the final state of the other. (Of course, we must treat all the reactions as the result of the operation on the imaginary part of the potential which violates the conservation of probability in the elastic scattering channel). Thus we can look for a phenomenological one-body potential which depends on relative coordinates and some parameters describing the two-particle system, and which gives the motion of one of the scattered particles. This is just the standpoint of the optical model approach. The question however arises, what is the extent of ambiguity in the choice of the phenomenological one-body potential and how is it connected with the two-body potential, because this connection is not such an immediate one as in the non-relativistic case. Thus the quantitative connection between the optical potential and the quantities describing the nucleon structure is not quite clear—although, of course, some qualitative conclusions can be drawn.

5.2. NATURE OF THE QUASI-RESONANCE

Whether the result of Markov and others is due to a quasi-resonance can be checked experimentally by performing similar experiments at energies in the neighbourhood of 8.5 GeV. By the word "quasi-resonance" we mean that a rapid change of phase shift as function of energy may take place here, which, we expect, is probably due to pion-pion interaction (some kind of meson-cloud excitation). We do not imagine that a single intermediary unstable particle is formed: the relations (57) have only an illustrative meaning. It would be of interest to examine whether and, if so, under what conditions a sufficiently rapid change of phase shifts can occur when there are in the intermediary state several particles, at least one of them being unstable.

If we employ a naive picture of pion-pion interaction, on the other hand, and assume that quasi-free pions in the peripheral part of the cloud surrounding the nucleons interact with each other very strongly in a certain energy region, a corresponding effect could be observed in pion-nucleon collison. If we further assume that these virtual pions have masses not much different from free pions, the corresponding energy would be $\mu/m \times 8.5$ GeV ≈ 1.25 GeV. In this connection it may be of some interest to notice that the experimental data of pion-proton collisions at 1.37 GeV show a somewhat similar behaviour: the last two columns of table 1 show that $(\mathrm{d}\sigma/\mathrm{d}\Omega)_{\max}$ is in this case comparable with $(\sigma_{\mathrm{tot}}/4\pi\lambda)^2$ and our criterion B) or III) of sect. 2.1 may be violatad if measurements for smaller angles are performed.

One of us (Z. K.) is very grateful to the Polish Academy of Sciences, to Professor L. Infeld, Professor M. Danysz and Professor J. Werle for their hospitality extended to him during his stay in Warsaw.

Note added in proof: After completing this work, we were informed by Dr. G. Domokos from Budapest that he and his coworker had obtained independently a result identical to the one described in subsection 2.3. Their work will appear in JETP.

References

1) V. I. Veksler, Report at the 9th International Conference on High Energy Physics (Kiev, July 1959)
2) D. Ito, S. Minami and H. Tanaka, Nuov. Cim. **8** (1958) 135
3) P. Markov, E. Tsiganov, M. Shafranova and B. Shahbazyan, Work presented at the 9th International Conference on High Energy Physics (Kiev, July 1959)
3a) B. A. Shahbazyan, preprint of the Joint Institute for Nuclear Research, Dubna (1959)
4) V. G. Grishin, I. S. Saitov and I. V. Chuvilo, JETP **34** (1958) 1221
5) L. I. Lapidus, JETP **34** (1958) 1148
6) D. I. Blokhintsev, V. S. Barashenkov and B. M. Barbashev, Usp. Fiz. Nauk **63** (1959) 417
7) See for instance: E. T. Whittaker and G. N. Watson, Modern Analysis (Cambridge, 1946) p. 315
8) S. Fernbach, R. Serber and T. B. Taylor, Phys. Rev. **75** (1949) 1352
9) R. N. Sternheimer, Phys. Rev. **101** (1956) 384

10) M. L. Goldberger, Y. Nambu and R. Oehme, Ann. of Phys. **2** (1957) 226
11) O. Chamberlain, E. Segrè, R. D. Tripp, C. Wiegand and T. Ypsilantis, Phys. Rev. **105** (1957) 288
12) H. R. Stapp, T. I. Ypsilantis and N. Metropolis, Phys. Rev. **105** (1957) 302
13) J. Smorodinski, Report at the 9th International Conference on High Energy Physics (Kiev, July 1959)
14) W. N. Hess, Rev. Mod. Phys. **30** (1958) 368
15) E. Segrè, Report at the 9th International Conference on High Energy Physics (Kiev, July 1959)
16) N. Horwitz, B. Miller, I. Murray and R. Tripp, Phys. Rev. **115** (1959) 472
17) I. S. Ball and J. R. Fulco, Phys. Rev. **113** (1959) 647
18) J. Pomeranchuk, JETP **34** (1958) 725
19) R. I. N. Phillips, Proc. Roy. Soc. **70** (1957) 721
20) W. Rarita, Phys. Rev. **104** (1950) 221
21) H. R. Stapp, Phys. Rev. **103** (1956) 425
22) S. Tamor, Phys. Rev. **97** (1955) 1077

1.E.4:
3.B

Nuclear Physics **19** (1960) 221—224; © *North-Holland Publishing Co., Amsterdam*
Not to be reproduced by photoprint or microfilm without written permission from the publisher

M1/E2 MIXING RATIO IN THE Fe^{57} 14.41 keV γ-TRANSITION

G. T. EWAN, R. L. GRAHAM and J. S. GEIGER

Physics Division, Atomic Energy of Canada Limited, Chalk River, Canada

Received 15 March 1960

Abstract: The M1/E2 mixing ratio of the 14.41 keV γ-transition in Fe^{57} has been deduced from a measurement of the $L_I/(L_{II} + L_{III})$ conversion line intensity ratio. The measured value $L_I/(L_{II} + L_{III}) = 10.9 \pm 0.8$ is compared with Rose's theoretical L sub-shell conversion coefficients extrapolated to 14.41 keV. This comparison indicates that the γ-transition has an E2 quantum admixture of less than 10^{-4}. This limit means that there is no strong enhancement of the E2 transition probability over the single particle estimate.

1. Introduction

The 14.41 keV γ-transition in Fe^{57} is of current interest since it is a particularly suitable transition for studying the "Mössbauer Effect", i.e., recoilless nuclear resonance scattering[1,2,3]). The detailed interpretation of the hyperfine structure observed in some of these experiments[4]) depends on the M1/E2 admixture of the 14.41 keV transition. Analysis of the published experimental data[5,6]) indicates that the 14.41 keV γ-transition is dominantly M1 but could have an E2 admixture of up to 2×10^{-2}. Such small E2 admixtures would not affect the interpretation of the hyperfine structure results to date. However, a single particle estimate[7]) of the E2 transition probability and the measured half-life of the state[5,8]) predict an E2 admixture of $\approx 2.5 \times 10^{-5}$ which is ≈ 1000 times less than the present limit. In view of the large amount of experimental information becoming available on the properties of this transition, it is of interest to determine whether the E2 transition probability is strongly enhanced over the single particle estimate as this would presumably indicate collective features of the $\frac{3}{2}^-$ state.

2. Experimental Procedure and Results

The low energy conversion electron spectrum of Co^{57} was studied in the Chalk River air-cored $\pi\sqrt{2}$ β-spectrometer, adjusted to operate at 0.1 % resolution[9]). The source was prepared from "carrier-free" material supplied by the Nuclear Science and Engineering Corporation. The Co^{57} was further purified by passing through a series of anion exchange columns. The Co^{57} in the chemical form $CoCl_2$ was then sublimed in vacuo from a boat-shaped tantalum filament through a slot 1.5 mm wide and 12.5 mm long on to a

backing of Al foil 800 μg/cm^2 thick. The resultant source had an estimated activity of $\approx 5\,\mu$c and was invisible to the eye.

The detector used in this study was a continuous flow proportional counter with a methane filling at an absolute pressure of 7.5 cm. The methane pressure was kept constant by a Cartesian manostat. The counter window was a thin film of VYNS $\approx 100\,\mu$g/cm^2 thick supported by a metallic grid of 87 % open area. The transmission of this film was not measured directly but was assumed to be the same as that determined experimentally in the spectrometer for a film of similar thickness. Due to non-uniformity of the surface densities of the films, the effective thickness can vary up to 15 % and could lead to an uncertainty in intensity measurements. In this experiment, where the intensities of the L_I (13.56 keV) and ($L_{II} + L_{III}$) (13.70 keV) conversion lines are compared, the film transmission is $\approx 90\,\%$ and the relative transmission correction is negligible. For the K-line (7.31 keV), where the transmission is only $\approx 40\,\%$, there is an uncertainty of $\pm 25\,\%$ in the relative intensity determination.

The observed conversion electron spectrum is shown in fig. 1. The experi-

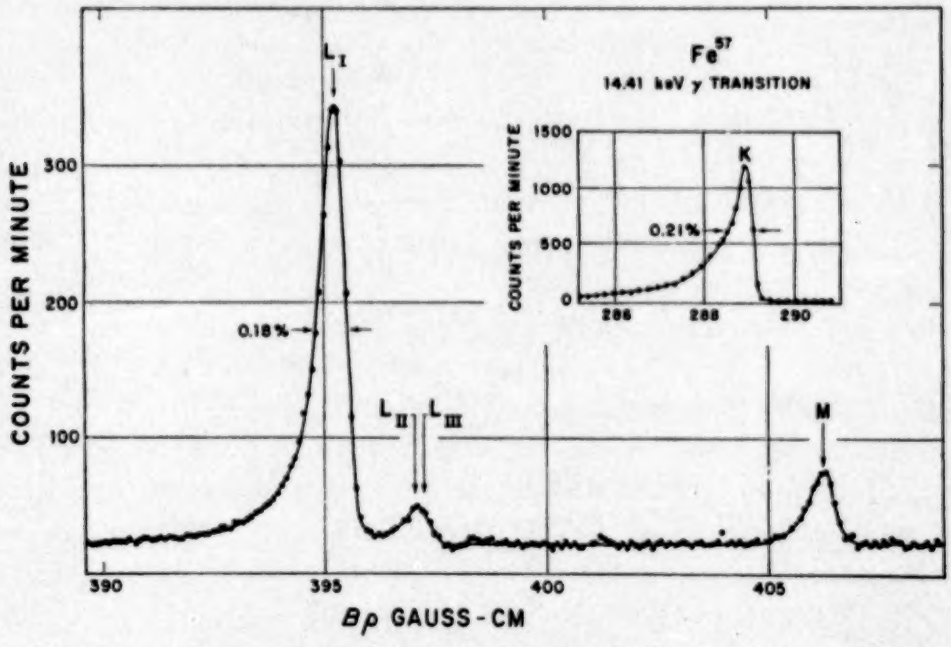

Fig. 1. The conversion line spectrum of Co^{57} from 13.2–14.6 keV. The points are not corrected for counter window transmission ($\approx 90\,\%$ at L_I and ($L_{II} + L_{III}$) lines). For the K-line (7.31 keV) shown in the inset the transmission is $\approx 40\,\%$.

mental line width of 0.18 % is considerably wider than the 0.10 % expected from the spectrometer settings. This increased width and the asymmetric low energy tail on the lines are attributed to energy degradation in the source which appears to have a surface density of $\approx 5\,\mu$g/cm^2. The fraction of the ($L_{II} + L_{III}$) line not resolved from the L_I line is $\approx 12\,\%$ and was estimated by a method described in a previous paper[10]).

The relative intensities of the lines, determined from the relative areas on a N/p versus p plot, are listed in table 1.

The errors quoted include allowance for statistical errors, uncertainties in the subtraction of background, and possible errors in the transmission curve

TABLE 1

Relative conversion line intensities of 14.41 keV transition

K	L_I	$(L_{II} + L_{III})$	M + N	$L_I/(L_{II} + L_{III})$
107 ± 25	10	0.92 ± 0.07	1.75 ± 0.2	10.9 ± 0.8

assumed for the $\approx 100\ \mu g/cm^2$ VYNS film used in this experiment. As discussed previously the last effect is only significant in determining the relative intensity of the K-line.

3. Discussion

The M1/E2 mixing ratio of the transition has been estimated using Rose's theoretical L sub-shell conversion coefficients[11]) for $Z = 26$. No values are tabulated for energies less than 25.5 keV ($k = 0.05\ mc^2$) and so it was necessary to extrapolate down to 14.41 keV ($k = 0.028$). The $L_I/(L_{II} + L_{III})$ ratio varies less rapidly than the individual conversion coefficients. The theoretical ratio was extrapolated for pure M1 radiation and also M1 with assumed admixtures up to 10 % E2. While it is difficult to estimate the errors in an extrapolation

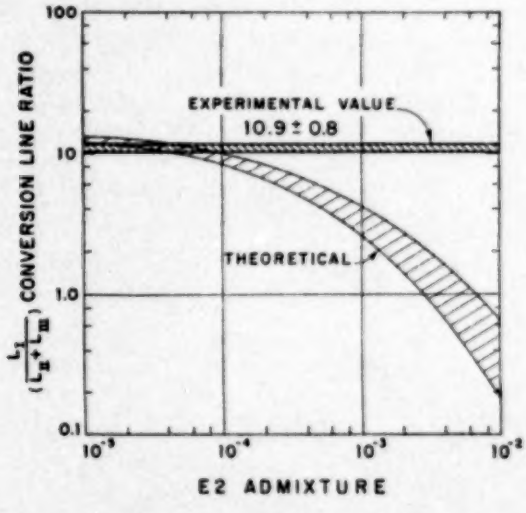

Fig. 2. Comparison of the experimental value of the $L_I/(L_{II} + L_{III})$ conversion line ratio with the theoretical predictions for small E2 quantum admixtures in the 14.41 keV M1 transition. The theoretical values were deduced by extrapolating Rose's theoretical L sub-shell conversion coefficients for $Z = 26$. The shaded area represents the limits of error we estimate assuming a smooth variation of the conversion coefficients with energy. The experimental value $L_I/(L_{II} + L_{III}) = 10.9 \pm 0.8$ indicates that the E2 quantum admixture is $< 10^{-4}$.

process, if the curve is smoothly varying the estimated errors in the extrapolated ratios are $\approx \pm 5\,\%$ at 10^{-5} E2 admixture up to $\approx \pm 50\,\%$ at 10^{-2} E2 admixture. The resulting theoretical ratios for a 14.41 keV transition are plotted in fig. 2 as a function of E2 admixture. Our experimental value of 10.9 ± 0.8 does not exclude the possibility that the transition is pure M1. The theoretical ratio deduced by extrapolation is, of course, subject to considerable error. However it seems unlikely that the E2 admixture can exceed 10^{-4}, i.e. the E2/M1 quantum ratio is less than 10^{-4}.

This result together with the measured half-life of the 14.41 keV state enables an estimate to be made of the E2 transition probability. The measured half-life[8]) of the state is $(1.0 \pm 0.1) \times 10^{-7}$ sec and the total conversion coefficient[5]) ≈ 15. This means that the transition probability for quantum emission is $\approx 5 \times 10^5$ sec^{-1}. Comparison with the single particle M1 estimate ($\approx 8 \times 10^7$ sec^{-1}) shows an M1 hindrance factor of ≈ 160. The present experiments indicate an E2/M1 quantum ratio $< 10^{-4}$. This implies an E2 quantum rate > 50 sec^{-1} to be compared with the single particle estimate[7]) of ≈ 20 sec^{-1}. It is thus apparent that there is no strong E2 enhancement attributable to collective effects in the 14.41 keV transition.

References

1) R. L. Mössbauer, Z. Physik **151** (1958) 124; Z. Naturforsh **14a** (1959) 211
2) R. V. Pound and G. A. Rebka Jr., Phys. Rev. Letters **3** (1959) 554
3) J. P. Schiffer and W. Marshall, Phys. Rev. Letters **3** (1959) 556
4) S. S. Hanna *et al.*, Phys. Rev. Letters **4** (1960) 177
5) H. R. Lemmer, G. J. A. Segaert and M. A. Grace, Proc. Phys. Soc. A **68** (1955) 701
6) J. B. Bellicard and A. Moussa, J. Phys. Radium **18** (1957) 115
7) S. A. Moszkowski, in Beta and Gamma-Ray Spectroscopy (North-Holland Publishing Company, Amsterdam, 1955) p. 373
8) W. C. Middelkoop *et al.*, Physica **21** (1955) 897
9) R. L. Graham, G. T. Ewan and J. S. Geiger, in preparation
10) G. T. Ewan, J. S. Geiger, R. L. Graham and D. R. MacKenzie, Phys. Rev. **116** (1959) 950
11) M. E. Rose, Internal Conversion Coefficients (North-Holland Publishing Company, Amsterdam, 1958)

1.D.1:
1.E.1

Nuclear Physics **19** (1960) 225—242; © *North-Holland Publishing Co., Amsterdam*
Not to be reproduced by photoprint or microfilm without written permission from the publisher

ENERGY LEVELS AND CONFIGURATION INTERACTION IN Zr^{90} AND RELATED NUCLEI

I. TALMI and I. UNNA

The Weizmann Institute of Science, Rehovoth, Israel†

Received 17 February 1960

Abstract: Proton and neutron $p_{\frac{1}{2}}$ and $g_{\frac{9}{2}}$ configurations (and in particular the interaction of the two 0^+ states in Zr^{90}) are considered without any specific assumptions on the two-body nuclear interaction and radial functions. Matrix elements of the effective nuclear interaction are determined by the analysis of energy levels in Zr^{90} and several neighbouring nuclei (e.g. Sr^{88} which has the same configurations). Good agreement is obtained between calculated and experimental level spacings. The one non diagonal matrix element is determined along with the diagonal elements and the amount of admixture is calculated in all cases. The ground state of Zr^{90} is found to be 75 % in the $p_{\frac{1}{2}}^2$ configuration and 25 % in the $g_{\frac{9}{2}}^2$ configuration in agreement with the rough experimental findings. The seniority is found to be a good quantum number for the effective interaction obtained in the $g_{\frac{9}{2}}$ shell of identical nucleons. This interaction gives rise to the low lying $\frac{1}{2}+$ level in Sr^{85}. Level schemes predicted by the present calculation are given for several nuclei.

1. Introduction

In a recent paper[1]), Bayman, Reiner and Sheline presented some shell model calculations for Zr^{90}. These authors take the observed levels with $J = 2, 4, 6, 8$ in Zr^{90} to belong to the $g_{\frac{9}{2}}^2$ configuration of protons outside the closed shells of 38 protons (and 50 neutrons). The two observed states with $J = 0$ are assumed to be due to admixtures of the $g_{\frac{9}{2}}^2$ and $p_{\frac{1}{2}}^2$ proton configurations. They assume a phenomenological interaction and harmonic oscillator wave functions and attempt to fit both the level spacings and the amplitudes of the interacting configurations in the two $J = 0$ states. Their main result seems to be the calculation of the amount of admixture in the $J = 0$ states which agrees with the experimental findings. On the other hand, the level spacings they obtain do not agree very well with the experimental data. Far worse is the nuclear interaction in the $g_{\frac{9}{2}}^n$ configurations of identical nucleons obtained with their interaction. It has a rather large attractive quadratic term in addition to attractive linear and pairing terms. This is in sharp contradiction with the established behaviour of nuclear binding energies. This is not surprizing since it is hardly conceivable that the *same* simple-minded potential interaction will give

† The research reported in this document has been sponsored by the Aeronautical Research Laboratory, Wright Air Development Center of the Air Research and Development Command, United States Air Force, through its European Office.

accurately enough both diagonal and non-diagonal elements of the energy matrix.

In the present paper it is shown that the configuration admixture in the two $J = 0$ states of Zr^{90} can be obtained without assuming a specific ad hoc interaction and special radial wave functions. It can be deduced from the energy levels of Zr^{90} and neighbouring nuclei by using only the general framework of the shell model. In such a shell model analysis, we assume only that the potential energy of the nucleus is due to two-body effective interactions between nucleons. The unknown matrix elements of those interactions, taken to be the same for all nuclei in which the same subshells are being filled, are determined by comparison with the experimental data. This method has been applied successfully to lighter nuclei in cases which exhibited rather pure configurations[2]). Configuration interaction, however, can also be incorporated into this approach. This is achieved by taking the non-diagonal matrix elements as unknown quantities which have the same values in all nuclei in which the same subshell is being filled. These non-diagonal elements are determined along with the diagonal elements by comparison with the experimental data. The calculation is considered to be successful if a certain number of such matrix elements reproduces accurately a larger number of experimental energies.

We consider the first 38 protons and first 50 neutrons to be in closed shells. The orbits available between numbers 38 and 50 are the $p_{\frac{1}{2}}$ and $g_{\frac{9}{2}}$ orbits. Since we shall always refer to the second $p_{\frac{1}{2}}$ shell and the first $g_{\frac{9}{2}}$ shell we shall omit the radial quantum numbers. In order to make the analysis possible we limit our treatment to configurations with either protons or neutrons outside closed shells. We thus consider nuclei with a few protons outside the closed shells of 38 protons and with exactly 50 neutrons. On the other hand we find the same *neutron* configurations in Strontium nuclei with exactly 38 protons and neutron number between 38 and 50. The possible configurations for identical nucleons are very simple. There can be n protons, say, in the $g_{\frac{9}{2}}$ orbit, i.e. in the $g_{\frac{9}{2}}^n$ configuration, or two of them can be in the $p_{\frac{1}{2}}$ orbit, i.e. in the $p_{\frac{1}{2}}^2 g_{\frac{9}{2}}^{n-2}$ configuration. These two configurations for any value of n have even parity and therefore can interact. On the other hand the $p_{\frac{1}{2}} g_{\frac{9}{2}}^{n-1}$ configuration has odd parity and its states cannot interact with states of the preceding two configurations. The fact that two identical nucleons in the $p_{\frac{1}{2}}$ orbit form a closed shell gives rise to another simplification. All states of the $p_{\frac{1}{2}}^2 g_{\frac{9}{2}}^{n-2}$ configuration have the spins and parities found in the $g_{\frac{9}{2}}^{n-2}$ configuration. The two protons (or neutrons) in the $p_{\frac{1}{2}}$ orbit must be always coupled to $J = 0$. Furthermore, there is only one non diagonal matrix element in the two particle configuration. It is the matrix element between the two $J = 0$ states of the $p_{\frac{1}{2}}^2$ and the $g_{\frac{9}{2}}^2$ configurations.

Our analysis gives very good agreement between calculated and experimental energies, which justifies our assumptions. As a result we obtain the best values

for the matrix elements of the effective nuclear interaction. In particular, we obtain the unperturbed energy levels of the $g_{\frac{9}{2}}^2$ configuration which determine completely the interaction energies in all $g_{\frac{9}{2}}^n$ configuration. The $g_{\frac{9}{2}}$ shell is of particular theoretical interest since $j = \frac{9}{2}$ is the lowest j value for which the seniority might not be a good quantum number (for identical nucleons). We obtain, as explained in detail in sect. 3, the non-diagonal matrix elements that connect states with the same J and different seniorities. We find that these are very small compared to a typical distance between such levels. Actually they are smaller than the statistical errors of our calculation and might well be considered to vanish. Even if, however, they should be twice (or more) as large, their contribution would still be negligible. As a result, the actual states we consider are almost pure states with definite seniorities. For example, the lowest state with $J = \frac{9}{2}$ in the $g_{\frac{9}{2}}^3$ configuration is found to be the state with $v = 1$. The probability of $J = \frac{9}{2}$, $v = 3$ in this state is only 3×10^{-4}. Another nice feature of this interaction is the occurrence of a very low lying $J = \frac{7}{2}$ state in the $g_{\frac{9}{2}}^3$ configuration. The experimental occurrence of such a $\frac{7}{2}+$ level used to be a difficulty for many shell model calculations. This point is discussed in detail in sect. 4.

The non-diagonal matrix element between the $J = 0$ states of the $p_{\frac{1}{2}}^2$ and $g_{\frac{9}{2}}^2$ configurations is determined along with the other matrix elements. The fact that this element is rather large gives rise to configuration interaction which modifies the energies of the pure configurations. The amount of admixture in Zr^{90} is larger than in the other cases considered. The amount of admixture obtained in the ground state of Zr^{90} is in agreement with numbers derived from the experimental data. These numbers, however, should have very large limits of error. In the other cases there are no experimental results on the amount of admixture. However, we obtain good agreement for the energy levels only by taking into account configuration interaction.

With the interaction parameters obtained from the analysis we can determine the level schemes of many nuclei. Unfortunately, there is no experimental information on these level schemes. We give in the following some of the theoretical predictions. We hope that possible experiments will be undertaken to clarify the situation further in this interesting region of nuclei.

2. The Experimental Data

The success of our approach depends on considering as many experimental data as possible. As will become clear later there is not enough experimental information either in nuclei with $p_{\frac{1}{2}}$ and $g_{\frac{9}{2}}$ protons and 50 neutrons or in the Sr isotopes with the corresponding neutron configurations. We shall be able to carry out our program only if we use the information of both the proton and neutron configurations taking the interaction between two neutrons to be

the same as the mutual nuclear interaction between protons. This seems a rather strong assumption in view of the strong additional Coulomb field which acts on the protons. However, in practice we shall use a less drastic approximation which is justified by the results obtained.

Unfortunately, binding energies of nuclei in this region are not known accurately enough. Several different sets of binding energies are given in the literature which differ in some cases by many times the quoted error. Therefore it does not seem safe to use binding energies in the analysis. The only experimental data that we can use are the *differences* in energies of states of various configurations. Luckily the parities of $p_{\frac{1}{2}}$ and $g_{\frac{9}{2}}$ nucleons are opposite, so that a configuration assignment can easily be made once the spin and parity of a level are known experimentally. There is another advantage in using only level spacings in the analysis. It is very probable that the difference in the nuclear interaction between protons and neutrons (due to the difference in radial functions) will be less important when considering differences of energies. Furthermore, the mutual electrostatic interaction between the protons is, owing to the long range of the Coulomb potential, roughly the same in all states of a certain number of protons in the same shell. Thus, when considering only differences of energies, we shall ignore throughout the mutual Coulomb interaction of the protons and use the same matrix elements for protons and neutrons.

The experimental data are from level schemes of several nuclei and were taken from a review article[3]) and the detailed experimental paper[4]) on Zr^{90}. In Y^{89} the extra proton can be in either the $p_{\frac{1}{2}}$ or the $g_{\frac{9}{2}}$ orbit. This gives rise to two experimentally obseved levels with spins $\frac{1}{2}-$ and $\frac{9}{2}+$. The difference between these two levels was taken as one of the data. The next simple nucleus is Zr^{90} with two extra protons. The two configurations $p_{\frac{1}{2}}^2$ and $g_{\frac{9}{2}}^2$ give rise to two states with $J=0$ which are pushed apart by configuration interaction. On the other hand, there are no states with $J>0$ of the $p_{\frac{1}{2}}^2$ configuration, and hence the observed levels with spins $2+$, $4+$, $6+$ and $8+$ must belong to the pure $g_{\frac{9}{2}}^2$ configuration. The $p_{\frac{1}{2}}\, g_{\frac{9}{2}}$ configuration has odd parity and thus does not interact with the other configurations. (It has two states with spins $4-$ and $5-$ of which one is known experimentally.) Thus, we take the spacings of the levels with $J=2, 4, 6, 8$ to be exactly those of the $g_{\frac{9}{2}}^2$ configuration. As data for our analysis we make use of the spacings between the two $0+$ levels and the $2+$ level. In Nb^{91} there are three extra protons with possible configurations $p_{\frac{1}{2}}^2\, g_{\frac{9}{2}}$, $p_{\frac{1}{2}}\, g_{\frac{9}{2}}^2$ and $g_{\frac{9}{2}}^3$. There are two experimentally observed levels in this nucleus and their spacing is included in our work. One level with spin $\frac{1}{2}-$ must be due to the $p_{\frac{1}{2}}\, g_{\frac{9}{2}}^2$ configuration whereas the other has spin $\frac{9}{2}+$ and is due to an admixture of the $p_{\frac{1}{2}}^2\, g_{\frac{9}{2}}$ and $g_{\frac{9}{2}}^3$ configurations. The one other nucleus with a proton configuration giving some information is Tc^{93}. The possible configurations in this nucleus are $p_{\frac{1}{2}}^2\, g_{\frac{9}{2}}^3$, $p_{\frac{1}{2}}\, g_{\frac{9}{2}}^4$ and $g_{\frac{9}{2}}^5$. The experimental

level with spin $\frac{1}{2}-$ we attribute to the $p_{\frac{1}{2}} g_{\frac{9}{2}}^4$ configuration whereas the observed $\frac{9}{2}+$ level is taken to be due to an admixture of the $p_{\frac{1}{2}}^2 g_{\frac{9}{2}}^3$ and $g_{\frac{9}{2}}^5$ configurations. The separation of the two experimental levels with $\frac{1}{2}-$ and $\frac{9}{2}+$ is also taken into consideration.

The better known Sr isotopes where the corresponding neutron configurations occur have neutron number close to 50. It is therefore more convenient to consider $p_{\frac{1}{2}}$ *and* $g_{\frac{9}{2}}$ *neutron holes* in the closed shell of 50 neutrons. In Sr^{87} there is just one hole which can be either a $g_{\frac{9}{2}}$ or a $p_{\frac{1}{2}}$ hole. Two levels with $\frac{1}{2}-$ and $\frac{9}{2}+$ are experimentally known in Sr^{87} and their separation is taken into our analysis. It is worth while to mention here that this separation is not simply related to the corresponding separation in Y^{89}. The neutrons (or neutron holes) in Sr^{87} interact with the closed shells of 38 protons whereas the 39th $p_{\frac{1}{2}}$ or $g_{\frac{9}{2}}$ proton in Y^{89} interacts with the closed shells of 50 neutrons. The difference in single particle energies in the two cases is due to proton-neutron interactions which are not considered in the present work. Therefore we shall have to determine also the single neutron hole energies from the experimental data.

The next nucleus we consider is Sr^{86} with two neutron holes. The level scheme of the $g_{\frac{9}{2}}^{-2}$ configuration of two holes should be the same as in the $g_{\frac{9}{2}}^2$ configuration. The states with $J = 2, 4, 6, 8$ cannot be perturbed by another configuration, whereas the $J = 0$ state of the $g_{\frac{9}{2}}^{-2}$ configuration can interact with the $J = 0$ state of the $p_{\frac{1}{2}}^{-2}$ configuration. Experimentally a $2+$ level is observed 1.08 MeV above the ground $0+$ state. Comparing this to Zr^{90} we can immediately see the effects of configuration interaction. In the latter nucleus the $2+$ level is 2.18 MeV above the $0+$ ground state and 0.43 MeV above the first excited $0+$ level. Our analysis will show that in Sr^{86} the unperturbed $J = 0$ state of the $p_{\frac{1}{2}}^{-2}$ configuration is much higher than both $J = 0$ and $J = 2$ of the $g_{\frac{9}{2}}^{-2}$ configuration. On the other hand in Zr^{90} the $p_{\frac{1}{2}}^2$ $J = 0$ state is lower than the $g_{\frac{9}{2}}^2$ $J = 0$ state. Thus configuration interaction increases the separation between the $J = 0$ and $J = 2$ states of the $g_{\frac{9}{2}}^{-2}$ configuration in Sr^{86} to 1.08 MeV. On the other hand it decreases the corresponding spacing in Zr^{90} to 0.43 MeV. This state of affairs is presented graphically in fig. 1, which will be introduced in the following. Also the observed 1.08 MeV separation in Sr^{86} is included in the analysis.

The one other Sr isotope with a neutron configuration to be used is Sr^{85}. The three neutron holes can be in the $g_{\frac{9}{2}}^{-3}$, $g_{\frac{9}{2}}^{-2} p_{\frac{1}{2}}^{-1}$ or $g_{\frac{9}{2}}^{-1} p_{\frac{1}{2}}^{-2}$ configurations. The experimentally observed $\frac{1}{2}-$ level must be attributed to the $g_{\frac{9}{2}}^{-2} p_{\frac{1}{2}}^{-1}$ configuration whereas the observed $\frac{9}{2}+$ ground state is taken to be due to an admixture of the $g_{\frac{9}{2}}^{-3}$ and $g_{\frac{9}{2}}^{-1} p_{\frac{1}{2}}^{-2}$ configurations. The measured distance between these levels is included in the experimental data in our work. However the $J = \frac{9}{2}$ state of the $g_{\frac{9}{2}}^{-3}$ configuration is lower than that of the $g_{\frac{9}{2}}^{-1} p_{\frac{1}{2}}^{-2}$ configuration as will be demonstrated later. This is unlike the situation in Nb^{91} and this fact gives rise to an additional experimentally known level in

Sr^{85}. A low lying $\frac{7}{2}$ level is observed in Sr^{85} and its measured height above the $\frac{9}{2}+$ state is also added to the experimental data to be used in the analysis. The relation between the level schemes of Sr^{85} and Nb^{91} is clearly seen in fig. 2 in the following. Such $\frac{7}{2}+$ states have long ago been attributed to the $g_{\frac{9}{2}}^3$ configuration[5]) and this was also the configuration assignment[6]) of this state in Sr^{85}. As we shall see later the position of the $J=\frac{7}{2}$ state in the $g_{\frac{9}{2}}^3$ configuration is a rather sensitive test of the two-body nuclear interaction.

3. The Spectroscopic Calculations

There are altogether nine experimental energy differences available. Under our assumptions, these energies can be expressed by theoretical formulae which involve six undetermined parameters. There are two parameters which involve single-particle energies. One of them is the difference between the single-proton energies in the $p_{\frac{1}{2}}$ and $g_{\frac{9}{2}}$ orbits, outside the closed shells of 38 protons and 50 neutrons,

$$\beta = E_{p_{\frac{1}{2}}} - E_{g_{\frac{9}{2}}} .$$

The other parameter of this type is the difference in single neutron hole energies in the $p_{\frac{1}{2}}$ and $g_{\frac{9}{2}}$ orbits,

$$\beta' = E_{g_{\frac{9}{2}}^{-1}} - E_{p_{\frac{1}{2}}^{-1}} .$$

These holes are in the closed shells of 50 neutrons when the proton number is 38. As explained earlier these two parameters cannot be correlated in the present work and must be considered as independent. Thus, we do not have to assume anything about the equality of the difference of protons and neutrons single particle energies. In this way we also avoid the danger that such differences would still be appreciable. We shall assume equality of the proton and neutron differences of matrix elements only in the case of the effective two-body interaction. The other parameters involve this effective mutual interaction and are taken to be the same for the proton configurations and the neutron hole configurations. The energy difference between the $J=2$ and $J=0$ states of the $g_{\frac{9}{2}}^2$ (or $g_{\frac{9}{2}}^{-2}$) configuration,

$$\gamma = V(g_{\frac{9}{2}}^2,\ J=0) - V(g_{\frac{9}{2}}^2,\ J=2) = V_0 - V_2 ,$$

is one of the parameters which describe the effective mutual interaction. Another such parameter is the difference in interaction energy of the (unperturbed) $J=0$ states of the $g_{\frac{9}{2}}^2$ and the $p_{\frac{1}{2}}^2$ configurations, i.e.

$$\delta_2 = V(g_{\frac{9}{2}}^2,\ J=0) - V(p_{\frac{1}{2}}^2,\ J=0) .$$

The third such parameter is the non-diagonal matrix element of the effective mutual interaction between these two states,

$$V = \langle p_{\frac{1}{2}}^2,\ J=0 \mid V \mid g_{\frac{9}{2}}^2,\ J=0 \rangle .$$

The last parameter appears when we consider the difference in interaction energy in the three particle configurations $g_{\frac{9}{2}}^3$ and $p_{\frac{1}{2}} g_{\frac{9}{2}}^2$. This parameter is defined as the difference $V(p_{\frac{1}{2}} g_{\frac{9}{2}}^2, J = \frac{1}{2}) - V(g_{\frac{9}{2}}^3, J = \frac{9}{2}, v = 1)$. In the $p_{\frac{1}{2}} g_{\frac{9}{2}}^2$ configuration the two $g_{\frac{9}{2}}$ particles must be coupled to $J = 0$ in order that the total J will be equal to $\frac{1}{2}$. On the other hand the three $g_{\frac{9}{2}}$ particles in the $g_{\frac{9}{2}}^3$ configuration are coupled to the state with $J = \frac{9}{2}$ and seniority $v = 1$. There is another state with $J = \frac{9}{2}$ in this configuration which has the higher seniority $v = 3$. The non-diagonal matrix element between these two states with $J = \frac{9}{2}$ can be calculated in terms of V_J. These V_J are the interaction energies in the states with the various J in the $g_{\frac{9}{2}}^2$ configuration. The interaction energy V_0, in the $J = 0$ state, cannot appear in this matrix element since the two states have different seniorities. Furthermore, for all the V_J equal, this non-diagonal matrix element vanishes. Thus, it can be expressed in terms of differences of the V_J with $J > 0$. We take in the present analysis these differences directly from the level scheme of Zr^{90} and can therefore calculate right away the value of this non-diagonal matrix element. Using the appropriate c.f.p.[7]) we obtain the value 0.03 MeV for this matrix element. This in itself is sufficient to guarantee that the shift due to this $J = \frac{9}{2}, v = 3$ level is less than 0.03 MeV which is smaller than the standard deviation of our results and therefore could be ignored. However we can put a much lower limit on the effect of this level on the ground, $J = \frac{9}{2}, v = 1$ state. The energy difference between the two states with $J = \frac{9}{2}$ depends also on the $0 - 2$ separation of the $g_{\frac{9}{2}}^2$ configuration. However, even if we take for this $0 - 2$ separation the lower limit of 0.43 MeV from Zr^{90}, we obtain that the distance between the two $J = \frac{9}{2}$ levels is more than 1 MeV and that the shift of the energy of the $J = \frac{9}{2}, v = 1$ state due to the upper level is less than 0.001 MeV. The actual results of our analysis show that this difference is more than 1.5 MeV so that the effect of the state with $v = 3$ is even smaller and definitely negligible. In this case, when the seniority is a good quantum number, the interaction energy of the ground states of the $g_{\frac{9}{2}}^n$ configurations is given by the simple expression[8])

$$\tfrac{1}{2} n(n - 1)\, a + [\tfrac{1}{2} n]\, b\,, \tag{1}$$

where the step function $[\frac{1}{2} n]$ which multiplies the pairing term b is the largest integer not exceeding $\frac{1}{2} n$. The energy of the $J = 0$ state of the $g_{\frac{9}{2}}^2$ configuration is $a + b$ whereas the energy of the state $J = \frac{9}{2}, v = 1$ of the $g_{\frac{9}{2}}^3$ configuration is $3a + b$. If we denote the interaction of a $p_{\frac{1}{2}}$ particle with the two particles in the state $g_{\frac{9}{2}}^2, J = 0$ by W we obtain for our last parameter the expression

$$\delta_3 = V(p_{\frac{1}{2}} g_{\frac{9}{2}}^2, J = \tfrac{1}{2}) - V(g_{\frac{9}{2}}^3, J = \tfrac{9}{2}, v = 1) = W - 2a\,. \tag{2}$$

The calculation of the theoretical expressions for the experimental energies is a straightforward procedure. The differences in single-particle energies taken

from Y^{89} and Sr^{87} should be made equal to our first two parameters β and β' respectively: these two equations are (A1) and (A2) of the appendix. The two and three particle configurations involve diagonalizations of two by two matrices. In Sr^{86}, for example, the shift of the ground state due to configuration interaction is obtained by diagonalizing the matrix

$$\begin{pmatrix} 2\beta' + \delta_2 & V \\ V & 0 \end{pmatrix}. \tag{3}$$

The energy shift thus obtained, as well as the shifts due to all matrices to be described, is a theoretical expression which contains (quadratically) the parameters which appear in the matrix under consideration. The shift obtained by diagonalizing (3) should be subtracted from the actual spacing of 1.08 MeV and the result, in itself a theoretical expression, equated to the parameter $\gamma = V_0 - V_2$ (we adopt throughout the convention that binding energies are positive so that $V_0 - V_2$ is also positive). The equation obtained in this case is (A3) given in the appendix.

The analogous shift in Zr^{90} is obtained from the corresponding matrix with the appropriate single-particle parameter. This (theoretical) shift when *added* to 0.43 should be equated to $\gamma = V_0 - V_2$: cf. eq. (A5). On the other hand this same shift should be subtracted from 2.18 and the result equated to $2\beta + \delta_2 + \gamma$: cf. eq. (A4).

A similar procedure is applied to configurations with more than two particles. In Nb^{91} there is a two by two matrix to be diagonalized. This matrix corresponds to the two states $p_{\frac{1}{2}}^2 g_{\frac{9}{2}}$, $J = \frac{9}{2}$ and $g_{\frac{9}{2}}^3$, $J = \frac{9}{2}$, $v = 1$. This matrix has the form

$$\begin{pmatrix} 2\beta + V(p_{\frac{1}{2}}^2 g_{\frac{9}{2}}) - V(g_{\frac{9}{2}}^3) & \dfrac{2V}{\sqrt{5}} \\ \dfrac{2V}{\sqrt{5}} & 0 \end{pmatrix}. \tag{4}$$

The absolute value of the energy shift obtained from this matrix should be subtracted from the experimental energy difference (0.105 MeV) of the $\frac{9}{2}+$ and $\frac{1}{2}-$ levels. The result should be made equal to the unperturbed difference between the $J = \frac{9}{2}$ state of the $p_{\frac{1}{2}}^2 g_{\frac{9}{2}}$ configuration and the $J = \frac{1}{2}$ state of the $p_{\frac{1}{2}} g_{\frac{9}{2}}^2$ configuration, giving eq. (A6). The latter difference is simply $\beta - \delta_2$ since the interaction between a $p_{\frac{1}{2}}$ proton and two protons in the state $g_{\frac{9}{2}}^2$, $J = 0$ is the same as between a $g_{\frac{9}{2}}$ proton and two $p_{\frac{1}{2}}$ protons (this interaction was denoted above by W). Using this result, namely

$$V(p_{\frac{1}{2}}^2 g_{\frac{9}{2}}) - V(p_{\frac{1}{2}} g_{\frac{9}{2}}^2) = V(p_{\frac{1}{2}}^2) - V(g_{\frac{9}{2}}^2),$$

we can express the non-vanishing diagonal element in the matrix (4) in terms

of our parameters. In fact we obtain

$$V(p_{\frac{1}{2}}^2 g_{\frac{9}{2}}) - V(g_{\frac{9}{2}}^3) = V(p_{\frac{1}{2}}^2 g_{\frac{9}{2}}) - V(p_{\frac{1}{2}} g_{\frac{9}{2}}^2) + V(p_{\frac{1}{2}} g_{\frac{9}{2}}^2) - V(g_{\frac{9}{2}}^3) = -\delta_2 + \delta_3 .$$

In Sr^{85} the corresponding matrix is diagonalized and the energy shift obtained is subtracted from the observed energy difference of 0.233 between the $\frac{9}{2}+$ and $\frac{1}{2}-$ levels. The result in this case is made equal to the unperturbed difference between the states of the $g_{\frac{9}{2}}^{-3}$ and $p_{\frac{1}{2}}^{-1} g_{\frac{9}{2}}^{-2}$ configurations which is $\beta' - \delta_3$. The resulting equation is (A7). In the only configuration with 5 particles, in Tc^{93}, the matrix which should be diagonalized is also a two by two matrix. This simplification is due to the fact that there can be no more than two identical particles in the $p_{\frac{1}{2}}$ orbit. The two interacting configurations in the $J = \frac{9}{2}$, $v = 1$ state are $p_{\frac{1}{2}}^2 g_{\frac{9}{2}}^3$ and $g_{\frac{9}{2}}^5$. Taking the seniority to be a good quantum number, the unperturbed energies of the $J = \frac{9}{2}$, $v = 1$ states of these two configurations are given by using eq. (1) as

$$2E_{p_{\frac{1}{2}}} + 3E_{g_{\frac{9}{2}}} + V(p_{\frac{1}{2}}^2) + 3a + b + 3W \text{ and } 5E_{g_{\frac{9}{2}}} + 10a + 2b .$$

Thus their difference can be expressed in terms of our parameters and the matrix to be diagonalized has the form

$$\begin{pmatrix} 2\beta - \delta_2 + 3\delta_3 & \sqrt{\frac{6}{5}}\, V \\ \sqrt{\frac{6}{5}}\, V & 0 \end{pmatrix}. \tag{5}$$

The experimental difference of 0.39 MeV between the $\frac{9}{2}+$ and $\frac{1}{2}-$ levels, from which the energy shift obtained from the matrix (5) is subtracted, is equated to the unperturbed energy difference of the

$$p_{\frac{1}{2}}^2 g_{\frac{9}{2}}^3 \,(J = \tfrac{9}{2}\,,\, v = 1) \quad \text{and} \quad p_{\frac{1}{2}} g_{\frac{9}{2}}^4 \,(J = 0\,,\, v = 0)$$

states, yielding eq. (A9). This latter difference is also given in terms of the parameters as $\beta - \delta_2 + \delta_3$.

The last equation (A8) between an experimental energy difference and a theoretical expression comes from the difference between the $\frac{9}{2}+$ and $\frac{7}{2}+$ levels in Sr^{85}. The shift of the ground $J = \frac{9}{2}$ state which is obtained from the diagonalization of the two by two matrix as explained above should be subtracted from the experimental difference of 0.225 MeV. The result should be made equal to the theoretical difference between the states $J = \frac{9}{2}$, $v = 1$ and $J = \frac{7}{2}$ of the $g_{\frac{9}{2}}^3$ configuration. This theoretical difference can be calculated using the appropriate c.f.p.[7]) in terms of the energy differences in the $g_{\frac{9}{2}}^2$ configuration. The differences $V_J - V_2$ for $J > 2$ are taken directly from Zr^{90} whereas the one other difference $\gamma = V_0 - V_2$ is one of our parameters. The calculated difference between the $J = \frac{9}{2}$, $v = 1$ and $J = \frac{7}{2}$ states obtained in this way is equal in MeV to $\frac{4}{5}(V_0 - V_2) - 0.64$.

4. Results and Discussion

We obtain in the way described above the nine equations, given in the appendix, between experimental energies and theoretical expressions involving six undetermined parameters. We attempt to find the values of these parameters which will best reproduce the experimental data. Apart from the first two, these equations are not linear in the parameters. Therefore the least squares fit analysis involves several iterations. We start from certain initial values of the parameters and, using them, linearize the equations. Better values of the parameters are obtained from the linearized equations which are used as initial values for the next iteration etc. The actual computations were greatly facilitated by using the WEIZAC electronic computer. The procedure converges rapidly and yields the following final best values of the parameters:

$$\begin{aligned}
&\beta = E_{p_{\frac{1}{2}}} - E_{g_{\frac{9}{2}}} = 0.992 \pm 0.043 \text{ MeV}, \quad \beta' = E^{-1}_{g_{\frac{9}{2}}} - E^{-1}_{p_{\frac{1}{2}}} = 0.372 \pm 0.048 \text{ MeV},\\
&\gamma = V(g^2_{\frac{9}{2}}, J = 0) - V(g^2_{\frac{9}{2}}, J = 2) = 0.866 \pm 0.032 \text{ MeV},\\
&\delta_2 = V(g^2_{\frac{9}{2}}, J = 0) - V(p^2_{\frac{1}{2}}, J = 0) = 1.164 \pm 0.073 \text{ MeV},\\
&|V| = |\langle g^2_{\frac{9}{2}}, J = 0 \,|\, V \,|\, p^2_{\frac{1}{2}}, J = 0 \rangle| = 0.708 \pm 0.039 \text{ MeV},\\
&\delta_3 = V(p_{\frac{1}{2}} g^2_{\frac{9}{2}}, J = \tfrac{1}{2}) - V(g^3_{\frac{9}{2}}, J = \tfrac{9}{2}, v = 1) = W - 2a = 0.320 \pm 0.058 \text{ MeV}.
\end{aligned} \tag{6}$$

The numbers with $\pm$ signs following the numerical values (6) are the statistical errors on the parameters. It is obvious that the statistical errors are much smaller than the values of the parameters so that they can be safely used.

When these best values of the parameters are introduced into the theoretical expressions we obtain the calculated values which should be compared to the experimental data. The agreement obtained between the calculated and the experimental energy differences is demonstrated in table 1. The agreement seems to be quite good in spite of the rather strong assumptions made. The r.m.s. deviation is defined by

$$\sqrt{\frac{\sum \Delta_i^2}{n - k}},$$

where the Δ_i are the deviations of the calculated from the experimental values, n the number of equations and k of unknowns. Its value is 0.082 MeV which is about 4% of the largest experimental value considered.

The level schemes of nuclei with two-particle (or two-hole) configurations are shown in fig. 1. The experimental levels of Zr^{90} and Sr^{86} are drawn in solid lines and the corresponding calculated levels in broken lines. The unperturbed level scheme of the $g^2_{\frac{9}{2}}$ configuration is given between the schemes of Zr^{90} and Sr^{86}. Along with it are given the unperturbed positions of the $p^2_{\frac{1}{2}}$ configuration in Zr^{90} and the $p^{-2}_{\frac{1}{2}}$ configuration in Sr^{86}. We see that the shift of the ground

state of Zr^{90} due to configuration interaction amounts to 0.41 MeV whereas in Sr^{86} the corresponding shift is only 0.23 MeV. The admixture of the $p_{\frac{1}{2}}^2$ and $g_{\frac{9}{2}}^2$

TABLE 1

Experimental and calculated energy differences

Nucleus	Levels considered		Energy difference in MeV	
			Experimental	Calculated
$_{39}Y_{50}^{89}$	$\frac{1}{2}-$	$\frac{9}{2}+$	0.915	0.99
$_{38}Sr_{49}^{87}$	$\frac{9}{2}+$	$\frac{1}{2}-$	0.388	0.37
$_{38}Sr_{48}^{86}$	0+	2+	1.079	1.10
$_{40}Zr_{50}^{90}$	(ground st.) 0+	2+	2.182	2.09
	(first excit.) 0+	2+	0.430	0.46
$_{41}Nb_{50}^{91}$	$\frac{9}{2}+$	$\frac{1}{2}-$	0.105	0.11
$_{38}Sr_{47}^{85}$	$\frac{9}{2}+$	$\frac{1}{2}-$	0.233	0.27
	$\frac{9}{2}+$	$\frac{7}{2}+$	0.225	0.27
$_{43}Tc_{50}^{93}$	$\frac{9}{2}+$	$\frac{1}{2}-$	0.39	0.44

configurations in the ground state of Zr^{90} can be easily calculated from the interaction matrix. The squares of the amplitudes of the two configurations in

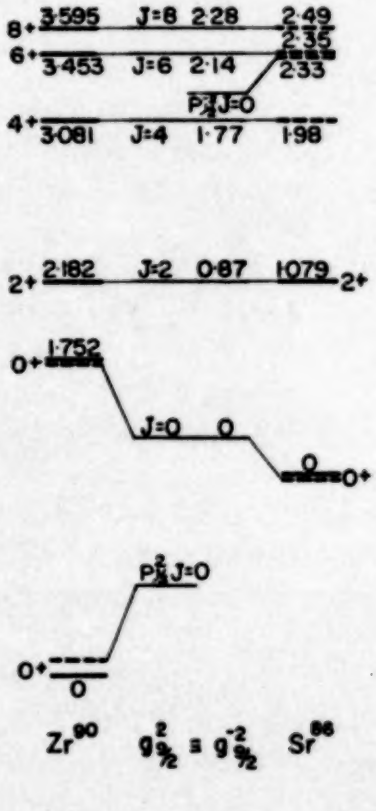

Fig. 1. Two-nucleon configurations.

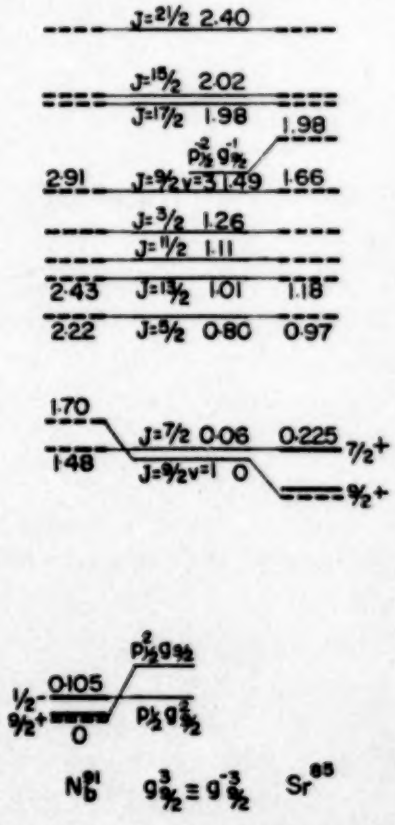

Fig. 2. Three-nucleon configurations.

the normalized wave function are 0.75 and 0.25 respectively. Thus the ground state of Zr^{90} is 75 % of the $p_{\frac{1}{2}}^2$ configuration and 25 % of the $g_{\frac{1}{2}}^2$ configuration. These percentages roughly agree with the values calculated in ref. [1]); in that paper an admixture of 65 % and 35 % is quoted. However these numbers are based on various estimates of experimental data not directly measured. Hence the error which goes with these percentages could be 15 % or more. In another experimental paper[9]), the same percentages are estimated to be 78 % and 22 %. The case of Zr^{90} is the one in which configuration interaction is most important. All the shifts of the ground states together with the percentages of the interacting configurations are given in table 2.

TABLE 2

The effect of configuration interaction in the ground states

Nucleus	Ground state	Energy shift (MeV)	Per cent admixture of configurations	
$_{40}Zr_{50}^{90}$	0+	0.41	$p_{\frac{1}{2}}^2$ 75	$g_{\frac{1}{2}}^2$ 25
$_{41}Nb_{50}^{91}$	$\frac{9}{2}$+	0.28	$p_{\frac{1}{2}}^2 g_{\frac{1}{2}}$ 83	$g_{\frac{1}{2}}^3$ 17
$_{43}Tc_{50}^{93}$	$\frac{9}{2}$+	0.29	$p_{\frac{1}{2}}^2 g_{\frac{1}{2}}^3$ 88	$g_{\frac{1}{2}}^5$ 12
$_{38}Sr_{48}^{86}$	0+	0.23	$g_{\frac{1}{2}}^{-2}$ 90	$p_{\frac{1}{2}}^{-2}$ 10
$_{38}Sr_{47}^{85}$	$\frac{9}{2}$+	0.22	$g_{\frac{1}{2}}^{-3}$ 89	$g_{\frac{1}{2}}^{-1} p_{\frac{1}{2}}^{-2}$ 11

The level scheme of the unperturbed $g_{\frac{1}{2}}^3$ configuration is uniquely determined by the energy levels of the $g_{\frac{1}{2}}^2$ configuration. It is shown in detail in fig. 2. Of particular interest is the spacing between the (unperturbed) state with $J = \frac{9}{2}$, $v = 1$ and the $J = \frac{7}{2}$ state which is given in MeV by $\frac{4}{5}(V_0 - V_2) - 0.64$. Using the value obtained for $V_0 - V_2$ we obtain for this unperturbed energy difference 0.06 MeV. The existence of a very low lying $J = \frac{7}{2}$ state in the $g_{\frac{1}{2}}^3$ configuration was in the past the subject of several papers[7]). Those attempts were always in the search of a simple phenomenological potential interaction that will give such a low lying state. No such simple potential interaction could, however, be found, which makes the $J = \frac{7}{2}$ state low lying whereas the $J = \frac{5}{2}$ and $J = \frac{3}{2}$ states are still higher. For example, the level spacings of the $g_{\frac{1}{2}}^2$ configuration in the region of best fit in ref. [1]) lead to a $J = \frac{7}{2}$ state at 0.5 MeV above the unperturbed $J = \frac{9}{2}$, $v = 1$ state in the $g_{\frac{1}{2}}^3$ configuration. The use of a Yukawa potential makes things even worse. All these features occur in spite of the rough agreement obtained in ref. [1]) for the $g_{\frac{1}{2}}^2$ levels. It seems that the position of the $J = \frac{7}{2}$ state in the $g_{\frac{1}{2}}^3$ configuration is a more severe and sensitive test to the agreement obtained with a phenomenological two-body interaction. On the other hand, the present analysis yields such a low lying state provided we take a certain effective interaction in the $g_{\frac{1}{2}}$ shell. This is the

interaction which is defined by the $g_{\frac{9}{2}}^2$ energies given in fig. 1. The $J = \frac{5}{2}$ and $J = \frac{3}{2}$ states of the $g_{\frac{9}{2}}^3$ configuration are predicted according to our results to be found 0.74 MeV and 1.21 MeV above the $J = \frac{7}{2}$ state respectively. These levels along with the other ones in the $g_{\frac{9}{2}}^3$ configuration are drawn in the middle of fig. 2. The unperturbed position of the $p_{\frac{1}{2}}^{-2}\, g_{\frac{9}{2}}^{-1}$, $J = \frac{9}{2}$ state is also given. This state interacts with the $g_{\frac{9}{2}}^{-3}$, $J = \frac{9}{2}$, $v = 1$ state so that the level scheme of Sr^{85} is obtained. The calculated and experimental levels of Sr^{85} are also given in fig. 2. The odd parity state $p_{\frac{1}{2}}^{-1}\, g_{\frac{9}{2}}^{-2}$, $J = \frac{1}{2}$ was left out since its experimental as well as calculated position practically coincides with that of the $\frac{7}{2}+$ level. The corresponding calculated levels of Nb^{91} are also obtained from the interaction of the $g_{\frac{9}{2}}^3$, $J = \frac{9}{2}$, $v = 1$ state with the $p_{\frac{1}{2}}^2\, g_{\frac{9}{2}}$, $J = \frac{9}{2}$ state. The calculated and observed levels of Nb^{91} are also given in fig. 2. Looking at fig. 2 it is clear that the only levels shifted by configuration interaction are those with $J = \frac{9}{2}$, $v = 1$. All other levels, including the $g_{\frac{9}{2}}^3$, $J = \frac{9}{2}$, $v = 3$ level, retain their relative positions. It is interesting that the level structure of the $g_{\frac{9}{2}}^2$ and $g_{\frac{9}{2}}^3$ configurations is very similar to that of the $f_{\frac{7}{2}}^2$ and $f_{\frac{7}{2}}^3$ configurations[2]). Also in the $f_{\frac{7}{2}}^3$ configuration there appears a rather low lying $J = \frac{5}{2}$ state, the position of which is obtained theoretically from the observed levels scheme of the $f_{\frac{7}{2}}^2$ configuration.

The unperturbed level scheme of the $g_{\frac{9}{2}}^2$ configuration in fig. 1 does not give all interaction constants. Obviously, an addition of the same constant energy to all states will not change the level scheme. Such an addition of a constant energy would change the value of the parameter a in (1). Therefore this parameter cannot be determined from the present analysis before accurate binding energies will be available. On the other hand, the parameter b can be determined from the level spacings in the $g_{\frac{9}{2}}^2$ configuration. In general, the position of the centre of mass of the levels with $J = 2, 4 \ldots, 2j - 1$ above the $J = 0$ state is equal to

$$\frac{2j+1}{2j+2}\, b\,.$$

Thus in the present case

$$\tfrac{10}{11}\, b = \tfrac{1}{44}\,[44(V_0 - V_2) + 9(V_2 - V_4) + 13(V_2 - V_6) + 17(V_2 - {}_8V)] = V_0 - V_2 + 1.105\,.$$

Inserting the actual value of the $V_0 - V_2$ energy spacing from (6) we obtain $(10/11)b = 1.97$, from which follows

$$b = 2.17 \text{ MeV}\,.$$

This value of the pairing term is reasonable and smaller than the pairing term in the lower $f_{\frac{7}{2}}$ shell which has the value of 3.2 MeV[8]).

We can utilize this value of b obtained from our analysis in order to treat the two-proton configuration with odd parity in Zr^{90}. This is the $p_{\frac{1}{2}}\, g_{\frac{9}{2}}$ configuration

which has two states, one with $J = 5$ and the other with $J = 4$. A state with spin 5— is actually observed in Zr^{90} at 2.315 MeV above the ground state. From our parameters we can calculate the centre of mass of the 5— and 4— levels. Thus we can use the observed energy of the 5— state to obtain the position of the 4— level. It can be easily shown[10]) that

$$\langle V(p_{\frac{1}{2}} g_{\frac{9}{2}}) \rangle = \tfrac{1}{20}[9V(p_{\frac{1}{2}} g_{\frac{9}{2}}, J = 4) + 11V(p_{\frac{1}{2}} g_{\frac{9}{2}}, J = 5)] = \tfrac{1}{2} V(p_{\frac{1}{2}}^2 g_{\frac{9}{2}}) = \tfrac{1}{2} W.$$

We now write down the energy difference between the $J = 0$ state of the $g_{\frac{9}{2}}^2$ configuration and the centre of mass of the 5— and 4— states. The difference is

$$2E_{g_{\frac{9}{2}}} + V(g_{\frac{9}{2}}^2) - E_{p_{\frac{1}{2}}} - E_{g_{\frac{9}{2}}} - \langle V(p_{\frac{1}{2}} g_{\frac{9}{2}}) \rangle$$
$$= E_{g_{\frac{9}{2}}} - E_{p_{\frac{1}{2}}} + a + b - \tfrac{1}{2} W = -\beta + b - \tfrac{1}{2} \delta_3$$

and can be immediately calculated with the values of b and the two other parameters. Inserting these values we obtain for this energy difference 1.02 MeV which corresponds to 2.332 MeV above the ground state of Zr^{90}. Using the observed position of the 5— state this leads to a 4— state at 2.353 MeV above the ground state. Although this 4— state is predicted to lie above the 5— state their calculated distance is rather small (0.04 MeV) and is well within the standard deviation. We can compare this result to similar spectra in lighter nuclei. There is some information on the level scheme of the $p_{\frac{1}{2}} s_{\frac{1}{2}}$ and $p_{\frac{1}{2}} d_{\frac{5}{2}}$ configurations. In C^{14} we find in both cases that the state with the higher spin (which is at the same time the odd spin) lies lower than the other state.— The actual separation is 0.8 MeV between the 1— and 0—states (of the $p_{\frac{1}{2}} s_{\frac{1}{2}}$ configuration) and 0.6 MeV between the 3— and the 2— states (of the $p_{\frac{1}{2}} d_{\frac{5}{2}}$ configuration). In view of these values one would expect the 4— state to lie somewhat higher above the 5— level. A separation of 0.1 to 0.2 MeV would still be consistent with the limits of error of our parameters. The problem of finding experimentally this 4— state is discussed in detail in ref. [1]). The centre of mass of the 5— and 4— states in Sr^{86} is calculated to be at 2.61 MeV above the ground state. The 5— level should lie slightly below this position and the 4— level slightly above it. The separation between the 5— and 4— levels should be the same in Zr^{90} and Sr^{86}.

5. Predicted Level Schemes

The interaction parameters obtained in our analysis are sufficient to determine the positions of many levels of nuclei with 38 protons or 50 neutrons. In the following we shall discuss the positions of levels, not yet known experimentally, in some interesting cases. We shall first consider proton configurations in nuclei with 50 neutrons. Of these, Y^{89}, Zr^{90} and Nb^{91} were already considered in detail in sect. 3.

Mo^{92}

We find that the unperturbed $p_{\frac{1}{2}}^2 g_{\frac{9}{2}}^2$, $J = 0$ state lies 1.46 MeV below the $J = 0, v = 0$ state of the $g_{\frac{9}{2}}^4$ configuration. Since the seniority is a good quantum number, the spacings between the corresponding $v = 2$ states of the unperturbed $p_{\frac{1}{2}}^2 g_{\frac{9}{2}}^2$ and $g_{\frac{9}{2}}^4$ configurations are also equal to 1.46 MeV. The non-diagonal matrix element between the two $J = 0, v = 0$ states is $\sqrt{\frac{8}{5}}V$. Due to the interaction through this matrix element the separation between the 0+ ground state and the next 0+ level is increased and predicted to be 2.32 MeV. The ground state is found to be 82 % in the $p_{\frac{1}{2}}^2 g_{\frac{9}{2}}^2$ configuration. The various $v = 2$ states are less shifted by configuration interaction since the non-diagonal matrix elements are only $\sqrt{\frac{3}{5}}V$. Thus, the first excited 2+ level is predicted to lie 1.12 MeV above the ground state of Mo^{92}. The positions of the other $v = 2$ states above this $J = 2$ state should be the same as in Zr^{90}.

Tc^{93}

The configuration interaction between the $J = \frac{9}{2}, v = 1$ states of the $p_{\frac{1}{2}}^2 g_{\frac{9}{2}}^3$ and the $g_{\frac{9}{2}}^5$ configurations was calculated above. The height of the $\frac{1}{2}-$ state above the ground $\frac{9}{2}+$ state was calculated to be 0.44 MeV which well agrees with the experimental value of 0.39 MeV. The two $J = \frac{7}{2}, v = 3$ states of the same configurations are connected by the non-diagonal matrix element $\sqrt{\frac{2}{5}}V$. Since the seniority is a good quantum number their unperturbed spacing is the same as for the $J = \frac{9}{2}, v = 1$ states. Therefore the lower $\frac{7}{2}+$ state is shifted less than the ground $\frac{9}{2}+$ state. This $\frac{7}{2}+$ state is predicted to lie 0.24 MeV above the ground state of Tc^{93}. In this position it might have escaped experimental detection.

Sr^{84}

This case is very similar to Mo^{92}. The unperturbed states of the $g_{\frac{9}{2}}^{-2} p_{\frac{1}{2}}^{-2}$ configuration lie 1.27 MeV above the corresponding unperturbed states of the $g_{\frac{9}{2}}^{-4}$ configuration. Taking into account the non-diagonal matrix elements, the first excited 2+ level is predicted to lie 1.14 MeV above the ground state. Levels with $v = 2$ and $J = 4, 6, 8$ should lie above this $J = 2, v = 2$ state at the same spacings as in Zr^{90}.

Sr^{83}

The states of the unperturbed $g_{\frac{9}{2}}^{-3} p_{\frac{1}{2}}^{-2}$ configuration are calculated to be 0.95 MeV above the corresponding unperturbed $g_{\frac{9}{2}}^{-5}$ states. The non-diagonal matrix elements are the same as in the case of Tc^{93}. Due to configuration interaction the ground state becomes $\frac{9}{2}+$, with the $\frac{1}{2}-$ level of the $g_{\frac{9}{2}}^{-4} p_{\frac{1}{2}}^{-1}$ configuration 0.17 MeV above it. The first excited $\frac{7}{2}+$ level is predicted to lie 0.32 MeV above the ground state of Sr^{83}.

Ground States of the Odd-mass Sr Isotopes

In fig. 3 some calculated levels in the odd-mass Sr isotopes are presented. All levels are drawn relative to the $\frac{1}{2}-$ states of the $p_{\frac{1}{2}} g_{\frac{9}{2}}^{n-1}$ configurations (we find it simpler in this section to refer to neutron configurations rather than

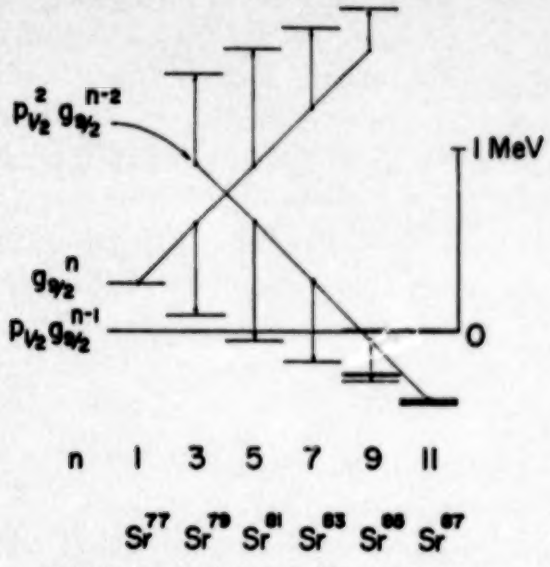

Fig. 3. Ground states of the Sr isotopes.

to neutron holes). The interaction energy in the $\frac{1}{2}-$ states of these configurations is

$$V(p_{\frac{1}{2}} g_{\frac{9}{2}}^{n-1}) = \tfrac{1}{2}(n-1)(n-2)a + \tfrac{1}{2}(n-1)b + \tfrac{1}{2}(n-1)W .$$

The interaction energy in the $J = \frac{9}{2}$, $v = 1$ states of the $g_{\frac{9}{2}}^{n}$ configurations is given by eq. (1) as

$$V(g_{\frac{9}{2}}^{n}) = \tfrac{1}{2}n(n-1)a + \tfrac{1}{2}(n-1)b .$$

The difference in energies between these unperturbed $\frac{1}{2}-$ and $\frac{9}{2}+$ states is therefore a linear function of n. The same holds also for the $J = \frac{9}{2}$, $v = 1$ state of the $p_{\frac{1}{2}}^{2} g_{\frac{9}{2}}^{n-2}$ configurations since in this case

$$V(p_{\frac{1}{2}}^{2} g_{\frac{9}{2}}^{n-2}) = \tfrac{1}{2}(n-2)(n-3)a + \tfrac{1}{2}(n-3)b + V(p_{\frac{1}{2}}^{2}) + (n-2)W .$$

The unperturbed positions of the $J = \frac{9}{2}$, $v = 1$ states of the $g_{\frac{9}{2}}^{n}$ configurations are indicated by dots connected by a straight line. Another straight line connects the unperturbed positions of the $J = \frac{9}{2}$, $v = 1$ states of the $p_{\frac{1}{2}}^{2} g_{\frac{9}{2}}^{n-2}$ configurations. The slope of the first line is $\frac{1}{2}(W - 2a) = \frac{1}{2}\delta_3$, whereas the slope of the second line is $-\frac{1}{2}(W - 2a) = -\frac{1}{2}\delta_3$. The shift of levels by configuration interaction is indicated by arrows leading from the corresponding dots to the calculated positions of levels. The experimental level spacings in Sr^{85} and Sr^{87} are indicated by heavier lines.

The ground state of Sr^{77} is $\frac{1}{2}-$ since the $p_{\frac{1}{2}}$ neutron level is lower by 0.26 MeV than the $g_{\frac{9}{2}}$ neutron level. However, also Sr^{79} is predicted to have a $\frac{1}{2}-$ ground state and this is possibly true also for Sr^{81} (since the difference between the calculated $\frac{1}{2}-$ and $\frac{9}{2}+$ levels is less than the r.m.s. deviation). Only from Sr^{83} on the ground states of the odd-mass Sr isotopes are definitely predicted to have $\frac{9}{2}+$ spin.

It is worth-while to notice that the lower $J = \frac{9}{2}$ states in fig. 3, after being shifted by configuration interaction, still lie fairly well on a straight line (with the exception of Sr^{77}). Assuming that this really reproduces the experimental spacings, this feature could lead to the simple yet wrong conclusion that these $J = \frac{9}{2}$ states belong to pure configurations, say $p_{\frac{1}{2}}^2\, g_{\frac{9}{2}}^{n-2}$. In other words, taking the $\frac{9}{2}+$ states to belong to *effective* $p_{\frac{1}{2}}^2\, g_{\frac{9}{2}}^{n-2}$ configurations, their energies could be well reproduced by *effective* two-body forces which have the same matrix elements in the nuclei considered. This is true in spite of the fact that the perturbing configurations, i.e. the $g_{\frac{9}{2}}^n$ configurations, are rather low lying. This example demonstrates clearly the fact that shell model wave functions may well include considerable admixtures of other configurations.

The authors would like to express their thanks to Dr. A. S. Reiner for helpful discussions about the results of ref. [1]) before its publication, and to Mr. J. B. Sanders for helpful discussions concerning binding energies.

Appendix

The equations used in least squares fit are:

$$\beta = 0.915\,, \tag{A1}$$

$$\beta' = 0.388\,, \tag{A2}$$

$$\gamma + \tfrac{1}{2}\{\sqrt{(2\beta' + \delta_2)^2 + 4V^2} - (2\beta' + \delta_2)\} = 1.079\,, \tag{A3}$$

$$\gamma + \tfrac{1}{2}\{\sqrt{(2\beta - \delta_2)^2 + 4V^2} + (2\beta - \delta_2)\} = 2.182\,, \tag{A4}$$

$$\gamma - \tfrac{1}{2}\{\sqrt{(2\beta - \delta_2)^2 + 4V^2} - (2\beta - \delta_2)\} = 0.430\,, \tag{A5}$$

$$\tfrac{1}{2}\{\sqrt{(2\beta - \delta_2 + \delta_3)^2 + 3.2V^2} - (\delta_2 + \delta_3)\} = 0.105\,, \tag{A6}$$

$$\tfrac{1}{2}\{\sqrt{(2\beta' + \delta_2 - \delta_3)^2 + 3.2V^2} - (\delta_2 + \delta_3)\} = 0.233\,, \tag{A7}$$

$$0.8\gamma + \tfrac{1}{2}\{\sqrt{(2\beta' + \delta_2 - \delta_3)^2 + 3.2V^2} - (2\beta' + \delta_2 - \delta_3)\} = 0.865\,, \tag{A8}$$

$$\tfrac{1}{2}\{\sqrt{(2\beta - \delta_2 + 3\delta_3)^2 + 4.8V^2} - (\delta_2 + \delta_3)\} = 0.390\,. \tag{A9}$$

References

1) B. F. Bayman, A. S. Reiner and R. K. Sheline, Phys. Rev. **115** (1959) 1627
2) cf. I. Talmi, Proceedings of the Rehovoth Conference on Nuclear Structure (North-Holland Publishing Company, Amsterdam 1958) p. 31, where further references are given
3) D. Strominger, J. M. Hollander and G. T. Seaborg, Rev. Mod. Phys. **30** (1958) 585
4) S. Bjørnholm, O. B. Nielsen and R. K. Sheline, Phys. Rev. **115** (1959) 1613
5) M. Goldhaber and A. W. Sunyar, Phys. Rev. **83** (1951) 906
6) A. W. Sunyar, J. W. Mihelich, G. Scharff-Goldhaber and M. Goldhaber, Phys. Rev. **86** (1952) 1023
7) B. H. Flowers, Proc. Roy. Soc. **A215** (1952) 398, where also other references are given
8) I. Talmi, Phys. Rev. **107** (1957) 326
9) N. H. Lazar, J. H. Hamilton, L. M. Langer and W. G. Smith, Phys. Rev. **110** (1958) 513 in Table II
10) For example, I. Unna and I. Talmi, Phys. Rev. **112** (1958) 452

4.E *Nuclear Physics* 19 (1960) 243—247; © *North-Holland Publishing Co., Amsterdam*
Not to be reproduced by photoprint or microfilm without written permission from the publisher

DECAY OF Y^{88}

M. K. RAMASWAMY and P. S. JASTRAM

Physics Department, Ohio State University, Columbus, Ohio, USA†

Received 22 April 1960

Abstract: The weak positon spectrum in the decay of 105-day Y^{88} has been measured in coincidence with the 1.86-MeV gamma ray and annihilation radiation. The spectrum has an end-point energy of 560 ± 30 keV. The spectral shape is found to be characteristic of a unique first-forbidden transition ($\Delta J = 2$, yes), thus confirming a 4^--spin assignment for the ground state of Y^{88}.

A search was made for a possible 0^+ excited level below the 1.86 MeV (2^+) level in Sr^{88} with negative results. An upper limit of 100 keV can be set on any possible E2 transition to such a state.

1. Introduction

Although the gamma spectrum following the decay of 105-day Y^{88} is well known, there is much less information on the weak position spectrum leading to the 1.86-MeV level (fig. 1). For some time the end-point energy of the positon spectrum was believed to be 830 keV[1]). Recently, however, Stirling and

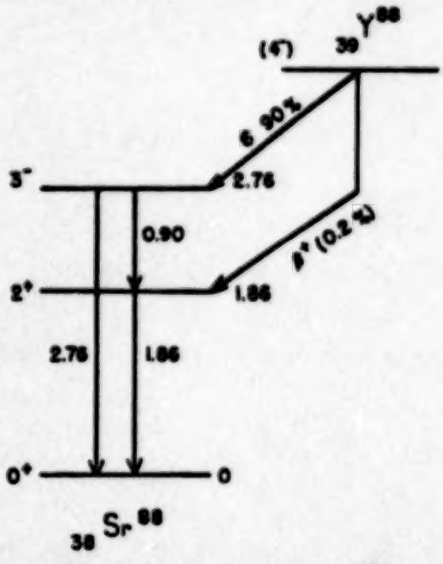

Fig. 1. Decay Scheme of Y^{88}.

Goldberg[2]) showed that the end-point energy was 580 keV and pointed out that the positon spectrum due to internal pair creation by the 1.86-MeV gamma ray was responsible for the erroneous higher end-point estimate. In order to obtain the positon end-point energy. Stirling and Goldberg had to subtract from the

† Work supported by the U.S. Atomic Energy Commission.

observed beta-spectrum the theoretically computed internal-pair positon spectrum.

We have determined the positon end-point energy, first, by determining the decay energy for the electron-capture transition to the 2.76-MeV level from a measurement of the L/K capture ratio using the sum-coincidence technique[3]) and, secondly, by measuring the positon spectrum directly in coincidence with the 1.86-MeV gamma ray and annihilation radiation. This procedure eliminates the contribution of the internal pair spectrum.

Incidental to these studies, a search was made for a 0^+ excited level in Sr^{88} below the 1.86-MeV level. It is known that $^{40}Zr^{90}_{50}$ has a 0^+ excited level at 1.73-MeV. Since 0^+ levels are found to occur in doubly closed-shell or closed-subshell nuclei, it seemed likely that Sr^{88} with 38 protons (presumably closing the $f_{\frac{5}{2}}$ subshell) and 50 neutrons may also have an accessible 0^+ excited level.

2. Decay Energy Measurement

The L/K ratio in a low-energy capture transition yields an accurate value of the decay energy. On the other hand, one can still obtain an approximate value even if this energy is large, as in the Y^{88} decay. To obtain an estimate for the end-point energy of the positon spectrum leading to the 1.86-MeV level, the L_1/K ratio was measured for the capture-transition to the 2.76-MeV level. This was accomplished by determining the ratio of the number of K X-rays in coincidence with the 0.90-MeV gamma ray to the number of 0.90-MeV gamma ray decays. The ratio of probabilities of L to K capture is given in this case by

$$P_{L_1}/P_K \approx [(N_{0.9}/N_{0.9,X})\,\varepsilon_K S_K \omega_K - 1]\,\frac{1}{1.15}\,,$$

where ε_K is the efficiency for detecting the K X-ray, S_K the solid angle subtended by the X-ray counter and ω_K the K-fluorescence yield.

The factor 1.15 in the denominator arises from taking account of capture from higher shells[4]). The decay energy is given in keV by the expression[5])

$$W = \frac{W_{L_1} - xW_K}{1 - x}\,,$$

where W_{L_1} is the L_1 binding energy, W_K the K binding energy and

$$x = \sqrt{\frac{(P_{L_1}/P_K)}{g^2_{L_1}/g^2_K}}\,, \quad \text{with } g^2_{L_1}/g^2_K = 0.10\,.$$

From the measured value of 0.104 for P_{L_1}/P_K, we compute the decay energy for the transition to the 2.76-MeV level to be 540 ± 160 keV. This then gives a positon end-point energy of 420 ± 160 keV.

3. Positon Spectrum Measurement

A 4π plastic scintillation counter can be effectively used[6]) to measure the shapes of beta-spectra, especially when the beta-branching is rather small as in the present case. The 4π counter consisted of two plastic cylinders 2 mm thick and 1 cm in diameter. A slot $\frac{1}{2}$ mm deep and $\frac{1}{2}$ cm in diameter was cut in one of the cylinders. An Y^{88} source† was made up by evaporating a drop on 0.0006 cm thick mylar foil and covering with a similar foil. This was then placed in the slot and sandwiched between the two cylinders. The 4π assembly was mounted on an EMI 9536B multiplier phototube.

The singles spectrum observed in this system is shown in fig. 2. In addition to the positon spectrum there is a substantial contribution from the Compton processes due to the 0.90 and 1.86-MeV gamma rays. Figure 3 shows the

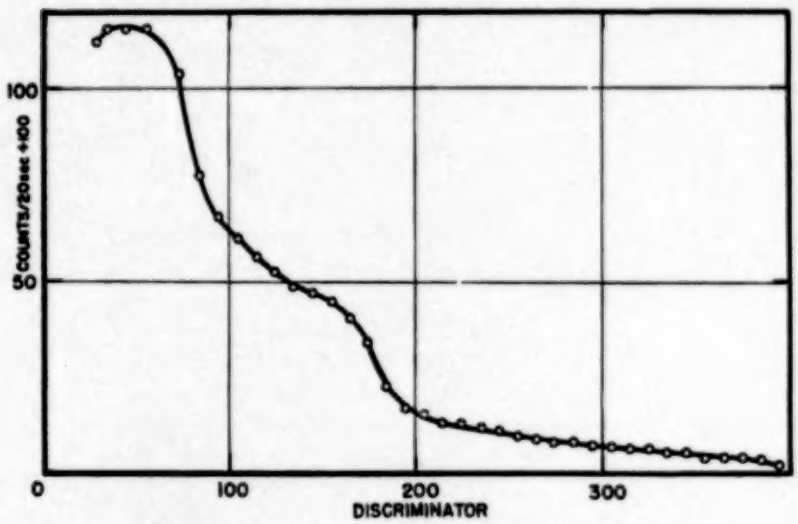

Fig. 2. Spectrum of Y^{88} measured in a 4π plastic scintillator.

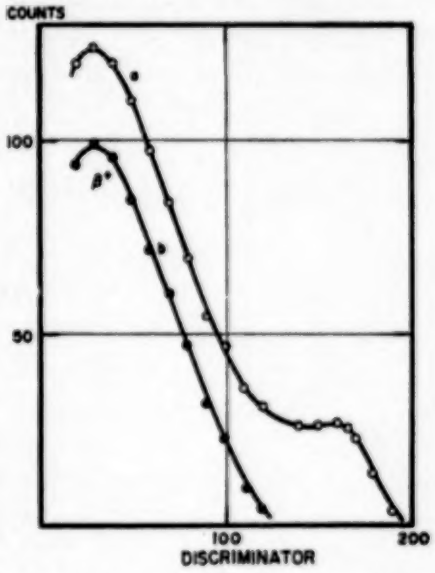

Fig. 3. Positon spectrum of Y^{88} in coincidence with the 1.86-MeV gamma ray (curve a) and both annihilation radiation and the 1.86-MeV gamma ray (curve b).

spectrum coincident with the 1.86-MeV gamma ray (curve a). The Compton spectrum due to the 1.86-MeV gamma ray is eliminated. To obtain the positon spectrum only, the spectrum was measured in coincidence with the 1.86-MeV gamma ray and annihilation radiation. The result is also shown in fig. 3 (curve b). A Fermi plot of this spectrum, after correcting for finite detector resolution, is shown in fig. 4 (curve a). The energy calibration was obtained by observing the 194-keV K-conversion line in the decay of Hg^{203}, and the Compton edges of the annihilation radiation and 0.90-MeV gamma rays. Curve b in fig. 4 shows the same Fermi plot when divided by $a_1^{\ddagger}$, the shape correction factor for unique first-forbidden spectra. An alternative presentation of essentially the

† Obtained from Nuclear Science and Engineering Corporation, Pittsburgh, Pa.

same information is shown in fig. 5, in which the first-forbidden unique shape correction factor

$$a_1 = (W^2 - 1) + (W_0 - W)^2$$

computed for an assumed end-point energy $W_0 = 2.14$ (solid line), is compared with values determined from the measured coincidence positon spectrum. The

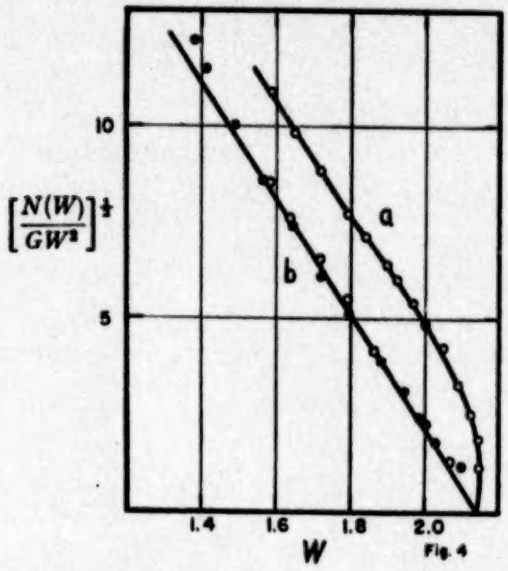

Fig. 4. Curve a: Fermi plot of the Y^{88} positon spectrum. Curve b: result of applying unique first-forbidden shape correction factor to the Y^{88}-plot (dividing by $a_1^{\frac{1}{2}}$) and the Na^{22} positon spectrum (open points).

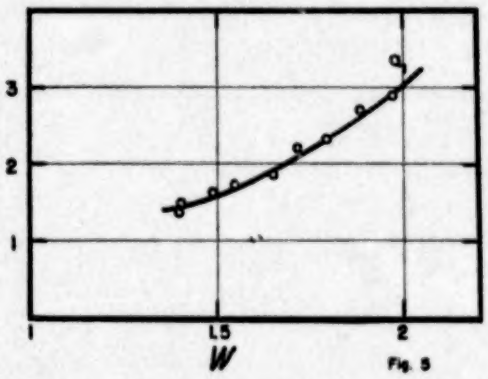

Fig. 5. Comparison of the computed (solid curve) and empirically determined (open points) energy dependence of the first-forbidden unique shape correction factor a_1 for Y^{88}, with an assumed end-point energy $W_0 = 2.14$.

experimental values of a_1 are determined as follows. The computed correction is first applied to the measured spectrum, and the best straight line (fig. 4) is drawn through the corrected points and the assumed end-point. This straight line is then taken to be the true corrected spectrum, which is then compared with the (uncorrected) measured positon spectrum to obtain a set of empirical a_1 values. The extent to which these values agree with the computed a_1 curve (fig. 5) is a measure of the correctness of the choice of end-point energy and of the validity of the assumption that the shape-corrected Fermi plot is indeed a straight line.

One notes that indeed a division by $a_1^{\frac{1}{2}}$ linearizes the Fermi plot. Also plotted for comparison in curve b of fig. 4 is the Fermi plot of a Na^{22} spectrum, which is known to be allowed, measured with the same counter under identical conditions. From the corrected Fermi plot one obtains for the positon spectrum of Y^{88} an end-point energy of 560 ± 30 keV.

4. Search for a 0^+ Excited Level in Sr^{88}

On the assumption that if a 0^+ state existed below the 1.86-MeV level in Sr^{88} one might observe a corresponding weak gamma transition, a search for additional gamma rays was made in the singles spectrum and in the gamma spectrum coincident with the 0.90-MeV gamma ray. No additional gamma rays were found. Using the Weisskopf-Moszkowski single-particle formula to estimate the E2 transition probabilities, an upper limit of 100 keV can be set on the energy of any possible gamma ray from the 1.86-MeV level to a 0^+ excited state.

5. Discussion

The fact that the beta spectrum of Y^{88} can be linearized by the first-forbidden unique shape correction factor confirms the spin assignment of 4^- for the ground state of Y^{88}. The assignment is consistent with a single-particle configuration in which the 39th proton is assumed to be in a $p_{\frac{1}{2}}$ state and the 49th neutron in a $g_{\frac{9}{2}}$ state, or *vice-versa*. Our positon end-point energy of 560 ± 30 keV agrees well with the value of 580 keV obtained by Stirling and Goldberg, and is also, within statistical error, in agreement with the rather approximate value obtained from the L/K capture ratio measurement.

References

1) Way, King, McGinnis and Van Lieshout, Nuclear Level Schemes $A = 40 - 92$ (U.S. Government Printing Office, 1955.
2) W. L. Stirling and N. Goldberg, Bull. Am. Phys. Soc. 6 (1956) 291
3) Gupta, Jha, Joshi and Madan, Nuovo Cim. 8 (1958) 48
4) Wapstra, Nijgh and Van Lieshout, Nuclear Spectroscopy Tables (North-Holland Publishing Company, Amsterdam, 1959) p. 61
5) H. Brysk and M. E. Rose, Revs. Mod. Phys. 30 (1958) 1169
6) M. K. Ramaswamy, Ind. J. Phys. 33 (1959) 285

1.D.2 *Nuclear Physics* **19** (1960) 248—263; © *North-Holland Publishing Co., Amsterdam*
Not to be reproduced by photoprint or microfilm without written permission from the publisher

COMPARISON OF THE THEORY OF NON-AXIAL NUCLEI WITH EXPERIMENTS

E. P. GRIGORIEV and M. P. AVOTINA

Physical Research Institute of the Leningrad University, Leningrad

Received 9 December 1959

Abstract: Experimental data on the energy levels and relative γ-transitions probabilities are compared with the theory of non-axial nuclei. It is shown that within the limits of applicability of the theory none of the data contradict it. In a number of cases it yields a better explanation of the experimental data than the generalized Bohr-Mottelson model.

1. Theory

The Bohr-Mottleson theory of deformed nuclei[1]) has been very fruitful in explaining a number of regularities of nuclear spectra in the range $150 < A < 190$ and $A > 222$. In many cases satisfactory agreement between predictions of the theory and the experimental results is observed.

Disagreement between the theory and experiments is found at the boundary of the deformed nucleus region. An appreciable divergence from the theoretical predictions is observed in the Sm^{152}, Gd^{154} and $Os^{186, 188, 190}$ spectra, the rotational nature of which is firmly established[2–4]).

Rotational levels of even nuclei have been treated by Davydov, Filippov and Rostovsky[6–9]) under the assumption that the nuclei possess equilibrium shapes which are not axially symmetric. The parameter of transverse deformation of the nucleus is an angle γ which can vary between 0° and 60°. When $\gamma = 0°$ or 60° the nucleus is axially symmetrical and at $\gamma = 30°$ the deviation of the shape of the nucleus from that of an ellipsoid of rotation is largest.

Relative values of the ellipsoid axes as a function of γ for a deformation parameter $\beta = 0.3$ are presented in table 1.

TABLE 1

Relative magnitude of ellipsoid axes as a function of γ ($\beta = 0.3$)

γ	R_1	R_2	R_3
0	1.189	0.906	0.906
10	1.183	0.935	0.879
20	1.177	0.967	0.857
30	1.163	1.000	0.837

Attempts have been made in a number of papers[7, 10, 11 etc.]) to show that if the nucleus contains a few nucleons beyond those in filled shells the potential energy will be minimum when the nucleus deviates from an axially symmetric shape. However this can be proved only if some certain assumptions are made.

1.1. LEVELS OF NON-AXIAL NUCLEI

Besides levels possessing total angular momenta 0^+, 2^+, 4^+, 6^+ etc. the theory of non-axial nuclei yields several other rotational levels with even and odd spins which are not encompassed by the Bohr-Mottelson theory. The levels were termed anomalous by the authors[6–9]), in distinction to the ground rotational band 0^+, 2^+, 4^+ etc.

The ratio of the level energies of the ground state differs from the ratio $1 : 3.3 : 7 : 12$ found for rotational levels of axial even nuclei. The latter ratio is obtained only in the limiting cases of $\gamma = 0°$ and $\gamma = 60°$.

Formulae for the level energies as a function of γ have been derived by Davydov and Filippov[6]). The energy in these formulae is expressed in units of $\hbar^2/4B\beta^2$, where β is the deformation parameter and B is the inertia parameter.

The formulae for levels with angular momenta 2^+, 5^+ (two levels) and 3^+ are

$$E_{1,2}(2) = \frac{9}{\sin^2 3\gamma}\left(1 \pm \sqrt{1 - \tfrac{8}{9}\sin^2 3\gamma}\right), \tag{1}$$

$$E_{1,2}(5) = \frac{1}{\sin^2 3\gamma}\left(45 \pm 9\sqrt{9 - 8\sin^2 3\gamma}\right), \tag{2}$$

$$E(3) = \frac{18}{\sin^2 3\gamma}. \tag{3}$$

The energies of spin 4^+, 6^+ and 8^+ levels are the roots of the following respective equations of the third, fourth and fifth degree:

$$E^3 - \frac{90\,E^2}{\sin^2 3\gamma} + \frac{48\,(27 + 26\sin^2 3\gamma)\,E}{(\sin^2 3\gamma)^2} - \frac{640\,(27 + 7\sin^2 3\gamma)}{(\sin^2 3\gamma)^2} = 0, \tag{4}$$

$$E^4 - \frac{252\,E^3}{\sin^2 3\gamma} + \frac{1764\,(9 + 4\sin^2 3\gamma)\,E^2}{(\sin^2 3\gamma)^2} - \frac{2592\,(81 + 235\sin^2 3\gamma + 24\sin^4 3\gamma)\,E}{(\sin^2 3\gamma)^3} + \frac{36288\,[162 + 163\sin^2 (3\gamma)]}{[\sin^2 (3\gamma)]^3} = 0, \tag{5}$$

$$E^5 - \frac{540\,E^4}{\sin^2 3\gamma} + \frac{108\,(819 + 232\sin^2 3\gamma)\,E^3}{(\sin^2 3\gamma)^2}$$

$$- \frac{864\,(5535 + 7362\sin^2 3\gamma + 452\sin^4 3\gamma)\,E^2}{(\sin^2 3\gamma)^3}$$

$$+ \frac{248832\,(243 + 1413\sin^2 3\gamma + 599\sin^4 3\gamma)\,E}{(\sin^2 3\gamma)^4} \qquad (6)$$

$$- \frac{17915904\,(162 + 363\sin^2 3\gamma + 50\sin^4 3\gamma)}{(\sin^2 3\gamma)^4} = 0\,.$$

The level energies as a function of γ are plotted as full lines in fig. 1.

The quantity γ which defines the degree of deviation of the nucleus from an axial shape can most easily be determined from the ratio of the energies of two levels with angular momenta $I = 2$.

The relation between single particle motion in the nucleus and collective motion can be taken into account by introducing corrections for non-adiabaticity. The correction in the Bohr-Mottelson theory has the form

$$B\,I^2\,(I+1)^2\,. \qquad (7)$$

According to the theory of Davydov and coworkers the adiabatic approximation is valid if the equality

$$E_1(2) = E(3) - E_2(2) \qquad (8)$$

is fulfilled.

1.2. PROBABILITIES FOR TRANSITIONS BETWEEN LEVELS

The ratio of the probabilities for electric transitions to rotational levels of a band can be determined for axially symmetric nuclei[5]) (Alaga rule)

In the theory of non-axial nuclei the probabilities of E2 transitions between all rotational levels can be determined. These probabilities depend on γ and for $\gamma = 0°$ they are identical to the results of Alaga.

The following formulae for the transition probabilities have been derived in ref. [6,8]):

$$b(\mathrm{E2};\,2_1^+ \to 0) = \tfrac{1}{2}\left(1 + \frac{3 - 2\sin^2 3\gamma}{\sqrt{9 - 8\sin^2 3\gamma}}\right), \qquad (9)$$

$$b(\mathrm{E2};\,2_2^+ \to 0) = \tfrac{1}{2}\left(1 - \frac{3 - 2\sin^2 3\gamma}{\sqrt{9 - 8\sin^2 3\gamma}}\right), \qquad (10)$$

$$b(\mathrm{E2};\, 2_2^+ \to 2_1^+) = \frac{10 \sin^2 3\gamma}{7(9 - 8 \sin^2 3\gamma)}\,, \tag{11}$$

where

$$b = \frac{16\pi^2}{e^2 Q_0^2} B\,;$$

B is the reduced transition probability.

The probabilities for transition between other rotational levels are also presented in the papers mentioned above.

The full lines in fig. 2 and 3 denote the ratio of the transition probabilities

$$\frac{(b\mathrm{E2};\, 2_2^+ \to 2_1^+)}{b(\mathrm{E2};\, 2_2^+ \to 0)} \text{ and } \frac{b(\mathrm{E2};\, 3^+ \to 2_1^+)}{b(\mathrm{E2};\, 3^+ \to 4_1^+)}$$

(the subscripts designate the number of a rotational level possessing a given spin).

1.3. FRACTION OF E2 AND M1 MULTIPOLES IN THE $2_2^+ \to 2_1^+$ TRANSITIONS

At present only the theory of non-axial nuclei permits one to determine numerically the ratio between M1 and E2 multipolarities in transitions between 2_2^+ and 2_1^+ levels. The following formula for the quantity $\delta^2 = I(\mathrm{E2})/I(\mathrm{M1})$ is given in ref. [9]):

$$\delta^2 = \frac{0.21\, E_\gamma^2}{80\, \hbar^2 c^2} \left(\frac{eZR_0^2}{\mu_0 g_R}\right)^2, \tag{12}$$

where

$$\mu_0 = 5.05 \times 10^{-24}\ \mathrm{erg \cdot G^{-1}}\,,\quad g_R = 0.4\,,\quad R_0 = 1.2 \times A^{\frac{1}{3}} \times 10^{-13}\ \mathrm{cm}\,.$$

Inserting the values of these quantities and expressing E_γ in keV we get

$$\delta^2 = 8.1 \times 10^{-11} E_\gamma^2 Z^2 A^{\frac{4}{3}}, \tag{13}$$

For sufficiently heavy nuclei and γ-rays of not very small energy the M1 contribution is not very large. Qualitative estimations based on the generalized model also indicate that E2 transitions are preponderant between the 2_2^+ and 2_1^+ levels[17]).

Up to the present three investigations have appeared in which the experimental data are compared with the theory of non-axial nuclei[12, 13, 14])†. The results of these studies are used in the present paper.

† *Editor's Note*: See further papers listed in ref. [82]).

2. Comparison with Experiment

2.1. LEVEL ENERGIES

Familiar decay schemes of radioactive isotopes have been considered from the viewpoint of the theory of non-axial nuclei[2, 3, 15, 16]). The deformation parameter γ was determined from the ratio of the energies of levels possessing characteristics 2^+. The positions of the rotational levels of various nuclei are denoted by the points in fig. 1. Satisfactory agreement between theory and experiment is found to hold from Gd^{156} to Pt^{192}. It should be noted that the

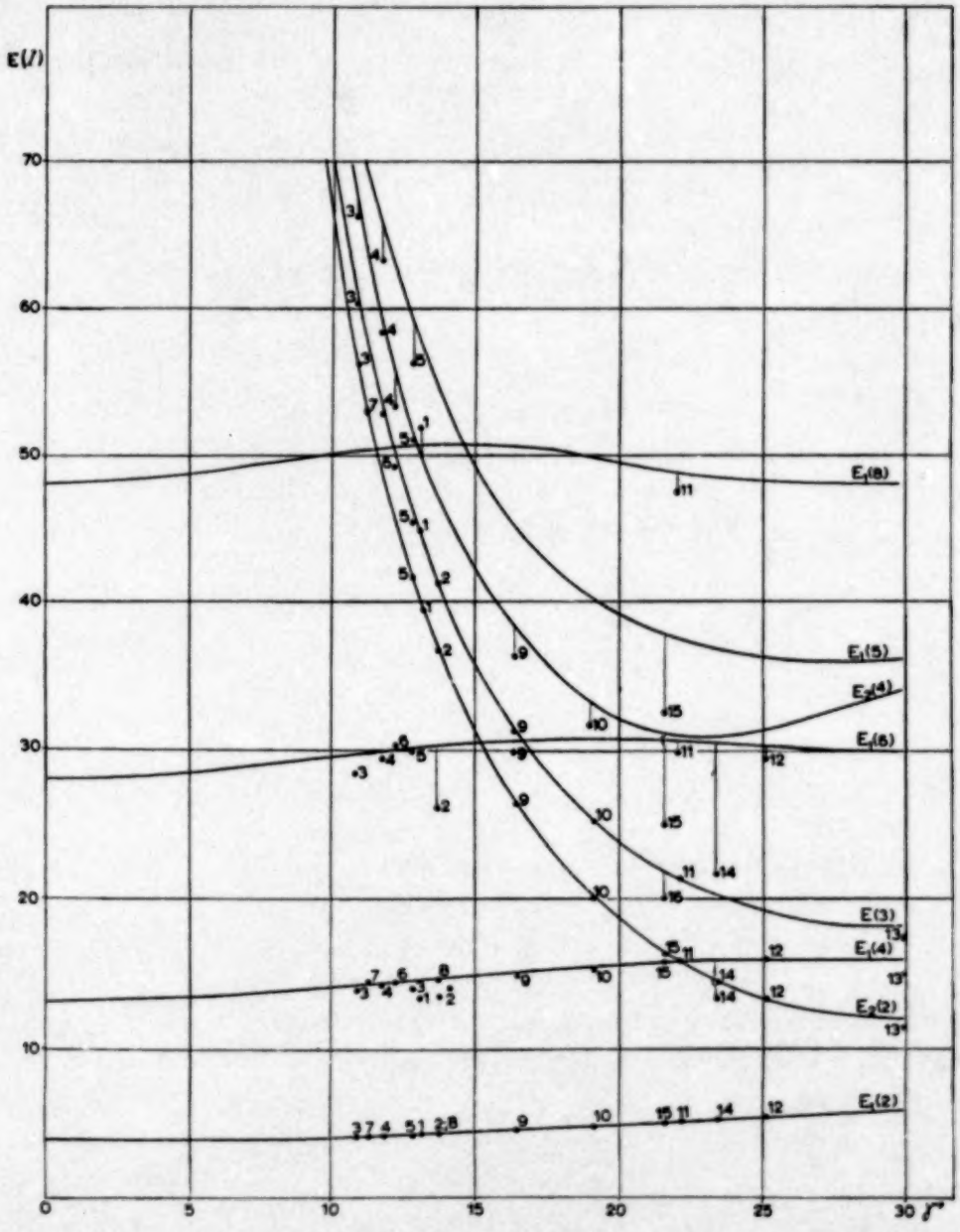

Fig. 1. Dependence of level energies (in $\hbar^2/4\beta\beta$ units) on γ according to non-axial nuclear theory and comparison with the experimental data. 1: Sm^{152}. 2: Gd^{154}. 3: Gd^{156}. 4: Dy^{160}. 5: Er^{166}. 6: Er^{168}. 7: W^{182}. 8: W^{184}. 9: Os^{186}. 10: Os^{188}. 11: Os^{190}. 12: Os^{192}. 13: Pt^{192}. 14: Hg^{198}. 15: Mg^{24}.

levels of nuclei lying between Gd^{156} and W^{184} can be satisfactorily explained by the Bohr-Mottleson model if two parameters A and B are introduced by the formula

$$E^* = AI(I+1) + BI^2(I+1)^2 .$$

However, no choice of A and B can make the theory agree with the experimental data for $Os^{188,190,192}$ and Pt^{192} (table 2). As can be seen from fig. 1 the

TABLE 2

Corrections to energy levels

Nucleus	γ	$B(4)$	$B(6)$	$B(8)$	$\frac{B(4)}{B(6)}$	$E(3)-E_2(2)$	$E_1(2)$	$\frac{\Delta E}{E_1(2)}$ %
1	2	3	4	5	6	7	8	9
Sm^{152}	13.2	0.143				138	122	13
Gd^{154}	13.8	0.125	0.078		1.67	132	123	9.0
Gd^{156}	11.0	0.036	0.022		1.63	94	89	5.6
Dy^{160}	11.8	0.018	0.011		1.63	83	86.6	—5
Er^{166}	12.9	0.011	0.006		1.84	74	80.7	—7
Er^{168}	12.3	0.004	0.002		1.75	75	80	—6
Hf^{178}	0	0.008	0.012	0.011			93	
Hf^{180}	0	0.006	0.006				93	
W^{182}	11.35	0.023				110	101	9.0
W^{184}	13.8	0.018				102	111	—8
Os^{186}	16.5	0.039 (0.079)	0.017 (0.054)		2.3	141	137	3
Os^{188}	19.2	0.039 (0.079)				162	155	4.5
Os^{190}	22.2	0.037 (0.25)	0.014 (0.17)	0.010 (0.12)	2.6	193	186	3.8
Os^{192}	25.2	0.034 (0.31)	0.022 (0.25)		1.55		206	
Pt^{192}	30.0	0.20 (0.95)				308	316	2.5

$B(I)$ is defined by the formula

$$E(I) + I^3(I+1)^3 B = \left[\frac{E(I)}{E(2)}\right]_t [E(2) + 2^3 3^3 B]$$

where $I = 2,4,6$. Between parentheses are given corrections B computed by the Bohr-Mottelson theory.

positions of the levels of these nuclei are quite close to the predictions of the theory of Davydov and coworkers.

The positions of the levels of nuclei Mg^{24} and Hg^{198} differ appreciably from the theoretical predictions. The level scheme of these nuclei can be explained from the same viewpoint although the conditions of the hydrodynamic and

adiabatic approximation are not fulfilled so well and the corrections should be large.

Many nuclei exist which have two levels with angular momenta 2^+ and an energy of the first level which is approximately twice as small as the energy of the second level. At present such nuclei are treated as spherical ones. They could be explained by the non-axial theory by assigning $\gamma = 30°$. However not one level of other spin is known in these nuclei which would be consistent with the theory in respect to energy and quantum characteristics. Final conclusions concerning these nuclei can be drawn only after more complete experimental data are obtained and a method for introduction of corrections in the theory is developed.

An analysis of the experimental data has led us to the conclusion that corrections to energy levels computed by the non-axial theory cannot be of the form $BI^2(I+1)^2$. Corrections computed for levels 4^+, 6^+ of a number of nuclei (columns 3 and 4) are presented in table 2. On the average, the corrections to the 4^+ level is 1.7 times larger than that for the 6^+ level (column 6). The corrections are the same for the 4^+, 6^+ and 8^+ levels of the Hf^{178} and Hf^{180} nuclei. Correction B calculated from the Bohr-Mottelson theory are given between parentheses. They are much greater in magnitude than the corrections which the non-axial nuclear theory yields for $\gamma > 13°$. The corrections are practically the same in both theories for $\gamma < 13°$. It should be noted once again that by no choice of the corrections to B can the experimental data for $Os^{186-192}$ and Pt^{192} nuclei be made to agree with the theory of axial nuclei.

The relation between the energy of the first level and the energy difference $E(3) - E_2(2)$ was also verified. If the adiabatic approximation is valid these quantities should be the same according to the non-axial nuclear theory.

The energies $\Delta E = E(3) - E_2(2)$ and $E_1(2)$ are presented in columns 7 and 8 and their difference relative to the level energy $E_1(2)$ is given in column 9. The ratio $\Delta E/E_1(2)$ varies over a brodd range and is independent of corrections $B(4)$ and $B(6)$. This signifies that the fulfilment of equality (8) cannot be considered as a good criterion of applicability of the adiabatic approximation. The results in table 2 indicate that corrections to the level energies cannot only be due to violation of the adiabaticity condition but must also depend on other factors.

2.2. TRANSITION PROBABILITIES

At present it is possible to compare the experimental data on the relative transition probabilities with the theory, especially for transitions from the levels $E_2(2)$ and $E(3)$ to levels $0^+.2^+$, 4^+. The ratio of the reduced transition probabilities $b(\mathrm{E2};\ 2_2^+ \to 2_1^+/b(\mathrm{E2};\ 2_2^+ \to 0)$ is shown in fig. 2. According to calculations performed by Alaga[5]) the value of this ratio is 1.43. The full curve corresponds to the non-axial nuclear theory and the points refer to the experi-

mental data. It can be seen from fig. 2 that almost all experimental points lie between the values of the two theories. In the theory of axial nuclei the comparatively large probability for the transition $2_2^+ \to 2_1^+$ was explained by an

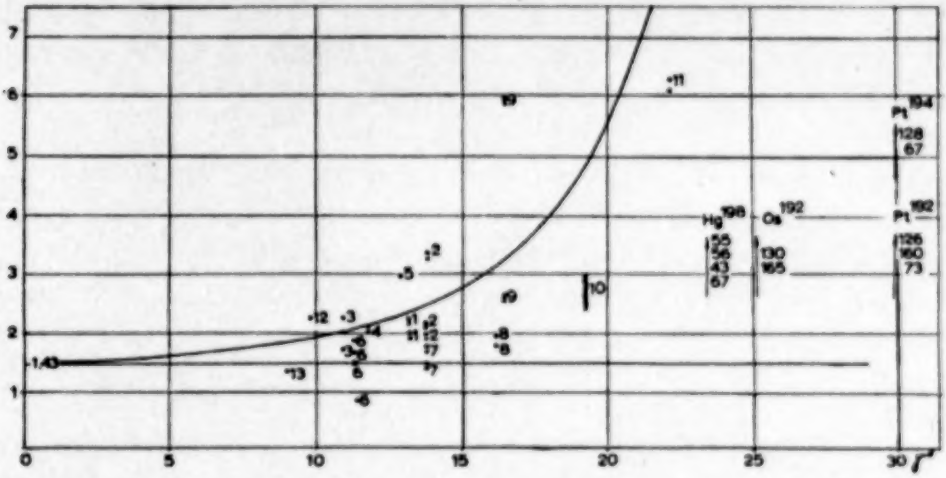

Fig. 2. Comparison of the experimental values of the ratios of the reduced transition probabilities $b(E2;\ 2_2^+ \to 2_1^+)$ and $b(E2;\ 2_2^+ \to 0)$ with the theories of Bohr and Mottelson and of Davydov and colleagues. 1: Sm^{152}. 2: Gd^{154}. 3: Gd^{156}. 4: Dy^{160}. 5: Er^{166}. 6: W^{182}. 7: W^{184}. 8: W^{186}. 9: Os^{186}. 10: Os^{188}. 11: Os^{190}. 12: Th^{228}. 13: Th^{230}.

admixture of the 2_2^+ state to the 2_1^+ state with the same total angular momentum. This admixture has been taken into account by Davydov. Moreover, an M1 transition is possible between these states. An admixture of this type would also enhance the observed intensity of the $2_2^+ \to 2_1^+$ transition and

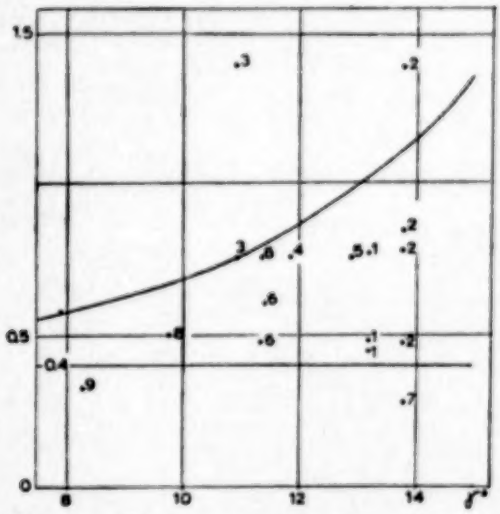

Fig. 3. Comparison of the experimental values of the ratios of the reduced transition probabilities $b(E2;\ 3^+ \to 4_1^+)$ and $b(E2;\ 3^+ \to 2_2^+)$ with the theories of Bohr and Mottelson and of Davydov and colleagues. 1: Sm^{152}. 2: Gd^{154}. 3: Gd^{156}. 4: Dy^{160}. 5: Er^{166}. 6: W^{182}. 7: W^{184}. 8: Th^{228}. 9: Pu^{240}.

thus lead to a discrepancy between the experiments and non-axial theory.

For a more rigorous comparison of the theory with the experiments the E2 component of the $2_2^+ \to 2_1^+$ transition should be taken and the M1 transition

admixture should be taken into account on basis of conversion coefficient or $\gamma - \gamma$ angular correlation measurements. The crosses in fig. 2 denote those cases in which the M1 admixture was taken into account.

A circumstance which speaks in favour of the theory of non-axial nuclei is that the experimental ratio $b(\mathrm{E2};\ 2_2^+ \to 2_1^+)/b(\mathrm{E2};\ 2_2^+ \to 0)$ increases appreciably with increase of γ and for nuclei with $\gamma > 15°$ it greatly differs from the value 1.43.

The experimental ratio of the reduced probabilities for transitions from levels with an angular momentum 3^+ to levels 4_1^+ and 2_1^+ is shown in fig. 3. Here the experiments are in somewhat better agreement with the new theory (full curve). In this case the preceding causes of divergence between Davydov's

TABLE 3

Reduced probability ratio $\dfrac{b(\mathrm{E2};\ 4_2^+ \to 2_1^+)}{b(\mathrm{E2};\ 4_2^+ \to 4_2^+)}$ for Er^{166} and Dy^{160}

Nucleus	Exper[18,19]	Davydov	Alaga
Er^{160}	0.20	0.10	
Dy^{160}	0.14	0.10	0.34

theory and the experimental data do not arise.

The reduced probability ratio $b(\mathrm{E2};\ 4_2^+ \to 2_2^+(/b(\mathrm{E2};\ 4_2^+ \to 4_1^+)$ is known for the Er^{166} (ref. [18])) and Dy^{160} (ref. [19])) (table 3). In this case an admixture

TABLE 4

Ratio of reduced transition probabilities $\dfrac{B(\mathrm{E2};\ 2_2^+ \to 2_1^+)}{B(\mathrm{E2};\ 2_1^+ \to 0)}$ for some nuclei

Nucleus	γ	Exper.	Non-axial nuclear theory	Axial nuclear theory
W^{184}	13.8	0.074	0.12	
W^{186}	16.15	0.12	0.18	
Os^{188}	19.2	0.19	0.33	2.0
Os^{190}	22.2	0.53	0.57	
Os^{192}	25.3	0.68	0.94	
Pt^{194}	30	0.59	1.43	

of M1 to the $4_2^+ \to 4_1^+$ transition is possible and this may increase the ratio of the probabilities of the E2 components of the transitions under consideration. An admixture of the 4_2^+ state to the 4_1^+ state should lower this ratio.

The ratio of the reduced probabilities can be determined from measurements on the level lifetimes and transition intensities. According to the vibrational model of Scharff-Goldhaber and Weneser[20]) this ratio should equal 2.0. whereas the experimental data[21] significantly differ from this value. The values which the non-axial nuclear model yields are much closer to the experimental values (table 4).

Thus, on the basis of relative transition probabilities it is difficult to draw any conclusions regarding the superiority of any of the theories. The experimental data, which, however, are not sufficiently accurate at present, do not explicitly contradict the theory of non-axial nuclei.

2.3. RATIO $\delta^2 = I(\mathrm{E2})/I(\mathrm{M1})$ for $2_3^+ \to 2_1^+$ TRANSITIONS

In a paper by Malik *et al.*[14]) the experimental results are compared with results of calculations performed on the basis of formula (12). The ratio $\delta^2_{\mathrm{exp}}/\delta^2_{\mathrm{theor}}$ which would be unity if the experimental and theoretical data were identical, is given in table 5. Besides, data taken from ref.[14]), table 5 contain other information on multipolarities in $2_2^+ \to 2_1^+$ transitions likewise derived from $\gamma - \gamma$ angular correlation data. In many cases large differences in the experimental data of various authors and the large experimental errors do not permit one to draw any final conclusions regarding the agreement between the theory and experiment.

The experimental results can conventionally be divided into three groups. In the first part of table 5 are presented values of $\delta^2_{\mathrm{exp}}/\delta^2_{\mathrm{theor}}$ which sharply differ from unity. Evidently the 2_2^+ levels in these nuclei are single-particle levels and the nuclei themselves are spherical. Their shells are almost filled up.

For the second group of nuclei the value of δ^2 as a whole is in agreement with the results of the theory of Davydov and colleagues. Such are the nuclei Fe^{58}, Ni^{60}, Te^{126}, Os^{186}, Os^{188}, Pt^{192}.

The third group of nuclei includes those for which δ^2 has not been measured with sufficient accuracy and hence no definite conclusions can be drawn. However within the accuracy of the measurements the data for these nuclei are not inconsistent with the theory of non-axial nuclei.

2.4. LIMITS OF APPLICABILITY OF THE THEORY

The experimental data considered above show that the theory can be applied to nuclei which at present are regarded as deformed. However, the authors of the theory also attempt to use it to explain such nuclei as Se^{76}, Fe^{122} and others which are now regarded as spherical. At present the data available on these nuclei are too sparse to permit any conclusion to be drawn concerning the rotational nature of their levels. As a matter of fact the only data which speak in favour of the theory of Davydov and colleagues or of any other collective model is the presence in these nuclei of two levels with quantum characteristics 2^+ and the small admixture of M1 multipolarity in transitions between them

TABLE 5

Comparison of the experimental values of $\delta^2 = I(E2)/I(M1)$ with the theoretical ones for $2_2^+ \to 2_1^+$

Nucleus	E_r(Wi)	δ^2Wi	δ^2WM	$\frac{\delta^2 Wi}{\delta^2 WM}$	Ref.
S^{34}	1160	0.016 0.017 ± 0.011	3.1	0.005 0.005 ± 0.004	22) 23)
Fe^{56}	1810	0.026 0.004 0.023 ± 0.020	38	0.0007 0.0001 0.0006 ± 0.00005 0.00002	24) 25) 14, 26)
	2100	0.087 0.036 0.078 ± 0.017 0.073	53	0.0017 0.0007 0.0015 ± 0.0003 0.0014	26) 27) 24) 25)
	2490	0.017	73	0.0002	24)
Zr^{92}	900	<0.002 <0.008	43	<0.00005 <0.0002	28) 14, 23)
Pd^{106}	1045	0.04	94	0.00043	29)
Ce^{140}	920	<0.015	170	<0.00009	23)
Hg^{198}	675	0.92 ± 0.4 1.5	270	0.0034 ± 0.0015 0.0055	14, 30) 31)
Po^{214}	1238	0.014	1100	0.00012	32)
Fe^{58}	805	5.3 ± 1.0	8.0	0.66 ± 0.12	14, 33)
Ni^{60}	850	⩾9.0	11	⩾0.84	24)
Te^{126}	740	41 ± 6	75	0.54 ± 0.07	52)
Os^{186}	627	100 ± 40	200	0.51 ± 0.20	34)
Os^{188}	480	250 ± 20	120	2.1 ± 0.2	14, 35, 36)
Pt^{192}	296	42 ± 16 19 ± 7	48	0.9 ± 0.4 0.40 ± 0.15	38)
Ge^{72}	630	⩾32	9.9	⩾3.3	39)
Se^{76}	640	>14 332 49 ± 20	13	>1.1 26 4 ± 2	14, 23) 40) 34)

TABLE 5 (*continued*)

Nucleus	E_r(Wi)	δ^2Wn	δ^2WM	$\frac{\delta^2\text{Wi}}{\delta^2\text{WM}}$	Ref.
Sn^{116}	800	12 $\pm$ 8	73	0.17 $\pm$ 0.1	14, 41)
Te^{122}	686	10 $\div$ 21 10	62	0.16 $\div$ 0.34 0.16	23) 14, 34)
Sm^{152}	970	$\geq$80 50	240	$\geqslant$0.3 0.2	42) 43)
Gd^{154}	875	>10	210	>0.05	45)
Dy^{160}	880	24	240	0.10	45)
W^{182}	1122	>9	575	>0.02	46)
Os^{190}	374	49	72	0.67	47, 48)
Pt^{194}	293	850 (<3000)	47	18 (0.2 — 63)	14. 49
Pt^{196}	331	30 $\pm$ 6 22 $\pm$ 4	61	0.5 $\pm$ 0.1 0.36 $\pm$ 0.07	14, 50) 51)

and the large value of the transition probability ratio $b(E2; 2_2^+ \to 2_1^+/b(E2; 2_2^+ \to 0)$ ($\approx$ 100).

Up to now these levels have been explained by one and two-phonon excitaiton of nuclei[17]). Besides the 2_1^+ and 2_2^+ levels no levels have been detected in any of the nuclei considered above which could be interpreted as rotational levels of non-axial nuclei.

It should be noted that, in our opinion, the statement made in ref. [11]) to the effect that γ vibrational levels should always lie by an order of magnitude above the usually observed 2_1^+ levels, is not very convincing. Comparison of the theory of Davydov *et al.* with the experiments shows that the theory correctly reflects some of the features of nuclear phenomena. The theory of non-axial nuclei is the next step in the development of model conceptions of the nuclei.

The present paper shows that no model is in complete agreement with experiment, some phenomena being better explained by one model, others by another. Yet none of them can in principle offer an exhaustive picture of the nuclei. On the contrary, the applicability of a model should have its explanation in the general theory of interaction of nuclear particles.

The authors express their appreciation to L. K. Peker and M. A. Listengarten for aid and interest in the work.

Appendix

Experimental data on nuclei whose spectra can be explained by the theory of non-axial nuclei (level energies in keV)

Nucleus	γ	$E_1(2)$	$E_1(4)$	$E_1(6)$	$E_1(8)$	$E_2(2)$	$E(3)$	$E_2(4)$	$\frac{b(E2; 2_2^+ \to 2_1^+)}{b(E2; 2_2^+ \to 0)}$	$\frac{b(E2; 3^+ \to 4_1^+)}{b(E2; 3^+ \to 2_1^+)}$	Ref.
Sm^{162}	13.2	121.2	366			1087	1235	1423	1.96 2.2 2.2	 0.46 0.78 0.48	53) 54) 55) 56)
Gd^{154}	13.8	123.02	371.06	718.1		996.6	1128.4		1.94 ± 0.27 2.11 3.29	0.85 ± 0.12 0.48 0.78 1.4	44) 57) 58) 54) 59)
Gd^{156}	10.95	89	288	584		1152	1246	1365	1.64 2.2	1.4 0.77	61) 59, 60)
Dy^{160}	11.85	86.6	283	580		966	1049	1156	2.04 ± 0.04	0.77	19)
Er^{166}	12.90	80.7	264.9	546		787.4	861	966	2.9	0.2 0.76	18, 62)
Er^{168}	12.28	80	265	548		822	897	996			62)
W^{182}	11.35	100.9	329.36			1222	1332	1481	0.8 1.6 1.8	 0.48 0.77	63) 64) 54, 82)
W^{184}	13.81	111.2	364			899	1006		 1.72 1.45	 0.28	15) 66) 63)
W^{186}	16.55	125				730			1.75 1.9		67) 63)
Os^{186}	16.5	137	434	869		769	910	1060	2.6 5.9		68) 69)

Nucleus	γ	$E_1(2)$	$E_1(4)$	$E_1(6)$	$E_1(8)$	$E_2(2)$	$E(3)$	$E_2(4)$	$\frac{b(E2;\ 2_2^+ \to 2_1^+)}{b(E2;\ 2_2^+ \to 0)}$	$\frac{b(E2;\ 3^+ \to 4_1^+)}{b(E2;\ 3^+ \to 2_1^+)}$	Ref.
Os^{188}	19.2	155	479			634	796	987	2.56 2.71 2.92 2.79		68) 70) 35) 71)
Os^{190}	22.2	186	548	1048	1662	557	754	956	2.5 6.2		72) 48)
Os^{192}	25.2	206	580	1065		489				130.0 165	73) 74)
Pt^{192}	30	316.5	784			613	921		160.5 73	22.9	75)
Pt^{194}	30	327				621			127.5 66.9		73) 76)
Hg^{198}	23.5	411.8	999	1636		1090.7			55 42.5 66.5		77) 78) 79)
Th^{228}	9.75	58	187.0			966	1018		2.2	0.5	80)
Th^{230}	9.0	52.8	174			1060			1.3		81)
Ra^{224}	22.3	84.47	253	487							15, 16)
Ra^{226}	19.9	67.76	210	416							15, 16)
U^{232}	9.3	47	156	321		869	943				15, 16)
U^{234}	14.4	43.5	143.3	296.4	499						15, 16)
Pu^{238}	8.4	44.2	145.8	303.4	514.0	1032	1076				15. 16)
Pu^{240}	8.3	42.87	141.77	292		1020				0.329	15, 16)

References

1) A. Bohr and B. Mottleson, Problems of Modern Physics **9** (1955); **1** (1956)
2) B. S. Dzhelepov and L. K. Peker, Excited States of Deformed Nuclei (Publishing House of Joint Institute of Nuclear Research, Dubna 1959)
3) B. S. Dzhelepov and L. K. Peker, Deformed Nuclei in the Nd-Os Region (Publishing House of Joint Institute for Nuclear Research, Dubna, 1958)
4) B. Mottleson and C. G. Nilsson, Mat. Fys. Skr. Dan. Vid. Selsk. **1**, No. 8 (1959)
5) G. Alaga, K. Adler, A. Bohr and B. Mottleson, Mat. Fys. Medd. Dan. Vid. Selsk. **29**, No. 9 (1955)
6) A. S. Davydov and G. F. Filippov, JETP **35** (1958) 440; Nuclear Physics **10** (1959) 654
7) A. S. Davydov and V. S. Rostovsky, JETP **36** (1959) 1788; Nuclear Physics **12** (1959) 58
8) A. S. Davydov, Izv. Acad. Nauk SSSR (Ser. Fiz.) **23** (1959) 792
9) A. S. Davydov and G. F. Filippov, Nuclear Physics **8** (1958) 237
10) D. A. Zaikin, JETP **35** (1958) 529
11) A. S. Davydov and D. A. Zaikin, JETP **36** (1959) 233
12) D. M. Van Patter, Bull. Am. Phys. **4** (1959) 233
13) V. R. Potnis, S. S. Malik and C. E. Mandeville, Bull. Am. Phys. **4** (1959) 233
14) S. S. Malik, V. R. Potnis and C. E. Mandeville, Nuclear Physics **11** (1959) 691
15) B. S. Dzhelepov and L. K. Peker, Decay Schemes of Radioactive Nuclei (Publishing House of the Academy of Sciences of the USSR, Moscow-Leningrad, 1958)
16) D. Strominger, J. M. Hollander and G. T. Seaborg, Rev. Mod. Phys. **30** (1958) 585
17) K. Adler, A. Bohr, F. Huus, B. Mottleson and A. Winter, Rev. Mod. Phys. **28** (1956) 432
18) K. Ya. Gromov, B. S. Dzhelepov and V. N. Pokrovsky, Izv. Acad. Nauk SSSR (Ser. Fiz.) **23** (1959) 821
19) E. P. Grigoriev, B. S. Dzhelepov, A. V. Zolotavin, B. Kratsik and G. Bitterlich, Izv. Acad. Nauk SSSR (Ser. Fiz.) **23** (1959) 868
20) G. Scharff-Goldhaber and J. Weneser, Phys. Rev. **98** (1955) 212
21) F. K. Gowan, Compt. Rend. du Congress International de Phys. Nucleaire Paris, (1958) p. 233
22) G. G. Shute and P. S. Fisher, Phil. Mag. **3** (1958) 726
23) C. F. Coleman, Nuclear Physics **7** (1958) 488
24) N. Levine, H. Frauenfelder and A. Rossi, Zs. Phys. **151** (1958) 241
25) M. J. Stimac, W. L. Skeel and P. S. Jastram, Bull. Am. Phys. Soc. **4** (1959) 56
26) F. R. Metzger and W. B. Todd, Phys. Rev. **92** (1953) 904
27) F. Asima, F. T. Kokoska, D. R. Cargwright and F. D. Kurbatov, Bull. Am. Phys. Soc. **3** (1958) 103
28) H. I. West, L. G. Mann and G. M. Iddings, Phys. Rev. **113** (1959) 881
29) E. D. Klema and F. K. McGowan, Phys. Rev. **92** (1953) 1469
30) C. D. Shrader, Phys. Rev. **92** (1953) 928
31) D. Schiff and F. R. Metzger, Phys. Rev. **90** (1953) 849
32) G. R. Bishop and F. Madaule, J. Phys. Rad. **19** (1958) 41
33) H. Frauenfelder, N. Levine, A. Rossi and S. Singer, Phys. Rev. **103** (1956) 352
34) T. Lindqvist and J. Marklund, Nuclear Physics **4** (1957) 189
35) V. R. Potnis, V. S. Dubey and C. E. Mandeville, Phys. Rev. **102** (1956) 459
36) W. J. King and M. W. Johns, Can. J. Phys. **37** (1959) 755
37) J. Mraz, Nuclear Physics **4** (1957) 457
38) W. H. Kelly and M. L. Wiedenbeck, Phys. Rev. **102** (1956) 1130
39) R. G. Arns and M. L. Wiedenbeck, Phys. Rev. **112** (1959) 229
40) E. G. Fink Jr., and M. L. Widenbeck, Phys. Rev. **109** (1958) 922
41) R. P. Scharenberg, M. G. Stewart and M. L. Wiedenbeck, Phys. Rev. **101** (1956) 689
42) S. Ofer, Nuclear Physics **4** (1959) 477
43) R. W. Lide and M. L. Wiedenbeck, Phys. Rev. **113** (1959) 840
44) C. D. Hickman and M. L. Wiedenbeck, Phys. Rev. **111** (1958) 539
45) R. G. Arns, R. E. Sund and M. L. Wiedenbeck, Nuclear Physics **11** (1959) 410
46) R. C. Williams and K. I. Roulstpn, Can. J. Phys. **34** (1956) 1087
47) F. Coppelani, U. Farineli, F. Ferrero and R. Maliano, Physica **24** (1958) 765

48) O. B. Nielsen, N. O. Poulsen, R. K. Sheline and B. S. Jensen, Nuclear Physics **10** (1959) 475
49) C. R. Mandeville, J. Varma and B. Saraf, Phys. Rev. **98** (1955) 1186
50) V. R. Potnis, Indian J. Phys. **30** (1956) 375
51) R. M. Steffen, Phys. Rev. **89** (1953) 665
52) M. Sakai (see ref. [14]))
53) L. Grodsins and H. Kendall, Bull. Am. Phys. Soc. **1** (1956) 163; NSA 10 N24B (1956)
54) B. S. Dzhelepov, N. N. Zhukovsky and G. E. Shchukin, Izv. Acad. Nauk SSSR (Ser. Fiz.) **21** (1957) 966
55) B. S. Dzhelepov, N. N. Zhukovsky and V. G. Nedovesov, Izv. Acad. Nauk SSSR (Ser. Fiz.) **19** (1955) 296
56) S. K. Bhattacherjee, T. D. Nainan, S. Raman and B. Sahai, Nuovo Cimento **7** (1958) 501
57) J. O. Juliano and F. S. Stephens, Jr., Phys. Rev. **108** (1957) 341
58) O. Nathan, Nuclear Physics **5** (1958) 401
59) S. Ofer, Phys. Rev. **114** (1959) 870
60) P. G. Hansen, N. O. Lassen, O. B. Nielsen and R. K. Sheline, Nuclear Physics **12** (1959) 389
61) K. B. Jacob, J. W. Mihelich, B. Harmatz and T. H. Handley, Bull. Am. Phys. Soc. **3** (1958) 358
62) C. J. Gallagher Jr. and J. O. Rasmussen, Phys. Rev. **112** (1958) 1730
63) J. J. Murray, F. Boehm, P. Marmier and J. W. M. DuMond, Phys. Rev. **97** (1955) 1007
64) B. V. Bobykin and K. M. Novik, Izv. Acad. Nauk SSSR (Ser. Fiz.) **21** (1957) 1556
65) C. J. Gallagher, D. Strominger and J. P. Unik, Phys. Rev. **110** (1958) 725
66) A. J. Poe, Phil Mag. **46** (1955) 1165
67) M. W. Johns, C. C. McMullen, I. R. Williams and S. V. Nablo, Can. J. Phys. **34** (1956) 69
68) F. T. Porter, M. S. Freedman, T. B. Novey and F. Wagner Jr., Phys. Rev. **103** (1956) 921
69) C. C. McMullen and M. W. Johns, Phys. Rev. **91** (1953) 418
70) V. R. Potnis, Phys. Rev. **104** (1956) 722
71) P. S. Fisher and R. A. Naumann, Phys. Rev. **112** (1958) 1717
72) M. W. Johns and S. V. Nablo, Phys. Rev. **96** (1954) 1599
73) L. L. Baggerly, P. Marmier, F. Boehm and J. W. M. DuMond, Phys. Rev. **100** (1955) 1364
74) V. Shiel, L. D. Wyly and C. H. Braden, Phys. Rev. **105** (1957) 1521
75) M. L. Thieme and E. Bleuler, Phys. Rev. **102** (1956) 195; **99** (1955) 1646
76) L. G. Elliot, M. A. Preston and J. L. Wolfson, Can. J. Phys. **32** (1954) 153
77) B. S. Dzhelepov, N. N. Zhukovsky, V. P. Prikhodtseva and Yu. V. Kholnov, Nuovo Cimento Suppl. **1** (1956) 49
78) J. Volpe and G. Minman, Phys. Rev. **104** (1956) 753
79) S. Bjrholm, O. Nathan, O. B. Nielsen and R. K. Sheline, Nuclear Physics **4** (1957) 313; NSA 11 N24 B (1957)
80) T. O. Passel (1954) NSA 9, N24B (1955)
81) V. S. Gvozdev and Yu. Khazov, Izv. Acad. Nauk SSSR (Ser. Fiz.) 24 (1960)
82) D. M. van Patter, Nuclear Physics **14** (1959/60) 42;
N. Macdonald, Nuclear Physics **14** (1959/60) 70;
C. A. Mallmann and A. K. Kerman, Nuclear Physics **16** (1960);
T. Tamura and T. Udagawa, Nuclear Physics

2.G *Nuclear Physics* 19 (1960) 264—279; © *North-Holland Publishing Co., Amsterdam*
Not to be reproduced by photoprint or microfilm without written permission from the publisher

ANGULAR CORRELATION STUDIES OF THE $Be^9(\alpha, n\gamma)C^{12}$ REACTION

J. B. GARG, J. M. CALVERT and N. H. GALE

The Physical Laboratories, University of Manchester

Received 1 April 1960

Abstract: Several angular distributions and (n, γ) correlations of the neutron group corresponding to the 4.43 MeV level of C^{12}, produced in the reaction $Be^9(\alpha, n\gamma)C^{12}$, have been measured using time-of-flight techniques. Bombarding energies of 3.35 MeV and 5.10 MeV were used. Results have been analysed in terms of direct interaction mechanisms. The angular distributions show forward peaking and can be fitted reasonably well by Butler's theory assuming contributions from $l = 1$ and $l = 3$ but require a rather large value of the radius parameter.

Angular correlation measurements have been done in the reaction plane for neutrons emitted at 10°, 20° and 75° to the direction of the incident beam at energies of 3.35 MeV and 5.10 MeV. These have been fitted by a sum of even order Legendre polynomials. The correlations show marked changes both with neutron angle and bombarding energy, but the symmetry axis is in most cases not very far from the direction of momentum transfer. These results would suggest interference either from different reaction mechanisms, different l-values or both.

1. Introduction

It is now well established that the differential cross section of emitted particles in a wide variety of nuclear reactions at medium energies shows marked variations from the prediction of a compound nucleus process in which the incident particle is said to interact strongly with all nucleons of the target nucleus and thus forming a compound state as an intermediate step in the reaction. Hence many investigators have suggested that such nuclear reactions could proceed by some sort of direct reaction mechanism in which the incoming particle interacts with only few nucleons of the target nucleus. It is probably true that many reactions take place in some kind of intermediate way and hence show features of both types of process.

Of reactions of the type X(a, b)Y where a is any bombarding particle and b is an emitted particle, the reactions most extensively studied which show direct interaction features are those in which the deuteron is the bombarding particle. At bombarding energies greater than about 1 MeV, (d, n) and similarly (d, p) reactions invariably proceed by a direct reaction mechanism called stripping. The theoretical analysis[1–3]) of such reactions in terms of a stripping process is now a well established tool for determining the spins and parities of levels involved in the particular reaction. Other reactions like (p, b), (α, b), (He^3, b), (t, b) etc. have not been investigated to the same extent but their theoretical

analysis in terms of direct interaction mechanisms has been given by many theoreticians[4–10]). Although such theories are necessarily based on simplified models, still they seem to give surprisingly good agreement with many experiments[11–15]).

Considering an X(a, n)Y reaction as representative of the above reactions it could proceed in the following possible ways:

1). Stripping of the incident α particle. Here the α particle is considered as a combination of a He^3 core and a neutron and hence in this type of reaction the neutron is stripped off as the He^3 constituent is captured by the target nucleus.

2). Stripping of a neutron from the target nucleus, called heavy particle stripping by Owen and Madansky. Here the target nucleus is assumed to consist of a heavy core plus an odd loosely bound neutron which is stripped off as the α particle is captured by the nucleus.

3). Direct knock-on collision of the incident α particle with a loosely bound neutron of the target nucleus. Here the α particle is captured and the neutron is knocked out.

4). Compound nucleus formation and its subsequent decay by the emission of a neutron.

The first process is similar to deuteron stripping in (d, p) and (d, n) reactions. However, in the case of α induced reactions, as the α-particle is a tightly bound nucleus, stripping seems rather improbable. The second process is expected to show a large intensity of the outgoing neutrons at backward angles. The third type of process is characterized by forward peaking of the angular distribution similar to deuteron stripping, whereas in a compound nucleus process the angular distribution is expected to be either symmetric about 90° or isotropic, if many levels are excited in the compound nucleus and if the assumptions of the statistical theory are valid.

According to current theories the shape of the angular distributions of emitted particles, arising from all forms of these direct processes, is given by a term $j_l^2(qr)$ where j_l is the spherical Bessel function of order l and q is the momentum transfer vector, whose values in the cm. system for direct processes 1), 2) and 3) are given as follows:

1) α-particle stripping: $q = k_a - \frac{M_X}{M_Y} k_n$;

2) heavy particle stripping: $q = -\left(k_a + \frac{M_a}{M_Y} k_n\right)$;

3) knock-on: $q = \left(\frac{M_X - M_n}{M_X}\right)\left(k_a - \frac{M_X}{M_Y} k_n\right)$.

Hence it is seen that angular distributions from processes 1) and 3) are not distinguishable from each other, though process 2) would be different from these and could be distinguished experimentally.

It was thought that a study of the $Be^9(\alpha, n)C^{12}$ reaction might be useful in understanding these reaction mechanisms, particularly because of the suggestion by Madansky and Owen[7]) that this reaction might show features of heavy particle stripping. This hypothesis has been successfully applied in the analysis of the neutron angular distributions from $B^{11}(d, n)C^{12}$ reaction[16-17]) and might well be applicable in this reaction as well.

Previous measurements of neutron angular distributions from this reaction at rather low energies of α particles from 0.4 to 1.3 MeV have been made by James *et al.*[18]), but their results do not support any stripping mechanism. Tanner[19]) has also measured the (n, γ) correlation from this reaction at α particle energies of 1.15 and 2.8 MeV. The neutrons were observed in the direction of the hypothetical stripping maximum (assumed to arise from heavy particle stripping) and γ rays were observed in coincidence at a few angles chosen to show the maximum anisotropy of the expected correlation. However, his results also did not show any positive evidence for this reaction mechanism, as the observed correlation was found to be isotropic.

Risser, Price and Class[20]) have also measured the angular distributions of the neutron groups n_0, n_1 leading to the ground and first excited states of C^{12}, using alpha particle energies of 2 to 5 MeV for n_0 and 4 to 5 for n_1. The results for the n_0 group were interpreted on a compound nucleus picture but no analysis was made of the n_1 distributions because there were too many uncertainties in the angular momenta involved. However, it is significant that the neutron group to the 4.43 MeV level was significantly more intense than that to the ground state and its angular distribution and energy dependence quite different.

In the experiments described here, we have made a more detailed study of the $Be^9(\alpha, n)C^{12}$ reaction to see if it does show any features of the direct interaction mechanisms mentioned in 1), 2) and 3). Although the experiments of Risser *et al.* show that the angular distribution of neutrons of the n_1 group is not strongly peaked at these bombarding energies, nevertheless the neutrons are emitted predominantly in the forward direction and the distribution does not change rapidly with bombarding energy, so that a direct process such as stripping or knock-on might not be an unreasonable explanation. While a strongly peaked angular distribution of outgoing particles is a well known characteristic of direct interaction, this alone is not sufficient to define the mechanism without ambiguity. However, it has been suggested by Satchler[21]) and Sherr[22]) that a reliable criterion is to be found in the examination of the angular correlation between the outgoing particle and the associated γ-decay.

We have carried out a series of $(\alpha, n\,\gamma)$ correlation measurements at two different energies. From these, the neutron angular distributions have been found and also the (n, γ) correlation function for different directions of the outgoing neutron. These measurements are discussed below.

2. Experimental Arrangement Details

The experimental arrangement is shown in fig. 1. Singly charged alpha particles from the University of Manchester's Van de Graaff accelerator were analysed by a 90° bending magnet and refocused by magnetic quadrupole lenses. The energy spread of the analysed beam was stabilized to better than ½ % using the conventional slit arrangement.

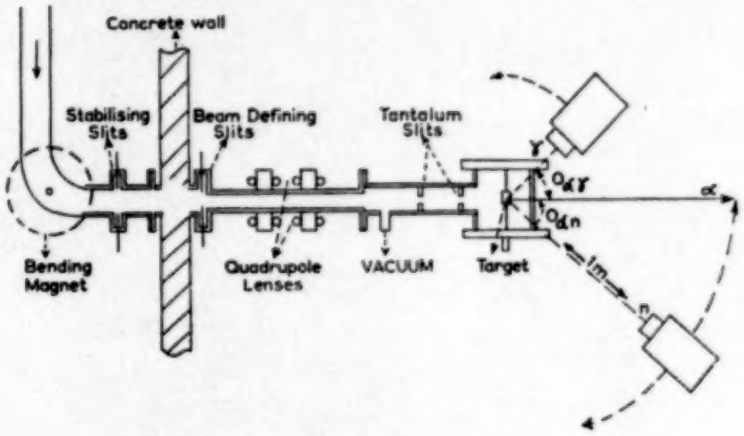

Fig. 1. Experimental arrangement.

The target chamber was made from a 5.1 cm diameter brass cylinder with a perspex lid for visual observation of the beam and target. The target was a foil of beryllium about 300 μg/cm² thick and about 1 cm in diameter. It was supported on a gold backing, 0.0025 cm thick, fixed in a holder at the centre of the target chamber. A time-of-flight spectrometer was used for the measurement of neutron energies. This spectrometer has been described in detail previously[23]).

The apparatus can only record neutrons in association with γ-rays, i.e., those neutron groups giving rise to excited states of the residual nucleus. The time-of-flight of neutrons over a given path was measured with respect to the emission of the associated γ-ray. The time interval between emission and detection of the γ-ray is negligible. The schematic diagram of the electronics is shown in fig. 2. It comprises a fast-slow coincidence system of conventional type. The discriminator bias in each channel of the slow coincidence unit can be adjusted to select the minimum energy of the radiation detected. This enables elimination of unwanted pulses from low energy radiations but also cuts out a fraction of the useful pulses, since the radiations under investigation produce a continuous spectrum of pulses from the detector from zero pulse height to a maximum determined by the energy of the radiation. It was therefore important to know the pulse height versus energy calibration in the neutron channel so that the relative detection efficiency determined by the setting of the discriminator bias could be calculated. The calibration was carried out using γ-rays of known

energies, the relative response of the scintillator to neutrons and γ-rays being known from the investigation of Hardy[24]).

Both the γ-ray and neutron detectors consisted of plastic scintillator NE 102, 5.1 cm diameter × 5.1 cm thick mounted on an RCA photomultiplier, type 6810A. The neutron counter was mounted on a trolley which could sweep out an arc from +150° to —150° on a 1 m radius. For one set of measurements the γ-detector was fixed with its axis perpendicular to the α-n reaction plane and with

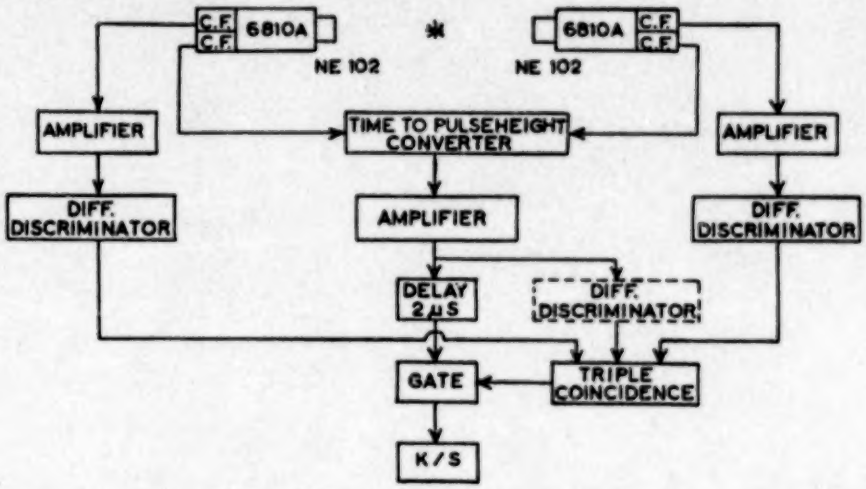

Fig. 2. Schematic diagram of the electronics used.

the front face of the scintillator at 4 cm from the target, while measurements were taken at about 15° intervals of the angle between α-particle and neutron directions. For the second set of measurements, the neutron counter was fixed, at a given angle, ($\theta_{\alpha n}$) and measurements were taken for different settings ($\theta_{\alpha\gamma}$), of the γ-counter with respect to the α-particle beam, the axis of the γ-detector now being in the α-n plane.

Monitoring was carried out using a scintillation counter adjusted to detect the 4.43 MeV γ-ray from the reaction, background being virtually eliminated by using a high discriminator bias. Charge reaching the target was measured with a current integrator. These two sets of readings were quite consistent throughout the experiments. The experimental geometry was checked by measuring the 3.56 MeV γ-ray angular distribution from the $Be^9(p, \alpha\gamma)Li^6$ reaction, which was found to be isotropic within 1 %.

3. Results

3.1. SPECTRUM

Fig. 3 shows a neutron spectrum taken with the time-of-flight spectrometer from the reaction at an angle of 10° to the direction of the incident α-particle beam of energy 5.1 MeV. The spectrum shows a prominent group at 6.2 MeV leading to the first excited state of C^{12} and signs of a weaker group which is

only just statistically significant corresponding to the 7.76 MeV state of C^{12}. The peak labelled as γ-ray arises mainly from coincidences due to neutrons detected in the γ-ray detector and γ-rays detected in the neutron counter. The full-width at half maximum of the main neutron group corresponds to an

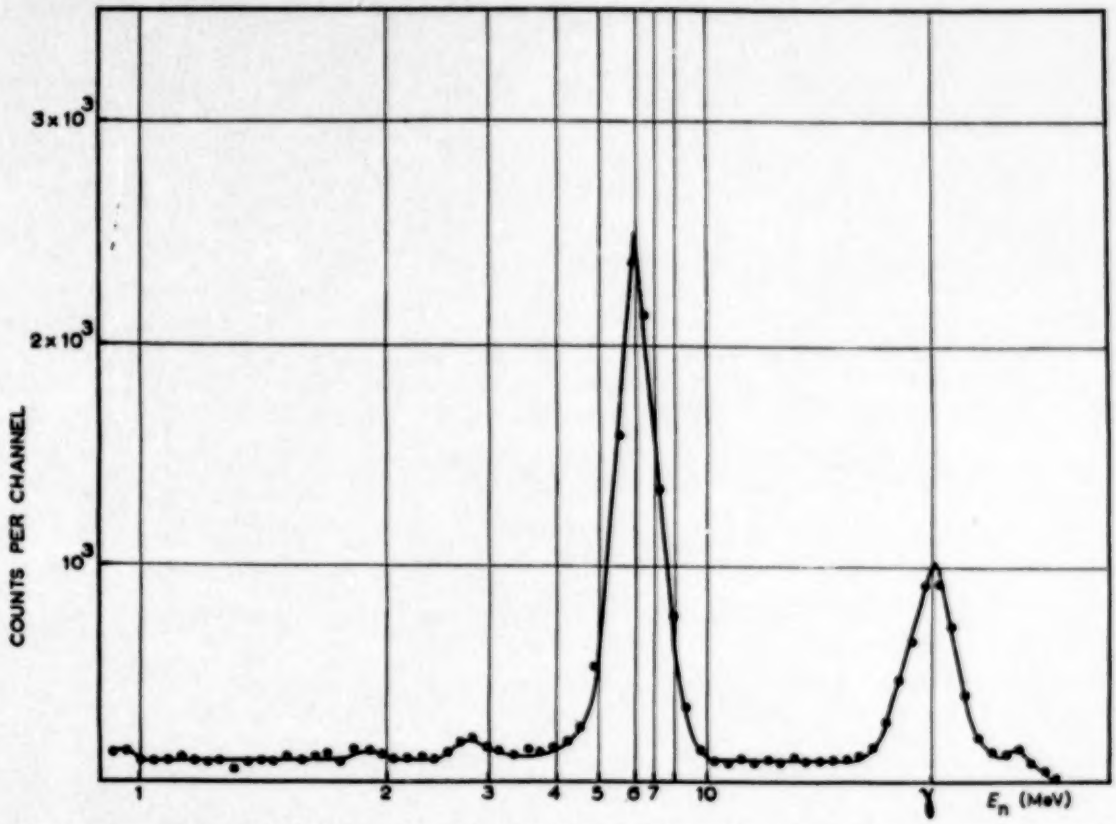

Fig. 3. Neutron time-of-flight spectrum in coincidence with associated γ-ray, measured at an angle of 15° from the bombardment of a thick target of Berylium with 5.1 MeV α-particles.

energy resolution of about 15 %, which was quite adequate for this experiment.

Since the levels of C^{12} higher in excitation than the first (4.43 MeV) are unstable to decay into $Be^8 + \alpha$, we would not expect to observe a large intensity of the corresponding lower energy neutron groups. As one such group is just observable in our spectra, it seems that the probability of this level decaying by γ-emission is not negligible.

3.2. ANGULAR CORRELATIONS

We have studied the (n, γ) correlations, mentioned previously, between the n_1 neutron group and the associated 4.43 MeV γ-ray from C^{12} at bombarding energies of 3.35 MeV and 5.10 MeV. According to the measurements of Bonner *et al.*[25]), the neutron yield curve is fairly flat at the lower energy whereas it shows a broad resonance at the higher one, corresponding to an excitation energy in C^{13} of 14.1 MeV. The width of this resonance has been estimated to be about 300 keV.

The results of these correlations are shown in figs. 5 to 11, the experimental conditions for each determination being quoted on the diagrams. The correlations can be described generally in terms of three angular variables [figs. 4(a)

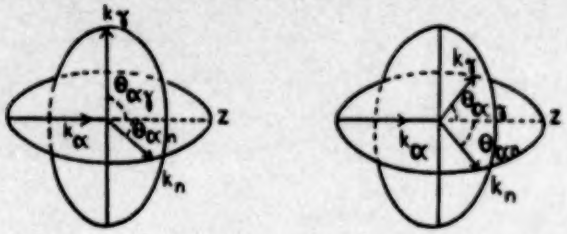

Fig. 4. Diagram showing different wave vectors.

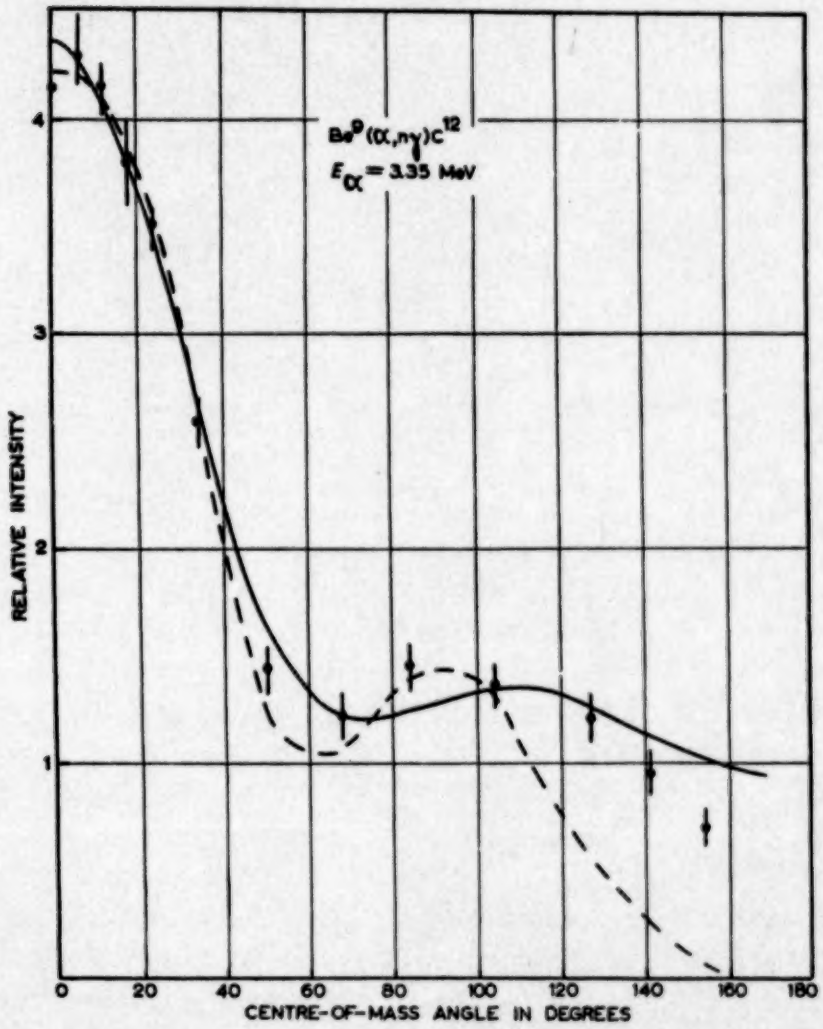

Fig. 5. The angular distribution of neutron groups corresponding to 4.43 MeV state of C^{12} from the reaction $Be^9(\alpha, n)C^{12}$ at incident energy of α-particles of 3.35 MeV. The solid curve is calculated from Butler's formula of direct interaction for a mixture of l values of 0 and 2 and $R = 6.0 \times 10^{-13}$ cm. The broken curve is Butler's curve for a mixture of $l = 1$ and $l = 3$ and $R = 8.8 \times 10^{-13}$ cm.

and (b)]: the angle $\theta_{\alpha n}$ between the momentum vectors k_α and k_n of the incoming α-particle and the outgoing neutron; the angle $\theta_{\alpha\gamma}$ between k_α and the direction of the outgoing γ-ray; and the angle ϕ between the normals to the α-n and α-γ planes (if k_α denotes the $+z$ direction, and k_α and k_n define the x-z plane, then $\theta_{\alpha\gamma}$ and ϕ are the polar coordinates of the γ-direction). Two sets of (n, γ) angular correlation measurements were made.

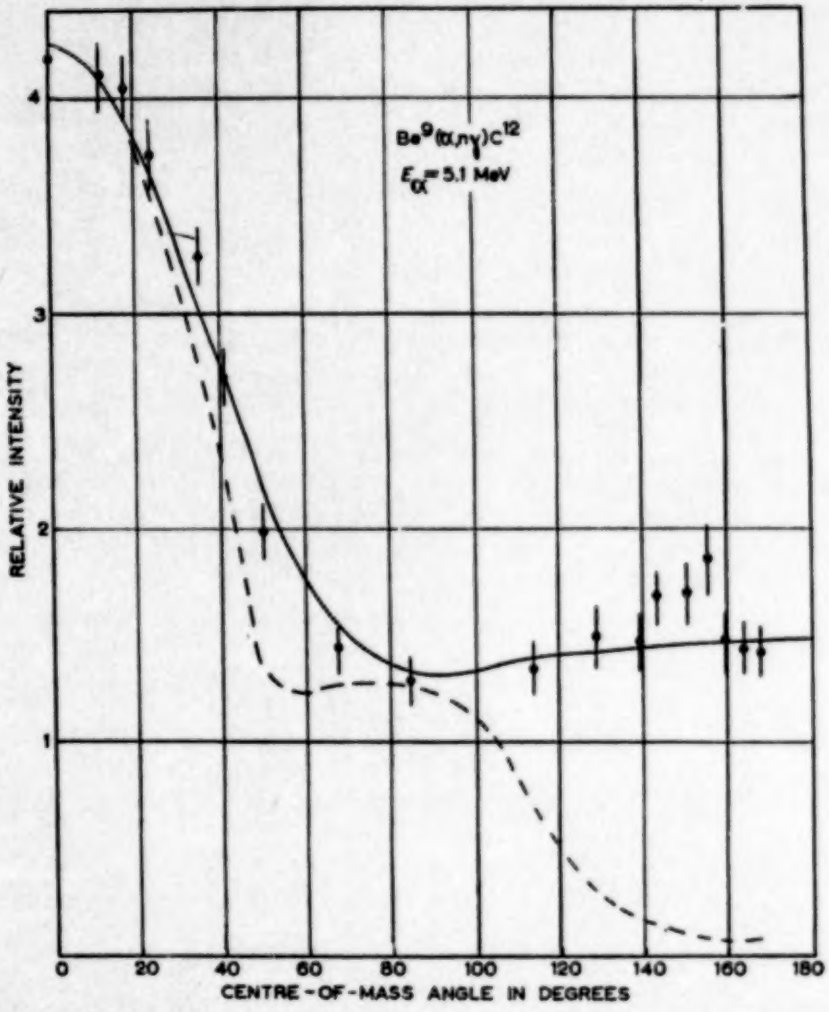

Fig. 6. The angular distribution of neutron groups (— 4.43 MeV) from $Be^9(\alpha, n)C^{12}$ at $E_\alpha = 5.1$ MeV. The solid curve is Butler's curve for a mixture of $l = 0$ and $l = 2$ and $R = 4.1 \times 10^{-13}$ cm. The broken curve is for a mixture of $l = 1$ and $l = 3$ and $R = 7.0 \times 10^{-13}$ cm.

In the first set of measurements the γ-counter was kept fixed in the vertical direction ($\theta_{\alpha\gamma} = \phi = 90°$) and the neutron counter was rotated in the horizontal plane. As will be discussed below these measurements yield essentially the neutron angular distribution.

In the second set of measurements the neutron counter was kept at a fixed angle ($\theta_{\alpha n}$), whose value was chosen from the results obtained in the first set of measurements, and the γ-counter was rotated in the plane defined by (α, n).

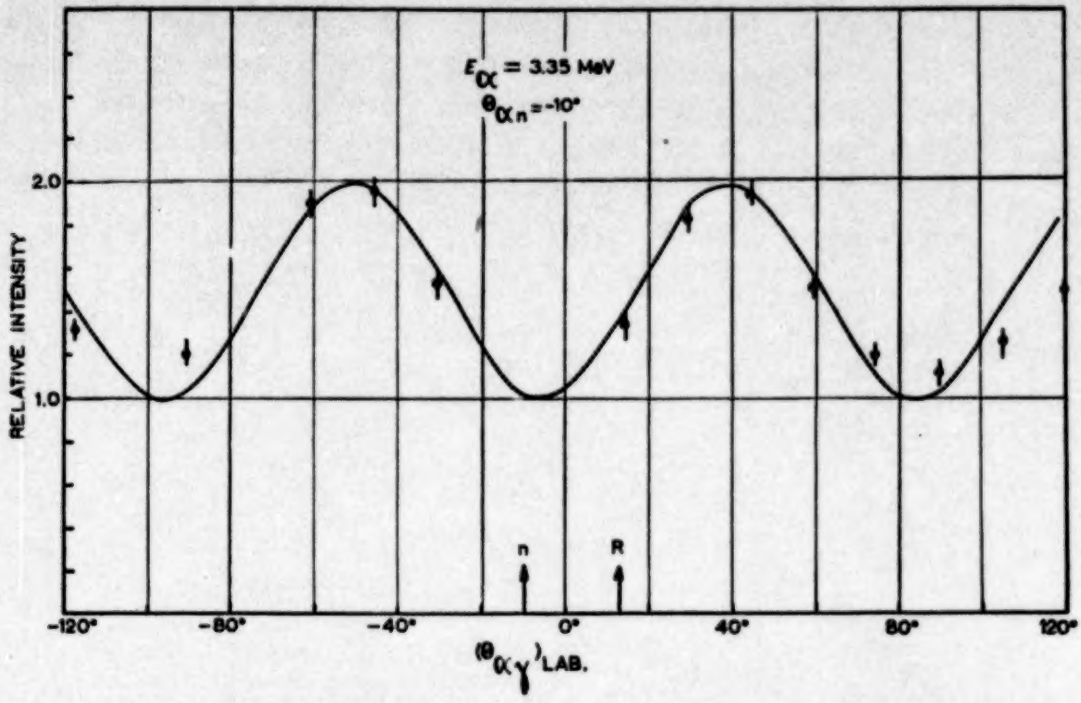

Fig. 7. (n, γ) angular correlation for neutron group and associated γ-rays (4.43 MeV) from Be^9 (α, n)C^{12} reaction at $E_\alpha = 3.35$ MeV. The neutron angle is fixed at 10°. The solid curve is calculated from least square analysis of the experimental results and is of the form $W(\theta) = 1 + 4\cos^2(\theta_{\alpha\gamma} + 5°) - 4\cos^4(\theta_{\alpha\gamma} + 5°)$. If the symmetry axis is taken at 40°, the best fitting function is $W(\theta) = 1 - 1.68\cos^2(\theta_{\alpha\gamma} - 40°) + 1.68\cos^4(\theta_{\alpha\gamma} - 40°)$.

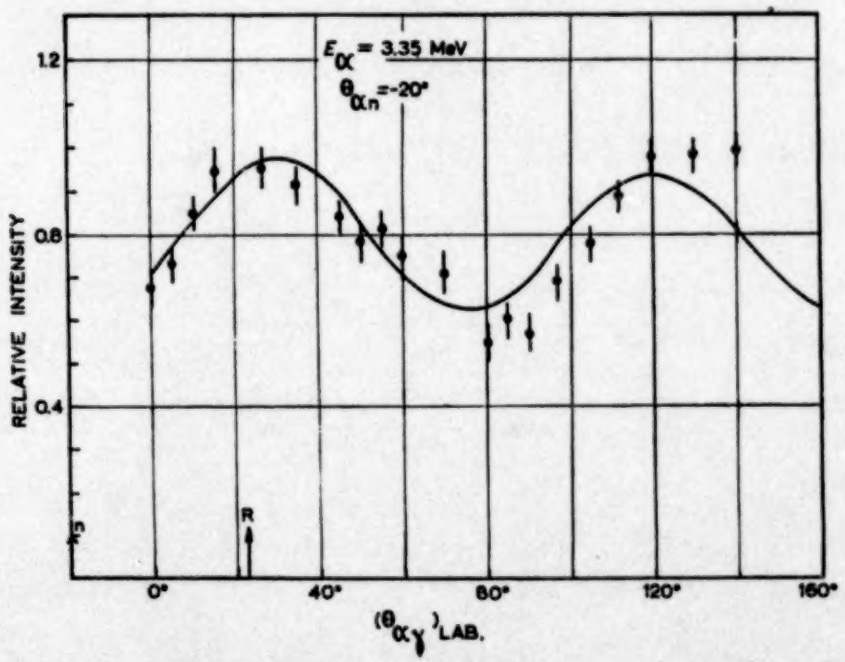

Fig. 8. (n, γ) correlation from $Be^9(\alpha, n\gamma)C^{12}$ (4.43) reaction at $E_\alpha = 3.35$ MeV. The neutron counter is fixed at 20°. Solid curve is a least square analysis curve and is of the form $W(\theta) = 1 - 1.50\cos^2(\theta_{\alpha\gamma} - 30°) + 1.53\cos^4(\theta_{\alpha\gamma} - 30°)$.

Values of θ_{an} of 10°, 20° and 75° were chosen, the former two angles corresponding to a maximum in the angular distribution and the latter to a minimum. It was

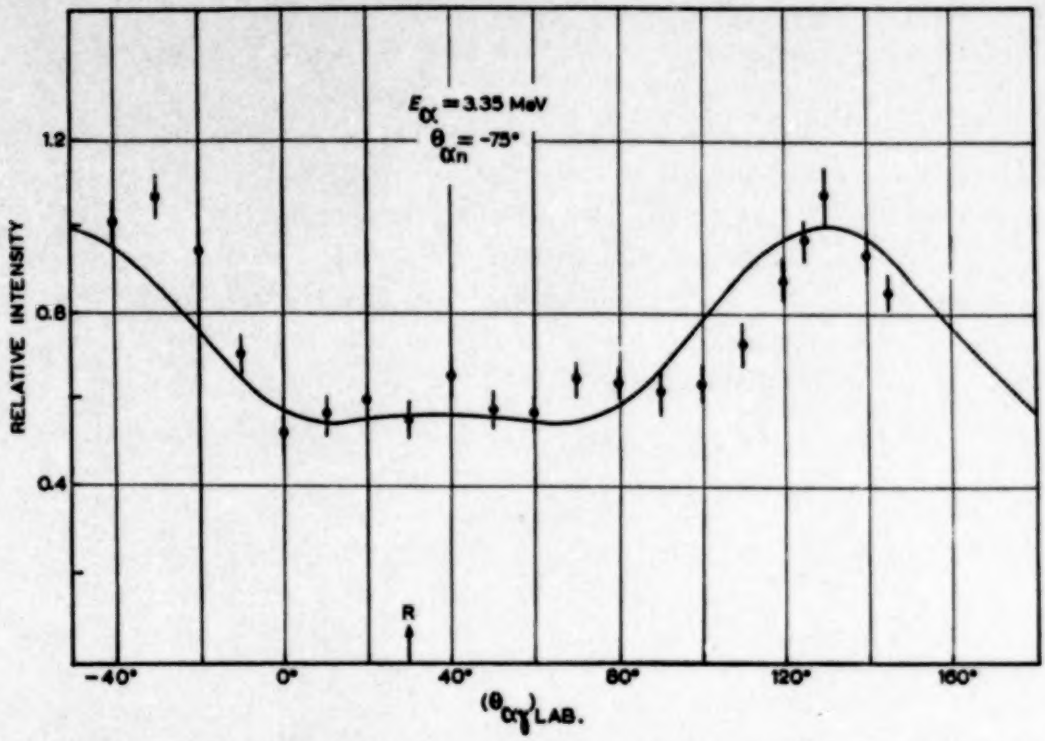

Fig. 9. (n, γ) correlation from $Be^9(\alpha, n)C^{12}$ (4.43 MeV) reaction at $E_\alpha = 3.35$ MeV. The neutron counter is fixed at 75°. The correlation function is $W(\theta) = 1 - 1.12\cos^2(\theta_{\alpha\gamma} - 40°) + 0.68\cos^4(\theta_{\alpha\gamma} - 40°)$.

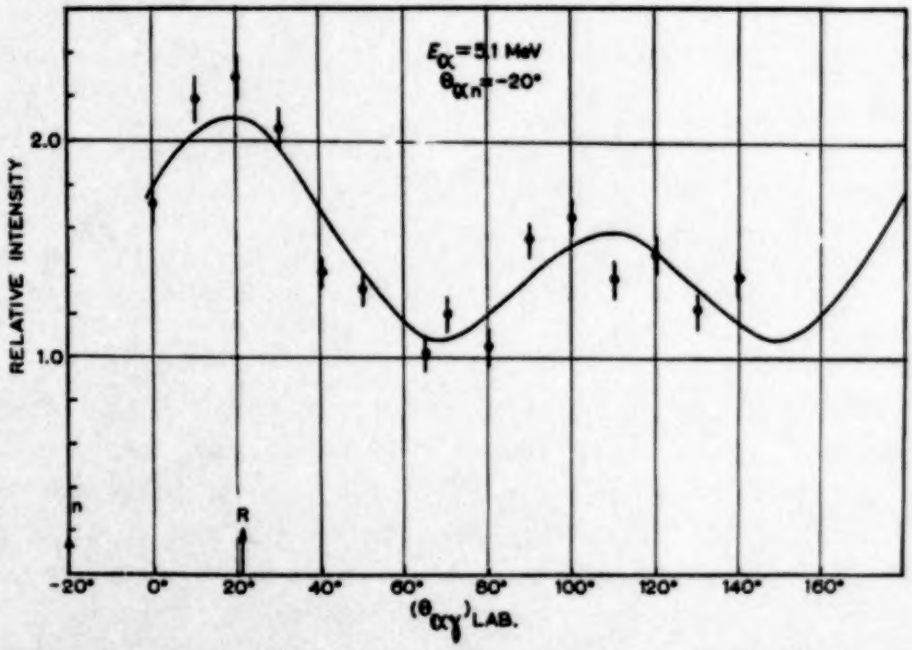

Fig. 10. (n, γ) correlation from $Be^9(\alpha, n)C^{12}$ (4.43 MeV) reaction at $E_\alpha = 5.1$ MeV. The neutron counter is fixed at 20°. The best fitting function is $W(\theta) = 1 - 1.54\cos^2(\theta_{\alpha\gamma} - 19°) + 1.87\cos^4(\theta_{\alpha\gamma} - 19°)$.

thought that by choosing these angles some information could be obtained about the reaction mechanisms contributing to the emission of neutrons in different directions.

The experimental points in each curve have been corrected for background due to random coincidences and have been normalized to the monitor. The effect of any shielding of the neutron counter by the γ-counter when the angle between their axes was small, was allowed for by careful analysis of the single channel rates in each counter with respect to the monitor.

The experimental data shown in figs. 5, 6 and 7 were taken when the γ-counter subtended a solid angle of 0.5 sr at the target. Similarly for figs. 8, 9, 10 and 11, the solid angle was 0.2 sr. No corrections have been made to the curves for this finite solid angle.

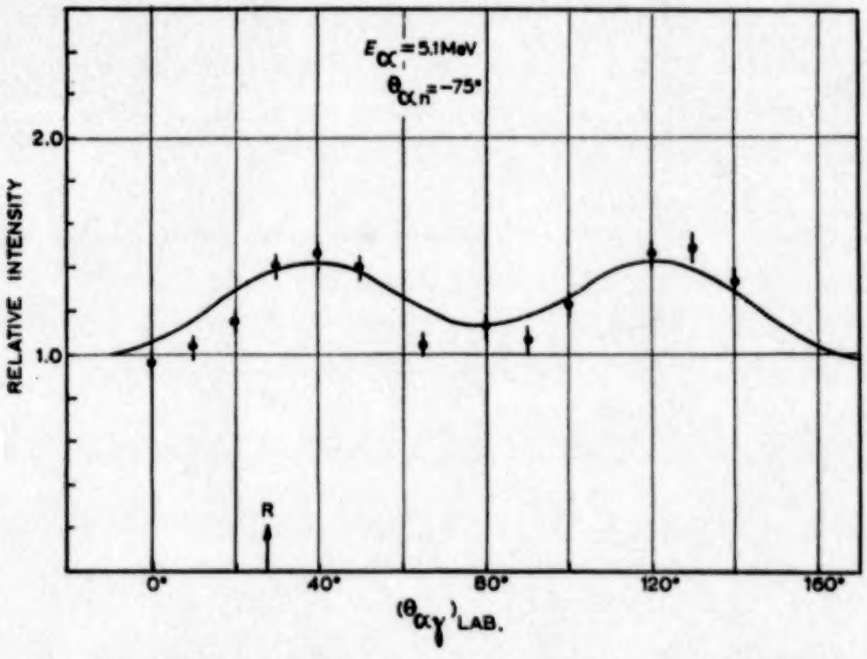

Fig. 11. (n, γ) correlation from $Be^9(\alpha, n)C^{12}$ (4.43 MeV) reaction at $E_\alpha = 5.1$ MeV. The neutron counter is fixed at 75°. The best fitting function is $W(\theta) = 1 + 1.14 \cos^2(\theta_{\alpha\gamma} + 10°) - 1.25 \cos^4(\theta_{\alpha\gamma} + 10°)$. If the symmetry axis is taken at 40°, the best fitting function is $W(\theta) = 1 - 1.21 \cos^2(\theta_{\alpha\gamma} - 40°) + 1.20 \cos^4(\theta_{\alpha\gamma} - 40°)$.

The solid curves in the figs. 7 to 11 are the result of a least-squares analysis, based on the assumption that only even powers of $\cos\theta_{\alpha\gamma}$ up to $\cos^4\theta_{\alpha\gamma}$ are present. All the curves can be represented by an expression of the form $A + B\cos^2(\theta_{\alpha\gamma} - \theta_0) + C\cos^4(\theta_{\alpha\gamma} - \theta_0)$, where A, B and C are coefficients to be determined and θ_0 is the angle between the symmetry axis and the direction of the α-beam. These were determined by assuming a value for θ_0 (nearest to the recoil axis) from inspection of the results and calculating A, B and C by least-squares fitting. Using these calculated values of A, B and C, the angle θ_0 was then adjusted by further least-squares fitting. Arrows in the figures

indicate the angles ($\theta_{\alpha n}$) of outgoing neutron and the corresponding classical recoil direction (θ_R).

The results shown in the figures and the best fitting curves are quoted in table 1.

TABLE 1

Best fitting correlation functions

E_α (MeV)	$\theta_{\alpha n}$	Correlation function $W(\theta_{\alpha\gamma})$	θ_R	θ_0
3.35	—10°	$1 + 4\cos^2(\theta_{\alpha\gamma} + 5°) + 4\cos^4(\theta_{\alpha\gamma} + 5°)$	+12°54	—5°
		$1 - 1.68\cos^2(\theta_{\alpha\gamma} - 40°) + 1.68\cos^4(\theta_{\alpha\gamma} - 40°)$		+40°
3.35	—20°	$1 - 1.50\cos^2(\theta_{\alpha\gamma} - 30°) + 1.53\cos^4(\theta_{\alpha\gamma} - 30°)$	+22°48	+30°
3.35	—75°	$1 - 1.12\cos^2(\theta_{\alpha\gamma} - 40°) + 0.68\cos^4(\theta_{\alpha\gamma} - 40°)$	+29°42	+40°
5.10	—20°	$1 - 1.54\cos^2(\theta_{\alpha\gamma} - 19°) + 1.87\cos^4(\theta_{\alpha\gamma} - 19°)$	+20°42	+19°
5.10	—75°	$1 - 1.21\cos^2(\theta_{\alpha\gamma} - 40°) + 1.20\cos^4(\theta_{\alpha\gamma} - 40°)$	+27°52	+40°
		$1 + 1.14\cos^2(\theta_{\alpha\gamma} + 10°) - 1.26\cos^4(\theta_{\alpha\gamma} + 10°)$		—10°

4. Discussion

4.1. NEUTRON ANGULAR DISTRIBUTIONS

If the angular distribution of the neutron group n_1 with respect to the direction of incidence of the α-particle is given by some function $f(\theta_{\alpha n})$, then the counting rate in the first set of measurements would be proportional to $f(\theta_{\alpha n})\, g(\theta_{\alpha n}, \theta_{\alpha\gamma}, \phi)$, where $g(\theta, \theta, \phi)$ is the correlation function between neutrons and gammas†. Under the conditions chosen, the mean value of $\theta_{\alpha\gamma}$ and ϕ was kept at 90° independent of $\theta_{\alpha n}$, so that if $g(\theta, \theta, \phi)$ were independent of the neutron direction $\theta_{\alpha n}$ the measured correlation would be exactly equivalent to the neutron angular distribution (if the correlation function is isotropic, the equivalence is obvious and further the limitation on $\theta_{\alpha\gamma}$ is not required). However, if the nuclear reaction leading to the excited state is a mixture of different mechanisms, e.g. direct interaction and compound nucleus formation, then $g(\theta, \theta, \phi)$ would generally be expected to depend on $\theta_{\alpha n}$. Then only from a knowledge of this dependence could the angular distribution be calculated from the angular correlation.

We have made no attempt in the present measurements to find the detailed dependence of $g(\theta_{\alpha\gamma}, \theta_{\alpha n}, \phi)$ on $\theta_{\alpha n}$, apart from showing that there is a dependence, as this would take a great deal of effort without being fruitful, and since angular distributions can be measured by more straightforward methods. The deviation of our measurements from the true angular distributions can be estimated using

† More precisely the counting rate should be proportional to

$$f(\theta_{\alpha n}) \int_{\text{crystal}} g(\theta_{\alpha n}, \theta_{\alpha\gamma}, \phi)\mathrm{d}\omega / \int_{4\pi} g(\theta_{\alpha n}, \theta_{\alpha\gamma}, \phi)\mathrm{d}\omega$$

where in principle the integral over the solid angle of the crystal could also include a function of detection efficiency.

our limited knowledge of the dependence of g on $\theta_{\alpha n}$ and making the reasonable assumption that $g(\theta, \theta, \phi)$ should vary slowly with $\theta_{\alpha n}$. With these reservations, figs. 5 and 6 show the angular distributions of the neutrons measured at 3.35 and 5.10 MeV respectively. Angles are in the centre of mass system while the ordinates represent relative intensities. The experimental points have been corrected for the variation of efficiency of the neutron detector as a function of energy while the measured counts extracted from the neutron spectra were corrected for the uniform background due to random coincidences.

From the arguments given in the last paragraph it is clear that a straightforward measurement of the angular distribution of neutron groups would be useful for comparison with the results obtained by the (n, γ) coincidence method. Hence a pulsed-beam time-of-flight method was used to study this distribution. The results obtained at $E_\alpha = 3.35$ MeV are shown in fig. 12

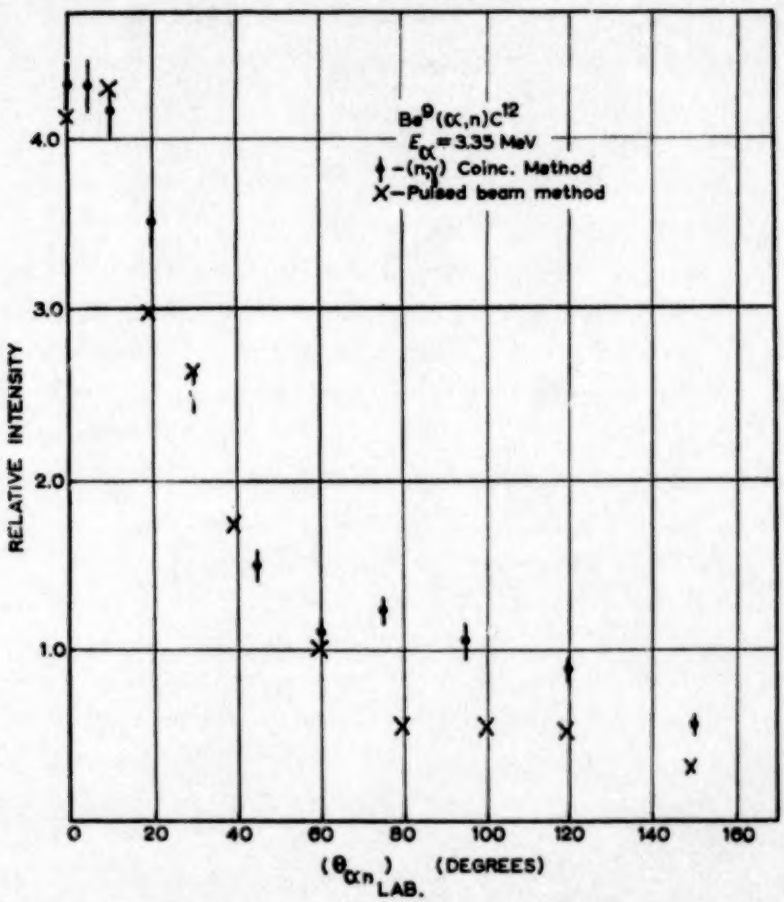

Fig. 12 Comparison of angular distribution of neutrons from $Be^9(\alpha, n)C^{12}$ for $E_\alpha = 3.35$ MeV obtained from (γ, n) coincidence method with that obtained from pulsed beam method.

and are compared with previous results of our measurements. As can be seen the two distributions are exactly alike in the forward direction with some difference in the magnitude of the contribution at large angles.

These angular distributions have been analysed in terms of Butler's direct interaction theory for a knock-on process, the broken curves in figs. 5 and 6 being the theoretical curves obtained from Butler's detailed formula[5]), taking into account the form factor.

As the Be^9 nucleus has spin $\frac{3}{2}$ and odd parity and the 4.43 MeV level of C^{12} has spin 2 and even parity, conservation of angular momentum and parity restricts the possible l-values of the captured particle which can contribute to this reaction to $l = 1$ or $l = 3$.

Although the forward peak in each case can be closely fitted with a curve with $l = 1$ a better fit to the experimental points over a larger angular range is obtained with a mixture of $l = 1$ and $l = 3$.

Although the addition of the $l = 3$ contribution gives a closer fit to the experimental points, this evidence alone does not justify its inclusion and the intensity at larger angles may equally be ascribed to compound nucleus formation. It is unusual for the theory of direct interactions to give a close fit to angular distributions over the full angular range, and the closeness of fit in this case is therefore not unreasonable.

It is seen that a rather large value of the radius is required to fit the experimental results by Buler's theory with a mixture of $l = 1$ and $l = 3$. In fact, a closer fit to the experimental points can be found for a mixture of $l = 0$ and $l = 2$, with a smaller value of the radius. However this would be inconsistent with the known parities of the Be^9 ground-state and the C^{12} first excited state. Difficulties of assigning parities from similar analysis have been experienced by other investigators, notably Silver[26]) on $Li^7(\alpha, \alpha')Li^7$ and Hinds *et al.*[27]) on Be^9 (He^3, p).

4.2. NEUTRON-GAMMA ANGULAR CORRELATIONS

It has been pointed out by Satchler[21]), Sherr[22]) and others that a test for distinguishing between the direct interaction and compound nucleus processes consists in the measurement of the angular correlation between the outgoing particle and the radiation emitted by the excited residual nucleus. Using plane waves to describe the initial and final states of incoming and outgoing particles, Satchler has shown that according to a surface interaction theory, the γ-ray angular correlation is symmetric about the momentum transfer direction, whereas in the case of compound nucleus formation in a definite state, the angular correlation does not have this symmetry axis. If the incoming particle is captured in an S state, the direction of the wave vector k_f of the outgoing particle becomes the symmetry axis, and if the outgoing particle is emitted from an S state, the direction of the wave vector k_i of the incident particle becomes the symmetry axis. When many levels are excited with random phase relationship among them, the γ-angular correlation tends to become isotropic.

Several experimental investigations of such correlations have shown the

validity of these predictions. Sherr and Hornyak[28]) measured the angular correlation of γ-rays from the 4.43 MeV level of C^{12} to the ground-state in coincidence with inelastically scattered protons at bombarding energies of 16.2 MeV. The angular correlation function was found to be of the expected form, but the symmetry axis only coincided approximately with the recoil direction.

However, this difficulty in the observed shift of symmetry axis was removed by Levinson and Bannerjee[29]) by taking into account the distortion of plane waves. They argued that plane waves are a poor description of the initial and final states of the nucleons and were able to show that the correlation is essentially unchanged in form from that predicted by plane waves but that distorted waves in general lead to a shift in the symmetry axis. Our measured correlations are all symmetrical over a 180° angular range, and in three cases the axis of symmetry is fairly close to the recoil axis. The departure from the axis of momentum transfer is not unexpected because of the shortcomings of the plane wave theory. The change in the correlation function both with incident energy and with angle of emission of the observed neutrons is remarkable.

This may indicate that the reaction mechanism is not a simple one and that either of the following mode-mixtures is occurring:

(1) a mixture of l-values of the captured particle,

(2) a mixture of mode (1) and compound nucleus,

(3) a mixture of (1) with different direct interaction mechanisms[30]).

In each case the relative amplitudes which appear in the theoretical expression for the correlation depend on θ_{an}. Hence the correlation function would be expected to vary with θ_{an} for this reason.

Attempts to analyse these results on a simple model have been unsuccessful. Considering an α-stripping process in which a He^3 particle is captured by the target, an angular momentum transfer of $l = 1$ is not compatible with the observation of a $\cos^4\theta$ term in the correlation function. While a mixture of $l = 1$ and $l = 3$ is consistent with the $\cos^4\theta$ term (the highest cosine power in the correlation being presumably limited by the E2 transition) there are too many unknowns to make an analytical fit of theory to experiment.

5. Conclusion

The purpose of this investigation was to examine the presence of a direct interaction mechanism at low energies in this particular reaction. The study of the angular distribution indicates the presence of a direct reaction mechanism. However, compound nucleus formation cannot be excluded completely from the angular distribution study alone.

The angular correlation experiments definitely show that compound nucleus

formation is not the dominant process as no angular correlation seems to be symmetric either about the incoming beam direction or the outgoing neutron direction. The angular correlation results definitely indicate the presence of some direct reaction processes, possibly a mixture of them, even at these low energies of incident particles.

Detailed analysis would be very complicated and in any case would require more experimental data.

We are grateful to Dr. L. J. B. Goldfarb and Dr. J. O. Newton for useful discussions and to Mr. J. Shelmerdine, T. Moore and J. Iliffe for help in running the Van de Graaff machine. One of us (J. B. G.) gratefully acknowledges the tenure of a Turner and Newall Post-Doctoral Fellowship at the University of Manchester.

References

1) S. T. Butler, Proc. Roy. Soc. A**208** (1951) 599
2) Bhatia, Huang, Huby and Newns, Phil. Mag. **43** (1952) 485
3) W. Tobocman, Phys. Rev. **94** (1954) 1655
4) Austern, Butler and McManus, Phys. Rev. **92** (1953) 350
5) S. T. Butler, Phys. Rev. **106** (1957) 272
6) N. Austern and S. T. Butler, Phys. Rev. **109** (1958) 1402
7) L. Madansky and G. E. Owen, Phys. Rev. **99** (1955) 1608
8) G. E. Owen and L. Madansky, Phys. Rev. **105** (1957) 1766
9) Hayakawa, Kawai and Kikuchi, Progr. Theor. Phys. Japan **13** (1955) 415
10) S. Yoshida, Proc. Phys. Soc. A**69** (1956) 668
11) G. F. Pieper and N. Y. Heydenburg, Phys. Rev. **111** (1958) 265
12) C. E. Hunting and N. S. Wall, Phys. Rev. **108** (1957) 901; **115** (1959) 956
13) G. E. Fisher and V. K. Fisher, Phys. Rev. **114** (1959) 533
14) Lackner, Dell and Hausman, Phys. Rev. **114** (1959) 560
15) B. Zeidman and J. L. Yntema, Nuclear Physics **12** (1959) 298
16) Ames, Owen and Swartz, Phys. Rev. **106** (1957) 775
17) B. Zeidman and J. M. Fowler, Phys. Rev. **112** (1958) 2020
18) James, Jones and Wilkinson, Phil. Mag. (8) **1** (1956) 949
19) N. W. Tanner, Proc. Phys. Soc. A**72** (1958) 457
20) Risser, Price and Class, Phys. Rev. **105** (1957) 1288
21) G. R. Satchler, Proc. Phys. Soc. A**68** (1955) 1037
22) R. Sherr, Proceedings of the University of Pittsburgh Conference on Nuclear Structure, 1957, edited by S. Meshkov (Univ. of Pittsburgh and office of Ordnance Research, U.S. Army, 1957, 361)
23) J. B. Garg, Nuclear Instruments **6** (1959) 72
24) J. E. Hardy, Rev. Sci. Instr. **29** (1958) 705
25) Bonner, Kraus, Marion and Schiffer, Phys. Rev. **102** (1956) 1348
26) R. Silver, Thesis, University of California, Radiation Laboratory, Berkeley (1957)
27) S. Hinds and R. Middleton, Proc. Phys. Soc. A**73** (1959) 721
28) R. Sherr and W. F. Hornyak, Bull. Am. Phys. Soc. **1** (1956) 197
29) C. A. Levinson and M. K. Banerjee, Ann. of Phys. **2** (1957) 471
30) Steve Edwards, Jr., Phys. Rev. **113** (1959) 1277

2.L *Nuclear Physics* **19** (1960) 280—298; © *North-Holland Publishing Co., Amsterdam*
Not to be reproduced by photoprint or microfilm without written permission from the publisher

ON THE THEORY OF p-α SCATTERING

A. HERZENBERG

The Physical Laboratories, The University, Manchester 13

and

E. J. SQUIRES†

A.E.R.E., Harwell, Didcot, Berks††

Received 17 February 1960

Abstract: The differential cross-section for p-α scattering at 40 and 95 MeV is calculated with simple gaussian internucleon potentials. Effects due to distortion of the α-particle and to the antisymmetry of the wavefunction are included and shown to be essential in fitting the qualitative features of the experimental cross-sections. The results suggest a resolution of difficulties which have been encountered in recent attempts to calculate nucleon-nucleus scattering from nucleon-nucleon phase shifts, by means of multiple incoherent scattering effects which occur when centre of mass motion is treated correctly.

1. Introduction

Recent advances in the determination of the nucleon-nucleon potential[1]) have been followed by an increased interest in the scattering of nucleons by light nuclei. In the theoretical studies of these processes[2]) certain approximations are made, and it is the purpose of this paper to discuss some of the effects which are usually neglected. In particular, we consider effects due to the antisymmetry of the incident and bound nucleons, incoherent multiple scattering, and (in a rather different context) distortion of the incident plane wave (i.e. deviation from Born approximation) and of the nuclear wavefunction. (The latter is usually referred to as a "polarisation" effect but we avoid this term owing to confusion with other uses of the word).

In this preliminary survey we are concerned with general features of the scattering, rather than with obtaining precise agreement with experiment; we shall therefore simplify the problem as much as is possible without eliminating the desired effects. We consider the particular case of proton-alpha scattering at 40 and 95 MeV, and we shall, at first, assume that we have only central non-singular potentials designed to give approximate agreement with the low energy nucleon-nucleon scattering data. The relation to a more realistic treatment in which the potentials contain a hard core is discussed in sections 5 and 6.

The plan of the paper is a follows. Section 2 contains an account of the basic

† Now at Cavendish Laboratory, Cambridge.

†† Part of this work is incorporated in the Ph.D. thesis of one of the authors (E.J.S.) presented at Manchester in 1956.

theory and the approximations used. The results are quoted in section 3 and compared with experiment. The various contributions to the scattering amplitude are discussed in more detail in section 4, with particular emphasis on the qualitative features. The effects of several of these contributions can be clearly seen in the differential cross-section. In section 5 we consider the modifications which must be introduced to take account of a hard core in the nucleon-nucleon potential. Finally, in section 6 we discuss the relevance of our results to other calculations. Section 6.1 deals with optical model calculations, and, in particular, we make it plausible that incoherent multiple scattering can account for much of the large discrepancy between the theoretical and phenomenological optical potentials. In section 6.2 calculations using the resonating group method[3]) are discussed, and we give reasons for believing that the nuclear distortion corrections to these calculations are larger than has previously been supposed. A summary of the conclusions is given in section 7.

2. Basic Theory

The elastic scattering cross-section for p-α scattering in the C. of M. system is given by

$$\frac{\mathrm{d}\sigma}{\mathrm{d}\Omega} = |\, T\,(\boldsymbol{k}, \boldsymbol{k}_0)\,|^2\,,$$

where $\hbar\boldsymbol{k}$ and $\hbar\boldsymbol{k}_0$ are the final and initial relative momenta; T can be written in the form

$$T(\boldsymbol{k}, \boldsymbol{k}_0) = \gamma \,\langle\, \boldsymbol{k}(5)\alpha(5)p(5)\Phi_0(1234) \,|\, \{\, PV(5) + V(5)P(E - H + i\varepsilon)^{-1}\, V(5)\,\} \,|\, \boldsymbol{k}_0(5)\alpha_0(5)p(5)\,\Phi_0(1234)\,\rangle\,. \tag{2.1}$$

Here, $\gamma = 4\pi^2\mu/\hbar^2$, the quantity μ ($= \frac{4}{5}$ proton mass) being the reduced mass; $\Phi_0(1234)$ is the properly antisymmetric ground state of the α-particle made up of nucleons 1, 2, 3 and 4; $|\, \boldsymbol{k}_0 \,\rangle$ and $|\, \boldsymbol{k} \,\rangle$ are plane waves representing the incident and final relative momentum states; $|\, \alpha_0 \,\rangle$ and $|\, \alpha \,\rangle$ are initial and final proton spin states; $|\, p >$ is the isobaric spin state representing a proton; H is the total hamiltonian; $V(5) = \sum_{i=1}^{4} V_{5i}$, where V_{ij} is the interaction potential between nucleons i and j; and P is the antisymmetrising operator given by $P = 1 - \sum_{i=1}^{4} P_{5i}$, where P_{ij} exchanges all the co-ordinates of nucleons i and j.

Eq. (2.1) is exact. We denote the contribution of the first term between the braces { } by T_1, and that of the second by T_2. Then T_1 is the first Born approximation, and T_2 gives the contribution of distortion of the incident wave and of the α-particle due to the interaction $V(5)$. For T_1 it is convenient to write

$$T_1 = T_{1D} + T_{1E} + T_{1TE} + T_{1C}\,, \tag{2.2}$$

where

$$T_{1D} = 4\gamma \,\langle\, \Phi_0(1234)\boldsymbol{k}(5)\alpha(5)p(5) \,|\, V_{51} \,|\, p(5)\alpha_0(5)\boldsymbol{k}_0(5)\,\Phi_0(1234)\,\rangle\,, \tag{2.3a}$$

$$T_{1E} = -4\gamma \langle \Phi_0(5234)k(1)\alpha(1)p(1) \mid V_{51} \mid p(5)\alpha_0(5)k_0(5)\, \Phi_0(1234) \rangle , \quad (2.3b)$$

$$T_{1TE} = -12\,\gamma \langle \Phi_0(1534)k(2)\alpha(2)p(2) \mid V_{51} \mid p(5)\alpha_0(5)k_0(5)\, \Phi_0(1234) \rangle . \quad (2.3c)$$

We shall make the convention that the factors V_{51} in eqs. (2.3) are to contain only the potential of the nuclear forces, as distinct from the Coulomb forces. The first three terms in eq. (2.2) are called[2]) "direct" (eq. (2.3a)), "exchange" (eq. (2.3b)) and "target exchange" (eq. (2.3c)). The direct term T_{1D} represents scattering of the proton 5 from the potential $\langle \Phi_0(1234) \mid V(5) \mid \Phi_0(1234) \rangle$; it gives a forward peak. The exchange term T_{1E} represents a knock-on process in which the incident nucleon knocks on one of the nucleons in the α-particle and takes its place. The target exchange term T_{1TE} represents a pick-up process in which the incident nucleon picks up three of those in the α-particle, the fourth being left behind. The term T_{1E} gives a forward peak, and T_{1TE} a backward peak in the C. of M. system. The term T_{1C} in T_1 is due to the Coulomb potential; it contains three parts analogous to eqs. (2.3), but with the nuclear potential V_{51} replaced by the corresponding Coulomb interaction. We shall keep only the direct Coulomb term, because the exchange parts will be much smaller by analogy with the nuclear terms (see section 4).

To calculate T_2 we make two approximations. First, the exchange contributions to T_2 will be ignored. By analogy with the first order exchange terms (see section 4) these are expected to be small. Secondly, we put

$$\frac{1}{E - H + i\varepsilon} V(5) \to \sum_i \frac{1}{E_i - K + i\varepsilon} V(5) \mid \chi_i \rangle \langle \chi_i \mid , \quad (2.4)$$

where K is the kinetic energy operator for the five nucleons and $\mid \chi_i \rangle$ are its eigenstates (i.e. products of plane waves) such that

$$K \mid \chi_i \rangle = E_i \mid \chi_i \rangle . \quad (2.5)$$

Two things are involved in this approximation: (i) the dropping of $V(5)$ from the denominator means that we are only calculating T up to second order Born approximation, and (ii) we are using the "impulse approximation"[4]) to treat the propagation of the struck nucleons in the nucleus. These approximations should be adequate for our purposes in this paper.

For the α-particle wavefunction we have used the approximate form

$$\Phi_0(1234) = (4\alpha/\pi)^{\frac{3}{4}} \exp\left(-\tfrac{1}{4}\alpha \sum_{i,j=1}^{4} r_{ij}^2\right) D(1234) , \quad (2.5)$$

where r_{ij} is the distance between nucleons i and j, and D is a Slater determinant of spin and isobaric spin states of the 4 nucleons. The parameter α is adjusted to fit the r.m.s. radius r_α of the α-particle found from electron scattering[13]), i.e. we take

$$r_\alpha = (9/32\alpha)^{\frac{1}{2}} = (1.42 \pm 0.14) \times 10^{-13} \text{ cm}. \quad (2.6)$$

A small correction for the finite extent of the charge distribution of the proton has been made here. The spin dependence of the wavefunction (eq. (2.5)) is what one would get for purely central forces; this approximation should be acceptable because the D-state probability of the α-particle arising from tensor forces has been estimated to be only a few per cent[14]). Eq. (2.5) corresponds to a simple shell model with the centre of mass treated correctly.

For the nuclear potential we take

$$V_{ij} = -f(r_{ij})\,(V_0 + V_\sigma \boldsymbol{\sigma}_i\cdot\boldsymbol{\sigma}_j + V_\tau \boldsymbol{\tau}_i\cdot\boldsymbol{\tau}_j + V_{\sigma\tau}\boldsymbol{\sigma}_i\cdot\boldsymbol{\sigma}_j\boldsymbol{\tau}_i\cdot\boldsymbol{\tau}_j)\,, \tag{2.7}$$

with

$$f(r_{ij}) = \exp(-\beta r_{ij}^2)\,, \quad \beta = 0.37 \times 10^{26}\,\mathrm{cm}^{-2}\,, \tag{2.8a}$$

the other constants being adjusted to give a singlet-even strength

$$V_0 - 3V_\sigma + V_\tau - V_{\sigma\tau} = 37\ \mathrm{MeV}\,, \tag{2.8b}$$

and a triplet-even strength

$$V_0 + V_\sigma - 3V_\tau - 3V_{\sigma\tau} = 62\ \mathrm{MeV}\,. \tag{2.8c}$$

These parameters reproduce the experimental values of the singlet scattering length and effective range, and the triplet scattering length. Since the odd parity potentials have not been specified, we shall restrict the factor

$$(V_0 + V_\sigma \boldsymbol{\sigma}_i\cdot\boldsymbol{\sigma}_j + V_\tau \boldsymbol{\tau}_i\cdot\boldsymbol{\tau}_j + V_{\sigma\tau}\boldsymbol{\sigma}_i\cdot\boldsymbol{\sigma}_j\boldsymbol{\tau}_i\cdot\boldsymbol{\tau}_j)$$

in the potential to two possible forms:
the "modified Serber" potential

$$\tfrac{1}{2}(1 + aP_{x\,ij})\,(A + B\boldsymbol{\sigma}_i\cdot\boldsymbol{\sigma}_j)\,, \tag{2.9a}$$

and the "symmetric" potential

$$\boldsymbol{\tau}_i\cdot\boldsymbol{\tau}_j\,(A + B\,\boldsymbol{\sigma}_i\cdot\boldsymbol{\sigma}_j)\,. \tag{2.9b}$$

The symmetric potential has been chosen as an example of a potential which does not contain a direct force (i.e. has $V_0 = 0$), while the modified Serber one has a non-zero value of V_0, its strength being determined by the parameter a.

3. Comparison with Experiment

A detailed discussion of the properties of the different terms in T is given in the next section. Here we shall quote the results of the calculation and compare them with the experiments. These results are for the complete calculation with $T = T_1 + T_2$, making use of approximations (2.4) and (2.5).

The experimental values of $\mathrm{d}\sigma/\mathrm{d}\Omega$ for incident protons of energy 40 and

95 MeV are given by the points in fig. 1. The results of the calculation with the symmetric and Serber potentials are given by the curves. The parameter a in the Serber potential (e.g. eq. (2.9a)) has been adjusted so as to give the best possible fit. It will be seen that, although the calculated curves show an

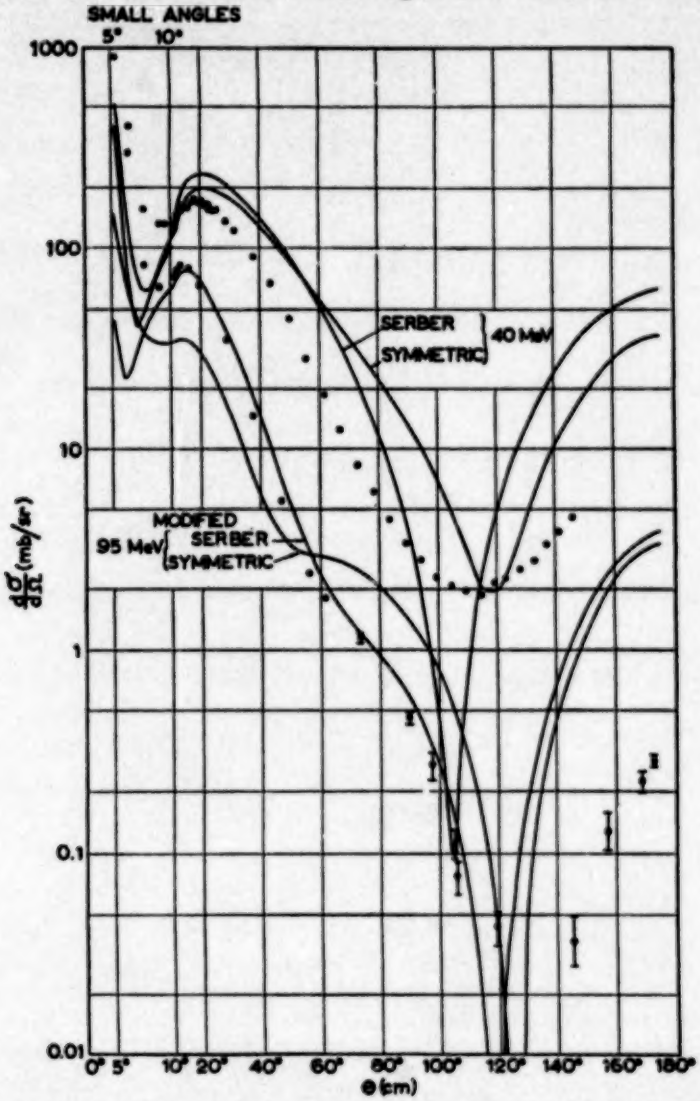

Fig. 1. Experimental and calculated values of $d\sigma/d\Omega$. The experimental points are taken from refs. [5,6]). The theoretical curves are calculated with the symmetric potential (2.9b) and with the modified Serber potential (2.9a) with $a = 1.8$.

appreciable deviation from the experimental ones at most places, the theory accounts for all the qualitative features. It gives the general drop in $d\sigma/d\Omega$ from 40 to 95 MeV, and the predominant forward peak followed by a deep minimum and a small rise in the backward direction. There is also a small kink in the 95 MeV curve, corresponding to that found experimentally, at about 60°.

The very good agreement between theory and experiment at 95 MeV from 10° to 100° is probably fortuitous, arising from an underestimate of Im T and an overestimate of Re T. This is suggested by the Coulomb interference region, if one

bears in mind that the Coulomb contribution to the scattering amplitude is real. (The slow shift of the phase of the wave of the incident proton as it traverses the atom does not matter because it affects the Coulomb and nuclear scattering amplitudes equally except at scattering angles less than about 1°.) The fact that the calculated $d\sigma/d\Omega$ is too small by about a factor 3 at the Coulomb minimum shows that Im T is too small by a factor $\sqrt{3} = 1.7$, whereas the position of the calculated Coulomb minimum at 95 MeV, at 6° instead of at 9° as found experimentally, shows that the nuclear part of Re T is too large by a factor $(\frac{9}{6})^2 \approx 2.3$. (This argument assumes the nuclear part of T to be nearly constant in the Coulomb interference region, and the calculations show this to be nearly true.) In view of the discrepancies, the value of a which we have obtained from the best fit is very uncertain.

4. The Effect of the Different Terms in T

In this section we shall discuss the terms in $T(\boldsymbol{k}, \boldsymbol{k}_0)$ one by one.

4.1. T_{1D}

One finds

$$T_{1D} = -4V_0\gamma\,(2\pi^{\frac{1}{2}}\beta^{\frac{1}{2}})^{-3} \exp\left[-\left(\frac{3}{64\alpha} + \frac{1}{4\beta}\right) |\,\boldsymbol{k}_0 - \boldsymbol{k}\,|^2\right]. \qquad (4.1)$$

This gives a forward peak, the value of T_{1D} being down to e^{-1} of the maximum at a scattering angle given by

$$k_0\theta \approx \sqrt{6}\left(\frac{3}{2\beta} + r_a^2\right)^{-\frac{1}{2}}. \qquad (4.2)$$

The width of this peak is thus determined not by $r_a = 1.4 \times 10^{-13}$ cm, but by $(r_a^2 + \frac{3}{2}\beta)^{\frac{1}{2}} = 2.5 \times 10^{-13}$ cm, the difference being due to the extension of the nuclear force field beyond the mass-distribution.

The term T_{1D} is proportional to V_0 and independent of V_σ, V_τ and $V_{\sigma\tau}$. This is due to the fact that the α-particle has spin and isobaric spin zero. If one considered tensor forces and spin orbit forces, there would be small contributions to T_{1D} from spin-dependent terms in the potential due to the presence of P and D states in Φ_0, but terms containing the isobaric spin of the α-particle nucleons would still not contribute. The proportionality to V_0 constitutes the reason for our choice of the two potentials in eq. (2.9). The fact that the symmetric potential gives $T_{1D} = 0$ implies that for this case, the fringe of the nuclear force field extending outside the α-particle's mass distribution does not contribute to T in first order. This, however, ceases to be true in higher orders which take distortion of the α-particle into account.

The value of T_{1D} at $\theta = 0$ is independent of the energy. We shall see later that there is a substantial contribution to the observed forward peak also

from T_2, but this falls off with energy. To get the correct energy variation, a substantial contribution from T_2 is needed. The calculated values of T_{1D} are shown in fig. 2.

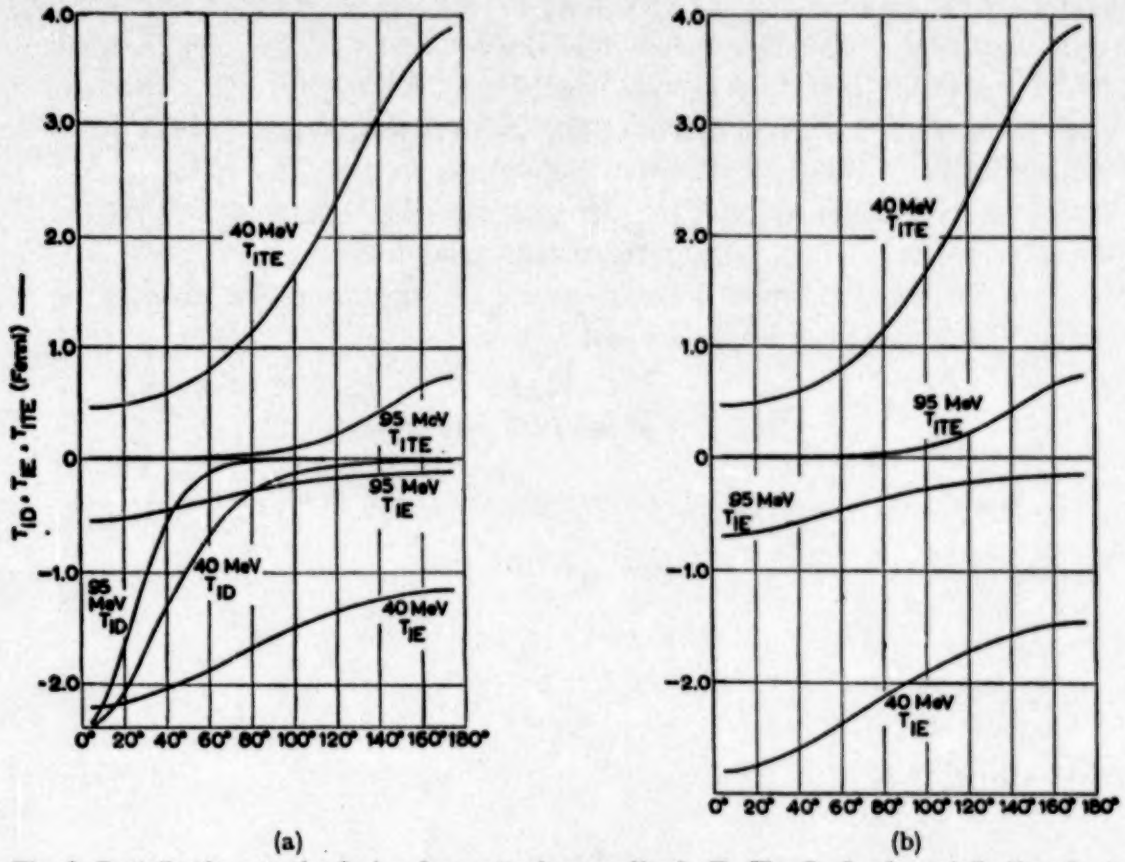

Fig. 2. Contributions to the first order scattering amplitude T_1. The Coulomb contribution T_{1c} is not shown. (a) Modified Serber potential with $a = 1.8$. (b) Symmetric potential.

4.2. T_{1E} AND T_{1TE}

One finds

$$T_{1E} = \gamma\,[4V_0 - \{\,3V_0 - 3(V_\sigma + V_\tau + 3V_{\sigma\tau})\,\}\,] \frac{\exp\left[-\frac{3}{64\alpha}\,|\,k_0 - k\,|^2 - \frac{25}{64(3\alpha+4\beta)}\,|\,k_0 + k\,|^2\right]}{\left[2\pi^{\frac{1}{2}}\left(\frac{3\alpha}{4}+\beta\right)^{\frac{1}{2}}\right]^3}, \quad (4.3)$$

$$T_{1TE} = \gamma\,[3V_0 - 3(V_\sigma + V_\tau + 3V_{\sigma\tau})\,] \frac{\exp\left[-\frac{(2\alpha+\beta)}{64\alpha(6\alpha+5\beta)}\,(9\,|\,k_0 - k\,|^2 + 25\,|\,k_0 + k\,|^2)\right]}{\left[2\pi^{\frac{1}{2}}\left(\frac{3\alpha}{4}+\frac{5\beta}{8}\right)^{\frac{1}{2}}\right]^3}. \quad (4.4)$$

The values of these expressions are given in fig. 2.

In the coefficients in eq. (4.3) and eq. (4.4) the expression $[3V_0 - 3(V_\sigma +$

$V_t + 3V_{\sigma\tau})]$ is proportional to the mean of the singlet-even and triplet-even strengths, whereas the term $4V_0$ in eq. (4.3) is relatively small, even for the biggest value of V_0 one might consider. It follows that T_{1E} and T_{1TE} have coefficients of the same order of magnitude, but of opposite sign, irrespective of how one chooses the central two-body potential. This is important because at large angles T_{1E} and T_{1TE} predominate and therefore their opposite signs leads to the minima observed in the 40 and 95 MeV data at 110° and 135° respectively. Beyond the minimum, the experimentally observed tail is due to T_{1TE}.

The exchange terms are strongly energy dependent. This follows already from eq. (2.3). Since the range of the nuclear forces is roughly equal to the radius of the α-particle, one can, to a very rough approximation, replace the factors V_{s1} in eqs. (2.3b) and (2.3c) by a constant. T_{1E} and T_{1TE} then reduce to the square of the Fourier transform of Φ_0 with respect to exp $(i\boldsymbol{k}\cdot\boldsymbol{x})$, and therefore fall off rapidly when the momentum of the incident proton in the CM frame exceeds the value $\hbar/r_\alpha$ corresponding to the internal momentum distribution in the α-particle. This occurs at an incident energy of about 30 MeV. The process can be seen qualitatively in fig. 3, where we have plotted

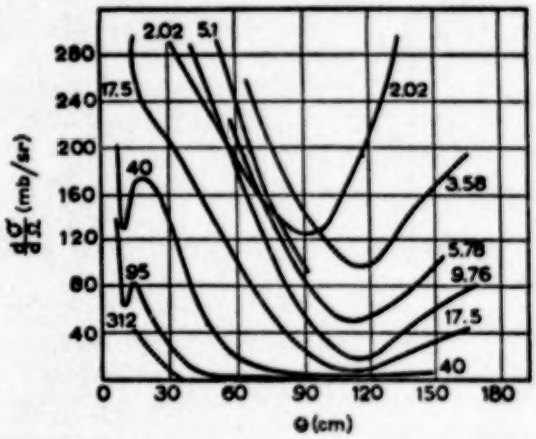

Fig. 3. Variation of $d\sigma/d\Omega$ with energy. (The numbers labelling the curves give the energy). The figure is taken from ref. [7]), except for the curves at 40 and 95 MeV, which are taken from refs. [5,6]).

the experimental values of $d\sigma/d\Omega$ for a range of energies. The backward peak, due to T_{1TE} is seen to disappear almost completely between 17.5 and 40 MeV (this argument is of course very crude because the Born approximation is very poor at low energies).

4.3. T_2

It is convenient to divide T_2 into two terms such that

$$T_2 = T_2^{(ii)} + T_2^{(ij)}, \tag{4.5}$$

where

$$T_2^{(ii)} = 4\gamma \langle \ldots | V_{s1} \ldots V_{s1} | \ldots \rangle, \tag{4.6}$$

$$T_2^{(ij)} = 12\gamma \langle \ldots | V_{s1} \ldots V_{s2} | \ldots \rangle , \tag{4.7}$$

the meaning of the dots being clear from eq. (2.1).

The values of $T_2^{(ii)}$ and $T_2^{(ij)}$ are shown in fig. 4. It turns out that $T_2^{(ii)}$ is proportional to $(V_0^2 + 3V_\sigma^2 + 3V_\tau^2 + 9V_{\sigma\tau}^2)$ and $T_2^{(ij)}$ to $(3V_0^2 - 3V_\sigma^2 - 3V_\tau^2 - 9V_{\sigma\tau}^2)$.

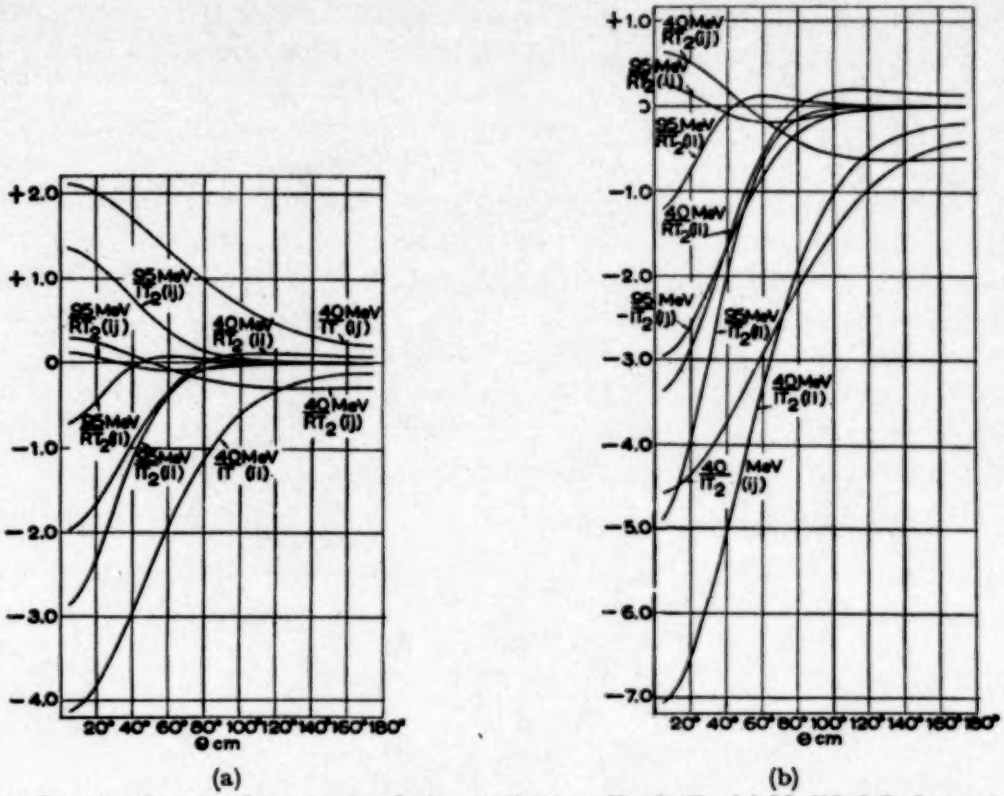

(a) (b)

Fig. 4. Contributions to the second order scattering amplitude T_2. (a) Modified Serber potential with $a = 1.8$. (b) Symmetric potential.

In T_2 one has the effect of the distortion of the α-particle by the interaction with the incident nucleon. This acts in two ways. Firstly, it causes the α-particle nucleons to be pulled towards or pushed away from the incident nucleon in a way depending on the relative orientation of the spins. Consequently, the $\boldsymbol{\sigma}_i \cdot \boldsymbol{\sigma}_j$ and $\boldsymbol{\tau}_i \cdot \boldsymbol{\tau}_j$ terms in the nucleon potential now contribute to the interaction, and the fringing field of the α-particle has an important effect even if $V_0 = 0$. Secondly, the V_0 part of the potential distorts the α-particle into a spheroid, and also distorts the wave function of the p-α relative motion. These two mechanisms give, respectively, the terms proportional to $(V_\sigma^2 + V_\tau^2 + 3V_{\sigma\tau}^2)$ and V_0^2 in T_2; they represent Van-der-Waals effects which are independent of the sign of the force acting. The presence of the first effect means that, even for $V_0 = 0$, a sharp forward peaking occurs. The V_0^2 effect is, of course, present only in the Serber potential. The relative importance of the two distortion mechanisms is indicated by the numbers in table 1.

Since we find the best fit with $a \approx 2$, it appears that the effect of the spheroidal distortion is insignificant in comparison with the effect of distortion due to space-spin correlation.

TABLE 1

The ratios of the contributions of spin-space correlation and spheroidal distortion to T_3

Term	Ratio	Serber ($a = 1$)	Modified Serber ($a = 2$)	Symmetric
$T_2^{(1)}$	$\frac{3V_\sigma^2 + 3V_\tau^2 + 9V_{\sigma\tau}^2}{V_0^2}$	1.9	31	∞
$T_2^{(2)}$	$\frac{3V_\sigma^2 + 3V_\tau^2 + 9V_{\sigma\tau}^2}{3V_0^2}$	0.6	10.3	∞

More insight into the distortion mechanism may be gained by calculating T_2 not with the "free particle" approximation (eq. (2.4)), but by introducing a fixed mean excitation energy ΔE for the α-particle in intermediate states. This amounts to replacing the energy denominator in T_2

$$E - H + i\varepsilon \equiv [E_0 - K(5) + V(5)] + (E_\alpha - H_\alpha) + i\varepsilon$$

by

$$[E_0 - K(5)] - \Delta E + i\varepsilon\,.$$

Here E_0 is the energy of the incident proton, $K(5)$ its kinetic energy operator, E_α the energy of the α-particle in the ground state and H_α its internal Hamiltonian. Besides introducing ΔE, we have dropped $V(5)$. The results of a calculation of T_2 with a fixed ΔE are given in table 2.

TABLE 2

Comparison of values of T_2 calculated with a fixed α-particle excitation energy ΔE and with the impulse approximation (eq. 2.4))

Angle	0°	10°	20°	30°	40°
$\Delta E = 20$ MeV	$-0.8 - 1.6i$	$-0.8 - 1.5i$	$-0.5 - 1.2i$	$-0.4 - 0.8i$	$-0.2 - 0.5i$
$\Delta E = 40$ MeV	$-1.4 - 1.3i$	$-1.4 - 1.3i$	$-1.1 - 1.1i$	$-0.8 - 0.8i$	$-0.5 - 0.6i$
Using eq. (2.4)	$-0.9 - 1.6i$	$-0.8 - 1.5i$	$-0.7 - 1.1i$	$-0.5 - 0.8i$	$-0.2 - 0.5i$

These values are for an α-particle radius given by $r_\alpha = 1.55 \times 10^{-13}$ cm and for the symmetrical potential. T is in units of 10^{-13} cm. These figures were calculated for $E_0 = 70$ MeV.

It appears that $\Delta E \approx 30$ MeV gives results not greatly different from those obtained with the free particle approximation (eq. (2.4)). This value is of the

order one would expect from the distortion picture, since the space-spin correlation requires the excitation of one nucleon from the 1s to the 1p state in the sense of the single particle model, whereas the spheroidal distortion implies the excitation of one nucleon into the 1d state.

The contribution T_2 turns out to be of the same order of magnitude as T_1. Both $T_2^{(ii)}$ and $T_2^{(ij)}$ have appreciable imaginary parts which are peaked in the forward direction, and have opposite signs unless V_0 is improbably large. Moreover,

$$| \operatorname{Im} T_2^{(ii)}(\theta = 0) | > | \operatorname{Im} T_2^{(ij)}(\theta = 0) | ,$$

while Im $T_2^{(ii)}$ is more narrowly peaked than Im $T_2^{(ij)}$, so that Im T_2 has a zero which shows up as a kink in the differential cross section at 95 MeV at about 55°. This kink is too weak to show at 40 MeV.

The compensation between the calculated values of Im $T_2^{(ii)}$ and Im $T_2^{(ij)}$ in the forward direction is somewhat too large, leading to the low calculated value of the differential cross-section at the Coulomb minimum, as previously pointed out.

4.4. THE QUANTITATIVE IMPORTANCE OF DISTORTION

To give a quantitative estimate of the effect of distortion of the incident wave we have calculated the scattering in first and second order (i.e. T_1 and $T_1 + T_2$) with the α-particle constrained to be in the ground state throughout.

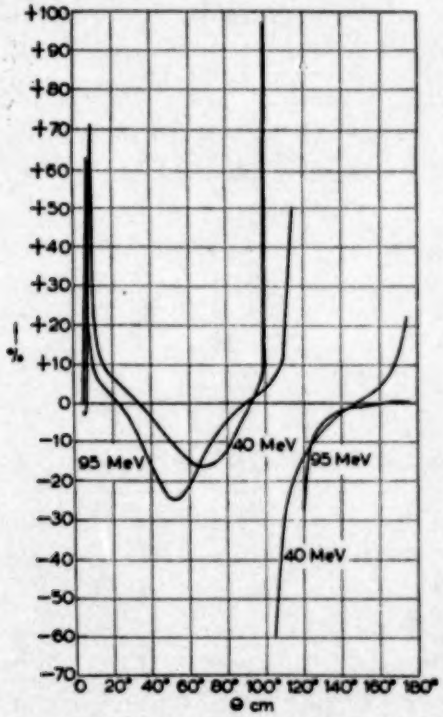

Fig. 5. Effect of distortion of the wave function of the incident nucleon. The curves give the ratio $\{(d\sigma/d\Omega)_1 - (d\sigma/d\Omega)_{\text{no dist.}}\}/(d\sigma/d\Omega)_{\text{no dist.}}$, where $(d\sigma/d\Omega)_1$ is calculated from T_1 alone and $(d\sigma/d\Omega)_{\text{no dist.}}$ from $T_1 + T_2$ with the α-particle constrained to the ground state. The potential used is the modified Serber with $a = 1.8$.

The results of this calculation are shown in fig. 5 for a Serber potential with $a = 1.8$ (i.e. $V_0 = 8$ MeV). Fig. 5 shows that the effect of distortion of the incident wave is small except near the minima of the differential cross-section. For example, at the maximum following the Coulomb dip, distortion of the incident wave raises the differential cross-section by about 4 % at 95 MeV.

The importance of distortion of the α-particle can be seen by comparing T_2 calculated as in section 2 with the corresponding values calculated when the α-particle is constrained to remain in its ground state. The result of this calculation is shown in fig. 6. We see that this distortion is much more important

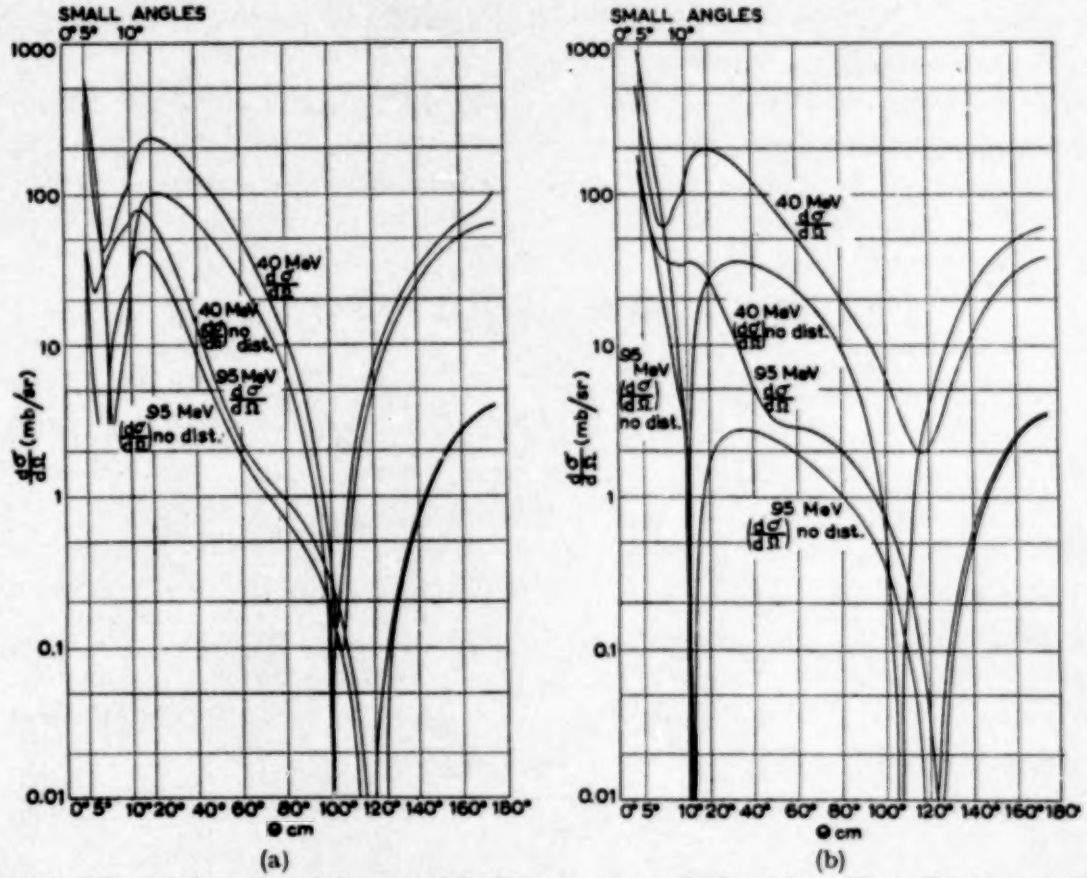

Fig. 6. Effect of distortion of the α-particle. The curves are calculated from $(T_1 + T_2)$, that marked $d\sigma/d\Omega$ using the impulse approximation for the intermediate states, while that marked $(d\sigma/d\Omega)_{\text{no dist.}}$ has the α-particle constrained to the ground state. (a) Modified Serber potential with $a = 1.8$. (b) Symmetric potential.

than that of the incident wave, since its neglect raises the differential cross-section by about a factor 2 just beyond the Coulomb dip. Moreover, if this distortion is neglected the negative factor $(3V_0^2 - 3V_\sigma^2 - 3V_\tau^2 - 9V_{\sigma\tau}^2)$ in $T_2^{(ij)}$ becomes replaced by the positive quantity $3V_0^2$, so that there is no longer destructive interference between Im $T_2^{(ii)}$ and Im $T_2^{(ij)}$ and the kink almost disappears. The very shallow dip which remains is due partly to T_{1E}, which has a wider forward peak than T_{1D} and Re T_{2D}, and partly to a slight diffraction effect due to the interference of T_{1D} and Re T_{2D}.

4.5. SUMMARY OF SECTION 4

We can now see which effects have to be taken into account to reproduce the qualitative features of the experimental points in fig. 1. The forward peak comes partly from T_{1D}, and partly from the α-particle distortion in T_2. The first shows too little energy variation (see fig. 6) and the second too much (see the symmetric potential curves in fig. 1); we find that we get about the right energy variation for $a \approx 2$. This also gives about the right values of $d\sigma/d\Omega$, whereas a reduction of a, i.e. of the fraction of space exchange force, makes the cross-section too high. (For example, $a = 1$ gives a post-Coulomb maximum of 321 mb/sr at 95 MeV (experimentally 82 mb/sr), and 622 mb/sr at 40 MeV (experimentally 170 mb/sr).

The backward peak comes from T_{1TE}, and the deep minimum preceding it requires the correct phase relation between this and T_{1E}. Lastly, the kink in the 95 MeV curve at 55° again requires the distortion of the α-particle in intermediate states.

5. The Effect of a Hard Core in the Nuclear Potential

It is generally accepted that the nuclear potential is not of the simple form used above[1]), but contains a strongly repulsive core of radius about 0.4×10^{-13} cm. In this section we indicate how the proton-alpha scattering problem would have to be formulated to take these repulsive cores into account, and consider how far our previous results are relevant. We then give a simple argument which suggests that the tail of the nuclear potential gives the principal effects in this problem—at least for forward angles.

When the potential contains a strongly repulsive core the Born approximation cannot be used, and it is therefore convenient[2]) to introduce the two-body scattering matrix t by an equation of the form†

$$t_{15} = V_{15} + V_{15}\,(E - H_0 + i\varepsilon)^{-1}\,t_{15}\,, \tag{5.1}$$

where it is understood that this is correctly antisymmetrised between particles 1 and 5, and where $H_0 = H_a + K(5) = H - V(5)$. The impulse approximation implies replacing this t matrix by the free nucleon-nucleon scattering matrix

† There are possible modifications to this definition of t, which, of course, have a corresponding effect on the series for T. For example, when using the optical model (see section 6.1) it may be convenient, to avoid $1/A$ difficulties (where A is the number of nucleons in the nucleus), to restrict the intermediate states to be those which are unoccupied in the nuclear ground state (considered in first approximation as a shell model). Kerman, McManus and Thaler[9]) go further than this and demand that when the right hand side of eq. (5.1) operates on an antisymmetric state of all nucleons, the intermediate states should also be antisymmetric. This makes the identification of their t matrix with the free scattering matrix unreasonable. It is only when the corrections to this are combined with the terms of the expansion corresponding to eq. (5.2) that one obtains a series which has a reasonable chance of being rapidly convergent.

which can, in principle, be obtained directly from nucleon-nucleon scattering experiments.

If we neglect target exchange terms the p-α transition operator can be expanded in powers of t. This expansion differs from that in V (see eq. (2.1)), since now successive interactions must not be with the same nucleon. Thus, up to second order we have

$$T(t) = \sum_{i=1}^{4} t_{5i} + \sum_{\substack{i,j=1 \\ i \neq 1}}^{4} t_{5i} (E - H_0 + i\varepsilon)^{-1} t_{5j} \tag{5.2a}$$

$$\equiv T_1(t) + T_2(t) . \tag{5.2b}$$

We use the notation $T(t)$ to distinguish the T in eq. (5.2) from that in eq. (2.1). This operator must be taken between states which are not antisymmetrised. We have not found a suitable formulation of the problem in this form which takes complete account of antisymmetry and of centre of mass motion, and we cannot therefore include the target exchange terms in this formulation. However, target exchange contributes mainly in the backward direction and may probably be ignored for forward angles.

We see that $T_1(t)$ is the analogue of $T_1 + T_2^{(ii)}$ in the previous treatment, while $T_2(t)$ is the analogue of $T_2^{(ij)}$. The operator $T(t)$ will thus contain all the qualitative features necessary to produce agreement with experiment as before. For example, the kink in the 95 MeV cross-section at 55° will still arise from a zero in Im T due to interference between Im $T_1(t)$ and Im $T_2(t)$ in the following way. In the forward direction Im $T(t)$ must be negative (from the theorem which relates it to the total cross-section) whereas Im $T_2(t)$ will be positive provided that the spin and isobaric spin independent part of t is not too large (this follows in the same way as the sign of $T_2^{(ij)}$. It follows that Im $T_1(t)$ is negative at $\theta = 0$. However, the angular spread of Im $T_1(t)$ is smaller than that of Im $T_2(t)$, since the first comes from single and the second from double scattering, so that somewhere the two must cancel.

We next give an argument which suggests that the repulsive cores are in fact not important in this problem. The idea is that the angular width of the forward diffraction peak is a measure of the radius of an effective potential seen by the incident nucleon, and that this radius is so much larger than the radius of the α-particle's mass distribution, that the long range part of the nucleon-nucleon potential must be of predominant importance.

We represent the nucleon-alpha interaction (in the rest of this section only!) by a potential $V_{p\alpha} \propto \exp [-3r^2/2r_{p\alpha}^2]$, where r is the distance of the incident nucleon from the mass-centre of the alpha particle, and

$$r_{p\alpha}^2 \equiv \frac{\int \mathrm{d}r\, r^2 V_{p\alpha}(r)}{\int \mathrm{d}r\, V_{p\alpha}(r)} .$$

We take $r_{p\alpha}^2 = r_\alpha^2 + r_V^2$, where

$$r_V^2 \equiv \frac{\int \mathrm{d}r\, r^2 V_{ij}(r)}{\int \mathrm{d}r\, V_{ij}(r)},$$

V_{ij} being the nucleon-nucleon potential as before. One then gets

$$\frac{\mathrm{d}\sigma}{\mathrm{d}\Omega} \propto \mathrm{e}^{-\theta^2/\theta_0^2}$$

in the first Born approximation and omitting the Coulomb interaction. Here, $1/\theta_0^2 = \frac{1}{3}k_0^2(r_\alpha^2 + r_V^2)$. We have made the approximation $2\sin\frac{1}{2}\theta \to \theta$, which involves an error of 5 % at $\theta = 60°$. To test this relation, and to determine θ_0,

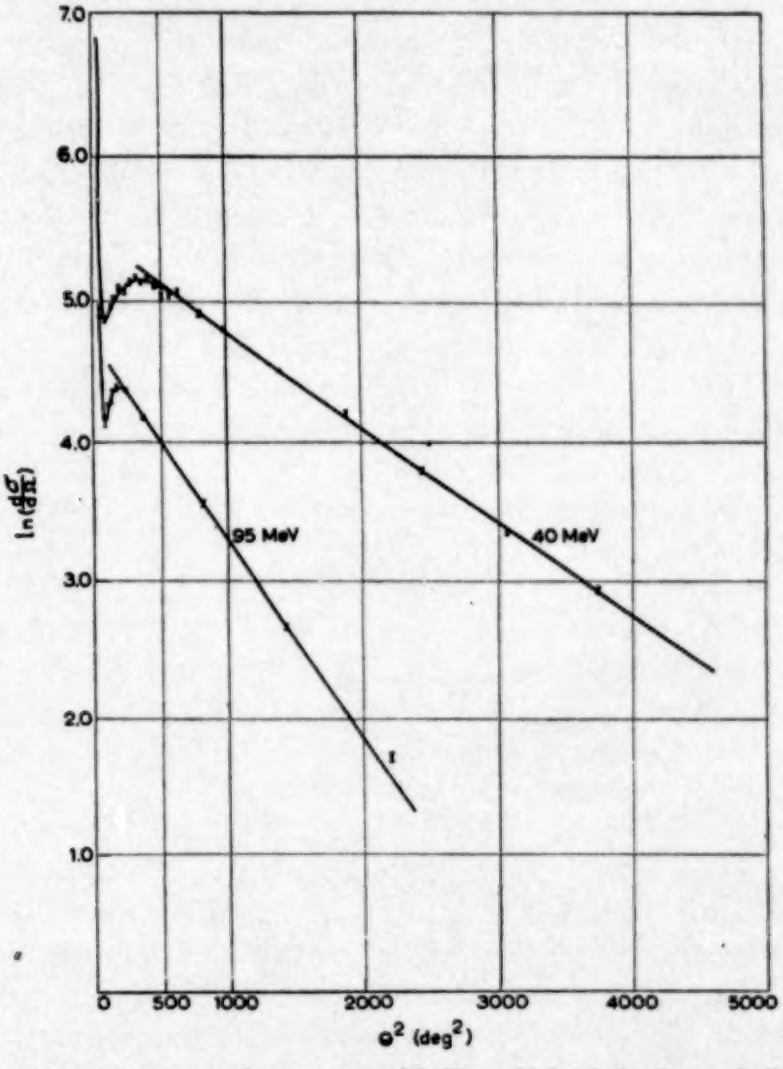

Fig. 7. Radius of the effective nucleon-α potential. The width of the forward diffraction peak gives the radius (see section 5).

we have plotted $\ln(\mathrm{d}\sigma/\mathrm{d}\Omega)$ against θ^2 in fig. 7. A linear relation is seen to hold from just beyond the Coulomb interference region out to angles where $\mathrm{d}\sigma/\mathrm{d}\Omega$ has fallen to a few per cent of the maximum attained just after the Coulomb

TABLE 3

Radius of the nucleon-nucleon potential required to give the correct width of the forward diffraction peak in nucleon -α scattering

E_{lab} (MeV)	θ_0	$k_0\theta_0$ (cm^{-1})	$r_V = \left(\frac{3}{k_0^2\theta_0^2} - r_\alpha^2\right)^{\frac{1}{2}}$ (cm)
40	0.68	0.75×10^{13}	$(1.7 \pm 0.2) \times 10^{-13}$ (average)
95	0.46	0.79×10^{13}	

dip. From fig. 7 one obtains the results given in table 3.

The error in r_V contains equal contributions from r_α and from $k_0\theta_0$ (estimated from the difference of the two values). The value of r_V is so large that it is unlikely that the repulsive core with its short range plays an important part in the scattering where the cross-section is appreciable. The repulsive core is probably more important at larger angles where the exchange effects predominate.

6. Comparison with other Calculations

6.1. NUCLEON—α SCATTERING

Analyses of the scattering at about 150 MeV have been made by Cromer[8]), and by Kerman, McManus and Thaler[9]) using the optical model with a potential derived from nucleon-nucleon scattering. This procedure starts from eq. (5.2) for T, using the t-matrix for free nucleon-nucleon scattering, and constraining the α-particle to its ground state in the intermediate states in the second term on the right in eq. (5.2). This constraint means that incoherent multiple scattering is neglected. The analyses were confined to angles less than 50°. A striking result is that the calculated cross-sections exceed the experimental values by roughly a factor 2, or from 50–100 mb/sr. A possible explanation of this is the neglect of the multiple incoherent scattering term. To calculate this term one would have to calculate $T_2(t)$ with the α-particle ground state excluded as an intermediate state of four nucleons. We have not done this, but, as a rough estimate, we have calculated the difference between $T_2^{(ij)}$ with no constraint on the intermediate states and with the intermediate state constrained to contain an alpha particle in its ground state. This difference gives a measure of the effect of the multiple incoherent scattering term (it would be exactly equal to the double incoherent scattering if the V_{ij} used were equal to t_{ij}). The results for the cross-section, with and without the constraint in $T_2^{(ij)}$, are shown in fig. 8. It will be seen that the effect of the multiple incoherent scattering is to lower the cross-section by the required order of magnitude. The effect arises from the cancellation of Im $T_2^{(ij)}$ and Im $T_2^{(ij)}$. The actual values we have

calculated are not significant beyond their order of magnitude because, as we saw in section 4.3, the cancellation is somewhat too large. However, we can show that the magnitude of the increase in the cross-section due to the con-

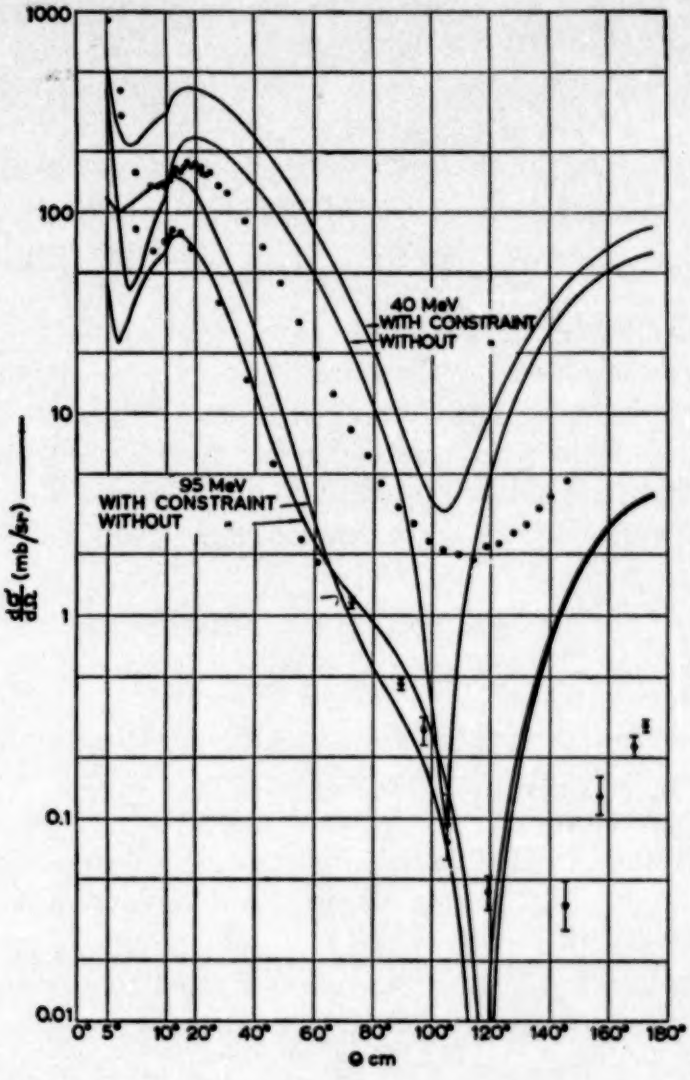

Fig. 8. Effect of neglect of incoherent multiple scattering. The curves are calculated from $(T_1 + T_2)$, those marked "without constraint" taking proper account of the distortion of the α-particle and the incident wave, those marked "with constraint" taking into account only the ground state of the α-particle in the multiple scattering term $T_2^{(1)}$, but leaving the α-particle free to distort in $T_2^{(0)}$, in other words neglecting incoherent multiple scattering.

straint is not sensitive to the parameter a which is very badly determined. In fig. 9 we give results calculated with and without constraint at the Coulomb minimum for a varying from $a = 1$ to $a = 3$, corresponding to a monotonic decrease of V_0 from 18.7 to 0 MeV.

Note that the incoherent multiple scattering would be zero if it were not for the correlations in the α-particle wave function. These correlations arise from these sources: (i) the centre of mass motion; (ii) the exclusion principle

(if we defined the t matrix with the restriction that in intermediate states target nucleons could be thrown only into initially unoccupied levels, as mentioned in the footnote to eq. (5.1), this type of correlation would not contribute here); (iii) the nuclear interactions (i.e. deviations from the shell model). We have only included correlations due to (i) and (ii).

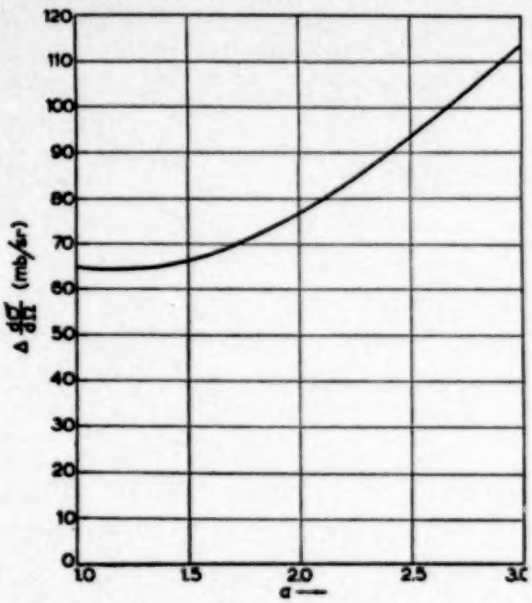

Fig. 9. Dependence of the correction for multiple incoherent scattering on the parameter a. The curve gives $\Delta(\mathrm{d}\sigma/\mathrm{d}\Omega)$, the increase of $(\mathrm{d}\sigma/\mathrm{d}\Omega)$ at the Coulomb minimum when multiple incoherent scattering is neglected.

An attempt to find an optical potential in a phenomenological way to fit nucleon-alpha scattering at 40 MeV has been made by Gammel and Thaler[10]). They find that the backward peak requires the inclusion of a space exchange part in the nucleon-alpha potential. A straightforward optical potential calculated according to the prescription of Riesenfeld and Watson[11]), which neglects target exchange, of course does not give a backward peak.

6.2. RESONANT GROUP CALCULATIONS OF THE SCATTERING OF NUCLEONS FROM DEUTERONS AND TRITONS

Our estimate of the effect of distortion of the α-particle in nucleon-alpha scattering has a bearing on these calculations. We have seen that there are two distortion mechanisms present: a correlation involving only the positions of the incident and the target nucleons, and a much more important correlation involving simultaneously the spins, isobaric spins, and positions. Such estimates as have been made of distortion in n-d and n-t calculations have taken only the first kind into account[3]), and are therefore probably too low.

There is one general feature of the results of resonant group calculations in whose interpretation the neglect of the spin-space type of correlation may be very misleading. One finds that in all nucleon scattering off very light nuclei at

$E \gtrsim 10$ MeV, there is a strong forward peak in the elastic scattering, analogous to the forward peak in the nucleon-alpha problem we have discussed here. This peak is sometimes interpreted as evidence for a strong V_0 component in the nuclear force, since as the calculations ignore distortion of the target it is mainly the V_0 component which gives the fringing field required by the strong forward peak. However, our calculations have shown that the Van-der-Waals effect arising largely from spin-space correlations can also produce a strong forward peak, and therefore the usual determinations of V_0 which ignore distortion are likely to be overestimates.

Drell[12]) has calculated the effect of distortion in producing a fringing field around heavy nuclei with a symmetric potential, and found an appreciable effect, although not sufficient to explain the observed field. This conclusion agrees with ours although we believe Drell's method of calculation to underestimate the effect (it corresponds to an effective ΔE (eq. (4.8)) of over 100 MeV, which seems rather too large).

7. Conclusions

(i) To give a qualitatively correct account of proton-alpha scattering at energies around 100 MeV it is necessary to include effects due to both nucleon exchange and target distortion. The importance of target distortion is considerably larger in reactions between light nuclei at energies up to 100 MeV than has often been assumed in calculations by the resonating group method. The estimates we have made of multiple incoherent scattering suggest that this correction is of importance in calculating the optical potential for light nuclei from free nucleon-nucleon phase shifts.

(ii) It is extremely difficult to deduce the exchange properties of the internucleon potential from the scattering of nucleons by the light nuclei because of the importance of the target distortion effect. The magnitude of the direct component is particularly liable to misinterpretation on this account.

References

1) A review is given by R. J. N. Phillips, Rep. Prog. Phys. **22** (1959) 562
2) K. M. Watson, Phys. Rev. **89** (1953) 573;
G. Takeda and K. M. Watson, Phys. Rev. **97** (1954) 1336;
H. Feshbach, Ann. Rev. Nucl. Sc. **8** (1958) 47
3) Reviews have been given by H. S. W. Massey and H. B. Bransden, Conference on the Few Nucleon Problem (London, 1959)
4) G. F. Chew and M. L. Goldberger, Phys. Rev. **87** (1952) 778
5) M. K. Brussel and J. H. Williams, Phys. Rev. **106** (1959) 286
6) W. Selove and J. M. Team, Phys. Rev. **112** (1959) 1658
7) P. E. Hodgson, Advances in Physics **7** (1958) 1
8) A. Cromer, preprint and private communication
9) A. K. Kerman, H. McManus and R. M. Thaler, preprint
10) J. L. Gammel and R. M. Thaler, Phys. Rev. **109** (1958) 2041
11) W. B. Riesenfeld and K. M. Watson, Phys. Rev. **102** (1956) 1157
12) S. D. Drell, Phys. Rev. **100** (1955) 97
13) R. Hofstadter, Rev. Mod. Phys. **28** (1956) 214
14) G. Abraham, L. Cohen and A. S. Roberts, Proc. Phys. Soc. A **68** (1955) 265

1.D.1: 4.D

Nuclear Physics **19** (1960) 299—302; © *North-Holland Publishing Co., Amsterdam*
Not to be reproduced by photoprint or microfilm without written permission from the publisher

THE DECAY ENERGY OF Ba^{133}

M. K. RAMASWAMY, W. L. SKEEL and P. S. JASTRAM

Department of Physics, The Ohio State University, Columbus, Ohio†

Received 28 March 1960

Abstract: We have redetermined the transition energy for the decay of Ba^{133} to Cs^{133} to be 489 keV, confirming Gupta's results, in disagreement with the estimate of 700 keV from beta-decay systematics. The log *ft* values for the orbital capture transitions to the 437 and 381 keV levels, as well as gamma cascade studies reported previously support a single-particle description for all of the low-lying levels of Cs^{133}, with the possible exception of the one at 158 keV. The doublet splitting between the $d_{\frac{3}{2}}$ and $d_{\frac{5}{2}}$ levels is found to be 300 keV. This splitting and the ground-state quadrupole moment are however not in good agreement with estimates based on a pure single-particle configuration.

1. Introduction

In a recent paper[1]) we reported results on gamma-ray studies in the decay of Ba^{133}. A level scheme for Cs^{133} was proposed with levels at 79 ($\frac{5}{2}^+$), 158 ($\frac{5}{2}^+$), 381 ($\frac{3}{2}^+$) and 437 ($\frac{1}{2}^+$) keV (fig. 1). This scheme can be satisfactorily described

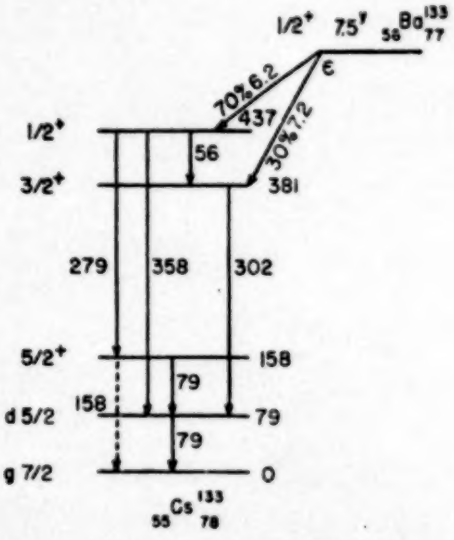

Fig. 1. Proposed decay scheme of Ba^{133} (see ref. [1])).

(except for the 158 keV level) in terms of the excitation levels of a single proton, if it is assumed that the 381 keV level is a $d_{\frac{3}{2}}$ state and the 437 keV level an $s_{\frac{1}{2}}$ state. The single-particle ground state of Ba^{133} is most likely to be an $s_{\frac{1}{2}}$ orbital[2]). From this assumption it follows that the electron-capture decays to the 381

† Supported by the U.S. Atomic Energy Commission.

and 437 keV levels in Cs^{133} should both be allowed, but that the transition to the 381 keV level should be l-forbidden ($\Delta l = 2$).

A more quantitative test of this picture may be made through comparison of estimated log ft values for the corresponding transitions with measured values. According to the beta-decay systematics of Way and Wood[3]) the energy available for Ba^{133}–Cs^{133} decay is approximately 700 keV. On the basis of the observed gamma-ray intensities the amount of electron-capture was estimated to be 70 % to the 437-keV level and 30 % to the 381-keV level. From these and the half-life of 7.5 years[4]) for Ba^{133}, the log ft values were calculated to be at least 8, which appeared rather large for allowed transitions. Recently Gupta *et al*[5]) measured the L/K ratio for orbital electron-capture de-excitation to the 437-keV level, and estimated the total decay energy to be about 490 keV. This results in log ft values of 6.1 and 7.2 respectively for transitions to the 437 and 381 keV levels.

If the energy released in the capture decay is correspondingly small, as it turns out to be in this case, it can be determined quite accurately from the L/K ratio; the result is in fact comparatively insensitive to errors in the necessary estimates of detector efficiency and solid-angle. The substantial discrepancy between the transition energy estimated from systematics and Gupta's experimental value led us to repeat the measurement, using summing and coincidence techniques to select transitions to the 437-keV level in Cs^{133}.

The experiment consists of determining the ratio of coincidences of K X-rays with the (358 + 79) keV sum-peak to the total number of sum-peak counts. Then if the solid-angle subtended by the X-ray counter S_K, the K-fluorescence yield ω_K and the efficiency for detecting the K X-ray ε_K are known, it follows that the ratio of probabilities of L to K capture is given by

$$\frac{P_{L_1}}{P_K} = [(N_{358+79}/N_{358+79,X})\,\varepsilon_K S_K \omega_K - 1]\,\frac{1}{1.207}$$

where the factor 1.207 in the case of Ba^{133} arises from taking account of capture from higher shells[6]). The decay energy is given in keV by the expression[7])

$$W = \frac{W_{L_1} - xW_K}{1 - x},$$

where $W_{L_1} = L_1$-binding-energy, $W_K = K$-binding-energy and

$$x = \sqrt{\frac{P_{L_1}/P_K}{(g_{L_1}^2/g_K^2)}},$$

with $g_L^2/g_K^2 = 0.13$ in our case.

2. Results

Table 1 summarizes the results of our measurements for two separate runs at different counter solid-angles. The average of these comes out to be 52 $\pm$ 1.6

keV for the decay energy to the 437-keV level, giving a total ground-state energy difference of 489 keV. The main uncertainty in the result arises from an estimated 6 % uncertainty in the determination of the X-ray counter solid-angle. The measured L/K ratio and probable error are plotted on the curve in

TABLE 1

Results on decay energy measurement

Run	$I_{437\ \mathrm{sum}}$ (counts per sec)	$I_{437,\ \mathrm{X}}$ (counts per sec)	S_K	ε_K	ω_K	P_L/P_K	W (keV)
1	180.0 ± 1.4	0.547 ± 0.016	0.013	0.60	0.876	1.098 ± 0.09	51.9
2	253.6 ± 1.6	3.51 ± 0.06	0.038	0.96	0.876	1.084 ± 0.08	52.1

fig. 2, showing the energy dependence. It is clear that in this region the transition energy is comparatively insensitive to variations in the capture ratio.

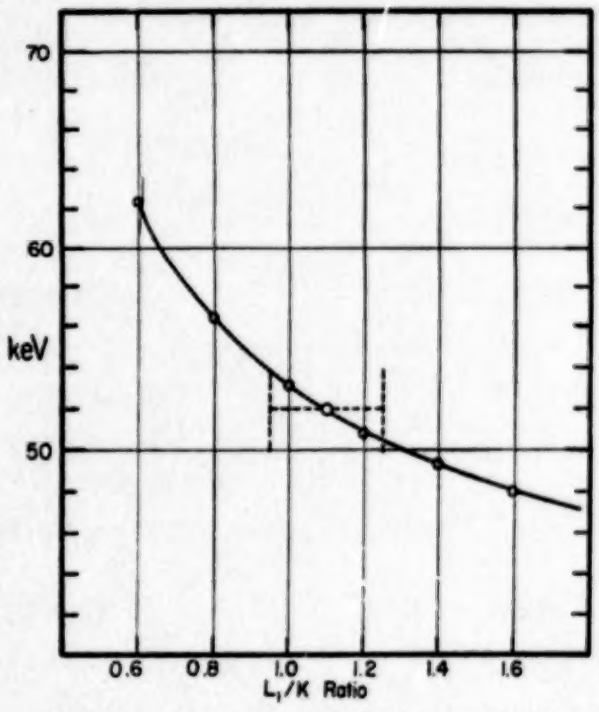

Fig. 2. Decay energy as a function of the L_1/K ratio. The experimental value is marked with the estimated error.

3. Discussion

The measured value of 489 ± 1.6 keV for the total decay energy is in excellent agreement with the work of Gupta *et al.*[5]) who, however, did not take into account the capture contributions from higher shells, which amount to about 20 % of the total. The present value yields log ft values of 6.1 and 7.2 for the

capture transitions to the 437 and 381 keV levels. These values are entirely reasonable for allowed transitions, provided we interpret the value 7.2 as indicating l-forbiddenness. This in turn is consistent with assigning single-particle orbitals for the 381 and 437 keV levels, as well as the ground state of Ba^{133}.

An interesting quantity that we can obtain from the proposed level scheme for Cs^{133} is the $d_{\frac{3}{2}} - d_{\frac{5}{2}}$ separation. Blin-Stoyle[8]) has calculated the spin-orbit splittings for a square well with triangular tail, obtaining a splitting of 980 keV for the 2d level in the region of the double-closed-shell nucleus Pb^{208}. The doublet separation is expected to vary as $A^{-\frac{1}{3}}$ where A is the mass number; accordingly for Cs^{133} the $d_{\frac{3}{2}} - d_{\frac{5}{2}}$ splitting is estimated to be 1250 keV, whereas the observed value is 300 keV. Table 2 gives a comparison of some of the known

TABLE 2

Comparison of properties of Cs^{133} with single-proton model

	Observed	Single-particle estimate
Magnetic moment (nuclear magnetons)	2.6	1.7
Quadrupole moment (in Q/R_0^2 units)	—0.003	—0.14
$d_{\frac{3}{2}} - d_{\frac{5}{2}}$ splitting (in MeV)	0.30	1.25

parameters of Cs^{133}, namely, magnetic moment, electric quadrupole moment and the $d_{\frac{3}{2}} - d_{\frac{5}{2}}$ splitting with the estimates from the single-particle shell model. From an examination of this table we note that although the level scheme follows closely the ordering expected from the single-particle shell model, one does not find quantitative agreement with this model for the properties listed.

It is a pleasure to thank Professor B. Margolis for discussions concerning the spin-orbit splittings.

References

1) M. K. Ramaswamy, W. L. Skeel and P. S. Jastram, Nuclear Physics **17** (1960) 619
2) M. Goldhaber and R. D. Hill, Revs. Mod. Phys. **24** (1952) 217
3) K. Way and M. Wood, Phys. Rev. **94** (1954) 119; revised
4) S. Katcoff; quoted by Beggs, Robinson and Fink, Phys. Rev. **101** (1956) 149
5) Gupta, Jha, Joshi and Madan, Nuovo Cim. **8** (1958) 48
6) Wapstra, Nijgh and Van Lieshout, Nuclear Spectroscopy Tables (North-Holland Publishing Co., Amsterdam, 1959) p. 61
7) H. Brysk and M. E. Rose, Revs. Mod. Phys. **30** (1958) 1169
8) R. J. Blin-Stoyle, Phil. Mag. **46** (1955) 973

1.D.2:
1.E.1

Nuclear Physics **19** (1960) 303—308; © *North-Holland Publishing Co., Amsterdam*
Not to be reproduced by photoprint or microfilm without written permission from the publisher

COLLECTIVE VIBRATIONS IN P^{31}

V. K. THANKAPPAN and S. P. PANDYA

Physical Research Laboratory, Ahmedabad-9, India†

Received 20 April 1960

Abstract: An attempt is made to explain the energy levels and the electromagnetic transitions in P^{31} in terms of the collective vibrational model. The results are found to be fairly satisfactory.

1. Introduction

The role of collective motion in explaining the properties of nuclei of mass $A \approx 30$ is recently being investigated with much interest, in view of the successful demonstration of the existence of the collective rotational motion of nuclei of mass $A \approx 25$, and the experimental observation of enhanced E2 transitions in some $A = 29$ and $A = 31$ nuclei[1]). In particular, it is found in these nuclei that the E2 cross-over transition from the second excited state of spin $J = \frac{5}{2}$ to the ground state of spin $J = \frac{1}{2}$ is about hundred times more intense than the possible M1 transition to the first excited state of spin $J = \frac{3}{2}$. This and other properties of these nuclei are explained with a fair amount of success by a model which describes them in terms of a single odd particle interacting with a deformed rotating nuclear core.

Analysis of nuclear stripping reaction data for these nuclei by French and Mcfarlane[2]) shows evidence of considerable mixing of shell model configurations in the ground state of P^{31}. However, detailed calculations on the basis of nuclear shell model including mixed configurations, predicting the energy levels, magnetic moments, etc., are not yet available.

It should be of interest to examine the predictions of the collective vibrational model for nuclei of $A \approx 30$, for several reasons. One of us has earlier described a preliminary calculation for the properties of Si^{29} in terms of this model[3]). In view of the considerably more detailed information now available for the energy levels of P^{31}, we present here results for this nucleus. Earlier calculations of Goldhammer[4]) on similar lines were based on assumptions quite different from those we adopt here; our emphasis is at present on detailed comparison of the predicted and observed energy level spectra.

† Supported by the Department of Atomic Energy, India and the University Grants Commission, India.

2. Energy Levels

We consider the P^{31} nucleus as a spherical core of 14 protons and 16 neutrons, filling up the nuclear subshells upto $1d_{\frac{1}{2}}$ and $2s_{\frac{1}{2}}$ respectively, and the last odd proton in the $2s_{\frac{1}{2}}$ or $1d_{\frac{3}{2}}$ subshell. The collective properties of the core are described in terms of quadrupole surface oscillations which are quantised. The single particle states of the odd proton are then coupled to the 0, 1 and 2 quanta states of the core. The mathematical formalism for such a model is well-known, and detailed calculations are exactly similar to those described in ref. [3]). We follow the notation described there.

It is implicit in the model that the collective properties of the core should be approximately the same as those observed in the Si^{30} nucleus. We interpret the first excited state of Si^{30} at 2.24 MeV[5]) as the one-quantum vibrational state of the core, which gives $\hbar\omega = 2.24$ MeV. Of course, on the basis of such a simple model we should expect to see in Si^{30} a degenerate triplet of states of spins 0, 2 and 4 arising from two-quanta excitation at 4.5 MeV. However, the experiments show only a close doublet at 3.51 and 3.79 MeV, and further excited states are not clearly known. This result should not be surprising as for excitation energies $\geqq 4$ MeV, this simple model may not be adequate; in particular, effects of inter-nucleon forces and particle excitations from the core may have to be taken into account more explicitly. It is for this reason that we confine our attention to (even parity) states of P^{31} below 4 MeV.

The other two parameters of the model, viz. the separation Δ of the single particle states $2s_{\frac{1}{2}}$ and $1d_{\frac{3}{2}}$, and the constant q indicating the strength of coupling of the odd particle to the collective oscillations of the core, are considered as free parameters, and are adjusted to obtain the best agreement of the calculated and the observed energy levels. The Hamiltonian matrices for $J = \frac{1}{2}, \frac{3}{2}, \frac{5}{2}$ and $\frac{7}{2}$ are constructed, and are explicitly diagonalised for various values of Δ and q. The results for the lowest few states of each J are shown in fig. 1. The experimental results are shown in fig. 2.

We note that qualitatively the order of the energy levels is correctly given by the theory. To find the best choice of the parameters Δ and q, we remark† that the separation of the states $\frac{3}{2}$ and $\frac{3}{2}^*$, and the splitting of the triplet $\frac{5}{2}^*$, $\frac{1}{2}^*$ and $\frac{3}{2}^{**}$ is quite sensitive to variation in the value of q and is relatively unaffected by variation of Δ; this enables us to choose the best value of q as ≈ 1.0. With this choice for q, the variation of the excitation energy of the $\frac{3}{2}$ state with Δ determines the best value for Δ viz., $\Delta \approx 2.0$ MeV. Fig. 2 also shows the predicted energy levels for $q = 1.0$, $\Delta = 2.0$ MeV. It may be noted that experimentally the spin of the 3.41 MeV state is not determined. Moreover, Simons[6]) assigns spin $\frac{1}{2}$ to the 3.51 MeV level, whereas Broude *et al.*[1]) find spin

† The notation here is that the unstarred, starred and double starred values refer to the lowest, the first and the second excited states of a given J.

$\frac{3}{2}$ for the same level. Though we have shown in fig. 2 the spin sequence of the triplet as $\frac{5}{2}$, $\frac{1}{2}$, $\frac{3}{2}$, the possibility that the 3.41 MeV state is $\frac{3}{2}$ and the 3.51 MeV state is $\frac{1}{2}$ cannot be ruled out from our calculations, as these levels cross in the

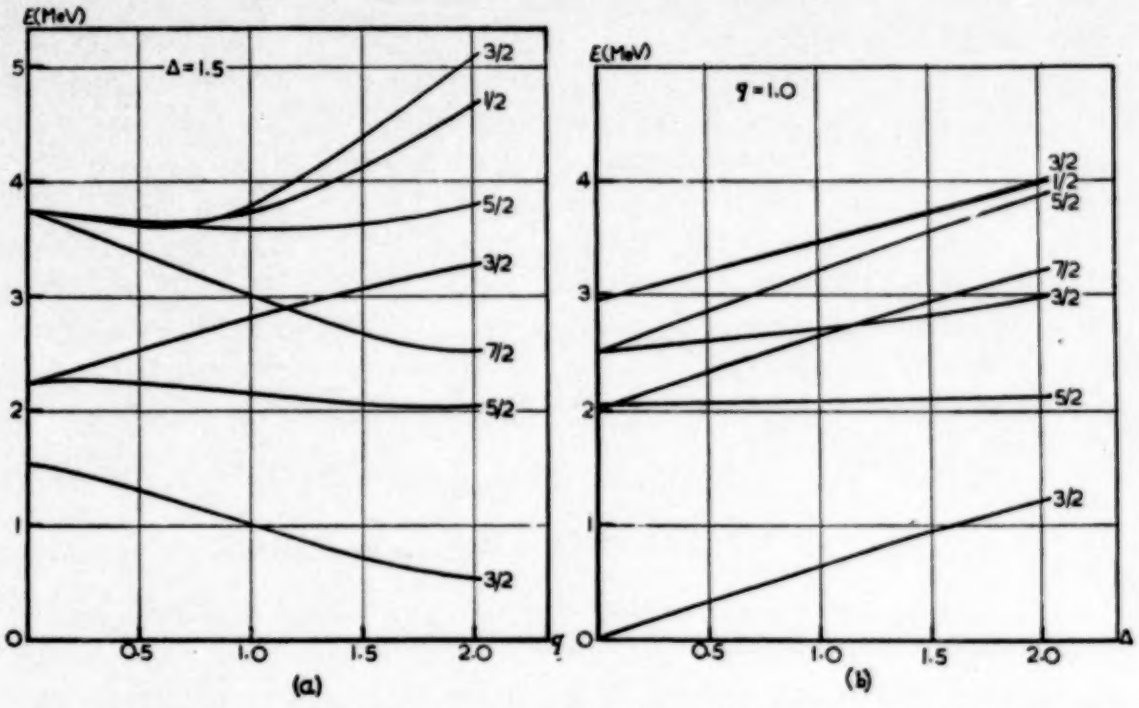

Fig. 1. Variation of the energy level scheme of P^{31} with q (fig. 1(a) and with Δ (fig. 1(b)). The levels are normalised to $E = 0$ for the ground state.

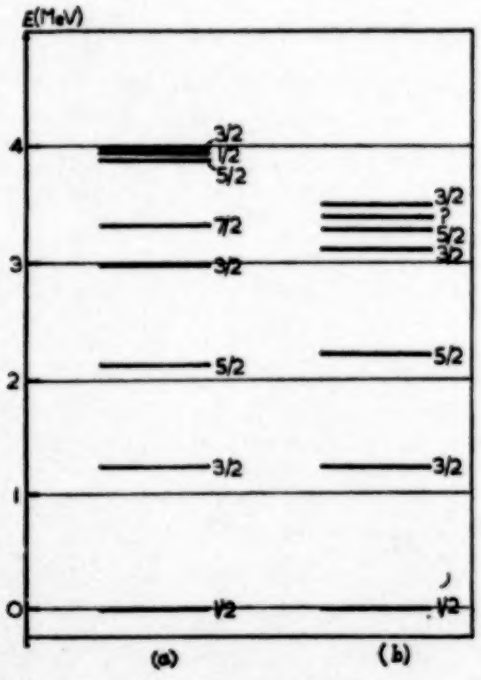

Fig. 2. Comparison of the calculated energy levels ($\Delta = 2.0$ MeV, $q = 1.0$ MeV) with the observed energy levels below 4 MeV. (a) Calculated levels. (b) Experimental levels.

neighbourhood of $q \approx 1.0$, as may be seen from fig. 1a. The close triplet of levels $\frac{5}{2}^*$, $\frac{1}{2}^*$ and $\frac{3}{2}^{**}$ is predicted about 0.5 MeV higher than the observed triplet. This discrepancy is not regarded as serious in view of the remark earlier made regarding the higher energy levels, and the availability of only two parameters in the calculation.

. The really serious difficulty in the predictions of this model is the presence of the $J = \frac{7}{2}$ level between the $\frac{3}{2}^*$ level and the higher triplet. This level is not seen experimentally. We stress this feature as important, since no reasonable variation of the parameters can avoid placing this level below ≈ 4 MeV. The only comment we make is that since the observed levels in this region are very close, the probability that the $\frac{7}{2}$ level is degenerate with $\frac{3}{2}^*$ or $\frac{5}{2}^*$ should be considered. Small changes in the parameters Δ and q may easily cause this to happen. It may be noted that for $q > 1$, this $\frac{7}{2}$ level would occur below 3 MeV, and would almost certainly have been detected. This is perhaps an additional argument against choosing $q > 1.0$.

3. Electromagnetic Transitions

It is characteristic of the collective vibrational model that although E2 transitions can be considerably enhanced by introducing even a small amount of collective vibrations, the static values of the electromagnetic moments are not changed very much from the simple shell model values. P^{31} belongs to that group of $s_{\frac{1}{2}}$ nuclei which show a very large deviation of the observed magnetic moment from the Schmidt value. It is thus not surprising that as in the case of Si^{29}, the vibrational model fails to predict the observed value of the magnetic moment of P^{31}. The calculated value for the magnetic moment is (for $q = 1.0$, $\Delta = 2.0$ MeV) $\mu = 2.56$ n.m., which may be compared to the observed value $\mu = 1.13$ n.m., and the Schmidt value $\mu = 2.79$ n.m.

The wavefunctions of the ground state and the first two excited states are listed in table 1. These show features very similar to those calculated for Si^{29}. The two important characteristics of the electromagnetic transitions in P^{31} are as follows:

a) large E2 component in the decay of the first excited state,

b) the possible M1 transition from the second excited state $\frac{5}{2}$ to the first excited state $\frac{3}{2}$ is less than 5 % of the crossover E2 transition to the ground state $\frac{1}{2}$.

Qualitatively these features are easily explained by the structure of the wavefunctions found for these states. We note that the ground state is ≈ 80 % pure single particle $s_{\frac{1}{2}}$ state, whereas the first excited state $\frac{3}{2}$ has a large admixture of the single particle state $d_{\frac{3}{2}}$, and the $s_{\frac{1}{2}}$ state coupled to one vibrational quantum. The presence of the latter large component would give rise to an enhanced E2 transition to the ground state. On the other hand the second

excited state arises almost entirely from the coupling of the $s_{\frac{1}{2}}$ state to one vibration quantum state of the core. Hence we should expect a strong E2 transition to the ground state, whereas the M1 transition to the first excited state is almost forbidden. We hope to report on detailed calculations of the

TABLE 1

Eigenfunctions of the states $J = \frac{1}{2}, \frac{3}{2}, \frac{5}{2}$ of P^{31} for $q = 1.0, \Delta = 2.0$ MeV

n	k	j	$J=\frac{1}{2}$	$J=\frac{3}{2}$	$J=\frac{5}{2}$
0	0	$\frac{1}{2}$	0.948	—	—
0	0	$\frac{3}{2}$	—	0.709	—
1	2	$\frac{1}{2}$	—	— 0.625	0.924
1	2	$\frac{3}{2}$	0.308	— 0.247	— 0.175
2	0	$\frac{1}{2}$	0.056	—	—
2	2	$\frac{1}{2}$	—	0.079	— 0.039
2	4	$\frac{1}{2}$	—	—	—
2	0	$\frac{3}{2}$	—	0.153	—
2	2	$\frac{3}{2}$	— 0.053	0.129	0.090
2	4	$\frac{3}{2}$	—	—	0.325

The tabulated quantity is the amplitude of the single particle state of spin j coupled to the state of the nuclear core with n quanta coupled to the resultant spin k.

electromagnetic transitions in such odd-proton nuclei later in another context. It may be emphasised in the meanwhile that absolute measurements of the various transition probabilities in these nuclei would be very useful.

We should like to add a remark on the interpretation of these electromagnetic transitions within the framework of simple shell model ideas, as we fear that this aspect has perhaps been misrepresented elsewhere. On the basis of the simple shell model, one would interpret the ground and the first excited states as pure single particle states $s_{\frac{1}{2}}$ and $d_{\frac{3}{2}}$, whereas the second excited state would be due to the excitation of a $d_{\frac{1}{2}}$ particle from the underlying closed shell to perhaps the $s_{\frac{1}{2}}$ shell, resulting in the configuration $(d_{\frac{1}{2}})^{-1}(s_{\frac{1}{2}})^2$ for this state. Even on the basis of such a simple model, it is clear that the $\frac{5}{2} \to \frac{3}{2}$ transition would be absolutely forbidden (as it involves two-particle transitions), whereas $\frac{5}{2} \to \frac{1}{2}$ transition can take place as d → s transition. The introduction of collective effects would serve to enhance the E2 transitions. It is therefore unfair to infer from the large crossover transition that the shell model fails, and deformation of the core must be invoked. Perhaps a proper shell model calculation taking into account the mixing of configurations would also give quite good results.

4. Conclusions

We conclude that the collective vibrational model explains satisfactorily the seven energy levels of P^{31} observed below 4 MeV, but predicts an unobserved

level $J = \frac{7}{2}$. We hope that further experimental observations may elucidate this point. One may compare the predictions of this simple two-parameter model to those of the collective rotational model of Broude *et al.*[1]) for the low lying energy levels. It appears that both models are about equally successful. It is important to remark that though the rotational model predicts the $\frac{7}{2}$ level above 4 MeV, the position of this level is displaced to a large extent by the rotation-particle coupling between the bands 8 and 11.

The values of the parameters Δ and q obtained here are also quite reasonable. In particular the small value of q and the calculated wavefunctions for all the states considered here show that the amplitudes of the two-quanta excitation states of the core are small, and the neglect of more than two-quanta excitations of the core is justified.

Finally, the observed features of the electromagnetic transitions in P^{31} are also quite easily understood, at least qualitatively, on the basis of this unified model.

References

1) D. A. Bromley, H. E. Gove, E. B. Paul, A. E. Litherland and E. Almquist, Can. J. Phys. **35** (1957) 1042;
D. A. Bromley, H. E. Gove and A. E. Litherland, Can. J. Phys. **35** (1957) 1057;
C. Broude, L. L. Green and J. C. Willmott, Proc. Phys. Soc. **72** (1958) 1097, 1115, 1122
2) M. H. Mcfarlane and J. B. French, NYO-2846, The University of Rochester, Rochester N.Y.
3) S. P. Pandya, Prog. Theor. Phys. **21** (1959) 431
4) P. Goldhammer, Phys. Rev. **101** (1956) 1375
5) P. M. Endt and C. M. Braams, Revs. Mod. Phys. **29** (1957) 683
6) L. Simons, Nuclear Physics **10** (1959) 215

2.H *Nuclear Physics* **19** (1960) 309—313; © *North-Holland Publishing Co., Amsterdam*
Not to be reproduced by photoprint or microfilm without written permission from the publihers

A REMARK ON THE COULOMB DISINTEGRATION OF ACCELERATED HEAVY IONS

Johannes M. HANSTEEN

Institute of Physics, University of Oslo, Blindern, Norway

Received 17 February 1960

Abstract: The Coulomb disintegration of heavy ions is treated by a semi-classical perturbation method, taking the repulsion of the bombarding particle in the Coulomb field of the target nucleus into account. The cross section for the electric break-up of ^{12}C nuclei into three α-particles in nuclear emulsions is found to be of the order of 10^{-27} cm^2 for projectile energies of approximately 100 MeV. This seems to be in conformity with the very scanty experimental data.

1. Introduction

Several authors have performed calculations on the disintegration of light nuclei in a Coulomb field[1-5]). The calculations in refs. [2-4]) are based on the assumption that the impinging particles follow straight-line paths. In ref. [4]) the order of magnitude of the cross section for the process of disintegration into two fragments at bombarding energies of about 100 MeV is given as 10^{-29} $(Z_1Z_2)^2$ cm^2, Z_1 and Z_2 being the charge number of the projectile and the target nucleus respectively. For carbon ions disintegrating via $^8Be + \alpha$ into three α-particles in the Coulomb field of the heavy components in photographic emulsions ($Z_2 \approx 42$) this would mean a cross section of about 0.6 b. It should be noted that this is more than twice the experimentally determined total cross section for production of three-prong stars by carbon ions of the mentioned energy in nuclear emulsions (cf. refs. [6,7])).

2. Outlines of the semi-classical perturbation treatment of the process

It is thought to be of interest to apply to this process the semi-classical methods developed in connection with the investigation of Coulomb excitation of nuclei[8]).

We notice first that the inequality

$$\varkappa = \frac{2Z_1Z_2e^2}{\hbar v} \gg 1 , \tag{1}$$

where v is the projectile velocity, is satisfied by the phenomenon under consideration: for a ^{12}C-projectile with energy 100 MeV impinging on a Ag nucleus, $\varkappa \approx 31$. The approximation of using a classical orbit for the projectile is thus well justified[9]).

We apply an extremely simple model for the process. The unpolarized disintegrating projectile of mass M_1 is thought of as being composed of the two fragments into which it is broken up, i.e. $M_1 = M_1^{(1)} + M_1^{(2)}$ and $Z_1 = Z_1^{(1)} + Z_1^{(2)}$, the interaction between the two being represented by a square well potential. (One should in this connection recall that the cluster model of atomic nuclei has recently been successfully applied to several of the light nuclei, cf. ref. [10]).) The movement of the centre-of-mass of the two fragments is described by a classical hyperbolic path.

Let b_{if} be the probability amplitude for the Coulomb disintegration to take place from an initial state i of the projectile with angular momentum l to a final state f of the two free fragments, whose relative energy we denote by E_r. The differential cross section for electric disintegration can then be written as

$$\frac{\mathrm{d}^2\sigma}{\mathrm{d}E_r\,\mathrm{d}\sigma_R} = \frac{1}{2l+1}\int \mathrm{d}\Omega_k \mid b_{if} \mid^2 , \tag{2}$$

where

$$\mathrm{d}\sigma_R = \tfrac{1}{4}d^2 \sin^{-4}\tfrac{1}{2}\vartheta\,\mathrm{d}\Omega \tag{3}$$

is the Rutherford scattering cross section. The latter is expressed in eq. (3) by half the distance of closest approach in a head-on collision $d = Z_1 Z_2 e^2/M_0 v^2$ where $M_0 = M_1 M_2/M_1 + M_2$, and by the scattering angle ϑ of the projectile in the centre of mass system of the projectile and the target nucleus, $\mathrm{d}\Omega$ being the corresponding solid angle. In eq. (2) $\mathrm{d}\Omega_k$ corresponds to the angular coordinates of the relative wave vector k of the two fragments. From this

$$\frac{\mathrm{d}\sigma}{\mathrm{d}E_r} = \tfrac{1}{4}d^2 \frac{1}{2l+1}\int \mathrm{d}\Omega_k \int_0^{\vartheta_{max}} \mathrm{d}\Omega \mid b_{if} \mid^2 \frac{1}{\sin^4 \tfrac{1}{2}\vartheta} . \tag{4}$$

Here, ϑ_{max} is the angle corresponding to scattering just on the nuclear surface, i.e.

$$\vartheta_{max} = 2 \arcsin\left(\frac{1}{2\dfrac{E}{E_B} - 1}\right) , \tag{5}$$

with E_B = height of the Coulomb barrier and $E = \tfrac{1}{2}M_0 v^2$. Particles passing outside the nucleus will be Coulomb scattered into angles less than ϑ_{max}.

The Coulomb interaction between the target nucleus, pictured as a point charge, and the two fragments is given by

$$V = Z_2 e^2 \sum_{n=1}^{2} \frac{Z_1^{(n)}}{\mid (-1)^{n-1} a_n \mathbf{r} - \mathbf{r}_{pt} \mid} . \tag{6}$$

Here $\mathbf{r}_{pt}$ is the position vector of the projectile centre of mass measured from

the centre of mass of the target nucleus. The relative position vector of the two fragments is denoted by r and

$$a_1 = \frac{M_1^{(2)}}{M_1^{(1)} + M_1^{(2)}}, \quad a_2 = \frac{M_1^{(1)}}{M_1^{(1)} + M_1^{(2)}}. \tag{7}$$

The probability amplitude is then, according to first order time-dependent perturbation theory, given by[8])

$$b_{if} = \frac{4\pi Z_2 e^2}{i\hbar} \sum_{\lambda,\mu} \left(\sum_{n=1}^{2} a_n^{\lambda} Z_1^{(n)} \right) \frac{1}{2\lambda + 1} S_{E\lambda,\mu} \langle \mathrm{f} \mid r^{\lambda} Y_{\lambda\mu}(\theta, \varphi) \mid \mathrm{i} \rangle , \tag{8}$$

where $S_{E\lambda,\mu}$ are the orbital integrals known from the Coulomb excitation studies, and the angles θ and φ are measured from a fixed polar axis in the disintegrating nucleus. The final state wave function representing the two fragments is taken as a plane wave normalized with respect to energy. (See also ref. [4]). In the matrix element $\langle \mathrm{f} \mid r^{\lambda} Y_{\lambda\mu}(\theta, \varphi) \mid \mathrm{i} \rangle$ we insert square well wave functions and the mentioned plane wave.

We only consider the dipole case, i.e. $\lambda = 1$. By a straightforward calculation it is found that in this case ($\lambda = 1$)

$$\frac{1}{2l+1} \int \mathrm{d}\Omega_k \, |\langle \mathrm{f} | r^{\lambda} Y_{\lambda\mu}(\theta, \varphi) | \mathrm{i} \rangle|^2 = \frac{\hbar k}{(2\pi\hbar)^3} (4\pi)^2 \left\{ \frac{l+1}{2l+1} D_{l,l+1}^2 + \frac{l}{2l+1} D_{l,l-1}^2 \right\} , \tag{9}$$

with

$$D_{l,l\pm1} = C_l \int_0^R \mathrm{d}r \, r^3 j_l(\beta r) j_{l\pm1}(kr) + C_l \frac{j_l(\beta R)}{k_l(\alpha R)} \int_R^{\infty} \mathrm{d}r \, r^3 k_l(\alpha r) j_{l\pm1}(kr) ; \tag{10}$$

R is the radius of the square well potential. The quantities α, β and C_1 are related to the depth of the well and the binding energy of the constituents of the light nucleus before disintegration; they are defined in eqs. (16) and (18) of ref. [4]). In this paper there also occurs a term very similar to the one within brackets in eq. (9), with the difference that the coefficients before the D-integrals are the squares of ours. The j_l and k_l in eq. (10) are spherical Bessel and Hankel functions respectively.

The remaining angular integration in eq. (4) can easily be carried out[8]). We have finally

$$\sigma = \frac{1}{3\pi} \left(\frac{Z_1 Z_2 e^2}{\hbar v} \right)^2 \left(\frac{\sum_{n=1}^{2} a_n Z_1^{(n)}}{Z_1} \right)^2 \times \int_0^{k\max} \mathrm{d}k \, k^2 \left\{ \frac{l+1}{2l+1} D_{l,l+1}^2 + \frac{l}{2l+1} D_{l,l-1}^2 \right\} \mathrm{e}^{-\pi\xi} (\xi\varepsilon_{\min}) K_{i\xi}(\xi\varepsilon_{\min}) K'_{i\xi}(\xi\varepsilon_{\min}) . \tag{11}$$

Here $\xi = d\Delta E/\hbar v$ (ΔE is the energy loss in the collision) and $\varepsilon_{min} = 1/\sin \frac{1}{2}\vartheta_{max}$ is the eccentricity of the hyperbolic path corresponding to the maximum Coulomb angle ϑ_{max}. The value of k_{max} is determined from the maximum momentum transfer associated with this angle. The symbol $K_{i\xi}$ denotes modified Bessel functions of the third kind and of imaginary order.

3. Discussion

From eq. (11) we have calculated the total cross section for the Coulomb disintegration process $^{12}C \rightarrow {}^{8}Be + \alpha \rightarrow 3\alpha$ caused by collisions with the silver and bromine atoms in nuclear emulsions. The values for the modified Bessel functions of the third kind are obtained from ref. [11]). The results are shown in fig. 1.

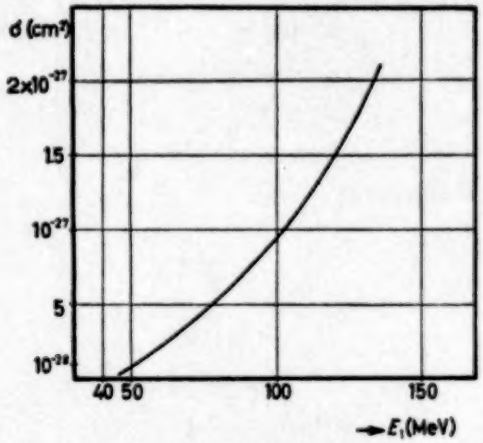

Fig. 1. The cross section as a function of the bombarding energy for the Coulomb disintegration of ^{12}C into three α-particles in the fields of the heavy components in nuclear emulsions. The depth of the square well potential used is 28.2 MeV and its radius 3.43×10^{-13} cm.

The results obtained from eq. (11) may be compared to existing measurements. Miller[6]) has studied the so-called impact disintegration of ^{12}C in three α-particles in photographic emulsions. The projectiles in this experiment had an initial energy of 110 MeV. A certain fraction of the observed impact disintegrations represent probably Coulomb disintegrations. One can pick out events which might be electric disintegrations, by studying Miller's data, especially his table 5.4, and using the following criteria:

1) The recoil energy of the heavy target nucleus in a Coulomb process cannot exceed a certain value which is simply related to the angle ϑ_{max} in eq. (5).

2) In a Coulomb disintegration process (e.g. the carbon disintegration mentioned above) the number of events per unit of the relative energy of the produced fragments increases strongly with decreasing values of this energy (cf. eq. (11)).

Considerations of this kind lead to the conclusion that about one fourth of

the events tabulated by Miller may have been caused by electric break-up. The very meager data in each suitable energy interval down to the Coulomb barrier give cross sections not incompatible with the values calculated from eq. (11).

The values for σ given here should not be considered as more than a rough guide to what may be expected experimentally. It is hoped, however, that this note will stimulate further measurements of the total cross section for Coulomb disintegration of heavy ions, and also of the angular distribution of the fragments produced in the process.

This work was started under the auspices of Nordita, Nordisk Institut for teoretisk Atomfysik, in Copenhagen. Its completion was made possible by a research grant from the Royal Norwegian Council for Scientific and Industrial Research. To both institutions the author offers his sincere thanks.

Note added in proof. Very recently[12]) Anderson *et al.* have observed the α-particles produced by bombardment of a gold target with ^{6}Li ions. The authors assume the observed disintegration products to originate from 1) Coulomb excitation of ^{6}Li ions to unbound levels with subsequent disintegration and 2) nuclear stripping, i.e. capture of a deuteron from the projectile by the target nucleus. Total cross sections for α-particle production at bombarding energies of 60, 34 and 25 MeV are given as approximately 500, 400 and 40 mb respectively. By application of eq. (11) above and representing the ^{6}Li nucleus by an α-particle and a deuteron put in a square well potential of radius 2.73×10^{-13} cm and a depth of 9.65 MeV, the Coulomb disintegration cross sections at 60, 34 and 25 MeV are found to be 400, 300 and 60 mb respectively. These results seem to give some support to the idea of the existence of substructures in light nuclei.

References

1) J. R. Oppenheimer, Phys. Rev. **47** (1935) 845
2) S. M. Dancoff, Phys. Rev. **72** (1947) 1017
3) J. Sawicki, Acta Phys. Polon **14** (1955) 135
4) V. I. Mamasakhlisov and G. Chilashvili, JETP **32** (1956) 806
5) M. Z. Maksimov, JETP **36** (1959) 1582
6) J. F. Miller, Thesis, University of California, published as Report U.C.R.L. 1902 (1952)
7) J. H. Fremlin in Nuclear Reactions, editors P. M. Endt and M. Demeur (North-Holland Publishing Company, Amsterdam 1959) vol. I, Ch. III
8) K. Alder, A. Bohr, T. Huus, B. Mottelson and A. Winther, Rev. Mod. Phys. **28** (1956) 432
9) Niels Bohr, Mat. Fys. Medd. Dan. Vid. Selsk. **18** no. 8 (1948)
10) K. Wildermuth and Th. Kanellopoulos, The Application of the "Cluster" Model to Nuclear Physics, mineographed lecture notes Cern 59-23, Theoretical Study division, Geneva 1959
11) S. P. Morgan, Tables of Bessel Functions of Imaginary Order and Imaginary Argument (California Institute of Technology, 1947)
12) C. E. Anderson, W. J. Knox and A. R. Quinton, Bull. Am. Phys. Soc. **5** (1960) 292

1.E.1: 3.A

Nuclear Physics **19** (1960) 314—326; © *North-Holland Publishing Co., Amsterdam*
Not to be reproduced by photoprint or microfilm without written permission from the publisher

GAMMA RADIATION FROM EXCITED STATES OF F^{18}, Na^{22} AND Ne^{22}

T. A. RABSON, T. W. BONNER, R. CASTILLO-BAHENA, M. V. HARLOW, Jr.,
H. P. HAENNI and W. A. RANKEN

The Rice Institute, Houston, Texas†

Received 28 March 1960

Abstract: Gamma radiation from the proton bombardment of O^{18}, the He^3 bombardment of O^{16}, and the alpha bombardment of F^{19} have been studied by means of a magnetic lens photo conversion spectrometer and a NaI spectrometer. Gamma rays from the bombardment of an O^{18} target with protons were observed with energies 0.511 ± 0.004, 0.666 ± 0.005, 0.938 ± 0.006, 1.043 ± 0.008, 1.082 ± 0.010 and 1.990 ± 0.010 MeV. Gamma rays from the bombardment of an O^{16} target with 2.83 MeV He^3 particles were observed with energies of 0.189 ± 0.005, 0.66 ± 0.02, 0.95 ± 0.02, 1.07 ± 0.02, 1.71 ± 0.03, 2.14 ± 0.03, 2.54 ± 0.03, and 3.11 ± 0.05 MeV. The internal conversion coefficient of the 0.189 MeV radiation was measured to be $(2.86 \pm 0.4) \times 10^{-3}$. The energies of the gamma radiation from the alpha particle bombardment of a F^{19} target were observed to be 0.073 ± 0.002, 0.109 ± 0.002, 0.586 ± 0.004, 0.892 ± 0.005, 1.275 ± 0.008, 1.530 ± 0.010 and 2.090 ± 0.016 MeV. The internal conversion coefficients of the 0.073, 0.109 and 0.586 MeV gammas were observed to be $(4.5 \pm 0.4) \times 10^{-3}$, $(2.8 \pm 0.5) \times 10^{-3}$ and $(1.14 \pm 0.3) \times 10^{-4}$, respectively.

1. Introduction

A study of the γ radiation from $O^{18} + p$, $O^{16} + He^3$ and $F^{19} + \alpha$ has been made in an effort to learn more about the energy level structure of F^{18}, Na^{22} and Ne^{22}. The photoconversion electron spectrum from the proton bombardment of an O^{18} target backed with thorium foil was observed in an intermediate image magnetic lens spectrometer. The photoconversion electron spectrum from the α particle bombardment of CaF_2 backed with a gold foil was also observed. The γ-ray spectrum from the bombardment of a thin SiO target with He^3 particles was observed with a NaI spectrometer. Internal conversion electron-spectra from the same target and from a thin CaF_2 target bombarded with α-particles were also observed.

2. Apparatus

The magnetic lens spectrometer used in this work has been described previously in its application as a pair spectrometer[1]) and as a photoconversion and an internal conversion spectrometer[2]). For observing electrons of energy less than 0.300 MeV a thin walled end window Geiger counter was used as the detector in place of the plastic scintillator.

† Work supported by the U.S. Atomic Energy Commission.

To facilitate the pulse-height analysis of the data from the NaI spectrometer, an RCL 256-channel pulse-height analyzer was used.

3. Excited States of F^{18}

There is still some uncertainty concerning the spins and parities of the four excited states of F^{18} at an excitation of about 1 MeV. In order to gain more knowledge about these levels the γ radiations emitted upon the decay of these states were observed. The target used in studying the $O^{18}(p, n)F^{18}$ reaction was a 12.7 mg/cm² thorium foil which had been oxidized on the surface. The foil was oxidized by heating in an induction heater to approximately 1000° C in an atmosphere of heavy water 85 % enriched in O^{18}.

The photoelectron spectrum obtained when the target described above was bombarded with 4.6 MeV protons is shown in fig. 1. The reactions which are energetically possible are:

$$O^{18}(p, p')O^{18}, \qquad Q = 0 \text{ MeV};$$
$$O^{18}(p, n)F^{18}, \qquad Q = -2.453 \text{ MeV};$$
$$O^{18}(p, \alpha)N^{15}, \qquad Q = 3.969 \text{ MeV}.$$

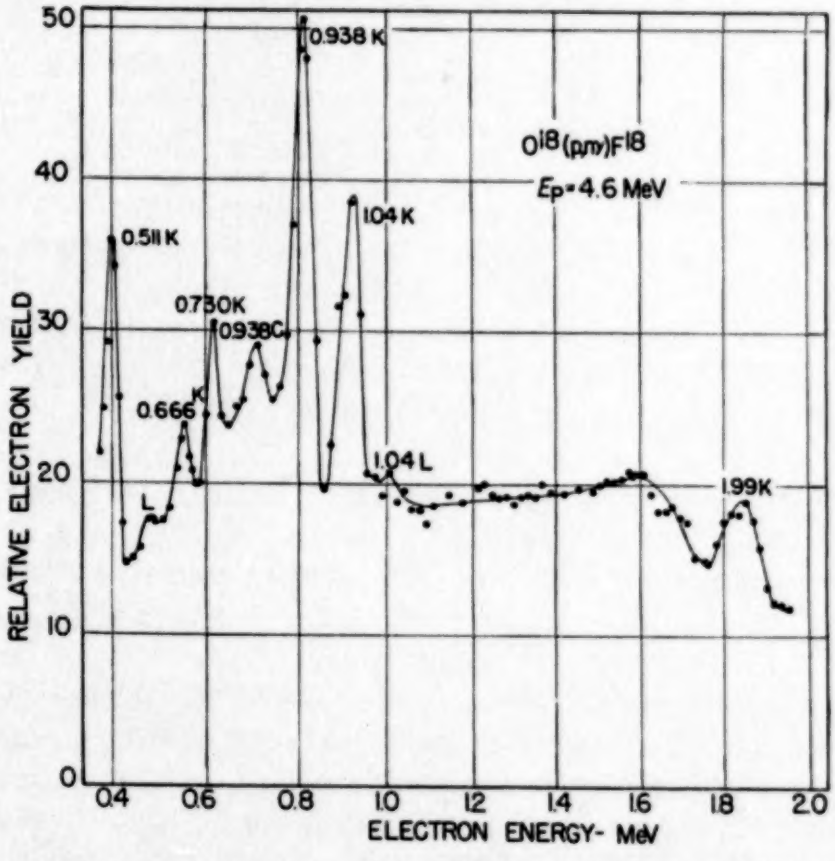

Fig. 1. Photoconversion electron spectrum obtained by bombarding O^{18} on a 12.7 mg/cm² thorium foil with 4.6 MeV protons.

No γ radiation was observed from N^{15} in the energy range which was studied. The energies of the observed γ radiations are 0.511 ± 0.004, 0.666 ± 0.005, 0.730 ± 0.006, 0.938 ± 0.006, 1.043 ± 0.008 and 1.990 ± 0.01 MeV. An energy level diagram of the states of F^{18} below 3.2 MeV is shown in fig. 2. The energy

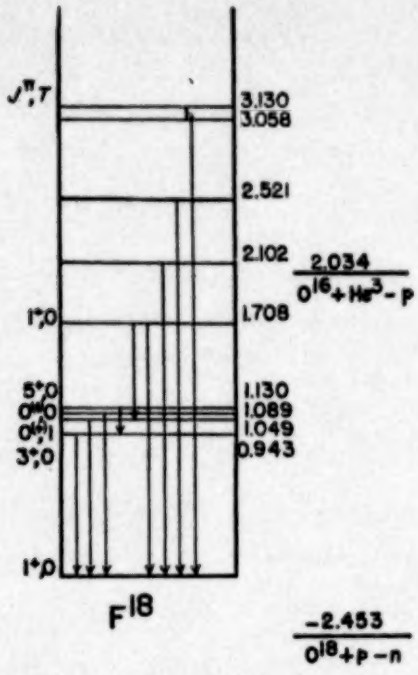

Fig. 2. Energy level diagram of F^{18}. Arrows represent gamma radiations observed in this experiment.

levels are those observed by Rao *et al.*[3]) by means of magnetic analysis of the protons from $O^{16}(He^3, p)F^{18}$. The spins and parities are those which seem to be consistent with all the data available at the present time.

The 0.511 MeV radiation is annihilation radiation from the positons emitted by F^{18}. The 0.666 MeV gamma is from a cascade between the 1.708 MeV level and the 1.049 MeV level in F^{18}. The 0.730 MeV radiation is from the Coulomb excitation of Th^{232}.

The 0.938 and 1.043 MeV radiations are from ground state transitions in F^{18} which have been observed previously[4, 5]). The Saclay group reported a Doppler shift for the 1.043 MeV γ radiation but no shift in the case of the 0.938 MeV radiation[6]). The 1.990 MeV radiation is from the inelastic scattering of protons in O^{18}.

Because a level in F^{18} was known to exist at 1.08 MeV[7]), the region around 1 MeV was inspected at various proton energies. At a bombarding energy of 4.0 MeV a 1.082 ± 0.010 MeV γ-ray was observed. The photoconversion electron-spectrum obtained at this bombarding energy is shown in fig. 3. The excitation curves for the 0.666, 0.938, 1.043 and 1.082 MeV γ-rays are shown in fig. 4, together with a curve showing resonances in the yield of neutrons

which was obtained by R. A. Chapman[8]). The relative yields of the gamma excitation curves have been corrected for the efficiency of detection. A pronounced resonance structure is observed for the four γ-rays and for the total

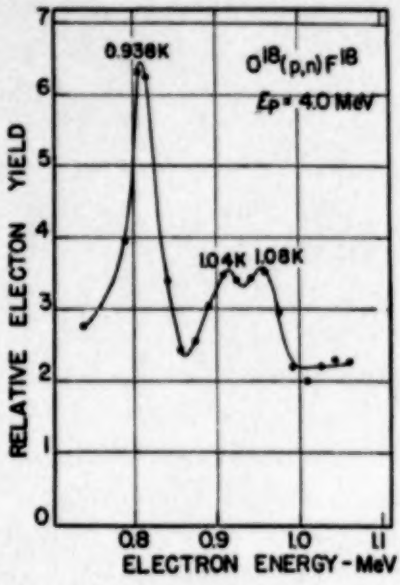

Fig. 3. Photoconversion electron spectrum obtained by bombarding O^{18} on a 12.7 mg/cm^2 thorium foil with 4.0 MeV protons.

yield of neutrons. The relative yields of the several γ-rays vary markedly from resonance to resonance and this accounts for the fact that the 1.08 MeV radiation was not originally observed.

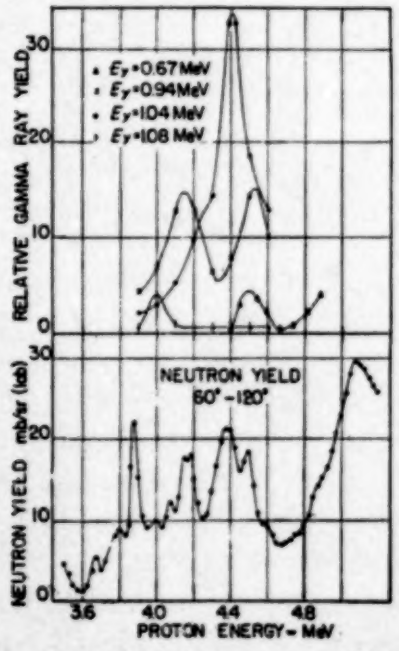

Fig. 4. Excitation curves of the neutrons and the gamma radiations produced by bombarding an O^{18} target with protons. The relative intensities of the several γ-rays were measured with a photoconversion spectrometer.

No γ radiation was seen from the 1.130 MeV level in F^{18}. A search was made with a NaI crystal for a possible cascade between this level and one of the lower levels. This proved inconclusive, however, because F^{19} contamination in the target produced 0.109 and 0.197 MeV γ-rays from inelastic scattering of protons. However, comparison of the spectrum with another obtained from protons incident on a thorium blank did indicate the presence of γ radiation of about 0.185 MeV.

A more conclusive experiment on the cascade γ radiations was carried out with the reaction $O^{16}(He^3, p\gamma)F^{18}$. A SiO target was used; it was made by evaporation onto a 2.5×10^{-4} cm nickel sheet which was mounted on an aluminium holder. The nickel was then etched off with an acid solution leaving a self-supporting SiO film approximately 0.1 mg/cm^2 in thickness. The use of this technique in the fabrication of thin carbon foils has been described by Kashy *et al.*[9]). A coating of silver was evaporated onto the back of the target to help cool the foil when it was under bombardment and to prevent the beam from building up electrostatic charges which might break the foil.

The internal conversion electron-spectrum obtained when this target was bombarded by 2.83 MeV He^3 particles is shown in fig. 5. The only detectable

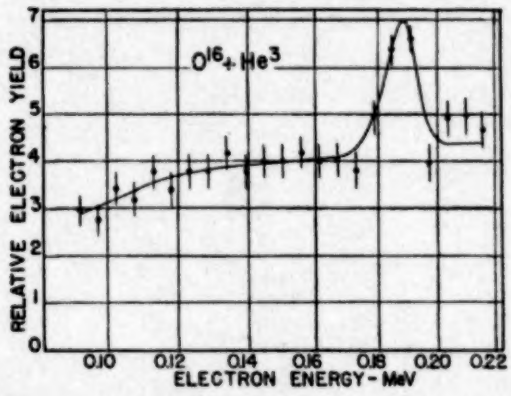

Fig. 5. Internal conversion electrons from a thin SiO target bombarded with 2.83 MeV He^3 particles.

radiation is at 0.189 ± 0.004 MeV and this radiation is almost certainly from the $1.130 \rightarrow 0.943$ MeV cascade in F^{18}. The low energy gamma spectrum obtained from this same target with a NaI crystal is shown in fig. 6. The 0.070 MeV and 0.144 MeV radiations are from the Ta used to stop the beam. From these data the total internal conversion coefficient of the 0.189 MeV radiation was calculated to be $(2.86 \pm 0.4) \times 10^{-3}$. In order to calculate the K internal conversion coefficient 11 % of the total electron yield was subtracted to account for conversion in other than the K shell[10]). The K shell internal conversion coefficient of the 0.189 MeV radiation was calculated to be $(2.5 \pm 0.4) \times 10^{-3}$. Table 1 gives the ratio of the experimental value to the theoretical value of the coefficient for E1, M1, E2, M2, E3 and M3 radiation. An E2 transition is strongly indicated although an M2 transition cannot be excluded.

The higher energy γ-ray spectrum obtained by bombarding a thick quartz target with 2.83 MeV He^3 particles is shown in fig. 7. The energies of the radiations observed are 0.66 ± 0.02, 0.95 ± 0.02, 1.07 ± 0.02, 1.71 ± 0.03,

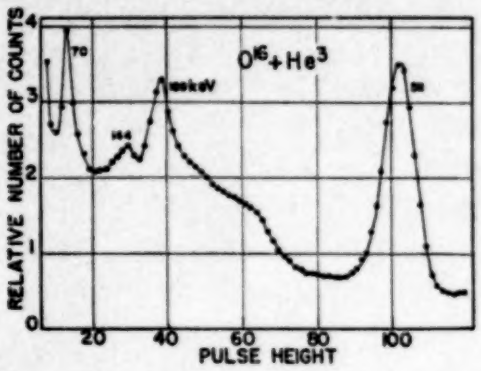

Fig. 6. Low energy γ-ray spectrum from bombarding a thin SiO target with 2.83 MeV He^3 particles, taken with a 2.5 cm by 2.5 cm NaI crystal.

TABLE 1

Ratio of the experimental to the theoretical K internal conversion coefficient for the 0.189 MeV gamma radiation for different multipolarities

E1	M1	E2	M2	E3	M3
5.8 ± 1.2	9.3 ± 1.9	1.02 ± 0.2	1.46 ± 0.3	0.13 ± 0.03	0.30 ± 0.06

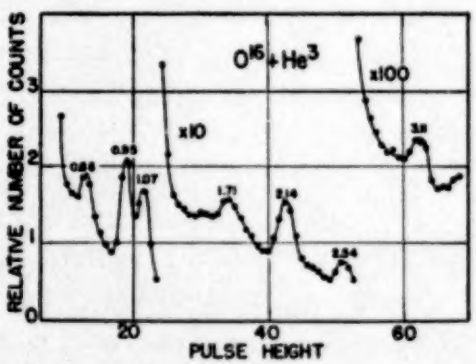

Fig. 7. Gamma ray spectrum from bombarding a thick quartz target with 2.83 MeV He^3 particles taken with a 5.1 cm by 5.1 cm NaI crystal. The γ-ray energies are given in MeV.

2.14 ± 0.03, 2.54 ± 0.03 and 3.11 ± 0.05 MeV; all of these γ-rays are from transitions in F^{18}. The energies and relative yields of these γ-rays are shown in table 2.

TABLE 2

Relative yields of gamma radiation from $O^{16}(He^3, p)F^{18}$ at $E_{He^3} = 2.83$ MeV with NaI detector

E_γ (MeV)	0.66	0.95	1.07	1.71	2.14	2.54	3.11
Relative yield	537	1580	1330	75	178	89	19

The ratio of the intensities of the 1.708 → 1.049 MeV cascade to the 1.708 MeV ground state transition is 7.1.

4. Discussion of Results

Lifetime measurements and angular distribution measurements from $O^{16}(He^3, p)F^{18}$ by Bromley *et al.*[11]) imply that $1 \leqq J \leqq 3$ for the 0.943 MeV state. Angular distribution measurements of the deuterons from $F^{19}(p, d)F^{18}$ imply even parity for the 0.943 and 1.708 MeV states[12]). These results together with the fact that no Doppler shift was observed for the 0.943 MeV radiation[6]) suggest that the 0.943 MeV state is that predicted by Elliott and Flowers[13]) with $T = 0$ and $J^\pi = 3^+$.

The data in the literature concerning the 1.049 MeV level and the 1.089 MeV level are rather confused because of the difficulty in distinguishing these closely spaced levels. Also, early observers did not know that there were two states with a small energy differen . One of these states is apparently the analog of the $T = 1$, $J = 0^+$ ground state of O^{18}. Both the 1.049 and 1.089 MeV states are believed to have $J = 0$ on the basis of the angular distribution of the gamma radiation from the reaction $O^{16}(He^3, p)F^{18}$ and from the proton-γ-ray angular correlation measurements[7]). The 1.049 MeV state was given a $J = 0$ assignment from the analysis of the $F^{19}(p, d)F^{18}$ pickup reaction[12]).

The level at 1.708 MeV is believed to have an isobaric spin of zero because it is populated by the reaction $Ne^{20}(d, \alpha)F^{18}$ which can only lead to $T = 0$ states[4]); this state is believed[14]) to have a spin and parity of 1^+. A γ-ray with an energy of 0.666 MeV is observed; this now is known to be a cascade from the 1.708 level to the 1.049 MeV level. The errors in the energy determinations are not sufficient to allow this radiation to be between the 1.708 and 1.089 MeV levels. The maximum possible Doppler shift for the 0.666 MeV radiation in this case would be 5 keV. Further proof that this radiation could not be a 1.708 → 1.089 MeV cascade is obtained from the result that the 0.666 MeV radiation is of greater intensity than the 1.082 MeV gamma radiation for proton bombarding energies of 4.4 to 4.6 MeV. This result would be clearly impossible if the cascade were between the 1.708 and 1.089 MeV states. The 0.666 MeV radiation is not, however, more intense than the 1.043 MeV γ-ray at any bombarding energy for which measurements were made.

Calculations were made to determine the parity and isobaric spin assignments of the 1.049 and 1.089 MeV levels which would be compatible with the observed branching ratios from the decay of the 1.708 MeV level in F^{18}. To do this transition probabilities were calculated for the various types of transitions possible from this state. The following assumptions were made in these calculations:

A. Allowed E1 transitions have a speed of about $|M|^2 = 0.032$ Weisskopf units[15]).

B. Allowed M1 transitions have a speed of about $|M|^2 = 0.15$ Weisskopff units[15]).

C. There is a strong tendency for E1 and M1 transitions of low energy to be relatively faster and the distribution of R (the ratio of the reduced strengths of the higher and lower energy members of competing branches of dipole de-excitation) shows $R \approx 0.35$ with a spread of an order of magnitude either way[15]).

D. Isobaric spin forbidden E1 and M1 transitions show a decrease of a factor of 30 in their speed[15, 16]).

On the basis of these calculations the most probable assignments are + parity for both levels and $T = 1$ for the 1.049 MeV level and $T = 0$ for the 1.089 MeV level, although negative parity for either or both levels is not ruled out.

The internal conversion coefficient measured for the 0.189 MeV radiation from the reaction $O^{16}(He^3, p)F^{18}$ agrees closely with that expected for E2 radiation. Since this gamma radiation is from the $1.130 \rightarrow 0.943$ MeV cascade, it follows that the 1.130 MeV level is the 5^+, $T = 0$ state predicted by Elliott and Flowers[13]).

The energies of the 2.14, 2.54 and 3.11 MeV γ-rays lead one to believe they are ground state transitions from levels observed at these energies.

5. Gamma Radiation from $F^{19} + \alpha$

Gamma radiation from the excited states in Na^{22} has been observed in a number of experiments. Excited states of Na^{22} have also been observed in the reaction $Mg^{24}(d, \alpha)Na^{22}$ where only $T = 0$ isobaric spin states are expected to be formed. Until the recent experiments of Temmer and Heydenburg[17]) there was no evidence for the excited $T = 1$ state in Na^{22} predicted to have an energy of about 0.6 MeV. One of the principal objects of the present investigation was to search for this state in Na^{22}.

The photoconversion electron spectrum observed when a 1.6 mg/cm² thick CaF_2 target, evaporated on a 16 mg/cm² gold radiator, was bombarded by 4.9 MeV alpha particles is shown in fig. 8. The energies of observed γ-rays are 0.586 ± 0.004, 0.892 ± 0.005, 1.275 ± 0.008, 1.530 ± 0.010 and 2.090 ± 0.016 MeV. The three reactions which might yield gamma radiation are:

$$F^{19}(\alpha, \alpha')F^{19}, \qquad Q = 0 \text{ MeV};$$

$$F^{19}(\alpha, p)Ne^{22}, \qquad Q = 1.705 \text{ MeV};$$

$$F^{19}(\alpha, n)Na^{22}, \qquad Q = -2.061 \text{ MeV}.$$

The level schemes for Ne^{22} and Na^{22} are shown in fig. 9. The Ne^{22} levels shown are those observed by Fader through magnetic analysis of proton groups from the $F^{19}(\alpha, p)Ne^{22}$ reaction[18]).

The Na^{22} levels are those observed by Browne and Cobb[19]) by magnetic analysis of alpha particles from the reaction $Mg^{24}(d, \alpha)Na^{22}$, with the exception

of the 0.666 MeV level whose 0.073 MeV cascade gamma to the 0.595 MeV level was first observed by Temmer and Heydenburg[17]). The most accurate determination of the energy of the first excited state of Ne^{22}, 1.275 ± 0.0005

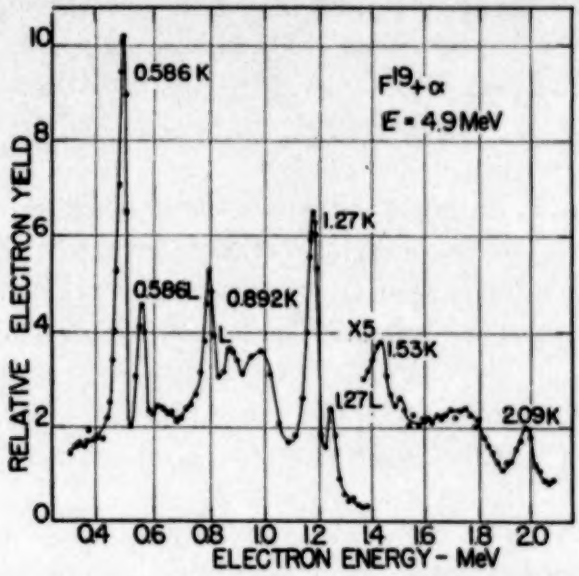

Fig. 8. Photoconversion spectrum from bombarding a 1.6 mg/cm² CaF_2 target on 16 mg/cm² gold with 4.9 MeV alpha particles.

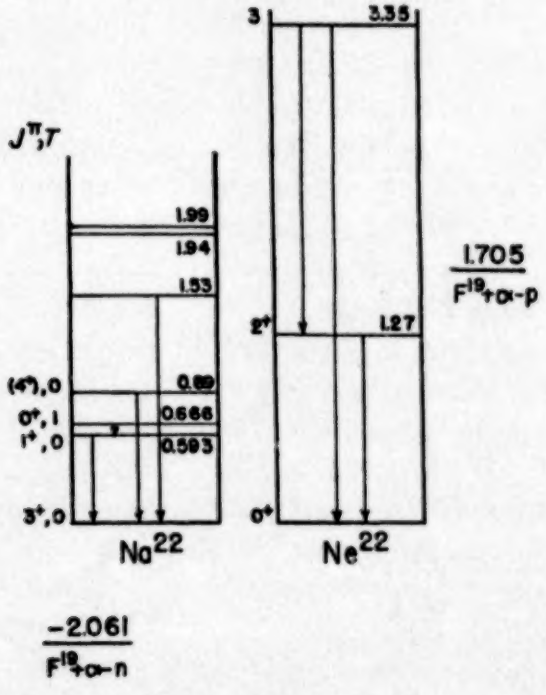

Fig. 9. Energy level diagrams of Na^{22} and Ne^{22}. Arrows represent γ-rays seen in the present experiment.

MeV, has been obtained by magnetic spectrometer measurements of the energy of the γ-rays from this state through the use of a Na^{22} source[20]). This γ-ray was used in the present experiment for calibration purposes.

The energies of the γ-rays given above agree very well with the known levels shown in fig. 9. The 0.586 MeV γ-ray is a ground state transition from the first excited state of Na^{22} and the 1.275 MeV γ-ray is from the first excited state of Ne^{22}. The 2.090 MeV γ-ray is a cascade between the 3.35 and 1.275 MeV levels in Na^{22}. This γ-ray is thought to have either an E1 or M1 multipolarity and hence should be Doppler shifted. The Doppler corrected energy of this γ-ray is 2.075 MeV, which gives a value of 3.350 ± 0.020 MeV for the energy of the second excited state of Ne^{22}.

The 0.892 and 1.530 MeV γ-rays agree well in energy with the states in Na^{22} observed by Browne and Cobb at 0.89 and 1.53 MeV[18]). The Doppler corrected energies of these γ-rays are 0.886 and 1.519 MeV. However, it is not clear whether the Doppler corrections should be applied since the multipolarities of the γ-rays are not known. The fact that there are no strong cascades from the 1.53 MeV state indicates that a Doppler correction should probably be made for this radiation. The threshold energy of producing Na^{22} in the 1.94 MeV state is 4.84 MeV. Consequently very little radiation of 1.94 MeV and no radiation of 1.99 MeV is expected, in agreement with the experimental results.

The relative intensities and the Doppler corrected energies of the observed γ-rays are listed in table 3. The intensity of the 3.35 MeV gamma radiation was

TABLE 3

Relative intensity of gamma radiation from $F^{19} + \alpha$ for $E_\alpha = 4.9$ MeV

E_γ (MeV)	0.586	0.886	1.275	1.519	2.075	3.350
Relative intensity	36	25	100	6	10	4

obtained from a separate experiment which made use of a NaI spectrometer. Gamma radiation from the 1.35, 1.46 and 1.56 MeV states in F^{19} populated by the inelastic scattering of alpha particles was too weak to be observed in the present experiments.

The level postulated by Temmer and Heydenburg at 0.666 MeV is believed to be the 0^+ first $T = 1$ state in Na^{22}, since it occurs at the energy predicted by isobaric spin considerations[17]) and its lifetime of less than 0.5×10^{-9} sec, as measured by Holland and Lynch[21]), is compatible with this assignment. If it is a 0^+ state and the ground state and first excited state assignments of 3^+ and 1^+ are correct, then the 0.666 MeV level would decay by a 0.073 MeV M1-E2 cascade with very few direct transitions to the ground state. A search was made to detect γ-rays or internal conversion electrons caused by ground state transitions from this level. No gamma radiation with an intensity greater than 5 % of the 0.586 MeV gamma radiation was observed between 0.600 and 0.700 MeV when a 1.2 mg/cm^2 CaF_2 target on 12 mg/cm^2 silver foil was bombarded

TABLE 4

Internal conversion coefficient of the gamma radiation from $F^{19} + \alpha$

E_γ (MeV)	Experimental internal conversion coefficient	Ratio of the experimental conversion coefficient to the theoretical value					
		E1	M1	E2	M2	E3	M3
0.073	$(4.5 \pm 0.4) \times 10^{-3}$	3.52 ± 0.7	1.02 ± 0.2	0.097 ± 0.004	0.0725 ± 0.015		
0.109	$(2.8 \pm 0.5) \times 10^{-3}$	1.31 ± 0.4	3.6 ± 1.1	0.112 ± 0.03	0.35 ± 0.1		
0.586	$(1.14 \pm 0.3) \times 10^{-4}$	4.16 ± 1.7	3.23 ± 1.3	1.35 ± 0.5	1.14 ± 0.4	0.45 ± 0.18	0.45 ± 0.18

with 3.7 MeV alpha particles. No internal conversion electrons were observed in this same energy range with an intensity greater than 25 % of that of the internal conversion electrons from the 0.586 MeV gamma radiation when a 1.5 mg/cm² CaF_2 target on 6.8 mg/cm² aluminium was bombarded with 4.9 MeV alpha particles. The γ-ray and internal conversion electron yield from the 0.586 MeV transition to the ground state were measured when the above target was bombarded by 3.7 MeV alpha particles and the total internal conversion coefficient was found to be 1.14×10^{-4}. Table 4 indicates that this result is consistent with the 0.586 MeV γ-ray being E2 or M2.

In order to determine the multipolarity of the 0.073 MeV γ-ray, a measurement was made of its internal conversion coefficient. Because the internal conversion coefficient of the 0.109 MeV gamma radiation from the first excited state of F^{19} had been accurately measured by Mills[22]), it was decided to remeasure this coefficient as a check on the method of measurement.

A 0.2 mg/cm² CaF_2 target evaporated on a 0.2 mg/cm² aluminium foil was used for the measurements. The angular distribution of the 0.073 MeV and 0.109 MeV gamma radiation was found to deviate from isotropy by less than 10 % when the target was bombarded by 3.7 MeV alpha particles. The pulse height spectrum obtained using a 2.5 cm by 2.5 cm NaI crystal is shown in fig. 10. The internal conversion electron-spectrum obtained with the same

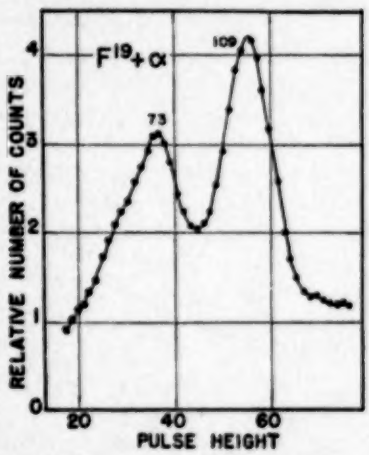

Fig. 10. Gamma rays from bombarding a 0.2 mg/cm² CaF_2 target on 0.2 mg/cm² aluminium with 3.7 MeV alpha particles, taken with a 2.5 cm by 2.5 cm NaI crystal.

energy alpha particles and the same target is shown in fig. 11.

The total internal conversion coefficient of the 0.073 MeV radiation was found to be $(4.5 \pm 0.4) \times 10^{-3}$ and that of the 0.109 MeV radiation was $(2.8 \pm 0.5) \times 10^{-3}$. From table 4 one can see these values are in agreement with M1 and E1 radiation, respectively. The results of this experiment are consistent with assignments of 3^+, 1^+ and 0^+ for the ground, first and second excited states of Na^{22}.

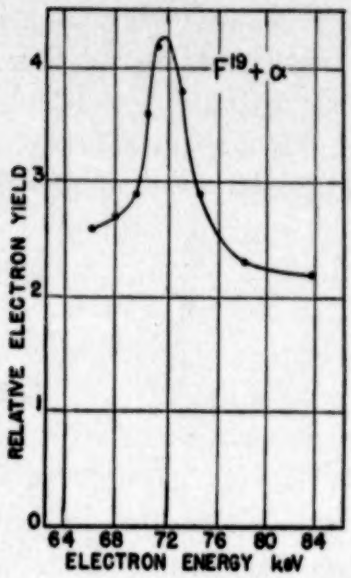

Fig. 11. Internal conversion electrons from bombarding a 0.2 mg/cm² CaF_2 target with 3.7 MeV alpha particles.

References

1) Bent, Bonner and Sippel, Phys. Rev. **98** (1955) 1237;
Ranken, Bonner, McCrary and Rabson, Phys. Rev. **109** (1958) 917
2) Ranken, Bonner, Castillo-Bahena, Harlow and Rabson, Phys. Rev. **112** (1958) 239
3) Rao, Young, Spencer, Beckner and Phillips, Bull. Am. Phys. Soc. **4** (1959) 96
4) R. Middleton and C. T. Tai, Proc. Phys. Soc. **A64** (1951) 801
5) P. C. Price, Proc. Phys. Soc. **A68** (1955) 553
6) Naggiar, Roclawski-Conjeand, Szteinsznaider and Thirion, Compt. Rend. **244** (1957) 445
7) Kuehner, Almquist and Bromley, Bull. Am. Phys. Soc. **3** (1958) 27;
Kuehner, Almquist and Bromley, Phys. Rev. Let. **1** (1958) 260
8) R. A. Chapman, Ph. D. Thesis (Rice Institute, 1957)
9) Kashy, Perry and Risser, Nuclear Instruments **4** (1959) 167
10) W. R. Mills, Ph. D. Thesis (Cal. Inst. Tech., 1955
11) Bromley, Kuehner and Almquist, Bull. Am. Phys. Soc. **3** (1958) 27
12) E. F. Bennett, Bull. Am. Phys. Soc. **3** (1958) 26
13) J. P. Elliott and B. H. Flowers, Proc. Roy. Soc. **229** (1955) 536
14) F. Ajzenberg-Selove and T. Lauritsen, Nuclear Physics **11** (1959) 239
15) D. H. Wilkinson, Phil. Mag. **1** (1956) 127;
Proceedings of the Rehovoth Conference on Nuclear Structure, edited by H. J. Lipkin (North-Holland Publishing Company, Amsterdam, 1958) Session IV, p. 175
16) E. K. Warburton, Phys. Rev. **113** (1959) 545
17) G. M. Temmer and N. P. Heydenburg, Phys. Rev. **11** (1958) 1303
18) W. J. Fader, M.I.T. Progress Report (May, 1954)
19) C. P. Browne and W. C. Cobb, Phys. Rev. **99** (1955) 644 A
20) F. Ajzenberg and T. Lauritsen, Rev. Mod. Phys. **27** (1955) 77;
P. Marmier, private communication
21) P. E. Holland and F. J. Lynch, Bull. Am. Phys. Soc. **3** (1958) 380
22) Mills, Hilton and Barnes, Phys. Rev. **100** (1955) 1794 A

1.D.4:
1.E.1

Nuclear Physics **19** (1960) 327—336; © *North-Holland Publishing Co., Amsterdam*
Not to be reproduced by photoprint or microfilm without written permission from the publisher

LOWER EXCITED STATES OF W^{185}

H. MORINAGA† and K. NAGATANI††

Department of Physics, Tohoku University, Sendai, Japan

Received 28 March 1960

Abstract: The decays of Ta^{185} and W^{185m} were investigated with a scintillation spectrometer with a coincidence circuit. The sources were prepared from photodisintegration of metallic tungsten. Gamma rays observed were essentially the same as previous results by Pöe except for a few new lines. A decay scheme is proposed for both decays. The decay of Ta^{185} is consistently explained with the unified model for strongly deformed nuclei. The isomer, however, is difficult to explain from the unified model. It is suggested that the isomeric state may represent a spherical state.

1. Introduction

The decay schemes of nuclei with well developed deformation have been accounted for by unified model[1–3]) surprisingly well. According to the recent analysis of odd-mass nuclei by Mottelson and Nilsson[3]), every decay scheme in the deformed region is quantitatively explained without any violation. In the deformed region around lanthanide elements the analysis has been extended from $A = 153$ to 185. The model, however, does not apply well outside of this region where deformation becomes less or more. On the heavier side of this region the deformation diminishes more gradually; this gives us more chance to examine the nature of the break-down of the strong coupling unified model.

At W^{183} the levels seem to be quite well explained by the unified model. But around $A = 190$ the situation seems to be very obscure. In the detailed study of the level scheme of Os^{190}, G. Scharff-Goldhaber *et al.*[4]) and O. B. Nielsen *et al.*[5]) point out definitely the unstability of the deformation.

The level scheme of W^{185} is not known so far, although some of the decay characteristics of Ta^{185} and W^{185m} have been studied[6,7]). The ground state spin is estimated from its decay to Re^{185} and is accounted for by the unified model well[3,8]). However, the known isomer with a half life of 1.6 min is very difficult to explain from the unified model (cf. section 4). Therefore, it was thought that the investigation of the decay characteristics of Ta^{185} and W^{185m} would give useful information for elucidating the situation in this transition region.

2. Experimental Procedures and Results

2.1. Ta^{185}

Natural tungsten metal of 99.9% purity was irradiated for 60 minutes by the 25-MeV bremsstrahlung in the internal target of the Tôhoku University betatron.

† Present address: Department of Physics, University of Tokyo, Bunkyoku, Tokyo, Japan.
†† Present address: Department of Physics, Yale University, New Haven, Connecticut, U.S.A.

The decay of the beta rays from this activated sample was first detected by a Geiger-Müller counter. It was separated into the 50-min Ta^{185} and the 5.2-d Ta^{183} produced by the (γ, p) reactions of tungsten-186 and -184, respectively.

The end-point energy of the beta ray from Ta^{185} was determined to be 1.7 MeV using a conventional multi-channel scintillation spectrometer with an anthracene crystal of 1.9 cm diameter and 0.42 cm thick. This value was in good agreement with the previous investigation[6]).

The gamma rays were observed with a NaI(Tl) scintillation spectrometer. The size of the crystal was 3.8 cm diameter and 3.8 cm thick. In order to analyse the gamma spectra, the energy calibration and the spectral shapes were obtained in the same geometry from the well known Hg^{203}, Se^{75}, In^{114} and Na^{22} sources. Following the decay of the gamma spectra, it was found that there were some confusing activities such as 1.6-min W^{185m}, 7-min W^{179m}, 40-min W^{179} and Ta^{183}. For obtaining the gamma spectrum of Ta^{185}, the measurement began after the shorter lived W^{185m} and W^{179m} had decayed away. And the longer lived Ta^{183} and W^{179} were corrected later in the spectrum. Such corrected spectrum is shown in fig. 1. The relative intensity of each photopeak was measured from the photopeak area after the subtraction of the back-scattering

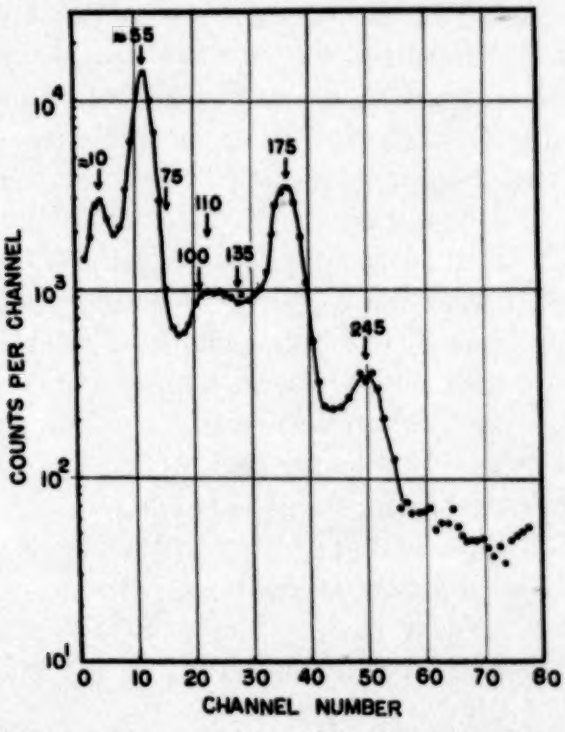

Fig. 1. Scintillation spectrum of the gamma rays from Ta^{185}.

and the Compton tails of higher energy components. In the spectrum, sharp peaks at about 10 and 55 keV were observed. These were considered to be L and K x-rays, respectively. The relative intensity ratios of these peaks, how-

ever, were rather ambiguous because of the rough estimations of the photopeak efficiencies against such low energies. At about 110 keV a broad peak was found. This was too broad to assign a single peak. We might regard it to be a peak due to piling up of three weak components, e.g., 100, 110 and 135 keV (cf. section 3). A peak at 175 keV was very strong. It is estimated that its relative intensity ratio to the beta ray was (60 ± 25) % by counting the beta rays with a Geiger-Müller counter and the gamma spectrum with the NaI(Tl) scintillation counter simultaneously. A weak peak was found at 245 keV as a gamma ray belonging to Ta^{185}. At 75 keV in the spectrum, a peak was indistinguishable because the 55-keV peak was very strong, but there might be a weak gamma ray. For surveying high energy gamma rays, we tried to observe gamma spectra using a large NaI(Tl) crystal (10.2 cm diameter and 10.2 cm thick). With this measurement, however, no other gamma ray was found. The results are listed in table 1. These gamma rays were slightly different from the previous investigation[6]) in which gamma rays have been reported at 125, 175 and 235 keV.

TABLE 1

Gamma rays of Ta^{185}

Energy (keV)	Intensity ratio of the γ-rays	Classification of the transition type	Relative intensity of the K conversion electrons
55	≈ 150	K x-ray	
75	8	M1.h. (+ E2.h.)	71
100	16	M1.u. (+ E2.u.)	62
110	1	M1.h. (+ E2.h.)	3
135	5	M1.u. (+ E2.u.)	10
175	100	E2.h.	25
245	8	M1.h. (+ E2.h.)	3

These values are estimated using the theoretical conversion coefficients.

The gamma spectrum coincident with the 175-keV gamma ray was observed using a slow coincidence circuit ($2\tau = 5\mu$ s). It was shown qualitatively that the 110-, 135- and 245-keV gamma rays were coincident with each other. But no quantitative estimation of intensities were made because the 175-keV gamma

ray transition rate might be rather slow and comparable to the resolving time of this circuit (cf. section 3).

2.2. W^{185m}

The same tungsten metal used for producing Ta^{185} was irradiated for 2 minutes in this case.

The gamma spectra were obtained with the scintillation spectrometer of which NaI(Tl) crystal had a diameter of 3.8 cm and was 3.8 cm thick. From the gamma spectra, it was recognized that the sample contained mainly W^{185m} and Ta^{185}. The gamma-ray spectrum corrected for the contribution of Ta^{185} is shown in fig. 2. In the spectrum, the L and K x-rays were observed and their

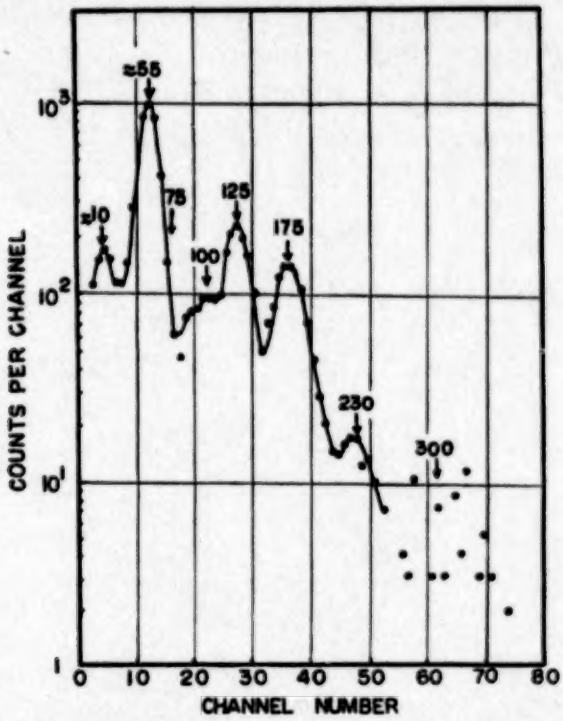

Fig. 2. Scintillation spectrum of the gamma rays from W^{185m}.

intensities were stronger than in the spectrum of Ta^{185}. There might be a weak peak at 100 keV, and there was a very strong peak at 125 keV which was not observed in Ta^{185}. At 175 keV, a strong peak was found. This might be considered to be the gamma ray due to the same transition in the decay of Ta^{185} (cf. section 3). In the previous investigation[6]), the 165- and 130-keV gamma rays were reported which probably correspond to the 175 and 125 keV in the present measurement. A weak peak was observed at 230 keV. However, if we assume a level scheme given later, this could well be assigned to a sum peak, e.g., the sum of the K x-ray due to the conversion electron of the 125-keV transition and the 175-keV gamma-ray. The sum of the 125-keV gamma ray and the 100-keV gamma ray may contribute to this peak, but with much smaller extent. Similarly, a

weaker counting rate at about 300 keV can be regarded as being a sum peak of the 125-keV gamma ray and the 175-keV gamma ray. Since it should be considered that the peak at about 100 keV was contributed by sum peaks of the K x-rays from all cascade transitions (cf. section 3), its relative intensity ratio was corrected for such effects in the final result. A weak 75-keV gamma ray was seen as the case of Ta^{185}. The results are listed in table 2.

TABLE 2

Gamma rays of W^{185m}

Energy (keV)	Intensity ratio of the γ-rays	Classification of the transition type	Relative intensity of the K conversion electrons
55	≈ 250	K x-ray	
75	8	M1.h. (+ E2.h.)	71
100	16	M1.u. (+ E2.u.)	62
125	70	E3.u.	105
175	100	E2.h.	25
225	8	sum peak	

These value are estimated using the theoretical conversion coefficients.

3. Decay Scheme

3.1. Ta^{185}

Every ground state of odd-mass tantalum isotope whose spin parity has been known is being assigned to the $\frac{7}{2}^+[404]$ Nilsson level. In Ta^{179}, the $\frac{9}{2}^-[514]$ Nilsson level is found very close to the $\frac{7}{2}^+[404]$ ground state, namely, 30 keV apart. However, this difference increases by 152 keV in Ta^{181}. We can expect this difference to increase in Ta^{183} and Ta^{185} from the Nilsson diagram given in fig. 3 since the deformation is expected to decrease with the neutron number in this region. The $\frac{5}{2}^+[402]$ Nilsson level is found also in Ta^{181} at 480 keV from the ground state and this difference is not expected to change with the deformation. Another level which lies close to the $\frac{7}{2}^+[404]$ Nilsson level is the $\frac{1}{2}^+[411]$ Nilsson level. This is seen in Ta^{181} at 612 keV above the ground state. This level should come down with decreasing deformation but since it is so high above the $\frac{7}{2}^+[404]$ intrinsic state at Ta^{181}, the order will not reverse. It is therefore postulated that the ground state of Ta^{185} is also the $\frac{7}{2}^+[404]$ intrinsic state. The assignment to the $\frac{1}{2}^+[411]$ intrinsic state would not make such a consistent decay scheme as described below.

The ground-state of W^{185} has been explained as the $\frac{3}{2}^-[512]$ intrinsic state on the basis of the observed beta decay directly to the Re^{185} ground state[3,8]).

We may assume that the eccentricity δ is about 0.2 in W^{185}. From the

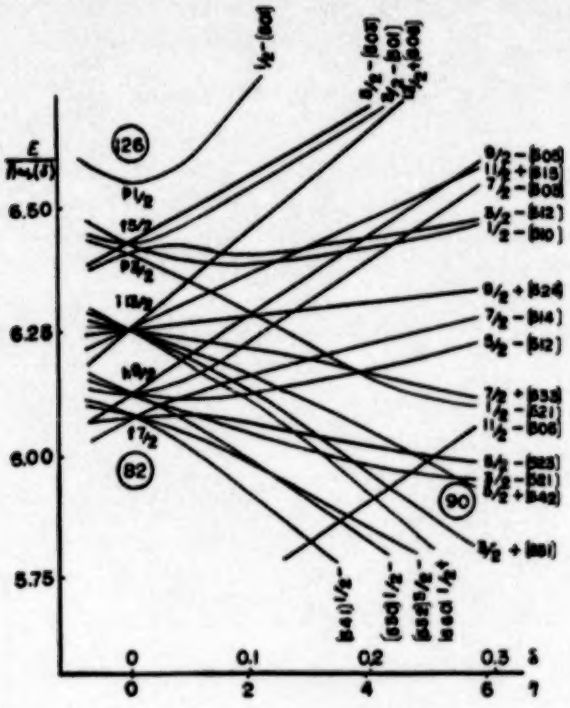

Fig. 3. Single-particle levels for odd neutron nuclei in the region $82 < N < 126$. This is reproduced from ref. [3]).

Nilsson diagram, we find the $\frac{1}{2}^-[510]$, $\frac{7}{2}^-[505]$, $\frac{9}{2}^-[503]$ and $\frac{11}{2}^+[615]$ Nilsson levels in the vicinity of the $\frac{3}{2}^-[512]$ Nilsson level. Here, the $\frac{3}{2}^-[512]$ intrinsic state is the right level expected for the ground state of W^{185}. From these levels, we can expect the $\frac{1}{2}^-[510]$ or $\frac{7}{2}^-[503]$ Nilsson levels to be the next appearing intrinsic state as in W^{183}. The former will not be reached by a beta transition from the $\frac{7}{2}^+[404]$ intrinsic state but the latter is attained by a first forbidden and unhindered transition (abbreviated as l.u.) from the $\frac{7}{2}^+[404]$ intrinsic state. A similar situation exists in the beta decay from Ta^{183} to W^{183} and is parallel to this example; it may be appropriate to place the $\frac{7}{2}^-[503]$ Nilsson level as the nearest intrinsic state to the $\frac{3}{2}^-[502]$ ground state. In W^{183}, this intrinsic state lies at 224 keV from the $\frac{3}{2}^-[512]$ intrinsic state. As the difference of these two levels tends to decrease with decreasing deformation in the Nilsson diagram, the present 175-keV gamma ray can be assigned to the transition between these intrinsic states in W^{185} following the major beta transition. This gamma transition is classified from the asymptotic quantum numbers as E2 and hindered (abbreviated as W2.h.). From the single particle estimate, the 175-keV E2 transition has a half-life of about 10^{-7} sec. The present transition is moderated by a hindrance factor, and is probably slower than 10^{-7} sec.

As in the case of W^{183}, this transition should be in competition with a transition to the first rotational $\frac{5}{2}^-$ state of the $\frac{3}{2}^-[512]$ intrinsic state, even though the latter transition is M1 and is hindered by the *K*-selection rule (abbreviated as M1.h.). In this transition, we may expect some amount of mixing of E2.h. transition. We can expect that the moment of inertia of the $\frac{3}{2}^-[512]$ intrinsic state decreases in W^{185} compared with W^{183}, because in the even tungsten isotopes the moment of inertia decreases rapidly between W^{182} and W^{184}. According to such systematics of the moment of inertia, the first rotational $\frac{5}{2}^-$ state may be placed about 100 keV above the ground state. If we assume this, the 75-keV gamma ray can be explained as such a competing M1.h. transition. Then the 100-keV gamma ray can be assigned to the M1.u. (+ E2.u.) transition from the first rotational $\frac{5}{2}^-$ state to its $\frac{3}{2}^-[512]$ intrinsic state. The ratio of these branchings from the $\frac{7}{2}^-[503]$ state is consistent with the same branchings in W^{183} after corrections for the energies. The cascade transitions from the $\frac{7}{2}^-[503]$ intrinsic state, i.e. the 75- and 100-keV transitions, should have equal intensity, and using the theoretical conversion electrons in addition to the observed gamma rays, we could confirm that this is actually so (cf. table 1).

A 1.u. beta decay should take place to the first rotational $\frac{9}{2}^-$ state of the $\frac{7}{2}^-[503]$ intrinsic state. Then the M1.u. (+ E2.u.) gamma transition to the $\frac{9}{2}^-$ intrinsic state has to occur following this beta decay. Probably the 135-keV gamma ray corresponds to it. This energy difference is exactly what is expected for such a spacing from the systematics of the moment of inertia of $\frac{9}{2}$ states.

The 245-keV gamma ray coincident with the 175-keV gamma ray cannot be assigned to any transition between the above states. Consequently, we are forced to introduce another state. As mentioned above, the $\frac{9}{2}^-[505]$ or $\frac{11}{2}^+[615]$ Nilsson level may possibly be expected in the neighbourhood. The beta decay selection rule permits only the former level. It is considered, therefore, that the $\frac{9}{2}^-[505]$ intrinsic state may be placed at 420 keV above the ground state. Then the 245-keV gamma ray can be assigned to a gamma transition from the $\frac{9}{2}^-[505]$ intrinsic state to the $\frac{7}{2}^-[503]$ intrinsic state by a M1.h. (+ E2.h.) transition. This state should decay also to the first rotational $\frac{9}{2}^-$ state of the $\frac{7}{2}^-[503]$ intrinsic state with a M1.h. (+ E2.h.) transition. The 110-keV gamma ray may correspond to it. However, the transition may scarcely occur from this state to another state because of their higher multipole order and the selection rule. In table 1, these assumed transition characteristics and the intensities of the K conversion electrons estimated from Rose's table are summarized.

From the above level scheme, the beta component to the $\frac{7}{2}^-[503]$ intrinsic state is 90 %. The log *ft* value turns out to be 6.5, using the branching ratio and the half life in addition to the measured end-point energy. In the cases of the electron-capture transition from Ta^{177} to Hf^{177} and the beta decay from Ta^{183}

to W^{183}, the same types of transition are found, e.g., from the $\frac{7}{2}^+[404]$ intrinsic state to the $\frac{7}{2}^-[503]$ intrinsic state. Their log *ft* values are about 6.5 and 6.9, respectively: this is consistent with the value 6.5 obtained above.

The beta component to the first rotational $\frac{9}{2}^-$ state of the $\frac{7}{2}^-[503]$ intrinsic state is estimated to be about 5 %, and the component to the $\frac{9}{2}^-[505]$ intrinsic state is found to be about 5 %. This gives for their lof *ft* values about 7.3 and 7.5, respectively. These are in agreement with the systematics of the beta transitions classified as 1.u. In the above consideration, we introduced the $\frac{9}{2}^-[505]$ intrinsic state for the beta component to the 420-keV state. But if, instead, we assume that the first rotational $\frac{9}{2}^-$ state of the $\frac{7}{2}^-[503]$ intrinsic state appears at 110 keV above and the second rotational $\frac{11}{2}^-$-state appears at 245 keV above the $\frac{7}{2}^-[503]$ intrinsic state, and assume the 135-keV transition above the 110-keV gamma ray, the height of the rotational states fits with the $I(I+1)$ law. However, this assignment is less plausible since the lof *ft* value of the beta transition to the $\frac{11}{2}^-$-state is 7.3, which is too high for first forbidden α-type (unique forbidden) transition. Also the moment of inertia of the $\frac{7}{2}^-[503]$ intrinsic state becomes too low. The fact that the $\frac{9}{2}^-[505]$ intrinsic state must then appear higher is another difficulty of this assignment, since we have no other gamma ray in spite of the rather high decay energy available.

3.2. W^{185m}

The gamma rays of W^{185} at the 75, 100 and 175 keV can be assigned well to the same transitions in the decay of Ta^{185}. It is more natural to consider that the W^{185m} isomeric state decays via the $\frac{7}{2}^-[503]$ intrinsic state. Consequently, the 125-keV gamma ray seems to be the rate-determining transition of this

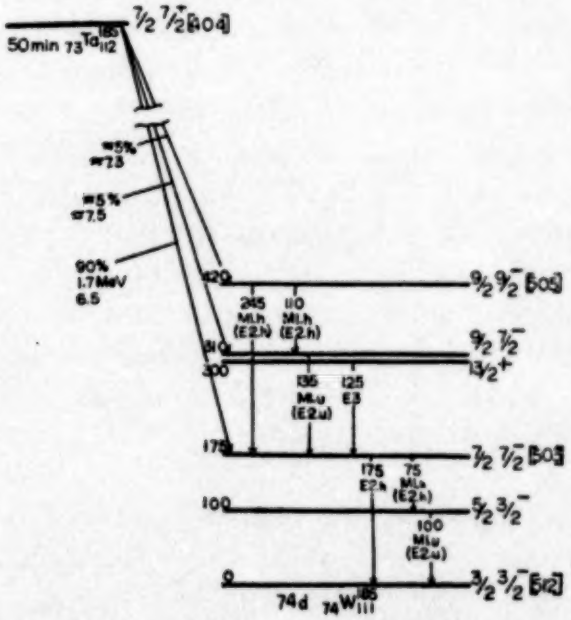

Fig. 4. Tentative decay scheme of Ta^{185} and W^{185m}.

isomer. The half life and the energy require this transition to be an E3 or an M3 type on the basis of the single particle estimate. The K conversion coefficients of 125-keV E3 and M3 transitions are 1.2 and 48, respectively, Since the observation excludes the K conversion coefficient to be greater than 3, the E3 assignment is strongly favoured. This has been also pointed out by Pöe[6]). Even if we assume this transition to be M2, the K conversion coefficient is 28 and this assignment cannot be possible. Therefore, it is necessary that this isomeric state should be placed at 300 keV above the ground state and the 125-keV rate-determining transition is a E3 transition to the $\frac{7}{2}^-[503]$ intrinsic state. Assuming the above level order (shown in fig. 4), all the gamma rays can be explained without any conflict. If we assume another level order, that is, if the 175-keV transition is placed above the 125-keV transition and is E3, the weak 230-keV sum peak cannot be explained. And if the 230 keV is a real gamma ray and the rate-determining transition, the intensities of the other two gamma rays are too strong.

The classification of the gamma rays and intensities of the K conversion electrons estimated from Rose's table are summarized in table 2.

4. Existence of both Spherical and Deformed States in W^{185}

As discussed in the preceding section, the gamma rays observed in the decay of Ta^{185} are quite consistently fitted into a decay scheme which postulates the $\frac{3}{2}^-[512]$, $\frac{7}{2}^-[503]$ and $\frac{9}{2}^-[505]$ intrinsic states and their rotational states as the lower states of W^{185}.

However, it is extremely difficult to fit the 1.6 min isomer in such a level scheme. The discussion in the former section results in an assignment of $\frac{13}{2}^+$ character for this isomer. Of course a $\frac{13}{2}^+[606]$ Nilsson level is expected from the Nilsson diagram, but then, there must be a $\frac{11}{2}^+[615]$ Nilsson level below this level. Since there are a few levels in between for $\delta \geqq 0.1$, the $\frac{11}{2}^+[615]$ Nilsson level cannot be the 111th neutron state and it is not possible to think that the $\frac{11}{2}^+[615]$ intrinsic state comes higher, as a hole state, than the $\frac{13}{2}^+[606]$ intrinsic state. Below this mass number, as is beautifully seen in Mottelson and Nilsson's work, no serious violation of the unified model is found in odd mass nuclei. All the levels seen in the Nilsson diagram are found in actual nuclei in their right order except for *minor* exceptions.

It seems, therefore, to be necessary to assign a configuration for this $\frac{13}{2}^+$ level which is not expected from Nilsson's scheme. Actually, one is forced to describe this state as a spherical state in which the last odd neutron is in the $\frac{13}{2}^+$ *shell model state*. Since this nucleide is at the end of the deformed region, where deformation begins almost to disappear, it is not completely strange that this may happen. The fact that for other states the Nilsson model still works, in other words, that there are still stably deformed states, does not argue against

to W^{183}, the same types of transition are found, e.g., from the $\frac{7}{2}^+[404]$ intrinsic state to the $\frac{7}{2}^-[503]$ intrinsic state. Their log *ft* values are about 6.5 and 6.9, respectively: this is consistent with the value 6.5 obtained above.

The beta component to the first rotational $\frac{9}{2}^-$ state of the $\frac{7}{2}^-[503]$ intrinsic state is estimated to be about 5 %, and the component to the $\frac{9}{2}^-[505]$ intrinsic state is found to be about 5 %. This gives for their lof *ft* values about 7.3 and 7.5, respectively. These are in agreement with the systematics of the beta transitions classified as 1.u. In the above consideration, we introduced the $\frac{9}{2}^-[505]$ intrinsic state for the beta component to the 420-keV state. But if, instead, we assume that the first rotational $\frac{9}{2}^-$ state of the $\frac{7}{2}^-[503]$ intrinsic state appears at 110 keV above and the second rotational $\frac{11}{2}^-$-state appears at 245 keV above the $\frac{7}{2}^-[503]$ intrinsic state, and assume the 135-keV transition above the 110-keV gamma ray, the height of the rotational states fits with the $I(I+1)$ law. However, this assignment is less plausible since the lof *ft* value of the beta transition to the $\frac{11}{2}^-$ state is 7.3, which is too high for first forbidden α-type (unique forbidden) transition. Also the moment of inertia of the $\frac{7}{2}^-[503]$ intrinsic state becomes too low. The fact that the $\frac{9}{2}^-[505]$ intrinsic state must then appear higher is another difficulty of this assignment, since we have no other gamma ray in spite of the rather high decay energy available.

3.2. W^{185m}

The gamma rays of W^{185} at the 75, 100 and 175 keV can be assigned well to the same transitions in the decay of Ta^{185}. It is more natural to consider that the W^{185m} isomeric state decays via the $\frac{7}{2}^-[503]$ intrinsic state. Consequently, the 125-keV gamma ray seems to be the rate-determining transition of this

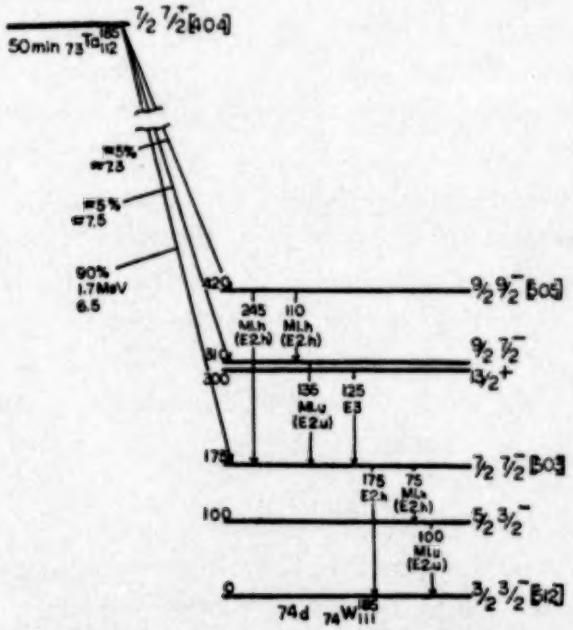

Fig. 4. Tentative decay scheme of Ta^{185} and W^{185m}.

isomer. The half life and the energy require this transition to be an E3 or an M3 type on the basis of the single particle estimate. The K conversion coefficients of 125-keV E3 and M3 transitions are 1.2 and 48, respectively, Since the observation excludes the K conversion coefficient to be greater than 3, the E3 assignment is strongly favoured. This has been also pointed out by Põe[6]). Even if we assume this transition to be M2, the K conversion coefficient is 28 and this assignment cannot be possible. Therefore, it is necessary that this isomeric state should be placed at 300 keV above the ground state and the 125-keV rate-determining transition is a E3 transition to the $\frac{7}{2}^-$[503] intrinsic state. Assuming the above level order (shown in fig. 4), all the gamma rays can be explained without any conflict. If we assume another level order, that is, if the 175-keV transition is placed above the 125-keV transition and is E3, the weak 230-keV sum peak cannot be explained. And if the 230 keV is a real gamma ray and the rate-determining transition, the intensities of the other two gamma rays are too strong.

The classification of the gamma rays and intensities of the K conversion electrons estimated from Rose's table are summarized in table 2.

4. Existence of both Spherical and Deformed States in W^{185}

As discussed in the preceding section, the gamma rays observed in the decay of Ta^{185} are quite consistently fitted into a decay scheme which postulates the $\frac{9}{2}^-$[512], $\frac{7}{2}^-$[503] and $\frac{9}{2}^-$[505] intrinsic states and their rotational states as the lower states of W^{185}.

However, it is extremely difficult to fit the 1.6 min isomer in such a level scheme. The discussion in the former section results in an assignment of $\frac{13}{2}^+$ character for this isomer. Of course a $\frac{13}{2}^+$[606] Nilsson level is expected from the Nilsson diagram, but then, there must be a $\frac{11}{2}^+$[615] Nilsson level below this level. Since there are a few levels in between for $\delta \geqq 0.1$, the $\frac{11}{2}^+$[615] Nilsson level cannot be the 111th neutron state and it is not possible to think that the $\frac{11}{2}^+$[615] intrinsic state comes higher, as a hole state, than the $\frac{13}{2}^+$[606] intrinsic state. Below this mass number, as is beautifully seen in Mottelson and Nilsson's work, no serious violation of the unified model is found in odd mass nuclei. All the levels seen in the Nilsson diagram are found in actual nuclei in their right order except for *minor* exceptions.

It seems, therefore, to be necessary to assign a configuration for this $\frac{13}{2}^+$ level which is not expected from Nilsson's scheme. Actually, one is forced to describe this state as a spherical state in which the last odd neutron is in the $\frac{13}{2}^+$ *shell model state*. Since this nucleide is at the end of the deformed region, where deformation begins almost to disappear, it is not completely strange that this may happen. The fact that for other states the Nilsson model still works, in other words, that there are still stably deformed states, does not argue against

this since the deformation starts and disappears suddenly, as illustrated by some examples[9, 10]).

That such an isomer is not found in the odd-mass osmium isotopes is probably due to their low-lying $\frac{9}{2}^-$ state. In platinum there are many $\frac{1}{2}^+$ states in the very low energy region.

The hindrance factor ($\approx 10^3$) for the isomeric transition also seems to support this fact. If the state were the $\frac{1}{2}^+$[606] Nilsson level, the isomeric transition would be classified as unhindered and the observed hindrance factor would be too high. This large hindrance factor may be due to the large change in the quadrupole deformation.

The energy between the deformed state and the spherical state may be calculated by adding up the energy levels in Nilsson's diagram. We have performed such additions using both Nilsson's old[2]) and revised diagram[3]). The result, however, shows that the spherical $\frac{1}{2}^+$ state is still higher than the deformed ground state of W^{185} by several MeV. But this is not a serious argument against the former assumption since in this way we do not take the effect of pairing energy into account. The latter has been considered to be the effect which counteracts the growth of deformation[11, 12]). The pairing energy becomes large when there are more components of the $\frac{1}{2}^+$ state in the nuclear wave function. It is easily expected that the $\frac{1}{2}^+$ spherical state has more pairing energy than the deformed states around the ground state of W^{185}.

References

1) A. Bohr and Ben R. Mottelson, Mat. Fys. Medd. Dan Vid. Selsk. **27**, No. 16 (1953)
2) S. G. Nilsson, Mat. Fys. Medd. Dan. Vid. Selsk. **29**, No. 16 (1955)
3) Ben R. Mottelson and S. G. Nilsson, Mat. Fys. Skr. Dan Vid. Selsk. **1**, No. 8 (1959)
4) G. Scharff-Goldhaber, D. E. Alburger, G. Harbottle and M. McKeown, Phys. Rev. **111** (1958) 913
5) O. B. Nielsen, N. O. Roy Poulsen, R. K. Sheline and Skytte Jensen, Nuclear Physics **10** (1959) 475
6) A. J. Pöe, Phil. Mag. **46** (1955) 611
7) R. B. Duffield, L. Hsiao and E. N. Sloth, Phys. Rev. **79** (1950) 1011
8) I. R. Williams and M. W. Johns, Nuovo Cimento **6** (1957) 18
9) P. Brix, Z. Ph. **132** (1952) 579
10) G. Scharff-Goldhaber, Phys. Rev. **90** (1953) 587
11) B. L. Birbrair, JETP, 33 (1957) 1235
12) S. T. Belyaev, Mat. Fys. Medd. Dan. Vid. Selsk. **31**, No. 11 (1959)

1.E.5: 8.B

Nuclear Physics **19** (1960) 337—345; © *North-Holland Publishing Co., Amsterdam*
Not to be reproduced by photoprint or microfilm without written permission from the publisher

CHARGE DISTRIBUTION IN NUCLEI AND ENERGY LEVELS OF μ MESONIC ATOMS

G. E. PUSTOVALOV and M. S. KRECHKO

Faculty of Physics, Moscow State University, Moscow

Received 14 December 1959

Abstract: The $2P_{\frac{3}{2}} \rightarrow 1S_{\frac{1}{2}}$ transition energies of μ mesonic atoms are calculated using Hofstadter's nuclear charge distribution. Numerical solutions of the Schroedinger equation for μ mesonic atoms for uniform charge distribution inside a sphere of radius R_0 are used as zero-order approximation. Corrections due to modifications of uniform charge distribution and relativistic effects are taken into account by perturbation theory. It is shown that the trapezoidal and the smoothed uniform (Fermi type) models, which are equivalent for electron scattering, are not equivalent for the determination of the $2P_{\frac{3}{2}} \rightarrow 1S_{\frac{1}{2}}$ transition energy of μ mesonic atoms. Agreement between the experimental transition energies and those calculated for the smoothed uniform model is satisfactory for heavy μ mesonic atoms. As for light mesonic atoms the value r_0 occurring in the formula for the uniform equivalent model radius $R_{eff} = r_0 A^{\frac{1}{3}} \times 10^{-13}$ cm and determined from the experimental transition energy values of μ-mesonic atoms proves to be smaller than that obtained from electron scattering.

1. Introduction

Most experiments on the determination of the proton distribution in nuclei offer a possibility to find only one parameter characterizing this distribution. The radius of the uniformly charged sphere whose size is chosen so as to agree with experiment can be taken as this parameter. The dependence of the effective "electromagnetic" radius on the mass number A, found from the experiments in which the interaction is mainly determined by electric forces, essentially follows the formula[1–3]

$$R_{eff} = r_0 A^{\frac{1}{3}} \times 10^{-13} \text{ cm}, \tag{1}$$

where $r_0 \approx 1.2$.

After the experiments of Hofstadter *et al.*[4,5]) on high energy electron scattering on nuclei it was found possible to describe the nuclear charge distribution by two-parameter models which differ little from the uniform model for medium and heavy elements ($Z \gtrsim 20$). One of the parameters, c, is the distance from the nuclear centre at which the charge density $\rho(r)$ decreases to half its centre value. The other, d, is the skin thickness, i.e. the distance at which the density decreases from 90 % of its maximum value to 10 %. The values of these parameters were obtained in particular for some spherical nuclei with Z from 20 to 83 for the smoothed uniform model (the Fermi model)

$$\rho(r) = \rho_1 \left(1 + \exp \frac{r - c_1}{z_1}\right)^{-1}, \tag{2}$$

and for the trapezoidal model

$$\rho(r) = \begin{cases} \rho_3 & (0 \leq r \leq c_3 - z_3)\,, \\ \rho_3(2z_3)^{-1}(c_3 + z_3 - r) & (c_3 - z_3 \leq r \leq c_3 + z_3)\,, \\ 0 & (r \geq c_3 + z_3)\,. \end{cases} \tag{3}$$

Here $z_1 = d/4.40$, $z_3 = d/1.60$, $c_3 = 0.98$; c_1 and ρ_1 and ρ_3 are the normalization factors found from the condition $\int \rho(r)\, d\tau = eZ$. As is emphasized by Hofstadter[4]), both models describe high energy electron scattering on nuclei equally well. On averaging the experimental values of parameters it was found that the skin thickness d was roughly the same for all nuclei except the lightest ones and was equal to 2.4×10^{-13} cm, the dependence of c_1 on A being

$$c_1 \approx 1.08\, A^{\frac{1}{3}} \times 10^{-13} \text{ cm}\,. \tag{4}$$

The aim of the present paper is the calculation of the $2P_{\frac{3}{2}} \rightarrow 1S_{\frac{1}{2}}$ transition energy for μ mesonic atoms with the charge densities (2) and (3) and the comparison of the results with the experimental data on X-ray energies of μ mesonic atoms[1]). It must be noted that so far only the $2P_{\frac{3}{2}} \rightarrow 1S_{\frac{1}{2}}$ transition energy for medium and heavy mesonic atoms has been measured. Therefore, it is impossible to determine from these experiments both parameters characterizing the nuclear charge distribution. If, however, these parameters have already been determined from some other experiments—from high energy electron scattering in the present case—the comparison of the calculated and experimental energies of even one transition is by no means useless, all the more so as the transition energy in mesonic atoms and the differential cross-section of electron scattering may be sensitive to different details of nuclear charge distribution, and the models equivalent for some experiments need not be equivalent for others.

2. Calculation of the $2P_{\frac{3}{2}} \rightarrow 1S_{\frac{1}{2}}$ Transition Energy in μ Mesonic Atoms

2.1. ZERO-ORDER APPROXIMATION

To calculate the $2P \rightarrow 1S$ transition energy in μ mesonic atoms we use a method[6]) for finding the energy levels of mesonic atoms, which consists in using as zero-order approximation the non-relativistic wave equation describing the meson motion in the field of the nucleus charged uniformly inside a sphere of radius R_0. In this case the solution is a function of one parameter $t = R_0 Z/a_\mu$ where $a_\mu = \hbar^2/me^2$ is the Bohr radius (m being the reduced mesonic mass). Let us use relative units

$$x = \frac{r}{R_0}\,, \quad \mathcal{E} = \frac{E}{E_0} \tag{5}$$

where $E_0 = -me^4Z^2/2\hbar^2$ is the non-relativistic energy of the ground mesonic atom state for the point nucleus. A numerical solution of the Schroedinger

equation obtained by using the continuity of the wave functions and their first derivatives on the nuclear edge was approximately represented in the following form, expressing the dependence of the quantum defect Δn on the parameter t:

$$\Delta n = A_0 + A_1 t + A_2 t^2 + A_3 t^3 + A_4 t^4 + A_5 t^5 + (C_0 + C_2 t^2)\, e^{-B_1 t - B_2 t^2 - B_3 t^3 - B_4 t^4}. \tag{6}$$

Here the exponential term may be disregarded for $t > 1$. For the 1S and 2P states the coefficients of this formula are given in table 1. The relative energy may be determined from

$$\mathscr{E} = (n + \Delta n)^{-2} \tag{7}$$

where n is the principal quantum number. The radial wave functions of the 1S and 2P states may be approximately expressed in the form of

$$R_{nl}(x) = \begin{cases} C_{nl}(1 - a x^{\frac{1}{2}}) x^l & (x \leqq 1), \\ C_{nl} u x^l\, e^{b(1-x)} & (x \geqq 1) \end{cases} \tag{8}$$

where l is the orbital quantum number and the parameters b and $u = 1 - a$ may be found according to the formula

$$\left.\begin{matrix} u^{-1} \\ b^{-1} t \end{matrix}\right\} = D_0 + D_1 t + D_2 t^2 + D_3 t^3 \tag{9}$$

whose coefficients are given in table 2; C_{nl} is the normalization factor.

TABLE 1

Values of the coefficients in formula (6)

	1S	2P
A_0	−0.032885	
A_1	0.165892	
A_2	0.013883	−0.0033673
A_3	−0.008312	0.0087840
A_4	0.001082	−0.0019263
A_5		0.0001244
B_1	5.0446	2.6086
B_2	0.9826	0.7091
B_3	−0.5560	0.7000
B_4	2.9875	
C_0	0.032885	
C_2		0.0033673

TABLE 2

Values of the coefficients in formula (9)

Levels	Parameters	D_0	D_1	D_2	D_3
1S	u^{-1}	1	0.4501	−0.0424	0.00580
	tb^{-1}	1	0.3068	0.0212	−0.00977
2P	u^{-1}	1	0.2650	0.0187	−0.00220
	tb^{-1}	2	0.0015	0.0388	−0.00333

If this approximate solution is known, the relativistic corrections, energy level changes caused by modifications to the uniform model, and some other corrections may be found on the basis of the perturbation theory. According to this theory the energy level shift in the first order approximation is equal to

$$\Delta E_{nl} = \int_0^\infty R_{nl}^2(x) x^2 \Delta U \mathrm{d}x \tag{10}$$

where ΔU is the addition to the potential energy of the uniform charge distribution U_0 which has the form

$$U_0 = \begin{cases} -\dfrac{e^2 Z}{R_0}\left[\tfrac{3}{2} - \tfrac{1}{2}\left(\dfrac{r}{R_0}\right)^2\right] = \dfrac{E_0}{t}(3 - x^2) & (0 \leqq x \leqq 1), \\ -e^2 Z/r = 2\dfrac{E_0}{tx} & (x \geqq 1). \end{cases} \tag{11}$$

In calculating integrals with the approximate wave functions it is convenient to use the symbols

$$F_m(a) = \int_0^1 (1 - ax^{\frac{1}{2}})^2 x^m \,\mathrm{d}x = \frac{1}{1+m} - \frac{4a}{5+2m} + \frac{a^2}{4+m},$$

$$G_m(\xi; x_1, x_2) = \int_{x_1}^{x_2} \mathrm{e}^{\xi(1-x)} x^m \,\mathrm{d}x$$

$$= \frac{m!}{\xi^{m+1}}\left[\mathrm{e}^{-\xi(x_1-1)} \sum_{k=0}^{m} \frac{(\xi x_1)^k}{k!} - \mathrm{e}^{-\xi(x_1-1)} \sum_{k=0}^{m} \frac{(\xi x_2)^k}{k!}\right]. \tag{12}$$

Taking into account the formulae (8), (10) and (12) one may see that the formulae determining the 2P level shifts have the same form as the 1S level formulae with F_{m+2}, G_{m+2} replacing F_m, G_m. The same will hold for the normalization factor of wave functions which for the 1S state has the form

$$C_{10} = [F_2(a) + u^2 G_2(2b; 1, \infty)]^{-\frac{1}{2}}. \tag{13}$$

2.2. CORRECTION DUE TO DISTRIBUTION FORM

Since the level energy of mesonic atoms is mainly determined by a root-means square (rms) radius of nuclear charge distribution, we took as R_0 for the zero-order approximation the radius of a uniform model for which the rms radius $\langle r^2 \rangle_{\text{unif.}} = \frac{3}{5} R_0^2$ is equal to that of the non-uniform distribution

$$\langle r^2 \rangle_{\text{non-unif.}} = \frac{4\pi}{eZ} \int_0^\infty \rho(r) r^4 \, \mathrm{d}r \,. \tag{14}$$

To simplify the calculation in the Fermi model case, we replace the charge density (2) with a polynomial at $r \leqq R_0$ and with an exponential expression at $r \geqq R_0$

$$\rho(x) = \begin{cases} \sum_i \alpha_i x^i & (0 \leqq x \leqq 1) \,, \\ \sigma \, \mathrm{e}^{\delta(1-x)} & (x \geqq 1) \,, \end{cases} \tag{15}$$

where $\sigma = \sum_i \alpha_i$; the polynomial power and its coefficients α_i were adapted so that the values $\rho(x)$ at $x \leqq 1$, found according to formulae (2) and (15), differ no more than by $0.01\, \rho_1$, and δ was adapted so that $\langle r^2 \rangle$ for (2) and (15) are equal. The values ρ_1 and $\langle r^2 \rangle$ for distribution (2) were determined by numerical integration. The meson potential energy for charge distribution (15) may be found by integrating Poisson's equation; then the addition to potential energy (11), due to the deviation of distribution (15) from the uniform distribution, will be

$$\begin{aligned} &\frac{E_0}{t} \left[(2\gamma - 3) + x^2 - \sum_i \frac{2\alpha_i x^{i+2}}{(i+2)(i+3)} \right] \quad (0 \leqq x \leqq 1) \,, \\ &- \frac{E_0}{t} \, 2\sigma\delta^{-3} (2x^{-1} + \delta) \, \mathrm{e}^{\delta(1-x)} \qquad\qquad (x \geqq 1) \,, \end{aligned} \tag{16}$$

where

$$\gamma = \sum_i \frac{\alpha_i}{i+2} + \sigma G_1 (\delta; 1, \infty) \,.$$

Finally, the 1S level shift for the Fermi model, for example, is obtained through eqs. (8), (10), (12) and (16):

$$\begin{aligned} \Delta\mathscr{E}_{10} = \frac{C_{10}^2}{t} \Big\{ &(2\gamma - 3) F_2(a) + F_4(a) - \sum_i \frac{2\alpha_i F_{i+4}(a)}{(i+2)(i+3)} \\ &- 2\sigma u^2 \delta^{-3} [2G_1(2b + \delta; 1, \infty) + \delta G_2(2b + \delta; 1, \infty)] \Big\} \,. \end{aligned} \tag{17}$$

Similar expressions have been derived for the trapezoidal model[7]).

2.3. OTHER CORRECTIONS

Other corrections to be taken into account in the final calculation of the $2P_{\frac{1}{2}} \rightarrow 1S_{\frac{1}{2}}$ transition energy include relativistic corrections, a correction caused by vacuum polarization and a correction due to nuclear polarization by a meson. The relativistic corrections were calculated according to ref. [6]). In our calculation we used the values determined in ref. [8]), for μ mesonic atom level shift due to vacuum polarization with taking into account the finite nuclear size.

We neglected the corrections (see e.g. ref. [9])) whose values greatly depend on the properties of individual nuclei due to their shells. These are a correction for nuclear charge polarization by a meson which increases transition energy by 0.25 to 0.5 % and a correction for level splitting caused by the influence of electrical quadrupole moment. Nor did we take into account the corrections whose values may be disregarded at the present calculation accuracy (≈ 0.1 %) such as the influence of nuclear magnetic moment, the screening of a nuclear charge by atomic electrons, etc.

3. Results

The $2P_{\frac{1}{2}} \rightarrow 1S_{\frac{1}{2}}$ transition energy of μ mesonic atoms in relative units, calculated for the Fermi and trapezoidal models with Hofstadter's average parameters, are shown in fig. 1. For comparison, here is also shown the transition energy calculated for uniform charge distribution with $R_0 = 1.18\, A^{\frac{1}{3}} \times 10^{-13}$ cm. In heavy nuclei ($Z > 50$) the transition energy for the trapezoidal model is by 2 to 3 % greater than that for the Fermi model. These models are therefore not equivalent for the transition energy of μ mesonic atoms, though they are equivalent for high energy electrons scattering. The reason probably is that the nuclear charge densities for both models nearly coincide in the skin region, the most essential for the scattering differential cross-section (see fig. 2), while the rms radii, which largely determine the position of the energy levels of mesonic atoms, if the distributions do not differ too much from the uniform one, differ rather strongly (about 4 %) for these models. For these nuclei an increase of therms radius by 1 % leads to about the same decrease in transition energy. A correction for deviation of distribution from the uniform for the same rms radius increases transition energy by 0.5 to 1.0 % for the Fermi model and by 0.2 to 0.5 % for the trapezoidal one.

For heavy nuclei the experimental transition energies[1]) as seen from fig. 1 lie lower than both curves. For these nuclei the trapezoidal model with Hofstadter's parameter values seems to disagree with experiments on mesonic X-ray energy measurements. Allowances for nuclear polarization by mesons may only increase this discrepancy.

The curve drawn for the Fermi model lies rather close to the experimental points, though outside the limits of experimental accuracy. It should be noted

that in general it is unjustified to expect that the calculations with such average models would completely coincide with experimental data, for considerable deviations due to the individual properties of nuclei are possible.

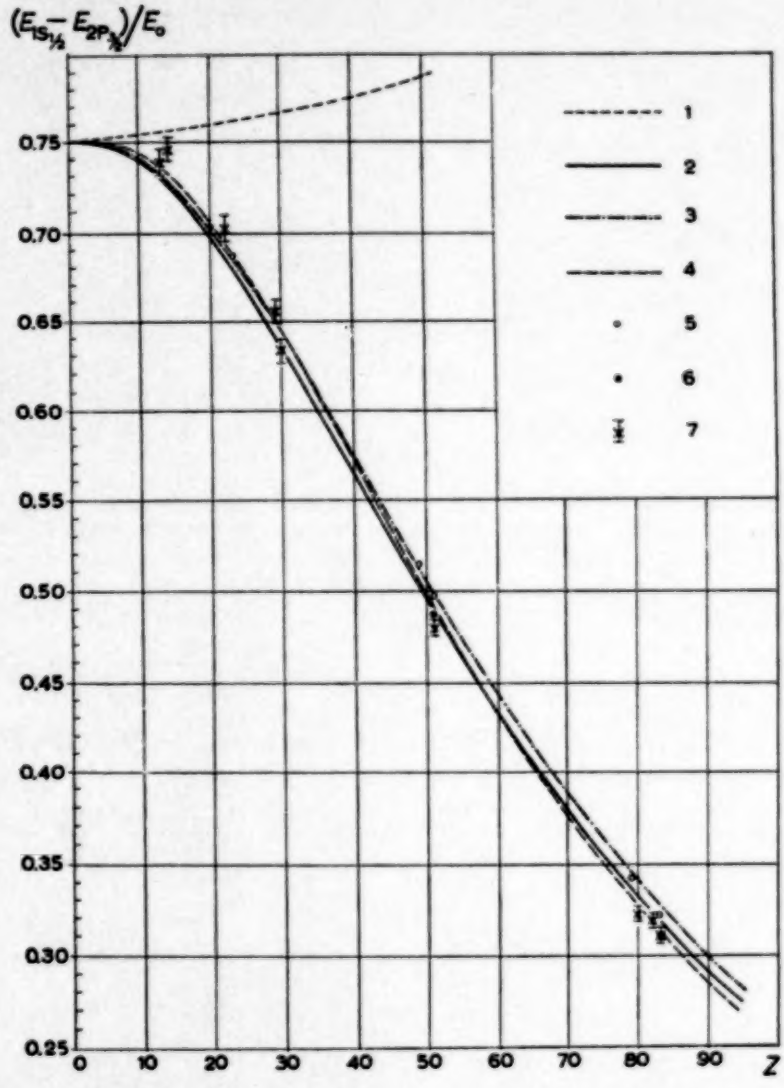

Fig. 1. The $2P_{\frac{1}{2}} \rightarrow 1S_{\frac{1}{2}}$ transition energy of μ mesonic atoms calculated
1) for point nuclei,
2) for the Fermi model with average parameters,
3) for the trapezoidal model with average parameters,
4) for the uniform model with $r_0 = 1.18$,
5) for the Fermi model with experimental parameters,
6) for the trapezoidal model with experimental parameters.
In addition is shown
7) the experimental transition energy (with accuracy limits equal to $\pm$ 1 %).

To gauge the magnitude of these deviations, fig. 1 represents the energies of some mesonic atoms calculated by using the nuclear charge densities whose parameter values were directly obtained in the experiments by Hofstadter *et al.*

For $_{83}Bi^{209}$ the Fermi model transition energy calculated with these parameter values coincides well with the experimental X-ray energy. Still, the average models may play an important part in bringing out various abrupt changes

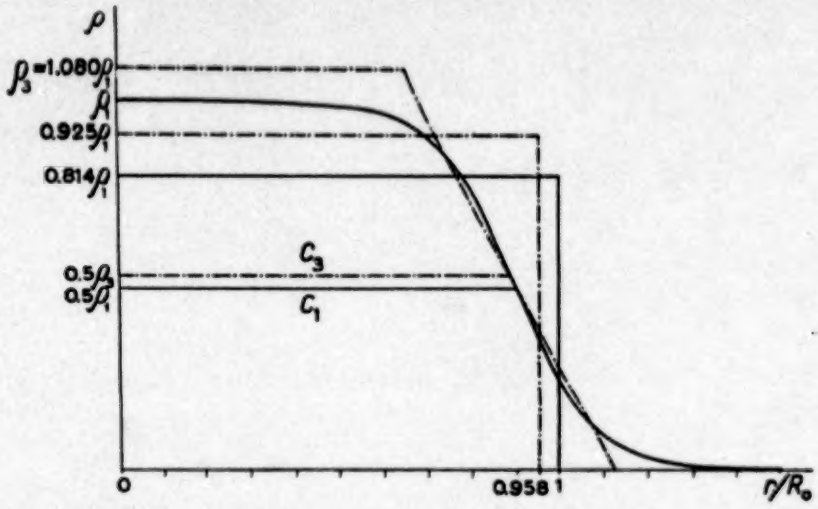

Fig. 2. Comparison of the Fermi, the trapezoidal and two uniform models (for $_{83}Bi^{209}$); one of the latter two models has an rms radius equal to that of the Fermi model, while the second one has an rms radius equal to that of the trapezoidal model.

and periodic regularities.

Let us now consider the nuclei with $Z > 30$. On the whole, the experimental points for them are situated above both curves. Hence the rms radii of the distributions used in calculating these curves are too large. This is quite clear from fig. 3 which shows the Z dependences of the coefficient r_0 in eq. (1) for the

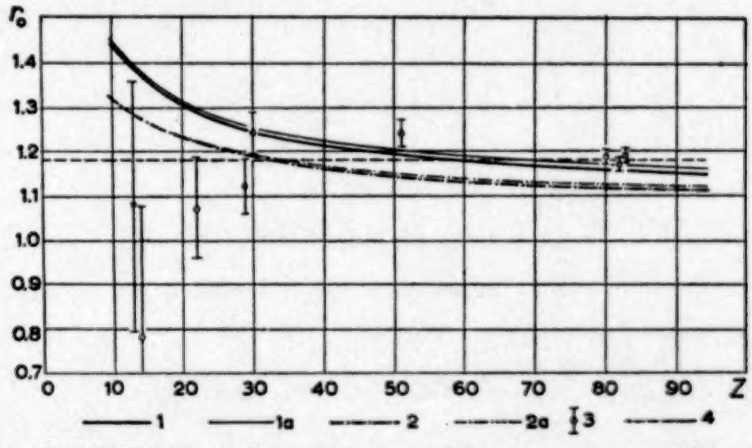

Fig. 3. The dependence of r_0 upon Z for the uniform model

1) equivalent to the Fermi model,
1a) having an rms radius equal to that of the Fermi model,
2) equivalent to the trapezoidal model,
2a) having an rms radius equal to that of the trapezoidal model,
3) yielding the experimental transition energy (the limits of accuracy for r_0 correspond to an accuracy of $\pm$ 1 % for the transition energy).

For comparison here is also drawn
4) the line for $r_0 = 1.18$.

radii of the uniform models equivalent to the Fermi and trapezoidal models, i.e. for the radii, with which the uniform models yield transition energies equal to those calculated with the non-uniform models. The same figure lists the values of r_0 for the equivalent radii of the uniform model, found from experimental data[1]), as well as the limits of accuracy in determining them, if the transition energy is measured with 1% accuracy. Though accuracy in determining the equivalent experimental radii decreases very much as Z decreases, their comparison with the equivalent radii for Hofstadter's models shows that they do not agree with Hofstadter's increase of r_0 from 1.2 up to 1.35 as Z decreases in eq. (1).

To sum up, it has been shown that

1) the nuclear charge distributions (trapezoidal and smoothed uniform), equivalent for the high energy electron scattering, are not equivalent for the $2P_{\frac{3}{2}} \rightarrow 1S_{\frac{1}{2}}$ transition energy of μ mesonic atoms with large Z;

2) of these two distributions only the smoothed uniform distribution agrees with experiments on the determination of the X-ray energy of μ mesonic atoms for large Z;

3) for μ mesonic atoms with $10 < Z < 30$ the uniform distribution radii found from mesonic atom experiments are smaller by 10 to 30% than those from experiments on high energy electron scattering.

In conclusion it will be noted that, in our opinion, it is desirable to carry out more systematic experiments on the determination of mesonic X-ray energy using many nuclei (enriched isotopes), since even a small increase in experimental accuracy will yield useful information on the influence of the nuclear quadrupole moments and nuclear shell filling on mesonic atom spectra.

The authors are indebted to Prof. D. Ivanenko for stimulating discussion of the results.

References

1) V. L. Fitch and J. Rainwater, Phys. Rev. **92** (1953) 789
2) K. W. Ford and D. L. Hill, Phys. Rev. **94** (1954) 1630
3) L. N. Cooper and E. M. Henley, Phys. Rev. **92** (1953) 801
4) R. Hofstadter, Revs. Mod. Phys. **28** (1956) 214
5) B. Hahn, D. G. Ravenhall and R. Hofstadter, Phys. Rev. **101** (1956) 1137
6) G. E. Pustovalov, JETP **36** (1959) 1806; translation: Soviet Phys. JETP **36** (1959) 1288
7) M. S. Krechko, Graduation Thesis, Moscow State University (1959)
8) G. E. Pustovalov, JETP **32** (1957) 1519; translation: Soviet Phys. JETP **5** (1957) 1234
9) E. M. Henley, Revs. Mod. Phys. **30** (1958) 438

2.J *Nuclear Physics* **19** (1960) 346—365; © *North-Holland Publishing Co., Amsterdam*
Not to be reproduced by photoprint or microfilm without written permission from the publisher

DIRECT PROCESSES AND COLLECTIVE EFFECTS IN HIGH ENERGY PROTON INDUCED FISSION

H. FAISSNER

CERN, Geneva, Switzerland

and

H. SCHNEIDER

Physikalisches Institut der Universität Tübingen, Tübingen, Germany

Received 4 April 1960

Abstract: Nuclear emulsions loaded with thorium have been exposed to the external 600 MeV proton beam of the CERN synchro-cyclotron. For each fission event both ranges, a characteristic angle relative to the proton beam and the angle between the two fragments was measured. From these data one computes, under certain assumptions, the longitudinal momentum imparted to the fissioning nucleus. The distribution of momentum transfers obtained falls off exponentially towards higher values; its maximum is estimated to lie around 170 MeV/c. At momentum transfers above 300 MeV/c the light fragment is emitted preferentially in the forward direction. This indicates the existence of a direct, fast fission mode. The fore-aft asymmetry is largest for fissions almost parallel to the proton beam; it increases with increasing momentum transfer. The range distribution is symmetric. Qualitatively the fast fission may be described as a deformation of a viscous liquid drop by the fast cascade. At momentum transfers below 300 MeV/c there is no significant fore-aft asymmetry. The angular distribution, instead, is peaked around 90° to the primary direction. It can be represented by $1 + \alpha \sin^2\theta$ with $\alpha = 0.64 \pm 0.10$. The range distribution has an asymmetric component. Angular anisotropy and mass asymmetry are consistent with the model of I. Halpern who assumes a collective rotation initiated by the capture of slow secondary nucleons.

1. Introduction

Radiochemical techniques have provided already valuable information about high energy particle induced fission (cf. ref. [1])†). The interpretation of these data, however, encounters severe difficulties. The primary particle in general deposits only a small fraction of its energy inside the nucleus. Therefore, one has a broad spectrum of excitation energies and consequently a great number of possibly quite different reactions eventually leading to fission. Also some nucleons of the target nucleus are ejected in the fast cascade, some others in the subsequent evaporation stage. Thus, there is a variety of nucleides which undergo fission, widely differing in Z and A. These ambiguities are also inherent in the interpretation of angular distributions measured by catcher techniques with or without chemical separation of the collected fragments[2–5]). Moreover,

† This paper gives a very competent and up to date review of the present status of fission physics.

this method seems to suffer from serious instrumental anisotropies[6]), which make a number of previous conclusions[4]) doubtful.

In order to study the mechanisms involved in high energy fission methods which permit the determination of the relevant parameters for every single event seem to be preferable. Indeed, Perfilov and co-workers[7–10]) have already obtained a number of surprising results using nuclear emulsions loaded with solutions of the target material. With 660 MeV protons on uranium they found[7]) an angular distribution (measured from 0° to 90°) which was peaked at 90°. They estimated the excitation energy E^* from the number of light charged particles accompanying each event and found the anisotropy increasing with E^*. On the other hand, the angular distributions found in low and medium energy particle induced fission[1, 11–14]) show maxima at 0° and 180° except very close to threshold[11]). This is readily explained within the framework of A. Bohr's model, which assumes that an appreciable fraction of the angular momentum imparted to the target nucleus is taken over by a collective rotation[1, 15–17]).

Meadows[2]), studying proton induced fission of U and Th, also found this "normal" anisotropy at 45 MeV, which decreased when the energy was raised to 80 MeV. At 155 MeV the anisotropy of symmetric mass pairs was still normal but very small, whereas asymmetric pairs showed a small anisotropy of reversed sign. Recently the existence of this "anomalous" anisotropy was confirmed by Vallinder and Tyrén[3]) in the fission of U by 185 MeV protons. If one believes that this anomalous anisotropy at high energies is also due to collective rotations, one has to assume some secondary process which changes the sign. This was done in a paper of Halpern[18]), which appeared shortly after the beginning of the present experiment. Halpern assumes the capture of slow *secondary* nucleons emerging under almost 90° to the primary direction, the primary proton leaving the nucleus again having lost only a small fraction of its kinetic energy. Of course, this explanation is at variance with the dependence of anisotropy on excitation energy reported by Perfilov[7]). One might remark that this is true for any explanation based on collective rotations. No matter what the details of the model are, collective effects should prevail at the lowest excitation energies involved.

It seemed worthwhile to repeat Perfilov's measurements with two improvements:

a) Instead of relying upon a rather indirect measure for the excitation energy, the momentum imparted to the fissioning nucleus was determined from the angle between the fragments.

b) The full angular distribution from 0° to 180° was measured whenever it was possible. The hope was to detect an asymmetry of fragment emission into the forward or backward hemisphere. The observation of such a fore-aft asymmetry would prove the existence of a fast, direct fission process. Previous attempts to find a fore-aft asymmetry have been made by Cohen *et al.*[12, 13]) with 22 MeV

protons, Fairhall and Halpern[1]) with 43 MeV α-particles, Protopopov and Eismont[19]) and Leachman and Ford[20]) with 14 MeV neutrons. All these experiments failed to show a fore-aft asymmetry exceeding the experimental errors of a few per cent†.

The present paper reports the experimental methods (section 2) and the results obtained with thorium. In particular the distribution of longitudinal momentum transfers is given in section 3. The angular distributions measured are discussed in some detail in section 4. The range distributions are presented in section 5. A brief comparison with the results of other authors follows in section 6. The interpretation of the measurements is given in section 7. They essentially confirm Halpern's model for the low momentum transfer events. The direct process found at very high momentum transfers is possibly describable by a simple hydrodynamical model. Preliminary results of this work have already been reported elsewhere[23]). Experiments with other nucleides are in progress.

2. Experimental Procedure

The *emulsions* were of the fine grained and rather insensitive Ilford L-0 type. They were loaded with thorium by soaking for 8 hours, in a 5 % thorium-nitrate solution containing 4 % glycerine. The low pH value of the solution (1.5) causes an additional reduction of sensitivity[24]). Consequently, only fission fragments and heavy fragments from spallation processes gave black and almost continuous tracks. α-particles from radioactive decay were registered at most as tracks of single grains; primary protons and fast cascade particles were not detected. This permitted fairly high proton fluxes to be used.

The *irradiation* was done in the regeneratively extracted external proton beam of the CERN 600 MeV synchro-cyclotron. The long edge of the photoplates was optically aligned parallel to the beam direction to within $\pm 2°$; it served as a reference for the angle measurements. The dose was about 10^{11} protons per cm^2. After irradiation the plates were soaked for 1½ hours in distilled water and developed with amidol, using a standard temperature gradient procedure.

For *scanning* as well as for *measuring*, a Leitz Ortholux with a magnification of 100 × 1.25 × 10 (oil) was used. The thorium fissions were selected according to the following *acceptance criteria*:

α) both long and short track must show the ionization typical for very heavy ions, i.e. an almost completely black, thick track at the beginning which thins down and/or gets resolved towards the end;

† A different problem has been studied by Sugihara *et al.*[21]) and Nicholson and Halpern[22]): they tried to measure the fraction of fissions *following* some direct process, such as deuteron stripping, instead of proceeding via the usual compound nucleus formation. Even if these experiments had shown an effect exceeding the experimental uncertainties, it could well be compatible with the fission process itself being slow.

β) the long track R_L must not be more than three times as long as the short one R_S;

γ) the total range $R = R_L + R_S$ ought to lie between 18.4 and 25.6 μm.

On the average about 2 thorium fissions were observed per microscope field. The frequency of Ag and Br fissions which could be confused with Th fissions was determined from an unloaded plate exposed and scanned under the same conditions. (Also the same pH of 1.5 was provided by treatment with HNO_3.) The frequency turned out to be (0.33 ± 0.08) % of the true events. Similarly the frequency of confusable thorium α-particle stars was found from a loaded, but unexposed control plate, to be less than 1 % too. Besides the ranges mentioned above the following angles were measured:

the angle θ between the long ranged (= light) fragment and the primary proton direction: θ was defined as shown in fig. 1, in order to account approxi-

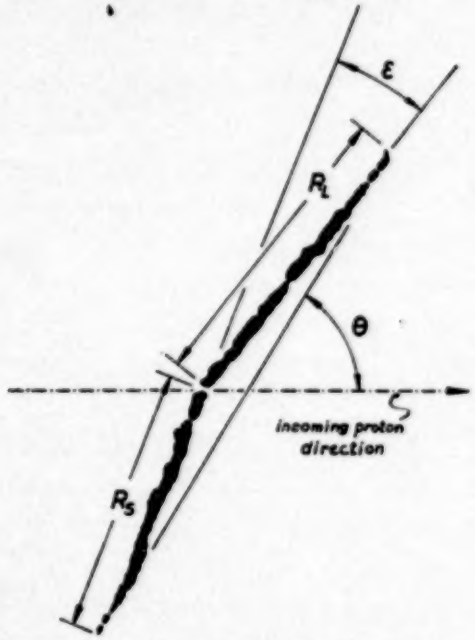

Fig. 1. Re-drawing of a typical event. The measured quantities are indicated.

mately for the centre-of-mass motion;

the angle $180° - \varepsilon$ between the two fission fragments which provides a measure for the momentum transferred to the fissioning nucleus.

All these quantities were measured as projections on the surface of the emulsions. However, the calculation of the true spatial quantities is straightforward as the dip D of each track was measured too. The details have been given in a previous publication[25]). In this paper it was also discussed how the true angular distribution $W(\theta)$ can be obtained from the distribution $W(\theta, \delta_0)$ which results from accepting only tracks with a dip angle δ smaller than a prescribed maximum value δ_0.

The *errors* (obtained as standard deviations of repeated measurements of

the same events) are $\pm$ 0.4 μm for R_L and R_S, $\pm$ 0.2 μm for R, $\pm$ 0.5° for θ and ε, provided the tracks show no appreciable curvature; otherwise the error might be twice as much.

3. The Distribution of Longitudinal Momentum Transfers

Because some deviation from collinearity could arise from multiple scattering of fragments and/or emulsion distortions, a deviation $|\varepsilon| > 4°$ was demanded for a momentum transfer measurement. Therefore, all events were divided into two classes.

Type A contains all events with $|\varepsilon| > 4°$. At $\theta = 90°$ an angle $\varepsilon = 4°$ corresponds (under the assumptions listed below) to a momentum transfer q of 300 MeV/c, i.e. $\frac{1}{4}$ of the primary momentum k_p. For $\theta \neq 90°$, $q(4°)$ is bigger than that (see eq. (2) below). Thus, type A comprises *only* events with $\eta \equiv q/k_p > 0.25$, *but not all of them.*

Type B correspondingly contains all events with $|\varepsilon| < 4°$. Therefore, type B includes *all* events with $\eta < 0.25$, but additionally *also a contamination of high momentum transfer* fissions which increases with $\theta \to 0°$ (or 180°).

A total of 786 type A and 1374 type B events was measured. Allowing for the different solid angle involved in both cases this yields a relative frequency of 27 % type A and 73 % type B events.

The longitudinal momentum transfer q of type A events was calculated under the following simplifying assumptions:

(a) the fissioning nucleus moves in the primary direction,

(b) the mass division is symmetric.

Assumption (a) would hold if the particle emission preceding fission were isotropic. It would still be correct if the total momentum of these particles K were parallel to the primary momentum k_p and if in addition $K < k_p$. As it turned out, even this is not always the case. However, in order to renounce (a) one would have to determine the momenta of *all* the emitted particles; and this is out of the question even in very sensitive emulsions. Assumption (b) is not essential, but it simplifies the calculation considerably†. It has not been made by Ostroumov[26]) who was first to determine q from ε. However, other uncertainties involved in his procedure make its advantages doubtful.

Under the assumptions (a) and (b), one obtains from the measured quantities the ratio of the velocity u of the fissioning nucleus in the lab. system to the fragment velocity v in the system of the moving nucleus

$$(u/v)^2 = 1 - 2\sin^2\theta \operatorname{ctg}^2\varepsilon \{ (1 + \operatorname{tg}^2\varepsilon/\sin^2\theta)^{\frac{1}{2}} - 1 \}. \qquad (1)$$

If one expands the square root, one gets in the first non-vanishing approximation

$$\frac{u}{v} \approx \frac{\operatorname{tg}\varepsilon}{2\sin\theta}. \qquad (2)$$

† There are calculations in progress, using an electronic computer, in which this assumption has been dropped.

From this expression one sees that ε gives a reliable measure of u/v near $\theta = \frac{1}{2}\pi$. For $\theta \approx 0°$ or 180° even a small ε may correspond to a large u/v. This introduces a large uncertainty of the momentum transfers determined in these regions. It is also the reason for the angular dependent contamination of high momentum transfers in type B events.

The fragments' velocity v is determined by the kinetic energy E_k released in the fission process and by the masses of the fragments. The energy E_k depends only a little upon the energy of the primary particle[1,27]). Therefore, one may use the value of E_k in thorium fission determined at lower energies[27]), provided one corrects for the differences in Coulomb energies resulting from the nucleon losses before fission. The proton loss is known from the work of Ivanova[28]), who found, on the average, 3 charged particles accompanying each fission. The number of emitted neutrons was assumed to be 12. With these numbers Jungerman's value leads to a value of $\bar{E}_k$ of 158 MeV. With the aid of these data the values of u/v as computed from eq. (1) were converted into momentum transfers q or relative momentum transfers $\eta \equiv q/k_p$.

Fig. 2 shows the distribution of longitudinal momentum transfers obtained.

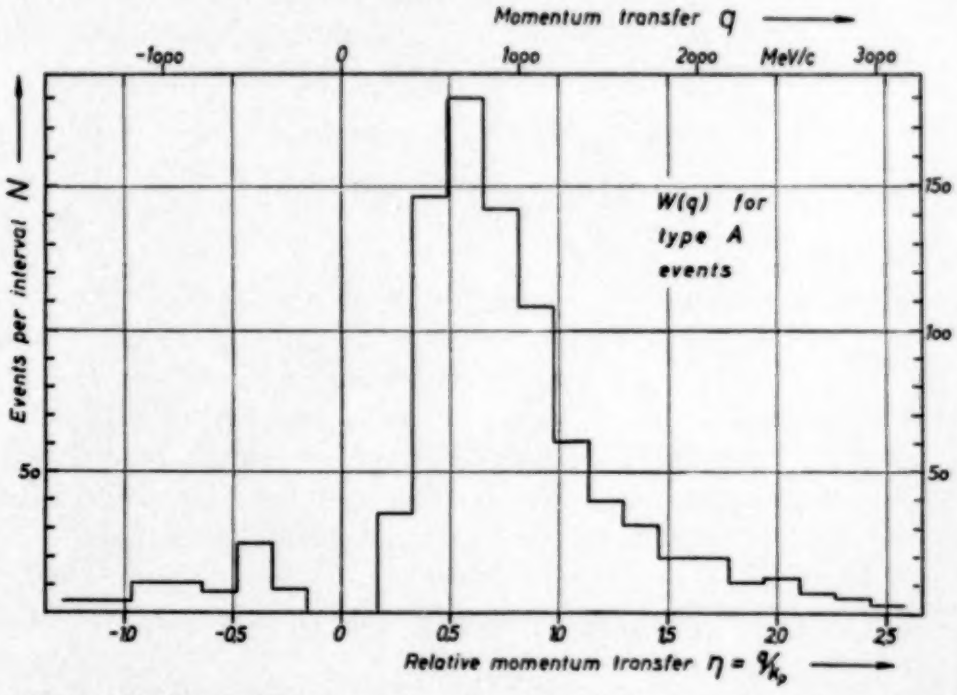

Fig. 2. Distribution of longitudinal momentum transfers for type A events formally calculated under the assumptions a) and b) stated in the text.

The curve falls off approximately exponentially towards high values. The maximum which one expects lies below the minimum observable value of $\eta = 0.25$. (The maximum appearing in fig. 2 is of experimental origin.) However, we can estimate its position if we assume a reasonable shape for the distribution, for instance

$$W(\eta) = \tfrac{1}{2}N\left(\frac{\eta}{\eta_0}\right)^2 \exp\left(-\frac{\eta}{\eta_0}\right). \tag{3}$$

Under the conditions $60° < \theta < 120°$ and $\delta < 15°$, where the counting losses discussed above are small, it was found that 30 % of all events had $\eta > 0.25$. From this it follows that $\eta_0 \approx \frac{1}{15}$ and therefore $\eta(\max) \approx \frac{2}{15}$ and $\bar{\eta} \approx \frac{1}{5}$, corresponding to 170 MeV/c for the most probable, and 250 MeV/c for the average momentum transfer.

There are some events with $\eta > 1$ and $\eta < 0$ in fig. 2. Of course, these unphysical values stem from a violation of at least one of the assumptions stated above. It is easy to see how very asymmetric fissions formally can lead to momentum transfers well above 1. The negative momentum transfers on the other hand show quite directly a violation of assumption (a): in these cases, the total momentum of the fast cascade exceeded the primary momentum, and the momentum of the residual nucleus had to compensate for that. In any case, the events in question have very high inelasticity.

In general, the rough division into types A and B was sufficient to decide whether the effects studied were due to high or low excitation energy events. In the case of the fore-aft asymmetry of fragment emission observed at high momentum transfers, the η-dependence of the effect was also studied.

4. The Angular Distributions

4.1. AT HIGH MOMENTUM TRANSFERS

Because of the relatively low frequency of measurable high momentum transfers, all events with a dip angle $\delta < 37°$ were accepted. The angular distribution measured under these conditions is given in fig. 3a. The minimum at 90° is of instrumental origin; it reflects merely the fact that larger angles θ are rejected by the limitation in dip angle with higher probability than smaller ones. As outlined previously, it is easy to correct for this effect[25]). This was done in fig. 3b. Although this curve represents the true angular distribution of type A events, (defined by $|\varepsilon| > 4°$), its shape has little physical significance. Its maximum at 90° comes essentially from the θ-dependence of ε discussed above.

Indeed, the curve of fig. 3a comes closer to the true angular distribution of fission at high momentum transfers ($\eta > 0.25$) than that of fig. 3b does, because here the two concurring instrumental effects tend to cancel each other. The most important feature of the angular distribution given in fig. 3 is independent of experimental limitations: both of them show a statistically significant fore-aft asymmetry. This means, according to the definition of θ, that at high momentum transfer the *light* fragment is emitted preferentially in the *forward* direction. The existence of this effect is not affected by the counting losses and

corrections discussed, as all of them are symmetric around 90°. The magnitude of the asymmetry, however, does depend upon them.

We define a fore-aft asymmetry A depending upon an arbitrarily chosen cut-off angle θ_0 by

$$A = \frac{N(\theta < \theta_0)}{N(\theta > \pi - \theta_0)} - 1 . \tag{4}$$

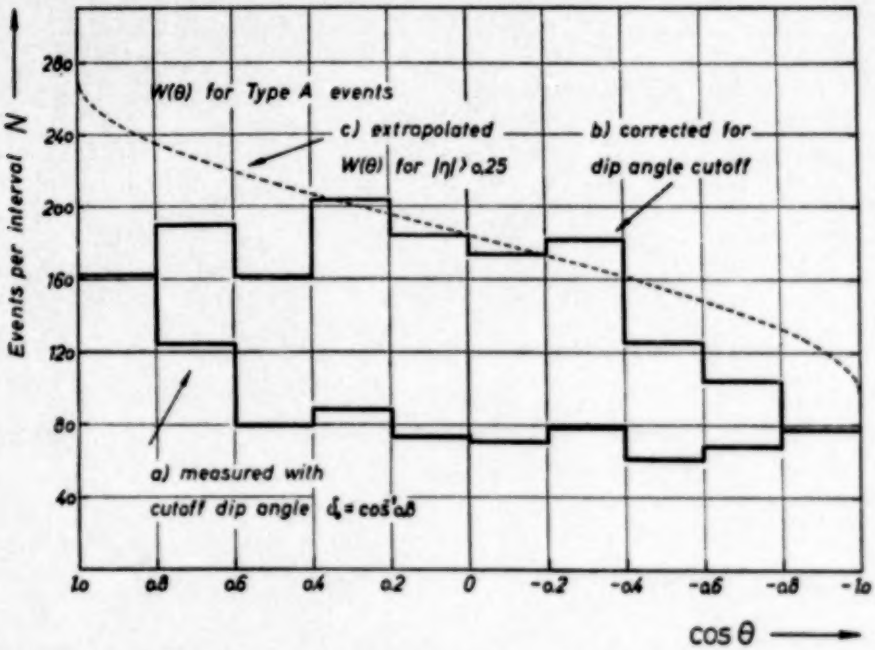

Fig. 3. Angular distribution for type A events. a) Measured with a cut-off dip angle of 37°. b) Corrected for dip angle cut-off. c) Extrapolated angular distribution for all events with momentum transfers above 300 MeV/c.

Some asymmetries deduced from figs. 3a and 3b respectively are given in table 1. In addition to the statistical error, also a more appropriate figure is given: the probability of the asymmetry in question being actually less than or equal to 0, as it results from application of Student's t-test. As one sees from these figures, the fore-aft asymmetry is statistically well established, the confidence level

TABLE 1

Fore-aft asymmetry A as a function of emission angle

θ_0	A measured	t	$P(t)$	A corrected for dip angle cut-off	t	$P(t)$
25.9°	1.00 ± 0.36	3.91	10^{-4}	1.00 ± 0.36	3.91	10^{-4}
45.5°	0.98 ± 0.23	6.14	$\ll 10^{-4}$	0.97 ± 0.23	6.22	$\ll 10^{-4}$
60.0°	0.91 ± 0.18	6.95	$\ll 10^{-4}$	0.86 ± 0.18	6.74	$\ll 10^{-4}$
90.0°	0.48 ± 0.10	5.72	$\ll 10^{-4}$	0.35 ± 0.10	4.44	$\ll 10^{-4}$

exceeding 99.99 % even for the (unrealistic) corrected values. The asymmetry is largest for fissions occurring almost parallel to the proton beam†.

The dependence of the asymmetry on the momentum transfer is given in table 2. The type A events were divided into four classes according to

TABLE 2

Fore-aft asymmetry A as a function of relative momentum transfer η ($\theta_0 = 90°$)

η	A measured	t	$P(t)$ %	A corrected for dip angle cur-off	t	$P(t)$ %
0.25 — 0.60	0.16 ± 0.15	1.14	12.7	0.09 ± 0.14	0.68	24.8
0.60 — 1.00	0.31 ± 0.16	2.17	1.5	0.27 ± 0.16	1.93	2.7
> 1	1.01 ± 0.26	5.50	$\ll 10^{-2}$	0.92 ± 0.25	5.14	$\ll 10^{-2}$
< -0.25	0.68 ± 0.34	2.61	0.5	0.54 ± 0.30	2.18	1.5

$0.25 < \eta < 0.6$, $0.6 < \eta < 1$, $\eta > 1$ and $\eta < -0.25$. As discussed in the preceding section, the latter two classes correspond to high inelasticity too. The limiting angle θ_0 was chosen to $\frac{1}{2}\pi$ in all cases. Again the two values quoted refer to omission or application of the dip-angle correction respectively. Apparently the asymmetry increases with increasing inelasticity. At momentum transfers below 730 MeV/c (i.e. $\eta < 0.6$), the asymmetry is not statistically significant. Actually, this dependence on momentum transfer and the angular dependence discussed above are to some extent the same thing: with our simplifying assumptions η becomes > 1 or negative preferentially for events with θ around 0° or 180°.

An attempt was made to get an angular distribution at high momentum transfers which is free from the counting losses mentioned above. For that purpose, type A events were selected which satisfied $60° < \theta < 120°$ and $\delta < 15°$. Because for a given momentum transfer ε does not vary much with θ in this region (see eq. (2)), this distribution should represent to a good approximation the true angular distribution of *all* events with $|\eta| > 0.25$. Within the (fairly large) statistical errors it could be fitted by (fig. 3c)

$$W(\theta) = 1 - 0.20\theta \qquad (\theta \text{ in radians}) . \tag{5}$$

Although this particular ansatz is of little significance, its qualitative features agree well with the conclusions drawn from the angular distribution of type A events measured under less restrictive conditions.

The main points are:

a) There is no genuine sideways-peaking at high momentum transfers.

† This shows incidentally that the centre-of-mass motion, which might not have been taken into account fully by the definition of θ, is rather irrelevant for the type of asymmetry found (see, however, the note added in proof).

b) The tendency for the light fragment being emitted into the forward hemisphere is greatest for small angles.

4.2. AT LOW MOMENTUM TRANSFERS

The angular distribution of events without measurable momentum transfer ($|\varepsilon| < 4°$) was obtained by selecting fission tracks with small dip angle only ($\delta \leqq 15°$). Then, apart from a small correction, the distribution of projected angles $W(\vartheta)$ (fig. 4) is identical with the true angular distribution $W(\theta)$. As

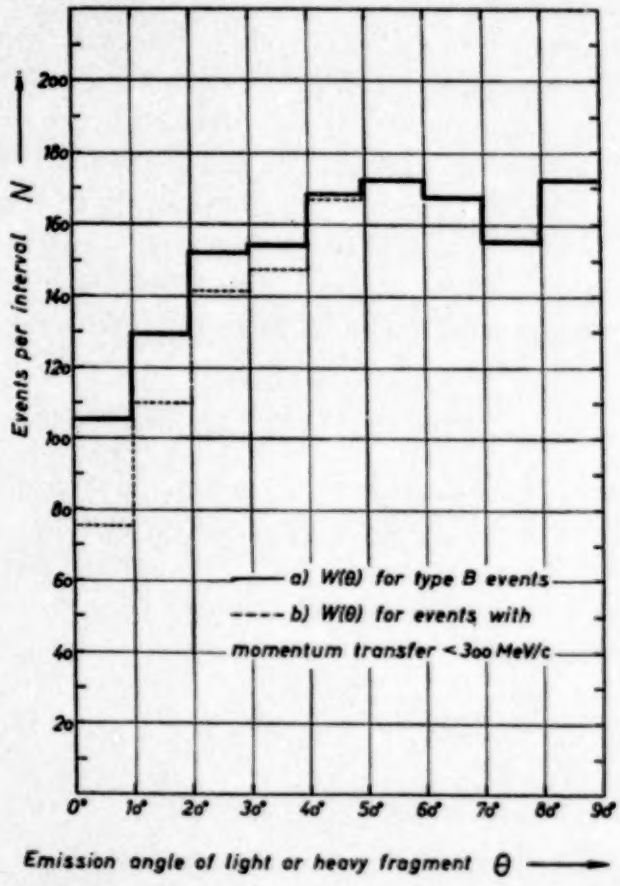

Fig. 4. a) Angular distribution for type B events (light and heavy fragment not distinguished). b) Angular distribution at momentum transfers below 300 MeV/c.

the origin of fission cannot be determined without further information, light and heavy fragments are indistinguishable. The angular distribution, therefore, extends from 0° to 90° only. It does show the "anomalous" angular anisotropy, a preferential emission of fragments around 90°. Its magnitude is (following the definition as used by Lozhkin *et al.*[7])

$$\alpha(30°) \equiv \frac{N(60° < \theta \leq 90°)}{N(\theta < 30°)} - 1 = 0.28 \pm 0.09\,. \qquad (6)$$

A least squares fit to the distribution of fig. 4a with an ansatz

$$W(\theta) = 1 + \alpha \sin^2\theta \tag{7}$$

gave

$$\alpha = 0.36 \pm 0.09 .$$

In any case the anisotropy is well established; the confidence level exceeds 99.9 %.

The distribution of fig. 4a contains with decreasing angle an increasing amount of high momentum transfer events. Therefore, the anisotropies deduced above are lower limits for the actual anisotropy at low momentum transfers. The correction was done simply by subtracting the difference of the curves of figs. 3c and 3b multiplied by the ratio of the two different solid angles involved. Even if the curve of fig. 3c deviated appreciably from the true distribution, the correction would be little affected, because the ratio of type A to type B events is small. The resulting angular distribution at low momentum transfers ($|\eta| < 0.25$) is given in fig. 4b. One deduces the following anisotropies:

$$\alpha(30°) = 0.51 \pm 0.11 , \quad \alpha = 0.68 \pm 0.10 .$$

The interpretation of the anisotropy in terms of a collective rotation implies the absence of any fore-aft asymmetry. In order to test this, one has to extend the angular distribution to 180°. This implies the knowledge of the origin of fission. As it was shown by our group[25, 29, 30]), the origin of fission can be determined under certain conditions from the ionization properties of the fission fragments: in about 50 % of all cases, the ionization of the two fragments near origin was found to differ appreciably from each other. The ionization of the originally less ionizing fragment, (which can be either the heavy or the light one) reaches a maximum a few μm after the origin. Under suitable development there is a gap at the beginning of this fragment's path, whereas all other parts of the two tracks (apart from the endings) are black. For practical purposes, the following procedure was adopted:

a) Only those tracks were accepted, which have a gap in the inner 50 % of the total track length, which exceeds the next smaller gap for at least a factor of two in length.

b) The origin was assigned to the middle of this long gap. This is not quite correct because it presumably lies at one edge of the gap. However, it is not known a priori at which one. The error introduced herewith is on the average 0.5 μm. This introduced in no case an ambiguity in the assignment of light and heavy fragment.

A more serious limitation of the method is caused by the gaps resulting from statistical fluctuations of development. (One of them may be seen in each of the

tracks of fig. 1). According to test measurements performed with type A events, there is a 30 % chance of confusing these gaps with the non-statistical ones[30]). But these 30 % wrongly identified origins should only add a constant background to the distributions.

The full angular distribution $W(\theta)$ of type B events determined by this method is given in fig. 5a. The 90° anisotropy is compatible with the more

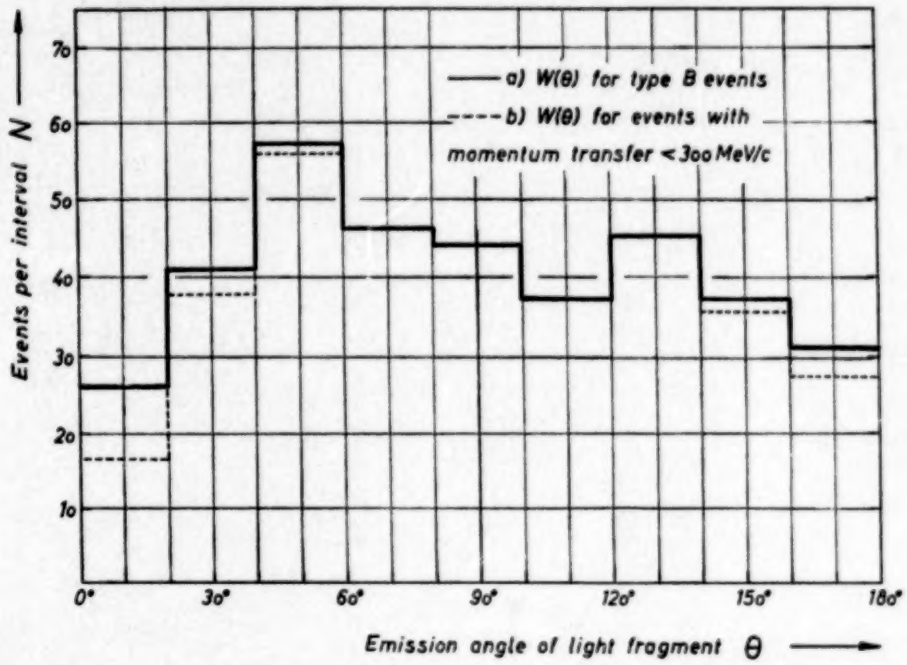

Fig. 5. a) Complete angular distribution of type B events which permitted discrimination between light and heavy fragment. b) The corresponding distribution for momentum transfers below 300 MeV/c.

accurate values from fig. 4. In addition, there is a slight fore-aft asymmetry $A = 0{,}17 \pm 0.12$, which however does not exceed the 95 % confidence level. A certain asymmetry is to be expected because of the high momentum transfer events included in type B. After the correction, the asymmetry has disappeared almost completely (fig. 5b). Thus, it has been shown that at low momentum transfer there is an appreciable sideways-peaking of the angular distribution; on the other hand, no forward-backward preponderance of fragment emission was found.

5. The Range Distributions

5.1. AT HIGH MOMENTUM TRANSFERS

The range distributions measured give a fairly reliable picture of the mass distributions. Considering energy loss by ionization and excitation only, N. Bohr[31]) obtained with some simplifying assumptions, the following expression

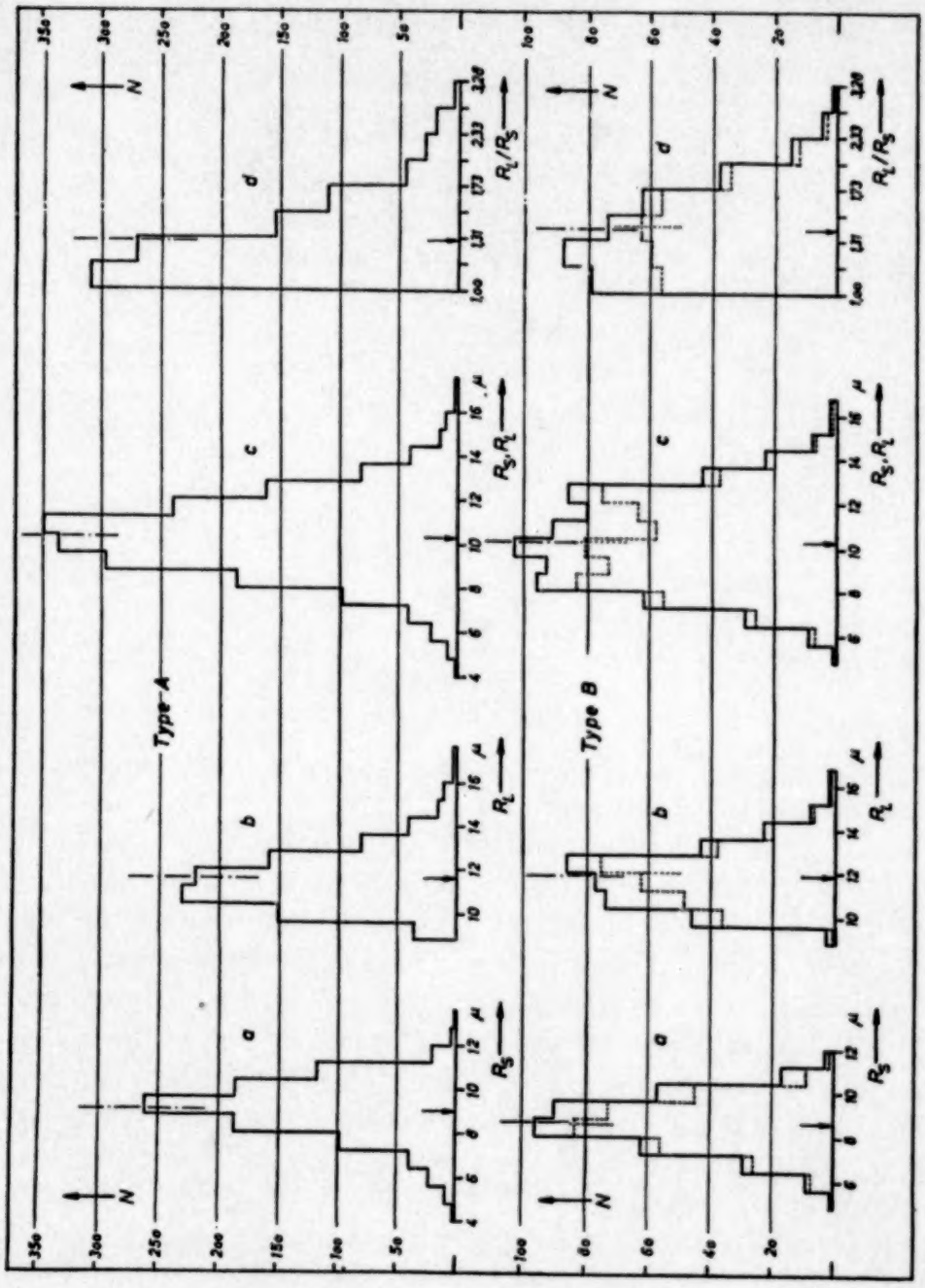

Fig. 6. Range distributions for type A and B. a) Range of heavy fragment. b) Range of light fragment. c) Sum of distributions a) and b). d) Distribution of range ratios.

for the range R of a fragment of mass M, charge Z and initial velocity v:

$$R = \text{const}\,\frac{Mv}{Z^{\frac{1}{2}}}\,. \tag{8}$$

For each fission event light and heavy fragment have practically the same momentum Mv, because the momentum transfer q is small by comparison to it. Even for different events the momenta do not differ too much from each other, as the variation of the kinetic energy released is not excessive. Therefore, the observed differences in the range stem mainly from the differences in Z. As Z/M is roughly constant, one expects the range scale in fig. 6 to be approximately a scale in $M^{-\frac{1}{2}}$. Indeed the average mass ratio of 1.19 ± 0.01 which one deduces from the observed average range ratio of 1.30 ± 0.01 is not far from the radiochemically determined value[32]) of 1.25. As one sees from these figures, the exponent of Z in eq. (9) actually lies somewhere between 0.7 and 1. In any case, the correlation between R and M is strong enough to allow definite conclusions about the preponderance of symmetric or asymmetric fission.

The distributions of type A events are plotted in the upper part of fig. 6. As we know for each event which one is the light and which is the heavy fragment, we can list the distributions for a) *the heavy fragments*, and b) *the light fragments* separately, and also obtain d) *the distribution of range ratios*. Additionally in c) *the sum of the distributions* a) and b) is given because it resembles the familiar mass yield curves most closely. From c) and d) it is clear that at high momentum transfers the mass division is symmetric. The spread in masses is large.

5.2. AT LOW MOMENTUM TRANSFERS

Although the separate distributions a) and b) displayed on the lower part of fig. 6 at first sight do not seem to differ from the distributions above very much, the curves c) and d) reveal an appreciable fraction of asymmetric fission to be present. This is statistically well established: attempts to fit the distribution of range ratios with monotonically decreasing smooth functions lead to a χ^2 of at least 19 for 7 degrees of freedom. Thus the existence of an asymmetric component is established with $> 99\,\%$ confidence. This is the more remarkable as the admixture of high momentum transfers obscures the effect considerably. The fraction of high momentum transfers admixtured was read directly from fig. 4. A numerically equal amount of events selected at random was suppressed in establishing the range distribution. The resulting distributions are indicated in fig. 6 by the dashed lines. They should represent to a fair extent the mass distribution of fissions with momentum transfers below 300 MeV/c ($\eta < 0.25$).

6. Comparison with the Results of Other Authors

The *distribution of momentum transfers* q obtained agrees well with the results of Ostroumov[26]), who used the same method but somewhat different assump-

tions in the calculation. The curve (fig. 2) shows the same general features as the distributions of excitation energies E^* calculated by Monte Carlo methods[33,34]: a preponderance of fairly low values and an approximately exponential decrease towards higher values. In order to make the comparison a little more quantitative we may use the correlation between q and E^* as given by Porile and Sugarman[5]) for 460 MeV protons on Bi. (The correlation for 600 MeV protons on Th should be almost the same [34]). The estimated average momentum transfer of 250 MeV/c (section 2), then corresponds to an average excitation energy of 83 MeV, whereas Metropolis *et al.*[34]) computed for 600 MeV protons on U an $\bar{E}^*$ of 180 MeV. The uncertainties involved are too great and the correlation between q and E^* is too loose for ascribing too much significance to this discrepance. However, it might be possible that by observation of binary fissions only one favours the low energy part of the total excitation energy spectrum. For instance it is conceivable that a sizeable fraction of the fissions proceeds through the excitation of discrete thorium levels slightly above threshold.

The *fore-aft asymmetry* in the angular distribution at high momentum transfers has not yet been observed before. The isotropic results at low energies[1,12,13,19,20]) are fully consistent with the results of the present paper: indeed, table 2 shows a significant asymmetry only for very high momentum transfers (> 700 MeV/c).

The *sideways-peaking* of the angular distribution was observed for the first time by Lozhkin *et al.*[7]) in uranium bombarded with 660 MeV protons. The existence of this anomalous anisotropy is confirmed by the present measurements. The magnitude of the anisotropies are roughly the same: from the data of Lozhkin *et al.*, one obtains without differentiating between high and low momentum transfers, $\alpha(30°) = 0.28 \pm 0.06$ for uranium; under the same conditions we get $\alpha(30°) = 0.29 + 0.08$ for thorium. On the other hand, the shape of the angular distribution found by the Russian group is quite different from ours: Lozhkin *et al.* fit their distributions with an ansatz $1 + \alpha \sin^m \theta$ with $m \gtrapprox 4$. Such a sharp peaking is not seen in our results (figs. 4 and 5).

Concerning the *dependence of the anisotropy on excitation energy*, our data are contrary to the conclusions of the Russian group. But this discrepancy seems to be rather one of interpretation than one of measurement. The method adopted in the present paper has one definite advantage: the events causing the excess at 90° in figs. 4 and 5 are *known* to have momentum transfers below 300 MeV/c, because a larger one would have produced a measurable ε. This limits their excitation energies E^* to values below $\approx$ 100 MeV[5]). The method of Lozhkin *et al.* apparently is far from this unambiguity. Using emulsions of moderate sensitivity they took the number of visible cascade particles n to be a measure for E^*. This method is generally believed to be reliable, provided n is large. In Lozhkin's measurements, however, the most frequent n were 0 and 1.

The frequency of events with $n \geq 2$ is only $\approx 70\,\%$ of the events with $n = 0$. Thus, statistical fluctuations and, more seriously, the possibility of the primary proton exchanging charge and/or producing neutral secondaries seem to destroy the correlation between n and E^* almost completely.

Range distributions in emulsions have been measured previously under conditions similar to ours. Ivanova and P'ianov[28]) in uranium fission by 660 MeV protons observed a "combined" range distribution which was symmetric and had practically the same shape as our curve of fig. 6 Ac. However, Ivanova's distribution is shifted for ≈ 1.5 μm to higher values. This is easily explained by the higher sensitivity of her emulsion, because we tend to lose 0.5 to 1 μm at each ending. Broad, symmetric distributions in U fission at 660 MeV were also obtained by Shamov and Lozhkin[8]) in emulsions which were only slightly more sensitive than ours. If one compares all events irrespective of the excitation energy assigned, then there is no significant discrepancy between their distribution and ours. Disagreement arises again because of their determination of E^* from n: Shamov and Lozhkin find an increasing importance of asymmetric fission with increasing E^*, whereas our measurements show definitely that range asymmetry as well as angular anisotropy is associated with low momentum transfers.

The *presence of an asymmetric component* in the range distribution at low momentum transfers is, of course, what one expects from the known energy dependence of asymmetric fission†. One has to remember, however, that the experiments in general yield the ratio of asymmetric to symmetric mass division as a function of *primary particle energy* only. (There is one exception: see ref. [1]). Our measurements provide rather direct support to the now generally accepted view that the ratio of asymmetric to symmetric fission is entirely determined by the excitation energy available.

7. Interpretation of Results

7.1. AT HIGH MOMENTUM TRANSFERS

Part of the high momentum transfer fissions certainly will occur according to the generally accepted two-stage process: the first stage is the emission of the fast cascade. The second one is the decay of a rather long lived (though highly excited) residual nucleus, which may emit a few neutrons and eventually fission according to the statistical competition of this particular channel with the other possible modes of de-excitation. These events provide no peculiarities; their mass distribution is symmetric, the angular distribution is, of course, isotropic.

† The term "asymmetric fission" refers to the *process* resulting in a double-humped mass distribution. Of course, this process can lead to symmetric mass division in a particular event.

In addition to these well understood events, however, there must be a sizeable fraction of fast, direct processes, in which the fission occurs in a single step, almost simultaneously with the ejection of the nuclear cascade. This is demonstrated by the fore-aft asymmetry observed. Even a life-time of the order of one nuclear oscillation period would delete any original asymmetry completely.

It seems natural to connect the asymmetry in fragment emission with the well-known asymmetry of the nuclear cascade, namely its pronounced peaking in the forward direction. The following simple hydrodynamic model possibly comprises the main features of the direct fission process observed. Let us consider a nuclear cascade initiated rather closely to the entrance point of the primary proton. The cascade may be pictured to represent a stream of nuclear matter moving through the nucleus with a fairly low angular spread with respect to the primary direction. Now it is well known that a detailed description of fission in terms of the liquid drop model necessitates the introduction of a finite viscosity of the nuclear fluid. Thus, the flow of nuclear matter initiated by the cascade may well extend over a sizeable fraction of the nuclear volume. In the rest system of the nucleus, then, one has the following situation: a stream of fluid flowing approximately in the primary direction, and a surrounding flow in the opposite direction. This clearly leads to a longitudinal deformation, which occasionally may be sufficient for fission†. According to this model, direct fission occurs preferentially parallel to the primary direction, in agreement with the observation (table 1).

The light fragment's emission into the forward direction is favoured because the cascade is initiated more probably in the inner region of the nucleus than just near the entrance point of the proton. In these cases, the amount of fluid moving in the primary direction is small and the resulting deformation asymmetric. If the cascade was orginated at the very beginning of the proton's path, then the situation might be reversed. Thus, the model predicts a decrease in asymmetry (possibly even a reversal of sign) for very large cascades. The results in table 2 may be taken as an indication for this effect, because the formally negative momentum transfers certainly correspond to events with the largest cascades. (For a better explanation see note added in proof).

7.2. AT LOW MOMENTUM TRANSFERS

The most outstanding feature of the low momentum transfer fissions is the peaking of their angular distribution at 90° to the primary direction. I. Halpern's very suggestive explanation[18]) combines two well established facts: i) the normal anisotropy observed in low energy particle induced fission; ii) the Serber

† Another conceivable source of longitudinal deformation is the interaction of the emerging cascade particles with the nuclear potential.

model of high energy nuclear reactions, according to which the primary particle interacts with the individual nucleons inside the target nucleus. As Halpern points out, primary particles with energies around 600 MeV have a very small chance to be absorbed in the nucleus. On the other hand, secondary nucleons with energies below say 15 % of the primary particle are captured with high probability. If one assumes them to result from single nucleon-nucleon collisions only, they emerge nearly under 90° with respect to the primary beam. The familiar forward anisotropy they induce upon being captured, therefore, is a sideways anisotropy, as seen from the primary direction.

The present measurements confirm Halpern's model in all essential points. In particular, they show that the anomalous anisotropy is indeed connected with low inelasticity. The magnitude of the effect also seems to be in rough agreement with the expectations. Halpern showed that under the assumptions mentioned above, an angular distribution $1 + \alpha \cos^2\theta$ at low energies leads approximately to a distribution $1 + \frac{1}{2}\alpha \sin^2\theta$ at high energies. The anisotropy found in the present work seems to be consistent with the values obtained at low energies[1]). One slight discrepancy remains as far as the shape of $W(\theta)$ is concerned. From the empirical sharp peaking of the low energy distributions (much higher powers than $\cos^2\theta$), Halpern expects a rather sharp peaking at 90°, similar to that reported by Lozhkin *et al.* (see section 6). Our distribution apparently is far from that. However, multiple scattering effects might well account for the observed smearing out of $W(\theta)$. In conclusion, one may say that the explanation of the anomalous anisotropy in terms of nuclear transparency and collective rotation seems to work quite well.

The collective rotation plays an important role in a model of nuclear fission recently proposed by Faissner and Wildermuth[35]). In the spirit of the cluster model of the nucleus[36]) they specify this rotation as the relative motion of two clusters with closed 82 and 50 neutron shells respectively. This is thought to be the common origin of mass asymmetry and angular anisotropy. The familiar decrease of the probability for asymmetric fission with increasing excitation energy (see section 5) is interpreted as loss of cluster structure. According to the model, asymmetric fission is not possible for nucleides with neutron numbers below 132. Also a collective rotation near threshold seems to be improbable for nucleides around lead. Preliminary results on bismuth, lead and thallium showed no anisotropy exceeding the statistical error[37]).

This work was done while one of the authors (H.F.) held a CERN Research Associateship. He wishes to express his gratitude to Professors Bakker†, Bernardini and Gentner for the hospitality extended to him, and for the permission to use the CERN facilities for this experiment. The exposures have been made possible through the kind co-operation of Doctors Harting and Kluyver and their group. Additional help was given by Dr. Goebel and by the

CERN emulsion group under the direction of Doctors Gibson and Combe. The authors are indebted to Professor H. Krüger for his interest in this work and for providing the facilities for processing and scanning of plates at Tübingen. This part of the work was supported by the Bundesministerium für Atomkernenergie und Wasserwirtschaft. Finally, it is a pleasure to acknowledge the stimulating discussions with Professors I. Halpern, L. Rosenfeld, V. L. Telegdi and J. A. Wheeler and an interesting correspondence with Dr. R. B. Leachman.

Note added in proof: The more detailed calculations done on an electronic computer revealed the importance of a kinematical effect which had been underestimated previously. It had always been assumed that in each fission event the fragment with the smaller mass has the longer range. However, for very high velocities of the fissioning nucleus a heavy fragment emitted in the forward direction can attain a longer range than a light one emitted backwards. As a consequence, the fore-aft asymmetry for events with $\eta > 0$ is, at least in part, a kinematical effect. On the other hand, it is hard to see how this effect could account for the fore-aft asymmetry of those events where the nucleus apparently travelled backwards ($\eta < 0$). Thus, there is still evidence for the direct fission mode discussed in the text. The details will be given in our forthcoming paper[37]).

References

1) I. Halpern, Ann. Rev. Nucl. Sci. **9** (1959) 245
2) J. W. Meadows, Phys. Rev. **110** (1958) 1109
3) U. L. Vallinder and H. Tyrén, Nuclear Physics **15** (1960) 152
4) R. L. Wolke and J. R. Gutman, Phys. Rev. **107** (1957) 850
5) N. T. Porile and N. Sugarman, Phys. Rev. **107** (1957) 1410
6) M. V. Ramaniah and N. Sugarman, Phys. Rev. (1960) to be published (EFINS 59-60)
7) O. V. Lozhkin, N. A. Perfilov and V. P. Shamov, JETP **29** (1955) 292; translation: Soviet Phys. JETP **2** (1956) 116
8) V. P. Shamov and O. V. Lozhkin, JETP **29** (1955) 286; translation: Soviet Phys. JETP **2** (1956) 111
9) G. F. Denisenko, N. S. Ivanova, N. R. Novikava, N. A. Perfilov, E. J. Prokofieva and V. P. Shamov, Phys. Rev. **109** (1958) 1779
10) V. F. Darovskikh and N. A. Perfilov, JETP **36** (1959) 652; translation: Soviet Phys. JETP **9** (1959) 456
11) R. L. Henkel and J. E. Brolley, Jr., Phys. Rev. **103** (1956) 1292
12) B. L. Cohen, W. H. Jones, G. H. McCormick and B. L. Ferrell, Phys. Rev. **94** (1954) 625
13) B. L. Cohen, B. L. Ferrell, D. J. Coombe and H. K. Hullings, Phys. Rev. **98** (1955) 685
14) C. T. Coffin and I. Halpern, Phys. Rev. **112** (1958) 536
15) A. Bohr, Proc. 1st Int. Conf. Peaceful Uses of Atomic Energy **2** (United Nations N.Y. 1956) 151
16) V. M. Strutinski, JETP **30** (1956) 606; translation: Soviet Phys. JETP **3** (1956) 638
17) I. Halpern and V. M. Strutinski, Proc. 2nd Int. Conf. Peaceful Uses of Atomic Energy **15** (United Nations, Geneva, 1958) 408
18) I. Halpern, Nuclear Physics **11** (1959) 522
19) A. N. Protopopov and V. P. Eismont, Atomnaya Energiia **4** (1958) 194; transl.: Consultants Bureau **4** (1958) 265
20) R. B. Leachman and G. P. Ford, Nuclear Physics **19** (1960) 366 (following paper)

21) T. T. Sugihara, P. J. Drevinsky, M. J. Troianello and J. M. Alexander, Phys. Rev. **108** (1957) 1264
22) W. J. Nicholson and I. Halpern, Phys. Rev. **116** (1959) 175
23) H. Faissner and H. Schneider, Physikal. Verhandl. **10** (1959) 70
24) H. Ackermann, Physikal. Verhandl. **10** (1959) 15;
H. Ackermann and H. Faissner, Nuclear Instruments and Methods, to be published
25) H. Faissner and F. Gönnenwein, Z. Physik **153** (1958) 257
26) V. I. Ostroumov, Doklady Akad. Nauk SSSR **103** (1955) 409
27) J. Jungerman and S. C. Wright, Phys. Rev. **76** (1949) 1112
28) N. S. Ivanova and I. I. P'ianov, JETP **31** (1956) 416; translation: Soviet Phys. JETP **4** (1957) 367
29) H. Faissner and F. Gönnenwein, Physikal. Verhandl. **9** (1958) 217
30) H. Faissner, F. Gönnenwein, H. Schneider and G. Wolf, Z. Physik. to be published
31) N. Bohr, Phys. Rev. **59** (1941) 270; Mat. Fys. Medd. Dan. Vid. Selsk. **18** no. 8 (1948)
32) Proc. Symp. Physics of Fission, Chalk River (Atomic Energy of Canada Lim., 1956) p. 44
33) N. Metropolis, R. Bivins, M. Storm, A. Turkevich, J. M. Miller and G. Friedlander, Phys. Rev. **110** (1958) 185
34) N. Metropolis, R. Bivins, M. Storm, J. M. Miller, G. Friedlander and A. Turkevich, Phys. Rev. **110** (1958) 204
35) H. Faissner and K. Wildermuth, Physikal. Verhandl. **10** (1959) 105; Proc. Amer. Phys. Soc. **5** (1960) 272; Nuclear Physics, to be published
36) K. Wildermuth and Th. Kannelopoulos, Nuclear Physics **7** (1958) 150, **9** (1958/59) 449; CERN Report 59–23 (1959)
37) H. Schneider, G. Wolf and H. Faissner, Physical. Verhandl. **10** (1959) 105; Nuclear Physics, to be published.

2.J *Nuclear Physics* **19** (1960) 366—369; © *North-Holland Publishing Co., Amsterdam*
Not to be reproduced by photoprint or microfilm without written permission from the publisher

FORE-AFT YIELDS OF FRAGMENTS FROM 14-MeV NEUTRON-INDUCED FISSION

R. B. LEACHMAN and GEORGE P. FORD

Los Alamos Scientific Laboratory, University of California, Los Alamos, New Mexico†

Received 30 January 1960

Abstract: The yield of Zr^{97} and Ba^{139} fission fragments in the direction of 14-MeV neutrons inducing fission of Np^{237} and U^{235} was measured relative to the yield in the opposite direction. The fore-aft isotropy found from these measurements agrees with the compound nucleus theory of fission.

1. Introduction

Nuclear fission induced by moderate-energy particles is believed to be a slow process arising from the excitation of many levels of the compound system. According to compound nucleus theory, the direction parallel to the beam of particles is not distinguished from the antiparallel direction for fragments from such fissions. Thus, in the centre-of-mass system, fore-aft isotropy of fragments relative to the beam is expected.

This fore-aft isotropy has been radiochemically confirmed within 2 % uncertainty for 22-MeV proton-induced fission[1]) and within 5 % for 43-MeV α-particle-induced fission[2]). Energy measurements distinguishing the light and heavy fragment groups have shown a fore-aft isotropy of the light fragment group from 14-MeV neutron-induced fission of U^{238} with the 7 % uncertainty in the measurements[3]). However, similar measurements[4]) on Np^{237} qualitatively showed an $\approx 20\%$ preference for the heavy fragment group to be emitted parallel to the beam relative to antiparallel.

In view of the importance of this reported fore-aft asymmetry to fission theory, fore-aft yield measurements of the nearly complementary Zr^{97} and Ba^{139} fragments from 14-MeV neutron-induced fission of Np^{237} and also of U^{235} were undertaken radiochemically to provide data on identified nucleides.

2. Experiment

The experiment was performed with a Cockcroft-Walton accelerator, using the T(d, n)He^4 reaction to provide $\approx 4 \times 10^{10}$ neutrons/sec of 14.1-MeV neutrons with a 0.1-MeV energy spread. Even with this source strength and irradiations of 4 h, the resulting low yield of fissions required larger solid angles

† Work performed under the auspices of the U.S. Atomic Energy Commission.

for detecting fragments than were used in previous experiments[1–4]). In the geometry used, the 1-cm diameter fission sources were 5.8 cm from the centre of the elliptically-shaped neutron source, which had axes of 0.6 and 0.9 cm. The fragment-catching foils of nickel, placed 3.6 cm fore and aft of the fission source, were either 2.6 or 3.8 cm in diameter, resulting in maximum catching angles θ_m from the fission source centre of 20° and 28°, respectively. The catching foils and fission source were perpendicular to the neutron beam axis and concentric on this axis. Fragments from the fission source proceeded in a vacuum to the catching foils, which were analyzed radiochemically[5]) for 17-h Zr^{97} and 84-min Ba^{139}. Even with these large solid angles of catching, the resulting β activities of Zr^{97} and Ba^{139} with 1.6-sr solid angles to the counters were low, always being less than 150 counts/min and often $\approx$ 10 counts/min for Ba^{139}.

The Np^{237} fission source consisted of 3 mg/cm² deposits on both sides of platinum foil, which was opaque to fragments. The two neptunium deposits were transparent to fragments proceeding toward the catchers and were shown by α activities to have a $3.5 \pm 0.9\%$ mass difference, for which corrections were made in the data.

For the case of the catching angle $\theta_m = 28°$, the results for Np^{237} were

$$Zr^{97} \text{ aft/fore yield ratio} = 0.998 \pm 0.030\,,$$

$$Ba^{139} \text{ fore/aft yield ratio} = 0.896 \pm 0.042\,.$$

Since these nucleides are nearly complementary in mass, the results can be combined to yield 0.966 ± 0.025 as the heavy fragment fore/aft yield ratio, or the light fragment aft/fore yield ratio, which is the equivalent. For $\theta_m = 20°$ the results for Np^{237} were

$$Zr^{97} \text{ aft/fore yield ratio} = 1.028 \pm 0.085\,,$$

$$Ba^{139} \text{ fore/aft yield ratio} = 0.77 \pm 0.24\,.$$

The combined result for $\theta_m = 20°$ is 0.998 ± 0.080 for the heavy fragment fore/aft yield ratio or the light fragment aft/fore yield ratio.

In the case of the runs with U^{235} fission, the 0.0025-cm (93 % isotopic abundance) fission source was thick compared to fragment ranges; therefore, the effective fission source mass of the fore side exceeded that of the aft side. This is because the compound nucleus velocity imparted by the 14-MeV neutrons increased the velocity, and thus range, of fragments proceeding to the fore catcher and decreased the velocity and range of fragments proceeding to the aft catcher. The ratio of these respective effective masses was estimated on the basis of range and velocity data[6]) to be 1.04 for Ba^{139} fragments and 1.06 for Zr^{97} fragments. Estimated 1.4 % uncertainties in these thickness ratios were included in the results.

To reduce the effect of the uncertainty in the effective masses of the U^{235} source on the results, the aft/fore yield ratio of Zr^{97} was multiplied by the nearly equivalent fore/aft yield ratio of Ba^{139}. The square root of this product gave for the aft/fore yield ratio of light fragments, or for the fore/aft yield ratio of heavy fragments, from U^{235} fission

$$0.953 \pm 0.027 \text{ for } \theta_m = 28°\,, \quad 0.966 \pm 0.031 \text{ for } \theta_m = 20°\,.$$

Yield uncertainties obtained from least squares fits[7]) of the activities to the known decay periods are the major part of the above uncertainties, which are standard deviations. All the data given above have been corrected for centre-of-mass effects on the solid angle of catching and small ($\leq 1\,\%$) errors in positioning the fission source between the catching foils. Each result is the weighted mean of two runs, except the Np^{237} result for Zr^{97} into $\theta_m = 28°$ is from three runs and for Ba^{139} into $\theta_m = 20°$ is from one run.

3. Discussion

The results from 14-MeV neutron-induced fission of Np^{237} and U^{235} are all within about two standard deviations of a fore/aft yield ratio of unity, which is the ratio expected from the compound nucleus theory of fission.

However, to make a comparison with results from measurements with better angular resolution[1–4]), it is necessary to consider whether any possible fore-aft anisotropy would be so sharply peaked in angle along the neutron beam as to be obscured by the relatively large acceptance angles of this experiment. In this connection, angular distributions of fragments from fission induced by 14-MeV neutrons[4, 8]) and by higher momentum particles[9]) are fitted by even terms of $\sum_n a_n \cos^n\theta$, where θ is the angle between the fragments and the incident particle, with a_n coefficients for $n > 4$ being unimportant. The fore-aft anisotropy result of Brolley *et al.*[4]) indicates $a_n/a_0 \approx 0.1$ for heavy fragments, where n is odd. Since the fore-aft anisotropy peaking from terms of as high an order as a_5 would for $a_n/a_0 = 0.1$ and $\theta_m = 28°$ reduce the observed fore-aft anisotropy by less than 30 % from the true 0°/180° anisotropy, it appears that the large acceptance angles of the present measurement would not obscure the observation of fore-aft anisotropy.

The authors are grateful to Mr. R. W. Davis for Cockcroft-Walton irradiations, to Miss Suzanne Kramnock for alpha counting, and to Mrs. Dorothy Copely and Mrs. Teresa Kelley for chemical separations.

References

1) Cohen, Ferrell-Bryan, Coombe and Hullings, Phys. Rev. **98** (1955) 685
2) A. W. Fairhall, as reported by I. Halpern, Annual Reviews of Nuclear Science **9** (1959) 245
3) A. N. Protopopov and V. P. Eismont, Atomnaya Energiia **4** (1958) 194; translation: Consultants Bureau **4** (1958) 265

4) Brolley, Dickinson and Henkel, Phys. Rev. **99** (1955) 159
5) J. Kleinberg, LA-1721, 2nd Ed. (Office of Technical Services, U.S. Department of Commerce, Washington 25, D.C., 1958)
6) J. M. Alexander and M. F. Gallagher, University of California Radiation Laboratory report UCRL-8978 (1959);
F. Suzor, Ann. de phys. **4** (1949) 269;
R. B. Leachman and H. W. Schmitt, Phys. Rev. **96** (1954) 1366
7) W. E. Deming, Statistical Adjustment of Data (Wiley, New York, 1938)
8) L. Blumberg and R. B. Leachman, Phys. Rev. **116** (1959) 102
9) C. T. Coffin and I. Halpern, Phys. Rev. **112** (1958) 536

1.G *Nuclear Physics* **19** (1960) 370—376; © *North-Holland Publishing Co., Amsterdam*
Not to be reproduced by photoprint or microfilm without written permission from the publisher

CAN THE NUCLEAR MANY-BODY PROBLEM BE SOLVED BY USING PERTURBATION THEORY?

J. S. LEVINGER

Department of Physics and Astronomy, Louisiana State University, Baton Rouge, La†

Received 29 April 1960

Abstract: A static two-body potential of Serber exchange character with a repulsive core fails to produce saturation in first-order perturbation theory, if the core is treated as a pseudopotential. (We are designating the order of the term in a joint expansion in powers of the strength of the attractive potential and in the range of the repulsive core). Second-order terms are estimated from the condition that saturation should be achieved at the observed density without invoking many-body forces. We conclude that any static potential that produces saturation at about the empirical density must have substantial second-order terms, of magnitude 10 MeV/particle or more. We discuss the use of a velocity-dependent two-body potential to replace the infinite repulsive core, and find that second-order terms may be much smaller if we use a velocity-dependent potential.

1. Introduction

It has been shown by many workers[1,2,3]) that perturbation theory converges rapidly if a well-behaved two-body potential is assumed in solving the nuclear many-body problem. (By "rapid convergence" we mean that the second-order terms are less than 5 MeV/particle so that terms beyond the second order can probably be neglected with an error of less than 1 MeV/particle in the nuclear binding energy.) If there is a strong tensor force, the second-order terms[4]) may give a contribution as large as 10 MeV/particle for a well-behaved potential that fits[5]) the low-energy two-body data. We shall not discuss this difficulty due to a strong tensor force further in this paper; but instead confine our attention to the simpler case of central forces.

These perturbation theory calculations have become unpopular in the past several years for two main reasons. First, measurements on the two-body system show that the two-body force has approximately a Serber character, and thus does not contain sufficient exchange force to give saturation. Second, the observed change in sign of the ^1S phase shift at about 200 MeV has supported the use of an infinite repulsive core.

Of course, ordinary perturbation theory cannot be used with this infinite repulsive core. But, if we replace the core by a pseudopotential[6]) we can develop a "modified perturbation theory" which gives us the nuclear energy as a joint expansion in powers of V_0 and c. (Here V_0 is the strength of the

† Supported in part by the National Science Foundation.

attractive part of the potential, and c is the radius of the repulsive core.) Application[4]) of modified perturbation theory to several different assumed two-body potentials with core gives large second-order terms, of order 20 MeV/particle.

One may wonder why we should be concerned with applications of perturbation theory: Why not solve the nuclear many-body problem with the more advanced methods used by Brueckner[7]) and others? Our main justification is that we wish to develop a method which is simple to apply to the many-body problem and which will not be excessively difficult to apply, *without further approximations*, to the problem of a finite nucleus.

Gomes, Walecka and Weisskopf[8]) discuss Brueckner theory and calculate the binding energy of nuclear matter using a pseudopotential to replace the infinite repulsive core. Their numerical work amounts to use of modified perturbation theory, including terms up to the third order in powers of c, but excluding terms beyond the first order in powers of V_0. Gomes, Walecka and Weisskopf find nuclear saturation, but achieve this saturation by using moderately large higher-order terms in the second and third powers of c.

Moszkowski[9]) has suggested another method for treating an infinite repulsive core by means of perturbation theory: part of the attractive potential near the core is cancelled against the pseudopotential of the core. The remaining part of the attractive potential is then treated by ordinary perturbation theory. Moszkowski's expansion will give smaller second-order terms than in our previous work[4]), but if it achieves nuclear saturation, it also must do this by means of moderately large second-order and higher terms†.

In the following section we discuss application of modified perturbation theory to the nuclear many-body problem. We shall show that *any static potential that produces saturation at about the empirical density must have substantial second-order terms*, of magnitude 10 MeV/particle or more. Of course, we are limiting ourselves to potentials that fit measurements on the two-body system. Various types of many-body forces could be invoked to produce, or help to produce, saturation: e.g. change of the dependence of the potential on the angular momentum, or introduction of a repulsive force depending on the co-ordinates of three or more particles[10]). We should like to solve the nuclear many-body problem without the introduction of many-body forces; but we have no assurance that such a solution is either possible or desirable.

The theorem just enunciated is established by the following argument: the two-body force assumed does not produce saturation in the first-order terms E_1. The kinetic energy is of the form $A\,k_f^2$, while the ordinary term for the potential energy is of the form $-B\,k_f^3$, where A and B are each positive, and the wave-number at the Fermi surface is denoted by k_f. The derivative

† *Note added in proof*: Moszkowski's separation method does introduce some velocity-dependence, but apparently not enough.

$dE_1/dk_f = S_1$ is negative, and can be evaluated at the empirical density of nuclear matter for any assumed two-body force. If saturation is to be achieved at or near the empirical density, then $dE_2/dk_f \equiv S_2 = -S_1$. (Here E_1 is the nuclear energy per particle up to terms of first order, while E_2 is the contribution from second and higher order terms.) If we make an assumption as to the form of the function $E_2(k_f)$, we can evaluate this function at the empirical density from the knowledge of its slope S_2. We estimate the value of E_2 for several different cases, obtaining at least 10 MeV/particle.

We note that if we replace the core by a pseudopotential (as done in refs. [4]) or [8]) the above argument still holds: we merely modify the value of the coefficient B, keeping it positive. Similarly, in Moszkowski's treatment[9]), only the long-range part of the attractive potential is used, but the ordinary term still gives a $-B\,k_f^3$ term, so that there is no saturation in first order. Saturation can be achieved only by the use of moderately large second-order terms.

The failure of a static potential to give a rapidly converging series suggests the use of a different type of two-body potential. In the third section we discuss the use of well-behaved velocity-dependent potential with which Razavy and Levinger[11]) have fitted observed ^1S phase shifts up to 310 MeV.

2. Failure of Perturbation Theory for a Static Potential

We shall assume a Serber exchange character for a central static potential. This potential consists of an attractive $v(r)$ and a pseudopotential $\hat{t}(r)$ which replaces the infinite repulsive core. The energy E_1 consists of 4 parts: a) the expectation value $\bar{T}$ of the kinetic energy; b) the Lenz term[6, 12]) due to the pseudopotential $\hat{t}$; c) the ordinary term $\bar{v}_0$ for the expectation value of the potential energy; d) the exchange term $\bar{v}_e$ for the expectation value of the potential energy. The first three of these quantities are given by the following simple formulae†:

$$\bar{T} = 12.5\,k_f^2\,, \tag{1}$$

$$\hat{t} = (\hbar^2 c/M\pi)k_f^3 = 5.3\,k_f^3\,, \tag{2}$$

$$\bar{v}_0 = \frac{1}{2\pi}\int v(r)r^2\,dr\,k_f^3 \tag{3}$$

In (2) we have used a core radius $c = 0.4 \times 10^{-13}$ cm.

Since we are not attempting precise calculations in this paper, we shall not include the exchange term $\bar{v}_e$. (Consider, for example, Euler's[1]) calculations for a Gaussian potential of form $\exp(-r^2/\beta^2)$ with $\beta = 1.7\,f$ and $k_f = 1.4\,f^{-1}$. We find from his table that $\bar{v}_e/\bar{v}_0 = 0.3$. We are actually interested in the effect of $d\bar{v}_e/dk_f$ on $S_1 = dE_1/dk_f$. Two effects operate in different directions, and we

† In these and the following formulae, numerical coefficients are expressed in MeV/particle, when the wave-number k_f is expressed in units of f^{-1}, where $f = 10^{-13}$ cm.

find that by coincidence $(d\bar{v}_e/dk_f)/S_1$ also equals 0.3. We note further that $d\bar{v}_e/dk_f$ is negative, so that if we did include this term we would make S_1 more negative, thus increasing the value of the second-order terms E_2 needed to produce saturation.)

We evaluate the integral in (3) for two different assumptions as to the shape of the two-body central potential: a) a square-well from 0.4 f to 2.3 f, with depth 28 MeV as used by Gomes, Walecka and Weisskopf[8]); b) the Gammel-Thaler-Brueckner potential[7]) which has a Yukawa shape outside the core, and is spin-dependent (note, that we neglect the poorly known central interaction in triplet odd states):

$$\bar{v}_0 = -18.6\, k_f^3 \text{ (Gomes-Walecka-Weisskopf)}, \tag{3'}$$

$$\bar{v}_0 = -16.1\, k_f^3 \text{ (Gammel-Thaler-Brueckner)}. \tag{3''}$$

If we (arbitrarily) average the two results to find a single number for E_1, we obtain from (1), (2), (3)

$$E_1 = 12.5\, k_f^2 - 12\, k_f^3 . \tag{4}$$

We see that the repulsive core, when evaluated as a pseudopotential for the first power in the core radius, merely changes the numerical value of the coefficient of the k_f^3 term, without changing the sign of the coefficient.

We now find the derivative of the first-order energy with respect to the Fermi wave-number, and substitute the empirical value $k_f = 1.4\ f^{-1}$:

$$S_1 = dE_1/dk_f = 25\, k_f - 36\, k_f^2 , \tag{5}$$

$$S_1(1.4) = -35 . \tag{6}$$

We shall use $S_1(1.4)$ to estimate the second-order (and higher-order) terms E_2. We *assume* that near the empirical density E_2 can be represented as a power law:

$$E_2 = Dk_f^n . \tag{7}$$

By logarithmic differentiation,

$$S_2 = dE_2/dk_f = (n/k_f)E_2 . \tag{8}$$

We assume that the saturation nuclear density occurs for $k_f = 1.4\ f^{-1}$, and solve (6) and (8) for the second-order energy $E_2(1.4)$ at the empirical density, where $S_2 + S_1 = 0$; we get

$$E_2(1.4) = -(k_f/n)\, S_1(1.4) \geqq 10 . \tag{9}$$

We have assumed that $n \leqq 5$, in order to obtain a numerical estimate of E_2. There are a variety of second-order terms, with different values of n; by choosing a plausible maximum value for n we have estimated a lower limit for the second-order terms.

Of course, (9) represents neither a precise numerical value nor a rigorous mathematical result, since it is based on the assumption of the validity of (7). We can check (9) for the Gomes-Walecka-Weisskopf calculation. (We note that these authors modify the Lenz term (2) by a factor $M/M^* = 1.5$, using their self-consistent value of the effective mass M^*. This modification changes the coefficient of the k_f^3 term from —12 to —10.6, changing $S_1(1.4)$ from —35 to —27, and reducing $E_2(1.4)$ by some 20 %.) Gomes, Walecka and Weisskopf (see their eq. (43)) also use an effective mass in E_2:

$$E_2 = (\hbar^2 k_f^2/2M^*)\left[\frac{12}{35\pi^2}(11 - 2\log 2)(k_f c)^2 + 0.26\,(k_f c)^3\right]. \qquad (10)$$

Substituting $c = 0.4\ f$ and $k_f = 1.4\ f^{-1}$, we find $E_2 = 9$ MeV particle. This result is in reasonable agreement with (9), with the 20 % modification due to use of an effective mass.

3. Discussion

Since a Serber potential with repulsive core gives a poorly convergent series in a modified perturbation theory, we shall consider as an alternative achieving saturation in first order by the use of a well-behaved potential that is velocity dependent[13]). Razavy and Levinger[11]) use a two-body potential of the form

$$V(r) + \beta\hat{\mathbf{p}}\cdot V(r)\hat{\mathbf{p}}\,. \qquad (11)$$

(Here $\hat{\mathbf{p}}$ is the operator $-i\hbar\nabla$.) In this preliminary work $V(r)$ was chosen as a square-well of range b and depth V_0. The three parameters b, V_0 and β were chosen so that the ^{1}S phase shifts calculated with this potential were in agreement with observations on proton-proton scattering: specifically, that the ^{1}S phase shift go through zero at a laboratory energy of about 200 MeV, and that the low energy calculations agree with effective range parameters.

This form of velocity-dependent potential involves no more free parameters than a potential involving a repulsive core, and either form can be derived from meson theory calculations[14]). The parameter c for the core radius is merely replaced by a parameter β for the strength of the velocity-dependent potential. It is not certain whether in practice, or even in principle, measurements on the two-nucleon system can determine if the change in sign of the ^{1}S phase shift is due to velocity-dependence, or to a very strong repulsion at very small distances. For instance, if the two-body potential were assumed to be *completely* static, the integrated cross section for the deuteron photoeffect[15]) would have a model-independent value. (We are here neglecting retardation, higher multipoles, and mesonic effects; and we are discussing the interaction in a spin-triplet state.) An experimental deviation from this value could give evidence as to the value of the parameter β of (11). However, physicists have already

abandoned the *completely* static Wigner (or Bartlett) potentials. The Majorana exchange force, which is a hidden complicated type of velocity dependence, gives a deviation from the model-independent sum-rule. We now need a numerical investigation to find whether the observed deviation[15]) is better explained by a Majorana exchange effect, with a static repulsive core, or by Majorana exchange combined with the potential of (11).

We note that in using a velocity-dependent potential, we are finding a replacement for the infinite repulsive core in the problem of an isolated pair of particles. In replacing the core by a pseudopotential we also find velocity-dependent terms[6]), but this pseudopotential should not be treated exactly in solving the two-particle Schrödinger equation, but only used in a Born approximation treatment. From the point of view of this paper we use the *same* velocity-dependent potential in the problem of two isolated nucleons, and in the problem of their interaction in nuclear matter. On the other hand, we would use different expressions for $\hat{t}$ for isolated nucleons and for nucleons imbedded in nuclear matter. (It is just this difference between two expressions for $\hat{t}$ that gives rise to the controversy[4, 16]) whether we should use the actual mass M or the effective mass M^* in (2) or (10).)

The velocity-dependent potential of (11) gives a first-order term proportional to k_f^5 in a perturbation treatment of nuclear matter. With β chosen negative[11]), the k_f^5 term is positive, thus making S_1 of (5) less negative and in turn decreasing the value of S_2 that is required. An order of magnitude estimate shows that the value needed for S_2 may be reduced by as much as a factor of five, so that second-order terms E_2 may be as small as 2 MeV/particle.

We have found above that a static potential of Serber exchange character is very unlikely to give a rapidly converging perturbation theory for nuclear matter. The value of 10 MeV/particle estimated for the second-order terms is too large to be tolerated in a calculation in which we are aiming at an accuracy of 1 MeV/particle. First, the second-order terms are sensitive to the energy denominator assumed in treating the unperturbed Hamiltonian. Second, the third-order terms would be likely to be several MeV/particle and are very hard to calculate accurately.

Both these objections are illustrated in the Gomes-Walecka-Weisskopf calculation[8]). Their modification of the Lenz term in first order, and in the second- and third-order terms as well, by the use of an effective mass is *essential* if they are to achieve saturation at about the observed density. This modification is controversial[4, 16]) and in any case cannot be regarded as a treatment sufficiently exact for our goal of 1 MeV/particle accuracy. Second, their third-order term quoted in (10) is almost 3 MeV/particle. (We should note that Gomes-Walecka-Weisskopf present their numerical work merely as an illustration of pedagogical value; so we should not be too critical of its failure to be an accurate method for obtaining numerical results.)

Moszkowski's method[9]) is an advance over the modified perturbation theory we have used[4]) in that he uses large terms to cancel each other before he performs the calculations of second-order perturbation theory. Nevertheless, he finds appreciable second-order terms (of order 10 MeV/particle) for the case in which he finds nuclear saturation.

In contrast to the work with a static potential, a velocity-dependent two-body potential can give saturation in a first-order calculation.

In summary, I answer the question I have posed in the title as follows: if the two-body potential is static and there is no many-body force, the answer is "no"; if the two-body potential is velocity dependent, the answer is "perhaps".

We are very grateful to R. E. Peierls, S. A. Moszkowski, V. J. Emery, M. Razavy and B. V. Paranjape for helpful discussions on various aspects of this problem.

References

1) H. Euler, Zeitschrift f. Physik **105** (1937) 553
2) R. Huby, Proc. Phys. Soc. **A62** (1949) 62
3) W. J. Swiatecki, Phys. Rev. **101** (1957) 1321; **103** (1957) 265
4) Levinger, Razavy, Rojo and Webre, Phys. Rev. **119** (1960) 230
5) Biedenharn, Blatt and Kalos, Nuclear Physics **6** (1958) 359
6) K. Huang and C. N. Yang, Phys. Rev. **105** (1957) 767
7) K. A. Brueckner and J. L. Gammel, Phys. Rev. **109** (1958) 1023
8) Gomes, Walecka and Weisskopf, Annals of Physics **3** (1958) 241
9) S. A. Moszkowski and B. L. Scott, Annals of Physics, in press
10) S. Drell and K. Huang, Phys. Rev. **91** (1953) 1527
11) M. Razavy, O. Rojo and J. S. Levinger, communication to Int. Conf. on Nuclear Structure, Kingston, Aug. 1960
12) W. Lenz, Zeitschrift f. Physik **56** (1929) 778
13) J. M. Blatt and V. F. Weisskopf, Theoretical Nuclear Physics (Wiley, New York, 1952) Ch. III, Section 2
14) S. Gartenhaus, Phys. Rev. **100** (1955) 900;
M. Sugawara and S. Okubo, Phys. Rev. **117** (1960) 605, 611
15) J. S. Levinger, Phys. Rev. **97** (1955) 970
16) C. de Dominicis and P. C. Martin, Phys. Rev. **105** (1957) 1419

4.D *Nuclear Physics* **19** (1960) 377—379; © *North-Holland Publishing Co., Amsterdam*
Not to be reproduced by photoprint or microfilm without written permission from the publisher

L TO K CAPTURE RATIO IN THE DECAY OF Ge^{68}

M. K. RAMASWAMY

Department of Physics, The Ohio State University, Columbus, Ohio†

Received 4 March 1960

Abstract: The L to K capture ratio in the decay of 270 day Ge^{68} has been determined by comparing the number of K X-rays emitted with the amount of annihilation radiation emitted in the decay of 68 minute Ga^{68}. This leads to a L/K ratio of 0.12 ± 0.07 in good agreement with theory.

1. Introduction

The ratio of probabilities of L to K capture is a theoretically well-defined quantity. Unfortunately, theory has been checked experimentally only in a few cases. In order to provide additional data, the L/K ratio has been measured in the decay of Ge^{68} by an indirect method. Ge^{68} (270 days) decays by pure electron-capture to 68 minite Ga^{68} which in turn decays by positon emission ($\approx 87\%$) and electron capture to stable Zn^{68}. The method employed here consists of comparing the number of K X-rays emitted in the decay of Ge^{68} with the amount of annihilation radiation following the decay of Ga^{68}. Incidentally, the results reported here arose as a byproduct of the author's studies[1]) on K-capture to positon branching ratios in the decay of Ga^{68}.

2. Experimental Procedure

Zinc was electroplated on to a copper backing and bombarded for 90 μA·h with 30-MeV alpha particles. 23 weeks after the bombardment the zinc layer on the copper backing was dissolved in a few cm^3 of concentrated HCl containing Ge carrier. $GeCl_4$ was distilled on to a receiver. Ge was separated from Ga using successive ether extractions from 6N HCl. Since an appreciable part (40 to 60%) of Ge is also extracted into the ether layer[2]) and since the number of extractions could not be done more than twice owing to the fast growth of 68 minute Ga^{68}, an efficiency of 50% or less was all that could be obtained for Ge. The Germanium thus separated was converted into the sulphide and rapidly transferred to the counting system. The 9-keV K X-ray was measured as a function of time by means of a 20-channel analyzer. A freshly-cleaved thin ($\approx$ 1 mm thick) NaI(Tl) crystal was used as the detector. At the same time a

† Supported by the U.S. Atomic Energy Commission. Work done at Johns Hopkins University, Baltimore.

second counter employing 3.8 cm × 2.5 cm NaI(Tl) crystal was set on the photopeak corresponding to the annihilation radiation and its growth in Ga^{68} was studied as a function of time.

3. Results

Fig. 1 (curve b) of ref. [1]) shows the X-ray spectrum immediately after chemical separation. The number of counts in the photopeak when extrapolated to zero time gives the total number of K X-rays emitted by Ge^{68}. The number of K X-rays is given by

$$N_K = N_0 \omega_K \varepsilon_K f_K , \tag{1}$$

where N_0 is the source strength, ω_K the K-fluorescence yield, ε_K the efficiency, and f_K the fraction of decays resulting in K-capture. Similarly when Ga^{68} is in equilibrium with Ge^{68}, the number of annihilation quanta is given by

$$N_{0.5} = 2N_0 f_+ \varepsilon_{0.5} , \tag{2}$$

where f_+ is the fraction of decays by positon emission and $\varepsilon_{0.5}$ the efficiency for detecting annihilation radiation. From eqs. (1) and (2) we get

$$f_K = \frac{2N_K f_+ \varepsilon_{0.5}}{N_{0.5} \omega_K \varepsilon_K} .$$

The experimental values were

$$N_K = 3200 \pm 30 \text{ min}^{-1} , \; N_{0.5} = 1002 \pm 12 \text{ min}^{-1} ;$$

ε_K was estimated to be 0.70, f_+ was assumed[3]) to be 0.87.

The fluorescence yield was taken to be 0.46[4]) and $\varepsilon_{0.5}$ was obtained from Bell[5]).

These values lead to $f_K = 0.88 \pm 0.07$ and

$$\frac{1 - f_K}{f_K} = \frac{f_L \left(1 + \frac{f_M}{f_L} + \frac{f_N}{f_L} + \dots\right)}{f_K} = \frac{0.12 \pm 0.07}{0.88 \pm 0.07} .$$

Taking $(f_M + f_N + \dots)/f_L = 0.11$ from tables of Wapstra, Nijgh and Van Lieshout[4]), the resulting L_1/K ratio was $L_1/K = 0.12 \pm 0.07$.

4. Discussion

The computed L_1/K ratio of 0.12 ± 0.07 is in good agreement with the theoretical value[6]) of 0.11 and consistent with a recently measured value[7]) of 0.09 ± 0.05 in Ge^{71} decay.

The author sincerely thanks Professor L. Madansky of Johns Hopkins University for valuable discussions.

References

1) M. K. Ramaswamy, Nuclear Physics **10** (1959) 205
2) E. J. Swift, J. Am. Chem. Soc. **46** (1924) 2375
3) Way, King, McGinnis and Van Lieshout, Nuclear Level Schemes $A = 40$–92 (U.S. Government Printing Office, Washington, 1955)
4) Wapstra, Nijgh and Van Lieshout, Nuclear Spectroscopy Tables (North-Holland Publishing Co, Amsterdam, 1959)
5) P. R. Bell in Beta and Gamma-ray Spectroscopy (North-Holland Publishing Co, Amsterdam, 1955), ch. 5
6) M. E. Rose and J. Jackson, Phys. Rev. **76** (1949) 1540
7) D. E. Rehfuss and B. Crasemann, Phys. Rev. **114** (1959) 1609

1.E.1: 4.E

Nuclear Physics 19 (1960) 380—388; © *North-Holland Publishing Co., Amsterdam*
Not to be reproduced by photoprint or microfilm without written permission from the publisher

INVESTIGATION ON THE DECAY SCHEME OF ThC (Bi^{212})

M. GIANNINI, D. PROSPERI and S. SCIUTI

Comitato Nazionale per le Ricerche Nucleari,
Istituto Nazionale Fisica Nucleare, Sezione di Roma,
Istituto di Fisica dell'Università, Roma

Received 7 May 1960

Abstract: The gamma rays emitted in the β-decay of Bi^{212} are investigated by means of α-γ, α-γ-γ and γ-γ-γ coincidences. New gamma rays of 0.13 and 0.19 MeV are found. The existence of 0.78 and 0.95 MeV transitions, recently reported, is confirmed, while no evidence of 1.3, 1.8, and 2.2 MeV transitions, reported by some authors, is found. An improved decay scheme of Bi^{212} is given. By means of semi-empirical calculations the spin and parity of the first excited level (0.73 MeV) turns out to be 2^+ as expected.

1. Introduction

The aim of the present work is to elucidate the decay scheme of Bi^{212} (β-branching) and to check some disagreements in the literature.

Although long under study, the decay schemes of some naturally occurring radioactive nucleides are not yet completely resolved. This is because of the large amount of γ-ray background coming from the other components of the family. In the present case the principal trouble arises from the high energy γ-rays of Pb^{208} due to the decay $Tl^{208} \rightarrow Pb^{208}$. This can be seen from fig. 1 in which the decay scheme of Bi^{212} (ThC) is shown. Reliable information can only be attained through $\alpha - \beta$ or $\alpha - \gamma$ coincidences[1,2]). These can be realized thanks to the 0.3 μs half-life of Po^{212}. Unfortunately most of the previous work[3-7]) deals with investigations carried out without coincidence systems and therefore cannot clearly establish which of the observed transitions belong to the nucleide under study.

Evidence of 0.72, 1.34, 1.60, 1.82 and 2.19 MeV levels in Po^{212} was found by means of $\alpha - \beta$ coincidences by Burde and Rozner[1]).

Long range α-particles coming from 0.73, 1.67 and 1.80 MeV levels in Po^{212} have been found by some authors[8-10]).

The following γ-transitions are reported in the majority of investigations dealing with Bi^{212} (β-branching): 0.73 MeV[2-5]); 0.89 MeV[2,5]); 1.1 MeV[2,3,5]); 1.34 MeV[2,3,5,6]); 1.5 MeV[2,5,6]); 1.61 MeV[2,3,5,6,7]); 1.80 MeV[2,3,5,6]).

The following γ-transitions are doubtful because only a few authors have reported them: 0.20 MeV[2]); 0.78 MeV[5]); 0.83 MeV[3]); 0.95 MeV[5]); 2.20 MeV[2,6]).

No evidence of 1.1, 1.3, 1.5, 1.8 and 2.2 MeV transitions has been found in

a work[7]) mentioned above. Furthermore in this work the intensity limits attributed to 1.3, 1.8 and 2.2 MeV γ-rays are noticeably less than the corresponding intensities reported in the other investigations.

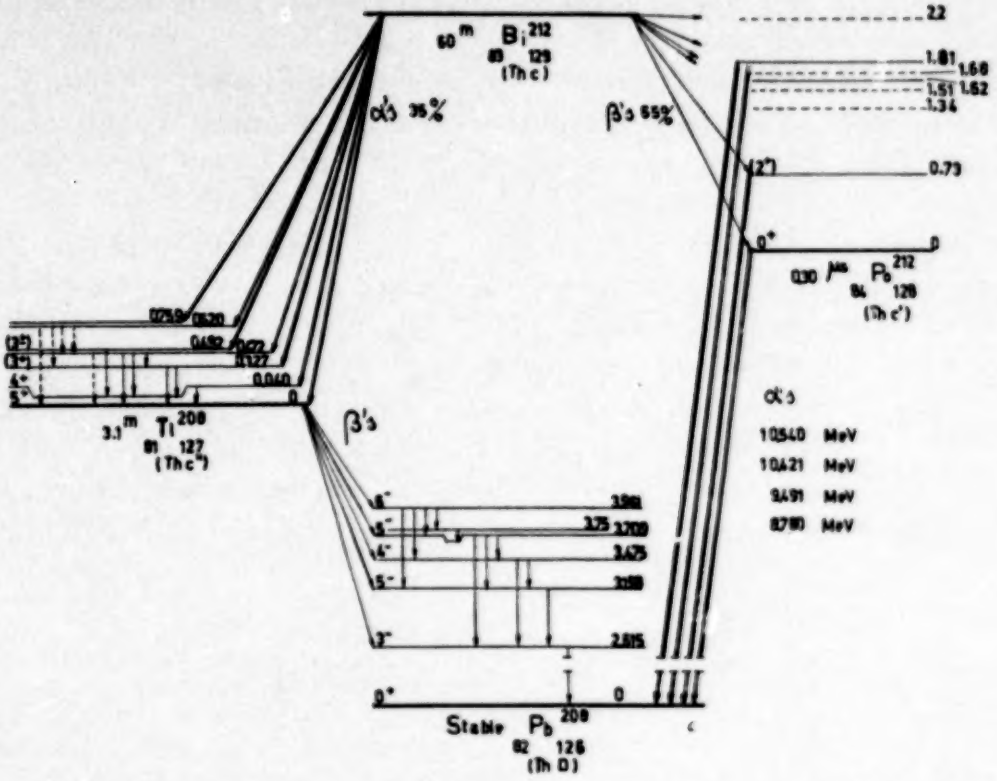

Fig. 1. Decay scheme of ThC deduced from literature. Data on Ti^{208} and Pb^{208} are reported from Nuclear Data Sheets (NRC 59-4-116).

The above stated discrepancies prompted us to re-examine Po^{212} levels by means of coincidence methods.

2. Experimental Methods and Results

The present work has been carried out by means of γ- and α-ray coincidences. Gamma quanta were detected by means of scintillation spectrometers employing 3.8 cm × 2.5 cm or 3.8 cm × 4.4 cm NaI(Tl) crystals; a gridded ionization chamber or a 0.013 cm thick CsI(Tl) crystal was employed for α-particle detection.

2.1. α-γ COINCIDENCES

The block diagram of the apparatus is shown in fig. 2. The source, ≈ 0.3 μc of RdTh (supplied by Amersham) in equilibrium with its daughter nuclei, was deposited in a thin layer on a polished aluminium disc constituting the ion chamber emitting electrode.

Coincidences between γ-rays and 8.78 MeV α's of Po^{212} were employed. The resolving time of the "fast" coincidence was kept > 0.2 μs because of the limitation imposed by the mean life of the selected α transition.

The data supplied by the γ-spectrometer were recorded by a LABEN 200-channel pulse-height analyser.

The experimental results are shown in fig. 3 in which curve a represents the total γ-ray spectrum of the source and curve b is the coincidence γ-ray spectrum following the β-decay in Bi^{212}. In fig. 4 curves c and d are expanded parts of curve b.

By inspection of curves b, c and d, 0.13, 0.19, 0.73, 0.78, 0.89, 0.95, 1.08, 1.51 and 1.62 MeV γ-rays are found, while there is no evidence for 1.8 or 2.2 MeV transitions. The existence of 1.3 MeV γ-rays is doubtful.

Dotted lines in figs. 3 and 4 represent the photopeaks obtained from curves b, c and d by decomposition and comparison with the standard peaks of Tm^{170}, Cr^{51}, Mn^{54}, Cs^{137}, Na^{22} and Y^{88}. In table 1 energies and relative intensities of γ-rays from Bi^{212} are reported (the photopeak efficiences were deduced from efficiency tables[11, 12]).

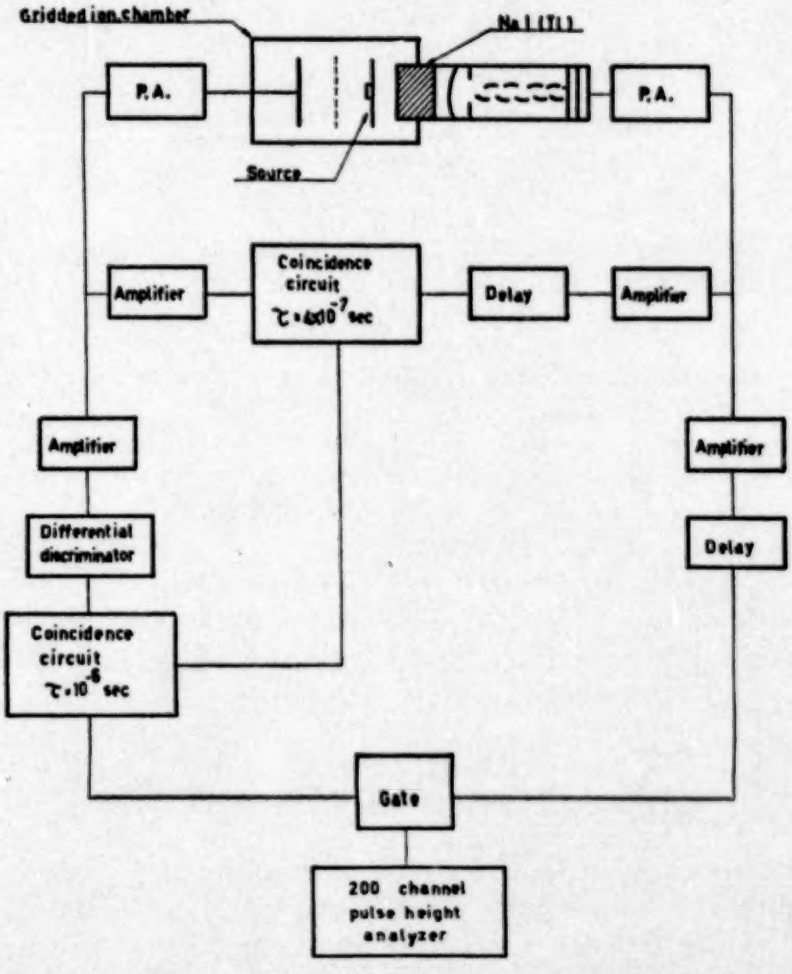

Fig. 2. Block diagram of the alpha-gamma coincidence arrangement.

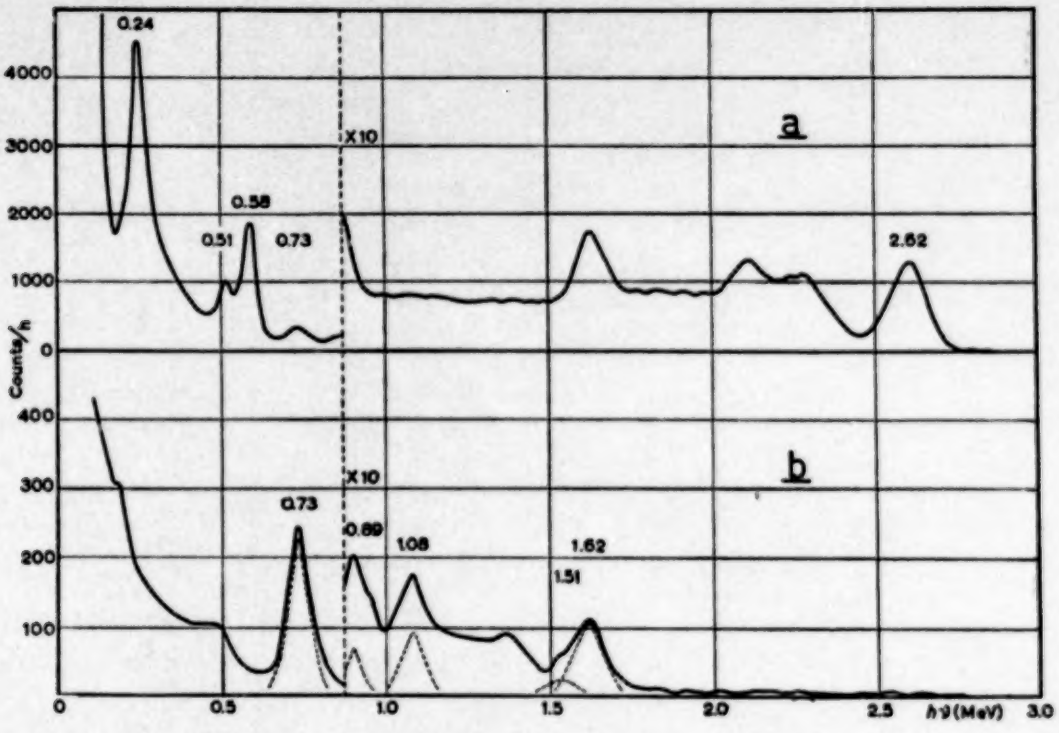

Fig. 3. Curve *a*: total gamma-ray spectrum of the RdTh source. Curve *b*: gamma-ray spectrum from Bi^{212}. The spectrum was obtained in coincidence with 8.78 MeV alpha-particles starting from the Po^{212} ground state. Dashed curves represent the photopeaks corresponding to the individual gamma-rays. In curve *b* the photopeaks of 0.78 and 0.95 MeV are not drawn.

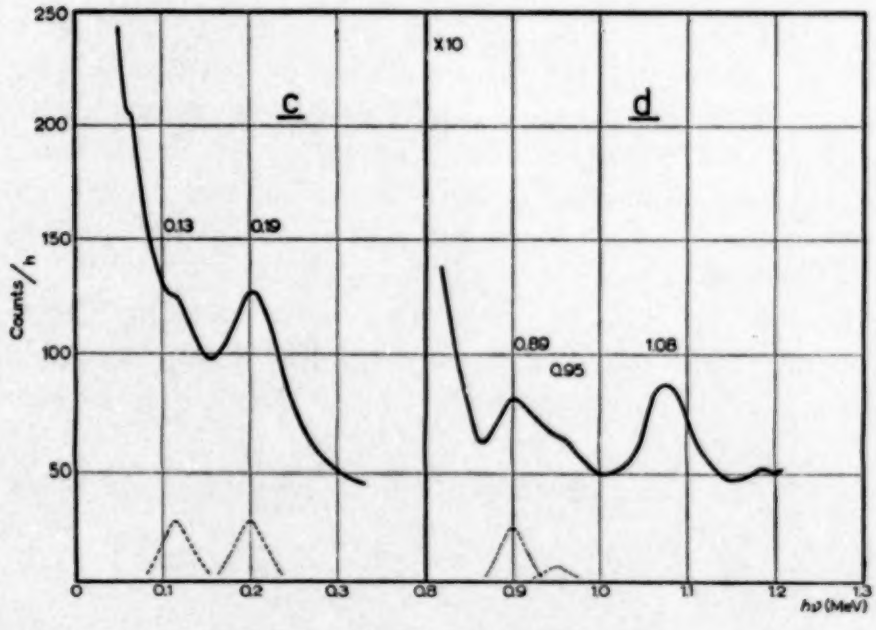

Fig. 4. Gamma-ray spectrum from Bi^{212}. Curve *c*: region below 0.3 MeV. Curve *d*: 0.8 to 1.3 MeV region.

TABLE 1

Intensities of γ-rays from Bi^{212}

γ-transition (MeV)	Relative intensity
0.13	3 ± 1
0.19	3 ± 1
0.73 + 0.78	100
0.89 + 0.95	6 ± 1
1.08	11 ± 1
1.3	< 2
1.51	4 ± 1
1.62	26 ± 1
1.81	no < 1
2.2	no < 0.5

The existence of 0.78 MeV γ-rays can be demonstrated by inspecting the 0.73 MeV peak-shape (curve b). From the peak asymmetry a relative intensity 10 ± 3 for 0.78 MeV transition is found. The 0.73 MeV transition should therefore have an intensity of ≈ 90.

From a similar procedure applied to the 0.9 MeV peak, the intensity ratio between 0.89 and 0.95 MeV transitions can be evaluated to ≈ 4.

2.2. α-γ-γ COINCIDENCES

The data obtained from the above measurements are not sufficient to fit univoquely the γ quanta energies in a decay scheme. In order to get further information on γ-cascades, we employed $\gamma - \gamma - \alpha$ coincidences. In fig. 5 is shown the block diagram of the experimental arrangement. In order to obtain a high overall efficiency, the RdTh source was sandwiched between two thin CsI(Tl) sheets backed up by an aluminium reflector and connected by means of a lucite light pipe to the photomultiplier.

The γ-ray spectrum in coincidence with the selected α's and the 0.73 MeV γ-quanta is drawn in fig. 6. By a careful analysis the γ-photopeaks were obtained. In table 2 the relative intensities are shown.

The intensity calculations are supported on the hypothesis that 1.08 MeV γ-rays belong entirely to a cascade between the 1.81, 0.73 and 0 MeV levels. Furthermore, 0.19, 0.89 and 0.95 MeV γ-rays turn out to be completely in coincidence with 0.73 MeV γ-quanta.

As far as the 0.78 MeV γ-ray intensity is concerned, the value given in table 2 is in agreement with that obtained from the above asymmetry considerations. A good agreement is also obtained by the absolute counting of 0.73 and 0.78 MeV two-fold coincidences.

The upper limits attributed by us to 1.3 and 1.51 MeV γ-rays show that $0.7 \rightarrow 0.2 \rightarrow 1.3$ and $0.7 \rightarrow 1.5$ cascades are very improbable.

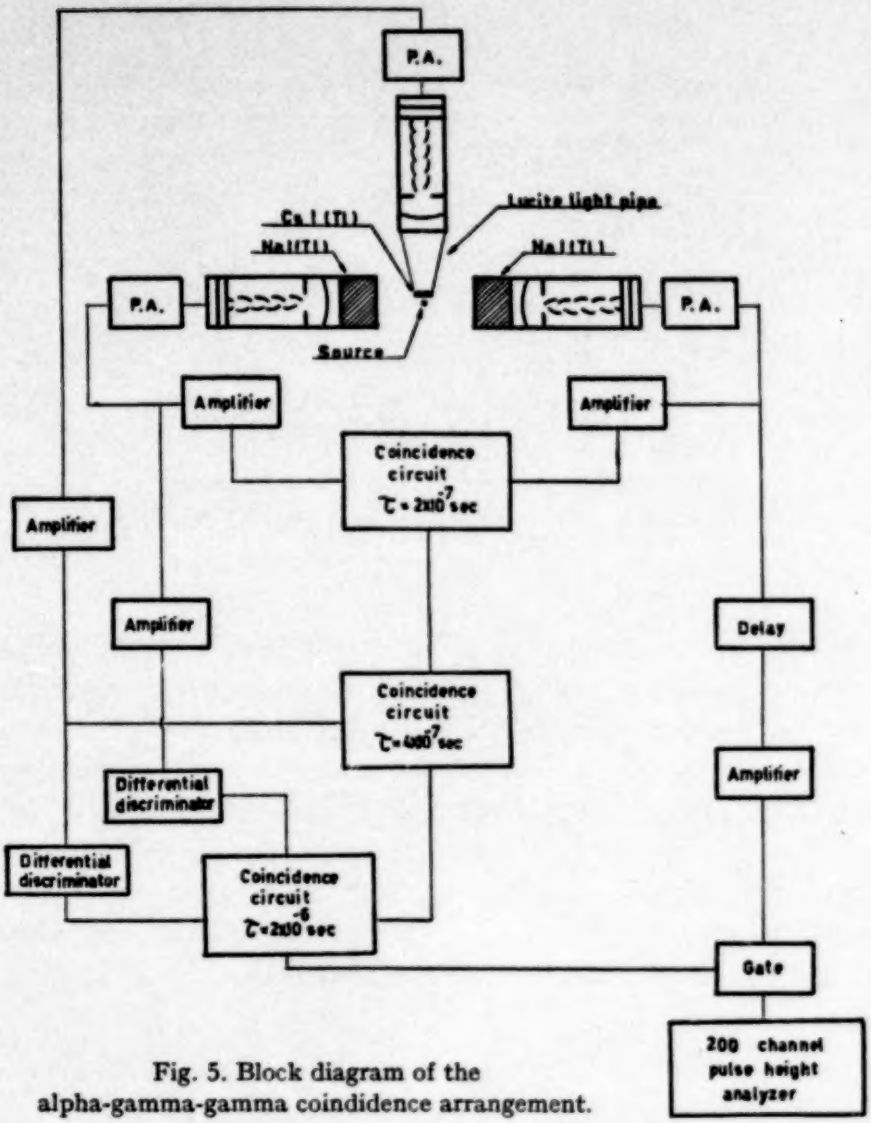

Fig. 5. Block diagram of the alpha-gamma-gamma coindidence arrangement.

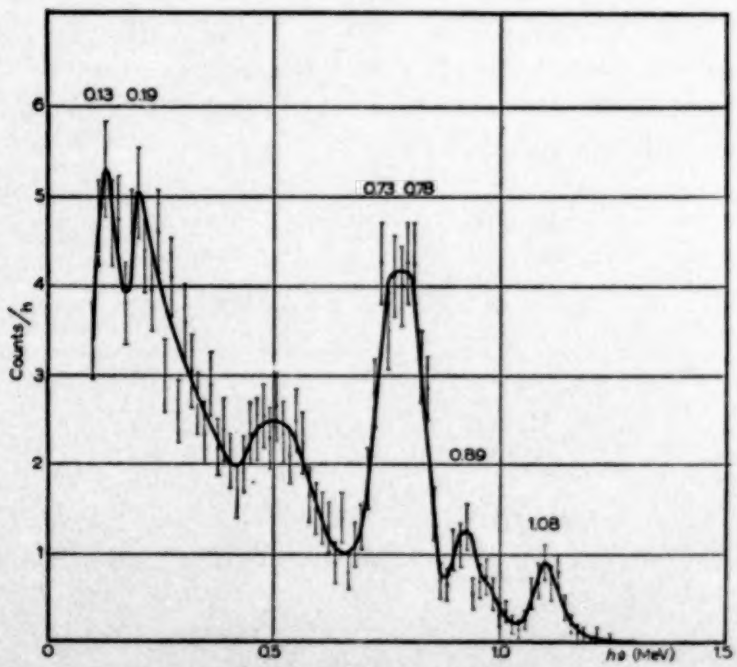

Fig. 6. Gamma-ray spectrum in coincidence with 8.78 MeV alpha-particles and 0.73 MeV gamma-rays.

TABLE 2

Intensities of γ-rays coincident with 8.78 MeV α-rays and 0.73 MeV γ-rays

γ-transition (MeV)	Relative intensity
0.13	3.5 ± 1
0.19	3.5 ± 1
0.78	11 ± 2
0.89 + 0.95	6.5 ± 1.5
1.08	11*
1.3	no < 0.5
1.51	no < 0.5

* All the intensities are referred to this transition

2.3. γ-γ-γ COINCIDENCES

As mentioned above, some authors have found evidence of a 2.2 MeV level. Since we found neither a direct transition nor cascade de-excitation involving 1.3 or 1.51 MeV γ-rays, there remained the possibility of a $0.7 \rightarrow 0.78 \rightarrow 0.73$ MeV cascades. An accurate analysis of the $\alpha - \gamma - \gamma$ coincidence results indicates that the probability of such a cascade is rather low. In order to obtain more quantitative data we employed a three-fold γ-ray coincidence in which the three channels were set to register the above mentioned γ-quanta. No evidence of coincidences was found. From our results, the upper limit for the relative intensity of the cascade under consideration is 1.

3. Conclusions

Elaborating the data obtained from our measurements, an improved decay scheme of Po^{212} can be given. This scheme, together with the β-disintegration intensities deduced from our γ-ray measurements, is shown in fig. 7. The β-rays percentage to the ground state was evaluated from the knowledge of ThC branching ratio[13])

$$\frac{\alpha}{\alpha + \beta} = 0.352 \pm 0.003 ,$$

and from the intensity ratio of 2.62 and 0.73 MeV γ-rays

$$\frac{I_{2.62}}{I_{0.73}} = 2.6 \pm 0.1 ,$$

as measured in the present work.

In the level scheme proposed by us a 1.68 MeV γ-ray is reported. Its existence, although not experimentally proved, because of the high intensity of the 1.62

MeV transition, seems to be essential for the de-excitation of the 1.68 MeV level.

An attempt was carried out in order to obtain information on the spins of levels from the knowledge of γ-ray and long range α-particle intensities. We employed the well-known formula

$$\tau_\gamma = \tau_\alpha \frac{I_\alpha}{I_\gamma},$$

where τ_γ and τ_α are the mean-lives of the γ-rays and long range α-particles starting from the same level[14]), and I_γ, I_α are the corresponding intensities. The τ_γ evaluation was compared with the Weisskopf estimate for different electric and magnetic polarities. In the case of Po^{212} the Weisskopf theory represents a zero order approximation. Such a rough estimate corresponds to

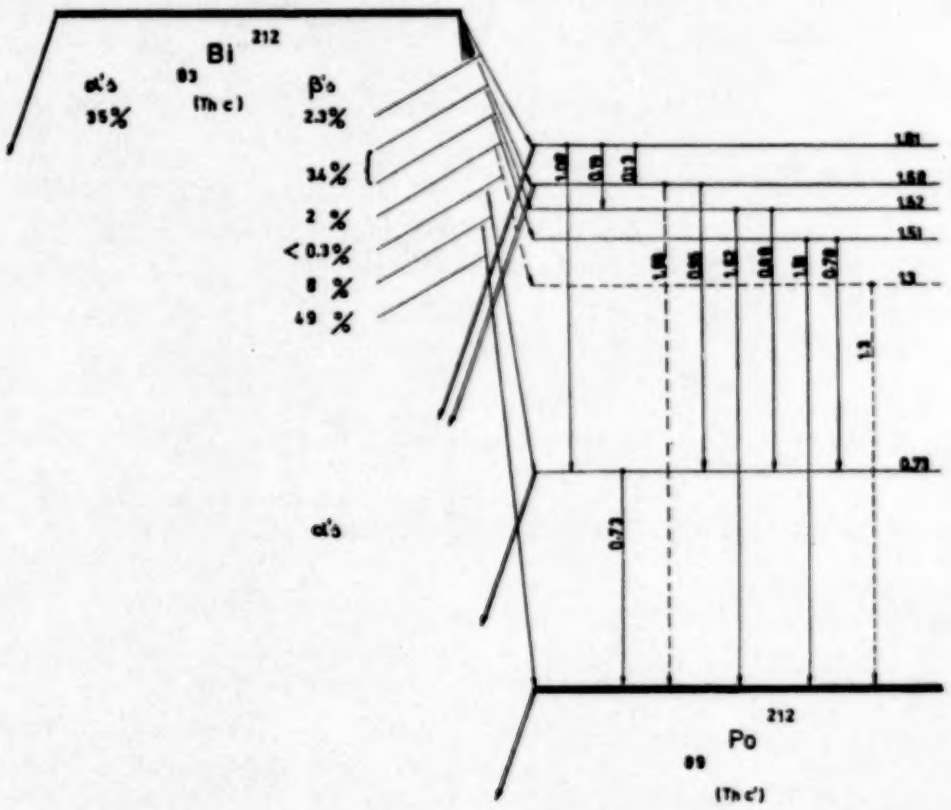

Fig. 7. Proposed level scheme of Bi^{212} (beta-branching). The intensities were calculated from tables 1 and 2.

neglecting the interactions between the four nucleons external to the closed shells $N = 126$ and $Z = 82$. We obtained a clearly interpretable result only for the 0.73 MeV first level (table 3). The best agreement occurs for an E2 radiation.

TABLE 3

Comparison of experimental values and theoretical estimates of τ_γ

$\tau_\gamma = \tau_\alpha \frac{I_\alpha}{I_\gamma}$ (sec)	Weisskopf estimate of τ_γ (sec)			
	E1	M1	E2	M2
1.1×10^{-11}	7×10^{-6}	9×10^{-14}	6×10^{-11}	7×10^{-9}

Assuming, as obvious, a 0^+ ground state for the Po^{212} the spin and parity of the 0.73 MeV level turn out[1,3]) to be 2^+.

Similar calculations, carried out for 1.68 and 1.81 MeV levels, gave ambiguous results. A more accurate analysis of the experimental results can give useful information about the limits of validity of the shell model in the lead region.

Note added in proof: Recently U. Hauser and W. Kerler[15]) published a work in which the decay scheme of Bi^{212} is studied by means of α-γ coincidences. The results attained by these authors are in a fairly good agreement with our data as far as it concernes energies greater than 0.7 MeV. The two γ-rays of 0.13 and 0.19 MeV found by us are not reported in the above mentioned work.

References

1) J. Burde and B. Rozner, Phys. Rev. **107** (1957) 531
2) B. Chinaglia and F. Demichelis, Nuovo Cimento **8** (1958) 365
3) A. Johansson, Arkiv Mat. Astron. Fysik **A34**, No. 9 (1947)
4) D. E. Muller, H. C. Hoyt, D. J. Klein and J. W. M. DuMond, Phys. Rev. **88** (1952) 775
5) V. D. Vorobev, K. I. Il'in, T. I. Kolchinskaia, G. D. Latyshev, A. G. Sergeev, Iu. N. Trofimov, and V. I. Fadeev, Izvest. Akad. Nauk. SSSR, Ser. Fiz. **21** 954; Columbia Tech. Trans. (1957) p. 956
6) G. D. Latyshev, Revs Mod. Phys. **19** (1947) 132
7) D. G. E. Martin and G. Parry, Proc. Phys. Soc. **A68** (1955) 1177
8) Values recalculated by G. H. Briggs, Revs. Modern Phys. **26** (1954) 1
9) A. Rytz, Compt. rend. **233** (1951) 790
10) A. Rytz, J. Recherches Centre Nat. Bellevue **25** (1953) 254
11) Stanley H. Vergos Jr., Louis L. Marsden and R. L. Heath, AEC Research and Development Report IDO-16370 (1958)
12) M. I. Kalkstein and J. M. Hollander, UCRL 2764 (1954)
13) D. Prosperi and S. Sciuti, Nuovo Cimento **9** (1958) 734
14) G. C. Hanna, in Experimental Nuclear Physics, ed. by Segrè (1959) Vol. III, Part IX, sect. 2
15) U. Hauser and W. Kerler, Z. Physik **158** (1960) 405

1.E.1: 4.E

Nuclear Physics **19** (1960) 389—399; © *North-Holland Publishing Co., Amsterdam*
Not to be reproduced by photoprint or microfilm without written permission from the publisher

DECAY SCHEME OF Tb^{152}

K. S. TOTH†, O. B. NIELSEN and O. SKILBREID

Institute for Theoretical Physics, University of Copenhagen

Received 12 May 1960

Abstract: The decay scheme $Tb^{152} \rightarrow Gd^{152}$ has been investigated with sources prepared in an isotope separator. In addition to obtaining γ-ray and conversion electron spectra, γ–γ and e–γ coincidence measurements were carried out. A disintegration scheme has been established that includes all transitions in Gd^{152} reported in earlier Eu^{152} β-decay studies. In addition, four new transitions which establish two excited levels in Gd^{152} were observed. One of these is a 0^+ state at 1047 keV and the other, at 929 keV, has probably spin 2^+. The 0^+ state decays with two monopole transitions to lower 0^+ states, and the transition from the 929 keV level to the 344 keV first excited level, seems to contain a considerable E0 admixture. The two new levels are tentatively interpreted as members of a three-phonon quintet.

1. Introduction

The isotope Tb^{152} was recently identified[1]). Its half life was found to be 18.5 h or quite similar to that of Tb^{151}, which is always produced simultaneously. A closer study of the decay scheme must thus preferably be done after an isotope separation.

The levels in the daughter Gd^{152} have been extensively studied from the β-decay of both Eu^{152} (13 y) and Eu^{152m} (9.3 h)[2–9]). The first excited state at 344 keV has spin 2^+ and, among other levels observed, a low lying 0^+ at 615 keV has been established[9]). These levels are probably of vibrational character, corresponding to one and two phonons, respectively. The vibrational energies, however, are lower than in most spherical nuclei and suggest that further vibrational states might be situated in the energy gap between the ground state and the intrinsic-particle excitations.

2. Experimental Technique

The source of Tb^{152} was prepared in an isotope separator[10]), the activity being collected on a 150 $\mu g/cm^2$ Al-foil that later served as a β-ray spectrometer source. A detailed description of the experimental methods used in producing and purifying the Tb activity is given in another publication[11]) that deals with a survey of the neutron-deficient Tb isotopes. The strength of the Tb^{152} source was about 5 μc.

† Present address: Electronuclear Research Division, Oak Ridge National Laboratory, Oak Ridge, Tennessee.

Two main instruments were used in the measurements. The first was a 100-channel pulse height analyzer that could be coupled to either a 3.8 cm × 3.8 cm or a 7.6 cm × 7.6 cm NaI(Tl) scintillation crystal detector. The two detectors were also used in a γ–γ coincidence set-up, where the spectrum in coincidence with the gating γ-ray was displayed on the 100-channel analyzer. The second instrument was a six-gap β-ray spectrometer[12]). It was used to obtain the conversion electron spectrum and, in conjunction with the 7.6 cm detector, to perform e–γ coincidence measurements. Details of the operation of the β-ray spectrometer have been published earlier[13]).

3. Experimental Data

A total of seven transitions can be identified in the conversion electron spectrum of Tb^{152} (fig. 1). Four of these were observed earlier by Toth[14]) who

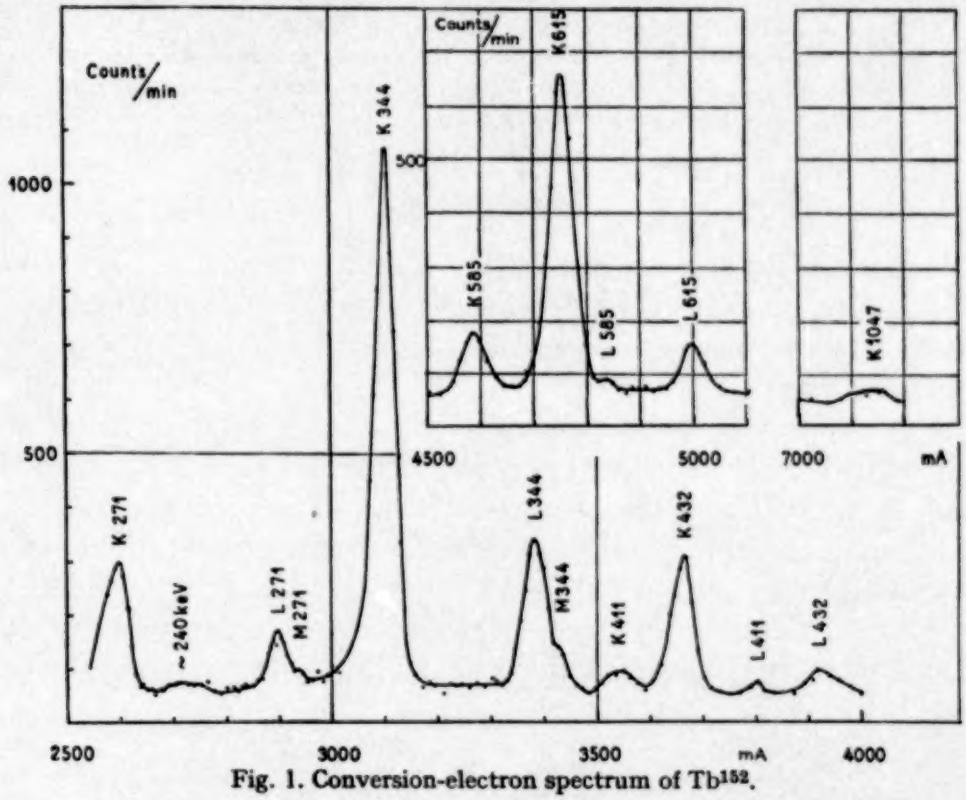

Fig. 1. Conversion-electron spectrum of Tb^{152}.

studied a mixture of Tb^{151} and Tb^{152}, using high resolution permanent magnet spectrographs. His energies were: 271.1, 344.1, 432.1 and 615.2 keV. At that time, the similarity of the Tb^{151} and Tb^{152} half-lives was not known and the four transitions were assigned to Tb^{151} decay. The 271, 344, 411 and 615 keV transitions are known from Eu^{152} studies, whereas the 432, 585 and 1047 keV transitions are seen only in the Tb^{152} decay. In addition, there is a weaker line at approximately 240 keV. The peak is rather broad and may consist of two electron lines, the first of which may be the K-line of the intense 287 keV transi-

tion of Tb^{151} [14,15]) present because of incomplete mass separation. The second may be the K-line of a weak Tb^{152} transition.

The singles γ-ray spectrum taken with the 7.6 cm NaI(Tl) detector, and shown in fig. 2, is divided into two sections, the first covering the energy range 80–800

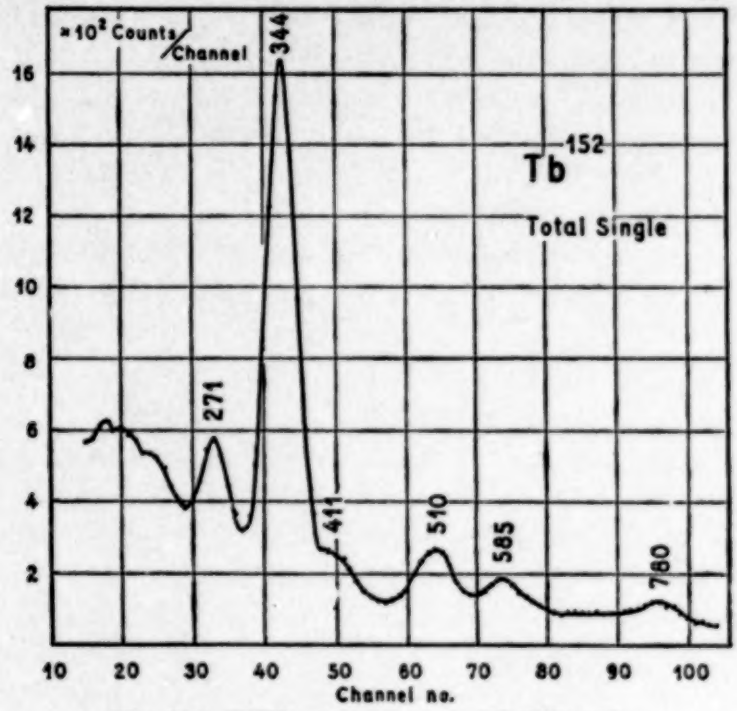

Fig. 2(a). Tb^{152} γ-ray spectrum (80–800 keV).

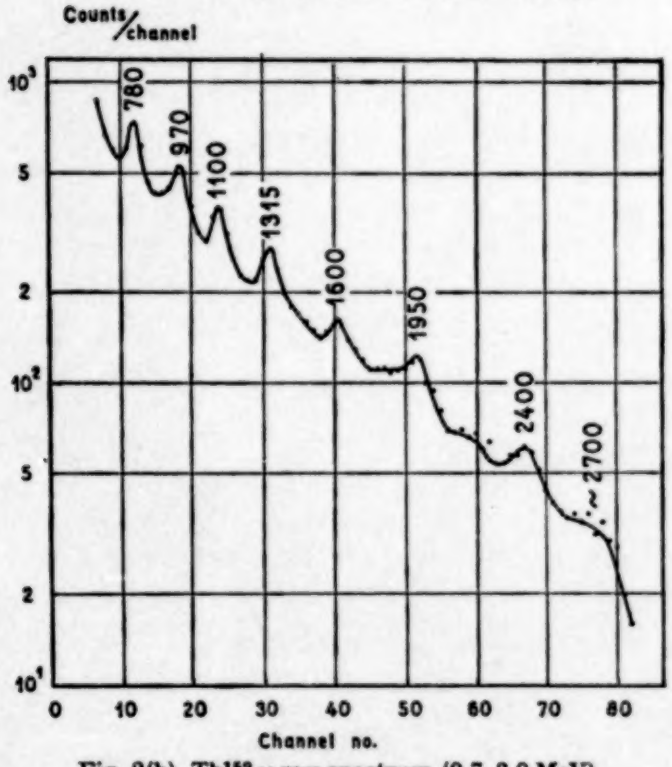

Fig. 2(b). Tb^{152} γ-ray spectrum (0.7–3.0 MeV).

keV, the second the range 0.7–3.0 MeV. Four transitions, of 271, 344, 411 and 585 keV, are clearly observable in both figs. 1 and 2, whereas the intensity of γ-rays corresponding to the relatively strong conversion lines of the 432, 615 and 1047 keV transitions is below the limit of detection. From a recent study of Eu^{152m} (9.3 h)[9]) it appears than the 615 keV transition is of monopole order. As will be discussed later, the same is probably true for the 432 and 1047 keV transitions. With the source strength available, none of the high energy transitions seen in fig. 2(b) is observed in the conversion electron spectrum. Three of the γ-rays seen in fig. 2(b), of 780, 970 and 1315 keV, are probably identical with γ-rays known from Eu^{152} decay studies.

The coincidence relations obtained in the e–γ coincidence measurements established, in connection with the previously known Gd^{152} levels, the position in the decay scheme (fig. 4) of the three new transitions of 432, 585 and 1047 keV. The line K_{585} is $\approx$ 100 % coincident with the 344 keV γ-ray and with no other strong γ-ray. It thus originates in a level at 929 keV, which must be excited by K-capture. K_{432} is $\approx$ 100 % coincident with the 271 as well as with the 344 keV γ-ray. The transition must thus connect a level at 1047 keV with the 615 keV level, the 1047 keV transition being the crossover to the ground state.

The γ-ray spectrum coincident with K_{615} is shown in fig. 3. The spectrum, aside from illustrating the type of spectra obtained in our e–γ coincidence

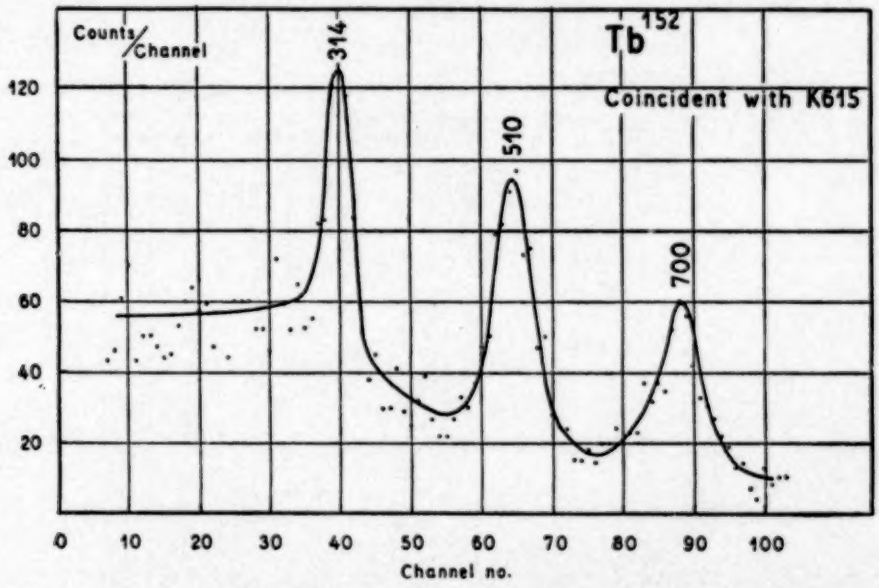

Fig. 3. γ-ray spectrum in coincidence with the K-electrons of the 615-keV transition.

measurements, clearly shows the presence of two transitions too weak to be identified in either fig. 1 or 2. The first γ-ray with an energy of 314 keV fits in between the above 929 keV level and 615 keV and has not been reported in earlier Gd^{152} studies. Its K-conversion line has an energy of 264 keV which

places this electron line in fig. 1 underneath the more intense L-line of the 271 keV transition. The second transition has an energy of 700 keV and has been reported in investigations of Eu^{152m} decay[9]).

γ–γ coincidence experiments were performed, but these were not as clear-cut and chiefly served to confirm the e–γ measurements. The spectrum coincident with the 510 keV γ-line showed only one intense peak again at 510 keV. No transition of this energy is apparent in the conversion electron spectrum, and the peak is thus undoubtedly due to annihilation radiation.

4. Numerical Results and Multipole Orders

Table 1 summarizes the conversion electron data. The experimental K/L ratios suggest the 271, 344 and 411 keV transitions to be of electric quadrupole order. The K-line of the 314 keV transition is known to be underneath the L-conversion peak of the 271 keV transition. The consequent increase in the

TABLE 1

Conversion electron data

Transition energy (keV)	Relative intensities*			K/L (exp.)	K/L ratios (theoretical)			Multipole assignment and remarks
	K	L	M+N		E1	E2	M1	
271	27.5	9	3	3.0 ± 0.3	7.3	3.8	7.1	E2; K of 314 keV transition under L line
344	100	27	9	3.7 ± 0.3	7.3	4.6	7.2	E2; K/L ratio known from Eu^{152} work to be 4.7
411	4.5	≈ 1		≈ 4.5	7.4	5.0	7.2	E2; the L-line is very weak and its intensity very approximate
432	24	3.5	≈ 1.5	7	7.4	5.1	7.2	
585	11	1.7		6.7	7.5	6.0	7.3	
615	50	7.5	3.5	6.5	7.5	6.1	7.3	
1047	2.5							

* The K-line of the 344-keV transition is assumed to be 100.

L-conversion line's intensity accounts for the discrepancy between the experimental and theoretical ratios. The K/L ratio for the 344 keV transition is known from Eu^{152} studies to be in agreement with the theoretical E2 ratio. The discrepancy in our case is too large to be due to incorrect analysis of the L + M + N peak, and probably there is another weak transition whose K-conversion line coincides in energy with L_{344}.

Numerical results of e–γ coincidence measurements are shown in table 2.

Knowing the crystal efficiencies for γ-rays of various energies, the relative intensities of the transitions represented by the conversion line and the coincident γ-rays can be estimated[13]). For each line listed in table 2 the energy of the coincident γ-rays is given as well as the percentage of the conversion electrons

TABLE 2

Results of e–γ coincidence measurements

Conversion line	Energies of coincident γ-rays (keV)	Percentage of conversion electrons accompanied by the coincident γ-ray
K 271	344	90
	314	≈10
K 344	271	12
	314	
	411	≈5
	585	12
K 432	271	100
	344	100
K 585	344	100
K 615	314	10
	700	15

accompanied by a particular γ-ray. Although the γ-ray intensities are accurate only to about 20 %, this is sufficient to distinguish between E1, E2 and M1 transitions whose K-conversion coefficients differ by a factor of two or more.

From the decay scheme one would expect that 1) gating in turn on the K-electrons of the transitions 271, 344 and 615 keV would reveal the 432 keV γ-ray in each of the three coincident γ-ray spectra, and 2) gating on the K-electrons of the 432 keV transition would reveal the 615 keV transition. Neither of the two transitions was observed in the coincident γ-ray spectra. Upper limits for the γ-ray intensity of the 432, 615 and of the 1047 keV transitions are given in table 3. The corresponding ratio between conversion electrons and γ-rays indicates either monopole nature or a high multipole order, M4 or higher. The latter possibility is improbable, among other reasons because levels of high spin at 615 or 1047 could deexcite to the 344 keV level with radiation of lower order. The level at 1047 keV then, no doubt, has spin 0^+ like that at 615 keV.

The coefficient α_K for the new 585 keV γ-ray is about 4 times the E2 and 2 times the M1 value. The transition probably takes place between two levels with spin 2^+, and a high multipole order is unlikely also in this case. As will be discussed later, the conversion coefficient may be due to a monopole admixture in a transition mainly of E2 nature.

The intensity of the K-line of the 314 keV transition was estimated to be

1.8 ± 0.9 ($K_{344} = 100$) by comparing the theoretical K/L ratio for the 271 keV transition with the observed value. The coefficient α_K of the 314 transition was then calculated to be 0.046 ± 0.023, which is closest to the theoretical E2 value.

TABLE 3

γ-ray intensities and conversion data

Transition energy (keV)	Relative K-line intensity	I_γ from e–γ measure-ments	I_γ from singles spectrum	α_K (exp.)	$\alpha_K \times 10^4$ (theoretical)			Assignment
					E1	E2	M1	
271	27.5	387	423[b])	0.071	180	650	1100	E2
314	1.8 ± 0.9	50		0.036	120	420	730	E2
344	100		3225[a])			310		E2
411	4.5	220	190	0.020	65	200	360	E2
432	24	< 15	< 60	> 1.5	58	170	320	E0
585	11	400	440	0.026	29	80	150	E0 + E2
615	50	< 50	< 160	> 1	26	70	130	E0
700	< 1	80	< 100					(E1)
780	< 1		440					(E1)
970			340					(E1)
1047	2.5		< 75	> 0.03	9	24	36	E0
1100			≈ 330					
1315			≈ 360					(E1)
1600			≈ 240					
1950			≈ 270					
2400			≈ 300					
2700			≈ 200					

The intensities of the high energy γ-rays are rough. Many of the lines in the scintillation spectrum are probably double.

[a]) The γ-ray intensities are normalized relative to the conversion lines by assuming the theoretical E2 conversion coefficient for the 344 keV transition.

[b]) This intensity is based on the line K_{271} and the theoretical E2 conversion coefficient.

Conversion lines for the 700, 970 and 1315 keV transitions were not observed. They are all known to be E1 in nature from previous investigation.

5. The Decay Scheme

In the decay of Tb^{152} (fig. 4) all the low lying levels of Gd^{152} are excited which have been observed in investigations of Eu^{152} and Eu^{152m}. In addition, a 0^+ level at 1047 keV and a level at 929 keV are established. The latter has probably spin 2^+, since the 314 keV transition to the 615 keV 0^+ level seems to be E2.

With the limited half-life of the source, measurements on the positon spectra could not be attempted. For this reason, the total energy release in the Tb^{152} disintegration was not determined, and information on the β^+ and K-capture

branches can only be found indirectly from the excess of γ-rays leaving the excited levels compared to those exciting them. The K-X ray is about two times the 344 keV γ-ray. This intensity cannot be accounted for by K-capture transitions to higher levels and indicates a group directly to the ground state about as intense as that to the 344 keV level.

The γ-rays coincident with the lines K_{344} and K_{615} are not sufficiently intense to account for all excitations of the 344 and 615 keV levels. Levels with spin 0^+ and 2^+ are thus directly excited with comparable half-lives, making 1^+

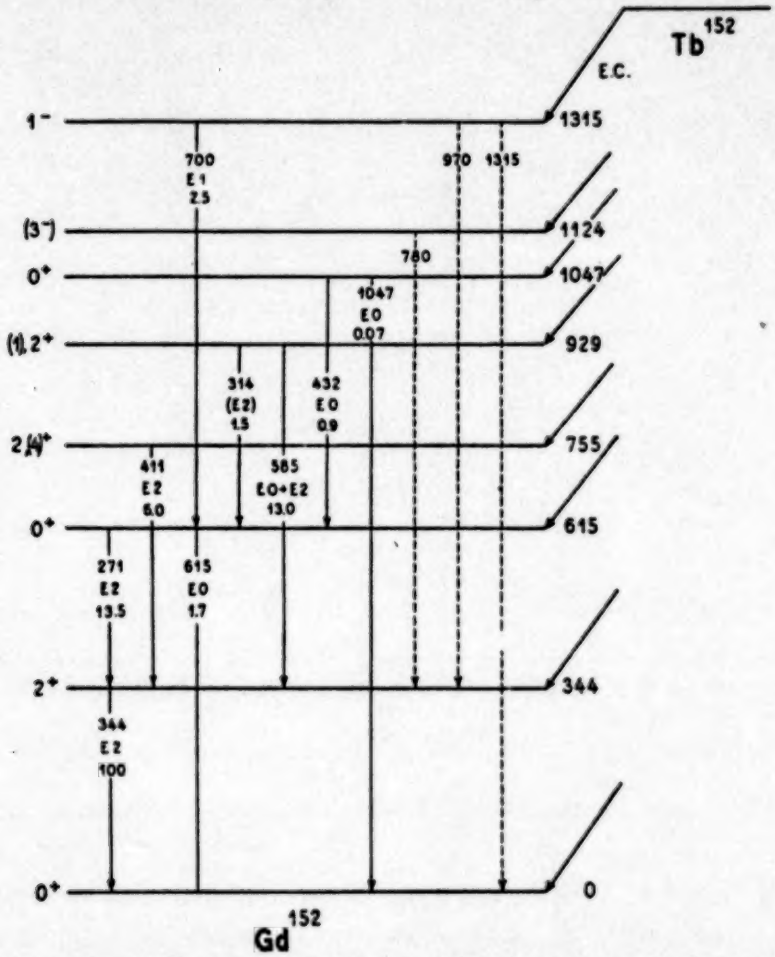

Fig. 4. Tb^{152} Decay scheme. For each transition the following information is given: a) the energy in keV, b) the multipolarity and c) the total intensity relative to the 344-keV transition which is assumed to be 100. Three transitions are drawn with dashed lines. These were observed only in singles γ-ray spectra. In addition, numerous levels of higher energy are excited.

the most probable spin assignment for Tb^{152}. This is between the value of 0 for Eu^{152m} and 3 for Eu^{152}, and explains why all transitions known from the decay of the two Eu isomers are observed simultaneously.

The 755 keV level is excited in the decay of Eu^{152}, 2^+ and 4^+ being possible spin assignments. The fact that it is excited in the Tb^{152} decay makes 2^+ the most likely.

The 1315 keV level is without much doubt identical with the level known from the decay of Eu^{152m}. The 700 keV γ-ray known to de-excite it was seen in coincidence with K_{615}; whereas a γ–γ coincidence measurement showed that the 980 keV γ-ray was coincident with 344 keV, but 1315 keV was not.

Also the strong 780 keV γ-ray was coincident with 344 keV and established a level close to 1124 keV, which is probably identical with the 3^- level known from the Eu^{152} decay.

6. Discussion

Gd^{152} with 88 neutrons lies close to the region of strongly deformed nuclei, which sets in at 90 neutrons. Gd^{152} itself is spherical as revealed by the position of the first excited 2^+ state. Its energy of 344 keV is definitely higher than that of the rotational states of the deformed even nuclei, although lower than in neighbouring spherical nuclei. The energy of the first excited level of even nuclei in the region under consideration is steadily increasing with decreasing neutron number, and Nd^{142} with a single closed shell has first excited state at 1.57 keV.

In general, the first excited level in an even spherical nucleus has spin 2^+ and is considered as a one-phonon quadrupole vibration of energy $\hbar\omega$[16, 17]. In a harmonic oscillator approximation, the two-phonon vibration with energy $2\hbar\omega$ will generate a degenerate triplet with spins 0^+, 2^+ and 4^+, whereas the three-phonon states will be 0^+, 2^+, 3^+, 4^+ and 6^+. In the actual nuclei the degeneracies seem removed by strong anharmonic terms. Furthermore, already the 2-phonon states, in most cases, have an energy in the same region as the lowest particle excitations in the even nuclei, making an identification difficult.

The two states of 615 and 755 keV have been interpreted as belonging to the two-phonon vibration[9]). It is natural to proceed along this line and to explain the 1047 keV 0^+ state and the 929 keV state with spin probably 2^+ as members of the three-phonon vibration. The interpretation can be tested by the branching of the E2 transitions de-exciting the two levels. E2 transitions involving a change of more than one phonon are expected to be strongly hindered and, in many cases, it has been confirmed experimentally that these transitions from a second 2^+ state to the ground state are much reduced in intensity compared to the E2 transitions to the first 2^+ state.

The multipole order of the γ-rays from the 929 keV level is not definitely established, but, if E2 nature is assumed, the 314 keV one-phonon transition is favoured 2.5 times compared to the 585 keV two-phonon transition. The ground state transition, assumed to involve a change of three phonons, is not observed and is hindered at least 40 times more than the 585 keV transition.

The most interesting new observations are the strong monopole transitions from the 1047 keV level to the two lower 0^+ states. The occurrence of such transitions between these 0^+ levels is not simply explained by the forbiddenness of γ-transitions. Since both the 615 and 1047 keV levels can de-excite by E2 radiation to lower levels, the monopole radiation strength must be comparable to the quadrupole radiation strength. As large monopole matrix elements are expected between vibrational levels[18, 19]), also the E0 transitions suggest the vibrational character of the two levels. A similar competition must also be expected for transitions between states with $I \neq 0$, $\Delta I = 0$. The abnormally high ratio between conversion electrons and γ-rays for the 585 keV transition connecting the 929 keV and 344 keV states, both with $I = 2^+$, is thus probably due to monopole conversion electrons.

Table 4 shows the ratios between E0 and E2 radiations from the same level.

TABLE 4

E0/E2 ratios

Initial level (keV)	Transitions	E0/E2 ratio
615	$\frac{615 \text{ keV E0}}{271 \text{ keV E2}}$	0.0058
1047	$\frac{1047 \text{ keV E0}}{703 \text{ keV E2}}$	$\gtrsim 0.05$
929	$\frac{585 \text{ keV E0}}{585 \text{ keV E2}}$	0.034
1047	$\frac{432 \text{ keV E0}}{703 \text{ keV E2}}$	$\gtrsim 2$

The 703 keV γ-ray could not be observed; it is weaker then 3% of the 344 keV γ-ray.

The data are those of table 3, but, in order to facilitate comparisons of the ratios in spite of the different energy dependence of the two multipole orders, all intensities are corrected so as to correspond to the energy $mc^2 = 511$ keV.

We should like to thank Professor Niels Bohr for the excellent working conditions at this Institute. Thanks are due also Å. Svanheden and the crew of the Uppsala synchrocyclotron who performed the bombardment. One of us (K.S.T.) is extremely grateful for the hospitality of the Institute for Theoretical Physics during his stay there. He would also like to thank the Fulbright Foundation that made it possible for him to spend a year at the institute.

References

1) K. S. Toth, K. T. Faler and J. O. Rasmussen, Phys. Rev. **115** (1959) 158
2) L. Grodzyns and H. Kenndall, Bull. Am. Phys. Soc. **1** (1956) 163, 164
3) O. Nathan and M. A. Waggoner, Nuclear Physics **2** (1957) 548
4) B. V. Bobykin and K. M. Novik, Izv. Akad. Nauk, SSSR **21** (1957) 1556
5) B. S. Dzelepov and N. N. Zhukovsky, Nuclear Physics **6** (1958) 655
6) G. T. Wood and O. Nathan, International Congress of Nuclear Physics, Paris (1958)
7) I. Marklund, Nuclear Physics **9** (1958) 83
8) O. Nathan and S. Hultberg, Nuclear Physics **10** (1959) 118
9) I. Marklund, O. Nathan and O. B. Nielsen, Nuclear Physics **15** (1960) 199
10) K. O. Nielsen and O. Skilbreid, Nuclear Instruments **2** (1958) 15
11) K. S. Toth, S. Bjørnholm, M. Jørgensen, O. B. Nielsen, O. Skilbreid and Å. Svanheden, J. Inorg. Nuc. Chem. **14** (1960) 1
12) O. B. Nielsen and O. Kofoed-Hansen, Mat. Fys. Medd. Dan. Vid. Selsk. **29** (1955) no. 6
13) P. Gregers Hansen, O. B. Nielsen and R. K. Sheline, Nuclear Physics **12** (1959) 389
14) K. S. Toth, Nuclear Studies in the Rare Earth Region (thesis), unpublished, UCRL-8192, March 1958
15) J. W. Mihelich, B. Harmatz and T. H. Handley, Phys. Rev. **108** (1957) 989
16) K. Alder, A. Bohr, T. Huus, B. R. Mottelson and A. Winther, Revs. Mod. Phys. **28** (1956) 432
17) G. Scharff-Goldhaber and J. Weneser, Phys. Rev. **98** (1955) 212
18) A. Reiner, Thesis, Amsterdam (1958)
19) E. L. Church and J. Weneser, Phys. Rev. **103** (1957) 1035

2.H *Nuclear Physics* **19** (1960) 400—425; © *North-Holland Publishing Co., Amsterdam*
Not to be reproduced by photoprint or microfilm without written permission from the publisher

COULOMB EXCITATION OF THE FIRST LEVELS OF SPHERICAL EVEN NUCLEI BY MULTIPLY CHARGED IONS

D. S. ANDREYEV, A. P. GRINBERG, K. I. EROKHINA and I. Kh. LEMBERG

Leningrad Physical-Technical Institute, Academy of Sciences USSR, Leningrad, USSR

Received 27 November 1959

Abstract: The Coulomb excitation of the first excited levels in the nuclei of Ne^{20}, Ne^{22}, Mg^{24}, Si^{28}, Ti^{46}, Ti^{48}, Cr^{54}, Fe^{58}, Ni^{58}, Ni^{60}, Ni^{62}, Ni^{64}, $Zn^{64+66+68}$, Se^{76}, Se^{78}, Se^{80}, Se^{82} and Zr^{92+94} was investigated by means of the cyclotron-accelerated multiply charged ions of $N^{14;3+}$ ($E = 16.3$ MeV), $N^{14;4+}$ (26 and 36 MeV), $O^{16;4+}$ (18.2 MeV), $Ne^{20;4+}$ (23.1 and 27.9 MeV) and $Ne^{22;4+}$ (25.2 MeV).

In the first two cases the nuclei investigated were present not in the target, but in the incident particles beam. The lifetime of the first excited level was determined for all above-mentioned nuclei. Merits and difficulties in using multiply charged ions for the investigation of Coulomb excitation are discussed.

1. Introduction

To develop the theory of nuclear levels it is highly desirable to study the Coulomb excitation of nearly spherical nuclei. Of special importance in this respect is the Coulomb excitation of even nuclei since the latter's inner structure has no effect on its spin. Refs. [1]) and [2]) discuss the results of investigating the Coulomb excitation of lower levels in nickel, zinc, cadmium, and tin with α-particles accelerated in a cyclotron.

In the even nuclei with $A < 70$ the energy of the first excited level (ΔE) exceeds 800 keV and in many cases 1 MeV. The Coulomb excitation of these high energy levels through α-particles proves to be possible only when the latter's energy (E_α) is sufficiently large. As E_α increases, however, the background from nuclear reactions sharply increases as well. The influence of this background arising at $E_\alpha \approx E_B$ (where E_B is the potential barrier of the nucleus) affects the measurements of Coulomb excitation in two ways.

First, in some cases the observation of γ-lines, attributable to the de-excitation of the levels excited through Coulomb interaction, proves to be impossible because of a considerable background. Second, the emission of the γ-quanta under investigation may occur not only through Coulomb excitation but also through non-elastic scattering reactions accompanied by the formation of a compound nucleus. In the latter case the values of the reduced probability $B(E2)\uparrow$ for transition from the ground state into the excited one, calculated from the experimental values of yield will prove erroneous.

Usually, the origin of the γ-lines is established by measuring the excitation function. At great values of ΔE it is difficult to determine the kind of an excitation function since the yield falls sharply as the energy of incident particles decreases, and measurements at small values of E_a become difficult. An increase in the values of E_a, on the other hand, involves a sharp increase in the interfering background from nuclear reactions, which strongly affects the accuracy of measurements.

For these reasons it might be worthwhile to study the Coulomb excitation of the first levels in even nuclei by heavy ions. In this case the probability of nuclear reactions accompanied by the formation of a compound nucleus decreases considerably as does the interfering effect of the background.

As follows from the data given below, the use of heavy ions (especially in bombarding nuclei with small A) makes it possible to study the Coulomb excitation of the levels a study of which with the help of α-particles or protons is extremely difficult or impossible because of considerable nuclear reaction background.

The relative role of non-elastic scattering processes accompanied by the formation of compound nuclei is much less in bombardement by heavy ions than in bombardement by protons or α-particles. The use of heavy ions, therefore, dispenses with such an uncertain operation as evaluating the contribution to the yield of the γ-rays from non-elastic scattering reactions. This is essential in those cases when high energy protons or α-particles have to be used owing to a high value of ΔE. Finally, it should be noted that in a number of cases there arises a need to investigate the nature of the γ-lines when using high energy incident α-particles or protons: whether these lines result from Coulomb excitation or from the nuclear reaction with the nuclei under investigation accompanied by the formation of a compound nucleus. The use of heavy ions makes it possible to answer the above question: if the γ-line observed in the experiment with α-particles (the yield of this line having been computed) does not appear with the corresponding yield in bombarding the same target by heavy ions, this line should not be ascribed to Coulomb excitation.

2. Certain Problems Connected with the Use of Multiply Charged Ions for Investigating the Coulomb Excitation of Nuclear Levels

In our former paper[3]) concerned with the Coulomb excitation of nuclear levels by heavy ions, triply charged 15.6 MeV nitrogen ions were used. To excite high energy levels, a higher energy of the incident ions is required in most cases.

Some special work has been done to increase the energy of ions accelerated in the PTI cyclotron. Beams of triply charged ions of C^{12}, triply and quadruply charged ions of O^{16} and N^{14} and the quadruply charged ions of Ne^{20} and Ne^{22} were obtained as a result. The intensity of the external beams varied from

0.1 to 0.001 μA in order of magnitude, depending on the type and the energy of the ions. The energy of the accelerated ions was altered by changing the magnetic field strength and, correspondingly, the frequency of the cyclotron accelerating field. The ions chiefly used in the investigation were 16.3, 26 and 36 MeV nitrogen ions, 23.1 MeV Ne^{20} ions and 25.2 MeV Ne^{22} ions.

Even during the initial studies of the γ-spectra emitted in bombarding various targets by 26 MeV nitrogen ions we discovered the presence of background γ-lines whose intensity in a number of cases by far exceeded that of the lines which might be ascribed to the Coulomb excitation of nuclear levels. To determine the origin of these background γ-lines, we investigated the γ-spectra of 40 various elements, their compounds and isotopes. To reduce the number of possible types of nuclear reactions with heavy ions, the nitrogen ions with relatively small energy (16.3 MeV) had originally been used. We investigated the γ-spectra in the interval from 0.1 to 2 MeV. It transpired that in irradiating each of the selected targets four background lines were observed with $E = 0.35$, 0.51, 0.59 and 1.37 MeV (the intensity of the 0.51 MeV line was much smaller than that of the 0.59 MeV line), apart from the γ-lines whose origin involves Coulomb excitation. It turned out that all above-mentioned γ-lines should be ascribed to the nuclear reactions with carbon which is contained in the targets as an impurity or, more probably, precipitates on the targets with oil vapours and is isolated in the subsequent disintegration in bombarding by a beam of accelerated ions. Fig. 1 shows the typical spectra of the background γ-lines emitted in bombarding nickel and carbon by nitrogen ions with $E = 16.3$ MeV. A study of the spectrum of the background γ-lines emitted in bombarding various targets by nitrogen ions with $E = 26$ and 36 MeV showed that the yield of the above lines increases as the energy of the incident particles rises. If the energy of ions increases to 36 MeV, the continuous background of γ-radiation in bombardment of light elements sharply increases too, while the relative yield of reactions occurring in a thin film of carbon diminishes as a result of a greater range of heavy ions in the target. This results in the disappearance of the 1.37 MeV peak in a number of cases (cf., for example, fig. 2) in the bombardment of light elements. In the bombardment of heavy elements the continuous γ-background is relatively small and the 1.37 MeV peak is quite noticeable.

As for the background γ-lines emitted in the reactions with other possible impurities, only those background lines which should be ascribed to the reactions between nitrogen and oxygen ions have a perceptible intensity, as was shown by our measurements. Background lines with $E = 0.51$, 1 and 1.78 MeV are observed in this case. The intensity of these lines sharply increases as the energy of nitrogen ions becomes greater, which in a number of cases makes it difficult to study Coulomb excitation in certain metals, if the latter contain oxides even in small quantities (which is quite common in separated isotopes)

In our experiments with Al, Mg and Si bombarded by nitrogen ions with $E \geq 25$ MeV weak γ-lines were observed, probably due to nuclear reactions. Since the content of impurities in the elements of our targets is insignificant, the influence of the practically occurring impurities with $Z > 8$ may probably be neglected. At any rate in all our experiments with a large number of elements

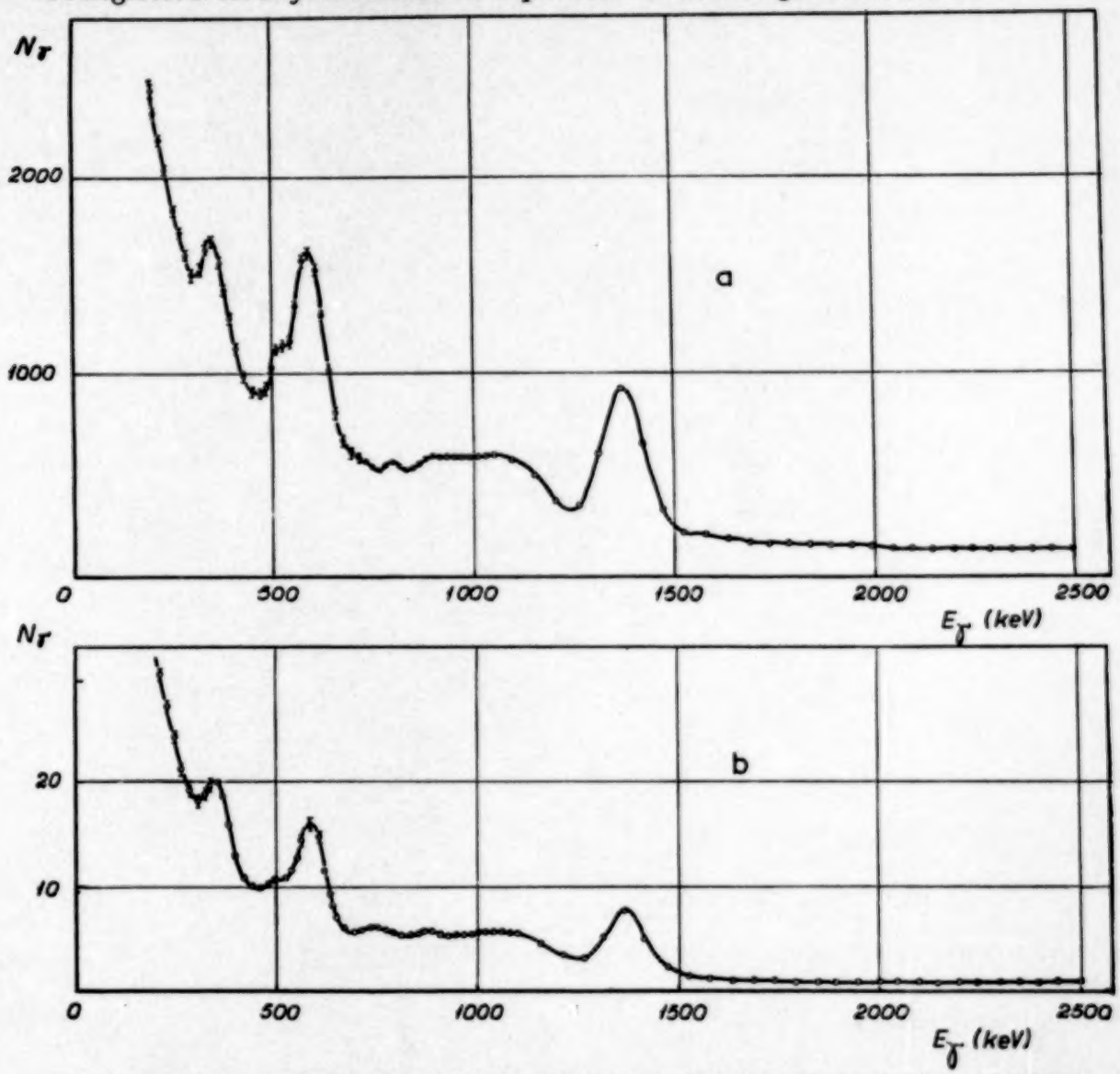

Fig. 1. Spectra of γ-radiation emitted in bombarding graphite (a) and nickel (b) by 16.3 MeV N^{14} ions. The yield of γ-rays related to 1 μC in an ion beam and to the width of the analyzer canal equal to 10 keV is marked off on the axis of the ordinates.

and compounds we have observed no lines (except those mentioned above) which may be ascribed to nulcear reactions with the nuclei of impurities.

The detailed data we have obtained on the energy and intensity of the background γ-lines make it possible to estimate the possibilities of investigating Coulomb excitation in various cases.

Using α-particles[4]) we find that there are no 562 and 590 keV γ-lines which formerly[3]) were ascribed to the excitation of levels in indium and manganese†. Now it is clear that an erroneous observation in these lines is connected with the bakground 590 keV line arising in the reaction C + N.

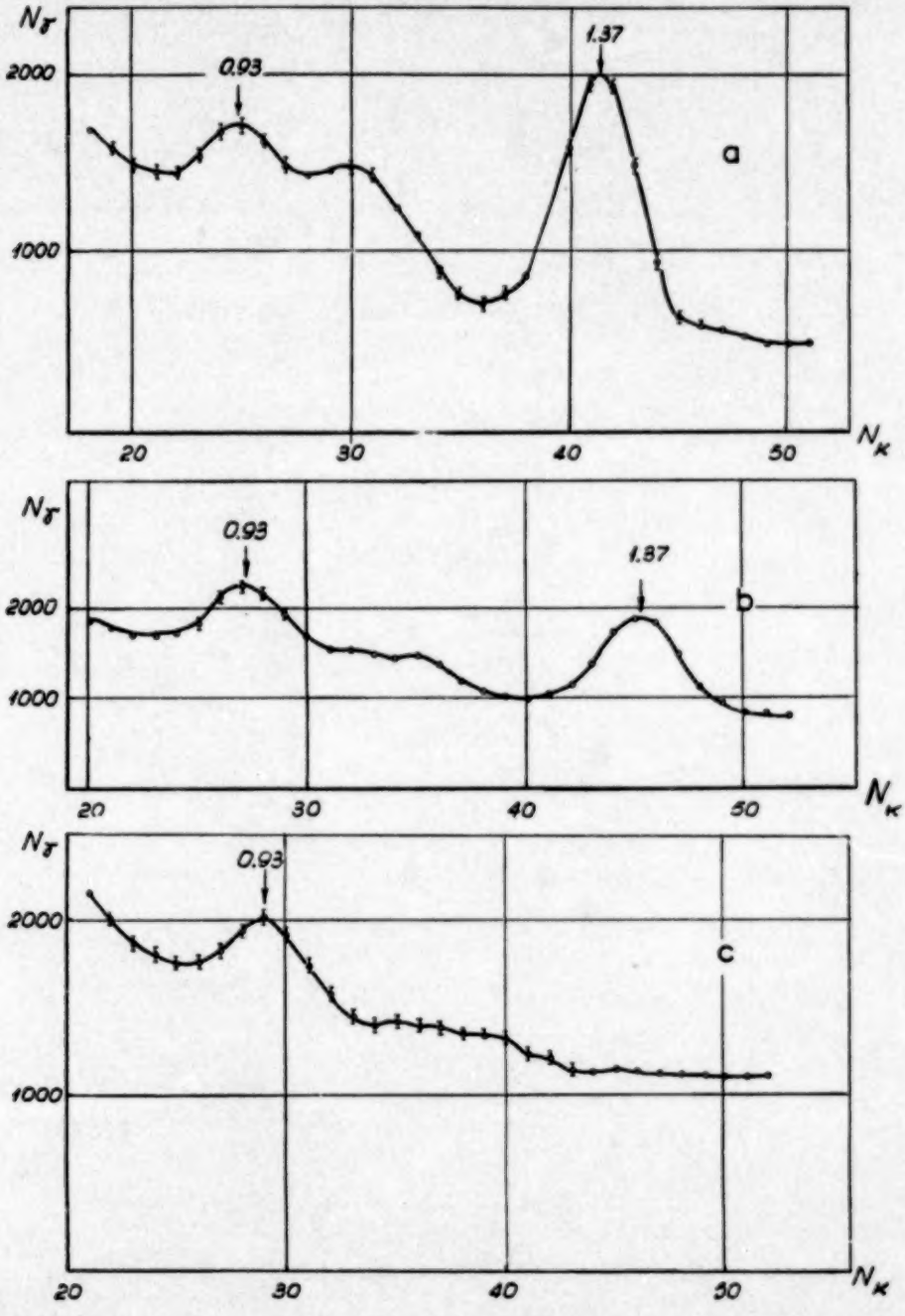

Fig. 2. Apparatus spectra of γ-lines obtained in the Coulomb excitation of vanadium by N^{14} ions with energies of (a) 16.3 MeV, (b) 26 MeV and (c) 36 MeV. N_k is the number of a canal, N the total number of counts by the counter in the canal related to 1 μC in an ion beam.

† Independently, the absence of the 590 keV γ-line in the Coulomb excitation of manganese was shown in a paper by Dr. Lehmann, France (private communication).

In the present paper the levels with $\Delta E > 700$ keV are investigated and the principal interference in the investigations with nitrogen ions was the background 1.37, 1 and 1.78 MeV γ-lines (the latter two if there was oxygen in the target). In bombardment by neon, carbon and oxygen ions at the energies we have used either the intensity of the background lines is small or their energy has a different value than in bombardment by nitrogen ions, which makes it possible to study certain regions of the spectrum despite the background lines, by using various ions for investigating Coulomb excitation. More detailed information on these lines and their connection with certain nuclear reactions is offered in ref.[5]).

3. Experimental Technique and Calculations of B(E2)

The methods and equipment used were described in refs. [2,6]) in detail. As in our previous work the yield of Coulomb excitation was determined by registering the γ-quanta emitted in the de-excitation of the excited levels; a "close" geometry (the distance between the target and the front surface of the crystal being 2.7 mm) and "thick" targets were used. In the present paper care should be taken to achieve a more accurate focussing of the ion beams on the target situated at the bottom of the Faraday cylinder. For this purpose the Faraday cylinder is replaced before measurements by a cylinder of the same length but with a glass bottom covered with a layer of ZnS. Careful focussing is especially essential with separated isotopes the targets of which had small sizes (in certain cases their diameter amounted to 5 mm). During the exposition of the target the focussing may be violated or the beam displaced, which may result in the latter hitting the bottom of the Faraday cylinder and being registered by the integrator, while the ions will not hit the target at all or will hit it only partially, which may lead to serious distortions in the current measurement. To prevent this the beam of ions is collimated by a lead diaphragm isolated from the Faraday cylinder and placed at 15 cm in front of the target. The diameter of the apperture can be changed from 5 to 15 mm depending on the size of a target. In control experiments it was shown that γ-radiation emitted by the lead diaphragm under the influence of the beam is not practically registered by the γ-spectrometer. The diaphragm reduced the consequences of defocussing or the displacement of the beam to merely a decrease in the current hitting the target. This did not distort measurements since in this case all the current registered by the integrator went into the target.

The γ-radiation emitted in bombardment of targets was registered by the scintillation spectrometer with a crystal of NaI (Tl) 40 mm in diameter and 40 mm in height, combined with a FEU-11 multiplier. The spectrometer was calibrated with respect to energy by sources of γ-radiation: Zn^{65} (1.12 MeV)

and Co^{60} (1.17 and 1.33 MeV) as well as with the help of the γ-line emitted in the Coulomb excitation of Ne^{20} (1.63 MeV).

The values of the reduced probability of excitation of levels was calculated according to the formula

$$B(\mathrm{E2})\uparrow = \frac{0.555 \times 10^{-10} Z_i S_p (1+\alpha_T) M Z_2^2 \dfrac{dE}{d\rho x}}{\eta \varepsilon_p \omega A_\gamma \mu n \displaystyle\int_0^{E\max} (E-\Delta E) f_2(\xi)\, dE}. \qquad (1)$$

Here, Z_i is the charge of ions in the external cyclotron beam (expressed in units of elementary charge), α_T the full coefficient of internal conversion, S_p the number of γ-quanta registered in the peak of full energy and related to 1μC of particles in the beam, M the molecular weight of the substance of the target in mass units, Z_2 the charge of the nucleus of the target atoms, $dE/d\rho x$ the specific losses of energy of ions in the substance of the target in MeV·$(mg/cm^2)^{-1}$, η the relative content of the given isotope in the element under investigation, ε_p the ratio between the number of γ-quanta registered in the peak of full energy and the total number of γ-quanta hitting the crystal, ω the relative solid angle, A_γ the fraction of the γ-quanta passing through the target and absorbers between the target and the crystal, μ the reduced mass in mass units, n the number of atoms of the element under investigation in the molecule of the target's substance, E the energy of collision in MeV ($E = \{m_2/(m_1+m_2)\} E_{lab}$, where m_1 and E_{lab} are the mass of the bombarding particle and its kinetic energy in the laboratory system of coordinates, while m_2 is the mass of the atom of the target), ΔE the energy of the excited level in MeV, $f_2(\xi)$ the function of Coulomb excitation, and ξ a parameter determined by the expression

$$\xi = 0.1575\, Z_1 Z_2 \sqrt{\mu} \left(\frac{1}{\sqrt{E-\Delta E}} - \frac{1}{\sqrt{E}} \right), \qquad (2)$$

where Z_1 is the charge of the nucleus of the incident particle.

Eq. (1) holds good in the lowest approximation of the perturbation theory; this approximation offers satisfactory results in those cases when the probability of excitation $\mathscr{P}$ in a separate collision is small as compared with unity. In the experiments with heavy ions the energy of incident particles is great and the values of $\mathscr{P}$ increase as compared with experiments in which protons or α-particles are used. Our numerical estimates showed that in all cases we have investigated the influence of higher orders of excitation remains small and eq. (1) valid†, which is due to the smallness of the value of B(E2) in all the cases we have investigated.

† In these calculations we have used the paper "Multiple Coulomb Excitation with Heavy Ions" by K. Alder and A. Winther. We are indebted to the authors for sending us this article before publication.

It should be noted that perceptible deviations from the results obtained according to eq. (1) may be expected in the excitation of the rotational levels for which the values B(E2) are by one or two orders larger than in the above-mentioned cases and the energy of heavy ions is the same ($E_N = 35$ MeV).

There are few data on the specific energy losses for heavy ions at E = 10—35 MeV passing through various substances. To calculate the values of $dE/d\rho x$ in various elements for nitrogen ions with energy up to 25 MeV we have used the range-energy relation for nickel of ref. [7]) as an initial experimental dependence; the values of $dE/d\rho x$ in other substances were determined through calculations based on the ratio of the experimental specific energy losses in nickel and in the element under investigation for the protons possessing the same speed as nitrogen ions. The values of $dE/d\rho x$ for nitrogen ions with $E > 25$ MeV in various elements were calculated in a similar manner, but preliminary a range-energy curve was plotted for nitrogen ions with $E = 0$—35 MeV for stopping in nickel according to the Longchamp method[8]). It should be noted that the values of $dE/d\rho x$ for the case in question calculated according to Longchamp are in good agreement with those calculated according to experimental data[7]). It was found that the values of $dE/d\rho x$ for nitrogen ions depend little on energy in the region of interest to us. We have used therefore the average values of $dE/d\rho x$ for nitrogen ions with $E = 15$—25 MeV and with $E = 20$—35 MeV. Fig. 3(a, b) represents the values $dE/d\rho x$ we have used for various elements and the two energy ranges of nitrogen ions mentioned above.

The values of $dE/d\rho x$ for the ions of Ne^{20} and Ne^{22} in passing through various elements were computed by the range-energy curve for neon ions stopped in lead, plotted by A. Papineau† on the basis of the method set down in ref. [9]). The values of $dE/d\rho x$ for the ions of Ne^{20} and Ne^{22} used in our paper are represented in table 1.

Ref. [10]) discusses the problem of evaluating the accuracy of the values $dE/d\rho x$ obtained by various calculating techniques. Errors in the values of $dE/d\rho x$ for nitrogen ions can hardly exceed 15 %; yet for neon ions they may probable reach 20 to 25 %.

An accurate evaluation of the energy of ions bombarding the targets as needed by calculations on eq. (1) is rather difficult. The energy of the ions accelerated in the cyclotron may be calculated according to the equation

$$E_{lab} = 0.0450 \frac{Z^2}{E_0} (H_k r)^2 \text{ MeV}, \tag{3}$$

where Z is the charge number of the accelerated ion, E_0 its rest energy in MeV, H_k the magnetic field strength in kOe at the point of entrance of the ion in the deflector channel and r is the radius in cm of the curvature of the orbit of the ion at the same point.

† We are indebted to A. Papineau who has kindly sent us a number of his graphs.

In calculating the values of B(E2), given in ref. [11]), the resonance strength of the field was adopted as the value of H_k and determined according to the equation

$$H_{res} = 0.2094 \frac{E_0}{Z\lambda} \text{ k0e}, \tag{4}$$

where λ is the length in m of the wave of the cyclotron accelerating field measured for this experiment, while E_0 is again measured in MeV.

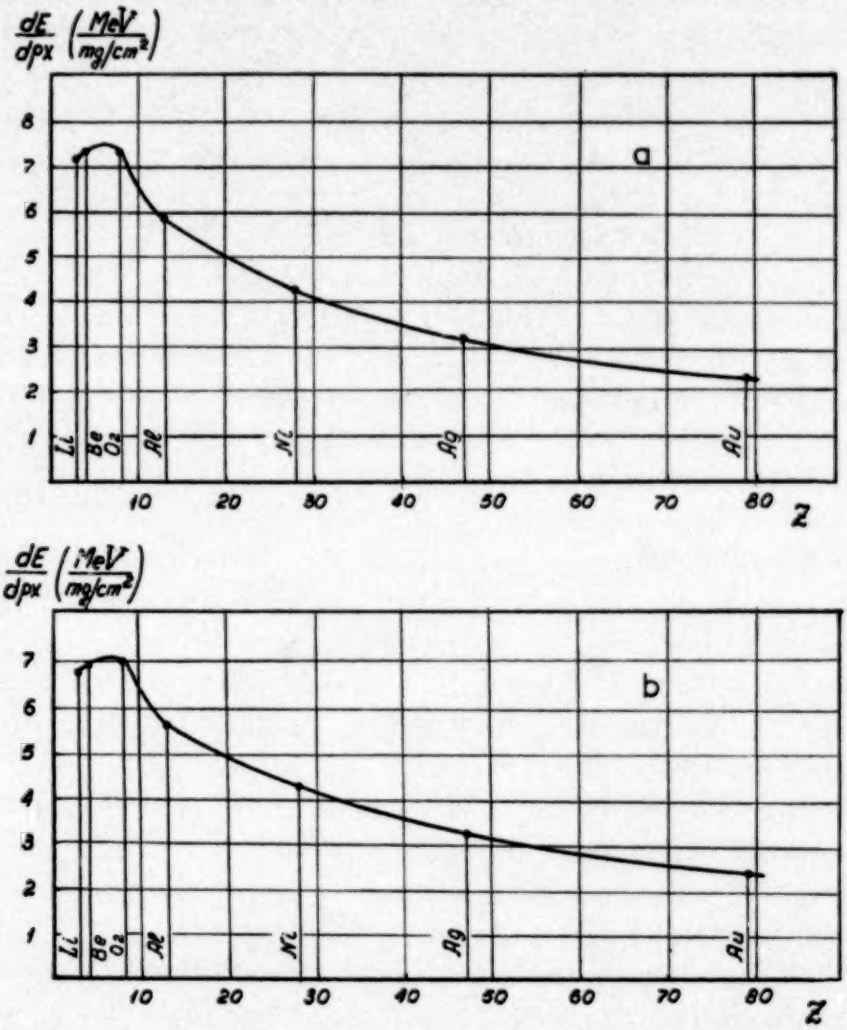

Fig. 3. Average value of specific energy losses of N^{14} ions in the range of energy (a) from 15 to 25 MeV and (b) from 20 to 35 MeV depending on the atomic number of the atoms of the stopping medium.

To obtain more accurate results the value of H_k at various currents in the cyclotron magnet winding was measured specially for the present paper. The measurements were taken by a magnetometer based on measuring the Hall effect in a germanium crystal. The magnetometer made it possible to measure H_k in the region of great field gradient with sufficient accuracy. The instrument

TABLE 1

Specific losses of energy of 23.1 MeV Ne^{20} ions and 25.2 MeV Ne^{22} ions in passing through various elements (in MeV.$(mg/cm^2)^{-1}$

Elements	Ne^{20}	Ne^{22}
C	12.8	12.2
O	12.5	11.9
Mg	10.4	9.8
Al	9.9	9.5
Si	9.7	9.3
Sc	8.1	7.8

was calibrated with the help of a nuclear magnetometer. The error in the measurement of H_k did not exceed 0.1 %.

Values of B(E2) were readjusted on the basis of the experimental data obtained before and on the basis of more accurate values of E_{lab} obtained as a result of the indicated measurement of H_k. In calculating E_{lab} according to eq. (3) the distance from the centre of the cyclotron chamber and to the "knife" of the deflector was assumed as being equal to r. The discrepancies between these new values of B(E2) and the former ones published in refs. [11-13]) come up to 40 and 50 % in two cases (Ne^{22} and Mg^{24}), do not exceed 35 % for all other levels, and are considerably less for a number of cases†.

It should be noted, however, that the radial coordinate of the "knife" of the deflector may not coincide with the radius of curvature of the orbit at the point of its entrance to the deflector channel as a consequence of the well-known precession of the ion orbit. Therefore, a certain error whose value it is difficult to appraise ramains in the reajusted values of E_{lab}. Repeated measurements of the cross-section of Coulomb excitation of even nuclei were undertaken to make the calculated values of B(E2) more accurate. The techniques of measurement differed in that a series of measurements with the target under investigation began and ended with determining the Coulomb excitation cross-section of a certain "reference" nuclear level for which the value of B(E2) was sufficiently well-known.

The values of B(E2) obtained experimentally for the nuclear level under investigation were normalized by the data found for the "reference" level. The normalization was effected by two methods. Under the first method it was assumed that if a discrepancy of the values of B(E2) for the reference level was observed between the data of our measurements and tables, this discrepancy is connected with an error in calculating the energy E_{lab} by eq. (3). In this case the true value of E_{lab} was determined by eq. (1) in which the table value of

† In ref. [11]) an erroneous value of B(E2) for Ti^{48} was given owing to a mistake in calculations. The correct result is B(E2) = 0.10 (instead of 0.14).

B(E2) for the reference level was substituted. The value of E_{lab} found in this way was used for calculating B(E2) of the nuclear level under investigation.

The second method of normalization was based on the assumption that the discrepancy between the experimental and table values of B(E2) for the reference level was connected with the inaccuracy in calculating the values of $dE/d\rho x$. Taking into account that there is a direct proportionality between the values of B(E2) and $dE/d\rho x$, the experimental value of B(E2) for the given level was re-calculated in this case through multiplying it by the ratio between the value B(E2) for the reference level according to table data and the one determined in our experiments. The reference levels were chosen in such a way as to make the dependence of B(E2) on the energy E_{lab} for the reference and investigated levels approximately equal. As a result, the discrepancy between the values B(E2) calculated by the two methods of normalization indicated above did not exceed 20 % and was less than 10 % in most cases. Therefore, the average values of B(E2) obtained in normalization under both methods were taken as true values of B(E2) in repeated measurements.

The nuclear levels of Mo^{100} ($E = 530$ keV) and $Zr^{92,94}$ ($E = 920$ keV) were taken as reference levels in measurements with nitrogen ions accelerated to $E_N = 36$ MeV. According to ref. [14]) the values of B(E2) for the excitation of these levels amount to $6.14 \times 10^{-49}\ e^2\ cm^4$ and $0.79 \times 10^{-49}\ e^2\ cm^4$ with errors amounting to 10 and 13 % respectively.

In measurements with $E_N = 16.3$ MeV the level of the nucleus of Ti^{48} ($\Delta E = 990$ keV) served as the reference level. According to our measurements B(E2) turns out to be $0.7 \times 10^{-49}\ e^2\ cm^4$, when $E_N = 16.3$ MeV and $E_N = 36$ MeV alike. This value is in good agreement with the one obtained in ref. [15]) according to the method of γ-ray resonance scattering.

The indications concerning the reference levels for Ne^{20}, Ne^{22} and some other nuclei are given below for each element separately.

4. Results of Measurements

These are presented in table 2. Column 1 represents the values of B(E2) we obtained in investigations with the ions of nitrogen and neon[11–13]), but recomputed with allowances for the measurements of H_k. Column 2 represents the values of B(E2) obtained for the same levels in a series of additional measurements in which the reference levels were used (experimental conditions in these measurements being represented in column 6). As is clear from the data of the table, the values of B(E2) calculated on the basis of additional experiments differ from the values represented in column 1 by no more than 35 % for all investigated levels except for Se^{82}, while in most cases this discrepancy does not exceed 25 %. Column 3 represents the values of B(E2) obtained as averages from those indicated in columns 1 and 2. Column 4 gives reajusted values

TABLE 2

Experimental results

Nucleus	ΔE (MeV)	$\frac{B(E2)\uparrow}{e^2} \times 10^{48}$ (cm^4)					Bombarding particles[a] and their energy in MeV	$\tau \times 10^{13}$ (sec)		F
		1	2	3	4	5	6	7	8	9
Ne^{20}	1.63	0.050	0.044	0.047				7.6	7.6 [18]	30
Ne^{22}	1.28	0.035	0.042	0.039				31		21
Mg^{24}	1.37	0.072	0.058	0.065			N (16, 3) Ne^{20} (27, 9)	13	19 [19]; 17 [20]; 2.6 [21]	30
Si^{28}	1.78	$\leq$ 0.041 [b]								
Si^{28}	1.78		0.046	0.046 [c]				5.0	6 [19]	19
Ti^{46}	0.89	0.094	0.072	0.083		0.15 [23]		88		17
Ti^{48}	0.99	0.079	0.061	0.070		0.083 [23]	N (16.3; 36.0)	61	60 $\pm$ 20 [15]	13
Cr^{54}	0.84	0.066	0.049	0.057			N (16.3)	170		9.3
Fe^{56}	0.855	0.058	0.064	0.061		0.10 [24]	N (16.3; 36.0)	150		9.5
Fe^{58}	0.815	0.13	0.088	0.11			N (16.3)	100		16
Ni^{58}	1.45	0.094	0.066	0.080	0.071			8.0		12
Ni^{60}	1.33	0.10	0.11	0.11	0.12		N (36.0)	8.9	11 $\pm$ 2 [26]; 10 $\pm$ 3 [25]	16
Ni^{62}	1.19	0.092	0.078	0.085	0.11			20		12
Ni^{64}	1.35	0.086	0.088	0.087	0.077			10		11
Zn^{64}	1.00				0.083	0.11 [24]		37		14
Zn^{66}	1.04	0.11	0.11	0.11	0.089	0.087 [24]	N (36.0)	30		14
Zn^{68}	1.08				0.084			25		13
Se^{76}	0.56	0.41	0.42	0.42		0.43 [24]	N (16.3; 36.0)	180		43
Se^{78}	0.615	0.41	0.30	0.36		0.36 [24]		130		36
Se^{80}	0.65	0.26	0.20	0.23		0.23 [24]	N (36.0)	150		22
Se^{82}	0.66	0.25	0.14	0.19				170		18
$Zr^{92,94}$	0.92	0.11	0.09	0.10		0.079 [14]	N (36.0)	62		8.0

[a] Column 6 lists the bombarding particles used for the excitation of the "reference" level.
[b] The result of measurements with N^{14} ions.
[c] The result of measurements with Ne^{20} ions.

of $B(E2)$, for calculation of which the data of our investigations with α-particles[1]) were used, and column 5, the values of $B(E2)$ according to investigations by other authors with α-particles. Column 7 represents the values of the lifetime τ of the nucleus in a corresponding excited state calculated according to the data given in column 3, while column 8 gives the values of τ according to the papers in which γ-ray resonance scattering and non-elastic electron scattering were investigated. Column 9 represents the values of the F-ratio between the value of $B(E2)\uparrow$ determined by experiment and the value of $B(E2)_{s.p.}$ caclulated by single-particle evaluation. The values of τ were calculated according to the equation

$$\frac{1}{\tau} = \frac{4\pi}{75 \cdot 5} \left(\frac{\Delta E}{\hbar c}\right)^5 \frac{1}{\hbar} B(E2)\uparrow$$

for all even nuclei whose spin and parity of the excited level are always equal to $2+$. The value of $B(E2)_{s.p.}$ was calculated by the equation

$$B(E2)_{s.p.} = 5 \frac{1}{4\pi} \left(\tfrac{3}{5} R_0^2\right)^2 ,$$

where R_0 was taken to equal $1.2 \times 10^{-13} A^{\frac{1}{3}}$ cm.

5. Remarks on Separate Elements

5.1. NEON ($Z = 10$)

From the investigations of β-decay of F^{20} and Na^{22} it is known that the energy of the first excited level of Ne^{20} and Ne^{22} amounts to 1.63 and 1.28 MeV respectively. The Coulomb excitation of these levels has not been observed so far since no noticeable yield of γ-rays due to this process may occur if the energy of incident α-particles or protons is large and comparable with that of the nuclear potential barrier. In this case measurements are much complicated by a considerable level of γ-ray background. It should also be noted that measurements of $B(E2)$ in the case of thick gaseous targets are more complex because an accurate measurement of the ion current to the target is more difficult. Thus, only relative values of the yield of γ-rays emitted in de-excitation are determined in refs. [16,17]) concerned with Coulomb excitation of crypton and xenon.

Yet, in investigating the Coulomb excitation of nuclei, the excitation of levels may be observed not only in the target nucleus but in the incident nucleus as well if the latter have levels for which the Coulomb excitation cross-section is sufficiently large. In most papers on Coulomb excitation the bombardment of targets was effected with protons and α-particles; since there are no appropriate levels in the nuclei of H^1 and He^4 phenomenon in qeustion has not been yet observed.

The use of heavy ions makes it possible to discover the excitation of nuclear

levels in the incident particles in certain cases and thereby to surmount the difficulties indicated above.

In this paper we have used accelerated ions of neon for investigating the Coulomb excitation of the first levels of Ne^{20} and Ne^{22}. Natural neon was supplied to the ion source of the cyclotron. The tuning of the cyclotron for the acceleration of certain ions was effected through changing the strength of the magnetic field with unchanged frequency of the accelerating field. The average beam-current of quadruply charged Ne^{20} ions amounted to 1.5×10^{-8} A and of the Ne^{22} ions to 1.5×10^{-9} A, since the content of Ne^{20} in natural neon is roughly ten times as high as that of Ne^{22}.

If we are dealing with the level excitation in the incident particle, to calculate the values of $B(E2)$ it is necessary to replace Z_2^2 with Z_1^2 in eq. (1) and substitute into eqs. (1) and (2) the values ΔE and ξ pertaining to the excitation of the first level in the nucleus of the incident particle (in the present case of neon). It is easy to see that the parameter ξ increases as the atomic number of the target increases. Since the function $f_2(\xi)$ sharply diminishes with the increase of ξ, the value of the integrand also diminishes as the charge of the atoms of the target increases, which is bound to lead to a sharp decrease in the value of S_p observed in experiment. Therefore, in experiments on the excitation of neon levels only those targets were used which contained light nuclei: Be, B, C, Mg, Al, Si, $Mg^{24}O$, $Mg^{25}O$, $Mg^{26}O$ and ScO. Fig. 4 represents the spectra of γ-rays emitted during bombardment by Ne^{20} ions of metallic magnesium, magnium oxide enriched by Mg^{26}, and aluminium. The 1.37, 0.84 and 1.01 MeV lines are connected with the Coulomb excitation of the respective levels in Mg^{24} and Al^{27} and the 1.63 MeV line with the Coulomb excitation of the first level of Ne^{20} with $\Delta E = 1.63$ MeV. Fig. 5 represents γ-spectra registered in bombarding carbon, magnesium oxide enriched by Mg^{25} and aluminium by Ne^{22} ions. The 1.28 MeV line is connected with the Coulomb excitation of the first level of Ne^{22} while the 0.84 and 1.01 MeV lines are a consequence of the Coulomb excitation of aluminium levels. Similar spectra verifying the excitation of the first levels of Ne^{20} and Ne^{22} are registered in bombarding the remaining targets mentioned above with the exception of boron and beryllium. In the two latter cases the 1.63 MeV peak was not discovered in bombarding the targets with Ne^{20} ions because of a very high background from nuclear reactions. In bombarding these targets by Ne^{22} ions a very well pronounced 1.28 MeV peak is observed, but the calculation of $B(E2)$ yields a value considerably exceeding (10 times in the case of beryllium) those which were obtained in experiments with other targets. Probably this is linked with the fact in the reactions Be + Ne^{22} and B + Ne^{22} the collision energy is near to the Coulomb barrier and most of γ-quanta with $E = 1.28$ MeV arises due to nuclear reactions and not to Coulomb excitation. The values of $B(E2)$ indicated in column 1 of table 2 for the excitation of the first levels of Ne^{20} and Ne^{22} in each case represent an

average of the results of 17 different bombardments. The standard deviation of the values of $B(E2)$ is equal to 35 % in experiments with Ne^{22} and to 40 % in experiments with Ne^{20}.

Repeated series of measurements with Ne^{20} and Ne^{22} were not undertaken, and for the appraisal of the values of $B(E2)$ with the aid of the reference level those experiments were used in which the lines corresponding to the Coulomb

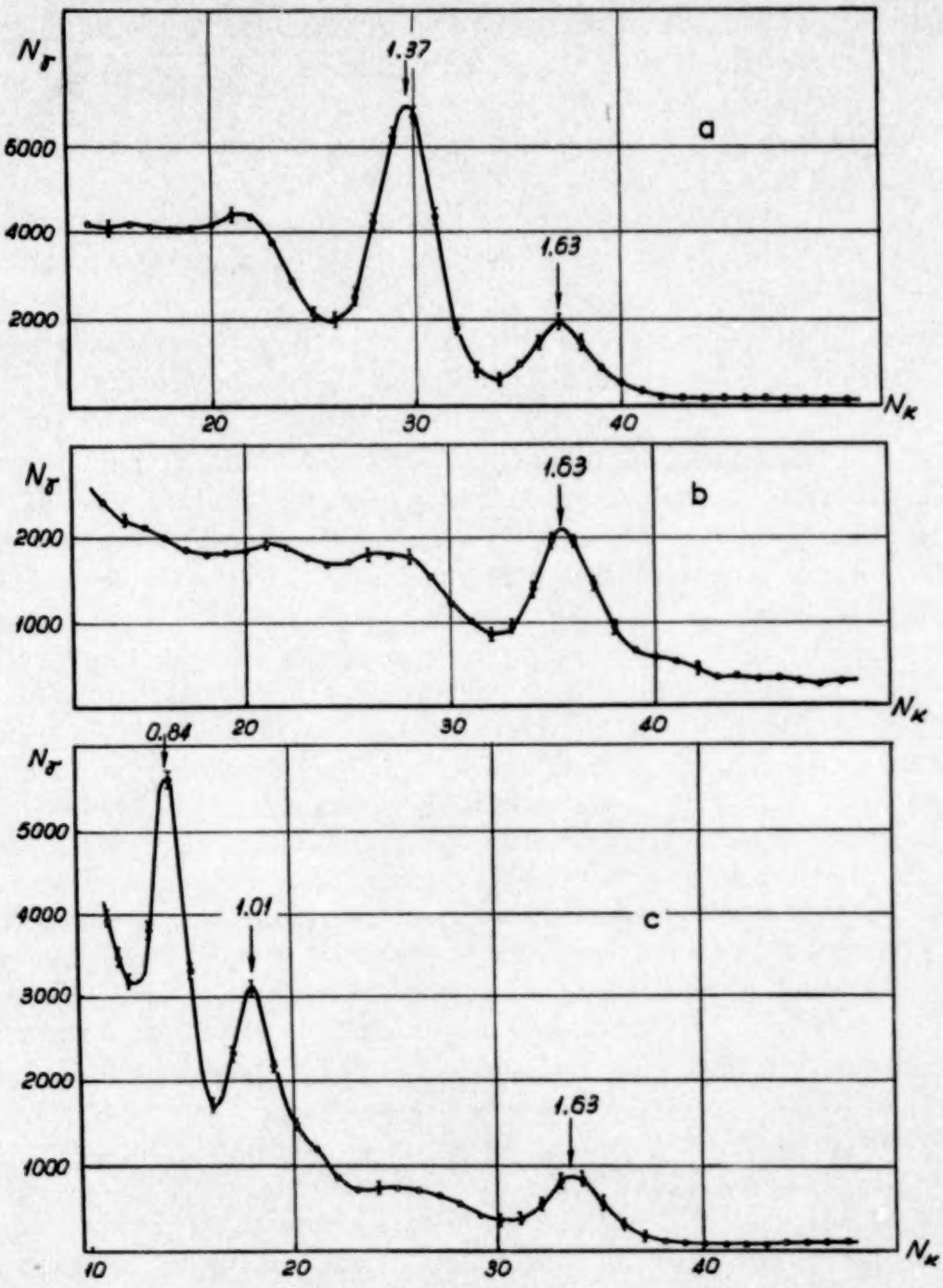

Fig. 4. Apparatus spectra of γ-lines obtained in the Coulomb excitation of Mg and Al by Ne^{20} ions: (a) Mg + Ne^{20}, (b) $Mg^{26}O$ + Ne^{20}, (c) Al + Ne^{20}.

excitation of the first level of Mg^{24} and that of the first level of Ne^{20} were measured simultaneously. Since both lines are measured simultaneously in these experiments an error in calculating $B(E2)$ for the isotopes of neon largely

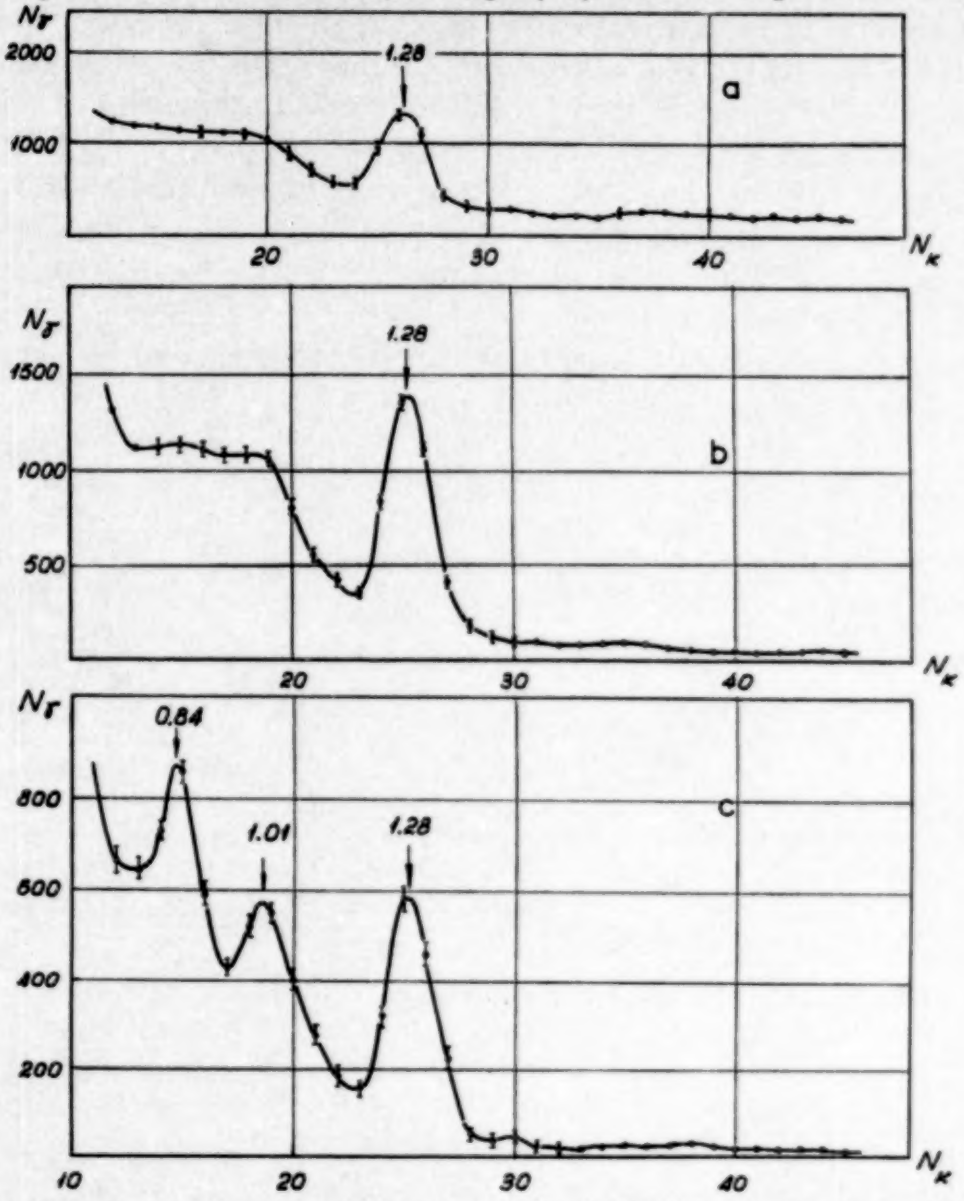

Fig. 5. Apparatus spectra of γ-lines obtained in bombarding various targets by Ne^{22} ions: (a) C + Ne^{22}, (b) $Mg^{25}O$ + Ne^{22}, (c) Al + Ne^{22}.

depends on the error in determining the values of $B(E2)$ for the excitation of the first level of Mg^{24}. The value of $B(E2)$ obtained in the present paper and equal to $0.065 \times 10^{-48}\, e^2\, cm^4$ was adopted for Mg^{24}.

The lifetime of the first excited level of Ne^{22} has not been determined before. The lifetime of the first excited level of Ne^{20} was determined in ref. [18]) by measuring the Doppler displacement of the γ-line and proved to be equal to $(7.6 \pm 3.3) \times 10^{-13}$ sec. Our value for the lifetime of the first excited level of Ne^{20} equal to 7.6×10^{-13} sec is in good agreement with this value.

5.2. MAGNESIUM ($Z = 12$)

According to the investigation of β-decay of Na^{24} the energy of the first excited level of Mg^{24} is equal to 1.368 MeV.

The content of Mg^{24} in natural magnesium amounts to 78.6%. Natural magnesium was used therefore as the target in our experiments on the Coulomb excitation of Mg^{24}. To make the results more precise, the targets of magnesium oxide enriched by Mg^{24}, Mg^{25} and Mg^{26} were used as well. The following ions were used as incident particles: triply charged N^{14} ions with $E = 16.3$ MeV, quadruply charged N^{14} ions with $E = 16.3$, 26 and 36 MeV, triply charged O^{16} ions with $E = 18.2$ MeV as well as quadruply charged Ne^{20} and Ne^{22} ions with energies 23.1 and 25.2 MeV respectively. Fig. 6 and fig. 4(a) represent γ-spectra obtained in bombarding the targets of natural magnesium by nitrogen ions

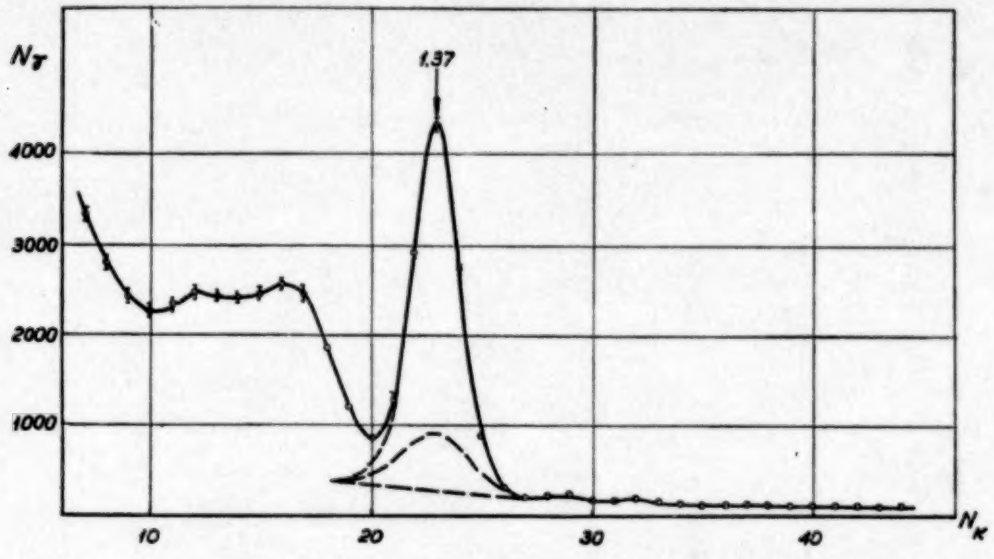

Fig. 6. Apparatus spectrum of γ-radiation obtained in bombarding Mg by N^{14} ions.

with $E = 16.3$ MeV and Ne^{20} ions with $E = 23.1$ MeV respectively. A study of the Coulomb excitation of the first level of Mg^{24} with the aid of nitrogen ions is made more complex by the fact that there is a 1.37 MeV background line, i.e., coinciding with the one under investigation, in the γ-spectra of the Coulomb excitation in a number of elements. It was established that despite the dispersion of absolute yields of γ-rays in the background peaks the ratio of the amplitude of the background peak to the intensity of a continuous background under the peak changes little in irradiating the targets of various substances with nitrogen ions. The dotted line of fig. 6 shows the contour of a background peak calculated on the basis of the above-mentioned observations. In our estimates the maximum error in determining the area of the peak under investigation does not exceed $\pm$ 5 % of this area.

There is no 1.37 MeV background peak in experiments with Ne^{20} and Ne^{22}. A study of the Coulomb excitation by neon ions when the targets are of mag-

nesium oxide enriched by Mg^{25} or Mg^{26} showed that under experimental conditions there arise no lines which could in irradiating natural magnesium have an effect on the yield of γ-quanta with $E_\gamma = 1.37$ MeV corresponding to the excitation of the first level of Mg^{24}.

The lifetime of the first excited level of Mg^{24} was evaluated in ref. [19]) by investigating the non-elastic scattering of electrons with $E = 187$ MeV on natural magnesium. According to ref. [19]) $\tau = 1.9 \times 10^{-12}$ sec; the author of the paper notices, however, that the method is not very accurate and the result may change by several times over. In refs. [20,21]) the lifetime of the first excited state of Mg^{24} was determined by investigating the resonance scattering of γ-rays. The values obtained in these papers differ markedly among themselves and amount to $(1.7 \pm 0.4) \times 10^{-12}$ sec and $(2.6 \pm 0.2) \times 10^{-13}$ sec respectively. Recently another value for τ was published in ref. [22]). It was measured in experiments with the resonance scattering of γ-rays and amounts to 0.95×10^{-12} sec. The value of τ we have obtained for the first excited level of Mg^{24} agrees, within the errors of experiment, with the data of ref. [20,22]).

5.3. SILICON ($Z = 14$)

According to the investigation of the β-decay of Al^{28} and P^{28}, the energy of the first excited level of Si^{28} amounts to 1.78 MeV.

High purity silicon used in semi-conductor engineering was employed in our experiments for the target (the content of Si^{28} in natural silicon is 92.3 %) and nitrogen ions with $E = 26$ MeV and ions of Ne^{20} with $E = 27.9$ MeV as bombarding particles. The investigation of the Coloumb excitation of the first level of Si^{28} with the aid of nitrogen ions is complicated by the fact that the value of the energy of this level coincides with the energy of γ-quanta emitted as a result of the nuclear reaction O + N. Small impurities of oxygen in the substance of the target may result in a sharp increase in the experimental values of the emission of γ-quanta under investigation. Our measurements with nitrogen ions therefore may offer only the upper limit of the value of B(E2). The results of measurement of the γ-spectrum emitted in bombarding natural silicon by nitrogen ions with $E = 26$ MeV are represented in fig. 7(a).

The 1.6 MeV line is probably connected with the nuclear reaction Si + N.

Column 1 of table 2 represents the average value of B(E2) obtained from four experiments with nitrogen ions with $E = 26$ MeV. The Coulomb excitation of the first level of Si^{28} was also investigated by Ne^{20} ions with $E = 27.9$ MeV. The γ-spectrum thus obtained is represented in fig. 7(b). In the present case measurement is made more difficult by the 1.63 MeV line arising from the excitation of the first level of Ne^{20}. Column 2 of table 2 represents the value of B(E2) for the excitation of the first level of Si^{28} calculated by the yield of the reference 1.63 MeV line stemming from the excitation of the first level of Ne^{20}. The value of B(E2) according to the experiments with Ne^{20} ions is determined less

accurately than the others since the calculation involves an analysis of the composite 1.63 + 1.78 MeV line of which the 1.78 MeV line is only a small portion. According to our estimates the true value of B(E2) hardly differs more than by 40 % from the value given in column 3.

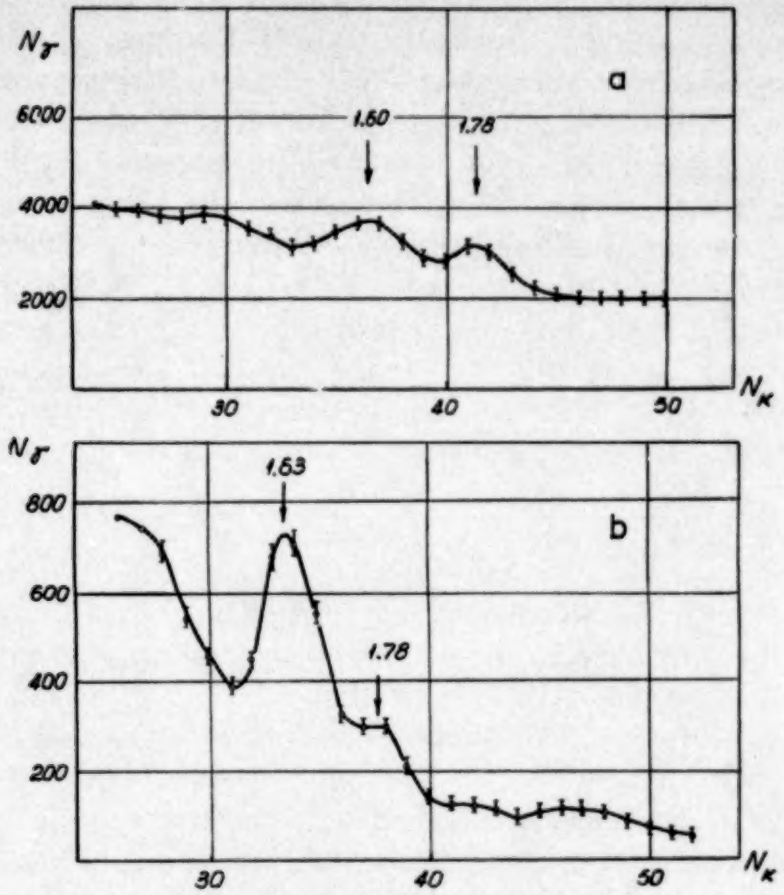

Fig. 7. Apparatus spectra of γ-lines obtained in the Coulomb excitation of silicon by (a) 26 MeV N^{14} ions and (b) 27.9 MeV Ne^{20} ions.

The lifetime of Si^{28} is measured in ref. [19]) with the aid of investigating electron non-elastic scattering. The value of τ agrees with that calculated by our data.

5.4. TITANIUM ($Z = 22$)

The Coulomb excitation of the first level of Ti^{46} was studied by us in experiments with titanium oxide enriched by Ti^{46} (in natural titanium a relative abundance η of this isotope amounts merely to 8 %). In the investigations of the Coulomb excitation of the first level of Ti^{48} the targets used were made from metallic titanium ($\eta = 73.5$ %), the oxide of natural titanium, and titanium oxide enriched by Ti^{48}. The experiments with natural titanium were carried out with nitrogen ions at $E_N = 16.3$, 26 and 36 MeV and the experiments with oxides at $E_N = 16.3$ MeV.

Fig. 8 represents the spectrum of γ-rays emitted in bombardment of metallic titanium by 16.3 MeV nitrogen ions. The levels of Mo^{100} with $E_N = 36$ MeV and of Se^{76} with $E_N = 16.3$ MeV were used as reference levels in the Coulomb excitation of Ti^{48}. For Se^{76} the value of $B(E2)$ was assumed to equal $0.42 \times 10^{-48}\ e^2\ cm^4$. This value is in good agreement with the data of ref. [23]).

The value of $B(E2)$ we have obtained for Ti^{48} is in good agreement with the data of ref. [23]). For Ti^{46} our value of $B(E2)$ is nearly one half that of ref. [23]).

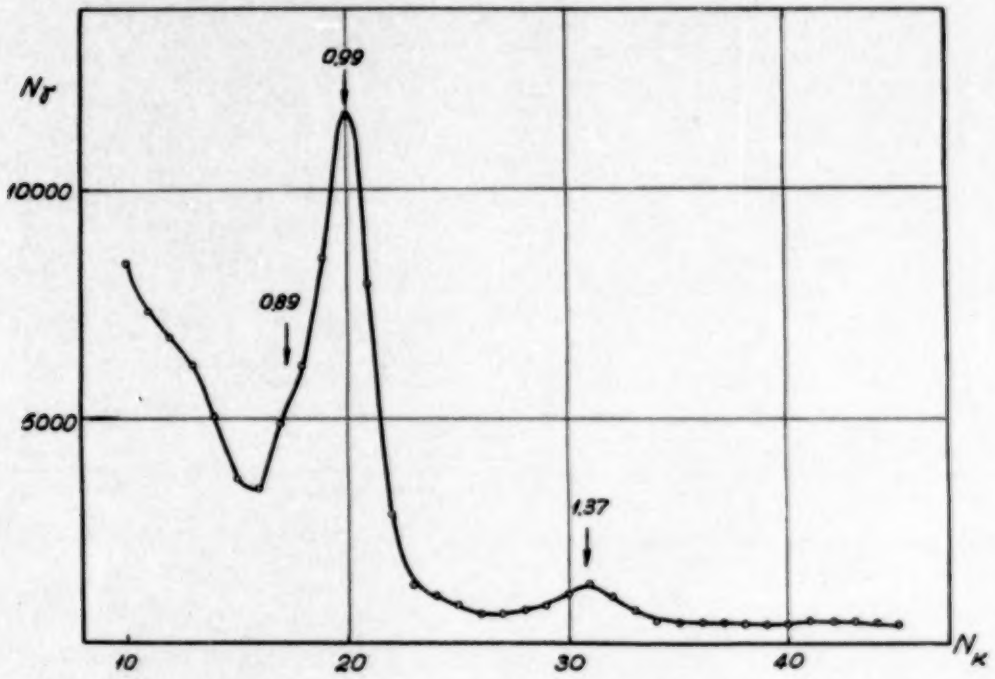

Fig. 8. Apparatus spectrum of γ-lines obtained in Coulomb excitation of titanium by 16.3 MeV N^{14} ions.

5.5. CHROMIUM ($Z = 24$)

The energy of the first excited level of Cr^{54} according to the data on the β-decay of Mn^{54} amounts to 0.84 MeV. A chromium oxide enriched by Cr^{54} was used for the target in investigating the Coulomb excitation of the first level of Cr^{54}. The value of $B(E2)$ represented in column 1 of table 2 was obtained in the experiments with triply and quadruply charged nitrogen ions with energies of 16.3 and 26 MeV respectively.

5.6. IRON ($Z = 26$)

The Coulomb excitation of the first level of the most abundant isotope of iron Fe^{56} was investigated in ref. [24]). Column 1 of table 2 represents the value of $B(E2)$ which is an average of the results obtained in bombardment of the target of metallic iron and ferric oxide by 16.3 and 26 MeV nitrogen ions. The level of Sn^{118} for which $B(E2) = 0.23 \times 10^{-48}\ e^2\ cm^4$ according to ref. [14]) was used as the reference level at $E_N = 36$ MeV.

The Coulomb excitation of the first level of Fe^{58} has not been investigated before. In our experiments this study was carried out with 16.3 and 26 MeV nitrogen ions. Metallic iron enriched by the isotope Fe^{58} was used as the target. Fig. 9 represents the spectrum of γ-rays registered in bombarding Fe^{58} by 26 MeV nitrogen ions. Our value of $\Delta E = 815$ keV is in good agreement with the one known from the investigation of the β-decay of Co^{58} ($\Delta E = 814$ keV).

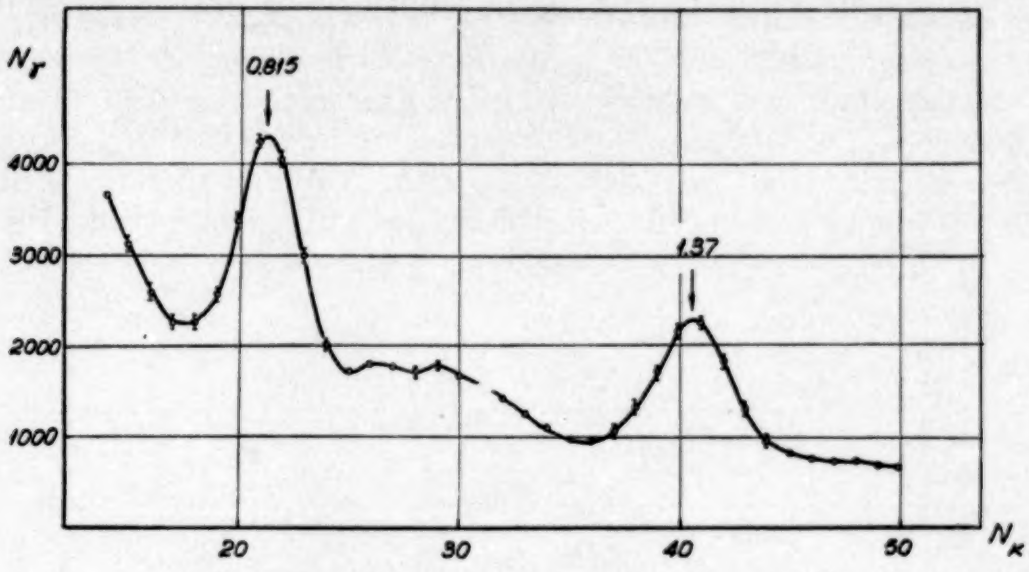

Fig. 9. Apparatus spectrum of γ-lines obtained in Coulomb excitation of Fe^{58} by 26 MeV N^{14} ions.

5.7. NICKEL ($Z = 28$)

The results of investigating the Coulomb excitation of the first levels of even nickel isotopes: Ni^{58}, Ni^{60}, Ni^{62} and Ni^{64} with the aid of α-particles is set down in ref. [1]). Investigations with nitrogen ions were undertaken to check the results we obtained in investigations with α-particles. Separated isotopes of nickel in the form of metallic samples were used as targets. As was indicated above, the 1.37 MeV background line vanishes in the continuous background when the energy of nitrogen ions amounts to 36 MeV, which makes it possible to determine the yield of 1.45, 1.33 and 1.35 MeV lines in the excitation of levels in Ni^{58}, Ni^{60} and Ni^{64} respectively.

Fig. 10 represents γ-spectra registered in bombarding the targets enriched with Ni^{58}, Ni^{60}, Ni^{62} and Ni^{64} by 36 MeV nitrogen ions.

The lifetime of the first excited level of Ni^{60} was investigated with the aid of resonance scattering of γ-rays in refs. [25, 26]). Our results are in good agreement with the data of these papers.

5.8. ZINC ($Z = 30$)

As in the case of nickel, a study of the Coulomb excitation of zinc by nitrogen ions was undertaken to check up our results[1]) obtained in investigations with α-particles. The energies of the first levels of Zn^{64}, Zn^{66} and Zn^{68} amount to

1.00, 1.04 and 1.08 MeV respectively. A study of the Coulomb excitation of all these levels is difficult owing to a background line with $E_\gamma \approx 1$ MeV arising in the reaction O + N. As the case was all targets enriched by zinc isotopes contained considerable admixtures of oxides (which follows from the fact that a very intense background line of 1.78 MeV was observed in all cases when zinc isotopes were irradiated). Column 1 of table 2 therefore contains only the average value of B(E2) obtained in investigating the Coulomb excitation of natural zinc by nitrogen ions with $E = 16.3$ and 26 MeV ($\eta = 50$, 27 and 18 % for the isotopes Zn^{64}, Zn^{66} and Zn^{68} respectively).

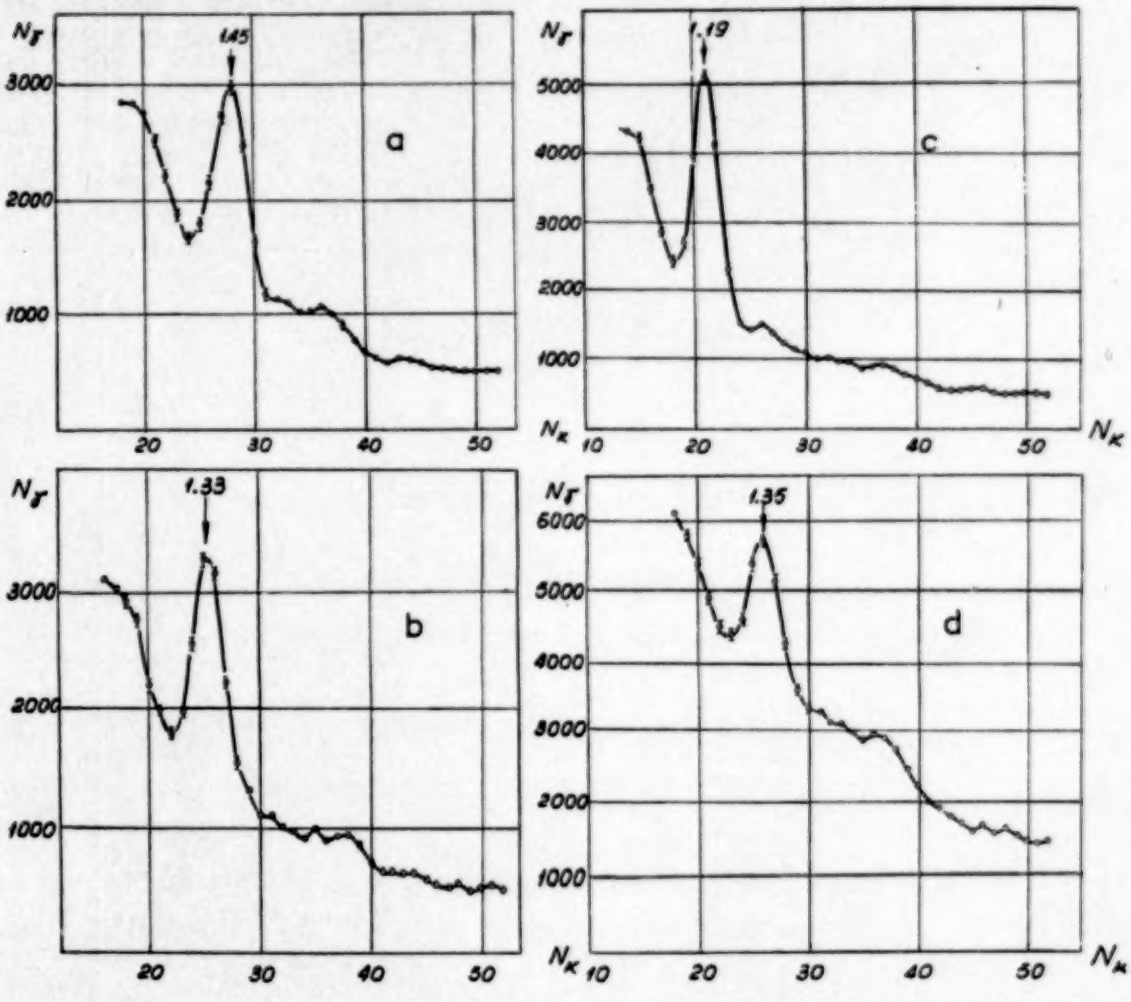

Fig. 10. Apparatus spectra of γ-lines obtained in bombarding nickel by 36 MeV N^{14} ions: (a) Ni^{58} + N, (b) Ni^{60} + N, (c) Ni^{62} + N, (d) Ni^{64} + N.

5.9. SELENIUM ($Z = 34$)

Values of B(E2) for the excitation of the first levels of Se^{76}, Se^{78} and Se^{80} are measured in ref. [24]) in bombarding selenium by α-particles. For comparison column 1 of table 2 lists the values we have obtained with enriched samples in investigating the Coulomb excitation of the first levels of selenium even isotopes by nitrogen ions with $E = 36$ MeV, and for Se^{76} also with $E = 16.3$ MeV.

The yield of the background 0.59 MeV γ-line is extremely small if compared with that of γ-lines attributable to the Coulomb excitation of the first levels of selenium isotopes and practically does not affect the accuracy of measurements of B(E2) values.

According to ref. [24]) the energy of the first excited level of Se^{82} amounts to 880 keV. According to our data $\Delta E = (660 \pm 10)$ keV.

5.10. ZIRCONIUM ($Z = 40$)

Fig. 11 represents the γ-spectrum registered in bombarding metallic zirconium with 36 MeV nitrogen ions. According to refs. [27,28]) the energy of the first excited level of Zr^{92} and that of Zr^{94} are equal and amount to 920 keV.

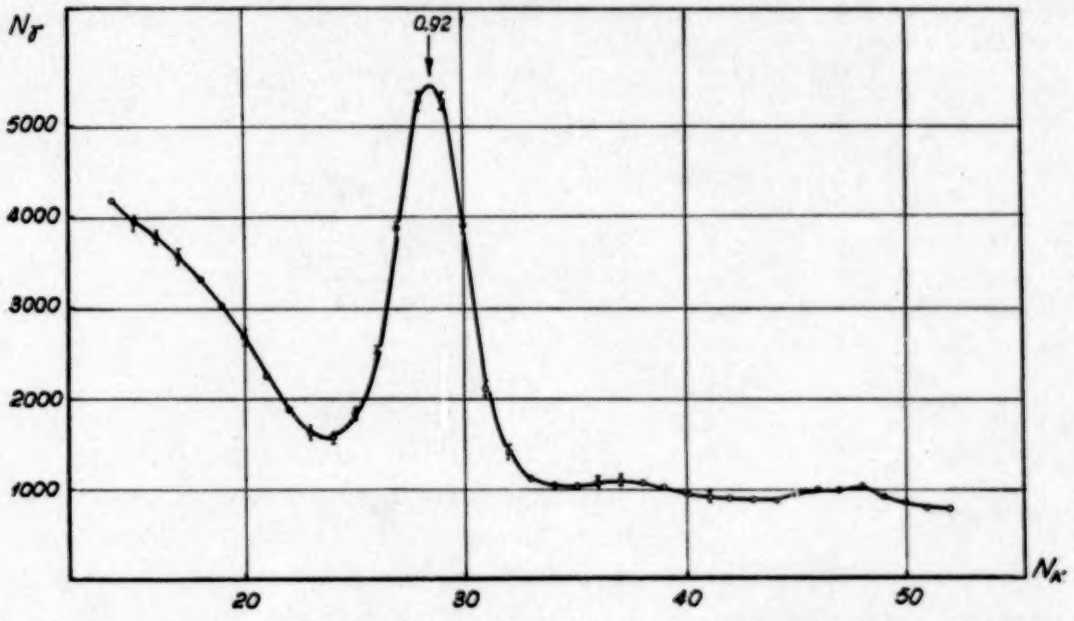

Fig. 11. Apparatus spectrum of γ-lines obtained in the Coulomb excitation of zirconium by 36 MeV N^{14} ions.

Column 1 of table 2 represents an average value of B(E2) for the nuclei of Zr^{92} and Zr^{94} we have obtained in irradiating natural metallic zirconium (which contains 17 % of Zr^{92} and as much of Zr^{94} by 26 and 36 MeV nitrogen ions.

6. Conclusion

The use of heavy ions as incident particles has made it possible to study the Coulomb excitation of such light nuclei as Ne^{20}, Ne^{22}, Mg^{24} and Si^{28}. The Coulomb excitation of the levels of the isotopes Ti, Cr, Fe, Ni and Zn with α-particles was studied in refs. [1,24]). The background γ-lines due to the nuclear reactions of α-particles with the nuclei under investigation were often observed in the process. These background lines interfered with an interpretation of the results in a number of cases. When using the heavy ions (N^{14}, for example)

quite definite background lines were observed, due to the nuclear reactions of the C + N and O + N types only (there were carbon and oxygen in the targets as impurities). Thus in investigating the Coulomb excitation of Ti^{48} we did not observe the 750 keV γ-line which was reported by ref. [24]) and which the authors of that paper ascribed to the reaction Ti^{48} $(\alpha, n\gamma)$ Cr^{51}. Similarly, investigating the Coulomb excitation of Ti^{46} we observed no activity with the period of 42 minutes which the authors of ref. [24]) ascribe to a similar reaction with Ti^{46}. Nor have we observed those background lines which we have registered in investigating the Coulomb excitation of Ni and Zn under the influence of α-particles with energy up to 8 MeV.

Table 2 represents data which make it possible to compare the results obtained in experiments with α-particles, on the one hand, and heavy ions on the other, the data of other authors being drawn upon in the former case as well. In 10 out of 12 cases the discrepancy between the values of B(E2) lies entirely within the errors of experiment and does not exceed 30 %. In two cases (Ti^{46}, Fe^{56}) the discrepancy is large. For Ti^{46} the value of B(E2) according to ref. [24]) is 1.8 times as high and for Fe^{56} 1.5 times as high as according to our data. Since the conditions of the excitation of levels in these two cases as well as cases we have investigated do not differ, the above mentioned discrepancies can hardly be ascribed to the transition from α-particles to heavy ions. Probably these discrepancies stem from some errors in the measurement of B(E2) in ref. [1]) or ref. [24]). Repeated measurements of the values of B(E2) for the above-mentioned two levels are therefore desirable.

In certain cases (Mg^{24}, Ti^{48} and Ni^{60}) it is possible to compare the values of τ found by two different methods: Coulomb excitation and resonance γ-ray scattering. In the case of Mg^{24} such comparison is made more difficult since there is a considerable dispersion of values of τ found by the resonance scattering method in various papers. The value B(E2) determined in our paper is rather close to an average of the values found in the papers on resonance scattering. In two other cases (Ni^{60} and Ti^{48}) our results are in good agreement with the data obtained in experiments on γ-ray resonance scattering.

In ref. [15]) the data available to the author enabled him to conclude that the values of τ determined in the studies of γ-ray resonance scattering are always less than those obtained in investigating Coulomb excitation. The greatest difference from the data of ref. [15]) was observed in the case of the first excited level of Ti^{48} with $\Delta E = 990$ keV. In the same work a hypothesis was made that the difference is probably due to the nucleus of Ti^{48} with 22 protons and 26 neutrons being near to a closed shell configuration. It is clear from table 2 that our value of τ for the first excited level of Ti^{48} is in good agreement with that obtained in ref. [15]). It also follows from table 2 that for the first excited level of Ni^{60} the value of τ we have determined in investigating Coulomb excitation *is less* than that determined by γ-ray resonance scattering. Thus, the

indication of ref. [15]) on the systematic excess of $\tau_{coul.\ excit.}$ over $\tau_{res.\ scat.}$ is not confirmed.

For the nuclei mentioned in fig. 2 and for heavier nuclei investigated in refs. [24,14,2]) the value of the factor F exceeds unity by one or two orders. This circumstance points to the role of collective interactions in the excitation of the first levels of even nuclei. It is notworthy that the value F exceeds 10 even in the case of nickel isotopes. The nickel nucleus possesses, as is wellknown, a closed shell with respect to protons ($n_p = 28$) and in this case it might be expected that the probability of excitation will be close to that of single-particle excitation. It will also be noted that in the case of Ni^{58} the number of neutrons is likewise close to the magic number ($n_n = 30$). It was observed before[14,2]) that in the case of tin isotopes for which a closed shell of protons ($n_p = 50$) is also characteristic the experimental values of $B(E2)$ are similarly more than 10 times as high as those calculated in single-particle estimate. In the case of isotopes of nickel, zinc as well as tin, the energy of levels and the values of $B(E2)$ in the excitation of the first levels differ little as the number of neutrons changes.

Usually results obtained in investigating the Coulomb excitation of even nuclei situated in the region of non-deformed nuclei are used for computing the parameters B_2 and C_2 describing the excitation of the oscillations of the quadrupole type. Yet the introduction of these parameters is worthwhile in those cases when it might be proved that the excitation levels are the vibrational ones. It is hardly possible to separate the vibration levels from single-particle levels in the nuclei of the above-mentioned type.

The data obtained in the investigation of the Coulomb excitation of the first levels of even nuclei situated outside the deformed nuclei region still await a theoretical substantiation.

References

1) D. G. Alkhazov, D. S. Andreyev, L. N. Galperin, A. P. Grinberg, G. M. Gusinsky, K. I. Erokhina and I. Kh. Lemberg, Nuclear Reactions at Low and Intermediate Energies (Publishing House of the Academy of Sciences, USSR) p. 257
2) D. G. Alkhazov, D. S. Andreyev, K. I. Erokhina and I. Kh. Lemberg, JETP **33** (1957) 1347
3) D. G. Alkhazov, D. S. Andreyev, A. P. Grinberg and I. Kh. Lemberg, Nuclear Physics **2** (1956) 65; Izv. Akad. Nauk. (Ser. Fiz.) **20** (1956) 1365
4) D. G. Alkhazov, A. P. Grinberg, K. I. Erokhina and I. Kh. Lemberg, Report at the Eighth Annual Conference for Nuclear Spectroscopy, Leningrad, 1958
5) D. G. Alkhazov, A. P. Grinberg, G. M. Gusinsky and I. Kh. Lemberg, Izv. Akad. Nauk. (Ser. Fiz.) **23** (1959) No. 11 (in print)
6) D. G. Alkhazov, A. P. Grinberg, G. M. Gusinsky, K. I. Erokhina and I. Kh. Lemberg, JETP **35** (1958) 1325
7) H. L. Reynolds, D. W. Scott and A. Zucker, Phys. Rev. **95** (1954) 671
8) J. P. Longchamp, J. Phys. et Radium **14** (1953) 89
9) A. Papineau, Compt. Rend. **242** (1956) 2933
10) A. P. Grinberg and I. Kh. Lemberg, Izv. Akad. Nauk SSSR (Ser. Fiz.) **23** (1959) 887

11) D. G. Alkhazov, A. P. Grinberg, K. I. Erokhina and I. Kh. Lemberg, Izv. Akad. Nauk. SSSR (Ser. Fiz.) **23** (1959) 223
12) D. G. Alkhazov, A. P. Grinberg, G. M. Gusinsky, K. I. Erokhina and I. Kh. Lemberg, JETP **35** (1958) 1056
13) D. G. Alkhazov, A. P. Grinberg, I. Kh. Lemberg and V. V. Rozhdestvensky, JETP **36** (1959) 322
14) P. H. Stelson and F. K. McGowan, Phys. Rev. **110** (1958) 489
15) V. Knapp, Proc. Phys. Soc. **71** (1958) 194
16) N. P. Heydenburg, G. F. Pieper and C. E. Anderson, Phys. Rev. **108** (1957) 106
17) G. F. Pieper, C. E. Anderson and N. P. Heydenburg, Bull. Am. Phys. Soc. **3** (1958) 38
18) S. Devons, G. Manning and J. H. Towle, Proc. Phys. Soc. A **69** (1956) 173
19) R. H. Helm, Phys. Rev. **104** (1956) 1466
20) N. N. Delyagin and V. S. Shpinel, Izv. Akad. Nauk SSSR (Ser. Fiz.) **22** (1958) 861
21) N. A. Burgov and Yu. V. Terekhov, JETP **35** (1958) 932
22) R. G. Arns, R. E. Sund and M. L. Wiedenbeck, Phys. Rev. Letters **2** (1959) 50
23) N. P. Heydenburg and G. M. Temmer, see the survey of literature by K. Alder *et al.* in: Deformation of Atomic Nuclei (Foreign Literature Publishing House, 1958)
24) G. M. Temmer and N. P. Heydenburg, Phys. Rev. **104** (1956) 967
25) N. A. Burgov, Yu. V. Terekhov and G. E. Bizina, JETP **36** (1959) 1612
26) F. R. Metzger, Phys. Rev. **103** (1956) 983
27) G. L. Griffith, Phys. Rev. **103** (1956) 643
28) R. W. Hayward, D. D. Hoppes and H. Ernst, Phys. Rev. **98** (1955) 231

1.E.4 *Nuclear Physics* **19** (1960) 426—435; © *North-Holland Publishing Co., Amsterdam*
Not to be reproduced by photoprint or microfilm without written permission from the publisher

NUCLEAR RESONANCE SCATTERING OF BREMSSTRAHLUNG

E. C. BOOTH

Department of Physics, Boston University, Boston, Massachusetts†

Received 5 May 1960

Abstract: Nuclear resonance scattering of bremstrahlung has been observed in six cases of light to medium weight nuclei. The results agree with previous measurements for the known cases. Mean lifetimes not previously reported are:

	τ/g (10^{-13} sec)
F^{19} (1.34 MeV)	0.5 ± 0.3
P^{31} (1.26 MeV)	3.4 ± 1.5
Cu^{65} (0.77 MeV)	3.3 ± 1.5

where $g = (1 + 2I)/(1 + 2I_0)$.

1. Introduction

This paper reports the measurement of several nuclear lifetimes in the 0.5 MeV to 2.2 MeV region, using bremsstrahlung from a Van de Graaff electron accelerator as a source of resonance radiation.

The past decade has seen the development of the technique of nuclear resonance fluorescence as a means of measuring the lifetimes and angular momenta of excited nuclear states. In the usual procedure gamma radiation from an excited nuclear state is scattered by a target of the same nucleus. In order that the gamma ray energy be precisely at resonance, the energy lost to the recoiling nucleus must be compensated by providing sufficient relative velocity to the nucleus before emission. This can be done mechanically, thermally, or by using the recoil from some previous interaction.

The use of a continuous spectrum to provide resonance photons was suggested by Schiff[1]). The experiment was attempted unsuccessfully by Gaertner and Yeater[2]), using a 100 MeV betatron, and successfully in the case of Li^7 by Beckman and Sandstrom[3]), using a 0.8 MeV Van de Graaff accelerator. Recently resonance scattering in the 5 MeV to 15 MeV range has been observed by Seward *et al.*[4]), using a 20 MeV linear accelerator. Energy levels in the range 0.5 to 3 MeV have not yet been explored in a systematic way.

Bremsstrahlung excitation has certain advantages over gamma ray excitation.

† Work supported by the National Science Foundation.

No extra energy must be supplied to insure resonance. The incident photon intensity varies slowly with energy and can be calculated or measured, whereas this may be difficult in the gamma ray case. Any energy level, including possible unknown levels, may be explored without the difficulty of finding gamma rays of sufficient relative intensity. On the other hand, the bremsstrahlung method suffers from a large background, since the fraction of incident photons falling into the resonance region is much smaller than that obtainable using gamma rays, so that the measurable lifetimes are somewhat shorter than those measured by the resonance scattering of gamma rays.

2. Relation of Lifetime to Resonance Intensity

The resonance absorption cross section is given by the Breit-Wigner formula

$$\sigma(E) = (8\pi)^{-1}\,[(E_r - E)^2 + \tfrac{1}{4}\Gamma^2]^{-1} g\lambda^2\Gamma^2\,,$$

where Γ is the level width and $g = (1 + 2I)/(1 + 2I_0)$ is the statistical factor. Doppler broadening of the natural line width produces a cross section with the form[5,6])

$$\sigma_D(E) = (2\Delta)^{-1}\sigma_0\pi^{\frac{1}{2}} \exp\,[-(E - E_r)^2/\Delta^2]\,,$$

where Δ is the Doppler width $\Delta = E(2kT/Mc^2)^{\frac{1}{2}}$ and $\sigma_0 = (2\pi)^{-1}g\lambda^2$. Since the target is a solid, T is replaced by the effective temperature given by Lamb[7]). The integral cross section is then

$$\int \sigma dE = \int \sigma_D dE = \tfrac{1}{2}\pi\sigma_0\Gamma\,,$$

where $\Gamma = h\tau^{-1}$. The incoming resonance photons will be scattered by nuclear resonance and electronic processes, but the outgoing fluorescence radiation is so far off resonance that it suffers only electronic scattering.

The yield of resonance radiation from a thick target is given by[8])

$$Y = (\mu_1 + \mu_2 \cos\theta \sec\phi + \delta k)^{-1}\pi^{\frac{1}{2}}N(E)\Delta k \\ \{\,1 - \exp\,[-(\mu_1 + \mu_2 \cos\theta \sec\phi + \delta k)b \csc\theta]\,\}\,,$$

where $N(E)$ is the incident photon flux per unit energy near resonance, $k = (4\pi^{\frac{1}{2}}\Delta)^{-1}ng\lambda^2\Gamma$; n is the number of atoms per gram; θ and ϕ are the incidence and exit angles; μ_1 and μ_2 are mass absorption coefficients for electronic absorption on incidence and exit, $\delta = 0.66$; and b is the target density in g/cm^2. If a self absorption measurement is made by placing an absorber between source and target, the yield is reduced by the factor $\exp\,[-(\mu_1 + \delta k)a]$, where a is the absorber density. The errors in this approximation are only a few per cent, much less than the experimental errors. The yield Y is the counting rate in the scintillation spectrometer photoelectric peak divided by the product of solid angle, absorption in lead and crystal efficiency.

If the spins of the states are unknown, the measurement yields the value of $\tau/gW(\theta)$, where $W(\theta)$ is the angular distribution factor. The angular distribution of the emitted resonance radiation is the same as for a $I_0 - I - I_0$ angular correlation, so that the spin of the excited state I can be found in principle by measuring the angular distribution. The small amount of resonance scattering relative to background makes the angular correlation experiment difficult when bremsstrahlung excitation is used.

3. Experimental Procedure

The experimental arrangement is shown in fig. 1. The electron beam from the Van de Graaff generator passes through a 76 μm aluminium window and a 25 μm platinum foil. The energy of the electron beam is about 10% above that

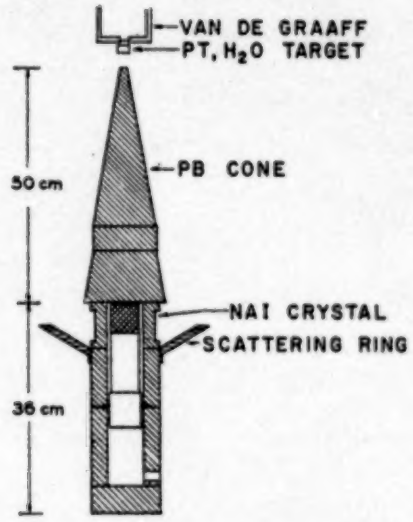

Fig. 1. Experimental arrangement showing lead absorbing cone, scattering ring and NaI counter.

of the resonance to be investigated. This insures that $N(E)$ will be large, and yet the background is comparatively low. The electrons are stopped in the cooling water of the electron target. The resonance photons are absorbed in the ring scatterer and reradiated at a mean angle of about 100° toward the 5.1 cm NaI detector. The energy of the Compton scattered photons is lower than the resonance energy by a factor of about 3; thus, they are heavily attenuated in the 2 cm lead absorber. An extra centimeter of lead was added when gamma rays above 1 MeV were studied. The resonance radiation appeared superimposed on an exponentially rising background produced by elastic scattering and by bremsstrahlung from photo and Compton electrons produced in the scattering ring.

A dummy scattering ring with the same mass and nearly the same Z was used to obtain the background, which was subtracted from the resonance scattering distribution plus background. The subtraction photo-peaks appear

at the same position when the energy of the Van de Graaff is increased, but they are lost in the statistics of the background when the electron energy is greater than 1.5 E_r. The electron beam current is usually 100 μA except above 2 MeV, where pile-up and photomultiplier saturation become serious.

An absorption measurement of k is more reliable in principle than a direct measurement, since the errors involved in estimating bremsstrahlung intensity, solid angles and counter efficiency are eliminated. However, the absolute measurement is possible with lower k values, since Y goes a E^{-2}, whereas k goes as E^{-3}. It should always be possible to measure k by absorption, provided that k is not much smaller than the electronic absorption coefficient.

Lifetime measurements at energies above 2 MeV are difficult, owing to the E^{-2} dependence of the resonance scattering cross section. The transition probabilities are supposed to have an $E^2{}_L{}^{+1}$ dependence using the single-particle model, but experience indicates that the energy dependency is not this strong. Above 1 MeV the absorption coefficient of lead changes slowly, making the lead filter relatively inefficient. The result is an increase in the total counting rate which causes pile-up and photomultiplier instability.

The pulse-height distribution from the NaI crystal was taken with a single-channel analyzer. The upper end of the spectrum was monitored by an integral discriminator located in the linear amplifier, permitting corrections for small energy and current fluctuations.

The density of the ring scatterer and absorbers ranged up to 20 g/cm^2, so that the correction for electronic absorption was important, especially in the absorption measurements.

Absorption coefficients were measured directly, using the appropriate geometry, and were found to be 5 to 10% lower than the good geometry values obtained from tables.

A correction to the lifetime obtained by direct measurement was made for Compton scattering into the resonance region. For low Z materials most of the beam attenuation was due to Compton scattering; and since there was a large flux above resonance, a considerable fraction of the incident bremsstrahlung distribution was scattered into the resonance region. Although a precise calculation of this scattered intensity is difficult, an upper limit to the correction may be obtained by assuming that the bremsstrahlung distribution is rectangular and that the Compton scattering cross section is independent of the energy of the scattered photon. In this case the ratio of Compton scattered intensity to primary intensity near resonance at a depth X is

$$N'/N = 2e^{\mu x}(1 - e^{-\mu x})\,(E_{max} - E_r)/E_{max}\,.$$

For a scatterer of thickness d, the fraction of resonance scattering due to the Compton effect is

$$e^{\frac{1}{2}\mu d}(1 - e^{-\frac{1}{2}\mu d})\,(E_{max} - E_r)/E_{max}\,,$$

where the factor of two is dropped to account for the decrease in $N(E)$ above E_r. The correction is less than 10% for the scattering rings used in this experiment.

The Compton scattering correction described above does not apply to the absorption measurements since the absorbers were placed at the tip of the cone, so that most of the Compton scattered photons missed the ring scatterer. Although the effect is diminished, it may be important, since the absorption measurements of k depend critically on the electronic absorption coefficients. In order to estimate the correction necessary in the absorption measurements, the attenuation of Cu^{63} 0.67 MeV resonance radiation by iron absorbers was observed. It was found to agree with the attenuation of the 0.67 MeV gamma from Cs^{137} to within the statistical uncertainty of 15%, so no correction was made. The situation is more serious for the case of large k, as in Li^7 where $k \approx 1.0$. In this case three absorbers were used with densities 0.25, 0.53 and 1.02 g/cm^2, which gave k values of 0.64, 0.58 and 0.54. The extrapolated value of k at zero absorber thickness was $k = 0.72$. The fact that k is still too low may be attributed to Compton scattering from the lead cone.

Nuclei with low Z and 100% abundance are particularly favourable, since elastic scattering has a Z^3 dependence and electronic absorption also increases with Z. Under favourable conditions lifetimes as long as 10^{-12} sec are measurable using the present techniques. The high background limits the method to the study of transitions to the ground state or to a level near the ground state.

The flux $N(E)$ was measured directly, using a small NaI crystal, and the results were found to agree within 30% with thin target data extrapolated from the review article by Koch and Motz[9]). This agreement is surprising, since the multiple scattering of electrons in the target should produce considerably more bremsstrahlung than that given by assuming a thin target. This may account for the fact that the lifetimes obtained by direct measurement are found to be smaller than those measured previously using gamma rays.

The electronic absorption, crystal efficiency, and solid angle subtended by the crystal were interpolated from direct measurements, using gamma rays from Cs^{137} and Na^{22}.

The size and shape of the lead scattering cone were varied until the background without the scattering ring was small. The lead absorber between the scattering ring and the crystal was increased until the slope of the background remained relatively unchanged. The present arrangement of cone, scatterer and absorber is probably near that required for the maximum ratio of resonance to background radiation.

4. Results

The lifetimes measured by the bremsstrahlung method are shown in table 1. The energies shown in the table are the known energies which coincide with

TABLE 1

Mean lifetimes measured by resonance scattering of bremsstrahlung

Nucleus	Energy (MeV)	$\tau(gW(\theta)$ $(10^{-13}$ s)	Spins assumed	$\tau \pm 50\%$ $(10^{-13}$ s)	Previous measurement
Li^7	0.477	(2.8)*	$\frac{3}{2}-\frac{1}{2}$	(1.4)*	0.77 ± 0.08[a]
		2.0		1.0	1.09 ± 0.07[b]
B^{11}	2.14	0.064	$\frac{3}{2}-\frac{1}{2}$	0.032	0.047 ± 0.06[c]
F^{19}	1.34	0.55			
P^{31}	1.26	3.4	$\frac{1}{2}-\frac{3}{2}$	4.6	
Cu^{63}	0.67	(5.3*)	$\frac{3}{2}-\frac{1}{2}$	(2.65)*	3.3 ± 1.3[d]
		3.1		1.6	
Cu^{63}	0.96	4.6	$\frac{1}{2}-\frac{1}{2}$	6	≈ 6[e]
Cu^{63}	1.89	> 4.5			
Cu^{65}	0.77	3.3			
Cu^{65}	1.114	> 2.9			

* Absorption method.

[a] D. Bunbury, S. Devons, G. Manning and J. Towle, Proc. Phys. Soc. **69**A (1956) 165.

[b] C. Swann, V. Rasmussen and F. Metzger, Phys. Rev. **114** (1959) 862.

[c] F. Metzger, C. Swann and V. Rasmussen, Phys. Rev. **110** (1958) 906.

[d] A. Sunyar, J. Cumming, L. Grodzins, N. Porile and A. Schwarzschild, Bull. Am. Phys. Soc. **4** (1959) 57.

[e] K. Ilakovac, Proc. Phys. Soc. **67**A (1954) 601.

the observed resonance energies. The experimental uncertainty in the energy of the resonance scattered photons is about 3%. The experimental error in the lifetime measurement is about 50% in all cases. Satisfactory agreement with previously measured values is obtained. Comments on the individual cases are made below.

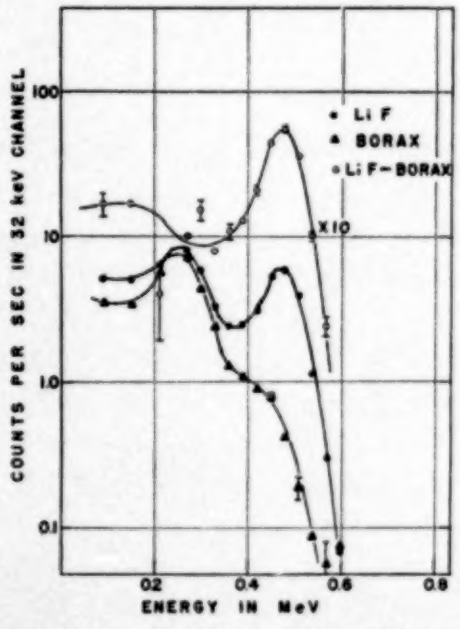

Fig. 2. Resonance scattering from the 0.477 MeV state in Li^7 using a thick scattering of LiF.

Li^7 (fig. 2)

The 0.477 MeV resonance in Li^7 is particularly easy to observe because of its short lifetime and low energy. The lifetime agrees with the previous measurements. Both scattering ring and absorber were thin in order to avoid errors due to Compton scattering. One has $\Delta = 0.77$ eV.

B^{11} (fig. 3)

The 2.14 MeV state of B^{11} has by far the shortest lifetime of those measured in these experiments. The resonance peak is unmistakable, despite the fact

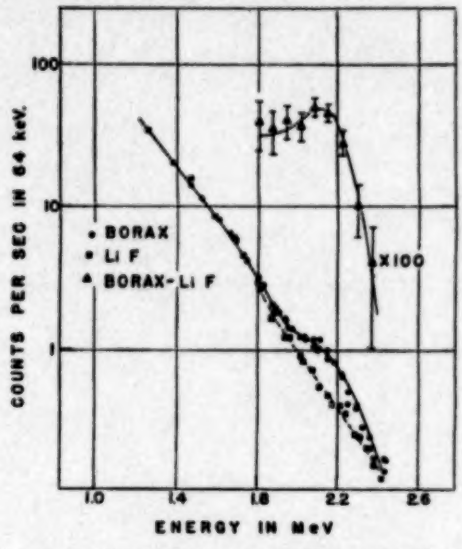

Fig. 3. Resonance scattering from the 2.14 MeV state of B^{11} using $Na_2B_4O_7 \cdot 10H_2O$ as the scatterer.

that borax ($Na_2B_4O_7 \cdot 10H_2O$) was used. Boron carbide (B_4C) would have given a much more prominent resonance. The dummy scatterer was lithium fluoride. One has $\Delta = 3.0$ eV.

F^{19} (fig. 4)

The resonance scattering from F^{19} is shown as a function of changing electron energy. The energy of the resonance radiation is 1.37 ± 0.04 MeV. If the intensity of the resonance radiation is plotted as a function of electron energy, the cut-off comes between 1.4 MeV and 1.5 MeV. This indicates that the resonance is with the 1.46 MeV state of F^{19} which decays to the 0.109 MeV state. The lifetime given in table 1 assumes that the branching ratios are as reported by Toppel, Wilkinson and Alburger[10]). The fact that the resonance is observed indicates a dipole transition between the 1.46 MeV state and the 0.109 MeV state, giving spin $\frac{3}{2}$ for the 1.46 MeV state. One has $\Delta = 2.3$ eV.

P^{31} (fig. 5)

The resonance here is clearly due to the 1.264 MeV transition. The lifetime confirms the choice of $I = \frac{3}{2}$ for the 1.264 MeV state. One has $\Delta = 2$ eV.

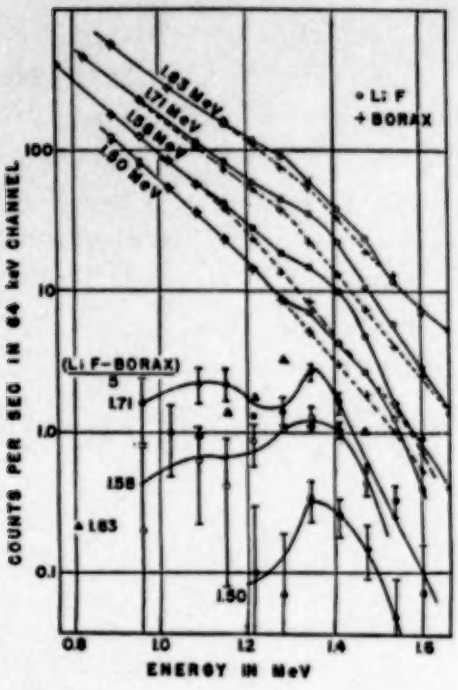

Fig. 4. Resonance scattering from F^{19} found at different electron energies. Resonance scattering begins at 1.45 $\pm$ 0.05 MeV. The resonance radiation has an energy of 1.37 $\pm$ 0.04 MeV.

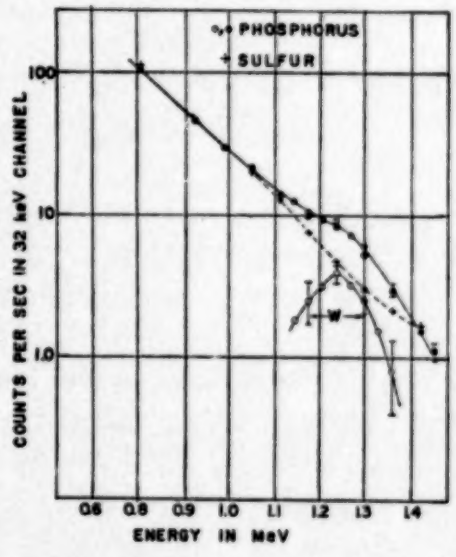

Fig. 5. Resonance scattering from the 1.264 MeV state of P^{31}.

Cu^{63} (fig. 6)

Copper was the first and most thoroughly studied case. Excited states following beta decay are 0.67, 0.960, 1.89 and 2.60 MeV in Cu^{63} and 0.769, 0.82 and 1.14 MeV in Cu^{65}. Both iron and zinc have been used as dummy targets, but iron is more satisfactory, since zinc has several energy levels near those in copper. The 0.67 MeV resonance was observed on many occasions, and the life-

time was measured by the absolute method and by the absorption method. The results of the absorption method agree with the previous measurement, but the lifetime found by the absolute method is somewhat less than that warranted by experimental error. The difference in lifetime is understandable on the assumption that the thin target calculation of bremsstrahlung intensity gives too low a value. A correction of the absorption measurement for Compton scattering into resonance would decrease the value of τ. One has $\Delta = 0.72$ eV.

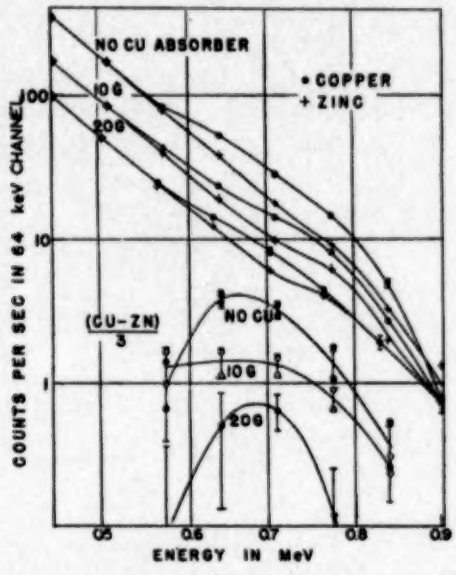

Fig. 6. Resonance scattering from the 0.67 MeV state of Cu^{63} found with increasing amounts of copper absorber. The assymetry and width of the subtraction peak show the presence of another resonance near 0.77 MeV.

The 0.96 MeV resonance appeared at the proper energy and gave a lifetime agreeing with the previous measurements. In this case, as in all other cases, the resonance was observed at the proper position when the electron energy was increased. One has $\Delta = 1.02$ eV.

The 1.89 MeV resonance was not observed, but it was established that the lifetime is greater than about 5×10^{-13} s. Assuming an E^3 dependence for $L = 1$ transitions, the lifetime would be 2.5×10^{-14} s if the 1.89 MeV state is $I = \frac{1}{2}$ or $I = \frac{5}{2}$, making these angular momenta unlikely for the 1.89 MeV state. One has $\Delta = 2.02$ eV.

Cu^{65}

Fig. 6 shows evidence for a gamma ray slightly above 0.67 MeV. Data taken at higher energies clearly show a resonance with an amplitude about half that of the 0.67 MeV resonance and with an energy of 0.77 ± 0.03 MeV. This indicates that the resonance is due to the 0.769 MeV state of Cu^{65}, although the 0.82 MeV state cannot be definitely excluded, since the 0.82 MeV state was observed under Coulomb excitation but the 0.769 MeV state was not. The ground state

of Cu^{65} has $I = \frac{3}{2}$; hence, the 0.769 MeV state is expected to have spin $\frac{1}{2}$ or $\frac{5}{2}$. One has $\Delta = 0.83$ eV.

A search for the 1.114 MeV state of Cu^{65} yielded no results. A lower limit of $\tau > g \times 2.9 \times 10^{-13}$ s was found for the lifetime.

5. Conclusion

The resonance scattering of bremsstrahlung from a Van de Graaff generator offers a flexible method of measuring nuclear lifetimes of the order $\tau < 10^{-12} E^{-2} g$ (abundance) for $Z < 50$ and $E < 3$ MeV. Because of the large background, the experimental errors are somewhat greater than those occurring when lifetimes are measured by resonance scattering of gamma rays.

The author is pleased to acknowledge the kindness of Dr. J. G. Trump of Massachusetts Institute of Technology for allowing us to use the electron Van de Graaff. Thanks are also due to Mr. Kenneth Wright for his help in operating the Van de Graaff machine and for his many valuable suggestions.

References

1) L. Schiff, Phys. Rev. **70** (1946) 761
2) E. Gaertner and M. Yeater, Phys. Rev. **76** (1949) 363
3) O. Beckman and R. Sandstrom, Nuclear Physics **5** (1958) 595
4) F. Seward, H. Koch, R. Shafer and S. Fultz, Bull. Am. Phys. Soc **5** (1960) 68
5) F. Metzger, Phys. Rev. **101** (1956) 286
6) F. Metzger, Phys. Rev. **103** (1956) 9830
7) W. Lamb, Phys. Rev. **55** (1939) 190
8) S. Ofer and A. Schwarzschild, Phys. Rev. **116** (1959) 725
9) H. Koch and J. Motz, Revs. Mod. Phys. **31** (1959) 920
10) B. Toppel, D. Wilkinson and D. Alburger, Phys. Rev. **101** (1956) 1485

2.A.1:
3.A

Nuclear Physics 19 (1960) 436—441; © *North-Holland Publishing Co., Amsterdam*
Not to be reproduced by photoprint or microfilm without written permission from the publisher

THERMAL AND RESONANCE NEUTRON CAPTURE GAMMA RAYS FROM Nd^{144} AND Nd^{146}

J. E. DRAPER and R. L. HICKOK†

Yale University, New Haven, Connecticut††

Received 7 May 1960

Abstract: A number of neutron capture gamma rays following thermal and resonance neutron capture forming Nd^{144} and Nd^{146} have been investigated in the gamma-ray energy range below 1 MeV. Absolute intensities and isotopic assignments are reported.

The low energy gamma-ray spectra following resonant (4.37-eV) and thermal neutron capture in neodymium have been investigated with a single crystal scintillation spectrometer and with an anticoincidence NaI(Tl) spectrometer. Preliminary account of this work has already been reported[1]). Since that account a preliminary report of the measurements on thermal neutron capture in elemental Nd by Campion *et al.* has appeared[2]), and the measurements of Kalinkin *et al.* have appeared[3]). The present work affords isotopic assignments of several of the transitions.

The 6-MeV electron linear accelerator was used as the pulsed source of neutrons, and the neutron energy range of interest was selected by the time-of-flight method. The experimental methods were like those which have already been described in detail[4]). The problem of sample purity was made difficult by the low thermal neutron capture cross section[5]) of Nd (46 b) and the large cross-section of the rare earth impurities Sm (5600 b) and Gd (46000 b). The isotopic identification of the capture gamma rays is complicated by the large number of Nd isotopes. The various compound nucleides formed by thermal capture in the natural element[5]) are A = 143 (9.2 %), 144 (75 %), 145 (2.2 %), 146 (9.4 %), 147 (3.2 %), 149 (0.4 %) and 151 (0.4 %) For these reasons several Nd samples were used including samples of natural Nd from three commercial suppliers and a 100 mg sample enriched from 12.2 % to 68.7 % in Nd^{143}. Of the three samples of natural Nd, one showed large spectral peaks from Sm, another sample was similarly contaminated with Gd, and the third showed only structure common to all three samples. Fig. 1 shows a thermal capture spectrum[6]) from this sample, and fig. 2 shows the spectrum from the 4.37-eV resonance with a 7.6 cm × 7.6 cm scintillator.

† Socony Mobil Postdoctoral Fellow. Present Address: Socony Mobil Stony Brook Research Laboratory, Princeton, N.J.

†† Research supported in part by the U.S. Atomic Energy Commission.

With these samples it was possible to make the isotopic assignments of the transitions shown in table 1. Nd^{146} was formed exclusively by capture in the 4.37-eV resonance[5]), while Nd^{144} was formed in 98 % of the thermal captures

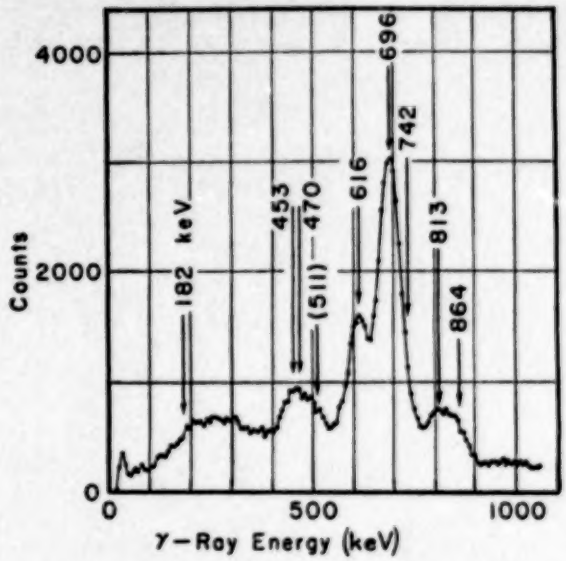

Fig. 1. Thermal neutron capture spectrum of Nd_2O_3 (2 gcm^{-2}) using the 20 cm × 30 cm anti-coindidence NaI(Tl) annulus. The arrows are located at the more intense peaks ($I_{\gamma e} > 1.6$) found, by Campion *et al.*, except for that at 182 keV reported by Kalinkin *et al.*

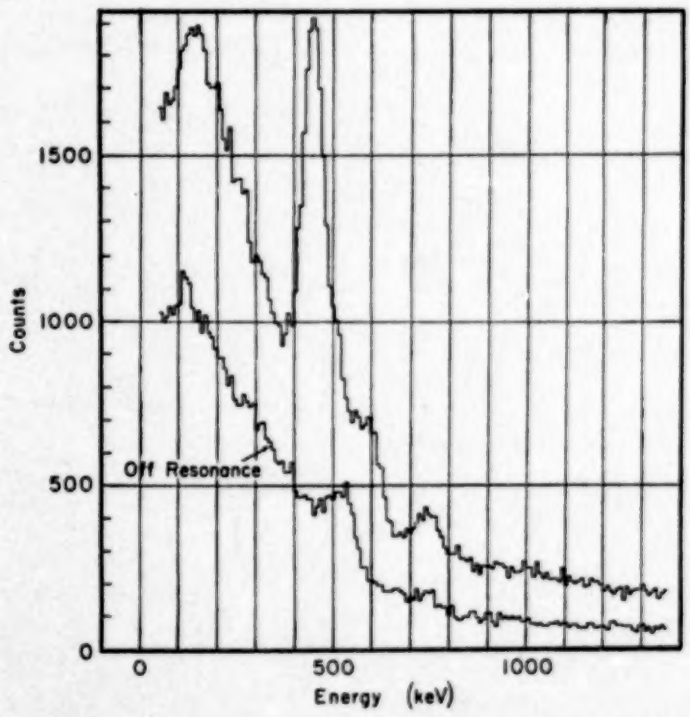

Fig. 2. Spectrum from the 4.37-eV resonance forming Nd^{146} using a 7.6 cm × 7.6 cm scintillator and 2 gcm^{-2} of Nd_2O_3. The lower curve was taken for the same duration with the time gate moved off of the 4.37-eV resonance.

TABLE 1

Experimental Results

Photon energy (keV)	A (cpd.) this work	Elemental Nd thermal $I_{\gamma e}$	Nd^{146} resonance $I_{\gamma i}$	Nd^{144} thermal $I^*_{\gamma i}$	Elemental Nd thermal $I_{\gamma e}$ (deduced from $I_{\gamma i}$ and $I^*_{\gamma i}$)	Results from ref. [2])		Results from ref. [3]) $I_{\gamma i}$
						E_γ (keV)	$I_{\gamma e}$	
460 ± 10	146	10 ± 3	52 ± 8		4.9 ± 0.8	453	5.2	40 (146)
470 ± 30	(144)			< 6	< 4			
605 ± 20	146	22 ± 4	15 ± 4		1.4 ± 0.4	590	1.6	≈ 100 (146)
615 ± 10	144			27 ± 5	20 ± 4	616	22	
695 ± 10	144	53 ± 8		71 ± 11	53 ± 8	696	46	85 ± 13 (144)
750 ± 30	146		6 ± 2		0.55 ± 0.2	not 742	5.4	
810 ± 15	144	7 ± 2	< 3	20 ± 11	15 ± 9	813	6.6	20 ± 4 (144)
860 ± 15	144	7 ± 2	< 3			864	7.5	

$I_{\gamma e}$ is the intensity in photons per 100 neutrons captured in the element.
$I_{\gamma i}$ is the intensity in photons per 100 neutrons captured in the isotope.
$I^*_{\gamma i}$ is the relative intensity normalized at 695 keV to indicate absolute isotopic intensity.

in the enriched sample and in 75 % of thermal captures in the natural isotopic mixture.

The results are summarized in table 1. The third column lists the elemental intensities $I_{\gamma e}$ of gamma rays (photons per 100 captures) measured for thermal neutron capture in natural Nd. The fourth column lists the isotopic intensities $I_{\gamma i}$ of gamma rays from capture in the 4.37-eV resonance forming Nd^{146}. The fifth column gives the relative intensities of photons from thermal capture by the sample enriched in Nd^{143}. These relative intensities are so normalized that they represent absolute isotopic intensities for Nd^{144} under the assumptions that all transitions in column five are in Nd^{144} and that all of the 695-keV intensity in column three is from Nd^{144}. The sixth column lists the elemental intensities for thermal capture in natural Nd as deduced from the fourth and fifth columns and from the assumption that isotopic intensities for Nd^{146} are the same for thermal neutrons and for the 4.37-eV resonance.

Comparison of the third and sixth columns with the seventh[2]) shows that these results are compatible as to intensities and energies (within the limitations of the energy resolution of our scintillator). The arrows in fig. 1 indicate the location of the stronger transitions ($I_{\gamma e} > 1.6$) found by Campion *et al.*[2]), with the exception of the 182-keV arrow which indicates a transition reported by Kalinkin *et al.*[3]). The 511-keV photons are presumed to arise from positon annihilation. The 813- and 864-keV transitions are not resolved in fig. 1, but the composite peak is almost twice the width of a single peak.

Comparison of the present results with those of Kalinkin *et al.*[3]) shows several points of reasonable agreement. However, their assignment of a 610 ± 10 keV transition to Nd^{146} with $I_{\gamma i} \approx 100$ appears to be in error since for the natural element the contribution from Nd^{144} to this peak is 14 times that from Nd^{146}. Their reported peak at 182 ± 3 keV with an $I_{\gamma e}$ of 0.1 that for the 615-keV peak is not apparent in fig. 1. However, the small intensity and the calculated sample absorption for this gamma ray would give a predicted peak height of only 80 counts per channel in fig. 1 and no conclusion is possible in this case.

Fig. 3 gives energy level diagrams of Nd^{144} and Nd^{146} which are consistent with the transitions observed in this work. The diagram for Nd^{144} is part of the one suggested by Campion *et al.*[2]). The levels at 696, 1313, 1783 and 2181 keV have been investigated with radioactive isotopes[7,8]). The results of Campion *et al.*, give strong evidence for the levels at 1560 and 2373 keV through the 6259- and 5441-keV gamma rays from the capturing state. Electron capture by Pm^{144} results in a 475-keV transition[7]) from a 6^+, 1.78-MeV level of Nd^{144}. The thermal capture intensity of this transition is listed in table 1 as $I^*_{\gamma i} < 6$, but recent investigations by Campion *et al.*[9]) would reduce this upper limit by an order of magnitude. Mallmann and Porter[8]) have suggested that Nd^{144} does not show the "vibrational pattern" but state that their analysis does not preclude the 1560-keV level as a second (2^+) level.

In Nd^{146} the levels at 0.46, 1.21 and 1.95 MeV have been assigned[10]) through beta decay of Pr^{146}. The dashed level at 1.06 MeV is only suggested to account for the 0.60-MeV gamma ray of table 1. A similar level was suggested by Kalinkin *et al.*[3]), but apparently it was suggested to account for the 615-keV

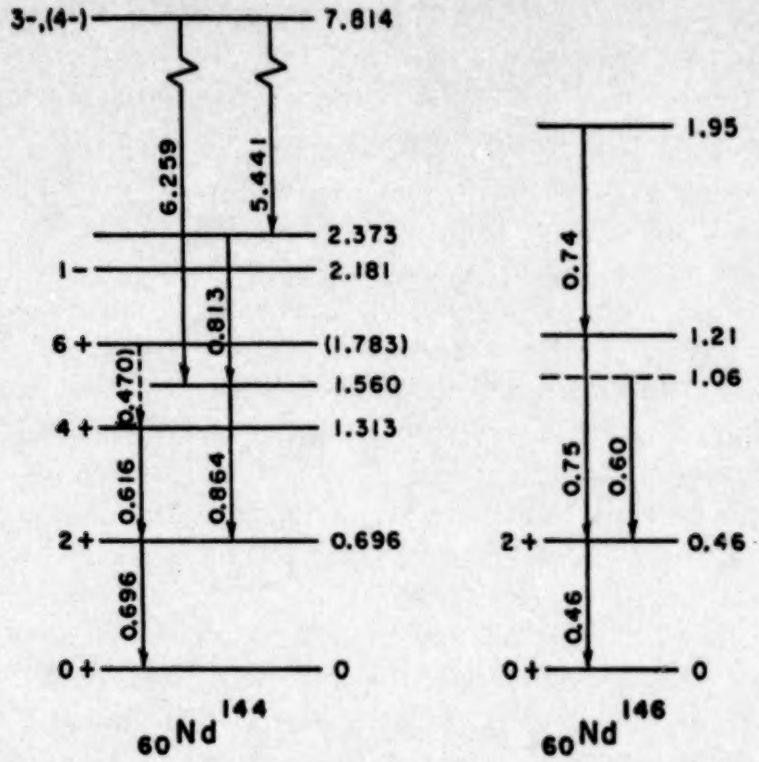

Fig. 3. Energy levels of Nd^{144} and Nd^{146} which can account for the transitions observed here. The levels at 1.56, 2.37 and 7.81 MeV are given in the results of Campion *et al.* The level at 1.06 MeV is suggested by the present results. The other levels were previously reported in radioactive source experiments.

transition which was erroneously assigned to Nd^{146}. The suggested location of the 605-keV transition as feeding the 460-keV level is only by analogy with Nd^{144}. The question of the relation of the possible 1.06- and 1.21-MeV levels of Nd^{146} to the 1.31- and 1.56-MeV levels of Nd^{144} can not yet be answered.

We acknowledge with pleasure the assistance of Mr. Carl Bostrom in obtaining the spectrum with the anticoincidence spectrometer.

References

1) R. L. Hickok and J. E. Draper, Bull. Am. Phys. Soc. 3 (1958) 382
2) Campion, Knowles and Bartholomew, Bull. Am. Phys. Soc. 4 (1959) 247
3) Kalinkin, Melioranskii and Estulin, JETP (USSR) 36 (1959) 1613
4) Draper, Fenstermacher and Schultz, Phys. Rev. 111 (1958) 906;
Fenstermacher, Draper and Bockelman, Nuclear Physics, 10 (1959) 386

5) D. J. Hughes and R. B. Schwartz, Neutron Cross Sections, Brookhaven National Laboratory Report BNL-325, Second Edition (U.S. Government Printing Office, Washington, D.C., 1958)
6) J. E. Draper and C. O. Bostrom, Bull. Am. Phys. Soc. **5** (1960) 17
7) Graham, Geiger and Eastwood, Can. Jour. Phys. **36** (1958) 1084;
Hickok, McKinley and Fultz, Phys. Rev. **109** (1958) 113;
S. Ofer, Phys. Rev. **113** (1959) 895;
K. S. Toth and O. B. Nielsen, Phys. Rev. **115** (1959) 1004
8) C. A. Mallmann and F. T. Porter, Bull. Am. Phys. Soc. **4** (1959) 324
9) Campion *et al.*, private communication
10) Bernstein, Markowitz and Katcoff, Phys. Rev. **93** (1954) 1073

2.B *Nuclear Physics* **19** (1960) 442—447; © *North-Holland Publishing Co., Amsterdam*
Not to be reproduced by photoprint or microfilm without written permission from the publisher

THE OBSERVATION OF p′-γ ANGULAR CORRELATION AT A NUCLEAR RESONANCE

H. YOSHIKI and N. M. NIKOLIC

Pegram Nuclear Physics Laboratories, Columbia University, New York, New York†

Received 7 May 1960

Abstract: p′-γ angular correlation in the $C^{12}(p, p'\gamma)C^{12}$ reaction was measured on nuclear resonances between 5.3 MeV and 6.1 MeV of incident proton energy. The excitation curve of this reaction shows a weak resonance at 5.69 MeV, which corresponds to an excitation of 7.17 MeV in N^{13}. The correlation measurements indicate a large discrepancy from the compound theory on the 5.93 MeV resonance.

Strong proton-gamma angular correlations have been observed in various direct (p, p′γ) processes with medium[1,2]) or low incident proton energy[3]). Generally speaking, the measured correlations[4]) have the form $A + B \sin^2 2\theta$, where θ is the angle between the gamma ray direction and the recoil nucleus direction. Our attention is focused on the question of the correlation to be expected if the incident proton energy is set on or off resonance corresponding to compound nucleus formation. An isolated resonance must be concerned only with a single state in contrast to the surface interaction with which many levels are associated. A measurement by Seward on Mg^{24} at 6.66 MeV resonance of (p, p′) process yields a correlation of the form $A + B \sin^2 2\theta$. However, not only because of the paucity of our knowledge about the level corresponding to this resonance in Al^{25}, but also because of the large background in yields over the resonances and the relatively high excitation energy, it is unclear to us to what extent we can safely speak of the idea of "compound nucleus resonance" and "direct interaction" in this case. Carbon was chosen in the present experiment in order to investigate this problem, since the excitation function had been measured in detail showing fairly good separation between isolated resonances.

The target used was a thin polystyrene target ($\approx$ 3 keV thick for 1.9 MeV protons). In order to avoid the recoil carbon ions and protons from p—p scattering the proton counter was fixed at backward angles. The detector for the protons was a 0.023 cm CsI crystal, exposed to the scattered protons inside a 20 cm diameter aluminium scattering chamber. For gamma ray detection, a 7.6 cm × 7.6 cm NaI crystal was used outside the chamber on a rotating arm. The axis of rotation was adjusted to the scattering centre by placing a weak Co^{60} source at the centre.

† This work was partially supported by the U.S. Atomic Energy Commission.

Fig. 1 shows some examples of the ungated inelastic proton spectrum displayed on a 256-channel pulse-height analyzer. At $E_p = 5.21$ MeV, no peak is present. At 5.37 MeV, a N^{13} level is excited and one sees the inelastic peak from

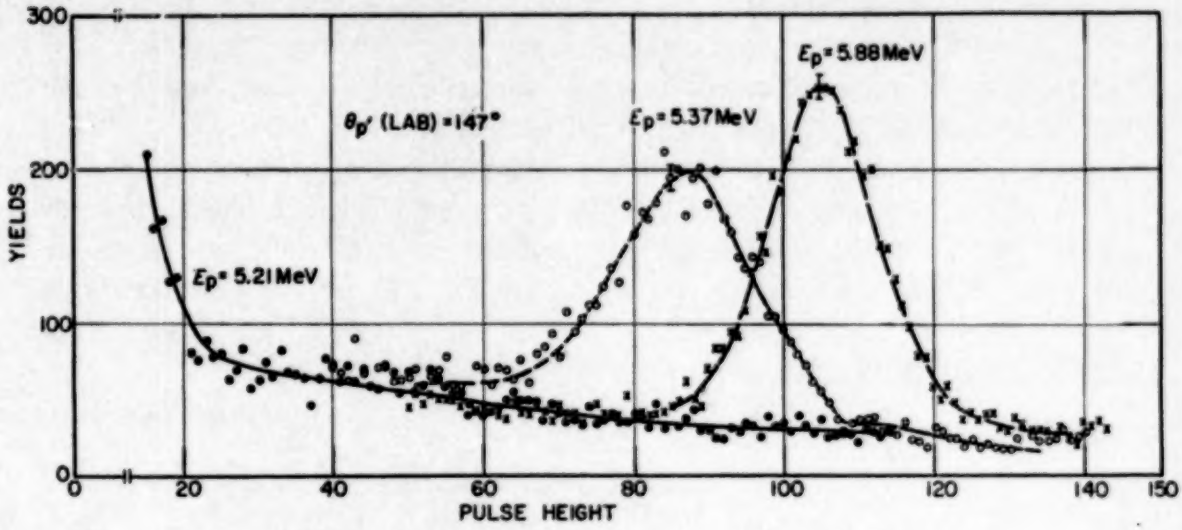

Fig. 1. Spectrum of inelastic protons from carbon.

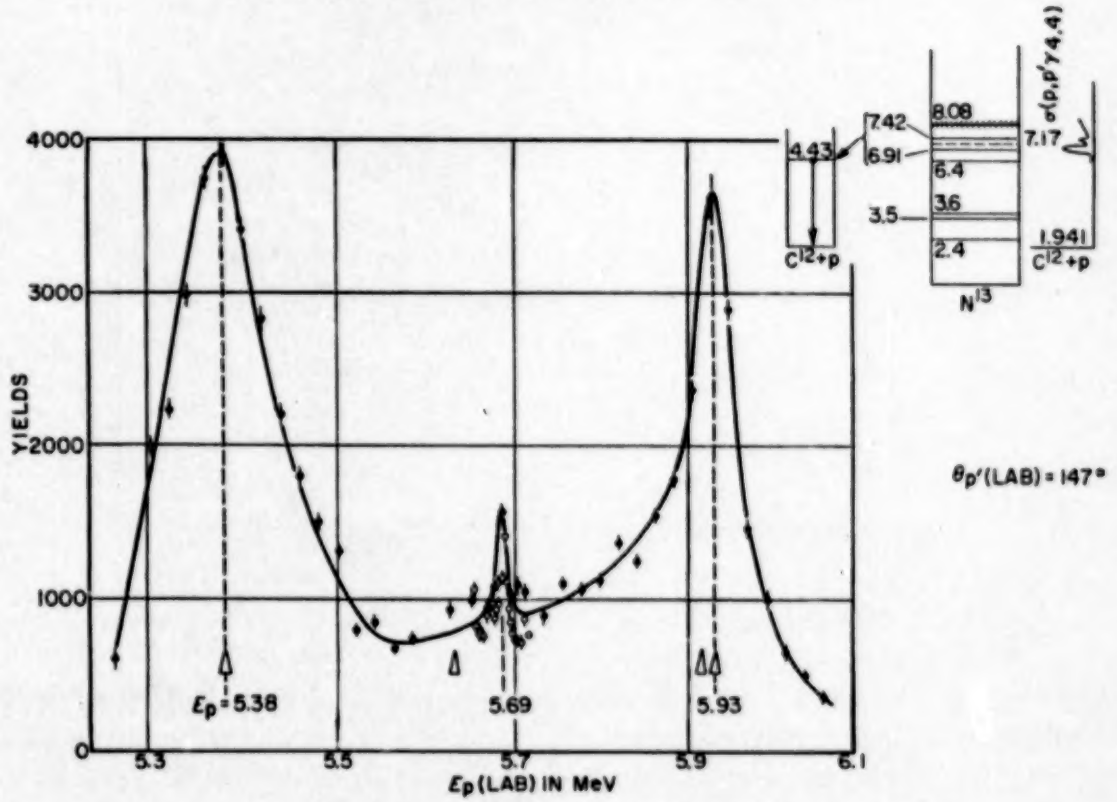

Fig. 2. Excitation curve for $C^{12}(p, p'\gamma)C^{12}$.

the subsequent decay to the first excited state of C^{12}. Another example is shown at 5.88 MeV.

Fig. 2 shows the excitation function for the inelastic protons at 147° in the

laboratory system. The curve is similar to the previously reported papers of several authors[5]), except for a weak peak present at 5.69 MeV about 20 keV wide. The resonance corresponds to an excitation of 7.17 MeV in N^{13}.

For correlation measurements the usual fast-slow coincidence method was used. The correlations were measured at the four different energies indicated by triangles in fig. 2. In particular, those measured at 5.38 MeV and 5.93 MeV are on resonances, corresponding to $\frac{3}{2}^+$, 6.91 MeV and $\frac{5}{2}^+$, 7.42 MeV levels in N^{13}. The proton counter was fixed at 111° throughout the measurement. Background counting rates varied from 0.2 to 1 % of the yield. The geometrical corrections due to the finite dimensions of the counters are[2]) for the gamma counter $J_2^\gamma/J_0^\gamma = 0.963$, $J_4^\gamma/J_0^\gamma = 0.890$, and for the proton counter J_2^p/J_{00}^p, $J_4^p/J_0^p > 0.99$. Figures to be shown in the next paragraph are, however, not corrected for such errors.

In fig. 3, the observed angular correlation is shown at the resonance corre-

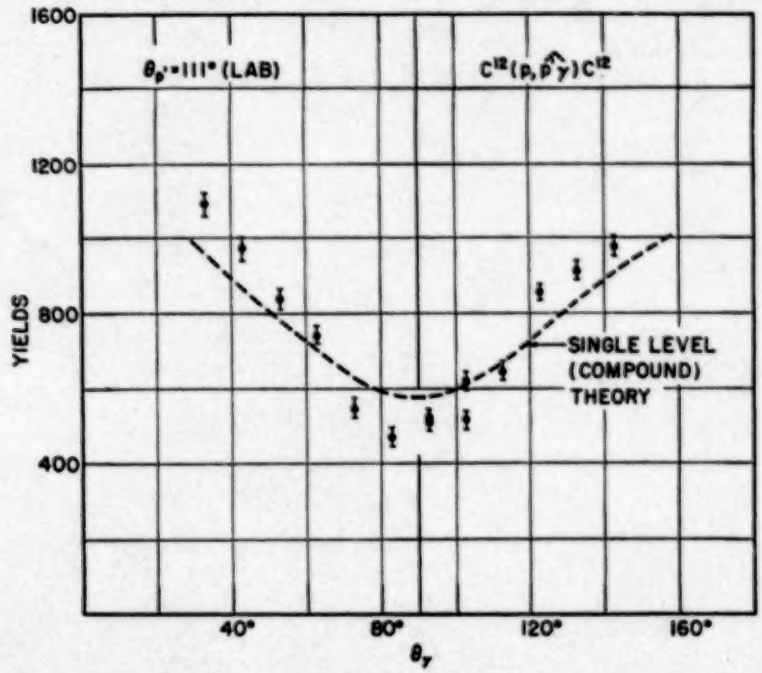

Fig. 3. Observed angular correlation at $E_p = 5.38$ MeV at the $\frac{3}{2}^+$ resonance.

sponding to the $\frac{3}{2}^+$ level in N^{13}. Experimental points show a slightly stronger correlation than is expected by compound nucleus theory[6]) taking an isolated $\frac{3}{2}^+$ level as an intermediate state. However, generally speaking, the fit is fairly good. Fig. 4 shows a correlation at 5.63 MeV, where the yields of (p, p') process are almost a minimum. At this energy the contribution from various levels can be considered. However, if we take only the s-waves for the inelastically scattered protons, the compound theory tells us that the correlation should be the same as the gamma distribution. The broken line is the experimentally

obtained gamma distribution at this energy. The correlation is still stronger than the gamma distribution, and there is a deviation from it at both ends of the curve. However, at 5.93 MeV, where $\frac{5}{2}^+$ resonance occurs, the correlation

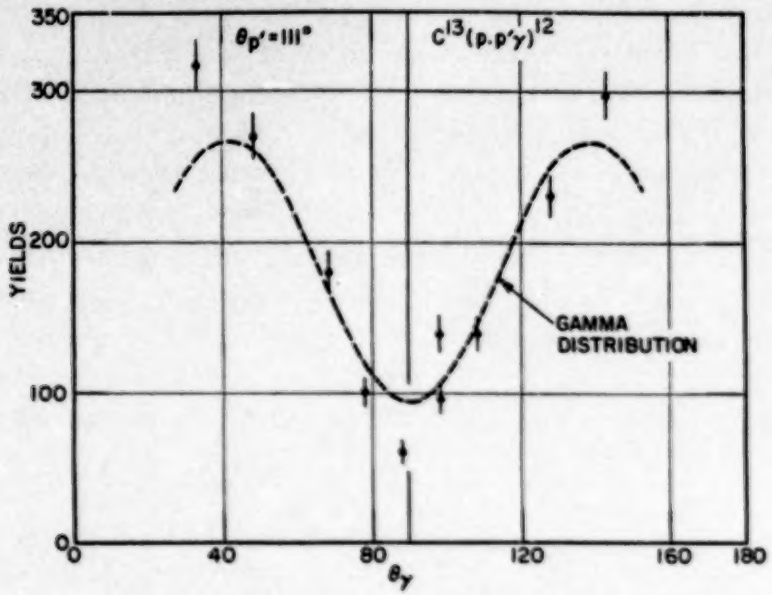

Fig. 4. Observed angular correlation at $E_p = 5.63$ MeV.

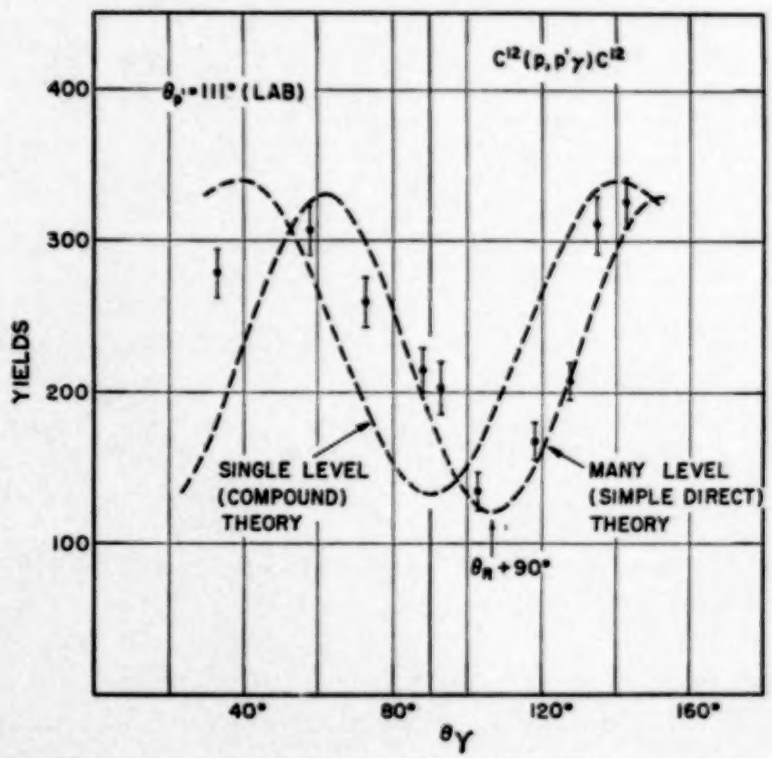

Fig. 5. Observed angular correlation at $E_p = 5.93$ MeV at the $\frac{5}{2}^+$ resonance.

pattern (as shown in fig. 5) no longer shows symmetry about 90°. The position of the minimum in the correlation coincides with the direction of the recoil

nucleus, a feature usually associated with the direct interaction. However, the whole distribution is asymmetric even around the recoil axis direction. In terms of the direct interaction theory, this signifies the presence of a large distortion of the incoming and outgoing proton wave. It may not necessarily be appropriate, however, to insist on direct interaction or the "incoherent" compound theory at this point. One of the adequate explanations would be that this state is mixed coherently with some other state. Yet, the gamma distributon at this energy can be almost entirely explained by $\frac{5}{2}^+$ assignment. From the excitation curve, and in order to meet the observed direct type character, this level overlaps a broad resonance which contains many resonances. We simply emphasize that at least one more level is involved in the present reaction at this particular resonance. If we go down in energy by 150 keV from the $\frac{5}{2}^+$ resonance (about 20 % of the half width), the correlation pattern changes considerably as shown in fig. 6. The tendency observed in the previous figure becomes more

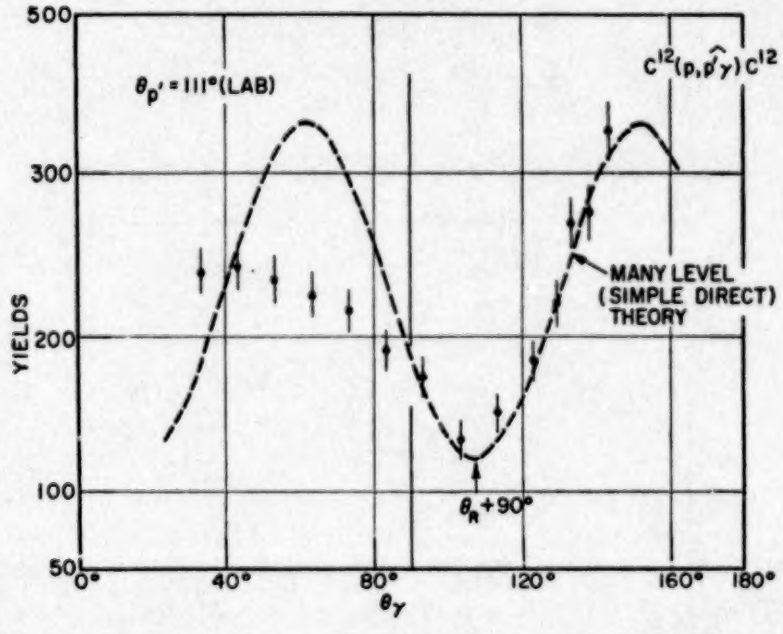

Fig. 6. Observed angular correlation at $E_p = 5.93$ MeV at the point 150 keV below the $\frac{5}{2}^+$ resonance.

pronounced: namely, the points in the forward angle flatten out whereas those in the backward angle are still steep.

The authors wish to express their sincere appreciation to Professor L. J. Lidofsky, Dr. T. H. Kruse and Dr. M. Morita for helpful discussions during the entire course of the experiment. Thanks are also due to Professor C. S. Wu, whose comments from time to time were illuminating. The authors are also obliged to Mr. H. D. Dieselman and Mr. R. A. Streeter, Jr., for taking part of the data.

References

1) R. Sherr and W. F. Hornyak, Bull. Am. Phys. Soc. **1** (1956) 197
2) H. Yoshiki, Phys. Rev. **117** (1960) 773
3) F. D. Seward, Phys. Rev. **114** (1959) 514
4) C. A. Levinson and M. K. Banerjee, Ann. Phys. **2** (1957) 471;
J. Sawicki, Nuclear Physics **7** (1958) 503
5) H. Schneider, Helv. Phys. Acta **29** (1956) 55;
C. Browne *et al.*, Phys. Rev. **104** (1956) 1099;
L. J. Lidofsky *et al.*, Bull. Am. Phys. Soc. **2** (1957) 29;
C. W. Reich *et al.*, Phys. Rev. **104** (1956) 143
6) A. A. Kraus *et al.*, Phys. Rev. **104** (1956) 1667;
W. T. Sharp *et al.*, Chalk River Report CRT-556

2.L *Nuclear Physics* **19** (1960) 448—452; © *North-Holland Publishing Co., Amsterdam*
Not to be reproduced by photoprint or microfilm without written permission from the publisher

GAMMA RAYS FROM THE INTERACTION OF 14-MeV NEUTRONS WITH CARBON

J. BENVENISTE, A. C. MITCHELL, C. D. SCHRADER and J. H. ZENGER

Lawrence Radiation Laboratory,
University of California, Livermore, California†

Received 21 April 1960

Abstract: The cross section for the $C^{12}(n, n')C^{12*} \rightarrow C^{12} + \gamma$ (4.43 MeV) reaction has been measured near 14 MeV by detecting the gamma rays at scattering angles of 30° to 150°. A time-of-flight technique was used to distinguish the gamma rays from the high neutron background. A least-squares fit to the data gives

$$\sigma(\theta) = (13.3 \pm 0.6) + (40.0 \pm 4.7)\cos^2\theta - (34.1 \pm 5.1)\cos^4\theta$$

for the angular distribution. The integrated cross section is $\sigma_{n,n'\gamma} = 249 \pm 28$ mb.

1. Introduction

When this work was begun there existed two serious measurements of the cross section for inelastic scattering of 14-MeV neutrons from C^{12}. The first[1]), an observation of the 4.43-MeV gamma rays with a three-crystal spectrometer, gave $\sigma_{n,n'\gamma}$ (4.43 MeV) = 245 ± 35 mb. The second[2]), a direct observation of the inelastically scattered neutrons by a time-of-flight technique, gave, for the group leaving C^{12} in its first excited state, $\sigma_{n,n'\gamma}$ (4.43 MeV) = 220 ± 30 mb. Since it has been demonstrated[3]) that no cascades occur from higher states to the level at 4.43 MeV, one expects that these two measurements will yield the same number. The reported agreement, however, is fortuitous.

The reason for this appears when one notes that in the first experiment gamma rays were observed at an angle of about 130° to the incident neutron direction. Isotropy was assumed in order to obtain the reported cross section. This means that the measured differential cross section was 19.5 mb/sr. In the second experiment, the complete angular distribution of the gamma rays was observed. When normalized to the measured cross section for inelastic scattering of neutrons to the 4.43-MeV level, this gave, for the gamma rays, a differential cross section which ranged from 13.1 mb/sr at 90° to 21.5 mb/sr at 150°.

To resolve this discrepancy, an absolute measurement of the differential cross section for the production of 4.43-MeV gamma rays was undertaken.

† This work was performed under the auspices of the U.S. Atomic Energy Commission.

2. Design of the Experiment

The Livermore Cockcroft-Walton accelerator employing the D-T reaction was used as the source of 14-MeV neutrons. Since the experimental techniques used have been described in detail in a previous report[4]), only brief mention of the important features will be made.

The method utilizes short bursts of neutrons incident on the scattering ring at a rate of 5 MHz. By using a flight path of about 2 m between the ring and the detector it was possible to separate in time gamma rays from any direct or scattered neutrons reaching the detector after each burst. Suitable timing, discriminating, and gating electronics enabled us to obtain a clean gamma spectrum on a multichannel analyzer.

The source neutrons were monitored by an alpha counter with an absolute precision of better than 2 %. A plastic scintillator was used as an auxiliary monitor to provide an additional check on the neutrons.

The gamma-ray detector consisted of a 4.45 cm diameter by 5.1 cm deep NaI scintillator on an RCA 6810A photomultiplier which was temperature controlled to minimize possible gain shifts. The efficiency of the detector was measured using the $N^{15}(p, \alpha)C^{12*}$ reaction to obtain 4.43-MeV γ rays.

The carbon ring was 2.5 cm thick, and had an inside diameter of 11.5 cm and an outside diameter of 16.5 cm. It could be moved by remote control so that the angle θ, between the incident neutron and the detected gamma ray, could be varied continuously between 30° and 150°. As a consequence of moving the ring with respect to the source, the energy of the incident neutrons also changed with angle over a range of about 1 MeV.

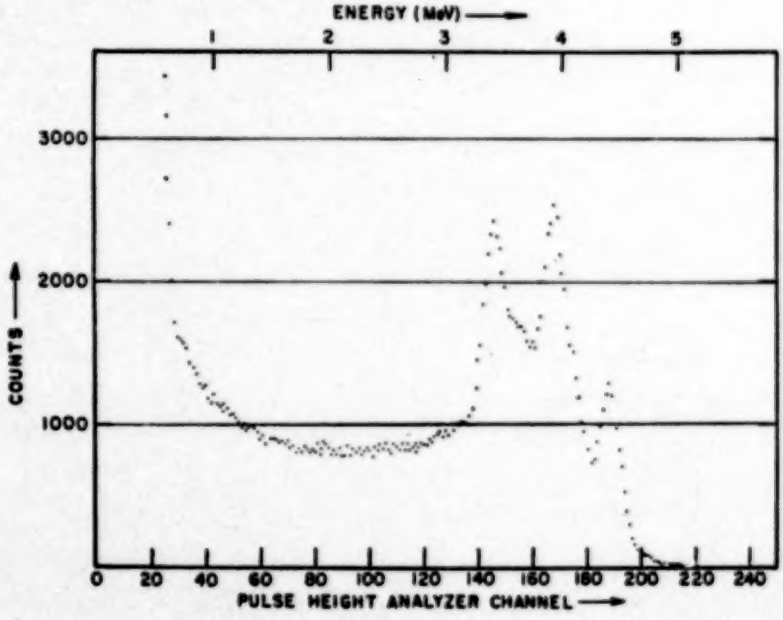

Fig. 1. 4.43-MeV gamma-ray spectrum.

Fig. 1 shows a typical spectrum of the $C^{12}(n, n'\gamma)C^{12*}$ gamma ray. It was known from a previous measurement that about 1% of the counts below 1.5 MeV is due to gamma rays originating in the Cockcroft-Walton target and subsequently Compton scattered into the detector by the carbon ring. We were able to correct for the Compton-scattered contribution by means of observations on a Be scatterer. The corrected spectra gave the same results at several bias levels.

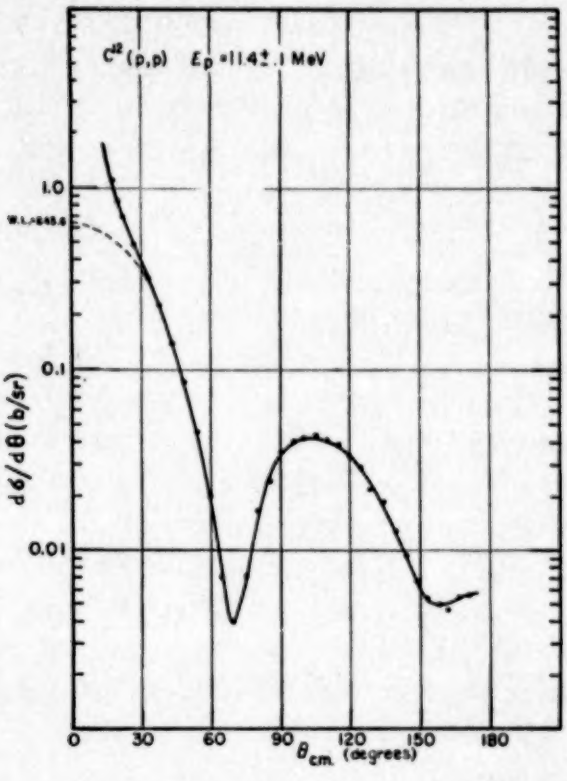

Fig. 2. Use of Wick Limit to derive neutron distribution from proton data.

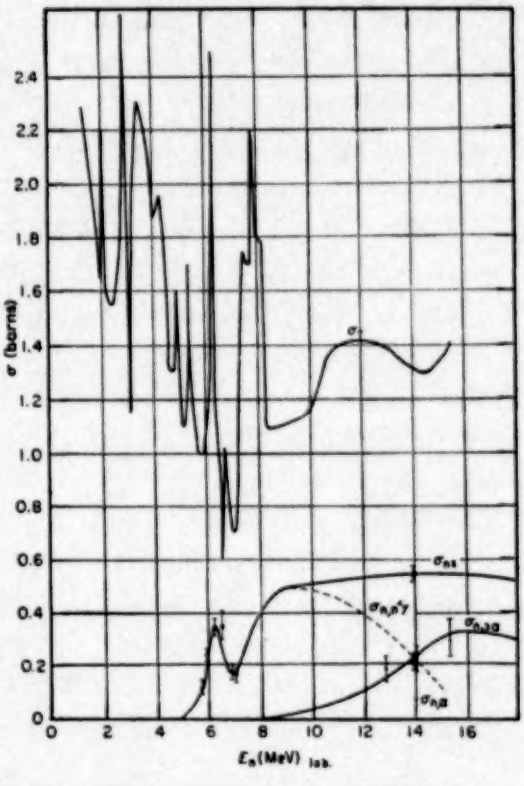

Fig. 3. Inference of $\sigma_{n,n'\gamma}$ (4.43 MeV) from available carbon cross sections.

The multiple-scattering problem was handled in much the same way as described in the earlier report. Because the threshold for producing the reaction in question is 4.8 MeV, however, it was necessary to follow all neutrons that had suffered an elastic or inelastic scattering in the primary interaction, until their energies had dropped below threshold or they had escaped the ring scatterer. Only those neutrons that had scattered inelastically from the 4.43-MeV state in C^{12} were considered, because of the small probability of exciting the 7.6-MeV state and because excitation of the higher states (e.g., 9.5 MeV, 11.2 MeV, etc.) leaves the neutron with less than the threshold energy.

To calculate the correction to the observations due to secondary interactions it is necessary to know the differential cross sections for elastic and inelastic scattering for a range of energies from 4.8 to 14.7 MeV. Unfortunately there is a dearth of data in this region.

Neutron elastic-scattering data are readily available at 14.2[5]), 7.0[6]), 6.3[6]), 6.0[6]) and 5.0[7]) MeV. At intermediate energies it is possible to use proton-scattering data by treating the differential cross section so that at 0° it smoothly approaches the "Wick Limit"[8]) $(k\sigma_T/4\pi)^2$. Proton data were obtained at 14.7[9]), 13.2[10]), 12.3[10]), 12.0[11]), 11.4[10]), 10.1[10]), 9.5[12]), and 8.5[10]) MeV. An example of this treatment is presented in fig. 2.

Inelastic neutron-scattering information at 14.2[2]) MeV was supplemented with proton data at 14.7[9]), 13.2[10]), 12.3[10]), 12.0[11]), 11.4[10]) and 10.1[10]) MeV. Only angular distributions were used; cross sections were derived from available data on non-elastic[13]), (n, n'3α)[14,15]) and (n, α)[15]) reactions. Fig. 3 summarizes the available information.

The use of proton data is not completely defensible, especially in the resonance region where neutron cross sections and angular distributions should not be expected to closely follow the proton behaviour. However, the multiple-scattering correction applied to our observations is typically 5 to 10 %, so that even a 20% uncertainty in the input data contributes only a 1 to 2 % uncertainty to the measurements.

3. Results and Discussion

The measured differential cross sections appear in fig. 4. The errors shown reflect the contributions that affect the angular distribution, namely, (1) the uncertainty of locating a specified bias level, (2) the uncertainty in our knowledge of the angular dependence of the neutron source strength, and (3) the correction due to absorption of incident neutrons, multiple scattering, and the

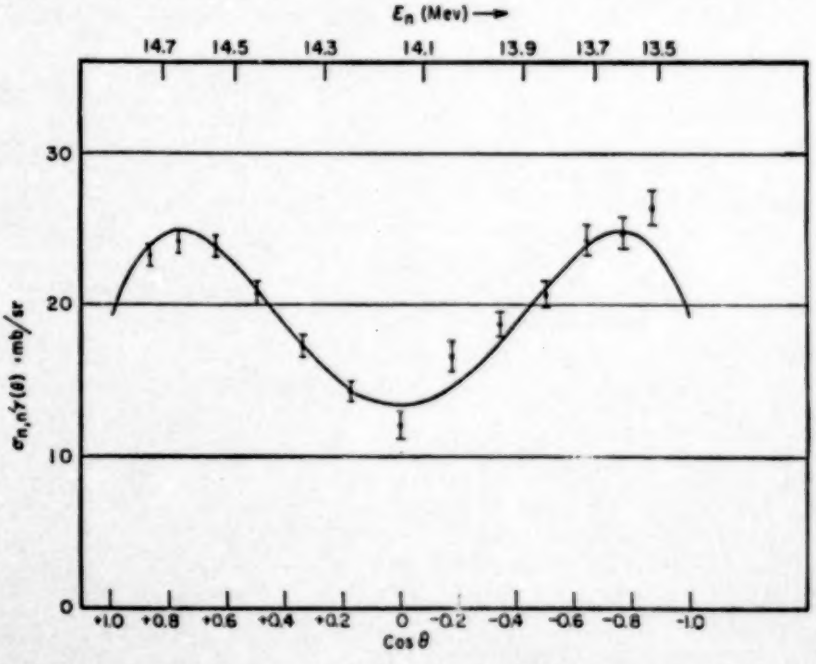

Fig. 4. Differential cross section for production of 4.43-MeV gamma rays by 14.1-MeV neutrons.

absorption of gamma rays emerging from the scattering ring. A least-squares fit to these data yields

$$\sigma(\theta) = (13.3 \pm 0.6) + (40.0 \pm 4.7)\cos^2\theta - (34.1 \pm 5.1)\cos^4\theta \text{ (mb/sr)} .$$

The integrated cross section is

$$\sigma_{n,\,n'\gamma}(4.43 \text{ MeV}) = 249 \pm 28 \text{ mb} ,$$

where the indicated uncertainty includes contributions from the absolute source-strength calibration and detector efficiency, in addition to those mentioned above.

We must confess to some surprise at finding such a high degree of symmetry in the differential cross section. We had expected considerable asymmetry to be displayed in view of the facts that the incident-neutron energy changes by about 1 MeV in the angular interval observed, and that the cross section seems to be falling with energy in the vicinity of 14 MeV. The observed symmetry suggests that the cross section does not vary as rapidly as we had expected from fig. 3, or else that the angular distribution is changing rapidly with energy.

It is our pleasure to acknowledge the help of Dr. Donald H. Davis in the determination of the multiple-scattering corrections. We would also like to express our gratitude to Chief Operator Roy V. Cedarlund and to Eric H. Carson, Alfred J. Horn, George L. Low, Darrell D. Malone, Edward J. Zaharis and Frank Ziskind, Jr., who operated the Cockcroft-Walton accelerator.

References

1) M. E. Battat and E. R. Graves, Phys. Rev. **97** (1955) 1266
2) J. D. Anderson, C. C. Gardner, J. W. McClure, M. P. Nakada and C. Wong, Phys. Rev. **111** (1958) 572;
J. B. Singletary and D. E. Wood, Phys. Rev. **114** (1959) 1595 (this paper confirms the observations of Anderson *et al.*)
3) R. D. Bent, T. W. Bonner, J. H. McCrary and W. A. Ranken, Phys. Rev. **100** (1955) 771
C. W. Cook, W. A. Fowler, C. C. Lauritsen and T. Lauritsen, Phys. Rev. **107** (1957) 508
C. D. Moak, A. Galonsky, R. L. Traughber and C. M. Jones, Phys. Rev. **110** (1958) 1369;
S. F. Eccles and D. Bodansky, Phys. Rev. **113** (1959) 608
4) J. Benveniste, A. C. Mitchell, C. D. Schrader and J. H. Zenger, UCRL-5596, June 9, 1959
5) M. P. Nakada, J. D. Anderson, C. C. Gardner and C. Wong, Phys. Rev. **110** (1958) 1439
6) Haddad and J. A. Phillips, WASH-1021, p. 20; private communication
7) R. W. Hill, Phys. Rev. **109** (1959) 2105
8) G. C. Wick, Atti Reale Acad. Italia Mem. Classe Sci, Fis. Mat. e Nat. **13** (1943) 1203
9) R. W. Peele, Phys. Rev. **105** (1957) 1311
10) J. Benveniste, R. Booth, A. C. Mitchell, C. D. Schrader and J. H. Zenger, unpublished
11) H. E. Conzett, Phys. Rev. **105** (1957) 1324
12) Burcham, Gibson, Hasaim and Rotblatt, Phys. Rev. **92** (1953) 1266
13) M. H. MacGregor and R. Booth, Phys. Rev. **112** (1958) 486;
J. R. Beyster, M. Walt and E. W. Salmi, Phys. Rev. **104** (1956) 1319
14) G. M. Frye Jr., L. Rosen and L. Stewart, Phys. Rev. **99** (1955) 1375;
L. L. Green and W. M. Gibson, Proc. Phys. Soc. **A62** (1949) 296;
Y. Tsuneoka, J. Phys. Soc. Japan **14** (1959) 869
15) E. R. Graves and R. W. Davis, Phys. Rev. **97** (1955) 1205

2.I *Nuclear Physics* **19** (1960) 453—460; © *North-Holland Publishing Co., Amsterdam*
Not to be reproduced by photoprint or microfilm without written permission from the publisher

PHOTOPROTONS FROM Cs AND I

R. B. TAYLOR

Research School of Physical Sciences, Australian National University, Canberra

Received 4 April 1960

Abstract: A study has been made of photoprotons emitted from Cs and I by irradiating a thin CsI(Tl) crystal with a bremsstrahlung beam and detecting the protons in the same crystal. The photoproton spectra for different bremsstrahlung end point energies all show a broad peak at 8 MeV after correcting for "escape" protons. The proton yield was also measured and a peak cross section of (18 ± 2) mb found at 25 MeV while the integrated cross section to 32 MeV was measured as (136 ± 30) · MeV · mb.

1. Introduction

The study of photoprotons arising from nuclei bombarded with bremsstrahlung has been hampered by the difficulty of detecting the protons in the presence of an accompanying electron background. As a result the data available are few compared with those for (γ, n) reactions and, in the region $Z > 50$, knowledge of (γ, p) reaction is confined to a few isolated elements. This region is important as it is here that the statistical model of the nucleus breaks down and direct processes play an important part in the mechanism of (γ, p) reactions[1]).

Some work has been carried out by measuring proton spectra and yields from bremsstrahlung radiation using photographic emulsions[2]) and with these it is possible to detect protons with energies as low as 3 MeV. ZnS detectors, which are insensitive to electrons but do not allow determination of proton energies, have also been used extensively by Halpern and Weinstock[3]) to measure the proton yields from many nuclei spread throughout the periodic table. Another method of obtaining the (γ, p) yields and cross sections is by activation methods but this is limited to the few nuclei which lead to radioactive end products on emission of a proton; they give no information about the proton energy spectra. Some work has been done in this laboratory using CsI crystals as detectors[4]) in an endeavour to determine the proton energies but this was limited to energies greater than 10 MeV.

The present paper describes a method of measuring both the (γ, p) yield and the proton spectra from Cs and I using a CsI(Tl) crystal scintillation counter and the bremsstrahlung from the Canberra 33 MeV synchrotron. The method uses the scintillation crystal both as the target and as a proton detector. A very thin crystal is employed and although this means that some protons are not stopped in the crystal accurate "escape" corrections can be applied.

The method is suitable for most scintillating crystals and CsI was used initially as both Cs and I have $Z > 50$ ($_{55}Cs^{133}$; $_{53}I^{127}$) and are close together on the periodic table. CsI also has the advantage of being an easy crystal to prepare as it is not deliquescent. It would be expected that the results from Cs and I would be similar owing to the similarity of Z values and the binding energies for proton emission, which differ[5]) by only 5 keV (see table 1). Also the

TABLE 1

Comparison of some properties of Cs and I

	Cs	I
Z	55	53
A	133	127
Coulomb barrier (MeV)	10.7	10.6
Binding energy of the last proton (MeV)	6.462	6.467
(γ, np) threshold (MeV)	15.4	15.3
(γ, α) threshold (MeV)	2.3	2.0

known systematics[3, 6]) of (γ, p) reactions do not suggest large variations between neighbouring nuclei and it will therefore be assumed that they have similar (γ, p) cross sections and that the protons have the same energy distribution.

2. Method and Procedure

The scintillation counter consisted of a 1.9 × 1.9 × 0.051 cm CsI(Tl) crystal mounted on a perspex disk attached to an E.M.I. (type 6097) photomultiplier. The entire counter was enclosed in a light tight Al can which had a thin Al window (3 mg/cm^2) for the beam to enter. The pulses from the photomultiplier were amplified and sorted in a Hutchison-Scarrott pulse-height analyser which was gated so that it only accepted pulses when the synchrotron beam was on; this reduced spurious background pulses to a negligible level.

The choice of the crystal dimensions was determined by the electron background which arises in two ways. An electron of long path length in the crystal will give a pulse like that of a low energy proton while if two or more electrons travel simultaneously through the crystal the pulses will add together and also look like a proton pulse. To overcome the first effect a very thin crystal was used and since electrons are emitted mainly in the forward direction[7]) the probability of an electron travelling any distance in the crystal was very small. The problem of pile-up was overcome by keeping the beam down to a suitable intensity. The crystal could not be made too thin or the number of protons actually stopping in the crystal would be too small to allow accurate "escape" corrections to be applied.

The number of electron pulses compared to proton pulses was further reduced by passing the γ-ray beam through 127 cm of graphite to harden it as shown in fig. 1. Also the length of the pulses from the counter was kept to a minimum (1 μs) while the beam pulse was lengthened to 200 μs. A check was made to see if there were any pulses due to multiple electron events in the crystal. This was

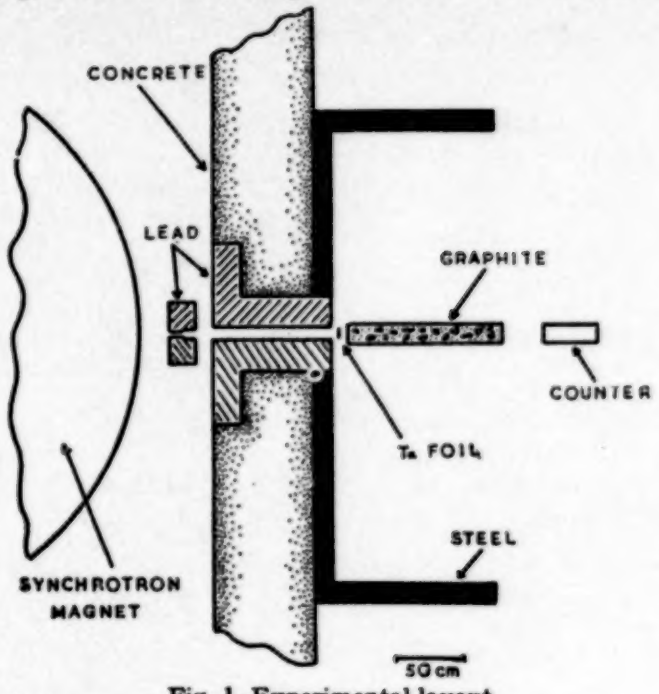

Fig. 1. Experimental layout.

possible because the number of multiple events was proportional to the beam intensity whereas single events are independant. Therefore by conducting several runs at different beam intensity (same total dose) multiple events would be seen as extra pulses in the high intensity runs. No such pulses were observed greater than 3 MeV.

The counter was calibrated with 8.8 MeV alpha-particles from ThC. The relative light response for α-particles and protons was measured by comparing the α peak with the known proton peaks from the (γ, p) reaction in CsI using 17.6 and 14.8 MeV γ-rays from the Li(p, γ) reaction[8]). The light response of the CsI crystal for protons is known to be linear up to 11 MeV[9]) and has been assumed to be linear up to 26 MeV. The resolution for 8.8 MeV α-particles was 6 %.

The total bremsstrahlung dose was monitored by activity induced in Ta foils placed in front of the graphite and was measured by detecting the 55 keV K-capture X-ray from the 8.15 h Ta^{180m} with a scintillation spectrometer. Each disk was left for at least 1 hour after irradiation to allow the 10 min activity from Ta^{178} from the $Ta^{181}(\gamma, 3n)$ to decay away (see Carver and Turchinetz[10])). Absolute yields were obtained by comparing the Ta activity with the $Cu^{63}(\gamma, n)$ activity and using the $Cu^{63}(\gamma, n)$ cross section measured by Berman and Brown[11]).

Spectra were obtained at 1 MeV steps of the bremsstrahlung end point from 14–32 MeV, each spectrum being the sum of 10 one-hour runs. The final spectra were corrected for protons escaping from the crystal.

3. Correction for Protons Escaping from the Crystal

The equations for determining the number N of particles of range R that are stopped completely in an infinite thin crystal are

$$\left.\begin{aligned} N &= N_0\left(1-\frac{R}{4t}\right) && (R<2t)\\ N &= N_0\left(\frac{t}{R}\right) && (R>2t)\end{aligned}\right\}\ \text{isotropic distribution,}$$

$$\left.\begin{aligned} N &= N_0\left(1-\frac{R}{8t}\right) && (R<2t)\\ N &= N_0\left(\tfrac{1}{3}+\frac{t}{R}-\frac{2t^3}{3R^3}\right) && (R>2t)\end{aligned}\right\}\ \sin^2\theta \text{ distribution.}$$

where, $2t$ is the thickness of the crystal and it is assumed that the particles are produced uniformly throughout the crystal. From these formulae it is possible to derive the number of particles of maximum range R in the crystal that will travel a distance r before leaving the crystal. For the case of an isotropic distribution of particles this is given by

$$N' = N_0\frac{1}{4t} \quad (r<2t,\ r<R)\,,$$

$$N' = N_0\frac{t}{r^2} \quad (r>2t,\ r<R)\,.$$

By using the range-energy relation for protons in CsI derived from Arron's tables[12]) the observed spectra were corrected.

The main problem associated with such corrections was that they are dependent on the angular distribution of the protons (see above) which is at present unknown. However, by taking the two extreme angular distributions (i.e. isotropic and $\sin^2\theta$) it can be shown that the difference in the calculated proton yields is only 4 % for the crystal that was used while the difference in the spectral shape was less than the statistical uncertainty. Since any error due to uncertainty of the angular distribution will be 4 % or less it will be neglected and all the present data were calculated assuming an isotropic distribution of the protons.

4. Results and Discussion

Fig. 2 shows some of the uncorrected photoproton spectra and all show evidence of a pronounced "valley" at 4 MeV. The sharp rise in counting rate below 4 MeV is due to electrons and protons which leave the crystal. To con-

sider how far the electron edge extended several runs were done at low bremsstrahlung energies (12–15 MeV, fig. 1) where the proton emission was negligible. Pulses greater than 4 MeV were not observed although it was energetically

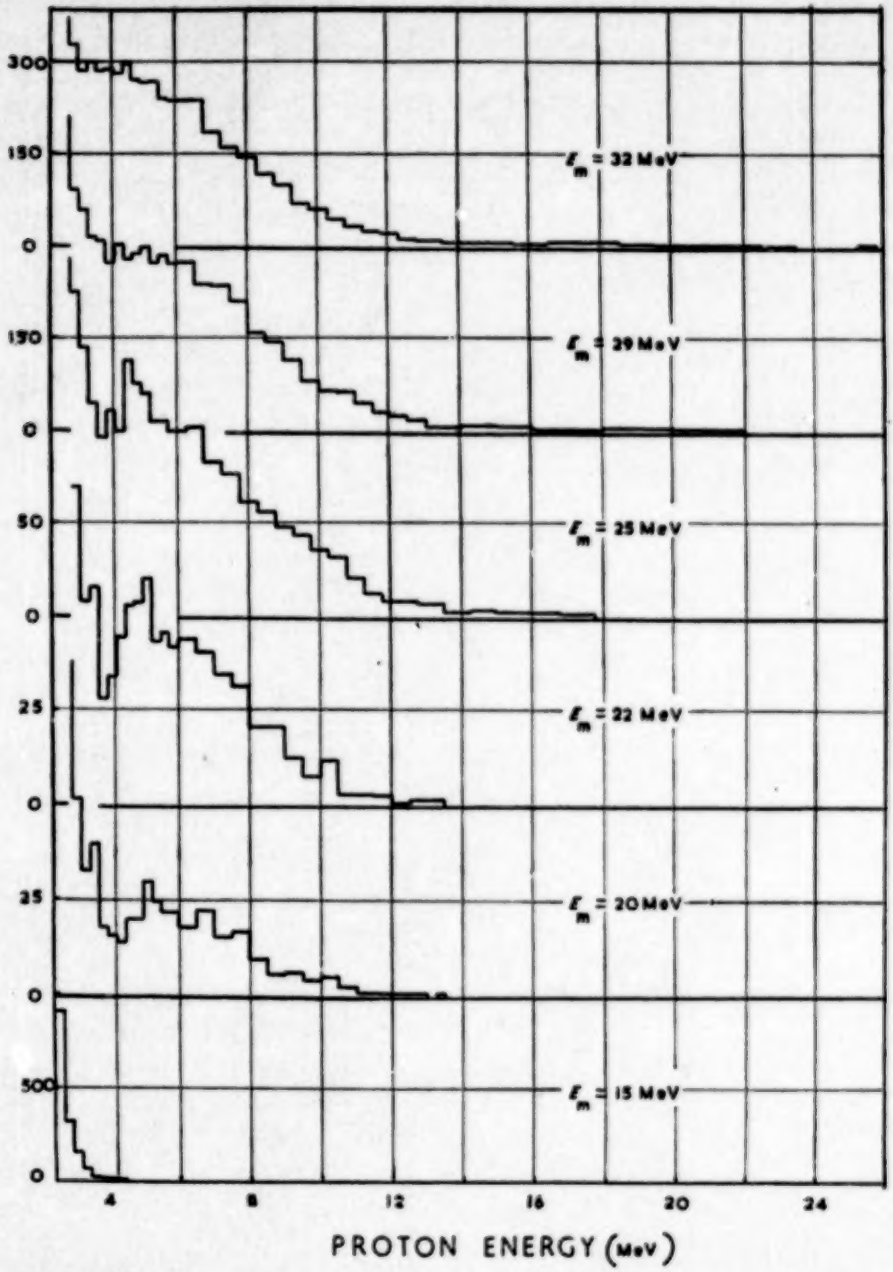

Fig. 2. Photoproton spectra with correction for escaping protons. Numbers on the ordinate indicate the number of protons per $\frac{1}{4}$ MeV interval.

possible to get pulses up to 15 MeV from the electrons. Using the shape of the electron edge obtained at low energies it was possible to estimate the effect of the electron edge at higher bremsstrahlung energies, and the number of pulses greater than 4 MeV caused by electrons was estimated to be less than 2 % for a bremsstrahlung energy of 30 MeV and less than 4 % at 17 MeV.

The possibility that the observed pulses were due to other effects than the (γ, p) in CsI was considered. Any reaction which leads to the emission of a charged particle could give pulses and the following were considered to be the most important: (n, p), (γ, α), $(\gamma, np + d)$ in Cs and I, and the (γ, p) in the perspex mount. The effect of the (n, p) reaction was obtained by measuring

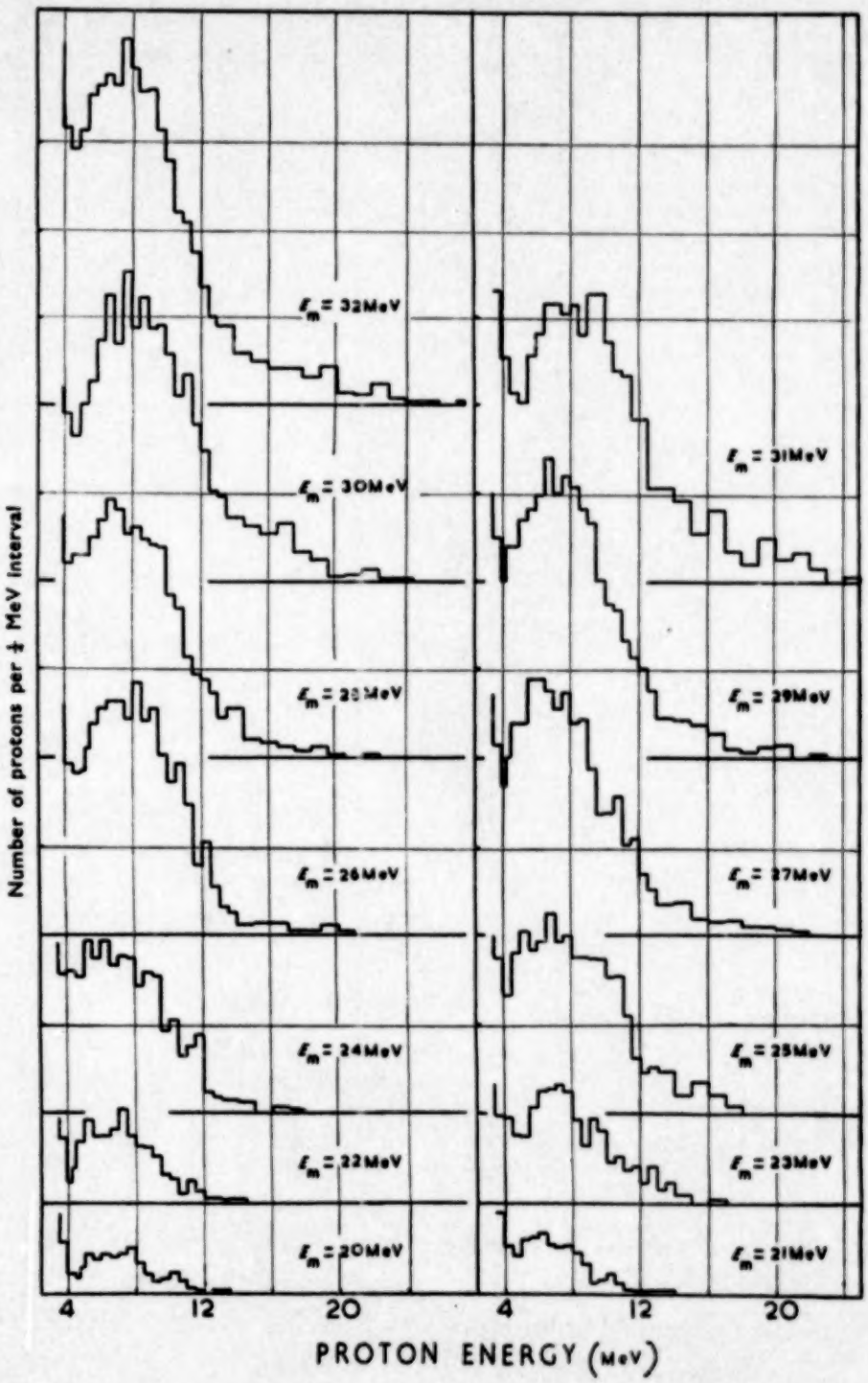

Fig. 3. Photoproton spectra corrected for proton losses and normalised to the same γ-ray beam

the number of (n, p) events using a standard Ra-Be source and normalising to the number of neutrons in the gamma-ray beam; it was found to be small (0 ± 1 %). The effect of the (γ, α) reactions was considered negligible from the known systematics of these reactions and the 20 MeV Coulomb barrier which the α-particles would have to penetrate. The (γ, p) reaction in the perspex would arise from the C^{12} content and an estimate of this effect was made using the results of Halpern and Mann[6]). The number of protons emitted from the nucleus with energy greater than 4 MeV is very small due to the high binding energy of the proton (16 MeV) and the shape of the (γ, p) cross section (peak at 21.5 MeV, being 1.7 MeV wide). The (γ, np + d) reaction in Cs and I has never been measured, but from other (γ, np) + d) results it is reasonable to suppose that the effect would be negligible at low energies although it may be important in the region 27–32 MeV.

Fig. 3 shows the corrected spectra normalised to the same γ-ray dose. These show that there are very few protons emitted from the nuclei of Cs and I with an energy less than 4 MeV and this is consistent with a Coulomb barrier of 10 MeV. The position of the peak increases only slightly with increasing bremsstrahlung energy which is what is expected from both the statistical model and Wilkinson's "resonance-direct" model[1]); its position fits in well with the known systematics of (γ, p) reactions[2]).

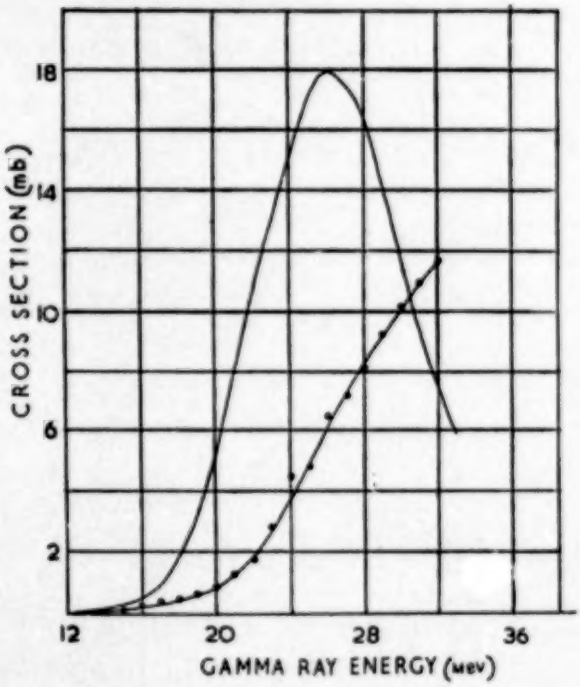

Fig. 4. Measured cross section and yield curve for Cs and I.

The (γ, p) cross section (fig. 4) was obtained from the measured yield curve using the method described by Carver and Lokan[13]) making allowances for the change in bremsstrahlung shape due to the absorption of the graphite. The

peak in the cross section is found at 25 MeV, the maximum cross section being 18 ± 2 mb and the integrated cross section to 32 MeV $(136 \pm 30) \cdot$ MeV. A comparison with other (γ, p) measurements cannot be made because the only other work in this region ($Z > 50$) has not gone beyond 25 MeV. This is unfortunate as a large proportion of the yield comes from γ-rays of energy 25 MeV. The fact that the proton yield beyond 25 MeV, measured in this experiment, is large makes is desirable to obtain more data in this region (nuclei with $Z > 50$) to obtain a better picture of the roles the various nuclear models play in the process.

The measured value of 17×10^4 protons $(\text{mole} \cdot \text{R})^{-1}$ at 23 MeV agrees with the proton yields measured by Weinstock and Halpern[3]) for nearby nuclei. To compare the results with the theoretical value obtained by Wilkinson[1]) it is necessary to make an assumption about the total absorption of gamma-rays at 23 MeV. It will be assumed that 80 % of the absorption leads to the emission of a neutron. This gives a value of 1 % for the proton emission to total absorption. The value of 14×10^6 neutrons $(\text{mole} \cdot \text{R})^{-1}$ for the yield at 23 MeV for the (γ, n) reaction in I was used to calculate the total absorption. It will be of great interest to measure proton yields for other heavy nuclei using bremsstrahlung energies in the region of 30 MeV.

The author wishes to thank Dr. J. Carver for many helpful discussions. He is grateful to the Australian National University for a Scholarship which enabled him to carry out the work.

References

1) D. H. Wilkinson, Physica **22** (1956) 1039
2) E. M. Toms and W. E. Stephens, Phys. Rev. **92** (1952) 363
3) E. Weinstock and J. Halpern, Phys. Rev. **94** (1954) 1651
4) K. H. Lokan, Proc. Phys. Soc. **73** (1959) 697
5) A. H. Wapstra, Handbuch der Physik **38** 10
6) J. Halpern and A. K. Mann, Phys. Rev. **83** (1951) 370
7) R. D. Evans, The Atomic Nucleus, p. 695
8) I. Wright, private communication
9) I. Wright, private communication
10) J. H. Carver and W. E. Turchinetz, Proc. Phys. Soc. **81** (1958) 613
11) A. I. Berman and K. L. Brown, Phys. Rev. **96** (1954) 83
12) W. A. Arron, B. C. Hoffman and F. C. Williams, A.E.C.U.-663
13) J. H. Carver and K. H. Lokan, A. J. Phys. **10** (1957) 312
14) Montalbetti, Katz and Goldenberg, Phys. Rev. **91** (1953) 659

1.E.1:
4.E

Nuclear Physics 19 (1960) 461—481; © *North-Holland Publishing Co., Amsterdam*
Not to be reproduced by photoprint or microfilm without written permission from the publisher

THE DECAY OF Ir^{194}

J. KERN† and G. BÄCKSTRÖM

The Institute of Physics, Uppsala

Received 5 May 1960

Abstract: The decay of Ir^{194} has been investigated by means of a double focusing spectrometer, mostly by the photo-electron technique. A total of 32 transitions has been observed, and their energies and intensities have been measured. An internally converted transition of 1480 keV, for which no gamma ray could be detected, showed that a 0+ state of this energy is populated. The log *ft* values for the beta branches showed that all the 18 levels excited are of even parity. By comparision of the measured gamma intensities with the conversion intensities of corresponding transitions in the decay of Au^{194}, spin values could be assigned for many levels. Evidence for a new 0+ state at 1547 keV was obtained in this manner. Indications were found for E0 admixture in competition with M1 and E2 multipolarities. A state at 923 keV may be interpreted as the 3+ level in the asymmetric rotor theory.

1. Introduction

The decay of Ir^{194} proceeds by negaton emission with a halflife of 19 hours. The most comprehensive investigation of this radioactivity has been made by Johns and Nablo[1]), and their work comprises measurements with a double focusing spectrometer of the continuous beta-spectrum, which was carefully separated into components, and of the photo-electron spectrum from gold and uranium radiators. The momentum resolution varied between 0.8 % and 2 %. In the region below about 1 MeV there was considerable interference from the longer-lived isotope Ir^{192} and the contribution of this activity was subtracted from the total spectrum. Photo-lines from 16 gamma rays were discovered (table 1). A level scheme of Pt^{194}, involving 10 excited states, was proposed on the basis of transition energies and of scintillation coincidences between a few of the strongest lines. Levels at 328 keV, 621 keV and 1265 keV were especially well established and have also received support from a later coincidence work[2]).

The level scheme of Pt^{194} may alternatively be studied through the decay of Au^{194}. A recent paper by Bäckström, Bergman, Burde and Lindskog[3]) reports an extensive study of this isotope, resulting in a decay scheme of 29 levels. A summary of important findings in earlier investigations is also found in this article.

There is evidence that the spins of the iridium and gold nuclei are the same, and hence, the same levels are expected to be populated, with allowance for the difference in mode of decay and disintegration energy (2236 keV for Ir^{194}

† On leave of the University of Fribourg, Switzerland.

and 2509 keV for Au^{194}). However, there are 15 additional levels in platinum, as observed in the gold decay, which for energy reasons could also be populated by the iridium decay. Furthermore, two of the levels proposed by Johns and Nablo (1836 keV and 1946 keV) have no correspondence in the gold decay scheme. There is also some doubt as to the identification of a few transitions.

Some problem has arisen concerning the 1480 keV level, which, according to evidence found by Bäckström *et al.*, should have spin zero and even parity. Johns and Nablo, however, report a gamma ray fitting as a ground state transition. The present work was initiated partly in order to investigate the origin of this transition. It was also considered worth while to remeasure regions of the gamma spectrum where more lines were found in the gold spectrum than has been reported for iridium. Apart from indicating whether additional levels are populated through the decay of Ir^{194}, such a study may actually help to assign positions for a few transitions observed but not located in the decay of Au^{194}, since any transition appearing in the iridium spectrum has to originate from a level lower than about 2.2 MeV. In particular, it helps to decide which of the possible alternative locations of a transition is associated with the highest intensity. The lower Q-value, and also other factors, induce a different population of levels, in this case, than in the Au^{194} decay. The consistency of the decay schemes may accordingly be checked by comparing the transition branching from corresponding levels in both types of decay.

2. Internal Conversion Experiments

All experiments reported in this paper were carried out by means of a 50 cm radius double focusing spectrometer[4]). Fairly thin sources ($\approx 100\ \mu g/cm^2$) were prepared by electroplating iridium, irradiated in the pile at a flux of $3 \times 10^{12}/cm^2 \cdot sec$, onto a palladium foil. The resulting source strengths were of the order of 1 mc. An attempt was made to determine conversion coefficients by measuring the internal conversion lines and by comparing these to the published gamma-ray intensities. The observation of these lines was, however, found to be exceedingly difficult because of the intense ground state beta branch (68 %). Only with the strongest transitions, of 328 keV and 294 keV, was the height of the K conversion lines comparable to that of the beta background at the resolution employed (≈ 0.4 %). A considerable improvement could be obtained by increasing the resolution, but this would require much higher specific activities than presently available.

The 1480 keV transition was the only one in the MeV region for which an accurate conversion measurement could be carried out. The line is shown in fig. 1 together with 328.5 K† which was used as an intensity standard. The

† In this paper the symbol 328 K means: the K conversion line of the 328 keV transition. By 328 alone is meant the transition of 328 keV.

position of 1480 K coincided well ($\frac{1}{10}$ of a half-width) with the previously measured line in the spectrum of Au^{194}. The conversion intensity ratio was found to be $I_K(1480)/I_K(328) = 0.037$. On the basis of the theoretical conversion coefficient for 328 ($\alpha = 0.048$) and the gamma intensities given by Johns and Nablo, the conversion coefficient of 1480 may be computed: $\alpha = 0.24$. This

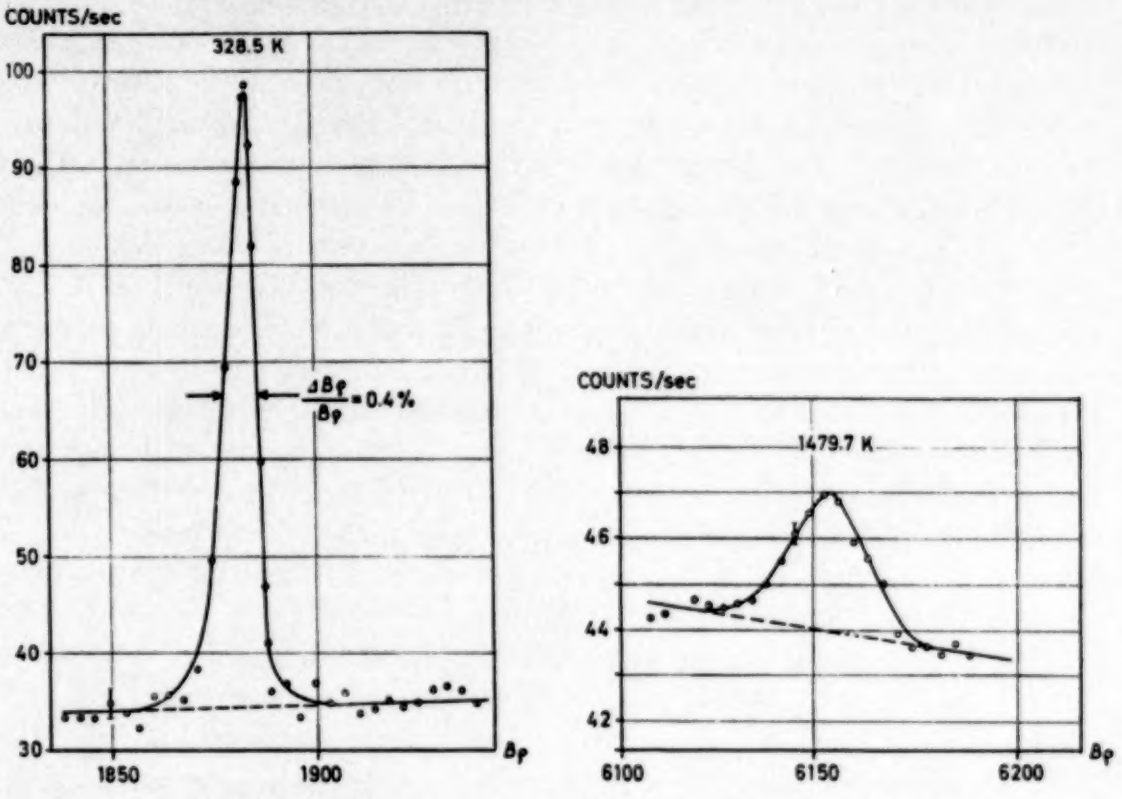

Fig. 1. Conversion lines measured in order to ascertain the multipolarity of 1480.

value is higher by a factor of 6 than that calculated for M5, and, since there can be no population in this decay of states with such high spin, it must be concluded that the observed 1480 K is an E0 transition.

Using the published gamma-ray intensities and the theoretical conversion coefficient (E2) for 1151, one finds $I_K(1480)/I_K(1151) = 5$, while in the decay of Au^{194} this ratio has been found to be 11. Considering the errors involved in measuring gamma intensities by the method of Johns and Nablo, this deviation need not be significant, however.

3. Photo-electron Experiments

The sources consisted of rods, 15 mm long by 1.5 mm diameter, of spectroscopically pure iridium, that had been activated in a pile for one or two days at fluxes ranging from 10^{12} to 10^{13}/cm^2·sec. In the measurements the sources were kept in beta-absorbing copper capsules with a wall thickness of 1 mm.

The source strengths varied between 1 and 15 curies, the strongest sources being used at high energy. Samples of a well chosen intermediate strength had to be used for the experiments designed to yield the intensity ratio between the low and high energy lines.

A twin Geiger tube was used for electron detection. The two parts, which are separated by a thin separating wall (1 mg/cm^2), can be operated in coincidence, and this arrangement was used in all experiments involving energies > 500 keV. The obvious advantage of this detector is that the counting background is suppressed, and this was found quite important when measuring lines in the region of 2000 keV. At lower energies than this, the Compton distribution is the predominating bakground, and therefore no suppression was actually achieved. However, the coincidence arrangement eliminates the spurions counts that a Geiger tube is liable to produce at high counting rates and thus reduces the counting errors to a well known statistical fluctuation. Consequently, useful data have taken with a statistical deviation of a few part in 10^3.

Use was made of both uranium and lead radiators, the latter element being used in cases where a K line from uranium would have coincided with an L or M group of another transition. The radiator thickness was chosen with regard to the energy and intensity of the lines to be observed, and the weight varied between 3 and 25 mg/cm^2. The resulting relative half-width of the lines was between 0.4 and 1.0 %.

The aim of the experiments was to conduct a thorough search of the whole region of energies > 850 keV and, furthermore, a search for isolated lines of lower energy which had been reported to exist in the decay of gold. The time spent per point was usually 5 to 15 min, and each point was corrected for the 19 hours decay. It was always attempted to cover as large an energy region as possible with the same source, since this gives more accurate information on the variation of the Compton background. It was not considered worthwhile to measure separately the continuous background, especially since the use of different converter materials often made it possible to measure the background of K-lines. The spectra were analyzed in such a manner that L and M groups were reconstructed on the basis of position and height of the corresponding K-line, the necessary intensity ratios being taken from empirical data. New transitions were actually discovered by this procedure. In some cases, K-lines were found to possess an unusual shape, and the components were then resolved purely graphically, the spectrum of Au^{194} being used as a guide in deciding the number and the spacing of the components. Examples of spectra are shown in figs. 2a–l.

In the present investigation, transition energies were determined mainly with the intention of establishing the identity of transitions relative to those found in the electron capture decay[3]), since the accuracy generally is lower in the photo-electron experiments. It was preferred, therefore, to utilize the

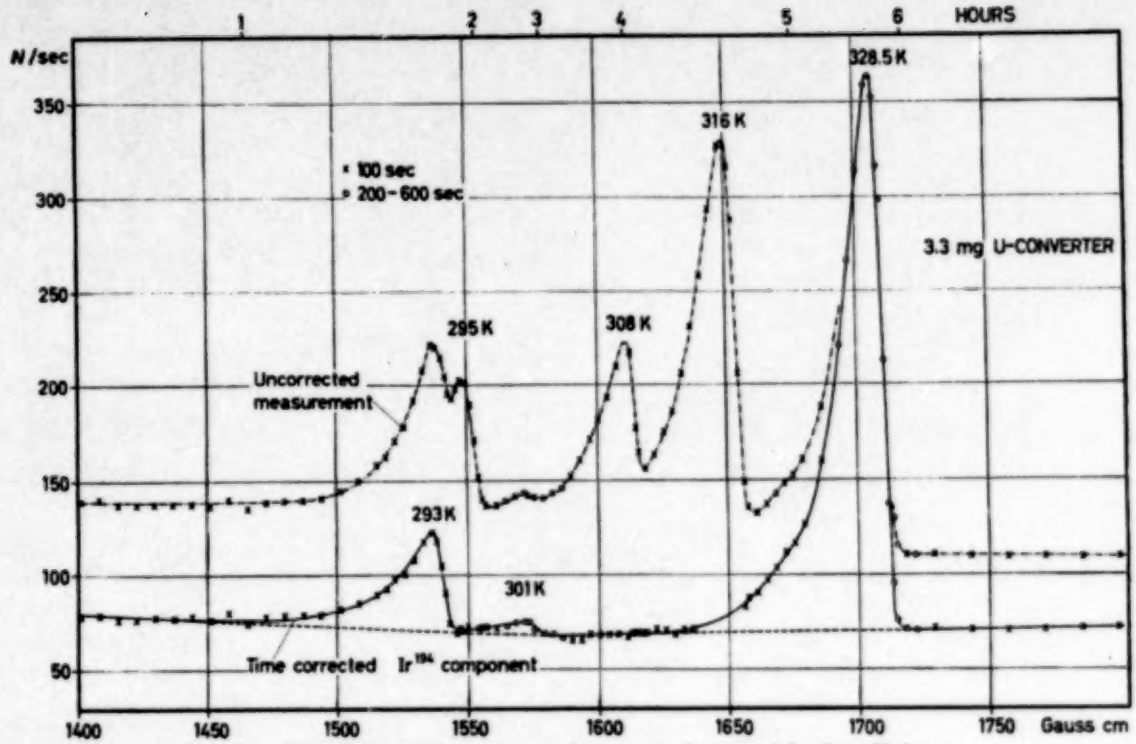

Fig. 2a. Photo-electron spectrum from uranium and lead radiators.

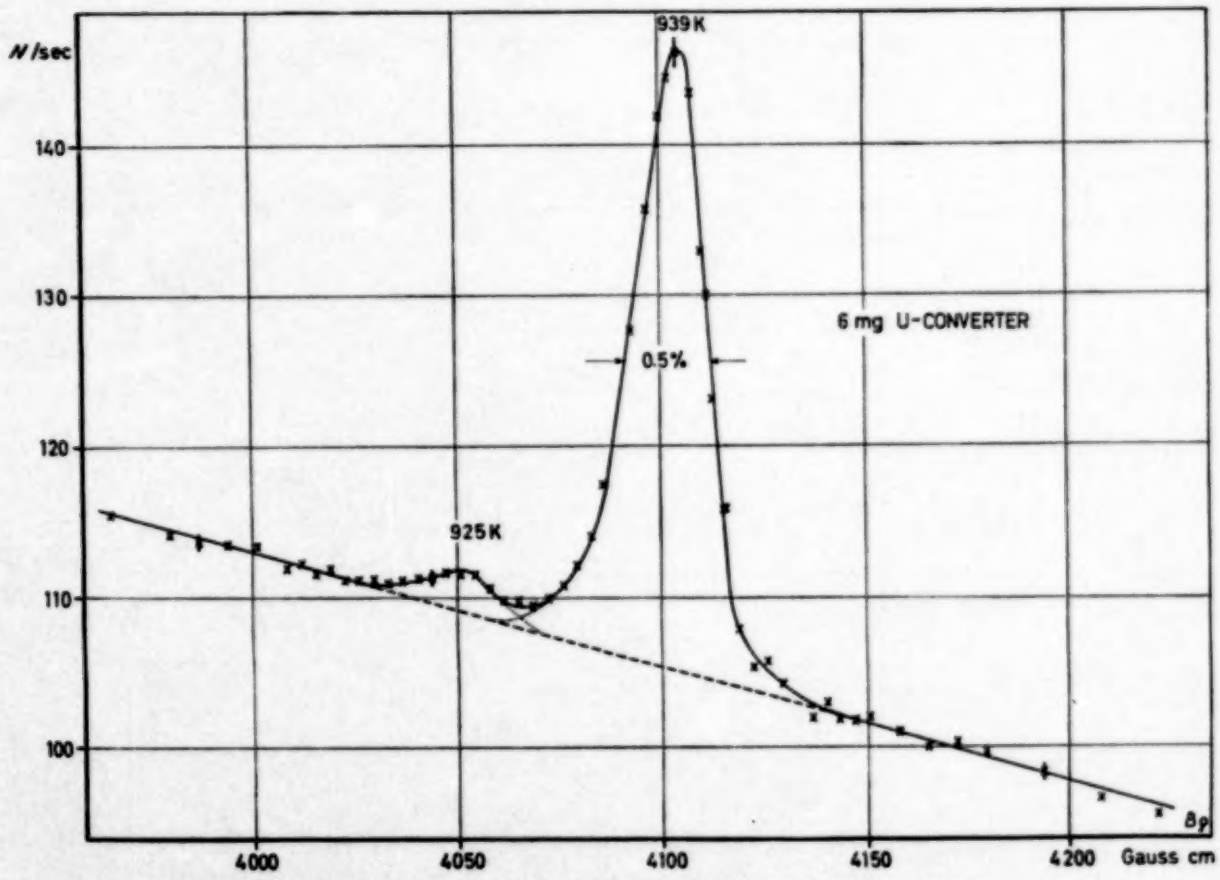

Fig. 2b. Photo-electron spectrum from uranium and lead radiators.

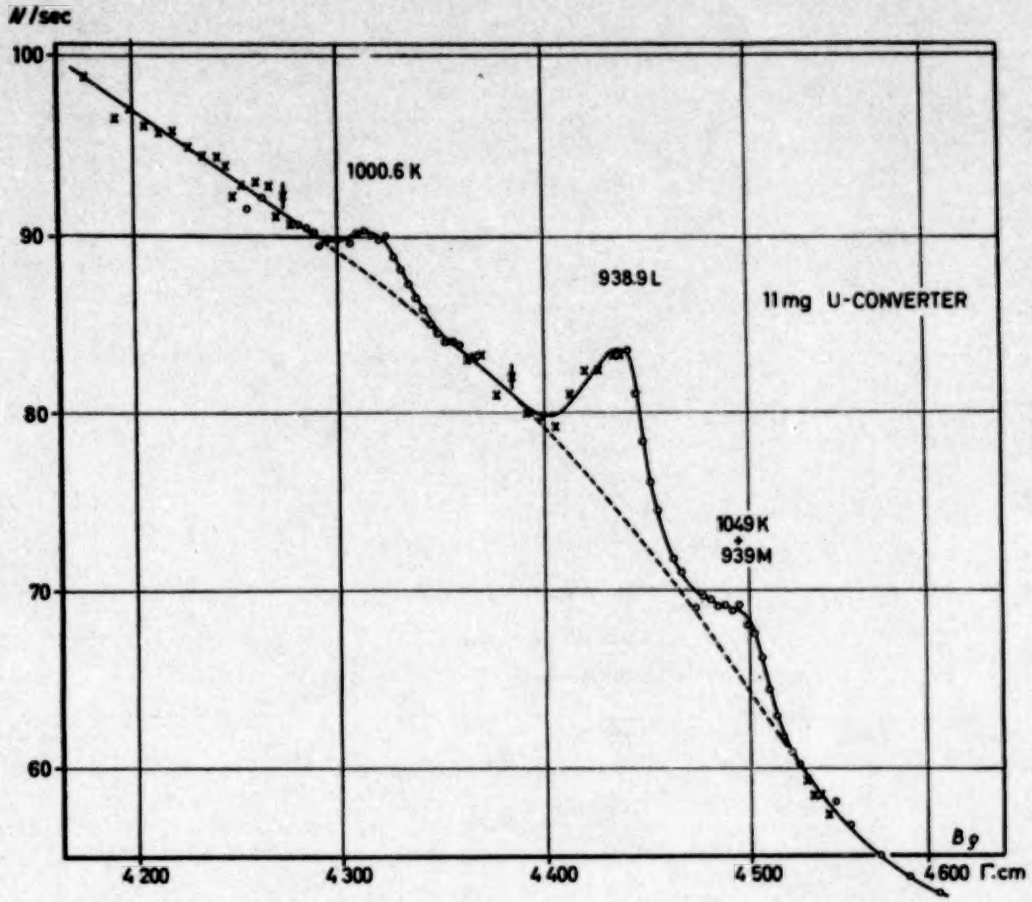

Fig. 2c. Photo-electron spectrum from uranium and lead radiators.

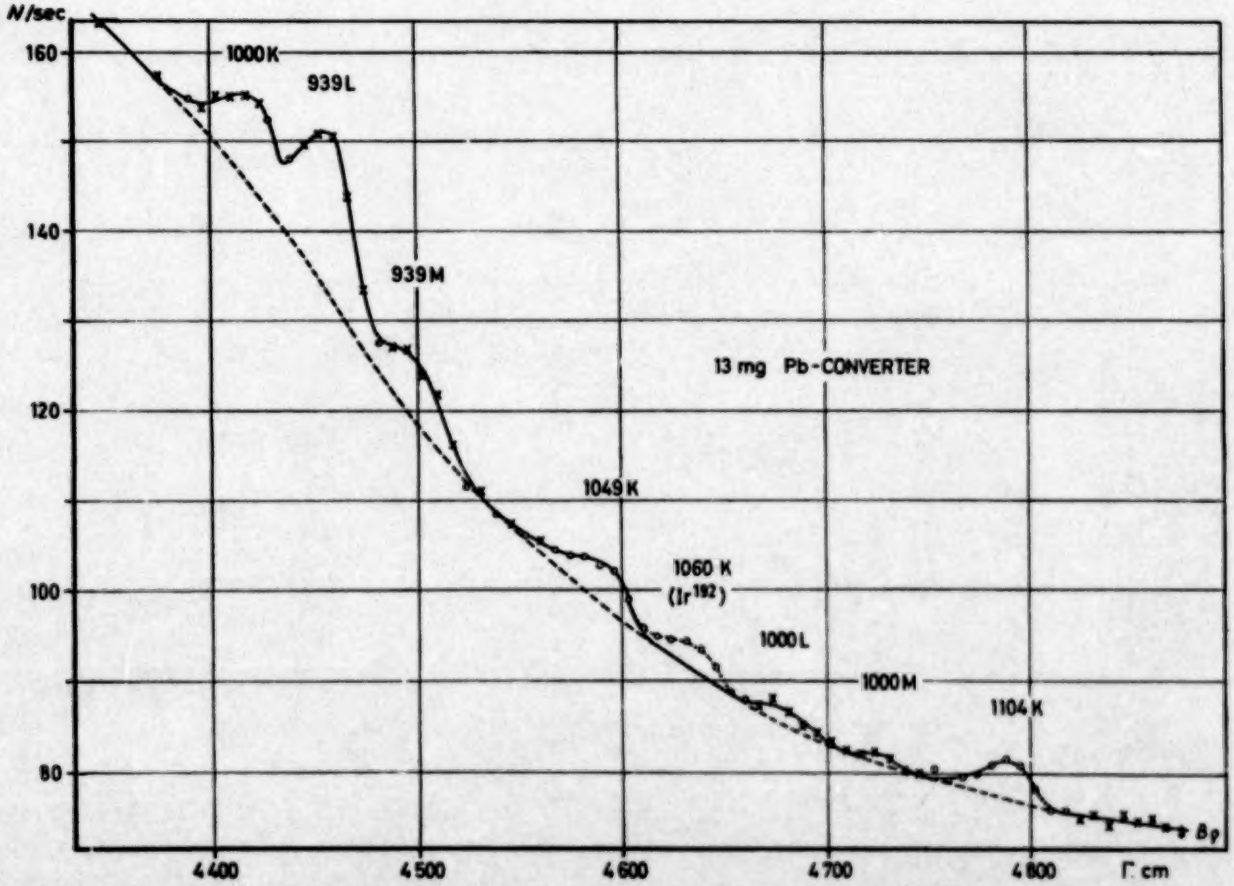

Fig. 2d. Photo-electron spectrum from uranium and lead radiators.

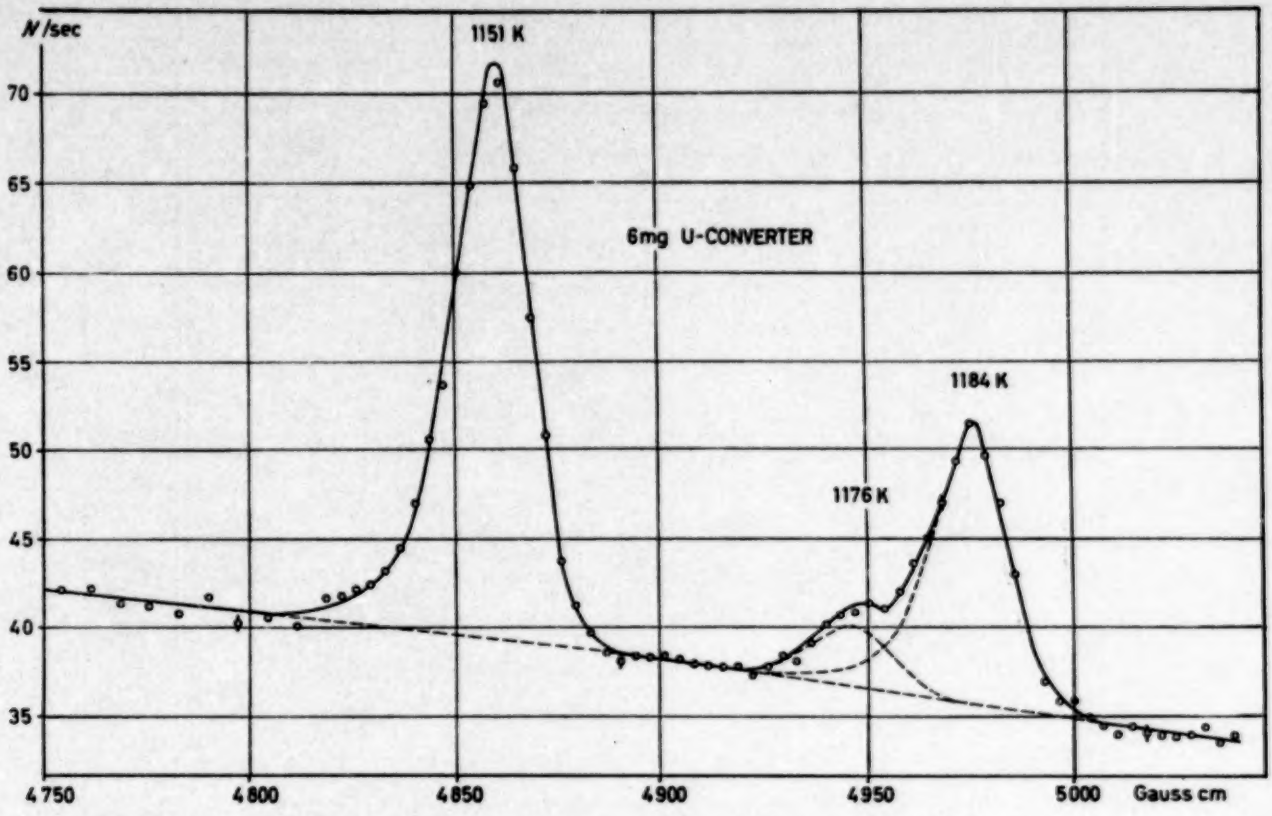

Fig. 2e. Photo-electron spectrum from uranium and lead radiators.

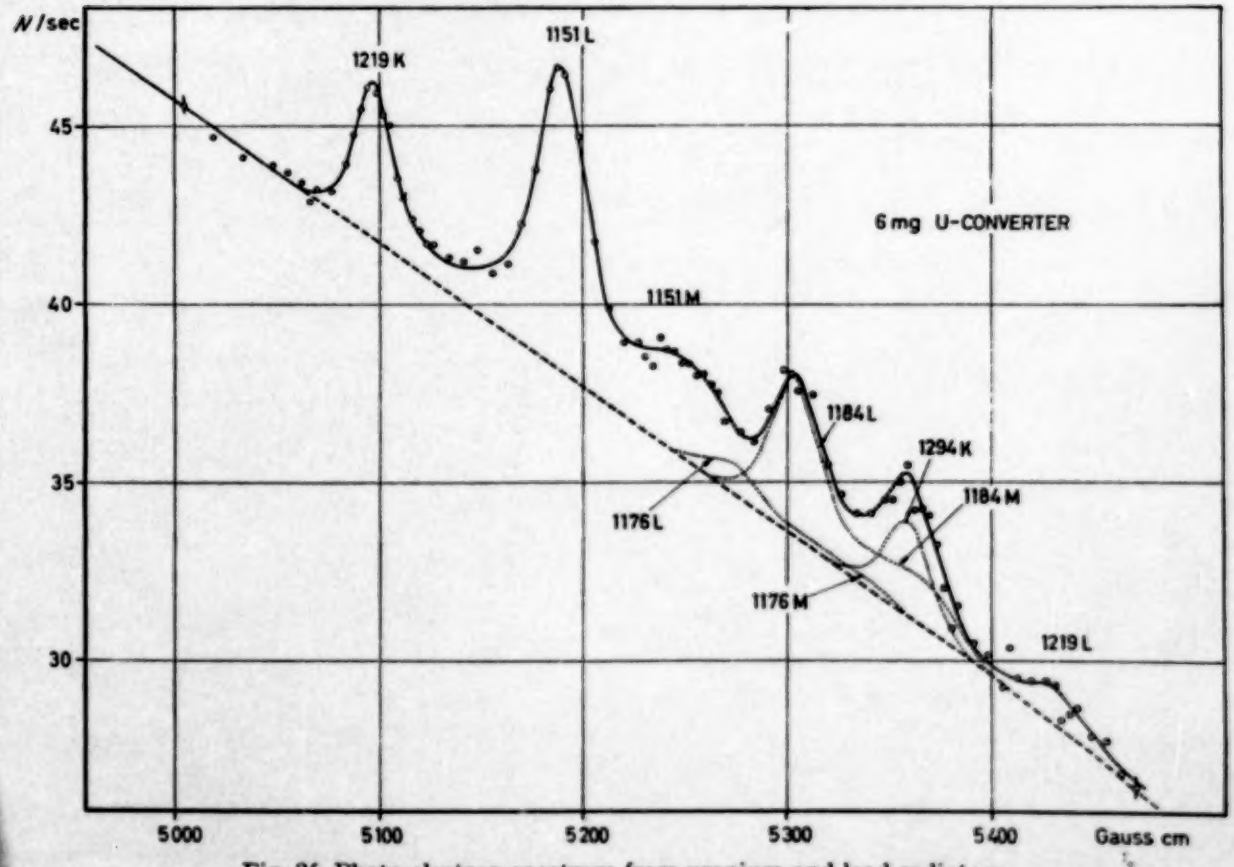

Fig. 2f. Photo-electron spectrum from uranium and lead radiators.

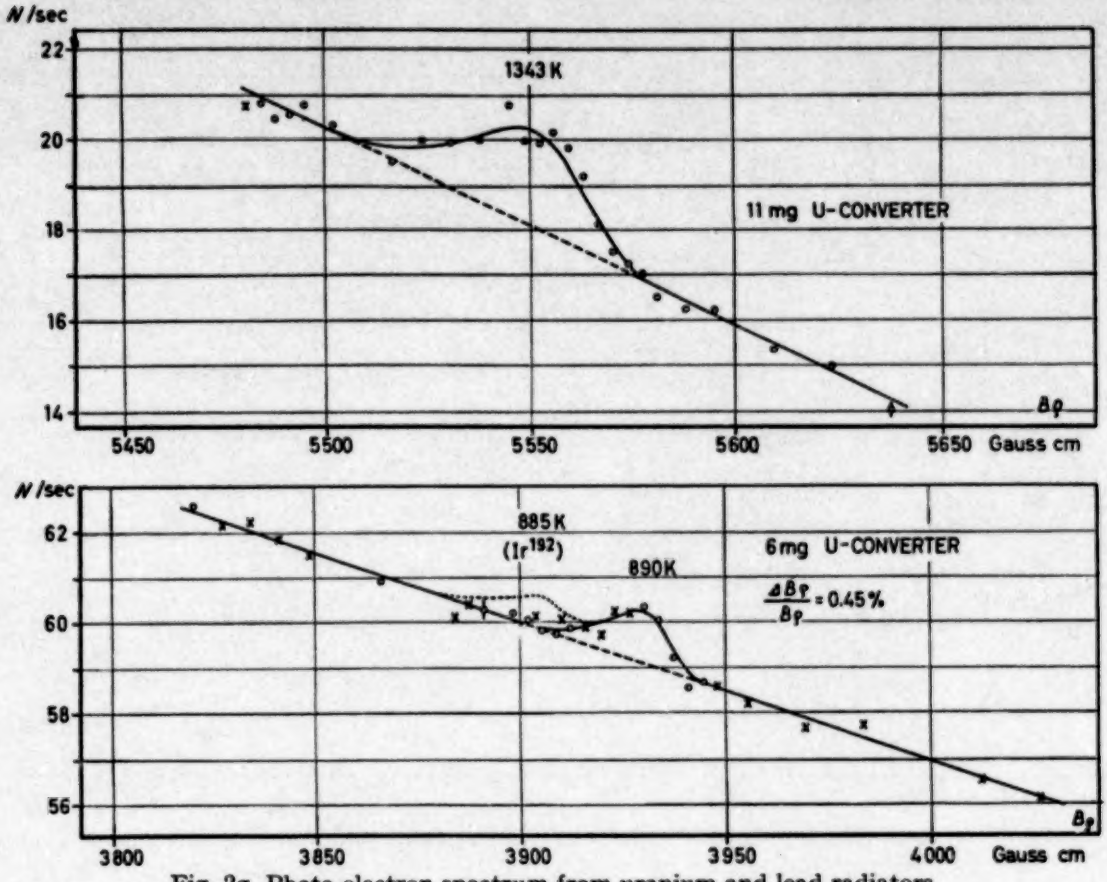

Fig. 2g. Photo-electron spectrum from uranium and lead radiators.

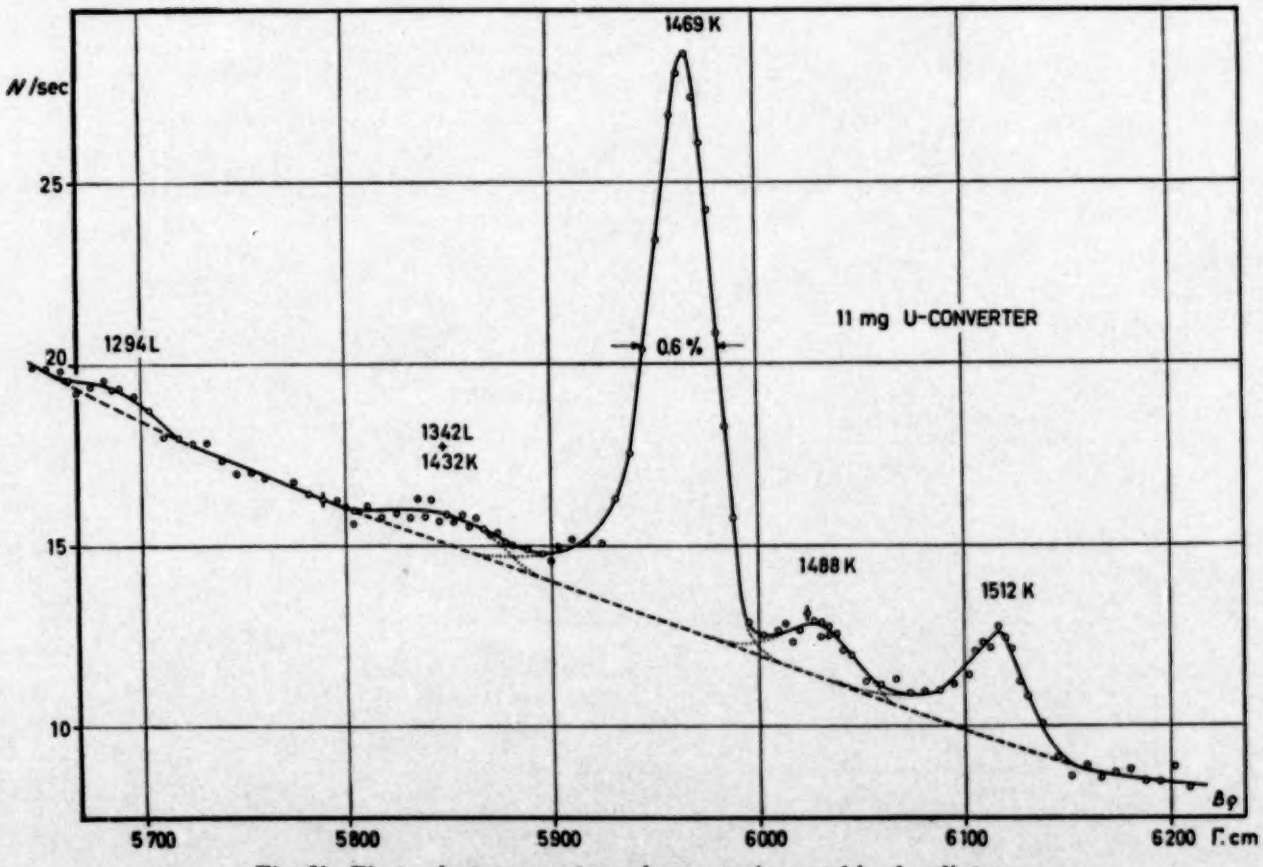

Fig. 2h. Photo-electron spectrum from uranium and lead radiators.

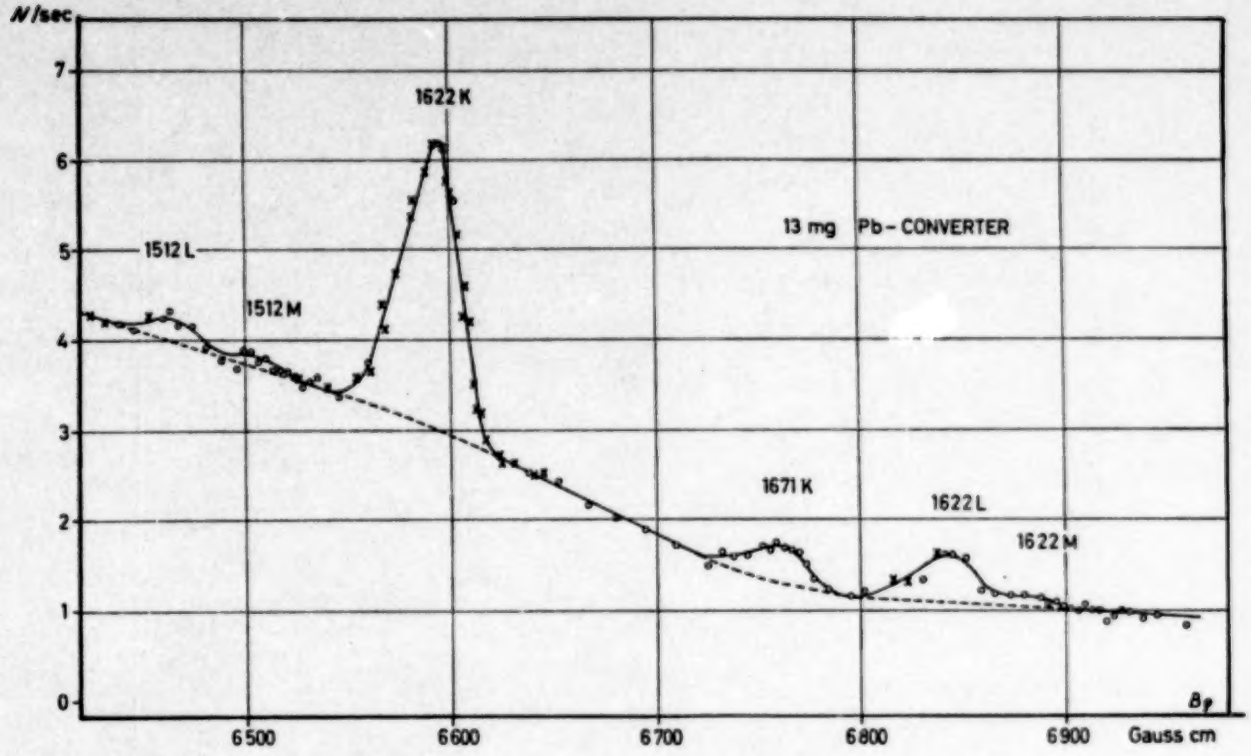

Fig. 2i. Photo-electron spectrum from uranium and lead radiators.

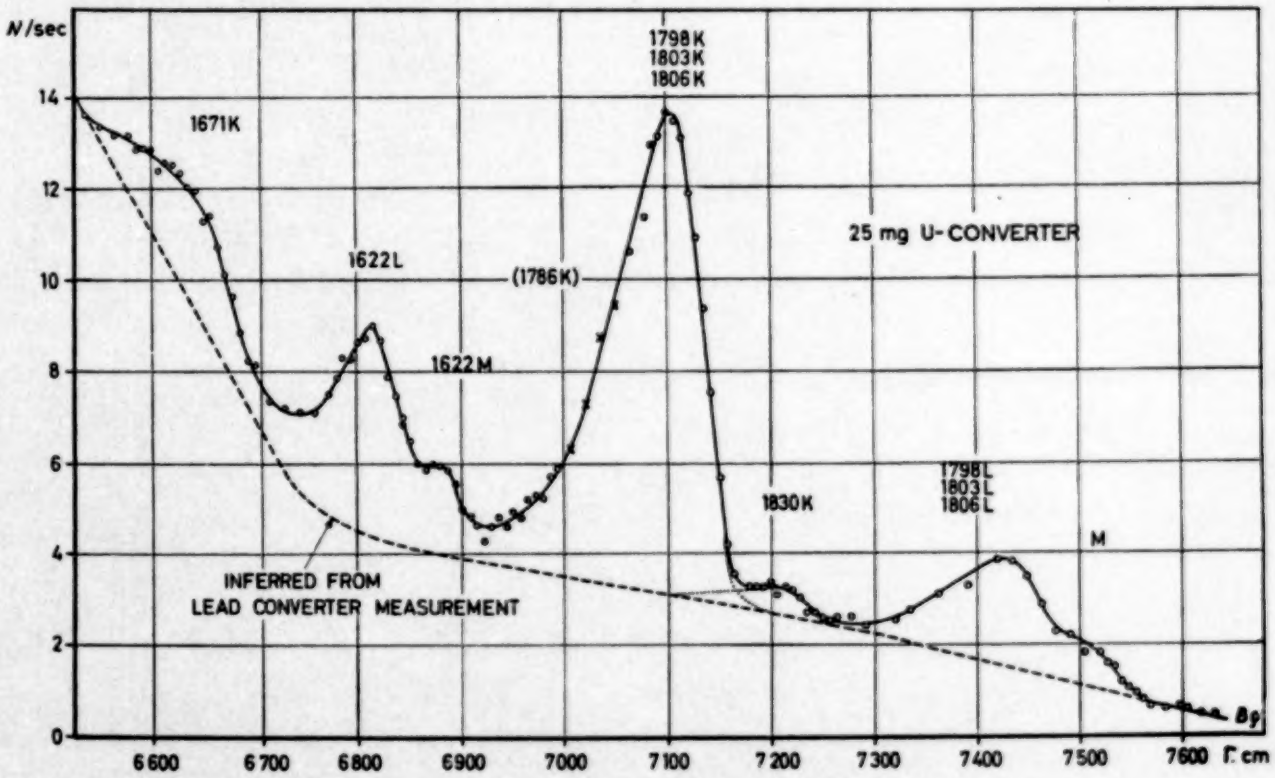

Fig. 2j. Photo-electron spectrum from uranium and lead radiators.

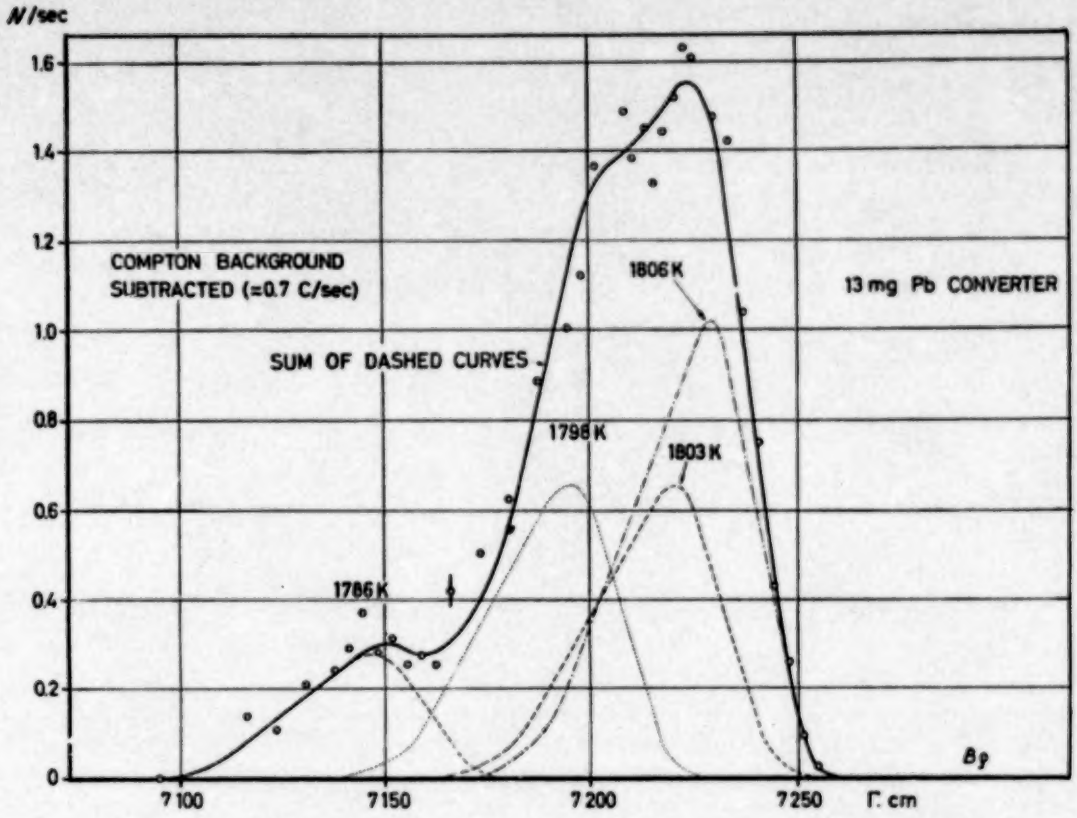

Fig. 2k. Photo-electron spectrum from uranium and lead radiators.

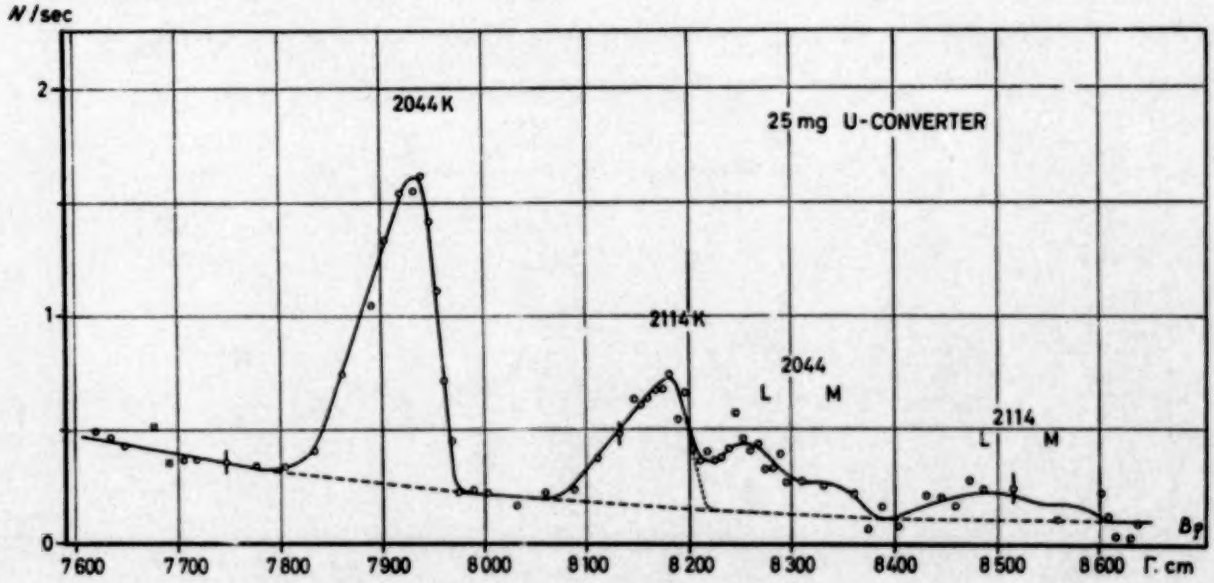

Fig. 21. Photo-electron spectrum from uranium and lead radiators.

TABLE 1

Gamma energies and intensities obtained in this investigation, compared to those obtained in a previous work

Johns and Nablo			Present investigation				Comments
E_γ	I_γ	Assignment	E_γ	I_γ (relative scale)		Assignment	
293.0 ± 0.3	5.1	621–328	293.44 ± 0.15	**11.8 ± 2**	(0)	622–328	1)
			300.66 ± 0.5	1.68 ± 0.4	(0)	923–622	2)
328.1 ± 0.2	27	328–0	328.5 ± 0.03	**59.5 ± 6**	(0)	328–0	3)
620.0 ± 1.0	1.7	621–0	622.3 ± 0.4	1.53 ± 0.3	(0)	622–0	
643.3 ± 0.6	6.2	1265–621	645.32 ± 0.06	4.9 ± 0.4	(0)	1267–622	
			890.29 ± 0.3	1.9 ± 0.2	(—1)	1512–622	1)
			924.7 ± 0.8	1.6 ± 0.2	(—1)	1547–622	4)
937.4 ± 0.4	2.9	1265–328	938.87 ± 0.1	2.7 ± 0.1	(0)	1267–0	
			1000.6 ± 0.4	1.5 ± 0.3	(—1)	1622–0	
			1048.34 ± 0.7	1.34 ± 0.1	(—1)	1671–622	5)
			1104.5 ± 0.7	1.1 ± 0.1	(—1)	1433–328	5)
1149.2 ± 0.6	2.9	1477–328	1151.3 ± 0.3	2.90 ± 0.1	(0)	1480–328	
			1176.1 ± 0.6	3.0 ± 0.5	(—1)	1798–622	6)
1180 ± 1	1.7	1802–621	1184.1 ± 0.4	1.44 ± 0.1	(0)	1806–622 **1512–328**	
1216 ± 1	0.4	1836–621	1219.4 ± 0.5	6.3 ± 0.5	(—1)	**1547–328**	
			1294.1 ± 0.7	4.8 ± 0.5	(—1)	1622–328	7)
1339 ± 2	0.3	1665–328	1343.0 ± 0.7	2.0 ± 0.3	(—1)	1671–328	8)
			1430.5 ± 3	4 ± 2	(—2)	1433–0	9)
1466 ± 1	0.8	1794–328	1469.5 ± 0.5	**1.70 ± 0.1**	(0)	1798–328	
			1480.2 ± 0.7	< 5	(—2)	1480–0	Int. converted
1478 ± 1	0.2	1477–0	**1488.0 ± 0.9**	1.6 ± 0.3	(—1)	1817–328	10)
1507 ± 2	0.3	1836–328	**1512.4 ± 0.5**	3.3 ± 0.5	(—1)	**1512–0**	10)
1618 ± 2	0.3	1946–328	1622.8 ± 0.6	4.4 ± 0.3	(—1)	**1622–0**	
1662 ± 3	0.2	1665–0	**1670.9 ± 0.6**	**6.0 ± 1**	(—2)	1671–0	11)
			1784.0 ± 3	4.6 ± 1.5	(—2)	2114–328	12)
1802 ± 2	0.3	1802–0	1798.0 ± 2	1.1 ± 0.2	(—1)	1798–0	12)
			1805,1 ± 2	1.1 ± 0.2	(—1)	1803–0	12)
			1807.5 ± 1.5	1.7 ± 0.2	(—1)	1806–0	12)
			1832.0 ± 3	1.6 ± 0.5	(—2)	1830–0	
			1925.9 ± 2	2.2 ± 1	(—2)	1925–0	
2048 ± 4	0.05	2048–0	2044.1 ± 0.8	4.1 ± 0.2	(—2)	2044–0	
			2115.5 ± 1.5	1.7 ± 0.2	(—2)	2114–0	13)

The location that has been given to the transitions in the level scheme is also indicated. Where data or assignments differ from those of the earlier work, the new information is given in bold figures. Intensities are relative values, normalized so that the data agree in the case of 1151. The figures should be multiplied by a power of ten, as indicated in a separate column. The errors given for the intensities represent an estimate of the combined effect of counting statistics, and of uncertainties in converter efficiency and gamma absorption calculations.

1) The line was not fully resolved from a line of Ir^{192}, but the contribution of the latter was measured after the decay of Ir^{194} (fig. 2).

2) 301 K clearly remains after subtraction of the longer-lived background, but it should be noted that its existence is shown beyond doubt already in the composite spectrum (fig. 2a).

(*Comments continued on next page*).

transitions of 328 keV and 939 keV as energy standards and to adopt for these lines the energy values published. The energies so obtained are given in table 2 together with the more precise date from Au^{194}.

Relative intensities were obtained from the areas of the photopeaks after correction for the converter efficiency. This efficiency was calculated for a cylindrical source geometry by means of an electronic computer, on the basis of the experimental photo-electron distributions of Hultberg[5]). In addition, a correction had to be applied for the gamma ray absorption in the copper capsule and in the iridium rod itself. This correction was not computed in an exact manner but was obtained by one-dimensional integration. Absolute intensities were obtained by normalization, utilizing the known percentage[1]) of beta-transitions proceeding to the ground state. These intensity data are included in tables 1 and 2.

4. Comparison with the Decay of Au^{194}

As mentioned before, the decay of Ir^{194} should populate the levels observed in the decay of Au^{194} to an extent set by the disintegration energy. Ir^{194} decays with a lower Q-value. It is satisfactory then that no transitions have been discovered in the present decay that cannot be identified with the transitions reported for the decay of Au^{194}. Furthermore, no transitions have been observed, which, according to the work of Bäckström *et al.*, should originate from levels higher than the Q-value. Conversely, evidence has been found in the iridium

---

3) The self-absorption effect makes the intensities of the low energy lines very uncertain.

4) The shape of the adjacent 939 K was inferred from the shape of the strong 1151 K (fig. 2b).

5) The shape required for the analysis was obtained from 1060 K, which belongs to Ir^{192} and could be studied after the decay of Ir^{194} (fig. 2d).

6) The analysis of the doublet 1176 K — 1183 K was made on basis of the line profile of 1151 K (fig. 2e).

7) The shapes and heights of 1176 L and 1184 L were inferred from 1151 L. Subtraction of these two L lines from the composite spectrum revealed the shape of the whole LM group of 1151, and this shape was then used for the construction of 1176 M and 1184 M. After subtraction of the known lines, 1294 K remained. The success of the graphical procedure shows that the background is linear under these lines, as was assumed. A possible curvature would not much affect the intensity of 1294. The 1294 L line is distinctly seen (fig. 2h).

8) The line profile was analysed by comparison with a line from Co^{60} (fig. 2g).

9) An additional measurement with a lead converter also gave evidence for the existence of this transition (fig. 2h).

10) The Compton background was re-constructed on the assumption that 1512 K is a single line. The line shape was taken from 1469 K (fig. 2h).

11) This line was reported by Johns and Nablo from an experiment using a uranium radiator. As is seen from fig. 2g, the line can hardly be discovered without a separate study of the background. With lead as a radiator, on the other hand, it is easily detected (fig. 2i).

12) The line group was resolved into components by aid of the shape of 1623 K. The positions of corresponding lines in Au^{194} were used as a guide in the graphical analysis (fig. 2k).

13) The line was separated graphically from 2044 L by the use of the shape of 2044 K (fig. 2l).

decay for nearly all levels that seem to be directly populated by Au^{194} and which have not too high energy. In addition, some transitions observed here have been observed in Au^{194} but not located in the decay scheme, and now conclusions may be drawn from this fact. A comparison of gamma-ray branching ratios from corresponding levels in the different types of decay would be a sensitive test of the level schemes. At the present stage, mostly conversion intensities are known for the gold isotope, although gamma-ray work is underway. The transitions have been listed in table 2 in the order of the levels they de-populate, in such a manner that conversion and gamma intensities may be compared. It is seen that these intensities show the same trend, and this is significant in so far as the transitions may generally be expected to have low multipolarity, and the conversion coefficients should not be widely different. It is justified then to identify the levels with those reported for the decay of Au^{194}.

The decay scheme of Ir^{194} is shown in fig. 3. It includes the transitions 1803, 1806 and 1830 for which definite locations could not be found in the decay of Au^{194}. In the present decay, 1803 can proceed to the ground state or to the first excited state, but not to a higher level. A level at 1803 keV could be populated by a beta branch of log $ft \approx 8.8$, which is normal for a first forbidden transition. If 1803 is assumed to lead to the 328 keV state, however this would require a log ft value about two units lower, and the level should be strongly populated in the decay of Au^{194}, which is not the case. Also, the ground state transition would have been observed even if its intensity were only 10 % that of 1803. On the other hand, a transition from a 1803 keV state to the first excited state may well exist in the gold spectrum, masked by 1469 K and 1480 K. The alternative of a 1803 keV level is consequently the more probable one, and a similar argument holds in the case of 1806. This level may be partly de-populated by 1184, which also is assumed to proceed from the 1512 keV state. The transition 1830 is much weaker than 1803 and 1806, and hence the arguments concerning log ft values seem less conclusive. However, an assignment as a ground state transition is still the more probable one. A transition of 1208 keV, which had been observed in Au^{194}, is also accomodated by this decay scheme, as a transition from the 1830 keV state to the second excited state (cf. table 2).

The log ft value for each branch of the beta decay may be calculated from the measured and normalized gamma intensities. The results are given systematically in table 3. The ft values generally correspond well to those expected theoretically for first forbidden transitions in this type of nuclei, and none is low enough to require a classification as an allowed transition.

The gamma intensity data may be combined with conversion intensities from ref. [3]) to yield relative conversion coefficients. These relative values contain surprisingly much information concerning the spin of the level from which the

TABLE 2

Transitions found in the decay of Ir^{194} and of Au^{194} arranged in order of depopulated levels

Initial state	Final state	ΔE	This work		Bäckström *et al.*		Comments
			E_γ	I_γ (abs.)	E_γ	$I_{e(K)}$	
2114.4 ± 0.4	0	2114.4 ± 0.4	2115.5 ± 1.5	9.3 (—3)	2114.0 ± 0.4	1.9(—2)	
	328.5 ± 0.03	1785.9 ± 0.4	1784.0 ± 3	2.5 (—2)	1786.3 ± 0.4	4.4(—2)	
	622.05 ± 0.06	1492.35 ± 0.4		< 2(—2)	1492.7 ± 0.5	2.9(—2)	
	1267.37 ± 0.1	847.0 ± 0.4			847.42 ± 0.2	3.0(—2)	
2044.0 ± 0.3	0	2044.0 ± 0.3	2044.1 ± 0.8	2.2 (—2)	2044.1 ± 0.4	2.8(—1)	
	328.5 ± 0.03	1715.5 ± 0.3		< 8(—3)	1715.7 ± 0.3	6.4(—2)	
	622.05 ± 0.06	1421.95 ± 0.3		< 1(—2)	1421.77 ± 0.2	6.6(—2)	
	1816.9 ± 0.4	227.1 ± 0.5			226.94 ± 0.1	3 (—1)	
1924.6 ± 0.2	0	1924.6 ± 0.2	1925.9 ± 2	1.2(—2)	1924.6 ± 0.2	1.8(—1)	
	328.5 ± 0.03	1596.1 ± 0.2		< 1(—2)	1596.2 ± 0.4	2.9(—1)	
	622.05 ± 0.06	1302.55 ± 0.2		< 5(—2)	1302.55 ± 0.15	5.1(—2)	
	1816.9 ± 0.4	107.7 ± 0.2			107.24 ± 0.06	$I_e(L) = 2.4$	
1830.3 ± 0.3	0	1830.3 ± 0.3	1832.0 ± 3	8.8 (—3)	1830.1 ± 0.3	2.8(—2)	4)
	622.05 ± 0.06	1208.25 ± 0.3		< 2(—2)	1208.47 ± 0.35	6.4(—3)	4)
1816.9 ± 0.4	328.5 ± 0.03	1488.4 ± 0.4	1488.0 ± 0.9	8.8 (—2)	1487.9 ± 0.5	2.2(—2)	
	622.05 ± 0.06	1194.85 ± 0.4		< 6(—2)	1195.1 ± 0.35	6.6(—3)	
	922.75 ± 0.1	894.15 ± 0.4		< 2(—2)	894.4 ± 0.4	1.0(—2)	
1806.4 ± 0.8	0	1806.4 ± 0.8	1807.5 ± 1.5	9.2 (—2)	1805.9 ± 0.8	1.2(—2)	
	622.05 ± 0.06	1184.35 ± 0.8	1184.1 ± 0.3	7.9 (—1)	1183.63 ± 0.2	1.2(—1)	1)
1803.4 ± 0.8	0	1803.4 ± 0.8	1805.1 ± 2	6.0 (—2)	1803.1 ± 0.8	1.3(—2)	4)
1797.8 ± 0.2	0	1797.8 ± 0.2	1798.0 ± 2	6.0 (—2)	1798.0 ± 0.4	2.6(—2)	
	328.5 ± 0.03	1469.3 ± 0.2	1469.5 ± 0.5	9.3 (—1)	1469.36 ± 0.25	2.6(—1)	
	622.05 ± 0.06	1175.75 ± 0.2	1176.1 ± 0.6	1.65(—1)	1175.46 ± 0.2	1.2(—1)	
	1432.6 ± 0.2	365.2 ± 0.3		< 1(—1)	364.97 ± 0.06	2.5	
	1512.2 ± 0.2	285.6 ± 0.3		< 3(—1)	285.34 ± 0.05	2.4(—1)	
1670.9 ± 0.2	0	1670.9 ± 0.2	1670.9 ± 0.6	3.3 (—2)	1670.9 ± 0.6	1.8(—2)	
					1342.44 ± 0.2	3.2(—1)	

	1512.2 ± 0.2	285.6 ± 0.3		< 1(—1)	364.97 ± 0.06	2.5	
				< 3(—1)	285.34 ± 0.05	2.4(—1)	
1670.9 ± 0.2	0	1670.9 ± 0.2	1670.9 ± 0.6	3.3 (—2)	1670.9 ± 0.6	1.8(—2)	
	328.5 ± 0.03	1342.4 ± 0.2	1343.0 ± 0.7	1.1 (—1)	1342.44 ± 0.2	3.2(—1)	
	622.05 ± 0.06	1048.85 ± 0.2	1048.34 ± 0.7	7.3 (—2)	1048.72 ± 0.15	3.5(—1)	
1622.3 ± 0.2	0	1622.3 ± 0.2	1622.8 ± 0.6	2.4 (—1)	1622.6 ± 0.5	1.3(—2)	
	328.5 ± 0.03	1293.8 ± 0.2	1294.1 ± 0.7	2.6 (—1)	1293.9 ± 0.5	7.3(—2)	
	622.05 ± 0.06	1000.3 ± 0.2	1000.6 ± 0.4	8.2 (—2)	1000.17 ± 0.2	5.7(—2)	
1547.4 ± 0.2	0	1547.4 ± 0.2		<2(—2)	1547.9 ± 0.4	8.1(—2)	
	328.5 ± 0.03	1218.9 ± 0.2	1219.4 ± 0.5	3.4 (—1)	1219.0 ± 0.2	1.6(—1)	
	622.05 ± 0.06	925.35 ± 0.2	924.7 ± 0.8	8.8 (—2)	925.3 ± 0.1	6.8(—2)	
1512.2 ± 0.2	0	1512.2 ± 0.2	1512.4 ± 0.5	1.8 (—1)	1512.8 ± 0.6	9.0(—3)	
	328.5 ± 0.03	1183.7 ± 0.2	1184.1 ± 0.4	7.9 (—1)	1183.6 ± 0.2	1.2(—1)	1)
	622.05 ± 0.06	890.15 ± 0.2	890.29 ± 0.3	1.04(—1)	890.1 ± 0.15	5.3(—2)	
	922.75 ± 0.1	589.45 ± 0.2			589.4 ± 0.1	1.8(—1)	2)
1479.6 ± 0.2	0	1479.6 ± 0.2		< 2(—2)	1479.75 ± 0.25	2.2	3)
	328.5 ± 0.03	1151.1 ± 0.2	1151.3 ± 0.3	1.6	1150.9 ± 0.2	2.0(—1)	
1432.5 ± 0.2	0	1432.5 ± 0.2	1430.5 ± 3	2.2 (—2)	1432.3 ± 0.3	1.8(—2)	
	328.5 ± 0.03	1104.0 ± 0.7	1104.5 ± 0.7	6.0 (—2)	1104.1 ± 0.2	1.7(— 1)	
	622.05 ± 0.06	810.4 ± 0.2		< 5(—2)	810.9 ± 0.5	1.5(—2)	
1267.37 ± 0.1	0			< 6(—2)	1267.37 ± 0.15	8.0(—2)	5)
	328.5 ± 0.03		938.87	1.48	938.87 ± 0.10	2.2(—1)	
	622.05 ± 0.06		645.32	2.68	645.32 ± 0.08	9.0(—1)	
922.75 ± 0.1	622.05 ± 0.06		300.66 ± 0.5	9.2 (—1)	300.7 ± 0.05	1.8	
622.05 ± 0.06	0		622.3 ± 0.4	8.4 (—1)	622.05 ± 0.06	7.7(—1)	
	328.5 ± 0.03		293.44 ± 0.15	6.45	293.55 ± 0.04	24	
328.5 ± 0.03	0		328.5	32.6	328.5 ± 0.03	100	

The level energies are quoted from ref. [3]). Gamma ray intensities have been transformed to absolute values, i.e. photons per disintegration.
1) Transition shared between 1806 — 622 and 1512 — 328. 2) Masked by Ir^{192}. 3) Internally converted, cf. section 2.
4) New assignment. 5) Upper limit of intensity estimated on basis of L-line.

TABLE 3

Log *ft* values of beta branches from Ir^{194} to levels of Pt^{194}

Level	Beta intensity (%)	log *ft*	Spin and parity
2114	0.034	7.28	1+
2044	0.022	8.16	
1925	0.012	9.12	
1830	0.009	9.66	
1817	0.09	8.61	
1806	0.09	8.64	
1804	0.06	8.82	
1798	1.15	7.61	1+
1671	0.22	8.65	2+
1622	0.58	8.33	2+
1547	0.43	8.65	0+
1512	1.07	8.31	2+
1480	1.66	8.22	0+
1432	0.07	9.66	2+ (1+)
1267	4.16	8.17	0+
923	0.92	9.32	(3+)
622	3.06	9.14	2+
328	20.5	8.60	2+
0	66	8.32	0+

Spin values are quoted from table 4.

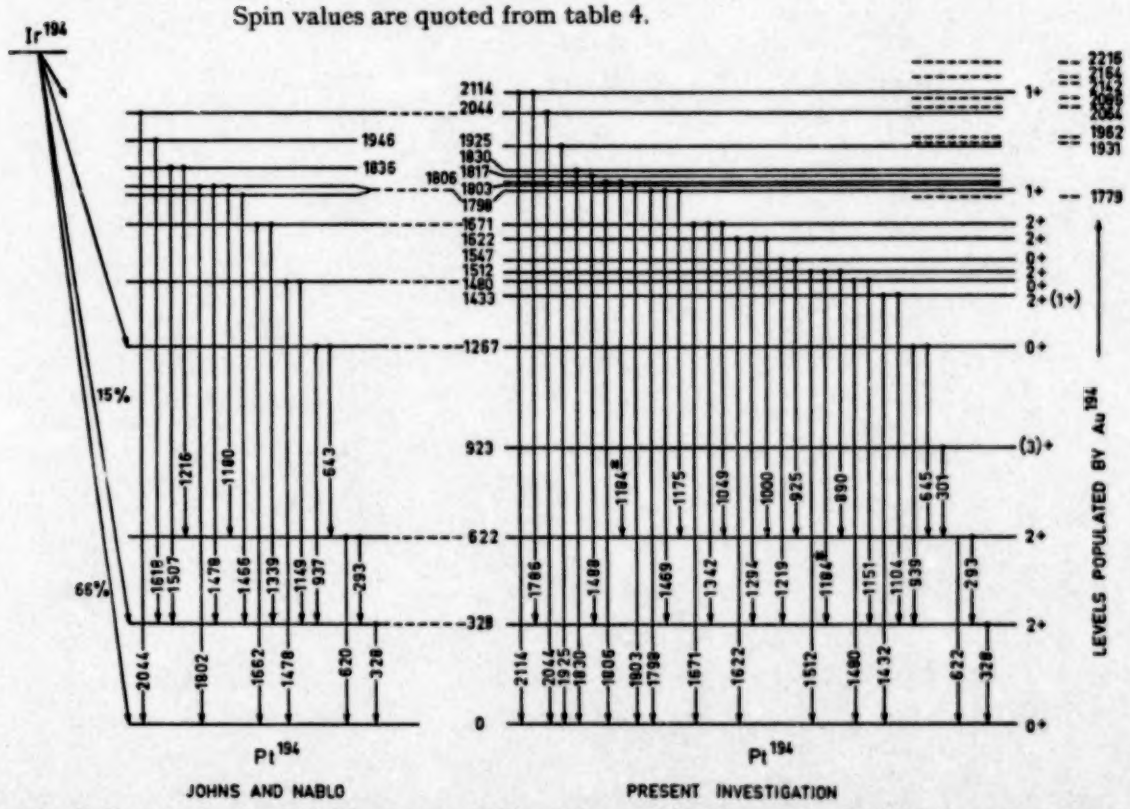

Fig. 3. Decay schemes of Ir^{194} as presented by Johns and Nablo and as obtained from the present work. Levels populated by Au^{194} but not by Ir^{194} are indicated by dashed lines to the right.

TABLE 4

Conversion coefficients and multipolarities

Initial level	Energy of transition (keV)	Multi-polarity	I_K/I_γ (normalized)	Theoretical conv. coeff.		Spin, parity
				M1	E2	
2114	2114	M1	1.75 ± 0.2 (−3)	1.67(−3)	1.13(−3)	1+
	1786	E2	1.50 ± 0.5 (−3)	2.6 (−3)	1.55(−2)	
1798	1798	M1	3.0 ± 0.6 (−3)	2.5 (−3)	1.52(−3)	1+
	1469	E2	1.95 ± 0.1 (−3)	4.1 (−3)	2.2 (−3)	
	1176	M1+E2	5.1 ± 0.8 (−3)	7.3 (−3)	3.3 (−3)	
1671	1671	E2	1.75 ± 0.3 (−3)	3.0 (−3)	1.75(−3)	2+
	1342	M1+E2+E0	9.3 ± 1.4 (−3)	5.2 (−3)	2.6 (−3)	
	1048	M1+E2+E0	1.55 ± 0.12(−2)	9.8 (−3)	4.1 (−3)	
1622	1622	E2	1.85 ± 0.15(−3)	3.2 (−3)	1.85(−3)	2+
	1293	M1+E2+E0	9.3 ± 1 (−3)	5.7 (−3)	2.8 (−3)	
	1000	M1+E2+E0	2.4 ± 0.5 (−2)	1.1 (−2)	4.4 (−3)	
1547	1547	E0	> 2.5 (−2)	3.7 (−3)	2.0 (−3)	0+
	1219	E2	2.9 ± 0.25(−3)	6.6 (−3)	3.05(−3)	
	925	E2	4.8 ± 0.6 (−3)	1.33(−2)	5.1 (−3)	
1512	1512	E2	2.06 ± 0.3 (−3)	3.8 (−3)	2.07(−3)	2+
	1184[a])	(M1)	> 6.2 (−3)	7.2 (−3)	3.25(−3)	
	890	M1+E2(+E0)	2.1 ± 0.2 (−2)	1.47(−2)	5.5 (−3)	
1480	1480	E0	> 3 (−1)	4.1 (−3)	2.15(−3)	0+
	1151	E2	3.4 ± 0.12(−3)	7.6 (−3)	3.4 (−3)	
1433	1433	E2	$2.46^{+2.5}_{-1.2}$ (−3)	4.4 (−3)	2.3 (−3)	2+(1+)
	1104	M1	8.5 ± 1 (−3)	8.5 (−3)	3.7 (−3)	
	810	(M1)	> 9 (−3)	1.85(−2)	6.6 (−3)	
1267	1267	E0	> 4.5 (−2)	5.9 (−3)	2.85(−3)	0+
	939	E2	5.1 ± 0.2	1.28(−2)	5.3 (−3)	
	645	E2	1.15 ± 0.1 (−2)	3.4 (−2)	1.05(−2)	
622	622	E2	1.4 ± 0.3 (−2)	3.7 (−2)	1.15(−2)	
	294	E2	5.7 ± 1 (−2)	2.75(−1)	6.5 (−2)	

[a]) Shared between two locations.

transitions emerge. It is concluded from the log *ft*-values in table 3 that only even parity needs to be considered. Levels which possess ground state transitions and which are directly fed by the beta decay must then be of the character 1+, 2+, or, possibly, 3+. The relative conversion coefficients were normalized by tentative assignments of the ground state transition as pure M1, E2, and

M3. It was then found that a possible multipolarity of the transitions to the first and second excited states (2+) could only be obtained for a certain spin of the level. The normalized conversion coefficients are listed in table 4. The spin and multipolarity assignments are formally unambiguous, provided that the conversion lines really correspond to single transitions. If this were not true, the corresponding conversion coefficient would have to be reduced. It is worth noticing that this effect could not be the explanation of the observed E0 admixtures, since a similar reduction of several conversion coefficients would be necessary.

5. Conclusions and Discussion

As seen from table 1, all 16 transitions reported by Johns and Nablo have been confirmed by the present work, although in 6 cases the results are in considerable disagreement concerning energies or intensities. The intensity deviation at low energies is no doubt due to the more accurate analysis used here to evaluate these intensities. An additional reason to believe that the new values are more accurate is given by the fact that the discrepancy mentioned at the end of section 2 concerning the branching from the 1480 keV level is completely removed when these intensity values are introduced.

The difference in both energy and intensity of 1671 is probably caused by a slight misinterpretation in the earlier work. When uranium is used as a converter, 1671 K coincides with the Compton edge of a higher line (cf. fig. 2j); and this may not have been taken into account in the interpretation.

In the present paper, 16 additional transitions are reported which could all be identified with transitions reported from the decay of Au^{194}.

The decay scheme may be compared in fig. 3 with that of Johns and Nablo (see also table 1). The position of the transitions has been modified here in four cases, and appreciable correction of the transition energy was associated with this change in three of the cases. Evidence has been found for a total of 18 excited states, and these are identical with those found in the decay of Au^{194}, except two levels, for which the depopulating lines were known before but not located. The remaining levels known from the decay of Au^{194}, have been indicated in fig. 3 (dashed lines). The lowest of these states, of energies 1779 keV, 1931 keV and 1962 keV, probably have spins of 3 units or more, as indicated by the decay pattern (cf. ref. [3])). The fact that the 5 highest states are not observed here is fully explained by the low disintegration energy and the associated poor intensities. Thus, the decay scheme of Au^{194} has been well confirmed. It is especially interesting to note that the existence of the level at 1547 keV has been verified. In the decay of Au^{194}, this level was found to be de-populated by three transitions: 1547, 1219 and 925, but two of these (1219 and 925) had been given the alternative assignments 2142–923 and 2358–1432 respectively. As the value 2358 keV is higher than the Q-value of Ir^{194}, the

assignment of 925 as a de-populating transition of the 1547 keV state is the only possible one in the present case. The presence of 1219 confirms this assignment.

It is shown, in tables 3 and 4, how the lof *ft* values and the available relative values of the conversion coefficients can be used to supply spin and parity information. It has to be remembered that the conclusions are subjected to some uncertainty, because the decay of the gold isotope, from which the conversion data are drawn, is much more complicated, and, consequently, a line which seemed to be a single one may possibly correspond to two different transitions. Such accidents should, however, be very rare with transitions of 1 MeV energy or more.

As seen from table 3, the constancy of log *ft* for the levels of 0+ parity is quite remarkable: $8.2 \leqslant \log ft < 8.7$. There are two beta branches, leading to the states of 2114 keV and 1798 keV, which possess a log *ft* value clearly lower than the others (7.3 and 7.6) and the states have been independently classified as 1+. This is in accord with the often observed fact that the beta transitions of $\Delta I = 0$ are somewhat faster than those of $\Delta I = 1$.

The remaining log *ft* values exhibit more scattering, with a variation from 8.3 to 9.7, and it could be that the highest of these values correspond to first forbidden unique transitions (level character 3+). A high spin value for the 923 keV level already suggested itself from the transition pattern in the decay of Au^{194}, and the parity is definitely even, since the depopulating transition to a 2+ state has E2 multipolarity[3]). The log *ft* value for the decay to this level is fairly high (9.3), but not significantly higher than for the transition to the second excited state (2+). However, no ground state transition corresponding to the 923 keV state has been observed ($I_\gamma < 0.16$ relative scale), i.e. this transition is forbidden by a factor of 7000 in comparison with 301. Consequently it is very unprobable that the spin is 2, because even if the special selection rules of the collective model are supposed to operate, the inhibition is rarely so strict. Thus, if the possibility of 2+ may be excluded, there remains only one alternative, i.e. 3+, the spin of 4 being completely incompatible with the log *ft* value obtained. It should be pointed out that the possibility of gamma-ray feeding to the 923 keV state has been examined, and it was found that, although the presence of some yet undetected gamma transition may increase the log *ft* value to some extent, the feeding of the level can not be accounted for by gamma-rays only.

In the theory of Davydov and Filippov[6]), the nucleus Pt^{194} should be regarded as having $\gamma = 30°$. The theory predicts, for this case, a 3+ level at 951 keV, a value which deviates by only 3 % from the energy actually found. Furthermore, the theory requires that the cross-over transition to the first excited state be forbidden, and it was indeed not observed in the decay of Au^{194}. The transition which was found to mask the possible cross-over line in Au^{194}

would be eliminated in the decay of Ir^{194}, and the inhibition could be studied closer, but, unfortunately, a line from Ir^{192} made this prohibitively difficult.

It is tempting to attach some significance to the increase in log *ft* for the beta transitions to the ground, to the first and to the second excited states. Such a trend is to be expected if the excited states are assumed to be one and two phonons of vibration respectively, and some retardation should also be predicted from the theory of the assymetric rotor.

Spin values could be inferred (table 4) for 10 levels, and, usually, also the multipolarity of associated transitions. Two of these results, for the 1267 keV and 1480 keV level, are just confirmations of earlier assignments. In all, three 0+ states are found to exist an energy interval of approximately 300 keV and another such level is known[3]) at 2164 keV. This fact should not be surprising in view of the possibility of two-nucleon excitation. Very roughly, the density of 0+ levels should be equal to the mean density of neutron and proton single particle states. An inspection of, for instance, the level scheme of Pt^{193} shows that the number of 0+ levels found is not at all unreasonably high from this point of view. Collective motion may, of course, also produce such states.

The conversion coefficients connected to the 1671 keV and 1622 keV states can only be explained with the assumption of an admixture of E0 in the transitions to the first two excited states. The magnitude of this admixture in these four transitions is 1 to 2 %. It was pointed out before that, although the risk of misinterpretation generally exists with these conversion coefficients, there can hardly be any doubt concerning a deviation in this sense. The fact that this admixture is encountered in two transitions from each level with about the same intensity suggests a plausible theoretical interpretation. The levels of 1671 keV and 1622 keV may be assumed to be produced by intrinsic excitation of the ground state, involving a net change of nuclear radius. The first and second excited states (2+) are, according to current theories, of the same intrinsic structure as the ground state. Consequently, the decay to the low 2+ states proceeds by change of intrinsic state, and the associated volume change creates a certain probability for E0 transition, and an admixture of E0 should then occur for both transitions to the 2+ states.

In the decay of states of 1+ or 2+ character, an admixture of M1 and E2 is formally possible in the transitions to the first and second excited states. In several cases there is evidence of appreciable E2 intensity, suggesting a cooperative mode of excitation. The 1433 keV level seems to be an exception, but the uncertainly is quite large here.

It is satisfactory that the transition 645 and 939 both appear to be E2 as expected. On the other hand, the conversion coefficients for 294 and 622 do not agree well. The explanation may be that 622 K, as observed in the decay of Au^{194}, is a very close doublet.

It is interesting to compare the probabilities for transition from a certain

level to the low 2+ states. It had been noticed before[3]) that selection rules operate in the case of the levels at 622 keV, 923 keV, 1267 keV and 1480 keV. When corrected for an E_γ^5 variation, the transition probabilities from the levels at 1547 keV and 1622 keV to the two 2+ states come out as almost equal. The corresponding matrix elements for the levels at 1512 keV, 1671 keV and 1798 keV are different by approximately a factor of 2.

The authors thank Professor Kai Siegbahn for the interest he has taken in this work. One of us, J. Kern, is much indebted to him for the generous hospitality shown during his stay at the Institute of Physics. He further wishes to thank Professor O. Huber for giving him the opportunity to visit this institute and the Fonds National Suisse de la Recherche Scientifique for financial support. The assistance of Per Andersson and N. E. Holmberg in the collection of data is gratefully acknowledged.

References

1) M. W. Johns and S. V. Nablo, Phys. Rev. **96** (1954) 1599
2) C. E. Mandeville, J. Varma and B. Saraf, Phys. Rev. **98** (1955) 94
3) G. Bäckström, O. Bergman, J. Burde and J. Lindskog, Nuclear Physics, **15** (1960) 566
4) A. Hedgran, K. Siegbahn and N. Svartholm, Proc. Phys. Soc. **A63** (1950) 960
5) S. Hultberg, Ark. f. Fysik **15** (1959) 307
6) A. S. Davydov and G. F. Filippov, Nuclear Physics **8** (1958) 237

1.E.2 *Nuclear Physics* **19** (1960) 482—495; © *North-Holland Publishing Co., Amsterdam*
Not to be reproduced by photoprint or microfilm without written permission from the publisher

ON NEUTRON-DEFICIENT ISOTOPES OF LIGHT NUCLEI AND THE PHENOMENA OF PROTON AND TWO-PROTON RADIOACTIVITY

V. I. GOLDANSKY

P. N. Lebedev Physical Institute, USSR Academy of Sciences, Moscow

Received 14 March 1960

Abstract: Application of isobaric invariance principles to light nuclei leads to a very simple relation between the Z-th proton binding energy E_p in nucleus 1 (${}_ZM_N^A$) and the Z-th neutron binding energy E_n in the miror nucleus 2 (${}_NM_Z^A$). With an accuracy of the order of a few per cent their difference $E_{n2} - E_{p1} = \Delta E_{np}$ is independent of N for a given Z and is given by

$$\Delta E_{np} \approx E_n({}_Z M_Z^{2Z}) - E_p({}_Z M_Z^{2Z}) \approx 1.2\,\frac{Z-1}{(2Z-1)^{\frac{1}{3}}}\,,$$

which is more correct than the usual expression $1.2\ (Z-1)/(Z+N-1)^{\frac{1}{3}}$. By exploiting this fact one can predict the existence and properties of almost ninety new neutron-deficient isotopes of light nuclei (up to $Z = 34$) and establish the limits of stability of the isotopes with respect to decay with proton emission. Among the specific properties of neutron-deficient isotopes, proton and two-proton radioactivity effects which may occur are of special interest. Some nuclei are indicated in which these effects may be observed. The main features of a very curious phenomenon of two-proton radioactivity are discussed.

1. Fundamental Energy Relations

As is well known, the difference in the neutron and proton binding energies in neighbouring mirror nuclei ${}_{Z-1}M_Z^A$ and ${}_ZM_{Z-1}^A$ equals the proton Coulomb energy $1.2\ (Z-1)/(A-1)^{\frac{1}{3}}$ MeV.

At first glance it would seen that the corresponding difference between the Z-th neutron binding energy in a nucleus 2, $E_n({}_NM_Z^A)$, for which the condition $N = Z - 1$ does not hold, and the Z-th proton binding energy in the mirror nucleus 1, $E_p({}_ZM_N^A)$, should equal the Coulomb energy of the Z-th proton in nucleus 1, which is $\approx 1.2\ (Z-1)/(Z+N-1)^{\frac{1}{3}}$, i.e. it should depend not only on Z but also on N (and hence on A).

It can readily be shown, however, that if the isobaric invariance principle is applied, the quantity ΔE_{np} under consideration is defined by the following relation†:

† Another simple corollary of isobaric invariance principles is, as can be readily proved, the following relation characterizing the mass difference between remote mirror nuclei:

$${}_ZM_N^A - {}_NM_Z^A \approx (Z-N)\,\Delta M_0\,,$$

where

$$\Delta M_0 = \begin{cases} {}_{\frac{1}{2}A+\frac{1}{2}}M^A_{\frac{1}{2}A-\frac{1}{2}} - {}_{\frac{1}{2}A-\frac{1}{2}}M^A_{\frac{1}{2}A+\frac{1}{2}} & \text{for odd } A\,, \\ \frac{1}{2}\left\{ {}_{\frac{1}{2}A+1}M^A_{\frac{1}{2}A-1} - {}_{\frac{1}{2}A-1}M^A_{\frac{1}{2}A+1} \right\} & \text{for even } A\,. \end{cases}$$

In some cases this formula may be useful and even more convenient than the relation (2) employed by us in this work.

$$\Delta E_{np} \approx E_n({}_N\mathrm{M}_Z^A) - E_p({}_Z\mathrm{M}_N^A)$$
$$= [E_{\mathrm{Coul}}({}_Z\mathrm{M}_N^A) - E_{\mathrm{Coul}}({}_{Z-1}\mathrm{M}_N^{A-1})] - [E_{\mathrm{Coul}}({}_N\mathrm{M}_Z^A) - E_{\mathrm{Coul}}({}_N\mathrm{M}_{Z-1}^{A-1})]$$
$$\approx 1.2 \left\{ \frac{Z-1}{A^{\frac{1}{3}}} - \tfrac{1}{2}(Z-N-1)\,(A-2) \left[\frac{1}{(A-1)^{\frac{1}{3}}} - \frac{1}{A^{\frac{1}{3}}} \right] \right\}, \qquad (1)$$

and to within a few per cent is in general independent of N. For $Z < N$ as well as $Z > N$, one has also

$$\Delta E_{np} \approx \Delta E_0 \equiv E_n({}_Z\mathrm{M}_Z^{2Z}) - E_p({}_Z\mathrm{M}_Z^{2Z}), \qquad (2)$$

where

$$\Delta E_0 \approx 1.2 \frac{Z-1}{(2Z-1)^{\frac{1}{3}}}. \qquad (3)$$

Besides the usual first two terms in squared brackets, account has also been taken in (1) of the change in the Coulomb energy due to decrease of the size of the nucleus as a result of the removal of a neutron (the last two terms in squared brackets).

Since a uniform distribution of the nuclear charge is a rough approximation, especially for light nuclei, relation (3) becomes correct with sufficient accuracy (not worse than $\pm$ 10 %) for $Z \geqslant 6$. Relation (2), on the other hand, is satisfactorily fulfilled for all values of Z, as can be seen from the experimental data presented in fig. 1 on ΔE_{np} and ΔE_0 for nuclei up to scandium. Only two

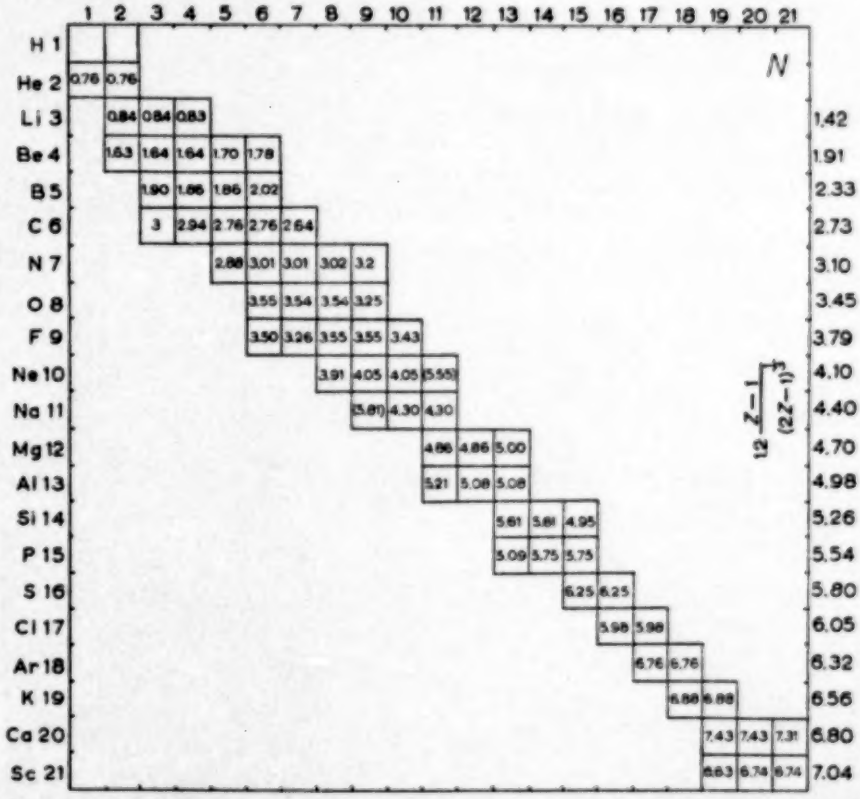

Fig. 1. Difference of binding energy of Z-th neutron in a ${}_N\mathrm{M}_Z^A$ nucleus and binding energy of Z-th proton in a ${}_Z\mathrm{M}_N^A$ nucleus (the numbers in the small squares are the values of ΔE_{np}).

TABLE I

Summary of the predicted isotopes and their properties

Z	Element	N	A	$M - A$ (MeV)	E_p (MeV)	E_n (MeV)	E_β (MeV)	$T_{\frac{1}{2}\beta}$ (sec)	Note
2	Helium	5	7	29.4 ± 0.5		-1.6			
		6	8	$< 36.1 \pm 3$		> 1.7	12.8	0.01	$T_{\frac{1}{2}\beta}$ refers to transition to 3.2 MeV level of Li^8 (1^+). Also see refs. [4,5]). (β^-)
4	Beryllium	8	12	< 30.3		> 1.5	< 13.4	$\gtrsim 0.01$	Predicted in ref. [4]). (β^-)
5	Boron	2	7	31.5 ± 0.5	-3.6				
6	Carbon	2	8	$< 40.4 \pm 4$	$-(< 1.3)$				
		10	16	< 17.5		> 4.6	< 4.5	? depends on N^{16} levels	Predicted in ref. [4]). (β^-)
7	Nitrogen	4	11	28.6	-2.5				
8	Oxygen	4	12	< 38.3	$-(< 2.1)$				
		5	13	27.3	1.4	< 19.4	17.1	0.01	
10	Neon	6	16	27.7—29	0.5—1.8		11.1—12.4	? depends on F^{16} levels	
		7	17	21.4	1.8	< 16	13.4	0.05	Questionable in ref. [3]). $T_{\frac{1}{2}\beta}$ refers to transition to $\frac{1}{2}^-$ level of F^{17} (3.1 MeV)
11	Sodium	8	19	18.3	-0.3		(9.9)	(0.7)	Questionable in ref. [3]). $T_{\frac{1}{2}\beta}$ refers to transition to $\frac{1}{2}^+$ level in Ne^{19} (0.2 MeV)
12	Magnesium	8	20	23.1	2.8		9.4	0.7	Predicted in ref. [4])
		9	21	17	3.4	14.5	12	0.3	Predicted in ref. [3])
14	Silicon	10	24	17.9	3.3		9.7	0.2	$T_{\frac{1}{2}\beta}$ refers to transition to 1^+ level of Al^{24} (0.5 MeV)
		11	25	11	3.7	15.2	11.6	0.4	Predicted in ref. [3])
		19	33	$-(< 12.4)$		< 6.1	> 4.2	?	(β^-)
15	Phosphorus	12	27	7.5	0.7		10.9	0.3	Questionable in ref [3]). $T_{\frac{1}{2}\beta}$ refers to transition to $\frac{1}{2}^+$ level of Si^{27} (0.9 MeV)
16	Sulphur	12	28	12.1	2.2		10.5	0.2	$T_{\frac{1}{2}\beta}$ for transition to 1.5 MeV level in P^{28}
		13	29	5	3.1	15.5	12.4	0.4	Predicted in ref. [3]) $T_{\frac{1}{2}\beta}$ for transition to $\frac{3}{2}^+$ level in P^{29} (1.4 MeV)
		14	30	-5.2	4.4	18.5	5.1	2	Predicted in ref. [3]). $T_{\frac{1}{2}\beta}$ for transition with $\Delta T = 0$
		23	39	$-(< 12.7)$		< 5.5	> 5.6	?	(β^-)
[illegible]	[illegible]	14	31	1.8	0.6		10.6	2	Questionable in ref. [3])
18	Argon	14	32	6.9	2.5		< 20	1	$T_{\frac{1}{2}\beta}$ for transition with $\Delta T = 0$

		14	31	1.8	0.6		10.6	2	Questionable in ref. [2])
18	Argon	14	32	6.9	2.5		< 20	1	$T_{\frac{1}{2}\beta}$ for transition with $\Delta T=0$
		15	33	0.2	3.3	15.1	10.8	0.7	Predicted in ref. [3])
		16	34	— 8.6	4.6	17.2	4.7	1	Predicted in ref. [3]). $T_{\frac{1}{2}\beta}$ for transition with $\Delta T = 0$
		24	42	—(> 20)		> 6.5	< 2.6	?	(β^-)
19	Potassium	14	33	> 15.3	—(> 0.8)		(> 14.1)	(< 0.1)	
		15	34	8.1	— 0.3	> 15.6	(15.7)	(0.1)	
		16	35	— 1.1	0.1	17.6	10.6	0.7	Questionable in ref. [3])
		17	36	— 6.7	1.7	14	< 12	0.8	Predicted in ref. [3]). $T_{\frac{1}{2}\beta}$ for transition with $\Delta T = 0$
20	Calcium	16	36	4	2.5		9.7	0.5	$T_{\frac{1}{2}\beta}$ for transitions with $\Delta T = 0$
		17	37	— 2	2.9	14.4	10.9	0.5	Predicted in ref. [3])
21	Scandium	16	37	14	— 0.7		(15)	(0.05)	$T_{\frac{1}{2}\beta}$ for transition to ≈ 2.7 MeV Ca^{37} level
		17	38	6.3	— 0.2	16.1	(15.9)	(0.5)	$T_{\frac{1}{2}\beta}$ for transition with $\Delta T = 0$
		18	39	— 2.9	0.6	17.6	11.7	0.5	Predicted in ref. [3]). $T_{\frac{1}{2}\beta}$ refers to transition with $\Delta T = 0$
22	Titanium	16	38	21	0.6		13.7	0.3	For all subsequent isotopes $T_{\frac{1}{2}\beta}$ is that for transition with $\Delta T = 0$
		17	39	13.1	0.8	16.3	15	0.3	
		18	40	2.0	2.6	19.5	10.2	0.4	
		19	41	— 4.4	2.8	14.8	11.6	0.4	
		20	42	— 13.7	4.2	17.7	5.6	0.5	
23	Vanadium	16	39	> 29.6	—(> 1)				
		17	40	22.2	— 1.7	> 16.4			
		18	41	10.9	— 0.6	19.6	14.3	0.2	
		19	42	3.2	— 0.1	16.1	16	0.2	
		20	43	— 6.5	0.4	18.2	9.5	0.3	
		21	44	— 11.5	2.2	13.5	12.1	0.3	
		22	45	— 19	1.9	15.8	5.7	0.3	
24	Chromium	18	42	< 18	—(< 0.2)		(< 13.8)	($0_{\frac{1}{2}}$)	
		19	43	9	1.9	< 17.4	14.5	0.2	
		20	44	— 2.3	3.4	19.7	8.2	0.2	
		21	45	— 7.6	3.6	13.7	10.4	0.2	
25	Manganese	19	44	16.6	0		(17.9)	(0.2)	
		20	45	5.9	— 0.6	19.1	(12.5)	(0.2)	
		21	46	— 0.8	0.8	15.1	15	0.2	
		22	47	— 10.1	0.9	17.7	10	0.2	
		23	48	— 16.1	2.5	14.4	11.8	0.2	
26	Iron	20	46	11.3	2.2		11.1	< 0.2	
		21	47	4.4	2.4	15.3	13.5	< 0.2	

TABLE 1 (*Continued*)

Z	Element	N	A	$M - A$ (MeV)	E_p (MeV)	E_n (MeV)	E_β (MeV)	$T_{\frac{1}{2}\beta}$ (sec)	Note
		22	48	— 5.8	3.4	18.6	9.3	< 0.2	
		23	49	— 11.9	3.4	14.5	10.8	0.2	
		24	50	— 20.9	4.7	17.4	6.3	0.2	
		25	51	— 25.7	5.1	13.2	6.4	0.2	
27	Cobalt	20	47	20	— 1.1				
		21	48	12.2	— 0.2	16.2	(17)	(< 0.2)	
		22	49	2.1	— 0.3	18.6	(13)	(< 0.2)	
		23	50	— 5.2	0.9	15.4	14.7	< 0.2	
		24	51	— 14.1	0.8	17.3	10.6	< 0.2	
		25	52	— 20.2	2.1	14.5	< 12	< 0.2	
		26	53	—(< 27.4)	> 1.9	15.5	6.6	< 0.2	
28	Nickel	20	48	25.8	1.4		12.6	0.1	
		21	49	18.2	1.5	16	15.3	0.1	
		22	50	7.1	2.3	19.5	11.3	0.1	
		23	51	— 0.1	2.4	15.6	13.1	0.1	
		24	52	— 10	3.4	18.3	9.3	0.1	
		25	53	— 16.2	3.4	14.6	10.2	< 0.2	
		26	54	— 24.8	5	17	6	< 0.2	
		27	55	— 30	6.6	13.5	6.9	< 0.2	
29	Copper	20	49	37	— 3.7				
		21	50	27.9	— 2.2	17.5			
		22	51	17.1	— 2.5	19.2			
		23	52	9	— 1.5	16.5			
		24	53	— 1.6	— 0.9	19	(13.6)	(0.1)	
		25	54	— 8.8	0.1	15.6	15.1	0.1	
		26	55	— 17.8	0.4	17.4	11.2	0.1	
		27	56	— 23.6	1.1	14.2	< 13.2	0.1	
30	Zinc	23	53	16.2	0.4		16.8	< 0.1	
		24	54	5.3	0.7	19.3	13.1	< 0.1	
		25	55	— 2.4	1.2	16	14.4	< 0.1	
		26	56	— 12.4	2.2	18.4	10.2	< 0.1	
		27	57	— 18.7	2.7	14.7	12	< 0.1	
		28	58	— 26.8	2.7	16.5	< 6.8	< 0.1	
		29	59	— 30.6	> 3.6	12.2	7.3	< 0.1	
31	Gallium	24	55	16.1	— 3.2				
		25	56	7.2	— 2	17.3			
		26	57	— 3.2	— 1.6	18.8			
		27	58	— 10.1	— 1	15.3	(15.7)	(< 0.1)	
		28	59	— 18.9	— 0.3	17.2	(10.7)	(< 0.1)	
		29	60	— 23.7	0.7	13.2		< 0.1	Hitherto undiscovered isotopes with $A = 62, 63$ also stable

		29	60	— 23.7	0.7	13.2		< 0.1	Hitherto undiscovered isotopes with $A = 62.63$ also stable
		30	61	— 29.5		14.2		< 0.1	
32	Germanium	25	57	15.6	— 0.8		(17.8)	(< 0.1)	
		26	58	3.9	0.5	20.1	13	< 0.1	
		27	59	— 3.5	1	15.8	14.4	< 0.1	
		28	60	— 13.2	1.9	18.2	9.5	< 0.1	
		29	61	— 18.4	2.3	13.6	10.1	< 0.1	Hitherto undiscovered isotopes with $A = 63$–65 also stable
		30	62	— 25.5	3.6	15.5		< 0.1	
33	Arsenic	26	59	14.5	— 3				
		27	60	6.3	— 2.2	16.7			
		28	61	— 3.7	— 1.9	18.4			
		29	62	— 10	— 0.8	14.8	(14.5)	(< 0.1)	
		30	63	— 17.4	— 0.5	15.7	15.7	(< 0.1)	Isotopes with $A = 64$–67 also evidently stable
34	Selenium	27	61	14.7	— 0.8		(17.4)	(< 0.1)	
		28	62	3.2	0.7	20	12.2	< 0.1	
		29	63	— 3.3	0.9	15	13.1	< 0.1	Hitherto undiscovered isotopes with $A = 65$–69 also stable
		30	64	— 11.7	1.9	16.8		< 0.1	
35	Bromine	27	62	25.3	— 3				
		28	63	14.1	— 3.3	19.7			
		29	64	6.5	— 2.2	16.0			Isotopes beginning from $A = 73$ known at present
		30	65	— 2	— 2.1	16.9			
36	Krypton	28	64	22.3	— 0.6		(14.8)	(< 0.1)	
		29	65	14.5	— 0.4	16.3	(15.5)	(< 0.1)	Isotopes beginning from $A = 76$ known at present
		30	66	4.9	0.7	18		(< 0.1)	
37	Rubidium	28	65	34.3	— 4.4				
		29	66	25.5	— 3.4	17.2			Isotopes beginning from $A = 81$ known at present
		30	67	15.9	— 3.4	18			
38	Strontium	29	67	34.6	— 1.5				
		30	68	24	— 0.5	19		(< 0.05)	Isotopes beginning from $A = 81$ known at present
39	Yttrium	30	69	36	— 4.4				Isotopes beginning from $A = 82$ known at present
40	Zirconium	30	70	45.4	— 1.8				Isotopes beginning from $A = 86$ known at present

significant deviations from (2) (for the pairs F^{20}–Na^{20} and Ne^{21}–Na^{21}) are observed. The discrepancies are evidently due to the fact that the mass defect value of Na^{20} presented in ref. [1]) (see also ref. [2])) is too high by about 1.5 MeV (it should be 12.7 MeV), as a result of a very rough estimation of the end point energy of the β-spectrum.

2. Neutron-deficient Isotopes

By applying (2) and, in those cases when ΔE_0 is unknown, by applying (3), one can predict the properties of a large number of neutron-deficient isotopes

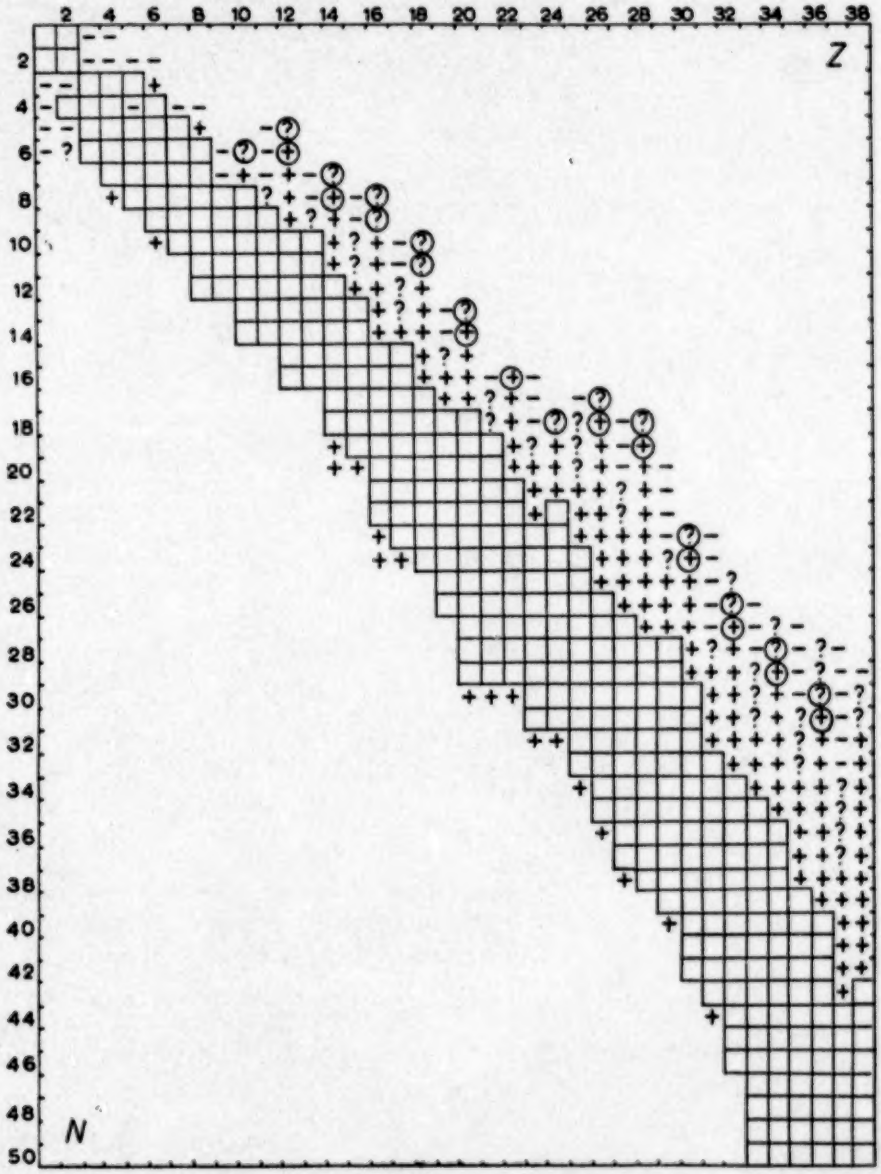

Fig. 2. Data on known and predicted isotopes. The region of previously known isotopes is outlined. The meaning of the different symbols is: + predicted isotopes stable with respect to p and n emission; ? p-stability questionable; O 2p-activity possible; — isotopes which beyond doubt are unstable with respect to n or p emission.

of light nuclei on the basis of known properties of the corresponding mirror nuclei with surplus neutrons. Some predictable properties are the neutron and proton binding energies, mass defects, β-decay half-periods and mechanism of the decay (transition to the ground or excited states), possibility of observing proton or two-proton radioactivity. A summary of all predicted isotopes (including proton-unstable ones), and their properties is presented in table 1 and fig. 2. Isotopes whose existence have been previously predicted by Baz[3]) or Zeldovich[4]) are correspondingly designated.

The values of $(M - A)$, E_p, E_n and E_β presented in the table are correct within an accuracy of 1 MeV. The values of $T_{\frac{1}{2}\beta}$ should be regarded as order of magnitude values.

The accuracy of the energy values was such that it was meaningless to take into account in the numerical calculations corrections for the increase of nuclear dimensions with the rise of Z at given A or for the proton Coulomb exchange energy of the type considered, for example, in ref. [6]).

With account of these corrections we obtain

$$\begin{aligned}
\Delta E_{np} &= E_n({}_N\mathrm{M}_Z^A) - E_p({}_Z\mathrm{M}_N^A) \\
&= [E_{\mathrm{Coul}}({}_Z\mathrm{M}_N^A) - E_{\mathrm{Coul}}({}_{Z-1}\mathrm{M}_N^{A-1})] - [E_{\mathrm{Coul}}({}_N\mathrm{M}_Z^A) - E_{\mathrm{Coul}}({}_N\mathrm{M}_{Z-1}^{A-1})] \\
&= 0.6\,[(Z-N)\,(Z+N)^{\frac{1}{3}} - (Z-1-N)\,(Z-1+N)^{\frac{1}{3}}] \\
&\quad - 0.6\left[C_Z\frac{Z^{\frac{1}{3}}}{(Z+N)^{\frac{1}{3}}} - C_{Z-1}\frac{(Z-1)^{\frac{1}{3}}}{(Z-1+N)^{\frac{1}{3}}}\right. \\
&\quad \left. - C_N\frac{N^{\frac{1}{3}}}{(Z+N)^{\frac{1}{3}}} + C_N\frac{N^{\frac{1}{3}}}{(Z+N-1)^{\frac{1}{3}}}\right], \qquad (4)
\end{aligned}$$

where

$$C_m = 0.7636 - \mathrm{e}^{-0.38\,m}. \qquad (5)$$

It should be noted that to a large extent the correction terms compensate each other.

With an accuracy of a few percent,

$$\Delta E_{np} \approx 0.6\,(2Z-1)^{\frac{1}{3}} - C_Z Z^{\frac{1}{3}}\,\frac{\frac{4}{3Z} - \frac{1}{3(Z+N)}}{(Z+N-1)^{\frac{1}{3}}} \qquad (6)$$

and, owing to the insignificant role of the correction, one can express ΔE_{np} in the form

$$\Delta E_{np} \approx 0.6\left[(2Z-1)^{\frac{1}{3}} - C_Z\frac{7}{6.2^{\frac{1}{3}}}\right] \approx 0.6\,[(2Z-1)^{\frac{1}{3}} - C_Z] \qquad (7)$$

by assuming that $N \approx Z$ in the correction term. It is easy to verify that corrections for Coulomb exchange interaction of the protons decreases ΔE_{np} with respect to (1), (2) or (3) by less than ≈ 0.4 MeV.

3. β-Decay

The data presented in the table require some additional explanation which will be now given. In the mass defect calculations based on the nucleon binding energies computed from (2) and (3), use was made of the data presented in the summary tables in ref. [1]) and [2]). Besides neutron-deficient isotopes some isotopes with an excess of neutrons are presented at the beginning of the table. Data pertaining to these isotopes were derived from information on the pairing energy of neutrons in neighbouring isotopes with even values of Z (see ref. [5])). The properties thus derived were then employed to supplement the main list of neutron-deficient isotopes by the corresponding mirror nuclei.

The β^+ decay energies refer to a ground state transition. These energies are related to similar β^- transitions in mirror nuclei by the simple relationship

$$E_{\beta^+}({}_Z\mathrm{M}_N^A) - E_{\beta^-}({}_N\mathrm{M}_Z^A) \approx 1.2\left[\frac{N}{(2N-1)^{\frac{1}{3}}} + \frac{Z}{(2Z-1)^{\frac{1}{3}}}\right] - 2.6\ \mathrm{MeV} \qquad (8)$$

(where 2.6 MeV $= 2m_e + 2(m_n - m_{\mathrm{H}})$. In the calculations of the half-period for β^+-decay one should keep in mind the possible existence of "super-allowed" transitions not involving a change of isobaric spin. In such transitions

$${}_{Z+1}\mathrm{M}_N^A \rightarrow {}_Z\mathrm{M}_{N+1}^{*A}$$

the β^+ decay energy is given simply as

$$E_{\beta^+}(\Delta T = 0) \approx 1.2\frac{Z}{A^{\frac{1}{3}}} - 1.8\ \mathrm{MeV} \qquad (9)$$

(where 1.8 MeV $= 2m_e + m_n - m_{\mathrm{H}}$) and varies slowly with A for a fixed value of Z.

If E_{β^+} exceeds the threshold defined by (9), the "super-allowed" transitions begin to compete with transitions to the ground state, the rate of transitions with $\Delta T = 0$ increasing with increasing Z as a result of the increase of their energy. Many of the neutron-deficient isotopes predicted here (practically all of them beginning at $Z \approx 20$) should undergo β^+-decay with $\Delta T = 0$ and subsequent cascade emission of γ-quanta or of delayed protons (or couples of protons). In such cases the values of E_β presented in table 1 characterize the sum of the maximum positon energy and energies of the subsequent γ-transitions. The peak positon energies for "super-allowed" transitions vary from ≈ 5 MeV for calcium to ≈ 8 MeV for selenium and the half periods (for $\log ft \approx 3.5$) change from ≈ 0.5 to ≈ 0.07 sec.

The values of the lifetimes of a number of known β^+ active isotopes with $Z = 13 - 25$ for which $E_\beta > 1.2\,Z/A^{\frac{1}{3}} - 1.8$ MeV (e.g. Al^{24}, Ca^{38}, V^{46} and Mn^{50}) confirm this assumption.

Because of the low value of the energy, "super-allowed" transitions are

found to be quite slow for lighter nuclei and hence transitions to ground states more frequently become dominant. For such light nuclei the half-lives were mainly computed on the basis of available data on "mirror" β^- decay.

4. Proton Radioactivity

The following is a list of stable isotopes which are located, according to our estimations, on the boundary of stability with respect to proton emission: Li^6, Be^7, B^8, C^9, N^{12}, O^{13}, F^{17}, Ne^{17}, $Na^{20(19?)}$, $Mg^{19(18?)}$, Al^{23}, $Si^{23(22?)}$, P^{27}, S^{26}, Cl^{31}, Ar^{30}, K^{35}, $Ca^{35(34?)}$, $Sc^{40(39?)}$, Ti^{39}, $V^{43(42?)}$, Cr^{43}, Mn^{46}, Fe^{45}, $Co^{50(48?)}$, Ni^{48}, Cu^{54}, $Zn^{55(54?)}$, $Ga^{60(59?)}$, Ge^{59}, $As^{64(?)}$, $Se^{62(61?)}$.

A comparison of this list with that of isotopes known at present indicates that approximately ninety new neutron-deficient isotopes of light nuclei may yet be discovered.

The next problem we consider is that regarding the possibility of detecting proton radioactivity[7]). It can easily be shown that the probability of observing this process is quite small. In fact, if the half life for p-decay is less than $10^{-4} - 10^{-3}$ sec it should already be difficult to record the events by delay coincidence techniques under the conditions of an accelerator. On the other hand, if the lifetime with respect to p-decay exceeds 1–10 sec the effect will be strongly obscured by β^+-decay. The half-life of proton-radioactive isotopes can approximately be determined from the formula

$$\log T_{\frac{1}{2}}\,(\text{sec}) \approx 0.43\, Z^{\frac{1}{2}} f(x) - 22\,, \tag{10}$$

where x is the ratio of the emitted proton energy to the height of the Coulomb barrier; for $x \ll 1$ we have

$$f(x) = 0.6\, x^{-\frac{1}{2}} [\arccos x^{\frac{1}{2}} - x^{\frac{1}{2}} (1 - x^{\frac{1}{2}})] \approx 0.6\, [\tfrac{1}{2}\pi x^{-\frac{1}{2}} - 2]\,. \tag{11}$$

For the interval $T_{\frac{1}{2}} = 10 - 10^{-4}$ sec the corresponding energies of the emitted protons are $0.03 - 0.04$ MeV (for $Z = 10$), $0.1 - 0.15$ MeV (for $Z = 20$), $0.2 - 0.3$ MeV (for $Z = 30$) and $0.35 - 0.5$ MeV (for $Z = 40$).

The energy range of recorded proton radioactivity events, however, can be appreciably broadened by observing the emission of delayed protons occurring after reactions on photographic emulsion or cloud chamber vapors nuclei. If protons with a lag of $\approx 10^{-12}$ sec are assumed to be distinguishable under such conditions from instantaneous protons, the upper limit for the energy of observed radioactive p-decays will increase up to 0.35 MeV ($Z = 20$), 0.70 MeV ($Z = 30$) and 1.1 MeV ($Z = 40$).

Of course the accuracy of our calculations of the masses is much too small to permit us to predict whether proton radioactivity will be observed at all, not speaking of predicting in exactly which isotopes it should be observed. The only

thing that is clear is that this phenomenon should be sought near the aforementioned stability boundaries (which is also true for some heavier nuclei not considered by us here).

5. Two-Proton Radioactivity

Owing to the very large neutron binding energy for all isotopes considered here the latter will all be stable with respect to α-decay from the ground state. However, a very curious effect, the two-proton radioactivity, can now be observed. Even at a positive proton binding energy instability with respect to emission of two protons may appear in even-Z isotopes. A well-known example[8]) of such two-proton instability is Be^6, but in this case the energy of $Be^6 \rightarrow Li^5 + p$ decay is less than the half width of the ground state of Li^5 and therefore the decay of Be^6 cannot be treated as two-proton radioactivity. The general condition for two-proton radioactivity is that the positive binding energy of the first proton must be larger than the half width of the emission of the second one. Therefore, the two-proton radioactive decay should be distinguished from possible $p\beta^+$- or p-decay chains, e.g.

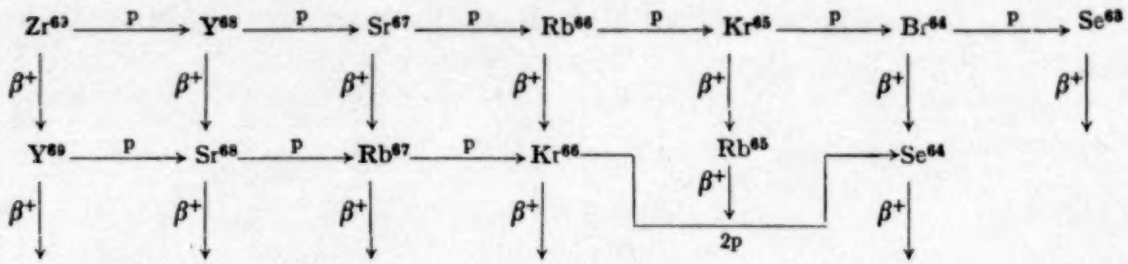

though in the p-decay chains the possibility of two-proton emission may essentially decrease the lifetime of p-radioactive isotopes with even $Z = 2m + 2$ in those rare cases when the energy of 2p-decay

$$E_{pp}(2m + 2 \rightarrow 2m) > 8E_p(2m + 2 \rightarrow 2m + 1) .$$

Variants of two-proton emission are illustrated in fig. 3(a, b, c), fig. 3c representing the "pure" case of two-proton radioactivity.

Thus, in such isotopes which are stable against proton and alpha decay, two-proton decay may be observed. This effect, which can also be conveniently observed with photographic emulsions of in the cloud chamber may occur in Ne^{16}, $Mg^{17(18?)}$, $Si^{21(22?)}$, $S^{25(24?)}$, $Ar^{29(28?)}$, $Ca^{25(24?)}$, Ti^{38}, Cr^{42}, $Fe^{44(43)}$, $Ni^{46(47?)}$, $Zn^{53(54?)}$, $Ge^{59(58?)}$, $Se^{63(62?)}$, $Kr^{67(66?)}$.

The probability for simultaneous sub-barrier emission of two protons includes the product of the two barrier penetration factors for the protons or the product of the penetration factor for a doubly charged particle and a preexponential factor which characterizes the probability for two-proton correlation in the nucleus. The lifetimes of the isotopes, therefore, assume values

convenient for measurement, which lie in a much broader energy interval in the case of two-proton decay than in the case of proton radioactivity. The possibility of two-proton emission from a nucleus which is stable against single-proton decay is a direct result of the binding energy of the even proton exceeding that

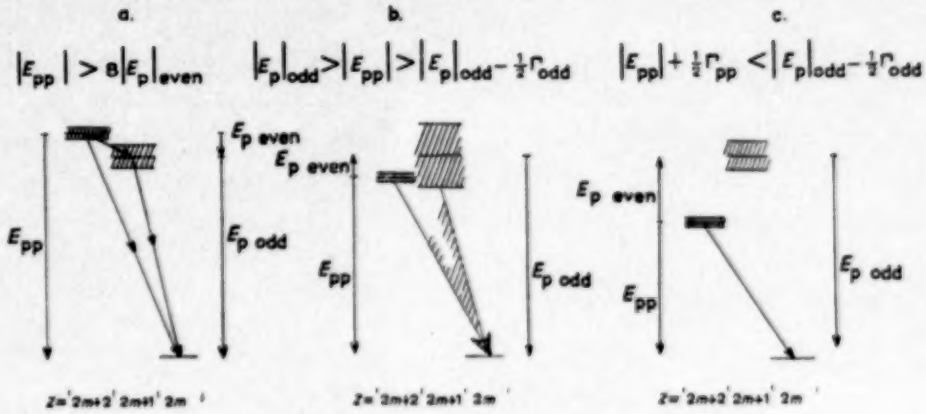

Fig. 3. Two-proton radioactivity.

of the preceding odd proton, i.e., it is thus clear that the properties of a stable diproton within the nucleus should become apparent in two-proton radioactive decay. Moreover, the angular and energy distributions and correlations of the emitted protons are found to be dependent on the nature of pair interaction of the protons in the initial nuclei. On the other hand, since break-up of the diproton occurs in a "tunnel" through the barrier it determines the effective height of the barrier and its penetration.

Thus, the simplest approach to the theory of two-proton decay would consist in using the product of two usual barrier factors, that is, in introducing an exponential factor of the type

$$w(E) = \exp\left\{\frac{-2\pi\,(Z-2)\,e^2\sqrt{M}}{\hbar\sqrt{E_{pp}}}\left[\frac{1}{\sqrt{x}} + \frac{1}{\sqrt{1-x}}\right]\right\}, \qquad (12)$$

where E_{pp} is the sum of the energies of the two protons (energy of emitted diproton), x and $(1 - x)$ are the fractions of energy referring to each of the protons.

It can easily be seen that the total barrier factor $w(E)$ is maximum for $x = 0.5$, i.e., when the proton energies are equal. It will be noted that the value in the exponent is just the same as for the sub-barrier emission of a diproton with the energy E_{pp} as a whole.

Thus, the break-up of the sub-barrier diproton does not change the permeability of the barrier if no additional interaction (such as Coulomb repulsion) between two protons are considered. The probability $w_x(E)$ for such two-proton decay when the energy imparted to one of the protons is $(0.5 - x)E_{pp}$

($\varkappa \ll 0.5$) and that imparted to the other proton is $(0.5 + \varkappa)E_{pp}$ is related to $[w(E)]_{max} = w_0(E)$ by the relation

$$\frac{w_\varkappa(E)}{w_0(E)} \approx \exp\left\{-\frac{6\pi\,(Z-2)\,e^2\sqrt{M}}{\hbar\sqrt{E_{pp}}}\,\varkappa^2\right\}.$$

It is evident that the energy correlation between the two protons during two-proton decay, which leads to their energies being almost equal, is quite strong. This correlation offers the possibility of detecting two-proton radioactivity even for almost immediate two-proton decays (by observing the equality of energies for two sub-barrier protons). The interesting problem concerning two-proton radioactivity of neutron-deficient isotopes of even elements certainly deserves a more detailed special study.

6. Further Remarks

It may be noted here that the most feasible way of obtaining neutron deficient isotopes of light nuclei is to bombard the lightest stable isotopes of neighbouring nuclei with protons or He^3 nuclei possessing energies close to the threshold value and also to use the heavy-ion nuclear reactions. However, one should keep in mind that owing to the low energy of the Coulomb barrier "boiling away" of protons will not be inhibited and hence the cross sections for production of neutron-deficient isotopes should be small.

In conclusion we shall note that in the case of neutrons a phenomenon similar to two-proton radioactivity may occur. The excitation energy of nuclei with large neutron excess and even number of neutrons, at which the emission of neutrons becomes possible, may prove to be lower than the threshold for the emission of one neutron owing to pairing effects. Therefore, for such nuclei there may be an excitation energy interval corresponding to the emission of neutron pairs correlated in angle and energy, without emission of single neutrons. Still more frequent must be the cases when the strongly excited states of neutron-saturated nuclei with an even number of neutrons may break up emitting one neutron as well as a correlated neutron pair. If similar excited states arise after a preceding β-decay, they can be observed by the coincidence-delayed neutron pairs.

7. Conclusions

1) The difference between the Z-th neutron and Z-th proton binding energies for any pair of mirror nuclei is determined by the formula

$$\Delta E_{np} = E_n({}_N\mathrm{M}^A_Z) - E_p({}_Z\mathrm{M}^A_N) \approx E_n({}_Z\mathrm{N}^{2Z}_Z) - E_p({}_Z\mathrm{M}^{2Z}_Z) \approx 1.2\,\frac{Z-1}{(2Z-1)^{\frac{1}{3}}}\ \mathrm{MeV},$$

which shows that it is independent of N.

2) With the aid of this formula it is possible to predict the existence of almost 90 new neutron-deficient isotopes of light nuclei ($Z = 8 - 34$) and also their properties (mass-defects, neutron and proton binding energy, β-decay energy and half-period). The limits of stability of neutron-deficient isotopes of light nuclei against proton and two-proton decay are indicated.

3) Proton-radioactive decay and also the specific phenomenon of two-proton radioactivity can be observed near the indicated stability boundaries.

4) The main features of two-proton radioactivity are discussed.

The author is sincerely thankful to Ya. B. Zeldovich for useful discussions.

References

1) F. Ajzenberg-Selove and T. Lauritsen, Nuclear Physics **11** (1959) 1
2) V. A. Kravtsov, Uspekhi Fiz. Nauk **65** (1958) 451
3) A. I. Baz, Atomnaya Energia **6** (1959) 571
4) Ya. B. Zeldovich, JETP **38** (1960) 1123
5) V. I. Goldansky, JETP **38** (1960) 1637
6) N. Swamy and A. Green, Phys. Rev. **112** (1958) 1719
7) B. S. Dzhelepov, Izvestija Akad. Nauk. SSSR Ser.-Fiz. **15** (1951) 498
8) G. F. Bogdanov, N. A. Vlasov, S. P. Kalinin, B. V. Rybakov and V. A. Sidorov, Atomnaya Energia **3** (1957) 204, no. 9

1.C:
1.E.1

Nuclear Physics **19** (1960) 496—499; © *North-Holland Publishing Co., Amsterdam*
Not to be reproduced by photoprint or microfilm without written permission from the publisher

PAIRING INTERACTION IN NUCLEI

G. ABRAHAM

Atomic Energy Establishment Trombay, Bombay, India

and

K. K. GUPTA

Tata Institute of Fundamental Research, Bombay, India

Received 16 May 1960

Abstract: The first excited levels of O, Ca and Pb isotopes have been calculated, using a constant pair interaction between particles outside the doubly closed shells. Quantitative agreement with experiment is obtained only for the Pb isotopes.

1. Introduction

In the Bardeen, Cooper and Schrieffer[1]) model of superconductivity one derives the energy gap above the ground state, making use of interactions between pairs of electrons of opposite momenta and spins. It was suggested by Bohr, Mottleson and Pines[2]) that pair interactions between nucleons which differ only in the sign of their magnetic quantum numbers could be responsible for the fact that in some heavy even nuclei the energy of the first excited state (> 1 MeV) is much larger than for neighbouring odd-mass nuclei (≈ 150 keV). Belyaev[3]) has shown that if the pairing interaction has a coherent character, this energy gap can be derived. Unfortunately the states considered in this model are not eigenstates of the number of nucleons; even the mean number of nucleons in the ground and the excited states are not the same. There is so far no theory which avoids this difficulty in the general case of an arbitrary number of particles in several non-degenerate states. In the case of a single degenerate level and a constant pairing interaction, Mottelson[4]) has derived a spectrum for any even number of similar particles, which agrees in a rough way with experiment, for low lying levels of the Pb isotopes. With several non-degenerate levels, the eigenvalue calculation can be carried out without difficulty provided we restrict ourselves to 2 and 3 particles. This has been done in this paper with special references to the Pb, Ca and O isotopes.

2. The Interaction Hamiltonian

The success of the shell model shows that the total interaction between the nucleons can be separated into two parts: a spherically symmetric self-consistent single-particle potential, and a weak residual two-body interaction.

With the help of creation and annihilation operators, we can thus write the total Hamiltonian as a sum of two parts, H_0 giving the energy in the single particle potential and H' defining the residual interaction between pairs of particles:

$$H_0 = \sum_{j,m} a^+_{jm} a_{jm} \varepsilon_j \,, \tag{1}$$

$$H' = \tfrac{1}{2} \sum_{jm} < j'_1 m'_1, j'_2 m'_2 \mid g \mid j_1 m_1, j_2 m_2 > a^+_{j'_1 m'_1} a^+_{j'_2 m'_2} a_{j_1 m_1} a_{j_2 m_2} \,. \tag{2}$$

Here ε_j is the single particle energy in the self-consistent potential, and a^+_{jm}, a_{jm} are creation and annihilation operators satisfying the commutation relations

$$[a_{jm}, a^+_{j'm'}]_+ = \delta_{jj'}\delta_{mm'}, \; [a_{jm}, a_{j'm'}]_+ = [a^+_{jm}, a^+_{j'm'}]_+ = 0 \,; \tag{3}$$

j and m denote the total angular momentum and one of its components. Following Mottelson[4]) we now assume that the residual interaction is between pairs only and is a constant for all pairs:

$$H' = -g \sum a^+_{j'm'} a^+_{j' \, -m'} a_{jm} a_{j \, -m} \,. \tag{4}$$

We shall now outline the method of calculation for the Pb isotopes. The same procedure applies generally for two and three identical particles outside a closed shell.

For $_{82}\mathrm{Pb}^{207}_{125}$ the single-hole levels which are taken into account are shown in fig. 1. The energy matrix for $_{82}\mathrm{Pb}^{206}_{124}$ is

$$\begin{pmatrix} -g\,(1) & & & & \\ & -g + 2a_1\,(3) & & & \\ & & -g + 2a_2\,(2) & & -g \\ & & & -g + 2a_2\,(7) & \\ & -g & & & -g + 2a_4\,(4) \end{pmatrix}. \tag{5}$$

Here the rows and columns are labelled by indices $(jm, j - m)$. The unpaired states are of course not affected by the interaction. The a_1, a_2, . . . are the single-particle excitation energies, and the numbers in square brackets denote the number of times that the corresponding element occurs on the diagonal. All non-diagonal elements are $-g$. The secular determinant is

$$\begin{aligned} \lambda_1^2 \lambda_2 \lambda_3^6 \lambda_4^3 \, (\lambda\lambda_1\lambda_2\lambda_3\lambda_4 + 4g\,\lambda\lambda_1\lambda_2\lambda_3 + 7g\,\lambda\lambda_1\lambda_2\lambda_4 + \\ + 2g\,\lambda\lambda_1\lambda_3\lambda_4 + 3g\,\lambda\lambda_2\lambda_3\lambda_4 + g\lambda_1\lambda_2\lambda_3\lambda_4) \,, \end{aligned} \tag{6}$$

where we have put

$$(\lambda - 2a_1) = \lambda_1 \,, \; (\lambda - 2a_2) = \lambda_2 \,, \; (\lambda - 2a_3) = \lambda_3 \,, \; (\lambda - 2a_4) = \lambda_4 \,. \tag{7}$$

In deriving eq. (6) we have used the fact that terms having less than 16 products of λ and λ_i vanish, on account of all nondiagonal elements being the same.

The roots of eq. (6), in addition to $2a$, $2a_2$, $2a_3$ and $2a_4$, are obtained by finding the roots of the fifth degree polynomial in the brackets in eq. (6).

For ${}_{82}Pb^{205}_{123}$ one has three neutron holes. The states which are affected by the interaction are designated by $(jm, j-m, j'm')$, denoting two paired particles and one odd particle. The total Hamiltonian in this case can be reduced to direct sums of 16×16 sub-matrices, each sub-matrix acting only on the states in which the odd particle is in a fixed state jm. The sub-matrices are all of the same form as eq. (5). The secular determinant can therefore be written down in the same way.

3. Results and Discussion

The observed single particle spectra of Pb^{207}, Ca^{41} and O^{17} and the observed and calculated first excited levels of Pb^{206}, Pb^{205}, Ca^{42}, Ca^{43}, O^{18} and O^{17} are given in figs. 1, 2 and 3. With no residual interaction and no change in the single-particle potential H_0 (eq. (1)), the nergy of the first excited levels would be the

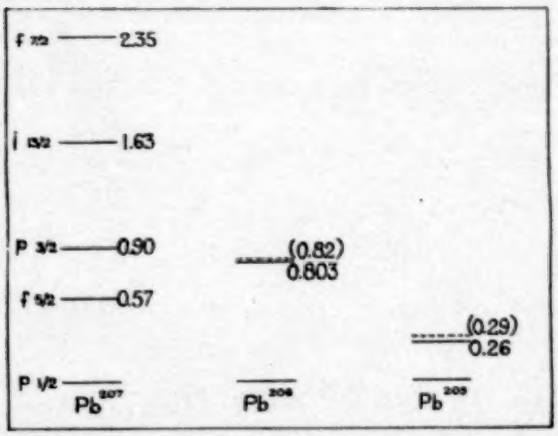

Fig. 1. Single-particle states of Pb^{207}, and calculated (indicated by dashed lines) and experimental first excited levels of Pb^{206} and Pb^{205}.

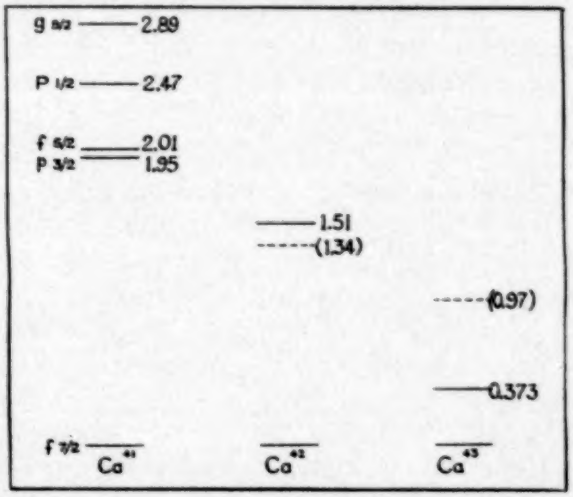

Fig. 2. Single-particle states of Ca^{41}, and calculated (indicated by dashed lines) and experimentalfirst excited levels of Ca^{42} and Ca^{43}.

same for one, two or three similar nucleons outside the closed shell. We assume here that the variation of the first excited level is entirely due to the pair interaction (4). The levels of Pb^{205} and Pb^{206} have been calculated for the value 0.1 MeV of the parameter g in (4), and are shown by dashed lines in fig. 1. The agreement with the observed levels is remarkably good. In fig. 2, the calculated levels of Ca isotopes are for $g = 0.2$ MeV. The calculated energies decrease, but not to the extent of the experimental levels. In the case of O isotopes we have chosen $g = 0.5$ MeV to fit the O^{18} level. The calculated first excited level in

O^{19} is then less than the corresponding O^{17} level but still much larger than the observed level at 0.096 MeV, which presumably is the first excited state due to the three nucleons outside the closed shell.

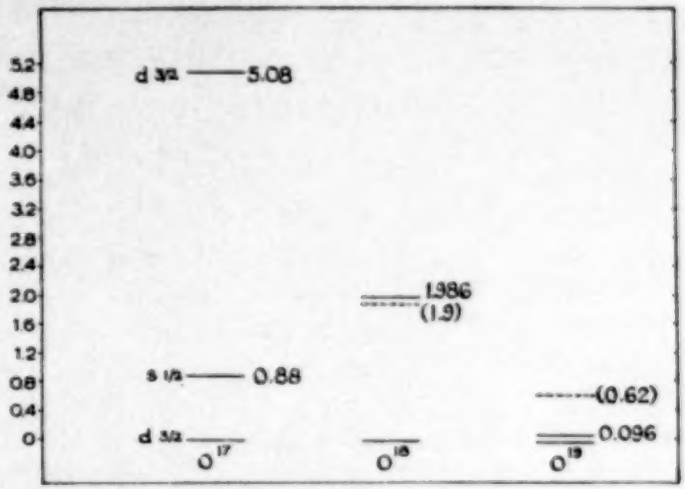

Fig. 3. Single-particle states of O^{17}, and calculated (indicated by dashed lines) and experimental firstexcited levels of O^{18} and O^{19}.

The constant pair interaction is therefore able to explain the first excited intrinsic state not only in the rotational region of heavy nuclei but also in Pb. A further confirmation would be to calculate the levels of nuclei just after Pb, but the experimental information here is insufficient. The pairing approximation is inadequate for light nuclei, where the single-particle levels are fewer and can be expected to change appreciably on adding a few more nucleons.

References

1) J. Bardeen, L. N. Cooper and J. R. Schrieffer, Phys. Rev. **108** (1957) 1175
2) A. Bohr, B. R. Mottelson and D. Pines, Phys. Rev. **110** (1958) 936
3) S. T. Belyaev, Mat. Fys. Medd. Dan. Vid. Selsk. **31** no. 11 (1959)
4) B. R. Mottelson, in The many body problem (Wiley, New York, 1959), p. 283

2.E *Nuclear Physics* **19** (1960) 500—510; © *North-Holland Publishing Co., Amsterdam*
Not to be reproduced by photoprint or microfilm without written permission from the publisher

THE INTERACTION OF 40-160 MeV NEUTRONS WITH HELIUM NUCLEI

M. ARNOLD†, P. E. HODGSON and D. F. SHAW

Clarendon Laboratory, Oxford

and

D. M. SKYRME

Atomic Energy Research Establishment, Harwell

Received 25 April 1960

Abstract: The collisions of 40–160 MeV neutrons with helium nuclei have been observed in a high pressure diffusion cloud chamber in a magnetic field of 12 kG. Results are presented for the angular distribution of elastically scattered neutrons in the energy ranges 40–80, 80–120 and 120–160 MeV. These are analysed using an optical model of the interaction with the Bjorklund-Fernbach radial variation and potentials adjusted to give the measured absorption and total cross-section. The calculated distribution falls below the experimental at backward angles due to the neglect of exchange reactions by the optical model. Agreement may be obtained by using an abnormally small value of the diffuseness of the nuclear surface. The energy distribution is given for the identified He^3 recoils resulting from neutron stripping. Although it has not been possible to carry out a detailed analysis of the observed inelastic events it is concluded that the inelastic cross section is approximately constant at about 100 mb over the energy range 80–160 MeV.

1. Introduction

During the last ten years a considerable number of experimental studies have been made of the fundamental nucleon interactions at bombarding energies above 20 MeV. While it has not proved possible to give a complete theoretical interpretation of these results in terms of a unique nucleon-nucleon potential, fair agreement has been obtained using a static potential with spin-orbit coupling up to about 300 MeV, when meson production begins to affect the character of the interaction.

The interaction of nucleons with heavier nuclei should in theory be capable of description in terms of the forces between the bombarding nucleon and the individual particles in the target nucleus, but unfortunately the problem is at present insoluble since there is no known exact method of treating the many body problem. The results of n-He^4 scattering experiments, representing a comparatively simple case of a many-body interaction, have recently been reviewed by Hodgson[1]). He showed how the differential cross-sections for elastic scattering up to about 20 MeV have been conveniently expressed in terms of a series of energy dependent phase shifts for the various partial waves.

† Now at A.E.E., Winfrith, Dorchester, Dorset.

The theoretical problem is then reduced to one of explaining the phase shift-energy variation in terms of the nucleon-nucleon interactions. At bombarding energies above 20 MeV there is the possibility of disintegration in one of the following ways:

$$\begin{aligned} n + He^4 &\rightarrow n + n + He^3 && \text{(threshold 20.5 MeV), (i)} \\ &\rightarrow n + H + T && \text{(threshold 23.9 MeV), (ii)} \\ &\rightarrow D + T && \text{(threshold 22.4 MeV), (iii)} \\ &\rightarrow n + D + D && \text{(threshold 30.1 MeV), (iv)} \\ &\rightarrow n + n + H + D && \text{(threshold 32.9 MeV), (v)} \\ &\rightarrow n + n + n + H + H && \text{(threshold 35.5 MeV), (vi)} \end{aligned}$$

as well as the elastic scattering process

$$n + He^4 \rightarrow n + He^4 . \qquad \text{(vii)}$$

The latter reaction might alternatively take place inelastically with the excitation of the target nucleus which subsequently decays by γ-emission thus

$$n + He^4 \rightarrow n + He^{4*} \rightarrow n + He^4 + \gamma . \qquad \text{(viii)}$$

Although reaction (viii) has not been observed, there have been several reports of possible states of He^4 which could contribute to it (see, for instance, Taschek *et al.*[2]), Argo *et al.*[3]) and Tyrén *et al.*[4])), whereas other investigators (Benveniste and Cork[5]), Wickersham[6]) and Eisberg[7])) conclude that no such state exists.

Heidmann[8,9]) has computed cross-sections for reactions (i), (ii), (iii), (v) and (vii) for incident neutron energies of 90 and 200 MeV by analysing the interaction between the incoming neutron and the nucleons in the He^4 nucleus. In order to make a solution possible the Born approximation was used together with gaussian wave-functions for the deuteron, triton and He^4 and a charge independent nucleon-nucleon potential of the Serber type was assumed.

2. Previous Experimental Work

Tracy and Powell[10]) analysed 14 two-prong helium stars produced by 90 MeV neutrons in a cloud chamber filled with an oxygen-helium gas mixture. In a similar cloud chamber study Swartz[11]) found evidence for preferential forward scattering of 50–200 MeV neutrons, whereas below 50 MeV the scattering was found to be approximately isotropic. Tannewald[12]) made a detailed study of the elastic and inelastic collisions of 40–90 MeV neutrons using a magnetic cloud chamber filled with pure helium at about 1 atmosphere pressure. His observations are in fairly good agreement with Heidmann's calculations for 90 MeV neutrons. However, the neutron beam used had a broad distribution with an effective energy of about 70 MeV. The results were mainly analysed as a

single energy group and so represent an average picture of the n-He^4 interaction over this energy range.

3. The Present Experiment

In our investigation the incident neutrons extended in energy up to 170 MeV and so we have obtained results in a region for which no detailed information was previously available.

The neutrons were produced by bombarding a LiD target with 175 MeV protons in the 280 cm Harwell synchrocyclotron. The beam was collimated by 2.5 × 2.5 cm channels in iron. The first channel was 150 cm long and the second one in the main 180 cm thick concrete shielding wall. The beam subsequently passed through a 0.02 cm steel window into a 45 cm diameter diffusion cloud chamber filled with helium gas at 18 atmospheres pressure. The relative number of high energy neutrons was increased by 53 g-cm^{-2} of polythene filtration. The resulting energy distribution is plotted in fig. 1. This spectrum was determined from the independent measurements of Randle

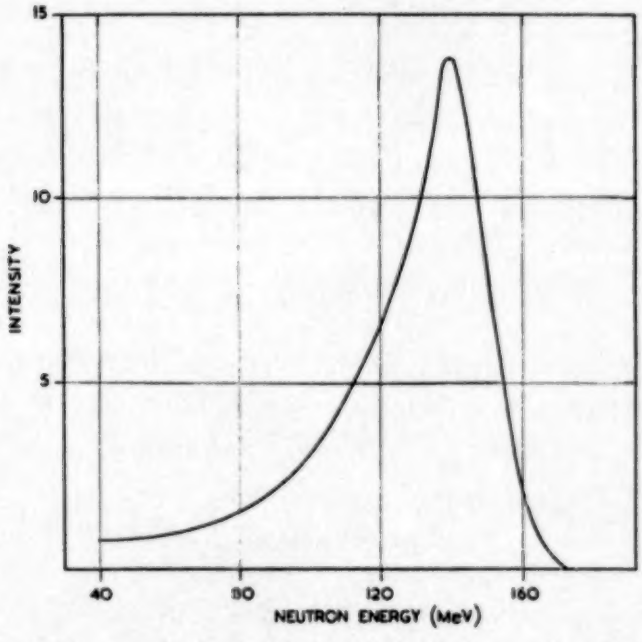

Fig. 1. Energy distribution of the neutrons in the beam traversing the cloud chamber.

et al.[13]) without filtration and correcting for the latter using total neutron cross sections for carbon and hydrogen taken from the measurements of Taylor and Wood[14]).

The cloud chamber was situated in a pulsed magnetic field of 12 kG and the proton pulse from the cyclotron was synchronized with the magnetic field by means of an electronic fluxmeter developed by Snelling and Lewis[15]). This ensured that the neutron pulse traversed the chamber at a predetermined value

of the magnetic field. The tracks of He^4 recoils and disintegrations were photographed on 70 mm Kodak R55 recording film using a stereoscopic camera.

Each photograph showed on average one or two single tracks due to He^4 or He^3 recoils and about two or three two-prong events due to the disintegration of He^4 into two charged nuclei, possibly with the emission of one or more neutrons. These events were analysed by reprojecting the stereoscopic pair to original size through the respective camera lenses on to a movable table. The plane of the table could be tilted to $\pm 45°$ from the horizontal about an axis corresponding to the direction of the incoming neutron. This means that the number of single recoils recorded must be doubled, whereas the count or two-prong events covered all possible directions.

In the case of single tracks the following measurements were made: visible length, radius of curvature, angle between the initial direction and the line of the neutron beam and the tilt angle of the table. Only tracks of length greater than 0.5 cm were measured. Shorter recoils were just counted.

For the two-prong events these measurements were made separately on the individual tracks. In the majority of cases the two tracks were not coplanar with the direction of the incoming neutron.

900 photographs were analysed in this way and measurements were made on 403 single tracks and 1678 two-prong events. It has so far been possible to identify only relatively few of the two-prong events since only a small proportion of these tracks ended in the sensitive region of the chamber and although the particle momentum could be found another parameter would be required before a mass assignment could be made. However, in the majority of cases, the reaction could be reduced to one of two possibilities by applying conservation of energy and linear momentum. Some of the two-prong events may be due to neutron-induced reactions in C and O in the methylalcohol. Assuming an average total cross-section of 20 mb we calculate that 3 such events would have been observed in our experiment.

20 of the 403 single recoils were identified from range and momentum as due to singly charged particles. They could have been proton recoils from neutron-proton scattering by hydrogen in the methylalcohol vapour or could arise from disintegration of the carbon or oxygen. A rough estimate shows that these reactions would have contributed about 30 protons in our experiment of which rather less than half would have been measured. It seems reasonable therefore that the remaining 383 recoils were correctly identified as doubly charged.

Range-energy curves were plotted from the data of Aron *et al.*[16]) for He^4 and He^3 recoils. Ranges could be measured to an accuracy of $\pm \frac{1}{2}$ mm. The temperature gradient in the sensitive region resulted in a difference in stopping power of 10 % between the top and bottom. Since all the recoils started within 1.25 cm of the centre of this volume which was 6–8 cm deep the maximum error due to our using range-energy curves for a gas mixture at the mean

temperature would be $\pm 4\,\%$. In the majority of cases the error was less than 2 %.

Three criteria were applied to test whether the doubly charged recoils were mass three or four:

(a) Elastic neutron scattering must project the He^4 at an angle less than 90° in the laboratory system relative to the incoming neutron direction.

(b) The incoming neutron energy calculated from the observed range and direction of the recoil should not exceed 170 MeV (the end point of the incident spectrum).

(c) For tracks longer than 4 cm it was possible to distinguish between He^3 and He^4 by a measurement of momentum together with range-energy data.

119 tracks were identified by means of (c), 16 definitely of mass 3 and 103 most probably mass 4. Altogether 51 tracks were found which failed to meet one of these criteria and hence must be due to the $He^4(n, 2n)He^3$ reaction.

4. Results and Discussion

4.1. THE REACTION $He^4(n, 2n)He^3$

On the basis of calculations performed for the analogous reaction $He^4(n, pn)T$, Heidmann[8,9]) deduced that He^3 production should account for 3 % of the total n-He^4 cross-section at 90 MeV and 5 % at 200 MeV. Tannenwald[12]) has suggested that these figures should be increased by a factor of 3. It is further predicted that the energy of most of the He^3 should be less than 2 MeV, only a few per cent having energies exceeding 5 MeV in the case of 90 MeV incident neutrons. Our results shown in fig. 2 do not entirely agree with these conclusions even

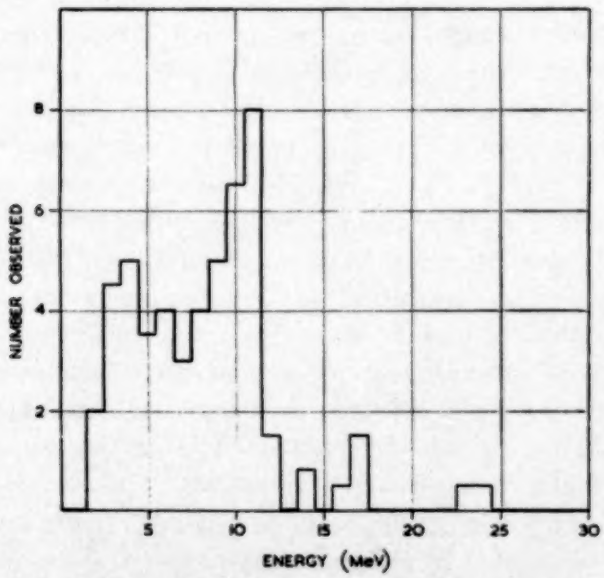

Fig. 2. Energy distribution of identified He^3 recoils produced in the reaction $He^4(n, 2n)He^3$.

after allowing for the higher energy of the neutrons in our experiment. We have found very few He^3 nuclei with energy less than 5 MeV although we were able to measure down to 2 MeV and detect down to 0.5 MeV. This is in accordance with the results obtained by Tannenwald who worked with somewhat lower energy neutrons. We have however detected He^3 nuclei with energies up to 15 MeV and more. Tannenwald, who detected these events by the characteristic ending to the He^3 track could not identify these high energy nuclei since their range is too great for them to be stopped in his cloud chamber. Comparison of the elastic and computed He^3 cross-sections leads us to set an upper limit of 42 to the number of He^3 events which could have been wrongly identified as He^4. Assuming that we have in fact failed correctly to identify all of these 42 tracks, our value for the He^3 production is only 5 % of the total n-He^4 cross-section. This is in rough agreement with Heidmann's original figure but much less than Tannenwald's amended value.

4.2. ELASTIC SCATTERING

For this part of the analysis we have assumed for the reasons given above that the remaining doubly charged recoils not identified as He^3 are in fact He^4 projected by elastic scattering of the incoming neutron. We believe the small number of He^3 events possibly included in error has little influence on the validity of the results described in this section.

The energy of the incoming neutron was deduced, knowing the energy and direction of the recoil nucleus, by applying energy and momentum conservation. The recoil angles could be measured to $\pm \frac{1}{2}°$ and allowing for the errors in the calculated recoil energies, the neutron energy could be determined to $\pm$ 5 MeV in the range 40–160 MeV. The data were divided for analysis into four groups due to neutrons < 40, 40–80, 80–120 and 120–160 MeV. The fraction due to neutrons below 40 MeV was small (59 out of 332) and these events have been excluded from the analysis. Angular distributions for the remaining three groups are plotted in figs. 3, 4 and 5, and discussed below.

(A) 40–80 MeV (figure 3)

84 of the events were ascribed to neutrons in this energy range. They were divided into 20° angular intervals (for the scattered neutron in the centre-of-mass system) and normalised to the same incident neutron flux per 10 MeV interval as in the peak energy interval of 140–150 MeV. Owing to our selection criterion of only measuring recoils greater than 0.5 cm length, events for neutrons scattered at angles less than 30° were excluded. The first point in fig. 3 has been corrected for the fact that the cut-off angle was greater than 30° for neutrons below 60 MeV.

Our experimental distribution shows the general features exhibited in previous work at intermediate energies, viz. a strong forward maximum

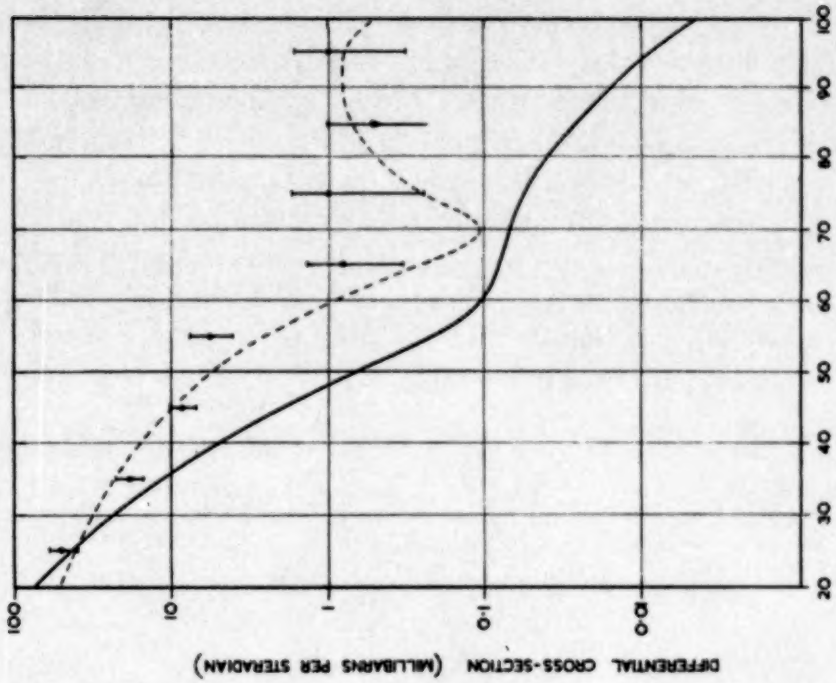

Fig. 4. Experimental and theoretical angular distributions for the elastic scattering (centre-of-mass system) of neutrons by He^4. Energy range 80–120 MeV. Curves and points have the same meaning as in fig. 3.

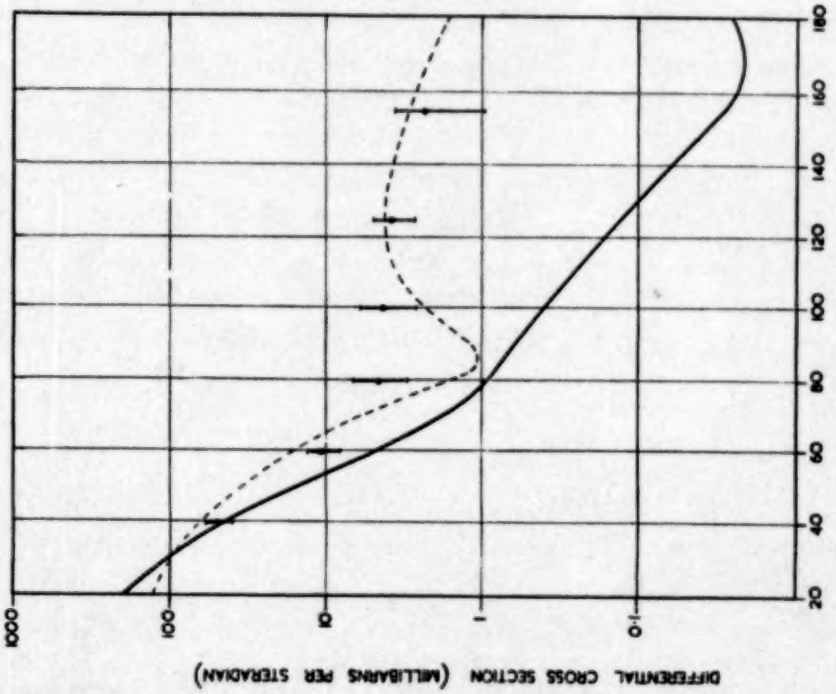

Fig. 3. Experimental and theoretical angular distributions for the elastic scattering (centre-of-mass system) of neutrons by He^4. Energy range 40–80 MeV. Black points are experimental values showing standard deviation; the solid curve is an average theoretical curve using the optical model with $a = 0.65 \times 10^{-13}$ cm, and the broken curve a theoretical curve with $a = 0.1 \times 10^{-13}$ cm.

and an approximately constant differential cross-section in the backward direction, but there is no pronounced rise like that at 14–16 MeV observed by Seagrave[17]) and Alston *et al.*[18]). Our results give a ratio of approximately 12:1 for the forward/backward scattering.

(B) 80–120 MeV (figure 4)

This energy range includes 89 events and since the majority were for small neutron scattering angles it was possible to divide them into 10° intervals. As before the numbers were normalised to the 140–150 MeV neutron flux. The backward scattering for this energy range was observed to be about 2 % of the total.

(C) 120–160 MeV (figure 5)

The data in this energy range were analysed in a similar manner to the preceding one. In this case the backward scattering was about 1 %.

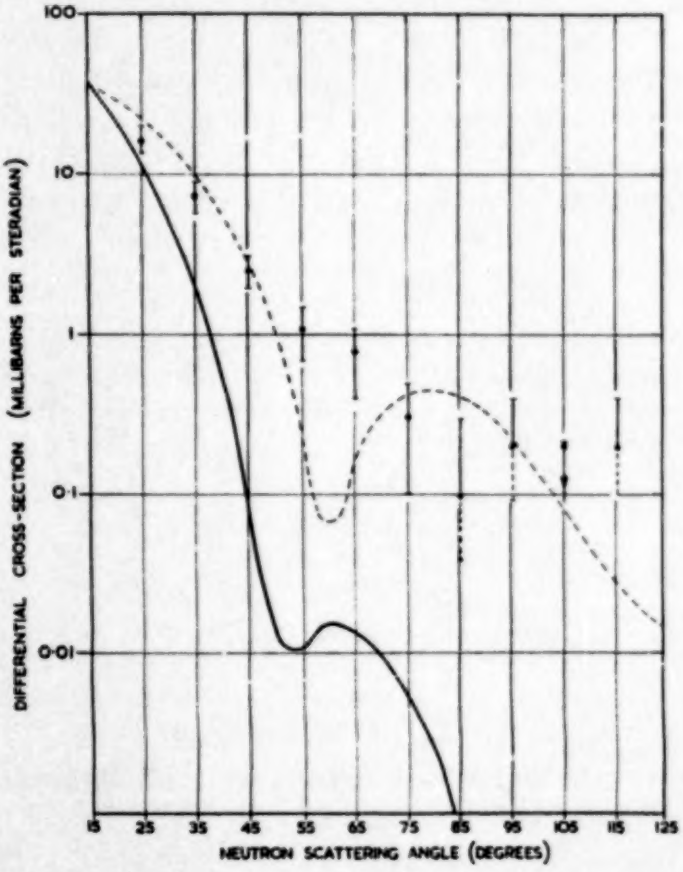

Fig. 5. Experimental and theoretical angular distributions for the elastic scattering (centre-of mass system) of neutrons by He^4. Energy range 120–160 MeV. Curves and points have the same meaning as in fig. 3.

As a first approximation in using the optical model the many nucleon-nucleon interactions in the scattering of neutrons by alpha-particles may be replaced by a two-body optical potential of the form

$$V = U\rho(r) + iW\rho(r) + \left(\frac{\hbar}{m_\pi c}\right)^2 (U_s + iW_s)\frac{1}{r}\frac{d\rho}{dr}\, l\cdot\sigma ,$$

where ρ(r) is the Saxon-Woods potential $\{ 1 + \exp((r - R)/a) \}^{-1}$, and U, W, U_s and W_s are the strengths of the real and imaginary spin-orbit potentials respectively, using the notation of Bjorklund and Fernbach[19]).

An analysis of neutron-nucleus scattering at 96 MeV by Hodgson[20]) has shown that if Bjorklund and Fernbach's values of the parameters of the Saxon-Woods potential ($a = 0.65 \times 10^{-13}$ cm, $R = 1.25A^{\frac{1}{3}} \times 10^{-13}$ cm), and of the spin-orbit potentials ($U_s = 4.4$ MeV, $W_s = 0$) are adopted, and U and W are determined from the absorption and total cross-sections, then the differential cross-section calculated from this potential agrees well with that measured by Salmon[21]), at least out to the first diffraction minimum.

A similar procedure was used to analyse the present data, with modifications to take account of the broad energy spectrum of the incident neutrons. The fitting procedure was first carried out for each of the three broad energy groups, and the corresponding potentials found are given in table 1. The optical potentials at intermediate energies were found by interpolation from these values, and the corresponding differential cross-sections calculated for energies from 40 to 160 MeV in 10 MeV steps. The average of these distributions was then computed to give the curves that are compared with the experimental data in figs. 3–5.

TABLE 1

Optical model potentials used to analyse the experimental data

	Normal surface model ($a = 0.65 \times 10^{-13}$ cm)		Sharp surface model ($a = 0.1 \times 10^{-13}$ cm)	
Energy range (MeV)	U	W	U	W
40–80	— 30.1	— 3.3	— 39.8	— 6.5
80–120	— 19.7	— 8.4	— 22.3	— 23.7
120–160	— 10.8	— 9.6	≈ 0	≈ — 27

All other parameters were taken from Bjorklund and Fernbach[19]), including the spin-orbit potentials they found from their analysis of proton-nucleus interactions.

The full curves were calculated using the above form of nuclear potential. They agree fairly well out to the first diffraction minimum, but the calculated scattering is far too small in the backward direction. The physical reason for

this is that the optical model does not take proper account of exchange interactions, which account for most of the observed cross-section in the backward direction. The optical model can be artifically adjusted to simulate this process by giving the alpha particle an abnormally sharp surface. This greatly increases the number of neutrons scattered in the backward direction, and improves the agreement with experiment, as shown in the dashed curves in figs. 3, 4 and 5. It is, however, so unphysical that it must be concluded that the optical model cannot give a realistic account of neutron-alpha scattering at high energies. It is interesting that Gammel and Thaler[22]), analysing the results of p-He^4 elastic scattering in the energy range 0–40 MeV, fitted the backward scattering by choosing a potential whose magnitude depended on **l**.

All these optical model calculations were performed on the Oxford Ferranti Mercury Computer, and details of the numerical methods used will be published elsewhere[23]).

4.3. TOTAL CROSS-SECTIONS

It has not proved possible to obtain absolute cross-sections from our measurements since the method of monitoring the neutron beam gave only a very rough value for the total number of incident neutrons. We consider a more satisfactory result can be achieved by normalising to independent values of the n-He^4 total cross-section. Measurements have been made at 21 MeV (Los Alamos) and 47.5 and 88 MeV (Hillman *et al.*[24])). No measurements have been reported above these and so we have extrapolated the curve assuming $\sigma_t \propto E^{-1}$ which is consistent with the available data between 20 and 90 MeV.

Extrapolating to zero scattering angle distributions of the gaussian form derived by Heidmann with parameters chosen to give a least squares best fit to our forward scattering data we have computed the number of elastic events excluded from the experimental analysis by our selection criteria.

The results and derived cross-sections are given in table 2. Errors in the cross-section arise from the statistics of track counting together with a $\pm 20\,\%$ allowance for extrapolation errors. We deduce that the integrated neutron flux in our experiment in the range 40–160 MeV was $(9.1 \pm 0.3) \times 10^5$. The inelastic cross-sections are calculated from $\sigma_{\text{total}} - \sigma_{\text{el}}$.

We are grateful to the Director of the Atomic Energy Research Establishment, Harwell, for facilities granted to us, to Mr. Frank Uridge for his assistance in maintaining the cloud chamber, and to the crew who operated the cyclotron. We also thank Dr. B. Buck and Mr. R. N. Maddison for their work on the computer programme, the Director of the Oxford University Computing Laboratory for the use of the computer, and Miss N. Reynolds, Miss S. Tilley and the staff of the Computing Laboratory for their assistance.

TABLE 2

Summary of observed events and experimental cross-sections

	Energy range (MeV)	Effective energy (MeV)	Observed number (× 2)	Corrected number	σ_{el}(mb)	σ_{inel}(mb)
Elastic events	40–80	60	168	334 ± 35	230 ± 35	≈ 65
	80–120	104	178	300 ± 25	64 ± 11	≈ 100
	120–160	138	200	318 ± 25	25 ± 3.5	≈ 100
	total		546	952 ± 50		

Inelastic events	number of two-prong stars	1678
	number of He^3's identified (× 2)	102
	total number of inelastic events	1780
	number attributed to C and O	3
	total number of inelastic He^4 events	1777

Total number of elastic and inelastic events 2729 (± 53)

References

1) P. E. Hodgson, Advances in Physics **7** (1958) 1
2) R. F. Taschek, H. V. Argo, A. Hemmendinger and G. A. Jarvis, Phys. Rev. **76** (1949) 325
3) H. V. Argo, H. T. Gittings, A. Hemmendinger, G. A. Jarvis and R. F. Taschek, Phys. Rev. **78** (1950) 691
4) H. Tyrén, G. Tibell and Th. A. Maris, Nuclear Physics **4** (1957) 277
5) J. Benveniste and B. Cork, Phys. Rev. **89** (1953) 422
6) A. F. Wickersham, UCRL Report no. 2662 (1954)
7) R. M. Eisberg, Phys. Rev. **102** (1956) 1104; Bull. Am. Phys. Soc. **1** (1956) 19
8) J. Heidmann, Phil. Mag. **41** (1950) 444
9) J. Heidmann, Comptes Rendus **234** (1952) 1446
10) J. Tracy and W. Powell, Phys. Rev. **77** (1950) 594
11) C. Swartz, Phys. Rev. **85** (1952) 73
12) P. E. Tannenwald, Phys. Rev. **89** (1953) 508
13) T. C. Randle, Proc. Phys. Soc. A**69** (1956) 760
14) A. E. Taylor and E. Wood, Phil. Mag. **44** (1953) 95
15) Snelling and Lewis, AERE Report no. G/M 131 (1952)
16) W. A. Aron, B. G. Hoffman and F. C. Williams, AECU 663 (1951)
17) J. D. Seagrave, Phys. Rev. **92** (1953) 1222
18) M. H. Alston, A. V. Crewe, W. H. Evans, L. L. Green and J. C. Wilmott, Proc. Phys. Soc. A**67** (1954) 657
19) F. Bjorklund and S. Fernbach, Phys. Rev. **109** (1958) 1295; Communication to the 2nd International Conference on the peaceful uses of atomic energy
20) P. E. Hodgson, Nuclear Physics (1960), to be published
21) G. L. Salmon, Nuclear Physics (1960), to be published
22) J. L. Gammel and R. M. Thaler, Phys. Rev. **109** (1958) 2041
23) B. Buck, R. M. Maddison and P. E. Hodgson, Phil. Mag. (1960), to be published
24) P. Hillman, R. H. Stahl and N. F. Ramsey, Phys. Rev. **96** (1954) 115

1.E.1: 3.A

Nuclear Physics **19** (1960) 511—522; © *North-Holland Publishing Co., Amsterdam*
Not to be reproduced by photoprint or microfilm without written permission from the publisher

GAMMA RAYS FROM THE 351-keV $C^{14}(p, \gamma)$ RESONANCE

D. F. HEBBARD†

W. K. Kellogg Radiation Laboratory, California Institute of Technology, Pasadena, California††

Received 29 March 1960

Abstract: Measurements have been made on the energies and the angular distributions of gamma rays from the 351-keV resonance in $C^{14}(p, \gamma)$. The observed transitions in N^{15} are the cascades 10.543 → 7.309 → 0 MeV, 10.543 → 5.276 → 0 MeV and 10.543 → 7.164 → 5.276 → 0 MeV. These transitions are consistent with the decays of the 7.309-MeV and 7.164-MeV levels observed in the $N^{14}(d, p)$ and $N^{14}(n, \gamma)$ reactions. The angular distribution measurements are consistent with a $\frac{1}{2}$ spin assignment for the 10.543-MeV level, a $\frac{1}{2}$ spin assignment for the 7.309-MeV level, a $\frac{1}{2}$ assignment for the 5.276-MeV level, and a $\frac{1}{2}$ assignment (with less certainty) for the 7.164-MeV level.

1. Introduction

The number of excited states of N^{15} in the energy region around 7 MeV is of astrophysical interest, because the corresponding region of excitation in O^{15} overlaps the threshold for breakup of O^{15} into N^{14} + p. The one-to-one correspondence of the O^{15} and N^{15} levels may be used in discussing the probability that the N^{14} + p capture reaction has a resonance at low proton energies in the region of 10 to 100 keV.

There has been some apparently contradictory evidence on the N^{15} levels near 7 MeV. Sperduto *et al.*[1]) have observed proton groups to levels in N^{15} at 7.164 and 7.309 MeV, among others, by means of the $N^{14}(d, p)$ reaction. The conflicting evidence relates to the decay of the 7.16-MeV level. Following the $N^{14}(d, p)$ reaction, no direct transition to the ground state of N^{15} has been observed[2]). A 1.88-MeV gamma ray has been observed by Thompson[3]), and this has been attributed to a transition from the 7.16-MeV level to one of the levels near 5.3 MeV. A similar situation exists for the $N^{14}(n, \gamma)$ reaction. The 7.16-MeV level is heavily populated by cascade gamma rays following thermal neutron capture by N^{14}, but only a weak 7.16-MeV gamma ray is observed[4]). On the other hand, the 351-keV resonance in the $C^{14}(p, \gamma)$ reaction has a cascade through a level close to 7.2 MeV, that has a relatively high probability of making a ground state transition[5, 6]). From a measurement of the energies of several of the gamma rays associated with this transition, the level near 7.2 MeV was tentatively identified with the 7.16-MeV level[6]), mainly because the observation of a 1.91-MeV gamma ray to one of the 5.3-MeV levels appeared to be in-

† Now at the Australian National University, Canberra, A.C.T., Australia.

†† Supported in part by the joint program of the Office of Naval Research and the U.S. Atomic Energy Commission.

consistent with the 7.2-MeV level having an excitation as high as 7.31 MeV.

Honsaker[7]) has investigated the region of excitation in N^{15} from 7.1 to 7.6 MeV with high resolution by observing, with magnetic analysis at backward angles, the proton groups from N^{14}(d, p), using a relatively oxygen-free target bombarded by 700-keV deuterons. The only observed proton groups are those already tabulated[1]) by Sperduto *et al.* Further, no other proton groups with an intensity greater than one per cent of the intensity of the group to the 7.31-MeV level have been observed in the vicinity of the proton group to the 7.16-MeV level. If two unresolved proton groups are present with comparable intensity, the level separation must be less than 10 keV.

Because of the existence of the inconsistencies in the 7.16-MeV level de-excitation referred to above, and because of the importance, to astrophysics, of the number of energy levels in this region of excitation, further measurements have been made on the gamma-ray cascades from the 10.543-MeV level in N^{15} (the 351-keV resonance in C^{14} + p). The gamma-ray energies and yields have been remeasured, and angular distributions have been measured for all gamma rays involved in the cascades.

2. Experimental Arrangements

The C^{14} target used has been described previously[6]). This target was bombarded by 356-keV protons from the 600-kV electrostatic accelerator in the W. K. Kellogg Radiation Laboratory. The gamma rays were detected in a 10.2 × 10.2-cm NaI(Tl) crystal mounted on a Dumont 6364 photomultiplier. The detector in its cylindrical lead shielding was able to rotate about a vertical axis through the target, so that the front surface of the crystal was 7.6 cm from the target during angular distribution measurements. No shielding extended past the plane of the front surface of the crystal. For this geometry, the smoothing factor for the $P_2(\cos\theta)$ coefficient of an angular distribution is 0.840, and the smoothing factor for the $P_4(\cos\theta)$ coefficient is 0.536. The target, deposited on a backing of 0.051-cm tantalum sheet, was held at 45° to the proton beam, inside a cylindrical target chamber with an 0.204-cm glass wall. The target chamber and a similar target have been tested, and have been found to introduce no appreciable anisotropy into the corrected angular distribution of radiation at the 460-keV $\frac{1}{2}^+$ resonance in C^{12}(p, γ).

Amplified pulses from the detector were sorted in a 100-channel pulse-height analyzer. From the spectra so obtained, angular distributions were calculated for the radiations able to be resolved. Correction was made for absorption of radiation traversing the target, and for the contribution of the tails of the high energy peaks. The latter corrections were particularly troublesome for the 1.9-MeV radiation as the appreciable layer of C^{12} in the target backing contributed a large amount of 2.25-MeV radiation.

3. Results

3.1. ENERGY MEASUREMENTS

The gamma-ray energy measurements with the detector close to the target to obtain improved counting statistics show the existence of gamma rays of energies 7.24 $\pm$ 0.15 MeV, 5.28 MeV, 3.30 $\pm$ 0.05 MeV and 1.89 $\pm$ 0.05 MeV. The 5.28-MeV gamma ray and the 7.96-MeV gamma ray from the $C^{13}(p, \gamma)$ resonance at a proton energy of 448 keV[8]) were used for energy calibration, to supplement gamma rays from radioactive sources. The only significant difference of these gamma-ray energies from those previously reported is for the 3.30-MeV gamma ray originally reported as 3.38 $\pm$ 0.05 MeV.

It is known that the 7.24-MeV gamma ray is in coincidence only with the 3.30-MeV gamma ray. Also the 5.28-MeV gamma ray is in coincidence with 1.89-MeV and 3.30-MeV gamma rays as well as with 5.28-MeV radiation. The 3.30-MeV gamma ray is in coincidence with 1.89-MeV and 5.28-MeV gamma rays as well as with the 7.24-MeV radiation[6]). These facts are consistent with a cascade from the 10.543-MeV level through a level (or levels) at 5.3 MeV to the ground state, competing with a cascade through a level (or levels) near 7.2 MeV excitation. The 7.2-MeV level has a further transition to the 5.3-MeV level. This is the 1.89-MeV transition, which identifies the 7.2-MeV level with the level at 7.164 MeV, if it is assumed that only known levels are contributing to

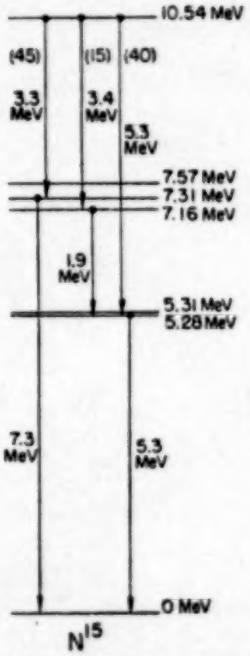

Fig. 1. Gamma-ray cascades from the 10.543-MeV level of N^{15}. The transitions shown from the 7.16-MeV and 7.31-MeV levels are consistent with the results from other reactions. The numbers in parentheses are the branching ratios for gamma transitions from the 10.543-MeV level. These branching ratios are used to estimate the strength of the unresolved 3.4-MeV radiation in the 3.3-MeV gamma-ray angular distribution. The branching ratios also give the strength of the triple cascade leading to 5.3-MeV radiation.

the gamma-ray cascades. There is, however, no reason to suppose that the level giving rise to 7.24-MeV radiation is necessarily the same level that gives rise to 1.89-MeV radiation. The energy measurement of the 7.24-MeV radiation is not

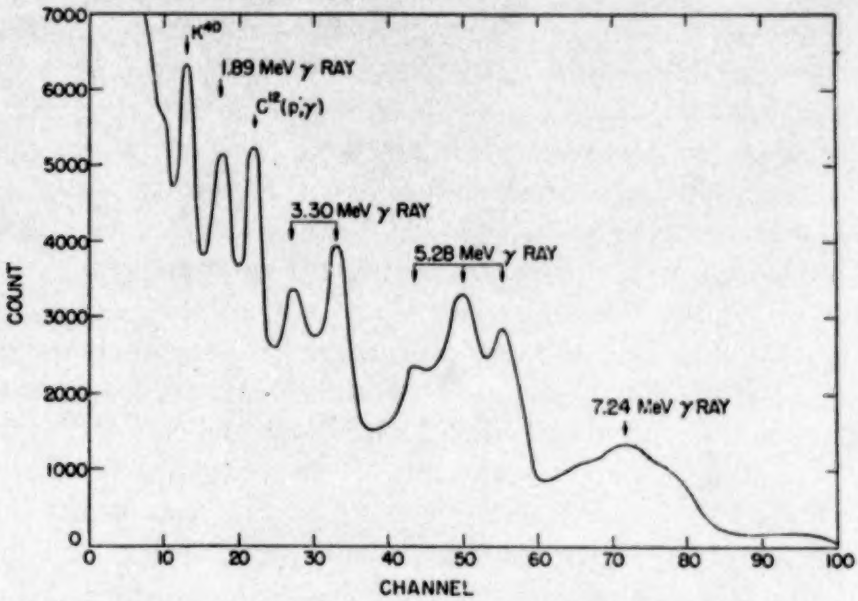

Fig. 2. The gamma-ray spectrum at the 351-keV $C^{14}(p, \gamma)$ resonance. The source of extraneous gamma rays is marked, as well as the energies of the gamma rays at the resonance. The pulses above channel 84 are caused by simultaneous detection of two members of a gamma-ray cascade.

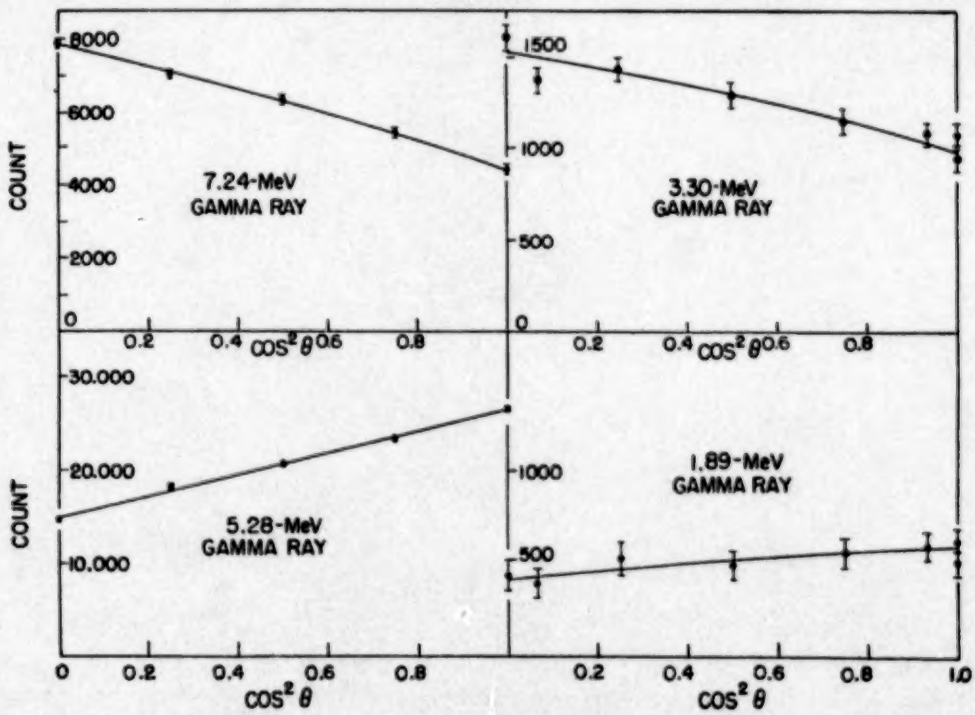

Fig. 3. Angular distributions for the gamma rays labelled in fig. 2. The full curves are least squares fits up to $P_4(\cos\theta)$. The errors are standard deviations based on the count under the various peaks of fig. 2, with an estimate of the error incurred during the subtraction of the low energy tails of high energy gamma rays.

sufficiently accurate to distinguish between the 7.164-MeV and 7.309-MeV states, while the 3.30-MeV gamma-ray energy measurement is intermediate between the transition energies to these two states. The 3.30-MeV gamma ray could be an unresolved mixture of transitions to both the 7.164-MeV and the 7.309-MeV states. It is known that the 7.309-MeV state decays mainly by a ground state transition. If the relative strengths of the 7.24-MeV and 1.89-MeV radiations are taken to indicate the relative populations of the 7.309-MeV and 7.164-MeV levels respectively, then the 3.3-MeV transitions, if unresolved, would have an energy of 3.27 MeV, which is consistent with the experimental value of 3.30 ± 0.05 MeV. The possibility that the observed 7.24-MeV and 1.89-MeV gamma rays come from two distinct levels has confirmation from the observed angular distributions. If the assumption is made that only the lowest order multipole contributes significantly to the transition amplitude, then the angular distribution results indicate that two different spins are required for the states giving rise to 7.24-MeV and 1.89-MeV gamma rays. Fig. 1 shows the N^{15} levels now assumed to be involved in the gamma-ray cascades from the 10.543-MeV state, in order that consistency may be obtained between the $C^{14}(p, \gamma)$ results and those of $N^{14}(d, p)$ and $N^{14}(n, \gamma)$.

3.2. ANGULAR DISTRIBUTIONS

The gamma-ray spectrum from the 351-keV resonance in $C^{14}(p, \gamma)$ is shown in fig. 2. Fig. 3 shows the angular distributions. These have been fitted by sums of even Legendre polynomials, up to the fourth order, and the least squares

TABLE 1

Normalized angular distribution coefficients

Gamma energy (MeV)	Angular distribution[a]
7.3	$P_0 - (0.327 \pm 0.015)P_2 - (0.01 \pm 0.02)P_4$
5.3	$P_0 + (0.400 \pm 0.010)P_2 + (0.000 \pm 0.010)P_4$
3.3	$P_0 - (0.24 \pm 0.04)P_2 - (0.02 \pm 0.04)P_4$
1.9	$P_0 + (0.22 \pm 0.16)P_2 - (0.03 \pm 0.15)P_4$
10	$P_0 - (0.07 \pm 0.05)P_2 + (0.08 \pm 0.05)P_4$

[a] The angular distributions quoted are experimental, corrected for target absorption, but not corrected for the effect of the finite solid angle of the detector.

[b] The 10-MeV gamma-ray distribution refers to the pulses above the 7.3-MeV peak in the spectrum. It is believed that these pulses do not represent a true 10-MeV gamma ray, but are caused by a simultaneous detection of two members of a gamma-ray cascade.

fits are also shown on the figures. Table 1 gives the normalized coefficients for the least squares fits. Attention has been confined to the even Legendre polynomials because the resonance is isolated, with no appreciable non-resonant

background. Taking the measured angular distributions into account, the absolute yields of the various gamma rays agree within five per cent with the yields quoted previously[6]).

4. Spin Assignments

Although the 10.543-MeV state in N^{15} is believed to have[6]) the spin and parity assignment $\frac{5}{2}^{\pm}$ or $\frac{7}{2}^{-}$, for completeness, all possible spins up to $\frac{9}{2}$ and both parities have been investigated. The measured anisotropies lead to the immediate rejection of $\frac{1}{2}^{\pm}$. For the intermediate state giving ground state radiation, believed to be the 7.31-MeV level, the possible spins[1]) considered are $\frac{3}{2}$, $\frac{5}{2}$, and $\frac{7}{2}$. Once again, a spin $\frac{1}{2}$ assignment is not allowed because of the anisotropic 7-MeV radiation. The ground state is known to have spin $\frac{1}{2}$. Thus, for the two gamma-ray cascade through the 7.31-MeV state, twelve possible radiation patterns have been calculated for the 7-MeV gamma ray. These patterns take into account the interference of the two lowest allowed multipole orders in both gamma-ray transitions. Fortunately, the channel spin of the pair C^{14} + p is unique, and the radiation pattern depends only on the spins, not the parities of the levels involved. Of the twelve angular distributions calculated, those involving the 7.3-MeV intermediate state with spins $\frac{5}{2}$ or $\frac{7}{2}$ may be rejected immediately. Each of these eight rejected distributions leads to a $P_2(\cos\theta)$ coefficient far outside the range of values obtained experimentally. In all eight cases, with all possible multipole amplitude mixing parameters, the $P_2(\cos\theta)$ coefficient is either always positive or not sufficiently negative. Thus, the level from which the 7-MeV ground state transition orginates has the unique spin assignment $\frac{3}{2}$.

Further information may be obtained from the 3.3-MeV gamma-ray angular distribution leading to the 7.31-MeV level. This case is, however, more complicated, because, in addition to the interference of multipole orders, there is a contribution of 25% in intensity of an unresolved 3.4-MeV radiation leading to the 7.16-MeV level. Only four cases of the original twelve need to be treated; i.e., those corresponding to a $\frac{3}{2}$ spin for the 7.31-MeV state. Of these, two may be rejected because they are sufficiently different from the observed angular distribution for all values of the multipole mixing parameter. The difference is so great that no unresolved radiation with a physically possible pattern (differential cross section always positive) present to the extent of 25% of the total intensity can reproduce the observed angular distribution. The two distributions rejected for this reason correspond to the spin assignments $\frac{7}{2}$ and $\frac{9}{2}$ for the 10.543-MeV state. Of the two remaining possibilities, the assignment $\frac{3}{2}$ for the 10.543-MeV state is improbable, as the 7-MeV and 3.3-MeV gamma-ray angular distributions can only be reproduced if the quadrupole intensities in both members of the cascade exceed the dipole intensities. In addition, the low

intensity of the ground state gamma-ray transition from the 10.533-MeV level suggests that the spin is greater than or equal to $\frac{5}{2}$.

The assignment of $\frac{5}{2}$ for the 10.543-MeV level is the most likely one, as both radiation paterns may be fitted with small mixing parameters. Fig. 4 shows the

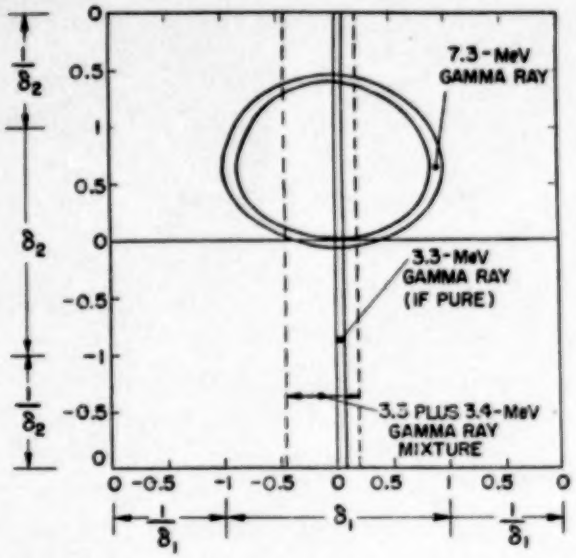

Fig. 4. From the double cascade through the 7.31-MeV state, the acceptable region of the amplitude mixing parameters δ_1 and δ_2 is shown. The spin sequence assumed is $\frac{1}{2}$ for the 10.543-MeV level and $\frac{3}{2}$ for the 7.31-MeV level. The parameter δ_1 is the quadrupole to dipole amplitude ratio for the first gamma-ray transition and δ_2 is a similar parameter for the second transition.

regions of acceptable amplitude ratios δ_1 and δ_2 for the first and second transitions, assuming the 10.543-MeV state has a spin $\frac{5}{2}$ and cascades through a spin $\frac{3}{2}$ state at 7.3 MeV.

Upon turning to the cascade from the 10.543-MeV state through the 5.3-MeV state, the available information is reduced, because the two 5.3-MeV gamma rays are unresolved. In addition, there is the complexity of 15 % intensity of 5.3-MeV radiation resulting from the triple gamma-ray cascade via the 7.16-MeV and 5.3-MeV levels. All the possibilities $J \leqq \frac{7}{2}$ have been considered for the 5.3-MeV state[1]) involved in the double cascade, and radiation patterns have been calculated for spins $\frac{3}{2}$ and $\frac{5}{2}$ for the 10.543-MeV state. In calculating the angular distribution of the 15 % of 5.3-MeV radiation from the triple gamma-ray cascade, it has been assumed that the same 5.3-MeV level is involved for both the triple and the double cascade.

The spin assignment $\frac{1}{2}$ for the 5.3-MeV state may be ruled out, because either the experimental value of the $P_2(\cos\theta)$ coefficient cannot be matched, or else the $P_2(\cos\theta)$ coefficient may be matched with the experimental value, but the $P_4(\cos\theta)$ coefficient is then far outside the experimental limits. Table 2 contains comments on the six remaining spin sequence assignments, and shows that the $\frac{3}{2}$ assignment for the 10.543-MeV state is again improbable. The $\frac{5}{2}$ assignment

for the 10.543-MeV state is again the probable one, and this is combined with a $\frac{5}{2}$ assignment for the 5.3-MeV state. For this combination of spins, fig. 5 shows the region of acceptable amplitude mixing ratios δ_1 and δ_2 for the two transitions. There is a good intersection of the regions defined by $P_2(\cos\theta)$ and

TABLE 2

Angular distribution of 5.3-MeV radiation

Spin sequence		Comment
10.5 MeV level	5.3 MeV level	
$\frac{3}{2}$	$\frac{3}{2}$	Possible if for first transition $\delta_1 \geqq 0.5$. No restriction on the second transition δ_2
$\frac{3}{2}$	$\frac{5}{2}$	Possible only if $\delta_1 = -0.4$ and $\delta_2 = -1.4$; the 15% mixture in intensity of the triple cascade must have a favourable distribution, as the experimental P_2 coefficient cannot otherwise be achieved
$\frac{3}{2}$	$\frac{7}{2}$	The experimental value of the P_2 coefficient cannot be achieved. No 2^4-pole transition is calculated. This spin sequence is unlikely from intensity considerations
$\frac{5}{2}$	$\frac{3}{2}$	The P_2 coefficient can be fitted if $\delta_1 \geqq 0.25$, $\delta_2 \leqq -1$. Under these conditions, the P_4 coefficient (smoothed) $\geqq +0.010$. The probability that this is the true value of the P_4 coefficient is 12%
$\frac{5}{2}$	$\frac{5}{2}$	Probable assignment. Both P_2 and P_4 coefficients can be matched with the experimental values for small δ_1 and δ_2. See fig. 5
$\frac{5}{2}$	$\frac{7}{2}$	The P_2 coefficient can be fitted if $\delta\text{-} \leqq -0.5$. Under these conditions, the P_4 coefficient (smoothed) $\geqq +0.014$. The probability that this is the true value of the P_4 coefficient is 7%. No 2^4-pole transition is calculated

$P_4(\cos\theta)$ coefficients in a part of the diagram where the amplitude mixing ratios are small. The $\frac{5}{2}$ assignment for the 5.3-MeV state is in agreement with our knowledge from other sources. The 5.28-MeV state has, from N^{14}(d, p) stripping results[1]), a spin $\leqq \frac{7}{2}$, probably $\frac{5}{2}$ or $\frac{7}{2}$. The 5.31-MeV state, from C^{15} beta decay[9]), has a spin of $\frac{1}{2}$ or $\frac{3}{2}$, probably $\frac{1}{2}$ by comparison with the corresponding O^{15} state[10]). The shell model predicts the presence of a state of spin $\frac{1}{2}$ and a state of spin $\frac{5}{2}$ which are usually correlated with the two 5.3-MeV states[11]).

The angular distribution of 1.9-MeV radiation has been calculated only for the $\frac{5}{2}$ assignment of the 10.543-MeV level. The energy measurement of this radiation suggests that the transition is from the 7.16-MeV level to the 5.27-

MeV level. The only final states considered are the shell model predictions $\frac{1}{2}$ or $\frac{5}{2}$. The 7.16-MeV intermediate state is assumed to be $\frac{3}{2}$, $\frac{5}{2}$, or $\frac{7}{2}$, in accordance with N^{14}(d, p) stripping data[1]), but eliminating spin $\frac{1}{2}$ because the 1.9-MeV radiation is anisotropic. All six angular distributions calculated are able to match the experimental distribution within the rather large errors. However, the pattern calculated for the assignment $\frac{5}{2}:\frac{5}{2}:\frac{5}{2}$, for the 10.543-MeV, 7.16-MeV and 5.3-MeV states respectively, gives the experimental coefficients for small values of the amplitude mixing parameters. Except for the assignment $\frac{5}{2}:\frac{5}{2}:\frac{1}{2}$ (which also predicts spin $\frac{5}{2}$ for the 7.16-MeV state), the amplitude mixing parameters required are considerably larger. Taking into consideration the fact that

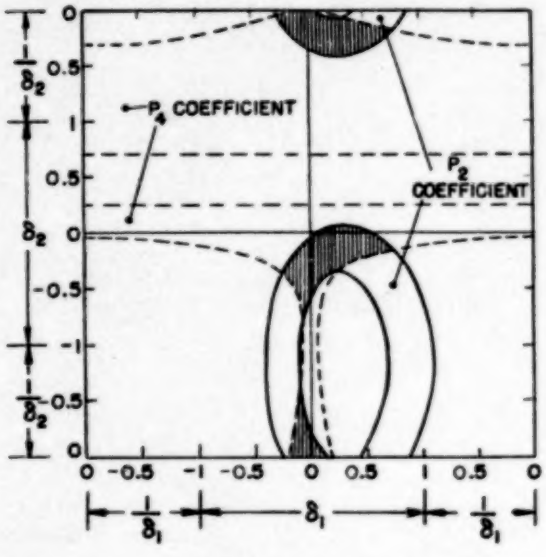

Fig. 5. From the double cascade through the 5.3-MeV state, the acceptable region of the amplitude mixing parameters δ_1 and δ_2 is shown. The spin sequence assumed is $\frac{1}{2}$ for the 10.543-MeV level and $\frac{5}{2}$ for the 5.3-MeV level. The shaded area is common to the bands defined by the P_2 and P_4 coefficients. The width of these bands is largely due to the 15% of 5.3-MeV radiation from the triple cascade. The possibilities $\frac{1}{2}$, $\frac{3}{2}$, or $\frac{7}{2}$ are covered for the 7.16-MeV state in the triple cascade. All possible relative intensities of multipoles in the two unobserved transitions of the triple cascade are considered. It has been assumed that both the double and triple cascade involve the same 5.3-MeV level, but the possibility that the triple cascade occurs through a level of spin $\frac{1}{2}$ is also covered.

small amplitude mixing ratios are expected, and that all other transitions in these gamma-ray cascades can be explained satisfactorily with small mixtures, the $\frac{5}{2}$ spin assignment for the 7.16-MeV level is the most probable one. This assignment agrees with the shell model predictions of $\frac{5}{2}$ or $\frac{7}{2}$ for the 7.16-MeV state[11]) in N^{15}.

The portion of the spectrum above the 7-MeV gamma-ray peak does not have the shape expected of a 10-MeV gamma ray. The calculated number of pulses expected from the simultaneous conversion in the NaI crystal of both gamma rays from a cascade is of the same order of magnitude as the observed

number of pulses. Furthermore the observed pulses have an almost isotropic angular distribution. This is inconsistent with a ground state transition from a $\frac{5}{2}$ state but is consistent with the distribution of double pulses if there are equal contributions from cascades through a $\frac{5}{2}$ intermediate state and through a $\frac{3}{2}$ intermediate state. It may be concluded from this that the number of true 10-MeV gamma rays is small, but the upper limit to the radiative width is not appreciably altered from the previous measurement[6]). An allowance of 25 % error is again made in estimating the number of double pulses, and it is this error that provides the upper limit to the radiative width for ground state radiation.

5. Conclusion

To summarize:

a. The 10.543-MeV level in N^{15} has spin $\frac{5}{2}$ or $\frac{3}{2}$, with spin $\frac{3}{2}$ being improbable because of the low intensity of 10-MeV radiation, and the large amplitude mixing ratios which would be required for the higher multipoles in the gamma-ray transitions.

b. The level from which the 7-MeV $C^{14}(p, \gamma)$ radiation comes must have spin $\frac{3}{2}$. The spin assignment and the gamma-ray energy measurements are consistent

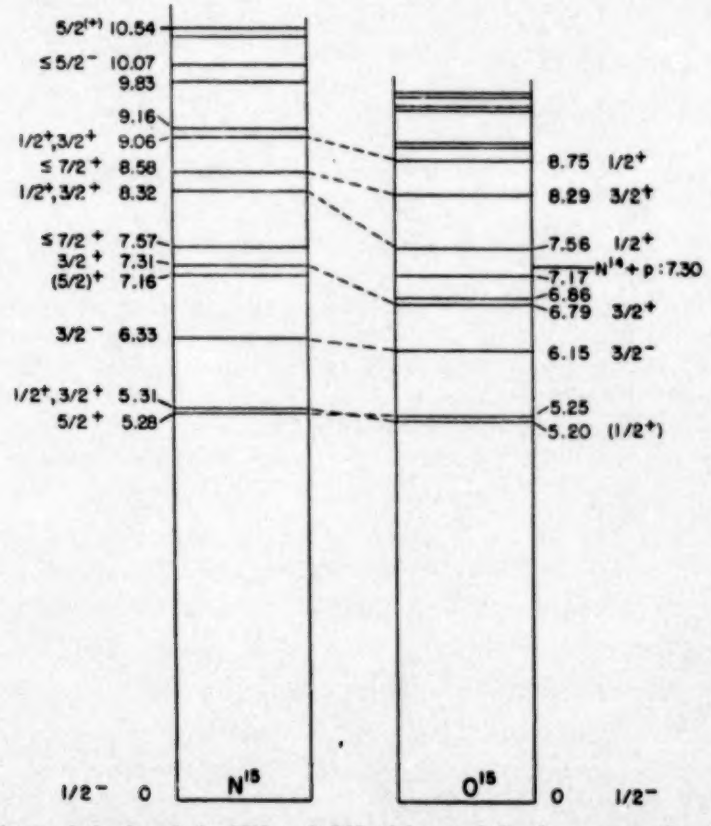

Fig. 6. A comparison of the levels in N^{15} and O^{15} with special reference to the energy region near 7 MeV. The spins and parities determined in this experiment and in others are shown on the diagram as well as the probable correlation of N^{15} and O^{15} levels.

with our knowledge of the 7.31-MeV level. The correlation between the 7.31-MeV level in N^{15} and the 6.79-MeV level in O^{15} is strengthened, since the 6.79-MeV level in O^{15} has also been shown[10]) to have spin $\frac{3}{2}$.

c. The 5.3-MeV level involved in the gamma-ray cascade from the 10.543-MeV state is probably the 5.28-MeV level. It has spin $\frac{5}{2}$. The other possible spins are unlikely because of the large amplitude multipole mixing ratios which would be required.

d. The 7.16-MeV level is best fitted with a $\frac{5}{2}$ assignment. This is consistent with the low intensity of ground state radiation, from this level, observed in other reactions.

The favoured spin assignments are incorporated into fig. 6 which also shows the comparison with the energy levels of O^{15}. There is now no evidence for any extra levels in N^{15} in the region around 7-MeV excitation apart from the ones shown in fig. 6. This implies that all the O^{15} levels near the N^{14} + p threshold have been identified[12]). Hence present calculations of the $N^{14}(p, \gamma)$ cross section at low proton energies[13]), assuming non-resonant capture as the dominant process, are acceptable.

Table 3 gives the revised radiative widths $\Gamma_p\Gamma_\gamma/\Gamma$ for the 10.543-MeV level.

TABLE 3

Revised radiative widths of the 10.543-MeV level in N^{15}

Transition	10.543 to 7.31 MeV	10.543 to 7.16 MeV	10.543 to 5.28 MeV
Radiative widths[a] $\frac{\Gamma\gamma\Gamma_p}{\Gamma}$ (eV)	0.006	0.002	0.006

[a] The statistical factor ($\omega = 3$ for $J = \frac{1}{2}$) has been removed.

The revision is required because two transitions to N^{15} levels at 7.31 and 7.16 MeV are now postulated, instead of a transition to a single N^{15} level near 7.2 MeV, with subsequent branching of the cascade.

The author wishes to thank Professor W. A. Fowler and Professor T. Lauritsen for their helpful comments on the manuscript.

References

1) R. D. Sharp and A. Sperduto, M.I.T. Annual Progress Report (1955) 125
2) Bent, Bonner, McCrary, Rabson and Sippel, Phys. Rev. **99** (1955) 710
3) L. C. Thompson, Phys. Rev. **96** (1954) 369
4) G. A. Bartholomew and P. J. Campion, Can. J. Phys. **35** (1957) 1347
5) Bartholomew, Brown, Gove, Litherland and Paul, Can. J. Phys. **33** (1955) 441

6) D. F. Hebbard and D. N. F. Dunbar, Phys. Rev. **115** (1959) 624
7) J. Honsaker, private communication
8) F. Ajzenberg-Selove and T. Lauritsen, Nuclear Physics, **11** (1959) 1
9) Alburger, Gallmann, and Wilkinson, Phys. Rev. **116** (1959) 939
10) B. Povh and D. F. Hebbard, Phys. Rev. **115** (1959) 608
11) E. C. Halbert and J. B. French, Phys. Rev. **105** (1957) 1563
12) D. F. Hebbard and B. Povh, Nuclear Physics **13** (1959) 642
13) W. A. Fowler, Mémoires Soc. Roy. Sciences de Liège, in publication

1.E.3:
1.E.6
2.H

Nuclear Physics **19** (1960) 523—534; © *North-Holland Publishing Co., Amsterdam*
Not to be reproduced by photoprint or microfilm without written permission from the publisher

INELASTIC SCATTERING FROM EVEN RARE EARTH ISOTOPES

B. ELBEK, M. C. OLESEN and O. SKILBREID

Institute for Theoretical Physics, University of Copenhagen

Received 16 December 1959

Abstract: The Coulomb excitation cross sections for the first excited state of 15 even-mass nuclei in the region of the rare earths have been determined from measurements on inelastically scattered protons and deuterons. From the cross sections, reduced E2-transition probabilities are obtained, in general in good agreement with those derived from the directly measured lifetimes of the nuclear states. The intrinsic quadrupole moments determined from the transition probabilities show, for each element, a regular variation with the mass number, but discontinuities occur when passing from one element to another. This behaviour appears to be correlated with the variation in the moment of inertia for the same nuclei. The individual intrinsic quadrupole moments of odd-mass nuclei in the same region often deviate from the moments of the neighbouring even isotopes, but on the average the quadrupole moments of odd-mass nuclei are almost the same as those for even nuclei.

1. Introduction

This paper reports measurements of the Coulomb excitation cross sections for the first excited state in some even nuclei in the region of rare earths. Most of the nuclei investigated are strongly deformed and the first excited state is therefore a $2+$ rotational state which can be reached from the ground state by an E2 Coulomb excitation. Under the experimental conditions employed, this is the only state appreciably populated by Coulomb excitation of an even nucleus. The excitation cross section is proportional to the reduced electric quadrupole transition probability, usually designated as $B(\mathrm{E2})$. This transition probability is again determined by the intrinsic nuclear quadrupole moment Q_0, if one assumes the validity of the rotational description for the levels in question. The intrinsic quadrupole moment can also be expressed in terms of the nuclear deformation, a parameter having considerable influence on the nuclear properties[1,2]).

The investigation covers all even isotopes of Sm, Dy, Er, and Yb, except the very rare isotopes Dy^{156} (0.05%), Dy^{158} (0.09%), Er^{162} (0.14%), and Yb^{170} (0.14%). The cross sections for the even isotopes of Gd (except Gd^{152}) have been reported earlier[3]).

The present results together with our earlier measurements[4–6]) on odd-mass nuclei in the same region of the periodic table allow a comparison of the intrinsic quadrupole moments of odd-mass and even-mass nuclei.

The properties of the odd-mass nuclei are determined to a considerable extent

by the orbit of the last odd particle[2]), whereas the properties of the even nuclei are expected to vary more regulary from specimen to specimen. Recent theoretical developments[7,8]) indicate that pairing correlations of a type similar to those considered in the theory of superconductivity may smoothen out contributions from the individual nucleons. This expectation about nuclar deformations is to some extent confirmed by our measurements.

2. Experimental method

The method used in our experiments has been described earlier[3–6]). 4.5-MeV protons and deuterons from an electrostatic generator were scattered from thin targets of the separated rare earth isotopes and were recorded at a scattering angle of 145° in a high resolution magnetic spectrograph on photographic plates. The inelastic cross section was then determined from the ratio of inelastic to elastic scattering, the elastic scattering being a pure Rutherford scattering under the experimental conditions employed.

3. Targets

The targets for the investigation were prepared in an electromagnetic isotope separator[9]). The separated beams impinged on a slightly curved surface of pure reactor graphite (fig. 1). A considerable fraction of the heavy atoms will by a

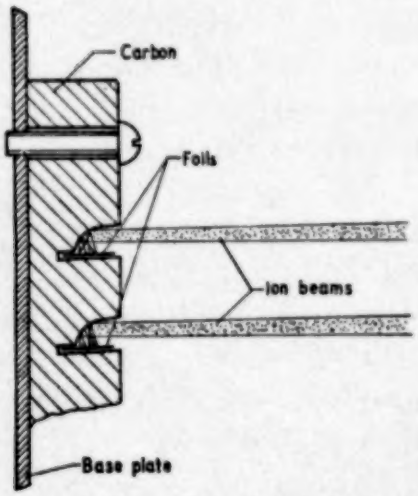

Fig. 1. Arrangement for collecting the separated isotopes on thin carbon foils.

scattering or sputtering effect again leave the surface and be caught on a thin carbon foil mounted in a frame. The foil was facing the beam spot on the graphite, but was protected against the direct beam.

All the even isotopes of one element could be collected at one time. Normally it took about two hours to prepare a target of sufficient thickness (about 30 $\mu g/cm^2$) of a 20% abundant isotope.

The purity of the collected isotopes was not determined directly, but according to earlier experience[5]) an abundant isotope should contain less than 1 per cent of a neighbouring isotope of the same abundance. However, the relatively rare isotopes Dy^{160}, Er^{164}, and Yb^{170} each have an isobar, namely Gd^{160}, Dy^{164}, and Er^{170}. As the charging materials used were never absolutely pure and as the ion source of the isotope separator had been used earlier for separation of rare earth elements, the above mentioned isotopes were contaminated by the isobar which, in all cases, is an abundant isotope. The appropriate correction for the contaminant, which contributes to the elastic group used in the evaluation of the cross section, was determined from the intensity of the inelastic group belonging to the contaminant. Only in the case of Yb^{170} was this procedure difficult and uncertain, as the inelastic groups of Er^{170} and Yb^{170} almost coincide.

The most heavily contaminated target was Er^{164} which contained about 25 % of the isobar Dy^{164}; this indicated a contamination of the charging material of about 1 per cent. This figure is in agreement with the contamination actually observed during the separation by means of a beam scanning device.

4. Results

As an example of the particle spectra recorded in the heavy particle spectrograph, fig. 2 shows the spectrum of deuterons scattered from an Yb^{172} target.

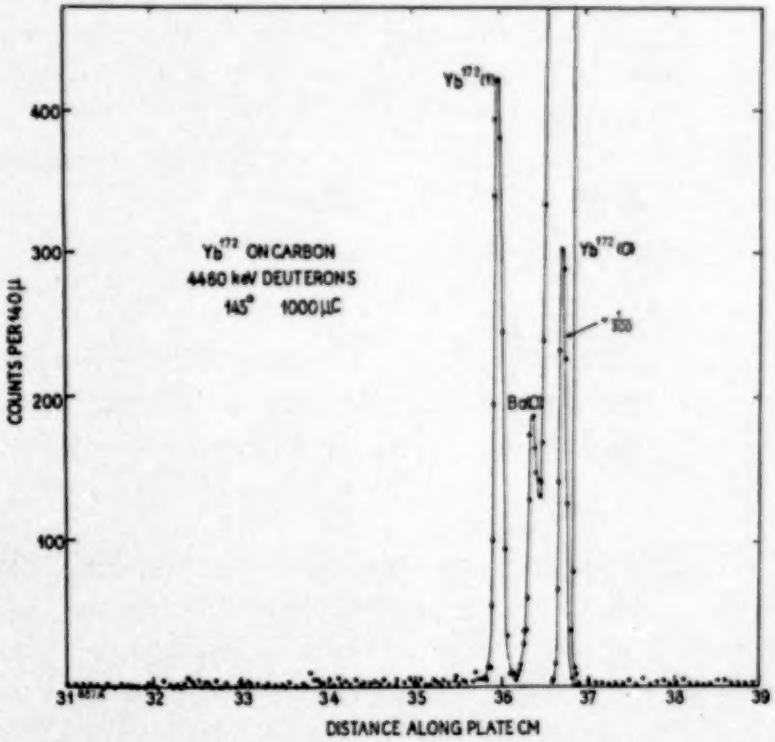

Fig. 2. Spectrum for deuterons scattered from an Yb^{172} target.

The other spectra had a similar appearance. Frequently elastic groups belonging to various contaminants were found, but they happened in no case to interfere with the determination of the intensity of the inelastic group. The peak labelled Ba(0) is due to elastically scattered deuterons from a Ba-contamination. Ba^{135} and Ba^{137} can together with Cl^{37} and Cl^{35}, respectively, form ions with mass 172 in the ion source of the isotope separator, and these ions will of course be collected together with the Yb^{172}-ions. As far as possible, each target was investigated with deuteron scattering as well as proton scattering or with different energies of the incoming particles. The shifts of the groups relative to each other obtained in this way served to reveal any impurity group that might be concealed under the inelastic group.

4.1. EXCITATION ENERGIES

Mostly as a check on isotopic constitution and bombarding conditions, we have determined the excitation energy for each of the groups for which the cross section was determined. Most of the energies are believed to be accurate within 1 keV, but the error may be somewhat larger in those few cases where the excitation energy is high.

The energies of most of the nuclei have been accurately measured by a bent crystal spectrometer[11]). We have listed the values from these measurements in table 1 for the sake of comparison and also because they are of importance for the determination of the nuclear moment of inertia used in the following discussion. The accurate energies should also be used in the evaluation of the lifetime of the nuclear state from the reduced transition probability. as the lifetime depends on the energy to a high power—up to the fifth—dependent on the conversion coefficients.

The nuclear moments of inertia $\mathcal{J}$ were obtained from the excitation energies ΔE by means of the simple rotational formula

$$E = \frac{\hbar^2}{2\mathcal{J}} I(I+1)\,, \tag{1}$$

where I is the spin of the excited state, which in all cases considered is 2. The moments of inertia are given in table 1 expressed as the ratio $\mathcal{J}/\mathcal{J}_{rig}$, where $\mathcal{J}_{rig}$ is the moment of inertia of a rigid spheroid determined from the approximate formula[1])

$$\mathcal{J}_{rig} = \tfrac{2}{5} AMR_0^2 (1 + 0.31\beta)\,. \tag{2}$$

Here A is the mass number of the nucleus and M the nucleonic mass. The nuclear radius R_0 was taken as $1.2 \times 10^{-13} A^{\frac{1}{3}}$ cm. β is the nuclear deformation which was derived from the observed transition probabilities (cf. below).

From table 1 it is seen that most of the energies determined in this experiment are in good agreement with the more accurate ones. In several of the cases the energy level was assigned earlier to a certain isotope only on the basis of

systematics. The direct isotopic assignment obtained here has in all cases been in agreement with the earlier assignments.

4.2. TRANSITION PROBABILITIES

The measured cross sections were used for the evaluation of the reduced transition probability with the assumption of pure E2-excitation and with use of the classically evaluated function $f(\xi, \theta)$ appearing in the expression for the

TABLE 1

Measured excitation energies and reduced electric quadrupole transition probabilities in even rare earth isotopes†

Nucleus	ΔE (keV)	ΔE (keV)	$B(E2)/e^2$ (10^{-48} cm^4)	Q_0 (10^{-24} cm^2)	β	$\mathcal{J}/\mathcal{J}_{rig}$
$_{62}Sm^{148*}$	549	—	0.89 ± 0.10	—	—	—
Sm^{150}	333	—	1.32 ± 0.06	3.65	0.184	0.147
Sm^{152}	122	121.85	3.40 ± 0.15	5.86	0.290	0.380
Sm^{154}	82	81.99	4.61 ± 0.20	6.83	0.336	0.551
$_{64}Gd^{154}$	123	—	3.43 ± 0.30	5.88	0.280	0.373
Gd^{156}	89	88.97	4.57 ± 0.25	6.79	0.320	0.498
Gd^{158}	79	79.51	5.44 ± 0.25	7.41	0.346	0.547
$_{66}Gd^{160}$	75	75.26	5.80 ± 0.25	7.65	0.354	0.561
Dy^{160}	85	—	4.46 ± 0.30	6.72	0.301	0.490
Dy^{162}	81	80.65	5.11 ± 0.15	7.19	0.320	0.512
Dy^{164}	74	73.39	5.64 ± 0.25	7.55	0.334	0.558
$_{68}Er^{164}$	90	—	5.04 ± 0.35	7.14	0.306	0.456
Er^{166}	80	80.57	5.66 ± 0.25	7.56	0.323	0.496
Er^{168}	79	79.80	5.72 ± 0.20	7.60	0.320	0.496
Er^{170}	79	79.31	5.44 ± 0.15	7.42	0.310	0.484
$_{70}Yb^{170}$	84	84.26	5.53 ± 0.25	7.48	0.304	0.455
Yb^{172}	79	78.70	5.89 ± 0.20	7.72	0.311	0.477
Yb^{174}	77	76.46	5.89 ± 0.20	7.72	0.308	0.475
Yb^{176}	83	82.16	5.78 ± 0.20	7.60	0.301	0.445

* Not rotational.

The first column of energies are those determined in this experiment. The second column gives the more accurate energies of the same states[11]). The $B(E2)$ are determined in this experiment, the errors being standard deviations from the mean. The intrinsic quadrupole moments Q_0 were derived from the transition probabilities by means of eq. (3) and the nuclear deformation parameter β by means of eq. (4). The ratio $\mathcal{J}/\mathcal{J}_{rig}$ was obtained from the excitation energies by means of eqs. (1) and (2).

Coulomb excitation cross section[1]). The exact quantal calculation of this function has now been carried out[12]), but the difference between the classical and the quantal function is almost negligible in the cases considered here (less than 1 per cent).

† *Note added in proof*: We are grateful to Drs. E. M. Bernstein and E. Z. Skurnik for pointing out to us a slight error in the procedure used earlier by us in the evaluation of the $B(E2)$ from the experimental data. Due to this error, the $B(E2)$ values given in refs. [3-6]) are systematically about 1.5 % too low. The data given in table 1 have been corrected for the error.

The B(E2) for each element is given in table 1. Each value is the average of several determinations (3–5) of the inelastic cross section. In general the individual determinations of B(E2) did agree within a few per cent, although larger deviations occurred. When such cases were re-investigated, we usually were able to find a trivial explanation for the deviations. If not, all the experimental values were used in the averaging process. The errors given in the table are standard deviations from the mean when the individual determinations were given simple weights 1, 2 or 3 taking into account the several factors (statistical uncertainty, background etc.) of influence on the reliability of the result. The statistical uncertainty was of minor importance as the elastic and inelastic groups contained several thousand tracks each. One would expect that the manual plate-counting could introduce serious errors. Frequent control countings by persons not knowing the result of earlier countings have led us to believe that also this source of error is small for trained counting personnel.

It should be emphasized that the errors given in table 1 as well as those from earlier papers do not take into account systematic errors. However, the systematic errors are believed to be small, as the determination of the cross section is dependent only on the measurement of a ratio.

Summarizing the information on errors in table 1, the standard error in the transition probabilities should in most cases be less than 5%. The intrinsic quadrupole moment Q_0 of the nucleus is proportional to the square root of the transition probability. The standard error on Q_0 is then less than 2.5%.

4.3. COMPARISON WITH LIFETIMES

For a number of the nuclei in table 1 the lifetime for the first excited state has been determined by delayed coincidence techniques[13–15]) in studies of radioactive decays. Recently an extensive survey of lifetimes in the same region of the periodic table has been published by Birk, Goldring and Wolfson[22]). These authors have directly measured the lifetime of Coulomb excited states by means of a beam sweeping technique.

From the measured lifetimes one can calculate the B(E2) by means of the theoretical conversion coefficients. Since the method of inelastic scattering is completely different from the lifetime method, it is very interesting to compare the B(E2) values that have been determined in both ways. We have therefore calculated B(E2) for the cases in which the lifetime has been measured, using the most recent K and L conversion coefficients of Rose[16]). The total (M + N + ...) conversion coefficient was taken as one third of the total L conversion coefficient. The B(E2) values obtained in this way are collected in table 2 together with our results for the same nuclei. When several measurements of the same lifetime have been made, a simple arithmetical mean has been used in the comparison.

In general, agreement between the two methods is satisfactory, the largest discrepancy being found for the nuclei of Dy^{160} and Er^{164}, for which the value

from the lifetime is about 25% larger than the result from the scattering experiments. Although our values for these nuclei are less reliable than the rest, it appears unlikely that the difference is due to errors in the cross section determinations alone. It should be mentioned that the value for the lifetime

TABLE 2

Transition probabilities derived from measured half-lives compared with transition probabilities derived from inelastic scattering cross sections

Nucleus	$\tau_{\frac{1}{2}}$	α	$B(E2)_{\tau}$	$B(E2)_{i.sc.}$	ref. for τ
Sm^{152}	1.43	1.18	3.34	3.40	13) 22)
Sm^{154}	2.74	4.84	4.76	4.61	22)
Gd^{154}	1.22	1.13	3.85	3.43	13) 22)
Gd^{156}	2.05	3.93	4.98	4.57	21) 22) 23)
Gd^{158}	2.79	5.98	4.55	5.44	22)
Gd^{160}	2.52	7.30	5.55	5.80	22)
Dy^{160}	1.8	4.62	5.57	4.46	13)
Dy^{162}	2.22	6.09	5.26	5.11	22)
Dy^{164}	2.42	8.93	5.48	5.64	22)
Er^{164}	1.4	4.37	6.46	5.04	13)
Er^{166}	1.75	6.73	6.11	5.66	13) 22)
Er^{168}	1.84	6.82	6.04	5.72	22)
Yb^{170}	1.57	6.34	5.73	5.53	14)

$\tau_{\frac{1}{2}}$ is a simple average of the measurements of the lifetime in units of 10^{-9} sec. α is the total internal conversion coefficient from the tables of Rose[16]). The reduced transition probability from the lifetime and from the inelastic scattering measurements is in units of 10^{-48} cm^4.

in these two cases is based on one measurement only. A discrepancy of the same order of magnitude was earlier found in the case of Gd^{156}, but the recent very accurate determination of this lifetime[15]) is in much closer agreement with our value[3]).

On the average the transition probabilities determined from the lifetimes are about 5% larger than our values. If Dy^{160} and Er^{164} are not included in the comparison, the difference is reduced to about 1%. This result indicates a considerable accuracy of the low energy E2-conversion coefficients used. Application of the conversion coefficients of Sliv and Band[17]) instead of those of Rose would reduce the average $B(E2)$ from the lifetimes by about 2%.

4.4. QUADRUPOLE MOMENTS

The intrinsic quadrupole moments were derived from the reduced transition probabilities by means of the formula of the rotational model[1]). In the case of an even nucleus, one finds the simple relation

$$B(E2, 0 \rightarrow 2)/e^2 = \frac{5}{16\pi} Q_0^2 \qquad (3)$$

between the reduced transition probabilities and the quadrupole moment. In fig. 3 the moments obtained are shown as a function of the mass number. For comparison we have included the moments of the gadolinium isotopes[3]) as well

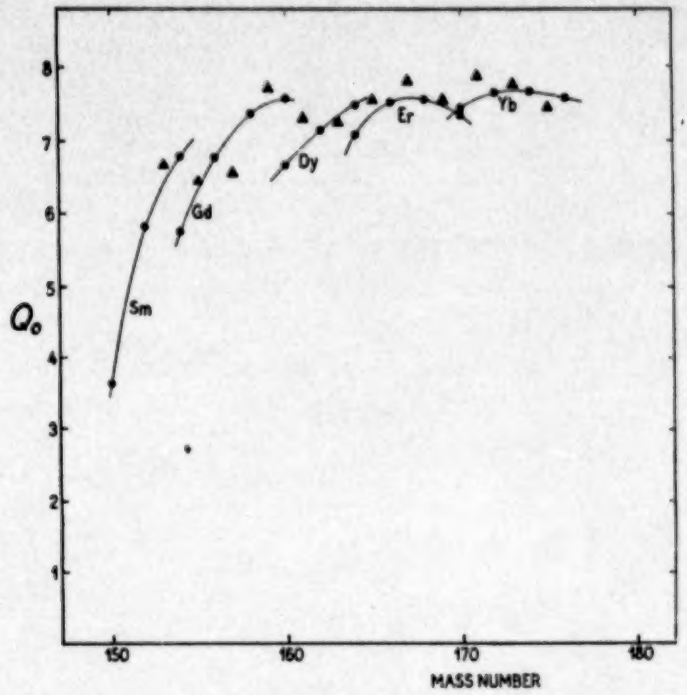

Fig. 3. Intrinsic quadrupole moments of rare earth isotopes as a function of the mass number. The points marked with ▲ correspond to the odd isotopes while the even ones are marked with ●.

as those of the odd-mass nuclei in the same region[4–6]). The numerical values of Q_0 are collected in table 1. The determination of $B(E2)$ from the cross section is essentially exact, as it involves only the theory of Coulomb excitation, whereas the derivation of the intrinsic quadrupole moment is dependent upon the use of the rotational model. Of the nuclei considered here Sm^{148} and Sm^{150} do not show rotational spectra and therefore require special treatment. Sm^{150} is probably just on the verge of being deformed, and for the sake of comparison we have determined the Q_0 as if the 2^+ state were a rotational state.

It is apparent from fig. 3 that the intrisic quadrupole moments of the even isotopes of each element show a quite regular behaviour. The moments of the odd-mass isotopes, although on the average hardly different from those of the even isotopes, seem to scatter a little with respect to the neighbouring even nuclei.

A noticeable feature of fig. 3 is the break when passing from one element to another. Fig. 4 shows again the intrinsic quadrupole moments of the even nuclei, but now as a function of the neutron number. The breaks have here disappeared to some extent, except in the case of gadolinium-dysprosium. It is thus indicated that the intrinsic quadrupole moment (or the almost equivalent nuclear de-

formation parameter β, cf. below) in the region considered is determined principally by the number of neutrons.

This fact can be understood qualitatively on the basis of Nilsson's wave functions for nucleons in a deformed potential[2]). In this model the ground state deformation corresponds to the configuration having the lowest total energy when the nucleons are filled pairwise into the Nilsson orbits[2, 18]). For the nuclei considered here, preliminary theoretical estimates show that the deformation decreases when going from Sm to Gd and from Gd to Dy, while it is rather independent of the proton number above Dy[19]). On the other hand, the energy in the neutron orbits is strongly decreasing with increasing deformation. The deformation corresponding to the energy minimum will therefore be increasing

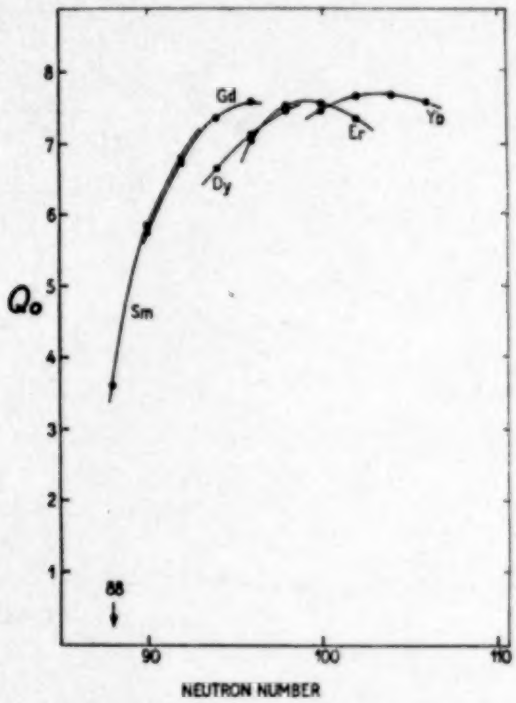

Fig. 4. Intrinsic quadrupole moments of even rare earth isotopes as a function of the neutron number.

when neutrons are added, but will not to any large extent vary with the proton number. The gross behaviour of fig. 4 is therefore in agreement with the theoretical expectations.

4.5. NUCLEAR DEFORMATION

The nuclear deformation can be expressed by various parameters. We have here used the parameter β, which to second order is related to the intrinsic quadrupole moment Q_0 through the approximated expression[1])

$$Q_0 = \frac{3}{\sqrt{5\pi}} ZR_0^2 (1 + 0.16\beta) , \qquad (4)$$

where Z is the atomic number and R_0 the nuclear radius. The deformations obtained with $R_0 = 1.2 \times 10^{-13}\, A^{\frac{1}{3}}$ are collected in table 1 and are shown as

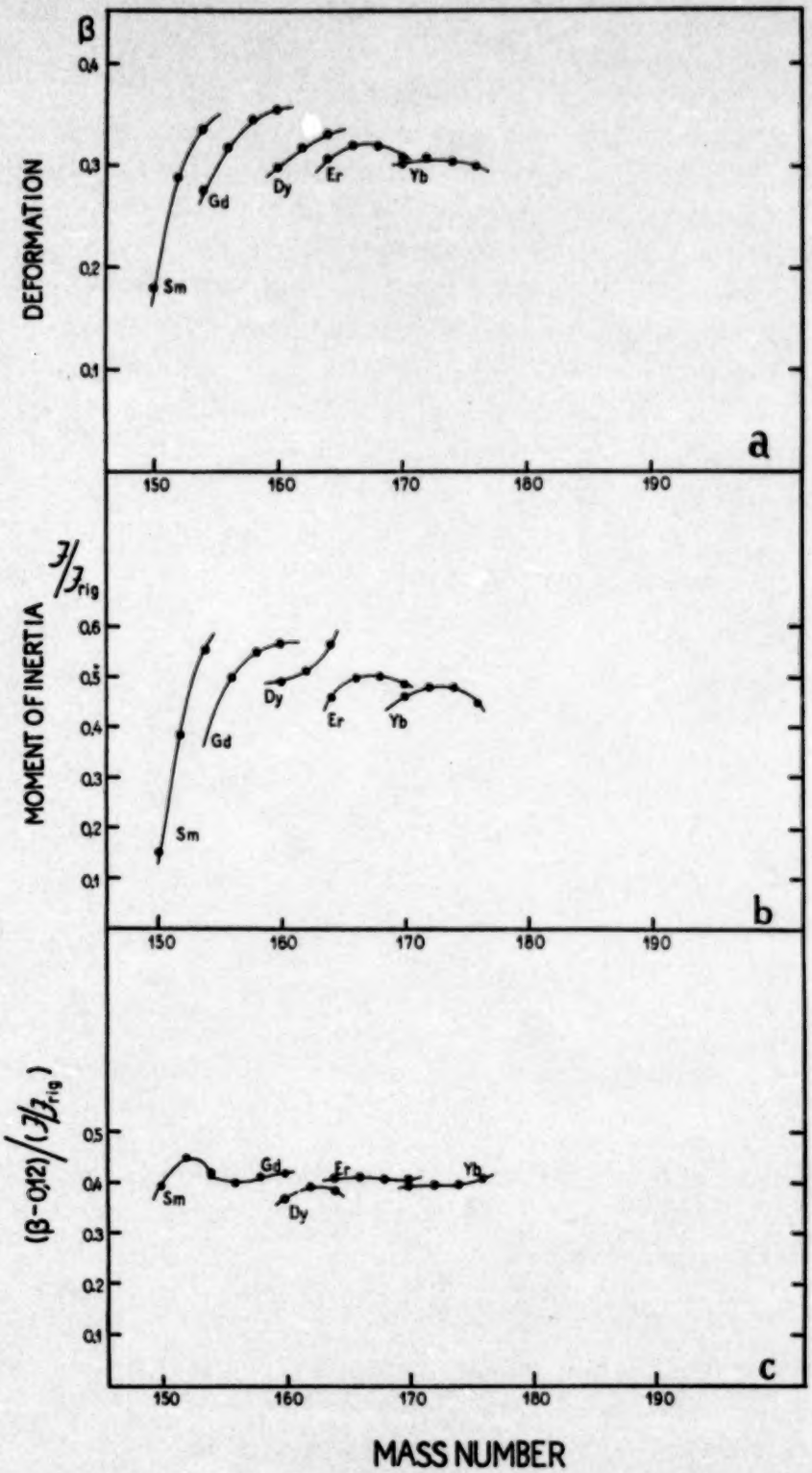

Fig. 5. The figure shows as a function of the mass number: a) the nuclear deformation parameter β, b) the ratio of the nuclear moment of inertia to the rigid moment of inertia, c) correlation between β and $\mathcal{J}/\mathcal{J}_{\text{rig}}$.

a function of the mass number in fig. 5a. Except for scale and for the slight dependence on mass taken into account by (4) the plot is similar to fig. 3.

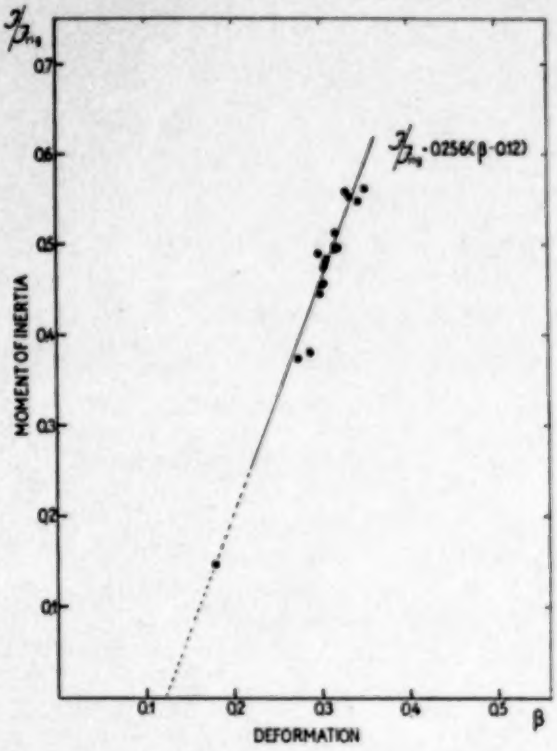

Fig. 6. The nuclear moment of the inertia versus deformation. The point on the dotted line is obtained from Sm^{150}, which does not have a pure rotational spectrum.

It is interesting to compare the variation of β with the variation of the moment of inertia for the same nuclei as shown in fig. 5b. It is apparent that the two parameters are strongly correlated. This correlation is also evident from fig. 6 where $\mathcal{I}/\mathcal{I}_{rig}$ and β are plotted against each other. The variation in β for the nuclei under consideration is quite small and it is difficult to say anything about the nature of the correlation. The deviations from the straight line shown on fig. 6 are more clearly seen in fig. 5c. It should be stressed that the line drawn on fig. 6 is thought merely as a help to the eye and in no way implies that the relation between moment of inertia and deformation is a linear one. In fact the points would equally well admit a parabola of the type $\mathcal{I}/\mathcal{I}_{rig} =$ const. $\times \beta^2$, the more so because the point on the dotted part of the line is obtained from Sm^{150} that does not show a pure rotational spectrum.

Theoretically one would expect a connection of some kind between the moment of inertia and the deformation, a connection also seen from earlier data on the transition probabilities[20]). It is, however, interesting to note how detailed this correspondence is. Preliminary data on the isotopes of Hf and W indicate that the correspondence is preserved when the deformation starts to

decrease. A somewhat similar behaviour is found for the very heavy elements in the deformed region[21]); however, the curve corresponding to fig. 6 for these elements does not coincide with ours, but is displaced towards smaller deformations. This could possibly indicate some kind of mass dependence of the relation between the moment of inertia and the deformation, not properly taken into account when displaying $\mathcal{I}/\mathcal{I}_{rig}$ against β.

We wish to thank Professor Niels Bohr for the excellent working conditions at his Institute and Professor Aage Bohr and Dr. S. G. Nilsson for stimulating discussions. We also wish to thank Mr. P. Ambrosius-Olesen for invaluable help in the experiment and Miss G. Bertram-Hansen and Miss E. Jensen for counting the tracks on the photographic plates.

References

1) K. Alder, A. Bohr, T. Huus, B. R. Mottelson and A. Winther, Revs. Mod. Phys. **28** (1956) 432
2) S. G. Nilsson, Mat. Fys. Medd. Dan. Vid. Selsk. **29**, no. 16 (1956)
3) V. Ramšak, M. C. Olesen and B. Elbek, Nuclear Physics **6** (1958) 451
4) B. Elbek, K. O. Nielsen and M. C. Olesen, Phys. Rev. **108** (1957) 406
5) B. Elbek, M. C. Olesen and O. Skilbreid, Nuclear Physics **10** (1959) 294
6) M. C. Olesen and B. Elbek, Nuclear Physics **15** (1960) 134
7) A. Bohr, B. R. Mottelson and D. Pines, Phys. Rev. **110** (1958) 936
8) S. T. Belyaev, Mat. Fys. Medd. Dan. Vid. Selsk. **31**, no. 11 (1959)
9) K. O. Nielsen and O. Skilbreid, Nuclear Instruments **2** (1958) 15
10) K. O. Nielsen and O. Skilbreid, Nuclear Instruments **1** (1957) 159
11) E. L. Chupp, J. W. M. Du Mond, F. J. Gordon, R. C. Jopson and Hans Mark, Phys. Rev. **112** (1958) 518
12) J. Bang, Mat. Fys. Medd. Dan. Vid. Selsk. **32**, no. 5 (1960)
13) A. W. Sunyar, Phys. Rev. **98** (1955) 653
14) R. L. Graham, J. L. Wolfson and R. E. Bell, Can. J. Phys. **30** (1952) 459
15) R. E. Bell and M. H. Jørgensen, Nuclear Physics **12** (1959) 413
16) M. E. Rose, Internal Conversion Coefficients (North Holland Publishing Company, Amsterdam 1958)
17) L. A. Sliv and J. M. Band, Internal Conversion Coefficient Tables circulated by the University of Illinois, Report 55 ICC K1 (1957) and ICC L2 (1958)
18) B. R. Mottelson and S. G. Nilsson, Mat. Fys. Skr. Dan. Vid. Selsk. **1**, no. 8 (1959)
19) D. Bès and Z. L. Szymanski, private communication
20) A. Bohr and B. R. Mottelson, Mat. Fys. Medd. Dan. Vid. Selsk. **30**, no. 1 (1955)
21) R. E. Bell, S. Bjørnholm and J. Severiens, Mat. Fys. Medd. Dan. Vid. Selsk. **32**, no. 12 (1960)
22) M. Birk, G. Goldring and Y. Wolfson, Phys. Rev. **116** (1959) 730
23) O. Nathan, Nuclear Physics **5** (1958) 401

2.A.1: 2.D

Nuclear Physics **19** (1960) 535—549; © *North-Holland Publishing Co., Amsterdam*
Not to be reproduced by photoprint or microfilm without written permission from the publisher

NEUTRON CROSS-SECTIONS IN ALUMINIUM

G. S. MANI†, G. J. McCALLUM†† and A. T. G. FERGUSON

Atomic Energy Research Establishment, Harwell, Berkshire, U.K.

Received 31 March 1960

Abstract: The (n, p) and (n, α) cross-sections in aluminium have been measured for neutron energies from 12 to 21 MeV; the cross-section for the (n, 2n) reaction leading to the 228 keV isomeric state in Al^{26} has been determined from the threshold to 21 MeV. The relative cross-sections in the above mentioned neutron energy ranges have been determined by measuring the gamma ray activity associated with the beta decay of the residual nucleus; the absolute cross-sections have been obtained by normalising to the values measured by other workers at 14 MeV. These results are compared with the statistical theory of nuclear reactions.

1. Introduction

Though in the past few years there has been a large accumulation of information on total neutron cross-sections, very little information is available on reaction cross-sections[1]). The optical model has been applied with great success to the total and elastic scattering cross-section data, however the finer details of the model can be tested only by polarization measurements and through the determination of reaction cross-sections which can be found by summing the partial cross-sections. Measurements on reaction cross-sections similarly would be useful in testing the validity of the statistical theory of nuclear reactions and in determining the contribution of direct interactions to the cross-sections.

The neutron reaction cross-sections for aluminium have been measured only up to 9 MeV[2]) and from 13.0 to 15.7 MeV[3]) in the case of (n, α) reaction and up to 17 MeV in the case of the (n, p) reactions[4]). The absolute cross-sections for these two reactions have been determined at 14 MeV by several workers[3, 5]); there has been no measurement of the (n, 2n) cross-section. In this paper we present results for the (n, p), (n, α) and (n, 2n) cross-sections of aluminium for neutron energies between 12 and 21 MeV.

2. Experimental Procedure

Deuterons accelerated in the Harwell Van de Graaff accelerator were allowed to strike an air cooled Titanium Tritide target to yield neutrons. The deuteron

† Atomic Energy Establishment, Trombay, Bombay, India. Present address: Rice Institute, Houston, Texas.

†† Institute of Nuclear Sciences, Wellington, New Zealand. Present address: Atomic Energy of Canada Limited, Chalk River, Ontario, Canada.

energies were either 2 or 4 MeV and the various neutron energies were obtained by using the variation of energy with angle in the (d, t) reaction. The aluminium samples were 5.08 cm in diameter and were placed on circular brass rings concentric with the target, with the deuteron beam a diameter and the samples at a distance of 30 cm from the target. The samples could be placed at 13 positions on the brass ring, thus exposing the samples to neutron energies ranging from 12 to 20.8 MeV. The size of the samples introduced a maximum spread of about 250 keV in neutron energy. The target thickness also gave about the same spread in neutron energy. The samples could be placed on either half of the ring so that any error in alignment could be detected.

The relative cross-sections for the various reactions were determined by measuring the activity of the gamma rays emitted by the residual nuclei formed in these reactions, as mentioned in detail below. The samples were placed on either a 2.54 cm high by 3.81 cm diameter or a 7.62 cm high by 12.7 cm diameter NaI (Tl) crystal and the gamma ray spectrum displayed on a 100-channel pulse-height analyser. The samples were counted for a definite time after irradiation, and the activity calculated by determining the area under the photopeak characteristic of the particular reaction. Since only relative cross-sections were determined the effects of self absorption were unimportant and we were able to use 2.5 cm thick samples which yielded high induced activities after irradiation. Most impurities were automatically avoided since we measured only the area under a particular photopeak.

2.1. (n, p) REACTION IN ALUMINIUM

This reaction in Al^{27} leads to the residual nucleus Mg^{27} which is beta active with a half life of 9.5 minutes, decaying to various levels in Al^{27}. The decay scheme of Mg^{27} to Al^{27} is shown in fig. 1. A 70 % branch goes to the 843 keV

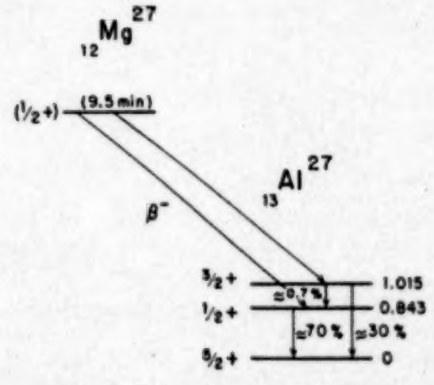

Fig. 1. Decay scheme of Mg^{27}.

level and the rest to the 1015 keV level in Al^{27}. The 1015 keV level decays with 98 % probability directly to the ground state and with about 2 % probability to the first excited state, that is, the 843 keV level. Hence the gamma rays

from this reaction with their relative abundances are as follows: 843 keV (70 %), 1015 keV (30 %) and 172 keV (0.7 %). The Q-value for this reaction is calculated to be —1.812 MeV[6]).

To measure the (n, p) cross-section we adopted the following procedure. The samples were irradiated (one at a time) at any one of the 13 positions on the brass ring. Only 8 of these 13 positions were used in the experiment. The samples were placed on both halves of the ring to correct for errors due to misalignment. It was found that such errors were much smaller than the total experimental errors. The samples were irradiated for 15 minutes and the counting started 1 minute after irradiation. A 5 minute count sufficed to give good counting statistics. A 2.5 cm thick, 3.8 cm diameter NaI (Tl) crystal was used in this experiment since the gamma rays of interest had an energy of 843 keV. After each measurement a background count was taken and in all cases the background was found to be about 3 % of the actual counting rate in the energy region of interest. When measurements are made using deuterons and a Titanium Tritide target a background of low energy neutrons is observed arising from the D(d, n)He^3 reaction; this increases with time due to the absorption of deuterons in the target. The effect of this source of low energy neutrons on the cross-section measurements can be determined by making use of the fact that the yield of neutrons produced by this mechanism rises rapidly with deuteron energy. We employed two deuteron energies for the experiment, namely, 2 MeV and 4 MeV. The samples were so arranged that the cross-sections at some neutron energies were obtained using both deuteron energies. The two deuteron energies yielded the same activities, showing thereby, that the effect of (d, d) neutrons was negligible. The gamma spectrum due to this reaction is shown in fig. 2. By using the time of flight method to determine the

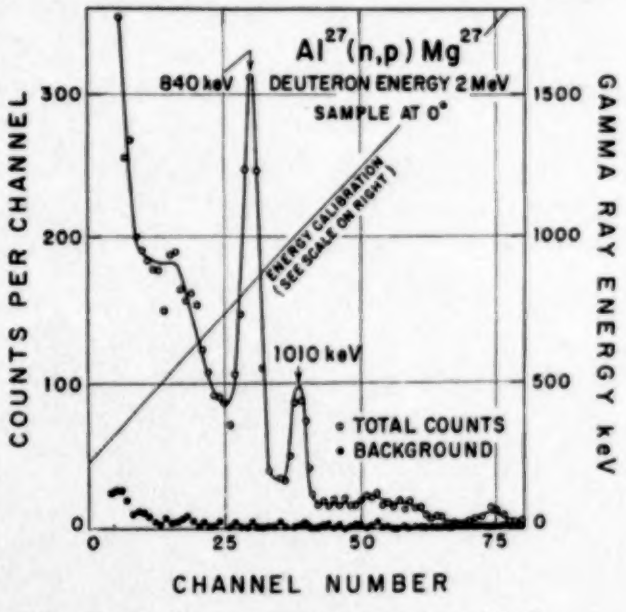

Fig. 2. Gamma ray spectrum from Mg^{27}.

neutron energy spectrum, the background neutrons due to the scattering from the walls and from the air were found to be negligible. The activity due to the (n, α) reaction was found to be very small since the Na^{24} nucleus produced in this reaction has a half life of the order of 15 hours. Further, the decay of the 843 keV gamma rays was followed through several half lives; the half life thus determined gave a value of ten minutes.

The area under the 843 keV photopeak was measured after subtracting the background. The method of subtracting the background from below a photopeak is complicated if the escape peaks and Compton continua from higher energy gamma rays are important. Since in our measurement the only higher energy gamma ray of sufficient intensity to enter into the background correction was the 1010 keV gamma also formed in the (n, p) reaction no correction for this was necessary. The area obtained was assumed to be proportional to the initial activity since in all cases the irradiation time, the waiting time before counting and the counting time were the same.

The neutron yield was continuously monitored by a biassed proton recoil counter. The sample activities were normalised to the monitor counts and the relative cross-section was then obtained by normalising the results to the variation of the (d, t) neutron intensity with angle. This angular distribution was taken from the Los Alamos report on changed particle cross-sections[7]). The actual counting errors were of the order of 1 % and the main source of error arose from the finite size of the samples which introduced uncertainties due to the variation in intensity and energy with angle. Since the angular distribution becomes more peaked in the forward direction with deuteron energy, the error due to this is larger for the results obtained with the 4 MeV deuterons than with the 2 MeV deuterons. The maximum error was about 10 %.

The absolute cross-section was obtained by normalising to the value at 14 MeV obtained by other workers[5]): a value of 82 mb at 14.1 MeV has been used. In giving the final errors, the following errors have not been taken into account: (1) the error in angular distribution measurements in (d, t) neutrons since this error cannot be very definitely obtained and since it was felt that it is smaller than the error due to the size of the samples; (2) the error in absolute cross-section at 14 MeV since any change in the 14 MeV value would only shift our curve without changing its shape.

The absolute cross-section for the (n, p) reaction in aluminium is shown in fig. 3. It will be seen that there is good agreement with values obtained by Hudson and Morgan[4]). Table 1 gives the values of the cross-section for various energies.

2.2. (n, α) REACTION IN ALUMINIUM

This reaction in Al^{27} leads to the residual nucleus Na^{24} which is beta active with a half life of 15 hours decaying to various levels in Mg^{24}. The decay

scheme of Na^{24} to Mg^{24} is shown in fig. 4. Na^{24} has an isomeric state 472 keV above the ground state. The isomeric state decays to the ground state with a half life of the order of 20 msec[8]). There is no conclusive evidence[9]) for its direct beta decay to Mg^{24}. The ground state of Na^{24} decays mainly to the 4.122 MeV

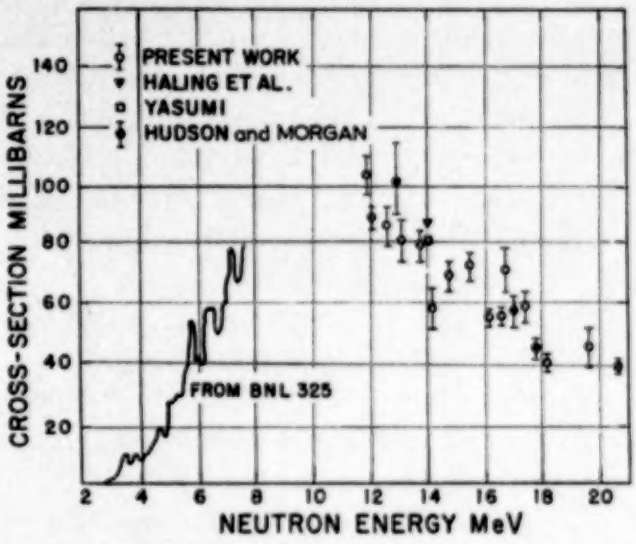

Fig. 3. Cross-section for the reaction $Al^{27}(n, p)Mg^{27}$.

level of Mg^{24}. This level de-excites by gamma emission to the 1.368 MeV level which then decays by gamma emission to the ground state. There is evidence[9]) that 0.003 % of the beta transitions go directly to the 1.368 MeV level in Mg^{24}. The gamma rays associated with this reaction therefore have energies of 2.54

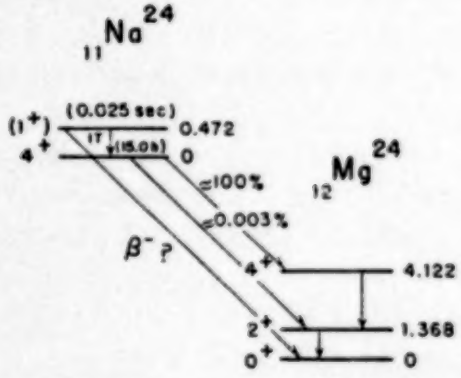

Fig. 4. Decay scheme of Na^{24}.

MeV and 1.368 MeV. The Q-value for this reaction is calculated[6]) to be —3.139 MeV.

In the case of the (n, α) reaction, samples were irradiated simultaneously at all the positions for a duration of 12 hours. The various samples were then counted with different waiting times after irradiation, the counting time in all cases being ten minutes. The samples for counting were chosen at random to

avoid any systematic errors. A 7.62 cm thick and 12.7 cm diameter NaI (Tl) crystal was used since the gamma rays involved were of higher energies. The background was about 8–10 % of the actual counts. To estimate errors due to (d, d) neutron background, two deuteron energies were used as before and it was found that within experimental errors there was no difference in results obtained at the same neutron energy but using different deuteron energies. The induced activity was determined by measuring the area under the 1.368 MeV photopeak. No correction was made for the escape peaks or the Compton continua from the higher energy gamma rays for the same reason as before. Fig. 5 shows the gamma spectrum obtained from this reaction. Since, in this case, the waiting time after irradiation varied from sample to sample the appropriate correction was applied to account for this. The relative cross-section was obtained after correcting for the angular distribution of the (d, t) neutrons.

The absolute cross-section was then obtained by normalising the results to the 14 MeV value, determined by other workers[3, 5]). A figure of 125 mb at 14.1 MeV was used. The errors quoted were obtained in the same way as in the (n, p) cross-section. Fig. 6 gives the excitation function for the (n, α) reaction in aluminium. Table 1 lists the (n, α) cross-section obtained at various energies.

2.3. (n, 2n) REACTION IN ALUMINIUM

This reaction in Al^{27} leads to the residual nucleus Al^{26} which is positon active. The decay scheme of Al^{26} to Mg^{26} is shown in fig. 7. The ground state has a half life of 8×10^5 years and so could not be observed by us. The 228 keV isomeric state has a half life of 6.7 sec and decays to the ground state of Mg^{26}. This reaction can therefore be detected by measuring the 511 keV annihilation radiation produced by the positons from the isomeric state. However it should be noted that the cross-section obtained is that for the production of the isomeric state only.

Samples were irradiated one at a time for 1 minute, and 10 seconds after irradiation were counted for 20 sec. The Q-value for this reaction is —13.27 MeV. For neutron energies below the (n, 2n) threshold no 511 keV photopeak was observed. It was also noted that the decay rate of the 511 keV gamma rays in the photopeak, produced following activation by neutrons of energies above the (n, 2n) threshold was of the order of a few seconds. These two facts confirmed that the 511 keV gamma rays were produced following the (n, 2n) reaction. Due to the very short irradiation time the Compton continuum arising from the 843 and 1015 keV gamma rays produced in the (n, p) reaction contributed only slightly to the background subtracted from below the 511 keV photopeak. The activity obtained was normalised to the neutron monitor counts. The relative cross-section was calculated as before. The absolute cross-section was determined as follows: Two samples were irradiation for 5 minutes at different neutron energies and counted for 2 minutes. The activities produced

following the (n, 2n) and (n, p) reactions were determined by measuring the areas under the 511 and 843 keV photopeaks; in this case the known shape of the gamma ray spectrum arising from the (n, p) reaction alone was used to

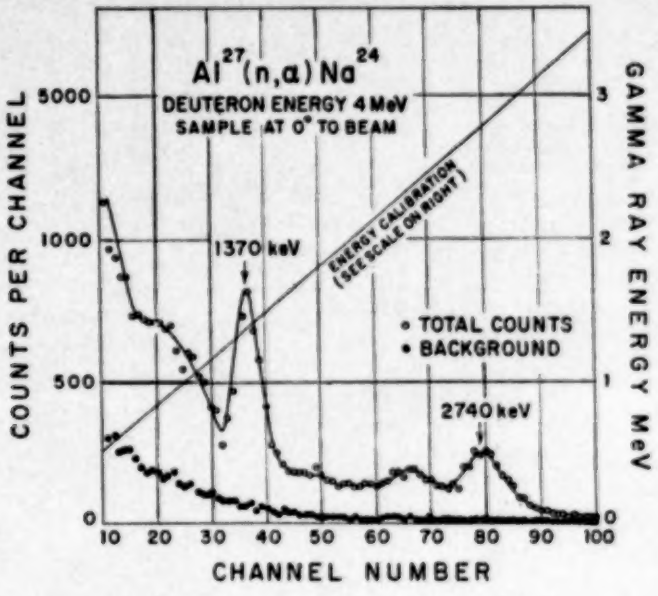

Fig. 5. Gamma ray spectrum from Na^{24}.

correct for the Compton gamma rays lying below the 511 keV photopeak. The ratio of the cross-sections was then obtained after correcting for differences

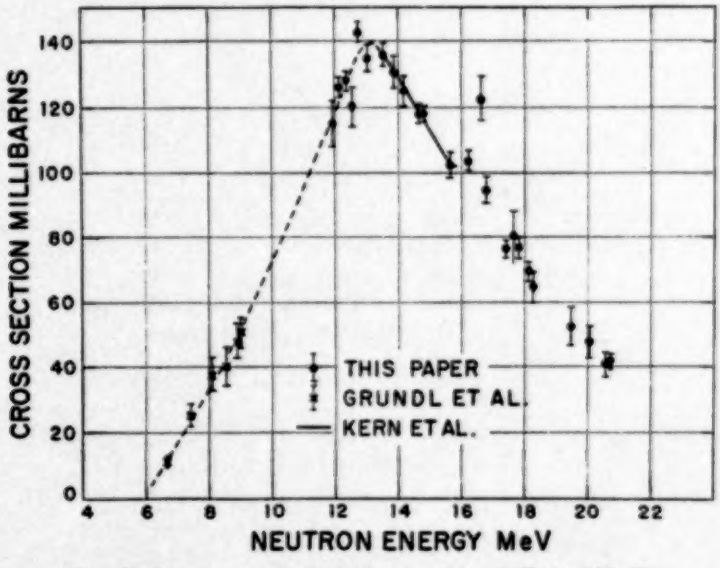

Fig. 6. Cross-section for the reaction $Al^{27}(n, \alpha)Na^{24}$.

in the photopeak efficiencies[10]) and the effects of self absorption in the samples. The internal consistency between the two measurements was good. Since the absolute cross-section of the (n, p) reaction had already been determined, it

was possible to calculate the absolute (n, 2n) cross-section. Fig. 8 shows the variation of the (n, 2n) cross-section with neutron energy. It should be noted that this cross-section is only for the production of the isomeric state in Al^{26}. Table 1 lists the values of the (n, 2n) cross-section for the neutron energies used in the experiment.

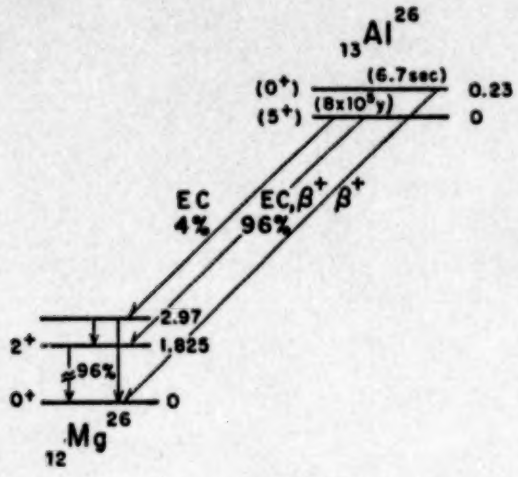

Fig. 7. Decay scheme of Al^{26}.

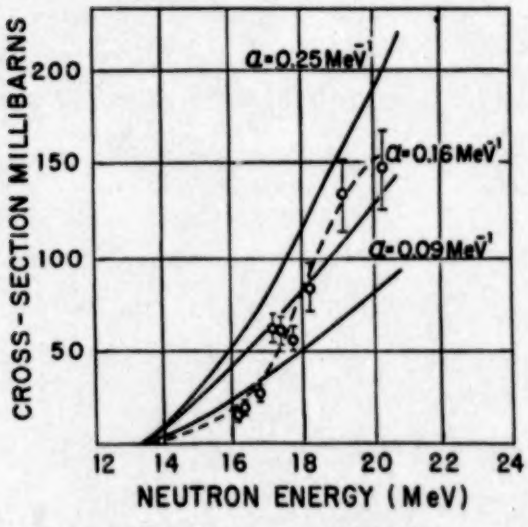

Fig. 8. Cross-section for the reaction $Al^{27}(n, 2n)Al^{26}$.

3. Discussion of Results

3.1. RATIO OF LEVEL DENSITIES

Following Blatt and Weisskopf[11]) we have attempted to obtain from the (n, p) and (n, α) cross-sections the ratio of the level densities in the corresponding residual nuclei and the nuclear temperatures.

Any partial cross-section can be expressed as

$$\sigma(\mathrm{n}, \mathrm{x}) = \sigma_c(E_n)\, G_x(E_n)\,, \qquad (1)$$

TABLE 1

Neutron reaction cross-sections in aluminium

E (MeV)	σ(n, α) (mb)	σ(n, p) (mb)	σ(n, 2n) (mb)
20.72	39 ± 1	32 ± 1.3	
20.57	38 ± 4		
20.20			144 ± 22
20.15	45.5 ± 5	29.5 ± 5.2	
19.48	50 ± 6.5		
19.60		44 ± 6.4	
19.05			131 ± 20
18.30	61.5 ± 5		
18.19			85 ± 13
18.13	65.7 ± 3	38 ± 3	
17.83	72 ± 3	42.5 ± 3.3	54 ± 8
17.66	76 ± 9		
17.45	72 ± 2.5	60 ± 2	
17.40			60 ± 9
17.24			60 ± 9
16.84	89 ± 4	69.5 ± 8.2	27 ± 4
16.63	115.5 ± 7.5	53 ± 3	
16.29			19 ± 3
16.20	97.5 ± 3	54.5 ± 3	15 ± 2
15.61	96.5 ± 4		
15.50		70.5 ± 4.5	
14.75	111 ± 3	68 ± 5	
14.66	111 ± 2		
14.16	117.5 ± 5	57 ± 7	
13.82	123 ± 5	78.5 ± 5	
13.56	128 ± 4		
13.05	127 ± 4	80 ± 7	
12.63	134.5 ± 3		
12.55	113 ± 6	85 ± 6.5	
12.33	121 ± 3.5		
12.13	118.5 ± 4	87.5 ± 3	
11.92	108 ± 7.5	103 ± 7	

where $\sigma_c(E_n)$ is the cross-section for the formation of the compound nucleus from an incident neutron of energy E_n and the target nucleus, and $G_x(E_n)$ is the probability of the decay of the compound nucleus into the residual nucleus and the emitted particle. We have assumed the formation cross-section for the compound nucleus to be given by

$$\sigma_c(E_n) = \pi(R + \lambda)^2 , \tag{2}$$

where λ is the wave length of neutrons of energy E_n divided by 2π and R is the radius of the target nucleus and is given by $R = r_0 A^{\frac{1}{3}}$ where we have used for r_0 the value 1.5×10^{-13} cm.

Blatt and Weisskopf have given the following expression for $G_x(E_n)$:

$$G_x(E_n) = \frac{F_x^0(E_n)}{\sum_v F_v(E_n)}, \tag{3}$$

where the summation is over all competing reactions. In eq. (3) we introduced

$$F^0 = \int_{E_0}^{E_{by}} E\sigma_c(E)\omega(E_{by} - E)\,dE\,, \quad F = \int_0^{E_{by}} E\sigma_c(E)\omega(E_{by} - E)\,dE\,, \tag{4}$$

where E_{by} is the maximum energy of the emitted particle for an incident neutron energy E_n and $E_0 = E_{by} - B_n$, the quantity B_n being the binding energy of the last nucleon in the residual nucleus. The first integral in (4) has the limit at E_0 rather than zero to exclude any other particle emission following the emission of particle x. Further, $\omega(E)$ is the density of levels in the residual nucleus at an excitation energy E, and $\sigma_c(E)$ is the cross-section for the formation of a compound nucleus by a collision, with energy E between the particle under consideration and the excited nucleus, the latter having an excitation energy $E_{by} - E$. The cross-section for the formation of the compound state can be calculated from the following expression:

$$\sigma_c(E) = \pi\lambda^2 \sum_{l=0}^{\infty} (2l + 1)\, T_l(E)\,, \tag{5}$$

where $T_l(E)$ is the transmission coefficient and can be obtained from standard tables[12]). In the computation we have used 1.5×10^{-13} cm for the value of r_0 and the correction suggested by Blatt and Weisskopf[11]) for the case involving an alpha particle, that is, the channel radius is taken to be the sum of the radius of the target nucleus and the alpha particle radius, a value of 1.2×10^{-13} cm being used for the latter.

For the nuclear level density we have used the very approximate expression

$$\omega(E) = C \exp\left[2a^{\frac{1}{2}} E^{\frac{1}{2}}\right], \tag{6}$$

where a is the constant in the expression $E = a\Theta^2$ which relates the excitation energy to the nuclear temperatuur Θ. Introducing (6) into (1) and using (3) and (4) we get for the (n, p) and (n, α) cross-sections

$$\sigma(\mathrm{n, p}) = \sigma_c \frac{f_p^0(E_n)}{\frac{C_n}{C_p} f_n(E_n) + f_p(E_p) + \frac{C_\alpha}{C_p} f_\alpha(E_n)}, \tag{7}$$

$$\sigma(\mathrm{n}, \alpha) = \sigma_c \frac{f_\alpha^0(E_p)}{\frac{C_n}{C_\alpha} f_n(E_n) + \frac{C_p}{C_\alpha} f_p(E_n) + f_\alpha(E_n)}, \tag{8}$$

with

$$f_x^0 = \frac{F_x^0}{C_x}, \quad f_x = \frac{F_x}{C_x}.$$

Here C_n, C_p and C_α are the values of the constant C in the level density formula for neutron, proton and alpha emission. The nuclear temperature as given by the quantity a is not expected to change appreciably for these nuclei. It will be seen that the cross-sections depend only on the ratios C_n/C_p and C_n/C_α if the effects of the competing reactions omitted from the denominators of equations (7) and (8) are small, and if the contributions to the cross-section by direct interaction can be neglected. The important contribution to the cross-section by processes such as (n, pn) have been taken into account by using the f_x factors in the denominator of equations (7) and (8) rather than the f_x^0, but reactions such as (n, d), (n, t) and (n, He^3) have been neglected. In a light element such as aluminium the principal mechanism leading to these reactions is probably pick-up rather than compound nucleus formation, and thus, they are not amenable to the type of analysis we are considering. However it is important to estimate the magnitude of their contribution to the total reaction cross-section. The (n, d) cross-section will be higher than the (n, t) and (n, He^3) independently of the Q-values for the reactions, since pick-up of one particle is more probable than two. The order of magnitude of the (n, d) cross-section can be obtained by comparison with the Al^{27}(p, d)Al^{26} data of Reynolds and Standing[13]) obtained using 18 MeV protons. Their results yield a total (p, d) cross-section of $\approx$ 5 mb and indicate that the contributions of the reactions (n, d), (n, t) and (n, He^3) to the total reaction cross-section at the energies we are considering, are small.

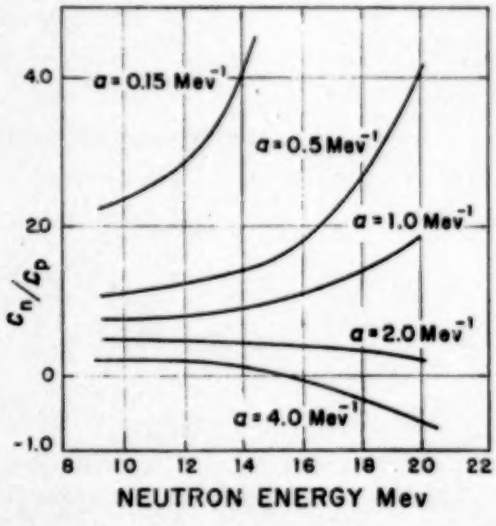

Fig. 9. C_n/C_p as a function of neutron energy.

If the level density formula used is valid and if the statistical theory can be applied to these reactions, the ratios C_n/C_p and C_n/C_α should not vary with

energy for the correct choice of the constant a. We have calculated these two ratios as a function of neutron energy for various values of a using the experimental values of the cross-section; the results are presented in figs. 9 and 10. It can be seen from the figures that the ratios C_n/C_p and C_n/C_α are approximately

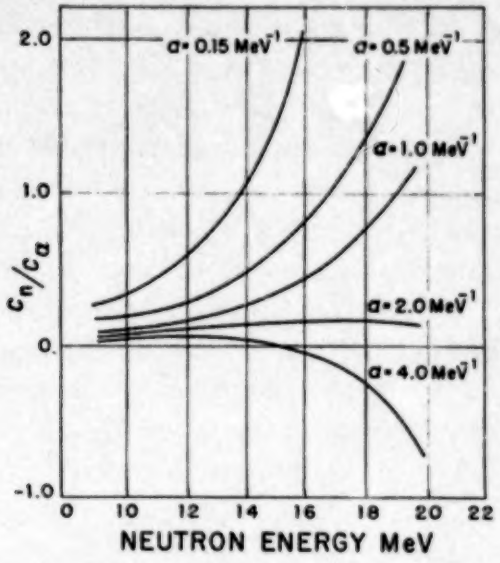

Fig. 10. C_n/C_α as a function of neutron energy.

constant with neutron energy for $a = 2$, which yields a nuclear temperature of 1.5 MeV. This value for the nuclear temperature agrees well with those obtained[14]) from the energy distribution of reaction products at an incident neutron energy of 14 MeV, and is consistent with Zucker's measurements[15]) on neighbouring nuclei using heavy ions. This latter agreement is perhaps fortuitous since differential energy measurements are more sensitive to admixtures of direct interaction processes than our value obtained by integration over the energy spectrum. The ratios C_n/C_p and C_n/C_α give an indication of the ratio of the level densities in the corresponding residual nuclei. From our results we get the following values:

$$\text{Level density in } {}_{13}\mathrm{Al}^{27}_{14} = 0.4 \text{ times level density in } {}_{12}\mathrm{Mg}^{27}_{15}$$
$$= 0.1 \text{ times level density in } {}_{11}\mathrm{Na}^{24}_{13}.$$

From very approximate considerations using the rather scanty experimental data available up to an excitation energy of 8 MeV Brown and Muirhead[16]) have obtained a value of 2.5 for the ratio of level densities of odd-odd to odd-even nuclei. Their evaluation is only an average and does not take into account effects like shell structure. Considering then the errors involved in the above computation and in the analysis of Brown and Muirhead, the above values seem fairly reasonable.

3.2. RELATIVE INTENSITY OF TRANSITIONS TO ISOMERIC AND GROUND STATE OF Al^{26}

Segrè and Helmholtz[17]) have suggested that in a reaction which may lead to either a ground state or an isomeric state the ratios of the population of these states should tend towards a limiting value. The limiting value should depend only on the statistical weights $(2I + 1)$ of the final states. Levy[18]), Meadows *et al.*[19]) and others have found that in a number of cases the ratio does tend to a limiting value but this value differs from the ratio of the statistical weights. In some cases arguments can be produced based on the known special properties of the nuclear states which account qualitatively for the observed value. More recently Huizenga[20]) has obtained good quantitative agreement with experimental data by consideration of the reaction mechanism through all stages of formation and decay of the compound nucleus.

Since no data on the intensity of transitions to the ground state of Al^{26} exist, a calculation of the total (n, 2n) cross-section has been made on the basis of the simple treatment of Blatt and Weisskopf. They show that

$$\sigma(\mathrm{n}, 2\mathrm{n}) = \sigma_c[1 - (1 + Z)\,\mathrm{e}^{-Z}]\,, \tag{9}$$

where σ_c is the cross-section for the formation of the compound nucleus, and

$$Z = E_c \left(\frac{a}{E_n}\right)^{\frac{1}{2}}$$

using $E_c = E_{by} - B_n$. Here, B_n is the binding energy of the last neutron in Al^{28} and E_{by} is the maximum energy of neutrons that can be emitted, which in this case is E_n.

In fig. 8 the calculated cross-section curves derived from equation (9) using various values of a are shown together with the experimental results. As expected the excitation function shows a pronounced curvature; however, even at a neutron energy of 20 MeV, the value of a required to fit the data ($a \approx 0.2$ MeV^{-1}) is too small, yielding a value of about 10 MeV for the nuclear temperature. This low value implies that the contribution to the total (n, 2n) cross-section by transitions to the ground state in Al^{26} is important. We have attempted to compute the ratio of the cross-section going to the ground state to that going to the isomeric state, as follows.

Using the value of $a = 2$ obtained from the (n, p) and (n, α) cross-sections, the total (n, 2n) cross-section can be estimated using equation (9). This estimate is an upper limit since it does not take into account the competing (n, np) reaction. From this we can get an upper limit for the ratio of the cross-section going to the ground state and the isomeric state. This is given by

$$\frac{\sigma^{gs}}{\sigma^{is}} = \frac{\sigma^{cal}(\mathrm{n}, 2\mathrm{n}) - \sigma^{exp}(\mathrm{n}, 2\mathrm{n})}{\sigma^{exp}(\mathrm{n}, 2\mathrm{n})}\,, \tag{21}$$

where σ^{gs} is the cross-section to the ground state, σ^{is} that to the isomeric state, σ^{cal} the calculated value of the total (n, 2n) cross-section taking $a = 2$ and σ^{exp} is the experimental value for the isomeric state. This ratio is plotted in fig. 11 as a function of neutron energy. The ratio is high at low energy due to

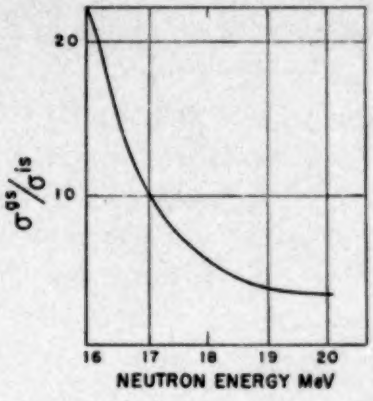

Fig. 11. Ratio of the (n, 2n) cross-section in Al^{27} going to the isomeric state and ground state in Al^{26}

the effect of neglecting the (n, np) reaction as mentioned above, but tends to a limiting value of about 3. This is very much less than the value of 11 predicted by the statistical weights. Since the γ-ray cascade will consist of several γ-rays, in general its course will be greatly influenced by the available low lying states in Al^{26}. The known states[6]) below 7 MeV tend to have low spin and hence should favour transitions to the ground state.

It is a pleasure to thank Dr. E. B. Paul for the interest he took in this work and for the many valuable discussions with him. Two of us (G.S.M. and G.J.M.) wish to express our gratitude to AERE, Harwell and to all the members of the Van de Graaff group for their hospitality and kindness. Finally the unstinting cooperation of the operating staff of the accelerator is gratefully acknowledged.

References

1) R. J. Howerton, UCRL-5420 (1958)
2) Grundl *et al.*, Phys. Rev. **109** (1958) 425
3) Kern *et al.*, Nuclear Physics **10** (1959) 226
4) Neutron Cross-sections, BNL 325 (1958);
Hudson and Morgan, Bull. Am. Phys. Soc. **4** (1959) 97
5) S. Yasumi, J. Phys. Soc. Japan **12** (1957) 443;
S. G. Forbes, Phys. Rev. **88** (1952) 1309;
Haling *et al.*, Phys. Rev. **106** (1957) 971
6) P. M. Endt and C. M. Braams, Rev. Mod. Phys. **29** (1957) 683
7) Charged Particle Cross-sections, LA-2014 (Los Alamos Report)
8) J. P. Dropesky and A. W. Schardt, Phys. Rev. **102** (1956) 426
9) D. Strominger *et al.*, Rev. Mod. Phys. **30** (1958) 585
10) W. E. Mott and R. B. Sutton, Handbuch der Physik XLV, 86
C. M. Davisson, in Beta and Gamma Ray Spectroscopy, ed. by K. Siegbahn (North-Holland Publishing Company, Amsterdam, 1955), p. 857

11) Blatt and Weisskopf, Theoretical Nuclear Physics (Wiley, New York, 1952)
12) Feshbach and Shapiro, NYO-3077 (1953);
Bloch *et al.*, Rev. Mod. Phys. **23** (1951) 147
13) J. B. Reynolds and K. G. Standing, Phys. Rev. **101** (1956) 158
14) D. Allan, Proc. Phys. Soc. **70** (1957) 195;
I. Kumabe, Phys. Rev. **106** (1957) 155
15) A. Zucker, Proceedings of the Conference on Reactions between Complex Nuclei, ORNL-2606 (1958), unpublished
16) Brown and Muirhead, Phil. Mag. **2** (1957) 473
17) Segrè and Helmholz, Rev. Mod. Phys. **21** (1949) 271
18) H. B. Levy, Thesis, University of California
UCRL-2305 (1953), unpublished
19) Meadows, Diamond and Sharp, Phys. Rev. **102** (1956) 190
20) J. R. Huizenga (private communication)

1.E.1:
3.A

Nuclear Physics **19** (1960) 550—554; © *North-Holland Publishing Co., Amsterdam*
Not to be reproduced by photoprint or microfilm without written permission from the publisher

INVESTIGATIONS OF THE DECAY-SCHEME OF Rh^{101}

B. L. SHARMA

Department of Physics, Ohio State University, Columbus†

Received 2 May 1960

Abstract: Enriched Ru^{101} bombarded with 6 MeV protons was observed to emit 75, 310, and 545 keV gamma rays each decaying with a 4.4 d half-life. However, the lead and copper absorption measurements strongly indicated that the 75 keV photo peak, observed in well crystal measurements, was actually due to the Pb K X-ray, produced by the photo-electric absorption of the 310 keV gamma ray in the lead shield around the crystal. A weak 235 keV gamma ray was observed to be in coincidence with the 310 keV gamma ray previously assigned to Rh^{101}. The latter was not in coincidence with 545 keV.

After the decay of 4.4 d activity, gamma rays of 127 and 198 keV were observed to be in coincidence and have a very long half-life. The 127 keV gamma ray was associated with Rh^{101} from the reported Coulomb excitation of Ru^{101} and the decay of Tc^{101}. The proposed decay scheme, having levels at 127, 310, 325 and 545 keV, is presented in this paper.

1. Introduction

The activity of Rh^{101} was first reported, among others, by Lindner and Perlman[1]) and by Eggen and Pool[2]). In 1951, Sullivan *et al.*[3]) reported the half-life of Rh^{101} to be 5.9 d. Later the radiation from Rh activity produced by the bombardment of pure Ru metal with protons were examined in a beta ray spectrometer by Scoville, Fultz and Pool[4]). According to them, the observed internal conversion peaks, decaying with a half-life of 4.5 d, were attributed to K and L conversion electrons from the 148 and 305 keV gamma rays of Rh^{101}.

More recently, Pd isotopes were prepared by α particle bombardment of Ru metal powder, and the radiation from these isotopes and their Rh daughters were investigated with scintillation coincidence spectrometer by Katcoff and Abrash[5]). After the decay of the shorter lived components in all the Rh and Pd samples, they observed that Rh^{101} decayed by electron capture with a half-life of 4.7 d and the only gamma ray was at 310 keV.

Farmer[6]) was the first to report that the 127 and 198 keV gamma rays did not, as previously reported by Avingnon[7]) and others, belong to Rh^{102}, but were due to a long-lived (half-life 5 ± 1 y) isotope of Rh with $A < 102$. Since then several workers have studied the decay of this long-lived isotope of Rh. Hisatake *et al.*[8]) and Perrin *et al.*[9]) have assigned the 5 year activity to Rh^{101}.

Because of the considerable disagreement in the reported data about the

† Present address: Defence Science Laboratory, Delhi-6.

half-life and the number and energies of the gamma rays in the decay of Rh^{101}, it was believed that a reinvestigation might be desirable. Furthermore, a research on this isotope was also suggested by the fact that enriched Ru^{101}, formerly not available, could be obtained from Oak Ridge. Hence these investigations were undertaken with the view of obtaining detailed information regarding the decay of Rh^{101}.

2. Experimental

2.1. SOURCE

In order to produce radioactive Rh^{101}, the enriched Ru^{101} (91.1 %) was bombarded with 6 MeV protons at the Ohio State University Cyclotron. Shortly after the irradiation, a number of samples were prepared in order to perform all the different types of measurements simultaneously. The well crystal sample was made by pouring molten paraffin over a small portion of the original sample in the bottom of a 0.64 cm × 5.1 cm glass test tube.

2.2. SCINTILLATION DETECTORS

The detector, known as well type crystal, consisted of a 7.6 cm × 7.6 cm cylindrical NaI (Tl) crystal with a 0.95 cm hole which extended along the longitudinal axis to the centre of the crystal, a DuMont 6394 (12.7 cm) photomultiplier tube and a preamplifier. The pulses from this detector were fed into a 100-channel pulse height analyzer. Essentially a 4π geometry was obtained by placing the sample inside the well of the crystal. For studying the effects of geometry variation, a source holder was provided outside the crystal. In order to reduce the back ground radiation the whole assembly was placed in a lead and iron shield.

Another type of scintillation detectors, used mostly for gamma-gamma coincidence measurements, were composed of a 4.44 cm × 5.1 cm cylindrical NaI (Tl) crystal, a DuMont 6292 photomultiplier tube, and a white cathode follower designed by the Oak Ridge National Laboratory.

3. Results and Conclusion

The early measurements showed the presence of 0.075, 0.310, 0.442, 0.545, 0.823, 1.10, 1.36, 1.56, 1.93 and 2.38 MeV gamma rays. All except the 75, 310 and 545 keV gamma rays decayed with a half-life of 20 h. This 20 h activity was attributed to the decay of Rh^{100}, obtained by the proton bombardment of Ru^{100} present in the enriched Ru^{101}. These values were found to be in close agreement with those reported by Marquez[10]).

In order to follow the decay of the Ru^{101} + p sample more accurately from geometrical considerations, measurements using the 7.6 cm × 7.6 cm well

type crystal were made. A typical gamma ray spectrum, obtained 5.5 days after the irradiation, is shown in fig. 1. With the source placed in the well, the Compton continuum accompanying the 310 keV photo-peak was much reduced. The 545 keV photo peak was initially observed to decay on a relatively shorter half-life of 20 h. However, after the decay of this 20 h activity of Rh^{100}, this 545 keV photo-peak was observed to decay with a 4.4 d half-life. From

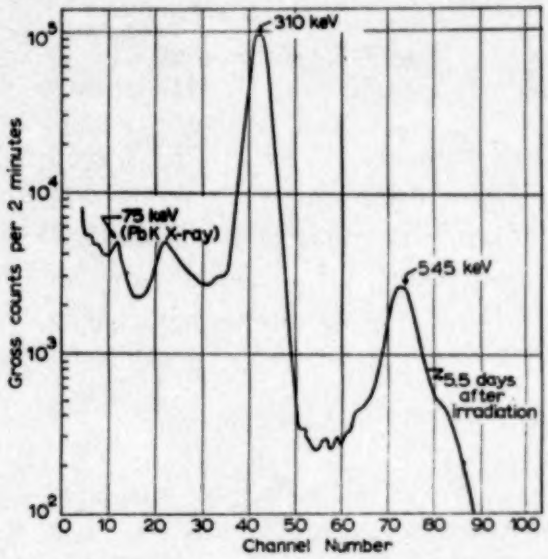

Fig. 1. Gamma ray spectrum of Rh^{101}.

the very beginning of the measurements, the 310 keV gamma ray was observed to decay with a 4.4 d half-life. The logarithmic decay curve of the 310 keV photo-peak was linear for 5 half-lives with a half-life of 4.4 d, and is shown in fig. 2. Although the 75 keV photo-peak, observed in well crystal measurements, decayed on the same half-life as 310 keV gamma ray, but the lead and copper

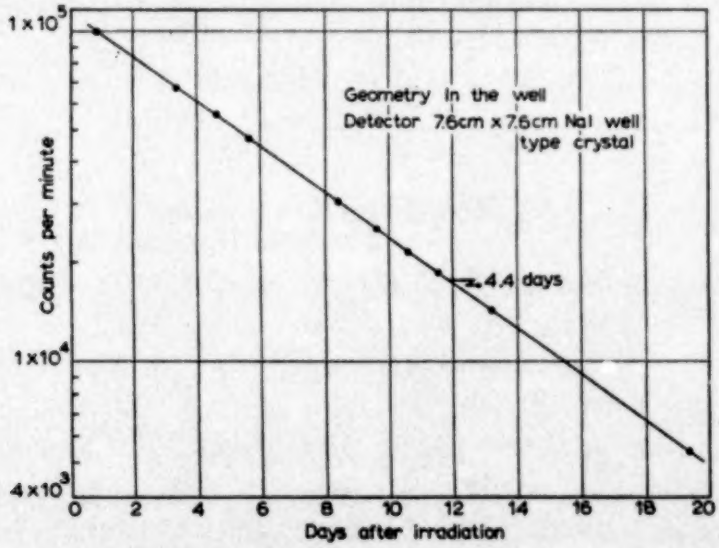

Fig. 2. 310 keV gamma decay of Rh^{101}.

absorption measurements strongly suggested that the 75 keV photo peak was actually due to Pb K X-ray, produced by photoelectric absorption of 310 keV gamma ray in the lead shield around the crystal.

The gamma-gamma coincidence measurements were carried out in order to determine the decay scheme of this isotope. Coincidences between successive gamma transitions in the Ru^{101} + p sample were observed by placing the sample between the two scintillation heads, each containing a 4.44 cm × 5.1 cm NaI(Tl) crystal. In the first gamma-gamma coincidence measurements, the single-channel analyzer was gated to accept the pulses corresponding only to 310 keV gamma ray, while the 100-channel analyzer viewed the entire spectral region upto 1 MeV. This measurement revealed that a weak 235 keV gamma ray was in coincidence with the 310 keV gamma ray. However, the latter was not in coincidence with 545 keV gamma ray. The lead and copper absorption measurements also proved beyond doubt that the 545 keV peak was not a sum peak of 235 and 310 keV gamma rays.

After the decay of the 4.4 d activity, photo-peaks at 127, 198 and 325 keV were found to have a very long half-life. A sample of Ru + d, which was allowed to decay for 13 y, strongly showed these above mentioned radiations. It was evident from the well crystal measurements that the 325 keV photo-peak was nothing but a sum peak of 127 and 198 keV gamma rays. This fact was further verified by coincidence measurements. The 127 and 198 keV gamma rays were found to be in coincidence with each other. Hence these results suggested that the 127 and 198 keV gamma rays were in cascade.

In order to help identify this 4.4 d activity, its gamma ray spectrum was compared with that of Tc^{101}. Since both these nuclides decay to stable Ru^{101}, it was expected that some of the gamma rays might be identical on both. As expected, the energies of the gamma rays, observed to decay with a 4.4 d half-life, were identical, within experimental uncertainty, with the energies of 3 of the Tc^{101} gamma rays[11]). As the nuclear energy states of Ru^{101} have been studied in a number of reactions and processes, the de-excitation gamma ray spectrum, obtained by Coulomb excitation of Ru^{101}, has been studied by Temmer *et al.*[12]), who observed 127, 180, 307 and 520 keV gamma rays. However, McGowan *et al.*[13]) observed a number of additional transitions in Ru^{101}, most of them only by coincidence detection. They also had evidence that the 307 keV state was really a doublet one member of which decayed directly by ground state transition and the other only by cascade via the 127 keV state. Therefore, the 127 keV radiation was assigned to Rh^{101} from the reported Coulomb excitation of Ru^{101} and the decay of Tc^{101}. Among others, Goldberg[14]) has also assigned this long-lived (half-life 5 ± 1 y) activity to Rh^{101}.

The results of the present investigations[15]), together with the above mentioned results of various workers, suggest a possible decay scheme of Rh^{101}, shown in fig. 3. The spin of the ground state of Ru^{101} has been previously measured[16])

as $\frac{5}{2}$. The other spin assignments are tentative, and are based on the theory of nuclear shell structure. An attempt was made to observe the gamma-ray associated with the internal transition between the 4.4 d and 5 y levels of Rh^{101}. However, it was not observed in the present investigations.

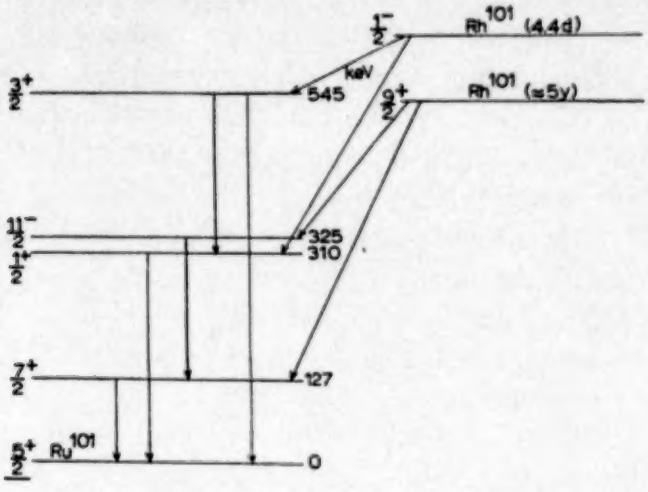

Fig. 3. Proposed decay scheme of Rh^{101}.

In conclusion the author wishes to express his sincere appreciation to Professor M. L. Pool for his interest, suggestions and encouragement throughout this work.

References

1) M. Lindner and I. Perlman, Phys. Rev. **73** (1948) 1202
2) D. E. Eggen and M. L. Pool, Phys. Rev. **75** (1949) 1464
3) W. H. Sullivan, N. R. Sleight and E. M. Gladrow, NNES-PPR **9** (1951) 1949
4) C. L. Scoville, S. C. Fultz and M. L. Pool, Phys. Rev. **85** (1952) 1046
5) S. Katcoff and H. Abrash, Phys. Rev. **103** (1956) 966
6) D. J. Farmer, Phys. Rev. **99** (1955) 659A
7) P. Avingnon, Compt. Rend. **240** (1955) 176
8) K. Hisatake, J. T. Jones and J. D. Kurbatov, Bull. Am. Phys. Soc. **1** (1956) 271
9) N. Perrin, L. Dick, R. Foucher and J. J. Vartapetian, J. Phys. et Radium **17** (1956) 593
10) L. Marquez, Phys. Rev. **92** (1953) 1511
11) G. D. O'kelley, Q. V. Larson and G. E. Boyd, Bull. Am. Phys. Soc. **2** (1957) 24
12) G. M. Temmer and N. P. Heydenburg, Phys. Rev. **104** (1956) 967
13) F. K. KcGowan and P. H. Stelson, footnote in G. M. Temmer and N. P. Heydenburg, Phys. Rev. **104** (1956) 967
14) N. Goldberg, Bull. Am. Phys. Soc. **2** (1957) 230
15) B. L. Sharma and M. L. Pool, Bull. Am. Phys. Soc. **4** (1959) 151
16) J. H. E. Griffiths and J. Owen, Proc. Phys. Soc. A **65** (1952) 951

1.D.3 *Nuclear Physics* **19** (1960) 555—578; © *North-Holland Publishing Co., Amsterdam*
Not to be reproduced by photoprint or microfilm without written permission from the publisher

TWO-BODY CLUSTER STATES IN NUCLEI

G. C. PHILLIPS and T. A. TOMBRELLO

The Rice Institute, Houston, Texas†

Received 16 May 1960

Abstract: A number of experimental results for nuclear states are cited that require a description of the nucleus as the interaction of two clusters of nucleons. The types of experiments that yield information about states of two-cluster parentage are considered. The clusters identified and discussed consist of such bodies as deuterons, excited deuterons, α-particles, tritons, helium-3, and nuclei in an excited state such as ^{8}Be and ^{12}C. The general nature of the nuclear forces necessary to produce clustering is discussed, and a phenomenological model describing these cluster states in terms of coupled Schrödinger equations is presented. The model is compared with other current models of nuclear structure. Several definite predictions of the model for the dynamical behaviour of nuclear systems are given.

1. Introduction

One of the central problems of nuclear physics is the study of nuclear structure. To establish the structure of nuclei experimentally, one must measure all the stationary and dynamical properties of the nuclei. Of particular importance in a proper description of nuclear structure is the treatment of the stable or semi-stable energy eigenstates of nuclei. It has been pointed out that there are a number of examples of dynamical properties of light nuclei that show strong evidence for the clustering of nucleons into two sub-groups within the nucleus, and a model for the nucleus has been proposed in which the interactions of these two-body clusters play an important role in nuclear structure[1]). The purpose of this paper is to cite some of the experimental evidence that reveals cluster structure within the nucleus and to give a model that describes these features and allows the prediction of new results.

Since the arguments for or against the existence of clustering within the nucleus must rest upon experimental evidence, it is important to emphasize the ways in which experiments may be interpreted as revealing clustering. To show that there is a spatial ordering of the nucleons within the nucleus for certain nuclear states, it is necessary by the uncertainty principle that the momentum, or energy, of the nucleons is suitably dispersed. Thus the evidence for clustering must come from studies of the energy properties of nuclear states.

The energy-characteristic nuclear wave function $\Psi(E)$ for an excited nucleus consisting of n nucleons, may be represented as the sum of all possible two-cluster wave functions $\psi_2(E)$, three-cluster wave functions $\psi_3(E)$, etc. for

† Work supported by the U. S. Atomic Energy Commission.

separation distances between clusters greater than the range of the nuclear forces. Thus it is possible to write, in this region of space,

$$\Psi = \sum_{\lambda} \theta_{2,\lambda}\psi_{2,\lambda} + \sum_{\mu} \theta_{3,\mu}\psi_{3,\mu} + \ldots .$$

Each of these wave functions is an energy characteristic function for the same total energy. The members of this set of wave functions may be considered in practice to be orthogonal and complete in this spatial region, as will be discussed in sec. 3. The θ are expansion parameters that are functions of the energy and may be related to the decay widths. A measurement of these θ, then, allows a determination of the state of spatial ordering of the nucleons.

The usefulness of the cluster expansion lies in the fact that it explicitly gives the wave functions that are physically observable as the outgoing reaction products of the nuclear interaction. However, this set of wave functions *must* also include *bound*, or negative energy, cluster arrangements in this spatial region since the bound wave functions are in principle observable. Each one of these wave functions, representing a particular arrangement of the nucleons into clusters, is called a parentage, channel, or cluster wave function, and gives the probability that the nucleus will be found in that parentage form for distances of cluster separation greater than or equal to the range of nuclear forces.

Sometimes it is possible to measure the $|\theta_{2,\lambda}|^2$ for fairly well defined energy eigenstates by the approximate relationship

$$|\theta_{2,\lambda}|^2 \approx \gamma_\lambda^2 / [3\hbar^2/2\mu_\lambda a_\lambda^2] ,$$

where the reduced width γ_λ^2 is related to the observed decay width Γ_λ for decay into the two cluster channel λ by[2])

$$\gamma_\lambda^2 = [\Gamma_\lambda A_\lambda^2/2k_\lambda r]_{r=a_\lambda} .$$

In these expressions k_λ is the wave number in channel λ outside the nucleus, whose nuclear forces extend only to $r = a_\lambda$; μ_λ is the reduced mass, and $A_\lambda^2 = F_\lambda^2 + G_\lambda^2$, where F_λ and G_λ are the two linearly independent solutions of the wave equation for the external region. Now $\sum_{n,\lambda} |\theta_{n,\lambda}|^2 = 1$, so that if at a certain resonance of energy E_λ, a certain $|\theta_{2,\lambda}|^2 \approx 1$, it follows that the other $|\theta_{2,n\neq\lambda}|^2$ of the system are very small and that the wave function is almost purely of the form $\psi_{2,\lambda}$ outside and on the nuclear surface. This argument allows the examination of nuclear states for their fractional, two-body parentage, $|\theta_{2,\lambda}|^2$.

Another very important type of experimental observation available for determining the fractional parentage of nuclear states is the total cross section in reaction channels. If the total cross section for formation of a reaction particle group shows a resonance whose cross section is near the

geometrical limit, the state may be inferred to be of a two-body character.

Techniques similar to those given above allow an experimental evaluation of all of the θ_λ corresponding to *open* two-body channels. However, when a channel is energetically closed, other techniques must be employed. The only method that is currently available and which gives unambiguous results involves the measurement of γ-ray transition probabilities: when the initial and final wave functions involved in a γ-ray transition are written in parentage form for all distances and when the initial and final wave functions are assumed to be of almost pure and similar parentage, then if the observed transition probability is near the calculated value, it may be inferred that the assumed parentages of the states are correct. In such calculations it frequently occurs that the wave functions for the region inside the nuclear surface are immaterial in that they contribute very little to the cross sections. This result is a consequence of the fact that electro-magnetic wavelengths are usually much larger than nuclear dimensions. This later type of experimental information has not been very carefully examined except in cases where single nucleon transitions have been considered[3]).

In the methods mentioned above one must compare the reduced width of a nuclear state to the Wigner limit[2]) $\gamma_\lambda^2 < (3\hbar^2/2\mu_\lambda a_\lambda^2)$. This limit is only an approximate one since it is fundamentally a restatement of the Heisenberg uncertainty principle, asserting that the decaying waves of the semi-stable state are somewhat confined inside the channel radius a_λ and that their momentum and energy are thus dispersed.

In addition, simple two-body type calculations, using reasonable potential wells, show that for the case of pure parentage λ, the value of $|\theta_{2,\lambda}|^2$ deduced from the energy-width argument may lie between about 0.1 and 2.0. Thus there is apparently no perfectly sharp way to show with measurements that a state is of pure parentage. Nevertheless, if one of the above techniques is applied to a given sharp or semi-sharp nuclear state and if it is found that the experimental evidence shows that a particular θ^2 is near unity, it may be inferred that the resonant state is described rather purely by that two-body cluster form in the external region. Furthermore, each of the external wave functions may be supposed continuous across the surface where strong inter-cluster interactions commence, and these external (observable) functions may be continued into the inner region. It may be inferred that the dominant channel wave function will continue to be largest over some distance within the region of strong intercluster interactions and that the resonant state may be approximately described as a two-body interaction in that channel. It is this type of interpretation of observation that shows there are two-body cluster arrangements of nucleus within the nucleus.

In section 2 these methods of obtaining information about the fractional parentage coefficients will be examined for the states of a number of nuclei.

2. A Survey of Some Experimental Evidence for Clustering

The states of several nuclei will now be discussed briefly. The examples will be principally taken from the light elements since the energy level structure is simpler and the experiments are usually of higher accuracy. However, certain other anomalous features that show evidence of clustering in the heavier nuclei will also be discussed.

2.1. NUCLEI WITH $A = 5$

The mirror nuclei He^5–Li^5 have a very simple level structure with only three well defined states observed below about 20 MeV of excitation. It is known that the two lower states have large single-particle widths for decay into He^4 and a nucleon[4]), while the narrow state near 17 MeV has a very large width for decay into a deuteron and either a triton or a He^3 nucleus[5]). These data are given in table 1 and fig. 1, and the observed decay widths are compared to the Wigner limit.

TABLE 1

The low-lying states of the mass-5 nuclei

	E_{ex}	J^π	T	θ^2_{1+4}	θ^2_{2+3}	Reference
He^5	0	$\frac{3}{2}^-$	$\frac{1}{2}$	1		a
	3–6	$\frac{1}{2}^-$	$\frac{1}{2}$	1		a
	16.69	$\frac{3}{2}^+$	$\frac{1}{2}$	0.04	1.5	b
Li^5	0	$\frac{3}{2}^-$	$\frac{1}{2}$	0.4		c
	5–10	$\frac{1}{2}^-$	$\frac{1}{2}$	1.0		c
	16.81	$\frac{3}{2}^+$	$\frac{1}{2}$	0.01	0.74	d

The energy of excitation E_{ex}, the total angular momentum J and parity π, the isobaric spin T and the two-body reduced widths in ratio to the Wigner limit are given. θ^2_{1+4} is this ratio for α-particle + nucleon, and θ^2_{2+3} for deuteron + mass-3 particle.

[a] F. Ajzenberg-Selove and T. Lauritsen, Nuclear Physics **11** (1959) 6

[b] Conner, Bonner and Smith, Phys. Rev. **88** (1952) 468

[c] P. D. Miller and G. C. Phillips, Phys. Rev. **112** (1958) 2043

[d] Bonner, Conner and Lillie, Phys. Rev. **88** (1952) 473

Thus all of the states of the mass-five system that have been identified to date show large two-body widths. It is indeed remarkable that *the most stable state of these systems is at the high excitation energy of about* 17 MeV *and is of nearly pure deuteron parentage.*

2.2. Li^6–He^6 STATES

The energy level diagram of Li^6, shown in fig. 2, along with the widths tabulated in table 2, shows that there is evidence for cluster states in this nucleus. Three excited states of Li^6 are quite purely of d + α parentage as is

shown by d + α scattering[6]). It is possible that the ground state of Li^6 is also of the form d + α with considerable purity[6]). It seems necessary to describe the

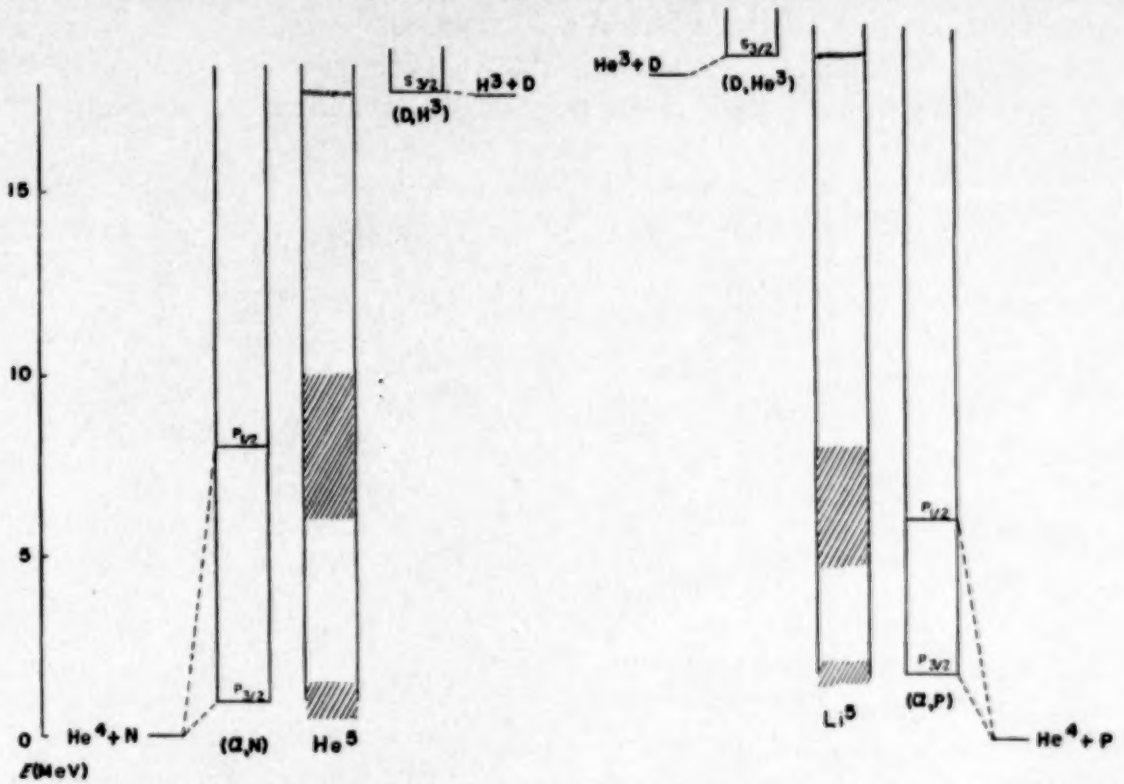

Fig. 1. Two-body cluster parentage of the mass-5 nuclei. The energy level diagrams for the nuclei He^5 and Li^5 are shown alongside the proposed two-body cluster parentage of the levels labeled (α, n), (α, p), (D, H^3), etc. The energy at which the nuclei may be decomposed into two-body clusters is shown. The ground states of the mirror pair have been arbitrarily adjusted to coincide. The dashed lines indicate the principle parent of each level and the designations $P_{\frac{3}{2}}$, etc., indicate the relative orbital angular momentum and total angular momentum of the two-body cluster arrangement assigned. Where appropriate the isobaric spin of each state is also given. The cross-hatching indicates, qualitatively, the energy-widths of states.

TABLE 2

The low-lying states of the mass-6 nuclei

	E_{ex}	J^π	T	θ^2_{trip}	θ^2_{sing}	Reference
Li^6	0	1^+	0	0.5	0	a
	2.18	3^+	0	0.8	0	a
	3.56	0^+	1	0	1.0	b
	4.52	2^+	0	1.0	0	a
	5.35	(1^+)	0	≈ 1	0	a
He^6	0	0^+	1	(0)	(≈ 1)	b
	1.71	(2^+)	1	(0)	(≈ 1)	b

See table 1 for the meaning of symbols. θ^2_{trip} and θ^2_{sing} refer to the ratio of partial widths to the Wigner limit for the two-body configurations α-particle + triplet (or singlet) *di*-nucleon.

[a] A. Galonsky and M. T. McEllistrem, Phys. Rev. **98** (1955) 590

[b] F. Ajzenberg-Selove and T. Lauritsen, Nuclear Physics **11** (1959) 20

$T = 1$ states as a similar group of states based upon the parentage of an excited (singlet) deuteron + α-particle. Each of these groups of states has an s-wave interaction at the lowest energy and a d-wave next lowest.

In a similar manner it seems reasonable that the ground and first excited ($T = 1$) states of He^6 consist of the two-body configuration α + *di*-neutron.

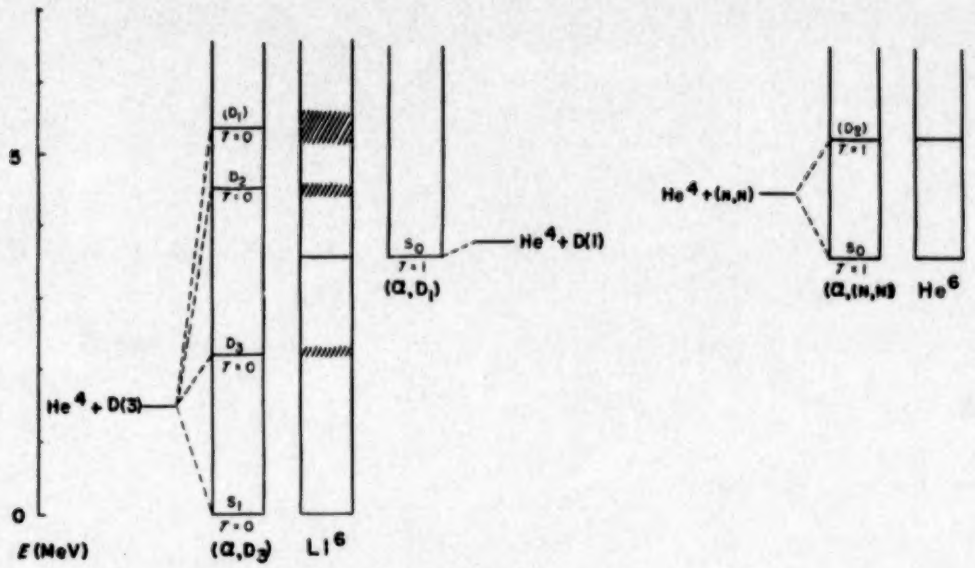

Fig. 2. Two-body cluster parentage of the mass-6 nuclei. See fig. 1 for the meaning of symbols. The symbols D_1 and D_3 refer to singlet or triplet deuteron structures while (n, n) refers to a (singlet) *di*-neutron structure.

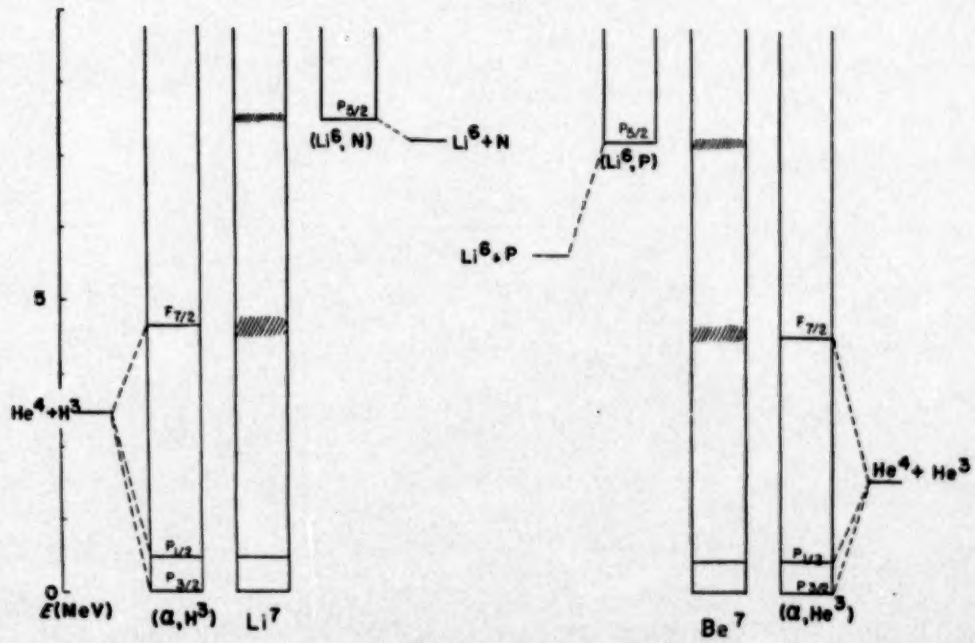

Fig. 3. Two-body cluster parentage of the mass-7 nuclei. See fig. 1 for the meaning of symbols. The reported state at about 6.5 MeV has not been included; see references of table 3.

TABLE 3

Low-lying states of the mass-7 nuclei

	E_{ex}	J^π	T	θ^2_{3+4}	θ^2_{1+6}	Reference
Li^7	0	$\frac{3}{2}^-$	$\frac{1}{2}$	($\approx$ 1)		a
	0.478	$\frac{1}{2}^-$	$\frac{1}{2}$	($\approx$ 1)		a
	4.63	$\frac{7}{2}^-$	$\frac{1}{2}$	($\approx$ 1)		a
	7.47	$\frac{5}{2}^-$	$\frac{1}{2}$	0.008	0.26	b
Be^7	0	$\frac{3}{2}^-$	$\frac{1}{2}$	0.1–1.0		c
	0.431	$\frac{1}{2}^-$	$\frac{1}{2}$	0.01–1.0		c
	4.53	$\frac{7}{2}^-$	$\frac{1}{2}$	0.36		c
	7.18	$\frac{5}{2}^-$	$\frac{1}{2}$	0.05	0.24	b

See table 1 for the meaning of symbols. The excited state reported at about 6.5 MeV[a,b] has been omitted[d]).

[a] F. Ajzenberg-Selove and T. Lauritsen, Nuclear Physics **11** (1959) 28

[b] Marion, Weber and Mozer, Phys. Rev. **104** (1956) 1402

[c] P. D. Miller and G. C. Phillips, Phys. Rev. **112** (1958) 2048

[d] E. W. Hamburger and J. R. Cameron, Phys. Rev. **117** (1960) 781

2.3. NUCLEI WITH $A = 7$

Reference to fig. 3, the level diagram for Li^7–Be^7, and to table 3 shows that these nuclei in their ground and first and second excited states have large values of θ for the configuration $He^3 + \alpha$ or $T + \alpha$[7]), while the third excited state has a large width for the nucleon + Li^6 configuration[8]). The ground and first excited states have been shown[9]) to be strongly populated by the processes $T + \alpha \rightarrow Li^7 + \gamma$ and $He^3 + \alpha \rightarrow Be^7 + \gamma$. The cross section for $He^3 + \alpha$ capture may be calculated to be about 0.7 microbarns at $E_{lab} = 1$ MeV by assuming that Be^7 is of pure $He^3 + \alpha$ parentage in both the initial (S) state and final (P) state. The observed yield is 0.5 microbarns. Thus the $\theta^2_{3+\alpha}$ is ≈ 0.3 Similarly for $T + \alpha$ capture the $\theta^2_{3+\alpha} \approx 0.16$. Thus the first three states of the mass 7 nuclei are of an almost pure mass $3 + \alpha$ cluster form, while the 7 MeV state has a large nucleon + Li^6 amplitude.

2.4. Be^8 STATES

The three lowest states of Be^8 have been noted[10]) to have large $\alpha + \alpha$ widths which are shown in fig. 4 and table 4. Below about 15 MeV of excitation the cluster description of Be^8 as two α-particles seems to be both necessary and sufficient. The effective potential of interaction for two α-particles has been discussed[10]), and the effective α–α potential has been shown to be attractive in the region near 5×10^{-13} cm and more repulsive than the Coulomb interaction at closer distances.

It is important to note that Be^8 has no excited states other than that of almost pure $\alpha + \alpha$ parentage until an energy approximately equal to the Li^7 + p threshold is reached.

TABLE 4

The low-lying states of Be^8

E_{ex}	J^π	T	$\theta^2_{\alpha+\alpha}$	Reference
0	0^+	0	0.15	a
2.9	2^+	0	0.7	a
11.8	4^+	0	0.95	a

[a] Russell, Phillips and Reich, Phys. Rev. **104** (1956) 135

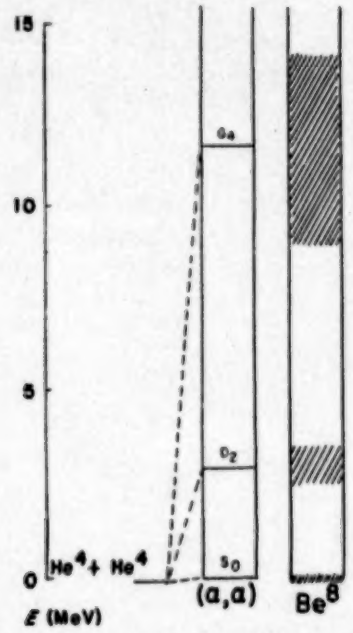

Fig. 4. Alpha particle parentage of Be^8. See fig. 1 for the meaning of symbols.

2.5. NUCLEI WITH $A = 9$

Studies[11]) of the reaction $B^{10}(He^3, \alpha)B^9$ have allowed the comparison of the mirror pair Be^9–B^9 as is shown in fig. 5 and table 5. There is no evidence for a

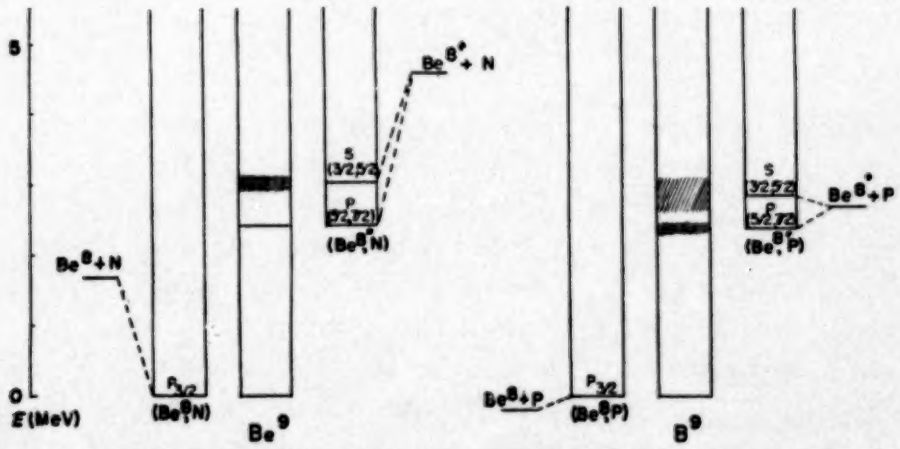

Fig. 5. Two-body cluster parentage of the mass-9 nuclei. See fig. 1 for the meaning of symbols. It should be noted that the states in Be^8 are not sharp but are in the continuum.

proper state near 1.7 MeV in B^9. The anomalous "cusp" at 1.666 MeV in Be^9 and the continuous excitation of any energy in B^9 between its sharp "ground state" and its state at about 2.34 MeV is most easily explained in terms of a "generalized density of states" function. Spencer *et al.* have proposed that the anomalous change of width of the mirror 2.43 MeV state of Be^9 and 2.34 MeV state of B^9 can only be understood in terms of these states having the almost pure parentage form of nucleon + Be^8 (excited to the 2^+ level at 3 MeV)[11]). A similar remark holds for the 3.1–2.7 MeV Be^9–B^9 pair of mirror levels. Thus

TABLE 5

The low-lying levels of the mass-9 nuclei

	E_{ex}	J^π	T	θ_{1+Be^8}	$\theta_{1+Be^{8*}}$	Reference
Be^9	0	$\frac{3}{2}^-$	$\frac{1}{2}$	(?)	(?)	
	2.43	$(\frac{1}{2}^-, \frac{5}{2}^-)$	$\frac{1}{2}$	$\leqslant 10^{-3}$	$\leqslant 0.75$	a, b
	3.10	$(\frac{1}{2}^+, \frac{3}{2}^+)$	$\frac{1}{2}$	(small)	≈ 1	b
B^9	0	$\frac{3}{2}^-$	$\frac{1}{2}$	(?)	(?)	
	2.34	$(\frac{1}{2}^-, \frac{5}{2}^-)$	$\frac{1}{2}$	(small)	0.7	a
	2.79	$(\frac{1}{2}^+, \frac{3}{2}^+)$	$\frac{1}{2}$	(?)	> 0.4	a

See table 1 for the meaning of symbols. The reported state at about 1.7 MeV in Be^9 has not been included since it is apparently not a state in the usual sense but rather is a manifestation of sequential two-body decay (see section 5).

[a] R. R. Spencer, Ph. D. Thesis, The Rice Institute (1958); Spencer, Phillips and Young, Nuclear Physics (to be published)

[b] J. B. Marion, private communication

the low excited states of the mass 9 system show strong evidence for clustering; and the clusters are of a rather unexpected sort: Be^8 (ground, 0^+) + nucleon and $^*Be^8$ (2.9 MeV, 2^+) + nucleon.

2.6. NUCLEI WITH $A = 13$

The mirror pair N^{13}–C^{13} show at least seven and possibly eight states of the cluster form. The energy level diagram of fig. 6 and table 6 presents this data. Reich *et al.*[12]) have pointed out that the two important nuclear parents, up to an energy of about 8 MeV of excitation, appear to be the configurations $C^{12}(0^+)$ + nucleon and $C^{12*}(4.43\ \text{MeV}, 2^+)$ + nucleon. Apparently the ordering of states is the same, and the strength of the interactions is almost the same in each configuration.

2.7. CERTAIN HIGH ENERGY NUCLEAR REACTIONS

A number of interesting observations concerning the intensity of nuclear particle emission have been recently reported. For example, Cohen[13]) in studies of (p, α) reactions for 32 MeV protons observed anomalously large intensities of low energy α-particles leaving the nucleus in highly excited states. Although

TABLE 6

The low-lying states of the mass-13 nuclei

	E_{ex}	J^π	T	$\theta^2_{1+C^{13}}$	$\theta^2_{1+\bullet C^{13}}$	Reference
C^{13}	0	$\frac{1}{2}^-$	$\frac{1}{2}$	0.07		a
	2.09	$\frac{1}{2}^+$	$\frac{1}{2}$	0.25		a
	3.68	$\frac{3}{2}^-$	$\frac{1}{2}$	0.02		a
	3.85	$\frac{3}{2}^+$	$\frac{1}{2}$	0.10		a
	6.86	$\frac{3}{2}^+$	$\frac{1}{2}$	0.006		b
	7.64	$\frac{1}{2}^+$	$\frac{1}{2}$	0.038		b
	8.33	$\frac{1}{2}^+$	$\frac{1}{2}$	0.51		b
N^{13}	0	$\frac{1}{2}^-$	$\frac{1}{2}$	(large)		c, a
	2.36	$\frac{1}{2}^+$	$\frac{1}{2}$	0.54		d
	3.51	$\frac{3}{2}^-$	$\frac{1}{2}$	0.031		d
	3.56	$\frac{3}{2}^+$	$\frac{1}{2}$	0.21		d
	6.38	$\frac{3}{2}^+$	$\frac{1}{2}$	0.003	(large)	e
	6.91	$\frac{1}{2}^+$	$\frac{1}{2}$	0.012	0.2	e
	7.42	$(\frac{1}{2}^+)$	$\frac{1}{2}$	(?)	(large)	f
	8.08	$(\frac{3}{2}^+)$	$\frac{1}{2}$	(0.11)	(?)	g

See table 1 for the meaning of the symbols.

[a] F. Ajzenberg-Selove and T. Lauritsen, Nuclear Physics **11** (1959) 146
[b] Wills, Bair, Cohn and Willard, Phys. Rev. **109** (1958) 891
[c] A. M. Lane, Handbuch der Physik, Vol. 39 (Springer, Berlin, 1957), p. 241;
A. M. Lane, Phys. Rev. **92** (1953) 839
[d] H. L. Jackson and A. I. Galonsky, Phys. Rev. **89** (1953) 370
[e] Reich, Phillips and Russell, Phys. Rev. **104** (1956) 143
[f] Lidofsky, Bent, Weil and James, Bull. Am. Phys. Soc. **2** (1957) 29
[g] Schneider, Helv. Phys. Acta **29** (1956) 55;
C. P. Browne and J. R. Lamarsh, Phys. Rev. **104** (1956) 1099

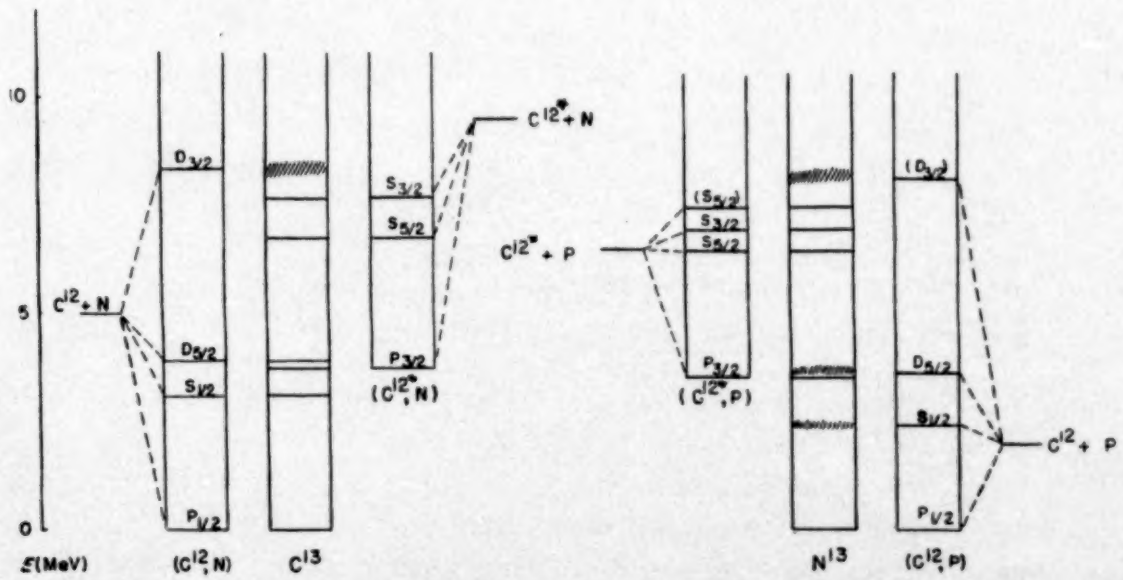

Fig. 6. Two-body cluster parentage of the mass-13 nuclei. See fig. 1 for the meaning of symbols.

attempts are being made to explain these results in terms of the excited nucleus being enlarged and the Coulomb barrier thereby lowered, these experiments may also be interpreted in terms of nuclear parentage. If the compound nucleus, at any energy, exists principally in two-body parentage states, where the two clusters have a low relative kinetic energy, then the experimental observation that low energy processes are the most likely must follow from the nature of the wave function.

Another striking example of evidence for clustering occurs in the experiments reported by Ball *et al.*[14]) in which $Ni^{58}(\alpha, \gamma)Zn^{62}$ and $Xe^{136}(\alpha, \gamma)Ba^{140}$ have been studied. It is easy to show that the only reasonable way to explain the very large observed cross sections is to assume that the very highly excited states of Zn^{62} and Ba^{140} are largely of α-particle parentage and that the decay by γ-radiation proceeds to other alpha parentage states. It is also a remarkable result of these experiments that, when corrected for Coulomb barrier penetration, the cross sections show the largest values for low energy α-particle capture.

Much more evidence could be cited[15, 16]) that shows cluster states in nuclei: $N^{14}(n, \alpha)B^{11}$, $O^{16}(He^3, \alpha)O^{15}$, etc.; however, a model will now be presented that correlates these experimental facts in a phenomenological way and allows predictions to be made simply about a number of nuclear properties.

3. A Cluster Model for Nuclear States

Consider a nucleus composed of n nucleons. At the lower energies of excitation it may be decomposed into various pairs of nuclear clusters and, at higher energies, into three of more clusters. These various two, three, or many body arrangements of the n-body system allow the expansion of the energy-characteristic wave function of the system into energy-characteristic, parentage wave functions:

$$\Psi(E) = \sum \psi(E)_{\text{two-body}} + \sum \psi(E)_{\text{three-body}} + \cdots \tag{1}$$

This expansion as it stands is useful for describing nuclear reactions in the region of space where the clusters are not strongly interacting. However, this expansion would apparently not be very useful for interaction distances less than the range of strong interactions between the clusters since a very large number of terms would apparently be needed. At low enough energies, only the two-body channels (both open and closed) will be necessary to describe adequately the system in that region of space exterior to the range of the nuclear forces acting between clusters; these two-body wave functions may be considered in practice a complete-orthonormal set of wave functions in this region of space. It is clear that for sufficiently small distances of separation of all of the nucleons that a very much larger number of wave functions must be

included to produce an effectively complete set. However, the experimental observations that there are stable and semistable nuclear states of high two-body purity *requires that there be a spatial region of strong interaction between two-body clusters where these two-body wave functions continue to be a complete* (or almost complete) *set of functions*. The experimental identification of rather pure bound states of two-cluster motion requires also that the bound two-body channels be included in this description. There is considerable evidence, such as listed in section 2, that two-body states have large amplitudes in nuclei; there is very little evidence for three or more body states. In the discussion that follows, for the sake of definiteness and simplicity, it will be assumed that only the two-body clusters need to be considered. This assumption is a fundamental aspect of the model.

Inquiry may be made, however, as to what is the general nature of the nuclear forces that allows stability to such two-body cluster states. Consider the interaction of two nuclear clusters, labeled a and b, of internal energy E_a and E_b to form a state, $\psi_\alpha(E)$, of parentage α and energy E, then

$$\psi_\alpha(E) = \chi_{\alpha,a}(E_{\alpha,a})\chi_{\alpha,b}(E - E_{\alpha,a} - E_{\alpha,r})\phi_\alpha(E_{\alpha,r}) , \tag{2}$$

where the quantities χ represent the internal coordinate wave functions of the clusters and $\phi_\alpha(E_{\alpha,r})$ represents the relative motion wave function of relative energy $E_{\alpha,r}$. Now if $\chi_{\alpha,a}$ and $\chi_{\alpha,b}$ describe clusters, each containing in its own centre of mass coordinates some particles whose wave functions represent identical states, the Pauli principle would be violated for certain relative motion wave functions, and such states will not occur. The states that do occur will have wave functions such that the clusters do not overlap strongly. Thus, in some sense the Pauli principle may be looked on as supplying a sort of short range repulsive force that will force the clusters apart, if they have identical nucleons in similar states, and aid in stabilizing them: this short range repulsive force would prohibit a large overlap of the two wave functions and thus prohibit the exchange of nuclear matter between the two clusters. In addition, the attractive features of nuclear forces, operative within each cluster, will serve to stabilize the structure of each cluster.

However, to have any temporary stability, this two-cluster structure must interact *via* a somewhat longer range attractive force. Even this type of force law between clusters is not enough to allow stability: there must be a restriction placed upon the relative energy of the two clusters; that is, the relative energy must be near resonance. If the relative energy of the clusters is too large (and positive), their wave functions will interpenetrate more and increase the probability of the exchange or nuclear matter, and the structure will decay to other cluster states; or the system may decay by emission. On the other hand, very large attractive forces between clusters would not be expected, and the

binding energy of the eigenstates of relative motion of the clusters would probably be only a few MeV.

The low energy states of the Be^8 system are a good example of these arguments: if two alpha particles collide with low energy, they may not interpenetrate as alpha particles because of the Pauli principle. Thus the allowed orbits of the two alpha particles must correspond to a fairly large average spatial separation. Yet the two alpha particles attract each other and form eigenstates, semistable against emission. The non-overlapping nature of the orbits of the two alpha particles reduces the chance of rearrangement. At high enough energies other cluster forms may become more stable, and the system may spend a large fraction of time in some other cluster form such as $p = Li^7$.

Thus, if it is postulated that two-body clusters perhaps composed of nucleons in similar states interact with a short-range repulsive, longer-range attractive potential, it seems reasonable that the two-body structure will have an enhanced stability, provided that the clusters have only a few MeV of relative energy. It is the proposal of the cluster model that these resonances for relative motion of two-body clusters provide a simple, physical interpretation for many of the observed sharp, or semi-sharp, energy states of nuclei.

These arguments, along with the experimental evidence for clustering cited above, lead to the proposal for a clustering model for nuclear states that is given below.

Consider the nucleus that at a set of energies E_n can be decomposed into two-body parents $A_n + B_n$ whose wave function is ψ_n. The particles A_n and B_n can be well-defined, stable nuclei or nucleons, or they may be the excited states of nuclei that are either bound against particle emission or free to emit particles. In the two-body approximation the wave function may be written

$$\Psi = \begin{pmatrix} \theta_1\psi_1 \\ \theta_2\psi_2 \\ \vdots \end{pmatrix}, \qquad \text{(A)}$$

where the $\psi_k(E)$ are two-body parentage functions as given in eq. (2), and the θ_k are the fractional parentage expansion coefficients.

The ψ_k of (A) are not orthogonal functions nor, of course, are they really complete. Nevertheless they are useful. In a practical sense, they may be considered orthogonal and complete for cluster separations outside the range of the inter-cluster forces. The inclusion of clusters that are unbound, when isolated, may be used to account for the cases when three-body decay may occur. In a sense (A) is similar to the assumption of the Wigner theory[17]) that free channel waves are a complete, orthogonal representation outside some radius R. However, there are three major differences in the assumption (A) and the well established channel-wave assumption. These differences are:

(a) the expansion of Ψ into the two-body functions ψ_k includes bound two-body channels as well as free two-body channels; (b) in addition a nuclear state may be composed of two clusters which, if isolated, would be unstable; (c) the spatial region of validity of (A) is assumed to extend *inside* the range of strong inter-cluster interactions. Of course, (A) will not be expected to apply at very short radii where a very much greater number of much more complicated wave functions would be needed. It has been suggested[18]) that these conditions can be met by assuming that the space be divided into three regions: (1) the "outer region" within which the clusters do not interact with each other or only interact *via* the well-known Coulomb law; (2) the "cluster region" within which a two-body cluster description of the system is still adequate, but where there are strong two-body cluster interactions; and (3) the "inner region" within which a much more complicated description of the system is necessary and where the wave functions are not known, but may only be discussed in terms of their logarithmic derivatives on the surface of this region. This "onion-skin" nucleus is different from the Wigner picture in that the "cluster region" has been inserted between the "inner" and "outer" regions.

In performing calculations with the cluster model, it does not seem to be necessary to include the "inner" region to obtain interesting results. Thus it will be assumed in most cases that (A) is a suitable wave function for all regions of space at sufficiently low energies. Now the general form of a *linear* Hamiltonian to represent these interactions may be written:

$$H = \begin{pmatrix} H_{1,1} & V_{2,1} & V_{3,1} \cdots \\ V_{1,2} & H_{2,2} & V_{3,2} \cdots \\ \vdots & & \end{pmatrix}, \tag{3}$$

where $H_{\alpha,\alpha} = h_{\alpha,a} + h_{\alpha,b} + H_{\alpha,r}$ and $h_{\alpha,a}\,\chi_{\alpha,a} = E_{\alpha,a}\,\chi_{\alpha,a}$, etc., and $H_{\alpha,r}\,\phi_\alpha = E_{\alpha,r}\,\phi_\alpha$. Thus the $V_{\alpha,\beta}$ represent the effects of the forces that cause the exchange of nuclear matter and change one cluster arrangement into another. It should be noted that each of the $V_{\alpha,\beta}$, $h_{\alpha,n}$, and $H_{\alpha,r}$ represents short range nuclear plus Coulomb interactions between clusters, and in general takes the form of an integral operator.

Thus the ψ_k obey a set of coupled Schrödinger equations such as

$$\ldots V_{n-1,n}\psi_{n-1} + H_{n,n}\psi_n + V_{n+1,n}\psi_{n+1} + \ldots = E_n\psi_n\,. \tag{B}$$

These equations are similar to the "resonating group" coupled equations of Wheeler[19]). It is noted that at any energy E, Ψ has eigenstates due to the channels that are bound at that energy, and in addition Ψ has eigenstates due to resonance in the channels having positive energy.

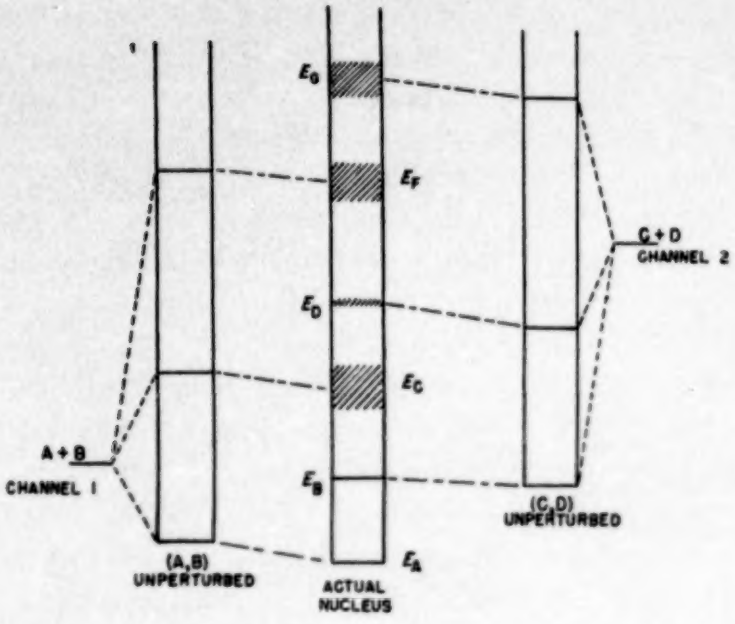

Fig. 7. Cluster states of a nucleus with only two important parents. See fig. 1 and text for the meaning of symbols.

The behaviour of such a system of coupled equations may be examined by considering the simple case of only two channels as shown in fig. 7. The system is represented by

$$\Psi(r,t) = \begin{pmatrix} \theta_1(t)\psi_1 \\ \theta_2(t)\psi_2 \end{pmatrix}, \tag{4}$$

where each ψ_n will be considered to be normalized so that $\int |\psi_n|^2 \, dV = 1$. The state Ψ obeys

$$\begin{pmatrix} (T_1 + V_{11}) & V_{12} \\ V_{21} & (T_2 + V_{22}) \end{pmatrix} \begin{pmatrix} \theta_1\psi_1 \\ \theta_2\psi_2 \end{pmatrix} = -\frac{\hbar}{i} \begin{pmatrix} \dot{\theta}_1\psi_1 \\ \dot{\theta}_2\psi_2 \end{pmatrix}. \tag{5}$$

In the limit of very small coupling, $V_{12} = V_{21}{}^* = 0$, each channel will have a set of unperturbed energy levels as shown in fig. 7.

The time dependence of eq. (5) is discussed in the following paper[20]) where it is shown that the amplitudes of the wave functions in the two channels oscillate and that fairly pure states of one cluster form will occur if either (a) the coupling between channels is small enough or (b) if the unperturbed energy eigenvalues of the pure cluster froms are sufficiently separated in energy.

For such a system of coupled equations, there are three interesting cases to consider.

Case I. *All Channels Bound.* If all channels are bound, the wave function representing a bound state of the system will oscillate among the various

parentage wave function. If the inter-cluster forces are as described above, the wave function will spend the largest fraction of its time in those free parentage states whose unperturbed eigenvalues are near to the actual energy of the nucleus. Thus it may be expected that those free parents that lie nearby in energy will have the largest fractional-parentage coefficients, θ. Since the elements $V_{n,m}$ in the Hamiltonian are not equal, it would not be expected that this statement will be exactly true, but will be true in an average over many states. Such bound states, at E_a and E_b, are schematically represented in fig. 7.

These large fractional parentage coefficients should be revealed by an enhancement of the γ-ray transition probability between states of similar parentage. In fact, the measurement of the γ-ray transition rates between a set of states of known parentage and a state of unknown parentage seems to be the most direct way of determining the fractional parentage of bound states.

Case II. *One Channel Unbound.* In general the remarks made for Case I apply here as well; however, the phenomenon of resonant scattering now becomes possible. Two types of resonant behaviour may be expected: there will be two-body type resonance in the free-parent channel and in addition other types of resonance showing the effects of bound states in the coupled channels. The former are expected to be the typical broad states that occur in two-body calculations, with widths γ^2 near the Wigner limit; the θ^2 for such states should be near unity at resonance. The resonance at E_c in fig. 7 is an example of such a state. Since this type of resonance behaviour is well understood, it will not be discussed here.

However, the coupling between channels will be evidenced in the free-parent channel by the occurrence of other types of resonances whose widths may be very small if the coupling is very small. The resonance at E_d in fig. 7 is an example of such a narrow state. The identification of the narrow resonances that may be due to bound, two-body parents is difficult, and the only obvious method of identification is by means of γ-ray transitions as discussed in Case I.

It has been shown[20]) that the effects of scattering in the free channel (designated 1) due to a bound state in one of the other channels (designated 2) will be the appearance of a resonance whose width may be very much less than the Wigner limit. The width of such resonance is shown to be

$$\Gamma_1 \approx \langle 1 \mid V_{12}V_{21} \mid 1 \rangle / E_d .$$

This width may be very much smaller than the Wigner limit provided either that V_{12} is sufficiently small or that the binding energy difference of the channels is large. This fact is an important consequence of the model since it provides a simple, physical mechanism for describing narrow resonances in terms of interactions that are primarily of a two-body type.

Case III. *More Than One Channel Unbound.* While most of the considerations

given above apply to this case as well, an interesting additional phenomenon may occur. Suppose a certain state has high purity for a certain cluster parentage, as is revealed in its large reduced-width for that parent. Suppose that some less energetic state is primarily of the same parentege, but is bound in its parent channel, although free in some other channel (such as discussed in Case II above). An enhanced transition by γ radiation from the upper to the lower state is expected and will very likely be *followed* by particle emission. This unusual process, enhanced by the parentage similarity of the states involved, may occur for highly excited states of nuclei and should be characteristic of the cluster nature of the states; its experimental identification should allow the widths or fractional parentage coefficients to be measured. An example of such a situation is shown in fig. 7 where an enhanced γ-ray transition from E_g to E_d will be *followed* by particle emission into channel 1. Similar arguments may be used to explain the large (α, γ) capture cross sections reported by Ball *et al.*[14]).

Nuclear Reactions in General. In each of the above discussions it has been found that near each free, two-body parent there is a group of cluster states which in the limit of zero coupling ($V_{n \neq k,k} = 0$) are purely of one parentage. With non-zero coupling each state should be a linear mixture of all possible parents, but the fractional parentage of any state would be expected to be in general highest for some, if not all, of the free parent configurations that are nearby in energy. This effect is shown schematically in fig. 8. This diagram exhibits most of the features of the proposed model and allows simple predictions of new phenomena.

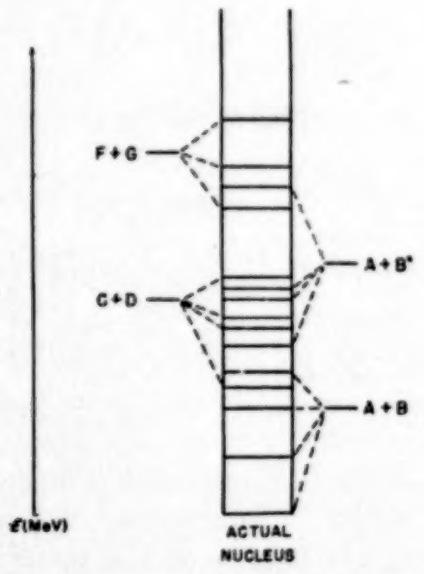

Fig. 8. General nuclear level diagram showing the energies of dissociation into all possible two-body clusters A + B, C + D, including clusters, (A + B*), where one (or both) is in an excited state. The principle parents are indicated schematically by a dashed line; however, each stable or semi-stable state of the nucleus is actually a linear combination of all possible parents.

4. The Relationship Between the Cluster Model and Other Models

4.1. THE SHELL MODEL

The cluster model must take over those features of the shell model related to the ordering and spacing of the low energy nuclear states. However, since the shell model treats all nuclear states as eigenstates in an infinitely deep potential well, the detailed ordering and spacing of the higher states should not be predicted accurately. In fact, the eigenfunctions of such a potential do not lend themselves easily or conveniently to the treatment of scattering or reaction problems.

The assumption of the independent particle model that the inter-nucleon forces are small cannot be maintained, and residual forces must be postulated which tend to favour the formation of clusters. This point is, perhaps, best shown by the following example.

It is instructive to consider whether the occurrence of deuteron clustering in the mass-5 nuclei may be described by a reasonable extension of the shell model. The mass-5 system is first viewed as five independent particles moving in a suitable realistic average potential; that is, the interaction must be *via* a potential of finite depth and resonable radius, adjusted so as to give the proper dissociation energies and binding energies for the eigenstates. The potential must be such that the lowest two eigenstates are $(s_{\frac{1}{2}})^4\,(p_{\frac{3}{2}})^1$ and $(s_{\frac{1}{2}})^4\,(p_{\frac{1}{2}})^1$ at positive energies of a few MeV. At higher energies one may expect a state $(s_{\frac{1}{2}})^3\,(p_{\frac{3}{2}})^2$ where an additional nucleon has been promoted to the $p_{\frac{3}{2}}$ shell. The additional energy for this excitation should be the energy to promote an $s_{\frac{1}{2}}$ nucleon in the α-particle to a $p_{\frac{3}{2}}$ level. Since there are no known bound states in the α-particle below the T + p or He^3 + n threshold[21]) and since there is the well-known p-wave nucleon capture process

$$p + T \rightarrow \alpha + \gamma\,,$$

which resonates at about 5 MeV bombarding energy, or at about 20 MeV of excitation in He^4, it is reasonable to suppose that the energy required to excite an $s_{\frac{1}{2}}$ nucleon to the $p_{\frac{3}{2}}$ level in He^4 is about 20 MeV.

Thus at about 20 MeV above the α + nucleon threshold for the mass-5 nuclei, there should be an eigenstate of the form $(s_{\frac{1}{2}})^3\,(p_{\frac{3}{2}})^2$. There are no obvious restrictions to the types of total angular momentum states that can be formed: states of total angular momentum $\frac{1}{2}^+$ to $\frac{7}{2}^+$ are formally possible. However, it is to be noted that the two excited nucleons may be in a relative S state so that a deuteron (triplet) or excited deuteron (singlet) structure may occur. In fact the residual interactions, not completely accounted for by the average forces assumed for the independent-particle model, will provide the

necessary forces: that is, the two-body forces between the two excited nucleons will produce a clustering of these two nucleons into a sort of deuteron structure. Even without the two-nucleon forces, the excited nucleon wave functions are similar and have a radial distribution that attains a maximum away from the centre-of-mass. The clustered deuteron-type wave function will have a similar shape, but will have a more peaked distribution owing to the neutron-proton attactive force in a relative S state. The deuteron (triplet) structure may then only move in even orbital states so that it may have S states of $J = \frac{1}{2}$ or $\frac{3}{2}$ and D states with $J = \frac{1}{2}$, $\frac{3}{2}$, $\frac{5}{2}$ and $\frac{7}{2}$. The excited (singlet) deuteron structure may have an S state of $J = \frac{1}{2}^+$ and D states with $J = \frac{3}{2}^+, \frac{5}{2}^+$.

It is clear that the effective potential of interaction of the deuteron with the mass-3 particle has an attractive region, but since the S wave deuteron wave function is excluded from regions near the center of mass, the effective potential must have a repulsive core. Furthermore, it is clear that the deuteron type states occur nearby in energy to the energy for dissociation into the configuration mass-3 + deuteron. These are the three necessary conditions, given earlier, for the formation of semi-stable two-cluster states.

These arguments, based on reasonable extensions of the independent-particle model, predict that $(s_{\frac{1}{2}})^3 (p_{\frac{1}{2}})^2$ states will have large amplitudes for deuteron type states and excited deuteron type states and should occur near the mass-3 + deuteron threshold. These types of states should have a large value for $\theta_{d+3}{}^2$ for the deuteron configuration, as is found experimentally and discussed in section 2. On the other hand, these states would be expected to show a small amplitude for the α + nucleon configuration, $(s_{\frac{1}{2}})^4 (p_{\frac{1}{2}})^1$, since the two $p_{\frac{1}{2}}$ nucleons have a wave function very different from an $s_{\frac{1}{2}}$ nucleon that is necessary to form an α-particle; thus $\theta_{1+\alpha}{}^2$ should be small. These conclusions describe the experimental facts quite well.

Thus reasonable extensions of the independent particle shell model should be able to describe all of the unusual physical features of the mass-5 system. It is important to notice, however, what these extensions consists of: (1) employing physically reasonable potentials to represent the average forces; (2) the residual interactions (in addition to the Pauli principle) must be included to provide the physical basis for the formation of semi-stable clusters.

The methods outlined above should allow simple calculations, and it seems that the arguments are capable of being extended to other nuclei so that the independent particle model may be generalized (with a loss of "independence" of the nucleons) to describe cluster states in nuclei.

4.2. THE COLLECTIVE MODEL

It seems promising to employ the cluster model to derive the rotational and vibrational levels of nuclei described so well by the collective model[22]). If the heavy nuclei are considered as having the rotational states of two nuclear

clusters of more or less equal size, then the quadrupole moments of 2^+ excited states of even nuclei would be expected to be large (of the order of $10e \times 10^{-24}$ cm^2) and should have a large overlap with the 0^+ ground state. These large quadrupole moments would give the large quadrupole excitation probabilities by Coulomb excitation observed for heavy nuclei. Furthermore, the even rotational states of such a two-cluster system would have a basic 0^+ to 2^+ energy separation of about 100 keV, as is observed.

4.3. THE OPTICAL MODEL

The simple cluster model for a system of coupled parentage-clusters, discussed above, provides a convenient way to discuss the optical-model potential in terms of the cluster model interactions: if the simultaneous Schrödinger equations of the form of (B) are resolved to the form $H_n\psi_n = E\psi_n$, then the form of H_n gives explicitly the appropriate optical potential. It is clear that H_n will in general have an imaginary part which will be energy dependent, even if all of the $V_{n,n}$ and $V_{n,m}$ are energy independent. It is interesting to note that the imaginary part of H_n employed in calculations to describe *low energy* reactions has a very small value[23]). This fact is consistent with the cluster model outlined above since the θ^2 in the parent channel at low energies will be expected to be large and all the other θ^2 small to that only a small imaginary interaction is needed.

Thus it seems that all the important features of the optical model have an interpretation in the cluster model, and indeed some assumptions of the optical model are derivable from the cluster model. In addition, the cluster model allows the inclusion of a detailed treatment of nuclear structure as well as the gross features described by the optical model.

4.4. DIRECT INTERACTION THEORY

The ideas of the cluster model presented here seem to coincide well with the direct interaction picture of nuclear processes. In the cluster model the interaction of a projectile with the target nucleus can be treated by the techniques outlined in section 3. However, if the reaction proceeds with high kinetic energy of the incoming and outgoing waves, then semi-stable resonating states will be unlikely since the relative kinetic energy is too large compared to the diagonal elements to allow resonance of two-body motion. The processes will have reaction cross sections and angular distributions whose behaviour will be determined by the off diagonal coupling terms $V_{n,m}$, and these effects will be very similar to the direct interaction picture of the same process. At lower relative kinetic energies of cluster motion, the resonant effects described above will be evident, although for energies of excitation between resonances the direct interaction effects may dominate.

5. Some Predictions of the Cluster Model

It is interesting to note that although the model predicts a direct type process for high energy reactions, it also predicts an anomalously large yield for *low energy* particle emission. Consider a nucleus X bombarded by a. The states formed will be of all possible parents such as (a + X), (a + X*), (b + Y), (b + Y*), etc., where X* is an excited state of X. Now as discussed in section 3, and fig. 8, the cluster arrangements having small relative energy are most likely to appear in any eigenstate. Thus cluster configurations of small relative energy, such as (a + X*) or (b + Y*), are more probable than the states (a + X) and (b + Y) where the relative energies are large. Now some of the states (a + X*) and (b + Y*), where the relative motion energy is small, may have large overlap integrals. It would then be expected that the reaction would proceed more strongly to (b + Y*) than to (b + Y). Thus there is predicted a distribution of particles a or b that shows an anomalously large yield for some low energy particle groups. Furthermore, the yields of those low energy particles should show discernable resonance even for rather high bombarding energies.

In addition, the model predicts, when the initial and final parentages are the same, that large reaction cross sections should result. For example $C^{12} + He^3$ may be considered $C^{12} + (p + d)$, and $C^{12} + d$ is known[24]) to have a large amplitude in certain states in N^{14}. Thus it is expected that the reaction $C^{12} + He^3 \rightarrow p + N^{14}$ will proceed very strongly for excited stated in N^{14} having the cluster arrangement $C^{12} + d$. Also it is expected that two-body resonances will occur in the low energy particle yields, while the high energy particles coming from the same system will behave as though a direct interaction process dominates.

The model also predicts the occurrence of two-body type resonances for heavy particle bombardment. Thus such resonances in the $Li^6 + Li^6$, or $C^{12} + C^{12}$ systems may be sought. Such resonance have been recently observed[25]).

Finally it seems reasonable to attempt to explain three-body decay as a succession of two-body emissions as has been discussed by Lane and Thomas[26]). It has been shown that such a process as $Be^9 + p \rightarrow d + \alpha + \alpha$ may be reasonably described by step-wise, two-body decay *via* the unstable nucleus Be^8 if a "generalized density of states" function is introduced[27]). Although it is not expected that such a treatment will describe all features of the many-body decay, it may be hoped that such a simple two-body description will account for many aspects of such transitions because of the apparent purity and stability of two-cluster states in nuclei. The general form of the energy spectrum of particles b for the three-body reaction

$$a + A \rightarrow D^* \rightarrow b + c + d \qquad (6)$$

may be easily determined when the important mechanism, according to cluster ideas, is the two-body sequential process

$$a + A \rightarrow D^* \rightarrow b + B^*, \quad B^* \rightarrow c + d. \tag{7}$$

Mechanism (7) suppose that particle b escapes *before* B* decays. Since the interactions of b and B* are of a very short range, R, it may be considered that B* will be localized at the time of emission of particle b. Thus B* represents the localized and energy-dispersed two body system c + d. As particle b is emitted, the localized system B* is decaying with a characteristic life-time $T(E_b)$. If the transition probability for emission of b from D* is $W(E_b)$, then the time integrated emission probability of particles b with energy E_b, is

$$P \approx W(E_b)T(E_b) .$$

The lifetime $T(E_b)$ may be considered a "generalized density of states" function in the sense that the more stable states of B* with larger values $T(E_b)$ will be strongly populated by the emission of particles b. It should be noted, however, that $T(E_b)$ *does not* necessarily correspond[28]) to the cross-section for formation of B* by c + d. Thus, even if no forces exist between c and b, there is still a non constant $T(E_b)$ that in fact is classically given by

$$T(E_b) \approx R/V_{cd} ,$$

where V_{cd} is the relative velocity of c and d. It may be shown, more generally, that

$$T(E_b) \approx \hbar \frac{d}{dE} (\delta + \phi) ,$$

where δ is the phase shift of interest for c + d scattering and $\phi = \tan^{-1}(F/G)_R$, where F and G are the regular and irregular solutions to the external ($r > R$) wave equation for the c + d scattering problem.

6. Conclusion

Perhaps the most radical assumption of the model is the discarding of three or more cluster interactions. This point needs both theoretical and experimental investigation. The ordering and selection rules for angular momentum characteristic states need to be worked out starting from the basic rules of the shell model: Wildermuth and Kanellopoulos have initiated this work[29]).

In addition, the optical and collective models need to be compared to the cluster model. Careful calculations need to be made, using the cluster model, to compare to experimental data. For example, at the present time calculations are being made for the mass-13 system, C^{13} and N^{13}, where the first seven states of the two nuclei seem to be well described[12]) as a nucleon + C^{12} or $*C^{12}(2^+)$.

Most important, however, more experimental evidence is needed to investigate

all aspects of the cluster model and to check the predictions of the model: (1) in particular the bound states of nuclei need to be re-examined by γ-ray studies to ascertain if their fractional parentage shows enhancement of nearby two-body parents (section 3, Case I); (2) of particular interest is the prediction of enhanced capture γ-ray resonances associated with scattering resonances due to bound states in other channels (section 3, Case II). Also (3) the prediction of enhanced capture γ-ray yields, *followed* by particle emission, should be more carefully investigated for high energy processes (section 3, Case III). In addition, the yields of particles predicted by the cluster model to be enhanced for certain low-energy transitions need to be further investigated for high energy interaction (section 5). These high energy nuclear reactions should exhibit simultaneously (4) resonances for low energy emission, (5) large enhancement of low energy particle emission, (6) and direct interaction type effects for high energy particle emission, and non-resonant low energy emission. (7) Two-body resonances for heavy particle interactions at low relative energies are predicted and should be investigated, and finally (8) the prediction of the shapes of spectra in many-body decay processes by employing the idea of successive two-body decays should be carried out.

The authors wish to thank Professor T. W. Bonner and Drs. R. Barloutaud, L. C. Biedenharn and W. Tobocman for helpful criticism in the formation of these ideas. The work of Drs. R. Spencer, T. Young, John Russell, P. D. Miller and C. Reich contributed many examples of the cluster structure in light nuclei. During the year 1957–1958, one of us (GCP) was aided by a Guggenheim Fellowship which allowed the development of some of these ideas; one of us (TAT) wishes to acknowledge the help of a National Science Foundation Fellowship during the course of this work.

References

1) G. C. Phillips, Bull. Am. Phys. Soc. **2** (1959) 99
2) E. P. Wigner and L. Eisenbud, Phys. Rev. **72** (1947) 29;
T. Teichmann and E. P. Wigner, Phys. Rev. **87** (1952) 123
3) A. M. Lane and D. H. Wilkinson, Phys. Rev. **97** (1955) 1199;
A. M. Lane, Phys. Rev. **92** (1953) 839
4) P. D. Miller and G. C. Phillips, Phys. Rev. **112** (1958) 2043;
Karl W. Brockman, Phys. Rev. **108** (1957) 1000
5) Conner, Bonner and Lillie, Phys. Rev. **88** (1952) 473;
Bonner, Conner and Smith, Phys. Rev. **88** (1952) 468
6) A. Galonsky and M. T. McEllistrem, Phys. Rev. **98** (1955) 590
7) P. D. Miller and G. C. Phillips, Phys. Rev. **112** (1958) 2048
8) Marion, Weber and Mozer, Phys. Rev. **104** (1956) 1402
9) H. D. Holmgren and R. L. Johnson, Phys. Rev. **113** (1959) 1556
10) Russell, Phillips and Reich, Phys. Rev. **104** (1956) 135;
N. P. Heydenburg and G. M. Temmer, Phys. Rev. **104** (1956) 123;
Nilson, Kerman, Briggs and Jentschke, Phys. Rev. **104** (1956) 1673;

Nilson, Jentschke, Briggs, Kerman and Snyder, Phys. Rev. **109** (1958) 850;
Jones, Phillips and Miller, Phys. Rev. **117** (1960) 525
11) R. R. Spencer and G. C. Phillips, Bull. Am. Phys. Soc. **2** (1959) 95;
R. R. Spencer, Ph. D. Thesis, The Rice Institute;
Spencer, Phillips and Young, Nuclear Physics (to be published)
12) Reich, Russell and Phillips, Phys. Rev. **104** (1956) 143
13) C. B. Fulmer and B. R. Cohen, Phys. Rev. **112** (1958) 1672
14) Ball, Fairhall and Halpern, Phys. Rev. **114** (1959) 305
15) Gabbard, Bichsel and Bonner, Nuclear Physics **14** (1959) 277
16) Bromley, Kuehner and Almqvist, Chalk River Report PD-309 (May, 1959)
17) E. P. Wigner, Am. Jour. Phys. **99** (1949)
18) We are indebted to Dr. L. C. Biedenharn for this interpretation
19) J. A. Wheeler, Phys. Rev. **52** (1937); **52** (1937) 1107
20) T. A. Tombrello and G. C. Phillips, to be published
21) J. E. Perry and S. J. Bame, Jr., Phys. Rev. **99** (1955) 1368
22) A. Bohr and B. R. Mottelson, Mat. Fys. Medd. Dan. Vid. Selsk. **27**, no. 16 (1953)
23) Feshback, Porter and Weisskopf, Phys. Rev. **96** (1954) 448
24) Kashy, Perry and Risser, Phys. Rev. **117** (1960) 1289;
Warburton, Rose and Hatch, Phys. Rev. **114** (1959) 214;
Warburton, Pinkston, Rose and Hatch, Bull. Am. Phys. Soc. **4** (1959) 219
25) Bromley, Kuehner and Almqvist, Phys. Rev. Lett., **7** (1960) 365
26) A. M. Lane and R. G. Thomas, Rev. Mod. Phys. **30** (1958) 257
27) G. C. Phillips and L. C. Biederharn, Bull. Am. Phys. Soc. **1** (1960) 44;
Phillips, Griffy and Biedenharn, Nuclear Physics (to be published)
28) K. M. Watson, Phys. Rev. **88** (1952) 1163;
E. W. Hamburger and J. R. Cameron, Phys. Rev. **117** (1960) 781
29) K. Wildermuth and T. Kanellopoulos, Nuclear Physics **7** (1958) 150

2.D *Nuclear Physics* **19** (1960) 579—588; © *North-Holland Publishing Co., Amsterdam*
Not to be reproduced by photoprint or microfilm without written permission from the publisher

(α, p) REACTIONS IN MEDIUM WEIGHT ELEMENTS

N. O. LASSEN and V. A. SIDOROV†

Institute for Theoretical Physics, University of Copenhagen

Received 16 May 1960

Abstract: Thin targets of V^{51}, Co^{59}, Ni^{58}, Ni^{60}, Cu^{63} and Cu^{65} were bombarded with α-particles of lab. energies of 19.3, 17.8, 16.3 and 11.9 MeV. The spectra of emitted protons at 45°, 90° and 135° were measured by means of an ionization chamber. Two groups of protons were seen. One group contains almost exclusively protons boiled off from the compound nucleus and only a very small number of protons created in direct interactions. The other group with energies below the Coulomb barrier contains protons emitted from daughters of the compound nucleus, i.e., secondary protons from (α, np), (α, 2p), and (α, αp) reactions. Both groups show symmetry around 90°. The first group is only slightly anisotropic, while the second group exhibits a considerably higher anisotropy, indicating higher angular momenta for the secondary emitted protons.

Using the formula from the statistical theory, the variation of the level density ρ with the excitation energy E^* was deduced from the spectral shape of the first group of protons. For the range of excitation energies 6–10 MeV, the spectra are consistent with a constant temperature of the order of one MeV. However, the values obtained for the temperature increase with increasing energy of the bombarding α-particles.

1. Introduction

One of the main results of the statistical theory of nuclear reactions[1]) is the shape of the spectrum of the particles emitted from the compound nucleus

$$N(E)\mathrm{d}E = \text{const.}\, E\sigma_c(E)\, \rho(E^*)\mathrm{d}E\,,$$

where $E^* = E^*_{\max} - E$ is the excitation energy of the residual nucleus, $\rho(E^*)$ is the level density of this nucleus, and $\sigma_c(E)$ is the cross section for formation of the compound nucleus in the inverse reaction.

The level density function is often written in the form

$$\rho(E^*) = C \exp{(aE^*)^\alpha}\,.$$

According to the model of the completely degenerate Fermi gas system[1]) most authors assume $\alpha = \frac{1}{2}$ and regard C as being approximately independent of the energy. There is, however, some evidence[2–4]) — partly from experimental work and partly from recent theoretical considerations on the effect of pairing correlations — that in a certain intermediate energy range a better approximation may be to put $\alpha = 1$, which corresponds to a constant temperature

$$\rho(E^*) = \text{const.} \exp\left(\frac{E^*}{T}\right).$$

† Present address: Institute of Atomic Energy, Moscow, U.S.S.R.

When comparing the statistical theory with experiments the best agreement is usually obtained when either the incoming or the outgoing particle is an α-particle[5]). This is to be expected, since a direct process in which an α-particle is exchanged with a nucleon would seem to be rather complicated and therefore unlikely to happen. From this point of view, (α, p) reactions are well suited for a determination of the parameters of the statistical theory. Accordingly, we have undertaken a thorough investigation of the energy spectra of protons created by α-bombardment of some medium weight nuclei, namely V^{51}, Co^{59}, Ni^{58}, Ni^{60}, Cu^{63} and Cu^{65}.

2. Experimental Arrangement

The external beam of about 20 MeV α-particles from the Copenhagen cyclotron was used. The beam handling system and the scattering chamber are described in a previous paper[2]).

As targets were used thin metallic foils of Vanadium and Cobolt and of separated isotopes of Nickel and Copper. The vanadium foil was prepared by electropolishing an 0.001 cm foil until the thickness was 1.85 mg/cm^2. The cobolt foil (1.2 mg/cm^2) was made by electroplating cobolt onto a molybdenum sheet from which it was afterwards peeled[6]). Foils of Ni^{58} (0.27 mg/cm^2, isotopic purity > 99 %) and Ni^{60} (0.24 mg/cm^2, > 99%) on a backing foil of gold (0.16 mg/cm^2) were made by electrolysis†. Selfsupporting foils of Cu^{63} (1.3 mg/cm^2, 99.7%) and Cu^{65} (1.75 mg/cm^2, 99.4%) were obtained from the Electromagnetic Separation Group, Isotope Division, Harwell, England.

The energies of the protons were measured by means of an ionization chamber, ThC + ThC′ α-particles being used for calibration. In order to distinguish between protons and scattered α-particles, a proportional counter was placed in front of the ionization chamber (fig. 1). This telescope could be connected to one of three ports in the scattering chamber, thus enabling us to measure the spectra of protons emitted at angles of 45°, 90° and 135° with the direction of the incoming α-particles.

The ionization chamber was of the fast, electron collecting type with a "Frisch"-grid; in construction it was rather similar to the one previously described[2]). It was filled with argon to about 10 atm, so that it would just stop 14 MeVp rotons. At this pressure, a rather long delay of the pulses was observed, but by adding a small amount of methane the delay was reduced to about 2 μs. It was found best to have no more than a fraction of 1 % of methane in the argon in order not to destroy the resolution which, for α-particles from ThC′ was found to be better than 3 %. The gas mixture was continuously purified by means of hot calcium. The window was equivalent to 1.4 mg/cm^2

† Our thanks are due Civilingeniør Mogens Jørgensen for preparing the vanadium and cobolt targets and Civilingeniør Bror Skytte Jensen for preparing the nickel targets.

aluminium in thickness. It was a mylar foil covered with a semi-transparent layer of aluminium, and it was supported by a stainless steel plate with a number of 1 mm diameter holes.

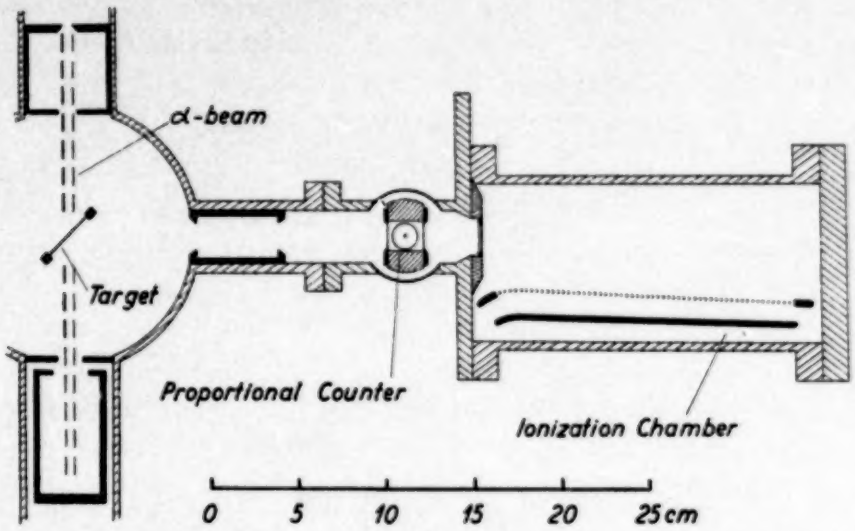

Fig. 1. Experimental arrangement.

The proportional counter had two side-windows of aluminium covered mylar foils of the same thickness as the ionization chamber window. It was filled with a mixture of argon and methane to a pressure of 20 cm Hg.

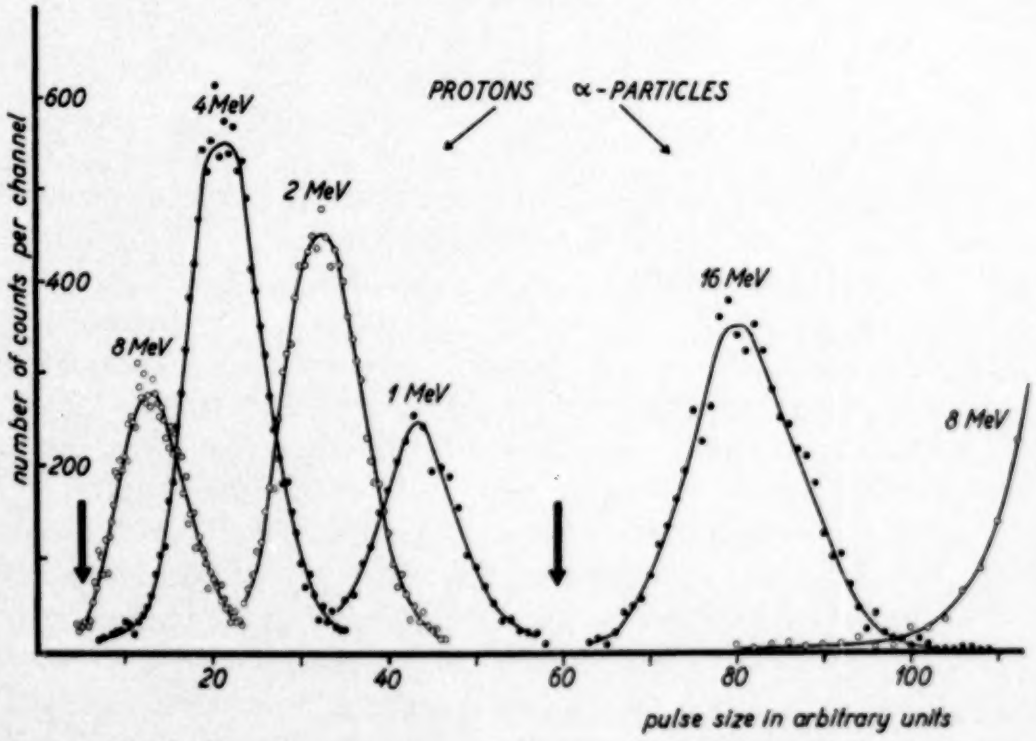

Fig. 2. Distributions of pulse sizes in the proportional counter for different values, written in the figure, of the corresponding energy loss inside the ionization chamber. The arrows indicate the range of pulses used for gating the 100-channel analyzer.

The pulses from the ionization chamber were analyzed by means of a 100-channel pulse height analyzer gated by the proportional counter. A single-channel analyzer was used to select proportional counter pulses corresponding to protons. The behaviour of the proportional counter was investigated in a separate run in which an inverse coincidence scheme was used. The counter pulses were fed to the 100-channel analyzer which was now gated by selected ionization chamber pulses. For each magnitude of the latter, the counter pulses showed two widely separated peaks corresponding to protons and α-particles; no deuterons were seen. Some such peaks are shown in fig. 2, in which is also indicated the range selected by the single-channel analyzer in the actual experiments. With this range good proton spectra were obtained for the energy interval 2–10 MeV, the lower limit corresponding to a residual energy of about 1 MeV inside the ionization chamber.

Experiments were done with the full α-energy as well as with beams degraded in energy by means of aluminium foils of various thicknesses. The average α-energies inside the targets were found to be 19.3, 17.8, 16.3 and 11.9 MeV for the various beams, respectively. The α-energies were determined from the ionization of the elastically scattered α-particles. The experimental set-up is thought to be closely linear in the energy range of importance for the proton spectra. However, after completing the measurements, it was realized that for higher energies there was, probably in the electronic system, a slight deviation from linearity. Thus, the value 19.3 MeV may be too low by about 2 %.

3. Results and Discussion

In fig. 3 are shown spectra of protons emitted at 90° from a target of Cu^{63} bombarded with α-particles. It may be seen that, at the high energy end, the intensity falls off smoothly, and even for still higher energies no indication of any proton groups corresponding to low lying levels in Zn^{66} were found, perhaps with the exception of some irregularities in the curve for $E_\alpha = 11.9$ MeV. Two proton groups are clearly seen. The one with the higher energy corresponds to the ordinary evaporation process in the reaction $Cu^{63}(\alpha, p)Zn^{66}$, and its shape is of the type expected from the statistical theory. The second group is peaked at about 2–3 MeV, which is much below the Coulomb barrier, the barrier penetrability for protons of this energy being about 0.01. Its intensity varies strongly with the energy of the incoming α-particles. The six nuclei investigated show this behaviour, though the curves for Cu^{63} are the most pronounced.

The origin of these sub-barrier protons may be readily understood from the following considerations. If, in the (α, p) reaction, the residual nucleus Zn^{66} has an excitation energy between 8.9 and 11.0 MeV, it may emit a second proton, but emission of a neutron is energetically impossible. Therefore, if the first proton is emitted in a certain energy range indicated in the figure, the

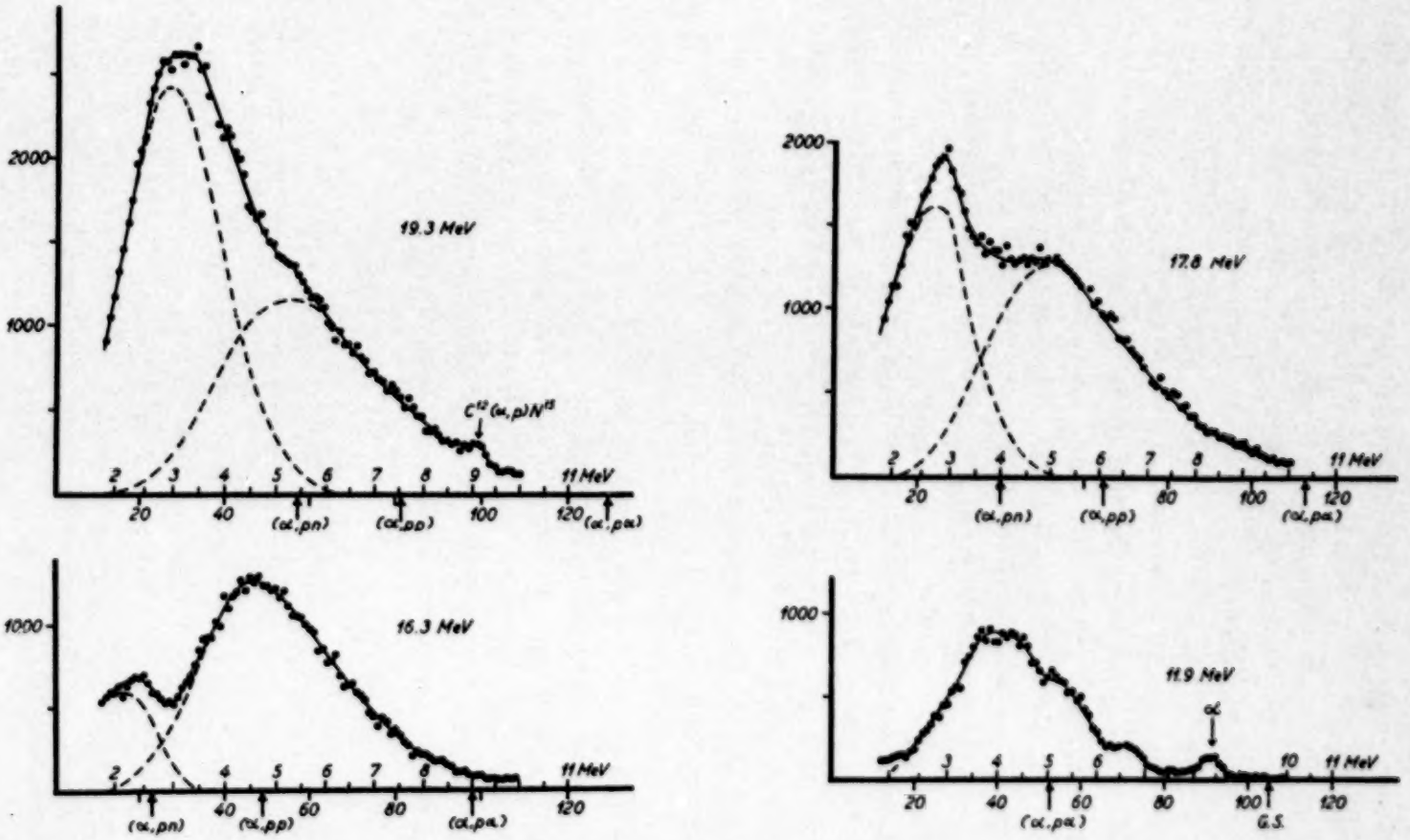

Fig. 3. Spectra of protons emitted at 90° from Cu^{63} bombarded with α-particles of lab. energies 19.3, 17.8, 16.3 and 11.9 MeV. The abscissa is the channel number; the corrected proton lab. energy is also indicated. The ordinate is the number of pulses per channel. The high-energy group consists of the protons emitted from the compound nucleus Ga^{67}. The low-energy group is formed by the protons emitted from a daughter of the compound nucleus. The arrows on the axis of abscissae marked (α, pn) indicate the upper proton energy for which successive neutron emission is possible. The arrows marked (α, pp) and (α, pα) have similar meanings. Thus, when the first proton has an energy in the range between the arrows (α, pn) and (α, pp), emission of a second proton does not have to compete with neutron emission. The arrow marked G.S. on the axis of abscissae for the 11.9 MeV curve indicates the position for a proton group corresponding to a transition from the compound nucleus Ga^{67} to the ground state of Zn^{66}. No such group is seen. The peak in this curve labelled "α" is due to chance coincidences between elastically scattered α-particles and protons. With the present gating time of 10 μs the number of α-particles counted is less than 2% of the actual number.

emission of a second proton will compete only with γ-ray de-excitation, which usually is a much slower process than emission of a nucleon. Just because in this case the secondary protons do not have to compete with neutrons, the Coulomb barrier is less effective in preventing low energy protons from escaping. However, the Coulomb barrier must strongly favour transitions to the ground state as compared to excited levels of the nucleus Cu^{65} formed by the secondary process.

Actually, not all the low energy protons observed are produced in an (α, 2p) reaction, but most of them are probably emitted from the Ga^{66} nucleus resulting from the (α, n) reaction, Again, one finds that, for a considerable range of excitation energies of the Ga^{66} nucleus, neutron emission is energetically forbidden, whereas protons may be emitted, although they will have energies which are only small compared to the barrier height. Similar conditions are exhibited after inelastic α-scattering.

In the above considerations we have neglected the possibility that α-particles may be emitted as secondary particles in competition with protons. Though this process is energetically possible it is usually of less importance as a result of the higher Coulomb barrier for α-particles.

Low-energy protons have earlier been observed after neutron bombardment by Allan[7]) and after proton bombardment by Cohen and Rubin[8]); these authors have offered a similar interpretation of them.

Table 1 gives the differences between the Q-values of reactions in which a proton or a neutron, respectively, is emitted after emission of a first particle, which may be either a proton, a neutron or an α-particle. This difference corresponds to the range of excitation energies of the intermediate nucleus for which proton, but not neutron, emission is energetically possible. A negative sign means that no such range exists. It is found that almost all nuclei must

TABLE 1

Q-value differences in MeV according to Ashby and Catron[9])

	V^{51}	Co^{59}	Ni^{58}	Ni^{60}	Cu^{63}	Cu^{65}
$Q(\alpha, pp) - Q(\alpha, pn)$	— 3.2[a])	— 0.5	7.1	4.7	2.1	0.2
$Q(\alpha, np) - Q(\alpha, nn)$	1.4	3.0	5.7[a])	2.5	3.9	1.8
$Q(\alpha, \alpha p) - Q(\alpha, \alpha n)$	3.0	3.1	4.0	1.9	4.7	2.5

[a]) Value obtained from Cameron[10]).

behave in a manner similar to the nuclei we have chosen, and that only in rare cases, viz. for especially neutron-rich nuclei, we should not expect to observe this group of sub-barrier protons.

In fig. 4 are shown, as an example, the spectra in the C.M. system of protons

emitted at three different angles from a target of Cu^{63} bombarded with 17.8 MeV α-particles. The points introduced in this figure were obtained from smooth curves drawn through the experimental points as shown in fig. 3.

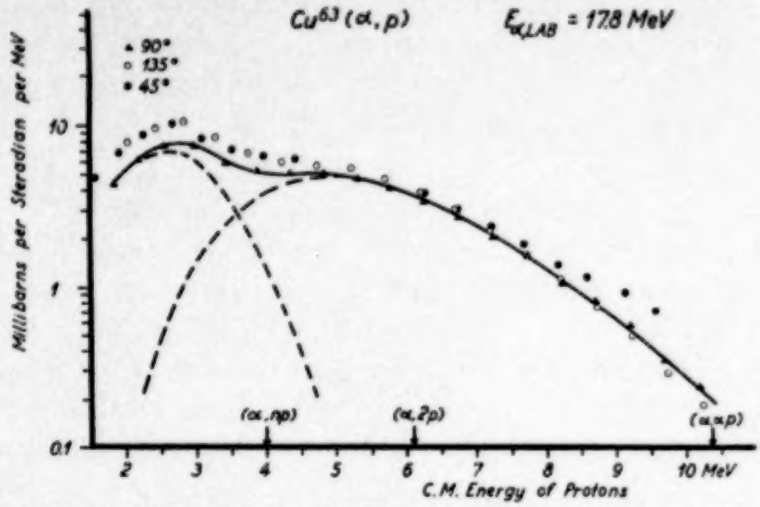

Fig. 4. C.M. spectra of protons emitted at 45°, 90° and 135° from Cu^{63} bombarded with 17.8 MeV α-particles. The arrows show the upper energy of protons from the indicated reactions. No 45° points are given in the neighbourhood of 5 MeV, because here a very high peak, corresponding to recoil protons from hydrogen impurities in the target, conceals the actual reaction protons.

Corrections for absorption in the material in front of the ionization chamber were applied. In all investigated cases, symmetry around 90° was observed for both proton groups. Only at the high energy end of the spectra, there was found an asymmetry giving evidence of the existence of some direct interactions. This asymmetry corresponds to a difference between the total probabilities for proton emission at 45° and 135° of the order of 1 %.

In accordance with the paper by Ericson and Strutinsky[11]), the average anisotropy $(\sigma_{135}/\sigma_{90°}) - 1$ for protons emitted as primaries in the (α, p) reaction can be estimated† to be a few per cent for $E_\alpha = 20$ MeV. Moreover, these authors predict an increase in anisotropy with increasing energy of the outgoing particles. We have not undertaken a special investigation of the angular distribution; however, our data indicate a somewhat higher anisotropy, for instance, for Cu^{63} about 10 %, and we do not find the predicted variation with proton energy; but the existence of direct interactions would, of course, tend to conceal this variation.

For the group of sub-barrier protons, the anisotropy is found to be significantly greater, for instance for Cu^{63} about 30 %, which is close to the $1/\sin\theta$ distribution to be expected if all the protons are emitted in a direction perpendicular to the angular momentum given to the compound nucleus by the incoming α-particles. As discussed by Ericson and Strutinsky[12]), the first emitted particle

† Using formulae (16) and (19) of this paper together with their value 15% for the anisotropy of scattered α-particles.

should be expected to carry away only a small angular momentum whereas, in the second transition going predominantly to the ground state of the residual nucleus, the proton must remove the main part of the angular momentum of the compound nucleus, which will result in higher anisotropy.

In fig. 5 is plotted the quantity $(d^2\sigma/dEd\Omega)/E\sigma_c(E)$ proportional to the level density $\rho(E^*)$ against the excitation energy E^*. Curves corresponding to the proton spectra at 90° from a target of Cu^{63} are given. Similar curves were obtained for the angles 45° and 135° and for the other targets. The 135° curves give essentially the same values for the temperature. This is also true for the 45° curves when one neglects the deviating points corresponding to the highest proton energies. $\sigma_c(E)$ was taken according to table 4 in Shapiro's paper[13]) using $r_0 = 1.41 \times 10^{-13}$ cm as in a previous paper[2]). As seen, for each value of the α-energy a straight line corresponding to a constant temperature, i.e. $\log \rho \propto E^*$ fits well with the experimental points for that part of the spectrum which is due entirely to the group of first emitted protons. The bending of the

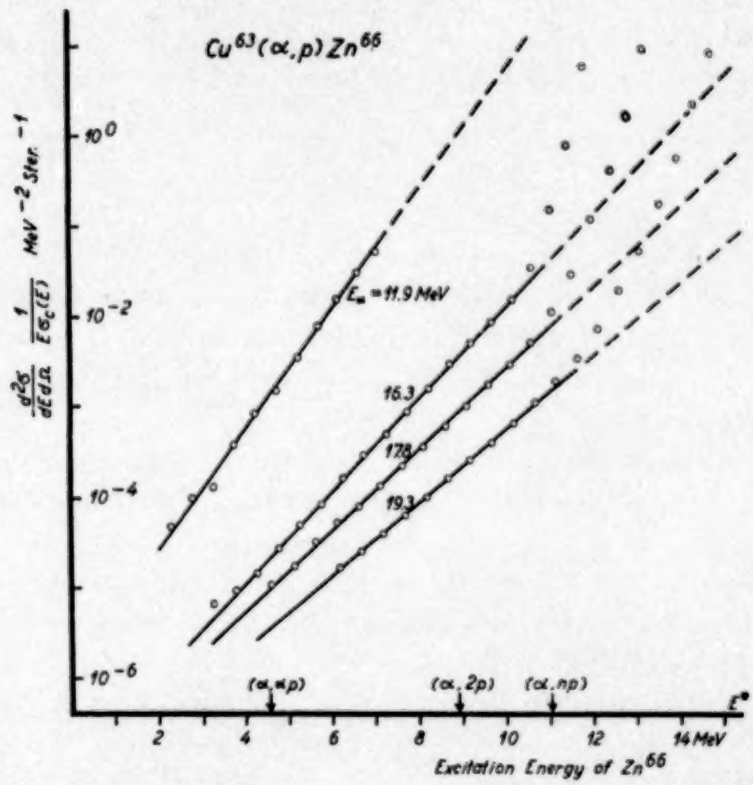

Fig. 5. Level density of Zn^{66} in arbitrary scale. Points from 90° proton spectra from α-bombardment of Cu^{63} for various energies $E_{\alpha,\mathrm{lab}}$ written in the figure.

curves for high excitation energies reflects the existence of the group of secondary protons. With the mentioned value of r_0 the fit to straight lines is definitely better when $\log \rho$ is plotted against E^* than when it is plotted against $\sqrt{E^*}$. However, this is not true if one uses a much higher radius as, for instance, $r_0 = 2 \times 10^{-13}$ cm, in which case it is difficult to decide which plot is the better.

In table 2 are given values of the temperature for various residual nuclei and for various energies of the incoming α-particles as obtained from curves similar to those in fig. 5. For the three highest α-energies the temperatures correspond to the same range, 6–10 MeV, of excitation energy of the residual nucleus, whereas for $E_\alpha = 11.9$ MeV it corresponds to lower energies and, in this case, the data are slightly less accurate. The figures indicate an increase in temperature with decreasing mass number in agreement with the statistical theory. However, they also show a strong decrease of the obtained values for the temperature with decreasing α-energy, an effect which is difficult to understand in terms of the statistical theory.

It is not possible to explain this peculiar energy dependence by assuming the use of too low a value for r_0, because a similar dependence is also found when using $r_0 = 2 \times 10^{-13}$ cm, though of course the temperature values are slightly changed. One might seek a possible explanation in the fact that

TABLE 2

Nuclear Temperatures in MeV

Target nucleus Residual nucleus	V^{51} Cr^{54}	Co^{59} Ni^{62}	Ni^{58} Cu^{61}	Ni^{60} Cu^{63}	Cu^{63} Zn^{66}	Cu^{65} Zn^{68}
Energy in MeV of incoming α's 19.3	1.35	1.17	1.10	1.05	1.07	1.05
Energy in MeV of incoming α's 17.8	1.22		1.04		0.97	0.92
Energy in MeV of incoming α's 16.3		0.99	0.98		0.85	0.83
Energy in MeV of incoming α's 11.9	1.00	0.74			0.65	0.62

Shapiro's tables are based upon simplified assumptions regarding the nuclear surface. One way to test this possibility might be to study the neutron spectra in similar reactions.

In principle, with different α-energies the compound nucleus has different angular momentum distribution and hence different levels are populated in the residual nucleus, but no proper explanation of the observed variation can be given in terms of existing theories. One might also consider the possibility that the main assumption in the statistical theory, viz., that transition takes place between equilibrium states in the compound and the residual nucleus, is not completely fulfilled.

The dashed lines in figs. 3, 4 and 5 correspond to the extrapolation, according to the statistical theory, of the experimental curves for the group of first emitted protons. By integration one obtains the cross sections for the latter group given in table 3 (errors in absolute values less than 20 %).

The values are in rough agreement with the statistical theory, the deviations never exceeding a factor of two, which is within the uncertainty to be expected

TABLE 3

Cross sections in mb

Target / E_α in MeV	V^{51}	Co^{59}	Ni^{58}	Ni^{60}	Cu^{63}	Cu^{65}
19.3	140	190	700	400	260	70
17.8	110		550		250	60
16.3		130	500		230	50
11.9	45	80			130	15

due to insufficient knowledge of the absolute cross section for formation of the compound nucleus and the absolute values of the level densities in different nuclei.

These experiments were carried out at the Institute for Theoretical Physics, University of Copenhagen, and the authors wish to express their deep gratitude to the Director of the Institute, Professor Niels Bohr. For valuable discussions our thanks are due Professor Aage Bohr and mag.sc. N. O. Roy Poulsen as well as many other members and guests of the Institute. We also thank Mr. Philip Dam for his help in operating the cyclotron.

References

1) J. M. Blatt and V. F. Weisskopf, Theoretical Nuclear Physics (John Wiley and Sons, New York, 1952)
2) H. W. Fullbright, N. O. Lassen and N. O. Roy Poulsen, Mat. Fys. Medd. Dan. Vid. Selsk. **31**, no. 10 (1959)
3) T. Ericson, Nuclear Physics **11** (1959) 481
4) V. Strutinsky, Comptes Rendus du Congrès International de Physique Nucléaire (Paris 1958) p. 617
5) P. C. Gugelot, Proc. Brookhaven Conference 1955, Statistical Aspect of the Nucleus, BNL-331, p. 89
6) I. Slaus and W. Parker Alford, Phys. Rev. **114** (1959) 1054; also private communication from Dr. Alford
7) D. L. Allan, Proc. Phys. Soc. A**70** (1957) 195
8) B. L. Cohen and A. G. Rubin, Phys. Rev. **113** (1959) 579
9) V. J. Asby and H. C. Catron, U.C.R.L.-5419
10) A. G. W. Cameron, Atomic Energy of Canada Limited, C.R.P.-690
11) T. Ericson and V. Strutinsky, Nuclear Physics **8** (1958) 284
12) T. Ericson and V. Strutinsky, Nuclear Physics **9** (1958) 689
13) M. Shapiro, Phys. Rev. **90** (1953) 171

2.L *Nuclear Physics* **19** (1960) 589—603; © *North-Holland Publishing Co., Amsterdam*
Not to be reproduced by photoprint or microfilm without written permission from the publisher

THE SCATTERING OF ALPHA PARTICLES AND DEUTERONS BY IODINE-127

I. J. VAN HEERDEN

Nuclear Physics Division of the National Physical Research Laboratory, C.S.I.R., Pretoria, South Africa

and

D. J. PROWSE

Department of Physics, University of California, Los Angeles 24, California

Received 1 April 1960

Abstract: The differential elastic scattering cross sections of 38 MeV α-particles as well as 8 and 19.5 MeV deuterons by I^{127} have been determined using nuclear emulsions. The angular distributions obtained have been analyzed according to Porter's model of absorption along classical undistorted Coulomb orbits. Information is thus obtained on the mean free path of the incident particles in nuclear matter. In the course of this experimental work, indications of the existence of a Cohen peak in the inelastic scattering have been observed; the evidence will be described and the implications discussed.

1. Introduction

The angular distributions of α-particles elastically scattered from various nuclei at several bombarding energies between 22 and 48 MeV have been previously reported[1–6]). Recently the elastic scattering cross sections of α-particles from a large number of nuclei ranging from Ni to Pu have been investigated as a function of beam energy[7]). The outstanding feature of the heavy nuclei results is the approximate exponential fall-off of the differential cross sections from pure Coulomb scattering, beginning at a certain critical angle or at a certain energy if the measurements are made at a constant angle as a function of energy. The results for medium weight nuclei begin to show diffraction patterns superimposed upon the decreasing cross sections; these become very marked for the light nuclei. Furthermore with decreasing atomic weight, the slope of the ratio of the elastic to pure Coulomb scattering becomes less and less, until for light nuclei it actually becomes an increase. To compare the energy and angle dependent data, the results can be plotted as a function of apsidal distance, i.e. the distance of closest approach of the classical hyperbolic Coulomb orbit to the centre of the nucleus. This is true, regardless of the nature of the bombarding particle.

In the paper, the angular distribution of 38 MeV α-particles elastically scattered from I^{127} is given, and analysed according to the model of Porter[8]).

There are rather few data in the literature on the elastic scattering of deuterons as a function of element and beam energy; however, results for nuclei of medium atomic number at energies from 3 to 22 MeV also show a similar fall-off from pure Coulomb scattering[9–11]). Some results on the angular distribution of 8 MeV deuterons elastically scattered from I^{127}, which were obtained earlier, are therefore also reported and compared with the α-particle data. Because of the lower energy, the range of apsidal distance over which the cross section differs from the Coulomb value is rather small; therefore a further deuteron experiment was performed at 19.5 MeV which extends the range of apsidal distance studied. The velocity of the particle inside the nucleus is not very different in these three cases; a comparison can thus be made between the mean free paths deduced via the Porter model for the deuterons and α-particles and the imaginary parts of the optical model potentials obtained from other work, which also give rise to certain mean free paths in nuclear matter.

2. Experimental Procedure and Results

2.1. α-PARTICLE SCATTERING

A modified version[12]) of the scattering camera originally described by Burrows, Powell and Rotblat[13]) was used to obtain the angular distributions. The camera was separately filled with hydrogen and methyl-iodide vapour at pressures of 5.48 and 4.87 cm Hg respectively and exposed to the 38 MeV α-particle beam of the 152 cm Birmingham cyclotron. The scattered particles were recorded in Ilford C2 emulsions, 200 μm thick. The thickness of the cylindrical tubes defining the scattering volume were very carefully measured on a reflecting microscope, and the volume defined at each scattering angle was computed from the measurements. The purpose of the first exposure was to determine the differential cross sections and the angular distribution of the protons from the $H^1(\alpha, p)He^4$ scattering reaction, and hence to calibrate the integrator used to measure the total beam current. The mean ranges of these knock-on protons at 24 angles from 15° to 72.5° in the laboratory system, corrected for the loss of energy in the gas and using the range energy curves of Gibson, Prowse and Rotblat[14]), gave a beam energy of 38.15 ± 0.35 MeV. In the second exposure, used to investigate the scattering from I^{127}, detailed measurements were made of the α-particle tracks at 53 angles between 12.5° and 150°; their true ranges were deduced and corrected for the loss of energy in the gas from the values of the differential stopping powers given by Wilkins[15]). A typical histogram of the α-particle tracks measured at a laboratory angle of 42.5° is shown in fig. 1. In addition to the elastic I^{127} group, there are five well-defined groups, four of which were identified as due to the ground and first three excited states of C^{12}. This was the case at most angles; the C^{12} results have been published separately. A value of 38.09 ± 0.13 MeV was derived for the beam

energy at the point of scattering from the mean ranges of the α-particles elastically scattered from C^{12} and I^{127} nuclei.

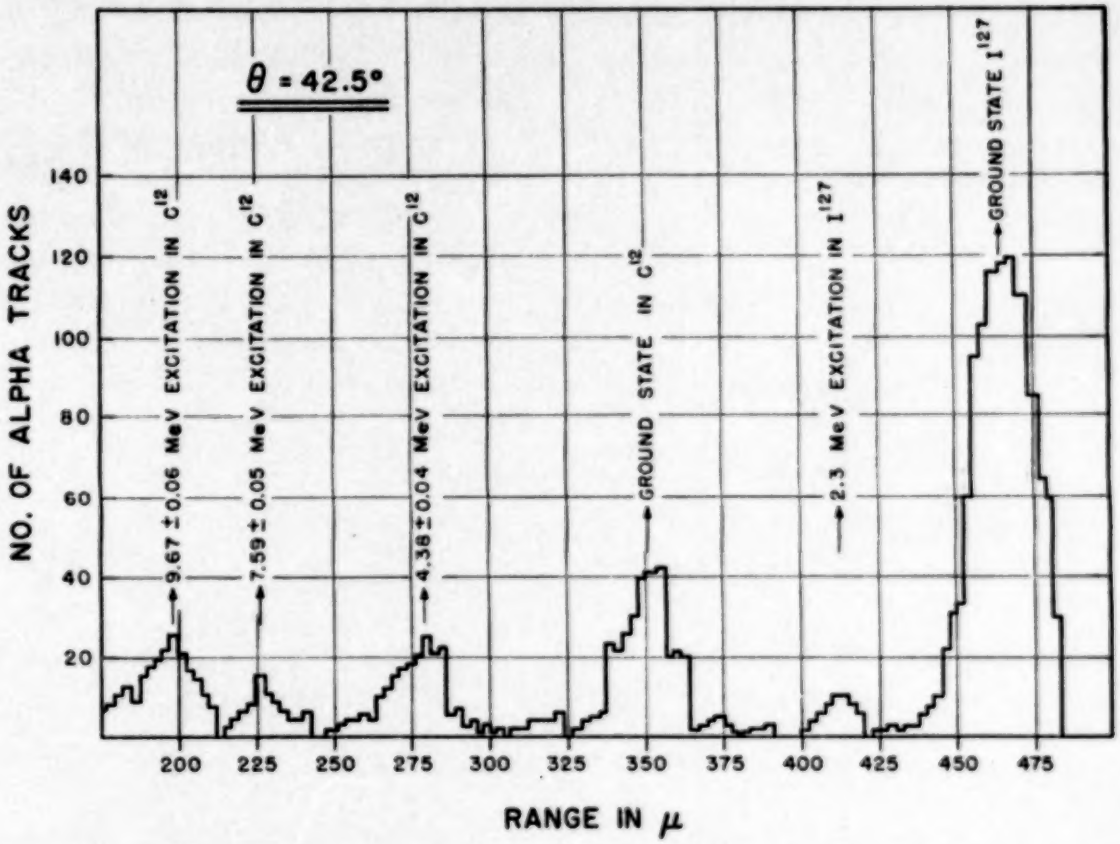
θ = 42.5°
NO. OF ALPHA TRACKS
RANGE IN μ
9.67 ± 0.06 MeV EXCITATION IN C12
7.59 ± 0.05 MeV EXCITATION IN C12
4.38 ± 0.04 MeV EXCITATION IN C12
GROUND STATE IN C12
2.3 MeV EXCITATION IN I127
GROUND STATE I127

Fig. 1. Range histogram of the α-particle tracks measured at 42.5° (lab.) for the 38 MeV α-particle exposure.

The absolute measurement of the beam intensity with the integrator used was somewhat erratic; to calculate the differential scattering cross sections in absolute units the following procedure was therefore adopted. In the centre-of-mass system the angular distribution of the knock-on protons produced in the bombardment of hydrogen nuclei by 38 MeV α-particles is the mirror image of the angular distribution for the elastic scattering of 9.5 MeV protons by Helium. Fig. 2 shows the differential cross sections obtained in the c.m. system for the knock-on protons. The errors shown are statistical only. The results of Williams and Rasmussen[16]) for the elastic scattering of 9.76 MeV protons by He^4 are also shown in fig. 2, but reflected about $\phi = 90°$. The two sets of data are very similar and provide an independent check on the correctness of the angular distribution. At small forward angles the ranges of the knock-on protons become very large, e.g., 2300 μm at an angle of 30° in the c.m. system. Great care was therefore taken to pick up all such tracks, as their grain density and consequent visibility in C2 emulsions is not high. Owing to the finite thickness of the emulsions, corrections were made to the numbers of such long

tracks to take into account the foreshortening in range of the small number of tracks which left the emulsion at the glass interface. The normalization of the two sets of data yielded a calibration for the differential cross section in absolute units and this was used to calculate the absolute cross sections in the second exposure. It is known that the variation of the p-α cross section with energy is small[17]; the difference in the effective beam energies therefore (9.76 and 9.50 MeV) is likely to have a very small effect. However, reliance is being placed on the stability of the integrator between the two exposures. That this is a fairly safe assumption is shown by two independent pieces of information: (a) at small forward angles the cross section of the elastic scattering from I^{127} is that expected from Coulomb effects alone—a very reasonable result; (b) at

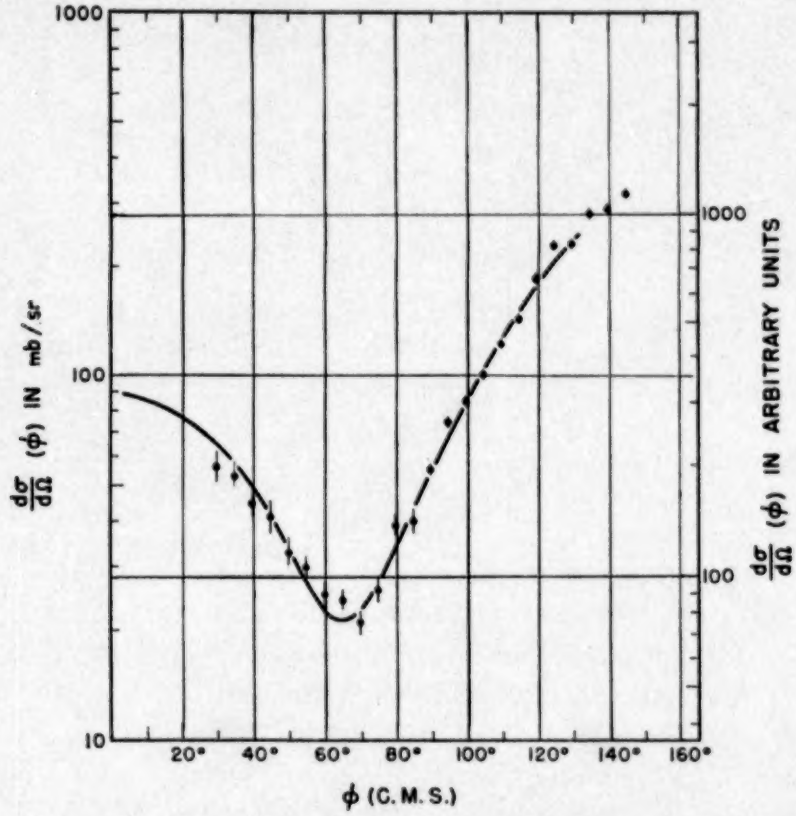

Fig. 2. Differential cross sections of the protons from the $H^1(\alpha, p)He^4$ reaction. The solid curve shows the angular distribution reflected about 90° of 9.76 MeV protons elastically scattered by He^4. This was obtained by Williams and Rasmussen.

the few angles where accurate measurements of the p-α cross section could be made in the second exposure itself, agreement was good between the two exposures.

The angular distribution in the c.m. system for the elastic scattering of α-particles from I^{127} is shown in fig. 3. The normal corrections for background tracks have been made at each angle but at very forward angles the energy resolution of the emulsion was insufficient to separate the elastic groups from I^{127} and C^{12}.

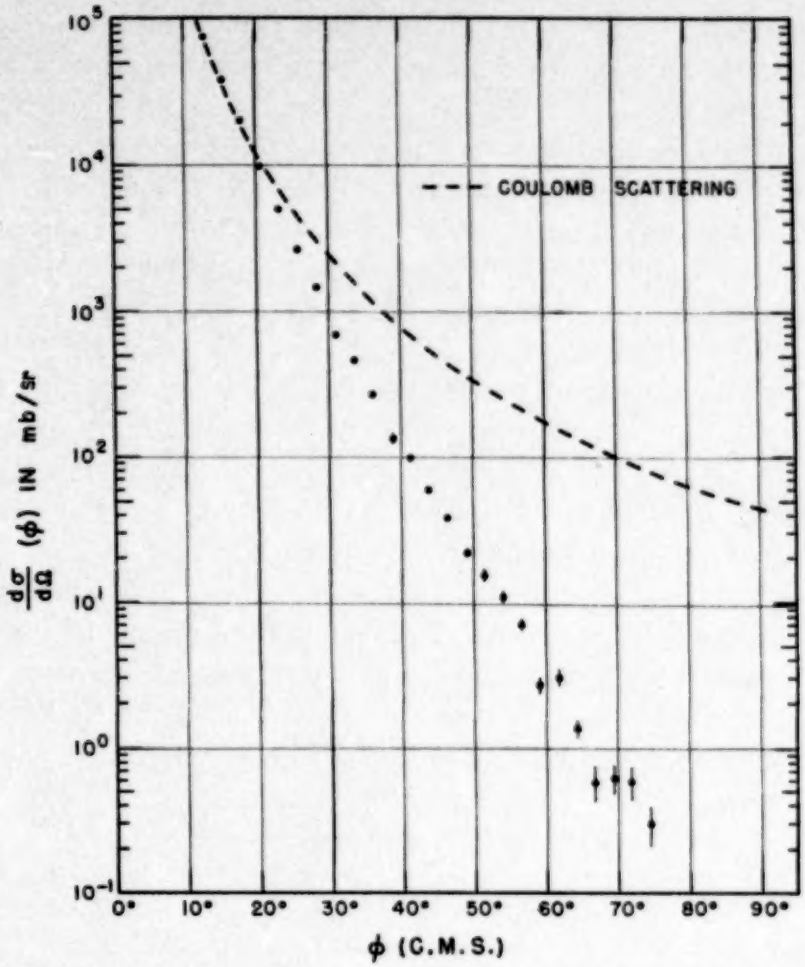

Fig. 3. Angular distribution of 38.09 MeV α-particles elastically scattered by I^{127}. The dashed line is the Coulomb scattering curve.

When this was the case the Coulomb value for carbon has been subtracted from the total cross section measured at each angle. Because the scattering from carbon is small compared to that from iodine, this procedure is unlikely to result in any large errors. A tacit assumption is made at all angles that inelastic scattering from the low lying excited states of iodine does not occur; levels within 500 keV of the ground state would not be resolved. Confirmation that such inelastic scattering from the slightly higher levels is indeed small is obtained from an examination of the number of "background" tracks between the I^{127} and C^{12} groups. There is, however, at a number of angles an apparent enhancement of this background into what appears to be a coherent group. These tracks form the sixth group visible for instance at 42.5° shown in fig. 1. The variation of the range of these tracks with angle indicates that they must be associated with iodine and not with carbon, or some gaseous impurity such as O^{16} or N^{14}. They correspond to an excitation in iodine of about 2.3 MeV; the implication of this group is discussed in a later section on inelastic scattering.

In fig. 3 the angular distribution is compared with that expected from pure Coulomb scattering; it is clear that beginning at $\phi \approx 20°$, there is a very rapid fall-off from the Coulomb value. The fall-off is in fact so rapid that at angles greater than 70° the number of particles scattered from iodine is too small to be measured with certainty. Above 80° the differential cross section is certainly less than 0.1 mb/sr and it never again rises above this value. In fig. 4 the ratio of the measured elastic differential cross section to the Coulomb value, i.e. $(\mathrm{d}\sigma/\mathrm{d}\Omega)_{\mathrm{elastic}}/(\mathrm{d}\sigma/\mathrm{d}\Omega)_{\mathrm{Coulomb}}$, is shown plotted as a function of angle. The weak oscillatory pattern characteristic of medium weight nuclei is shown more clearly in this figure than in the preceding one. If one assumes that the maxima are caused by diffraction scattering from a totally absorbing nucleus, a value of $7.73 \pm 0.36 \times 10^{-13}$ cm is obtained for the effective interaction radius of the I^{127} nucleus. This is consistent with the value 8.02×10^{-13} cm predicted for iodine, from the least squares line $R = (1.017\, A^{\frac{1}{3}} + 2.94) \times 10^{-13}$ cm proposed by Yavin and Farwell[5]). As the positions of the diffraction maxima are somewhat uncertain, the value of the interaction radius obtained is subject to rather a large error. In addition, the model of diffraction scattering from an opaque sphere with a sharp cut-off is not particularly realistic. If the finite transparency is taken into account together with the diffuseness of the nuclear surface, a somewhat larger value might be expected.

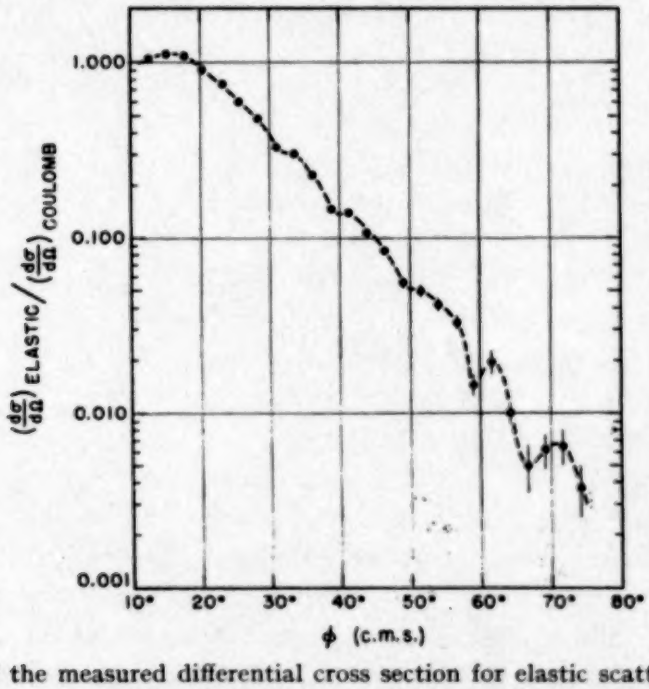

Fig. 4. The ratio of the measured differential cross section for elastic scattering of 38.09 MeV α-particles by I^{127} to the Coulomb value as a function of centre-of-mass angle.

2.2. DEUTERON SCATTERING

One set of deuteron data was obtained from an exposure of CH_3I vapour in the same scattering camera in the unmodified form[13]) to the 8 MeV deuteron

beam of the Liverpool cyclotron. The differential cross sections have been calculated in absolute units using the formula and calibration constant as derived from a comparison with d-p scattering data from other laboratories by Burrows, Gibson and Rotblat[18]). The correctness of the calibration constant of these workers is witnessed by the value of the ratio of the experimental

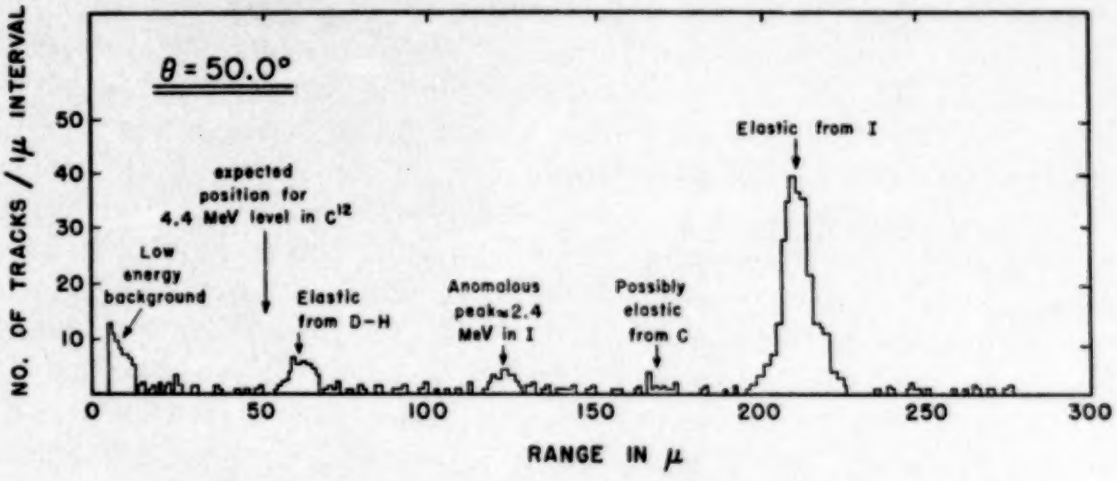
θ = 50.0°
NO. OF TRACKS / 1μ INTERVAL
RANGE IN μ
Low energy background
expected position for 4.4 MeV level in C12
Elastic from D-H
Anomalous peak≈2.4 MeV in I
Possibly elastic from C
Elastic from I

Fig. 5. Range histogram of the tracks measured at 50° in the laboratory system for the 8 MeV deuteron exposure.

scattering from iodine to that expected from Coulomb scattering alone. This value is unity up to about 70° in the c.m. system. A typical range histogram of the tracks obtained at 50° in the laboratory system is shown in fig. 5. In this histogram two large groups are visible, that due to the elastic scattering from iodine and that due to the knock-on protons from the d-p scattering process. The elastic scattering from carbon which would give rise to a group of particles

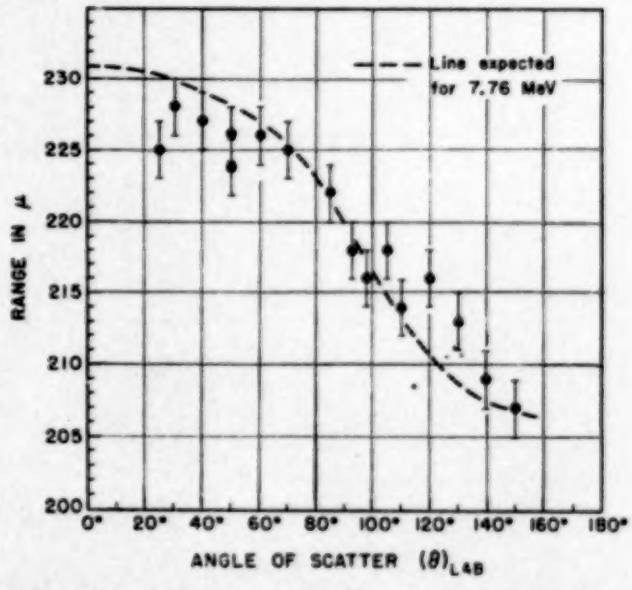

Fig. 6. Measured ranges of the deuterons elastically scattered from I^{127} plotted against angle. The dashed line is the expected kinematic curve for a deuteron energy of 7.76 MeV.

at about 170 μm in fig. 5, is very small compared to that from iodine and is in fact barely visible above the background. This is, of course, as expected; the ratio of the Coulomb scattering cross sections, observing particles at a constant c.m. system angle is about 80. Observing the particles at a constant laboratory angle (which is actually done) enhances this ratio, because a given laboratory angle is equivalent to a bigger c.m. angle for carbon than for iodine. The deuteron beam energy was calculated from the ranges of the elastically scattered particles at a number of angles. There is very little variation of range with angle as is exhibited in fig. 6, which shows the measured ranges plotted against angle with the expected kinematic curve for a deuteron energy of 7.76 MeV. In addition to the groups of particles which are readily explained there is a further semblance of a group at about 130 μm range. Slight indications of this group are present between 25° and 92.5°. It is a factor of three above the background level at 50° and decreases to background level at 25 °and 92.5°. The apparent range of this group is remarkably constant with angle indicating that it should be associated with iodine rather than with any other possible target. The excitation energy to which it would correspond if due to inelastic scattering from iodine is about 2.4 MeV. This is very close to the energy of a similar group observed in the α-particle scattering. The intensity of the group is much lower, however,

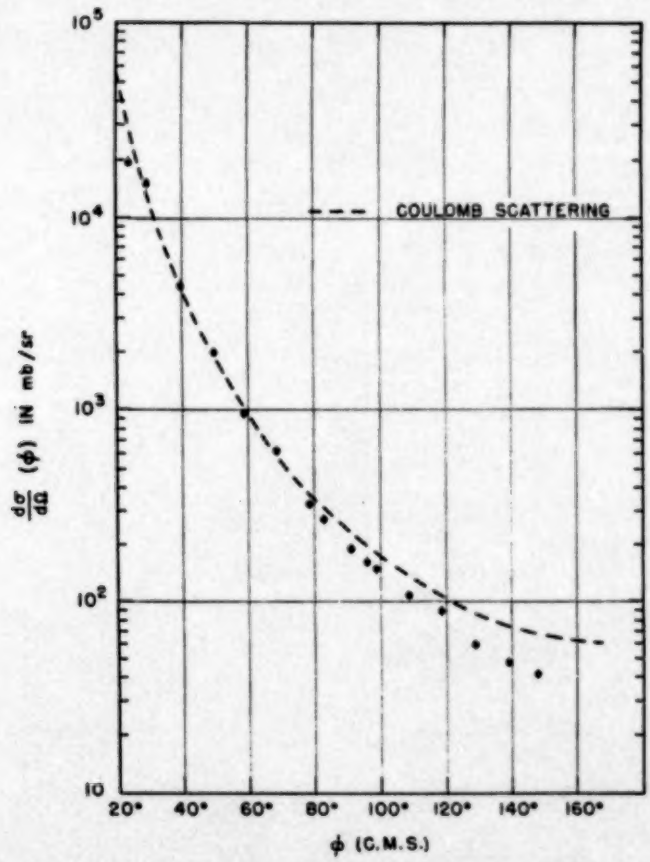

Fig. 7. Angular distribution of 7.76 MeV deuterons elastically scattered by I^{127}. The dashed line is the Coulomb scattering curve.

and not nearly so well established as the group of α-particles. Further work is obviously necessary before the existence of this anomalous peak is confirmed. We shall return to this question in a later section.

The other deuteron data were obtained in the modified camera used for the α-particle exposure. CH_3I-vapour was exposed to the 19.5 MeV deuteron beam of the Birmingham cyclotron. The beam energy as determined from the ranges of the elastically scattered particles was 19.45 ± 0.07 MeV. In this case the absolute differential scattering cross sections were determined from the values given by a calibrated integrator.

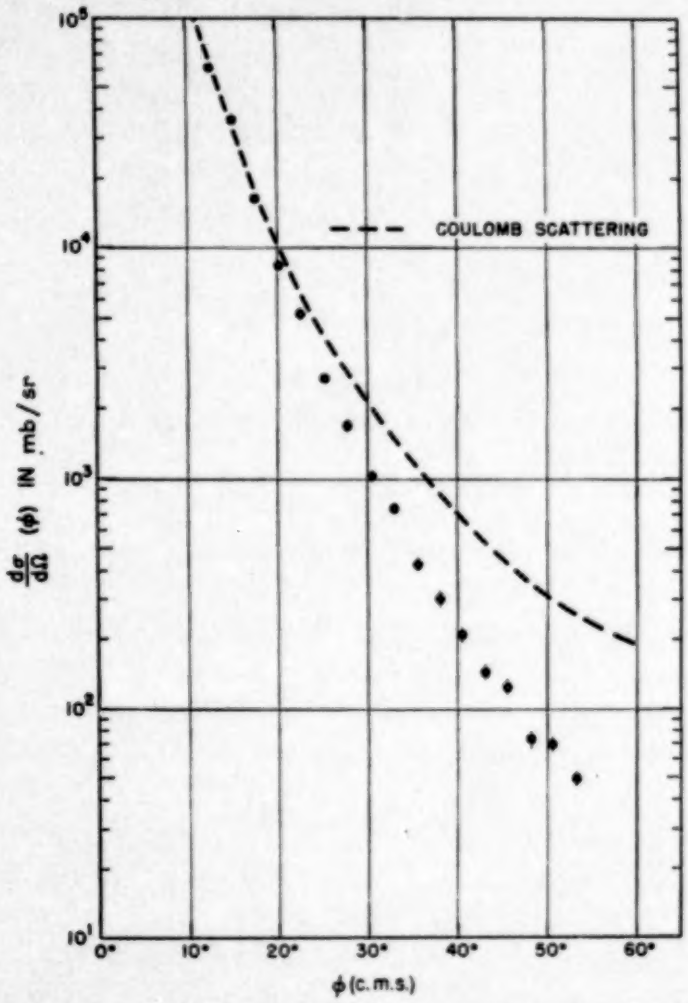

Fig. 8. Angular distribution of 19.45 MeV deuterons elastically scattered by I^{127}. The dashed line is the Coulomb scattering curve.

Figs. 7 and 8 show the angular distributions of 8 and 19.5 MeV deuterons elastically scattered from I^{127}. In common with other low energy deuteron scattering results[11]), the cross sections suddenly depart from the Coulomb values, at about 60° in the 8 MeV case and at about 16° in the 19.5 MeV case, and then continue to get smaller than these values. The immediate similarity to the α-particle data can easily be seen.

3. Analysis of the Angular Distributions using the Porter Model

According to the model of Porter[8]), which has been used by a number of authors[19]) in the last few years in varying degrees of refinement to obtain elastic angular distributions, the fall-off in the scattered intensity as a function of apsidal distance D is caused by absorption along the undistorted orbits of the particles as they traverse the nucleus. In the limit of a sharp cut-off for the nucleus, the sudden departure of the cross section from the Coulomb value at some critical angle is explained as being when the apsidal distance becomes exactly equal to the interaction radius. The rate of fall-off of the cross section now depends only on the mean free path of the particles in nuclear matter; for an infinite mean free path the fall-off is infinitely slow; for a zero mean free path it is catastrophic. The ratio of elastic to pure Coulomb scattering $(\mathrm{d}\sigma/\mathrm{d}\Omega)_{\text{elastic}}/(\mathrm{d}\sigma/\mathrm{d}\Omega)_{\text{Coulomb}}$ is the transmission factor T, i.e. the fraction of particles not absorbed by the nucleus. T has the form

$$T = \exp\left(-\int_x^\infty \frac{\mathrm{d}x}{l(x)}\right), \tag{1}$$

$l(x)$ being the mean free path as a function of the position co-ordinate along the path. The value of T is now derived assuming straight line paths through the nucleus, and is given by

$$T = \exp\left\{-\frac{R}{\delta l}\int_\xi^\infty (v^2-\xi^2)^{\frac{1}{2}}\,\mathrm{sech}^2\left(\frac{v-1}{\delta}\right)\mathrm{d}v\right\}, \tag{2}$$

in which $\xi = D/R$, R being the interaction radius; $v = r/R$, where r is the radial position of the particle on its path through the nucleus; $\delta = d/R$, where d is a measure of the thickness of the diffuse surface of the nucleus; and l is the mean free path in nuclear matter of full density.

Essentially we thus have three free parameters R, d and l. The initial apsidal distance at which T begins to differ from 1 is given largely by R. The initial gradient is determined by d and l and the gradient at smaller apsidal distances by l alone. If the data were of infinite precision it would be possible to determine all three parameters unambiguously; this, however, is not the case. All we can therefore do is to define a region in R, d and l space which gives a reasonable fit with the experimental data. There are a number of drawbacks to the model which have been pointed out by Eisberg and McCarthy[20]). These are essentially due to the finite size of the wave, a considerable fraction of the wave packet being outside the nuclear volume when classically the particle is inside. If this effect is serious it should lead to an apparent variation in the mean free path with apsidal distance because the finite size of the wave is only serious in this respect near the edge of the nucleus. The true mean free path in nuclear matter should be that as determined at very small apsidal distances.

In fig. 9 the ratio of the measured elastic α-particle scattering to Coulomb scattering is shown plotted as a function of apsidal distance, together with theoretical curves for $R = 10.7\,f$, $d = 2.7\,f$ and $l = 10.7$, 5.35, 2.68 and 1.34 f, where $f = 10^{-13}$ cm. Although a unique value of l fits the initial region of variation, it has to be successively decreased as the apsidal distance gets smaller. The variation of l with apsidal distance is as expected from the work of Eisberg and McCarthy. As is the case with optical model analyses (the Porter model is in any case just another way of looking at the optical model), it is not possible to fix the mean free path independently of R—essentially because it is the reaction cross section which is fixed and this can *only* be fixed by both R and l. The effective velocity of the α-particles inside the nucleus is that given by $V + E_\alpha$, where V is the real potential and E_α is the kinetic energy of the α-particles outside the nucleus. The optical model imaginary potential should thus be given by $W = \hbar\beta c/2l$; using the mean free path as determined at the lowest apsidal distances, one obtains a value of about 14 MeV, which is in accord with the accepted values for such potentials[21]).

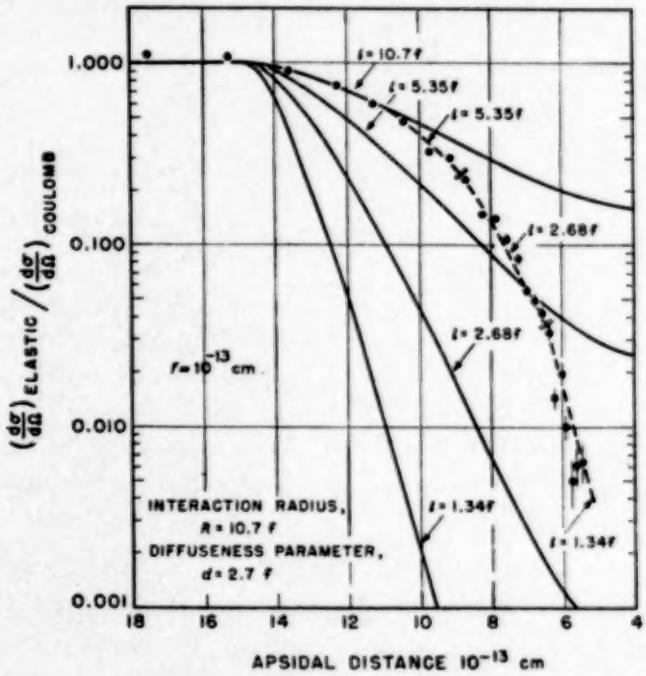

Fig. 9. Ratio of measured elastic scattering of α-particles by I^{127} to Coulomb scattering as a function of apsidal distance. Theoretical curves for $R = 10.7f$, $d = 2.7f$ and $l = 10.7$, 5.35, 2.68 and 1.34f are shown.

The ratio $(d\sigma/d\Omega)_{elastic}/(d\sigma/d\Omega)_{Coulomb}$ for the deuteron data is plotted against apsidal distance in fig. 10, together with theoretical curves for $R = 10.7\,f$, $d = 2.7\,f$ and $l = 17.8$ and $8.9\,f$. To fit the experimental data, l has to be successively decreased with decreasing apsidal distance. The same values were used for R and d for the α-particle and deuteron scattering data. The value of l

necessary to fit the initial region of variation is however greater for the deuterons than for the α-particles. This can also be explained by the work of Eisberg and McCarthy[20]). The wave packet spread will be worse for the deuterons than for the α-particles, and as that part of the wave outside the nucleus is not attenu-

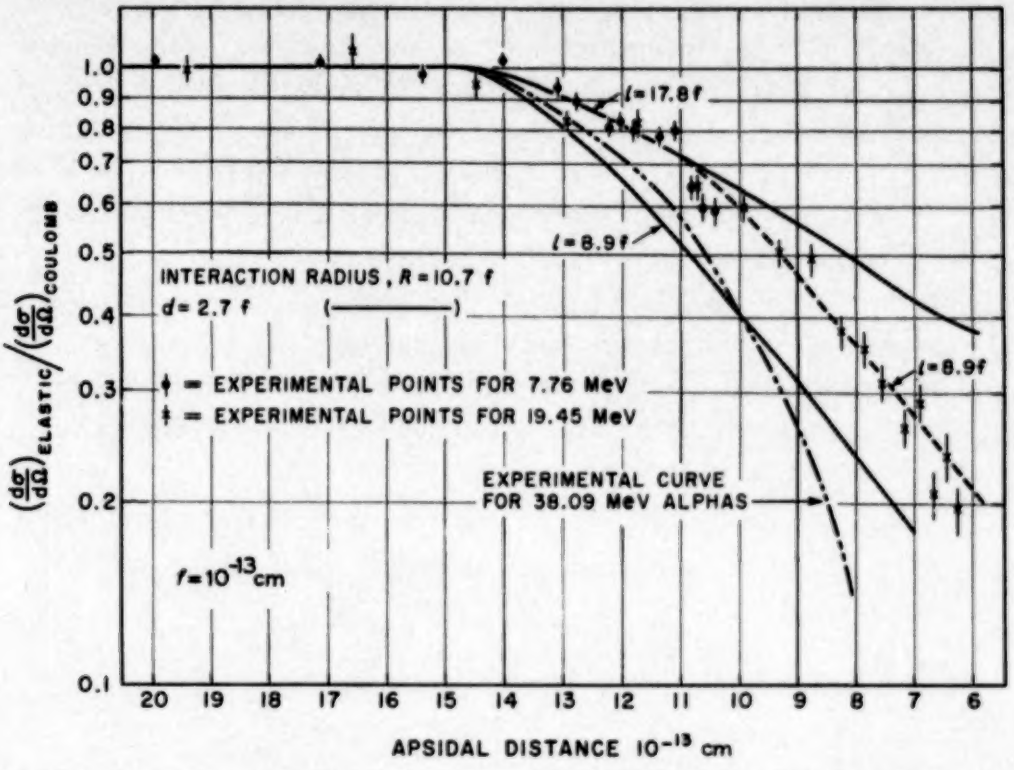

Fig. 10. Ratio of measured elastic scattering of deuterons by I^{127} to Coulomb scattering as a function of apsidal distance. Theoretical curves for $R = 10.7f$, $d = 2.7f$ and $l = 17.8$ and $8.9f$ are shown, as well as the experimental curve for the elastic scattering of 38.09 MeV α-particles by I^{127}.

ated, one therefore expects a greater initial mean free path for deuterons than for α-particles. To determine whether this situation persists at very small apsidal distances, it will be necessary to extend the 19.5 MeV deuteron measurements to backward angles. In the present results this was prohibited by the low intensity of the exposure. The imaginary part of the optical model potential for deuteron scattering corresponding to a mean free path of 8.9 f, is equal to about 2 MeV for the 8 and 19.5 MeV deuterons. The value needed to fit deuteron scattering angular distributions using the diffuse surface optical model is actually more than this[22]).

The interpretation of the deuteron data is also made more uncertain by the possibility of electric break-up of the deuteron in the Coulomb field of the nucleus. From a simple classical approach[19]), electric break-up becomes possible as soon as the energy gained by the deuteron in the Coulomb field of the nucleus exceeds the binding energy of the deuteron. The predicted angle at which the scattering cross sections suddenly depart from Coulomb scattering is independent of the nuclear charge, and will be equal to 42° and 22° for 8

and 19.5 MeV deuterons respectively. These are consistent with the experimental values. It has recently been pointed out by Yntema[10]) that for medium and heavy nuclei the total deviation from Coulomb scattering of the elastic scattering cross sections is several times larger than that expected from the electric break-up of the deuteron. This also applies to the present results.

In conclusion, it would appear that the Porter model is inadequate at apsidal distances corresponding to the region of the nuclear surface, but it is possible that it might give a reasonably accurate value of the mean free path in nuclear matter at very small apsidal distances. The effect of using undistorted Coulomb orbits instead of distorted ones is probably more serious for low energy particles when the kinetic energy is small compared with the real potential inside the nucleus. Further work with deuterons at smaller apsidal distances is required before it can be decided from this model whether or not the mean free path for deuterons is longer than that for α-particles. The general features of the experimental data can be explained by the model but care has to be taken in the interpretation of the parameters so derived.

4. Inelastic Scattering

Since the early work of Cohen[23]) in which anomalous peaks were found in the elastic scattering of 23 MeV protons, a considerable amount of effort has gone into the investigation of the effect using proton beams of various energies, e.g. refs. [24–26]). Rather less work has been done with deuteron or α-particle beams. Sweetman and Wall[27]) have investigated the inelastic scattering of 30 MeV α-particles and have found a structure which persists from element to element in the region $Z = 13$ to $Z = 48$. For Zr, they find a strong inelastic group corresponding to an excitation of about 3 MeV. The situation in Ni they find to be considerably more complicated while for Au they find no structure at all. The angular distributions of the groups corresponding to low excitation are strongly peaked forward, indicating a type of direct interaction. The anomalous group observed by us in the scattering of 38 MeV α-particles from I^{127} as shown in fig. 1, suggests that the effects observed by Sweetman and Wall for α-particle scattering at 30 MeV persist at 38 MeV and extend to I^{127} which has a higher atomic number than any nuclei apart from Au studied by these workers.

The energy spectra of protons in (d, p) reactions have also been found to contain anomalies[28]) and Yntema and Zeidman[29]) have found similar effects in the inelastic scattering of deuterons. The present results indicate that there might be an anomalous peak in 8 MeV deuteron scattering from I^{127}; no indications thereof were found at 19.5 MeV, but this might have been due to the low intensity of the exposure and further work is therefore needed to confirm these results. It will be interresting if it really exists, because it is known

from the work of Greenless, Lowe, Robbins and Ralph[25]) that all semblance of Cohen peaks at 2.3 MeV have disappeared when the bombarding energy in the case of protons is reduced below 10 MeV.

In an attempt to confirm the direct interaction nature of the peak in α-particle scattering we have measured the angular distribution; this is shown in fig. 11. In the angular region where measurements are possible it appears to

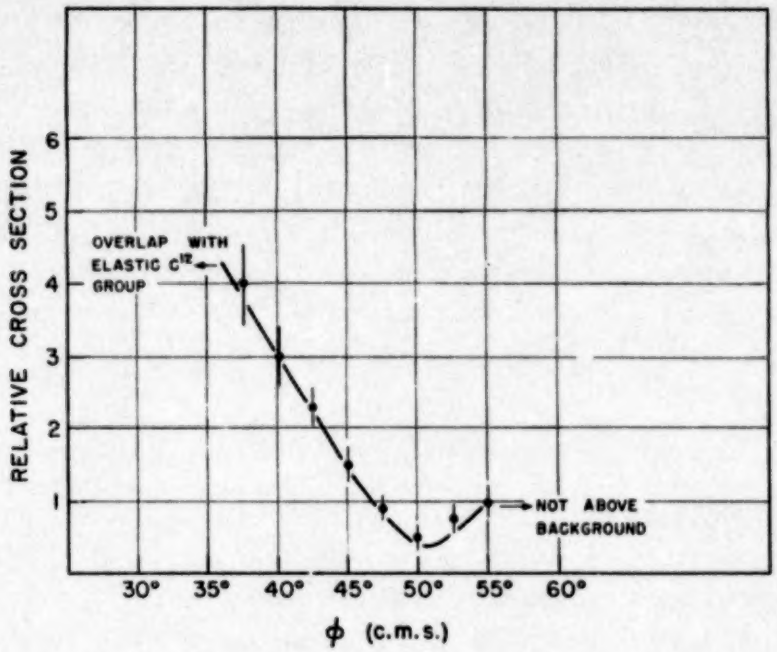

Fig. 11. Angular distribution of the anomalous group observed at 2.3 MeV excitation in the inelastic scattering of 38.09 MeV α-particles by I^{127}.

be peaked forward confirming the results of Sweetman and Wall. Lassen and Poulson[30]) have also observed forward peaking of anomalous groups in the scattering of 20 MeV α-particles from Copper isotopes. The direct interaction nature of the process would thus seem to be established.

The authors would like to thank Professor W. E. Burcham at Birmingham and Professor J. Skinner at Liverpool for their help and interest in this work. We also thank Dr. S. J. du Toit at Pretoria and Professor J. R. Richardson at Los Angeles for their encouragement. I. J. v. H. is deeply indebted to the South African Council for Scientific and Industrial Research for the facilities provided in their laboratories, while D. J. P. would like to express his thanks and appreciation to Professor C. M. G. Lattes and Professor A. Wataghin of the Centro Brasilerro de Pesquisas Fisicas for hospitality during his stay in Rio de Janeiro where much of this work was done. We also thank the scanners for their cooperation with the microscope work.

References

1) N. S. Wall, J. R. Rees and K. W. Ford, Phys. Rev. **97** (1955) 726
2) J. Aguilar, W. E. Burcham, J. Catala, J. B. A. England, J. S. C. McKee and J. Rotblat, Proc. Roy. Soc. A**254** (1960) 395
3) R. E. Ellis and L. Schechter, Phys. Rev. **101** (1956) 636
4) G. Igo and R. M. Thaler, Phys. Rev. **106** (1957) 126
5) A. I. Yavin and G. W. Farwell, Nuclear Physics **12** (1959) 1
6) L. Seidlitz, E. Bleuler and D. J. Tendam, Phys. Rev. **110** (1958) 682
7) D. D. Kerlee, J. S. Blair and G. W. Farwell, Phys. Rev. **107** (1957) 1343
8) C. E. Porter, Phys. Rev. **99** (1955) 1400
9) H. E. Gove, Phys. Rev. **99** (1955) 1353
10) J. L. Yntema, Phys. Rev. **113** (1959) 261
11) I. Slaus and W. P. Alford, Proceedings of the Paris Conference on Nuclear Physics (1958) 603
12) W. M. Gibson, D. J. Prowse and J. Rotblat, Proc. Roy. Soc. A**209** (1951) 237
13) H. B. Burrows, C. F. Powell and J. Rotblat, Proc. Roy. Soc. A**209** (1951) 461
14) W. M. Gibson, D. J. Prowse and J. Rotblat, Nature **173** (1954) 1180
15) J. J. Wilkins, A.E.R.E. Report G/R 664 (1951)
16) J. H. Williams and S. W. Rasmussen, Phys. Rev. **98** (1955) 56
17) R. G. Freemantle, T. Grotdal, W. M. Gibson, R. McKeague, D. J. Prowse and J. Rotblat, Phil. Mag. **45** (1954) 1090
18) H. B. Burrows, W. M. Gibson and J. Rotblat, Proc. Roy. Soc. A**209** (1951) 489
19) Y. Nishida, Prog. Theor. Phys. **19** (1958) 389
20) R. M. Eisberg and I. E. McCarthy, Proceedings of the Paris Conference on Nuclear Physics (1958) 98
21) G. Igo, Phys. Rev. Letters **1** (1958) 73
22) M. A. Melkanoff, private communication
23) B. L. Cohen, Phys. Rev. **105** (1957) 1549
24) S. W. Chen, R. M. Eisberg and N. M. Hintz, Proceedings of the Paris Conference on Nuclear Physics (1958) 377
25) G. W. Greenlees, J. Lowe, A. B. Robbins and P. M. Rolph, Proceedings of the Paris Conference on Nuclear Physics (1958) 424
26) B. L. Cohen and A. G. Rubin, Phys. Rev. **113** (1959) 579
27) D. R. Sweetman and N. S. Wall, Proceedings of the Paris Conference on Nuclear Physics (1958) 547
28) J. P. Schiffer and L. L. Lee, Bull. Am. Phys. Soc. **11** (1958) 211
29) J. L. Yntema and B. Zeidman, Phys. Rev. Letters **2** (1959) 309
30) N. O. Lassen and N. O. R. Poulsen, Proceedings of the Paris Conference on Nuclear Physics (1958) 477

1.E.1:
2.G

Nuclear Physics **19** (1960) 604—613; © *North-Holland Publishing Co., Amsterdam*
Not to be reproduced by photoprint or microfilm without written permission from the publisher

ENERGY LEVELS IN CHROMIUM ISOTOPES

F. A. EL BEDEWI† and S. TADROS

Faculty of Science, Alexandria University, U.A.R.

Received 26 April 1960

Abstract: A magnetic spectrograph with photographic detection is used to study the proton groups emitted from the deuteron interaction with a thin chromium target. Applying deuterons of energy 8.67 MeV, nine well-defined proton groups attributed to the isotope 52 of chromium yield Q-values of 5.73, 5.16, 4.72, 3.41, 3.04, 2.11, 1.60, 1.50 and 1.09 MeV with errors of $\pm$ 0.02 MeV. Four weak groups of protons having Q-values of 6.68, 6.26, 4.89 and 4.46 MeV with errors of $\pm$ 0.03 MeV may belong to the Cr^{53}(d, p)Cr^{54} reaction. In view of the present energy levels in Cr^{53} and Cr^{54}, interpretation of some gamma-ray groups emitted from previous work on neutron capture of chromium is given.

The angular distributions for the proton groups corresponding to the transition to the ground state and five low lying levels in Cr^{53} are compared with theoretical curves based on deuteron stripping mechanism. Odd parity is identified for all the examined energy levels and information about their possible spins, relative capture probabilities and relative reduced widths is obtained.

1. Introduction

Extensive work has been recently devoted to study the spectra and angular distributions of particle groups emitted from deuteron stripping reactions. Such experiments have been successful in identifying the energy levels of the residual nuclei, fixing their parities, limiting their spins and giving information about their capture probabilities and reduced widths. So far, most of these experiments are performed on light nuclei and very little attention has been given to those of atomic masses greater than 40. Applying deuterons of energy 8.67 MeV accelerated in the Liverpool 94 cm cyclotron together with a magnetic spectrograph, we have investigated some deuteron induced reactions with different medium heavy nuclei. The object of the present paper is to report results on a chromium target. Since chromium is known[1]) to have four stable isotopes of mass numbers 50, 52, 53 and 54 with natural abundances of 4.4 %, 83.7 %, 9.5 % and 2.4 % respectively, our investigation will be only confined to the most abundant isotopes Cr^{52} and Cr^{53}. The nucleus of the former isotope is even containing 28 neutrons supposed to fill the subshell $1f_{\frac{7}{2}}$ and it will be of interest to study the orbital angular momentum carried by the 29^{th} neutron when being captured in various excited states.

Previous to this work very little information has been reported concerning the excited levels of chromium isotopes. From neutron capture gamma rays

† Now at Nuclear Physics Laboratory, Atomic Energy Establishment, Cairo, Egypt.

Kinsey and Bartholomew[1]) measured gamma ray energies above 3.5 MeV by means of a magnetic pair spectrometer. Using a two-crystal Compton scintillation spectrometer, Braid[2]) observed few low energy gamma rays, but not in general agreement with those previously reported by Reier and Shamos[3]). Anyhow, it was rather difficult to assign with certainty the individual observed gamma rays to the appropriate transitions between unknown levels or even to relate them to the proper isotope. Interpretation of these results could be directly achieved if the energy levels of these nuclei are identified. No paper has been yet published in this field except some preliminary results reported by Elwyn and Shull[4]). These authors have used 10 MeV deuterons to bombard enriched targets of chromium isotopes 52 and 53 and the outgoing protons were detected by double proportional telescopes. Also, Van Patter *et al.*[5]) reported, from inelastic proton scattering, few low energy levels in chromium isotopes.

2. Procedure

A collimated deuteron beam, provided by the Liverpool 94 cm cyclotron, was used to bombard a chromium target of 0.5 mg/cm² areal density prepared by electrolysis onto a thin copper backing which was then dissolved by nitric acid. The collimation was achieved by a three slit system which defined the effective beam at the target to an area of $\frac{1}{2}$ mm wide and 3 mm high and reduced its energy spread to about 30 keV. For analysing the different charged particles emitted from the reactions taking place at the target a magnetic spectrograph depending on the focussing properties of an axially symmetrical field was used. The magnetic poles were semicircular of diameter 20 cm and accordingly the second order focussing was small. These poles were situated at about 120 cm from the centre of the target and the angle of acceptance of the instrument was 0.25°. The electro magnet was fed by a stabilised surrent of 12 A producing a field of 16 kOe across an air gap of 2.5 cm between the poles. This field was found to produce adequate dispersion and focus protons in the energy range of 3 to 18 MeV in a strip of width 15 mm of a photographic plate of length 30 cm. Ilford C_2 photographic emulsion of 100 μm thick was used and processed by standard methods. By examining such plates, the energy resolution was quite satisfactory since the width at half height of a single proton group was found to be less than 60 keV.

For angular distribution work, the focussing magnet was mounted so that it could be moved about an arc of a circle centred on the target and allowing exposures to be made at angles from 0° to 60°. For monitoring the exposures given at different angles, small photographic plates were placed on one side of the target at 90° to the incident deuteron beam. The experimental arrangement as well as the procedure were described in detail by Green and Middleton[6]) and El Bedewi[7]).

3. Scattered Deuterons

Elastically and inelastically scattered deuterons have been measured at different angles of observation. A typical deuteron spectrum at an angle of 57° is shown in fig. 1. Groups denoted by Cr, O and C are attributed to deuterons

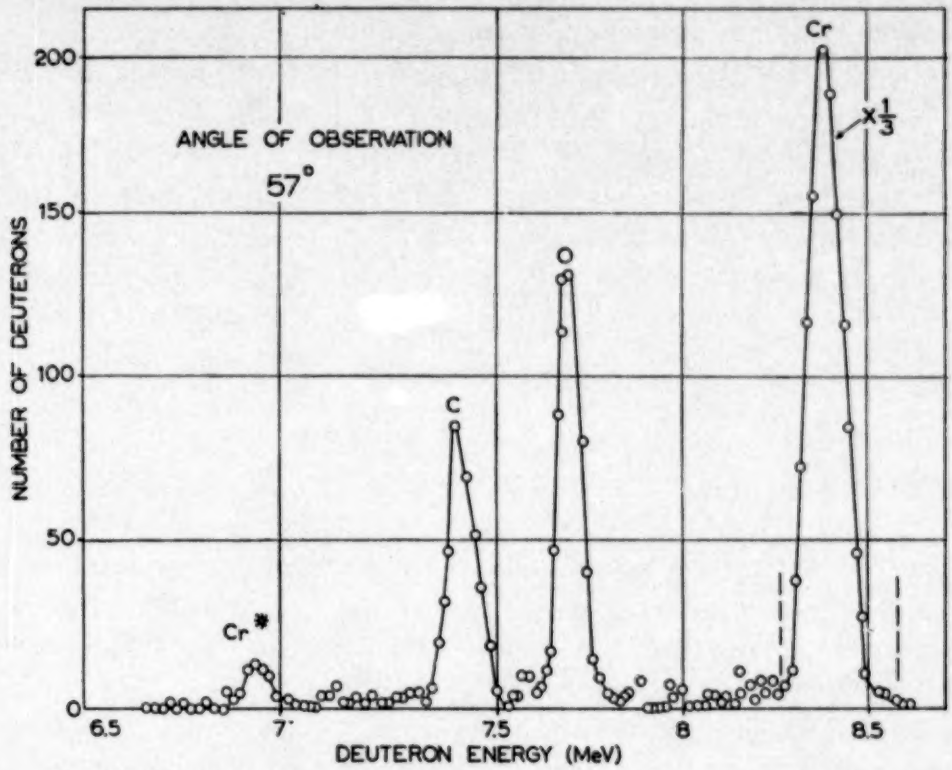

Fig. 1. Spectrum of the deuterons scattered from de deuteron bombardment of the chromium target.

elastically scattered from chromium isotopes, oxygen and carbon contaminations. From range measurement of individual tracks, the mean range of each of these groups at each angle of observation was estimated. Using the range energy curve of El Bedewi[8]), the mean energy of the incident deuterons was found to be 8.67 $\pm$ 0.02 MeV.

With regard to the weak group labelled Cr* our investigation which has been recently reported[9]) shows that it belongs to a level in Cr^{52} at 1.44 $\pm$ 0.02 MeV. The angular distribution of this group is found to be characterised by an angular momentum transfer $L = 2$ which, together with Glaubsman's rule[10]) for even nuclei, assigns an even parity and spin 2 for this level. This result is thus supporting the theoretical prediction of Lawson and Uretsky[11]).

4. Proton Energy Spectrum

A typical proton spectrum at an angle of observation of 20° is presented in fig. 2(A). Proton groups labelled by C_0, C_1, O_0 and O_1 are due to the reactions

$C^{12}(d, p)C^{13}$ and $O^{16}(d, p)O^{17}$ leaving the residual nuclei in the ground and first excited states as shown from their known Q-values and angular distributions. The remaining groups are thus attributed to the deuteron interaction with the chromium nuclei. Identification of the proper chromium isotope responsible for

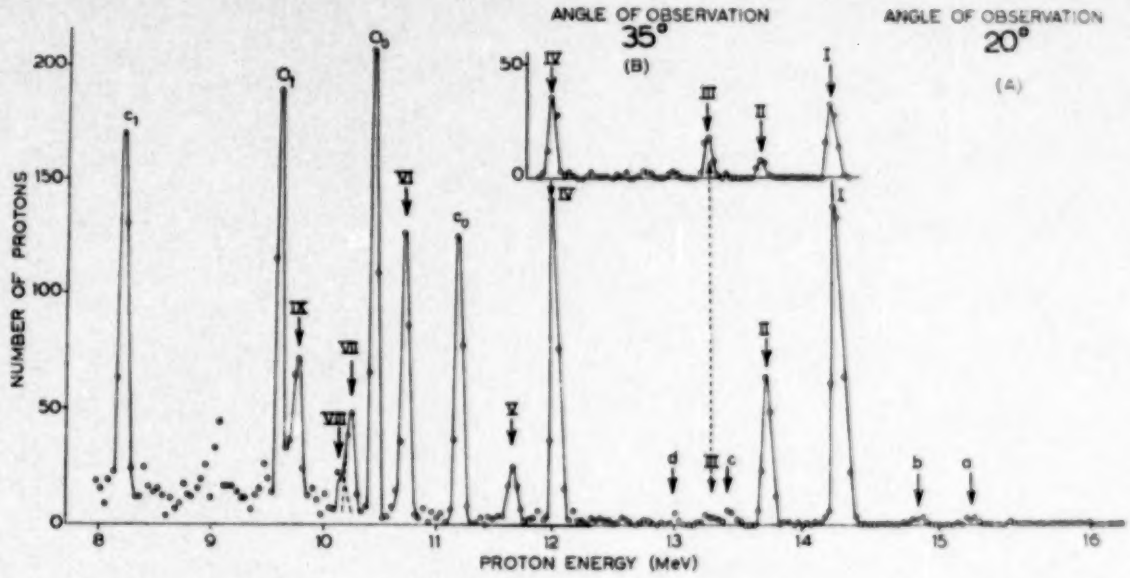

Fig. 2. Proton spectrum from the deuteron bombardment of chromium at angles of observation of 20° (A) and 35° (B).

each individual group is achieved on basis of the agreement of the Q-values calculated at different angles of observation. In general all the intense groups denoted by I, II, ..., IX are identified as arising from the interaction with the most abundant isotope Cr^{52}. Group III which appears so weak at angle 20° has a considerable intensity at angle 35° as shown in fig. 2(B). The Q-values for these groups are calculated from their positions in the spectra at the various angles of observation. The mean reaction energy Q_0 is found to be 5.73 $\pm$ 0.02 MeV in agreement with the value of 5.74 MeV given by Elwyn and Shull[4]) in their preliminary note. These authors have also observed three levels in Cr^{53} at 0.57, 0.97 and 2.31 MeV in excellent agreement with the present results, viz.: 0.57, 1.00, 2.32, 2.69, 3.62, 4.13, 4.23 and 4.64 MeV with errors of $\pm$ 0.02 MeV.

With regard to the weak groups in the high energy region of the spectrum it is difficult to find out the proper chromium isotope to which they may belong. However, assuming the second abundant isotope Cr^{53} to be responsible for their existence, the proton energy scales of the spectra at different angles of observation are transferred to the corresponding energy release Q of the reaction $Cr^{53}(d, p)Cr^{54}$. A superposition of all accepted tracks from the suspected weak groups at angles 15°, 20°, 25°, 30° and 35° reveals the existence of four well defined groups a, b, c and d as shown in fig. 3. The Q-values corresponding to these groups are found to agree with those reported by Elwyn and Shull[4])

using an enriched chromium target, as shown in table 1. In estimating the energy levels in Cr^{54} it is felt advisable to adopt the value for the reaction energy $Q_0 = 7.49 \pm 0.01$ MeV, calculated from the work of Kinsey and Bartholomew[1]) on the (n, γ) reaction. Applying this value, the transition to the ground state of Cr^{54} is represented by the weak group appearing at the arrow 0 in fig. 3.

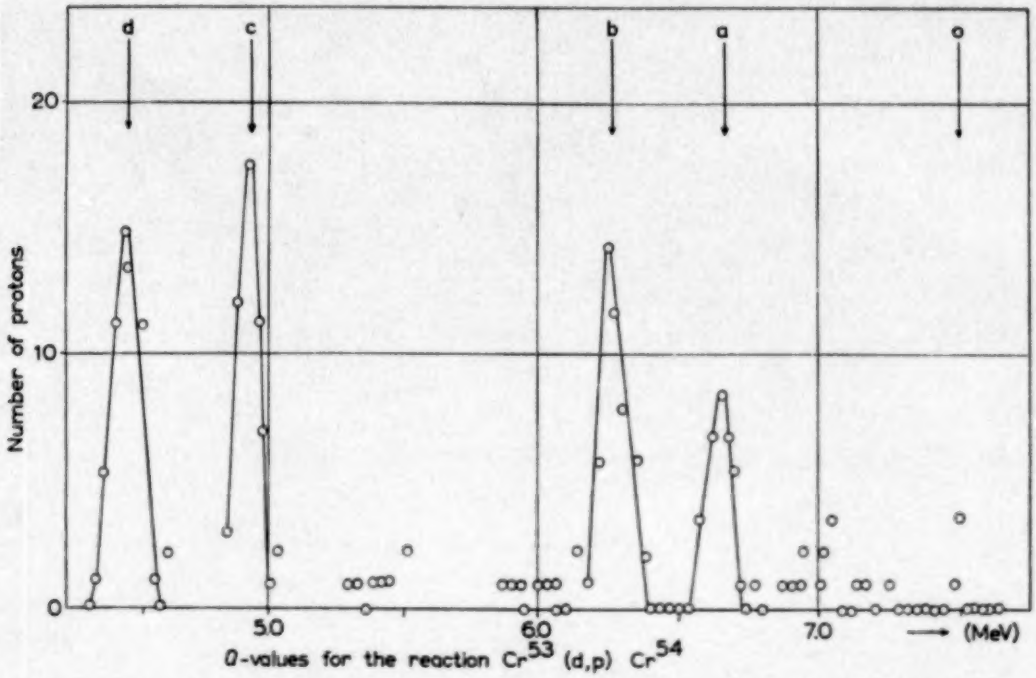

Fig. 3. Spectrum of the weak proton groups emitted from the deuteron bombardment of chromium (Superposition of the results obtained from the plates at angles of observation of 15°, 20°, 25°, 30° and 35°.

TABLE 1

Q-values for the reaction Cr^{53}(d, p)Cr^{54} at the different energy levels

Proton group	Q-values (MeV)		Level (MeV)
	Elwyn and Shull[4])	Present	
ground	7.55	(7.49 ± 0.01)	0
a	6.69	6.68 ± 0.03	0.81 ± 0.04
b	6.24	6.26 ± 0.03	1.23 ± 0.04
c	4.88	4.89 ± 0.03	2.60 ± 0.04
d	4.36	4.46 ± 0.03	3.03 ± 0.04

5. Angular Distributions of Proton Groups

The angular distributions for the proton groups corresponding to the transitions to the ground state and the five low lying levels in Cr^{53} are presented in

the centre-of-mass system as shown in fig. 4. The experimental errors are the statistical standard deviation. The theoretical curves are calculated from Butler's formula[12]) using generally a radius of interaction equal to the Gamow radius 6.25×10^{-13} cm and choosing the proper value for the orbital angular momentum l_n to give the best fit in each case. Except for the level at 1.00 MeV (III) which is found to have $l_n = 3$, all the other investigated proton groups are characterised by $l_n = 1$. The tentative results reported by Elwyn and Shull[4]) for the ground state and the three low lying levels show that their l_n-values are 1, 1, 3 and 1 respectively, in agreement with the present work. It should be pointed out that in case of the groups IV, V and VI better agreement is achieved when applying a smaller radius of interaction, viz. 5.5×10^{-13} cm. These results are consistent with those derived from the Born approximation stripping theory[13]) using a radius of interaction greater by one unit of 10^{-13} cm than that used in Butler's formula.

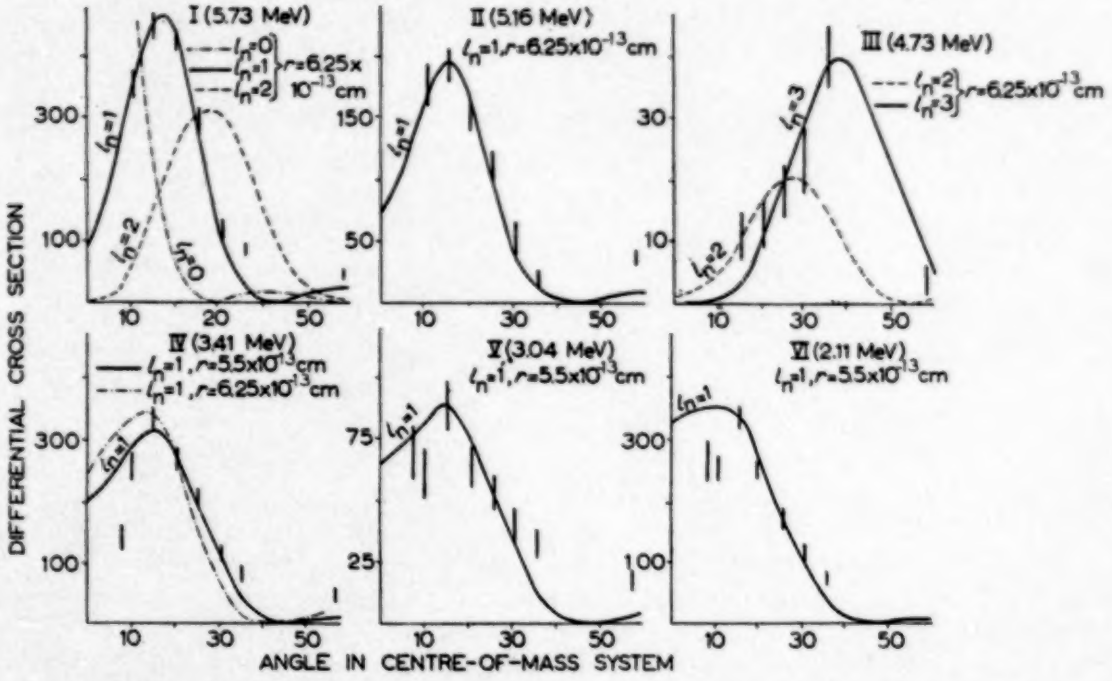

Fig. 4. Angular distribution of proton groups emitted from the reaction Cr^{52}(d, p)Cr^{53}.

The fact that the 29th neutron carries in the ground state of Cr^{53} one orbital angular momentum indicates that it is captured in the $2p_{\frac{3}{2}}$ state which seems to lie lower than the $1f_{\frac{7}{2}}$ state in the shell model. This conclusion supports our recent results in case of V^{51}(d, p)V^{52} in which we have reported[14]) similar evidence for the arrangement of these two states. Now, since the target nucleus $_{24}Cr^{52}$ contains even numbers of protons and neutrons, its ground state should have even parity and spin zero. According to selection rules, the value $l_n = 1$ indicates that the ground state of Cr^{53} should have odd parity and spin $\frac{1}{2}$ or $\frac{3}{2}$.

However, the shell model favours the latter value which agrees with the theoretical prediction of Halback[15]).

In case of the transition to the first excited state at 0.57 MeV, the value of $l_n = 1$ indicates that this state must have odd parity and spin $\frac{1}{2}$ or $\frac{3}{2}$. Wilkinson and Sheline[16]) pointed out that the relative intensities of the Cr^{52} neutron capture gamma rays (I) lead to the probability that this state in Cr^{53} is $2p_{\frac{1}{2}}$.

Also the value of $l_n = 3$ for the transition to the second excited state at 1.00 MeV indicates that this state must have odd parity and spin $\frac{5}{2}$ or $\frac{7}{2}$. The shell model rules out the latter value since the $1f_{\frac{7}{2}}$ state is supposed to be fully occupied and it is thus probable that the neutron is captured in the $1f_{\frac{5}{2}}$ state.

With regards to the remaining groups IV, V and VI corresponding to the transition to the excited states at 2.32, 2.69 and 3.62 MeV, the value of $l_n = 1$ indicates that each of these states in Cr^{53} has an odd parity and spin $\frac{1}{2}$ or $\frac{3}{2}$.

The results concerning all the energy levels observed in the present work for Cr^{53} together with their nuclear properties are summarised in table 2.

TABLE 2

Data concerning the energy levels in Cr^{53}

(1)	(2)	(3)	(4)	(5)	(6)	(7)	(8)
I	0	1	0dd	$\frac{3}{2}$	100	100	100
II	0.57	1	0dd	$\frac{1}{2}$	34	34	37
III	1.00	3	0dd	$\frac{5}{2}$	5	5	7
IV	2.32	1	0dd	$\frac{1}{2}$ or $\frac{3}{2}$	51	55	25
V	2.69	1	odd	$\frac{1}{2}$ or $\frac{3}{2}$	13	15	13
VI	3.62	1	odd	$\frac{1}{2}$ or $\frac{3}{2}$	35	40	
VII	4.13						
VIII	4.23						
IX	4.64						

(1) Group. (2) Energy level. (3) l_n-value. (4) Parity of final level. (5) Suggested spin value of the final nucleus J_B. (6) Relative neutron capture probability A. (7) Relative reduced width $\gamma^2 (2J_B + 1)$. (8) Relative intensities of gamma ray groups emitted from the neutron capturing level to the corresponding state.

6. Neutron Capture Gamma Rays

In view of the present data concerning the energy levels of Cr^{53} and Cr^{54}, information about the gamma transition between their various excited states may be derived from the experiments previously performed on neutron capture gamma rays from chromium[1-3]). Kinsey and Bartholomew[1]) investigated the high energy region and the gamma ray groups may be mainly attributed to direct transition from the capturing level to the different excited states of a nucleus. The energies and intensities of the chromium gamma rays as measured

by the authors are shown in table 3 together with some proposals on the level assignment for the chromium isotopes.

In case of Cr^{53}, these authors had assumed a value of 7.76 MeV for its neutron binding energy, as calculated from mass measurements, and accordingly it was

TABLE 3

Neutron capture gamma rays from chromium
(Results of Kinsey and Bartholomew[1]))

γ-ray group	Measurements of Kinsey and Bartholomew		Level assignment	
	Energy (MeV)	Relative intensity	Kinsey and Bartholomew	Present proposal
A	9.716 ± 0.007	7.0	Cr^{54} (ground)	
B	8.881 ± 0.007	19.0	Cr^{54} (0.835)	Cr^{54} (0.81)
C	8.499 ± 0.007	7.0	Cr^{51} (0.78)	Cr^{54} (1.23)
D	7.929 ± 0.008	8.0	Cr^{51} (1.17) or Cr^{53} (ground)	Cr^{53} (ground)
D′	7.67 ± 0.02	0.2	Cr^{51} (1.42) or Cr^{53} (ground)	
E	7.54 ± 0.02	0.2	Cr^{51} (1.53)	
F	7.364 ± 0.007	3.0		Cr^{53} (0.57)
F′	7.21 ± 0.02	0.2		
G	7.097 ± 0.006	2.6		Cr^{54} (2.60)
H	6.872 ± 0.008	0.6		Cr^{53} (1.00)
I	6.644 ± 0.006	3.0		Cr^{54} (3.03)
J	6.358 ± 0.007	0.3		
K	6.26 ± 0.02	0.9		
L	6.12 ± 0.01	0.7		
M	6.00 ± 0.01	1.0		
N	5.61 ± 0.01	2.0		Cr^{53} (2.32)
O	5.26 ± 0.02	1.0		Cr^{53} (2.69)
P	4.83 ± 0.01	0.6		
Q	3.72 ± 0.02	0.5		Cr^{53} (4.23)

uncertain to identify for the ground state transition of Cr^{53} either of the observed gamma ray groups D or D′ of energies 7.929 MeV and 7.67 MeV respectively. However, the present Q-value (5.73 MeV) for the reaction Cr^{52} (d, p)Cr^{53} implies that the neutron binding energy of Cr^{53} is 7.96 MeV. It thus follows that the gamma ray group D is attributed to the transition from the capturing level to the ground state of Cr^{53}. On this assignment, the gamma ray groups F, H, N, O and Q can be attributed to transitions from the capturing level of Cr^{53} to levels at 0.565, 1.057, 2.319, 2.669 and 4.209 MeV respectively in excellent agreement with our levels at 0.57, 1.00, 2.32, 2.69 and 4.23 MeV respectively.

With regard to energy levels in Cr^{54}, Kinsey and Bartholomew[1]) reported

that the gamma ray group A is due to direct transition from the capturing level to the ground level of Cr^{54}. With this assignment, groups B, C, G and I may thus arise from direct transitions to levels at 0.835, 1.217, 2.619 and 3.072 MeV respectively, in fair agreement with the present levels a, b, c and d at 0.81, 1.23, 2.60 and 3.03 MeV respectively. These assignments thus support our identification of the corresponding proton groups as arising from the reaction Cr^{53}(d, p)Cr^{54}. However, these authors, assuming the neutron binding energy of the isotope Cr^{51} to be 9.07 MeV, identified the gamma ray group C (8.499 MeV) as arising from a transition between the capturing level of this isotope and its first excited level at 0.78 MeV determined by Stelson *et al.*[17]) from their study on the reaction V^{51}(p, n)Cr^{51}. On this assumption the gamma ray energy for this group ought to be 8.29 MeV. It is thus obvious that our identification of this group C as arising from a transition between the capturing level of the isotope Cr^{54} and the second excited level at 1.23 MeV, which should be accompanied by gamma rays of energy 8.49 MeV, is more probable.

In addition, low energy gamma rays from the neutron capture of chromium have been measured by Braid[2]) and Reier and Shamos[3]) and their results are shown in table 4, together with their probable transitions.

TABLE 4

Results of the low energy gamma-ray groups from the neutron capture of chromium

E_γ (MeV)		Probable transition based on present result
Braid[2])	Reier and Shamos[3])	
0.52 ± 0.03		Cr^{53} $0.57 \rightarrow 0$
	0.740 ± 0.020	
0.83 ± 0.03	0.815 ± 0.016	Cr^{54} $0.81 \rightarrow 0$
	1.07 ± 0.06	Cr^{53} $1.00 \rightarrow 0$
1.84 ± 0.03		
	2.13 ± 0.05	Cr^{53} $2.69 \rightarrow 0.52$
2.28 ± 0.03		Cr^{53} $2.32 \rightarrow 0$
3.04 ± 0.03		Cr^{54} $3.03 \rightarrow 0$

In conclusion, we present in fig. 5 the energy level diagrams for the nuclei Cr^{53} and Cr^{54} with the proposed gamma ray transitions between the investigated levels. It is also of interest to point out as shown in table 2 the general similarity between the relative intensities of gamma rays emitted in the radiative neutron capture to the investigated states in Cr^{53} and the corresponding relative reduced widths and capture probabilities as derived from deuteron stripping theories.

One of the authors (F. B.) is grateful to Professor H. W. B. Skinner for his encouragement and advice during the performance of this experiment at the

Nuclear Physics Research Laboratories, Liverpool. The authors would also like to express their gratitude to Professor L. A. El Sherbini for his interest and discussion.

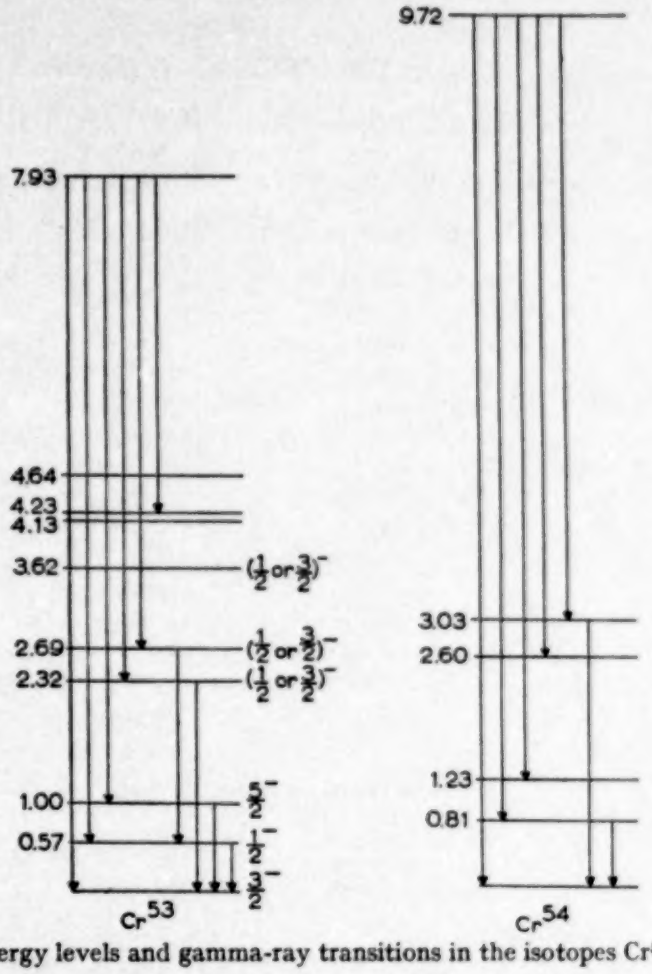

Fig. 5. Energy levels and gamma-ray transitions in the isotopes Cr^{53} and Cr^{54}.

References

1) B. B. Kinsey and G. A. Bartholomew, Phys. Rev. **89** (1953) 375
2) T. H. Braid, Phys. Rev. **102** (1956) 1109
3) M. Reier and M. H. Shamos, Phys. Rev. **100** (1955) 1302
4) A. J. Elwyn and F. B. Shull, Bull. Am. Phys. Soc. **1** (1956) 281
5) D. M. Van Patter, W. C. Porter, M. A. Rothman and C. E. Mandeville, Bull. Am. Phys. Soc. **3** (1958) 38
6) T. Green and R. Middleton, Proc. Phys. Soc. A**69** (1956) 16
7) F. A. El Bedewi, Proc. Phys. Soc. A**69** (1956) 321
8) F. A. El Bedewi, Proc. Phys. Soc. A**64** (1951) 1079
9) F. A. El Bedewi and S. Tadros, Nuclear Physics **6** (1958) 434
10) M. J. Glaubman, Phys. Rev. **90** (1953) 1000
11) R. D. Lawson and J. L. Uretsky, Phys. Rev. **106** (1957) 1369
12) S. T. Butler, Proc. Roy. Soc. A**208** (1951) 559
13) A. B. Bhatia, K. Huang, R. Huby and H. C. Newns, Phil. Mag. **43** (1952) 485
14) F. A. El Bedewi and S. Tadros, Nuclear Physics **8** (1958) 71
15) K. Halback, Helv. Phys. Acta **27** (1954) 259
16) J. R. Wilkinson and R. K. Sheline, Phys. Rev. **99** (1955) 752
17) P. H. Stelson, W. M. Preston and C. Goodman, Phys. Rev. **80** (1950) 287

2.G *Nuclear Physics* **19** (1960) 614—633; © *North-Holland Publishing Co., Amsterdam*
Not to be reproduced by photoprint or microfilm without written permission from the publisher

REACTION MECHANISM STUDIES ON $Si^{28}(d, p)Si^{29}$
(I) Distorted Wave Effects

J. A. KUEHNER, E. ALMQVIST and D. A. BROMLEY

Atomic Energy of Canada Limited, Chalk River, Ontario

Received 11 May 1960

Abstract: A study of the (p, γ) angular correlations involving the 1.28 and 2.03 MeV states in Si^{29} populated by the Si^{28}(d, p)Si^{29} reaction has been carried out for deuteron energies in the range from 6 to 9 MeV. In each case measurements were carried out in the (d, p) reaction plane with protons detected on the observed peak of the $l_n = 2$ stripping angular correlation. These data have been analysed within the framework of distorted-wave stripping formalism. The measurements on the 2.03-MeV state alone enable the statistical tensors for the reaction to be determined for each incident deuteron energy. These statistical tensors were then used to compute the angular correlation of the 1.28-MeV radiation, yielding results in good agreement with the experimental measurements and thus supporting the expectation that the matrix elements are essentially independent of the detailed nuclear structure of the final state. The statistical tensors have also been used to predict the general (p, γ) angular correlation function over the sphere as well as the magnitude of the proton polarization for the Si^{29*}-proton systems involving both the 1.28 MeV and 2.03 MeV excited states.

1. Introduction

The plane wave theory of stripping[1]) makes unique predictions about the form of both the angular distribution of protons from a (d, p) reaction and the angular correlation between protons leading to the formation of a given residual state and the gamma radiation de-exciting this state. The qualitative success of these predictions has encouraged attempts to improve on the simple theory by the use of distorted waves for the deuteron and the emergent particle[2]); with this approach it is possible to account for deviations from the plane wave predictions of the (d, p) differential cross sections and (d, pγ) angular correlations as well as to provide a mechanism by which the emergent protons may be polarized. The study of such deviations from the plane wave predictions can throw light on the nature of the reaction mechanism and provides a test of the validity of the distorted wave stripping theory.

The distorted wave stripping formalism can lead to two types of predictions; (i) those which are obtained for particular reactions by laborious numerical computations using an assumed distortion, such as have been carried out by Tobocman[3]) and (ii) more generally applicable theories such as discussed by Huby, Refai and Satchler[4]). The latter authors show that the distorted wave stripping assumptions result in relations among the (d, pγ) angular correlation coefficients and the spin polarization of the emergent protons which are not

dependent on the details of the distortion. This paper reports measurements which were made as part of a program undertaken to test the second, more general, consequences of the distorted wave stripping formalism and, in particular, to determine whether this gives an adequate description of the Si^{28}(d, pγ)Si^{29*} (2.03 MeV) and Si^{29*} (1.28 MeV) reactions.

Further measurements bearing upon the mechanism for the Si^{28}(d, p)Si^{29} reaction[5]), including measurements of differential and total excitation functions and of the proton angular distributions, will be reported in a companion paper in the near future. These measurements have demonstrated a dominant direct interaction amplitude, with, however, a small residual compound system amplitude reflected in interference terms in the cross section. In the present measurements the effects of the interfering compound system amplitude were minimized by the location of the proton counter on the peak of the stripping angular distribution. The distorted wave analysis reported herein is, of course, strictly valid only if the compound system effects are negligible.

The reaction Si^{28}(d, pγ)Si^{29} was selected as particularly suited to these measurements since it permits the study of two d-wave neutron capture situations, with $j = l_n \pm \frac{1}{2}$[6,7]) and essentially identical kinematics. In the $j = l_n + \frac{1}{2}$ case (2..03 MeV) the de-excitation gamma radiation is a pure E2 multipole[7]) to the spin $\frac{1}{2}$ ground state of Si^{29} so that, for a zero spin target, as in this case, the correlation is unique for plane wave stripping. In the $j = l_n - \frac{1}{2}$ case (1.28 MeV) an E2/M1 mixture is involved; however, since this amplitude mixture has been determined previously[8]) as 0.21 ± 0.03 a unique correlation prediction is again possible for plane wave stripping.

If no assumptions are made about the reaction mechanism it can be shown that in general the angular correlation between the gamma rays and the emitted protons from a (d, pγ) reaction involving an E2 transition, such as that involving the 2.03 MeV state of Si^{29}, requires eight independent theoretical parameters, apart from normalization of intensity, to describe it. The distorted wave stripping assumptions introduce relations among the parameters which reduce the number of independent parameters to four, while the Butler plane wave assumptions uniquely define the parameters, except for normalization, and thus lead to unique predictions for the correlations.

For the above reaction involving E2 de-excitation radiation the general form of the angular correlation in the reaction plane ($\theta = \frac{1}{2}\pi$ with the z-axis taken along $\boldsymbol{k}_d \times \boldsymbol{k}_p$) is

$$W(\tfrac{1}{2}\pi, \phi) = \sum A_n \cos n\,(\phi - \alpha_{nn}) \qquad (1)$$

with $n = 0, 2, 4$. This expression is independent of the reaction mechanism. A measurement of the correlation yields four experimentally determined constants, A_2/A_0, A_4/A_0, α_{22} and α_{44}. Thus sufficient data are available to obtain the four independent theoretical parameters appearing in the distorted

wave stripping theory and hence the statistical tensors[4]) which describe the final system in this formalism. Once determined, these statistical tensors allow unique predictions to be made of the general angular correlation over the entire sphere as well as of the magnitude of the proton spin polarization. Consequently measurements of these quantities provide experimental tests of the distorted wave theory.

The angular correlation data for the 2.03 MeV radiation has been analysed in the manner outlined above using the distorted wave formalism of ref. [4]) to obtain the statistical tensors as functions of the deuteron energy in the range 6.1 to 9.0 MeV. This analysis is described in detail in subsection 4.1. To the extent that the stripping reaction matrix elements are independent of the final state one expects that the same statistical tensors will apply equally well to the correlation of the radiation from the 1.28 MeV state. This expectation is tested by the comparison made between the computed and measured correlations for the 1.28 MeV radiation in subsection 4.2.

It should be noted that the analysis described herein is not possible if the correlation described by equation (1) has only the first two terms, as will be the case for reactions either to states of spin $\leqq \frac{3}{2}$ or involving neutron capture into s or p-states. In these cases (as illustrated by the 1.28 MeV case reported) the correlation measurements in the reaction plane alone do not suffice to determine the statistical tensors and must be supplemented by correlation measurements out of the reaction plane or by proton polarization measurements. These restrictions have applied to almost all previously reported (d, pγ) correlation measurements.

Correlation measurements have been reported previously on the Be^{9}(d, pγ) Be^{10} [9, 10]), B^{10}(d, pγ)B^{11} [9]), C^{12}(d, pγ)C^{13} [11]), Mg^{24}(d, pγ)Mg^{25} [9, 12]), Si^{28}(d, pγ) Si^{29} [13, 14]) and Ca^{40}(d, pγ)Ca^{41} [14]) reactions. In general the correlation data obtained have not deviated appreciably from the plane wave stripping predictions. Detailed distorted wave analyses of these data have not been presented†; in almost all cases, for the reasons noted previously, such analyses would require additional experimental data on proton polarizations or azimuthal correlations.

Preliminary reports of some of the results reported here in detail have been presented previously[15, 16]).

2. Apparatus

Figure 1 is a scale diagram of the experimental arrangement. The scattering chamber used a 25 μm Ti window (9°–120°), which permitted detection of protons outside the vacuum system, and a 0.16 cm brass wall (189°–351°) to allow simultaneous detection of gamma radiation from the reaction under study. The height of the Ti window was 4.44 cm and of the thin brass wall 8.89 cm.

† *Note added in proof*: Distorted-wave analysis of Mg^{24} (d, pγ) Mg^{25} data by Martin and Quisenberry (private communication)[12]) shows significant deviations from plane-wave stripping.

A system of four 0.32 cm diam. gold apertures served to define the deuteron beam on target; following traversal of the target the beam was allowed to pass through the chamber to a shielded beam catcher 7.5 m away. A 0.03 cm lead hood which partially surrounded the target, and lead lining of the chamber walls, helped to reduce the background reactions caused by scattered deuterons.

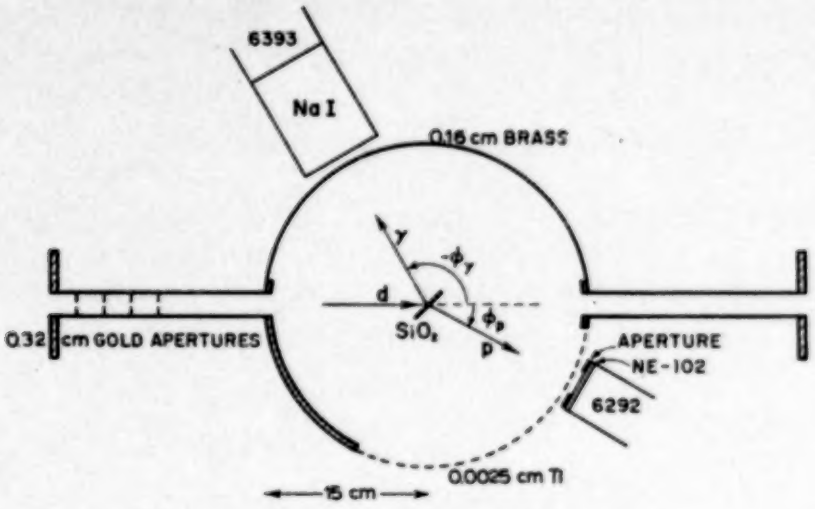

Fig. 1. Schematic arrangement of apparatus.

The gamma radiation was detected in a 7.6 cm by 7.6 cm NaI crystal whose front face was 16 cm from the target. The proton counter was a Nuclear Enterprizes NE-102 plastic scintillator with a thickness of 0.32 cm and an aperture of 3.2 cm. The aperture to target distance of 16 cm gave a half angle of acceptance of 5.7°. Sufficient absorber was used in front of the proton counter to stop scattered deuterons and, where necessary, to increase the apparent energy separation of the proton groups from the (d, p) reaction.

The chief limitation to the rate at which coincidence data could be accumulated was the very high total counting rate in the gamma-ray channel. The beam intensity on the target was adjusted to give the maximum counting rate that would be reliably handled by the electronic circuitry, which consisted of conventional fast-slow circuitry with incorporated provision for self-gate measurements[17]). A coincidence resolving time of $2\tau = 4 \times 10^{-8}$ s was used. The counting rate in the particle detector was not excessive and as large a geometric efficiency as possible consistent with good angular resolution was used. When running with the proton detector set on the stripping peak a real-to-chance coincidence ratio of about four was obtained. At angles other than on this peak the real coincidence rate drops making measurements considerably more difficult; no reliable data were obtained at these angles.

The targets† employed were sections of quartz bubbles (SiO_2) ranging in thickness from 5 to 25 μm. These thicknesses correspond roughly to 120 keV

† The authors are indebted to Mr. R. C. Bailey for preparation of the targets.

to 600 keV for 8 MeV deuterons. The SiO_2 flakes were mounted on metal frames and were inserted into the chamber through a vacuum lock.

Dual linear electronic channels were used allowing simultaneous setting of voltage gates on the proton groups leading to both the 1.28 MeV and the 2.03 MeV states of Si^{29}. After satisfying the requirements of particle pulse height and time coincidence the linear signal from the NaI crystal was fed into the appropriate one of two 100-channel analysers.

3. Experimental Results

Figure 2(a) is a typical proton spectrum, obtained at 35° to the deuteron beam and for a deuteron energy of 8 MeV. The shaded portions of the spectrum represent typical regions of pulse height used to open the gate circuits allowing pulse height analysis of the coincident gamma-ray spectra. The spectra of

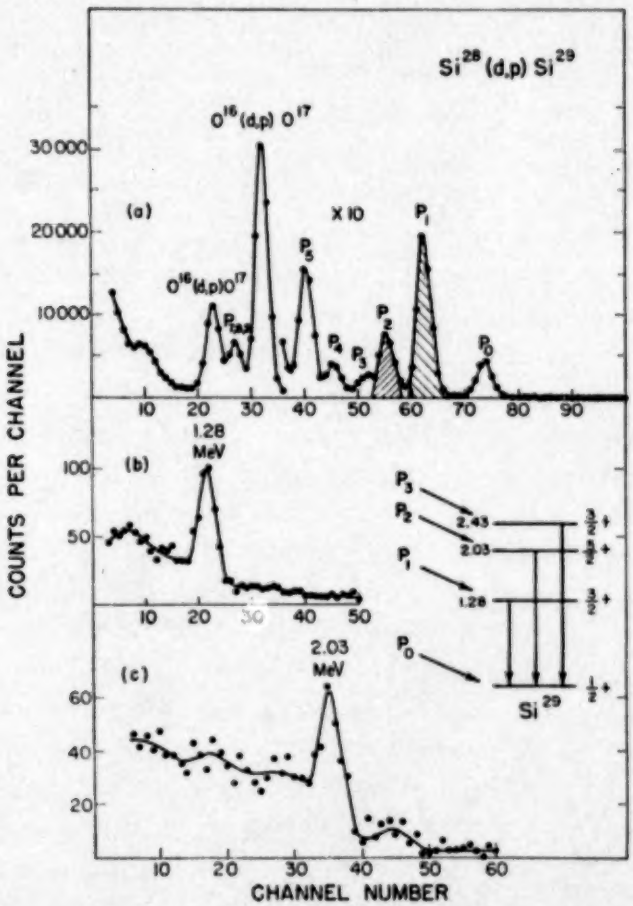

Fig. 2. Proton and coincident gamma-ray spectra from the Si^{28}(d, pγ)Si^{29} reaction at $E_d = 8.0$ MeV. (a) is a direct proton spectrum at $\phi_p = 35°$; typical voltage gates set on proton groups to the states in Si^{29} at 1.28 MeV (P_1) and 2.03 MeV (P_2) are superposed on this spectrum. Typical spectra of gamma radiation, at $\phi_\gamma = -90°$, coincident with the proton groups P_1 and P_2 are shown in (b) and (c), respectively. The inset level diagram shows the levels of Si^{29} involved, their spins and parities, and the relevant transitions.

gamma radiation at 90° gated by the proton groups P_1 and P_2 are shown in figs. 2(b) and 2(c) respectively. The inset level diagram shows the levels of Si^{29} involved, their spins and parities, and the relevant transitions.

Measurements made with a delay inserted between one detector and the coincidence circuit, to eliminate the events in true time coincidence, demonstrated that the pulses larger than those due to the 1.28 MeV total ab-

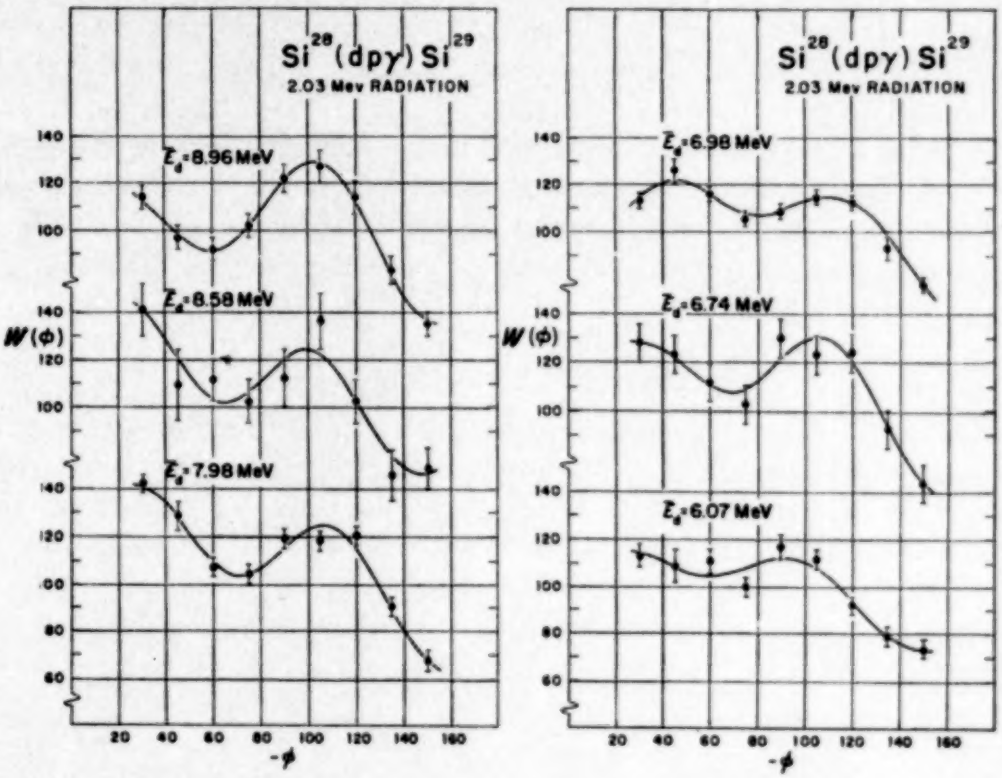

Fig. 3. Proton-gamma angular correlations in the de-excitation of the 2.03 MeV state in Si^{29}, measured in the reaction plane with the proton detector set in each case on the observed peak of the $l_n = 2$ stripping angular distribution. The angle ϕ is defined geometrically in fig. 1 and is measured with respect to a right handed coordinate system with z-axis directed along $\boldsymbol{k}_d \times \boldsymbol{k}_p$ and x-axis directed along $\boldsymbol{k}_d$. Values of the deuteron energy used are indicated in the figure.

sorption peak in fig. 2(b) were due to random events. Similar measurements, made periodically throughout the course of the experiment, were used to enable a correction to be made for these random events. In the case of the radiation coincident with P_2 an additional small correction was required to compensate for a small contribution from the state at 2.43 MeV in Si^{29}. This resulted from energy resolution inadequate to completely resolve the proton groups P_2 and P_3, with the result that a small fraction of the protons feeding the 2.43 MeV state were included in the voltage window set on the P_2 group.

Fig. 3 contains the angular correlation data obtained for the 2.03 MeV radiation measured at six different average deuteron energies. In this figure,

as elsewhere, the symbol $\bar{E}_d$ is used to denote the average deuteron energy as the beam passed through the target. $\bar{E}_d$ is obtained from

$$\bar{E}_d = E_d - \tfrac{1}{2}t\,, \tag{2}$$

where E_d is the initial deuteron energy and t is the energy loss in the target for deuterons of the energy being used. This energy loss was $\approx$ 120 keV for deuterons for all measurements except those made with $\bar{E}_d = 6.74$ MeV, in which case the target used was $\approx$ 600 keV thick. The data in fig. 3 represent the average of at least three complete sets of data measured for each value of incident deuteron energy.

In the analysis of the data discussed in the following section it was found convenient to express the angular correlation functions in a coordinate system with the z-axis along $\boldsymbol{k}_d \times \boldsymbol{k}_p$. For the sake of definiteness the x-axis has been chosen along the deuteron beam direction. The data are then reduced to an angular correlation function

$$W(\tfrac{1}{2}\pi, \phi) = \sum A_n \cos n\,(\phi - \alpha_{nn})\,, \tag{3}$$

with $n = 0, 2, 4$. Least squares adjusted fits of this function to the experimental data are included in fig. 3. Values of the parameters of the correlation function are listed in table 1. For comparison the plane wave predicted values are included in the last row.

TABLE 1

Parameters in the expansion $W(\frac{1}{2}\pi, \phi) = \sum A_n \cos n(\phi - \alpha_{n,n})$ for the 2.03 MeV radiation ($n = 0, 2, 4$)

$\bar{E}_d$	A_2/A_0	A_4/A_0	$-\alpha_{22}$ (deg.)	$-\alpha_{44}$ (deg.)
6.07	0.16 ± 0.03	-0.12 ± 0.03	56 ± 9	59 ± 5
6.74	0.20 ± 0.05	-0.22 ± 0.03	70 ± 7	69 ± 4
6.98	0.22 ± 0.03	-0.16 ± 0.03	74 ± 3	79 ± 2
7.98	0.19 ± 0.02	-0.24 ± 0.02	57 ± 5	68 ± 2
8.56	0.18 ± 0.04	-0.24 ± 0.05	40 ± 12	60 ± 4
8.96	0.18 ± 0.04	-0.26 ± 0.02	75 ± 4	62 ± 2
Plane wave Theory	0.24	-0.29	58 — 62 [a]	58 — 62 [a]

[a] The plane wave theory predicts symmetry about the nuclear recoil axis. This axis varies from 62° for $E_d = 6$ MeV to 58° for $E_d = 9$ MeV.

From these data it should be noted that: (i) the parameters of the function do not show large fluctuations over the energy range studied and (ii) the values of the parameters are not markedly different from the plane wave values at the higher incident energies studied, but deviate from these with decreasing in-

cident energy. These observations are in accord with the assumption of a dominant direct interaction and suggest an analysis as a distorted wave stripping process. More detailed measurements on the differential and total excitation functions for these reactions and on the angular distributions of the proton groups have been analyzed to give a limit of less than 30 % to the compound system intensity in this reaction. These data will be presented in a forthcoming publication[5]).

Figure 4 contains the corresponding angular correlation data obtained for the 1.28 MeV radiation. In this case no measurement was made for $\bar{E}_d = 6.74$ MeV. With this one exception these data were measured simultaneously with the corresponding five sets of data for the 2.03 MeV radiation.

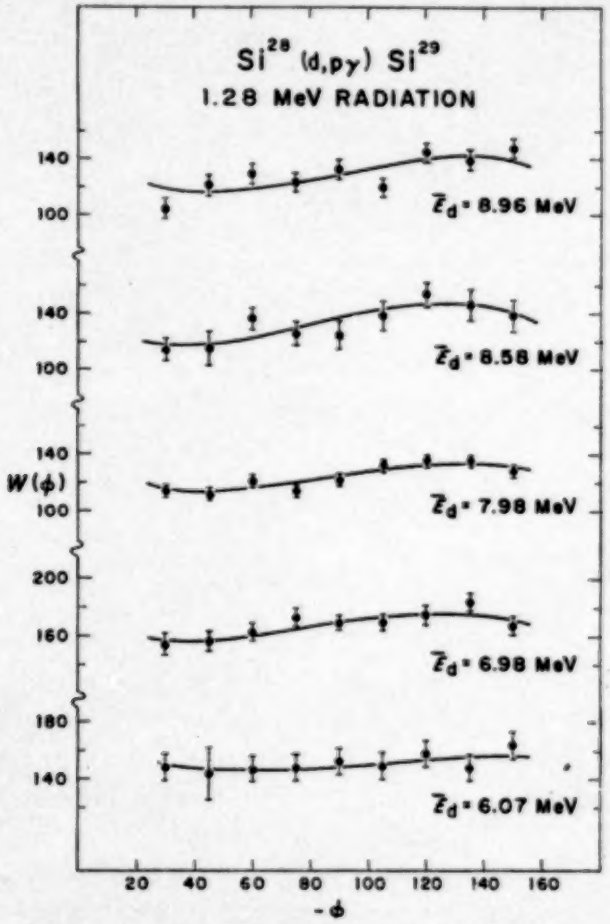

Fig. 4. Proton-gamma angular correlations in the de-excitation of the 1.28 MeV state in Si^{29}. The geometry used is identical to that described in the caption of fig. 3.

In this case the angular correlation function is limited to terms in $n = 0$ and 2 by the $\frac{3}{2}$ spin of the 1.28 MeV state in Si^{29}. The least squares adjusted fits are included in the figure and the corresponding parameters are listed in

table 2. Again, the last row gives the plane wave predicted values. Since the 1.28 MeV radiation is a mixed multipole the predicted value reflects any uncertainty in the mixture ratio. The experimental E2/M1 multipole amplitude

TABLE 2

Parameters in the expansion $W(\frac{1}{2}\pi, \phi) = \sum B_n \cos n(\phi - \alpha_{n,n})$ for the 1.28 MeV radiation ($n = 0, 2$)

$\bar{E}_d$	B_2/B_0	$-\alpha_{22}$ (deg.)
6.07	-0.035 ± 0.015	61 ± 16
6.98	-0.060 ± 0.015	31 ± 10
7.98	-0.084 ± 0.013	41 ± 8
8.58	-0.110 ± 0.029	35 ± 10
8.96	-0.097 ± 0.032	43 ± 13
Plane Wave Theory	-0.085 ± 0.037 [a]	61 — 65 [b]

[a] The error in the plane wave prediction arises from the uncertainty in the E2/M1 multipole mixture ratio.

[b] The plane wave theory predicts symmetry about the nuclear recoil axis. This axis varies from 65° for $\bar{E}_d = 6$ MeV to 61° for $\bar{E}_d = 9$ MeV.

ratio[8]) of 0.21 ± 0.03 has been used in calculating the plane wave parameters listed. The conclusions itemized for the angular correlation of the 2.03 MeV radiation apply equally well to the data for the 1.28 MeV radiation. Thus, again, an analysis in terms of distorted wave stripping suggests itself.

4. Discussion

4.1. THE STATISTICAL TENSORS

As noted previously, the similarity of the angular correlation data with the predictions of simple stripping and the relatively slow changes of the correlation function parameters suggest the feasibility of an analysis of the data in terms of a distorted wave stripping process. In this subsection such an analysis is presented for the 2.03 MeV data using the theoretical framework of distorted wave stripping considered by Huby *et al.*[4]) and expressing the data in terms of the statistical tensors for the final system. In the subsections to follow the consistency of the analysis is examined and further predictions are made.

Using the formalism and notational conventions of ref. [4]) it is possible to write the amplitude for an A(d, p)B stripping reaction as

$$I = \sum_{j,\mu_j,l,m,\mu_n} (J_A j M_A \mu_j \mid J_B M_B)\, (l\tfrac{1}{2} m \mu_n \mid j \mu_j) \times (\tfrac{1}{2}\tfrac{1}{2}\mu_p \mu_n \mid 1\, \mu_d)\, (2l+1)^{\frac{1}{2}}\, \theta_{jl} B_{lm}\,, \tag{4}$$

where the matrix elements are given by

$$B_{lm} = (2l + 1)^{-\frac{1}{2}} \int \{ \psi_p [u_l i^l Y_l^m]_n \}^* V_{np} \psi_d \, d\tau \tag{5}$$

and θ_{jl} is a "reduced width amplitude", which contains the main nuclear structure information. The subscripts A, B, n, p and d refer to the initial and final nuclei, the neutron, the proton and the deuteron, respectively; u_l is the radial wave function for the captured neutron. All observables in the reaction are parametrized by the θ_{jl}'s and the matrix elements B_{lm}. The B_{lm}'s are essentially independent of the nuclear structure, which enters them only through the u_l[4]). This relative insensitivity of the B_{lm}'s to the details of the structure of the final state permits the comparison of experimental data for reactions proceeding to different levels in the same or neighbouring nuclei, provided they have the same orbital momentum transfer and provided the cases are similar kinematically[4]). This assumption, that the u_l are independent of the $j = l \pm \frac{1}{2}$ of the captured neutron, is characteristic of the stripping analysis. Such a comparison is presented in this paper for the two Si^{28}(d, pγ) reactions proceeding via the levels of Si^{29} at 1.28 MeV and 2.03 MeV.

The distorted wave formalism is most conveniently parametrized by the statistical tensors for the reaction defined in the usual way as

$$\rho_{kq}(ll') = \sum_{mm'} (-1)^{l'-m'} (ll'm - m' \mid kq) \, B_{lm} B^*_{l'm'}. \tag{6}$$

With the z-axis chosen, as previously noted, along $k_d \times k_p$, the general requirement that the correlations exhibit symmetry relative to the reaction plane implies that all B_{lm} vanish when $l - m$ is odd. Consequently, in the case of d-wave capture as considered herein, the only non-zero matrix elements are B_{22}, B_{20} and $B_{2,-2}$. Since these are, in general, complex, a total of six real theoretical parameters is involved in the formalism. The normalization in magnitude and phase cannot affect the physical observables predicted and is thus arbitrary. Such normalization reduces the number of free parameters to 4 and implies the existence of functional relationships involving the 9 statistical tensors defined, for $l = 2$, by equation (6).

It should be noted that in the general correlation formalism, where no assumptions are included regarding the reaction mechanism, these relationships do not necessarily exist and a total of 8 theoretical parameters (tensor ratios of the form ρ_{kq}/ρ_{00}) are required to describe the system. The distorted wave formalism as involved here reduces this number of independent parameters to 4; the plane wave formalism reduces it further to zero.

The important point to note is that these 4 parameters appearing in the distorted wave formalism are, in principle, uniquely determinable from a single correlation measurement in the reaction plane since, as shown in equation (3), there are 4 experimentally determinable parameters in the correlation expansion.

In order to carry out this analysis it is convenient to use the normalized tensors[18])

$$d_{kq}(ll') = \rho_{kq}(ll') \{ (-1)^l (ll'00 \mid k0) (2l+1)^{\frac{1}{2}} \rho_{00}(ll') \}^{-1} . \tag{7}$$

The general angular correlation, for the reaction $J_A(j_n l_n) J_B(L) J_C$ and for the axes specified, is given by

$$W(\theta,\phi) = \sum_k g_k \left\{ d_{k0} P_k(\theta) + 2 \sum_{q>0} (-1)^q \left(\frac{(k-q)!}{(k+q)!} \right)^{\frac{1}{2}} P_k^q(\theta) \times \mid d_{kq} \mid \cos q(\phi - \alpha_{kq}) \right\} , \tag{8}$$

where

$$g_k = \eta_k(j_n j_n J_A J_B) \, F_k(L J_C J_B) \tag{9}$$

contains the dependence upon the angular momenta involved in the reaction. The parameter

$$\eta_k(abcd) = \hat{a}\hat{b}\hat{d} \, (-1)^{c-a-\frac{1}{2}} (ka0\tfrac{1}{2} \mid b - \tfrac{1}{2}) \, W(ddab;kc) \tag{10}$$

has been tabulated for low values of the quantum numbers by Satchler[19]) while the radiation parameters $F_k(abc)$ have been extensively tabulated by Biedenharn and Rose[20]).

The phase angles α_{kq} appearing in equation (8) are defined by

$$d_{kq} = \mid d_{kq} \mid e^{-iq\alpha_{kq}} . \tag{11}$$

It follows directly from equations (8) to (11) that a simple rotation of the correlation axis from the recoil direction (i.e. a single α_{kq}) is predicted only if one of l, J_B or L is less than 2. For $l = 2$ it can be simply shown that while $\alpha_{42} = \alpha_{22} + \frac{1}{2}\pi$, α_{44} is not related in any simple fashion and consequently no simple correlation rotation is expected, nor is any simple symmetry axis predicted for the reaction plane correlation.

From the definition (equation 7) and the relations[4]) between the ρ_{kq} it follows that

$$d_{42} = -\sqrt{\tfrac{5}{12}} \, d_{22} , \qquad d_{40} = \tfrac{7}{12} + \tfrac{5}{12} \, d_{20} . \tag{12}$$

In addition to the relations quoted in ref. [4]) it can be shown that

$$\tfrac{72}{35}(1 + d_{20}) \mid d_{44} \mid^2 - 2\sqrt{\tfrac{72}{35}} \mid d_{22} \mid^2 \mid d_{44} \mid \cos 4(\alpha_{22} - \alpha_{44}) - \tfrac{1}{4}(1 - d_{20})(1 - d_{20}^2) - (1 - d_{20}) \mid d_{22} \mid^2 = 0 . \tag{13}$$

In the correlation involving the 2.03 MeV state ($l_n = 2$; $j_n = \frac{5}{2}$), the coefficients are expressible in terms of the normalized tensors as

$$\frac{A_2}{A_0} = \mid d_{22} \mid (2.13 - 0.915 \, d_{20})^{-1} , \tag{14}$$

$$\frac{A_4}{A_0} = |\, d_{44} \,| \, (1.46 - 0.626\, d_{20})^{-1} \,. \tag{15}$$

Combination of equations (13) to (15), using the experimentally determined coefficient ratios as listed in table 1, results in a cubic equation in d_{20}.

Determination of the roots of this cubic equation for each deuteron energy studied leads to values of d_{20} and to the corresponding values of ρ_{20}/ρ_{00} plotted in fig. 5. The errors shown reflect the uncertainties in the least squares adjusted values of the correlation coefficient ratios and shift angles. For $E_d \leqq 7$ MeV there are two roots of possible physical significance, hence two sets of statistical tensors. For identification purposes these are labelled case 1 (open circles) and case 2 (closed circles). Data presented later, for the angular correlation of the 1.28 MeV radiation, strongly suggest that the case 2 root is extraneous, but since the argument depends on a further assumption, namely, that the statistical tensors apply equally well to both the 1.28 MeV and the 2.03 MeV data, both cases are retained here. For comparison purposes the plane wave value of ρ_{20}/ρ_{00} is included as a dashed line in fig. 5.

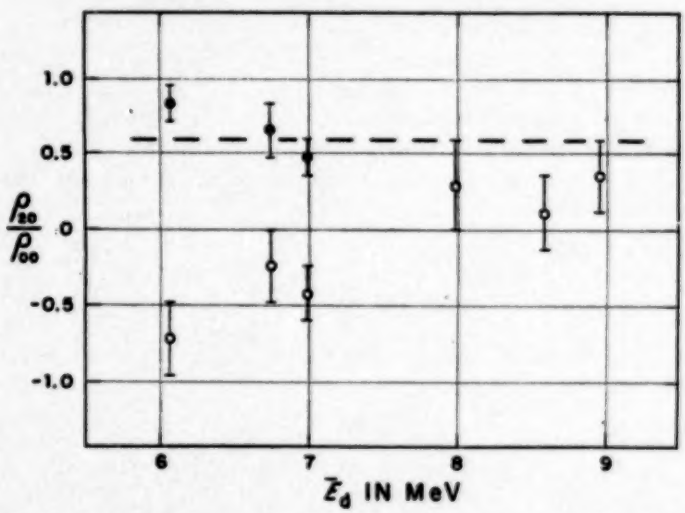

Fig. 5. Values of the statistical tensor ratios ρ_{20}/ρ_{00} obtained from the angular correlation data for the reaction Si^{28}(d, pγ)Si^{29} (2.03 MeV), are shown as a function of the incident deuteron energy. For $\bar{E}_d \leqq 7$ MeV two sets of statistical tensors of possible physical significance arise from the solution of a cubic equation for ρ_{20}/ρ_{00}. These are identified as case 1 (open circles) and case 2 (closed circles). The corresponding plane wave prediction is shown as the dashed line. In this and succeeding figures the errors shown reflect the uncertainties in the least squares adjusted values of the correlation coefficient ratios and shift angles.

Values of $|\, \rho_{22}/\rho_{00} \,|$ and $|\, \rho_{44}/\rho_{00} \,|$ are computed in a straightforward manner from equations (7), (14) and (15). The values obtained are plotted in figs. 6(a) and 6(b) respectively. Again the open circles denote case 1 and the closed circles denote case 2. The plane wave prediction is shown in each case as a dashed line.

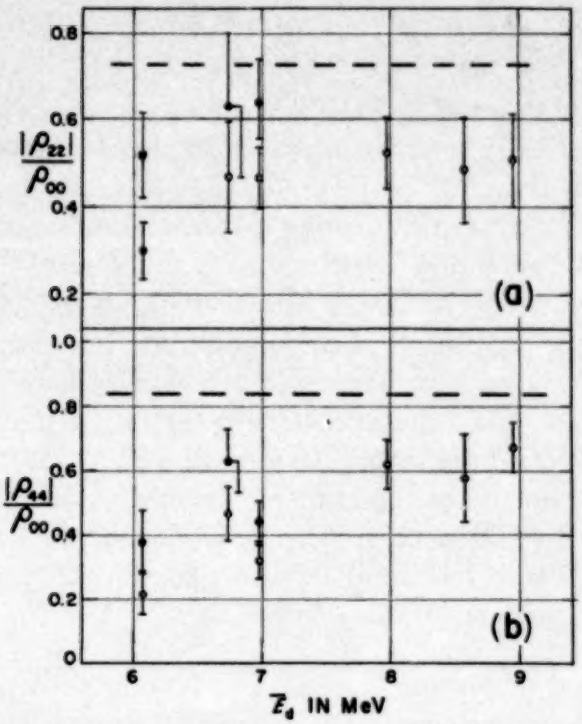

Fig. 6. Values of the statistical tensor ratios, $|\rho_{22}|/\rho_{00}$ and $|\rho_{44}|/\rho_{00}$, obtained from the angular correlation data for the reaction $Si^{28}(d, p\gamma)Si^{29}$ (2.03 MeV), are shown in (a) and (b), respectively, as functions of the incident deuteron energy. Both sets of tensor ratios, case 1 (open circles) and case 2 (closed circles), are included. The plane wave predictions are shown as dashed lines.

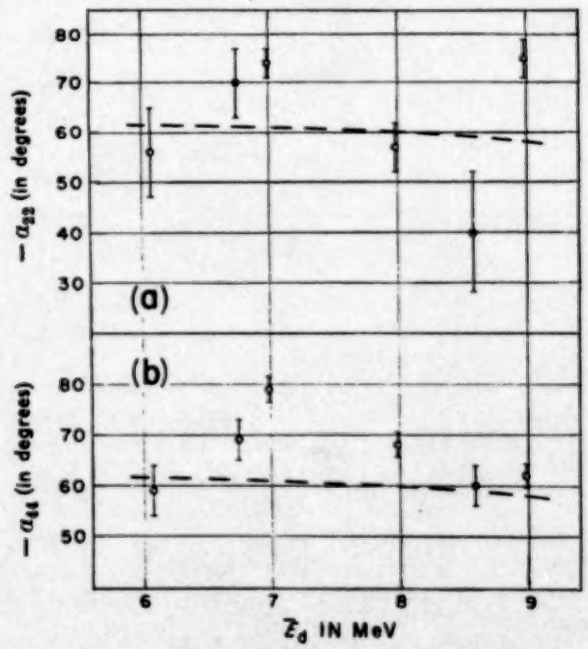

Fig. 7. The statistical tensor phase angles α_{22} and α_{44} are shown in (a) and (b) as functions of the incident deuteron energy. The plane wave prediction, which coincides with the nuclear recoil axis for each case, is included as a dashed line.

The phase angles α_{22} and α_{44} are plotted in figs. 7(a) and 7(b) respectively. Again, the plane wave prediction, which is the nuclear recoil angle for each case, is included as a dashed line. The tendency of the α_{22} to oscillate about the plane wave prediction as the energy is changed is suggestive of the oscillation found relative to the recoil axis as the proton angle is changed in the theoretical calculations of Tobocman and Satchler[18]).

The data of figs. 5, 6 and 7 constitute a complete set of statistical tensors obtained at each incident energy using the angular correlation data for the 2.03 MeV radiation measured in the reaction plane. Having obtained these tensors it is possible to compute the general azimuthal angular correlation as well as the polarization (to within a sign) for the protons detected on the stripping peak. The results of such computations are given in a later section. First, however, it is of interest to use these tensors to calculate the correlation parameters for the reaction via the 1.28 MeV state. To the extent that these calculations agree with the experimental correlation data they may be interpreted as supporting the assumption that the matrix elements are indeed independent of the detailed structure and total angular momentum of the final nuclear state.

4.2. 1.28 MeV CORRELATION

In this subsection the consistency of the analysis in terms of the distorted wave parameters is considered; the available experimental data overdetermine the relations if the 1.28 MeV angular correlation measurements are included. In addition to supporting the applicability of this analysis to the data, these comparisons verify the assumption that the statistical tensors are insensitive to the details of the nuclear state.

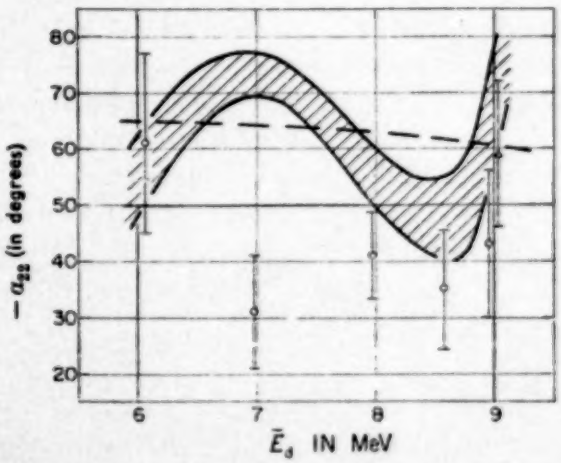

Fig. 8. The α_{22} phase predicted for the 1.28 MeV case, using the reaction tensors obtained from the 2.03 MeV de-excitation, on the assumption that the reaction tensors are independent of the $j = l \pm \frac{1}{2}$ of the final state involved, is shown as a band; the plane wave prediction is shown as a dashed line. Values of α_{22}, determined experimentally for the Si^{28}(d, pγ)Si^{29} (1.28 MeV) reaction, are shown as data points. The triangular point is from ref. [13]).

The angular correlation function, equation (8), for the case of the 1.28 MeV radiation in the reaction plane, is limited by the $\frac{3}{2}$ spin of the intermediate state to

$$W(\tfrac{1}{2}\pi,\phi) = B_0 + B_2 \cos 2\,(\phi - \alpha_{22})\,. \tag{16}$$

Fig. 8 shows the α_{22} phase predicted for the 1.28 MeV case as a band, the plane wave limit as a dashed line, and the measured α_{22}. The second measurement at 9 MeV was reported previously by Allen *et al.*[13]). In this case, the predicted value is obtained immediately as the measured α_{22} phase for the 2.03 MeV case.

The agreement is seen to be satisfactory for all cases except that at 7 MeV. This discrepancy may reflect residual interference effects which have been shown to be particularly prominent at this energy[5]). With the exception of this one datum, then, the α_{22} are correctly predicted.

The predicted value of B_2/B_0 is given by

$$\frac{B_2}{B_0} = \frac{\frac{3}{26}(x^2 + 12x - 1)\,|\,d_{22}\,|}{(1 + x^2) - \frac{1}{4}(x^2 + 12x - 1)d_{20}}\,, \tag{17}$$

where x is the multipole amplitude ratio E2/M1 for the 1.28 MeV radiation. Inserting the best available value[8]) for this ratio, $x = 0.21 \pm 0.03$, in (17) the expression may be written as

$$\frac{B_2}{B_0} = -\frac{(0.14 \pm 0.06)\,|\,d_{22}\,|}{1.04 + 0.057\,d_{20}}\,. \tag{18}$$

The predicted values of B_2/B_0 are shown as bands in figs. 9(a) and 9(b) for roots 1 and 2 respectively together with the experimentally determined values; the uncertainty in x has not been included in fig. 9 since, as seen from (18), the uncertainty in the multipole mixture enters as a multiplicative constant with the result that the variation with energy is predicted much more accurately than is the magnitude. The energy variation is sufficiently different for the two cubic roots to permit the exclusion of root 2 as extraneous. This root, shown in fig. 9(b), predicts larger $|\,B_2/B_0\,|$ for $E_d \leq 7$ MeV than for $E_d > 7$ MeV, contrary to the experimental data. Root 1, on the other hand predicts both the energy variation and the magnitude of the experimentally determined B_2/B_0.

The azimuthal angular correlation prediction for the 1.28 MeV radiation in a plane perpendicular to α_{22},

$$W(\theta,\tfrac{1}{2}\pi + \alpha_{22}) = C_0 + C_2 P_2\,(\cos\theta)\,, \tag{19}$$

is given in fig. 10. The plane wave limit (dashed line) predicts isotropy. Both roots 1 and 2 are retained in this and in further predictions because of the argument noted earlier. The triangular point at 9 MeV is from ref. [13]) and is based on measurements at only three angles. It is not clear whether this measurement represents a real discrepancy or not.

In summary, measurements of the 1.28 MeV angular correlation in the reaction plane, reported herein, are consistent with the predictions of the distorted wave theory.

Additional measurements would be desirable to further check the distorted-wave formalism used. In order to decide which measurements would be the most sensitive to the assumptions involved, predictions of the azimuthal

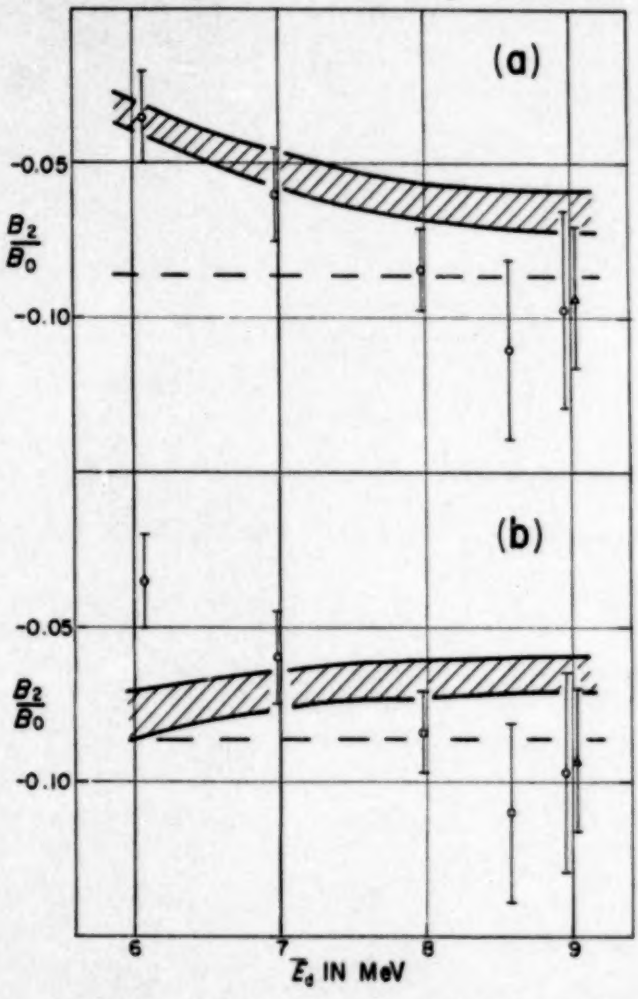

Fig. 9. The coefficient ratios predicted for the angular correlation in the de-excitation of the 1.28 MeV state in Si^{29}, calculated as noted in the caption to figure 8, are shown as bands for (a) case 1 and (b) case 2. Values of the coefficient ratios, as determined experimentally for the $Si^{28}(d, p\gamma)Si^{29}$ (1.28 MeV) reaction, are shown as data points. The plane wave predictions are included as dashed lines. The triangular point is from ref. [13]).

angular correlation of the 2.03 MeV radiation as well as of the proton polarization magnitude have been made. These predictions are presented in the following subsection.

4.3. FURTHER PREDICTIONS

Having the statistical tensors for the reaction as a function of the deuteron energy it is possible to compute the angular correlation over the entire sphere.

As well, the polarization magnitude can be computed. This subsection presents the results of such computations.

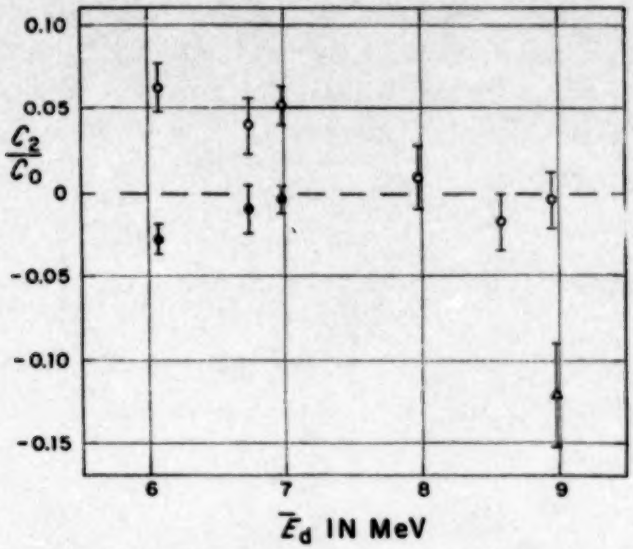

Fig. 10. Predicted ratios of coefficients for the azimuthal angular correlation in a plane perpendicular to $\overline{\alpha_{22}}$ in the de-excitation of the 1.28 MeV state in Si^{29}. For $\bar{E}_d \leqq 7$ MeV the open circles apply to case 1 and the closed circles apply to case 2. The plane wave prediction (isotropy) is shown as a dashed line. The triangular point at 9 MeV is from ref. [13]).

Using the general relation (8) the angular correlation for the 2.03 MeV radiation measured in the plane perpendicular to α_{22} can be written

$$W(\theta, \alpha_{22} + \tfrac{1}{2}\pi) = D_0 + D_2 P_2(\cos\theta) + D_4 P_4(\cos\theta), \tag{20}$$

where

$$\frac{D_2}{D_0} = \frac{0.572\, d_{20} + 0.078\, |d_{22}| + 0.455\, |d_{44}| \cos 4(\alpha_{44} - \alpha_{22})}{1 - 0.544\, |d_{22}| - 0.319\, |d_{44}| \cos 4(\alpha_{44} - \alpha_{22})} \tag{21}$$

and

$$\frac{D_4}{D_0} = -\frac{0.333 + 0.238\, d_{20} - 0.467\, |d_{22}| + 0.137\, |d_{44}| \cos 4(\alpha_{44} - \alpha_{22})}{1 - 0.544\, |d_{22}| - 0.319\, |d_{44}| \cos 4(\alpha_{44} - \alpha_{22})}. \tag{22}$$

Figs. 11(a) and 11(b) contain values for the angular correlation coefficient ratios plotted as a function of deuteron energy. The plane wave limit in this case is $D_2/D_0 = D_4/D_0 = 0$. It becomes immediately obvious that for the lower energies not only is the predicted angular correlation large but it is vastly different for roots 1 and 2. Measurements of this angular correlation would thus be a sensitive test of the theory and would also serve to distinguish unambiguously between the two roots. At the higher energies, on the other hand, the predicted angular correlation is hardly different from that given by the plane wave calculations.

The predicted azimuthal angular correlation for the 1.28 MeV state was given in the last subsection (fig. 10).

The polarization of the protons for the case $l_n = 2$ is given by

$$P = \pm \frac{0.5956}{(2j+1)} [1.25\,(1 - d_{20})^2 - 10.29\,|\,d_{44}\,|^2]^{\frac{1}{2}}\,, \tag{23}$$

where j is the spin of the state formed. It should be noted that the proton polarization is in general parametrized by the ρ_{10} statistical tensor. In equation (23) use has been made of the particular relationships existing between the ρ_{kq} (because of the stripping assumptions) to express ρ_{10} in terms of ρ_{20} and ρ_{44}, hence d_{20} and d_{44}. The general distorted wave theory is not able to predict the sign of the polarization without additional assumptions regarding the details of the wave functions and potentials.

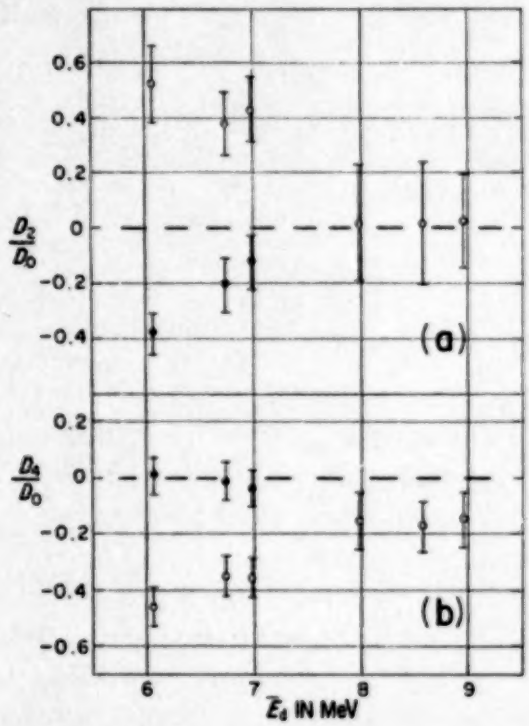

Fig. 11. Predicted coefficient ratios for the azimuthal angular correlation in a plane perpendicular to $\overline{\alpha_{zz}}$ in the de-excitation of the 2.03 MeV state in Si^{29}. For $\bar{E}_d \leqq 7$ MeV the open circles apply to case 1 and the closed circles apply to case 2. The plane wave predictions (isotropy) are shown as dashed lines. It should be noted that in this case the α_{zz} direction has no simple interpretation as a correlation symmetry axis; it is chosen for presentation here simply since such choice simplifies the resulting expressions.

Values of P are given in fig. 12 as a function of the deuteron energy. The scale used in the figure is appropriate to the $j = \frac{5}{2}$ (2.03 MeV) state. The predicted values of P for the protons leading to the $\frac{3}{2}$ (1.28 MeV) state are 50 % larger than those given in fig. 12. Again, at the higher energies the predicted values are consistent with the plane wave value $P = 0$, although the experimental errors are large enough to encompass larger values. For the lower energies,

however, the predicted polarizations are significantly different for the two roots, again suggesting a measurement to distinguish between the two.

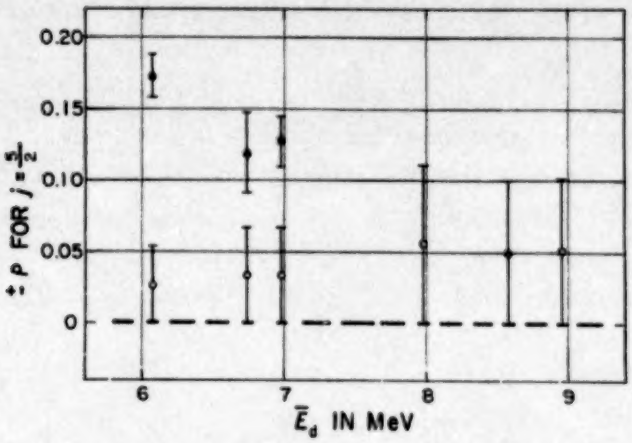

Fig. 12. Predicted polarization magnitude for protons at the peak of the $l_n = 2$ stripping angular distribution from the reaction Si^{28}(d, p)Si^{29} (2.03 MeV). For $\bar{E}_d \leqq 7$ MeV the open circles apply to case 1 and the closed circles apply to case 2. The predicted polarizations for protons leading to the $\frac{1}{2}+$ 1.28 MeV state in Si^{29}, because of the j dependence, are 50% larger than those given in the figure.

5. Conclusions

It has been found possible to fit the Si^{28}(d, pγ)Si^{29} angular correlation data assuming distorted wave stripping and the formalism of Huby, Refai and Satchler[4]). The measurements on the angular correlation in the reaction plane involving the 2.03 MeV state alone yield four real experimental parameters; these are enough to enable the statistical tensors for the reaction, as defined in ref. [4]), to be determined for each energy. These statistical tensors, in terms of which the magnitude of the proton polarization as well as the general (p, γ) angular correlation function over the entire sphere can be expressed, are then used to compute the angular correlation of the 1.28 MeV radiation yielding results in good agreement with experiment and thus supporting the expectation that the matrix elements are essentially independent of the detailed nuclear structure of the final state. This is particularly interesting since other evidence[21]) suggests that the 1.28 MeV state in Si^{29} has $K = \frac{3}{2}$ while the 2.03 MeV state is the $\frac{5}{2}+$ member of the $K = \frac{1}{2}$ rotational band based on the Si^{29} ground state.

Predictions of the azimuthal angular correlations of both the 1.28 MeV and the 2.03 MeV radiations are made as well as of the proton polarization magnitude. These predictions are essentially the plane wave limit predictions for deuteron energies greater than 7 MeV but deviate significantly for energies of 7 MeV and less.

The observed systematic trend of the statistical tensors approaching the plane wave limit as the incident energy is increased is consistent with the fact

that with increasing energy the Coulomb and nuclear forces are expected to have less effect in distorting the deuteron and proton waves.

Having the experimental values for the reaction tensors it is of considerable interest to test appropriate optical and shell model wave functions by substitution in equations (5), (6) and (7). Preliminary results of such a calculation have been reported by Tobocman and Satchler[18]).

Further measurements bearing upon the mechanism for the $Si^{28}(d, p)Si^{29}$ reaction, including differential and total excitation functions and studies on the proton angular distribution, will be reported in a companion paper in the near future.

The authors wish to thank Drs. G. R. Satchler, L. G. Elliott and H. McManus for helpful discussions concerning the analysis.

References

1) S. T. Butler, Proc. Roy. Soc. A **208** (1951) 559;
Biedenharn, Boyer and Charpie, Phys. Rev. **88** (1952) 517;
L. G. Gallagher and W. B. Cheston, Phys. Rev. **88** (1952) 684;
G. R. Satchler and J. A. Spiers, Proc. Phys. Soc. A **65** (1952) 980
2) H. C. Newns, Proc. Phys. Soc. **66** (1953) 477;
J. Horowitz and A. M. L. Messiah, J. Phys. et Rad. **14** (1953) 695;
W. Tobocman and M. H. Kalos, Phys. Rev. **97** (1955) 132
3) W. Tobocman, Phys. Rev. **115** (1959) 98
4) Huby, Refai and Satchler, Nuclear Phys. **9** (1958) 94
5) J. A. Kuehner, E. Almqvist and D. A. Bromley, Bull. Am. Phys. Soc. **5** (1960) 56; Nuclear Physics (to be published)
6) J. R. Holt and T. N. Marsham, Proc. Phys. Soc. A **66** (1953) 467
7) D. A. Bromley, H. E. Gove, A. E. Litherland, E. B. Paul and E. Almqvist, Can. Jour. Phys. **35** (1957) 1042
8) G. J. McGallum (private communication);
G. J. McGallum and A. E. Litherland, Bull. Am. Phys. Soc. **5** (1960) 56
9) S. A. Cox and R. M. Williamson, Phys. Rev. **105** (1957) 1799
10) R. T. Taylor, Phys. Rev. **113** (1959) 1293
11) Chase, Warburton and Johnson, Bull. Am. Phys. Soc. **5** (1960) 45
12) J. P. Martin and K. S. Quisenberry, Bull. Am. Phys. Soc. **4** (1959) 404
13) Allen, Collinge, Hird, Maglic and Orman, Proc. Phys. Soc. A **69** (1956) 705
14) H. A. Hill and J. M. Blair, Phys. Rev. **111** (1958) 1142
15) J. A. Kuehner, E. Almqvist and D. A. Bromley, Phys. Rev. Letters **4** (1960) 132
16) D. A. Bromley, J. A. Kuehner and E. Almqvist, Bull. Am. Phys. Soc. **5** (1960) 56
17) D. A. Bromley, E. Almqvist, H. E. Gove, A. E. Litherland, E. B. Paul and A. J. Ferguson, Phys. Rev. **105** (1957) 957
18) W. Tobocman and G. R. Satchler, Bull. Am. Phys. Soc. **5** (1960) 28; and to be published
19) G. R. Satchler, Proc. Phys. Soc. A **66** (1953) 1081
20) L. C. Biedenharn and M. E. Rose, Rev. Mod. Phys. **25** (1953) 729
21) D. A. Bromley, H. E. Gove and A. E. Litherland, Can. Jour. Phys. **35** (1957) 1057

1.E.1: 3.A

Nuclear Physics **19** (1960) 634—653; © *North-Holland Publishing Co., Amsterdam*
Not to be reproduced by photoprint or microfilm without written permission from the publisher

ENERGY LEVELS OF Re^{187}

R. G. ARNS† and M. L. WIEDENBECK

Harrison M. Randall Laboratory of Physics,
The University of Michigan, Ann Arbor, Michigan††

Received 15 August 1960

Abstract: The gamma rays of Re^{187} following beta decay of the 24-hr. W^{187} have been studied using prompt and delayed coincidence techniques. A total of 25 gamma rays was found. Relative intensities are given for the gamma transitions. The directional correlation of the 552-keV–134-keV cascade has been measured. A decay scheme is proposed on the basis of the coincidence measurements. Spins and parities of the principal levels are discussed.

1. Introduction

The decay of W^{187} ($\tau_{\frac{1}{2}} = 24$ hours) by beta emission to levels of Re^{187} has been studied by many authors[1–9]). There has been general agreement regarding transitions connecting the levels at 686 keV, 206 keV and 134 keV. The 206-keV

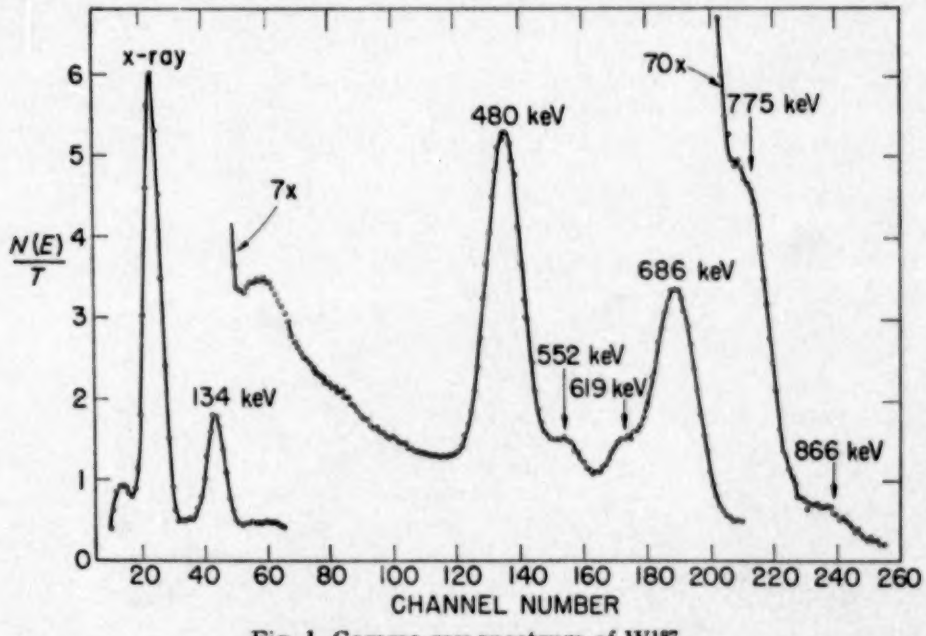

Fig. 1. Gamma-ray spectrum of W^{187}.

level is a metastable state with a halflife of 0.55 μsec[1]). A number of additional gamma rays have been known to exist[2–5]) but their position in a decay scheme has not been well established. The gamma ray spectrum of W^{187}, as shown in

† Present address: Department of Physics, The University of Buffalo, Buffalo, N.Y.

†† Work supported in part by the U.S. Atomic Energy Commission and the Michigan Memorial-Phoenix Project.

fig. 1, does not reflect this complexity. Hence it was felt that detailed coincidence measurements would be of value in establishing the existence and position of these weak gamma transitions.

Coulomb excitation of Re^{187} yields gamma rays of 134 keV, 167 keV and 301 keV[10-15]). Gamma-gamma coincidences have been observed following Coulomb excitation[13]). As a result of these measurements, a level has been proposed at 301 keV de-excited by a ground-state transition and a cascade through the 134-keV level. The 301-keV and 167-keV gamma rays have not previously been observed in the decay of W^{187}.

2. Experimental Procedure

The gamma coincidence measurements were made on samples of very pure tungsten foil which were irradiated at a flux of 2×10^{12} neutrons/cm^2·sec for periods of 1 to 8 hours in the Ford Nuclear Reactor. A dilute solution of lithium tungstate was similarly irradiated to provide sources for the directional correlation measurements. The gamma ray spectrum of both forms of source material was followed for a one month period. The only activity observed in addition to the W^{187} was the long-lived electron-capture isotope, W^{181}. All data were taken early in the decay of each source in order to eliminate interference from W^{181}.

The prompt coincidence measurements employed a fast-slow coincidence circuit with a resolving time of 35 ns. A resolving time of 20 ns was used in the delayed coincidence measurements. Pulses coincident with a selected energy range were fed through a linear gate and recorded on a 256-channel analyzer.

The detectors in all cases consisted of 5.1 cm by 5.1 cm NaI(Tl) crystals mounted on R.C.A. 6342A phototubes. A Compton shield of 6.4 mm thick lead surrounded by 0.8 mm cadmium and 0.4 mm copper was placed between the detectors in the coincidence measurements.

Differential analyzers provided energy selection and lateral lead shielding was used to prevent counter-to-counter scattering in the directional correlation measurement. Data were taken in a double quadrant sequence at seven angles (i.e., every 15°) in each quadrant. The real coincidence rate was corrected for source decay and electronic drift. After making a least squares fit[16]), the expansion coefficients were normalized and corrected for finite resolution[17]).

3. Results

3.1. COINCIDENCE SPECTRA

Measurements were made of the spectra of gamma rays in prompt coincidence with 18 energy ranges. Delayed coincidence spectra involving the metastable state at 206 keV were observed in two additional measurements.

The spectra were corrected for random coincidences. The source to crystal distance in all cases was 2.5 cm. In order to eliminate coincidences with beta particles, the detectors were shielded frontally with 6.5 mm teflon in addition to the (1 mm) aluminium crystal case.

The results of all of the measurements are summarized in subsection 3.2. Only the most significant of the coincidence measurements will be displayed and discussed in detail here. These are listed below according to the energy range selected. The observed gamma ray energies are expected to be correct to within 1 %.

Coincidence with 125 keV *to 145* keV

The spectrum of gamma rays coincident with the energy range from 125 keV to 145 keV is shown in fig. 2. The relative enhancement of the complex peak at 63 keV clearly illustrates the 72-keV–134-keV coincidence. The strong peak

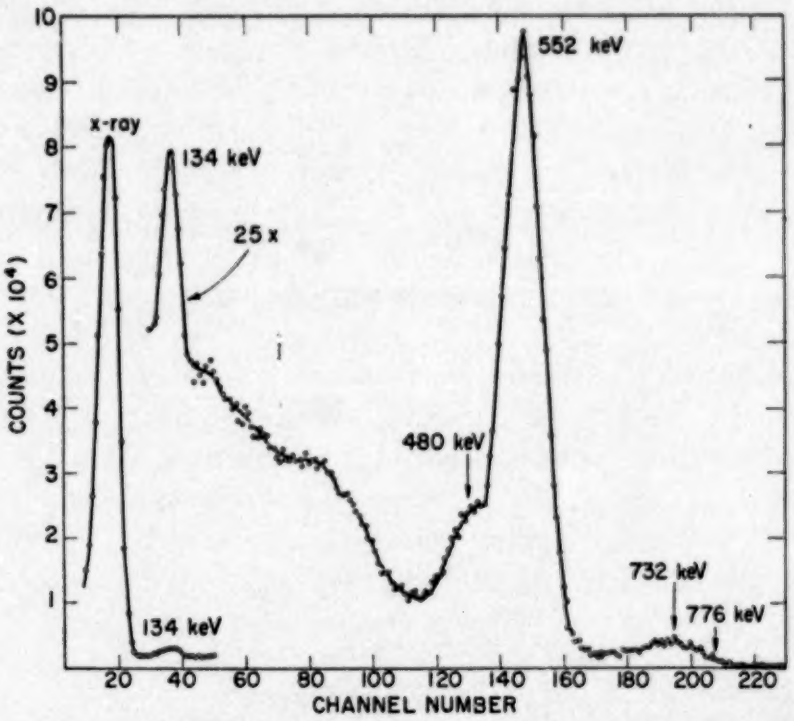

Fig. 2. Spectrum of gamma rays coincident with the energy range from 125 keV to 145 keV.

at 552 keV is interpreted as a transition from the 686-keV level to the level at 134 keV. The peak at 480 keV is due to coincidences which pass through the metastable state at 206 keV. Considering the resolving time of the coincidence circuit and the lifetime of the 206 keV level, the intensity of this peak is consistent with the assumption that essentially all of the 480-keV transition decays through the metastable state. A new line is observed at 732 keV which is interpreted as a transition from a level at 866 keV to the 134-keV level. This peak may also contain a contribution from a weak line at 776 keV. The strong 775-

keV line observed in the singles spectrum is a ground-state transition. The 866-keV transition to the ground state appears in the singles spectrum but was not found in any of the coincidence spectra. The "continuum" from 175 keV to 400 keV is much larger than would be expected from the Compton distribution of higher energy gamma rays. This clearly indicates the presence of a number of unresolved lines.

Coincidence with 158 keV *to 178* keV

Fig. 3 illustrates the gamma ray spectrum coincident with this energy range. A strong peak is observed at 301 keV. Fig. 6 will show this to be in coincidence with a line at 167 keV. New lines are noted at 440 keV and 485 keV. The bump

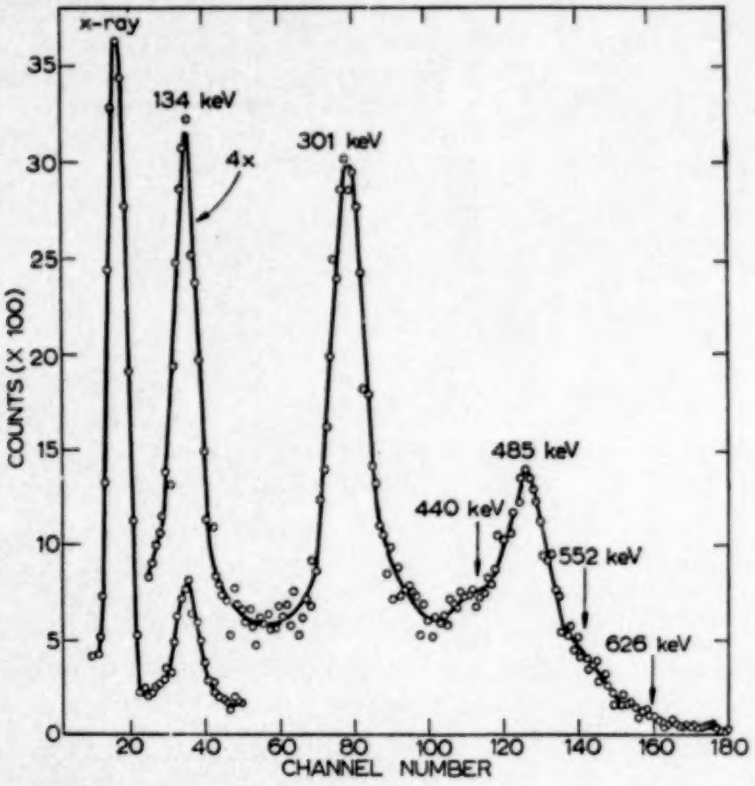

Fig. 3. Spectrum of gamma rays coincident with the energy range from 158 keV to 178 keV.

at about 364 keV is due to summing. The enhancement of the 63-keV peak and part of the 552-keV line are due to interference in the selectror channel from the tail of the 134-keV line.

Coincidence with 180 keV *to 225* keV

This coincidence spectrum is shown in fig. 4. The 485-keV line is quite strong. There is again a clear indication of a line at 440 keV. The 301-keV line is less intense since it is only coincident with the 167-keV transition. Lines of 552 keV, 626 keV, 686 keV and 760 keV are present, although quite weak. The 485-keV

line is clearly different from the 480 keV transition between the 686-keV and 206-keV levels. The presence of the 552-keV and 686-keV transitions indicates that a weak gamma ray of 180 keV (from the 866 keV level) feeds the 686-keV level. Again part of the 552-keV line appears to be the result of interference.

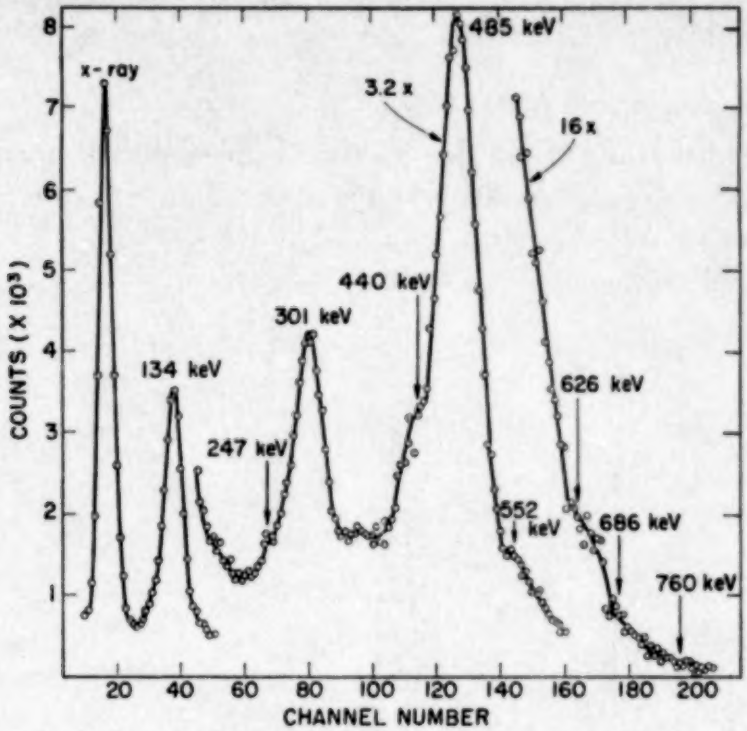

Fig. 4. Spectrum of gamma rays coincident with the energy range from 180 keV to 225 keV.

As will be seen below, the 485-keV line is apparently a ground state transition fed by a 201-keV transition from the level at 686 keV. The 760-keV line is probably also a ground state transition fed by a gamma ray in the energy range of this measurement. The 626-keV line is a transition from this new level to the first excited state. This was confirmed by other measurements.

Coincidence with 235 keV *to 265* keV

This coincidence spectrum is shown in fig. 5. The principal line which is seen to be in coincidence with this energy region is at 619 keV. Additional weak lines are seen at 179 keV, 247 keV and 440 keV. The presence of the 134-keV line and its internal conversion X-ray is mostly due to interference from the Compton distribution of the 552-keV line in the energy selecting channel. The 247-keV line in this spectrum may similarly be explained as due to interference from the 619-keV line.

If a level is placed at 619 keV, which is principally de-excited by a ground state transition, then a 247-keV transition from the 866-keV level to the 619 keV level will give the observed strong coincidence. The 440-keV transition is

apparently also a ground state transition fed by a 179-keV transition from the 619-keV level.

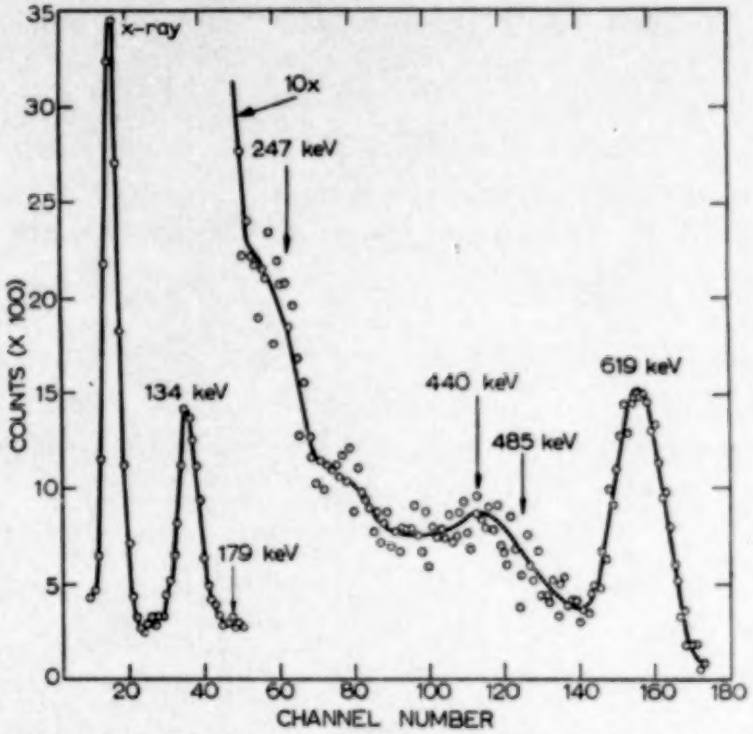

Fig. 5. Spectrum of gamma rays coincident with the energy range from 235 keV to 265 keV.

Coincidence with 285 keV *to 315* keV

The spectrum of gamma rays coincident with this energy range is shown in curve A of fig. 6. Again, as in many of these curves, most of the 134-keV line

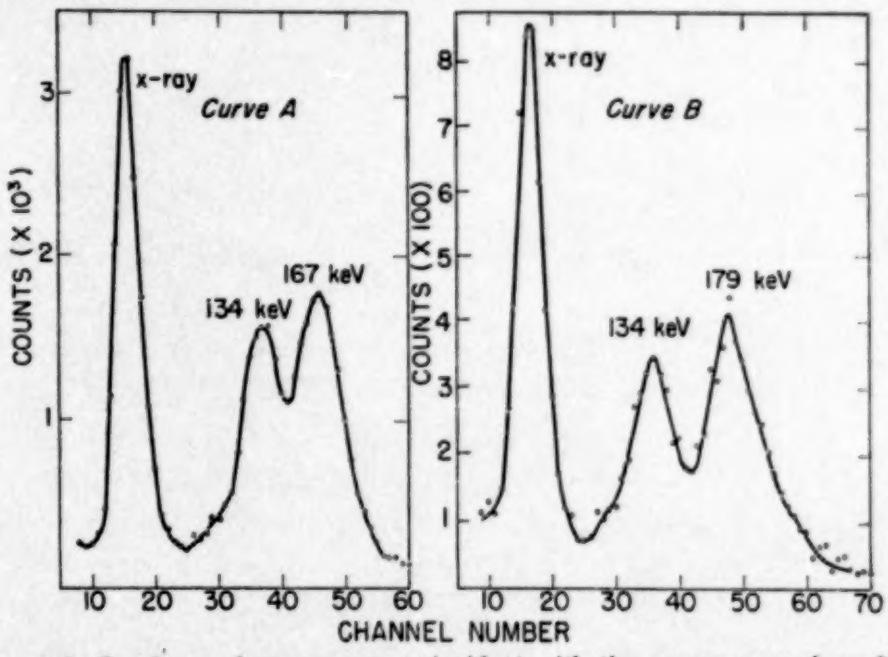

Fig. 6. Curve A: Spectrum of gamma rays coincident with the energy range from 285 keV to 315 keV. Curve B: Same for energy range from 425 keV to 455 keV.

and its internal conversion X-ray is due to interference from the Compton distribution of the 552-keV line in the energy selecting channel. An additional strong line is seen at 167 keV. This is in coincidence with the 301-keV line as was seen in fig. 3.

Coincidence with 425 keV *to 455* keV

This coincidence spectrum is shown in fig. 6, curve B. A strong coincidence is noted at 179 keV. The two parts of fig. 6 illustrate that the 167-keV and 179-keV lines are clearly distinct.

Coincidence with 455 keV *to 505* keV

The spectrum of gamma rays in prompt coincidence with this energy region is shown in curve A of fig. 7. Again the 134-keV line and X-ray appear as a result

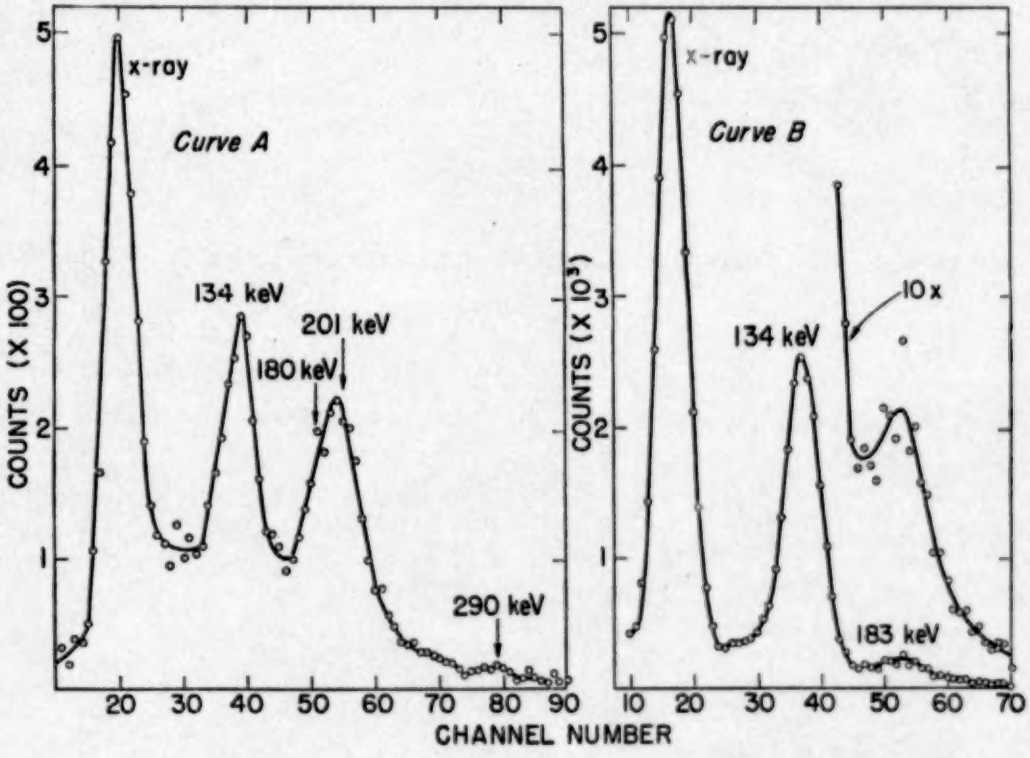

Fig. 7. Curve A: Spectrum of gamma rays coincident with the energy range from 455 keV to 505 keV. Curve B: Same for energy range from 535 keV to 585 keV.

of the interference. A complex line centered at $\approx$ 198 keV is found. The major part of this coincidence is due to the 201-keV transition to the 485-keV level. The remainder results due to the tail of the 440-keV line in the selector channel which permits the 179-keV line to appear. A weak line is seen at about 290 keV. This may indicate a weak transition of this energy from the 775-keV level to the 485-keV level.

Coincidence with 535 keV *to 585* keV

This coincidence spectrum is shown in fig. 7, curve B. The principal transition in coincidence with this energy range is the 134-keV transition from the first excited state to the ground state. This spectrum provides an excellent means of determining the K-conversion coefficient of the 134-keV transition as will be seen below. The additional weak line at about 180 keV is partly due to the transition from the 866-keV level to the 686-keV level and partly the result of interference from the 626-keV–185-keV coincidence (cf. below).

Coincidence with 610 keV *to 650* keV

This coincidence spectrum is shown in fig. 8. The 134-keV transition is seen to be in coincidence with a gamma ray in this energy range. In addition, coincidences are observed with gamma rays at 185 keV and 247 keV. The 247-keV gamma ray is interpreted as a transition from the 866-keV level to the 619-keV level and is in coincidence with the ground state transition from the latter level. A 626-keV gamma ray from a level at 760 keV to the first excited state gives rise to the coincidence with the 134-keV transition. The 185-keV gamma ray is probably a transition from a level at 945 keV to the 760-keV level.

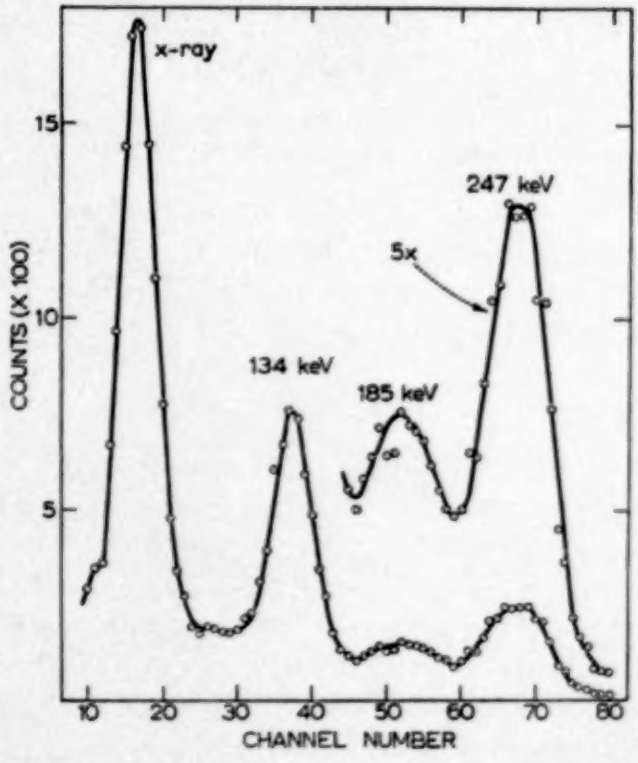

Fig. 8. Spectrum of gamma rays coincident with the energy range from 610 keV to 650 keV.

*Delayed coincidence with the 134-*keV *gamma ray*

Fig. 9, part A shows the coincidence spectrum which is observed by accepting the 134-keV gamma ray in the selector channel and delaying the pulses which

are to be displayed on the multichannel analyzer by 220 ns. In this way prompt coincidences are minimized and the gamma rays which pass through the

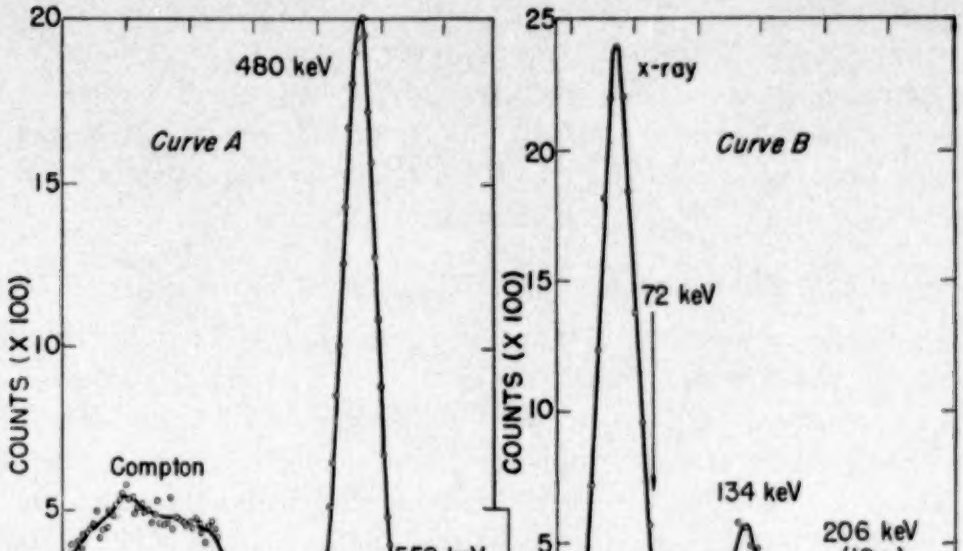

Fig. 9. Curve A: Spectrum of delayed coincidences with the 134-keV gamma ray. Curve B: Spectrum of delayed coincidences with the 480-keV gamma ray.

metastable state at 206 keV may be observed. The 480-keV transition from the 686 keV level to the metastable state is the only delayed coincidence which appears. A small peak is present at 552 keV due to prompt coincidences.

Delayed coincidences with the 480 keV *line*

If pulses from the detector in the range selector channel are delayed by 220 ns and if this channel is set to accept the 480-keV peak, then the multichannel analyzer will display only gamma rays from the decay of the metastable state. This is shown in part B of fig. 9. Some of the X-ray and 134-keV peaks will result from prompt coincidences due to interference from the 552-keV Compton distribution in the selecting channel. After this correction is made, this curve serves as a means of determining the unconverted relative intensity of the 206-keV crossover transition from the metastable state.

3.2. SUMMARY OF THE COINCIDENCE MEASUREMENTS

In addition to the coincidence spectra discussed in section 3.1, a number of other measurements were made. These are summarized, along with the data described above, in table 1.

TABLE 1

Summary of the coincidence measurements

Energy range (keV)	Observed coincident gamma ray energies (keV)																				
	x-ray + 72	134	167	179 + 180	185	201	206	247	290	301	440	480	485	552	619	626	686	732	760	775 + 776	866
65– 90	s	s										m		s		vw	x	m		vw	x
125–145	s	m			vw							m		s		vw	x	m		vw	x
158–178	s	s	x	x	x		x	vw		s	m		s	w		vw	vw		vw		
180–240	s	s	x				x	w		m	m		s	w		w	vw		vw		
180–225	s	s	x				x	w		m	m		s	w		m	w		w		
225–275	s	s	x	vw			x	vw		x	m		m		s						
235–265	s	s	x	vw			x	vw		x	m		w		s				vw		
280–340	s	s	s				x	vw		x	x		vw		vw						
285–315	s	s	s				x	vw		x	x		vw								
360–420	m	m		m		vw	x	vw		x	x										
425–455	m	m		s		vw	x			x	x										
455–505	m	m		w		s			w	x	x										
474–491	m	m		vw	vw	s			vw	x	x										
535–585	s	s		vw	w		x			x											
610–650	m	m			m		x	m		x											
675–697	vw	vw		vw			x			x											
740–800	vw	vw			vw		x														
840–880	x	x																			
Delayed 134												s		w							
Delayed 480	s	s					w														

s = strong coinc., m = medium coinc., w = weak coinc., v = very weak coinc., x = not in coincidence. A blank square does not indicate the absence of a coincidence. Often neighbouring strong peaks may overwhelm a weak transition or a number of close peaks may be unresolved.

3.3. INTERNAL CONVERSION MEASUREMENTS

A number of electron lines from W^{187} were observed by Cork *et al.*[3]) in photographic magnetic spectrometers. The W^{187} sources were produced by neutron bombardment of isotopically-enriched (97.5 %) W^{186}. Their data have been reinterpreted and the results are summarized in table 2. Many of the weak

TABLE 2

Energies of electron conversion lines as observed by Cork *et al.*[3])

Electron energy (keV)	Interpretation	Energy sum (keV)	Electron energy (keV)	Interpretation	Energy sum (keV)
34.5	K	106.2	134.5	K	206.2
41.9	K	113.6	167.5	K	239.2
46.6	Auger (α_1 — L_1)		174.6	K	246.1
48.7	Auger (α_1 — L_3)		194.2	L_2	206.2
50.3	Auger (α_2 — L_3)		203.3	M	206.2
59.5	L_1	72.0[b])	229[a])	K	301
61.5	L_3	72.0	395[a])	K	467
62.5	K	134.2[b])	408	K	479.5[b])
69.3	M	72.0	468	L	479.5
71.7	N	72.0	480	K	552
94.2	L_2	106.2	547	K	618.9[b])
101.6	L_2	113.6	554[a])	K	626
110.3[a])	K	182.0	607	L	619
121.7	L_1	134.2	614	K	686.1[b])
122.2	L_2	134.2	674	L	686.1
123.7	L_3	134.2	703	K	775
131.4	M	134.2	763	L	775
133.6	N	134.2	794	K	866

[a]) Weak and uncertain lines.
[b]) Crystal spectrometer values of Muller *et al.*[2]).

lines observed in the coincidence measurements are below the limit of observation of the internal conversion experiment. Similarly three of the lines found in internal conversion (106.2 keV, 113.6 keV and 467 keV) were not seen in the coincidence measurements.

Vergnes[8,9]) has summarized the measurements of K-shell internal conversion coefficients for the strong transitions in Re^{187}. These data are shown in table 3.

The spectrum of gamma rays coincident with the 552-keV transition in the present experiment provided an accurate determination of α_K for the 134 keV transition. Using the X-ray and 134-keV photopeak intensities, and correcting for absorption, crystal efficiency and X-ray fluorescence yield, a value of $\alpha_K = 1.75 \pm 0.14$ was determined. As is seen in table 3, this is consistent with the assumption that the 134 keV transition is predominantly M1 with a small E2 admixture.

TABLE 3

K-shell internal conversion coefficients for strong transitions in Re^{187}

E_γ (keV)	α_K (exp.)	α_K (theor.)				Multipolarity
		E1	E2	M1	M2	
72	1.4 ± 0.2	0.61	1.06	9.6	81	E1 + M2 (or E2 + M1)
134	1.5 ± 0.4	0.15	0.47	1.9	11.4	M1 + E2 (or E1 + M2)
	2.12 ± 0.32 [a])					
	1.75 ± 0.14 [b])					
480	0.0195	0.0067	0.018	0.056	0.16	E2
552	0.029	0.005	0.013	0.04	0.11	E1 + M2 or E2 + M1
619	0.06	0.004	0.01	0.03	0.08	E1, E2 or M1
686	0.0069	0.0032	0.0082	0.023	0.06	E1
775	0.047	0.0025	0.0065	0.017	0.042	M2

Unless otherwise noted, the experimental coefficients are due to Vergnes[8,9]). The theoretical values were obtained from the tables of Sliv and Band[18]).

[a]) McGowan and Stelson[14]). [b]) Present measurement.

It is not possible to assign a unique multipolarity to the 72-keV or 134-keV transitions on the basis of the K-shell conversion alone. The experimental L-shell internal conversion coefficients measured by Vergnes[8,9]) are compared to corresponding theoretical values in table 4. This comparison shows clearly that the 72 keV transition is predominantly E1 with a small M2 admixture ($M2 \leq 1.5\ \%$).

TABLE 4

L-shell internal conversion dats for the 72-keV and 134-keV transitions in Re^{187}

E (keV)	Experimental coefficient	Ref.	Theoretical coefficient			
			E1	E2	M1	M2
72	$\alpha_{L_1 + L_3} = 0.23 \pm 0.13$	[8,9])	0.083	4.5	1.396	28.6
134	$\alpha_L = 0.3 \pm 0.1$	[8,9])	0.026	0.66	0.31	3.4
	$K/L = 4.6 \pm 0.5$	[10])	5.8	0.71	6.1	3.3

Although the L-shell conversion data for the 134 keV transition supports an M1(+ E2) assignment for the 134 keV transition, it does not rule out an E1 + M2 mixture. However, the Coulomb excitation of the 134-keV level rules out the latter assignment and it can be concluded from the internal conversion data that the 134-keV transition is mostly M1 with an E2 content of $< 25\ \%$.

3.4. GAMMA-RAY RELATIVE INTENSITIES

The relative intensities of the observed gamma rays were determined from the singles and coincidence spectra. The results are summarized in table 5. The intensities have been corrected for efficiency and absorption due to the shields covering the front of the crystals. The relative intensities of the stronger transitions have been determined by a least-squares fitting of the individual gamma-ray distributions to the observed singles spectrum. Details of this

TABLE 5

Relative intensities of the gamma rays from W^{187}

E_γ (keV)	Relative intensity[a])	Estimated uncertainty (%)	Transition intensity (%)
72	65.7	± 20	21.5[b])
134	47.2	± 10	30.4[b])
167	4.8	± 20	≳ 1.1
179	2.6	± 40	≳ 0.61
180	0.05	± 50	≳ 0.012
185	0.05	± 50	≳ 0.012
201	4.1	± 40	≳ 0.96
206	2.2	± 50	1.9[c])
247	0.19	± 30	0.044
290	0.50	± 40	0.12
301	4.8	± 20	1.12
440	2.6	± 40	0.61
480	100		23.4
485	4.6	± 40	1.2
552	28.7	± 10	6.7
619	38.9	± 10	9.1
626	0.85	± 50	0.2
686	134	± 5	31.4
732	2.8	± 20	0.65
760	0.15	± 50	0.035
775	20.3	± 10	4.75
776	1.1	± 40	0.25
866	3.5	± 10	0.82

The relative intensities of the unconverted gamma rays are compared to the 480-keV gamma ray. An estimate of the uncertainty in the relative intensity is given in the third column. The transition intensities have been corrected for internal conversion wherever possible.

[a]) Unconverted gamma ray intensity.

[b]) Internal conversion from tables 3 and 4.

[c]) Theoretical M2 internal conversion.

method will be published elsewhere[19]). In this manner accurate relative intensity values were obtained for the 480 keV, 552 keV, 619 keV, 686 keV, 775 keV and 866 keV gamma rays. All of the other intensities were obtained by comparing photopeak areas in the singles and coincidence spectra.

3.5. DIRECTIONAL CORRELATION MEASUREMENT OF THE 552-keV–134-keV CASCADE

In measuring the directional correlation of this cascade, each of the differential analyzers was allowed to accept a narrow range of the full-energy peak of one of the gamma rays. The resultant expansion coefficients, after correction for finite angular resolution, were found to be $A_2 = 0.316 \pm 0.018$ and $A_4 = -0.086 \pm 0.027$. Some interference was present due to the tail of the 480-keV gamma ray in the channel accepting the 552-keV photopeak. The contribution from this source was found to be 3 ± 2 % of the total coincidence rate and can be expected to be isotropic due to the intermediate metastable state. As is clearly shown in fig. 2, interference from higher energy gamma rays in the 552-keV channel is also very small. No correction was made for these effects.

The ground state spin of Re^{187} has been measured[20]) to be $\frac{5}{2}$. Re^{187} has 75 protons. The ground state is logically characterized in terms of the Nilsson model[21, 22]) as $\frac{5}{2}^+$. This corresponds to an equilibrium deformation parameter of $\delta = 0.19$. The Nilsson diagram predicts that the next intrinsic excitation will have a spin and parity of $\frac{9}{2}^-$. This appears to correspond to the metastable state at 206 keV. The first excited state at 134 keV does not fit the Nilsson diagram as an intrinsic level. It is most easily characterized as the first rotational excitation of the ground-state configuration. If this is indeed the case, this level will have a spin and parity of $\frac{7}{2}^+$. This is consistent with the Coulomb excitation[10, 15]) of this level and with the internal conversion data. Thus it seems safe to assume that the 134-keV gamma ray is a $\frac{7}{2}$ (M1 + E2) $\frac{5}{2}$ transition with a quadrupole content of $Q \leq 0.25$ (from internal conversion data). If the above spin and parity assumptions are indeed correct, then the pattern of transitions from the 686-keV level to the ground state and first two excited states is only consistent with spin assignments of $\frac{5}{2}$, $\frac{7}{2}$, or $\frac{9}{2}$ to the 686-keV level. Of these possibilities only $\frac{7}{2}$ will fit the observed directional correlation expansion coefficients. The negative A_4 coefficient is inconsistent with the $\frac{5}{2}$ or $\frac{9}{2}$ assignments. If the quadrupole content of the second transition is assumed to be $Q_2 \leq 0.25$, then the $\frac{7}{2}(D_1, Q_1)\frac{7}{2}$ $(D_2, Q_2)\frac{5}{2}$ sequence will fit the measured coefficients over a considerable range of Q_1. This is shown in fig. 10[23]).

As is seen from the graphical analysis, the large A_2 coefficient requires a large partial coefficient for each transition ($A_2 = A_2^{(1)} A_2^{(2)}$). Measurements of the angular distribution of the 134-keV gamma ray following Coulomb excitation[14, 15]) have been found to be isotropic. As can be seen from the $\frac{7}{2}(D, Q)\frac{5}{2}$ curve in fig. 10, this requires a quadrupole content of about 3 % in the 134-keV transition. This is clearly in disagreement with the present directional correlation expansion coefficients. Mössbauer and Wiedemann[24]) have measured the halflife of the 134-keV level to be $\tau_{\frac{1}{2}} = (1.04 \pm 0.14) \times 10^{-11}$ sec. The sources used in the Coulomb-excitation experiment were metallic rhenium (which has a hexagonal crystal structure). It is possible that the angular distribution was perturbed in the Coulomb excitation measurement.

If the parity of the 686-keV level is even, this would then contradict the measured internal conversion of the ground state transition (E1, see table 3). A $\frac{7}{2}$— assignment for this level will make the 686-keV transition an E1, the 480-keV transition an E2 + M1 mixture, and the 552-keV transition an E1 + M2 mixture, in keeping with the internal conversion measurements. The mixing ratios implied for the 480-keV transition and the 552-keV transition are rather large. Vergnes[8]) has pointed out that the 686-keV E1 gamma ray is highly hindered. Re^{187} is in the transition region between the highly-deformed rotational nuclei and the nuclei with small equilibrium deformation. Here

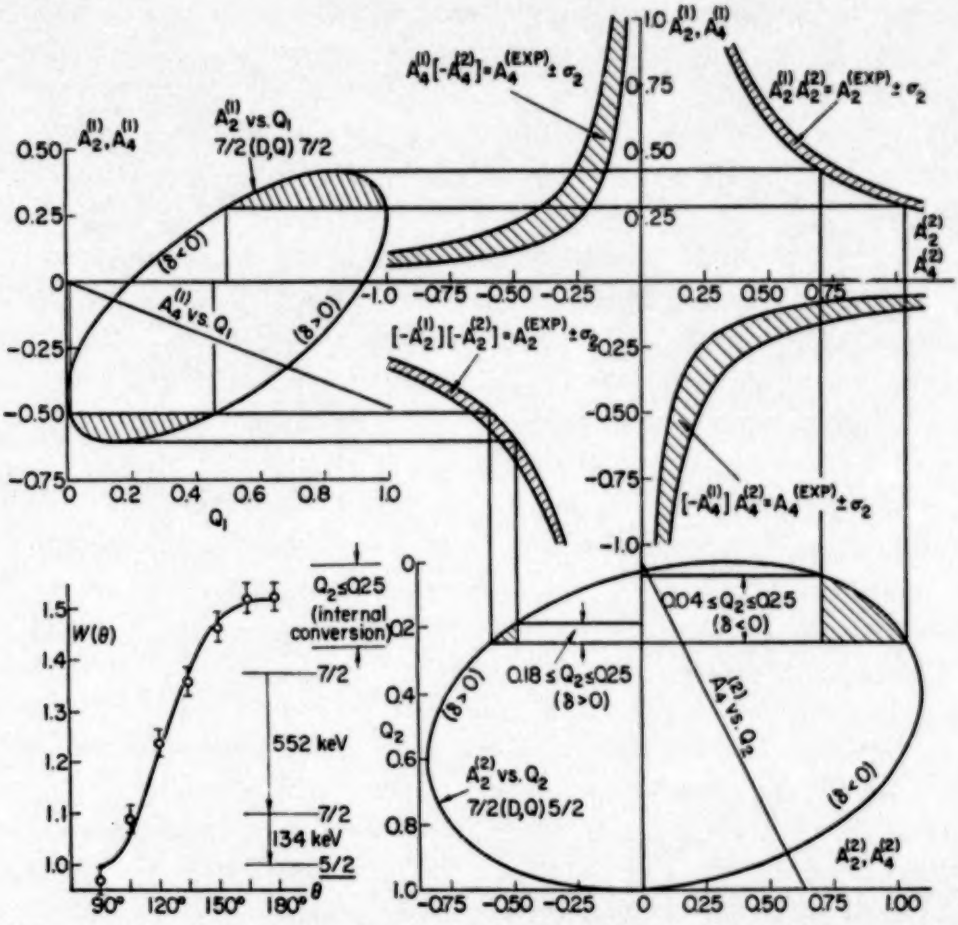

Fig. 10. Graphical analysis of the 552-keV–134-keV directional correlation data in terms of a $\frac{7}{2}(D, Q)\frac{7}{2}(D. Q)\frac{5}{2}$ sequence. Internal conversion data have been used to limit the allowed range of quadrupole mixture in the second transition. The insert in the lower left corner shows the corrected experimental points and the resultant least-squares curve for the correlation function $W(\theta)$.

intrinsic excitations may occur involving a change of nuclear deformation[22]). If the 686-keV level does involve an excitation of this nature, the observed mixing ratios would be entirely reasonable.

It does not seem possible that the observed A_4 coefficient is in error. Sufficient precautions were taken to avoid counter-to-counter scattering. A second measurement, made under different conditions, gave similar results although

attenuation was present due to source environment. The $\frac{7}{2}$ assignement to the 686-keV level is based on the presence of the A_4 coefficient. The A_2 coefficient alone would be consistent with sequences of the form $\frac{9}{2}(D, Q)\frac{7}{2}(D, Q)\frac{5}{2}$ or $\frac{5}{2}(D, Q)\frac{7}{2}(D, Q)\frac{5}{2}$.

Although directional correlation measurements on other cascades in Re^{187} would be desirable, intensity considerations or interference make these unprofitable. Previous measurements on the 72-keV–134-keV cascade[6,7]) suffer from the isotropic contribution of the unresolved X-ray in the channel accepting the 72-keV line. Due to these difficulties, no attempt was made to repeat the measurement.

4. Discussion

In subsections 3.1 and 3.2 the observed coincidence spectra were summarized and some arguments for the level structure of Re^{187} were given. The proposed decay scheme is shown in fig. 11. The levels and the transitions connecting them

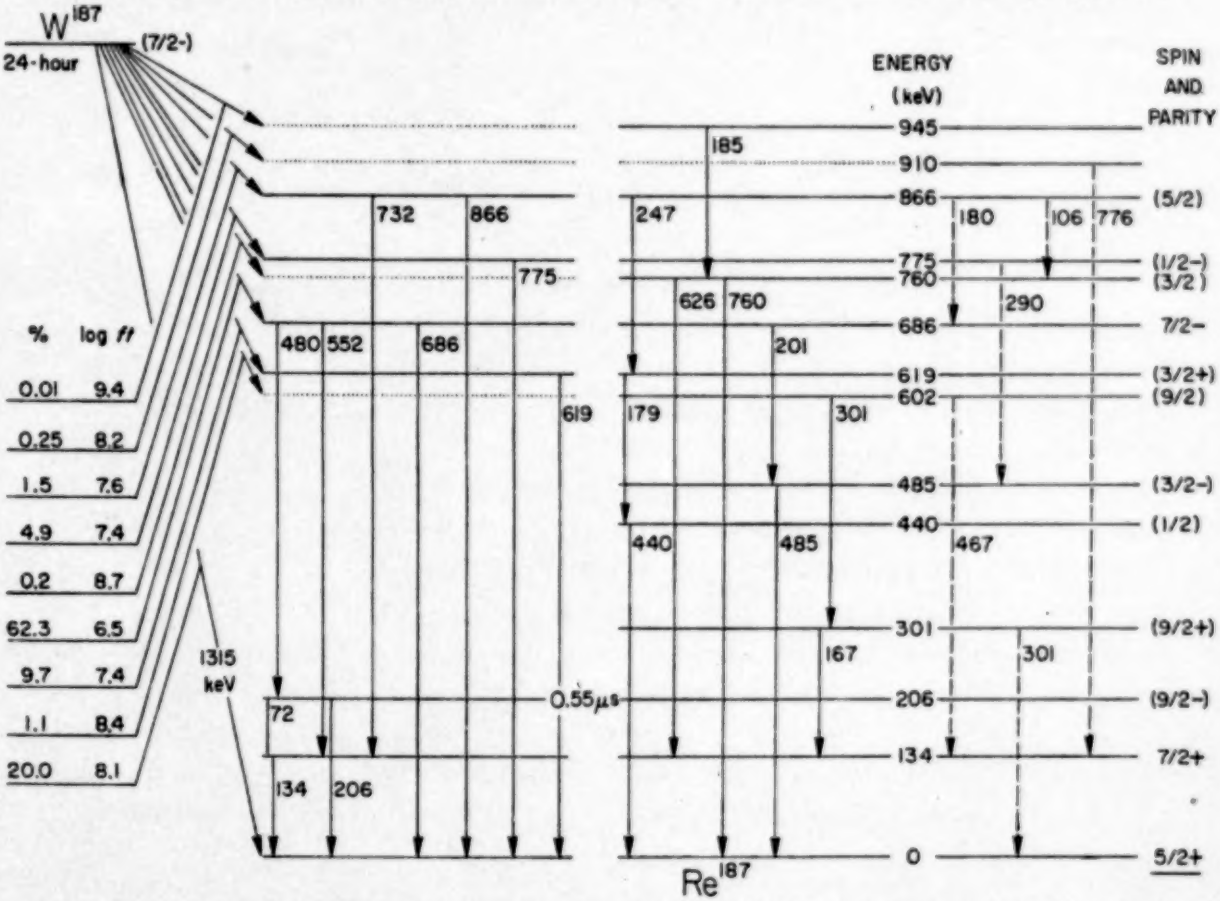

Fig. 11. Decay scheme of W^{187}. The level structure has been divided into three sections dependent upon the strength of the evidence for the proposed transitions and levels. The position and existence of transitions shown in the left-hand portion of the decay scheme are known with certainty. The position of gamma rays shown in the centre section of the decay scheme is probable. The gamma rays shown in the right-hand section of the decay scheme are very weak and the position proposed is not certain. The log ft values have been computed assuming a 20 % ground-state component[3,5]) and using the gamma transition intensities given in table 5.

have been divided into three groups dependent upon the strength of evidence for their existence and position. In order to clarify the arguments leading to this level structure and simplify the interpretation, each level will be discussed separately.

The 134-keV level

There is ample evidence that the first excited state of Re^{187} occurs at 134 keV The 134 keV gamma ray has been observed in Coulomb excitation[10–15]) and resonance fluorescence[24]) experiments, and following the beta decay of W^{187} [1–9]). The latter measurements have shown that this level is fed by gamma rays of 72 keV and 552 keV from the 206-keV and 686-keV levels respectively. The present coincidence measurements have shown the existence of weak feeding by gamma rays of 626 keV, 732 keV, 167 keV, and perhaps 776 keV. The possibility of additional beta feeding from W^{187} was investigated by Vergnes[8,9]). He placed an upper limit of 5 % on the portion of the total number of beta transitions which feed this level. This is in accord with the present measurements.

The probable spin and parity assignment for this level ($\frac{7}{2}^+$) has been discussed in detail in subsection 3.5.

The 206-keV level

The metastable state at 206 keV is fed by a 480-keV gamma transition from the 686-keV level. It is de-excited mainly by a 72-keV E1 transition to the first-excited state (cf. subsection 3.3). The ground state transition from the 206-keV level is quite weak. Again, as for the 134-keV level, there does not appear to be significant beta feeding of this level.

In accord with the E1 multipolarity of the 72-keV transition to the $\frac{7}{2}+$ first-excited state, possible spin and parity assignments for the 206-keV level are $\frac{9}{2}-$, $\frac{7}{2}-$, or $\frac{5}{2}-$. Thus the 206-keV transition can be M2 or E1. The relative weakness of this transition favors an M2 multipolarity and hence the $\frac{9}{2}-$ assignment for the 206-keV level. The Nilsson model predicts a $\frac{9}{2}-$ orbit in this region[21,22]). This has been observed at 496 keV in Re^{183} [25]).

The halflife of the 206-keV state is[1]) 0.55 μsec. This lifetime clearly shows that the 72-keV E1 transition is highly hindered. Presumably this is a K-forbidden transition in which case the observed retardation is as predicted.

The 301-keV level

Gamma rays of 134 keV, 167 keV and 301 keV have been observed in Coulomb excitation of Re^{187} [10–15]). As a result of these experiments, a level at 301 keV has been proposed which is deexcited by a ground-state transition and a cascade through the 134-keV level. This level has been interpreted as the third member ($\frac{9}{2}+$) of the ground-state rotational band.

In the present experiment gamma rays of 167 keV and 301 keV have been observed and have been shown to be in coincidence (cf. figs. 3 and 6A). Although the possibility that the 301-keV–167-keV cascade reaches the ground state directly cannot be ruled out on the basis of the coincidence measurements, it is probable that this cascade feeds the first-excited state. Aside from the 301-keV, 167-keV, and probably the 134-keV gamma rays, no other coincidences were observed in this sequence. If the 167-keV gamma ray is a transition from the 301-keV level to the first excited state, then the observed 301-keV gamma ray must feed the 301-keV level. It is possible that the 167-keV and 301-keV gamma rays observed in this experiment differ from those following Coulomb excitation. However, if the same levels are involved, one is forced to conclude that the crossover transition from the 301-level is weaker than had been supposed.

*The 440-*keV *level*

A new level is proposed at 440 keV which is fed by a 179-keV gamma ray from the 619-keV level and de-excited by a ground-state transition. Evidence for this cascade appears in figs. 4 and 6B. Fig. 5 supports the conclusion that this cascade deexcites the 619 keV level. Decay of the 440-keV level to the ground state but not to the 134-keV, 206-keV, or 301-keV levels favors a low spin, perhaps $\frac{1}{2}$, for this level.

*The 485-*keV *level*

Figs. 3 and 4 show the existence of a line of about 485 keV which is different from the 480-keV transition (between the 686-keV and 206-keV levels). Fig. 7A shows the origin of this coincidence as a 201-keV–485-keV cascade, which apparently de-excites the 686-keV level. Fig. 7A also indicated a weak 290-keV–485-keV coincidence. The 290-keV gamma ray is probably a transition between the 775-keV and 485-keV levels. As in the case of the 440-keV level, the direct decay to the ground state favors a low spin for the 485-keV level.

*The 602-*keV *level*

The 602-keV level has been postulated in order to explain the observed 301-keV–167-keV coincidence. The arguments regarding the position of this cascade have been given above in the discussion of the 301-keV level. A weak 467-keV gamma ray was observed in the internal-conversion measurements (cf. table 2) which may correspond to a transition between the 602-keV level and the first-excited state. Since no gamma rays are observed feeding the 602-keV level, it is presumably fed by a separate beta transition. The pattern of transitions from this level favors a spin of $\frac{3}{2}$.

*The 619-*keV *level*

The 619-keV level is de-excited by a strong ground-state transition and by a weak cascade through the 440-keV level. It is fed mainly by a beta transition

from W^{187}. Additional weak feeding by a 247-keV gamma ray from the 866-keV level is indicated in the coincidence spectra (cf. figs. 5 and 8).

A low spin is favored by the direct ground-state decay from this level. If the W^{187} ground state is characterized as $\frac{7}{2}-$ (cf. below), a $\frac{3}{2}+$ assignment to the 619-keV level would require a first-forbidden beta decay to this level in accord with observed log $ft = 7.4$.

*The 686-*keV *level*

The 686-keV level is fed mainly by a strong beta transition from W^{187} and de-excited by strong gamma rays of 480 keV, 552 keV and 686 keV. An additional weak 201-keV gamma ray from this level has been discussed above in regard to the 485-keV level. Evidence for a very weak 180-keV gamma ray feeding the 686-keV level appears in the coincidence measurements (cf. table 1).

The assignment of a spin and parity of $\frac{7}{2}-$ to the 686-keV level has been discussed in detail in subsection 3.5. In accord with the Nilsson model, possible spin and parity assignments for the W^{187} ground state are $\frac{1}{2}-$, $\frac{3}{2}-$, or $\frac{7}{2}-$. The observed log ft (6.5) of the beta transition to the 686-keV level ($\frac{7}{2}-$) rules out $\frac{1}{2}-$ and $\frac{3}{2}-$. A $\frac{7}{2}-$ assignment for the W^{187} ground state would characterize this beta transition as allowed hindered. Beta decay to the ground state and 134-keV and 206-keV levels also appears to be hindered.

*The 760-*keV *level*

The presence of a coincidence between the 134-keV gamma ray and a gamma ray in the region 610 keV to 650 keV was shown in fig. 8. It seems reasonable that this coincidence arises from the 626-keV gamma ray observed by Cork *et al.*[3]) (cf. table 2). This then necessitates the placing of a level at 760-keV. Both the 626-keV and 760-keV gamma rays appear in coincidence with a gamma ray in the region 180 keV to 225 keV (cf. fig. 4). Fig. 8 shows the energy of this transition to be 185 keV. The 760-keV level is partly fed by a beta transition. A weak transition 106 keV, observed only in internal conversion (cf. table 2), has been shown in the decay scheme feeding the 760-keV level.

The pattern of transitions from this level favor a spin assignment of $\frac{3}{2}$.

*The 775-*keV *level*

The observed M2 multipolarity of the 775-keV ground-state transition (cf. table 3) favors a spin and parity of $\frac{1}{2}-$ for this level. The log $ft = 7.4$ of the beta transition feeding this level is then difficult to explain.

*The 866-*keV *level*

Evidence for the placing of a level at 866-keV includes the presence of a ground-state transition and 732-keV and 247-keV transitions to the 134-keV and 619-keV levels respectively. An additional weak transition of 180-keV to

the 686-keV level has also been proposed. This level is apparently fed by a separate beta transition from W^{187}. A spin assignment of $\frac{1}{2}$ or $\frac{3}{2}$ seems to be favored by the observed gamma de-excitation.

*The 910-*keV *level*

The weak 776-keV–134-keV coincidence suggests the placing of a beta-fed level at 910 keV.

*The 945-*keV *level*

The 185-keV transition to the 760-keV level de-excites a beta-fed level at 945 keV.

References

1) McGowan, DeBenedetti and Francis, Phys. Rev. **75** (1949) 1761
2) Muller, Hoyt, Klein and DuMond, Phys. Rev. **88** (1952) 775
3) Cork, Brice, Nester, LeBlanc and Martin, Phys. Rev. **89** (1953) 1291
4) A. W. Sunyar, Phys. Rev. **90** (1953) 387A
5) Dubey, Mandeville, Mukerji and Potnis, Phys. Rev. **106** (1957) 785
6) H. J. Behrend and H. Neuert, Z. Naturforsch., **13a** (1958) 208
7) M. V. Klimentovskaya and P. I. Shavrin, JETP **36** (1959) 1360
8) M. Vergnes, J. Phys. Rad. **19** (1958) 947
9) M. Vergnes, Ann. de Phys. **5** (1960) 11
10) E. M. Bernstein and H. W. Lewis, Phys. Rev. **105** (1957) 1524
11) G. Goldring and G. Paulissen, Phys. Rev. **103** (1955) 1314
12) Davis, Divatia, Lind and Moffat, Phys. Rev. **103** (1956) 1801
13) Wolicki, Fagg and Geer, Phys. Rev. **105** (1957) 238
14) F. K. McGowan and P. H. Stelson, Phys. Rev. **109** (1958) 901
15) de Boer, Martin and Marmier, Helv. Phys. Acta **32** (1959) 377
16) M. E. Rose, Phys. Rev. **91** (1953) 610
17) Arns, Sund and Wiedenbeck, Univ. of Mich. Res. Inst. Report 2375-4-T, February 1959
18) L. A. Sliv and I. M. Bond, Leningrad Phys. Techn. Inst. Rep. 1956 (translations: Report 57 ICC Kl, Phys. Dep. University of Illinois, Urbana, Illinois)
19) J. Trombka and M. L. Wiedenbeck, Univ. of Mich. Res. Inst. Report 2863-2-P, September 1960
20) S. L. Segel and R. G. Barnes, Phys. Rev. **107** (1957) 638
21) S. G. Nilsson, Mat. Fys. Medd. Dans. Vid. Selsk. **29**, No. 16 (1955)
22) B. R. Mottelson and S. G. Nilsson, Mat. Fys. Skr. Dans. Vid. Selsk. **1**, No. 8 (1959)
23) R. G. Arns and M. L. Wiedenbeck, Phys. Rev. **111** (1958) 1631
24) R. L. Mossbauer and W. H. Wiedemann, Zeit. f. Phys. **159** (1960) 33
25) J. O. Newton and V. S. Shirley, Bull. Am. Phys. Soc. **2** (1957) 395

1.E.1
1.E.4

Nuclear Physics **19** (1960) 654—664; © *North-Holland Publishing Co., Amsterdam*
Not to be reproduced by photoprint or microfilm without written permission from the publisher

ON THE DECAY OF 5.8 d Sb^{120}, 5.1 h Sb^{118} AND 1 h Sb^{116}

B. SKYTTE JENSEN, O. B. NIELSEN and O. SKILBREID

Institute for Theoretical Physics, Copenhagen

Received 11 May 1960

Abstract: Activities of Sb^{116}, Sb^{118} and Sb^{120} were produced in the Sn(d, n)Sb or In(α, n)Sb reactions. Sources for β- and γ-ray spectroscopy were prepared in an isotope separator. The radiations were studied in two six-gap β-ray spectrometers and by scintillation spectrometers in connection with a 100-channel kicksorter.

The decay scheme of McGinnis for Sb^{120} is confirmed, and schemes for 1 h Sb^{116} and 5.1 h Sb^{118} are proposed. The level schemes of the single closed-shell nuclei Sn^{116}, Sn^{118} and Sn^{120} are compared with the calculation of Kisslinger and Sorensen.

1. Introduction

The assumption of a pairing correlation in the movement of the particles in the nucleus has led to an understanding of many nuclear properties[1, 2]). The ground state of even nuclei is considered to be a coherent superposition of many shell-model configurations, which is favoured energetically by 1 to 2 MeV relative to levels formed by the excitation of two particles in unpaired configurations. In the resulting energy gap, only collective excitations of the ground-state structure are found. The first excited level in spherical even nuclei has systematically spin 2^+, and the properties support an interpretation as a one-phonen vibrational state[3]). The degenerate two-phonen states with spins 0^+, 2^+ and 4^+ have in general an energy in the region of the intrinsic two-particle excitations and, although many levels have been observed which are believed to belong to this triplet, the nature of this second vibration is not fully established.

Recently, Kisslinger and Sorensen[4]) have included the effect of a pairing interaction in a calculation of the structure of the two-particle excitations in even nuclei with a single closed shell (s.c.s. nuclei). A detailed verification of the calculated scheme is scarcely possible, as present experimental means in general reveal only a smaller number of levels in the interesting region above the energy gap. Still, it can be tested how well the experimental data are contained in the calculated picture, and thus to which extent the parameters used in the calculation need revision.

Sn represents one of the s.c.s. regions, and the large number of isotopes available makes practicable a rather systematic comparison with the scheme of Kisslinger and Sorensen. In all the even isotopes from Sn^{112} to Sn^{124}, the collec-

tive 2^+ level is known from Coulomb excitation[5, 6]). Higher levels in Sn^{120}(ref. [7])) and Sn^{118}(ref. [8])) are excited in the K-capture decay of Sb^{120} and Sb^{118} and in the β-decay of In^{118}. The levels in Sn^{116} have been studied[9, 10]) from the β-decay of In^{116}. Two excited levels are reported[11]) on the decay of 15 min Sb^{116} and, furthermore, a 1 h isomer of this isotope has been reported[12]). Pure sources of this activity have not been prepared as more long lived Sb isotopes are produced simultaneously. In the present work, this difficulty was overcome by the preparation of sources in an isotope separator.

2. Experimental Methods

2.1. TARGET PREPARATION

The Sb activities were produced in the Copenhagen cyclotron either in the Sn(d, n)Sb reaction or in the In(α, n)Sb reaction with α-particles of 20 MeV or deuterons of 11 MeV. In most cases, the cyclotron targets consisted of the pure metals which were simply melted on a copper block. For the production of Sb^{116} in the (α, n) reaction, In_2O_3 enriched to about 30 % in In^{113} (supplied by the Electromagnetic Isotope Separator Group of Harwell) was used as target. It was dissolved in a small amount of concentrated nitric acid; the solution was neutralized with excess concentrated ammonia and transferred to a gold block. By carefully heating the bar with a small flame from underneath it was possible to evaporate the water, melt the NH_4NO_3 and sublime it off, leaving the Indium oxide as a yellow-brown, well adherent layer. The irradiated material could easily be scraped off after the bombardment. The same technique should be useful for many other metals.

2.2. SOURCE PREPARATION

The ion source of the isotope separator[13]) was charged with metallic antimone carrying the antimone activity. The charge was prepared from scrapings of the irradiated material, which was dissolved in conc. hydrochloric acid in the hood. Antimone carrier was added as $SbCl_3$ dissolved in concentrated HCl, giving about 10 mg precipitate in the succeeding reduction which was performed with tin filings, and the precipitate was centrifuged. After several washings with concentrated HCl, water, and finally alcohol, the precipitate was dried under an infra lamp and transferred to the oven of the ion source. The chemical steps were performed in 20–30 min, and the yield of the activity was about 70 %.

Sb^{118} and Sb^{120} were studied only on isotope separated sources, the intensity being 10–20 μc. Also the measurements of γ-rays and low energy conversion lines from Sb^{116} could be performed with isotopically pure sources, but the high energy conversion lines had to be studied with stronger sources prepared by a purely chemical procedure. In this case, enriched Indium oxide was irradiated with α-particles for one hour, and the bombarded material dissolved

in a few drops of concentrated HCl. The solution was filtered through glass wool and evaporated on a Teflon disc under an infrared lamp until a volume of about $\frac{1}{20}$ ml was obtained. This drop was transferred by means of a small pipette to the source backing consisting of a thin film formed by a mixture of polystyrene and stearylamine in $\frac{3}{1}$ ratio. Such a film has been found to adsorb many activites, among others antimony, from strong hydrochloric acid. After drying under the infra-lamp several washings with concentrated HCl removed the crystals of $InCl_3$, leaving in some cases up to 70 % of the activity. Sources of mc strength could be obtained in this way.

Due to the presence of In^{115} in the target material, these sources also contained a considerable amount of Sb^{118}. The conversion lines could be identified, however, from the lifetimes and from the known γ-ray energies.

2.3. APPARATUS

The conversion lines and e-γ coincidence spectra were studied in two six-gap β-ray spectrometers[14]). The experimental technique employed has already been described in detail[15]); the coincident γ-ray spectra were recorded by means of a 3.8 cm × 3.8 cm NaJ crystal. Single γ-ray spectra as well as γ-γ coincidence spectra were recorded in a conventional setup in connection with a 100-channel kick-sorter.

An attempt to estimate the lifetime of a state in Sn^{118} was made in a conventional fast-slow coincidence setup, which was also used for angular correlation measurements.

3. Experimental Methods

3.1. Sb^{120} (5.8 d)

The γ-ray spectrum of isotope separated Sb^{120} is seen on fig. 1. In addition to K X-rays, the spectrum consists of four lines of 90, 200, 1010, and 1170 keV. Intensities and conversion line data are collected in tables 1 and 2. The K-

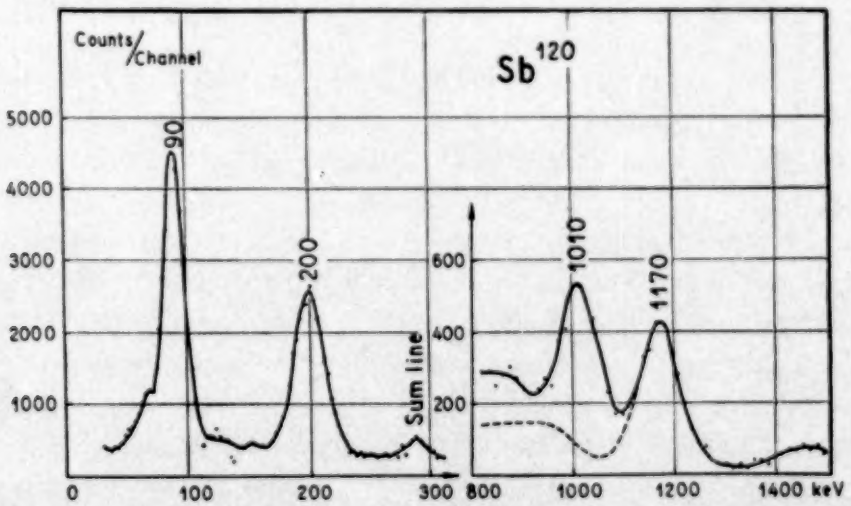

Fig. 1. Single-channel γ-ray spectrum of Sb^{120} with a NaJ-crystal.

conversion coefficients and K/L ratios classify the 90 keV transition as E1 and the remaining three as E2's. The quantitative results are in close agreement with those of McGinnis[7]).

TABLE 1

Data of Sn^{120}

E_γ (keV)	I_γ (%)	I_K ($\times 10^4$)	α_K (exp.)	Assignment	α_K (theor.)			I_{trans} (%)
					E1	E2	M1	
90	90	2260	0.25	E1	0.205	1.55	0.65	115
200	106	1750	0.165	E2	0.022	0.112	0.072	123
1010	84	12.6	0.0015	E2	0.00047	0.00110	0.00133	84
1170	100	(7.9)		(E2)		(0.00079)		(100)

The intensities are normalized with respect to the 1170 keV transition which is considered as pure E2.

TABLE 2

K/L Ratios of Sn^{120}

E_γ (keV)	Exp.	Theoretical		
		E1	E2	M1
90	7.7	7.8	2.8	8.1
200	5.8	8.4	5.7	8.4

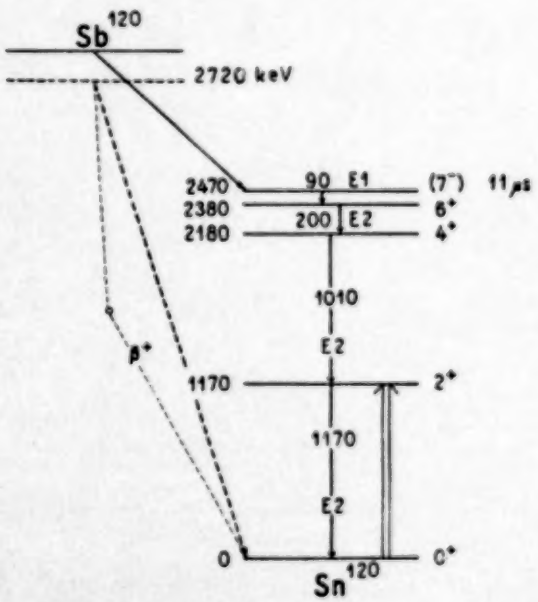

Fig. 2. The decay scheme $Sb^{120} \rightarrow Sn^{120}$. The data given with dotted lines refer to the short lived activity.

γ-γ coincidence experiments confirmed that all the γ-rays were coincident and thus forming one cascade. No coincidences with X-rays were observed; a lifetime of 11 μs for the state populated by K-capture was recorded by McGinnis.

The 1170 keV γ-rays have been observed in Coulomb excitation and must thus populate a 2^+ level at 1170 keV. The measurement of McGinnis of the angular correlation between the 1170 and 1010 keV γ-rays established a second excited level at 2180 keV with spin 4^+. The order of the 90 and 200 keV γ-rays was not uniquely determined. The position in the decay scheme, fig. 2, is consistent with the angular correlations.

An attempt to establish the order of the low energy transitions by looking for possible delayed coincidences between the 200 keV and the remaining γ-rays was not successful. We observed no lifetime larger than about 3×10^{-9} s. The 90 keV transition was placed above in fig. 2 by McGinnis, the argument being that a 11 μs lifetime is more likely to be connected with a 90 keV E1 than with a 200 keV E2 transition.

3.2. Sb^{118} (5.1 h)

The γ-ray spectrum (fig. 3) contains four lines of 40, 255, 1030 and 1220 keV. No annihilation radiation was observed, the upper limit for positron emission

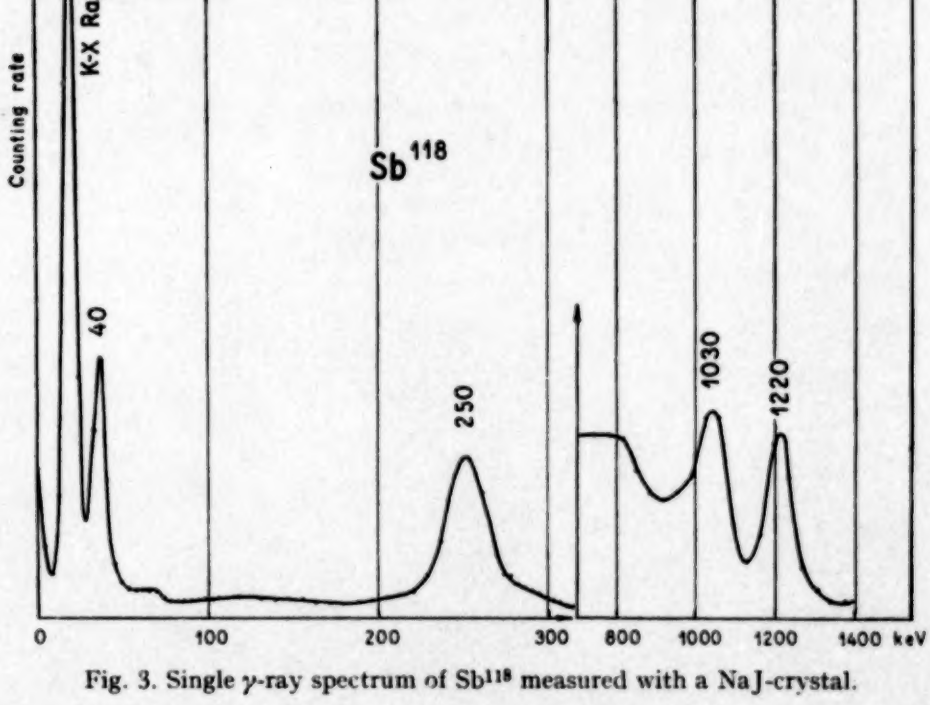

Fig. 3. Single γ-ray spectrum of Sb^{118} measured with a NaJ-crystal.

being 0.1 % of all decays. The data collected in table 3 specify the 40 keV transitions as E1, and the others as E2's. The E2 character of the 250 keV transition was confirmed by a K/L ratio of 5, in agreement with the theoretical

TABLE 3

Data of Sn^{118}

E_γ (keV)	I_γ (%)	I_K ($\times 10^4$)	α_K (exp.)	Assignment	α_K (theoretical)			I_{trans} (%)
					E1	E2	M1	
40*	29	740	0.25	E1	0.27	24	0.86	83
250	91	467	0.051	E2	0.012	0.054	0.040	97
1030	93	10.5	0.00118	E2	0.00045	0.00102	0.00125	93
1220	100	(7.0)		E2		(0.00070)		(100)

The intensities are normalized with respect to the 1220 keV transition which is considered as pure E2.

* The data refer to the L shell.

E2 value. Dipole transitions have K/L ratios larger than 8. The four γ-rays were coincident; the 1220 keV ray is known from Coulomb excitation and is thus the last in the cascade. The 40 keV transition was not coincident with X-rays, whereas coincidences between the other γ-rays and X-rays could be explained by the K-conversion of the 40 keV transition.

All these data are quite analogous to those of the Sb^{120} decay and suggest tentatively a similar decay scheme (fig. 4). To check this interpretation further,

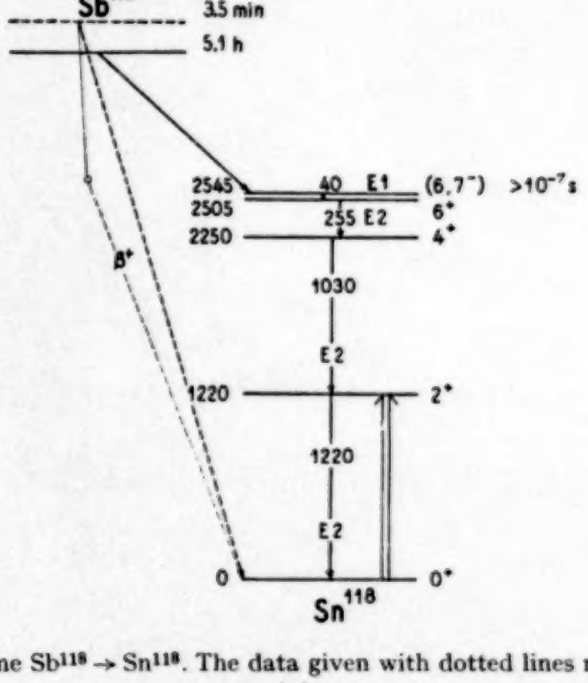

Fig. 4. The decay scheme $Sb^{118} \rightarrow Sn^{118}$. The data given with dotted lines refer to the short lived activity.

the angular correlations of the 1030–1220 keV cascade were measured. An attempt to measure the correlations between the 40 and 255 keV lines failed. Although the activity was dissolved in concentrated hydrochloric acid, which

was contained in a glass capillary, the correlation function seemed to be time-dependent. This is believed to be due to a gradual change in the chemical properties of the SnSb complexes.

The angular correlation coefficients for the 1030–1220 keV cascade were $A_2 = 0.11 \pm 0.02$ and $A_4 = 0.07 \pm 0.07$. This correlation is similar to that found by McGinnis for the 1010–1170 keV cascade in Sn^{120} and is consistent with the spin sequence 4–2–0. An unique spin determination on the basis of this measurement is not possible, partly because the M1 and E2 internal conversion coefficients differ by only 20 %.

Also the data on the decay of Sb^{118} are in agreement with those of McGinnis and Kundu[8]).

3.3. Sb^{116} (1 h)

The γ-ray spectrum (fig. 5) contains the six lines listed in table 4 in addition to the peak due to annihilation-radiation. Furthermore, there is some indication

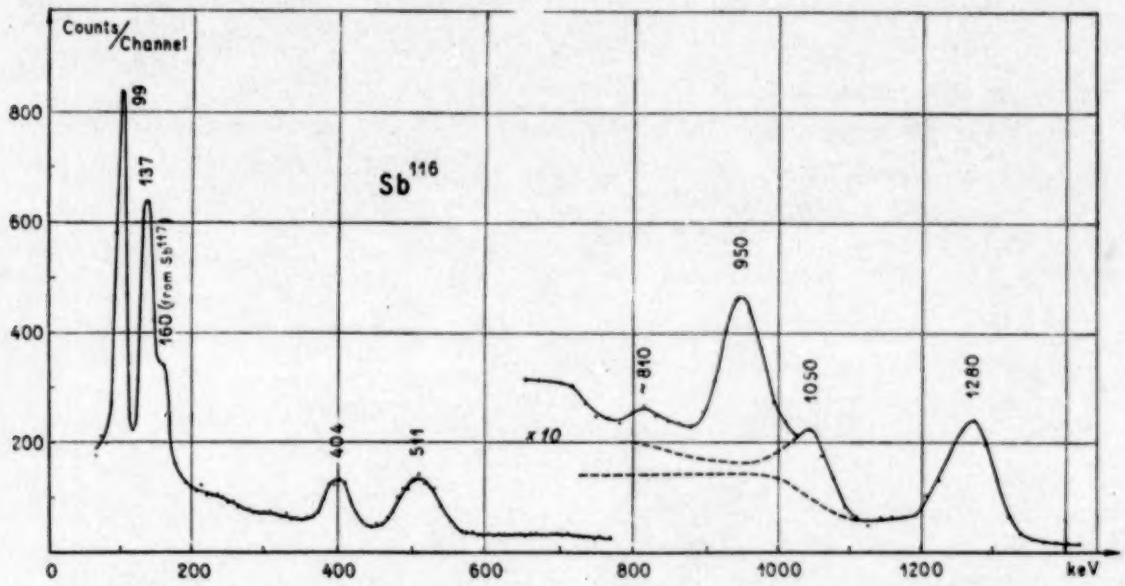

Fig. 5. Single γ-ray spectrum of Sb^{116} measured with a NaJ-crystal.

of a weak γ-ray 810 keV. The estimate of the relative intensities of the three high energy lines was facilitated by the fact that the contribution from the 1280 keV γ-ray could be found by measuring the 1280 keV γ-ray from Na^{22} in the same geometry. The conversion lines of these transitions were measured on unseparated sources containing Sb^{116} and Sb^{118} in about equal intensity, and the 1050 keV line was not resolved from the 1030 keV line of Sb^{118}. Since also the γ-ray intensity was measured with some difficulty, the α_K for this transition is given with less accuracy. The E2 character of the 99 keV transition was confirmed by a K/L ratio of 2.8.

The maximum energy of the continuous β^+ spectrum was found to be

1160 ± 40 keV, indicating a total energy difference between 1 h Sb^{116} and Sn^{116} of 4510 ± 50 keV. The measurement was performed in the β-ray spectrometer on a weak isotope separated source. Unseparated sources contained impurities of other β^+ emitters.

TABLE 4

Data of Sn^{116}

E_γ (keV)	I_γ (%)	I_K (× 10^4)	α_K (exp.)	Assignment	α_K (theoretical)				I_{trans} (%)
					E1	E2	M1	M2	
99	27	3800	1.4	E2	0.155	1.12	0.48		78
137	26	610	0.23	M1	0.063	0.40	0.20		33
404	32	54	0.017	M1 or E2	0.0034	0.0117	0.0115		32
953	66	4.7	0.00071	E1	0.00052	0.0012	0.0015		66
1055	28	5.3	0.0019	M2 (+E1)	0.00042	0.00095	0.00117	0.0030	28
1280	100	(6.7)		E2		(0.00067)			(100)

The intensities are normalized with respect to the 1280 keV transition which is considered as pure E2.

The 1280 keV γ-ray is known from Coulomb excitation as deexciting the first excited 2^+ level in Sn^{116}. It was coincident with the 99, 950 and 1050 keV transitions, whereas the 99 keV transition was coincident with 950, but not with 1050 keV. The energy fit would thus indicate a cascade of 99 and 950 keV

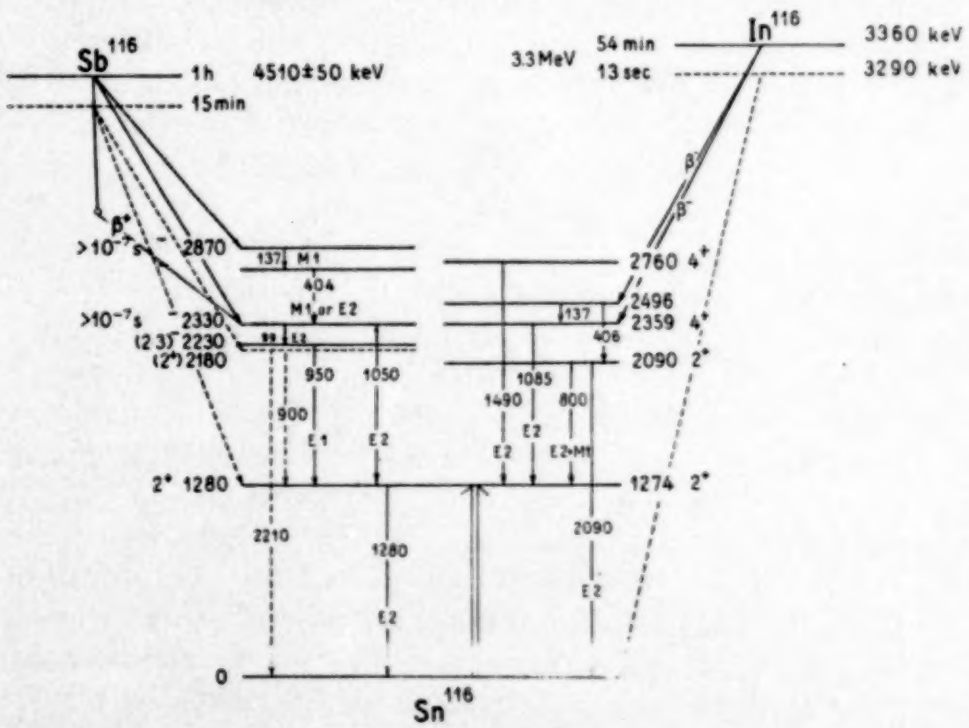

Fig. 6. The decay schemes $Sb^{116} \rightarrow Sn^{116}$ and $In^{116} \rightarrow Sn^{116}$. The data given with dotted lines refer to the short lived activities.

transitions with the 1050 as a crossover, suggesting levels with negative parity at 2230 and 2330 keV. An M2 (+E1) assignment for the 1050 keV transition is consistent with the conversion coefficient as well as with the fact that the partial halflife is about the same as that of a 99 keV E2-transition. The 140 and 404 keV lines were mutually coincident, but not with other γ-rays. Since levels in Sn^{116} with energies of 137, 404 or 541 keV are extremely unlikely, they are shown in the decay scheme as originating in a 2870 keV level.

The intensities of the transitions given in table 4 show that the 2870 and 2330 keV levels are fed by K-capture. No coincidences between any γ-rays and annihilation radiation or K X-rays were observed, and lifetimes $\gtrsim 10^{-7}$ s must be suggested for the two levels in question.

Also the levels of Sn^{116} observed in the decay of In^{116} and 15 min Sb^{116} are given in fig. 6.

4. Discussion

The results of Kisslinger and Sorensen regarding the excitation of two neutrons in the even Sn isotopes are shown in fig. 7. The complete level scheme generated by the splitting of the configurations is evidently very complex. Due to the fact that all the single-particle orbits in a major shell have the same parity, except the one with highest angular momentum, many levels are expected with low spin and even parity. Odd-parity levels occur only when one of the unpaired particles moves in this latter orbit and, consequently, they can in principle be identified with less ambiguity than the levels of even parity.

The levels observed in Sn^{120} have been discussed in ref. [4]). Whereas the 1170 keV 2^+ level clearly is the first collective state, the 2228 keV 4^+ level can be a member of either the two-phonon triplet or the $(h_{\frac{11}{2}})^2$ configuration, both of which are expected at this energy (fig. 7). The 6^+ level is also interpreted as a member of this configuration, and the 2570 keV level as the 7^- state of the $(h_{\frac{11}{2}}\, d_{\frac{3}{2}})$ combination. The E1 transition from this level thus represents a single-particle transition from a $d_{\frac{3}{2}}$ to a $h_{\frac{11}{2}}$ orbit. This is consistent with the long lifetime.

The levels observed in Sn^{118} are apparently quite analogous to those of Sn^{120} and, according to fig. 7, they can also be interpreted in an identical way. Also the slightly lower energies of the levels are understandable. In Sn^{114}, however, the configurations containing the $d_{\frac{3}{2}}$ and $g_{\frac{7}{2}}$ states are expected to introduce additional levels of low or medium spin below 3 MeV. Such a change relative to Sn^{120} and Sn^{118} seems already to be apparent in the level scheme of Sn^{116}, as negative parity states with spins as low as 2 or 3 can only be obtained by the coupling of a $h_{\frac{11}{2}}$ to a $g_{\frac{7}{2}}$ or $d_{\frac{3}{2}}$ particle. A correction to the calculation in this direction is already suggested by results from the odd Sn isotopes (ref. [4])), the experimental $\frac{7}{2}^+$ state in Sn^{115} being well below the calculated one.

A detailed comparison of experimental and calculated levels in Sn^{116} is

scarcely justified, also because the experimental material is still incomplete. The 2090 keV 2^+ level excited in the decay of In^{116} deexcites predominantly with E2 radiation to the 1280 keV vibrational level, the reduced transition probability of the ground state transition being about 100 times smaller, and thus favouring an interpretation as a two-phonon state. A level with similar

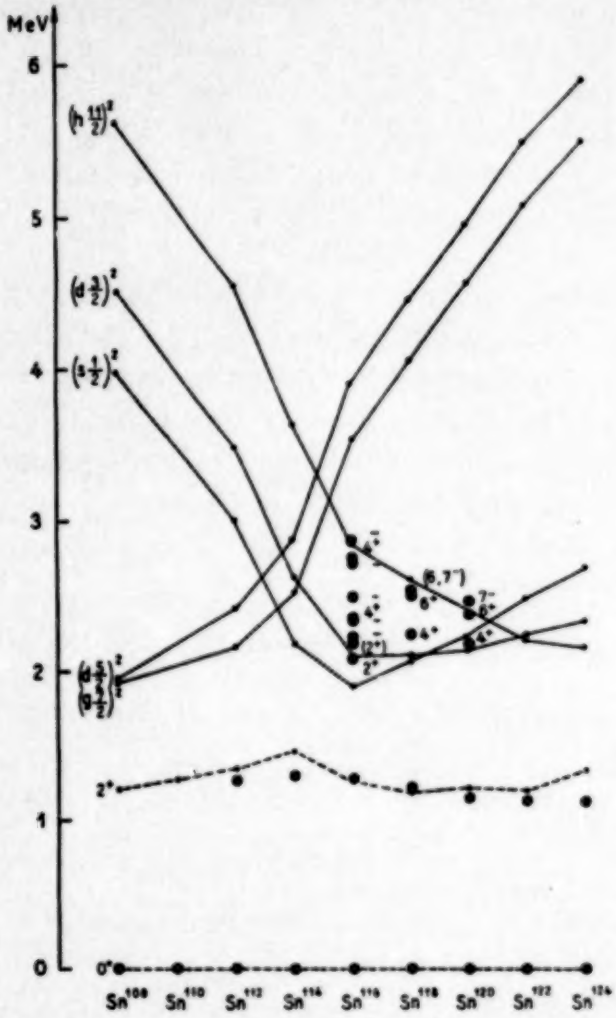

Fig. 7. The level schemes of the even Sn isotopes according to the calculation of Kisslinger and Sorensen. Only configurations with two neutrons in the same state are indicated. Combinations involving two particles from different states should be placed half way between the corresponding two curves. The splitting of the configurations has not been calculated. The $(h\,\frac{11}{2})^2$ state f. ex. generates levels with spins 10^+, 8^+, 6^+ ... and a $(h\,\frac{11}{2}\,d\,\frac{3}{2})$ state levels of 7^-, 6^-, 5^- and 4^-. The heavy dots indicate experimental levels.

properties is seen, however, at 2180 keV in the decay of 15 min Sb^{116}, and at least one of them is then probably a particle excitation. The relative intensities of the deexciting γ-rays is possibly the result of mixing with the two-phonon state. Due to the large E2 transition probability connected to a vibrational state, the γ-ray intensities can be largely determined by the admixed component.

A more complete discussion of the nuclear transformations of Sb and In isotopes into Sn isotopes would have to deal with the nature of the mother states. The structure of these states must be assumed to determine the β-decay not only in terms of spin selection rules, but also, more detailed, the transition probability to the individual daughter levels.

The odd proton in the odd Sb isotopes probably occupy a $g_{\frac{7}{2}}$ or $d_{\frac{5}{2}}$ orbit as indicated by the spin of the odd mass Sb isotopes. The low lying states for the odd neutron should correspond to those given in fig. 7. Still, there exists no quantitative calculation of the resulting configurations, but it is at least easy to understand the presence of close lying states of high and low spin demonstrated by the isomeric levels in Sb^{116} as well as Sb^{118} and Sb^{120}.

We wish to express our sincere gratitude to Professor Niels Bohr for the excellent working conditions in his Institute. We are indebted to Drs. R. A. Sorensen and L. S. Kisslinger for permission to read their manuscript prior to publication, and to Professor A. Bohr for illuminating discussions. One of us (B.S.J.) is grateful to the Danish Atomic Energy Commission, especially Dr. C. F. Jacobsen, for having given him the opportunity to participate in this work. We are indebted to Professor N. O. Lassen and the cyclotron crew for numerous bombardments.

References

1) A. Bohr, B. R. Mottelson and D. Pines, Phys. Rev. **110** (1958) 936
2) S. T. Belyaev, Mat. Fys. Medd. Dan. Vid. Selsk. **31,** no. 11 (1959)
3) G. Scharff-Goldhaber and J. Weneser, Phys. Rev. **98** (1955) 212
4) L. S. Kisslinger and R. A. Sorensen, Mat. Fys. Medd. Dan. Vid. Selsk **32,** No. 9 (1960).
5) P. H. Stelson and F. K. McGowan, Phys. Rev. **110** (1958) 489
6) D. G. Alkhazov, D. S. Andreev, K. I. Erokhina and I. Kh. Lemberg, JETP **33** (1957) 1347
7) C. L. McGinnis, Phys. Rev. **109** (1958) 888
8) C. L. McGinnis and D. N. Kundu, Bull. Am. Phys. Soc. **3** (1958) 62
9) H. Slätis, S. J. DuToit and K. Siegbahn, Ark. f. Fysik **2** (1951) 321
10) R. P. Scharenberg, M. G. Stewart and M. L. Wiedenbeck, Phys. Rev. **101** (1956) 689
11) P. Stähelin, D. Maeder and M. Pochon, Z. Phys. **140** (1955) 498
12) A. H. W. Aten, J. Manassen and G. D. de Feyfer, Physica **20** (1954) 665
13) K. O. Nielsen and O. Skilbreid, Nuclear Physics **2** (1958) 15
14) O. B. Nielsen and O. Kofoed Hansen, Mat. Fys. Medd. Dan. Vid. Selsk. **29,** no. 6 (1955)
15) P. Gregers Hansen, O. B. Nielsen and R. K. Sheline, Nuclear Physics **12** (1959) 389

9.B *Nuclear Physics* **19** (1960) 665—674; © *North-Holland Publishing Co., Amsterdam*
Not to be reproduced by photoprint or microfilm without written permission from the publisher

THE ANOMALOUS SCATTERING OF UNDERGROUND μ-MESONS

R. BURNSTEIN, T. KITAMURA† and D. D. MILLAR

The Falkiner Nuclear Department, School of Physics††, The University of Sydney, Sydney, Australia

Received 15 May 1960

Abstract: An experiment is described using a magnet cloud chamber and a multiplate chamber to investigate the scattering of underground μ-mesons of momentum < 1.5 GeV/c in iron and in lead. No evidence has been obtained for or against the existence of anomalous large-angle scattering. A computation of the effects of errors, as determined experimentally, on the theoretical scattering distributions indicates that these could easily simulate an apparent anomaly if not taken into account and that when they are taken into account the possibility of distinguishing between scattering from an extended nucleus and from a point nucleus becomes remote.

1. Introduction

The properties of the μ-meson appear to be well explained and understood save possibly in the observed scattering distribution of high energy μ-mesons traversing absorbers. Experimental determinations of the distribution of the angles of scatter of cosmic-ray μ-mesons up to 1957 have been discussed by Fowler and Wolfendale[1]) and further experiments have been reported since by Nash and Painton[2]), Fukui, Kitamura and Watase[3]) and by Alikhanian and Arutyunion[4]). Several experiments have indicated a frequency of occurrence of large angle scatters greater than is expected for a pure Coulomb interaction with an extended nucleus, such as accounts successfully for the observed analogous scattering of high energy electrons. Other experiments, however, have failed to confirm the anomaly. The question is a difficult one to resolve since the anomalous scattering occurs in the large-angle tail of the scattering distribution where the expected frequency of events is less than 1 % of the total number of scatters recorded and where the contribution to the scattering distribution from experimental uncertainties and errors may no longer be regarded as a second order effect; in this region it becomes of primary importance and must be rigorously taken into account. It has been recently stated by Lloyd and Wolfendale[5]), in criticising the work of Fukui *et al.*, that neither the experiment of these authors, nor any other experiment, has disproved the existence of the anomaly. It can also be questioned whether the experimental evidence substantiating the apparent anomaly would survive unscathed a similar detailed critical study.

† On leave of absence from Osaka City University, Osaka, Japan.

†† Also supported by the Nuclear Research Foundation within the University of Sydney.

The present paper does not aim to provide such a criticism, but rather gives a description of an experiment carried out on the scattering of the underground μ-meson flux using a magnet cloud chamber and a multiplate cloud chamber, together with an account of the methods whereby the experimental errors and their effects on the scattering distributions were investigated. The experiment provides no conclusive evidence for or against the existence of anomalous scattering and it was in fact discontinued when the investigation of the effects of the errors involved indicated that several years of recording with the apparatus would be required in order to arrive at a possibly significant answer.

2. Apparatus

The apparatus consisted of two cloud chambers placed one above the other. The upper chamber, of 30 cm diameter and 10 cm depth was placed between the poles of an electromagnet in an average field of 5500 Oe. This chamber was photographed stereoscopically by a camera inserted in a hole through one of the magnet pole pieces. The field of view of this camera was thereby restricted to a central region of the chamber of some 20 cm diameter. The illuminated depth of the chamber was 3.5 cm. The magnet current was continuously recorded.

Below this magnet chamber was a multiplate chamber of dimensions 55 cm $\times$ 45 cm $\times$ 20 cm illuminated depth. It contained 9 plates alternately of lead and of iron, each 1 cm thick.

A diagram of the apparatus is shown in fig. 1. Both chambers were triggered simultaneously by a coincidence between the three trays of Geiger counters located as shown in that figure. The apparatus was installed in an underground laboratory under 30 m of sandstone ($\approx$ 65 m water equivalent).

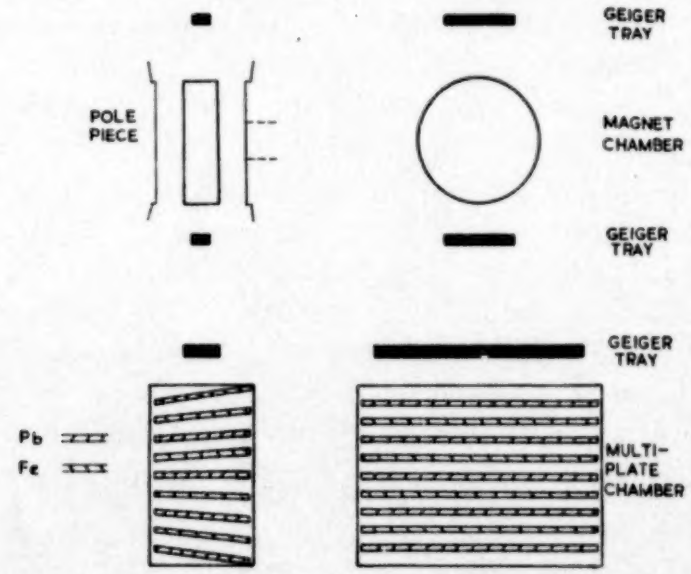

Fig. 1. Diagram of the apparatus to scale. The upper chamber has diameter 30 cm.

3. Measurements

For each event showing a track in both chambers the momentum was determined from the upper chamber photograph and the projected angle of scatter in each traversed plate from the lower chamber photograph.

The momentum of the particle is given by the relation $p = 300\ \bar{H}m/c_t$ eV/c where $\bar{H}$ (in Oe) is the appropriate average value of the magnetic field along the visible track, m is the magnification from object to image on the film and c_t is the curvature of the track image (in cm^{-1}). The first two quantities were determined by stereoscopic reprojection to find the position of the track within the chamber, together with a plot of the magnetic field strength, obtained with flip-coil and fluxmeter, throughout the sensitive volume of the chamber. Tracks were grouped together according to their depth in the chamber and to the distance of the track centre from the centre of the chamber. To each such group was ascribed a value of $\bar{H}$ using the approximate weighting function given by Thompson[6]). Such a procedure was necessary since the magnetic field varied between limits of 5700 and 5200 Oe within the sensitive volume. The correction was simplified by the narrowness of the illuminated volume of the chamber and the selection criterion that tracks must be at least 1.5 cm long on the film ($\approx$ 15 cm in the chamber) so that all tracks could be regarded as sufficiently close to the vertical that no correction for dip was required. For the same reason the location of the track in depth only was sufficient for the determination of m, the magnification.

Curvature of the track on the film was measured using a microscope with micrometer eyepiece. Successive settings of the eyepiece cross-hair were made on the track at half-millimeter intervals. Only tracks of length greater than 1.5 cm on the film were measured. A least-squares fit was then made of the measured data to the curve $Y_i = A + BX_i + CX_i^2$, where the Y_i are the micrometer readings at the points X_i along the track image. This least-squares computation was carried out for each measured track using the electronic computer "Silliac". The computation yielded the best value of the curvature of the track on the film, c_t, together with the quantity $\Sigma^2 = (Y_i - \bar{Y}_i)^2/n$, where n is the total number of readings Y_i along the track and $\bar{Y}_i$ is the corresponding value computed from the parabola of best fit. Σ^2 is then a measure of the goodness of fit of the computed parabola to the track.

The loss of momentum of each particle in traversing the material between the sensitive volumes of the chambers and in the plates in the lower chamber was corrected for. These losses were respectively 10 MeV/c and 20 MeV/c for relativistic μ-mesons.

The projected angles of scatter of the tracks in the multiplate chamber were measured using the method of McDiarmid[7]). Stereoscopic photographs were made

of the lower chamber but were used only to decide in cases of doubt whether a particle had left the illuminated volume of the chamber or had stopped in one of the plates.

4. The Theoretical Distributions

Theoretical scattering distributions have been computed on "Silliac" by Chartres[8]), for the scattering layers used here, employing a Monte Carlo technique. The cross-section for a single scatter by a μ-meson of given momentum is of the form

$$\sigma(\theta) = \text{const.}\ (\theta^2 + \theta_M^2)^{-\frac{3}{2}}\, h(\theta)\mathrm{d}\theta\,,$$

where θ is the total angle of deflection, θ_M is the Molière cut-off angle taking into account the effect of electron screening and $h(\theta)$ is the form factor given by Gatto[9]). The scattering distribution may be divided into roughly three regions. Small deflections upon traversal of the scattering medium result from the cumulative effects of many small deflections and in this region the distribution may be represented accurately by a gaussian distribution. Large total angles of deflection are more likely to arise from a single large angle of deflection and the distribution will then conform to the single scattering cross section. The intermediate region however may result from a combination of several moderate single scatters and it is in this region that the Monte Carlo computation is required.

The gaussian assumption for the multiple scattering region is equivalent to cutting off the single scattering cross section at some small angle θ_0, and assuming that the accumulated effect of all single scatters less than θ_0 can be replaced by one total scatter θ_g, which has a gaussian distribution. Then because of the sharp decrease of the cross-section with increasing angle only a very small number n of single scatters are greater than θ_0. In the case of the 1 cm thick absorbers as used in the experiment some 10^5 collisions are expected in one plate traversal while test computations showed that a suitable choice of θ_0 corresponded to $n\,(>\theta_0) \approx 4$ or 5; further reduction of θ_0, with a consequent increase in n, had no effect on the resulting computed distribution. The history of the particle traversing the plate was then simulated by choosing a number of deflections from a Poisson distribution of mean value $n(>\theta_0)$, and ascribing to each such collision a random angle of deflection chosen from the cross-section $\sigma(\theta > \theta_0)$ together with one further random deflection chosen from the small-angle gaussian. Each angle of deflection was decomposed randomly into two projected angles in two planes at right angles and the addition of the components yielded the final projected angles in the two planes.

Two distributions were obtained in this way corresponding to the case of an extended nucleus and of a point nucleus, the latter giving a predicted distribution with which the anomalous experimental results have in the past shown

agreement. The extended nucleus radius which is contained in the form factor h was taken as $1.3 \times 10^{-13} A^{\frac{1}{3}}$ cm. The point nucleus case was computed similarly by using a radius one-twentieth of the above, since it was found that further reduction had no effect upon the computed results.

The theoretical differential distributions of frequency versus the product $p\theta$, where p is the momentum of the particle and θ is the projected angle of scatter in traversing a 1 cm plate, was presented by the computer in the form of a histogram of interval width 0.125 (GeV/c) $\times$ deg. These distributions are shown in integral form in fig. 2. The distribution for the extended nucleus is labelled

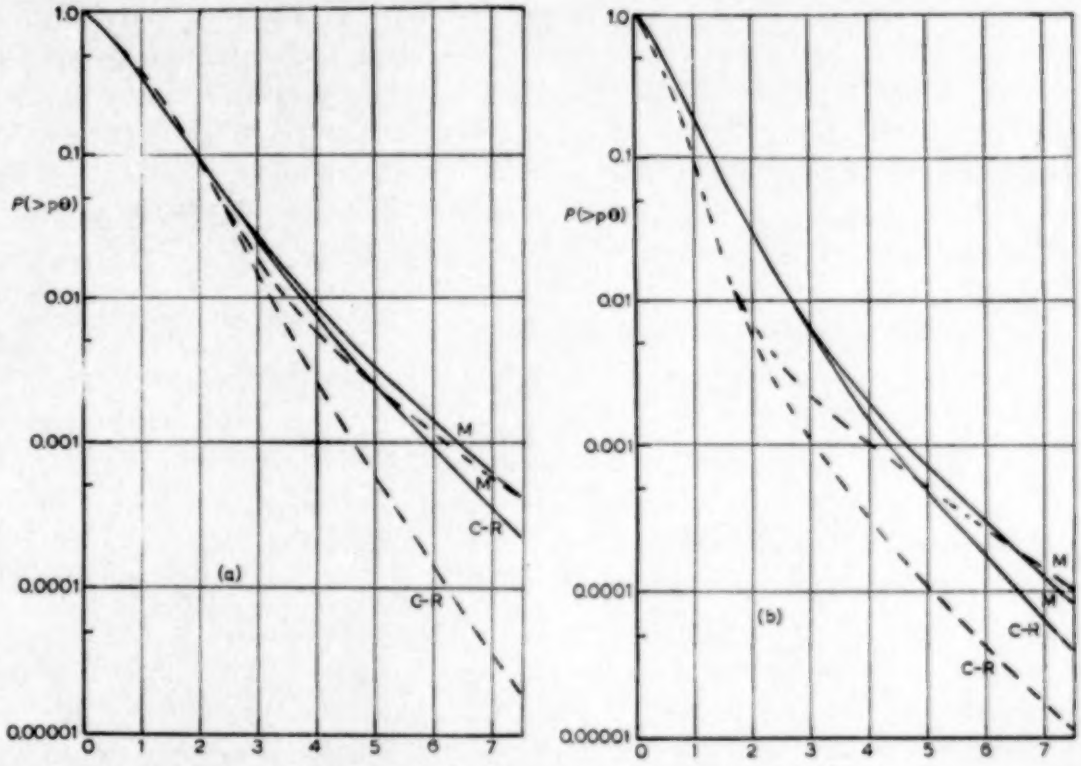

Fig. 2. The integral scattering distribution in 1 cm of lead (a), and in 1 cm of iron (b), as a function of $p\theta$ in units of (GeV/c) $\times$ deg. The broken lines are the theoretical distributions for scattering from a point nucleus (M) and from an extended nucleus (C–R). The full lines are the expected distributions when errors in determination of angle and momentum are included, for measured momenta < 2.3 GeV/c.

C–R since a repetition of the Monte-Carlo computation for a 2 cm thick lead plate yielded the same curve as obtained by Cooper and Rainwater[10]). The curve for the point nucleus is labelled M since it corresponds to the treatment of the problem given by Molière[11]).

5. The Effects of Errors on the Theoretical Scattering Distributions

For comparison with the experimental results the effects of errors in the measurements of p and of θ must be folded in to the theoretical distributions. These errors were determined as follows.

5.1. ERRORS IN MOMENTUM

The magnetic field was switched off at regular intervals throughout the period of recording. The photographs taken during these periods were scanned and those particles which showed no detectable scattering in the lower chamber, and which therefore were of sufficiently high energy to be unaffected by scattering in the gas of the upper chamber, had their curvatures in the upper chamber measured in the same way as described above. In this way a distribution of curvatures was obtained which, in the absence of the magnetic field, gives a measure of the effects of track distortion in the chamber and measurement errors. It is customary to fit the observed no-field curvature distribution with a gaussian distribution whose rms value gives the maximum detectable momentum of the apparatus, and in our case such a procedure yielded a value of 3.5 GeV/c. This low value was caused by the shortness of tracks available for measurements and by the presence of thermal convection currents in the chamber. The distortion distribution moreover, had a large tail whose presence invalidated, particularly in such an investigation as the present one, the gaussian approximation.

In view of the presence of track distortion an endeavour was made to detect and to exclude those tracks which were affected by distortion, by using the quantity Σ^2. In the absence of the magnetic field the measured tracks should be straight. A least-squares fit of a straight line was therefore made to each track and the corresponding quantity Σ_1^2 determined for each. As expected every track with a large measured curvature also possessed a large value of Σ_1^2; conversely, however, some events with small measured curvature still showed a large value of Σ_1^2, indicating the presence of third, and higher order terms in their curves. In the presence of such S-shaped distortions an analytical determination of the error in curvature obtained from the least-squares method of fitting a parabola would be of doubtful significance. A selection criterion was therefore introduced according to which the value of Σ^2 for any track must be less than some maximum value. This maximum value was such that $\Sigma \approx 10$ μm. By comparison, the error in each setting of the microscope on the track was found to be of order 5 μm, and the total track width on the film 100 μm. With this limitation, a new distortion curvature distribution was obtained for the no-field tracks whose rms value when fitted with a gaussian distribution yielded a maximum detectable momentum of $\approx$ 6 GeV/c. The observed no-field curvature distribution in the form of a histogram, and not the gaussian approximation to it, was folded in to the theoretical distribution.

The following selection criteria for inclusion of tracks in the analysis were consequently introduced:

i) the track image on the film must be greater than 1.5 cm ($\approx$ 15 cm in the chamber),

ii) the computed value of Σ^2 must be less than 100 μm^2, and

iii) the measured momentum of the particle must be less than 1.5 GeV/c, and alternatively, in order to gain some insight into the importance, of this momentum cut-off, 2.3 GeV/c.

These selection criteria had the effect of reducing considerably the number of usable events to around two or three out of a total of $\approx$ 80 recorded per day.

5.2. ERRORS IN SCATTERING ANGLE

The errors in θ, the projected scattering angle, were found to be entirely accounted for by measurement errors due to the finite width and length of the track segments between plates. All measurements of angles were repeated after a time, the measurements compared, and the distribution of the differences between corresponding measurements found. Here a gaussian distribution fitted the data well, and the standard deviation was 0.5°. Measurements of the scattering angles were also made of high energy particles which showed no detectable curvature in the magnetic field of the upper chamber. The distribution of scattering angles for these high energy particles was also determined. No difference was observed between these two distributions for the lead and the iron traversals, indicating the absence of any real scattering distribution from a low energy contamination, and again the rms value of the distribution was found to be 0.5°. The errors in θ were therefore taken to be normally distributed with standard deviation of 0.5°.

5.3. THE EFFECTS OF FOLDING IN THE ERROR DISTRIBUTIONS

If the theoretical differential frequency distribution of the product $\pi\theta$ is given by $\varphi(\pi\theta)$, where π and θ are the true momentum and projected angle of scatter, then the expected observed frequency distribution is given by $f(p\,t)$, where p and t are the measured momentum and projected angle of scatter.

The modified distribution $f(p\,t)$ was obtained by first computing the effects of errors in angle only assuming that the momenta were accurately determined to find the expected distribution, $f'(\pi\,t)$, over the observed momentum spectrum of particles. This new distribution was, as expected, broader than the theoretical distribution. Taking this new distribution the errors in determination of momentum were now included using the observed no field curvature distribution, and as momentum spectrum the observed spectrum smoothly joined to the underground spectrum for a depth of 65 m water equivalent[12]) at a momentum of 2 GeV/c. The computation was carried out on Silliac using histogram intervals of 0.25 (GeV/c) $\times$ deg. The effects of folding in the errors are shown in figs. 2 and 3. In fig. 2 the less stringent cut-off condition on the acceptable measured momentum ($p_0 = 2.3$ GeV/c) has been adopted. It will be observed that the theoretical distributions have been modified considerably by the effects of the errors and that in particular the difference between the

curves for the extended nucleus and for the point nucleus has been considerably reduced.

The importance of the cut-off momentum p_0 is indicated in fig. 3 where the corresponding computed curves are shown for a cut-off momentum of only 1.5 GeV/c. The resulting curves differ appreciably from those of figure 2 and in a

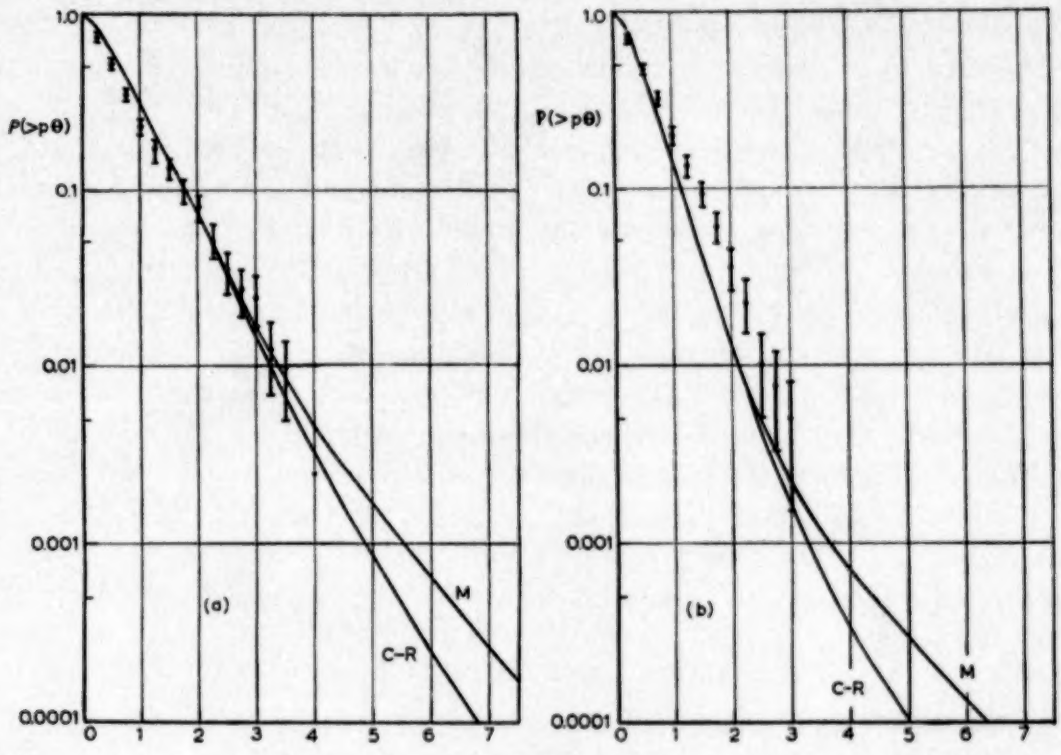

Fig. 3. The expected scattering distributions with errors folded in for lead (a) and for iron (b) for measured momenta < 1.5 GeV/c. The corresponding experimental results are shown.

non-obvious way which, however, may be accounted for by the asymmetry in the momentum error distribution, and by the shapes of the underground momentum spectrum and of the theoretical scattering distributions.

6. Results

Also plotted in fig. 3 are the frequency distributions of the measured values of the product $P\theta$ for $P < 1.5$ GeV/c for some 400 traversals of iron and of lead. For the particles stopping in the lower chamber, less than 10 % of the total, the appropriate variable $p\beta\theta$ was calculated and used. The error bars attached to each point refer to the statistical error only in the number of traversals represented by the ordinates. While it is clear that no evidence for anomalous scattering in lead exists, there is some discrepancy between the predicted curves and the experimental points for iron. It is considered more likely that this discrepancy is produced by insufficient rigour in the treatment of the errors, even

in the treatment as outlined above, rather than by an anomalous scattering in iron. Because of the more rapid decrease of the scattering distribution in iron than in lead the effects of errors not taken into account will show up more markedly in the former case. Sources of such errors could well lie in one or more of the following:

(i) The momentum error distribution is obtained from curvature measurements on some 150 no-field tracks only. A larger number of measurements might have increased the proportion of large curvatures in the tail of this distribution.

(ii) It has been assumed that the distortion level in the magnet chamber is the same with magnet field on and off.

(iii) It has been assumed in the analysis that each value of the product $p\theta$ for a plate traversal is independant. This is not so since for each particle whose momentum is measured there corresponds on average four traversals in each material. No evidence of such a correlation was found within the admittedly poor statistics. Of some 10 particles which showed a large angle scatter of $p\theta > 2$ (GeV/c) $\times$ deg. in one plate, 7 of these particles underwent a similar large angle scatter in another plate. This number is consistent with expectation on the assumption of the independance of each value of $p\theta$. π-meson contamination of the μ-meson flux would of course also give a correlation of large angle scatters.

While it is true that the above factors should certainly be taken into account in a rigorous treatment of this problem, it is also apparent from the curves of figs. 2 and 3 that some 10^5 traversals would be required in order to distinguish between the two possibilities of scattering from an extended nucleus and from a point nucleus in the case of lead, and an order of magnitude more for iron using the present arrangement. It is probable that a more rigorous treatment of the errors would result in a smaller separation of the tails of the distributions.

7. Conclusion

As a result of the analysis of the effects of errors upon the theoretical scattering distributions to obtain distributions with which the experimental results might be compared it became obvious that these errors were such as to make it highly doubtful that an anomaly of the magnitude so far claimed could be detected by this apparatus. It also became obvious that any experiment designed to look for the existence of such an anomaly should be less subject to measurement errors than the one described here and that the detailed determination of these errors and a rigorous treatment of them — more rigorous than has been presented here, according to the indications of our experimental results — will be required before the existence of the anomalous scattering of μ-mesors may be established.

We are grateful to Professor H. Messel and the Nuclear Research Foundation for the provision of the experimental facilities for carrying out this work. It is a pleasure to acknowledge the assistance of A. van Heugten, A. J. Webb and J. A. D. Stockdale in the installation and initial running of the apparatus.

References

1) G. N. Fowler and A. W. Wolfendale, in Progress in Elementary Particle and Cosmic Ray Physics, Vol. IV (North Holland Publishing Co., Amsterdam, 1958)
2) W. F. Nash and A. J. Pointon, Nuov. Cim. **9** (1958) 412
3) S. Fukui, T. Kitamura and Y. Watase, Phys. Rev. **113** (1959) 315
4) A. I. Alikhanian and F. R. Arutyunian, Nuclear Physics **10** (1959) 244
5) J. L. Lloyd and A. W. Wolfendale, Phys. Rev. **117** (1960) 247
6) R. W. Thompson, Nuov. Cim. **1** (1955) 735
7) I. B. McDiarmid, Phil. Mag. **45** (1954) 368
8) B. A. Chartres, Proceedings of Conference on Data Processing, Weapons Research Establishment, Salisbury, S.A. (1957)
9) R. Gatto, Nuov. Cim. **10** (1953) 1559
10) L. N. Cooper and J. Rainwater, Phys. Rev. **97** (1955) 492
11) G. Moliere, Z. Naturforsch. **2a** (1947) 133; **3a** (1948) 78
12) D. C. Peaslee, Nuov. Cim. **9** (1952) 56

1.E.8:
3.A

Nuclear Physics **19** (1960) 675—687; © *North-Holland Publishing Co., Amsterdam*
Not to be reproduced by photoprint or microfilm without written permission from the publihser

MEASUREMENT OF THE ROTATIONAL g-FACTOR (g_R) FOR SEVERAL NUCLEI

GEOFFREY MANNING† and JOHN ROGERS

California Institute of Technology, Pasadena, California††

Received 19 August 1960

Abstract: The g-factors of several excited states of nuclei have been measured by observing the rotation of the angular correlation for a source in a magnetic field. The results are: 122-keV state of Sm^{152} ($\tau = 2.0 \times 10^{-9}$ sec) $g = 0.28 \pm 0.07$; 123-keV state of Gd^{154} ($\tau = 1.7 \times 10^{-9}$ sec) $g = 0.4 \pm 0.5$; 81-keV state of Er^{166} ($\tau = 2.4 \times 10^{-9}$ sec) $g = 0.31 \pm 0.06$; 87-keV state of Dy^{160} ($\tau = 2.5 \times 10^{-9}$ sec) $g = (0.28 \pm 0.08)$; 118-keV state of Tm^{169} ($\tau = (9.0 \pm 1.5) \times 10^{-11}$ sec) $g = 0.20 \pm 0.06$. The assumptions used in deducing the g-factors from the observed rotations are discussed. A discussion of available evidence suggests that the rotational g-factor g_R is less than Z/A. The g-factor of the 118-keV state of Tm^{169} is discussed on the basis of the Nilsson model.

1. Introduction

The unified model as developed by Bohr and Mottelson[1]) and extended by Nilsson[2]) has enjoyed considerable success in quantitatively explaining the levels and properties of many nuclei. Perhaps the most marked single success has been the prediction, and accurate verification, of a series of rotational levels in even nuclei. A further consequence of the collective motion is that there should be a non-zero magnetic moment for these rotational states resulting from the collective motion of the nucleus. Approximate calculations indicate that if the nuclear matter moves as a uniformly charged medium the g-factor of the rotational state should be simply $g_R = Z/A$. This prediction is not expected to be an accurate one but only a first approximation. The Nilsson model yields predictions for the g-factors of states of odd-mass nuclei and these are also dependent upon the rotational g-factor, g_R. A further nuclear property that is dependent upon g_R is the magnetic dipole transition probability between rotational states in odd-mass nuclei. Both of the last mentioned properties, while dependent on g_R, also depend upon other nuclear parameters, and though such measurements give some indication of the magnitude of g_R, in general they are not a sensitive method of determining the parameter. The g-factor of rotational states of even nuclei are, on the other hand, a direct measure of g_R. Goldring and Scharenberg[3]) have determined three such g-factors, Nd^{150}, Sm^{152} and Sm^{154},

† Present address: United Kingdom Atomic Energy Research Establishment, Harwell, Didcot, Berkshire, England.

†† Work performed under the auspices of the U.S. Atomic Energy Commission.

obtaining g_R for these nuclei of 0.2 which is about 0.5 Z/A. An approximate measurement has also been made on the g-factor of the first excited state of Dy^{160} [5]) yielding a result which is also smaller than Z/A. However, a recent measurement on the first excited state of W^{184} [20]) gives a value about Z/A. Extensions of such measurements to other nuclei is clearly of considerable interest as they may give some insight into the form of the collective motion and it is hoped that in the near future more exact theoretical predictions can be made, using the "cranking model" of Inglis[6]) for example.

In the experiments below we have made measurements of the g-factors of first excited states of the following even nuclei, Sm^{152}, Gd^{154}, Er^{166} and Dy^{160}. We have also measured the g-factor of the 118-keV state of Tm^{169}. The Nilsson model predicts that the g-factor of this level should be predominantly dependent upon g_R, the other contributions canceling out.

2. Experimental Method

The method we have used to determine the g-factors was the observation of the rotation of a γ-γ angular correlation by a magnetic field applied perpendicular to the plane of the correlation measurement. This method is one which has been applied by many authors[7]). The detailed description of our equipment and method, together with the assumptions used and equations developed in order to obtain the g-factor from the observed rotation, are contained in a previous article Manning and Rogers[8]).

3. Experimental Results

3.1. 122-keV STATE OF Sm^{152}

The g-factor of the 122-keV state of Sm^{152} has been measured by Goldring and Scharenberg[3]), who populated the level by Coulomb excitation using protons. They obtained a value $g = 0.21 \pm 0.04$. Sugimoto[4]), using the same method, obtained $g = 0.36 \pm 0.16/\beta G$ (in our notation). (β and G are for a solid oxide target at 700° K).

We made our measurements using a γ-γ cascade following the decay of Eu^{152} by electron capture. The source was produced by dissolving neutron irradiated Eu oxide, enriched in Eu^{151}, in nitric acid. The cascade used for our measurement was the 1420 — 122 keV cascade. The angular correlation for this cascade has been measured by Hartmann and Wiedling[9]), and by Ofer[10]). Hartmann and Wiedling used aqueous solutions of $EuCl_3$ as sources and obtained

$$\overline{W(\theta)} = 1 + (0.219 \pm 0.005)\, P_2(\cos\theta) + (0.003 \pm 0.007) P_4(\cos\theta).$$

(At the time these authors carried out their measurements they incorrectly attributed the 1420 — 122 keV cascade to Gd^{154} but presumably their results

themselves, if not their conclusions, are still valid.) Ofer used a dilute aqueous solution of $Eu_2(SO_4)_3$ as a source and obtained

$$\overline{W(\theta)} = 1 \pm (0.21 \pm 0.02)P_2(\cos\theta) + (0.02 \pm 0.03)P_4(\cos\theta).$$

Our correlation measurements, after corrections for random coincidences and the finite solid angle subtended by the counters were in agreement with the above authors.

The g-factor measurements were made at an angle of 125° using a field of 12 000 G. A total of $\approx 2.5 \times 10^5$ counts were observed in the peak corresponding to the 1420 — 122 keV cascade. The value of R (see eq. 6 of ref. [8])) deduced was 2.1 % ± 0.5 % which gave $G_2\omega\tau = (3.7 \pm 0.9) \times 10^{-2}$ radians. The 122-keV γ-ray is K-converted and the value for R for the coincidences corresponding to the 1420 — K X-ray cascade was 0.0 % ± 0.2 % which indicates no significant systematic effect from the effects of the magnetic field on the detectors.

The value of G_2 for the 122-keV level of Sm^{152} in a liquid source of $Sm(NO_3)_3$ has been determined by Goldring and Scharenberg by comparison of the angular distribution they observed with the theoretical distribution for Coulomb excitation of a 2+ level. They obtained $G_2 = 1$. We made a direct measurement of G_2 for the same source as used for the g-factor experiments by measuring the angular correlation for the 244 — 122 keV 4-2-0 cascade. This cascade is a pure E2-E2 cascade and the true correlation is known. Our observed value of G_2 was 1.0 ± 0.13. The somewhat large error is mainly because of the difficulty in accurately estimating the contributions from tails of other γ-rays falling within the gate set on the 244-keV γ-ray. This effect was determined by measuring the angular correlation with the gate set just above and just below the 244-keV γ-ray.

The other factor required in order to determine the g-factor from the measured value of $G_2\omega\tau$ is the effective field parameter β (see appendix of ref. [8])). It has been pointed out by Sugimoto and Kanamori[22])† that the assumptions used in evaluating β in the appendix to ref. [8]) are not applicable to Sm and Eu, due to the small energy splitting to the first excited state. Their more accurate calculation gives $\beta = 1.15$ rather than $\beta = 1.9$ as deduced in ref. [8]). Goldring and Scharenberg used a value 1.7 ± 0.2.

Taking $\tau = 2.0 \times 10^{-9}$ sec, $G_2 = 1$ and $\beta = 1.15$, we obtain, using eq. 6 of ref. [8]), $g = 0.28 \pm 0.07$ for the 122-keV level of Sm^{152}. Using the same value of magnetic correction, Goldring and Scharenberg's value of $g = 0.20 \pm 0.04$ becomes $g = 0.30 \pm 0.06$. Sugimoto's measurement, with the assumptions $G = 1, \beta = 1.07$[22]) gives $g = 0.34 \pm 0.16$. These measurements are thus in good agreement. This agreement is pleasing to note in light of the different methods used to populate the 122-keV state, and furnishes some support for the assump-

† There are several numerical errors in this paper. Eq. 4 is correct. Eq. 5 when corrected gives the results of table 2 in ref. [8]).

tion that the electronic state of the Sm ion reaches a stable state as the initial excitation of the ion is no doubt markedly different in the two experiments.

3.2. 123-keV STATE OF Gd^{154}

The g-factor of the 123-keV state of Gd^{154} was measured using the 1280 — 123 keV cascade from the 1400-keV state. The 1400-keV state was populated by β-decay from 16 year Eu^{154}.

The angular correlation of the 1280 — 123 keV cascade has been measured by Hickman and Wiedenbeck[11]). They used a source of Eu_2O_3 dissolved in dilute HCl and obtained an angular correlation of

$$\overline{W(\theta)} = 1 + (0.191 \pm 0.010)P_2(\cos\theta) - (0.007 \pm 0.015)P_4(\cos\theta) .$$

These authors have measured the correlation of the 248 — 123-keV cascade from the 371-keV state as well. After correcting for competing cascades they obtained a correlation of

$$\overline{W(\theta)} = 1 + (0.098 \pm 0.018)P_2(\cos\theta) - (0.020 \pm 0.024)P_4(\cos\theta) .$$

This is in good agreement with the expected angular correlation from a $(4(Q)2(Q)O)$ cascade. On the basis of this measurement one can calculate the attenuation coefficient G_2 for the 123-keV state. One obtains from the above results, $G_2 = 0.96 \pm 0.18$. Goldring and Scharenberg[3]) have measured the attenuation coefficient G_2 for the 123-keV state of Gd^{154} in a dilute nitric acid solution by comparing the angular distribution of the 123-keV γ-ray following the Coulomb excitation with the theoretical prediction. They obtained $G_2 = 0.5 \pm 0.06$. They have measured the value of G_2 for similar states in Gd^{156} and Gd^{160} and conclude that the observed attenuation can be explained on the basis of a static magnetic hyperfine interaction and can not be explained on the basis of electric quadrupole interactions. Deutsch and Stiening[12]) have recently shown that the attenuation of the 123-keV level in Gd^{154} can be removed by application of a magnetic field parallel to one of the γ-rays, thus demonstrating that this attenuation is indeed due to magnetic hyperfine interactions.

We have measured the angular correlation of the 1280 — 123 keV cascade using a source of neutron irradiated Eu_2O_3 enriched in Eu^{153}, which was dissolved in dilute nitric acid. After correcting for random coincidences and finite solid angle of the counters, we obtained an angular correlation of

$$\overline{W(\theta)} = 1 + (0.170 \pm 0.008)P_2(\cos\theta) .$$

We have also measured the angular correlation of the 248 — 123 keV cascade. Interferences from competing cascades were determined by measuring the angular correlation with the gate just set above and just below the 248-keV γ-ray. We obtained an angular correlation of

$$\overline{W(\theta)} = 1 + (0.075 \pm 0.015)P_2(\cos\theta) ,$$

which gives an attenuation coefficient of $G_2 = 0.74 \pm 0.15$. The angular correlation we obtain from the 1280 — 123 keV cascade is consistent with the results of Hickman and Wiedenbeck when corrected by this factor.

Because this attenuation is due to a magnetic hyperfine interaction, it will be increased by a magnetic field applied perpendicular to the plane of the counters. To correct for this effect, we have measured the angular correlation of the 1260 — 123 keV cascade in a field of 13000 G perpendicular to the plane of the correlation measurement. After correction for randoms and finite solid angles of the counters we obtained

$$W(\theta) = 1 + (0.059 \pm 0.006)P_2(\cos\theta) .$$

Although the attenuation from magnetic hyperfines tructure does not have the exact time variation assumed in deriving the equations of section 2 of ref. [8]), it is a reasonable approximation, to the accuracy we require, to use the G_2 calculated on the basis of angular distribution in the magnetic field in those equations. Using our measurement of G_2 in the field-free source, and the measurement above in the magnetic field we obtain $G_2 = 0.24 \pm 0{,}05$.

We observed a value $R = (0.20 \pm 0.25)$ %, which gives a value

$$G_2\omega\tau = (1.25 \pm 1.56) \times 10^{-2} \text{ radians} = 0.7 \pm 0.9 \text{ degree} .$$

The g-factor of this state can be calculated from eq. 6 and the above measured values to be

$$g = \frac{0.5 \pm 0.6}{\beta} .$$

In the appendix of ref. [8]) we have estimated β for Gd to be 1.0. Using the known value for the hyperfine interaction in cerium magnesium nitrate crystals, a value of $\beta = 1.2$ is obtained. We use $\beta = 1.2$. The measured τ is 1.7×10^{-9} sec. On this basis we obtain

$$g = 0.4 \pm 0.5 .$$

3.3. 81-keV STATE OF Er^{166}

The cascade used in measuring the g-factor of the 81-keV state in Er^{166} was the 1370 — 81 keV cascade from the 1450-keV state. The 1450-keV state was populated from the β-decay of 27 hour Ho^{166}.

The angular correlation of this cascade has been measured by Fraser and Milton[13]) using a source of $Ho(NO_3)_3$ maintained above its melting point. Their observed angular correlation was

$$\overline{W(\theta)} = 1 + (0.137 \pm 0.006)P_2(\cos\theta) + (0.560 \pm 0.019)P_4(\cos\theta) .$$

This result demonstrated that the 1450-keV level was spin 0 and that the 81-keV level was spin 2. On the basis of this assignment attenuation coefficients $G_2 = 0.384 \pm 0.011$ and $G_4 = 0.490 \pm 0.017$ can be calculated.

Our source was prepared by dissolving neutron irradiated natural Holmium of 99.9 % purity in dilute nitric acid. We measured the angular correlation of the 1370 — 81 keV cascade for angles of 90° and 135°, and 90° and 180°. The results after correction for random coincidences and finite solid angle of the counters gave

$$W(\theta) = 1 + (0.159 \pm 0.03)P_2(\cos\theta) + (0.474 \pm 0.04)P_4(\cos\theta) .$$

Correcting for the 25% contribution of the 1570-keV γ-ray gives

$$G_2 = 0.78 \pm 0.12 \text{ and } G_4 = 0.55 \pm 0.05 .$$

The g-factor measurements were made at $\theta = 153°$ in a field of 5000 G. The X-ray peak in coincidence with the 1350-keV γ-ray was also observed as a check on the measurement. The observed value of R for the 1350 — 81 keV cascade after correcting for random coincidences was $R = (13.7 \pm 1.8)$ %. The observed value of R for the 1350-X-ray cascade, after correction for random coincidences, was $R = (0.3 \pm 2)$ %.

In calculating the g-factor from the above data it is necessary to use eq. 4 of ref. [8]) rather than eq. 6 because of the relatively large rotation observed and the presence of attenuation. Fig. 1 shows a plot of R versus $\omega\tau$ calculated from eq. 4 of ref. [8]) using our observed angular correlation (uncorrected for

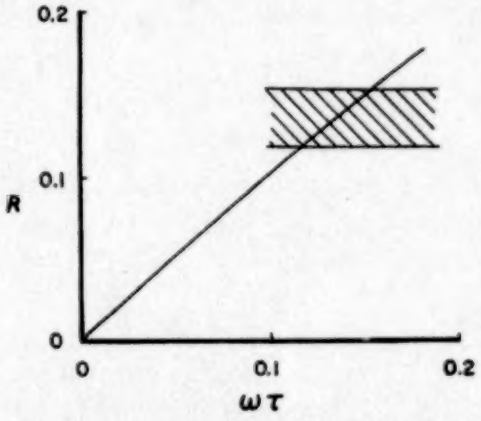

Fig. 1. The measured fractional difference R in counting rate with field up and field down, is plotted against the angular rotation $\omega\tau$ for the 81-keV state of Er^{166}. The curve is obtained from eq. 4 of ref. [8]) using the measured values of the angular correlation and attenuation coefficients.

finite solid angle). The attenuation coefficients found above have been used to calculate the curve shown in fig. 1. The cross hatched area denotes the observed value of R. A value $\omega\tau = 0.14 \pm 0.02$ is obtained.

Using this value, the measured lifetime of 2.4×10^{-9} sec and the calculated value $\beta = 7.7$, from the appendix of ref. [8]), we obtain

$$g = 0.31 \pm 0.06 .$$

3.4. 87-keV STATE OF Dy^{160}

The decay scheme of Dy^{160} is shown in fig. 2. A previous measurement of the g-factor of the 87-keV state was made by Debrunner *et al.*[5]). They measured the rotation of the angular correlation of the 880 — 87 keV cascade using a solid oxide source. The measurement was done at 300°K and at 700°K. From

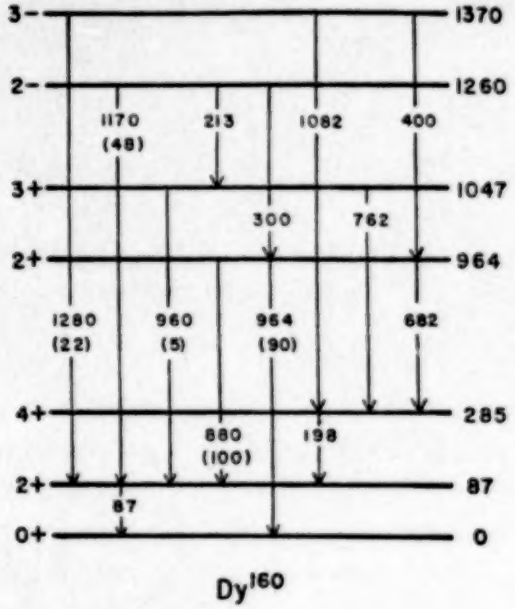

Fig. 2. Level scheme of Dy^{160}. Energies are in keV. Relative γ-ray intensities from ref. [14]) are shown in brackets.

these two measurements, a value of the g-factor, and of the effective field parameter β can be deduced. They obtained $g = 0.18 \pm 0.08$. The effective field parameter calculated from their results is $\beta = 6.3 \pm 0.7$. Interpreting their measurements in light of the recent work on the decay scheme discussed below would probably increase their value for g about 30 %, in agreement with our results discussed below.

Two groups have measured the angular correlations in Tb^{160}. Ofer[14], using $Tb_2(SO_4)_3$ dissolved in water as a source, measured correlations for most of the cascades. He obtained for the 1170 — 87 keV cascade.

$$\overline{W(\theta)} = 1 + (0.08 \pm 0.02)P_2(\cos\theta) + (0.07 \pm 0.015)P_4(\cos\theta),$$

and for the 1280 — 87 keV cascade

$$\overline{W(\theta)} = 1 + (0.011 \pm 0.02)P_2(\cos\theta) + (0.00 \pm 0.01)P_4(\cos\theta).$$

On the basis of his measurements, he obtained attenuation coefficients $G_2 = 0.40 \pm 0.15$ and $G_4 = 0.42 \pm 0.04$.

Arns, Sund and Wiedenbeck[15]), have also studied the angular correlations in Tb^{160} using a Tb_2O_3 source dissolved in dilute HCl. They conclude, on the

basis of their measurements, that the attenuation coefficients of the 87-keV state cannot be measured, but that the results they obtained are most compatible with the assumption that the attenuation is small. For the 1170 — 87 keV cascade, they obtained

$$\overline{W(\theta)} = 1 + (0.133 \pm 0.041)P_2(\cos\theta) + (0.008 \pm 0.083)P_4(\cos\theta) ,$$

and for the 1270 — 87 keV cascade

$$\overline{W(\theta)} = 1 + (0.148 \pm 0.065)P_2(\cos\theta) - (0.09 \pm 0.14)P_4(\cos\theta) .$$

Our g-factor measurements were made using the composite of the 1170 — 87 and 1280 — 87 keV cascades. The source used was Tb_2O_3 dissolved in HCl. The angular correlation obtained for the composite cascade after correction for random coincidences and finite solid angle of the counters was

$$W(\theta) = 1 + (0.091 \pm 0.010)P_2(\cos\theta) + (0.00 \pm 0.02)P_4(\cos\theta) .$$

Since it appeared that this angular correlation was somewhat lower than expected on the basis of the results of Arns *et al.* the angular correlations were measured for a dilute HCl solution of Tb_2O_3 and a dilute HCl and glycerine solution of Tb_2O_3 with a viscosity of about 10 centipoise. The results of these, after corrections for random coincidences and finite solid angles gave

$$\overline{W(\theta)} = 1 + (0.11 \pm 0.01)P_2(\cos\theta) + (0.02 \pm 0.02)P_4(\cos\theta)$$

for the aqueous solution, and

$$\overline{W(\theta)} = 1 + (0.10 \pm 0.01)P_2(\cos\theta) + (0.00 \pm 0.02)P_4(\cos\theta)$$

for the water and glycerine solution. This demonstrates that quadrupole attenuation is not large in these samples. From this we calculate $G_2 = 0.8 \pm 0.12$ for the source used in the g-factor experiment.

The g-factor measurement was done at $\theta = 135°$ in a field of 12000 G. The temperature was 340 °K. A total value of 2×10^5 counts was observed in the 87-keV coincidence peak for each direction of magnetic field. The K X-ray coincidence peak resulting from K-conversion of the 87-keV γ-ray was also observed to assure that there were no significant systematic effects. The value of R obtained was $R = (4.5 \pm 0.5)$ % which gave a value $G_2\omega\tau = 0.19 \pm 0.03$. Using $\tau = 2.5 \times 10^{-9}$ sec we obtain $g = (1.36 \pm 0.20)/\beta G_2$. Using $G_2 = 0.8 \pm 0.12$ from above, and $\beta = 6.0$, obtained by correcting the value in the appendix of ref. [8]) for the temperature of 340 °K, we obtain $g = 0.28 \pm 0.08$.

3.5. 118-keV STATE OF Tm^{169}

We have used the 198 — 110 keV cascade to measure the g-factor of the 118-keV state in Tm^{169}. The source was made by dissolving neutron irradiated Yb^{168}

oxide in dilute nitric acid. Fig. 3 shows relevant parts of the Tm^{169} level scheme.

The angular correlation of the 198 — 110 keV cascade has been measured by Cappeller and Klingelhöfer[17]), and by Koicki, Simic, and Kucoc[18]). The first mentioned authors obtained an angular distribution of

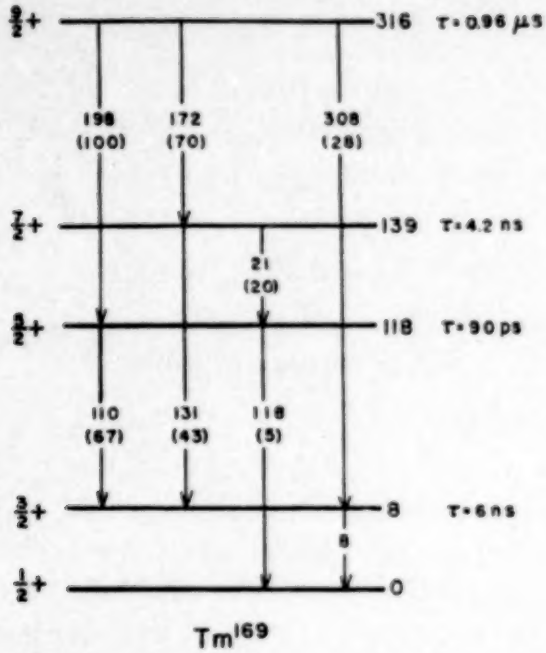

Fig. 3. Level scheme of Tm^{169} below the 316 keV level. Energies are in keV. Relative γ-ray intensities fro... ref. [21]) are shown in brackets. The lifetimes of the states are shown to the right. The spinvalue of the 316-keV level should be $\frac{3}{2}+$.

$$\overline{W(\theta)} = 1 + (0.250)P_2(\cos\theta) + (0.029)P_4(\cos\theta).$$

The second obtained

$$\overline{W(\theta)} = 1 + (0.314 \pm 0.003)P_2(\cos\theta) + (0.003 \pm 0.005)P_4(\cos\theta)\,.$$

The difference in these two values may possibly result from the difficulty of resolving the 198 — 110 keV cascade from the 177 — 130 keV cascade and the 177 — 110 keV coincidences through the intermediate 21-keV γ-ray. Our results are in agreement with those of Koicki *et al.* after correction for random coincidences and finite solid angles of the counters.

The g-factor measurements were made in a field of 13000 G at an angle of 135°. 3×10^6 counts in the 110-keV peak were observed for each field position. In addition, 4×10^6 counts in the coincidence peak corresponding to the K X-rays from the conversion of the 110-keV line were observed as a check that no systematic errors were present. We observed value of $R = (0.35 \pm 0.10)$ %. The value $G_2\omega\tau$ obtained for the 198 — 110 cascade using eq. 6 of ref. [8]) was

$$G_2\omega\tau = (0.56 \pm 0.17) \times 10^{-2} \text{ radians} = (0.32 \pm 0.11) \text{ degrees}\,.$$

The lifetime of this state has been measured by Blaugrund[19]) to be $\tau = (9.0 \pm 1.5) \times 10^{-11}$ sec. G_2 is expected to be 1 for lifetimes in this range. Therefore using eq. 6 of ref. [8]) we obtain

$$g = \frac{(1.1 \pm 0.3)}{\beta}$$

β is estimated to be 5.6 in the appendix to ref. [8]). Due to the fact that the lifetime of the 139-keV state, which feeds the 198 — 110 keV cascade, is 1 μsec, this is expected to be a good estimate. We therefore calculate that the g-factor of the 118-keV level of Tm^{169} is

$$g = 0.20 \pm 0.06 .$$

4. Discussion of Results

4.1. 118-keV STATE OF Tm^{169}

Several properties of the low lying levels of Tm^{169} have been interpreted on the basis of the unified model. Mottelson and Nilsson[19]) list the $\frac{5}{2}+$, 118-keV state as the second rotational state based on the $\frac{1}{2}+$ ground state, which is identified as the (411 $\frac{1}{2}$) orbital. The nuclear deformation δ is taken as 0.28 by these authors, and the decoupling parameter $a = -0.77$, calculated from the level spacing, is in good agreement with the theoretical value for this deformation. The ground state g-factor, $g = 0.41 \pm 0.04$, is in excellent agreement with the predicted value. Fig. 4 shows the g-factor of the 118-keV $\frac{5}{2}+$

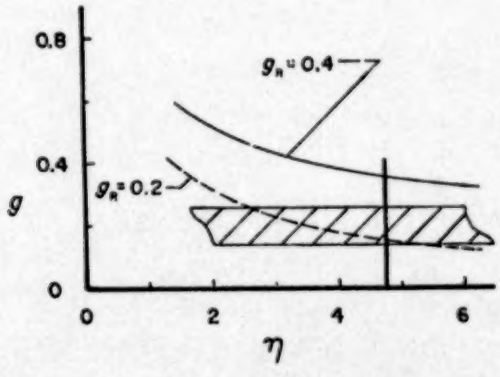

Fig. 4. The calculated g factor for the 118-keV state of Tm^{169} on the basis of the Nilsson model is shown for $g_R = 0.4$ (solid curve) and $g_R = 0.2$ (dashed curve). The cross hatched area shows the experimental value. The experimental deformation ($\eta = 4.8$) is indicated.

state as calculated from eq. 25 of ref. [20]) for various values of the deformation. Curves are shown for $g_R = 0.4$ and $g_R = 0.2$. The agreement for $g_R = 0.2$ is seen to be excellent.

This agreement must not, however, be taken as a demonstration that g_R is less than Z/A in this nucleus without some caution since the theoretical

predictions for the intrinsic part of the magnetic moment are not all verified to this accuracy in rotational nuclei (see for instance fig. 16 of ref. [20]).

4.2. VALUE OF THE ROTATIONAL g-FACTOR

The results in this paper which bear most significantly on the rotational g-factor are those for Er^{166}, Sm^{152} and Dy^{160}. The results for Gd^{154} are not significant. Table 1 summarizes our results and the results of other researches which bear on the problem of the rotational g-factor.

TABLE 1

Summary of experimental results, which bear on the rotational g-factor. The second column gives g_R assuming uniform nuclear flow. The third and fourth columns are estimates assuming a spherical core of 50 protons and 82 neutrons, and 50 protons and 50 neutrons respectively.

Nucleus	Z/A for whole	Z/A of outer shell with inner core of 50 protons and 82 neutrons	Z/A of outer shell with inner core of 50 protons and 50 neutrons	Experimental values of g_R
$_{60}Nd^{150}$	0.40	0.50	0.20	0.22 ± 0.04[a]
$_{62}Sm^{152}$	0.41	0.60	0.23	0.30 ± 0.04[a] [g]
				0.30 ± 0.06[b]
				0.34 ± 0.16[c] [g]
$_{66}Dy^{160}$	0.41	0.57	0.27	0.18 ± 0.08[e]
				0.28 ± 0.08[b]
$_{68}Er^{166}$	0.41	0.53	0.27	0.31 ± 0.06[b]
$_{74}W^{184}$	0.40	0.46	0.29	0.38 ± 0.05[d]
$_{72}Hf^{177}$	0.41	0.96	0.40	0.24 ± 0.16[f]

[a]) Goldring and Scharenberg [3])
[b]) Present paper
[c]) Debrunner *et al.* [5])
[d]) Bodenstedt *et al.* [20])
[e]) Sugimoto [4])
[f]) Manning and Rogers [8])
[g]) Corrected for effective field as discussed in ref. [22])

Except for the case of W^{184} [20]), the above measurements are dependent on a correction for the effects of paramagnetism of the electronic structure. This effect is discussed in the appendix to ref. [8]). Confirmatory evidence for the values of β tabulated in the appendix of ref. [8]) can be deduced from the measurements on Gd^{154}, where the anomalous results are readily explainable on the basis that the electronic structure is Gd 3+ during the lifetime of the intermediate state[12]), and in the experimental measurement of β on Dy^{160} by Debrunner *et al.*[14]) which agrees within the limits of error with our estimate.

The rotational g-factor can also be deduced from measurements of magnetic moments of odd-proton nuclei by using the ground state magnetic moment to compute the contribution from the single particle to the magnetic moment. From the equations developed in ref. [2]) it can be seen that for $I \neq \frac{1}{2}$

$$g_R = \frac{gI(I+1) - g^*(I^*)\,(I^*+1)}{I(I+1) - I^*(I^*+1)},$$

where g and I are the g-factor and spin for one level, and g^* and I^* are the g-factor and spin for another level of the same rotational band. Using the values quoted in ref. [8]) for Lu^{175} and Hf^{177} one obtains $g_R = 0.24 \pm 0.16$ for Hf^{177} and $g_R = 0.7 \pm 0.8$ for Lu^{175}. The calculation is not applicable to Yb^{169} since $K = \frac{1}{2}$ for that rotational band.

The results quoted in table 1 on the whole strongly favor a g_R somewhat less than Z/A for even nuclei. Similar results for odd-mass nuclei have recently been obtained by Bernstein and de Boer[23]) from an analysis of M1 transition probabilities.

Values of g_R substantially less than Z/A can be explained by assuming that the average radii of protons in nuclei are less than those of neutrons. While it is true that a comparatively small difference would explain the observed values of g_R, the large binding between neutrons and protons in nuclear matter makes such an explanation seem intuitively unlikely. Another possible way of accounting for values of g_R different from Z/A is to assume that nuclei in the rare earth region have a spherically symmetric core surrounded by an outer shell of ellipsodial shape. The Z/A of the outer shell would then be effective in producing the g_R. For the rare earth nuclei an inner spherical core of a closed shell of 50 protons and a closed shell of 82 neutrons would seem reasonable. Unfortunately this assumption produces larger effective Z/A. An inner core of 50 protons and 50 neutrons produces values in better agreement with experiment, see table 1.

The above suggestions are two possible ways of accounting for values of g_R less than Z/A. They are mentioned to indicate that further experimental and theoretical work on the problem may give some information on the collective motion of nuclear matter.

References

1) A. Bohr and B. R. Mottelson, Mat. Fys. Medd. Dan. Vid. Selsk. **16**, no. 27 (1953)
2) S. G. Nilsson, Mat. Fys. Medd. Dan. Vid. Selsk. **29**, no. 16 (1955)
3) G. Goldring and R. P. Scharenberg, Phys. Rev. **110** (1958) 701
4) K. Sugimoto, J. Phys. Soc. Japan **13** (1958) 240
5) P. Debrunner, W. Kundig, J. Sunier and P. Scherrer, Helv. Phys. Acta **31** (1958) 326
6) F. Villars, Ann. Rev. Nuclear Science **7** (1957) 185
7) H. Frauenfelder, in Beta- and gamma-ray spectroscopy, ed. by K. Siegbahn (North-Holland Publishing Co., Amsterdam, 1955)
8) G. Manning and J. D. Rogers, Nuclear Physics **15** (1960) 166
9) B. Hartmann and T. Weidling, Ark. Fys. **10** (1956) 355
10) S. Ofer, Nuclear Physics **4** (1957) 477
11) G. D. Hickmann and M. L. Weidenbeck, Phys. Rev. **111** (1958) 539
12) M. Deutsch, private communication
13) J. S. Fraser and J. C. D. Milton, Phys. Rev. **98** (1955) 117, 3A

14) S. Ofer, Nuclear Physics **5** (1958) 331
15) R. G. Arns, R. E. Sund and M. L. Wiedenbeck, Nuclear Physics **11** (1959) 411
16) U. Cappellar and R. Klingelhöfer, Z. Physik **150** (1958) 375
17) S. Koicki, J. Simic and A. Kucoc, Nuclear Physics **10** (1959) 412
18) A. E. Blaugrund, Phys. Rev. Letters, **3** (1959) 226
19) B. R. Mottelson and S. G. Nilsson, Mat. Fys. Medd. Dan. Vid. Selsk., **29**, no. 16 (1955)
20) E. Bodenstedt, E. Matthias, H. J. Körner, E. Gerdau, F. Frishus and D. Hovenstadt, Nuclear Physics **15** (1960) 239
21) Nuclear Data Sheets (National Academy of Sciences – National Research Council) 1958
22) J. Kanamori and K. Sugimoto, J. Phys. Soc. Japan, **13** (1958) 754
23) E. M. Bernstein and J. de Boer, to be published

AUTHOR INDEX

ABRAHAM, G. and K. K. GUPTA, Pairing interaction in nuclei 496

ALMQVIST, E., D. A. BROMLEY, H. E. GOVE and A. E. LITHERLAND, Low levels of Al^{27} 1

ALMQVIST, E., *see* KUEHNER . . . . . .

ANDREYEV, D. S., A. P. GRINBERG, K. I. EROKHINA and I. KH. LEMBERG, Coulomb excitation of the first levels of spherical even nuclei by multiply charged ions 400

ARMSTONG, ALICE H., and L. ROSEN, Mechanism of the Zn^{64} (n,p) Cu^{64} reaction at incident neutron energies of 8 and 14 MeV 40

ARNOLD, M., P. E. HODGSON, D. F. SHAW and D. M. SKYRME, The interaction of 40–160 MeV neutrons with helium nuclei 500

ARNS, R. G., and M. L. WIEDENBECK, Energy levels of Re^{187} 634

AVOTINA, M. P., *see* GRIGORIEV

BÄCKSTRÖM, G., *see* KERN

BARKER, F. C., Calculation of splitting of $3s_{\frac{1}{2}}$ neutron levels 110

BARKER, F. C., E. BRADFORD and L. J. TASSIE, The 9.63 MeV state of C^{12} 101

BEARD, G. B., *see* KELLY

BENVENISTE, J., A. C. MITCHELL, C. D. SCHRADER and J. H. ZENGER, Gamma rays from the interaction of 14-MeV neutrons with beryllium 52

BENVENISTE, J., A. C. MITCHELL, C. D. SCHRADER and J. H. ZENGER, Gamma rays from the interaction of 14-MeV neutrons with carbon . . 448

BONNER, T. W., *see* RABSON

BOOTH, E. C., Nuclear resonance scattering of bremsstrahlung 426

BRADFORD, E., *see* BARKER

BROMLEY, D. A., *see* ALMQVIST

BROMLEY, D. A., *see* KUEHNER

BROWNE, C. P. and J. T. RADZYMINSKI, Energy levels of Si^{29}, Si^{30} and Si^{31} from (d,p) reactions 164

BURLESON, G. R. and H. W. KENDALL, An experimental search for dipole structure of the electron 68

BURNSTEIN, R., T. KITAMURA and D. D. MILLAR, The anomalous scattering of underground μ-mesons 665

CALVERT, J. M., *see* GARG

CARVER, J. H. and G. A. JONES, Radiative proton capture in Ni^{58} . . . 184

CASTILLO-BAHENA, R., *see* RABSON

CHAFFEE, W. B., *see* KELLY

CHYLIŃSKI, Z., *see* KOBA
DEBRUNNER, P., *see* SUNIER
DRAPER, J. E., and R. L. HICKOK, Thermal and resonance neutron capture gamma rays from Nd^{144} and Nd^{146} 436
EDWARDS, W. F., *see* GALLAGHER, Jr.
EL BEDEWI, F. A., and S. TADROS, Energy levels in chromium isotopes . 604
ELBEK, B., M. C. OLESEN and O. SKILBREID, Inelastic scattering from even rare earth isotopes 523
EMERY, V. J., Reaction matrix singularities and the energy gap in an infinite system of fermions 154
EROKHINA, K. I., *see* ANDREYEV
EWAN, G. T., R. L. GRAHAM and J. S. GEIGER, M1/E2 mixing ratio in the Fe^{57} 14.41 keV γ-transition 221
FAISSNER, H., and H. SCHNEIDER, Direct processes and collective effects in high energy proton induced fission 346
FERGUSON, A. T. G., *see* MANI
FORD, G. P., *see* LEACHMAN
GALE, N. H., *see* GARG
GALLAGHER, C. J., Jr., W. F. EDWARDS and G. MANNING, The W^{187} decay scheme and possible vibrational levels in an odd-mass nucleus 18
GARG, J. B., J. M. CALVERT and N. H. GALE, Angular correlation studies of the $Be^9(\alpha, n\gamma)C^{12}$ reaction 264
GARVIN, H. L. and E. LIPWORTH, The nuclear spins of I^{126}, I^{132}, I^{133} and I^{135} 140
GEIGER, J. S., *see* EWAN
GIANNINI, M., D. PROSPERI and S. SCIUTI, Investigation on the decay scheme of ThC (Bi^{212}) 380
GOLDANSKY, V. I., On neutron-deficient isotopes of light nuclei and the phenomena of proton and two-proton radioactivity. 482
GONSER, J. M., *see* KELLY
GOVE, H. E., *see* ALMQVIST
GRAHAM, R. L., *see* EWAN
GRIGORIEV, E. P., and M. P. AVOTINA, Comparison of the theory of non-axial nuclei with experiments 248
GRINBERG, A. P., *see* ANDREYEV
GUPTA, K. K., *see* ABRAHAM
HAENNI, H. P., *see* RABSON
HANSTEEN, J. M., A remark on the Coulomb disintegration of accelerated heavy ions 309
HARLOW, Jr., M. V., *see* RABSON
HEBBARD, D. F., Gamma rays from the 351-keV $C^{14}(p, \gamma)$ resonance 511

HERZENBERG, A., and E. J. SQUIRES, On the theory of p-α scattering . . 280
HICKOK, R. L., *see* DRAPER
HODGSON, P. E., *see* ARNOLD
JASTRAM, P. S., *see* RAMASWAMY
JENSEN, B. SKYTTE, O. B. NIELSEN and O. SKILBREID, On the decay of 5.8 d Sb^{120}, 5.1 h Sb^{118} and 1 h Sb^{116} 654
JONES, G. A., *see* CARVER
KELLY, W. H., G. B. BEARD, W. B. CHAFFEE and J. M. GONSER, The 85 minute activity of Ba^{139} 79
KENDALL, H. W., *see* BURLESON
KERN, J. and G. BÄCKSTRÖM, The decay of Ir^{194} 461
KING, J. D. and W. J. MCDONALD, The $Mg^{24}(\gamma, n)Mg^{23}$ reaction 94
KITAMURA, T., *see* BURNSTEIN
KOBA, Z., A. KRZYWICKI, R. RĄCZKA and Z. CHYLIŃSKI, Elastic scattering of nucleons and pions at very high energy 199
KRECHKO, M. S., *see* PUSTOVALOV
KRZYWICKI, A., *see* KOBA
KUEHNER, J. A., E. ALMQVIST and D. A. BROMLEY, Reaction mechanism studies on $Si^{28}(d,p)Si^{29}$ (I) Distorted wave effects 614
LASSEN, N. O. and V. A. SIDOROV, (α,p) reactions in medium weight elements 579
LEACHMAN, R. B., and G. P. FORD, Fore-aft yields of fragments from 14-MeV neutron-induced fission 366
LEFORT, M., G. SIMONOFF et X. TARRAGO, Réactions secondaires de spallation 173
LEMBERG, I. KH., *see* ANDREYEV
LEVINGER, J. S., Can the nuclear many-body problem be solved by using perturbation theory? 370
LIPWORTH, E., *see* GARVIN
LITHERLAND, A. E., *see* ALMQVIST
MANI, G. S., G. J. MCCALLUM and A. T. G. FERGUSON, Neutron cross-sections in aluminium 535
MANNING, G. and J. ROGERS, Measurements of the rotational *g*-factor (g_R) for several nuclei 675
MANNING, G., *see* GALLAGHER, Jr.
MCCALLUM, G. J., *see* MANI
MCDONALD, W. J., *see* KING
MILLAR, D. D., *see* BURNSTEIN
MITCHELL, A. C., *see* BENVENISTE
MORINAGA, H., and K. NAGATANI, Lower excited states of W^{185} 327
NAGATANI, K., *see* MORINAGA
NATHAN, O., Multipole order of the 869 keV gamma ray in Sm^{152} . . . 148

NIELSEN, O. B., *see* JENSEN
NIELSEN, O. B., *see* TOTH
NIKOLIC, N. M., *see* YOSHIKI
OLESEN, M. C., *see* ELBEK
PANDYA, S. P., *see* THANKAPPAN
PHILLIPS, G. C. and T. A. TOMBRELLO, Two-body cluster states in nuclei 555
PROSPERI, D., *see* GIANNINI
PROWSE, D. J., *see* VAN HEERDEN
PUSTOVALOV, G. E., and M. S. KRECHKO, Charge distribution in nuclei and energy levels of μ mesonic atoms 337
RABSON, T. A., T. W. BONNER, R. CASTILLO-BAHENA, M. V. HARLOW, JR., H. P. HAENNI and W. A. RANKEN, Gamma radiation from excited states F^{18}, Na^{22} and Ne^{22} 314
RĄCZKA, R., *see* KOBA
RADZYMINSKI, J. T., *see* BROWNE
RAMASWAMY, M. K., L to K capture ratio in the decay of Ge^{68} 377
RAMASWAMY, M. K., and P. S. JASTRAM, Decay of Y^{88} 243
RAMASWAMY, M. K., W. L. SKEEL and P. S. JASTRAM, The decay energy of Ba^{133} 299
RANKEN, W. A., *see* RABSON
RASMUSSEN, J. O., Theory of E0 transitions of spheroidal nuclei 85
ROGERS, J., *see* MANNING
ROSE, H. J., The decay modes of the 9.17-MeV excited state in N^{14} . . 113
ROSEN, L., *see* ARMSTRONG
SCHERRER, P., *see* SUNIER
SCHNEIDER, H., *see* FAISSNER
SCHRADER, C. D., *see* BENVENISTE
SCIUTI, S., *see* GIANNINI
SHARMA, B. L., Investigations of the decay-scheme of Rh^{101} 550
SHAW, D. F., *see* ARNOLD
SIDOROV, V. A., *see* LASSEN
SIMONOFF, G., *see* LEFORT
SKEEL, W. L., *see* RAMASWAMY
SKILBREID, O., *see* ELBEK
SKILBREID, O., *see* JENSEN
SKILBREID, O., *see* TOTH
SKYTTE JENSEN, B., *see* JENSEN
SKYRME, D. M., *see* ARNOLD
SQUIRES, E. J., *see* HERZENBERG
SUNIER, J. W., P. DEBRUNNER and P. SCHERRER, β–γ correlation of the 3^-–2^+–0^+ cascade in the decay of Eu^{152} 62
TADROS, S., *see* EL BEDEWI

TALMI, I., and I. UNNA, Energy levels and configuration interaction in Zr^{90} and related nuclei 225
TARRAGO, X., *see* LEFORT
TASSIE, L. J., *see* BARKER
TAYLOR, R. B., Photoprotons from Cs and I 453
THANKAPPAN, V. K., and S. P. PANDYA, Collective vibrations in P^{31} . . 303
TOMBRELLO, T. A., *see* PHILLIPS
TOTH, K. S., O. B. NIELSEN and O. SKILBREID, Decay scheme of Tb^{152} . 389
UNNA, I., *see* TALMI
VAN HEERDEN, I. J., and D. J. PROWSE, The scattering of alpha particles and deuterons by iodine-127 589
WIEDENBECK, M. L., *see* ARNS
YOSHIKI, H., and N. M. NIKOLIC, The observation of p′–γ angular correlation at a nuclear resonance 442
ZENGER, J. H., *see* BENVENISTE

SUBJECT INDEX

1. Nuclear Structure

1.C *Many-particle systems*

Reaction matrix singularities and the energy gap in an infinite system of fermions, V. J. Emery 154
Can the nuclear many-body problem be solved by using perturbation theory?, J. S. Levinger 370
Pairing interaction in nuclei, G. Abraham and K. K. Gupta 496

1.D *Nuclear models*

1.D.1 *Shell model*

The nuclear spins of I^{126}, I^{132}, I^{133} and I^{135}, H. L. Garvin and E. Lipworth 140
Energy levels and configuration interaction in Zr^{90} and related nuclei, I. Talmi and I. Unna 225
The decay energy of Ba^{133}, M. K. Ramaswamy, W. L. Skeel and P. S. Jastram 299

1.D.2 *Collective model*

Low levels of Al^{27}, E. Almqvist, D. A. Bromley, H. E. Gove and A. E. Litherland 1
The W^{187} decay scheme and possible vibrational levels in an odd-mass nucleus, C. J. Gallagher, Jr., W. F. Edwards and G. Manning 18
Theory of E0 transitions of spheroidal nuclei, John O. Rasmussen . . . 85
The Mg^{24} (γ, n) Mg^{23} reaction, J. D. King and W. J. McDonald 94
Calculation of splitting of $3s_{\frac{1}{2}}$ neutron levels, F. C. Barker. 110
Multipole order of the 869 keV gamma ray in Sm^{152}, O. Nathan 148
Comparison of the theory of non-axial nuclei with experiments, E. P. Grigoriev and M. P. Avotina. 248
Collective vibrations in P^{31}, V. K. Thankappan and S. P. Pandya . . . 303

1.D.3 *Other models*

Two-body cluster states in nuclei, G. C. Phillips and T. A. Tombrello . . 555

1.D.4 *Relationship between different models*

Lower excited states of W^{185}, H. Morinaga and K. Nagatani 327

1.E *Properties of nuclei*

1.E.1 *Energy levels*

Low levels of Al^{27}, E. Almqvist, D. A. Bromley, H. E. Gove and A. E. Litherland 1
The W^{187} decay scheme and possible vibrational levels in an odd-mass nucleus, C. J. Gallagher, Jr., W. F. Edwards and G. Manning 18
The 9.63 MeV state of C^{13}, F. C. Barker, E. Bradford and L. J. Tassie. . 101
Calculation of splitting of $3s_{\frac{1}{2}}$ neutron levels, F. C. Barker. 110
The decay modes of the 9.17-MeV excited state in N^{14}, H. J. Rose . . . 113
The nuclear spins of I^{126}, I^{132}, I^{133} and I^{135}, H. L. Garvin and E. Lipworth 140
Energy levels of Si^{29} Si^{30} and Si^{31} from (d, p) reactions, C. P. Browne and and J. T. Radzyminski 164
Energy levels and configuration interaction in Zr^{90} and related nuclei, I. Talmi and I. Unna 225
Collective vibrations in P^{31}, V. K. Thankappan and S. P. Pandya . . . 303
Gamma radiation from excited states of F^{18}, Na^{22} and Ne^{22}, T. A. Rabson, T. W. Bonner, R. Castillo-Bahena, M. V. Harlow, Jr., H. P. Haenni and W. A. Ranken 314
Lower excited states of W^{185}, H. Morinaga and K. Nagatani 327
Investigation on the decay scheme of ThC (Bi^{212}), M. Giannini, D. Prosperi and S. Sciuti 380
Decay scheme of Tb^{152}, K. S. Toth, O. B. Nielsen and O. Skilbreid . . . 389
The decay of Ir^{194}, J. Kern and G. Bäckström 461
Pairing interaction in nuclei, G. Abraham and K. K. Gupta 496
Gamma rays from the 351-keV $C^{14}(p, \gamma)$ resonance, D. F. Hebbard . . . 511
Investigations of the decay-scheme of Rh^{101}, B. L. Sharma 550
Energy levels in chromium isotopes, F. A. El Bedewi and S. Tadros . . 604
Energy levels of Re^{187}, R. G. Arns and M. L. Wiedenbeck 634
On the decay of 5.8 d Sb^{120}, 5.1 h Sb^{118} and 1 h Sb^{116}, B. Skytte Jensen, O. B. Nielsen and O. Skilbreid 654

1.E.2 *Binding energies; masses*

On neutron-deficient isotopes of light nuclei and the phenomena of proton and two-proton radioactivity, V. I. Goldansky 482

1.E.3 *Elestric and magnetic moments*

Inelastic scattering from even rare earth isotopes, B. Elbek, M. C. Olesen and O. Skilbreid 523

1.E.4 *Transition probabilities; cross sections*

Multipole order of the 869 keV gamma ray in Sm^{152}, O. Nathan 148
M1/E2 Mixing ratio in the Fe^{57} 14.41 keV γ-transition, G. T. Ewan, R. L. Graham and J. S. Geiger. 221
Nuclear resonance scattering of bremsstrahlung, E. C. Booth 426
On the decay of 5.8 d Sb^{120}, 5.1 h Sb^{118} and 1 h Sb^{116}, B. Skytte Jensen, O. B. Nielsen and O. Skilbreid 654

1.E.5 *Nuclear radii; matter distributions*

An experimental search for dipole structure of the electron, G. R. Burleson and H. W. Kendall 68
Charge distribution in nuclei and energy levels of μ mesonic atoms, G. E. Pustovalov and M. S. Krechko 337

1.E.6 *Nuclear moments of inertia*

Inelastic scattering from even rare earth isotopes, B. Elbek, M. C. Olesen and O. Skilbreid 523

1.E.8 *Other properties*

Measurement of the rotational g-factor (g_R) for several nuclei, G. Manning and J. Rogers 675

2. Nuclear Reactions

2.A *General Properties*

2.A.1 *Cross-sections, energy relations*

Gamma rays from the interaction of 14-MeV neutrons with beryllium, J. Benveniste, A. C. Mitchell, C. D. Schrader and J. H. Zenger 52
Thermal and resonance neutron capture gamma rays from Nd^{144} and Nd^{146}, J. E. Draper and R. L. Hickok 436
Neutron cross-sections in aluminium, G. S. Mani, G. J. McCallum and A. T. G. Ferguson 535

2.B *Angular distributions; correlations; polarization*

The observation of p′–γ angular correlation at a nuclear resonance, H. Yoshiki and N. M. Nikolic 442

2.D *Statistical model*

Mechanism of the $Zn^{64}(n,p)Cu^{64}$ reaction at incident neutron energies of 8 and 14 MeV, Alice H. Armstrong and L. Rosen 40
Radiative proton capture in Ni^{58}, J. H. Carver and G. A. Jones 184
Neutron cross-sections in aluminium, G. S. Mani, G. J. McCallum and A. T. G. Ferguson 535
(α, p) reactions in medium weight elements, N. O. Lassen and V. A. Sidorov 579

2.E *Optical model*

The interaction of 40–160 MeV neutrons with helium nuclei, M. Arnold, P. E. Hodgson, D. F. Shaw and D. M. Skyrme 500

2.F *Direct interaction other than (stripping)*

Mechanism of the $Zn^{64}(n,p)Cu^{64}$ reaction at incident neutron energies of 8 and 14 MeV, Alice H. Armstrong and L. Rosen 40

2.G *Stripping and pick-up*

Energy levels of Si^{29}, Si^{30} and Si^{31} from (d,p) reactions, C. P. Browne and J. T. Radzyminski 164
Energy levels in chromium isotopes, F. A. El Bedewi and S. Tadros 604
Angular correlation studies of the $Be^{9}(\alpha, n\gamma)C^{12}$ reaction, J. B. Garg, J. M. Calvert and N. H. Gale 264
Reaction mechanism studies on $Si^{28}(d, p)Si^{29}$ (I) Distorted wave effects, J. A. Kuehner, E. Almqvist and D. A. Bromley 614

2.H *Coulomb excitation*

A remark on the Coulomb disintegration of accelerated heavy ions, J. M. Hansteen 309
Coulomb excitation of the first levels of spherical even nuclei by multiply charged ions, D. S. Andreyev, A. P. Grinberg, K. I. Erokhina and I. Kh. Lemberg 400
Inelastic scattering from even rare earth isotopes, B. Elbek, M. C. Olesen and O. Skilbreid 523

2.I *Photonuclear processes*

The $Mg^{24}(\gamma, n)Mg^{23}$ reaction, J. D. King and W. J. McDonald 94
Réactions secondaires de spallation, M. Lefort, G. Simonoff et X. Tarrago . . . 173
Photoprotons from Cs and I, R. B. Taylor 453

2.J *Fission and spallation*

Direct processes and collective effects in high energy proton induced fission, H. Faissner and H. Schneider 346
Fore-aft yields of fragments from 14-MeV neutron-induced fission, R. B. Leachman and G. P. Ford 366

2.L *Scattering processes (except two-nucleon system and meson scattering)*

On the theory of p–α scattering, A. Herzenberg and E. J. Squires 280
Gamma rays from the interaction of 14-MeV neutrons with carbon, J. Benveniste, A. C. Mitchell, C. D. Schrader and J. H. Zenger 448
The scattering of alpha particles and deuterons by iodine-127, I. J. Van Heerden and D. J. Prowse 589

3. Electromagnetic Radiation

3.A *Gamma radiation*

Gamma rays from the interaction of 14-MeV neutrons with beryllium, J. Benveniste, A. C. Mitchell, C. D. Schrader and J. H. Zenger 52
The decay modes of the 9.17-MeV excited state in N^{14}, H. J. Rose 113
Gamma radiation from excited states of F^{18}, Na^{23} and Ne^{22}, T. A. Rabson, T. W. Bonner, R. Castillo-Bahena, M. V. Harlow, Jr., H. P. Haenni and W. A. Ranken 314
Thermal and resonance neutron capture gamma rays from Nd^{144} and Nd^{146}, J. E. Draper and R. L. Hickok 436
Gamma rays from the 351-keV $C^{14}(p,\gamma)$ resonance, D. F. Hebbard 511
Investigations of the decay-scheme of Rh^{101}, B. L. Sharma 550
Energy levels of Re^{187}, R. G. Arns and M. L. Wiedenbeck 634
Measurement of the rotational g-factor (g_R) for several nuclei, G. Manning and J. Rogers 675

3.B *Internal conversion*

M1/E2 mixing ratio in the Fe^{57} 14.41 keV γ-transition, G. T. Ewan, R. L. Graham and J. S. Geiger 221

4. Beta Decay; Parity

4.C *Evaluation of matrix elements*

β–γ correlation of the 3^-–2^+–0^+ cascade in the decay of Eu^{152}, J. W. Sunier, P. Debrunner and P. Scherrer 62

4.D K-*capture*

The decay energy of Ba^{133}, M. L. Ramaswamy, W. L. Skeel and P. S. Jastram 299
L to K capture ratio in the decay of Ge^{68}, M. K. Ramaswamy 377

4.E *Analysis of data*

The 85 minute activity of Ba^{139}, W. H. Kelly, G. B. Beard, W. B. Chaffee and J. M. Gonser 79
Decay of Y^{88}, M. K. Ramaswamy and P. S. Jastram 243
Investigation on the decay scheme of ThC (Bi^{212}), M. Giannini, D. Prosperi and S. Sciuti 380
Decay scheme of Tb^{152}, K. S. Toth, O. B. Nielsen and O. Skilbreid 389
The decay of Ir^{194}, J. Kern and G. Bäckström 461

7. Quantum Field Theory

7.B *Quantum Field Theory*

An experimental search for dipole structure of the electron, G. R. Burleson and H. W. Kendall 68

7.C π-*meson field (scattering and nuclear forces)*

Elastic scattering of nucleons and pions at very high energy, Z. Koba, A. Krzywicki, R. Rączka and Z. Chyliński 199

8. Elementary Particles

8.B *Theory, interactions, transformation properties*

Charge distribution in nuclei and energy levels of μ mesonic atoms, G. E. Pustovalov and M. S. Krechko 337

9. Cosmic Radiation

9.B *Passage of particles through matter*

The anomalous scattering of underground μ-mesons, R. Burnstein, T. Kitamura and D. D. Millar 665